



**20<sup>th</sup> International Conference on  
Sustainable Energy Technologies  
15<sup>th</sup> to 17<sup>th</sup> August 2023, Nottingham, UK**

---

***Sustainable Energy Technologies 2023  
Conference Proceedings: Volume 3***

---

© 2023 Copyright University of Nottingham & WSSET

The contents of each paper are the sole responsibility of its author(s); authors were responsible to ensure that permissions were obtained as appropriate for the material presented in their articles, and that they complied with antiplagiarism policies.

Reference to a conference paper:

To cite a paper published in these conference proceedings, please substitute the highlighted sections of the reference below with the details of the article you are referring to:

Author(s) Surname, Author(s) Initial(s), 2023. 'Title of paper'. In: Riffat, Su,. ed., **Sustainable Energy Technologies**: Proceedings of the 20th International Conference on Sustainable Energy Technologies, 15th – 17th August 2023, Nottingham, UK. University of Nottingham: Buildings, Energy & Environment Research Group. Pp XX-XX. Available from: [nottingham-repository.worktribe.com/](https://nottingham-repository.worktribe.com/) [Last access date].

ISBN-13: 978 085358 357 8

Version: 15.12.2023

# CONTENTS

Paper Reference #	Title of Paper	Page Number
#201:	Power generation prediction of a new tower type thermal/photovoltaic (T/PV) power generation system based on spectral beam splitting .....	1
#202:	Designing ecological landscapes .....	14
#203:	Experimental investigation of concentrated triple junction solar cells under non-uniform illumination .....	23
#204:	Optimum scheduling by creating feeder scale islands for continuity of supply of critical loads in emergency network conditions .....	33
#205:	3-E analysis of plasma gasification combined cycle integrated molten carbonate fuel cell for power production based on refused derived fuel feedstock .....	40
#207:	Estimating energy savings in singapore’s building benchmarking policy for office buildings .....	48
#209:	Effect of diffuser proximity to buildings on wind energy potential .....	54
#211:	Analysis of suitability of national sustainability recommendations for thermal comfort in post-disaster social housing in Yucatan, Mexico .....	62
#213:	Robotic composite filament winding technology for ultra-lightweight I7e class electric vehicles: enabling cost-effective zero emission urban mobility solutions .....	71
#220:	A computational study into the charging of an agitated fluidised bed thermochemical energy storage system .....	79
#222:	Synthesis and characterization of doped magnesium hydroxide for medium heat storage application .....	88
#223:	Fifth generation district heating and cooling network coupled with geothermal energy source for a sustainable community: case study of embassy of sharing at Malmö .....	96
#232:	Field monitoring of indoor air temperature of 3D-printed house in the hot climate of Saudi Arabia .....	102
#233:	Building retrofit- an active influence on the residential building's energy consumption by changing the size of the windows .....	110
#235:	A numerical study on the effect of different roof shapes on the performance of an oscillating aerofoil energy harvester integrated into a building structure .....	121
#236:	A review on the state-of-the-art wind energy harvesting technologies and potential integration into building roof structure .....	129
#240:	Inter-unit transmission of pollutants in naturally ventilated buildings adjoining a street canyon: a parametric study .....	137
#241:	Operational tool for selecting energy systems for small buildings based on useful energy needs .....	148
#242:	Power quality impacts of grid-tied PV inverters on low voltage distribution networks .....	156
#244:	Exploring sustainable residential building solutions through green engineering: a Saudi Arabian case study .....	167
#245:	A renewable multigeneration energy system for a public school in Denmark .....	177
#247:	The impact of applying the new Saudi building code on residential buildings’ performance in Riyadh region .....	188
#249:	A BIM-based framework for designing sustainable structures through the reuse of precast concrete components .....	201
#251:	The role of the informal sector towards sustainable waste management practices in developing countries: case study in Jordan .....	210
#253:	The impact of courtyards and window designs on thermal and visual comfort conditions in adobe traditional buildings of Nigeria .....	217
#254:	Advancing thermal comfort research: evaluating indices for naturally ventilated residential buildings in diverse climatic zones .....	229
#255:	A hardware-in-the-loop simulation of a heat pump system for vehicle thermal management .....	240
#256:	The impact of PV, battery and immersun on the meadows community: data analysis of project sensible .....	249
#260:	Converting flood-risk areas to water-resilient and productive dryland production systems .....	259
#261:	Heat transfer optimization of a carnot battery using a partial cascade organic-steam rankine cycle .....	264
#263:	An assessment of the value of V2X for commercial car parks: a case study for East Midlands airport .....	273
#266:	Non-traditional social housing in the UK .....	281
#271:	Maximizing solar power harvest: experimental analysis of vacuum insulated photovoltaic/thermal (PVT) power module in subtropical climates .....	300
#275:	Performance study for selected HVAC systems .....	310
#277:	Challenges of climate change & resilient housing design solution .....	317
#281:	Smart responsive shading for enhanced energy efficiency in hot climates .....	329
#283:	Interpretable data-driven methods to automate energy model calibration .....	340
#286:	An experimental investigation on adsorption and regeneration performance of composite desiccants for building applications .....	351
#289:	Investigation on a novel thermoelectric ventilator system for retrofit in heritage buildings .....	359
#290:	Investigations on the retrofitting strategies coupling multiple targets on heritage dwellings located in Suzhou .....	372
#291:	Comparative study on a low-carbon house and common houses with post occupancy evaluation in rural area of China .....	383
#293:	Impact of various technologies on peak energy demand of residential building in the cold climate of UK .....	394
#295:	AI-based hourly electricity consumption prediction for households and residents .....	404
#298:	How window opening behaviour affect thermal comfort of low-cost apartment in Indonesia .....	413

---

# #201: Power generation prediction of a new tower type thermal/photovoltaic (T/PV) power generation system based on spectral beam splitting

---

Zhongzhu QIU<sup>1</sup>, Xingrui Ni<sup>2</sup>, Qunzhi ZHU<sup>3</sup>, Yongjian YE<sup>4</sup>, Tao ZHANG<sup>5</sup>, Jingyong CAI<sup>6</sup>, Ning XU<sup>7</sup>, Miaomiao ZHANG<sup>8</sup>, Chengyang LI<sup>9</sup>

<sup>1</sup> Shanghai University of Electric Power, Shanghai, China, qiuzhongzhu@shiep.edu.cn

<sup>2</sup> Shanghai University of Electric Power, Shanghai, China, 1181579260@qq.com

<sup>3</sup> Shanghai University of Electric Power, Shanghai, China, zhuqunzhi@shiep.edu.cn

<sup>4</sup> East China Electric Power Design Institute Co., Ltd. of China Power Engineering Consulting group, Shanghai, China, yyj1@ecepdi.com

<sup>5</sup> Shanghai University of Electric Power, Shanghai, China, taozhang@shiep.edu.cn

<sup>6</sup> Shanghai University of Electric Power, Shanghai, China, caijingyong@126.com

<sup>7</sup> Shanghai University of Electric Power, Shanghai, China, suepxn@163.com

<sup>8</sup> Shanghai University of Electric Power, Shanghai, China, 184790618@qq.com

<sup>9</sup> Shanghai University of Electric Power, Shanghai, China, 2111270992@qq.com

*Abstract: At present, photovoltaic power generation can only utilize a portion of the solar band, and the remaining bands entering the battery will not be used for power generation, but will instead increase the temperature of the battery, leading to a decrease in photoelectric conversion efficiency. Therefore, using frequency division to utilize some photons that do not respond to the battery for thermal utilization can effectively improve the energy conversion efficiency of solar energy. In this article, the author proposes a tower-type thermal/photovoltaic (T/PV) power generation system using spectral beam splitting technology. The spectroscopic glass is formed by plating a layer of spectral selective film on the surface of special glass, and then install the spectroscopic glass as a cover plate on the photovoltaic cell to replace the heliostat in the tower thermal power generation, so that specific wavebands enter the photovoltaic cell through the spectroscopic glass for photovoltaic power generation, and other wavebands are reflected onto the collector for thermal power generation. The mirror field arrangement was designed using the MUJEN algorithm, and the proposed system was analysed optically and thermodynamically at the AM1.5D solar spectrum as the incident irradiance flux density. Solar radiation data for a typical meteorological year were used to forecast and compare the full-year power generation of photovoltaic power, solar thermal power and this system. The results show that the combined power production of the tower-type T/PV power generation system based on spectral beam splitting is higher than the other two systems under the selected climatic conditions.*

*Keywords: solar energy; power generation system; solar tower; beam splitting technology; thermodynamic analysis*



# 1. INTRODUCTION

Solar energy is inexhaustible as well as clean and free of charge, making it a unique advantage and a huge potential for development and utilization. At present, the utilization of solar energy mainly includes thermal utilization and light utilization, where thermal utilization mainly includes solar water heater, solar thermal power generation and high temperature solar furnace, while light utilization is mainly photovoltaic power generation (Li, 2022). Solar thermal power generation in thermal utilization is the focus of solar radiation, using heat collection and heat exchange equipment to transfer heat to thermal fluid, and the thermal fluid drives the thermal machine to generate electricity. Solar thermal power generation is mainly divided into trough type, tower type and dish type according to the different forms of solar energy concentration. However, the annual power generation efficiency of this type of concentrating solar thermal power generation is only 11-25 %, while the tower power generation technology has higher concentrating multiplier, easier to reach higher working temperature, and higher thermal conversion efficiency, which makes it have more room for improvement (O'Neill, 2021). Today, photovoltaic power generation in the laboratory is capable of converting about 30% of simulated sunlight into electricity (Ju et al., 2012), while in engineering this efficiency is even lower, at 16-20% (Zhang, 2019). However, due to the characteristics of photovoltaic power generation, only a specific spectral range of solar radiation can be converted into electricity, the rest of the band is not only not conducive to photovoltaic power generation but will lead to an increase in cell temperature and thus reduce the efficiency of power generation.

In order to fully utilize solar energy in a wider range of solar spectral wavelengths, the concept of T/PV power generation system based on spectral beam splitting was proposed, i.e., a specific spectral range for photovoltaic power generation and other spectral ranges for photothermal power generation (Ju et al., 2017). Mahmoudinezhad et al. (2022) built a simple hybrid photovoltaic-thermoelectric generator beam splitter (PV-TEG-BS) system using photovoltaic cells, a temperature differential generator, and a beam splitter for spectral splitting. Experimentally, it was found that the use of the spectral beam splitting technique reduces the power generation of the solar thermal component but significantly increases the power generation of the PV cells in the system, and the total power generation of the system is also higher. In order to scale up the system and utilization efficiency, numerous scholars have tried to replace the temperature difference generator in the system with concentrated solar thermal power technology. Widyolar, Jiang and Winston (2018), Jiang et al. (2009), Liu et al. (2014), Segal, Epstein and Yogev (2004) combined trough, butterfly, linear Fresnel and tower with a split-spectrum photothermal -photovoltaic composite power system. The simulation results show that the power generation efficiency of the system is all improved than before. However, most of the current tower type T/PV power generation system based on spectral beam splitting are set up with a selective transmission mirror in the path of the sunlight reflected by the heliostat to the collector, so that the specified waveband reflection is used for photovoltaic power generation and the other wavebands are used for solar thermal power generation. However, this structure leads to increased path loss of sunlight and the construction difficulty of setting up a mirror surface between the heliostat and the collector is also relatively high.

Therefore, In this article, the author proposes a new tower type T/PV power generation system system based on spectral beam splitting. The system design is based on a spectral glass that is capable of transmitting completely in the specified wavelength band and reflecting completely in other wavelength bands. By combining the spectroscopic glass with the solar panel to form a spectroscopic photovoltaic panel and replacing the heliostat in a conventional tower-type solar thermal power system, the path loss of sunlight is reduced. After designing the arrangement of the mirror field, the optical and thermodynamic analysis of the system is carried out, and the power generation capacity of the system is estimated for each month of the year based on the meteorological data of a typical meteorological year in Lhasa and compared with conventional photovoltaic power generation and conventional tower-type thermal power generation.

## 2. A NEW TOWER-TYPE T/PV POWER GENERATION SYSTEM BASED ON SPECTRAL BEAM SPLITTING

### 2.1. Structure of tower-type T/PV power generation system based on spectral beam splitting

In this paper, the authors constructed a new tower-type T/PV power generation system based on spectral beam splitting as shown in Figure 1. Combining a spectral glass with a photovoltaic cell to replace the heliostat in a tower-type thermal power generation heliostat field allows specific wavelengths to pass through the spectral glass into the photovoltaic cell for photovoltaic power generation and other wavelengths to be reflected onto the collector for thermal power generation.

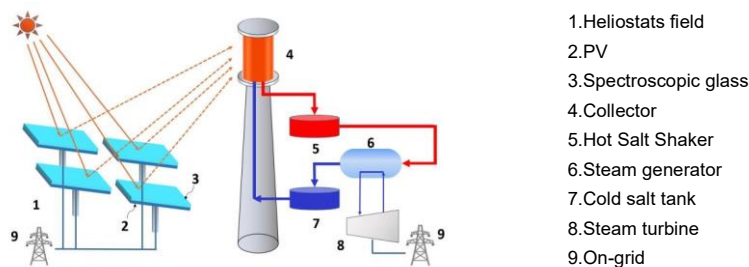


Figure 1 Construction of tower-type T/PV hybrid system based on spectral beam splitting

## 2.2. Spectral photovoltaic panels

A spectrally selective thin film is coated on the surface of the special glass to form a spectroscopic glass, and then the spectroscopic glass is mounted on the conventional solar panel as a cover to assemble a PV panel based on spectral beam splitting(SBS PV panel). The structure of the SBS PV panel is shown in Figure 2, and the materials of each layer from top to bottom are spectroscopic glass, first EVA sheet, conductive welding tape, cell, second EVA sheet and TPT back sheet.

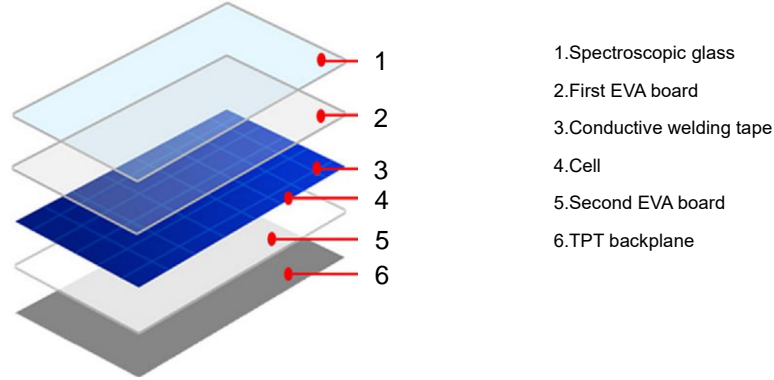


Figure 2 Structure of SBS PV panel

The photovoltaic cells in the SBS PV panels use monocrystalline silicon (c-Si) solar cells with a spectrally selective coating with a theoretical spectral reflectance of (Wang et al., 2019):

Equation 1: Theoretical spectral reflectance of coatings

$$\rho(\lambda) = \begin{cases} 0 & (500nm \leq \lambda \leq 900nm) \\ 1 & (\lambda \leq 500nm, \lambda > 900nm) \end{cases}$$

Where:

- $\lambda$  = wavelength of solar radiation (nm)

## 2.3. Arrangement of the heliostat field

In this study, the conventional radial interleaved layout is chosen for the heliostat field layout, which can effectively reduce the shadowing and occlusion loss of the heliostat field, and then an unobstructed heliostat field layout is established using the MUUEN algorithm (Siala and Elayeb, 2001).

The conventional radially staggered layout is shown in Figure 3, where the heliostats are distributed in concentric rings centered on the heat collection tower, and the distribution of the heliostats is centrosymmetric. The small circles distributed on each ring represent a heliostat. The intersection of the ring and the north axis is called the essential rings when there is a heliostat, and the intersection is called the staggered ring when there is no heliostat. The characteristic diameter DM of the heliostat is equal to the diagonal of the heliostat plus the separation distance :

Equation 2: Characteristic diameter of heliostat

$$DM = l_m(\sqrt{1 + f^2} + dS)$$

Where,

- $l_m$  = heliostat length (m)
- $f$  = heliostat width-to-length ratio
- $dS$  = ratio of heliostat separation distance to heliostat length

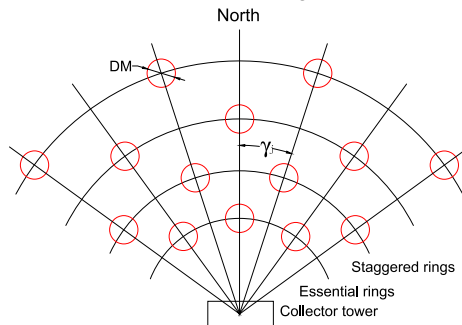


Figure 3 Traditional radial staggered layout

For no blocking, the minimum characteristic diameter  $DM_{min}$  of a square heliostat is (Collado and Turégano, 1989):

Equation 3: Minimum characteristic diameter of heliostat

$$DM = 2w_m$$

Where,

–  $w_m$  = heliostat width (m)

Angular direction unit: The angle between the distribution axes. In radians, this is given by:

Equation 4: The angle between the distribution axes

$$\gamma_j = \frac{DM}{2R_0}$$

Where,

–  $R_0$  = radius of the first ring (m)

The radius of the first circle in the heliostat column is given by:

Equation 5: Radius of the first ring

$$R_0 = R_{min} = 0.75 * H_t$$

Where,

–  $H_t$  = aim point height

Angular direction: The angle between the north axis and distribution axes. It is given by:

Equation 6: Angular direction

$$\Psi = \pm n\gamma_j$$

Where,

–  $n = 0, 2, \dots$  for essential rings,

–  $n = 1, 3, \dots$  for staggered rings

For no blocking radially staggered distribution the radius of the circle is designed as shown in Figure 4.

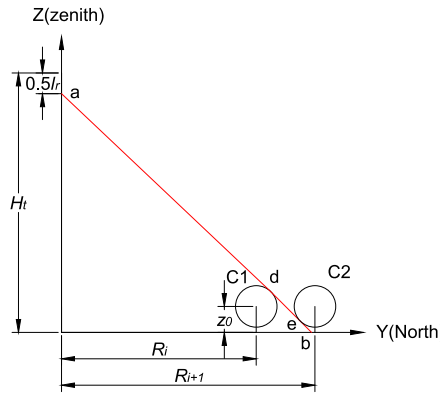


Figure 4 Schematic Diagram of No Blocking Radial Staggered Distribution

The radius of any other ring in the field is determined in accordance with the graphical field layout method. In Figure 4, C1 represents the front view of a known heliostat from the previous ring and ab represents the lowest limit of reflected rays originating behind C1 and striking the receiver with no blocking by C1. Then, the radius of the new ring, equal to  $R_{i+1}$ , is obtained by solving the equations of the line ab and circles C1 and C2.

The radius of each circle  $R_i$  on the horizontal surface can be solved by the geometric relationship shown in Figure 4. After obtaining the radius of each circle, the angle of the adjacent distribution axis, The coordinates of a single heliostat can be expressed as:

Equation 7 Coordinates of each heliostat

$$\begin{aligned} x_m &= R_i \sin \Psi_m \\ y_m &= R_i \cos \Psi_m \\ z_m &= z_0 \end{aligned}$$

In this paper, we assume that the height of the collector tower is 50 m, the length of both sides of the heliostat is 4 m, the height is 5 m, and the solar receiving angle of the collector tower is  $90^\circ$ . Under this condition, the efficiency of using the MUUEN algorithm is relatively high (Barberena et al., 2016). Using the above equation, the heliostats field arrangement can be calculated as shown in Figure 5. Each circle in the figure represents a fixed heliostat, with the positive x-axis pointing due east and the positive y-axis square pointing due north.

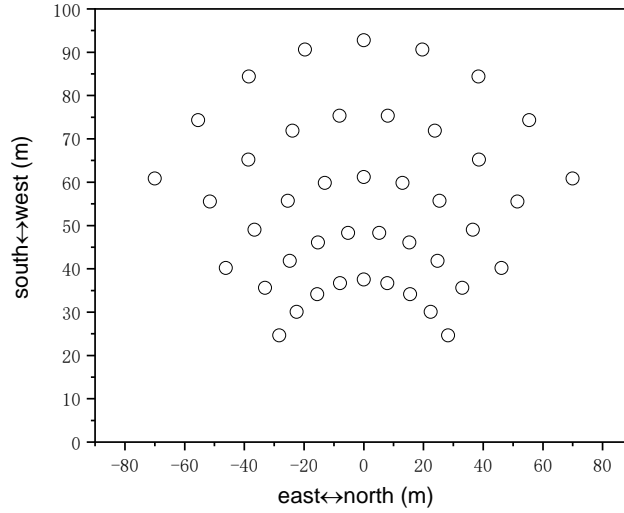


Figure 5 Heliostat field layout

### 3. MATHEMATICAL MODEL OF SYSTEM'S POWER GENERATION FORECAST

#### 3.1. Photovoltaic power generation mathematical model

For a tower-type T/PV hybrid system based on spectral beam splitting, the maximum power generated by the solar cells can be expressed as (Wang, 2022):

Equation 8: The maximum power generated by the solar cells

$$P_{PV,BS} = V_{OC,BS} \cdot I_{SC,BS} \cdot FF$$

Where,

- $V_{OC,BS}$  = open circuit voltage (V)
- $I_{SC,BS}$  = short circuit current (A)
- FF = fill factor

The open circuit voltage  $V_{OC,BS}$ , short circuit current  $I_{SC,BS}$  and fill factor FF of the solar cell in the system under  $\lambda_1$ - $\lambda_2$  band are given by:

Equation 9: Open circuit voltage

$$V_{OC,BS} = \frac{hc}{\lambda_2} \cdot \frac{V_{OC}}{E_g}$$

Equation 10: Circuit current

$$I_{SC,BS} = \int_0^{\infty} \tau(\lambda) \cdot E(\lambda) \cdot QE(\lambda) \cdot \frac{e\lambda}{hc} d\lambda$$

Equation 11: Fill factor

$$FF = \frac{v_{OC} - \ln(v_{OC} + 0.72)}{1 + v_{OC}} (1 - R_S)$$

Where,

- $h$  = planck constant ( $6.626 \times 10^{-23}$ )
- $c$  = velocity of light in the vacuum ( $3 \times 10^8$  m/s)
- $V_{OC}$  = open circuit voltage of the solar cell under  $1 \times \text{SUN}$  illumination condition (V)
- $E_g$  = bandgap energy of solar cell (1.4 eV)
- $\tau(\lambda)$  = spectral transmissivity of spectral photovoltaic panel
- $E(\lambda)$  = incident spectral irradiance at AM1.5D
- $QE(\lambda)$  = spectral external quantum efficiency of solar cells
- $e$  = charge of an electron ( $1.6 \times 10^{-19}$  C)
- $v_{OC}$  = open circuit voltage normalized to the thermal voltage  $V_{th}$
- $R_S$  = actual solar cell series resistance

The thermal voltage  $V_{th}$  can be expressed as:

Equation 12: Thermal voltage

$$V_{th} = \frac{\eta_f kT}{e}$$

Where,

- $\eta_f$  = diode ideality factor
- $k$  = boltzmann constant ( $1.38065 \times 10^{-23} \text{ m}^2\text{kg}\cdot\text{s}^{-2}\text{K}^{-1}$ )
- $T$  = operating temperature of solar cell ( $^{\circ}\text{C}$ )

The incident radiation received by the solar cell after spectral division  $Q_{PV,BS}$  is:

Equation 13: Incident radiation received by the solar cell after spectral division

$$Q_{PV,BS} = Q_{in} \int_0^{\infty} \tau(\lambda) d\lambda$$

Equation 14: Incident solar energy flux on the solar concentrator

$$Q_{in} = \eta_{cos} \int_0^{\infty} E(\lambda) d\lambda$$

Where,

- $Q_{in}$  = incident radiation of the system ( $\text{KWh}\cdot\text{m}^{-2}$ )
- $\eta_{cos}$  = cosine efficiency of the system

Thus the energy efficiency of the photovoltaic part of the tower-type hybrid system based on spectral beam splitting  $\eta_{PV}$  is:

Equation 15: Overall energy efficiency of the system

$$\eta_{PV} = \frac{P_{PV,BS}}{Q_Z}$$

Where,

- $Q_Z$  = total solar radiation ( $\text{KWh}\cdot\text{m}^{-2}$ )

The formula for calculating the power of conventional PV panels is as follows:

Equation 16: Power of conventional PV panels

$$P_{PV} = V_{OC} \cdot I_{SC} \cdot FF$$

The short-circuit current and the solar cell efficiency is:

Equation 17: Short circuit current of traditional photovoltaic panels

$$I_{SC} = \int_0^{\infty} E(\lambda) QE(\lambda) \frac{e\lambda}{hc} d\lambda$$

Equation 18: Solar cell efficiency

$$\eta_{PV} = \frac{P_{PV}}{Q_Z}$$

Where,  $P_{PV}$ ,  $V_{OC}$  and  $I_{SC}$  respectively represent the output power of the photovoltaic component without frequency division and their corresponding open circuit voltage and short circuit current values.

For a fixed inclination solar panel the received incident radiation is:

Equation 19: Incident radiation received by fixed tilt solar panels

$$Q_{in} = Q_Z \cdot \eta_{cos,pv}$$

The expression for the cosine efficiency of a fixed inclination PV panel is:

Equation 20: Cosine efficiency of a fixed-tilt PV panel

$$\eta_{cos,pv} = \sin\alpha\cos\beta - \cos\alpha\sin\beta\cos A$$

Where,

- $\alpha$  = Solar altitude angle ( $^{\circ}$ )
- $\beta$  = Tilt angle of photovoltaic panels ( $^{\circ}$ )
- $A$  = Solar Azimuth ( $^{\circ}$ )

The expressions for the solar altitude and azimuth angles are:

Equation 21: Solar altitude angle

$$\alpha = \arcsin(\sin\delta\sin\phi + \cos\delta\cos\omega\cos\phi)$$

Equation 22: Solar azimuth angles

$$A = \arcsin\left(\frac{-\cos\delta\sin\omega}{\cos\alpha}\right)$$

Where,

- $\delta$  = declination angle ( $^{\circ}$ )
- $\phi$  = latitude angle ( $^{\circ}$ )
- $\omega$  = hour angle ( $^{\circ}$ )

The latitude angle is usually the local latitude, the declination angle and the hour angle are calculated by the formula:

Equation 23: Declination angle

$$\sin\delta = 0.39795 \times \cos[0.98563 \times (N - 173)]$$

Equation 24: Solar hour angle

$$\omega = 15 \times (t_s - 12)$$

Where,

- N = the number of days into a leap year cycle with N = 1 being January 1 of each leap year
- $t_s$  = solar time in hours (h)

After choosing the local latitude as the inclination angle, the cosine efficiency of the fixed inclination PV panel can be found for the whole year.

### 3.2. Mathematical model of tower thermal power generation

The power generation capacity of the photothermal component of a tower-type T/PV hybrid system based on spectral beam splitting is usually determined by the total mirror area, solar irradiance per unit area time, optical efficiency and other influencing factors. The amount of electricity generated by the solar thermal fraction per unit area  $P_{TH,BS}$  and the amount of incident radiation received by the collector  $Q_{TH,BS}$  can be expressed as (Xie, 2017):

Equation 25: Electricity generated by the solar thermal fraction

$$P_{TH,BS} = Q_{TH,BS} \cdot \eta_{else}$$

Equation 26: Incident radiation received by the collector

$$Q_{TH,BS} = Q_{in} \cdot \int_0^{\infty} \rho(\lambda) d\lambda$$

Where,

- $\eta_{else}$  = other influencing factors, representing the various losses encountered in the actual operation of tower solar thermal power for example
- $\rho(\lambda)$  = spectral reflectance of the spectral photovoltaic panel

The most important factors in optical efficiency are the cosine efficiency of the heliostat and the shadowing and blocking losses. As the fixed heliostatic field is designed in this paper using the no blocking model, the shadow loss is small so it is not considered for the time being. The cosine efficiency, on the other hand, depends on the position of the solar rays and the individual heliostats relative to the receiver. Therefore, a coordinate system as shown in Figure 6 was established for calculating the cosine efficiency. The x-axis of this coordinate system points north, the y-axis points east, the collector is the coordinate origin, A is the collector coordinate, and B is the coordinate of a certain heliostat.

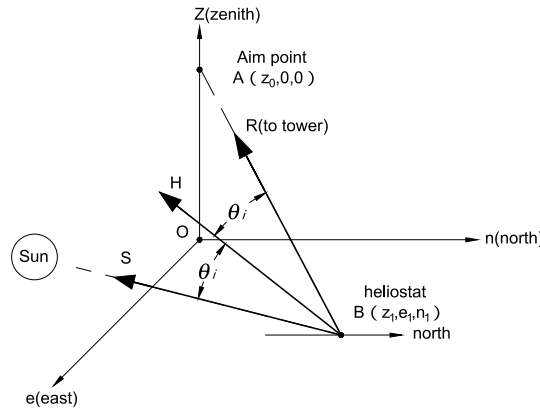


Figure 6 Coordinates of sunlight reflected by a single heliostat

The expression to calculate the cosine efficiency of the system is (Stine and Geyer, 2001):

Equation 27: Cosine efficiency of the system

$$\eta_{cos} = \cos\theta_i$$

Equation 28: Angle of incidence of the sun

$$\cos 2\theta_i = \frac{(z_0 - z_1) \sin \alpha - e_1 \cos \alpha \sin A - n_1 \cos \alpha \cos A}{\sqrt{[(z_0 - z_1)^2 + e_1^2 + n_1^2]}}$$

Where,

- $\theta_i$  = angle of incidence of sunlight (°)
- $z_0$  = height of collector (m)
- $z_1, e_1, n_1$  = coordinates of heliostat (m)

After determining the date, the time of the day, the local latitude, the collector, and the coordinates of the heliostat, the cosine efficiency of that heliostat can be found for any time of the year.

The literature (Yao, 2019) presents the estimation of power generation for the actual operation of tower solar thermal power, on the basis of which this paper assumes that the other influencing factors in the power generation process are 0.237, i.e.  $\eta=0.237$ .

Therefore, the efficiency of the photothermal component of the tower-type T/PV hybrid system based on spectral beam splitting  $\eta_{PV,BS}$  is:

Equation 29: Efficiency of the photothermal component

$$\eta_{TH,BS} = \frac{P_{TH,BS}}{Q_Z}$$

This gives the total generation capacity  $P_{total}$  and total generation efficiency  $\eta_{sys}$  of the tower-type T/PV hybrid system based on spectral beam splitting as :

Equation 30: Total generation capacity of the tower-type T/PV hybrid system

$$P_{total} = P_{PV,BS} + P_{TH,BS}$$

Equation 31: Total generation efficiency of the tower-type T/PV

$$\eta_{SYS} = \frac{P_{total}}{Q_Z}$$

### 3.3. Model solution

In this paper, we simulate a new tower-type T/PV hybrid system based on spectral beam splitting under AM1.5D ideal spectral (ASTM international, 2012) distribution using the equations presented in the previous paper.

The model solution first requires the assumption of the spectral transmittance profile of the system, i.e., which band is selected for complete transmission for photovoltaic power generation. Using the assumed spectral transmittance curves combined with Eqs. (13) - (28), the respective incident radiation amounts of the photovoltaic and photothermal components of the system can be obtained. The model solution is then divided into two parts: photovoltaic and solar thermal.

In the photovoltaic power generation section, c-Si solar cells are selected in this paper, and their open-circuit voltage, fill factor (Green et al., 2013), diode ideality factor  $\eta_i$ , and series resistance  $R_s$  (Green et al., 2021) under standard test conditions are shown in Table 1. Assuming the cell temperature of 30°C, the open-circuit voltage, short-circuit current and fill factor of the PV cell after spectral separation are calculated by Eqs. (9)-(11), respectively, and then the power generation of the PV part of the system at a given spectral transmittance and the power generation efficiency are calculated using Eqs. (8) and (15).

Table 1: Thermodynamic analysis constants

Parameters		Parameters	
Voc	0.7485	$\eta_i$	1.28
FF	0.855	$R_s$	0.012

In the solar thermal power generation section, Lhasa is chosen as the simulation site, and the solar altitude angle, solar azimuth angle, declination angle and hour angle of a single spectral photovoltaic panel can be calculated for each moment of the year using Eqs. (21)-(24). Based on the mirror field arrangement layout designed in Section 2.3 to obtain the relative coordinates between each spectral PV panel and the collector, the cosine efficiency of the mirror field can be calculated using Eq. (28). Using Eqs. (25) and (29), the amount of power generated by the photothermal part of the system for a given spectral transmittance and the power generation efficiency can be calculated. Finally, the total generation capacity and total generation efficiency of the tower-type split-spectrum composite power generation system are obtained using Eqs. (30) and (31). The solution process is shown in Figure 7.

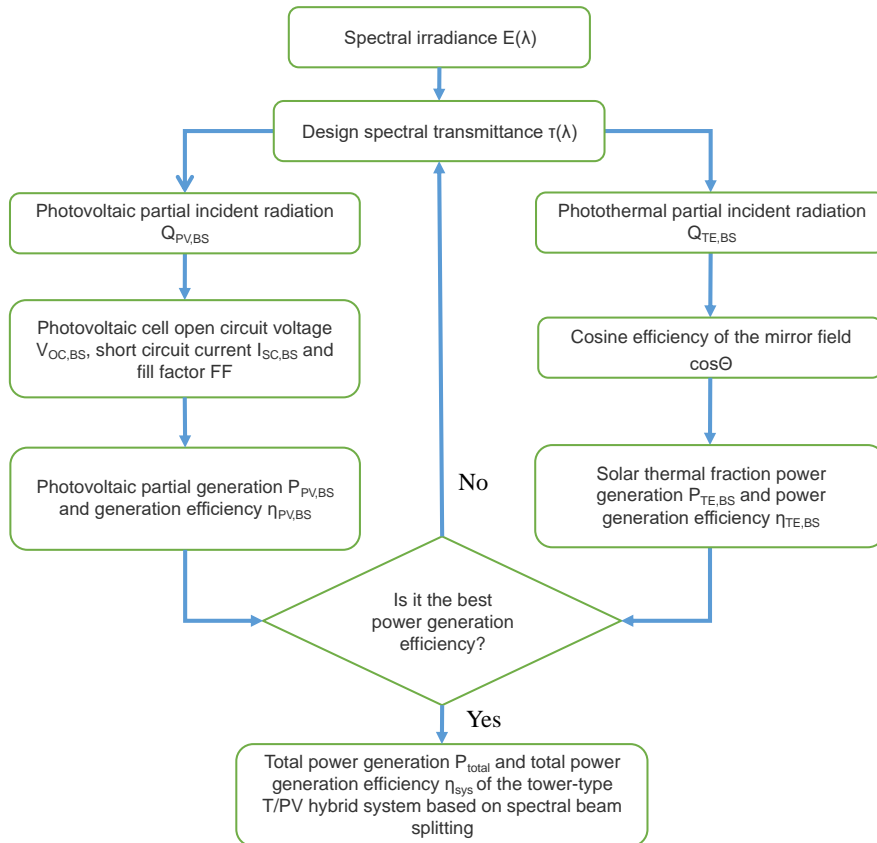


Figure 7 Solution process diagram of tower type hybrid power generation system based on spectral beam splitting

As shown in Figure 8, setting different spectral transmittance bands can calculate the total power generation efficiency of different tower-type T/PV power generation system based on spectral beam splitting. It can be seen that the total power generation efficiency of the system is highest when the starting band is 500 nm and the ending band is 900 nm, which is 21.31 %.

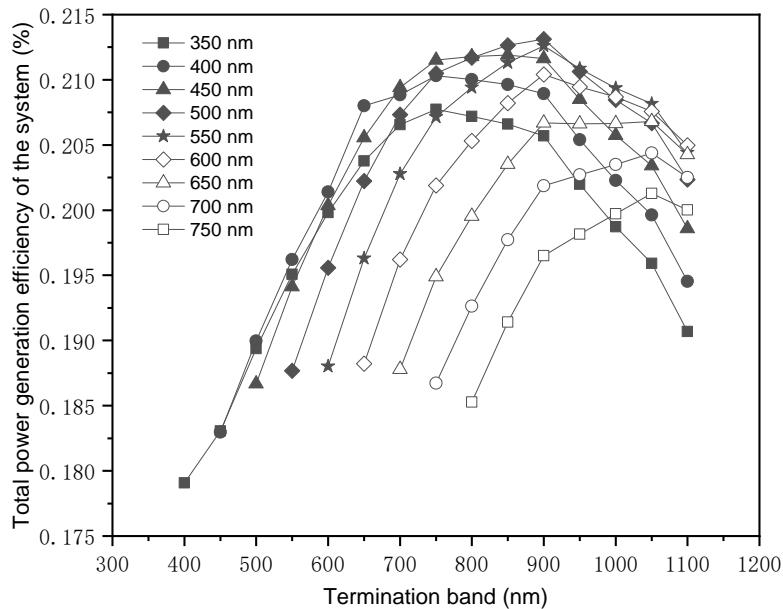


Figure 8 Total power generation efficiency of the system at different wavebands

When the starting band is 500-900 nm, the ideal spectral distribution of AM1.5D on the surface of the PV cell and collector after spectroscopic glass spectroscopy and the frequency division band are shown in Figure 9, and the total incident radiation on the surface of the spectroscopic glass can be obtained as 1000.37 W/m<sup>2</sup> by integrating the curve. The incident radiation received by the solar cell surface is 490.18 W/m<sup>2</sup> and the incident radiation reflected to the collector is 510.19 W/m<sup>2</sup>. The average transmittance of the spectroscopic glass is 49.08 % and the average reflectance is 50.92 %.



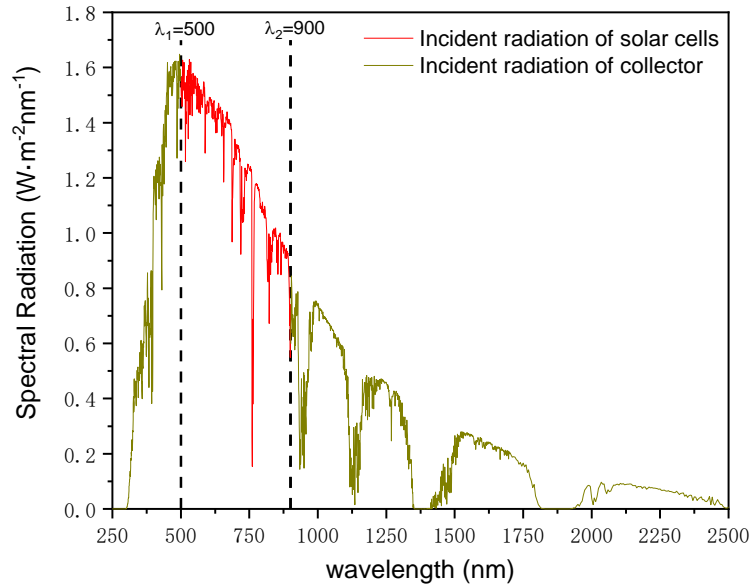


Figure 9 Spectral distribution of incident radiation

The quantum efficiency of c-Si solar cells versus the optimal spectral transmittance curve of the spectroscopic glass is shown in Figure 10. When the starting band is 500-900 nm, the power generation efficiency of the photovoltaic part of the tower-type T/PV power generation system is 33.17 %. By using Eqs. (16)-(19), it can be calculated that the power generation efficiency is 25.06 % when direct sunlight hits the photovoltaic panel, and the power generation efficiency of this c-Si solar cell given in the literature (Green et al., 2021) is  $25.3\pm 0.4$  %, which is consistent with the power generation efficiency calculated in this paper.

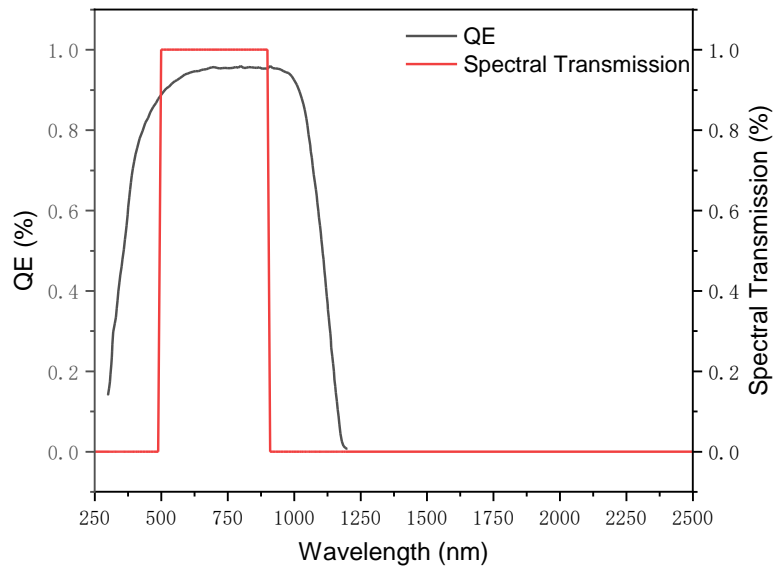


Figure 10 Quantum efficiency and spectral transmittance curves of c-Si solar cells versus spectroscopic glass

#### 4. RESULTS AND DISCUSSION

The total system power generation corresponding to different bands in the AM1.5D solar spectrum irradiation as defined by ASTM G173-03 (2012) can be obtained for the tower-type T/PV power generation system based on spectral beam splitting according to the equation given in the third part. This paper uses the solar direct radiation data in a typical meteorological year in Lhasa as the basis, assuming that the trend of direct radiation with wavelength in it is the same as the solar spectrum of AM1.5D, and the total power generation under each moment of the year when the system is in Lhasa can be calculated by the same way.

The month-by-month values of direct radiation for a typical meteorological year in Lhasa are shown in Figure 11, where the average value of the three months with the least direct radiation is  $142.9 \text{ KWh/m}^2$ , which is 72.60 % of the average value of the three months with the most total radiation of  $196.8 \text{ KWh/m}^2$ . It can be seen that the radiation levels in Lhasa do not vary much from season to season throughout the year, while the total radiation level is higher in summer due to the long sunshine hours.

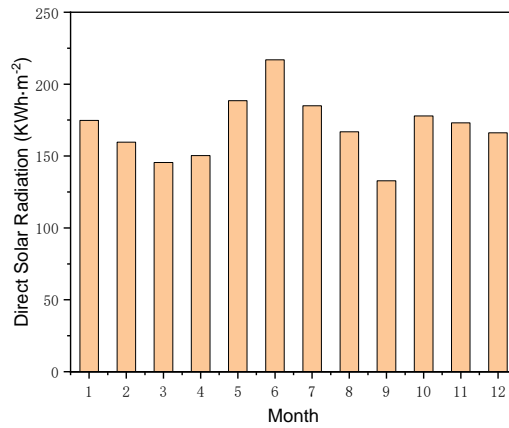


Figure 11 Monthly value of direct radiation

Bringing the data of direct radiation to Eqs. (26) and (27) gives the cosine efficiency of the spectral PV panel at each moment of the year for a given coordinate. Based on the coordinates of each mirror in the mirror field designed in section 2.3, the total incident radiation per unit area received by the mirror field can be calculated. The average cosine efficiency of the mirror field for each month of the year is shown in Fig. 12, and the average cosine efficiency of the mirror field for the year is 75.18 %. Using Eqs. (20)-(24), it can be calculated that the annual cosine efficiency of a fixed-tilt PV panel is approximately 65.97 % when the tilt angle is the local latitude.

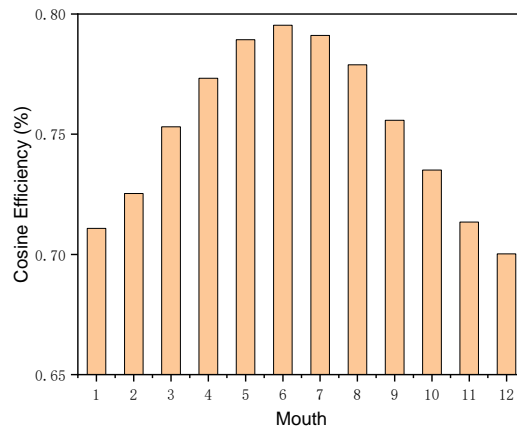


Figure 12 Monthly value of mirror field cosine efficiency

Using the introduction in section 3.3, the power production of the system can be obtained for monocrystalline solar cells at different moments of the year in the optimal band 500-900 nm. The full-year variation of power generation for tower-type T/PV hybrid system based on spectral beam splitting, fixed-tilt PV power generation system, and conventional tower-type solar thermal power generation system is shown in Figure 13.

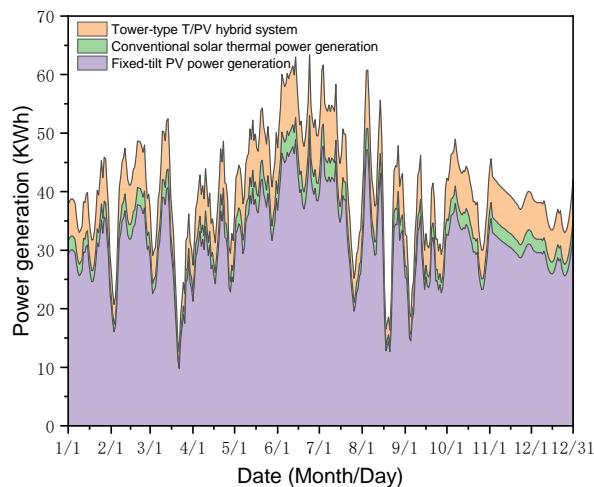


Figure 13 Daily power generation of the system throughout the year

The photothermal part of the tower-type T/PV hybrid system based on spectral beam splitting was obtained by bringing in parameters such as the average cosine efficiency, and the power generation efficiency of the photothermal part of the system after neglecting the shadow area was 17.83 %. The monthly average data of all calculated results in the tower-type T/PV hybrid system based on spectral beam splitting are shown in Table 2. The total power generation efficiency of the system is 21.32 %, which is higher than the power generation efficiency of both fixed-tilt PV power generation system and conventional tower-type solar thermal power generation system.

Table 2: Comparison of thermodynamic analysis results of the tower-type T/PV hybrid system based on spectral beam splitting, fixed-tilt PV power generation system and conventional tower-type solar thermal power generation. system.

Parameters	Tower type T/PV hybrid system	fixed-tilt PV generation system	Conventional tower type system
$Q_z/\text{kWh}\cdot\text{m}^{-2}$	7696.64	7696.64	7696.64
$Q_{in}/\text{kWh}\cdot\text{m}^{-2}$	5786.34	5077.47	5786.32
$Q_{PV,BS}$ or $Q_{PV}/\text{kWh}\cdot\text{m}^{-2}$	2839.81	5786.34	—
$Q_{TH,BS}$ or $Q_{TH}/\text{kWh}\cdot\text{m}^{-2}$	2946.53	—	5786.34
$P_{PV,BS}$ or $P_{PV}/\text{kWh}\cdot\text{m}^{-2}$	941.91	1272.41	—
$P_{TH,BS}$ or $P_{TH}/\text{kWh}\cdot\text{m}^{-2}$	698.91	—	1371.32
$P_{total}/\text{kWh}\cdot\text{m}^{-2}$	1640.82	1272.41	1371.32
$\eta_{PV}/\%$	12.24	16.53	—
$\eta_{TE}/\%$	9.08	—	17.83
$\eta_{SYS}/\%$	21.32	16.53	17.83

## 5. CONCLUSION

In this paper, we designed a spectral splitting glass that can completely transmit the specified wavelength band and completely reflect the other wavelength bands, and used it as a cover to lay on c-Si solar cells to form a spectral splitting PV module, and used the spectral splitting PV module to replace the heliostat in the tower power generation to obtain a new tower-type T/PV hybrid system based on spectral beam splitting. A preliminary model of no blocking mirror field distribution was established using the MUUEN algorithm, a mathematical model of the power generation of the system was constructed, and the model was analyzed optically and thermodynamically. The solar radiation data of a typical meteorological year in Lhasa were then used to predict the full-year power generation of the tower-type T/PV power generation system based on spectral beam splitting and compared with the fixed-tilt PV power generation system and conventional tower-type solar thermal power generation system. The results show that the proposed tower-based T/PV hybrid system based on spectral beam splitting has the highest power generation efficiency, which is 4.79 % and 3.49 % higher than the fixed-tilt PV power generation system and conventional tower-type solar thermal power generation system, respectively.

## 6. REFERENCES

- ASTM international. (2012) Standard tables for reference solar spectral irradiances : direct normal and hemispherical on 37° tilted surface. Available at: <https://www.astm.org/g0173-03r12.html> (Accessed: 21 September 2022)
- Barberena J G. et al. (2016) 'State-of-the-art of heliostat field layout algorithms and their comparison', Energy procedia, 93, pp. 31-38.
- Collado, F.J. Turégano, J.A.(1989) 'Calculation of the annual thermal energy supplied by a defined heliostat field', Solar energy, 42(2), pp. 149-165.
- Green, M.A. et al. (2013) 'Solar cell efficiency tables (Version 42)', Progress in photovoltaics: research and applications,21, pp. 827-837.
- Green M A. et al. (2021) 'Solar cell efficiency tables (Version 58)', Progress in photovoltaics: research and applications, 29, pp. 657–667.
- Jiang, S. et al. (2010) 'Optical modeling for a two-stage parabolic trough concentrating photovoltaic/thermal system using

- spectral beam splitting technology', *Solar energy materials and solar cells*, 94(10), pp. 1686-1696.
- Ju, X. et al. (2012) 'Numerical analysis and optimization of a spectrum splitting concentration photovoltaic- thermoelectric hybrid system', *Solar energy*, 86(6), pp. 1941-1954.
- Li, Y.F. et al. (2022) 'Efficient and comprehensive photovoltaic/photothermal utilization technologies for solar energy', *Power generation technology*, 43(03), pp. 373-391.
- Liu Y. et al. (2010) 'Thermodynamic and optical analysis for a CPV/T hybrid system with beam splitter and fully tracked linear fresnel reflector concentrator utilizing sloped panels', *Solar energy*, 103, pp. 191-199.
- Mahmoudinezhad, S. et al. (2022) 'Experimental investigation on spectrum beam splitting photovoltaic-thermoelectric generator under moderate solar concentrations', *Energy*, 238, pp. 121988.
- O'Neill, S.(2021) 'Perovskite pushes solar cells to record efficiency', *Engineering*, 7(8), pp. 1037-1040.
- Segal, A. Epstein, M. Yogev, A.(2004) 'Hybrid concentrated photovoltaic and thermal power conversion at different spectral bands', *Solar energy*, 76(5), pp. 591-601.
- Siala, F.M.F. Elayeb, M.E.(2001) 'Mathematical formulation of a graphical method for a no-blocking heliostat field layout', *Renewable energy*, 23(1), pp. 77-92.
- Stine, W.B. Geyer, M.(2001) Power from the sun. Available at: <http://powerfromthesun.net/index.html> (Accessed: 9 June 2022)
- Wang, B.T.(2022) 'Study on solar spectral beam splitting photovoltaic/concentrated solar thermal system', China: Northeast Electric Power University.
- Wang G. et al. (2010) 'Thermodynamic and optical analyses of a hybrid solar CPV/T system with high solar concentrating uniformity based on spectral beam splitting technology', *Energy*, 166, pp. 256-266.
- Widyolar, B. Jiang, L. Winston, R.(2018) 'Spectral beam splitting in hybrid PV/T parabolic trough systems for power generation', *Applied energy*, 209, pp. 236-250.
- Xie F.(2013) 'Optical simulation of heliostat field in solar tower power system and its application', China: Zhejiang University.
- Yao, L.S.(2019) 'Estimation of power generation of solar power tower plants', *Shanghai energy saving*, 12, pp. 974-979.
- Zhang, F.(2019) 'Modulation and related mechanism of dislocations in cast quasi-single crystalline silicos', China: Zhejiang University.

---

## #202: Designing ecological landscapes

### A case study of Amata City's smart environment

---

Fa LIKITSWAT<sup>1</sup>, Siwaporn KLINMALAI<sup>2</sup>

<sup>1</sup> Faculty of Architecture and Planning, Thammasat University, Pathum Thani, Thailand, [flikitsw@ap.tu.ac.th](mailto:flikitsw@ap.tu.ac.th)

<sup>2</sup> Faculty of Architecture and Planning, Thammasat University, Pathum Thani, Thailand, [siwaporn@tu.ac.th](mailto:siwaporn@tu.ac.th)

*Abstract: Rapid industrialization and urbanisation offer economic opportunities but also lead to the degradation of ecosystem functioning and ecosystem services, which affect local food security and the preservation of local habitats. The concept of Eco-Industrial Parks, which demonstrate the symbiotic relationship between factories within the same industrial estate to promote circularity of energy and material flows, has been implemented since 1998 in Europe, the United States, and Canada. In 2000, this concept was also adopted in Thailand, though it has yet to be fully realised. Amata City is one of the largest industrial estates in the Eastern Economic Corridor of Thailand (EEC), covering 43 square kilometres or 4,330 hectares. It is a part of Industrial Estate authority of Thailand plans towards the eco-industrial park and smart city development. This article presents a literature review based on three components: i) academic papers related to the concept of eco-industrial parks, ii) an analysis of the Sustainability Report of Amata City, with a focus on the smart environment section, and iii) landscape design proposals by a group of Landscape Architecture students at Thammasat University. In order to interpret the review material, 18 peer-reviewed academic papers, 2014 to 2022 Sustainability Reports of Amata City, and six landscape design proposals were analysed. The results indicate that there are essential characteristics for understanding and implementing the concept of eco-industrial parks, such as the flow of material and energy. Moreover, for a successful sustainability approach, the community and environment should be at the centre, with emphasis placed on the community participatory process and improving environmental quality in the estate and its surroundings. By offering alternative futures for ecological approaches and restoring ecological balance, the design proposals provide insights into designing with ecological approaches and community involvement. Based on these findings, we suggested developing a guideline plan for improving and designing sustainable approaches and practices, which takes into account ecosystem services and maintains the ecosystem function of the industrial landscape.*

*Keywords: Sustainable landscape, Eco-Industrial Park, Ecosystem Functioning, Smart Environment, Urban Biodiversity*

## 1. INTRODUCTION

The international movement on the sustainable development and green economy set up and define the sustainable development goals, framework, and strategies since 1987. The Brundtland Commission: World Commission on Environment and Development officially defines sustainable development definition. The current focus is shift to the complex issue as climate change. Possible environmental impacts of industrial estates (UNEP, 1997), lead to the concept of developing eco-industrial park. This framework is adopted worldwide throughout the regions. However, there are several limitation factors that obstruct the key success to implement this concept to achieve the ideal industrial ecology potentials.

Industrial estate in Asia developed without planning and usually mainly focused on economic driver (Chiu &Yong, 2004). In Thailand, some participating agencies include GTZ and IEAT are involve with the planning and implementing of eco-Industrial parks (Sakr et al., 2011). The example of Industrial estate authority of Thailand plans (Map Ta Phut, northern region, Amata Nakorn, eastern sea-board, Bang Poo); Samut Prakarn province CPIE, project (ADB-funded); Bangkok (Panapanaan).

Amata City has become one of the biggest industrial estate developments in Thailand since its foundation in 1989, through the promotion of the Eastern Economic Corridor of Thailand. As a part of the 5th National Economic and Social Development Plan (1982-1986) established Eastern Seaboard Development Program (ESB), the three provinces Chonburi, Rayong, and Chachoengsao were assigned to be strategic location for the mega-project development for economic driven to Thailand 4.0. Situated in the lower part of the Bangpakong River Basin near the coastal landscape of the Gulf of Thailand, Amata City has expanded over the years and now occupies an area of 43 square kilometres or 4,330 hectares in the provinces of Chonburi and Chachoengsao. With the vision of "Creating Perfect Cities where possibility happens", there has been a shift in focus towards a sustainable development plan, transitioning from an eco-industrial town to a smart city. Despite the socio-economic driven mechanism behind the development of the industrial park, there are existing ecological landscapes that consist of mudflats, mangrove forests, fishponds, paddy fields, and orchards. However, land-use conflicts have disconnected the food security and the preservation of local habitats. Community organising actions have been taken to protect farmland from the development of EEC at Ban Pho Chachoengsao. The question now is how to plan for ecological activity in such a humanised area. What will be the vision and strategic design for an embedded ecological landscape in an industrial town?



*Figure 1 Aerial photography over Amata City in Chonburi and Chachoengsao, Thailand  
Source: Author 28 Feb 2023*

To address these issues, the sustainable landscape design studio at the Faculty of Architecture and Planning at Thammasat University has conducted a study to analyse and redesign the ecological connection between Amata City and its surroundings. A macro-scale landscape vision plan aimed at redesigning the eco-industrial park to emphasis on the smart environment and ecological landscape design for the industrial sites. Six ecological visioning landscape design proposals were developed. These include: eco-industrial towns, eco-factory and manufacturing, eco-revitalization of local canals, revitalization of water networks, green linkages, and eco-mobility. This paper will discuss the concept of Eco-Industrial Parks, analyse the Sustainability Report of Amata City closely on the focus towards an environmental section,



as well as extend to discuss further on the visioning of ecological landscape design proposals proposed by the landscape architecture students from Thammasat University.

## 2. METHODOLOGY

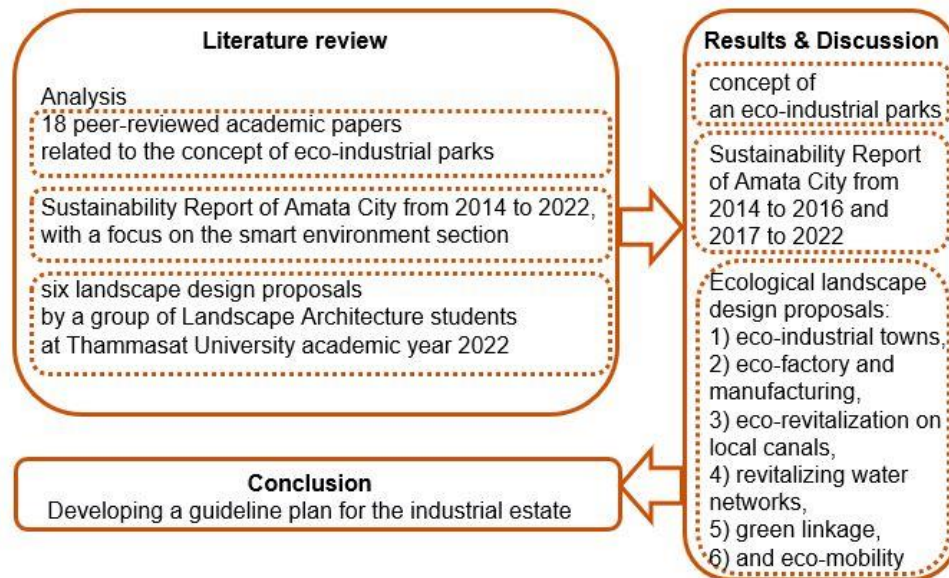


Figure 2 Methodology diagram

There are three material components which will be analysed for the literature review. From these three components will be linked and discussed with the result and discussion as well as the conclusion part to understand the vision and strategic design for an embedded ecological landscape in the case study area. The concept of methodology diagram is shown in Figure 2.

The first part based on 18 peer-review academic papers related to the concept of eco-industrial parks. This part of the research uses a narrative review approach based on 60 articles from the Scopus and Google Scholar search engines. Keywords, including 'Eco- Industrial park'; 'Eco- Industrial estate'; 'Eco- Industrial development'; 'Industrial Ecology'; 'Circular economy'; 'Green development'; 'Environmental protection'; ' Land protection'; 'Waste recycling'; 'Waste recycling'; 'Water resource recycling'; and 'Biodiversity' were used to search for the pertinent articles.

The second part based on the Sustainability Report of Amata City from 2014 to 2022 with a focus on the smart environment section. The Sustainability Report were downloaded online from the official website of Amata City under the Investor Resources tab to the Sustainability Report from this link <https://www.amata.com/th/sustainability/our-approach>. There are two main characteristics of the report structure from the early versions from 2014 to 2016 and the further versions from 2017 to 2022.

In addition, the last component based on the six landscape design proposals by a group of Landscape Architecture students at the Faculty of Architecture and Planning, Thammasat University academic year 2022. There are number of 24 landscape architecture students in their 3<sup>rd</sup> year of study attend the course "LN316 Landscape Architecture Studio". The six groups of four students per team develop the of their landscape vision plan as one of the projects in this class. The studio class is also a part of the research project funded by the Ministry of Labor, Government of Thailand to set up the study site at Amata City.

## 3. RESULTS AND DISCUSSIONS

There will be three points for illustrate the results and further discuss including, i) eco-industrial park concept to implementation, ii) Amata City's sustainability report, and iii) visioning landscape.

### 3.1. Eco-industrial park concept to implementation

The concept of an eco-industrial park involves not only economic efficiency but also a social dimension and ecological integrity. In the early state, the Kalundborg in Denmark was marked as the model of eco-industrial park, emphasising the symbiosis relationship between the industrial factories and the community since 1998. The concept has been adopted and implemented in the US and Canada, which follow certain characteristics. "If the goal is sustainability of the industrial community and ecosystem, a more comprehensive perspective involving ecological, economic and social aspects is necessary" (Co'te & Cohen-Rosenthal, 1998).

From the academic and research viewpoints, there is no agreement on essential characteristics of eco-industrial parks (Co`te & Cohen-Rosenthal, 1998). The current body of knowledge on industrial ecology is not sufficient to provide practical solutions (Sakr et al, 2011). The academic research focused on eco-industrial park which increases from 2014 with significant numbers (Vahidzadeh et al., 2020). Eco-Industrial Parks should be designed to encourage the water exchange between factories both for minimizing freshwater discharge and recycling on the wastewater (Tiu & Cruz, 2017). It should also emphasize on material and energy flow (Gibbs & Deutz, 2017). It should also emphasize on sustainable management of green areas in terms of biodiversity protection, landscape conservation and carbon fixing cycles (Daddi et al., 2015).

Table 1: Eco-industrial park concept and characteristic through the regions and countries

Regions, countries	Year	Concepts and Characteristics	References
European, Denmark	1960s	Regional self-organizing manufacturing and enterprise networks	Co`te & Cohen-Rosenthal, 1998
European, German		Industrial symbiosis and efficiency measures	Kechichian & Jeong, 2016
European, Italy	1998	A voluntary certification process	Taddeo, 2016
North America, the U.S.	1998	Regional self-organizing manufacturing and enterprise networks	Co`te & Cohen-Rosenthal, 1998
North America, Canada	1998	Industrial zones to supply of green and environmentally friendly technologies, products, and services and attracting and mobilizing investments	Co`te & Cohen-Rosenthal, 1998
Asia, Japan	2010	An optimization of material and energy use within the eco-city	Minoru et al., 2015
Asia, Republic of Korea	2000s	Mainstreaming an industrial symbiosis project through a public private partnership investment	Kechichian & Jeong, 2016
Asia, China	2000s	Focus on waste management and pollution mitigation	Kechichian & Jeong, 2016
Asia, India	2000s	Focus on waste management and pollution mitigation	Kechichian & Jeong, 2016
Asia, Vietnam	2014	Special Economic Zones to provide a catalytic platform to enhance business applications and opportunities for climate friendly investment	Kechichian & Jeong, 2016
Asia, Thailand	2014	Special Economic Zones with 5 characteristics defined by IEAT	Kechichian & Jeong, 2016

The concept of eco-industrial park first initiated in the European countries. The early state was the Kalundborg model in Denmark (Co`te & Cohen-Rosenthal, 1998). In Italy, the framework of Industrial Ecology was introduced in 1998 by a national law as the Ecologically Equipped Industrial Area (EEIA) (Taddeo, 2016). From the strict regulation and cost control perspective, the movement of relocating manufactures from the develop countries shift to the other part of the regions start since 1970.

In India, all monitoring sites adjacent to the industrial estate in India found very less diversity mostly with invasive species (Banerjee & Srivastava, 2009). The study also points out two recommendations on action and planning stages including, plant native species and setting up the species control and monitoring system as well as plan for greenbelt to filter air pollution.

In Thailand, this initiative was started in 2000 and still not reach the goals (Panyathanakun et al., 2013). According to Koenig's Criteria for Thai Eco-industrial Park, there should be an improvement on the criteria on the following issues. The points are concluded to these five recommendations (Kechichian & Jeong, 2016). "First, physically, the industrial parks must be developed with infrastructure in public utilities and facilities that is environmentally friendly, eco-sufficient, eco-efficient, and safe. Second, economically, the industrial park has to promote localized and provincial economies. Third, environmentally, within the industrial park, operating industries must utilize energy and resources in an efficient manner during production processes, promote waste reduction, and produce environmentally friendly goods. Fourth, socially, the managing organization has to execute human-focused management that makes the well- being of people in the organization the top priority and it must be a significant participant in creating a good quality of life for the community. Lastly, the park management must focus on collaboration and good governance for the benefit of all parties involved." For develop and implementing on the EEC, it still lacks community engagement in the decision-making involvement (Cheevapattananuwong et al., 2020). For Amata City sustainable development program missioned on "Promote CSR Programs of Amata City That Foster Both the Economy and the Environment" (Panthong & Taecharungroi, 2021).

### 3.2. Amata City's sustainability report

The eco-industrial park should not only focus on socio-economic development driven benefit but also plan for less environmental impact. From the concern negatively impact on the living environment of local communities (Panthong & Taecharungroi, 2021), the industrial estate should response to the existing community and local ecosystem. By looking from the management perspective, it is also critical and crucial for sharing the scientific data and information to the public.

There are two main structure shifts on the Sustainability Report of Amata City. The early version of the report from 2014 to 2016 focused on sustainability indicators of an eco-industrial town, such as eco-efficiency resource management, energy



management and conservation, water and wastewater management, pollution control, and air quality monitoring. Later year, the Sustainability Report of Amata City from 2017 to 2022 developed progress not only focused on environmental management onsite but also set indicators toward the other environmental issues and concerns such as biodiversity, climate change and climate resilience, responsible consumption of water resources, and natural resource protection and conservation. This is the progress development at least showing the concern and linkage to response with complex issue as climate change.

Table 2: Analysis on the Sustainability Report of Amata City from 2014 to 2022

Sustainability Report of Amata City (Year)	Theme	Environmental issues								
		eco-efficiency resource management	energy management and conservation	water and waste water management	pollution control	air quality monitoring	biodiversity	climate change and climate resilience	responsible consumption of water resources	natural resource protection and conservation
2014	Merging Innovative Technology with Environmental Sustainability	0	0	0	0	0				
2015	Strategic focus on AEC	0	0	0	0	0				
2016	Creating cities, driving Economies	0	0	0	0	0				
2017	Amata smart city	0	0	0	0	0	0	0	0	0
2018	Amata smart activation	0	0	0	0	0	0	0	0	0
2019	Safe earth, safe us with smart business	0	0	0	0	0	0	0	0	0
2020	Journey to challenge	0	0	0	0	0	0	0	0	0
2021	Collaboration for success	0	0	0	0	0	0	0	0	0
2022	Sustainable cities	0	0	0	0	0	0	0	0	0

While there are more environmental issues report from 2017 to 2022, the detail of data, activities, and environmental monitoring system seems focus on the other surrounding community through the CSR programs. The other potential to link back the issues on biodiversity, climate change and climate resilience, responsible consumption of water resources, and natural resource protection and conservation should somehow be considered within the boundary of the industrial estate as well.

There are common factors for key success and limited factor to develop the Eco-industrial parks (Baas & Huisingsh, 2008). Technological barriers and challenges for implementing the eco-industrial park as concept were mentioned (Li et al., 2015). If these barriers are not dealt with and green technology is not created, it will be even more difficult in the future to address climate change, loss of biodiversity, and other environmental problem. A long-term vision for eco-industrial park must highlight on the network and collaboration as well as focus on the surrounding community not co-located business (Gibbs & Deutz, 2017).

### 3.3. Visioning landscape

After the reading landscape and define the issues and future challenge for Amata City, the landscape visions were defined and proposed to the stakeholders who involve with the development plan of Amata City. The visioning ecological landscape design by the six teams of landscape architecture students from Thammasat University include 1) eco-industrial towns, 2) eco-factory and manufacturing, 3) ecological revitalization on local canals, 4) revitalising water networks with community engagement, 5) green linkage, and 6) eco-mobility.

The strategies and design proposals focused on sustainable energy management, developing a circular water management network, wastewater control, promoting local biodiversity, connecting with the local community, and preserving natural ecological patches. The vision landscape design proposals were review by the stakeholders including,

government agencies, the facility management team from Amata City, and CEO and managers of the factories within the industrial zone.

From the ecological perspective, the discussion on the linkage between the existing ecosystem to the industrial estate boundaries are highlighted and debated. For example, from the vision landscape on revitalizing water networks and preserving natural ecological patches with community engagement, the design scheme aims to emphasize not only on the preservation on the natural ecosystems but also greening and linking the green network back to the industrial sites. Figure 3 shows the analysis on the impact of urban heat islands and the proposed landscape vision design for providing the green corridors and patches to minimize the impact of the hard surface of the industrial sites. The discussion on the linkage between local and new coming community were also discussed with the new programming on the landscape design activities for ecotourism and recreation proposes.

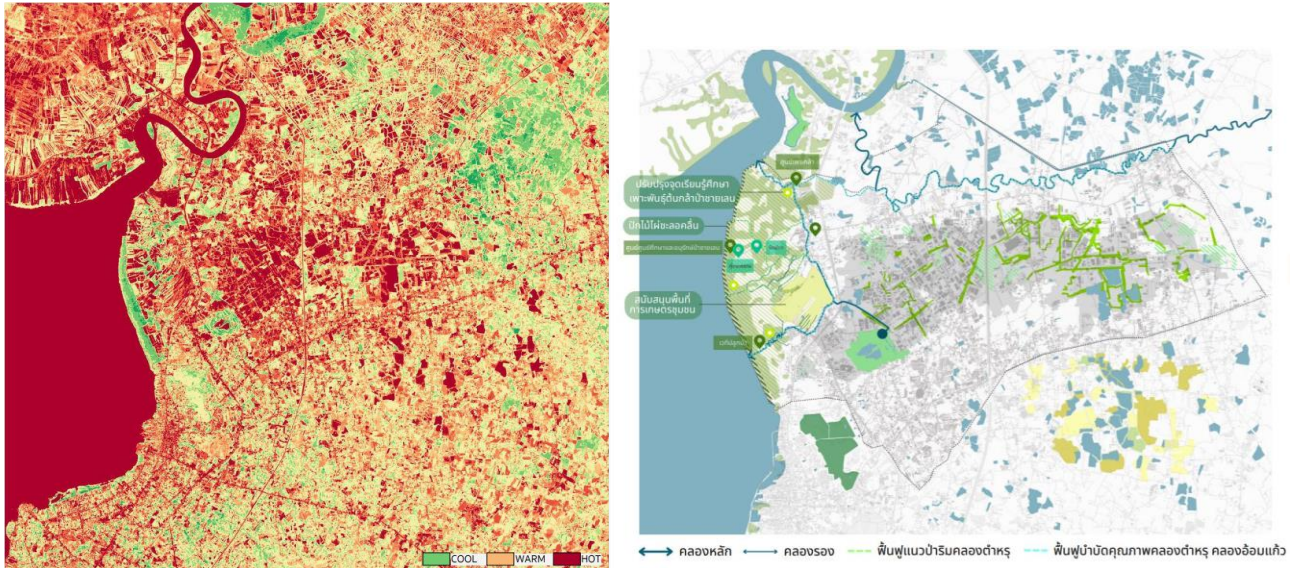


Figure 3 Urban heat island analysis (left), and vision landscape on revitalizing water networks and preserving natural ecological patches with community engagement (right). Source: The 3<sup>rd</sup> year Landscape Architecture students of Thammasat University, Academic year 2022

Figure 3 illustrates an analysis of the Industrial Estate Authority of Thailand (IEAT) initiatives (modified after Panyathannakun et al, 2013) overlay with the design response from landscape visionaries from Landscape Architecture students at Thammasat University. From the 5 main categories and 22 sub issues and themes, the design proposal of the students emphasises most of the initiative issues. The design proposal of the students covers the theme and subtheme on the physical (eco-design, and eco-center), environmental (water management, air pollution management, industrial waste management, energy, noise, health and safety, environmental monitoring, industrial process, and eco- efficiency), and societal (quality of life for workers and quality of life for those in community). The theme economical were response on these following subthemes including, economy of industries, local-growth, economy of community, and transportation and logistics. The other theme on managerial were response on these points including, collaboration, and improvement and maintenance of management system. The only two missing issues are from the economical theme on the marketing concern and managerial theme on the information and report.

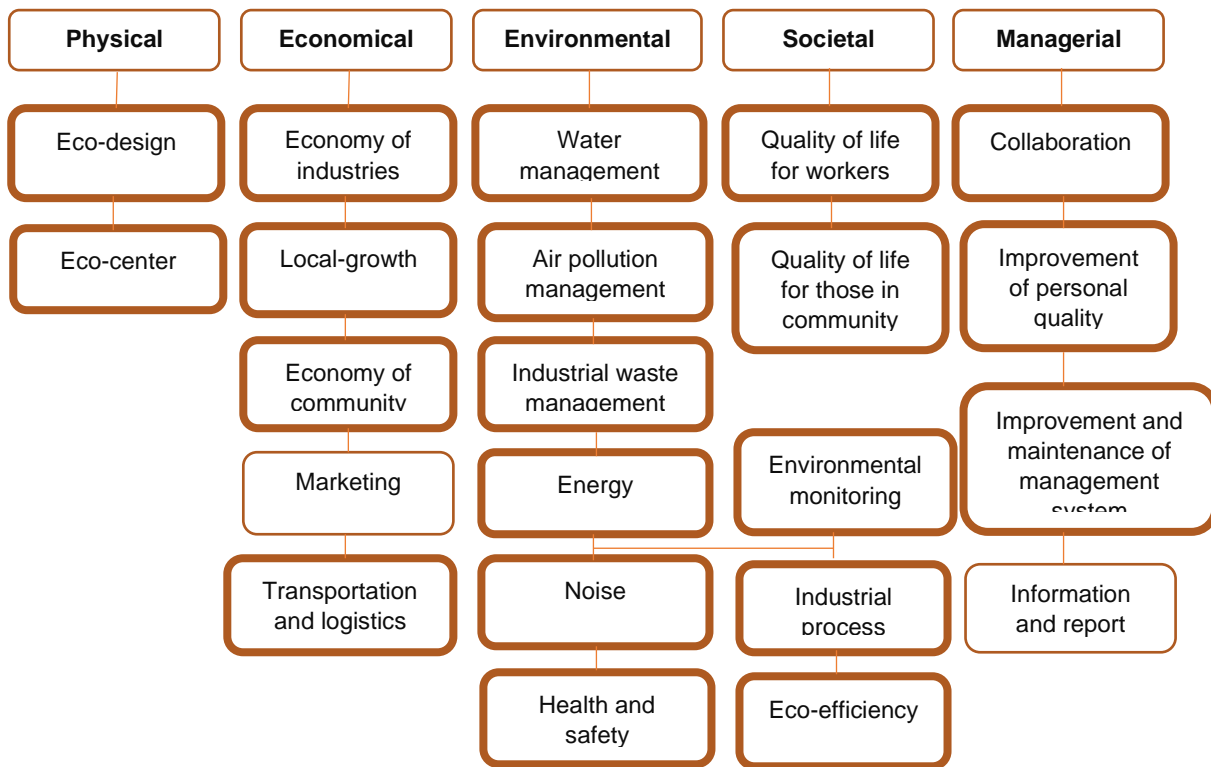


Figure 4 An analysis of the Industrial Estate Authority of Thailand (IEAT) initiatives (modified after Panyathannakun et al, 2013) overlay with the design response from landscape visionaries from Landscape Architecture students at Thammasat University  
Source: The 3<sup>rd</sup> year Landscape Architecture students of Thammasat University, Academic year 2022

#### 4. CONCLUSION

The concept of an eco-industrial park involves not only economic efficiency but also a social dimension and ecological integrity. In the early state, the Kalundborg in Denmark was marked as the model of eco-industrial park, emphasising the symbiosis relationship between the industrial factories and the community since 1998. The concept has been adopted and implemented in the US and Canada, which follow certain characteristics. Unlike industrial estates in Asia, where development offend occurs without planning focused on the benefits of economic drivers. In Thailand, the concept was adopted by the Industrial Estate Authority of Thailand (IEAT) starting in 2000, but it has not yet reached its goal (Panyathanakun et al., 2013).

Sustainability Report of Amata City from 2014 to 2016 focused on sustainability indicators of an eco-industrial town, such as eco-efficiency resource management, energy management and conservation, water and wastewater management pollution control, and air quality monitoring. Additionally, we found that the Sustainability Report of Amata City from 2017 to 2022 developed progress not only focused on environmental management onsite but also set indicators toward the other environmental issues and concerns such as biodiversity, climate change and climate resilience, responsible consumption of water resources, and natural resource protection and conservation.

The visioning ecological landscape design by the six teams of landscape architecture students ranged from eco-industrial towns, eco-factory and manufacturing, ecological revitalization on local canals, revitalising water networks with community engagement, green linkage, and eco-mobility. The strategies and design proposals focused on sustainable energy management, developing a circular water management network, wastewater control, promoting local biodiversity, connecting with the local community, and preserving natural ecological patches.

We suggest developing a guideline plan for the industrial estate involving community engagement and designing based on sustainable approaches. Ecosystem services should also be a focus for further discussion among all stakeholders.

#### 5. REFERENCES

Amata Corporation Public Company Limited, 2014, Sustainable Development Report 2014, Muang Chonburi, Amata Corporation PCL. Amata Nakorn Industrial Estate.

Amata Corporation Public Company Limited, 2015, Sustainable Development Report 2015, Muang Chonburi, Amata Corporation PCL. Amata Nakorn Industrial Estate.

Amata Corporation Public Company Limited, 2016, Sustainable Development Report 2015, Muang Chonburi, Amata Corporation PCL. Amata Nakorn Industrial Estate.

Amata Corporation Public Company Limited, 2016, Sustainable Development Report 2016, Muang Chonburi, Amata Corporation PCL. Amata Nakorn Industrial Estate.

Amata Corporation Public Company Limited, 2017, Sustainability Report 2017, Muang Chonburi, Amata Corporation PCL. Amata Nakorn Industrial Estate.

Amata Corporation Public Company Limited, 2018, Sustainability Report 2018, Muang Chonburi, Amata Corporation PCL. Amata Nakorn Industrial Estate.

Amata Corporation Public Company Limited, 2019, Sustainability Report 2019, Muang Chonburi, Amata Corporation PCL. Amata Nakorn Industrial Estate.

Amata Corporation Public Company Limited, 2020, Sustainability Report 2020, Muang Chonburi, Amata Corporation PCL. Amata Nakorn Industrial Estate.

Amata Corporation Public Company Limited, 2021, Sustainability Report 2021, Muang Chonburi, Amata Corporation PCL. Amata Nakorn Industrial Estate.

Amata Corporation Public Company Limited, 2022, Sustainability Report 2022, Muang Chonburi, Amata Corporation PCL. Amata Nakorn Industrial Estate.

Banerjee, T, Srivastava, R . K., 2010. Estimation of the Current Status of Floral Biodiversity at Surroundings of Integrated Industrial Estate-Pantnagar, India. *Int. J. Environ. Res.*, 4(1):41-48, Winter 2010 ISSN: 1735-6865

Baas, L W, Huisingh, D, 2008. The synergetic role of embeddedness and capabilities in industrial symbiosis: illustration based on 12 years of experiences in the Rotterdam harbor and industry complex. *Progress in Industrial Ecology* 5 (5-6), 399-421.

Boix, M, Montastruc, L, Azzaro-Pantel, C, Domenech, S, 2015, Optimization methods applied to the design of eco-industrial parks: a literature review. *Journal of Cleaner Production*, 87, 303-307.

<http://dx.doi.org/10.1016/j.jclepro.2014.09.032>

Cheevapattananuwong, P, Baldwin, C, Lathouras, A, Ike, N, 2020, Social Capital in Community Organizing for Land Protection and Food Security. *Land*, 9, 69, 1-19. doi:10.3390/land9030069

Chiu, A, Yong, G, 2004. On the industrial ecology potential in Asian developing countries. *Journal of Cleaner Production*. 12 (2004), 1037-1045.

Coˆte, R P, Cohen-Rosenthal, E, 1998, Designing eco-industrial parks: a synthesis of some experiences. *Journal of Cleaner Production*, 6, 181-188.

Daddi, T, Iraldo, F, Frey, M, Gallo, P, Gianfrate, V, 2015. Regional policies and eco-industrial development: the voluntary environmental certification scheme of the eco-industrial parks in Tuscany (Italy). *Journal of Cleaner Production*, 114, 62-70. <http://dx.doi.org/10.1016/j.jclepro.2015.04.060>

Gibbs, D, Deutz, P, 2007. Reflections on implementing industrial ecology through eco-industrial park development. *Journal of Cleaner Production*, 15, 1683-1695. doi:10.1016/j.jclepro.2007.02.003

Kechichian, E, Jeong, M H, 2016. Mainstreaming Eco-Industrial Parks, The World Bank Group.

Koenig, A, 2000. Development of Eco-Industrial Estates in Thailand, Project Development and Appraisal, June to December 2000. GTZ for Industrial Estate Authority of Thailand.

Li, J, Pan, S Y, Kim, H, Linn, J H, Chiang, P C, 2015. Building green supply chains in eco-industrial parks towards a green economy: Barriers and strategies. *Journal of Environmental Management*, 162, 158-170. <http://dx.doi.org/10.1016/j.jenvman.2015.07.030>

Minoru, F, Fujita, T, Ohnishi, S, 2015. "Eco-town and EIP." Center for Social and Environmental Systems Research. National Institute for Environmental Studies, JAPAN. Presented at the Eco-Industrial Park 2015 Conference

Panthong, S, Taecharungroj, V, 2021. Which CSR activities are preferred by local community residents? Conjoint and cluster analyses. *Sustainability*, 13, 1-16. <https://doi.org/10.3390/su131910683>

Panyathanakun, V, Tantayanon, S, Tingsabhat, C, Charmondusit, K, 2013, Development of eco-industrial estates in Thailand: initiatives in the northern region community-based eco-industrial estate. *Journal of Cleaner Production*, 51, 71-79.

Sakr, D, Baas, L, El-Haggar, S, Huisingh, D, 2011. Critical success and limiting factors for eco-industrial parks: Global trends and Egyptian context. *Journal of Cleaner Production*, 19, 1158-1169. doi:10.1016/j.jclepro.2011.01.001

Taddeo, R. 2016. Local industrial systems towards the eco-industrial parks: The model of the ecologically equipped industrial areas. *Journal of Cleaner Production*, 131, 189-197. <http://dx.doi.org/10.1016/j.jclepro.2016.05.051>

Tiu, B T C, Cruz, D E, 2017. An MILP model for optimizing water exchanges in eco-industrial parks considering water. *Resources, Conservation and Recycling*. 119, 89-96. <http://dx.doi.org/10.1016/j.resconrec.2016.06.005>

Vahidzadeh, R, Bertanza, G, Sbaffoni, S, Vaccari, M, 2020. Regional industrial symbiosis: A review based on social network analysis. *Journal of Cleaner Production*, 280, 124054. <https://doi.org/10.1016/j.jclepro.2020.124054>

---

## #203: Experimental investigation of concentrated triple junction solar cells under non-uniform illumination

---

Mahalakshmi K<sup>1</sup>, Reddy K.S<sup>1</sup>, Subrahmanyam A<sup>2</sup>

<sup>1</sup> Heat transfer and Thermal Power Laboratory, Department of Mechanical Engineering, Indian Institute of Technology Madras, Chennai-600036, mahalakshmikrishnan89@gmail.com

<sup>2</sup> GITAM Institute of Science, Vishakapatnam-530045

*Abstract: A concentrated multijunction solar cell offers good promise for high energy density. In a concentrated photovoltaic system, the solar cell's output power depends not only on the illumination energy but also on the spectral distribution and the uniformity of illumination. Under field operating conditions, non-uniformity is a major factor affecting the performance of concentrated solar cells. The present work is intended to address non-uniform illumination created on concentrated commercial triple junction solar cells. The study considered non-uniformity (both spatial and spectral) based on two cases (varying focal length and masking cell area). Both methods create non-uniformity, which affects the performance of triple-junction solar cells and is addressed here with experimental evaluation. The shadowing factor is a critical parameter considered for performance evaluation theoretically and experimentally. A Fresnel-based concentrating (commercial) photovoltaic system with InGaP/InGaAs/Ge triple-junction solar cells is employed for the purpose. The experimental results indicate that there is an 8 % ± 3 % reduction in overall efficiency with varying non-uniformity under 500-700 W/m<sup>2</sup>. The main parameters that are affected significantly are maximum power point voltage and current. Also, the influence of series resistance under increased non-uniformity plays a vital role in performance reduction. The experimental results are fitted to a proposed simple lumped diode model.*

*Keywords: non-uniform illumination, concentrated solar cell, equivalent circuit model, outdoor experiments*

## 1. INTRODUCTION

The High Concentrated Photo Voltaic (HCPV) systems have shown promise to yield high energy density and achieved 46 % efficiency using multi-junction solar cells made of III–V semiconductors [Dimroth et al., 2016] [ *NREL CPV Report 1.3, 2017*]. The multi-junction solar cells consist of several junctions in series and will typically operate under variable spectrum conditions, lower optical power, and higher temperature [Helmers, Schachtner, and Bett, 2013] [Liu et al., 2015]. Concentrated photovoltaics (CPV) uses an optical system, like the Fresnel lens, to collect the solar irradiance (power per unit area ( $W/m^2$ ), received from the Sun) and concentrate it on a small area of the solar cell [Kumar, Shrivastava, and Untawale, 2015].

Several research groups contributed to the understanding of the multi-junction concentrated solar cells [Alves et al., 2020] [Wiesenfarth, Anton and Bett, 2018] and its applications [P´erez-Higueras et al., 2018] [Zubi et al., 2009]. The HCPV modules based on the Fresnel lens show good promise and it is well known that the performance of HCPV multi-junction solar cells depends upon several growth and operating parameters. From among the parameters, the illumination concentration, operating temperature [Fern´andez and Almonacid, 2015], degradation influence [Mahalakshmi, Reddy and Subrahmanyam, 2022], optical properties of the concentrator [Guo et al., 2018], and atmospheric conditions significantly influence multi-junction cell efficiency.

The work reported so far on concentrated solar cells has been centered on improving the illumination energy on the cell, by improving the efficiency of the optical lens [Yang et al., 2013] [Languy et al., 2011]. Many researchers focused their attention on addressing the influence of chromatic aberration of the concentrator optics and the non-uniformity in incident illumination [Li et al., 2018] [Baig, Heasman, and Mallick, 2012]. These are the two parameters that have been considered crucial among performance-inhibiting parameters. Especially, the non-uniformity of illumination, which occurs due to the design deficiencies of the secondary concentrators [Ben´itez et al., 2010] [Zou and Yang, 2014] [Chen, Chiang, and Hsieh, 2015] and/or due to external factors such as shadowing. In particular, any non-uniformity in illumination affects adversely the electrical characteristics of the multi-junction solar cells [Ota and Nishioka, 2012] [Patanasemakul et al., 2017]. Accordingly, in this study, non-uniformity has been chosen as a performance-inhibiting factor in concentrated triple junction solar cells.

The present study aims at evaluating the solar cell performance under practical field (outdoor) conditions of the concentrated (commercial) triple-junction III–V solar cell on varying illumination and shadowing. Non-uniformity of illumination is achieved by (i) masking the primary concentrator and (ii) varying the focal length of the optical system; in both cases, the photon flux (both spectral and spatial) changes. The concept of shadowing factor  $S$  is borrowed from Bunthof et al., (2018). The impact on electrical characteristics under different DNI (Direct Normal Irradiance is measured at the surface of the Earth at a given location with a surface element perpendicular to the Sun) and shadowing factor is evaluated and presented.

## 2. METHODOLOGY

### 2.1. System description

A triple junction InGaP/InGaAs/Ge commercially procured solar cell (Azurspace CPV) of size: 10 mm×10 mm×0.2 mm, with a geometrical concentration ratio of 820 suns is employed in the present study. The optical band gaps of the sub-cells InGaP, InGaAs, and Ge are 1.91 eV, 1.42 eV, and 0.66 eV respectively. The concentrating optics consists of a point-focus Fresnel lens (286×286×2 mm active area with a focal length of 340 mm) made of Poly Methyl Metha Acrylate (PMMA) (M/s Rudra Optics, India). Since the optical efficiency of the concentrator under practical field conditions is as low as 37 %, the present study is conducted with a concentration of 300X. A 2.0 mm thick aluminum backplate is utilized as a heat sink for dissipating excess heat. The solar cell was pasted on the heat sink with Arctic Silver 5 compound thermal paste (8.5 W/mK thermal conductivity). For the evaluation of field results, ACR (Actual Concentration Ratio) is utilized and is represented in Equation 1.

Equation 1: ACR (Actual Concentration Ratio).

$$ACR = \frac{I_{sc}^{conc}}{I_{sc}^{1\ sun}}$$

Where:

- $I_{sc}^{conc}$  = short circuit current under concentration (A)
- $I_{sc}^{1\ sun}$  = short circuit current under 1 sun (A)

### 2.2. Experimental procedure

The present study is focused on evaluating the performance of the triple junction concentrator solar cell for non-uniformity in illumination and shadowing. The non-uniformity in flux distribution results in a fully illuminated region and a rarely illuminated region (shadowed region) on the surface of the solar cell. This shadowed region can be controlled by two

methods, i) by varying the irradiance by masking the Fresnel lens as shown in (Figure 1 (a)) and ii) by varying the exposed area with focal length by varying the distance between the Fresnel lens and solar cell (Figure 1(b)).

The shadowing factor (S) is the ratio of the shadowed region to the area of the cell. In this study, the shadowing factor is varied in the range of 0.25–0.9. For evaluating the non-uniformity with case (i), an aluminum sheet of 1 mm thickness is used for masking. On the other hand, for case (ii), the focal length (f) is varied by varying the distance between the Fresnel lens and the solar cell. At f=340 mm, the illuminated area of the solar cell is 0.85 mm<sup>2</sup> (S=0.7). Henceforth for case (ii) evaluation, the focal length is varied between 323 mm and 355 mm for S=0.5 and 0.9, respectively.

The experiments have been carried out in field conditions at the Indian Institute of Technology, Madras (Chennai, India; 12.9915 °N, 80.2337 °E) between December 2018 and June 2019. The Direct Normal Irradiance (DNI) varied in the range of 500–700 W/m<sup>2</sup> (measured with Pyrheliometer (Model LF Pyrheliometer, M/s Kaizen Imperial). The electrical characteristics of the multi-junction solar cell are evaluated with PV analyser PROVA 210 (Range: 0–10 V; 0.01– 12 A, Uncertainty: ± 1 %; M/s PROVA Instruments Inc.). The concentrated solar cell experimental setup with the Fresnel lens supported on a manual tracking system is shown in Figure.1 c).

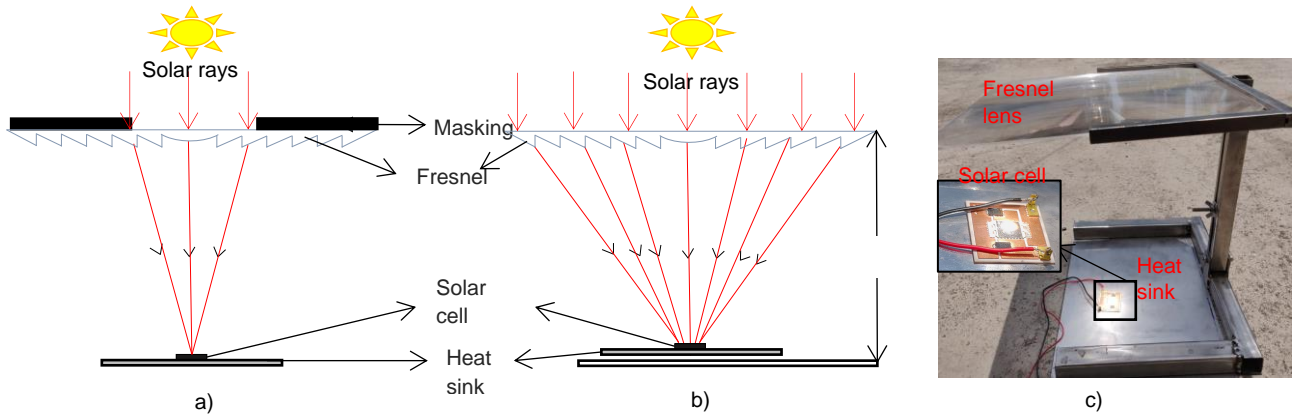


Figure 1 Schematic representation of Fresnel lens concentrating system a) Evaluation with the masking method by varying the irradiance exposure to solar cell (for S=0.25) b) Evaluation by varying the focal length (for S=0.9) c) Photograph of experimental setup depicting CPV system. The close-view picture depicts the shadowing factor S=0.5 at f=323 mm

### 2.3. Proposed lumped model for non-uniformity evaluation

The conventional five-parameter model as represented in Equation 2 has been modified as a lumped diode model for evaluating non-uniformity in concentrated triple-junction solar cells with some assumptions. A study by Bunthof et al.,(2018) evaluated the characteristics of non-uniformity and its influence on  $V_{oc}$  with a parameter termed as shading factor. To evaluate complete performance parameters, this study derived the influence of non-uniformity on electrical parameters such as  $I_{mpp}$ , and  $V_{mpp}$  by utilizing the shadowing factor, S. Shadowing factor represents non-uniformity on the surface of solar cells in terms of area fraction with effective illumination. Similarly, the prediction of  $I_{sc}$  as a linear dependence of solar cell illuminated area has been stated as early in the 1980s and is being utilized in this study.

Equation 2: Output current under uniform illumination.

$$I_{uniform} = I_{pv} - I_0 \left[ \exp \frac{V + I_{uniform}AR_s}{nV_t} \right] - \frac{V + I_{uniform}AR_s}{R_{sh}}$$

Where:

- $I_{uniform}$  = output current under uniform illumination (A)
- $I_{pv}$  = photocurrent (A)
- $I_0$  = diode saturation current (A)
- $V$  = output voltage (V)
- $A$  = total area of the solar cell (m<sup>2</sup>)
- $R_s$  = series resistance ( $\Omega$ )
- $R_{sh}$  = shunt resistance ( $\Omega$ )
- $V_t = \frac{nk_B}{T}$  = thermal voltage (V)
- $n$  = diode ideality factor
- $k_B$  = Boltzmann constant
- $T$  = temperature (K)
- $q$  = charge of an electron (C)



It is well known that any non-uniformity in flux on the surface of solar cells results in internal leakage current loss. This leakage current  $I_i$  can be considered as a diode connected in parallel to the load as represented in the equivalent circuit shown in Figure 2. This modifies the basic equation as Equation 3,

Equation 3: Basic equation for the lumped diode model

$$I_{non-uniform} = I_{uniform} - I_i$$

Where:

- $I_{non-uniform}$  = output current of a multi-junction solar cell subjected to non-uniform (A)
- $I_i$  = internal leakage current (A)

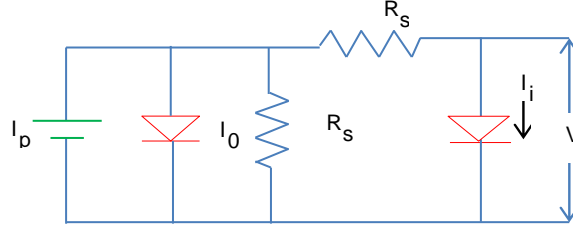


Figure 2 Lumped diode equivalent circuit model under non-uniform illumination

The internal leakage current is proportional to the non-illuminated area of the solar cell and can be substituted with a basic diode equation. For simplicity, the shunt resistance is assumed infinite. Hence the characteristic equation under non-uniform illumination can be represented as Equation 4,

Equation 4: Output current under non-uniform illumination.

$$I_{non-uniform} = A_l I_{pv} - A_l I_0 \left[ \exp \frac{V + IR_s}{nV_t} - 1 \right] - A_d I_0 \left[ \frac{V + IR_s}{R_{sh}} - 1 \right]$$

The shadowing factor  $S$  is taken as  $A_d/A_t$  and where  $A_d$  is the area of the solar cell under dark in  $m^2$  and  $A_t$  is the total area of the solar cell ( $A_d + A_l$ ) in  $m^2$  and  $A_l$  is the illuminated area of the solar cell in  $m^2$ . The electrical parameters can be derived from the basic equation (Equation 4) with initial conditions. The first initial condition considered is; at  $I = 0$ ;  $V = V_{oc}$ . Further simplifications result in open-circuit voltage,  $V_{oc}$  as in Equation 5.

Equation 5: The open circuit voltage

$$V_{oc} = V_t \ln(1 - S) \left[ \frac{I_{sc}}{I_0} - 1 \right]$$

The second condition for deriving maximum power point values is; at  $I = I_{mpp}$ ,  $V = V_{mpp}$  with an assumption  $V_t = I_{mpp} * R_s$ . The equation for current at maximum power point can be obtained by substituting the above-mentioned conditions in Equation 4 and is represented in Equation 6.

Equation 6: The maximum power point current

$$I_{mpp} = I_{sc} - I_0 \frac{\exp \left[ \frac{V_{mpp} + V_t}{nV_t} \right]}{1 - S} - 1$$

Similarly, substituting the second initial condition along with the value of  $I_{mpp}$  in Equation 4, results in maximum power point voltage,  $V_{mpp}$  as shown in Equation 7.

Equation 7: The maximum power point voltage

$$V_{mpp} = V_t \ln(1 - S) \left[ \frac{I_{sc} - \frac{V_t}{R_s}}{I_0} + 1 \right] - V_t$$

These equations are utilized here to evaluate the performance of solar cells under non-uniform illumination by substituting the area of solar cells exposed to irradiance in terms of the shadowing factor. The I-V characteristics were evaluated utilizing MATLAB (V 7.110.584) Simulink. The procedure utilized for evaluation has been represented in Figure 3. Here the parameter extraction by Carrero et al., (2012, pp. 2974-2976) has been utilized for evaluating the effect of non-uniformity on performance parameters such as  $I_{pv}$ ,  $I_0$ ,  $n$ ,  $R_s$ ,  $R_{sh}$  with derived basic parameters.

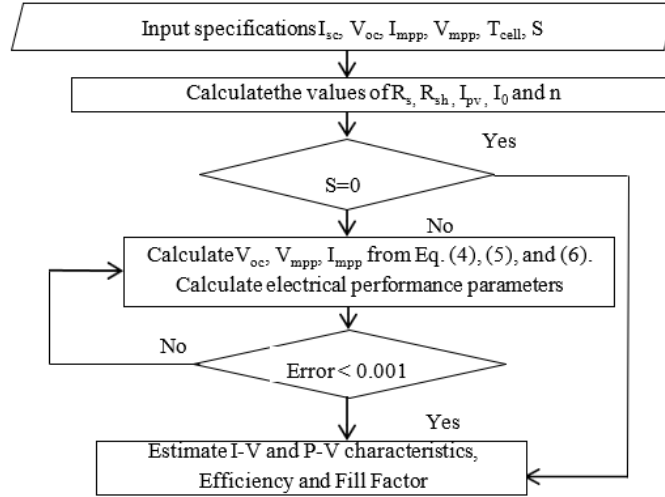


Figure 3 Flowchart explaining the procedure for calculating the non-uniformity effect on electrical performance

### 3. RESULTS AND DISCUSSIONS

#### 3.1. Non-uniform illumination-Varying the exposed area of the solar cell (by masking the primary concentrator)

The I-V characteristics of the triple junction solar cell measured at  $548 \text{ W/m}^2$  DNI under different masking conditions utilizing an aluminum sheet of 1mm thickness have been presented in Figure 4a (with the best values). It may be noted that the temperature of the triple junction solar cell is between 330 K to 345 K under illumination. As anticipated, the non-uniformity with masking influences  $I_{sc}$  and  $I_{mpp}$  values linearly till 0.25 of the masking, whereas non-linearity sets in with increased masking. Similarly,  $V_{oc}$  and  $V_{mpp}$  show logarithmic dependence until 0.75 masking thereafter exhibits almost independent behaviour.

The efficiency of the triple junction cell with uniform illumination at 300K is 31 % (4.6 W), however, it is 22 % at 345 K. The output power decreases (by 2 %) with non-uniformity in the illumination. Whereas fill factor values remain almost constant even under non-uniform illumination.

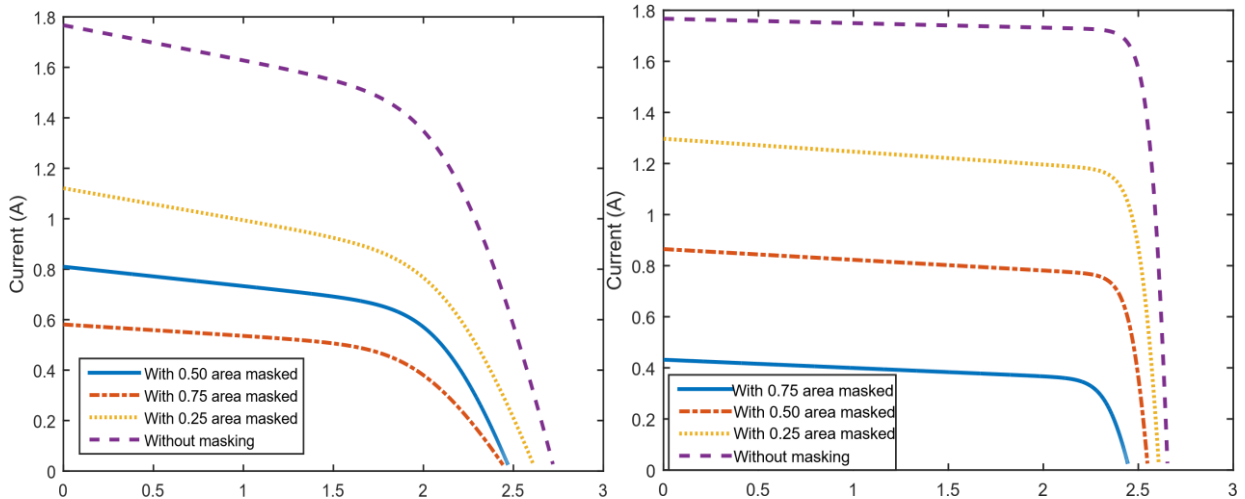


Figure 4 I-V characteristics a) measured at  $548 \text{ W/m}^2$  b) calculated at  $548 \text{ W/m}^2$  under different masking with the triple junction solar cell placed at the focal length of the Fresnel lens

The diode parameters for the triple junction solar cell under masking have been evaluated (Table 1). The performance parameters have been extracted based on curve fitting as given in Table 1 to understand the behaviour under non-uniform illumination detailedly. From the results, it is inferred that the characteristics show more dependency on series resistance. The other parameters such as the ideality factor and diode saturation current play a minor role. Though the ideality factor and saturation current decrease with non-uniformity, their decrease in values is proportionate to the illumination reduction due to masking. But the variation of parameters  $I_{sc}$  and  $V_{oc}$  are more dependent on illumination intensity and temperature conditions whereas, the non-uniformity in illumination has minimal influence. The performance characteristics subjected to

shadowing influence with case (i) show a similar trend as Figure. 4b for different DNI conditions. The behaviour of electrical characteristics under masking is proportional to illumination mostly and exhibits less dependency on non-uniformity.

Table 2: Extracted performance parameters for Case (i) at 548 W/m<sup>2</sup>, measured with different masking conditions.

Description	Diode saturation current I <sub>0</sub> (A)	Diode ideality factor (n)	Series resistance
Without masking	1.15×10 <sup>-17</sup>	2.60	0.29
With 0.25 area masked	8.55×10 <sup>-18</sup>	2.56	0.49
With 0.50 area masked	1.56×10 <sup>-18</sup>	2.45	0.33
With 0.75 area masked	2.11×10 <sup>-19</sup>	2.30	0.52
Without masking	1.15×10 <sup>-17</sup>	2.60	0.29

The theoretical I-V characteristics (calculated at 300 K) using a simple lumped model of the triple junction solar cells for illumination at 548 W/m<sup>2</sup> (210 suns concentration, shadowing factor varied in the range S=0.25 to 1) are given in Fig. 2b. The calculated values of V<sub>oc</sub> match well with the measured values. But V<sub>mpp</sub> shows a maximum deviation of 0.3-0.5 V, this can be justified with varying localized temperatures on the solar cell (333-358 K) due to long exposure to high-intensity radiation.

According to Ben and Appelbaum (2014), the reduction in n value and increased R<sub>s</sub> value (Table 1) justify the decreased V<sub>mpp</sub> values under the increased temperature of the solar cell. The higher current values at enhanced non-uniformity may also be attributed to increased temperature on the triple junction cell. There is a significant discrepancy in the R<sub>s</sub> values: calculated: 0.08 to 0.25 Ω to the measured values: 0.20 to 0.50 Ω. This infers that R<sub>s</sub> affects V<sub>mpp</sub> and I<sub>mpp</sub> values predominantly.

### 3.2. Non-uniform illumination- Varying the focal point on the solar cell (the concentration ratio varies)

The effect of non-uniformity on concentrated solar cells by varying the focal length has been evaluated for shadowing factors S=0.5, 0.7, and 0.9. This influence of focal length variation on flux distribution on the surface of solar cells is depicted in Figure 5.

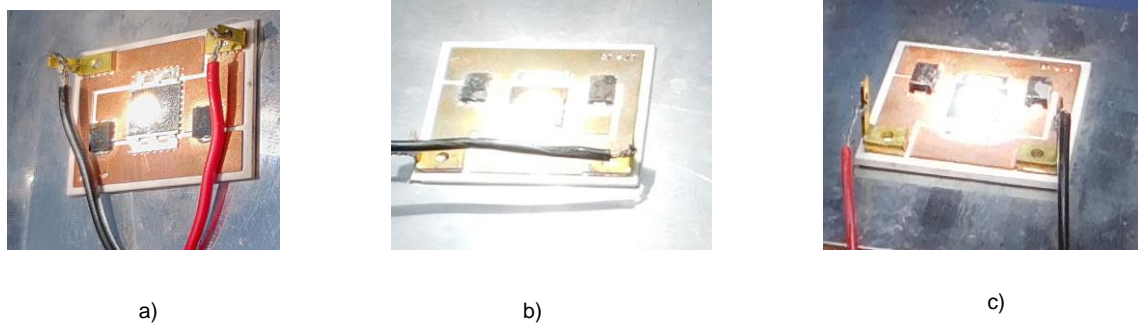


Figure 5 Picture of flux distribution on the solar cell by varying the focal length with a) S=0.5, b) S=0.7, and c) S=0.9

The performance characteristics of the triple-junction solar cell have been measured with different shadowing factors for the illumination in the range of 500-700 W/m<sup>2</sup> DNI are shown in Figure 5. The measured values of short circuit current (Figure 6a) do not vary linearly with shadowing factor. Moreover, this influence of I<sub>sc</sub> has its effect on the values of I<sub>mpp</sub> showing decreased dependency from linearity: due to the flow of electrons from the illuminated region towards the dark region creating additional electron-hole pairs that increase the conduction area under non-uniformity (Baig, Heasman, and Mallick, 2012).

Another perspective of understanding reveals that at S<1, the concentration ratio of solar cells increases (the illuminated area decreased under non-varying irradiance), but the influence of the shadowing factor decreases the illuminated area. Henceforth, the result should be a constant I<sub>sc</sub>. The actual decrease in I<sub>sc</sub> has been investigated based on the representation of external quantum efficiency by Nishioka et al. (2012), it is inferred that the spectral distribution has its influence on the triple-junction solar cell since the focal length has been varied. Meanwhile, a detailed analysis of the external quantum efficiency of multi-junction concentrated solar cells conducted by Gras et al. (2017) and Van Leest et al., (2019) reveals that when the solar cell is in shadow, the corresponding photon flux reduces at each wavelength. The materials are stacked in such a way that the high optical band gap InGaP (1.91 eV) is on the top followed by InGaAs (1.42 eV) and the bottom Ge (0.66 eV); thus, all the wavelengths with maximum photon flux are captured to generate the electron-hole pairs. With shadowing, the generation and recombination rate of the minority carriers affected is reflected mostly in I<sub>sc</sub> measurements.

Also, according to Helmers, Schachtner, and Bett, (2013), the triple-junction solar cell experiences a maximum temperature of about 340K under uniform illumination. Besides, if non-uniformity in irradiance is achieved by varying the focal length, the main parameter affected is the temperature of the solar cell. When the temperature is decreased due to focal length variation, both the effects of reduced photon flux in the selective wavelengths and the decrease in temperature result in the reduction of I<sub>sc</sub>.

Another observation from Figure 5a is a decreased dependency of  $I_{sc}$  with increased DNI values which infers that the effect of non-uniformity decreases at higher DNI values. Another parameter  $V_{oc}$  follows the usual trend of logarithmic proportionality with the shadowing factor (Figure 6b). It is anticipated that with increasing uniformity, the efficiency should increase but, on some occasions, it decreases as observed (Fig. 6e). This decrease may be due to the effect of localized temperature. The effect of non-uniformity in the concentrated solar cell decreases the efficiency up to a maximum of  $8\% \pm 3\%$  and the parameters affected by the shadowing factor predominately are the maximum power point values (Figure 6c, Figure 6d). Especially the  $V_{mpp}$  (Figure 6d) value varies arbitrarily under the influence of non-uniformity. This influences the efficiency and fill factor (Fig. 5f) proportionately. This behaviour invariably explains the crucial role of series resistance under non-uniform illumination. A detailed analysis of series resistance in the triple junction cells is given in reference (Nishioka et al., 2012).

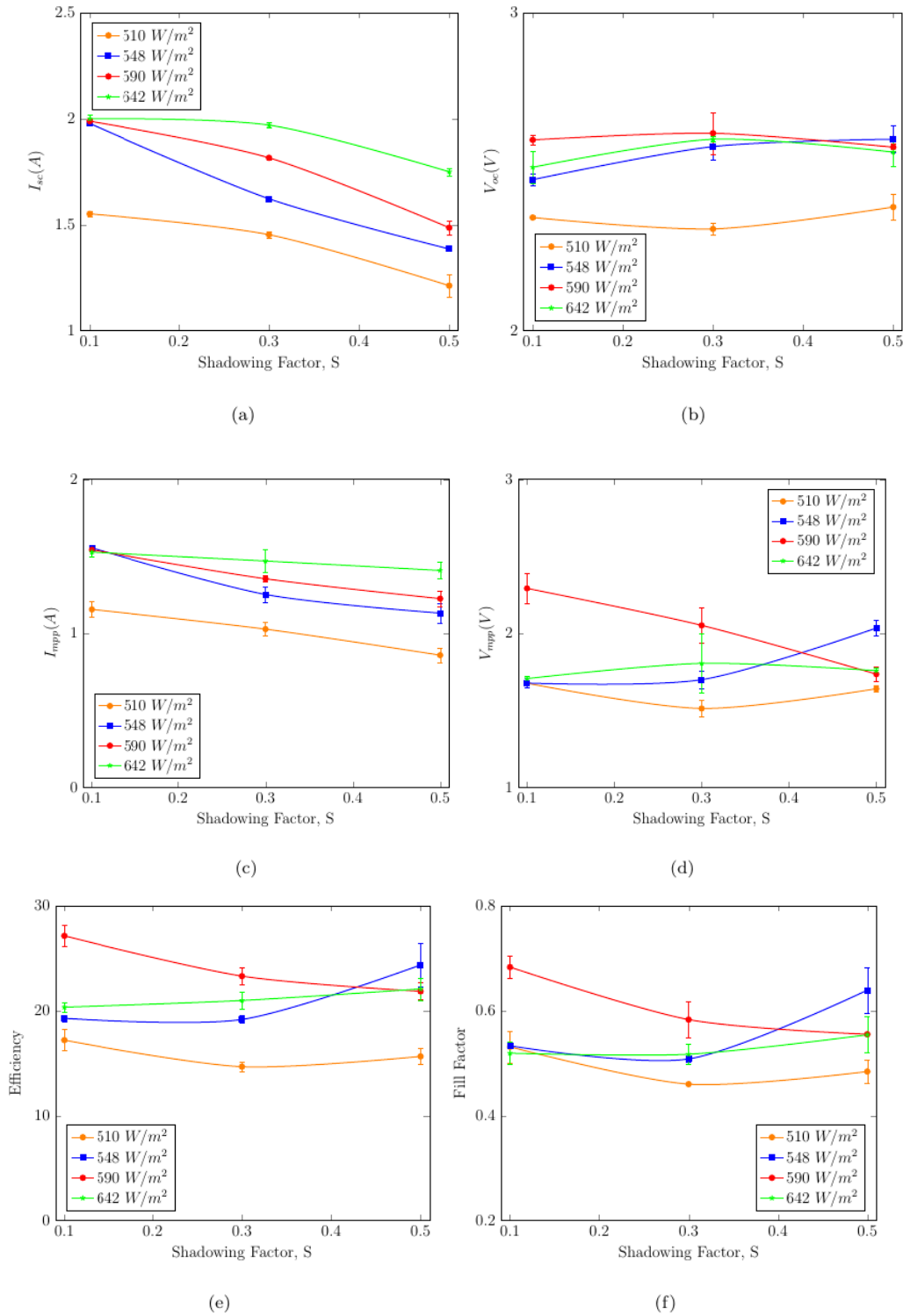


Figure 6 Measured parameters at different irradiance with varying shadowing factor

Several models are being used to analyse the triple and multi-junction solar cells [Rodrigo et al., 2013]. In this study, a simple yet robust model has been proposed and the theoretical I-V characteristics (calculated at 300 K) of the triple junction solar cells for illumination of  $548 \text{ W/m}^2$  for different shadowing factors (0.9 and 0.6) were calculated and compared against experimental measurements as given in Figure 7. The evaluated characteristics marginally differ from measured values, especially on  $V_{mpp}$  and  $I_{mpp}$  values which differ from measured values by 0.2-0.3 V and 0.2-0.4 A respectively. Because of this, the efficiency and fill factor get overestimated by 2-7 %. The calculated values at  $S < 1$ , underestimated the value of  $V_{oc}$  by 2-3 %. Also, there exists a similar behaviour of  $I_{sc}$  as explained with case (i) under increased non-uniformity. This may be due to the influence of non-uniformity on series resistance and diode saturation current as shown in Equation 8 (derived based on Equation 4).

Equation 8: The influence of non-uniformity in short circuit current 
$$I_{sc} = SI_{pv} - SI_0 \exp \left[ \frac{V + IR_s}{nV_t} - 1 \right] - (1 - S)I_0$$

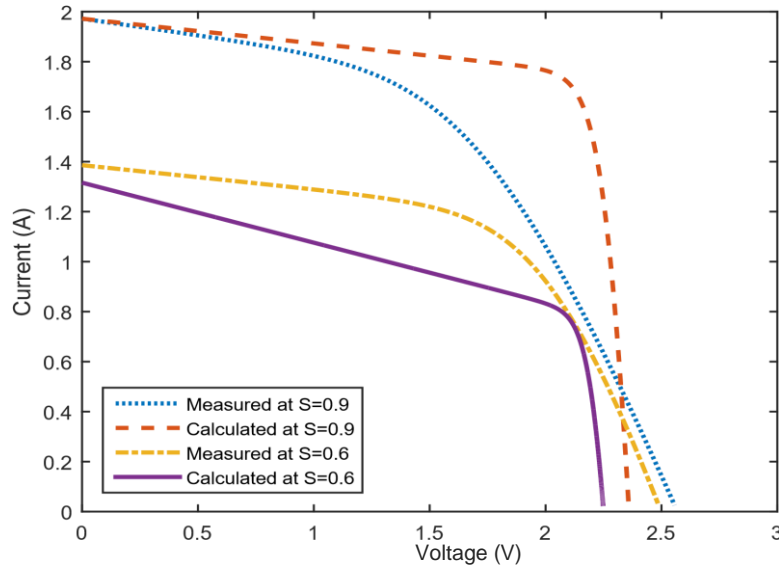


Figure 7 Comparison of characteristics measured and calculated at  $548 \text{ W/m}^2$

Though the comparison reveals that there exists uncertainty between evaluated and measured values, the proposed method correlates the impact of non-uniform illumination on performance with a simple procedure. Especially, the evaluation of spatial non-uniformity is accurate and the spectral non-uniformity estimates performance with an error of 10 %. Therefore, it can be claimed that the proposed model can be utilized as a simple tool to evaluate non-uniformity influence with incorporated experimental observations.

#### 4. CONCLUSION

The performance investigation of concentrated multi-junction solar cells under non-uniform illumination has been carried out with outdoor experimental conditions. The results show that the performance of CPV gets affected adversely by non-uniform illumination, especially under high concentration intensities. Based on experimental results, the findings are listed as follows,

- At varying illumination intensities, the  $I_{sc}$  of solar cells exhibits very less (nonlinear) dependency on non-uniformity. The decrease in  $I_{sc}$  is 0.5 A for a variation in the shadowing factor of 0.5 to 0.9, whereas  $I_{sc}$  shows linear dependency under masking.
- $V_{oc}$  shows less significant dependency on any type of non-linearity.
- The main parameters affected adversely are the maximum power point voltage and current. Also, the influence of series resistance under increased non-uniformity plays a vital role in performance reduction.
- Under the influence of non-uniformity created by focal length variation, the efficiency drops to about  $8 \% \pm 3\%$ , whereas it is linearly proportional to  $S$  under masking conditions.

Furthermore, the proposed theoretical model holds good at evaluating the masking influence on performance characteristics, on the other hand, if spectral influence comes into the picture by varying the focal length, due to the intertwined influence of illumination intensity and non-uniformity, it overpredicts the values of  $I_{sc}$ . Also, a 2–10 % error prevails in the calculated  $V_{mpp}$  values.

## 5. REFERENCES

- Alves, M., Pérez-Rodríguez, A., Dale, P. J., Domínguez, C., Sadewasser, S. (2020) 'Thin-film micro-concentrator solar cells', *Journal of Physics: Energy*, 2(1), 012001. Available at: <https://iopscience.iop.org/article/10.1088/2515-7655/ab4289>.
- Baig, H., Heasman, K. C., Mallick, T. K. (2012) 'Non-uniform illumination in concentrating solar cells', *Renewable and Sustainable Energy Reviews* 16 (8), pp. 5890–5909. Available at: <http://dx.doi.org/10.1016/j.rser.2012.06.020>
- Ben, A., Appelbaum, Or. J. (2014) 'Dependence of multi-junction solar cells parameters on concentration and temperature', *Solar Energy Materials and Solar Cells* 130, pp. 234–240. Available at: <http://dx.doi.org/10.1016/j.solmat.2014.07.010>
- Benítez, P., Miñano, J. C., Zamora, P., Mohedano, R., Cvetkovic, A., Buljan, M., Chaves, J., Hernández, M. (2010) 'High performance Fresnel-based photovoltaic concentrator', *Optic Express*, 18 (April) pp. 25–40. Available at: <https://opg.optica.org/oe/abstract.cfm?uri=oe-18-101-A25>
- Bunthof, L. A. A., Veelenturf, S., Haverkamp, E. J., Corbeek, W. H. M., Woude, D.V. D., Bauhuis, G. J., Mulder, P., Vlieg, E., Schermer, J. J. (2018) 'Partially shaded III-V concentrator solar cell performance', *Solar Energy Materials and Solar Cells*, 179, pp. 231–240. Available at: <https://doi.org/10.1016/j.solmat.2017.11.039>.
- Carrero, C., Ramírez, D., Rodríguez, J., Platero, C. A. (2011) Accurate and fast convergence method for parameter estimation of PV generators based on three main points of the I-V curve', *Renewable Energy*, 36 (11), pp. 2972–2977. Available at: <http://dx.doi.org/10.1016/j.renene.2011.04.001>.
- Chen, Y.-C., Chiang, H.-W., Hsieh, W.-H. (2015) 'Design of the Secondary Optical Elements for Concentrated Photovoltaic Units with Fresnel Lenses', *Applied Science*, 5, pp. 770–786. Available at: <http://dx.doi.org/10.3390/app5040770>.
- Dimroth, F., Tibbits, T. N. D., Niemeyer, M., Predan, F., Beutel, P., Karcher, C., Oliva, E., Siefert, G., Lackner, D., Fußkailuweit, P., Bett, A. W., Krause, R., Drazek, C., Guiot, E., Wasselin, E., Signamarcheix, T. (2016) 'Four-Junction Wafer-Bonded Concentrator', *IEEE 42nd Photovoltaic Specialist Conference (PVSC)*, 6 (1), pp.343–349. Available at: <https://ieeexplore.ieee.org/document/7342876>
- Fernández, E. F., Almonacid, F. (2015) 'A new procedure for estimating the cell temperature of a high concentrator photovoltaic grid connected system based on atmospheric parameters', *Energy Conversion and Management* 103, pp. 1031–1039. Available at: <http://dx.doi.org/10.1016/j.enconman.2015.07.034>.
- Fraunhofer ISE, 2017, NREL CPV Report1.3, Available at: <https://www.ise.fraunhofer.de/content/dam/ise/de/documents/publications/studies/cpv-report-ise-nrel.pdf> (Accessed :17 may 2018)
- Gras, A., Jungst, G., Campesato, R., Gori, G., Greco, E. (2017) 'External Quantum Efficiency and First Results Of Electric Performance Measurements On A Quadruple Junction Space Solar Cell', *E3S Web of Conferences*, 16, pp. 1-4. Available at: <http://dx.doi.org/10.1051/e3sconf/20171602006>
- Guo, Y., Liang, Q., Shu, B., Wang, J., Yang, Q. (2018) 'The III – V Triple-Junction Solar Cell Characteristics and Optimization with a Fresnel Lens Concentrator', *International Journal of Photon Energy*, 1–11, 7285849. Available at: <https://www.hindawi.com/journals/ijpe/2018/7285849/>
- Helmers, H., Schachtner, M., Bett, A. W. (2013) 'Influence of temperature and irradiance on triple-junction solar subcells', *Solar Energy Materials and Solar Cells*, 116, pp. 144–152. Available at: <http://dx.doi.org/10.1016/j.solmat.2013.03.039>
- Kumar, V., Shrivastava, R. L., Untawale, S. P. (2015) 'Fresnel lens: A promising alternative of reflectors in concentrated solar power', *Renewable and Sustainable Energy Reviews* 44, pp. 376–390. Available at: <http://dx.doi.org/10.1016/j.rser.2014.12.006>.
- Languy, F., Fleury, F., Lenaerts, C., Loicq, J., Regaert, D., Thibert, T., Habraken, S. (2011) 'Flat Fresnel doublets made of PMMA and PC: combining low cost production and very high concentration ratio for CPV', *Optic Express*, 19 (May), pp. 556–562. Available at: <http://dx.doi.org/10.1364/OE.19.00A280>
- Li, G., Xuan, Q., Pei, G., Su, Y., Ji, J. (2018) 'Effect of non-uniform illumination and temperature distribution on concentrating solar cell - A review', *Energy*, 144 pp. 1119–1136. Available at: <http://dx.doi.org/10.1016/j.energy.2017.12.067>.
- Liu, J., Yao, Y., Jiang, S., Jia, R. (2015) 'Analysis of the interdigitated back contact solar cells: The n-type substrate lifetime and wafer thickness', *Chinese Physics B*, 24(10), Available at: <http://dx.doi.org/10.1088/1674-1056/24/10/108801>.
- Mahalakshmi, K., Reddy K. S., Subrahmanyam A. (2022) 'Outdoor degradation evaluation of multi-junction solar cell for four Fresnel concentrated photovoltaic systems', *International Journal of Sustainable Energy*, 41(11), pp.1958-1972, Available at: <http://dx.doi.org/10.1080/14786451.2022.2125517>

- Nishioka, K., Takamotob, T., Aguib, T., Kaneiwab, M., Uraokac, Y., Fuyukic, T. (2006) 'Evaluation of InGaP/InGaAs/Ge triple-junction solar cell and optimization of solar cell's structure focusing on series resistance for high-efficiency concentrator photovoltaic systems', *Solar Energy Materials & Solar Cells*, 90 pp. 1308–1321. Available at: <https://www.sciencedirect.com/science/article/abs/pii/S0927024805002497>
- Ota, Y., Nishioka, K. (2012) 'Three-dimensional simulating of concentrator photovoltaic modules using ray trace and equivalent circuit simulators', *Solar Energy* 86 (1), pp. 476–481. Available at: <http://dx.doi.org/10.1016/j.solener.2011.10.021>.
- Patanasemakul, N., Rakkwamsuk, P., Chuangchote, S., Songprakorp, R., Kirtikara, K. (2017) 'Improved Radiation Uniformity in Concentrating Photovoltaic System using Reflective Secondary Optic', *Energy Procedia*, 138, pp. 598–603. Available at: <http://dx.doi.org/10.1016/j.egypro.2017.10.167>.
- Pérez-Higueras, P., Ferrer-Rodríguez, J. P., Almonacid, F., Fernández, E. F. (2018) 'Efficiency and acceptance angle of High Concentrator Photovoltaic modules: Current status and indoor measurements', *Renewable and Sustainable Energy Reviews*, 94 (June) pp.143–153. Available at: <http://dx.doi.org/10.1016/j.rser.2018.06.011>.
- Rodrigo P., Fernández E.F., Almonacid F., Pérez-Higueras, P.J. (2013) 'Models for the electrical characterization of high concentration photovoltaic cells and modules: A review', *Renewable and Sustainable Energy Reviews*, 26, pp- 752-760. Available at: <http://dx.doi.org/10.1016/j.rser.2013.06.019>.
- Van Leest, R. H., Fuhrmann, D., Frey, A., Meusel, M., Siefer, G., Reichmuth, S. K. (2019) 'Recent progress of multi-junction solar cell development for CPV applications at AZUR SPACE', *AIP Conference Proceedings* 2149. Available at: <http://dx.doi.org/10.1063/1.5124177>.
- Wiesenfarth, M., Anton, I., Bett, A. W. (2018), 'Challenges in the design of concentrator photovoltaic (CPV) modules to achieve highest efficiencies', *Applied Physics Reviews*, 5 (4), 041601. Available at: <http://dx.doi.org/10.1063/1.5046752>.
- Yang, G. H., Wei, M., Chen, B.-Z., Dai, M.-C., Guo, L.-M., Wang, Z.-Y. (2013) 'Design and research of equal-thickness slab Fresnel lens', *Journal of Applied Optics*, 34, pp. 898–902. Available at: <http://dx.doi.org/10.5768/JAO201334.0601003>.
- Zou, Y. H., Yang, T. S. (2014) 'Optical performance analysis of a HCPV solar concentrator yielding highly uniform cell irradiance', *Solar Energy*, 107 pp. 1–11. Available at: <http://dx.doi.org/10.1016/j.solener.2014.06.004>.
- Zubi, G., Bernal-Agustín, J. L., Fracastoro, G. V. (2009) 'High concentration photovoltaic systems applying III-V cells', *Renewable and Sustainable Energy Reviews*, 13 (9), pp. 2645–2652. Available at: <http://dx.doi.org/10.1016/j.rser.2009.07.002>.

---

## #204: Optimum scheduling by creating feeder scale islands for continuity of supply of critical loads in emergency network conditions

---

Fatma AVLI FIRIŞ<sup>1</sup>, Ali Osman KÖKSAL<sup>2</sup>

<sup>1</sup> AKEDAŞ Electricity Distribution Company, K.Maraş, Turkey, fatma.avlifiris@akedasdagitim.com.tr  
<sup>2</sup> AKEDAŞ Electricity Distribution Company, K.Maraş, Turkey, aliosman.koksal@akedasdagitim.com.tr

*Abstract: Because of the increase in distributed generation facilities based on renewable energy sources around the world, one-way energy flow in the electricity distribution network is replaced by multi-directional, multi-point to multi-point and changing according to the times of the day. The fact that most of the users in the electricity distribution network have sensitive loads makes it necessary for individual measures to be replaced by measures to be taken on the basis of the grid. This inevitableness put forward the concept of micro-grid with the approach of minimizing the impact of critical loads from interruptions and malfunctions in the interconnected grid. When analyse in the context of the main grid, the most important advantage of the microgrid is that it has the ability to operate in a controllable structure within the main grid and as a discrete energy source when necessary. From the user's point of view, the ability to meet individual energy needs by providing quality and uninterrupted energy and this situation to prevent possible damages stands out as the biggest advantage of the micro grid. In this study, the necessary technical criteria on the basis of distribution network level and distributed generation level, for the establishment of a distribution feeder-scale micro-grid (isolated island) over power plants connected to the distribution network and renewable energy sources, in order to improve supply continuity in emergency network conditions where the electricity distribution network is without energy, standards and regulatory needs were researched and criteria suitable for such a structure were developed. In this context, pilot feeders connected to a real electricity distribution network were determined on the DlgSILENT Power Factory program, and microgrid (isolated island) modelling was carried out at the scale of the distribution feeder with conventional and distributed generation plants on the feeder. With the study, it has been understood that microgrids to be operated in the distribution feeder scale island mode can be a rational and economical solution in improving the supply continuity indicators in emergencies that cause feeder interruption in medium voltage networks, as long as the necessary criteria are met.*

*Keywords: Distributed generation, Feeder, Isolated Island, Microgrid.*



## 1. INTRODUCTION

In recent years, the number of distributed generation (DG) connected to a distribution grid has increased significantly to meet the increase in power demand. Distributed production: It produces energy from 1 kW to 1000 MW using renewable energy sources such as water, solar, wind and biomass and non-renewable sources (Lopes et al., 2007). The benefits of distributed generation to the end user, power plants and DG owners include safety, reliability, efficiency, economy, etc. there is improvement. However, the connection of the DG to the grid changes the conventional power flow in a radial distribution system (source to load) and thus affects the existing protection coordination (Dalke et al., 2006; Committee, 2011). In addition, the interconnection connection introduced a number of technical problems. Isolated island or disconnection from mains (LOM) is among the problems that occur when a part of the grid system (load section) is energized by DG after being isolated from the rest of the grid system (Balaguer et al., 2011; Sao & Lehn, 2008; Caldón et al., 2008; Blaabjerg et al., 2006).

The principle of isolated island feeding microgrids of generation plants according to international standards; divided into planned and unplanned. Unplanned isolated island feeding; It is the situation in which a region isolated from the network continues to be fed by the DGs in the region after a failure in the network. According to the IEEE 1547.3 standard, in such a case, the isolated island supply conditions must be detected by the DGs within two seconds and the DGs should cut off their energy production. For planned isolated island supply, in order to provide these necessary issues, the capacities, equipment and controllers of the DGs feeding the isolated island must be designed in a way that can meet the active and reactive power balance in the isolated island within acceptable technical limits (Bose et al., 2007; Chowdhury et al., 2009; Best et al., 2009).

Recently, a regulation called IEEE 1547-4 (Guideline for Design, Operation and Integration of Electric Power Systems and Distributed Resource Island Systems) has been published by the IEEE Working Group. This code is a guide for businesses or independent power producers (IPPs) to design and operate the island operation and ensure grid reconnection. Once all technical issues are resolved, the isolated island business may be a viable solution. The solutions and important requirements for successful island business highlighted in the literature are summarized as follows (Best et al., 2009; Katiraei & Iravani, 2006; Jiayi et al., 2008; Mohamad et al., 2010):

- **Operation and management of the island system:** A well-planned island strategy is the most important requirement to run a smooth island business. The strategy should cover the island detection technique, operation on connection to the grid, island mode and reconnection to the grid.
- **Generator controller:** It stands out as the most important criterion in this island business. The controller is designed and modelled in two operating modes: grid connected and island mode. In island mode, the controller must be able to keep the island system's power quality within legal limits. To avoid simultaneous shutdown during reconnection to the mains, the synchronous DG must be equipped with the regulator controller designed to regulate the frequency, voltage and phasor of the island in close proximity to those in the mains. In addition, the controller must be able to improve the transient stability of the generator when subjected to mains loss. This should include applying load shedding when demands exceed the island's production capacity. Load sharing control (speed droop) for multiple DG units is included in the controller.
- **Communication management:** A fast and reliable communication link is required for the transfer of data and control information.

## 2. MODELING OF DISTRIBUTED GENERATION PLANTS IN ISLAND MODE OPERATION

In the international literature, conventional, small hydroelectric and other technology power plants up to 30 MW are considered as distributed generation sources. Such DGs have undertaken important tasks in the network structure with their proximity to the load, increasing the reliability of the region/facility they feed, voltage correction and increased efficiency (Kılınc & Arsoy, 2011).

In grid-connected mode, the mains connection provides strong support for microgrids and has lower risks compared to off-grid mode (island mode). Due to the lack of strong grid support in island operation mode, undesirable situations such as low inertia and short-circuit power occur. Due to the anti-islanding design of PV inverters, the grid disables the generation of solar power plants after switching to island mode. After the transition to the island state, there is a need for energy to re-commission the solar power plants (Bulatov & Kryukov, 2019).

DGs with energy source control and speed management system or preferably DG with single and largest rated power are selected in applicable islanding situations. In addition, it is assumed that every manufacturer hosting a synchronous machine has an automatic voltage regulator and can adjust the voltage of its connection busbars to reference values by drawing or giving reactive power. Manufacturers with asynchronous machines, on the other hand, do not have voltage or frequency regulation capabilities, although they can control a small amount of voltage with capacitor groups (Bulatov & Kryukov, 2019). The benefits of micro-grid systems to be created at the feeder scale are given below (Wang et al., 2016):

- They provide an advantage for micro-grid systems because they have easy disconnection from the grid and backup power sources (diesel generator, UPS, battery, etc.) for regions with critical loads (hospitals, data centers, financial institutions, industrial parks and campuses, etc.).

- Regions where distributed generation resources are concentrated offer opportunities for microgrid systems due to their ability to operate autonomously and as an isolated island.
- Regions whose network infrastructure is outdated and in need of modernization will be configured in accordance with the micro-grid, which will provide less cost and higher efficiency.
- Regions with access to energy efficient building technologies are likely to contribute to the microgrid system

In addition, the minimum technical conditions required for a part of the distribution system to operate as an isolated island are summarized below:

- The isolated island must have a generating plant or power plants with a synchronous generator.
- There must be a load within the island region (to be separated from the network by the distribution company and allocated to the isolated island)
- At least one switchboard must have a black start feature.
- The speed regulator system of the distributed generation plant should be able to operate in active power-frequency droop mode.
- The voltage control system of the distributed generation plant must be able to operate in reactive power-voltage droop mode.

The items mentioned above are the prerequisites for the isolated island system. Apart from these conditions, the presence of significant loads (such as a hospital) on the feeder was taken into consideration as a criterion while determining the pilot feeders in the project. The reason for this is that in an emergency with a large-scale power outage, priority loads are energized quickly with micro-feeder application. In addition, the dynamic modeling of conventional power plants in the region where the selected pilot feeders are located must be done perfectly.

## 2.1. Selection of Pilot Feeders

Considering the planned isolated island criteria, the Kahramanmaraş and Adıyaman distribution network models used in the GIS (Geographic Information System) -Digsilent PowerFactory (PF) integration study were examined in detail, within the scope of determining the most suitable pilot feeders for isolated island operation in the AKEDAŞ electricity distribution network. The geographical view of AKEDAŞ electricity distribution network modeled with Digsilent PowerFactory (PF) is given in Figure 1. As a result of the investigations, 4 potential pilot feeders were focused and selected. These feeders have the following characteristics:

- Feeder 1 → Being a power plant with network recovery (black start) feature
- Feeder 2 → Having critical loads (Kahramanmaraş city hospital and AFAD)
- Feeder 3 → To be able to feed with appropriate maneuvers to create an isolated island in the MV network
- Feeder 4 → Containing a power plant with a synchronous generator

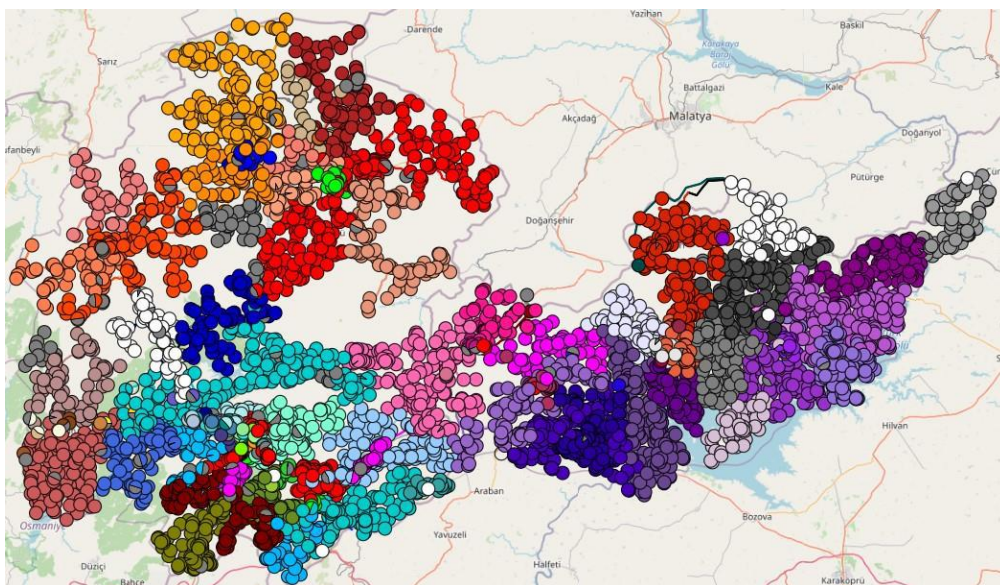


Figure 1 Geographical Based DigSilent PF Model of AKEDAŞ Network

## 2.2. Dynamic Modeling of Conventional Power Plants in the Pilot Region

Isolated island (off-grid) operating conditions differ significantly from on-grid operating conditions. The response of the power plant to the changes in the basic network parameters (voltage and frequency) under the operating conditions connected to the grid and the responses given in the isolated island conditions are different from each other. Especially in isolated island conditions, the main grid parameters (voltage and frequency) of the island fed by the unit directly depend on the dynamic response of the unit to changes in these parameters.

The dynamic reactions of conventional power plants on the pilot feeders under island feeding conditions were analyzed by computer simulations. Dynamic analyzes were carried out with generic models reflecting the general characteristics of conventional power plants. Generator, warning system and speed regulator-turbine models were created within the scope of modelling.

The power plant documents of the synchronous machine-based power plants on the pilot area were examined and the standard model, which was used for modeling the synchronous machine behaviors and referenced IEEE standards (IEEE, 2002), was used in the analyses. Although the required parameters for the generator model are generally design values, it is considered that they will reflect the dynamic behavior of the generator. Figure 2 shows the generator RMS parameters selection screen for dynamic simulation.

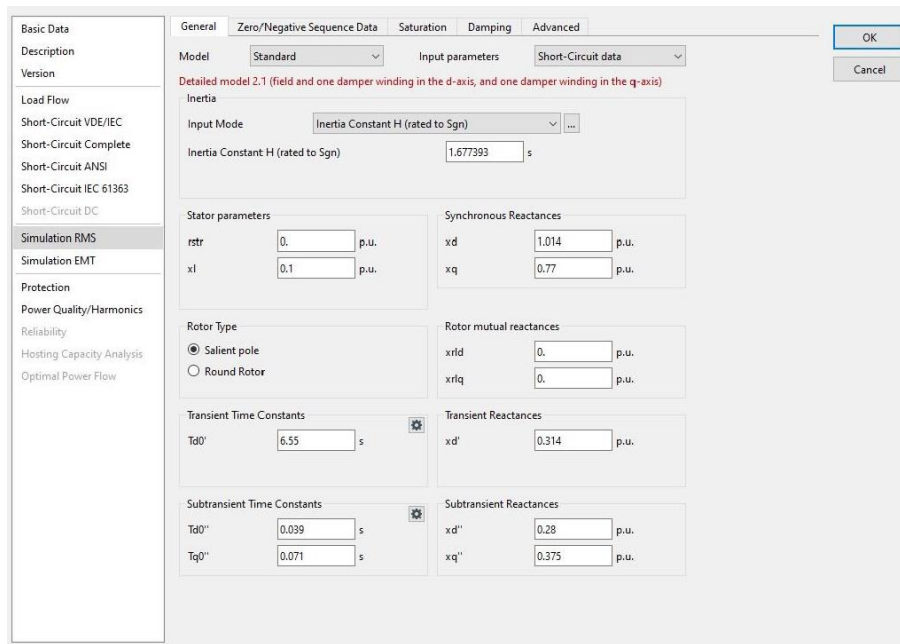


Figure 2 Generator RMS Parameters for Dynamic Simulations

Figure 3 shows the mathematical model of the IEEE Type 1 (AVR - Automatic voltage regulator IEEE T1) type warning system used for analysis in isolated island mode in the computer environment of the power plants on the pilot zone. In the dynamic analysis carried out, this warning system controls the reactive power according to the voltage change under the grid-connected and isolated island mode conditions of the plant. The AVR keeps the voltage changes that may occur against possible impacts during the operation of the plant in the isolated island mode, within the range of  $\pm 10\%$  of the voltage frequency value.

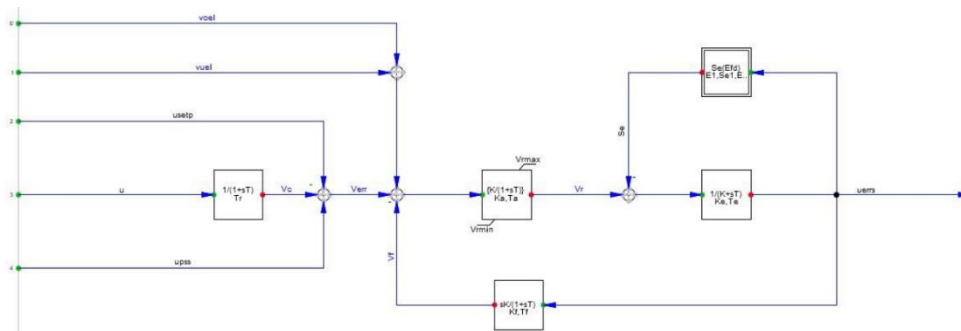


Figure 3 Warning System – IEEE T1 – IEEE Type 1

The mathematical model of the speed regulator (gov\_GENERAL – Generalized Turbine Governor) of conventional power plants on the pilot zone is shown in Figure 4. The speed regulator provides control by changing the setting parameters of

the turbine in order to keep the active power and frequency of the generator at the nominal level. After the power plant is disconnected from the network and switched to isolated island mode, there will be a change in the isolated island frequency in case of load changes in the isolated island. In these changes, the speed regulator should bring the turbine speed and frequency to its nominal value without triggering the protection relays.

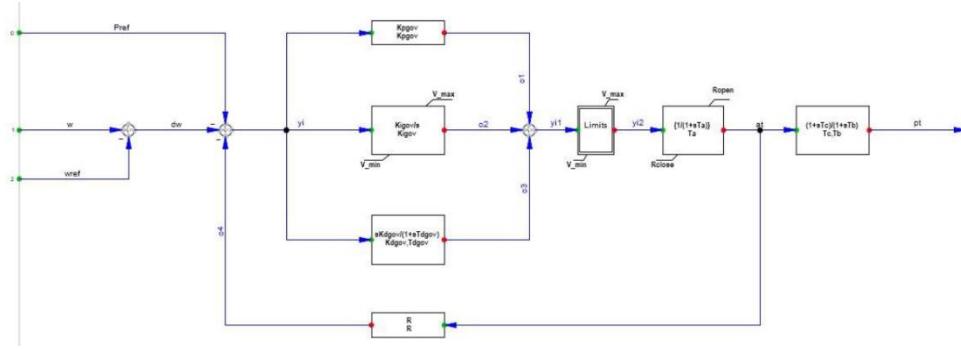


Figure 4 Speed Governor – gov\_General – Generalized Turbine Governor

Another critical issue within the scope of isolated island operation is the action plan to be implemented to operate the system and generation plant operators in isolated island operating conditions. This action plan, which was developed for the power plants on the pilot region discussed in the study, also includes scenarios where isolated island operation of generation power plants is applicable.

### 3. PRODUCTION PLANTS ACTION PLAN IN THE PILOT REGION

In the electricity distribution networks, the action plan for the conventional power plants connected to the distribution network to feed the network in the isolated island mode under emergency conditions is valid for the conventional power plants and the pilot region to which the conventional power plants are connected and is explained below in order of action phases.

**Stage 1 – Preliminary Evaluation:** The first step in the implementation of the isolated island operation plan is to ensure that a fault in the network is permanent and long-term. When generation plants (conventional power plants and SPPs embedded in distribution) fail after such a failure, the distribution company must make a preliminary assessment regarding the cause of the failure and the estimated time of removal. Because, it is not recommended to operate an isolated island in short-term interruptions (less than 4 hours). While determining the 4-hour limit, it was taken into account that the evaluation and total maneuver time required for the isolated island feeding system could reach 4 hours. This period has been calculated considering the situation where remote access is not possible, taking into account the state of being de-energized in the SCADA/DMS system, where the distribution companies can monitor the fault detection and production-consumption flow. In cases where SCADA/DMS systems are energized and necessary interventions can be made remotely, the 4-hour minimum downtime criterion can be reduced. Figure 5 shows the details of this decision and implementation process.

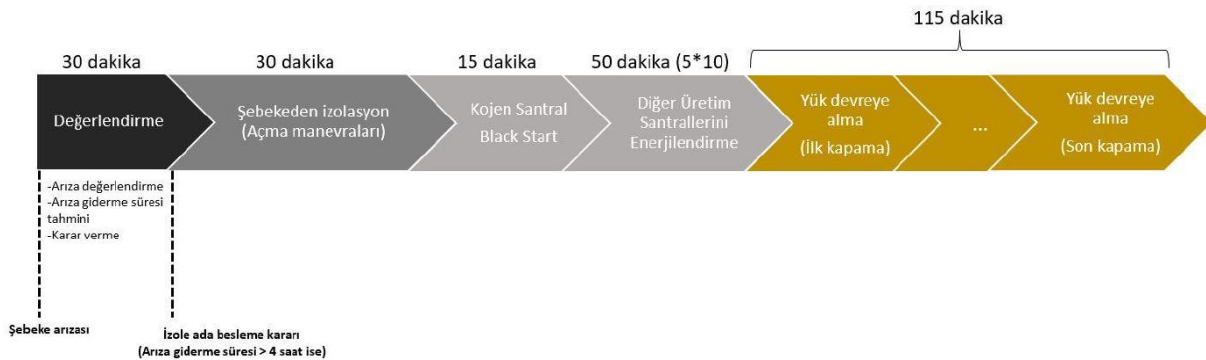


Figure 5 Isolated Island Supply Decision and Implementation Process

**Stage 2 – Isolation of the Pilot Area from the Network (Turn Off Maneuvers):** If it is decided by the conventional power plants and distribution company operators that the failure in the network is long-lasting (>4 hours) and that the conventional power plants can operate in isolated island conditions in this process, in the second stage, the pilot of the distribution company operator will be taken. Necessary maneuvers should be made in the region and the first conditions should be provided for isolated island feeding.

**Stage 3 – Commissioning the Cogen Power Plant with "Black-Start":** After the mains isolation, one of the isolated island conventional power plants should "black-start". For this, the internal requirement for "black-start" in a conventional power plant capable of "black-starting" must be provided by a diesel generator. Within the scope of black-start working preparation;

- It should be checked that the fuel level of the diesel generator is appropriate.
- Turbine-generator speed regulator and AVR controllers should be set to appropriate setting values for isolated island operating conditions.

In the pilot area study, after the diesel generator of the black-start power plant is started, SCADA, oil pumps, warning system, etc. In order to energize the internal demand loads, the diesel generator switch should be turned off and the turbine-generator should be warned under the feeding of the diesel generator and brought to synchronous speed. For this purpose, the following sequence is fulfilled:

- The mechanical torque is gradually increased until it reaches 60% of the rated speed, ie 30 Hz for a 50 Hz system.
- After the turbine speed reaches 60% of its nominal speed (steady state), the warning system is energized and the AVR set value is adjusted to 1 p.u.
- The mechanical torque is then gradually increased until the turbine reaches its rated speed.
- When the turbine-generator speed reaches the nominal speed, the power plant is ready to feed the isolated island.

**Stage 4 – Energizing Other Generating Plants in the Pilot Area (Partial Energizing):** Following the commissioning of the Black-start plant, other generating plants on the isolated island should be energized to feed as much load as possible.

**Stage 5 – Energizing Other Loads on the Pilot Zone:** In particular, the energizing of the isolated island in the pilot zone power plants is carried out by closing the switches. In isolated island supply, the switching sequence and the amount of load to be energized after switching are critical issues. During the closing of the switches, the criterion of change in frequency (due to dynamic factors) at each step must be taken into account.

**Stage 6 – Switching from Isolated Island Mode (Off-Grid) to Network Operation Mode (On-Grid):** After eliminating the fault in the network, it is necessary to switch from the isolated island mode to the network operation mode. The steps to be followed for this purpose are given below:

Step 1: Decommissioning of power plants

Step 2: Conversion of the controller setting set values of the switchboards back to the network mode

Step 3: Conversion of protection coordination set setpoints back to mains mode

Step 4: Transferring the pilot area to the grid with maneuvers

Step 5: Energizing from TM in coordination with TEIAS

After these steps, the power plants embedded in the distribution can be commissioned.

## 4. RESULTS AND DISCUSSION

According to current regulations, generation plants embedded in distribution are shut down in the event of a power outage in the grid. However, when the connection structures in the electricity distribution network and the power plants embedded in the distribution are examined, it is evaluated that it is possible to plan this combined structure to form a micro-grid and that micro-grids can deliver electrical energy to the users in case of interruptions. However, microgrids are an alternative solution for energizing the main grid in case of emergency, and in this respect, they add flexibility to the grid. While there are certain basic principles for performing isolated island work, work plans in isolated island mode must be adjusted and adapted to the pilot area. This is because possible grid configurations, number of generators available, control ranges etc. is the variation for different isolated islands. The first step to realize the advantages of isolated island study is to identify isolated islands. Here the term island means a region containing a certain amount of load and a certain number of controllable distributed generators, such as switching points for maneuvering purposes, fully or partially supplied by local generators (conventional power plants for this project).

Small-scale generation power plants connected to the distribution grid in Turkey are potential candidates for the "planned" isolated island application and the studies have shown that "planned" isolated island feeding can be implemented as long as an isolated island feeding decision and implementation process is implemented and the technical criteria are met. As a matter of fact, according to the computer simulations carried out on the pilot area within the scope of the study, it is understood that a planned isolated island feeding can be made as long as the relevant criteria are met. However, according to the current regulations and communiqués on the subject in Turkey, although the generation plants connected to the distribution network should be designed in accordance with isolated island supply, there is still a regulation/communiqué containing the rules for operating in the planned isolated island mode. and it is necessary to make legislative arrangements for the planned isolated island practice.

## 5. REFERENCES

- Balaguer, I.J., Lei, Q., Yang, S., Supatti, U. and F. Z. Peng., "Control for grid-connected and intentional islanding operations of distributed power generation," IEEE transactions on industrial electronics, vol. 58, pp. 147-157, 2011.
- Best, R.J., Morrow, D.J., Ten, C.F., Lavery, D.M. and Crossley, P.A., "Management of a multiple-set synchronous island," in Power & Energy Society General Meeting, 2009. PES'09. IEEE, 2009, pp. 1-6.
- Blaabjerg, F., Teodorescu, R., Liserre, M. And Timbus, A.V., "Overview of control and grid synchronization for distributed power generation systems," IEEE Transactions on industrial electronics, vol. 53, pp. 1398-1409, 2006.
- Bose, S., Liu, Y., Bahei-Eldin, K., De Bedout, J. and Adamiak, M., "Tieline controls in microgrid applications," in Bulk Power System Dynamics and Control-VII. Revitalizing Operational Reliability, 2007 iREP Symposium, 2007, pp. 1-9.
- Caldon, R., Stocco, A. and Turri, R., "Feasibility of adaptive intentional islanding operation of electric utility systems with distributed generation," Electric Power Systems Research, vol. 78, pp. 2017-2023, 2008.
- Chowdhury, S., Chowdhury, S and Crossley, P., "Islanding protection of active distribution networks with renewable distributed generators: A comprehensive survey," Electric Power Systems Research, vol. 79, pp. 984-992, 2009.
- Dalke, G., Baum, A., Bailey, B., Daley, J., Duncan, B., Fischer, J., et al., "Application of islanding protection for industrial and commercial generators-an IEEE industrial application society working group report," in Protective Relay Engineers, 2006. 59th Annual Conference for, 2006, p. 12 pp.
- IEEE, "Guide for Synchronous Generator Modelling Practices and Applications in Power System Stability Analyses," Tech. Rep. 1110-2002, IEEE, 2002.
- Jiayi, H., Chuanwen, J. and Rong, X., "A review on distributed energy resources and MicroGrid," Renewable and Sustainable Energy Reviews, vol. 12, pp. 2472-2483, 2008.
- Katiraei, F. and Iravani M.R., "Power management strategies for a microgrid with multiple distributed generation units," IEEE transactions on power systems, vol. 21, pp. 1821-1831, 2006.
- Kılınç, L., Arsoy, A.B., "Şebekede Yaşanan Bozucu Elektriksel Olayların Dağıtılmış Üretim Sistemleri Üzerindeki Etkilerinin İncelenmesi" 4. EMO Sempozyumu, EVK 2011.
- Lopes, J.P., Hatzigaryriou, N., Mutale, J., Djapic, P. and Jenkins, N., "Integrating distributed generation into electric power systems: A review of drivers, challenges and opportunities," Electric power systems research, vol. 77, no. 9, pp. 1189-1203, 2007.
- Mohamad, H., Bakar, A.A., Ping, H. and Mokhlis, H., "An adaptive controller of hydro generators for smart grid application in Malaysia," in Power System Technology (POWERCON), 2010 International Conference on, 2010, pp. 1-6.
- Sao, C.K. and Lehn, P.W., "Control and power management of converter fed microgrids," IEEE Transactions on Power Systems, vol. 23, pp. 1088-1098, 2008.
- Wang, J., Costa, L.M., Cisse, B.M., "From Distribution Feeder to MicroGrid: An Insight On Opportunities and Challenges", 2016.

---

## #205: 3-E analysis of plasma gasification combined cycle integrated molten carbonate fuel cell for power production based on refused derived fuel feedstock

---

Roni MALLICK<sup>1</sup>, Prabu VAIRAKANNU<sup>2</sup>

<sup>1</sup> Department of Chemical Engineering, Indian Institute of Technology Guwahati, Assam 781039, INDIA, roni@iitg.ac.in

<sup>2</sup> Department of Chemical Engineering, Indian Institute of Technology Guwahati, Assam 781039, INDIA, v.prabu@iitg.ac.in

*Abstract: Solid waste management is serious yet often overlooked, possibly due to the challenges it possesses worldwide. It is also a major source of greenhouse gas emissions in the form of methane, contributing to nearly half of global warming. Therefore, enhanced technologies have to be adopted that utilize the waste efficiently and recover valuable resources to safely dispose of waste and reduce environmental impact. This work focuses on using plasma gasification for clean syngas production and employing it for power production through the application of combined cycle i.e., gas and steam turbine (IPGCC) and molten carbonate fuel cell (MCFC). Refused Derived Fuel (RDF) is chosen as the feedstock for simulation using a thermodynamic model developed in Aspen Plus software. Steam is used as plasma gas at 4000 °C and oxygen as additional gas for gasification. The splitting ratios of syngas (25:75, 50:50 and 75:25) to IPGCC and MCFC based on the 3-E analysis (energy, exergy and economic) are studied to evaluate the performance of the system. It was observed that the plasma gasification could convert the RDF fuel into simpler compounds of H<sub>2</sub> and CO of >90 % among the syngas composition. Further, the maximum energy efficiency of 42.78% and exergy efficiency of 40.65% with carbon capture were found to be for a 25:75 [IPGCC: MCFC] ratio. While the economic assessment resulted in levelized cost of electricity (LCOE) values between 110-114 \$/MWh considering all the cases. Therefore, the 3-E analysis reported that IPGCC systems integrated with MCFC unit using RDF has the potential for producing good calorific value syngas, high power generation and a safe ecosystem.*

*Keywords: Plasma gasification; Refused Derived Fuel; Molten Carbonate Fuel Cell; Energy; Economic*



## 1. INTRODUCTION

Solid waste generation over the years grew rapidly due to population growth, economic prosperity and urbanization. Among the regions, countries in Europe and Central Asia and East Asia and Pacific accounts for nearly 45%. Despite having a low population count of 16% of world's, high-income countries produce 34% of global waste, whereas low-income countries generate only 5%. Successively, solid waste also emitted carbon dioxide equivalent greenhouse of 1.6 billion tonnes in 2016 and is expected to reach 2.6 billion tonnes by 2050 (Kaza *et al.*, 2018). On the other hand, the ongoing demand for energy in the power and transport sector increases the global greenhouse emissions to ~50% (IEA, 2022). The depletion of fossil fuel and the under-utilization capacity of waste possessed by many countries can be an alternative to induce waste-to-energy recovery techniques for waste management.

Most recently, researchers have studied the possibility of employing the waste feedstock as a source of fuel for end-use applications in the form of energy carrier, power, chemicals., etc. (Perkins 2020, Sajid *et al.*, 2022). Although the practical relevance of conventional technologies such as combustion and gasification in handling waste is demonstrated but generates high amount of pollutants (Conesa, Ortuño and Palmer, 2020). In this context, an emerging technology of plasma gasification is beneficial that decomposes the organic fraction of waste to syngas and inorganics to vitrified slag. The syngas produced through this method is environment friendly due to the breakdown of tars and pollutants drastically (Lemmens *et al.*, 2007). Further, the utilization of syngas for power generation by adopting fuel cell technique can improve the plant with higher efficiencies. It also allows the waste heat from the system to co-generate heat and power (Duan *et al.*, 2015, Wee, 2014).

The studies in plasma gasification have widened the scope for waste-to-energy technologies. Contemporary literatures based on plasma gasification includes exergoeconomic analysis of the combined cycle, thermodynamic analysis of solid oxide fuel cell (SOFC) integrated with chemical looping combustion, techno-economic assessment of integrating with coal-fired power plant using municipal solid waste (MSW). A maximum energy efficiency of 42.14% and exergy efficiency of 41.17% can be achieved with a payback period of 4.58 years (Pan *et al.*, 2022, Montiel-Bohórquez, Agudelo and Pérez, 2021, Jiang *et al.*, 2021). The other studies utilized bio-medical waste for combined power and heat generation (CHP), in internal combustion engines, etc. (Peng *et al.*, 2021, Paulino, Essiptchouk and Silveira, 2020). Even the plasma gasification of refused derived fuel (RDF) integrated with combined cycle and SOFC resulted in a lower efficiency of 31-33% (Minutillo, Perna and Di Bona, 2009, Galeno, Minutillo and Perna, 2011). Therefore, a more robust and detailed analysis is required to enhance the advantage plasma gasification imparts.

The objective of the present study is to provide a 3-E (Energy, Exergy and Economic) assessment of the power plant using Aspen plus 10 software. The overall plant combines a plasma gasification unit with the combined cycle and molten carbonate fuel cell (MCFC). Refused derived fuel (RDF), the combustible fractions of MSW is considered as feedstock. The syngas generated from plasma gasification is used as the main varying parameter for the simulation. This offer an insight of the optimum splitting ratios of syngas to combined cycle and MCFC.

## 2. SYSTEM DESCRIPTION

A basis of 100 MW of input chemical energy of the fuel is considered for the power plant study. Refused derived fuel (RDF) as shown in Figure 1 is chosen as the feedstock based on the Indian scenario (Mallick and Prabu, 2023). Table 1 illustrates the physical and chemical properties of the fuel. The Aspen plus simulation focuses on the integration of plasma gasification combined cycle (IPGCC) with molten carbonate fuel cell (MCFC) based on the splitting of syngas to the combined cycle (CC) and MCFC. In this regard, three cases are studied via syngas splitting from plasma gasification unit (PGU) in the ratio of [25:75], [50:50] and [75:25] to [CC:MCFC].



Figure 1 RDF feedstock used for this study.



Table 1: Proximate and ultimate analysis of RDF.

Proximate analysis (wt.%, dry basis)				Ultimate analysis (wt.%, dry-ash free basis)					LHV <sub>dry</sub> (MJ/kg)	
MC	VM	FC	Ash	C	H	N	S	O <sup>a</sup>	Energy	Exergy
14.57	83.04	3.01	13.95	62.74	6.69	3.12	0.21	27.24	22.16	23.49

<sup>a</sup> by difference; MC-Moisture content; VM-Volatile matter and FC-Fixed carbon.

## 2.1. Integrated plasma gasification combined cycle (IPGCC) with MCFC

The RDF feed is introduced in the plasma gasifier working under atmospheric pressure. Steam is used as the plasma gas and oxygen as a secondary gasifying agent. An air separation unit (ASU) separates the oxygen from air at a purity of 99% (Aneke and Wang, 2015), whereas certain portion of steam is recovered back from steam turbine unit for use in plasma generation. The plasma gasifier is divided into two parts (1) bottom half known as the high temperature reactor (HTR), working at 2500 °C and (2) low temperature reactor (LTR) is the top portion. The generated syngas exits the LTR at a temperature of 1250 °C followed by the heat recovery section (HRSG) where it is cooled to its operating temperature (Minutillo, Perna and Di Bona, 2009). The syngas exchange heat with water for steam generation at subcritical conditions. The cleaning of pollutants (H<sub>2</sub>S, COS, etc.) from raw syngas takes place in the acid gas removal (AGR) unit. Thereafter the clean syngas gets split into two streams in which one of the streams goes to gas turbine unit and the rest to the MCFC. After driving the gas turbine and MCFC to generate power, the residual heat from the flue gas of gas turbine and fuel cell is recaptured to create high-pressure steam in ST unit. Hence, the electricity is produced using a combined power system including GT, ST, and MCFC systems (Duan *et al.*, 2015). The conceptual schematic representation of the overall plant is shown in Figure 2.

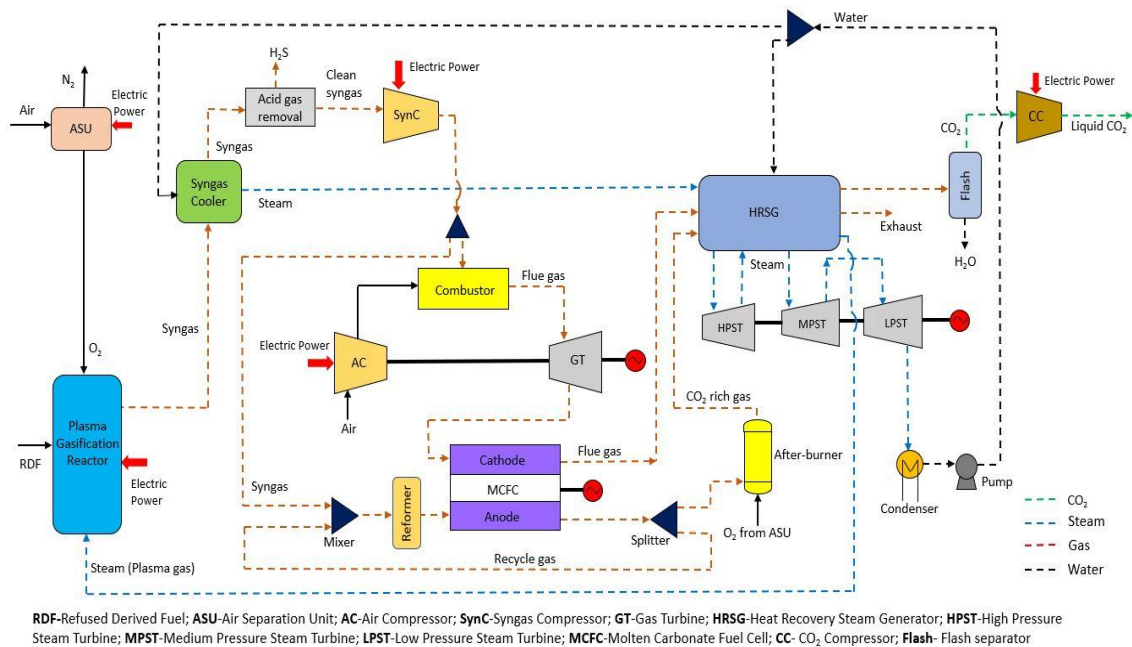
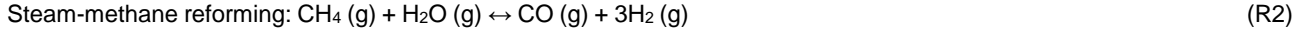
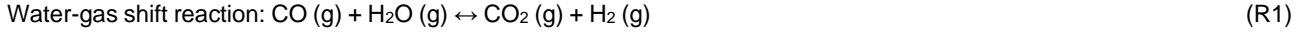


Figure 2 Schematic diagram of the IPGCC system combined with MCFC at various syngas ratio to CC and MCFC

The clean syngas primarily consists of H<sub>2</sub> and CO and small fractions of CO<sub>2</sub>, CH<sub>4</sub>, and H<sub>2</sub>O. Based on the literature (Ryzhkov, Bogatova and Gordeev, 2018), an optimal pressure ratio of 10.6 is set for the combustion chamber (CC) whereby the syngas is combusted at 10.6 bar and 1400 °C. To minimize the energy loss during compression of syngas to 10.6 bar, a double-stage compressor was located. The exhaust from the CC enters the gas turbine to derive electricity under the principle of expansion. Subsequently, the leftover flue gas from the GT at 1 bar and 600-700 °C (based on the flow rate of flue gas) flow into the cathode of the MCFC unit.

On the other hand, the separated syngas stream from AGR is sent to the anode of the MCFC section as inlet to the unit. A reformer was used before the anode to produce more H<sub>2</sub> by converting CO in the syngas via water-gas shift reaction (R1). The reaction consumes steam to liberate H<sub>2</sub> but also increases the CO<sub>2</sub> content of the product gas. A fraction of outlet anode stream is recycled back to the reformer to maintain the steam-to-carbon ratio and avoid carbon deposition. While the remaining stream is combusted in an after-burner using pure oxygen from ASU. The burnt gases comprising of CO<sub>2</sub> and H<sub>2</sub>O (steam) generates additional steam required for reformer. Further, the hot gas splits into two part based on the mass flow rate of CO<sub>2</sub> consumption in the electrochemical reaction of the MCFC. At the cathode, the CO<sub>2</sub> reacts with O<sub>2</sub> from air to form carbonate ions (CO<sub>3</sub><sup>2-</sup>) that reacts with H<sub>2</sub> at the anode and generate power. The following reactions (R2-R4) occurs in the MCFC. The remaining hot gas is cooled at room temperature to condense H<sub>2</sub>O and capture CO<sub>2</sub> for compression at 110 bar in 5 stages and store (Vairakannu and Kumari 2016). The energy from the exhaust stream of

cathode is passed through the HRSG section to generate steam that drives the high, medium and low-pressure steam turbines (HPST, MPST and LPST) and produces electricity.



### 3. METHODOLOGY

Table 2 provides the assumed operating parameters and COE for the simulation. The performance of the overall power plant is determined in terms of net energy efficiency ( $\eta_{en,net}$ ), which is described as the ratio of net power output ( $\dot{W}_{net}$ ) to the input chemical energy of feed (i.e., 100 MW) as given in Equation 1. The power output from MCFC is calculated based on the Nernst potential correlating the applied voltage and current as provided in the literature (Mallick and Prabu, 2023).

Table 2: Simulation parameters and COE assumptions.

Parameters	Unit	Value
Gasification pressure	bar	1.013
Syngas temperature	°C	1250
Gas turbine inlet pressure	bar	10.6
Gas turbine inlet temperature	°C	1400
Steam turbine pressure [HP/MP/LP]	bar	120/38/6
Steam turbine temperature [HP/MP/LP]	°C	530/560/307
Fuel utilization factor	%	75
CO <sub>2</sub> utilization factor	%	80
MCFC reaction temperature	°C	650
MCFC current density	A/m <sup>2</sup>	1500
RDF cost	M\$/year	4.06
Discount rate	%	8
Operating years	years	25
CO <sub>2</sub> transport and storage cost	\$/ton <sub>CO2</sub>	11.22
CO <sub>2</sub> emission tax	\$/ton <sub>CO2</sub>	27.22

Equation 2: Net energy efficiency

$$\eta_{en,net} = \frac{\dot{W}_{net}}{\dot{m}_F \times \text{LHV of solid fuel}}$$

The exergy analysis is performed on the basis of exergy destruction rate ( $\dot{E}_{xd}$ ) i.e., exergy inflow ( $\dot{E}_{xin}$ ) and outflow ( $\dot{E}_{xout}$ ) from the individual unit, and the net exergy efficiency ( $\eta_{ex,net}$ ) as per the Equation 2 and 3, respectively.

Equation 2: Exergy destruction rate

$$\dot{E}_{xd} = \sum \dot{E}_{xin} - \sum \dot{E}_{xout_{en,net}}$$

Equation 3: Net exergy efficiency

$$\eta_{ex,net} = \frac{\dot{W}_{net}}{\dot{m}_F \times \text{Specific exergy of fuel}}$$

For economic analysis, the specific cost of MCFC is considered as adopted by the literature (Spinelli *et al.*, 2020). Moreover, the cost of plasma gasifier ( $C_{plasma\ gasifier}$ ) using steam as plasma gas is estimated as given in Equation 4. The annuity factor is estimated in terms of the annual interest rate and payback period (Mallick and Prabu, 2023).

Equation 4: Plasma gasifier cost

$$C_{plasma\ gasifier} = (4800 * 1.25 * \dot{m}_F * \left(\frac{Quot_{US\$}}{Quot_{EURO}}\right))$$

Where:

- $\dot{m}_F$  = mass flow rate of fuel (kg/h)
- $Quot_{US\$}$  = dollar to euro quotation (US\$)
- $Quot_{EURO}$  = euro quotation (1 Euro)

The capacity factor method is used to measure the capital cost of other equipment's in Equation 5, considering the scaling parameter and reference component cost (Zang *et al.*, 2018, Duan *et al.*, 2015). While the other variables such as specific CO<sub>2</sub> emissions and cost of CO<sub>2</sub> avoided is estimated as per the reference (Mallick and Prabu, 2022).

Equation 5: Cost of the equipment's

$$C = C_0 \times (S/S_0)^f$$

Where:

- $C$  = equipment cost (M\$)
- $C_0$  = reference cost of same component from literature (M\$)
- $S_0$  = reference size
- $S$  = size of the equipment
- $f$  = scaling component

## 4. RESULTS AND DISCUSSION

### 4.1. Syngas from the plasma gasification unit

Based on the input chemical energy of the plant, the inlet feed flow rate is 4.51 kg/s, whereas the optimal inlet flow rates of plasma gas and oxidizing medium are 1.50 kg/s and 0.05 kg/s, respectively as given in Table 3. These flow rates were obtained following the sensitivity analysis of maximum H<sub>2</sub> and CO content in the syngas. The syngas obtained after the plasma gasifier has a molar concentration of 59.57% H<sub>2</sub>, 37.55% CO, 2.11% CO<sub>2</sub> and 0.59% CH<sub>4</sub>. The benefit of using steam as plasma gas is the higher concentration of H<sub>2</sub> via the water-gas shift reaction (R1). The reaction utilizes more CO to yield H<sub>2</sub> and thereby increases the H<sub>2</sub>/CO ratio. On the other hand, steam consumes more energy to generate plasma than other gases and results in high energy penalty of 16.32 MW in this study.

### 4.2. Energy analysis

The net energy efficiencies along with the power production and consumption components is summarized in Table 3. It is observed that the maximum energy consumption of 16.32 MW occurs in plasma generation as penalty, followed by air compression (7.35-16.08 MW) for combustion. The compression energy depends on the density of the gas i.e., denser gases consumes more power. The CO<sub>2</sub> power consumption is lower and varies in the range of 1.07-1.23 MW. This is mainly due to the utilization of CO<sub>2</sub> in the MCFC reactions (R3 and R4). Moreover, the direct capture and storage of CO<sub>2</sub> from the flue gas without any specific separation using physical and chemical solvents lowers penalty further. With the decrease in syngas flow rate ratio to MCFC i.e., [25:75] to [75:25], the syngas and air compression power increases. Accordingly, there is a decrease of 3.72% in net energy efficiency. The steam turbine (33.71 MW) and MCFC (17.12 MW) power output remains the highest for [CC:MCFC] ratio of 25:75. As the fuel utilization factor is set at 75%, excess syngas flow exits the MCFC unit and burns in after-burner to generate more steam for driving steam turbine. Subsequently, the oxygen flow rate increases to 0.8 kg/s (25:75) from 0.21 kg/s (75:25). In the clean-up section, the small amount of unwanted gases is removed, which results in 0.75-0.82% energy penalty of net power output. Despite the large power consumption components in the plant, the net energy efficiency is still higher than some already reported power plant studies on plasma gasification of RDF (Minutillo, Perna and Di Bona, 2009, Galeno, Minutillo and Perna, 2011). The optimized integration of the units with appropriate utilization of the heat and work energy increased the overall efficiency.

Table 3: Energy results for different systems of IPGCC-MCFC using RDF.

Syngas ratio [CC:MCFC]	[25:75]	[50:50]	[75:25]
<i>Flow rate [kg/s]</i>			
Feed rate	4.51	4.51	4.51
Steam plasma flow rate	1.50	1.50	1.50
Oxygen flow rate to gasifier	0.05	0.05	0.05
Oxygen flow rate to MCFC	0.80	0.70	0.21
<i>Power section [MW]</i>			
ASU power consumption	1.84	1.66	0.74
Syngas compression power	1.03	2.75	3.21
Air compression power	7.35	14.18	16.08
Plasma power consumption	16.32	16.32	16.32
Pump power consumption	0.24	0.22	0.19
Clean up power consumption	0.32	0.32	0.32

Gas turbine output power	20.12	33.95	42.98
Steam turbine output power	33.71	30.73	24.85
MCFC power output	17.12	13.01	9.32
CO2 power consumption	1.07	1.15	1.23
Net system power output	42.78	41.09	39.06
Net energy efficiency [%]	42.78	41.09	39.06

### 4.3. Exergy analysis

The input chemical exergy of RDF is estimated as per the literature mentioned in Section 3 and found to be 105 MW. A component wise exergy analysis is conducted to determine the exergy destruction rate occurring in all the units. Considering all the cases, around 74-81% of exergy destruction happens in the plasma gasifier, combustor and after-burner as shown in Figure 3. For CC:MCFC ratio of [75:25], the combustor has the largest exergy destruction of 26.48 MW, followed by plasma gasifier (18.42 MW) and after-burner (9.67 MW). This is attributed to the irreversible chemical reactions taking place inside the reactors, which generates entropy. Moreover, the use of excess air as moderator in the combustion chamber (CC) destroys a high portion of exergy. The addition of MCFC unit to the combined cycle for power generation becomes beneficial in terms of lower exergy destruction (6-9%) relative to the energy production reported in Section 4.2. Accordingly, the exergy efficiencies in Figure 4 show a negative deviation of 1.94-2.13% than the energy efficiencies. The low differences in efficiency values indicates the well-defined thermodynamic state of the overall system (Yazdanfar et al., 2015). However, all the units have potential to improve with optimization of the process parameters. Thus, combining the energy and exergy analysis together is useful in estimating the losses in the overall system.

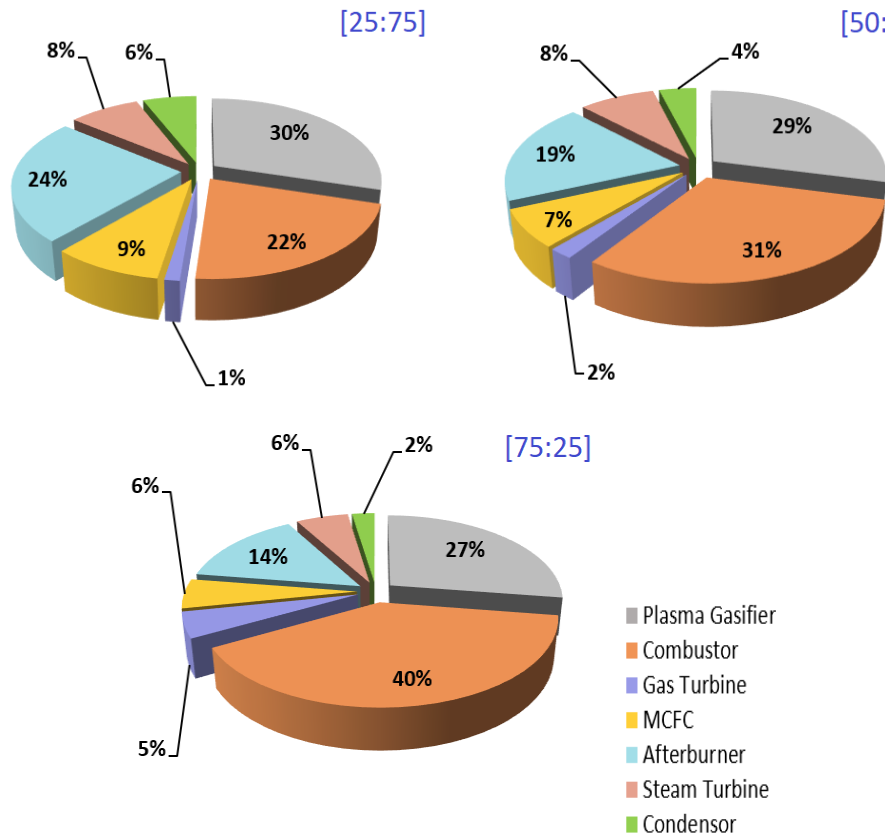


Figure 3 Percentage contribution in exergy destruction of RDF for various components based on syngas ratio to CC and MCFC.

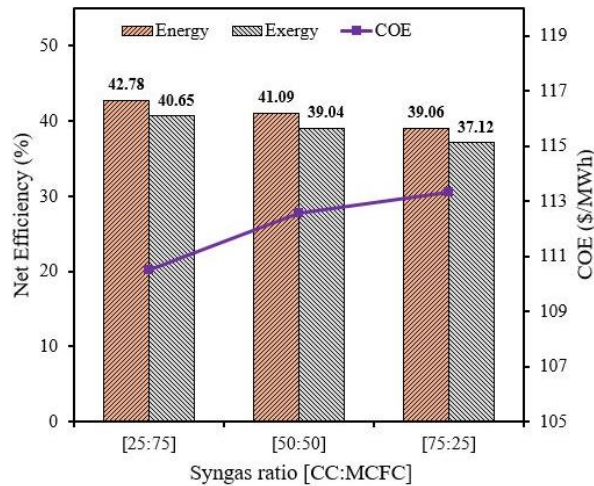


Figure 4 Net overall efficiencies and COE for different systems

#### 4.4. Economic assessment

Net present value (NPV) method and “bottom-up” approach is considered for estimating the values of economic analysis. The specific plant cost when RDF is evaluated for assessment lies between 6493.67–6518.45 \$/kW. The cost of electricity (COE) as shown in Figure 4 is found in the range of 110.50–113.33 \$/MWh for all scenarios. The higher plant cost and COE is due to the large initial investment of two units i.e., the plasma gasification and MCFC. However, it is viewed as short-term state and has the potential to reduce with more improvisation in thermodynamic efficiency and market acceptance. The COE strongly depends on the net energy output from the overall plant. The specific carbon emission of 45.07 kg/MWh is calculated for [CC:MCFC] ratio of 25:75 and increases up to 98.20 kg/MWh for 75:25 ratio. Despite additional CO<sub>2</sub> capture in the MCFC unit, the higher COE increases the avoided cost per ton of CO<sub>2</sub> to 40.90 \$/tonCO<sub>2</sub> for 75:25 (CC: MCFC) system. Therefore, regardless of its many advantages, the shortcoming of the plant in terms of cost analysis can be minimized by mixing RDF with high LHV fuel, increasing plant capacity, reducing avoidable exergy destruction and plasma gasifier and MCFC cost. The solutions may lead to an increase in the capital cost of the plant but will reduce the COE and carbon cost.

#### 5. CONCLUSIONS

The plasma gasification of RDF integrated with combined cycle and MCFC is proposed for power generation based on the splitting ratios of syngas. Further, a 3-E (energy, exergy and economic) analyses of the power plants are performed to draw the following conclusions:

- The high temperature (1250-2500°C) plasma gasification of RDF using steam (1.5 kg/s) and O<sub>2</sub> (0.05 kg/s) converts the feed to nearly 97% with H<sub>2</sub>/CO ratio of 1.6.
- The system with CC:MCFC ratio of 25:75 has the maximum net energy efficiency of 42.78%. Plasma power (16.32 MW) is one of the highest energy consumption unit, while CO<sub>2</sub> compression penalty is between 2.5-3.14% for all the cases.
- The net exergy efficiency deviates negatively by 1.94-2.13% than energy efficiency. Around 75-80% of the exergy destruction takes place in the plasma gasifier, combustor and afterburner due to the generation of entropy during chemical reactions.
- The economic assessment shown a higher COE of 100-114 \$/MWh for all cases. Further, the specific CO<sub>2</sub> emission rate varies between 45-98 kg/MWh and cost of CO<sub>2</sub> avoided has a lower value of 40.90 \$/ton CO<sub>2</sub> due to higher amount of CO<sub>2</sub> absorption in MCFC.

Hence, RDF waste has the potential to produce good calorific value syngas that encourages towards electricity generation via the integration of plasma gasification with MCFC based on the 3-E analyses.

#### 6. REFERENCES

- Aneke, M. and Wang, M., (2015). Potential for improving the energy efficiency of cryogenic air separation unit (ASU) using binary heat recovery cycles. *Applied Thermal Engineering*, 81, pp.223-231.
- Conesa, J.A., Ortuño, N. and Palmer, D., (2020). Estimation of industrial emissions during pyrolysis and combustion of different wastes using laboratory data. *Scientific Reports*, 10(1), p.6750.
- Duan, L., Sun, S., Yue, L., Qu, W. and Yang, Y., (2015). Study on a new IGCC (integrated gasification combined cycle) system with CO<sub>2</sub> capture by integrating MCFC (molten carbonate fuel cell). *Energy*, 87, pp.490-503.

- Galeno, G., Minutillo, M. and Perna, A., (2011). From waste to electricity through integrated plasma gasification/fuel cell (IPGFC) system. *International Journal of Hydrogen Energy*, 36(2), pp.1692-1701.
- IEA, (2022). World energy outlook 2022. Paris, France: IEA.
- Jiang, P., Parvez, A.M., Meng, Y., Dong, X., Xu, M., Luo, X., Shi, K. and Wu, T., (2021). Novel two-stage fluidized bed-plasma gasification integrated with SOFC and chemical looping combustion for the high efficiency power generation from MSW: A thermodynamic investigation. *Energy Conversion and Management*, 236, p.114066.
- Kaza, S., Yao, L., Bhada-Tata, P. and Van Woerden, F., (2018). *What a waste 2.0: a global snapshot of solid waste management to 2050*. World Bank Publications.
- Lemmens, B., Elslander, H., Vanderreydt, I., Peys, K., Diels, L., Oosterlinck, M. and Joos, M., (2007). Assessment of plasma gasification of high caloric waste streams. *Waste Management*, 27(11), pp.1562-1569.
- Mallick, R. and Prabu, V., (2022). 4-E analyses of plasma gasification integrated chemical looping reforming system for power and hydrogen co-generation using bakelite and acrylonitrile butadiene styrene based plastic waste feedstocks. *Energy Conversion and Management*, 271, p.116320.
- Mallick, R. and Prabu, V., (2023). Energy, exergy, economic and environmental (4-E) analyses of plasma gasification steam cycle integrated molten carbonate fuel cell for hydrogen and power co-generation based on residual waste feedstocks. *International Journal of Hydrogen Energy*, 48(45), pp.16971-16986.
- Minutillo, M., Perna, A. and Di Bona, D., (2009). Modelling and performance analysis of an integrated plasma gasification combined cycle (IPGCC) power plant. *Energy Conversion and Management*, 50(11), pp.2837-2842.
- Montiel-Bohórquez, N.D., Agudelo, A.F. and Pérez, J.F., (2021). Effect of origin and production rate of MSW on the exergoeconomic performance of an integrated plasma gasification combined cycle power plant. *Energy Conversion and Management*, 238, p.114138.
- Pan, P., Peng, W., Li, J., Chen, H., Xu, G. and Liu, T., (2022). Design and evaluation of a conceptual waste-to-energy approach integrating plasma waste gasification with coal-fired power generation. *Energy*, 238, p.121947.
- Paulino, R.F.S., Essiptchouk, A.M. and Silveira, J.L., (2020). The use of syngas from biomedical waste plasma gasification systems for electricity production in internal combustion: Thermodynamic and economic issues. *Energy*, 199, p.117419.
- Peng, W., Chen, H., Liu, J., Zhao, X. and Xu, G., (2021). Techno-economic assessment of a conceptual waste-to-energy CHP system combining plasma gasification, SOFC, gas turbine and supercritical CO<sub>2</sub> cycle. *Energy Conversion and Management*, 245, p.114622.
- Perkins, G., (2020). Production of electricity and chemicals using gasification of municipal solid wastes. In *Waste biorefinery* (pp. 3-39). Elsevier.
- Ryzhkov, A., Bogatova, T. and Gordeev, S., (2018). Technological solutions for an advanced IGCC plant. *Fuel*, 214, pp.63-72.
- Sajid, M., Raheem, A., Ullah, N., Asim, M., Rehman, M.S.U. and Ali, N., (2022). Gasification of municipal solid waste: Progress, challenges, and prospects. *Renewable and Sustainable Energy Reviews*, 168, p.112815.
- Spinelli, M., Di Bona, D., Gatti, M., Martelli, E., Viganò, F. and Consonni, S., (2020). Assessing the potential of molten carbonate fuel cell-based schemes for carbon capture in natural gas-fired combined cycle power plants. *Journal of Power Sources*, 448, p.227223.
- Vairakannu, P. and Kumari, G., (2016). CO<sub>2</sub>-Oxy underground coal gasification integrated proton exchange membrane fuel cell operating in a chemical looping mode of reforming. *International Journal of Hydrogen Energy*, 41(44), pp.20063-20077.
- Wee, J.H., (2014). Carbon dioxide emission reduction using molten carbonate fuel cell systems. *Renewable and Sustainable Energy Reviews*, 32, pp.178-191.
- Yazdanfar, J., Mehrpooya, M., Yousefi, H. and Palizdar, A., (2015). Energy and exergy analysis and optimal design of the hybrid molten carbonate fuel cell power plant and carbon dioxide capturing process. *Energy conversion and management*, 98, pp.15-27.
- Zang, G., Jia, J., Tejasvi, S., Ratner, A. and Lora, E.S., (2018). Techno-economic comparative analysis of Biomass Integrated Gasification Combined Cycles with and without CO<sub>2</sub> capture. *International Journal of Greenhouse gas control*, 78, pp.73-84.

---

## #207: Estimating energy savings in Singapore's building benchmarking policy for office buildings

---

Gu HAO<sup>1</sup>, Xiaoyu JIN<sup>2</sup>, Linda F. XIAO<sup>3</sup>

<sup>1</sup> The Hong Kong Polytechnic University, Hong Kong, [goodhao.gu@connect.polyu.hk](mailto:goodhao.gu@connect.polyu.hk)

*Abstract: As ever more countries commit to net-zero greenhouse gas emissions in official policy documents and laws, a series of relevant building energy policies have emerged in different areas to enhance building energy usage efficiency. However, the quantification of their effectiveness is challenging due to substantial uncertainty. Much of relevant research employ linear regression models to analyse the correlation between time and energy consumption, aiming to ascertain the energy savings linked to a specific policy. Nonetheless, these approaches may deviate to some extent due to priori unknown or underestimated interventions. In this study, we develop econometric models to investigate the causal link between energy savings and building benchmarking policy in Singapore for office buildings. Using matching and regression techniques, we find that Singapore's 2019 benchmarking policy contribute to 14% energy savings across all office buildings in 2020. However, we also find that the policy does not reduce energy consumption homogeneously in different buildings, exhibiting a more pronounced impact on buildings that are not certified as green buildings prior to 2019. These buildings have the potential to reduce their energy use intensity (EUI) by 19% if they can get certified in 2019, which is equivalent a reduction of 36.4 million dollars per year in electricity costs based on average electricity prices. These findings enable a better understanding of benchmarking policy impact and provide valuable insights for policymakers to conduct investment analyses related to building energy.*

*Keywords: Building Energy, Building Benchmarking Policy, Casual analysis, Energy savings*

## 1. INTRODUCTION

Buildings play a key role in achieving net-zero targets and mitigating climate change, accounting for 36% of global final energy consumption and 39% of energy and process-related CO<sub>2</sub> emissions (IEA, 2019). Many countries have implemented building energy policies to improve the energy performance and efficiency of buildings, such as mandatory energy audits, disclosure of energy consumption data, rating and labelling schemes, and minimum energy performance standards (Bouckaert et al., 2021). Although most policies prove effective, they occasionally yield unintended consequences, as seen in Hong Kong, where the OTTV requirements have adversely affected building energy efficiency (Jia and Lee, 2018). Nonetheless, measuring the actual impact of these policies on energy savings is challenging due to data limitations, methodological issues, and confounding factors. While linear regression models have been commonly employed in previous research to analyse the relationship between time and energy consumption, they may not fully capture the nuanced impacts of building energy policies due to the presence of unaccounted or underestimated interventions. Addressing this challenge requires robust econometric models that can establish causal links between energy savings and specific building energy policies. Singapore is one of the leading countries in promoting green buildings and implementing building energy policies. In 2019, it introduced a mandatory building benchmarking policy that requires all office buildings with a gross floor area of more than 5,000 square meters to submit their annual energy consumption data and obtain an energy performance certificate (BCA, 2019). The primary objective of this policy is to enhance energy efficiency throughout the commercial building sector, concurrently addressing the issue of data scarcity. Moreover, it presents a remarkable opportunity for evaluating the energy savings generated as a result of its implementation.

In this study, we engage in a technique that designs intricate econometric models to explore the cause-and-effect association between energy efficiency and Singapore's building benchmarking mandate for office infrastructures. The study employs matching and regression methods, thereby allowing us to uncover, with superior precision and reliability, the influence of the policy on energy consumption. The objective of this research is twofold: firstly, to quantify the energy savings achieved through Singapore's 2019 building benchmarking policy for office buildings, and secondly, to analyse the policy's varying impact in green-labelled and non-green-labelled buildings. By understanding the nuanced energy-saving patterns, policymakers can tailor future interventions to optimize energy efficiency efforts across the diverse spectrum of buildings. The subsequent sections of this paper are organized as follows: Section 2 provides the data description and econometric models, Section 3 presents the results, and Section 4 concludes the paper.

## 2. METHODOLOGY

### 2.1. Data description

The dataset used in this study is publicly available through Singapore's Building and Construction Authority (BCA) on the Building Energy Submission System. It comprises both basic information and energy performance details for commercial buildings. The basic information includes essential building characteristics such as the building name, address, main function, green mark rating and version, gross floor area, percentage of air-conditioned floor area, average occupancy rate, type of air conditioning system, age of chiller, and percentage usage of LED lighting. On the other hand, energy performance information is based on the annual average of energy use intensity (EUI) from January 2017 to December 2020. To ensure the quality and reliability of the data, some samples with missing EUI data for certain years and others with suspicious values showing significant fluctuations in EUI between adjacent years were excluded from the analysis. After applying these data quality measures, a total of 174 samples of office buildings were ultimately selected. Among these, 41 buildings received a green mark award (green labelled) in 2019, while 133 did not receive such an award (non-green-labelled). The statistical data for these selected buildings are presented in Table 1. Note that in the raw data, water system is a binary variable that indicates that the building uses water system when its value is 1 and vice versa.

Table 1: Basic information and energy performance statistics for different types of buildings

Parameters	Green mark award in 2019				No green mark			
	Mean	SD	Min	Max	Mean	SD	Min	Max
Gross Floor Area (m <sup>2</sup> )	62497	89566	6832	490000	20257	38299	1791	420000
Percentage of Air-conditioned Floor Area (m <sup>2</sup> )	0.78	0.21	0.08	1	0.69	0.27	0	1
Average Monthly Building Occupancy Rate (%)	88%	17%	8%	100%	88%	19%	7%	100%
Water system	0.63	0.49	0	1	0.46	0.5	0	1
Age of Chiller (year)	6.7	4.41	1	18	10.11	7.98	0	38
LED Percentage (%)	36%	34%	0%	100%	21%	30%	0%	100%
2017 EUI (kWh/m <sup>2</sup> .year)	227.33	111.46	25.06	703.43	245.51	252.69	3.97	1898.57
2018 EUI (kWh/m <sup>2</sup> .year)	228.77	124.72	24.75	743.53	240.93	251.58	3.77	1878.61
2019 EUI (kWh/m <sup>2</sup> .year)	232.54	135.60	23.48	768.10	239.31	251.22	1.87	1903.46
2020 EUI (kWh/m <sup>2</sup> .year)	193.39	132.03	19.96	805.56	216.90	259.29	2.34	2043.55



## 2.2. Econometric models

We employ econometric models to concurrently assess the impact of the building benchmarking policy on energy usage intensity. Unlike conventional linear regression, these models necessitate constructing counterfactual causality (Pearl, 2000) to forecast the policy's impact (commonly referred to as the treatment effect). This entails comparing the outcome of a unit when subjected to a specific treatment and the outcome of the same unit when not subjected to the treatment. In this study, we are concerned with examining the difference in EUI of a specific building at a given moment in time when it receives a green award and when it does not. Nonetheless, observing both states of a building, where it either receives a green award or does not, is not practically feasible. Therefore, a counterfactual value of EUI has to be predicted. The difference between the predicted value and the actual value represents the treatment effect of the policy, which is commonly measured using the mean value, thus called average treatment effect (ATE). To expound further, we define a binary variable  $D$ , which takes the value of 1 if a building obtains a green mark award in 2019 and 0 vice versa. The ATE of the policy is presented as Equation 3:

Equation 1: Average Treatment Effect.

$$ATE = \frac{1}{N_1} \sum_{i=1}^N D_i \cdot [Y_i - \hat{Y}_i]$$

Where:

- $N$ =the number of buildings
- $D$ =the binary variable indicates that if a building gets green mark award in 2019
- $Y$ =EUI of the building
- $\hat{Y}$ =Prediction of EUI of the building under counterfactual status

There are different ways to predict  $\hat{Y}$ . In this study, covariate matching (Zhao, 2004) is employed as a technique to mitigate bias and ensure comparability between the treatment and control groups. This involves identifying comparable observations from the control group that closely align with the characteristics of the treated group. Additionally, to further reduce bias and enhance the analysis's statistical consistency, a bias-corrected estimation (Abadie and Imbens, 2011) with 2 neighbours matching method is introduced, rendering the analysis  $N^{-\frac{1}{2}}$  consistent, as shown in Equation 2. By doing so, the analysis aims to create a more balanced and representative sample, enabling a reliable estimation of the causal effect of Singapore's building benchmarking policy on energy savings for office buildings.

Equation 2: Covariate matching.

$$\hat{Y}_i = \frac{1}{M} \sum_{j=1}^M Y_j$$

Where:

- $M$ =Number of nearest neighbor matches, which is 2 in this study
- $Y_j$ =EUI of sample  $j$  matched to sample  $i$

Another econometric model we used is propensity score matching (Caliendo and Kopeinig, 2008), as shown in Equation 3. This approach condenses all covariates into a single index-variable, namely the propensity-score, denoted as  $p(x_i)$ . The utilization of a heteroskedastic probit model helps control the error by constraining the upper and lower bounds of the propensity score to 0.1, while simultaneously considering the common support.

Equation 3: Propensity Score.

$$p(x_i) = E(D = 1|x_i)$$

$$\hat{Y}_i = Y_j, \min|p(x_i) - p(x_j)|$$

Where:

- $x$ =variant, including parameters listed in Table 1
- $E$ =the mathematical expectation
- $Y_j$ = EUI of sample  $j$  with the minimum absolute difference in  $p(x)$  from sample  $i$

When the treatment is not randomly assigned, there is a possibility that the distribution of the variables comprising  $x$  may become highly unbalanced. To rectify this issue and restore some balance in the covariates' distributions, a suitable approach is to assign weights to the observations and subsequently employ a weighted least squares (WLS) framework to estimate the ATE. In this context, we assign weights to each observation based on the inverse of its estimated propensity score (Hirano, Imbens and Ridder, 2003), as indicated in Equation 4. This means that observations with higher estimated propensity scores will receive lower weights, while those with lower estimated propensity scores will be assigned higher weights. By doing so, the analysis accounts for the imbalance in the covariates' distribution and gives more significance to observations that resemble the characteristics of the treated group, ensuring a more reliable estimation of the ATE.

Equation 4: Inverse probability weighting.

$$ATE = \frac{1}{N_1} \sum_{i=1}^N \beta_1(i) \cdot D_i \cdot Y_i - \frac{1}{N_0} \sum_{i=1}^N (1 - D_i) \cdot \beta_0(i) \cdot Y_i$$

$$\begin{cases} \beta_0 = \frac{1}{1 - p(x_j)}, & \text{if } D = 0 \\ \beta_1 = \frac{1}{p(x_i)}, & \text{if } D = 1 \end{cases}$$

Where:

-  $\beta$ =the reweighting coefficient

In summary, we employ covariate matching, propensity score matching, and IPW regression to investigate the causal link between Singapore's building benchmarking policy and energy savings in office buildings. By employing these advanced econometric techniques, we aim to provide policymakers and stakeholders with valuable insights into the effectiveness of the policy and its implications for enhancing building energy efficiency.

### 3. RESULTS

#### 3.1. Difference in EUI for different buildings in 2020

First, we present a graphical representation of the EUI trend from 2017 to 2020 for two distinct groups of buildings: those that received a green mark award in 2019 ( $D=1$ ) and those that did not ( $D=0$ ), as shown in Figure 1.

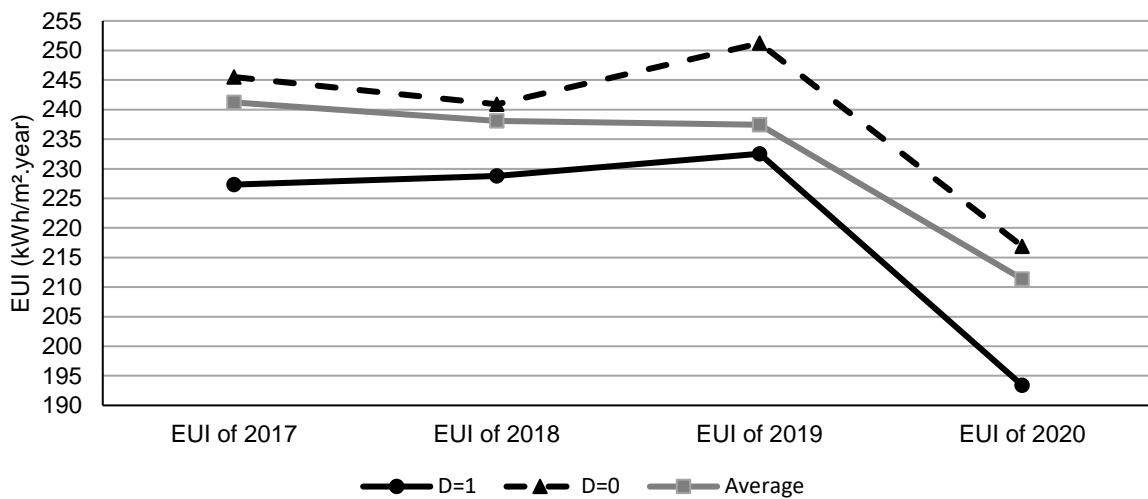


Figure 1 The EUI trend from 2017 to 2020

As depicted in the graph, the EUI keeps a general decreasing trend, with only a slight increase observed in 2019. It is essential to consider that buildings seeking the green mark award in 2019 would require time for the installation and commissioning of equipment. This process might lead to variations in air conditioning energy consumption due to various influencing factors. Therefore, the study employs the 2018 EUI as a reference point for comparison with the data from 2020.

In 2018, the average EUI is 238.07 kWh/m²·year, which subsequently decreased by 26.71 kWh/m²·year to 211.36 kWh/m²·year in 2020, signifying an approximate 11% reduction. Meanwhile, in buildings that received the green mark in 2019, their average EUI decreased from 228.77 kWh/m²·year to 193.39 kWh/m²·year, demonstrating a decrease of about 15%. On the other hand, in buildings that did not receive the green mark in 2019, their average EUI decreased from 240.93 kWh/m²·year to 211.36 kWh/m²·year, representing a reduction of about 10%. Notably, the relative reduction in the latter case is only two-thirds of the reduction observed in buildings with the green mark award.

It is crucial to recognize that this simple model, commonly used in government reports (BCA, 2022), may present positive results that please policymakers. However, these outcomes alone do not justify the conclusion that the green mark award policy in 2019 directly facilitated energy consumption reduction in buildings, as the building groups under consideration are not identical. Several possible reasons could contribute to this discrepancy. For instance, buildings receiving green mark award may have invested heavily in upgrading equipment initially. Consequently, to control ongoing costs, building owners may have reduced maintenance expenditures during the operational phase. This decision could result in the air conditioning system being turned off for repairs due to equipment failures, potentially leading to a lower EUI in 2020, which remains unobservable.

### 3.2. Estimated energy savings

To address the aforementioned issue, we designed econometric models represented by Equations 1 to 4. All three models evaluate the average treatment effect of the policy by controlling for the presence of a green mark award in 2019 as a single variable. These models calculate the difference in EUI between scenarios where the same building receives or does not receive the green mark award, thus ensuring there is no heterogeneity in building groups. The results are summarized in Table 2.

Table 2: Estimated energy savings by three econometric models

	Average energy savings(kWh/m <sup>2</sup> .year)	standard error	P> z
Covariate matching	31.35*	18.59	0.09
Propensity score matching	31.15*	21.89	0.085
IPW regression	36.47***	21.9	0.004
Average of three models	33.04	-	-

From the table, it is evident that the average energy savings attributed to the 2019 green mark award, obtained from the three model evaluations, are 31.35 kWh/m<sup>2</sup>.year, 31.15 kWh/m<sup>2</sup>.year, and 36.47 kWh/m<sup>2</sup>.year, respectively. The original hypothesis that the 2019 green mark award has no effect on building EUI is rejected since the P-values for the significant coefficients are below 10%. This means that the 2019 green mark award indeed contributed to a reduction in building EUI, and the results from the three models are consistent. On average, the EUI in 2019 is 237.44 kWh/m<sup>2</sup>.year, and the green mark award in 2019 helped buildings achieve an average reduction of approximately 33.04 kWh/m<sup>2</sup>.year, representing about 14% reduction. This improvement can be attributed to proactive measures taken by building owners, such as upgrading the building envelope, adopting newer and more efficient air conditioning equipment, and implementing other optimization measures to meet the green mark award requirements.

To gain further insight into the energy performance of buildings with and without the green mark award under counterfactual status, we employ propensity score matching as shown in Equation 3 to evaluate two other average treatment effects: Average Treatment Effect in Treated (ATET) and Average Treatment Effect in Untreated (ATEU). ATET assumes that buildings that received the green mark did not receive it in 2019, while ATEU assumes the opposite scenario. The results obtained through Equation 3 calculations are presented in Table 3.

Table 3: Estimated propensity scores

	EUI of treated group	EUI of control group	Average energy savings	P> z
ATEU	193.15	152.59	40.55	0.03
ATET	194.73	175.26	-19.47	0.75

From the table, it can be observed that the average energy savings under the ATEU assumption amount to 40.55 kWh/m<sup>2</sup>.year, which is statistically significant. This suggests that buildings without the green mark award, if they were to receive it in 2019, would experience an EUI reduction of 40.55 kWh/m<sup>2</sup>.year, equivalent to 19% of their 2020 EUI. Considering the total area of office buildings without the green mark award is about 2,847,000 m<sup>2</sup>, the total EUI reduction would be approximately 115 MWh/year. With the electricity price of commercial buildings estimated at around 0.315 dollars, the green mark award has the potential to save about 36.4 million dollars per year in office buildings. These results offer compelling evidence to support updating Singapore's building energy benchmarking policy and provide valuable insights for policymakers to conduct investment analyses related to building energy.

On the other hand, the average energy savings of buildings under the ATET assumption are negative, specifically -19.47 kWh/m<sup>2</sup>.year. This indicates that the green mark has seemingly worsened the energy performance of these buildings. However, it is crucial to note that this result requires further investigation, as the p-value of 0.75 is far from being statistically significant. Indeed, to obtain more accurate and comprehensive results, it is essential to conduct ongoing assessments for each subsequent year, considering the dynamic nature of building energy consumption patterns and policy effectiveness. While our current analysis provides valuable insights, it is vital to recognize the simplifications made in certain assumptions regarding building energy consumption. These assumptions may need further examination to evaluate their applicability to diverse buildings and the actual implications for the assessment process.

## 4. CONCLUSIONS

In this study, we take an approach by developing advanced econometric models to investigate the causal link between energy savings and Singapore's building benchmarking policy for office buildings. By utilizing covariate matching, propensity score matching and IPW regression techniques, our analysis demonstrates that the 2019 benchmarking policy in Singapore has led to significant energy savings of 15% across all office buildings in the subsequent year. However, it also brings to light the potential pitfalls of over-simplifying building energy analysis, emphasising the need for a more nuanced approach that accounts for the complex dynamics of building energy consumption.

Our study also reveals a nuanced picture of the policy's impact, showing that it does not uniformly reduce energy consumption across different buildings. Specifically, buildings that are not certified as green buildings prior to 2019 see a more considerable effect, suggesting that they have the potential to reduce their EUI by 19% if they acquire green mark award. This translates to a substantial reduction in electricity costs of approximately 36.4 million dollars, underscoring the economic benefits of energy-efficient practices.

In conclusion, our study's findings underscore the significant role of building energy benchmarking policies in fostering energy savings and reducing electricity costs. However, it also urges the need for a more nuanced understanding of building energy consumption and the impact of certification awards. While the green mark award has demonstrated positive results, we highlight the importance of continuous evaluation and refinement of these policies to maximize their effectiveness. These insights are valuable for policymakers striving to improve energy efficiency and sustainability in the built environment.

## 5. REFERENCES

- Abadie, A. and Imbens, G.W. (2011) 'Bias-Corrected Matching Estimators for Average Treatment Effects', *Journal of Business & Economic Statistics*, 29(1), pp. 1–11. Available at: <https://doi.org/10.1198/jbes.2009.07333>.
- BCA (2019) *Building and Construction Authority*. Available at: <http://www1.bca.gov.sg> (Accessed: 17 July 2023).
- BCA (2022) *BCA Building Energy Benchmarking Report 2022*. Building and Construction Authority. Available at: <https://www.bca.gov.sg/bess/benchmarkingreport/benchmarkingreport.aspx> (Accessed: 17 July 2023).
- Bouckaert, S. et al. (2021) *Net Zero by 2050: A Roadmap for the Global Energy Sector*. Available at: <https://trid.trb.org/view/1856381> (Accessed: 17 July 2023).
- Caliendo, M. and Kopeinig, S. (2008) 'Some practical guidance for the implementation of propensity score matching', *Journal of economic surveys*, 22(1), pp. 31–72.
- Hirano, K., Imbens, G.W. and Ridder, G. (2003) 'Efficient Estimation of Average Treatment Effects Using the Estimated Propensity Score', *Econometrica*, 71(4), pp. 1161–1189. Available at: <https://doi.org/10.1111/1468-0262.00442>.
- IEA, U. (2019) *Global Status Report for Buildings and Construction 2019*. UN Environment programme, p. 224.
- Jia, J. and Lee, W.L. (2018) 'The rising energy efficiency of office buildings in Hong Kong', *Energy and Buildings*, 166, pp. 296–304. Available at: <https://doi.org/10.1016/j.enbuild.2018.01.062>.
- Pearl, J. (2000) 'Models, reasoning and inference', *Cambridge, UK: CambridgeUniversityPress*, 19(2), p. 3.
- Zhao, Z. (2004) 'Using Matching to Estimate Treatment Effects: Data Requirements, Matching Metrics, and Monte Carlo Evidence', *The Review of Economics and Statistics*, 86(1), pp. 91–107. Available at: <https://doi.org/10.1162/003465304323023705>.

---

## #209: Effect of diffuser proximity to buildings on wind energy potential

---

Abdel Rahman ELBAKHEIT <sup>1</sup>

*1 King Saud University, College of Architecture and planning, Dept. of Architecture and building science, Riyadh, Saudi Arabia. P.O.Box 57448, Riyadh 11574, Abdel.elbakheit@hotmail.com*

*Abstract: Due to their promising augmentations of wind flows in a manner combating wind intermittency and turbulence, diffusers integration within the built environment is highly demanded. This paper investigated the effect of diffuser integration to a side of generic tall building. It examined diffuser's resulting velocities when varying diffuser's proximity to buildings. This proximity of diffusers provides one of the key factors affecting diffusers' performance within the Built environment. A generic diffuser is formed of an aerofoil profile following the NACA 1244 aerofoil. The diffuser is then subjected to an array of proximities to a generic tall building section ranging from 20cm-110cm. In addition to a range of velocities ranging from 1-16m/s. The paper concluded that optimum diffuser proximity to building is at 90cm from the building, which produced a resulting velocity of 29.8m/s with an increase of 86.6% over the resulting velocity in the same diffuser but as a stand-alone scenario. The study employed ANSYS FLUENT educational R1 CFD to model diffusers without incorporation of a turbine.*

*Keywords: wind energy augmentation; building integrated diffusers; wind energy optimization in buildings; diffuser optimization.*

## 1. INTRODUCTION

Building integrated wind turbines provides opportunities for obtaining valuable renewable energy within the built environment (Elbakheit A.R. 2021 pp 1-10). Thus, satisfying demand in a sustainable way and reducing CO<sub>2</sub> emissions simultaneously. Furthermore, reducing power transmission losses (Mahela, Khan et al. 2020 pp 2917-2925). The amalgamation of these efforts would hopefully reduce the production of CO<sub>2</sub>, slow global warming and climate change (Yoro and Daramola 2020 pp 3-28). However, many challenges are faced in this process (Juan, Wen et al. 2021) due to the variability of wind patterns and the low magnitude of wind speeds posed by the presence of buildings and other obstacles within the built environment. Shrouds, Diffusers and aerofoils (Elbakheit 2014 pp 417-437), (Elbakheit 2018 pp 365-371) are promising solutions within the built environment to solve wind variability and low wind speed. Therefore, the effect of low velocities and turbulence around buildings is reduced. Many researchers have provided theoretical and experimental studies on these diffusers or shrouds, their components (Nunes, Brasil Junior et al. 2020 pp 3-56), types (Agha 2018 pp 1370-1383), optimizations (Dighe, Avallone et al. 2019 pp 1655-1666) and underlying principles (Lilley and Rainbird 1956 pp 2-73). It is well known that these technologies have great potential of assisting various turbine technologies in achieving energy generation well beyond Betz Limit. (Betz 1966). However, this is true and valid for stand-alone diffusers. In this study a building integrated diffuser is investigated in an attempt to examine the effect of building presence on diffuser's performance. A series of diffuser's proximities to a side of a generic tall building are proposed and investigated using simulation tool Computational fluid dynamics (CFD).

## 2. PARAMETERS INTRODUCTION:

A free standing diffuser composed of a cross sectional profile made following the NACA 1244 aerofoil profile is simulated in two scenarios. First as a stand-alone entity and second at the side of a tall building to establish the effect of building proximity on expected wind acceleration within the diffuser. Figure 1 presents the diffuser cross section and dimensions.

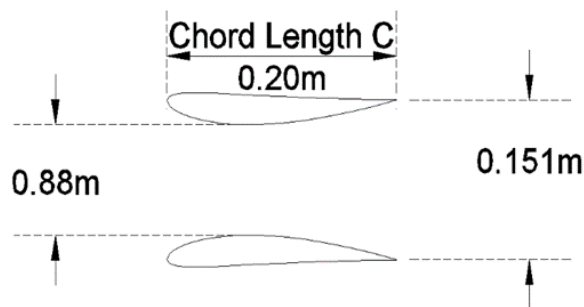


Figure 1 Diffuser cross sectional profile made of NACA 1244 profile.

## 3. SIMULATIONS

To simulate the diffuser in ANSYS FLUENT with plausible accuracy a domain of the size presented in figure 2 has been adopted. The domain size is built to be 12 times the chord length (i.e., distance C in Figure 1) before the diffuser from the front and sides and 24 times the cord in the leeside according to (Vinit et al. (al, 2019). Furthermore, domain grid is extra refined around the diffuser with 20 inflation layers to accurately describe the flow around the diffuser, as presented in figure 3.

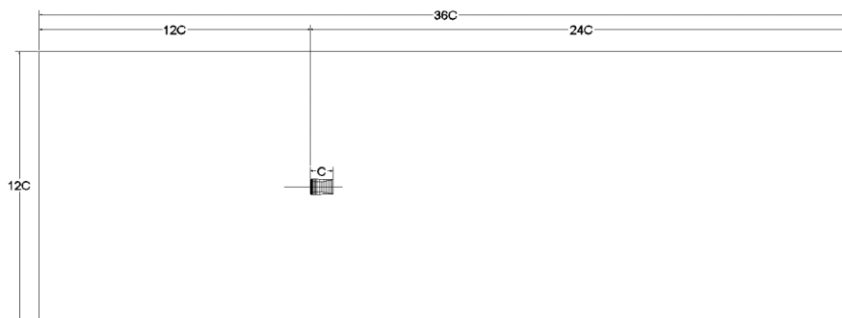


Figure 2 Domain size according to Vinit et al.

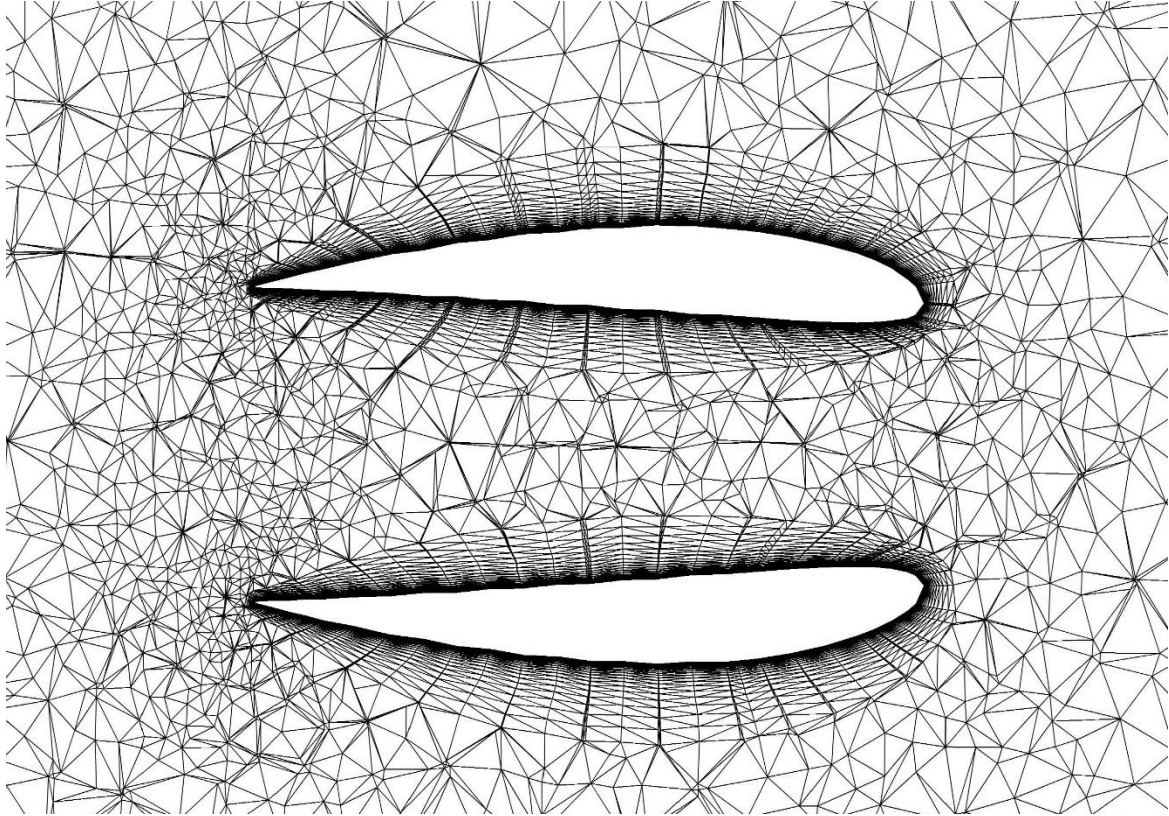


Figure 3 Inflation layers around the diffuser.

The other scenario of diffuser simulation is when fixing the diffuser to a side of a tall building. In this regard, diffuser's distance from the building is gradually increased to determine the optimum distance for higher diffuser resulting velocities. Here a generic block of a tall building of about 10 story high is proposed. The domain of simulation is increased to 10-times the height  $H$  of the tall building from the front and side and 20-times the height in the lee side figure 4, according to (Elbakheit, 2014 pp 417-437). Grid refinement is also introduced to areas around diffusers with 10 inflation layers figure 6, due to the distance between the diffuser and the building studied from as low as 20cm. Simulations parameters in CFD employed the Pressure- velocity coupling second order, coupled. Simulation is a Steady state, using turbulence model SST-K epsilon. The boundary layer conditions involved velocity inlet at the inlet and Pressure outlet. Convergence reached about 100-1000 iterations in majority of cases. The equation for turbulent kinetic energy  $k$  (Versteeg, 2007 pp 72-80)is:

$$\frac{\partial(\rho k)}{\partial t} \times \frac{\partial(\rho k \mu_i)}{\partial x_i} = \frac{\partial}{\partial x_i} \left[ \frac{\mu_t}{\sigma_k} \frac{\partial k}{\partial x_i} \right] + 2\mu_t E_{ij} E_{ij} - \rho \epsilon$$

for dissipation  $\epsilon$ (Versteeg, 2007) :

$$\frac{\partial(\rho \epsilon)}{\partial t} \times \frac{\partial(\rho \epsilon \mu_i)}{\partial x_i} = \frac{\partial}{\partial x_i} \left[ \frac{\mu_t}{\sigma_\epsilon} \frac{\partial \epsilon}{\partial x_i} \right] + C_{1\epsilon} \frac{\epsilon}{k} 2\mu_t E_{ij} E_{ij} - C_{2\epsilon} \frac{\epsilon^2}{k} \rho$$

where

$\mu_i$  is velocity in corresponding direction

$E_{ij}$  is rate of deformation

$\mu_t$  is eddy viscosity

$$\mu_t = \rho C_\mu \frac{k^2}{\epsilon}$$

Where,(Versteeg, 2007)

$C_\mu = 0.09$  ,  $\sigma_k = 1.00$  ,  $\sigma_\epsilon = 1.30$  ,  $C_{1\epsilon} = 1.44$  ,  $C_{2\epsilon} = 1.92$



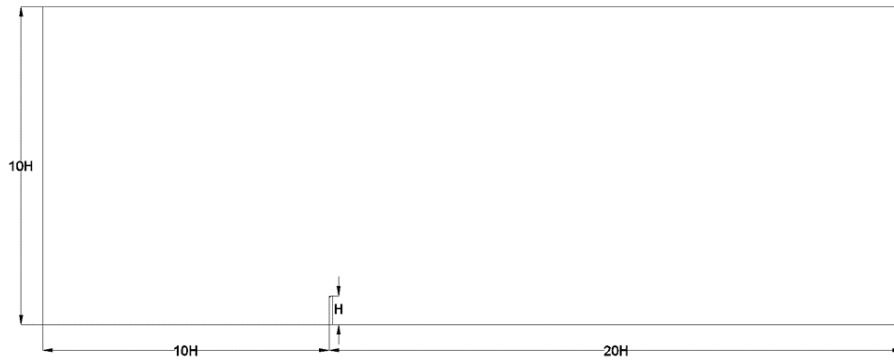


Figure 4 Longitudinal section to domain of diffuser proximity to building

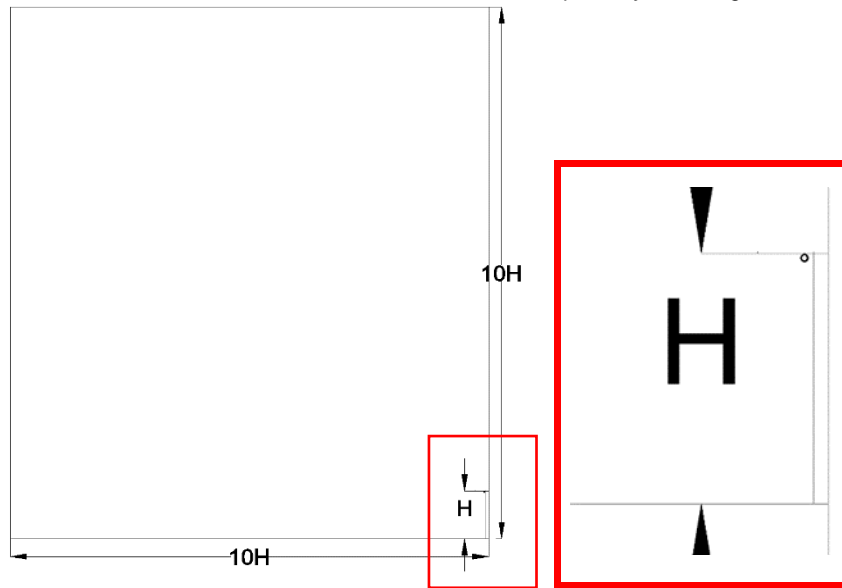


Figure 5 Side section to the domain of diffuser proximity to building and enlargement of diffuser at top of building

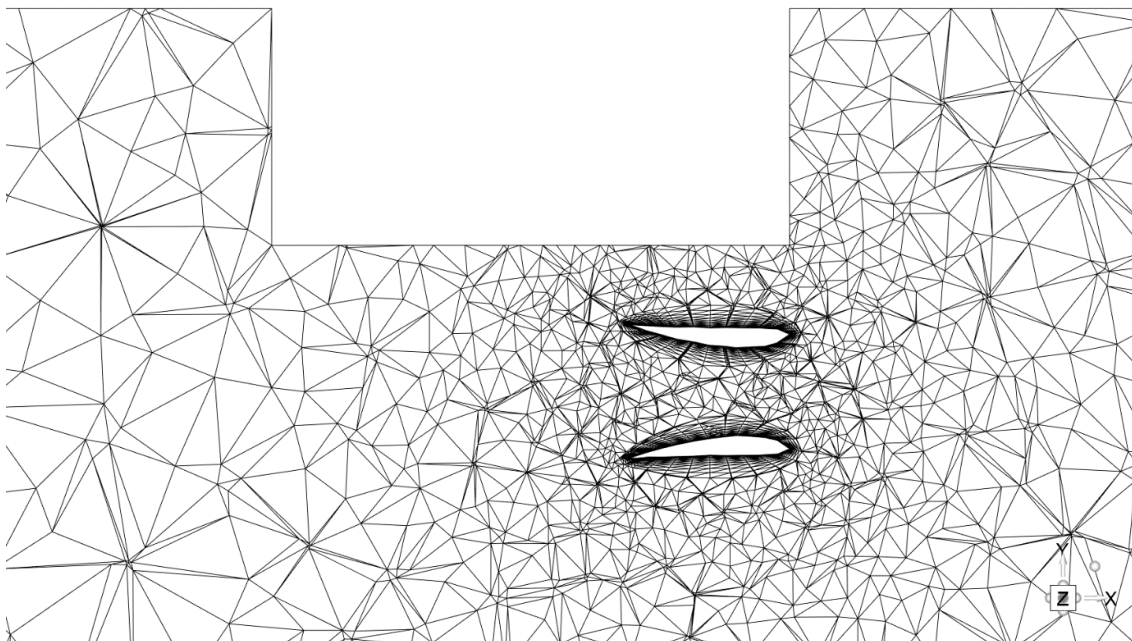


Figure 6 Inflation layers for diffuser with 90cm proximity to building.



#### 4. VALIDITY OF SIMULATION:

Validation to the simulation is accomplished by comparison to previously reported data. Igra's (Igra, 1977) experimental model (B) results were chosen due to similarity of their diffuser's design to the diffuser adopted in this study (i.e., without radial gaps, as depicted in Figure 1. The conditions of Igra's (Igra, 1977) experiment included an inlet velocity of 32 m/s that resulted in a thrust coefficient of 0.434. These conditions are employed to the constructed domain in Figures 2 and 3 to allow comparison to be made between this simulation and the published experiment as a validation to simulation.

In addition, an extra point to validate the simulation is to determine grid dependence of the results. A 3D domain grid is employed for its efficiency and accuracy. A number of three grids of varying sizes (i.e., small, medium and large number of cells) were used and their results are compared to Igra's experiment results to establish effect of grid size on results of simulation. The largest grid of cells just above 500,000 cells delivered most accurate results in the simulation with 0.444 for thrust coefficient. This matches results from Igra's experiment as table 1 shows.

Table 1: Grid study for validation of 3d model in ANSYS FLUENT

Grid	No. of cells	Force simulated Cp	Force experiment Cp
Coarse	153544	0.392	0.434
Medium	242885	0.415	0.434
Fine	502011	0.444	0.434

#### 5. RESULTS AND DISCUSSION:

Figure 7 below depicts the result of varying diffusers' proximity to building façade from 20cm to 110cm while subjecting each proximity position to a range of incident velocities from 1m/s-16m/s. It is evident from figure 7 that an increase in resulting velocities is observed through the entire resulting velocities with varying increase percentages. However, a diffuser proximity of 90cm has achieved the highest resulting velocities of 29.8m/s through the entire tested incident velocities. Therefore, this proximity distance is considered the optimum distance. When comparing this resulting velocity with the condition of a bare stand-alone diffuser position in figure 8 (right figure) , we can see that the latter achieved a resulting velocity of 25.8m/s. this gives the building integrated diffuser 86.6% increase in resulting velocity. Obviously, the increase is for the optimized case only.

When conducting a path-line plot of the flow around the building and through the diffuser as in figure 9 below for the optimum case with 90cm proximity as well as the flow patterns in table 2; it became clearer that the flow that deviated from the building was channeled through the diffuser. Therefore, the building became a source for extra-flow to the diffuser which resulted in further acceleration to the flow inside the diffuser. In addition, table 2, reveals that too close or too far proximity of diffuser to building will render the diffuser away from most of flow shed from the building. While proximity of 90cm would be the right position to capture most of the flow into the diffuser.

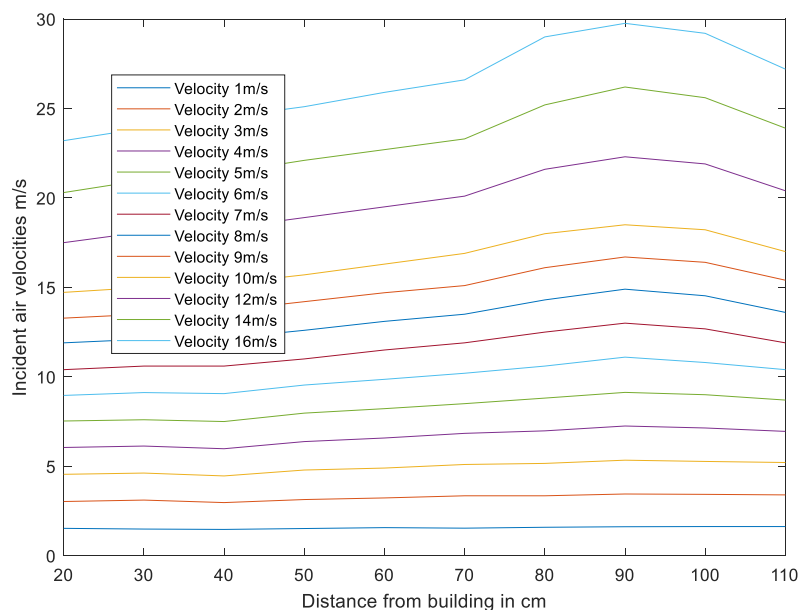


Figure 7 Resulting velocities from different diffuser's proximities to building

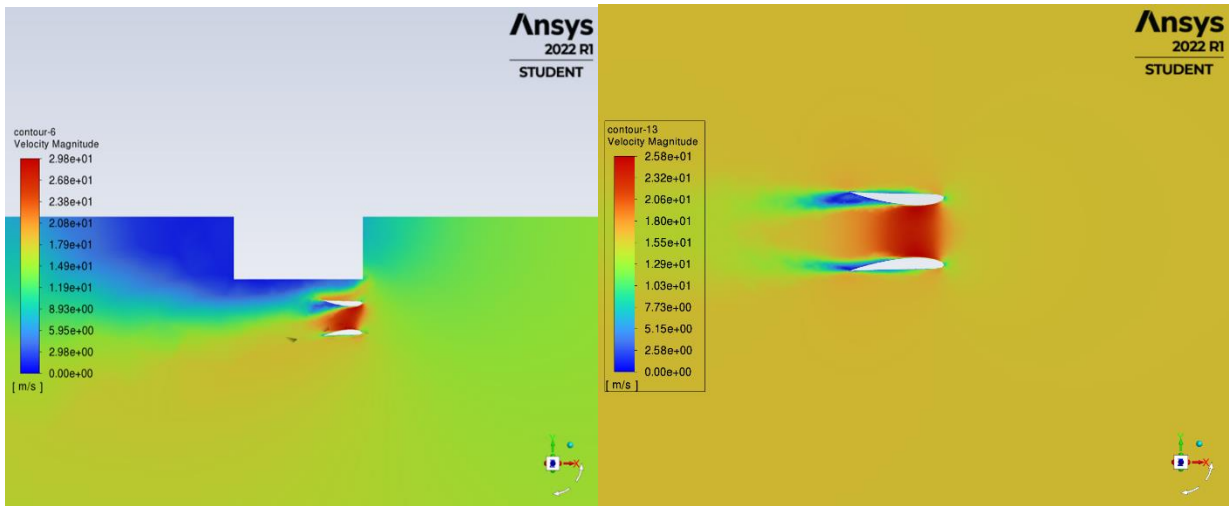


Figure 8 Comparison between resulting velocities from bare diffuser (right figure) and diffuser at 90cm proximity to building façade (left figure)

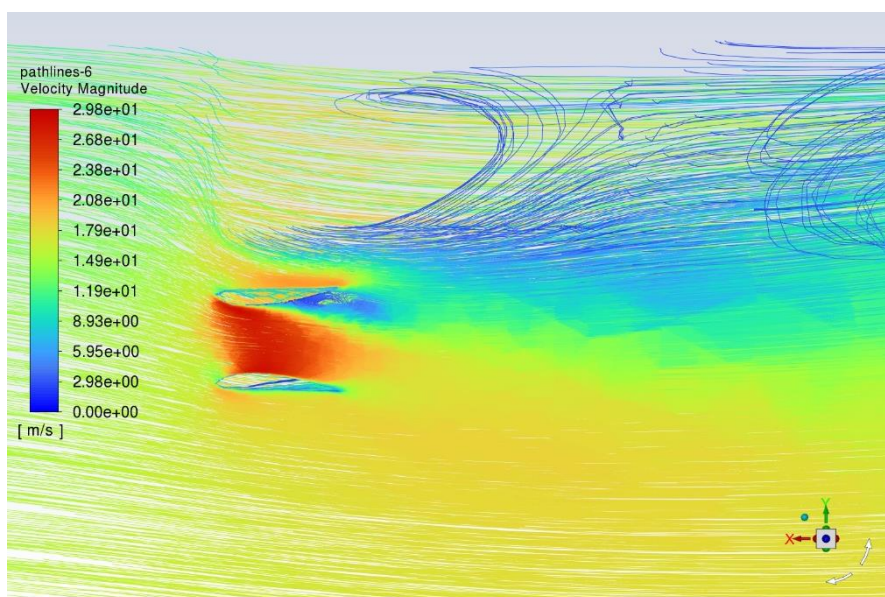
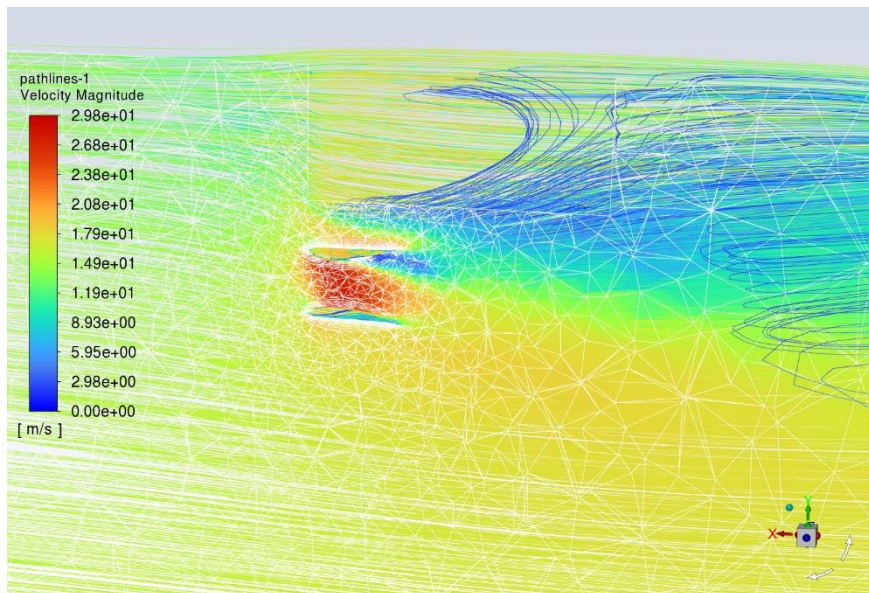
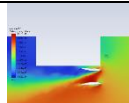
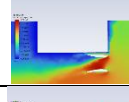
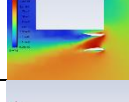
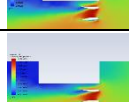
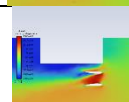
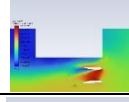
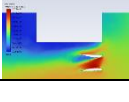
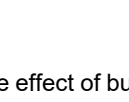


Figure 9: Path lines flow around the generic building and into diffuser with further acceleration.

Table 2: incremental velocity increase and flow patterns around building integrated diffuser.

Proximity to building	Resulting Velocity m/s for 16m/s	Incremental Increase %	CFD
20cm	23.2	-	
30cm	23.9	3	
40cm	24.5	2.5	
50cm	25.1	2.4	
60cm	25.9	3.2	
70cm	26.6	2.7	
80cm	29	9	
90cm	29.76	2.6	
100cm	29.2	-2	
110cm	27.2	-7	

## 6. CONCLUSIONS

Owing to the large successes of diffusers in augmenting wind flows. It is a logical step to investigate the effect of buildings' presence close to diffusers and their effect on diffusers' performance. Therefore, a generic diffuser design with NACA1244 cross section is employed with a generic block of a tall building to simulate this condition. A series of diffuser's proximities ranging from 20cm-110cm are studied by subjecting each to a range of incident velocities from 1-16m/s. The study concluded that optimum diffuser proximity to building is at 90cm from the building, which produced a resulting velocity of 29.8m/s with an increase of 86.6% over the resulting velocity in the same diffuser but as a stand-alone scenario. We can also conclude that incorporating diffusers within the built environment not only will help to reduce or eliminate wind turbulence and low wind velocities, but also through further optimization diffusers' performance could be enhanced.

Diffuser augmented wind flows provide a promising technology to harness wind energy within the built environment. It helps to eliminate the effect of turbulence and variability of wind flows within the built environment, which is a condition leading to an adverse decline in energy output from wind turbines.

## 7. REFERENCES

- Elbakheit A.R., (2021). Systematic Architectural Design for Optimal Wind Energy Generation. Bentham Science Publishers, Volume 5, DOI:10.2174/97816810885011210501.
- Agha, A. C., HN. Wang, F (2018). "Diffuser Augmented Wind Turbine (DAWT) Technologies: A Review." INTERNATIONAL JOURNAL OF RENEWABLE ENERGY RESEARCH 8(3): 1369-1385.

- al, V. V. D. e. (2019). "Multi-element ducts for ducted wind turbines: a numerical study." *Wind Energy Science*(4): 439–449.
- Betz, A. (1966). Introduction to the theory of flow machines, 1st Edition. Oxford; New York ,Pergamon Press. eBook ISBN: 9781483180908.
- Dighe, V. V., F. Avallone, O. Igra and G. van Bussel (2019). "Multi-element ducts for ducted wind turbines: a numerical study." *Wind Energ. Sci.* 4(3): 439-449.
- Elbakheit, A. R. (2014). "Factors enhancing aerofoil wings for wind energy harnessing in buildings." *Building Services Engineering Research & Technology* 35(4): 417-437.
- Elbakheit, A. R. (2018). "Effect of turbine resistance and positioning on performance of Aerofoil wing building augmented wind energy generation." *Energy and Buildings* 174: 365-371.
- Igra, O. (1977). "The shrouded aerogenerator." *Energy* 2(4): 429-439.
- Juan, Y. H., C. Y. Wen, W. Y. Chen and A. S. Yang (2021). "Numerical assessments of wind power potential and installation arrangements in realistic highly urbanized areas." *Renewable and Sustainable Energy Reviews* 135: 110165.
- Lilley, G. M. and W. J. Rainbird (1956). A preliminary report on the design and performance of ducted windmills. Cranfield (AGRAWAL), College of Aeronautics.
- Mahela, O., B. Khan, H. Haes Alhelou and P. Siano (2020). "Power Quality Assessment and Event Detection in Distribution System with Wind Energy Penetration Using S-transform and Fuzzy C-means Clustering." *IEEE Transactions on Industrial Informatics*.
- Nunes, M. M., A. C. P. Brasil Junior and T. F. Oliveira (2020). "Systematic review of diffuser-augmented horizontal-axis turbines." *Renewable and Sustainable Energy Reviews* 133: 110075.
- AGRAWAL, P. (1992). REVIEW OF PASSIVE SYSTEMS AND PASSIVE STRATEGIES FOR NATURAL HEATING AND COOLING OF BUILDINGS IN LIBYA. *International Journal of Energy Research*, 16(2), 101-117. doi:10.1002/er.4440160203
- al, V. V. D. e. (2019). Multi-element ducts for ducted wind turbines: a numerical study. *Wind Energy Science*(4), 439–449. doi:doi.org/10.5194/wes-4-439-2019
- Elbakheit, A. R. (2014). Factors enhancing aerofoil wings for wind energy harnessing in buildings. *Building Services Engineering Research & Technology*, 35(4), 417-437. doi:10.1177/0143624413509097
- Igra, O. (1977). The shrouded aerogenerator. *Energy*, 2(4), 429-439. doi:https://doi.org/10.1016/0360-5442(77)90006-8
- Versteeg, H. K. (2007). An introduction to computational fluid dynamics : the finite volume method. In W. Malalasekera (Ed.), (2nd ed. ed.). Harlow, England :: Pearson Education Ltd.
- Yoro, K. and M. O. Daramola (2020).,Chapter 1 - CO2 emission sources, greenhouse gases, and the global warming effect, *Advances in Carbon Capture*, Woodhead Publishing, Pages 3-28,ISBN 9780128196571,https://doi.org/10.1016/B978-0-12-819657-1.00001-3.

---

# #211: Analysis of suitability of national sustainability recommendations for thermal comfort in post-disaster social housing in Yucatan, Mexico

---

Yarely AGUILAR-PEREZ<sup>1</sup>, LUCELIA RODRIGUES<sup>2</sup>, Renata TUBELO<sup>2</sup> Paolo BECARELLI<sup>2</sup>

<sup>1</sup> Building, Energy and Environment Research Group, Faculty of Engineering, University of Nottingham, University Park, Nottingham NG7 2RD, UK

<sup>2</sup> Department of Architecture and Built Environment, Faculty of Engineering, University of Nottingham, University Park, Nottingham NG7 2RD, UK

*Abstract: This study focused on user s' thermal comfort in post disaster houses in Yucatan, México. FONDEN was the national fund in Mexico dedicated to reconstructing public infrastructure and social housing after disasters (World bank, 2012). An equivalent of eight hundred million American Dollars was invested yearly in reconstruction throughout Mexico. However, recent research has pointed out that the delivered poor thermal comfort, being one of the main causes of dissatisfaction in them (Carrasco et al., 2016) and in some cases led occupants to abandon or repurpose their houses (Castro del Río, 2009). The relevance of this study is that this house model has been mass produced to date in similar government-led housing programmes. This study aimed to assess the effectiveness of national recommendations for sustainability and thermal comfort in naturally ventilated buildings such as these social housing. This is relevant, given that economically restricted societies cannot rely on air conditioning systems to achieve comfortable environmental levels in their houses. The method utilised was a computer-aided simulation analysis using the Software IES Virtual Environment (2019). The strategies tested evaluated the national appropriate mitigation actions (NAMAs) for improving thermal comfort in the Mexican context. Results indicated that the common approaches for improvements including building insulation in naturally ventilated buildings might result in counterproductive effects. However, it has positive effects in energy demand reduction when considering the integration of air conditioning system. This study contributed to the scarce knowledge about thermal comfort in naturally ventilated buildings in Mexico.*

*Keywords: Thermal Comfort, Post-disaster Social Housing, IES-VE analysis*

## 1. INTRODUCTION

FONDEN was the national trust in Mexico which from 1996 to 2020 funded reconstruction of low-income housing and public infrastructure after disasters. In 2002, after Hurricane Isidore, 34 thousand homes were built in the disaster zones in Yucatan, Mexico (Castro del Rio, 2009: page 57), allocating approximately 100 thousand people according to the average household population reported by (CONEVAL, 2018). This reconstruction programme costed 8 thousand million USD to the FONDEN. However, previous studies have demonstrated the thermal comfort has not been achieved in these Government-led housing programmes in Mexico. In addition, beneficiaries' economic background restricts their access to active cooling mechanisms like air conditioning, making it critical to provide housing with enough control mechanisms for thermal comfort in their building envelope. The relevance of this study is that public recommendations for upgrading residential buildings for thermal comfort have questionable suitability for naturally ventilated buildings such as this type of housing. This is relevant considering that according to (INEGI,2018: page 29) only 12.4% of Mexico's population had air conditioning in their homes. The inability of inhabitants to customize their homes to their needs were one of the main causes of abandonment and repurpose (Castro del Rio, 2009: page 85). Discomfort in post-disaster social housing has been demonstrated to be the number one cause of dissatisfaction among beneficiaries at a global level (Carrasco et al., 2016).

The Mexican government has published guidelines for retrofitting and improve thermal comfort in residential dwellings, named the national appropriate mitigation actions (NAMAs). Previous studies in the Mexican context, including Davis et al. (2020) studied the energy efficiency of basic social-interest housing and compared them to similar NAMAs-approved houses. They reported no difference in thermal comfort or energy demand between similar houses from the same site, with a difference in wall insulation as an energy-efficiency upgrade. They were measured simultaneously throughout the days and months of the year. The reasons they found revealed that this was a consequence of leaving windows open throughout the day, nullifying the effect of the insulation outside. They also concluded that the energy-efficient upgrades proposed by NAMA CONAVI (2011) standards for sustainable housing are unlikely to pass a cost-benefit test (Davis et al., 2020).

The aim of this study was to analyse whether the public recommendations for thermal comfort are suitable for the housing typology in Yucatan. The impact of this research is to inform public stakeholders about the importance of assess the suitability of international strategies to the Mexican climatic context and the best strategies to retrofit and design future approaches to social housing or clarify in their policies that the suggested strategies are only suitable for mechanically ventilated buildings for future housing programmes.

The method for this research was computer-aided simulations considering NAMA's guidelines and analysed thermal comfort resulting from their implementation. The case study presented in this document analysed the model of the mass-produced homes in 2002 which followed a modern housing typology commonly built in near urban areas since 1960's when modernisation brought precast concrete beams and hollow concrete blocks and since has been inserted as the main building system in the zone (Perez and Rebollar, 2003).

### 1.1. Thermal Comfort

Thermal Comfort is defined by (ANSI/ASHRAE,2020: page 3) as "the condition of mind that expresses satisfaction with the thermal environment and is assessed by subjective evaluation" and proposes a method to determine the acceptable indoor operative temperatures  $t_o$  using the 80% of acceptability limits according to Equation 1 and Equation 2 based on ASHRAE (2020) [p. 20-21] and  $t_{pma(out)}$  according to Figure 1.

Equation 1

$$\text{Upper 80\% acceptable limit (}^\circ\text{C)} = 0.31 t_{pma(out)} + 21.3$$

Equation 2

$$\text{Lower 80\% acceptable limit (}^\circ\text{C)} = 0.31 t_{pma(out)} + 14.3$$

Where:

- $t_{pma(out)}$  is the prevailing mean outdoor temperature.

The local climate of the site (Figure 1) reveals a tendency of temperatures above thermal comfort acceptability according to ASHRAE index. The climate in this region is hot and humid.



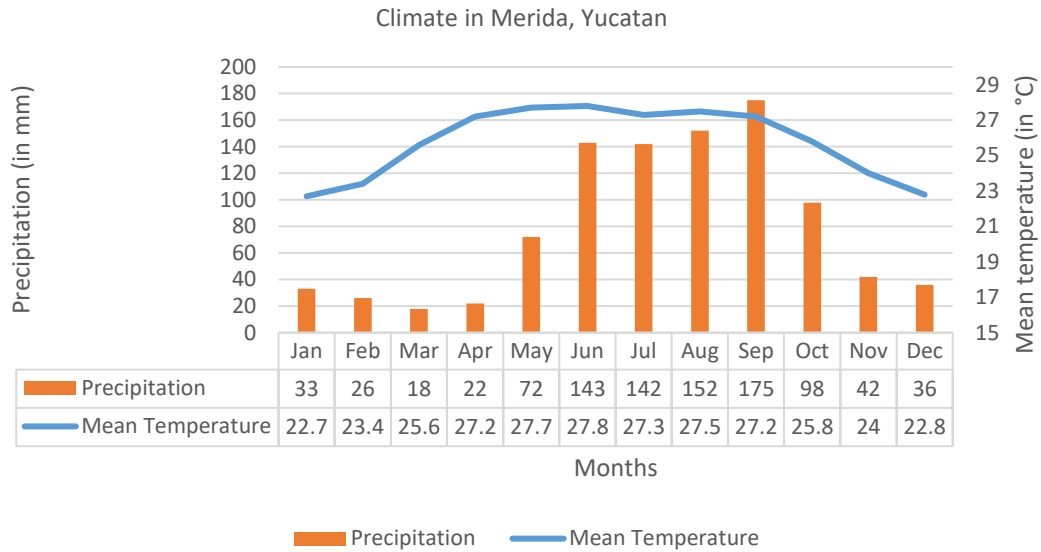


Figure 1 Climate in Merida, Yucatan.

The house model studied in this study was a roughly 25 m<sup>2</sup> detached house with flat roof (see Figure 2) which did not comply with the minimum requirements for habitable spaces according to the local construction manual for the state of Yucatan (Merida, 2004). Within the regulations that these houses did not comply was the window ratio of 5% minimum of glazing for natural lighting and 20% of wall area for natural ventilation.

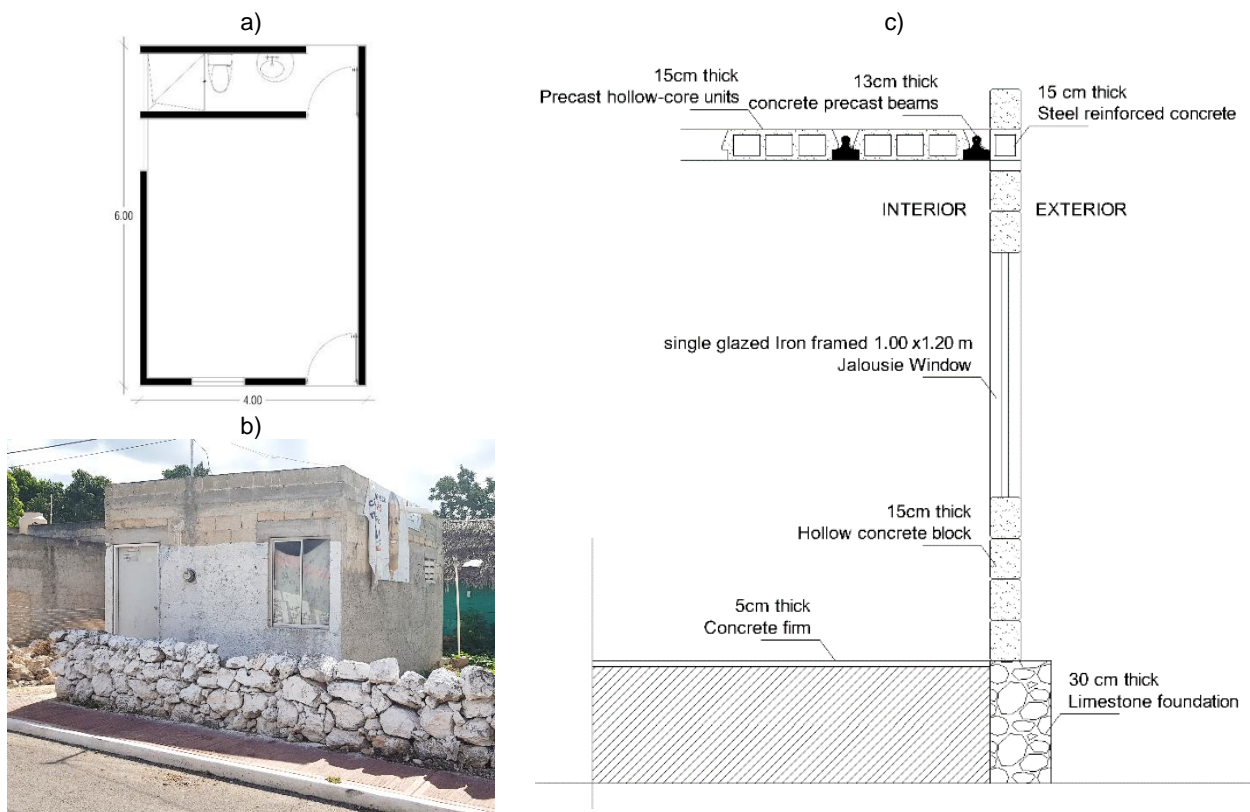


Figure 2 Description of the house a) Floorplan, b) Exterior façade, c) section.

## 1.2. Mexican Sustainability recommendations

According to CONAVI (2011), within the NAMAs actions in Mexico, they created the programmes “Hipoteca Verde” (Green Mortgage) and “Esta es tu casa” (This is your house). They are Mexico’s first programmes for more sustainable housing. They offer loans to cover extra costs derived from upgrading appliances to their more efficient version. Those are financed by the Federal Government and aim to enhance efficient use of water and energy. Within the requirements to access those

loans, are included the exclusive use of Light-Emitting Diode (LED) lights, water-saving taps, and solar water heaters, among other energy-efficient technologies.

Nationally appropriate mitigation actions (NAMAs) are the actions towards sustainable development that developing countries such as Mexico engaged in financially, technological and capacity-building support in a measurable, reportable and verifiable manner (Martínez et al., 2015: page 36). According to SEGOB (2014), in Mexico, NAMAs are actions in a pilot stage to reduce greenhouse gas emissions and enhance thermal comfort in the housing sector by making efficient designs and delivering efficient use of energy and other resources for the households. The NAMA recommendations (Martínez et al., 2015 pp.36) included three different levels of insulations: (i) Eco Casa 1, (ii) Eco Casa 2 and (iii) Eco Casa Max. The latter was based on the Passivhaus standard (Institute, 2017).

“Eco Casa 1”: Includes 25 mm of insulation to the roof and the south-facing external wall reflective paint and appliances like an efficient A/C unit and solar water heater.

“Eco Casa 2”: Involves the same features of “Eco casa 1” plus the insulation of all external walls and looks at window design.

“Eco Casa Max”: Look at the passive house certification criteria to reduce the energy demand based on passive strategies such as shading devices, extensive insulation ( $\leq 0.15 \text{ W/m}^2 \cdot \text{K}$ ) and airtightness ( $\leq 0.6$  air changes per hour @ 50 Pa) (McLeod, 2014 p.5)

Conduction occurs when two bodies with different temperatures are in direct contact, and the body with the highest temperature transfer energy to the body with the lowest temperature (Koeigsberger, 1973). Thermal conductivity is the characteristic of a material determined by the rate at which it conducts heat. The thermal transmittance or heat transfer coefficient (U-value) an is calculated as per Equation 3. The U-value is the coefficient on which insulation capacity is measured. A smaller number indicates that the heat transmissivity is slower.

Equation 3: Quantity of energy stored in water

$$Q_f = \sum UA (t_i - t_o)$$

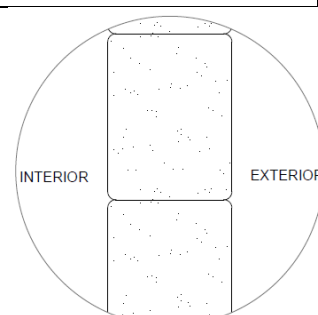
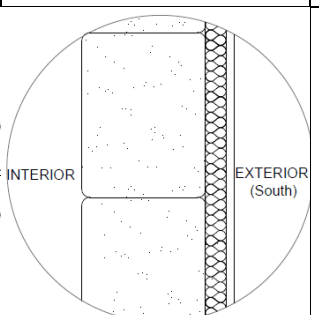
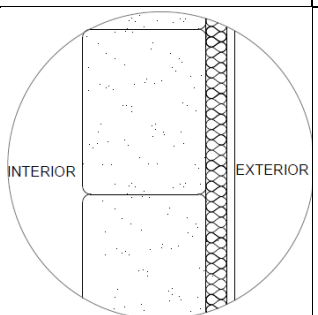
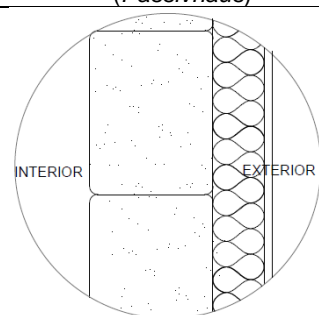
Where:

- $Q_f$  is the fabric heat flow for a wall
- A area ( $m^2$ )
- ( $t_i$ ) interior temperature ( $^{\circ}\text{C}$ )
- ( $t_o$ ) exterior temperature ( $^{\circ}\text{C}$ )

## 2. METHOD

The method used for this research was a computer aided simulation analysing the three proposed stages for envelope optimisation named Casa 1, Casa 2 and Casa 3 (McLeod, 2014: page 5). The envelope materials were analysed to evaluate the influence and potential improvement of thermal comfort delivered by potential insulation according to the national NAMA recommendations for sustainable housing. In Table 1 it is possible to see the construction material of the building envelope composed of 150 mm thick hollow concrete blocks in walls and roofs, with no plaster on the internal side of the walls or any render on the external side of the walls, without any insulation provided.

Table 1: Variations of Materials to the FONDEN house envelope. a) Original, b) Insulated roof (EcoCasa1), c) Insulated external walls (EcoCasa2), d) Eco Casa Max (Passivhaus standard).

a) Base Case	b) Eco Casa 1	c) Eco Casa2	d) Eco Casa Max (Passivhaus)
			



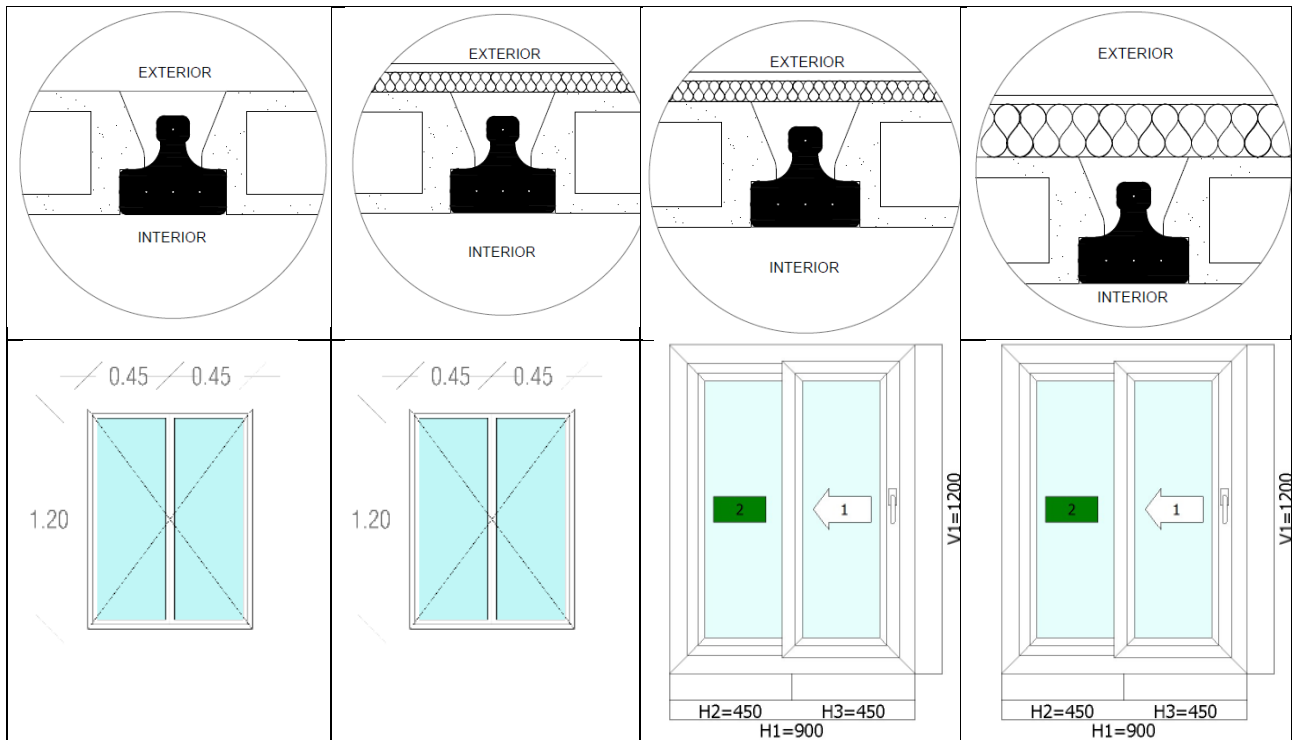


Table 2 summarises the U-value of the building fabrics element like Roof, External walls, South-facing external wall and windows that will be analysed to observe their impact on the thermal conditions indoors.

Table 2: U-values of each building element integrating the three alternative fabrics of the building.

	Base Case	Eco Casa 1	Eco Casa 2	Eco Casa Max
	W/m <sup>2</sup> ·K	W/m <sup>2</sup> ·K	W/m <sup>2</sup> ·K	W/m <sup>2</sup> ·K
Roof	1.88	0.49	0.49	≤0.15
External walls	1.06	0.44	0.44	≤0.15
South Façade	1.06	0.44	0.44	≤0.15
Windows	5.90	5.90	1.67	1.67

First, an extra layer of insulation available in the region was integrated into the roof construction materials following the specifications suggested by Eco Casa 1. Second, exterior walls were integrated with the same layer of insulation to compare the impact of insulating the walls against the insulation of the roof following the specifications of Eco Casa 2. Finally, airtightness and higher insulation were included in the external walls, roof, windows and doors to comply with the Eco Casa Max specifications. In all cases, the ventilation sources were considered off continuously throughout this set of simulations; only infiltration rates were considered in the model to observe the influence of the building fabrics clearly.

The results taken from IES-VE software were Dry-bulb temperature (°C) and Relative Humidity (%) to test thermal comfort and annual cooling Energy load (Kw) and heating energy load (Kw) for annual energy demand calculation assuming a potential integration of air conditioning and heating devices. The metrics used to evaluate the results were (i) percentage of time conditions were over, under and within thermal comfort thresholds, (ii) degree hours and (iii) energy demand.

#### Degree hours

Degree-hours is defined as the “hourly summation of temperature difference between a reference temperature and the temperature investigated, in which the reference temperature named as base temperature, is a reference thermal comfort limit temperature that does not need any heating or cooling systems in order to maintain comfort conditions” (CIBSE, 2006 P.23). This is considered an accurate method to calculate thermal comfort. The degree hours allow to evaluate not only how much time conditions were outside the comfort zone but also how far conditions were from its upper and lower thresholds. According to Li (2015) Cool Degree-hours (CDH) refer to the time when conditions are above the comfort threshold and Heating Degree-hours (HDH) refer to the time when conditions are below the comfort threshold. This metric delivered the number of hours when conditions were below and above comfort thresholds and is a suitable methodology for calculating the magnitude of the thermal discomfort in free-running buildings (Tubelo, 2016).

### 3. RESULTS

The Results from the parametric simulations considered the comfort criterion defined by Equation 1 and Equation 2. Figure 3 shows the level of comfort achieved by the base case. It is noticeable that the resulting conditions were mainly above thermal comfort from April to October, consistently above 70.6% of the time, reaching some comfort only from December to March, but never above 64.8%, even in the coldest months.

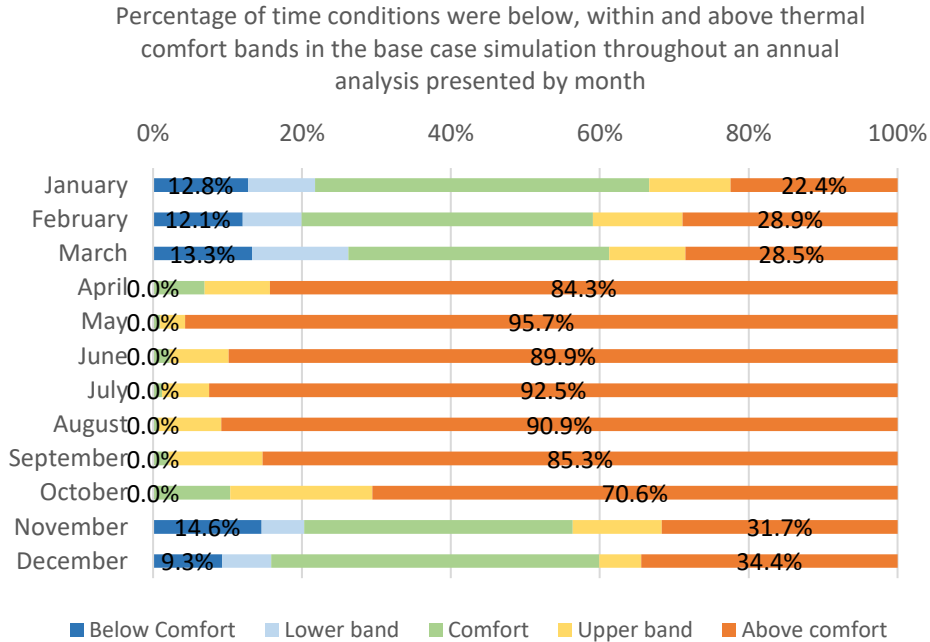


Figure 3 Percentage of time conditions were below, within and above thermal comfort bands in the base case (West orientation) simulation throughout an annual analysis presented by month

Figure 4 shows the impact of the recommendations suggested by Martínez et al. (2015) for a basic house envelope improvement Eco Casa 1 when comparing these results to the base case, it was possible to notice that overheating decreased in the coldest months (up to 4.8% in January), and overcooling decreased by 0.7% in February and November. However, in March, overcooling increased by 0.3% and overheating increased in the warmer months from March to October, with the highest impact found in September with an increase of 3.3%.

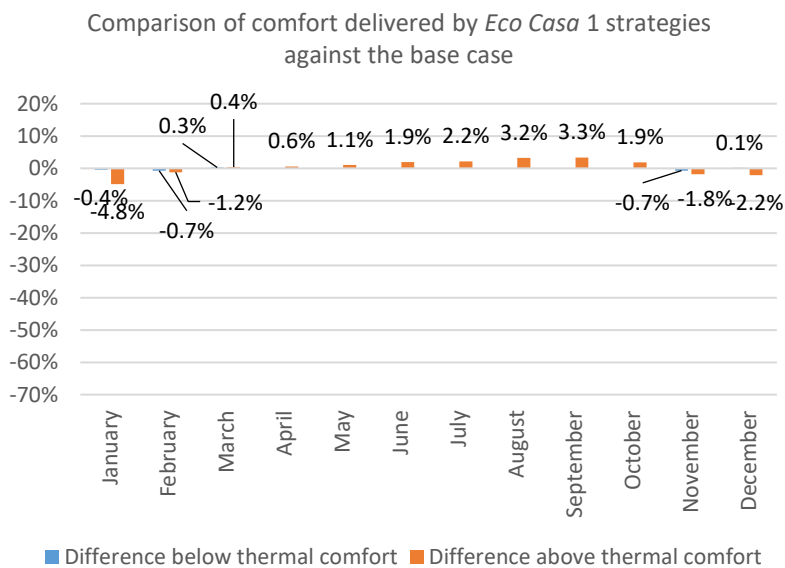


Figure 4 Comfort difference between the base case and building fabrics following Eco Casa 1 strategies

Figure 5 shows the impact of an intermediate envelope optimisation suggested by Martínez et al. (2015), named Eco Casa 2. It is possible to see that, compared to the base case, overheating was reduced up to 8.9% in the coldest months. However, in September, it increased by 11.9%. On the other hand, overcooling decreased 8.9% in February and increased by 1.1% in March.

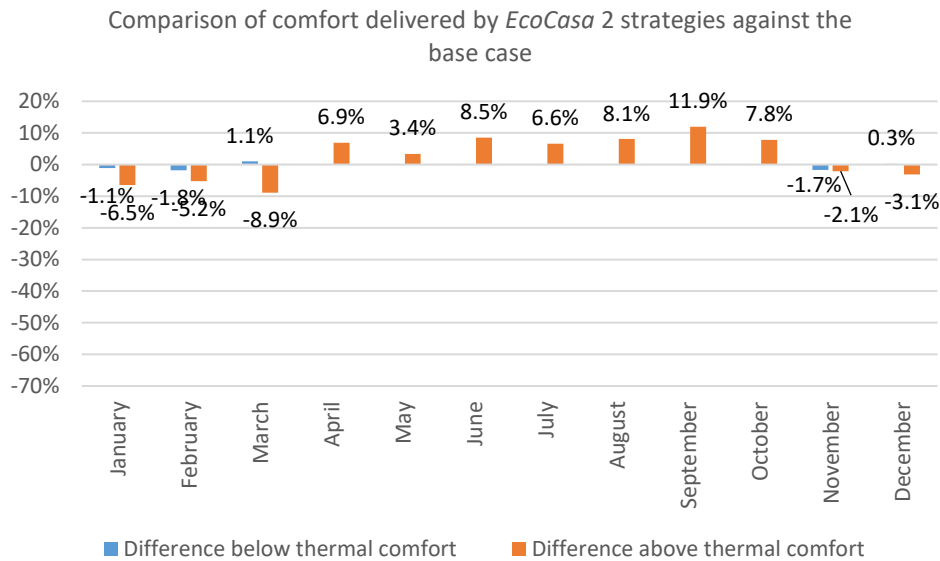


Figure 5 Comfort difference between the base case and building fabrics following Eco Casa 2 strategies.

Figure 6 shows the expected impact of the optimal insulation suggested by Martínez et al. (2015) named Eco Casa Max, which follows the Passivhaus standards. It was found a constant increase of overheating conditions up to 15.7% in October. However, during the coldest months, overheating decreased by 22.4%, keeping overcooling almost constant. The most contrasting variation was found in January at 3.2%.

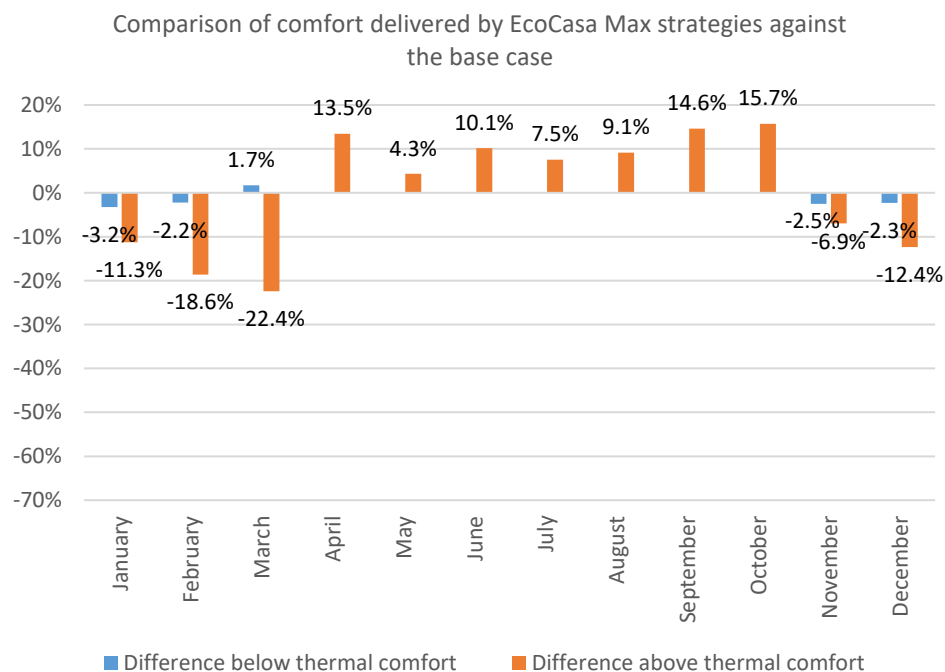


Figure 6 Comfort difference between the base case and building fabrics following Eco Casa Max strategies.

As it can be seen in Figure 7a) the Cooling Degree Hours decreased drastically in Eco Casa 1, in Eco Casa 2 they remained the same and in Eco Casa Max they even increased while Heating Degree hours remained the same across the three cases. Figure 7b) shows a constant reduction of annual energy demand required for cooling and heating across the three

cases. This reduction is positively correlated with the level of insulation. However, the energy demand related to cooling represented a greater impact to the energy demand for heating.

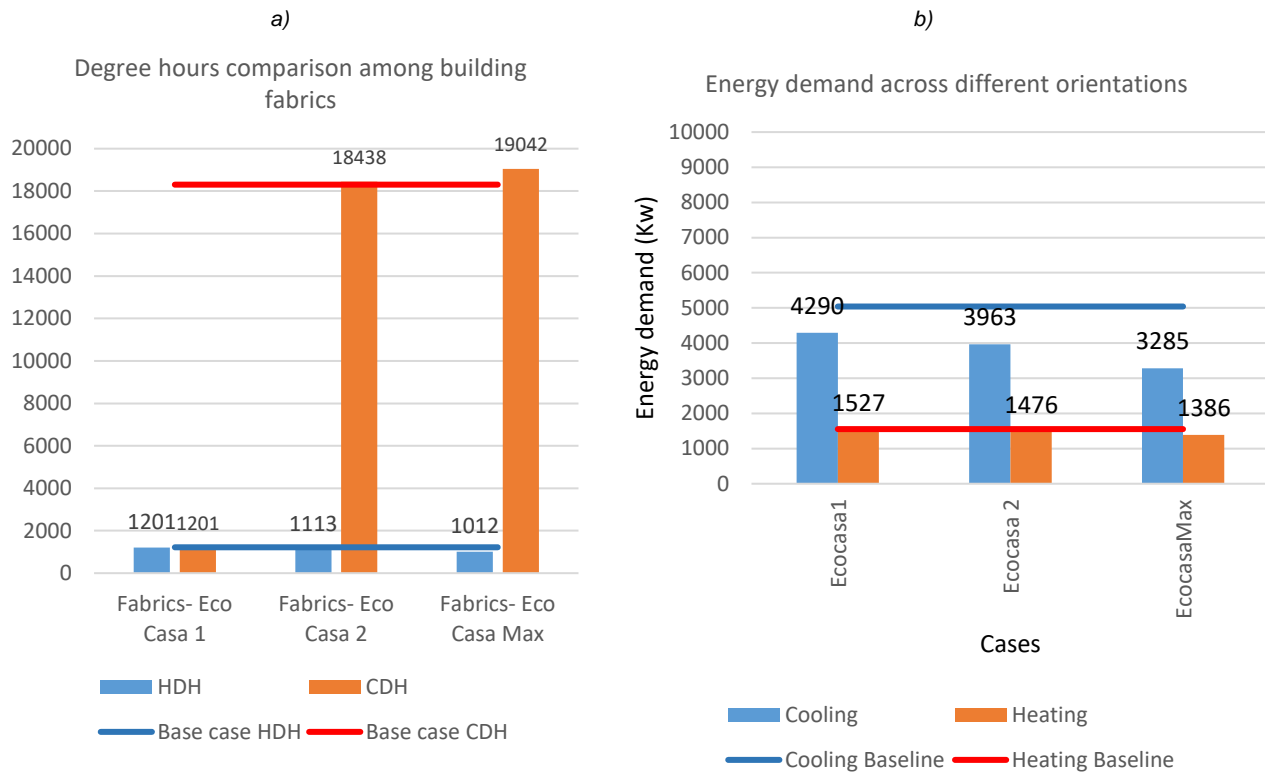


Figure 7 a) Degree hours comparison among building fabrics b) Energy demand across different cases

#### 4. CONCLUSION

The strategies suggested by NAMAs were found to be useful for reducing energy demand when assuming the integration of air conditioning or heating mechanisms (see Figure 7. b)). However, for naturally ventilated buildings they were counterproductive. It could be seen from Figure 3 to Figure 6 that the increasing U-value on the external walls had counterproductive effects on the thermal conditions inside the homes during the months with higher temperatures. However, in Figure 7. a) it was seen that insulation in one or two façades that received the higher heat gains alone could have a positive influence on the degree hours, meaning that temperatures were slightly over the comfort zone but not too far since they prevented heat gains from the most exposed facades and allowed heat loss from the less-exposed facades. The insulated envelope could be the source of this phenomenon, causing difficulties for heat loss in the building. Contrastingly, original FONDEN houses had walls with higher transmissivity allowing a more efficient heat loss. It can be assumed that some façades are the main surfaces for heat gain and others for heat loss. For that reason, it is important to identify which façades are convenient to insulate and which are not. Authors suggest that a cost-effectiveness analysis could complement this study with the aim of analysing which of the three levels of improvements could be convenient for the occupier to invest in.

#### 5. REFERENCES

ANSI/ASHRAE Standard 55-2020; Thermal Environmental Conditions for Human Occupancy. American Society of Heating, Refrigerating and Air Conditioning Engineers : Atlanta, United States of America, 2020.

ARNFIELD, A. J. 2020. Köppen climate classification [Online]. Encyclopedia Britannica. Available: <https://www.britannica.com/science/Koppen-climate-classification> [Accessed 13 May 2021].

Carrasco, S., Ochiai, C. & Okazaki, K. 2016. Residential satisfaction and housing modifications A study in disaster-induced resettlement sites in Cagayan de Oro, Philippines.

Castro del Río, J. 2009. El huracán "Isidoro" y la reconstrucción de la vivienda en Yucatán. Evaluación de las condiciones de habitabilidad en la zona rural, por la aplicación del Programa de Reconstrucción de Vivienda FONDEN

CONAVI, S. 2011. Supported NAMA for Sustainable Housing in Mexico-Mitigation Actions and Financing Packages. Mexico City.

- CONAVI. Reglas de Operación del Programa Nacional de Reconstrucción Para el Ejercicio Fiscal 2022; Gobierno de Mexico, 2022 Available at: <https://www.gob.mx/conavi/documentos/reglas-de-operacion-del-programa-nacional-de-reconstruccion-para-el-ejercicio-fiscal-2022?idiom=es> (Accessed 11 July 2023).
- CONEVAL. Informe de Pobreza y Evaluación 2020; Yucatan, Merida, Mexico: 2020. Available at: [https://www.coneval.org.mx/coordinacion/entidades/Paginas/Informes\\_Pobreza\\_Evaluacion\\_2020.aspx](https://www.coneval.org.mx/coordinacion/entidades/Paginas/Informes_Pobreza_Evaluacion_2020.aspx) (Accessed on 11 July 2023).
- CONEVAL. Pobreza 2018; Yucatan: Mexico City, Mexico, 2018 Available at: [https://www.coneval.org.mx/coordinacion/entidades/Yucatan/Paginas/Pobreza\\_2018.aspx](https://www.coneval.org.mx/coordinacion/entidades/Yucatan/Paginas/Pobreza_2018.aspx) (Accessed: 11 July 2023).
- Davis, L. W., Martinez, S. & Taboada, B. 2020. How effective is energy-efficient housing? Evidence from a field trial in Mexico. *Journal of Development Economics*, 143, 102390.
- INEGI 2018. PRIMERA ENCUESTA NACIONAL SOBRE CONSUMO DE ENERGÉTICOS EN VIVIENDAS PARTICULARES (ENCEVI)
- KOEIGSBERGER, O. 1973. *Manual of Tropical Housing and Building: Part One: Climatic Design*, Longman.
- LAC, U. Status of negotiations on NAMAs. 10-13 December 2013 2013 Mexico City.
- MARTÍNEZ, M. F. G., SCHMID, G. & GIZ, J. A. 2015. Deutsche Gesellschaft für Internationale Zusammenarbeit (GIZ) GmbH "Programa Mexicano-Alemán para NAMAs: mejores prácticas, impactos y perspectivas a futuro". Primera edición: Ciudad de México, noviembre 2015.
- MCLEOD, R. J., M.; CHEESEMAN, B.; TILFORD, A. ; MEAD, K. 2014. *Passivhaus primer: Airtightness Guide, Airtightness and air pressure testing in accordance with the Passivhaus Standard*. . BRE Trust.
- MERIDA, A. D. 2004. Reglamento de construcciones del municipio de Mérida. *Diario Oficial del Gobierno del Estado de Yucatán*, 14.
- PÉREZ, M. & REBOLLAR, S. 2003. Anatomía y usos de las hojas maduras de tres especies de Sabal (Arecaceae) de la Península de Yucatán, México. *Revista de biología tropical*, 51, 333-344.
- SEGOB 2014. Programa Nacional de Vivienda 2014-2018. In: FEDERACION, D. O. D. L. (ed.).
- Worldbank, T. 2012. FONDEN. Mexico's Natural Disaster Fund- A Review. In: DEVELOPMENT, T. I. B. F. R. A. (ed.). Washington DC.

---

## #213: Robotic composite filament winding technology for ultra-lightweight L7E class electric vehicles: enabling cost-effective zero emission urban mobility solutions

---

Assist. Prof. Dr. H. Ufuk GÖKÇE<sup>1</sup>, Assist. Prof. Dr –Ing. K. Umut GÖKÇE<sup>2</sup>

<sup>1</sup> EOS Sustainable Energy Solutions GmbH, Energie Effizienz Zentrum (EEZ) Bochum, Lothringer Allee 2, 44805 Bochum, Germany. E-mail: ufuk.gokce@eos-ses.de

<sup>2</sup> EOS Sustainable Energy Solutions GmbH, Energie Effizienz Zentrum (EEZ) Bochum, Lothringer Allee 2, 44805 Bochum, Germany. E-mail: umut.gokce@eos-ses.de

*Abstract: The pursuit of cost-effective electric vehicles (EVs) tailored for zero emission urban mobility solutions have gained significant momentum in recent years. The L7e class of EVs, specifically designed for urban transportation, presents a unique opportunity to address the challenges of polluted and congested city environments. However, the high costs of currently available EVs and lack of charging infrastructure remain significant barriers to their widespread adoption. This study explores the application of robotic composite filament winding technology with ISOGRID structure to develop an ultra-lightweight chassis for L7e class EVs, with the aim of achieving cost-effectiveness by reducing the weight, battery capacity and production costs of these advanced urban mobility solutions.*

*Composite filament winding offers a promising manufacturing method for producing structurally efficient and lightweight components. By combining high-strength fibres, such as carbon or glass, with a polymer resin matrix, composite materials can be engineered to exhibit superior mechanical properties while significantly reducing weight. Leveraging this technology for the construction of ultra-lightweight EV chassis in the L7e class vehicles can enhance energy efficiency, extend driving range, and contribute to cost reduction.*

*In this research which has been carried out within the frame of ZEUS (Zero Emissions Urban Mobility Solutions) R&D project led by authors, we investigate the design and manufacturing aspects of a robotic composite filament-wound ultra-light EV chassis for L7e class vehicles. Utilizing advanced computer-aided design and simulation tools, we optimize the composite layup configuration to meet stringent structural performance requirements while considering cost constraints. Extensive mechanical testing, including tensile, flexural, and impact evaluations, is performed to validate the performance and safety of the composite materials.*

*Additionally, we examine the feasibility of integrating composite filament-wound ultra-light EV chassis into L7e class vehicles from a manufacturing standpoint. Scalability, assembly processes, and the potential for mass production are evaluated, taking into account cost-effectiveness and efficient integration within existing production lines. The environmental impact and cost analysis encompass various factors, such as raw material selection, energy consumption, and waste management, to ensure sustainability in the manufacturing process.*

*Keywords: Robotic composite filament winding technology, ultra-lightweight EV chassis, L7e class electric vehicle, Polymer Exchange Membrane (PEM) Fuel-Cell Technology, Switched Reluctance Motor (SRM).*

## 1. INTRODUCTION

Since the beginning of the Industrial Revolution, the global annual mean CO<sub>2</sub> concentration has witnessed a 50% rise, soaring from 280 ppm to 420 ppm as of April 2021. This current concentration level represents the highest value observed in the past 14 million years. The escalation can be attributed to human activities, primarily the burning of fossil fuels and deforestation. Based on the assumption of a continued growth rate in energy consumption, it is projected that the CO<sub>2</sub> concentration will reach 550 ppm by 2050 (NOAA 2022).

For decades, the internal combustion engine (ICE) has been the dominant powertrain in the automotive industry. Globally, liquid fuels like petroleum have accounted for over 90% of transportation energy in 2020. Among various modes of personal mobility, light-duty vehicles have contributed to 44% of total transportation energy consumption. With increasing concerns about climate change and evolving needs and perceptions, the industry has started diversifying its powertrain portfolio (U.S. EIA 2016).

Within the European Union, the limit for CO<sub>2</sub> emissions from cars introduced to the market in 2020 was set at 95 g CO<sub>2</sub>/km, averaged across the brand's fleet sold within a year (EEA 2021). Studies on hybrid electric and electric vehicles with the lowest CO<sub>2</sub> emissions have gained momentum, and the transition to mass production is ongoing. Considering the current and anticipated issues related to petroleum and its derivatives, import dependency, carbon dioxide emissions from fossil fuels, and the constraints imposed by the Kyoto Convention on emissions, hydrogen is being considered as a readily available and unlimited alternative.

Germany's national climate change strategy, outlined in the Climate Action Plan 2050 and part of the "Energiewende (Energy Transition)" strategy, follows a similar approach. It sets long-term goals for sector-specific emissions reduction, including a shift from ICE to electric mobility. The key objectives compared to the base year of 1990 are to achieve a minimum 40% reduction in greenhouse gas (GHG) emissions by 2020, 55% by 2030, 70% by 2040, and 80-95% by 2050, with the aim of becoming predominantly GHG-neutral by then (BMU 2016).

Despite progress in reducing overall emissions, Germany has fallen short of its 2020 target of a 40% reduction. Even with a rapid increase in renewable electricity generation, total emissions in Germany have not experienced the expected decrease. As of 2018, Germany had only reduced its total GHG emissions by approximately 31% compared to 1990.

The growing momentum behind electric vehicle adoption, both from consumers and the automotive industry, indicates that electrified powertrains will play a crucial role in Europe's future mobility. However, the inadequate infrastructure of the electricity grid to accommodate the increasing number of electric vehicles has led to the consideration of using hydrogen fuel cell technology as a range extender, which is deemed a viable solution. In 2018, global hydrogen production reached 60 million metric tons, a figure projected to significantly rise to around 300 million metric tons by 2030. The current annual production is sufficient for 250 million fuel cell vehicles, and the annual growth rate stands at approximately 3.5%. The worldwide economic value of hydrogen production in one year amounts to 135 billion USD, with the economic size of fuel cell production alone expected to reach 180 billion USD by 2050. Hydrogen, as a synthetic energy carrier, has the highest energy content per unit weight (120,000 kJ/kg) among all known fuels. When liquefied, it occupies only 1/700th of its gaseous volume (IEA 2019).

Composite filament winding presents a compelling manufacturing approach to fabricate structurally optimized and lightweight components. Through the amalgamation of high-strength fibres, such as carbon or glass, with a polymer resin matrix, composite materials can be tailored to demonstrate exceptional mechanical characteristics while substantially minimizing mass. Utilizing this technique in the fabrication of ultra-light electric vehicle (EV) chassis for L7e class vehicles has the potential to augment energy efficiency, extend the driving range, and contribute to cost reduction.

This study focuses on researching, developing, and integrating a universal L7e class urban electric vehicle platform that incorporates robotic ISOGRID composite filament winding technology, methanol polymer exchange membrane fuel cell range extender technology, low-speed autonomous drive technology, and SRM (Switched Reluctance Motor) technologies. The ultimate aim is to create an innovative, cost-effective zero emission urban mobility solution. Described technologies and concepts are developed within the frame of EOS Sustainable Energy Solutions GmbH Company's ZEUS (Zero Emission Urban Solutions) R&D project that is led by authors with project partners, M. S. Pedersen and Roadrazer ApS.

The findings of this study demonstrate the potential of robotic ISOGRID composite filament winding for developing ultra-lightweight EV chassis in L7e class vehicles, paving the way for cost-effective and sustainable urban mobility solutions. The lightweight characteristics of composite materials contribute to increased energy efficiency, extended driving range, and reduced battery requirements. Furthermore, the manufacturing scalability and integration feasibility highlight the viability of this technology for large-scale production, facilitating the transition towards affordable and environmentally friendly urban transportation systems.

## 2. L7E CLASS ELECTRIC VEHICLE CONCEPT

A vehicle category serves as a regulatory classification for land vehicles or trailers. Within the European Union, the quadricycle category has been established for four-wheeled microcars, allowing these vehicles to adhere to less stringent requirements compared to standard cars. Quadricycles are defined based on limitations related to weight, engine power, and speed.

There exist two distinct categories of quadricycles: light quadricycles (L6e) and heavy quadricycles (L7e). The primary goal of the ZEUS project is to develop three separate urban electric vehicle (EV) segments within the L7e class, all of which will share a common platform and utilize similar technologies.

As per Framework Directive 2002/24/EC, heavy quadricycles (L7e), also known as heavy quadricycles, are characterized as motor vehicles with four wheels, distinct from light quadricycles. These vehicles have an unladen mass not exceeding 450 kg (600 kg for goods-carrying vehicles), excluding the weight of batteries in the case of electric vehicles. Additionally, they retain a design payload of no more than 200 kg for passenger vehicles or 1000 kg for goods vehicles, and their maximum net engine power does not exceed 15 kW. Such vehicles are considered motor tricycles and are required to meet the technical specifications applicable to motor tricycles of category L5e unless otherwise specified in individual directives.

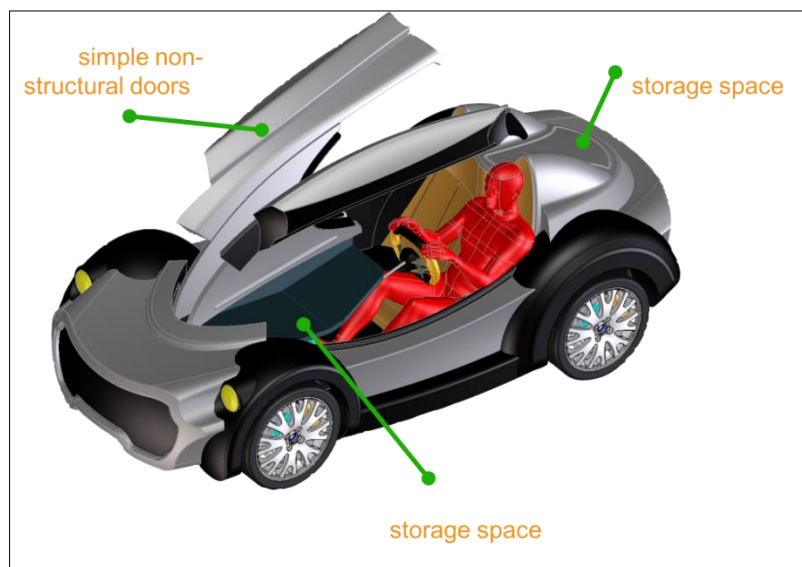


Figure 1 EOS ZEUS L7e Class Urban Passenger Electric Vehicle Concept (Gökçe 2022)

As part of the EOS Sustainable Energy Solutions GmbH company's ZEUS (Zero Emission Urban Solutions) project focused on electric vehicle (EV) development, a series of three distinct fuel-cell electric vehicles within the L7e class have been designed and developed in collaboration with project partners. These vehicles share a universal platform and are equipped with a SRM drive train, an off-the-shelf Panasonic lithium-ion battery pack, and Serenergy H3 5000 methanol-based PEM fuel-cell modules.

The developed L7e class passenger vehicle concept, illustrated in Figure 1, features a range of 1000 km with a methanol fuel-cell range extender. The specifications for this concept are as follows (Gökçe 2022):

- Dimensions: Length of 275 cm, Width of 175 cm, Height of 155 cm
- Weight: 680 kg, inclusive of the battery bank and fuel-cell modules
- Space: Accommodates three seats or can be configured with one seat and additional storage capacity
- Doors: 120 cm wide, positioned on both sides
- Drive Characteristics: Includes regenerative braking functionality and offers a turning radius of 5 meters

These design and technical details exemplify the advancements made in the development of the L7e class fuel-cell electric vehicles as part of the ZEUS project.

## 3. ULTRA-LIGHT ISOGRID STRUCTURE BY ROBOTIC COMPOSITE FILAMENT WINDING

Composite materials are made by combining two or more fundamental materials with dissimilar physical/chemical properties, resulting in a material that unveils unique characteristics do not originate in the individual components. These materials offer advantages such as increased strength, reduced weight, and cost-effectiveness compared to traditional materials. These find widespread application in various sectors including automotive, marine, and aerospace applications.



In aerospace applications, composite materials are extensively utilized in spacecraft and aircraft due to their superior performance (Frulloni et. al. 2007).

Fabrication methods for composite products vary, and the choice of method depends on design requirements and manufacturing challenges. Among these methods, filament winding has gained prominence in recent years (Gortner 2019). Filament winding is a cost-effective manufacturing process utilized for producing composite shapes, whether closed or open-ended. Originating as one of the earliest composite manufacturing techniques, filament winding gained prominence post-World War II for fabricating solid rocket motor cases. Its commercial adoption expanded during the 1960s and '70s, with the introduction of winding machines to create fibre-reinforced pipes, pressure vessels, and streetlight poles (Gardiner 2018).

It is a continuous production technique that enables high levels of automation, repeatability, and relatively low costs compared to hand lay-up methods. Filament winding excels in producing structures with exceptional stiffness-to-weight ratio, high fibre volume fraction, and impressive strength-to-weight characteristics, particularly in applications like pressure vessels and rocket motor cases. The application of filament winding technique not only enhances the usage of filament wound composite products but also drives advancements in filament winding machinery.

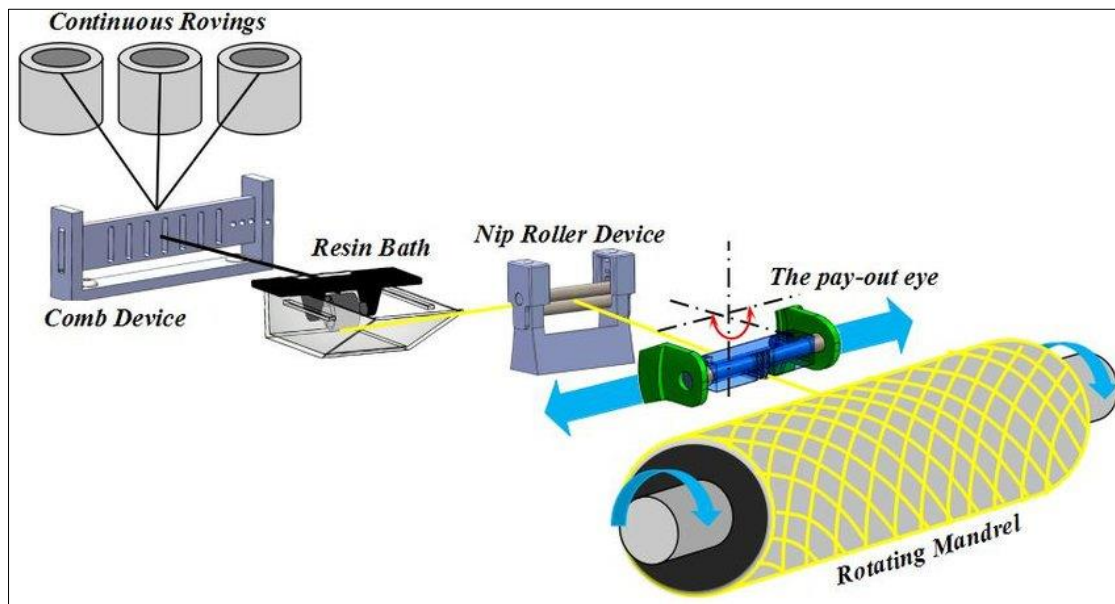


Figure 2 Schematic diagram of filament winding technique (Ma et. al. 2019)

Filament winding process entails the application of tensioned filaments onto a rotating mandrel as illustrated in figure 2. The mandrel revolves around the spindle (Axis 1 or X: Spindle), while a carriage with a delivery eye moves horizontally (Axis 2 or Y: Horizontal) along the mandrel's rotational axis, depositing the fibres in the desired pattern or angle. Commonly used filaments include glass or carbon, which are impregnated with resin as they are wound onto the mandrel by passing through a resin bath. After achieving the desired thickness, the resin is cured. Depending on the resin system and its curing characteristics, the mandrel may undergo autoclaving, heating in an oven, or rotation under radiant heaters until the part is fully cured. Once the resin has cured, the mandrel is extracted or removed, leaving behind the final product with a hollow interior. In certain cases, such as gas bottles, the 'mandrel' becomes a permanent component of the finished product, serving as a liner to prevent gas leakage or as a protective barrier for the composite material.

In order to maximize range and minimise battery size, electric vehicles require light and robust structures. This objective can be accomplished by developing ISOGRID structures made of composite material. In fact, such structures present both lightness and structural resistance. However, some problems can arise during the manufacturing process of these structures. In the ZEUS EV development project, the RFW (Robotic Filament Winding) technology is used for manufacturing an ISOGRID cylinder, made of composite material.

### 3.1 ISOGRID Structure for the ZEUS Chassis

In this section, we present a concise overview of the structural and manufacturing process design of ISOGRID structure for the vehicle chassis designed in the scope of the ZEUS project. The conceptual representation of the designed structure is depicted in figure 3. The primary objective was the creation of a cylindrical configuration characterized by a height of 800 mm and a diameter of 400 mm, engineered to withstand an axial compression load of no less than 75 kN. The Vasiliev method, as outlined in (Regi et. al. 2004), was employed to design the rib section, while finite element method (FEM) software was utilized to define the material composition and thickness of the skin. The choice for constructing the isogrid lattice fell upon carbon/epoxy composites due to their lightweight and high-strength properties. A MATLAB computational procedure was implemented to ascertain the structural dimensions.

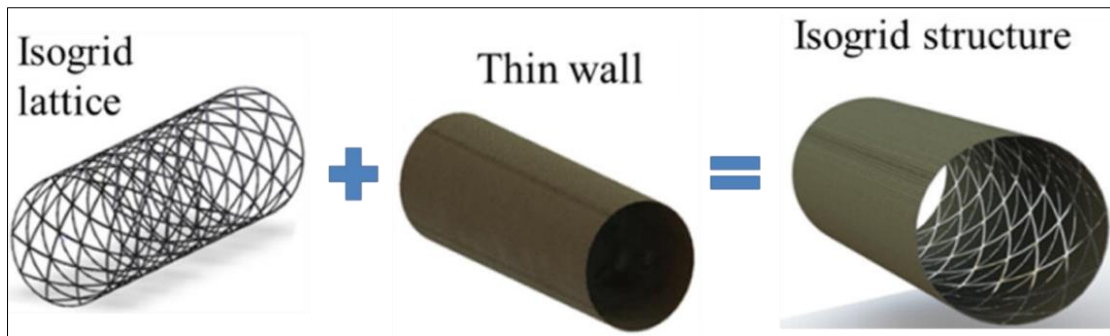


Figure 3 Conceptual Design of ISOGRID Structure (figure is modified from (Sorrentino et. al. 2017))

Based on the aforementioned data, the rib width and thickness were determined to be 6 mm and 3 mm, respectively, with an inter-rib spacing of 85 mm. To fabricate the ISOGRID lattice, it necessitated the application of 15 layers of 5 mm wide carbon/epoxy split tape.

The selection of the skin material was made among three options: carbon/epoxy, providing a homogeneous structure; glass/epoxy, offering cost-effectiveness; and kevlar, characterized by superior mechanical properties. A quarter-section of the cylinder was modelled in 3D using Ansys software. Boundary conditions involved a fixed support along one-quarter of the cylinder's length and a uniform load of 500 N applied across the entire skin surface. Numerical analysis outcomes were assessed according to the maximum stress criteria. The analysis was conducted employing the Margin of Safety (MoS), conventionally defined as the ratio of allowable loads to actual loads multiplied by the applicable Safety Factor.

FEM analysis results depict that, the central rib emerged as the region subject to the highest stress, and deformations occurred primarily out of the plane. Furthermore, all the considered materials exhibited robust strength characteristics, with all MoS values significantly exceeding unity. However, carbon/epoxy was ultimately selected due to its lighter weight and the assurance of uniform thermal and electrical behaviour within the structure.

An additional finite element analysis (FEM) simulation was conducted to determine the optimal skin thickness. In this instance, the entire cylinder was subjected to meshing, incorporating three distinct skin thickness values ranging from 1 mm to 2 mm. The boundary conditions entailed immobilization on one side while imposing a compressive axial load of 75 kN on the opposite side.

The examination of the FEM results revealed that a skin thickness of 2 mm should be selected, as it yielded consistently positive Margin of Safety (MoS) values. This specific thickness could be achieved by stacking four layers of prepreg material composed of epoxy resin and carbon balanced fabric.

Furthermore, it became evident from the FEM analysis that the region of the skin near the point of load application was subjected to the highest levels of stress. Figure 4 depicts the universal EOS ZEUS Chassis designed in the scope of ZEUS R&D project.

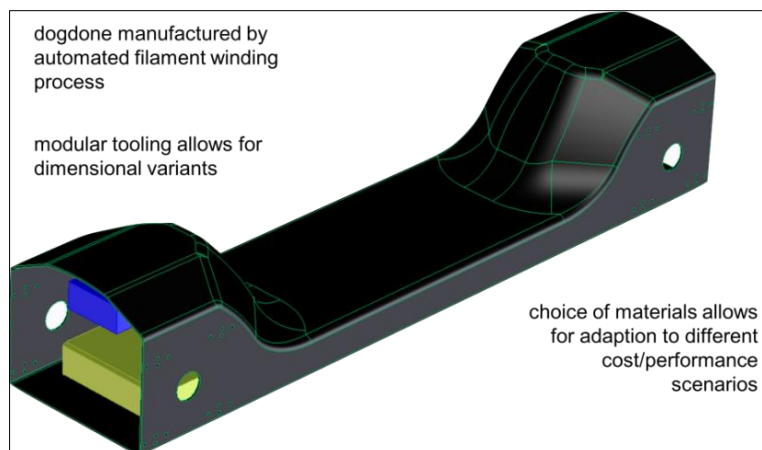


Figure 4 Universal EOS ZEUS Chassis (Gökçe 2022)

### 3.2 Robotic Filament Winding System for the ZEUS Chassis

The manual stratification method poses evident challenges, particularly concerning the stringent requirements of industrial production, where precision and repeatability of operations cannot be reliably maintained. Even with experienced operators, achieving layer consistency with the previous one is highly unlikely. Additionally, manual stratification lacks the capability to control tape tension within the desired range of 50–75 N. To address these issues, this study focuses on an automated layering process.

The automated deposition of fibres into the mould grooves for the ribs was accomplished using the RFW technology. This technique involves depositing fibre bundles along predefined trajectories with the assistance of a specialized end effector mounted on an industrial robot. To facilitate this process, a robotic cell was assembled, comprising an anthropomorphic robot equipped with an integrated deposition system and a positioner to hold the mould for the ISOGRID structure.

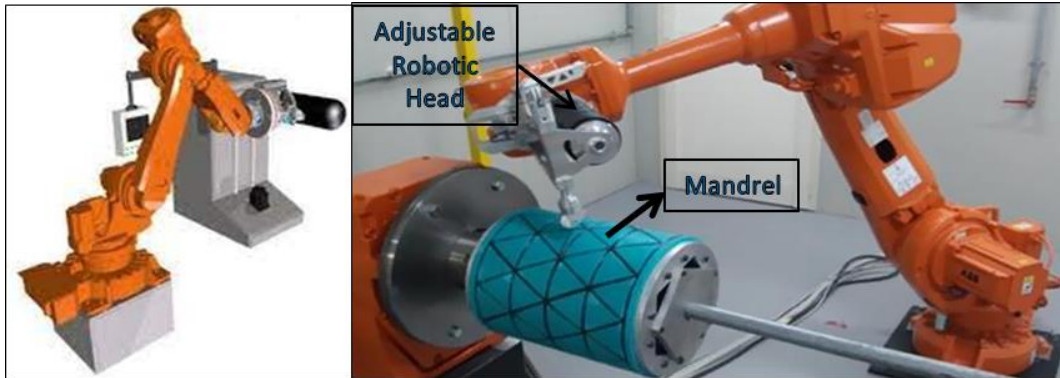


Figure 5 Robotic Filament Winding Application (figure modified from (Arrabiyeh et. al. 2021))

The deposition integrated RFW system, illustrated in Figure 5, exhibited a modular design comprising four crucial subcomponents or modules: the main frame, the tape-guide system, the winding tensioning system, and the deposition system. Mounting the deposition integrated system on the robot's end effector was critical to prevent tape torsion and ensure precise fibre placement on the mould, as well as to maintain the appropriate tape tension. Failure to execute these tasks correctly would result in defects that could compromise the reliability and strength of the produced parts. Furthermore, it is essential to keep both the overall dimensions and weight of the deposition system in check, as reducing these characteristics minimizes the inaccuracies (related to moments and inertias) that may arise during robot movement. The deposition system itself comprised various components, including the supporting base structure, the front pulley supports with roving locking flanges, the roving unwinding system, and the coil support group.

#### 4. RESULTS of ISOGRID STRUCTURE and RFW TECHNOLOGY APPLICATION for the ZEUS CHASSIS

The primary objective of this study is to implement robotic automation within the manufacturing process of ISOGRID structures, with the primary goal of enhancing product quality by leveraging the inherent advantages of process repeatability and reliability for the ZEUS vehicle chassis. Following the fabrication of structures using the robotic cell, a comprehensive assessment encompassing dimensional and structural evaluations was conducted, utilizing a combination of both destructive and non-destructive testing methodologies. Additionally, the findings derived from this automated production approach were juxtaposed with those derived from corresponding tests performed on manually crafted structures. Specifically, this study encompassed the production of five ISOGRID structures via automated stratification and an equivalent number of structures fabricated manually. Various tests and controls were conducted to the manufactured parts in order to compare manually wound and robotic wound parts. These tests/controls are; (i) Dimensional controls using Poli Galaxy Diamond CNC machine, (ii) non-destructive ultrasonic structural testing using Omniscan MX2 machine and (iii) load structural tests using dynamometric machine.

The test results for both manually manufactured structures and RFW process manufactured structures are depicted in table 1 below.

*Table 1: Test results for RFW and manual wound ISOGRID structures.*

		Mean
<b>RFW ISOGRID Structure</b>	Load	78,400 N
	Displacement	0.17 mm
<b>Manual ISOGRID Structure</b>	Load	61,200 N
	Displacement	0.19 mm

#### 5. CONCLUSIONS

In conclusion, an innovative, ultra-light and cost-effective L7e class electric vehicle chassis which is produced using RFW technology is described. RFW, an automated technology for creating ISOGRID structures, comprising a cylindrical skin reinforced by an internal lattice structure.

Innovative, efficient and cost-effective technologies are integrated into a universal vehicle platform to address future urban mobility requirements. In order to accomplish this objective, methanol based PEM fuel cell technology, robotic filament winding technology, 3D reinforced composite sandwich panel technology, switched reluctance motor technologies are researched, developed and integrated into different segments to create a cost effective, affordable zero emission urban mobility solution. Utilising methanol based PEMFC technology as a range extender not only eliminates range anxiety but also high pressure, low temperature storage of pure hydrogen that causes serious safety risks.

Application of RFW, ISOGRID structure and ultra-light 3D reinforced composite sandwich panel technology reduces the total vehicle weight which improves overall vehicle performance. To assess the benefits of RFW, isogrid structures were produced and subjected to various tests, with results compared to manually crafted counterparts. Initial structure designs were determined through numerical procedures and finite element simulations, specifying geometrical parameters (rib section: 2 x 6 mm<sup>2</sup>, skin thickness: 2 mm) and curing cycles for proper resin curing.

Geometric and structural tests were conducted post-production. Geometrically, RFW structures exhibited superior quality, with an average deviation of 0.65 mm compared to 0.9 mm for manual structures, representing a 28% improvement. Ultrasonic scans revealed no internal defects in both technologies. Density and matrix digestion tests showed increased average fibre content and reduced voids in RFW structures.

Destructive axial compression tests indicated a 22% improvement in the maximum load at break for RFW structures, from 61,199 N to 78,400 N, highlighting the efficiency and effectiveness of the automated approach. Also, utilisation of innovative composite filament winding process reduces the required man hour time and complexity of assembly processes since these materials do not require welding applications. At present, assembly and test processes of ZEUS L7e class passenger vehicle concept require a total of 7 man-hours. Moreover, the authors are further working on the application of 3D printing and additive manufacturing processes for the ZEUS project which will reduce waste raw materials, energy and man-hours required for assembly. Switched reluctance electric motor technologies with embedded transmission and brake systems with its compact design maximise space utilization while reducing vehicle weight. Also, 97% electric motor and 91% powertrain system efficiencies increase vehicle performance and reduce energy consumption.

## 6. ACKNOWLEDGEMENT

The authors would like to thank M. S. Pedersen, team members of Roadrazer ApS and EOS Sustainable Energy Solutions GmbH companies for their valuable technical contributions and efforts for researching, designing and developing the technologies described in this paper.

## 7. REFERENCES

Arrabiyeh, P. & May, D. & Eckrich, M. & Dlugaj, A., 2021. An overview on current manufacturing technologies: Processing continuous rovings impregnated with thermoset resin. *Polymer Composites*. 42. 10.1002/pc.26274.

BMUV, 2016. The Climate Action Plan 2050. [https://www.bmuv.de/fileadmin/Daten\\_BMU/Pool/Broschueren/klimaschutzplan\\_2050\\_en\\_bf.pdf](https://www.bmuv.de/fileadmin/Daten_BMU/Pool/Broschueren/klimaschutzplan_2050_en_bf.pdf). Last accessed on 15.07.2022.

EEA (European Environment Agency), 2021. CO<sub>2</sub> performance of new passenger cars in Europe. <https://www.eea.europa.eu/ims/co2-performance-of-new-passenger>. Last Access on 15.07.2022.

Gortner F., 2019. Bio-basierte und nachwachsende Füllstoffe für dichterduzierte Sheet Molding Compounds: Technische Universität Kaiserslautern.

Frulloni E, Kenny JM, Conti P, Torre L., 2007. Experimental study and finite element analysis of the elastic instability of composite lattice structures for aeronautic applications. *Compos Struct* 2007;78:519–28. <http://dx.doi.org/10.1016/>

Gökçe H.U. & Gökçe K.U., 2022. "L7e class urban electric vehicle platform based on methanol fuel cell range extender technology, ultra-light composite filament winding technology, low speed autonomous technology and permanent magnet synchronous AC motor technologies." In: Riffat, Su., ed., *Sustainable Energy Technologies: Proceedings of the 19th International Conference on Sustainable Energy Technologies*, 16th – 18th August 2022, Turkey. University of Nottingham: Buildings, Energy & Environment Research Group. Pp 233-241. Available from: [nottingham-repository.worktribe.com/](http://nottingham-repository.worktribe.com/) [Last access date: 19.10.2023].

IEA (International Energy Agency), 2019. The Future of Hydrogen. <https://www.iea.org/reports/the-future-of-hydrogen>. Last accessed on 15.07.2022.

Ma Q. & Rejab R. & Mat S. & Manoj N., 2019. Filament winding technique: SWOT analysis and applied favourable factors. 3.

NOAA Global Monitoring Lab, 2022. Climate Change: Atmospheric Carbon Dioxide. Accessible on: <https://www.climate.gov/news-features/understanding-climate/climate-change-atmospheric-carbon-dioxide>. Last accessed on 26.07.2022.

Regi M, Mancina F, Marchetti M, Sintoni F, Totaro G, De Nicola F, et al., 2014. Nano structured composite materials and isogrid lattice structures for aerospace applications. In: *Int. Astronaut. Fed. - 55th Int. Astronaut. Congr.*, vol. 3; 2004. p. 1944–52.

Sorrentino L., Marchetti M., Bellini C., Delfini A., del Sette F., 2017. Manufacture of high performance isogrid structure by Robotic Filament Winding. *Journal of Composite Structures*. 2017,164, 43.

U.S. EIA (Energy Information Administration), 2016. International Energy Outlook 2016. <https://www.eia.gov/outlooks/ieo/pdf/transportation.pdf>. Last accessed on 15.07.2022.

---

## #220: A computational study into the charging of an agitated fluidised bed thermochemical energy storage system

---

Mark WORALL<sup>1</sup>, Jo DARKWA<sup>1</sup>, John CALAUTIT<sup>1</sup>, Rabah BOUKHANOUF<sup>1</sup>, Weiguang SU<sup>2</sup>, Sarah ROGER-LUND<sup>1</sup>, Anti KUR<sup>1</sup>

<sup>1</sup> Department of Architecture and Built Environment, Faculty of Engineering, The University of Nottingham, Nottingham, UK

<sup>2</sup> School of Mechanical Engineering, Qilu University of Technology (Shandong Academy of Sciences), Jinan, China.

*Abstract: Waste heat of medium to high temperatures (150-500°C) is often dissipated directly to the atmosphere or used in low-temperature applications. However, much of this waste heat could be used in industrial, process and renewable energy applications. Sensible and phase change materials storage are generally, not suitable for these temperature ranges, but thermochemical energy storage (TCES) can store and release this heat at high temperatures, sufficient to drive industrial and process applications. TCES stores the energy in the form of chemical bonds, which are released with exothermal reactions. This enables heat to be stored without degradation until a reaction is activated and so can store the energy over long periods, allowing short-term and long-term storage.*

*An agitated fluidised bed thermochemical reactor is being developed to optimise the system and create an efficient and effective storage system. To gain a better understanding of the interaction between the fluidised bed, agitation and thermochemical reaction, computational fluid dynamics (CFD) simulations were developed. The process involved the integration of a multiphase gas-solid fluidisation model, a heterogeneous reaction model and a sliding mesh model. Key findings included successfully simulating water vapour dehydration, the change in volume fractions of the products and reactants as the simulations progressed and enabling us to gain an insight into the hydrodynamics of agitation, chemical reaction and fluidisation.*

*Keywords: Thermochemical energy, Energy storage, Energy efficiency, Waste heat, Agitated bed simulation*

## 1. INTRODUCTION

Global carbon dioxide emissions (CO<sub>2</sub>) from energy combustion and industrial processes grew to an all-time high of 36.8Gt CO<sub>2</sub> in 2022, according to the IEA (2023). Global warming and its effect on the climate are resulting in intergovernmental agreements to reduce or eliminate the generation of greenhouse gases. Energy combustion and industrial processes generate waste heat at medium to high temperatures (100-500°C), amounting to 35% of the total waste heat available, according to Forman et al (2016), so being able to utilise the waste heat will increase the efficiency of such processes and reduce the CO<sub>2</sub> emissions relative to the energy conversion and industrial production. Waste heat is often dissipated directly to atmosphere or used in low temperature applications. However, much of this waste heat could be used at relatively high temperatures in industrial and process applications, as well as high temperature renewable processes, such as solar power generation and waste to energy systems. Sensible and phase change materials storage are generally, not suitable for these temperature ranges. Alternatively, thermochemical energy storage (TCES) can store and release this heat at high temperatures, sufficient to drive industrial and process applications. TCES stores the energy in the form of chemical bonds, which are released with exothermal reactions. This enables heat to be stored without degradation until a reaction is activated and so can store the energy over long periods, allowing short-term and long-term storage. A simplified chemical reaction can be represented by equation 1, where chemical elements (reactants) A and B react when in contact to produce chemical element C (product of reaction) and release the heat of reaction  $\Delta H$ .



Thermochemical materials have high energy storage densities of 7-10 times that of sensible storage (Goetz, Elie, Spinner, 1993), but relatively low thermal conductivities, which present barriers to heat transfer. One of the most promising technologies for enhancing, storing, releasing and transferring the heat of thermochemical materials is by gas-solid fluidisation. Fluidisation has advantages over other processes; heat transfer can be 5 to 10 times that of a fixed bed; particles in motion, especially small particles can transport heat more efficiently than gas alone; and a fluidised bed can maintain an isothermal profile within a few degrees, even for the most extreme exothermal reactions (Cocco, R, Reddy Karri, S, B, Knowlton, 2014),

The thermochemical materials of interest to the authors are mainly metal hydroxides, and so the main reactant is water vapour. Although advantageous in terms of their energy density, heat of reaction, safety and temperature ranges, they present difficulties in a fluidised bed. Pardo et al (2014) described experimental results from a fluidised bed employing Ca(OH)<sub>2</sub>/CaO materials. Gas channelling was observed resulting in poor fluidisation. Inert Al<sub>2</sub>O<sub>3</sub> particles were mixed with the Ca(OH)<sub>2</sub>/CaO in proportions of up to 70%wt to produce fluidisation, Agglomeration is also a problem during hydration/dehydration processes. Particles tend to stick together and form clumps, which results in non-uniform particles and hinders fluidisation.

In this paper, to address problems of channelling and agglomeration, an agitated fluidised bed has been considered. Integrating a mechanical agitator into a fluidised bed will allow breakup of the gas bubbles that form and grow into large bubbles and channelling and reduce the problems of agglomeration of particles by enhancing particle motion and circulation. Zhang et al (2016) described a CFD simulation of an agitated gas-fluidised bed. A 3D gas-fluidised bed with a frame impeller was investigated using commercial CFD software Ansys Fluent. In this work, the thermofluidics of a gas-fluidised bed using a propeller type agitator and operating at high temperatures and with chemical reactions is presented.

## 2. BACKGROUND

### 2.1. Fluidisation

When a fluid is introduced into a packed bed of particles, the pressure drop across the bed increases with increasing velocity. When the drag force imposed by the upward-flowing gas on the particles is equal to the weight of particles, the particles become fluidised, and its velocity is known as the minimum fluidisation velocity (Kunii and Levenspiel, 1969). The minimum fluidisation velocity is usually determined experimentally, but empirical equations have been developed to estimate it for comparison with experimental values and for use in simulations. The minimum fluidisation velocity can be calculated using the Ergun equation (Ergun, 1952) with the assistance of the Archimedes number, which is defined as

$$Ar = \frac{d_p^3 \rho_g (\rho_s - \rho_g) g}{\mu_g^2} \quad (2)$$

Where  $d_p$  is the Sauter mean diameter of the particles (m),  $\rho$ , is the density (kg.m<sup>-3</sup>),  $g$  is the acceleration due to gravity (m.s<sup>-2</sup>) and  $\mu_g$  is the dynamic viscosity of the gas (kg.m<sup>-1</sup>.s<sup>-1</sup>). Subscripts g and s represent the gas and solid phases.

Defining the Reynolds number at minimum fluidisation velocity as

$$Re_{mf} = \frac{-b + \sqrt{b^2 + 4aAr}}{2a} \quad (3)$$

Where a and b are defined as

$$a = \frac{1.75}{\phi \varepsilon_{mf}^3} \quad (4)$$

$$b = \frac{150(1-\varepsilon_{mf})}{\varphi^2 \varepsilon_{mf}^3} \quad (5)$$

Where  $\varepsilon_{mf}$  is the porosity or gas void fraction of the bed at minimum fluidisation velocity and  $\varphi$  is the sphericity or shape factor.

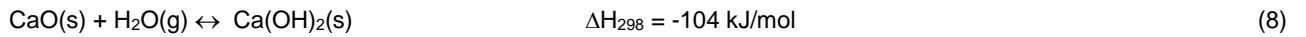
$$\varphi = \frac{\text{surface area of sphere}}{\text{surface area of particle}} \quad (6)$$

The minimum fluidisation velocity can then be calculated from equation 7.

$$Re_{mf} = \frac{\rho_g d_p u_{mf}}{\mu_g} \quad (7)$$

## 2.2. Reaction kinetics

The hydration and dehydration of CaO have been shown to be a suitable thermochemical material for reversible reactions (Criado *et al*, 2014), with high reaction enthalpy (-104kJ/mol) and a high temperature of heat release (450-500°C). The reversible reaction of CaO is shown below.



Criado, Alonso and Abanades (2014) reported the results of an experimental study of the kinetics of hydration and dehydration of CaO. For the dehydration reaction, Equation 9 gives the dehydration conversion rate as a function of time, based on a shrinking core model.

$$\frac{dX_{dehy}}{dt} = \frac{1}{d_p} A'_{dehy} \exp\left[-\frac{E_{dehy}}{RT}\right] (v_{eq} - v_{H_2O})^3 (1 - X_{dehy})^{2/3} \quad (9)$$

Where  $X_{dehy}$  is the conversion (mol H<sub>2</sub>O/mol CaO),  $d_p$  is the average particle size ( $\mu\text{m}$ ),  $A'_{dehy}$  is the pre-exponential factor ( $\mu\text{s}^{-1}$ ),  $E_{dehy}$  is the activation energy ( $\text{J}\cdot\text{mol}^{-1}$ ),  $R$  is the universal gas constant ( $\text{J}\cdot\text{mol}^{-1}\cdot\text{K}^{-1}$ ),  $T$  is the absolute temperature (K),  $v_{eq}$  and  $v_{H_2O}$  are equilibrium and steam volume fractions. Criado, Alonso and Abanades (2014) reported values for  $A'_{dehy}$  and  $E_{dehy}$  as  $7.3 \pm 0.6 \times 10^4 \mu\text{m/s}$  and  $60.8 \pm 0.3 \times 10^3 \text{ J/mol}$ , respectively.

The heterogeneous phase interaction rates are based on a modified Arrhenius type expression and, according the Ansys Fluent Theory guide (2021), can be expressed in the general form:

$$r_{dehyd} = \frac{dX_{dehy}}{dt} \prod_{i=1}^{NR} \left[ \frac{Y_{ip} \rho_p \alpha_p}{MW_{ip}} \right]^n \quad [10]$$

Where  $r_{dehyd}$  is the heterogeneous dehydration reaction rate ( $\text{kmol}\cdot\text{m}^{-3}\cdot\text{s}^{-1}$ )  $Y_{ip}$  is the mass fraction of reactant species  $i$  in phase  $p$ ,  $NR$  is the total number of reactants in a given inter-phase reaction,  $\rho_p$  is the bulk density of the phase  $p$ ,  $\alpha_p$  is the volume fraction of the phase  $p$ ,  $MW_{ip}$  is the molecular weight ( $\text{kg}\cdot\text{kmol}^{-1}$ ) of the reactant species  $i$  in the phase  $p$  and  $n$  is the rate exponent.

## 3. NUMERICAL MODEL

### 3.1. Multiphase model

The Eulerian-Eulerian multiphase model was used to simulate the gas-solids interaction during fluidisation. The gas and solid phases were treated as interpenetrating continua so that the laws of conservation of mass and momentum were satisfied for each phase. Ansys Fluent's multiphase model does not distinguish between fluid-fluid and fluid-solid flows. At least one phase must be designated as granular for fluid-solid multiphase flows to be modelled.

It is assumed that a single pressure is shared by all phases and that the momentum and energy equations are solved for all phases. The equations derived from the kinetic theory of granular flow (Lun *et al*, 1984) were used to describe the properties of granular phases.

Zang *et al* (2016) described a CFD study of the particle-particle collision coefficient for an agitated fluidised bed. The particle-particle collision coefficient is the ratio of the velocities of two colliding particles before and after the collision. The momentum exchange between fluid-solid and solid-solid phases is based on the fluid-solid and solid-solid interphase exchange coefficients, respectively. Equation 10 shows the general definition of a fluid-solid interphase exchange coefficient.

$$K_{sl} = \frac{\alpha_s \rho_s f}{\tau_s} \quad (11)$$



Where  $\alpha$  is the volume fraction,  $\rho$  is the density ( $\text{kg.m}^{-3}$ ), subscripts s and l represent solid and fluid phase properties,  $f$  is defined differently for the different exchange-coefficients and  $\tau_s$  is the “particulate relaxation time” and defined as

$$\tau_s = \frac{\rho_s d_s^2}{18\mu_l} \quad (12)$$

Where  $d_s$  is the diameter of particles of phase s and  $\mu$  is the dynamic viscosity  $\text{kg.m}^{-1}.\text{s}^{-1}$ ). All definitions of  $f$  include drag functions ( $C_D$ ) that are based on the relative Reynold number ( $\text{Re}_s$ ).

In these simulations the Gidaspow drag model (Gidaspow, 1984) was employed. The Gidaspow model combines the Wen-Yu model (Wen and Yu, 1966) and the Ergun equation (Ergun, 1952), and is reasonable at simulating dense fluidisation in comparison to the other models available in Ansys Fluent, according to Wang et al (2014).

When  $\alpha$  is  $\leq 0.8$ , the gas-solid exchange coefficient is

$$K_{sl} = 150 \frac{\alpha_s(1-\alpha_l)\mu_l}{\alpha_l d_s^2} + 1.75 \frac{\rho_l \alpha_s |\vec{v}_s - \vec{v}_l|}{d_s} \quad (13)$$

When  $\alpha$  is  $> 0.8$ , the gas-solid exchange coefficient is

$$K_{sl} = \frac{3}{4} C_D \frac{\varepsilon_s \varepsilon_g \rho_g |\vec{v}_s - \vec{v}_l|}{d_s} \varepsilon_g^{-2.65} \quad (14)$$

Where  $\vec{V}$  is the overall velocity vector ( $\text{m.s}^{-1}$ ),  $\varepsilon$  is the void fraction and subscript g represents the gas phase properties.

$$C_D = \frac{24}{(\varepsilon_g \text{Re}_s)(1+0.15(\varepsilon_g \text{Re}_s)^{0.687})} \quad \text{Re}_s < 1000 \quad (15)$$

$$C_D = 0.44 \quad \text{Re}_s \Rightarrow 1000 \quad (16)$$

### 3.2. Sliding mesh model

A sliding mesh model was developed to simulate the agitated fluidised bed reactor. A sliding mesh model allows the creation of separate mesh zones which can move relative to one another. Multiple cell zones are connected to each other through non-conformal interfaces, according to Ansys Fluent Theory Guide 2021. As the mesh motion is updated in time, the non-conformal interfaces are updated to reflect the new position for each zone. Mesh motion must be specified so that zones linked through non-conformal interfaces remain in contact with each other to allow for fluid flow from one mesh to another.

The integral form of the conservation equation or an arbitrary scalar  $\phi$  whose boundary is moving can be written as

$$\frac{d}{dt} \int_V \rho \phi dV + \int_{\partial V} \rho \phi (\vec{u} - \vec{u}_g) \cdot d\vec{A}_j = \int_{\partial V} \Gamma \nabla \phi \cdot d\vec{A} + \int_V S_\phi dV \quad (17)$$

Where  $\vec{u}$  is the flow velocity vector,  $\vec{u}_g$  is the mesh velocity of the moving mesh  $\Gamma$  is the diffusion coefficient and  $S_\phi$  is the source term of  $\phi$ . The time derivative of equation 16 can be written as

$$\frac{d}{dt} \int_V \rho \phi dV = \frac{(\rho \phi V)^{n+1} - (\rho \phi V)^n}{\Delta t} \quad (18)$$

Mesh motion formulation is rigid and so all cells retain their original shape and volume. The time rate of change of the cell volume is zero, therefore

$$V^{n+1} = V^n \quad (19)$$

Equation 18 becomes

$$\frac{d}{dt} \int \rho \phi dV = \frac{[(\rho \phi)^{n+1} - (\rho \phi)^n] V}{\Delta t} \quad (20)$$

And

$$\sum_j^{n_f} \vec{u}_{g,j} \cdot \vec{A}_j = 0 \quad (21)$$

Equation 17 together with the simplifications allows for the flow in the moving mesh zones to be updated, provided that suitable rigid mesh motion is defined for each zone. A numerical model has been developed using commercial software Ansys Fluent (v19.2) to simulate an agitated fluidised bed thermochemical energy store so that design and off-design conditions could be investigated.

### 3.3. Solution procedure

A model of an agitated bed reactor was developed in Ansys Fluent Design Modeler consisting of a cylindrical vessel and a stirrer. The vessel was 100mm in diameter and 750mm in height. A 4-bladed propeller stirrer was chosen with blade outer diameter and height of 50mm and 10mm, respectively. A hub 15mm in diameter and of the same height as the blade was included in the model. The stirrer centroid was located 55mm from the base. A stirrer rod was not included in the model to simplify the modelling and meshing. The geometry of the reactor is shown in Figure 1a.

The domain was divided into two sub-domains, a fixed domain consisting of the majority of the volume of the vessel, and a moving domain, consisting of the stirrer and some surrounding fluid. The moving domain was 60mm in diameter and 20mm in height, and its centroid position was 55mm from the base.

A mesh was developed based on a 7.5mm element size and adaptive sizing with a resolution of 7. The modelling created two zones with interfaces and interface zones at the boundaries. In order to refine the mesh at the interface, edge sizing was carried out at the two edges in both the moving and fixed domains, dividing the edges into 60 equal divisions. The number of nodes and cells created were 24,803 and 126,358, respectively. The mesh generated is shown in Figure 1b.

Three meshes were created consisting of element sizes of 5, 7.5 and 10mm to check on grid independence and convergence. The number of cells for each mesh was 245,844, 126,358 and 99,023, respectively. An absolute convergence tolerance of  $10^{-3}$  for the scaled residual components between successive iterations was chosen. At an element size of 10mm, the continuity residuals were found to be high and rising and did not converge to the specified tolerance. At 7.5mm, the residuals reduced to the convergence criteria rapidly, with the solution to the tolerance within 10-15 iterations. The results for the 5mm element showed quicker convergence but would result in an increase in computational time for similar results.

An absolute convergence tolerance of  $10^{-3}$  for the scaled residual components between successive iterations was chosen. Figures 2a and 2b show residuals for meshes of 7.5 and 10mm. At an element size of 10mm (Figure 2a), the continuity residuals were found to be high and rising and did not converge to the specified tolerance. At 7.5mm (Figure 2b), the residuals reduced to the convergence criteria rapidly, with the solution to the tolerance within 10-15 iterations. The results for the 5mm element showed quicker convergence but would result in an increase in computational time for similar results.

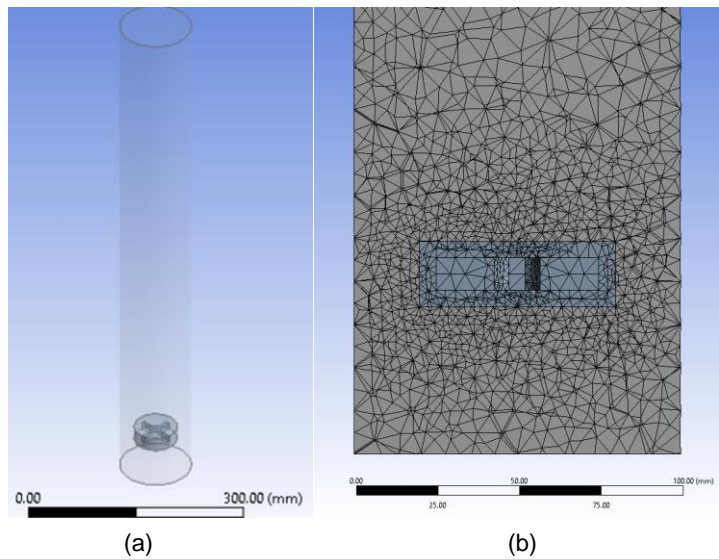
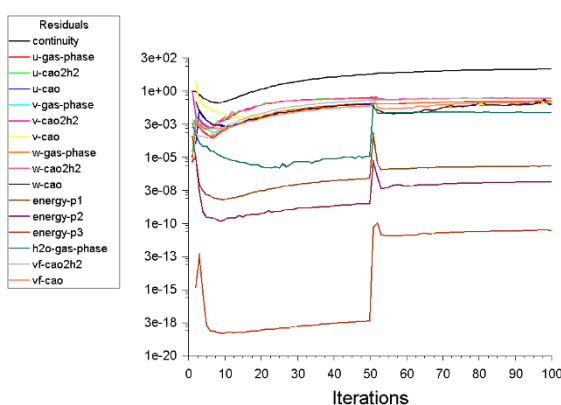
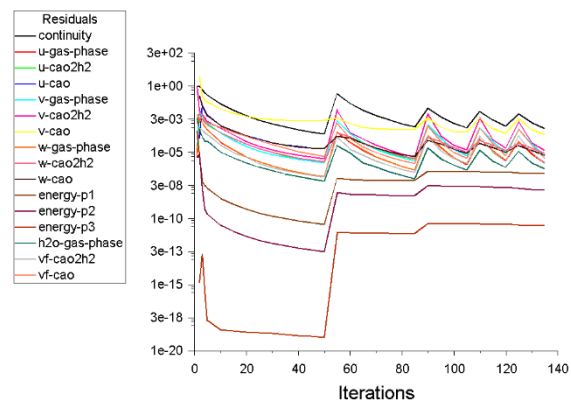


Figure 1a. 3D agitated reactor model. 1b. Two zone mesh



(a)

Figure 2a. Residuals for element size 10mm



(b)

Figure 2b. Residuals for element size 7.5mm

The fluidised bed simulation conditions and granular properties are described in Table 1.

<i>Table 1: Fluidised bed simulation conditions</i>		<i>Granular properties</i>	
Particle mean diameter ( $\mu\text{m}$ )	100	Granular viscosity ( $\text{kg}\cdot\text{m}^{-1}\cdot\text{s}^{-1}$ )	Syamial-O'Brien
Particle density ( $\text{Ca(OH)}_2$ ) ( $\text{kg}\cdot\text{m}^{-3}$ )	2210	Granular bulk viscosity ( $\text{kg}\cdot\text{m}^{-1}\cdot\text{s}^{-1}$ )	Lun et al
Minimum fluidisation velocity ( $\text{m}\cdot\text{s}^{-1}$ )	0.015	Solids pressure (Pa)	Lun et al
Void fraction at min fluidisation velocity	0.44	Granular temperature ( $\text{m}^2\cdot\text{s}^{-2}$ )	Algebraic
Bed height (m)	0.25	Frictional viscosity ( $\text{kg}\cdot\text{m}^{-1}\cdot\text{s}^{-1}$ )	Schaeffer
Sphericity	1	Frictional pressure (Pa)	Based-ktgf
Coefficient of restitution	0.9	Packing limit	0.63

Three phases were chosen to represent the fluidisation and reactions during dehydration. A primary gas phase consisting of a mixture of air and water vapour species and two solid, granular phases, namely, calcium oxide (CaO), and calcium hydroxide ( $\text{Ca(OH)}_2$ ). The three phases were created as mixture materials in order to enable volumetric reactions within the fluid domains, with CaO and  $\text{Ca(OH)}_2$  considered as single species mixtures. Table 2 shows the properties of the materials used in the simulations.

<i>Table 2: Properties of materials</i>				
	CaO(s)	$\text{Ca(OH)}_2$ (s)	$\text{H}_2\text{O(g)}$	Air (g)
$\rho$ ( $\text{kg}\cdot\text{m}^{-3}$ )	3340	2210	0.5542	1.225
$C_p$ ( $\text{J}\cdot\text{kg}^{-1}\cdot\text{K}^{-1}$ )	753	1181	piecewise-polynomial	1006.43
$k$ ( $\text{W}\cdot\text{m}^{-1}\cdot\text{K}^{-1}$ )	0.3	0.4	0.0261	0.0242
$\mu$ ( $\text{kg}\cdot\text{m}^{-1}\cdot\text{s}^{-1}$ )	$1.79 \times 10^{-5}$	$1.79 \times 10^{-5}$	$1.35 \times 10^{-5}$	$1.79 \times 10^{-5}$
$M$ ( $\text{kg}\cdot\text{kmol}^{-1}$ )	56	74	18	28.966
$\Delta H_{298}$ ( $\text{J}\cdot\text{mol}^{-1}$ )	$-635 \times 10^3$	$-986 \times 10^3$	$-241 \times 10^3$	-
$\Delta S_{298}$ ( $\text{J}\cdot\text{mol}^{-1}\cdot\text{K}^{-1}$ )	38.2	83.3	188.696	194.336

Table 3 describes the modelling parameters and solution controls used in Ansys Fluent simulation.

<i>Table 3: Modelling parameters</i>			
Solution Methods	Solution Controls: Under-relaxation Factors		
Scheme	Phase Coupled SIMPLE	Pressure	0.5
Gradient	Least squared cell based	Density	1
Pressure	Second Order	Body Force	1
Momentum	First Order Upwind	Momentum	0.5
Volume Fraction	First Order Upwind	Volume Fraction	0.5
Energy	First Order Upwind	Granular Temperature	0.2
Gas $\text{H}_2\text{O}$	First Order Upwind	Energy	1
Transient Formulation	First Order Implicit	Gas $\text{H}_2\text{O}$	1

Table 4 describes the boundary conditions used in the simulation.

<i>Table 4: Boundary and cell zone conditions</i>		
Name	Type	Conditions
Inlet	Velocity inlet	Gas phase velocity $v = 0.015\text{m/s}$ , $T = 623.15\text{K}$ , $MF_{\text{H}_2\text{O}} = 0$ , all other phases $v = 0$ , $T = 623.15\text{K}$
Outlet	Outlet	All phases zero backflow $VF$ , $T = 623.15\text{K}$
Wall	Wall	No slip - $T =$ zero heat flux
Wall	Moving wall	Via system coupling
Mesh interfaces	Contact region	Matching
Moving mesh domain	Mesh motion	rotational speed – 0/60/120rpm, clockwise from motor about y axis

#### 4. RESULTS

Figure 3 shows contour maps of gas and  $\text{Ca(OH)}_2$  volume fractions for a rotational speed of 60rpm at 2.5, 5 and 10 seconds. Expansion occurs in the 2.5 and 5-second images, but the bed conforms to a steady state at about 10 seconds.  $\text{Ca(OH)}_2$  volume fraction is highest surrounding the agitator and between the agitator and vessel wall, as the action interferes with the accumulation and growth of bubbles. Figure 3 shows that there is a region surrounding the stirrer that is more pronounced in the earlier times steps, but this region has been termed a cavern and represents an agitated volume surrounded by a stagnant fluid (Paul, Ateimo-Obeng, Kresta, 2003, Etchells, 1987). This is a behaviour observed in non-Newtonian fluids and pseudo-plastics.

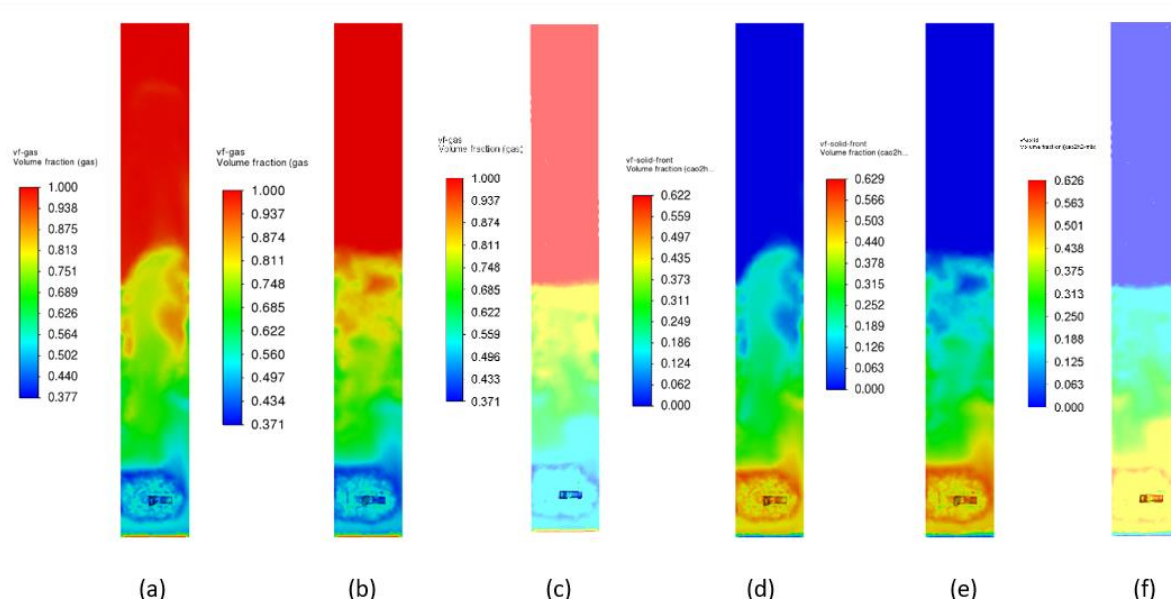


Figure 3 Volume fraction contours, a) gas at 2,5s, b) gas at 5s, c) gas at 10s, d)  $\text{Ca(OH)}_2$  at 2,.5s, e)  $\text{Ca(OH)}_2$  at 5sec, f)  $\text{Ca(OH)}_2$  at 10s

Figure 4 shows cross-sectional contour maps of gas temperature and heterogeneous reaction rate for a rotational speed of 60rpm and at 2.5, 5 and 10 seconds. The endothermic reaction causes a sensible decrease in temperature over time, with the minimum recorded being 608, 602 and 588K with increasing time. The temperature remains uniform in the majority of the bed, but there is a change toward the outlet as a constant temperature boundary condition was imposed. The heterogeneous reaction rate is greatest where the  $\text{Ca(OH)}_2$  volume fraction is highest and therefore where the gas bubbles are smallest. The values of the reaction rates ( $0.04$  to  $0.06 \text{ kmol}\cdot\text{m}^{-3}\cdot\text{s}^{-1}$ ) are consistent with experiments, such those reported by Criado, et al (2017).

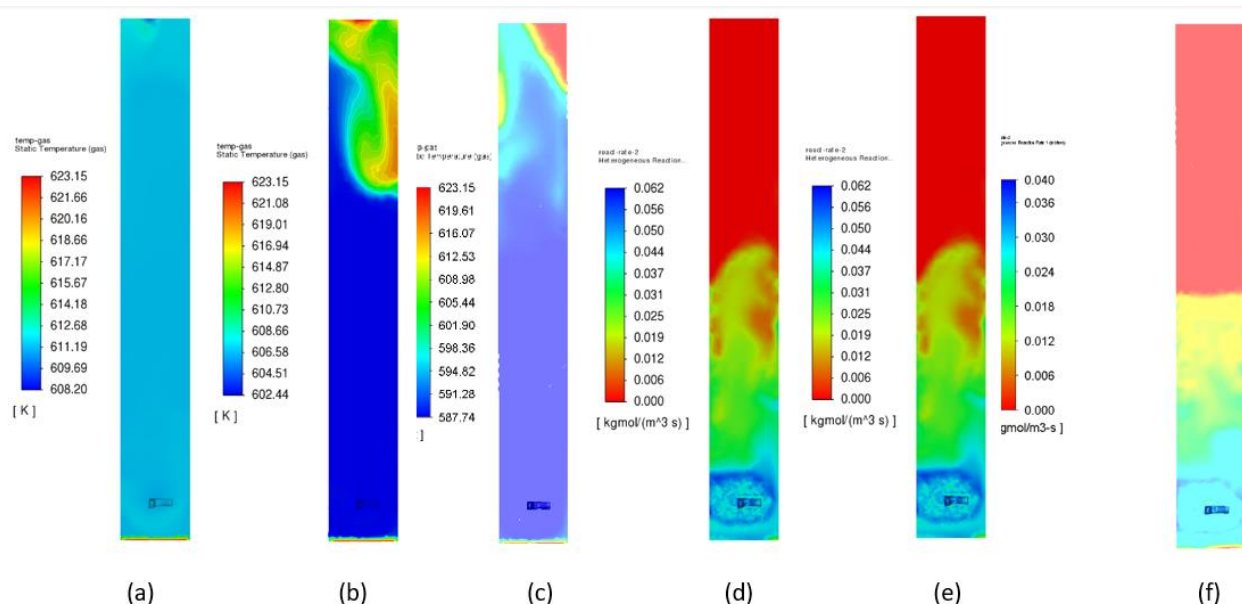


Figure 4 Gas temperature/reaction rate contours, a)  $T_{\text{gas}}$  at 2,5s, b)  $T_{\text{gas}}$  at 5s, c)  $T_{\text{gas}}$  at 10s, d)  $r_{\text{dehy}}$  at 2,.5s, e)  $r_{\text{dehy}}$  at 5sec, f)  $r_{\text{dehy}}$  at 10s

Figure 5 compares the volume fractions of both the gas and the  $\text{Ca(OH)}_2$  phases as a function of reactor height along the vertical centreline at zero rotational speed, 60 and 120rpm at 10 seconds. Figure 5a shows that the  $\text{Ca(OH)}_2$  phase expands further at zero rpm, reaching a reactor height of approximately 0.45m. At 60rpm, the bed expands less in comparison to a maximum of approximately 0.38m. The simulations at 60rpm and 120rpm show similar volume fraction curves with height. This shows that agitation reduces the expansion of the bed. The gas phase volume fraction shows a steady increase with height until the gas/solid boundary is reached. The  $\text{Ca(OH)}_2$  volume fraction increases but becomes fairly uniform in the region below the agitator. This suggests that the action of stirring the bed prevents the gas phase from expanding in that region and creates a uniform mixing zone. The difference in the height of the interface (also known as the freeboard) is reduced with agitation.

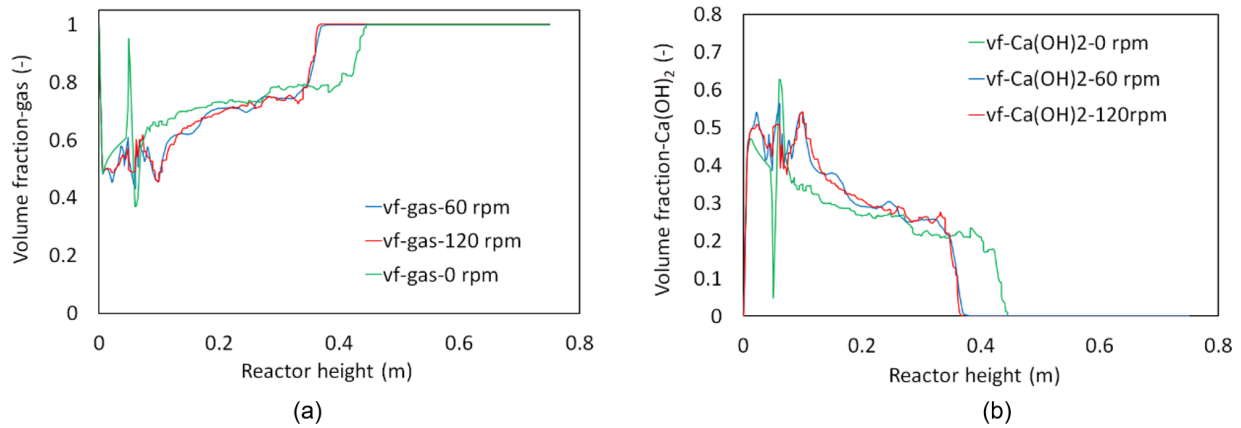


Figure 5 Variation in volume fraction with reactor height at centreline and agitator rotational speed. a) gas phase, b) Ca(OH)<sub>2</sub>

Figure 6 shows how the gas temperature (a) and heterogeneous reaction rate (b) vary with reactor height and agitator rotational speed at 10 seconds. The gas static temperature remains approximately uniform as the gas progresses through the particles of the bed. The approximately uniform temperature across the bed is a well-known characteristic of fluidised bed reactors (Coco, Reddy and Knowlton, 2014). The static temperatures for each case are similar but vary slightly. The average temperature within the bed for the three cases was determined to be 588.92K, 589.95K and 588.92K, respectively.

As the gas leaves the solids particles, the temperature increases with height. This was mainly because a constant temperature boundary condition at the outlet was specified to allow for the evaluation of agitation and fluidisation at very high temperatures.

At zero rpm, the reaction rate reduces steadily with reactor height until the gas exits the bed of particles. Agitation increases the reaction rate with height in comparison to the case of no agitation. The volume fractions in the region of the stirrer are more uniform, as observed in Figure 5, allowing for greater reaction rates in comparison the case of no agitation.

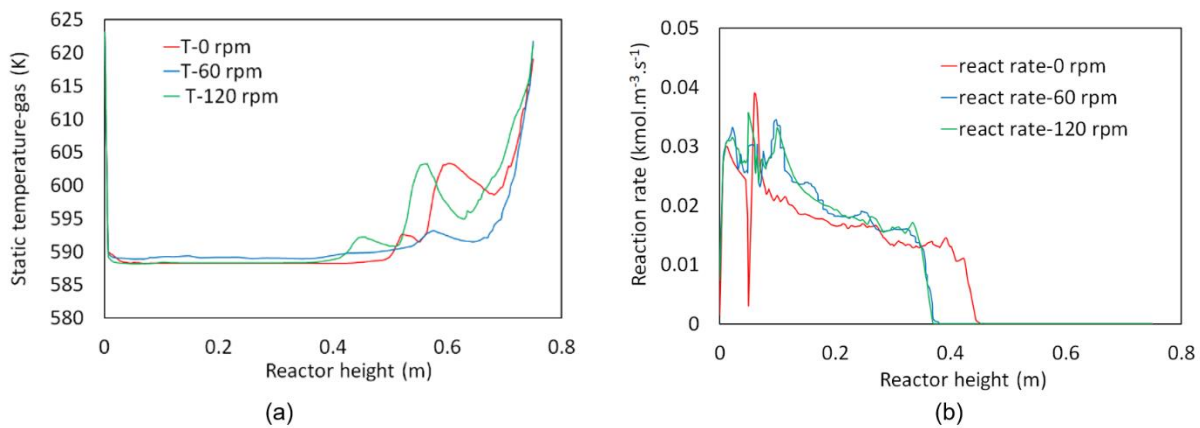


Figure 6 Variation in reaction rate (a) and gas temperature (b) with reactor height at centreline and agitator rotational speed

Figure 7 shows the variation in net mass flux and total net heat transfer between inlet and outlet for rotational speeds of 0, 60 and 120rpm. Mass flux varies from approximately 0.975 g.s<sup>-1</sup> at 0 rpm, to 0.965 g.s<sup>-1</sup> at 60rpm and 1.01 g.s<sup>-1</sup> at 120rpm. The net mass flux is the water vapour generated due to the reaction. It was expected that mass flux would increase with agitation speed, but as observed previously, the average static temperature in the bed at 60rpm is slightly higher than for the other rotational speeds. A difference in temperature will impact the calculation of the mass flux and heat transfer. The net total heat transfer rate varies from 14.57kW at 0 rpm, to 12.85kW at 60 rpm and to 17.18kW at 120 rpm. Only about 500W of the total is due to sensible heat transfer, so the majority is by latent heat due to water vapour generation.

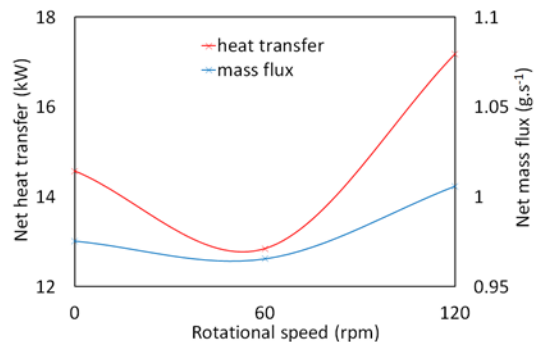


Figure 7. Net mass flux and heat transfer v rotational

## 5. CONCLUSION

This paper has presented preliminary results of computational fluid dynamics of an agitated fluidised bed for high-temperature thermochemical energy storage application. The study has shown that agitation enhances the fluidisation process of the bed by reducing the gas volume fraction, and this produces a more uniform bed temperature. The reduction in gas volume fraction, especially in the region below the stirrer, increases the average heterogeneous reaction rate because more material is available for reaction and less occupied by the inert gas. The heterogeneous reaction causes reductions in static temperature in the reactor of the order of 34K in 10 seconds. Simulations conform to the well-known uniform temperature that characterises fluidised beds. Heat transfer was found to be in the order of 12-17kW, mainly due to the release of latent heat.

## 6. ACKNOWLEDGEMENT

This work was supported by UK Engineering, Physical Sciences Research Council (EPSRC) (under Grant Award No. EP/V041452/1); Qing Chuang plan by Department of Education of Shandong Province (Sub-Title: Innovative Research Team of Advanced Energy Equipment).

## 7. REFERENCES

- Ansys Fluent Theory Guide 2021, Ansys Inc, p780.
- Cocco, R, Reddy Karri, S, B, Knowlton, 2014, introduction to fluidisation, AIChE, November, 21-29.
- Criado, Y, A, Alonso, M, Abanades, C, J, 2014, kinetics of the  $\text{CaO}/\text{Ca}(\text{OH})_2$  hydration/dehydration reaction for thermochemical energy storage applications, *Ind. Eng. Chem. Res.*, 53, 12594–12601.
- Criado, Y, A, Huille, H, Rougé, S, Abanades, C, J, 2017, experimental investigation and model validation of a  $\text{CaO}/\text{Ca}(\text{OH})_2$  fluidized bed reactor for thermochemical energy storage applications, *Chem. Eng. J.*, 313, 1194-1205.
- Ergun, S, 1952, fluid flow through packed columns. *Chem. Eng. Prog.* 48, 89–94.
- Etchels, A, W, 1987, mixing of bingham plastics on an industrial scale. *Fluid mixing III*, The Inst. Chem, Eng, Symposium series, pp.271-285.
- Forman, C, Muritala, I, K, Pardmann, R, Meyer, B, 2016, estimating the global waste heat potential, *Renew. Sustain. Energy Rev.* 57, 568-1579.
- Gidaspow, D, 1994. *multiphase flow and fluidization: continuum and kinetic theory descriptions*. Academic Press, New York.
- Goetz, V, Elie, F, Spinner, F, 1993, the structure and effect of single effect solid-gas chemical heat pumps, 23, 1, 79-96.
- Kunii, D, Levenspiel, O, 1969, *fluidisation engineering*, Wiley and Sons, Inc, New York, p.534.
- IEA, 2023, *CO2 emissions in 2022*, IEA Publications, France, p19.
- Lun, C, K, K, Savage, S, B, Jeffrey, D, J, Chepurny, N, 1984, kinetic theories for granular flow: inelastic particles in couette-flow and slightly inelastic particles in a general flow field. *J. Fluid Mech.* 140, 223–256.
- Pardo, P, Anxionnaz-Mincielle, Z, Rougé, S, Cognet, P, Cabassud, M, 2014,  $\text{Ca}(\text{OH})_2/\text{CaO}$  reversible reaction in a fluidized bed reactor for thermochemical energy storage, *Solar Energy*, 107, 605-616.
- Paul, E, L, Atiemo-Obeng, V, A, Kresta, S, M, 2003, *handbook of industrial mixing: science and practice*, John Wiley and Sons, New Jersey, p.59.
- Wang, J, J, Han, Y, Gu, X, P, Feng, L, F, Hu, G, H, 2013, effect of agitation on the fluidization behavior of a gas-solid fluidized bed with a frame impeller. *AIChE J.* 59, 1066–1074.
- Zhang, Y, J, Wang, J, J, Gu, X, P, Feng, L, F, Wu, B, 2016, CFD simulation of an agitated gas-fluidized bed: effects of particle–particle restitution coefficient on the hydrodynamics, *Chem. Eng. Res. Des.*, 111, 353-361.

---

## #222: Synthesis and characterization of doped magnesium hydroxide for medium heat storage application

---

Nawaf ALBELADI<sup>1</sup>, Anti KUR<sup>2</sup>, Robert MOKAYA<sup>3</sup>, Jo DARKWA<sup>4</sup>, Sarah ROGER-LUND<sup>5</sup>, Mark WORALL<sup>6</sup>, John CALAUTIT<sup>7</sup>, Rabah BOUKHANOUF<sup>8</sup>

<sup>1</sup> School of Chemistry, University of Nottingham, United Kingdom, Nawaf.Albeladi@nottingham.ac.uk

<sup>2</sup> Department of Architecture and Built Environment, University of Nottingham, United Kingdom, Anti.Kur@nottingham.ac.uk

<sup>3</sup> School of Chemistry, University of Nottingham, United Kingdom, Robert.Mokaya@nottingham.ac.uk

<sup>4</sup> Department of Architecture and Built Environment, University of Nottingham, United Kingdom, Jo.Darkwa@nottingham.ac.uk <sup>5</sup> Department of Architecture and Built Environment, University of Nottingham, United Kingdom, enysr5@exmail.nottingham.ac.uk <sup>6</sup> Department of Architecture and Built Environment, University of Nottingham, United Kingdom, lazmw@exmail.nottingham.ac.uk

<sup>7</sup> Department of Architecture and Built Environment, University of Nottingham, United Kingdom, ezzjkc@exmail.nottingham.ac.uk

<sup>8</sup> Department of Architecture and Built Environment, University of Nottingham, United Kingdom, lazrb@exmail.nottingham.ac.uk

*Abstract: A vast amount of waste heat is generated annually from the industrial and power sectors, estimated at approximately 391 TWh, equivalent to about 35% more than the UK's total annual electricity demand. It is therefore imperative to utilize efficiently all possible waste heat sources which may be classified according to their temperatures as; low grade (ambient–250°C), medium grade (250–500°C), and high grade (> 500°C). With appropriate technologies, a large proportion of this waste energy could potentially be recovered for useful applications. In this context, thermal energy storage (TES) technologies provide the best opportunities to recover waste heat at various temperatures for long-term storage and application. The potential of thermochemical energy storage (TCES) materials such as magnesium hydroxide, Mg(OH)<sub>2</sub>, has been established but it has a relatively high dehydration temperature thus limiting its potential for medium-temperature heat storage applications that account for a vast proportion of industrial waste heat. To this end, samples of doped Mg(OH)<sub>2</sub> with varying proportions (5, 10, 15, and 20 wt%) of potassium nitrate (KNO<sub>3</sub>) have been developed and characterized for evaluation. The results showed that the doped Mg(OH)<sub>2</sub> sample with 5 wt% KNO<sub>3</sub> achieved the best outcome and was able to lower the dehydration temperature by about 23°C with an increase of 6% in the energy storage capacity. The results also showed good surface topology and thermal stability in the non-isothermal test conducted on the sample and therefore appear to have the potential for medium heat storage applications ranging from 293°C to 400°C.*

*Keywords: thermochemical energy storage, magnesium hydroxide, composite material, characterization, dehydration temperature*



## 1. INTRODUCTION

According to published climate data, over 34 billion tonnes of CO<sub>2</sub> are currently being emitted as against 22 billion in 1990 (Ritchie *et al.*, 2020). One of the main factors contributing to this CO<sub>2</sub> output is the energy consumption in buildings which is responsible for 40% of global energy consumption. For instance, UK buildings account for about 35% of final energy consumption and CO<sub>2</sub> emissions (Adams *et al.*, 2019). A greater part of this energy consumption is for hot water and space heating purposes (Watson *et al.*, 2019). Meanwhile, a vast amount of waste heat is generated annually from the industrial and power sectors and is estimated at approximately 391 TWh, which is 35% more than the UK's total annual electricity demand (Stevenson and Hyde, 2014). It is therefore imperative to utilize efficiently all possible waste heat sources which may be classified according to their temperatures as; low grade (ambient–250°C), medium grade (250–500°C), and high grade (> 500°C). With appropriate energy storage technologies, a large proportion of this waste energy could potentially be recovered for useful applications in the building sector. Thermochemical energy storage (TCES) in inorganic oxides has attracted growing research interest due to their relatively higher energy storage density, smaller storage volume, and long-term storage capabilities (Chen *et al.*, 2018). However, most past studies were focused on exploring low-temperature (below 200°C) (Hongois *et al.*, 2011; Jarimi *et al.*, 2019; Scapino *et al.*, 2017; Yu *et al.*, 2013; Zhang and Wang, 2020) and high-temperature (above 500°C) (André *et al.*, 2016; Felderhoff *et al.*, 2013; Pardo *et al.*, 2014; Sunku Prasad *et al.*, 2019; Wu *et al.*, 2018) storage materials thereby creating a gap in materials for medium-temperature range applications.

Magnesium hydroxide (Mg(OH)<sub>2</sub>) has been identified as a potential material for such medium-temperature applications, but its dehydration temperature would have to be modified to enable it to cover a wider range of medium-grade waste heat sources. Investigation carried out by Ryu *et al.*, (2008) did indicate that it should be possible to modify the dehydration temperature by doping it with nitrate salts. Shkatulov *et al.* (2014) therefore doped Mg(OH)<sub>2</sub> with sodium nitrate (NaNO<sub>3</sub>) and achieved a reduction of up to 50°C in the dehydration temperature. In another investigation, Shkatulov and Aristov (2018) doped Mg(OH)<sub>2</sub> with lithium nitrate (LiNO<sub>3</sub>) and obtained a reduction of 76°C in the dehydration temperature. Sun *et al.* (2019) obtained a reduction of 29°C with cerium nitrate (Ce(NO<sub>3</sub>)<sub>3</sub>) as a dopant. Li *et al.* (2019) was also able to reduce the dehydration temperature of Mg(OH)<sub>2</sub> by 56°C with a 10 wt% of LiNO<sub>3</sub>. However, in all these investigations the respective heat storage capacities were very much reduced. There is, therefore, the need to further explore other types of nitrate salts which could protect the energy storage integrity of Mg(OH)<sub>2</sub>. Potassium nitrate (KNO<sub>3</sub>) appears to be an appropriate dopant since it possesses higher ionic mobility as compared to other alkali metal ions (Yoshinari *et al.*, 2019). The higher mobility level could therefore facilitate the diffusion of protons (H<sup>+</sup>) and hydroxide ions (OH<sup>-</sup>) during the dehydration process thereby contributing to the acceleration and lowering of the dehydration temperature. This study is, therefore, intended to synthesize and characterize composite Mg(OH)<sub>2</sub>/KNO<sub>3</sub> as a potential thermochemical energy material for industrial heat decarbonization.

## 2. MATERIALS AND METHODS

### 2.1 Materials development

A total of 5 samples (1 pure Mg(OH)<sub>2</sub> + 4 composite Mg(OH)<sub>2</sub>/KNO<sub>3</sub>) each weighing 10 g, were prepared in proportions of 5%, 10%, 15%, and 20% of KNO<sub>3</sub>. The powders were initially ground together in an agate mortar for about 10 min to ensure a uniform mixture before thoroughly mixing them in a beaker with 20 ml of distilled water. They were then stirred continuously while being heated at 90°C for 1.5 hours and finally dried in an oven at 120°C for 12 hours.

### 2.2 Materials characterization

#### *Powder x-ray diffraction*

Powder X-ray diffraction (XRD) test provides information on structures, phases, crystal orientations (texture), and other structural parameters within materials. It was therefore carried out for phase identification of various elements within the composite samples. The test was conducted at room temperature using a PANalytical X'Pert PRO diffractometer with CuK $\alpha$  radiation ( $\lambda = 1.5406 \text{ \AA}$ , 40 kV, 40 mA), for values of 2-Theta and 0.02 step size, 50s step time in the range 2°–70°.

#### *Differential scanning calorimetry*

Differential scanning calorimetry (DSC) measurements were taken to estimate the heat storage and dehydration temperatures for the samples. By using a TA Thermal Instrument, a baseline measurement was taken in the range of 25°C to 550°C at a heating rate of 10°C/min on each sample weighing 5 mg. Nitrogen was used as the purge gas at a volumetric rate of 20 ml/min under 1 atm pressure.

#### *Thermogravimetry analysis*

Thermogravimetric analysis (TGA) was performed on each sample weighing 20 mg with a vacuum-tight thermomicrobalance SDT600, to determine their thermal characteristics. This was achieved by measuring the amount of weight changes in the samples as a function of increasing temperatures under nitrogen gas protection covering a heating range of 25 °C to 600 °C at a heating rate of 10°C/min.

### Brunauer-Emmett-Teller analysis

Brunauer–Emmett–Teller (BET) analysis was conducted to measure the surface areas of the samples and to assess how they would interact with their environment. These were obtained via nitrogen sorption isotherm by using a Micromeritics 3Flex analyzer at  $-196^{\circ}\text{C}$ . Prior to the analysis, the samples were degassed at  $100^{\circ}\text{C}$  for 16 hours under a vacuum. The specific surface areas were calculated using the BET method from the nitrogen adsorption data within the relative pressure ( $P/P_0$ ) range of 0.05–0.30. The total pore volume was estimated using total nitrogen adsorbed at relative pressure close to saturation ( $P/P_0 \sim 0.99$ ). The pore size distribution (PSD) was determined using non-local density functional theory (NL-DFT) applied to nitrogen isotherm data.

### Scanning electron microscopy

The surface images of the samples were taken to observe their structure. This was achieved by means of a JEOL 6490LV scanning electron microscope (SEM), operated in high vacuum mode at 15 kV, and with a secondary electron detector. The electron beam in the vacuum excites electrons from the surface to create different signals of the material's topology.

### Energy dispersive X-ray spectroscopy

The energy-dispersive X-ray spectroscopy (EDX) is an extended functionality of the JEOL 6490LV (SEM) instrument used to obtain information on the chemical composition of the samples. To do this, the material was irradiated with a high-energy beam to stimulate X-ray emission. The characteristic of the emitted radiation was then compared to the atomic energy of the matched element. During the measurement, two different areas were sampled to assess the atomic weight distribution, and the corresponding peaks were obtained.

## 3. RESULTS AND DISCUSSION

### 3.1 Powder XRD

The XRD diffractograms for the pure and doped  $\text{Mg}(\text{OH})_2$  samples are shown in Figure 1. It can be seen that  $\text{Mg}(\text{OH})_2$  showed only a single phase (peak) whereas the doped composites showed two distinct peaks. The intensity of the peaks increased with an increase in the dopants' proportion. The highlighted areas show the peak positions of the  $\text{KNO}_3$ . Since the phases of both  $\text{Mg}(\text{OH})_2$  and  $\text{KNO}_3$  were clearly detected as intended, this confirms that the doping process was successful.

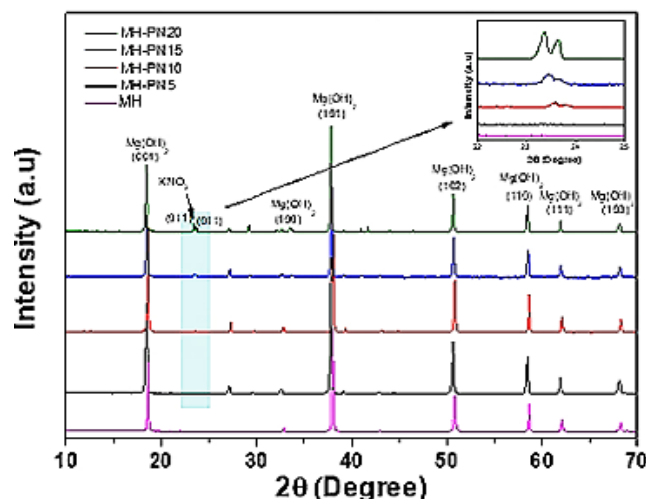


Figure 1 Powder XRD patterns for pure and doped  $\text{Mg}(\text{OH})_2$

### 3.2. DSC

The DSC overlay curves for pure and doped  $\text{Mg}(\text{OH})_2$  samples are shown in Figure 2, and the results are summarised in Table 1 showing the respective energy storage densities and the onset temperatures at which dehydration started. It can be clearly seen that the sample MH-PN5 with 5 wt%  $\text{KNO}_3$  achieved the lowest onset or dehydration temperature of  $293.82^{\circ}\text{C}$  which is about  $23^{\circ}\text{C}$  less than the dehydration temperature of pure  $\text{Mg}(\text{OH})_2$ . It also recorded the highest energy content of  $1317.90\text{ J/g}$  which is also about 6% higher than  $\text{Mg}(\text{OH})_2$ . Minute peaks were however observed at  $132^{\circ}\text{C}$  with progressing troughs as the dopant ratio increased beyond 10 wt%. A similar observation was reported in the literature and was attributed to the fusion of crystalline  $\text{KNO}_3$  around  $334^{\circ}\text{C}$  (Shkatulov and Aristov, 2017).

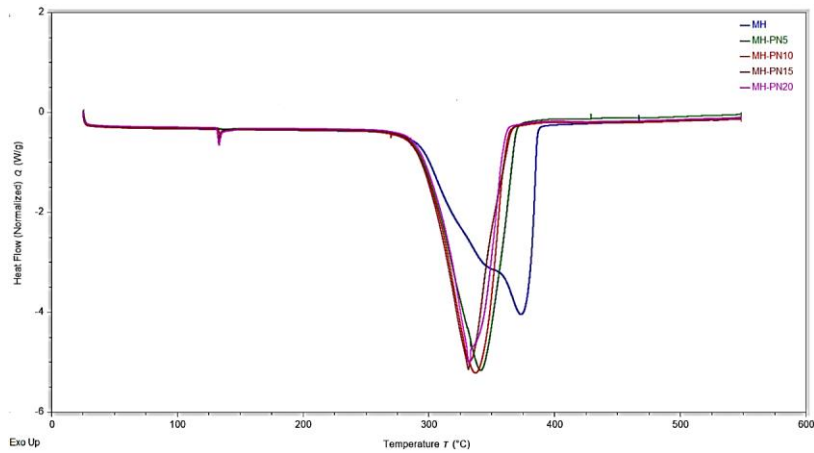


Figure 2 DSC overlay curves of pure and doped  $Mg(OH)_2$  samples

Table 1: The onset temperatures and heat storage densities of the pure and doped  $Mg(OH)_2$

Material	Onset temperature (°C)	Heat content (J/g)
MH	317.03	1246.40
MH-PN5	293.88	1317.10
MH-PN10	297.82	1171.60
MH-PN15	296.47	1103.40
MH-PN20	308.20	1044.00

### 3.3. TGA

The TGA overlay curves for pure and doped  $Mg(OH)_2$  samples are shown in Figure 3, while the summary of the results is presented in Table 2. For pure  $Mg(OH)_2$ , the weight loss at 295.25°C is 28.79% and for the composites, their thermal stabilities are closely related to that of pure material. For instance, the average difference in weight loss is around 4% whilst the average difference in onset temperature is ~3°C. These marginal differences suggest that the thermal integrity of the pure material is preserved even with the addition of  $KNO_3$ . Specifically, the MH-PN5 composite has a weight loss of 28.80% compared to 28.79% for pure material, MH.

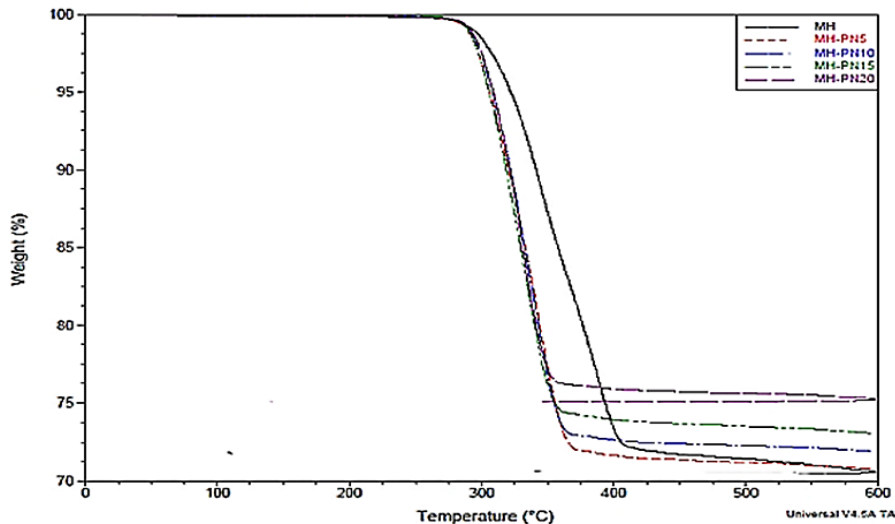


Figure 3 TGA overlay curves for the pure and doped  $Mg(OH)_2$

Table 2: TG onset temperatures and weight loss in the pure and doped Mg(OH)<sub>2</sub>

Material	Onset temperature (°C)	Weight loss (%)
MH	295.25	28.79
MH-PN5	291.65	28.80
MH-PN10	293.56	27.73
MH-PN15	292.00	26.56
MH-PN20	293.69	24.82

The overall analysis of the DSC/TGA results showed that sample MH-PN5, which represents Mg(OH)<sub>2</sub> with 5 wt% KNO<sub>3</sub> addition, is the only composite that could reduce the dehydration temperature as well as increase the energy storage capacity of the pure Mg(OH)<sub>2</sub>, whilst maintaining good thermal integrity. Therefore, further physical characterizations of the MH-PN5 composite were done.

### 3.4. BET analysis of MH-PN5

The BET surface area ( $S_{BET}$ ) of the pure (MH) and 5 wt% KNO<sub>3</sub>-doped (MH-PN5) samples are presented in Table 3. It showed pure hydroxide with a high  $S_{BET}$  value of 250 m<sup>2</sup>/g and the MH-PN5 composite with a value of 6 m<sup>2</sup>/g. The BET result for the doped sample (MH-PN5) showed a dramatic reduction in its surface area compared with the pure MH sample. This could be attributed to the pore-plugging effect of the dopant leading to the decline in porosity. In Figure 4, the nitrogen adsorption profile for pure MH appears as a type IV isotherm indicating some level of mesoporosity. However, the doped sample did appear as type III isotherms.

Table 3: BET surface areas of the samples

Sample	$S_{BET}$ (m <sup>2</sup> /g)
MH	250
MH-PN5	6

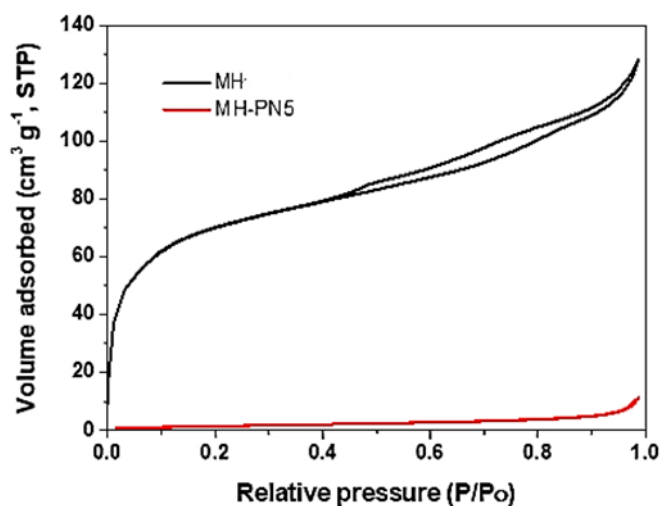


Figure 4 Adsorption isotherms for pure MH and MH-PN5 composite

### 3.5. PSD analysis of MH-PN5

The wide disparity in the  $S_{BET}$  values of samples was further investigated by comparing their pore size distribution (PSD) with and without doping. The PSD curves for the pure MH and the doped (MH-PN5) materials are shown in Figure 5. The curves show that MH contains some microporosity with pore sizes less than 2 nm and large mesoporosity with pore sizes between 2 and 40 nm. Thus, the dramatic reduction in the surface area is due to the dopant's pore-clogging effect, especially at the micropores as they become inaccessible to the probe molecule (N<sub>2</sub>) during adsorption. As can be seen in Figure 5, pores smaller than 20 nm are present in the MH but significantly reduced after doping. This could impede the

sorption capacity of this material since sorption depends on the degree of porosity, surface area, and pore volume (Daud *et al.*, 2016).

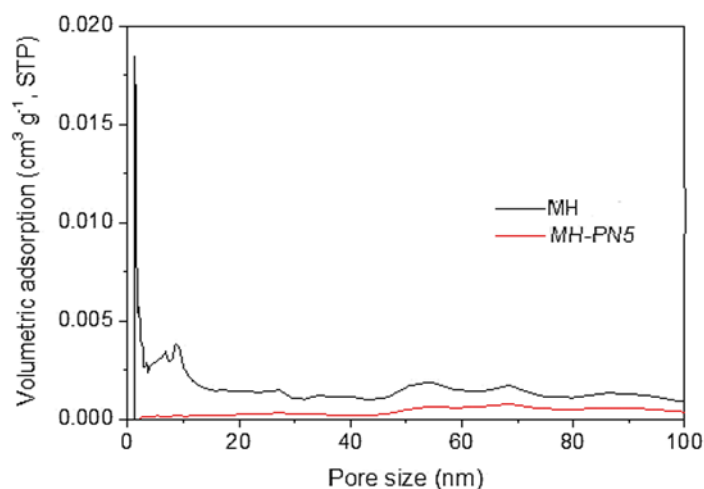


Figure 5 PSD for pure MH and MH-PN5 composite

### 3.6. SEM analysis of MH-PN5

The SEM image of the pure  $\text{Mg}(\text{OH})_2$  (MH) is shown in Figure 6 (a). This material had a fluffy or spongy morphology with closely arranged particles. This spongy texture is suggestive of a large surface area as adequately supported by the  $S_{\text{BET}}$  value of  $250 \text{ m}^2/\text{g}$ . This would have the advantage of adequate heat adsorption capacity. The addition of 5 wt%  $\text{KNO}_3$  (MH-PN5) results in monodisperse quartzite-shaped grains (Figure 6 (b)). The monodisperse is an indication that the constituent atoms are uniformly distributed in the material. However, the micropore spaces are fairly close which explains the low  $S_{\text{BET}}$  value that could negatively impact the heat adsorption capacity of the composite material.

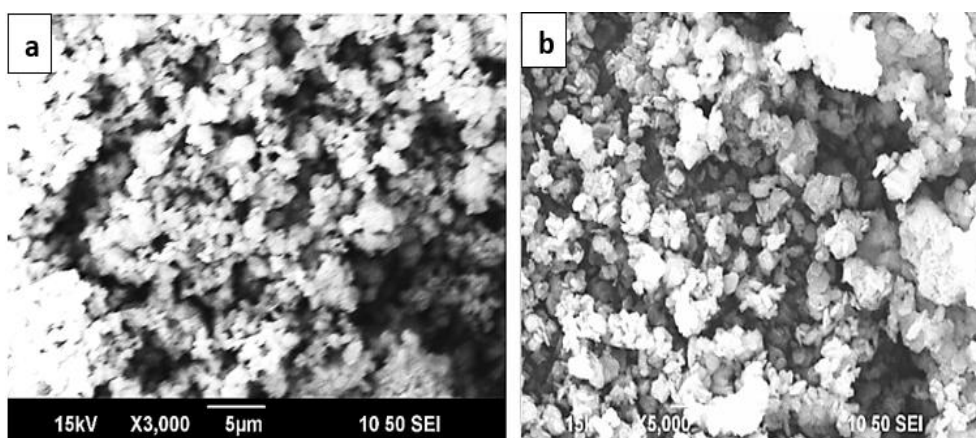


Figure 6 SEM images for (a) pure MH and (b) MH-PN5 composite

### 3.7. EDX analysis of MH-PN5

Figure 7 shows the EDX spectra for the MH-PN5 composite, consisting of quantitative data at each sampled point; spots 1 and 2. The EDX of the elemental compositions of Mg, O, and K have values of 39.72, 60.08, and 0.20% at sampled spot 1, and 39.95, 59.89, and 0.16% at spot 2 showing consistency (approximately the same values) in the sampled areas. These correspond to atomic weights of 49.92, 49.68, and 0.40% at spot 1, and 50.17, 49.50, and 0.33% at spot 2 for Mg, O, and K respectively. The nitrogen (N) element was not detected as is sometimes the case with small quantities of light atoms. The very small standard deviation values of 0.16, 0.13, and 0.03 for Mg, O, and K respectively are indicative of the uniform atomic weight distribution in the material. Thus, the EDX supports the monodisperse SEM topographic information about this composite material.



Figure 7 EDX spectra and data for the MH-PN5 composite

#### 4. CONCLUSION

This work was aimed at doping  $\text{Mg}(\text{OH})_2$  with  $\text{KNO}_3$  for medium-temperature heat storage application. The XRD results showed clear traces of the core materials and the doping agent thus confirming the success of the synthesis. The DSC/TGA results revealed that 5 wt%  $\text{KNO}_3$  had a more positive impact on the  $\text{Mg}(\text{OH})_2$  in terms of reduction in dehydration temperature, heat storage enhancement, and thermal stability and therefore found to possess the highest potential for heat storage within the medium-temperature range of 293–400°C. However, the BET test conducted on the MH-PN5 sample showed a reduction in the surface area and porosity which was attributed to the dopant's pore-plugging effect. Analysis of the SEM results also showed that the micropore spaces were fairly close and could therefore have a negative impact on the heat adsorption capacity of the composite material. The EDX results also supported the monodisperse topographic structure shown in the SEM. Despite the negative physical adsorption characteristics, the study has established sample MH-PN5 as a promising candidate for wide-range temperature medium-heat storage.

#### 5. REFERENCES

- Adams, M., Burrows, V. and Richardson, S. (2019), "Bringing embodied carbon upfront", *World Green Building Council*, September, available at: [https://worldgbc.s3.eu-west-2.amazonaws.com/wp-content/uploads/2022/09/22123951/WorldGBC\\_Bringing\\_Embodied\\_Carbon\\_Upfront.pdf](https://worldgbc.s3.eu-west-2.amazonaws.com/wp-content/uploads/2022/09/22123951/WorldGBC_Bringing_Embodied_Carbon_Upfront.pdf) (accessed 20 February 2023).
- André, L., Abanades, S. and Flamant, G. (2016), "Screening of thermochemical systems based on solid-gas reversible reactions for high temperature solar thermal energy storage", *Renewable and Sustainable Energy Reviews*, Elsevier Ltd, 1 October, doi: 10.1016/j.rser.2016.06.043.
- Chen, X., Zhang, Z., Qi, C., Ling, X. and Peng, H. (2018), "State of the art on the high-temperature thermochemical energy storage systems", *Energy Conversion and Management*, Elsevier Ltd, 1 December, doi: 10.1016/j.enconman.2018.10.011.
- Daud, F.D.M., Vignesh, K., Sreekantan, S. and Mohamed, A.R. (2016), "Improved  $\text{CO}_2$  adsorption capacity and cyclic stability of  $\text{CaO}$  sorbents incorporated with  $\text{MgO}$ ", *New Journal of Chemistry*, Vol. 40 No. 1, doi: 10.1039/c5nj02081f.
- Felderhoff, M., Urbanczyk, R. and Peil, S. (2013), "Thermochemical heat storage for high temperature applications-A review", *Green*, Walter de Gruyter GmbH, doi: 10.1515/green-2013-0011.
- Hongois, S., Kuznik, F., Stevens, P. and Roux, J.J. (2011), "Development and characterisation of a new  $\text{MgSO}_4$ -zeolite composite for long-term thermal energy storage", *Solar Energy Materials and Solar Cells*, Vol. 95 No. 7, pp. 1831–1837, doi: 10.1016/j.solmat.2011.01.050.
- Jarimi, H., Aydin, D., Yanan, Z., Ozankaya, G., Chen, X. and Riffat, S. (2019), "Review on the recent progress of thermochemical materials and processes for solar thermal energy storage and industrial waste heat recovery", *International Journal of Low-Carbon Technologies*, Oxford University Press, 22 January, doi: 10.1093/ijlct/cty052.
- Pardo, P., Deydier, A., Anxionnaz-Minvielle, Z., Rougé, S., Cabassud, M. and Cognet, P. (2014), "A review on high temperature thermochemical heat energy storage", *Renewable and Sustainable Energy Reviews*, April, doi: 10.1016/j.rser.2013.12.014.

- Piperopoulos, E., Fazio, M., Mastronardo, E., Lanza, M. and Milone, C. (2021), "Tuning Mg(OH)<sub>2</sub> structural, physical, and morphological characteristics for its optimal behavior in a thermochemical heat-storage application", *Materials*, MDPI AG, Vol. 14 No. 5, pp. 1–19, doi: 10.3390/ma14051091.
- Ritchie, H., Roser, M. and Rosado, P. (2020), "CO<sub>2</sub> and greenhouse gas emissions", *OurWorldInData.Org*, available at: [ourworldindata.org/co2-and-greenhouse-gas-emissions](https://ourworldindata.org/co2-and-greenhouse-gas-emissions) (accessed 20 February 2023).
- Ryu, J., Hirao, N., Takahashi, R. and Kato, Y. (2008), "Dehydration behavior of metal-salt-added magnesium hydroxide as chemical heat storage media", *Chemistry Letters*, Vol. 37 No. 11, pp. 1140–1141, doi: 10.1246/cl.2008.1140.
- Scapino, L., Zondag, H.A., van Bael, J., Diriken, J. and Rindt, C.C.M. (2017), "Sorption heat storage for long-term low-temperature applications: A review on the advancements at material and prototype scale", *Applied Energy*, Elsevier Ltd, doi: 10.1016/j.apenergy.2016.12.148.
- Shkatulov, A. and Aristov, Y. (2015), "Modification of magnesium and calcium hydroxides with salts: An efficient way to advanced materials for storage of middle-temperature heat", *Energy*, Elsevier Ltd, Vol. 85, pp. 667–676, doi: 10.1016/j.energy.2015.04.004.
- Shkatulov, A. and Aristov, Y. (2017), "Calcium hydroxide doped by KNO<sub>3</sub> as a promising candidate for thermochemical storage of solar heat", *RSC Advances*, Royal Society of Chemistry, Vol. 7 No. 68, pp. 42929–42939, doi: 10.1039/c7ra06639b.
- Shkatulov, A., Krieger, T., Zaikovskii, V., Chesalov, Y. and Aristov, Y. (2014), "Doping magnesium hydroxide with sodium nitrate: A new approach to tune the dehydration reactivity of heat-storage materials", *ACS Applied Materials and Interfaces*, American Chemical Society, Vol. 6 No. 22, pp. 19966–19977, doi: 10.1021/am505418z.
- Shkatulov, A.I. and Aristov, Y. (2018), "Thermochemical energy storage using LiNO<sub>3</sub>-doped Mg(OH)<sub>2</sub>: A dehydration study", *Energy Technology*, Wiley-VCH Verlag, Vol. 6 No. 9, pp. 1844–1851, doi: 10.1002/ente.201800050.
- Stevenson, P. and Hyde, R. (2014), "The potential for recovering and using surplus heat from industry", *Element Energy*, available at: [https://assets.publishing.service.gov.uk/government/uploads/system/uploads/attachment\\_data/file/294900/element\\_energy\\_et\\_al\\_potential\\_for\\_recovering\\_and\\_using\\_surplus\\_heat\\_from\\_industry.pdf](https://assets.publishing.service.gov.uk/government/uploads/system/uploads/attachment_data/file/294900/element_energy_et_al_potential_for_recovering_and_using_surplus_heat_from_industry.pdf) (accessed 20 February 2023).
- Sun, L., Wu, Q., Zhang, L., Li, Y., Li, M., Gao, T., Guo, S., *et al.* (2019), "Doping magnesium hydroxide with Ce(NO<sub>3</sub>)<sub>3</sub>: A promising candidate thermochemical energy storage materials", *IOP Conference Series: Earth and Environmental Science*, Vol. 295, Institute of Physics Publishing, doi: 10.1088/1755-1315/295/3/032068.
- Sunku Prasad, J., Muthukumar, P., Desai, F., Basu, D.N. and Rahman, M.M. (2019), "A critical review of high-temperature reversible thermochemical energy storage systems", *Applied Energy*, Elsevier Ltd, 15 November, doi: 10.1016/j.apenergy.2019.113733.
- Watson, S.D., Lomas, K.J. and Buswell, R.A. (2019), "Decarbonising domestic heating: What is the peak GB demand?", *Energy Policy*, Elsevier Ltd, Vol. 126, pp. 533–544, doi: 10.1016/j.enpol.2018.11.001.
- Wu, S., Zhou, C., Doroodchi, E., Nellore, R. and Moghtaderi, B. (2018), "A review on high-temperature thermochemical energy storage based on metal oxides redox cycle", *Energy Conversion and Management*, Elsevier Ltd, 15 July, doi: 10.1016/j.enconman.2018.05.017.
- Yu, N., Wang, R.Z. and Wang, L.W. (2013), "Sorption thermal storage for solar energy", *Progress in Energy and Combustion Science*, doi: 10.1016/j.pecs.2013.05.004.
- Zhang, Y. and Wang, R. (2020), "Sorption thermal energy storage: Concept, process, applications and perspectives", *Energy Storage Materials*, Elsevier B.V., 1 May, doi: 10.1016/j.ensm.2020.02.024.



---

## #223: Fifth generation district heating and cooling network coupled with geothermal energy source for a sustainable community: Case study of Embassy of Sharing at Malmö

---

Nischal CHAULAGAIN<sup>1</sup>, Ulla JANSON<sup>2</sup>, Saqib JAVED<sup>3</sup>

*1 Division of Building Services, Lund University, Sweden, nischal.chaulagain@hvac.lth.se*

*2 Division of Building Services, Lund University, Sweden, ulla.janson@hvac.lth.se*

*3 Division of Building Services, Lund University, Sweden, saqib.javed@hvac.lth.se*

*Abstract: With growing urbanization and increase in energy demand for space heating and cooling in buildings, reliability, security, distribution of energy and its efficient end use is of utmost importance particularly when emissions from energy use and indoor thermal comfort of the end users is of question. Numerous solutions have been put forth in the field of effective distribution of thermal energy to meet the space heating and cooling requirements of buildings to assure indoor comfort of which fifth generation district heating and cooling (5GDHC) is regarded as a viable solution in terms of low emissions, low distribution losses and effective energy supply. The challenges however lie in connecting the buildings in the network to facilitate the energy sharing between the buildings such that otherwise waste heat from one of the buildings can be used by another building connected to the same network. This paper presents the concept and design of such advanced 5GDHC network which facilitates energy sharing between connected buildings comprising of office spaces, residential complex, shopping centre and other occupying 61,901 square meters in Hyllie region of Malmö, Sweden. The system design consists of a bi-directional two pipe network with a local bore field consisting of 103 bore hole heat exchangers as the primary energy source for the network with heat pumps and dedicated direct cooling heat exchangers to alter the temperature of district heating and cooling fluid going into the buildings. The system as such is self-sufficient and requires electricity only to run the heat pumps and auxiliary control systems to meet the thermal demands of the connected buildings.*

*Keywords: 5GDHC, Geothermal, low-temperature network, sharing, sustainability*

## 1. INTRODUCTION

Thermal comfort is one of the basic human needs for a healthy lifestyle and productivity (Bueno et al., 2021; McCartney and Humphreys, 2002) and since an average human spends almost 90 % of time in indoor settings (Iii and Lan, 2011), globally, huge amount of energy is thus spent to maintain a thermally comfortable indoor environment (Mastrucci et al., 2021). These energies are accounted as energy use for heating and cooling of buildings.

The international Energy Agency (IEA) has reported that energy demand for space heating and domestic hot water usage in buildings accounts for approximately 50 % of the total energy use in buildings, 60 % of which comes from the fossil fuels-based energy sources (International Energy Agency, 2022). In Europe alone, fossil fuels-based energy sources contribute to almost 75 % of the total heating and cooling demands (Martinazzoli et al., 2023). The energy use for district heating and electricity in the residential buildings in Sweden was 44 TWh and 70 TWh respectively in the year 2020 which together comprises almost 80 % of the total energy demand in the residential sector, both of which being primarily used for space heating (Swedish Energy Agency, 2022). Amidst the growing urbanization and signs of severe climate change effects, these figures reportedly will increase sharply in near future, which has also been shown in the projection of the IEA stating that the space cooling will be tripled by 2050 owing to anthropogenic and environmental factors (Abugabbara et al., 2022; International Energy Agency, 2023). A smart, energy-efficient, and a sustainable energy supply solution is thus necessary to cope with this issue and ensure that thermal demands of the buildings are met without comprising the comfort of the occupants.

In that context, district heating and cooling systems has always been viewed as a sustainable energy supply solution for meeting the thermal demands of buildings in Europe and other western countries (Abugabbara et al., 2022; Martinazzoli et al., 2023). District heating and cooling systems has been implemented for over a century now leading to various developments and modifications in its supply systems, technology and materials, heat carrier fluids and working conditions in overall. This has led to the realization of the current fifth generation district heating and cooling systems (5GDHC) which is capable of providing both heating and cooling via the same pipe network and allows for integration of wide range of controls, energy mix and possibilities for energy sharing between connected buildings (Abugabbara et al., 2022; Lindhe et al., 2022; Sorknæs et al., 2020).

This paper describes the design and application of such an advanced 5GDHC system being built at Malmö, Sweden which integrates the onsite bore field with 103 Borehole Heat exchangers (BHEs) as its primary source of energy assisted with heat pumps at each building level to provide comfort heating and cooling to approximately 61,901 m<sup>2</sup> of space area comprising of office spaces, residential buildings, retail stores, and entertainment spaces. The network further facilitates energy sharing between these connected buildings via its bidirectional Geo-Energy Sharing Systems (GESS) to realise an independent and sustainable community colloquially termed as the “Embassy of Sharing”.

### 1.1. Embassy of Sharing

Driven by the vision of the “neighborhood of the future”, Embassy of Sharing is an ongoing urban planning project developed by Granitor Properties at Hyllie in Malmö, Sweden that encourages collaboration, sharing of spaces and energy between the buildings. The main aim is to create a sustainable community with a low carbon footprint, and that requires minimal use of purchased energy for its operation. The community houses seven unique buildings, hereafter referred to as Sub-Centrals (UC), comprising of the tallest wooden office building, residential apartments, cafes, restaurants, showrooms, co-working spaces, and others. In terms of thermal aspect of the community, each UC has its own unique energy demand profiles because of its dynamic and diverse use functions and building technology. The main concept is thus to utilize this diversity to facilitate energy sharing between these UCs via the GESS whereby, otherwise lost/excess heat/cooling, from one of the UC is utilized to provide heating/cooling to another UC in network thereby reducing the net active energy requirement.

Table 1: Representation of Sub-Central's energy demand and primary energy source specification in the form of Borehole heat exchanger depth

Sub-Central (UC)	Building Name	Peak energy demands (kW)		Borehole heat exchangers	
		Heating	Cooling	Numbers	Depth (meters)
UC 1	Fyrtornet and Drivbänken	500	600	30	9,000
UC 2	Levnadskonstnären	385	291	18	5,400
UC 3	Droppen	235	NA	12	3,600
UC 4	Skogslunden	285	NA	15	4,500
UC 5	Pinnen	187	NA	10	3,000
UC 6	Fabriken and Basaren	210	311	18	5,400

Table 1 shows the peak energy demands and the specification for the dedicated primary energy source i.e., BHEs for each sub-central. With a total of approximately 31,000 meters of single U-tube borehole heat exchanges, the six UCs are self-

reliant on their BHEs to meet its thermal energy requirements. Furthermore, since all UCs are connected to the GESS systems, each sub-central can also make use of BHEs of the other connected sub-centrals to extract or dump heat via the GESS system. The methodology on how the sharing is achieved is discussed in section 2 of this paper.

## 2. MATERIALS AND METHODS

This section of the article describes the concept behind energy sharing between connected buildings and how it is aimed to be realized in Embassy of Sharing.

The primary energy source is a shallow geothermal system in the form of series of single U-Tube BHE. The BHEs are connected to the Sub-central which houses a local heating/cooling setup comprising of heat pumps, circulation pumps, radiators, piping connections and associated controls. The BHEs are further connected to the GESS which is characterized by a closed loop two pipe network acting as an energy sharing vessel and fluid transport media for the connected sub-centrals.

The GESS which carries brine with 25 % by volume bioethanol has a year-round free-floating temperature ranging from 6°C to 30°C close to the ambient conditions. Apart from the scenarios where free cooling is possible from this low temperature fluid by directly supplying through a heat exchanger, heat pumps installed at the sub-centrals are activated to meet the thermal demands for both heating and cooling by altering the fluid temperature on the demand side of the sub-centrals. The low temperature heat from the BHEs can be fed either directly to the sub-central or re-directed towards the GESS to facilitate sharing with other sub-centrals.

Sub-centrals with heating demand will draw the heat either from its dedicated bore field or the GESS depending on the temperature of the fluid (whichever is greater) coming from these sources. The returning low temperature fluid either passes through the bore field, facilitating recovery of bore field and used again in the heating loop or dumped to the GESS where after sub-centrals with cooling demand is benefitted. In another working scenario, where the sub-centrals have a cooling demand, the returning high temperature fluid from the sub-central is again either passed through the boreholes to replenish the geothermal source or supplied to the GESS to be used by other sub-centrals running in heating mode. This process establishes each sub-centrals to act as a prosumer (i.e., both consumer and producer) of heat depending on its use function and outdoor environmental conditions.

The amount of energy available for sharing depends on the thermal needs of the sub-centrals. The sharing is maximized when one of the sub-centrals has cooling demand and the other has a heating demand. In all other modes of operation, the flow is prioritized to be regulated only between its dedicated BHEs and the sub-central.

## 3. RESULT AND DISCUSSION

This section describes the 5GDHC network with its associated system components, controls and working mechanism opted to realize energy sharing at the Embassy of Sharing.

### 3.1. System Design

Figure 1 shows the schematic layout of the 5GDHC network of Embassy of Sharing. The central loop is a 180 mm diameter high density Polyethylene (PE) pipe network connected to the expansion tanks which together resembles the overall mixing reservoir facilitating energy and flow exchange between the UCs. Each UC is equipped with dedicated BHEs as indicated in Table 1 and Figure 1.

Each building icon here represent a sub-central in the network. The corresponding notation used for the identification of sub-central and the numbers of dedicated BHEs for each sub-central are indicated in Figure 1. The two branch connections between the central loop and the sub-central which essentially represents the supply and return to and from the sub-central respectively is based on stainless steel pipes of variable dimensions for each UC depending on its thermal demand profile. For example, for UC 1, this branch connections to the sub-central is made of two Stainless Steel pipes of 168 mm diameter each. Similarly, the same for UC 3 is of 114 mm diameter.

Figure 2 represents the overall control system that regulates the flow between the central loop i.e., the GESS, BHEs in each UC and the sub-central itself. The control system is essentially placed before the local heat pumps units of the sub-centrals and the GESS. It is noteworthy to point out that the central loop or GESS is devoid of any centralized pumping unit and rather each UC is equipped with its own circulation pump that regulates the overall flow. Furthermore, the overall flow between the UC, BHE and the GESS is regulated by a combination of control valves represented as Val\_BHret, Val\_Bypass and the Three-way valve in Figure 2. These valves are regulated by the control signals which essentially depends on the feedback from the temperature's sensors as shown in the figure. Here, as the name suggests, the temperature sensors TSupp\_GESS measures fluid temperature at the supply side of the GESS. Similarly, TSupp\_DSS

records the actual fluid temperature that goes into the evaporator of heat pumps in the sub-central. Tret\_DSS shows the temperature of fluid returning from the heat pumps in the sub-central. And finally, TSupp\_BH represents the fluid temperature at the supply side of the borehole heat exchangers.

The controller shown in Figure 2 is essentially an electronic unit that sends the signals to open and close the valves depending on the pre-defined control logics based on the readings of the temperature sensors and operating mode (heating and cooling) of the sub-central.

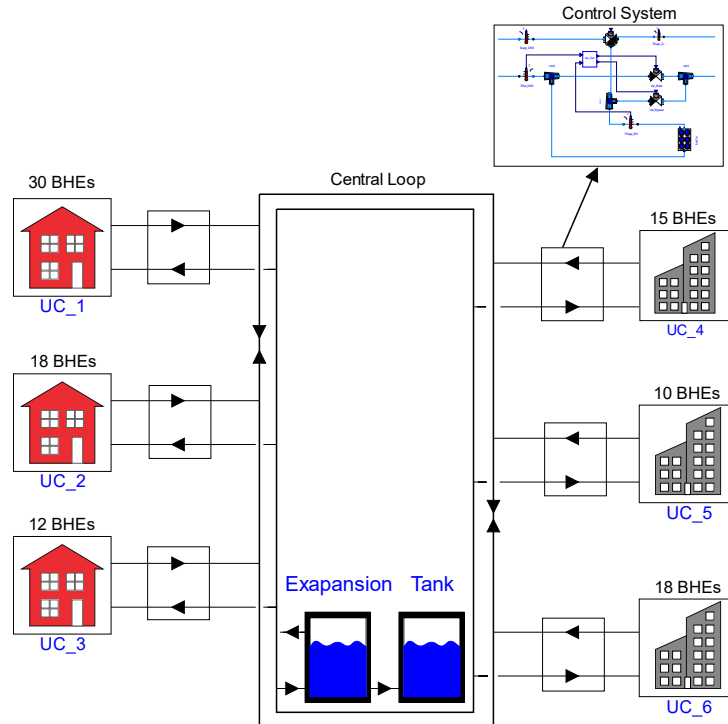


Figure 1 5GHDC network plan of Embassy of Sharing

To highlight on how the overall system is working at any instant, an example is presented as follows. When a subcentral has a heating demand, the flow to the building is regulated either from the GESS or the bore field via the three-way valve depending on the temperature readings at the temperature sensors TSupp\_GESS and TSupp\_BH. If the supply temperature from borehole is higher than that from the GESS, the flow is prioritized in the direction of B to AB (i.e., from the borehole field to the sub-central) in the three-way valve which continues until when TSupp\_GESS becomes higher than TSupp\_BH whereafter the flow is prioritized in the direction of A to AB (i.e., from the GESS to the sub-central) The returning fluid from the sub-central which is at lower temperature is then either sent back through the borehole loop for core replenishment or to the GESS where buildings with cooling demand is then able to use low temperature fluid from central loop.

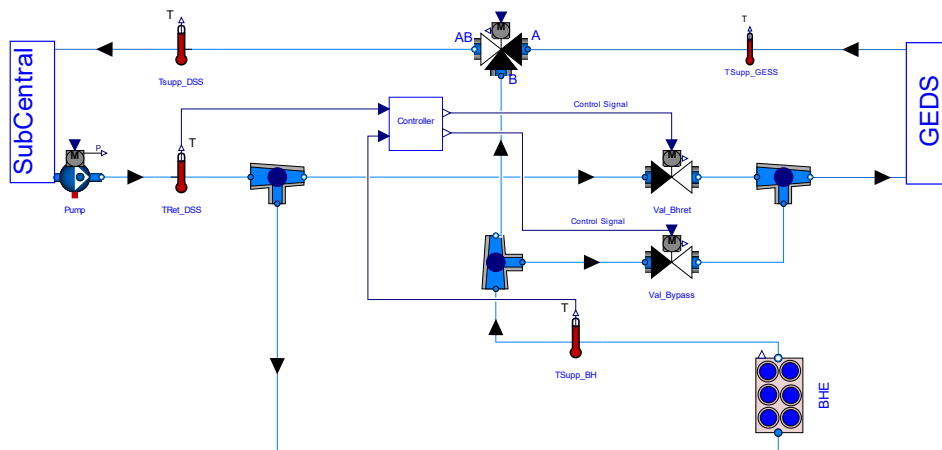


Figure 2 Control System depicting the flow interactions between the boreholes, sub-centrals and the GESS.

When the sub-central has a cooling demand, the flow is prioritized from B to AB in the three-way valve until TSupp\_BH is less than the TSupp\_GESS and from A to AB when the reverse scenario of temperature readings are realised. The main driving idea in the cooling mode is to receive as low temperature fluid as possible in the sub-central to facilitate free cooling through heat exchangers placed at the sub-central. When the potential for free cooling ceases to exist, active cooling is then initiated through the heat pumps whereby the outgoing high temperature fluid is returned through the boreholes for source replenishment and to the GESS where other UCs working in the heating demand mode gets to utilize this excess heat.

Here, UCs with both heating and cooling demands will both use and supply heating/cooling to the GESS while UCs with no cooling demand is either self-sufficient on their dedicated BHEs or requires heat from the GESS but does not have much to offer when it comes to energy sharing for net heating demand. It is evident from Table 1 that, UC 3, UC 4, and UC 5 does not have cooling demand thus is designed to not take part in energy sharing when there is net requirement of heat in the central loop. However, when UC 1, UC 2 and UC 6 are running on cooling mode, the excess heat dumped from these sub-centrals can be utilized by the UC 3, UC 4 and UC 6 depending on its thermal needs. However, the central connection to the GESS facilitates each individual UCs to make use of the BHEs of other UCs as well, which is regulated by a three-way valve control mechanism placed in each Sub-Central.

#### **4. CONCLUSION**

The article has presented a design concept for utilization of a shallow geothermal energy source in the form of borehole heat exchangers coupled in a fifth-generation district heating and cooling network with local heat pumps to meet the total thermal energy demand of a proposed community in Malmö, Sweden. The paper has further described the potential for energy sharing between buildings during their heating and cooling operations with use of flow control logics based on the temperature sensor's reading at multiple inlet and outlet positions in the network. The dual pipe central loop network with year-round free-floating temperature close to ambient conditions offers to meet both the heating and cooling needs of buildings through the same network with low distribution losses thus contributing to lower active energy requirements for the building's heating and cooling needs.

In the face of growing urbanization and climate change effects where the earth's atmosphere is rising leading to increasing cooling demands and consequently the global CO<sub>2</sub> emissions due to the higher energy requirements for heating and cooling of buildings, fifth generation district heating and cooling systems based on onsite geothermal energy production as presented in this article can offer a viable solution in terms of both energy sustainability and reduction in global GHG emissions.

#### **5. ACKNOWLEDGEMENT**

This study was financially supported by the Swedish Energy Agency under the project title "Energy Sharing within the Embassy of Sharing, Malmö- system, function and comfort".

#### **6. REFERENCES**

- Abugabbara, M., Javed, S., Johansson, D., 2022. A simulation model for the design and analysis of district systems with simultaneous heating and cooling demands. *Energy* 261, 125245. <https://doi.org/10.1016/j.energy.2022.125245>
- Bueno, A.M., de Paula Xavier, A.A., Broday, E.E., 2021. Evaluating the Connection between Thermal Comfort and Productivity in Buildings: A Systematic Literature Review. *Buildings* 11, 244. <https://doi.org/10.3390/buildings11060244>
- lii, H.H., Lan, Q., 2011. Indoor Air Pollution Attributed to Solid Fuel Use for Heating and Cooking and Cancer Risk.
- International Energy Agency, 2023. Space Cooling - Analysis and key findings. A report by the International Energy Agency. Available at: <https://www.iea.org/reports/space-cooling> (accessed 6.13.23).
- International Energy Agency, 2022. Heating - Analysis and key findings. A report by the International Energy Agency Available at: <https://www.iea.org/reports/heating>
- Lindhe, J., Javed, S., Johansson, D., Bagge, H., 2022. A review of the current status and development of 5GDHC and characterization of a novel shared energy system. *Sci. Technol. Built Environ.* 28, 595–609. <https://doi.org/10.1080/23744731.2022.2057111>

Martinazzoli, G., Pasinelli, D., Lezzi, A.M., Pilotelli, M., 2023. Design of a 5th Generation District Heating Substation Prototype for a Real Case Study. *Sustainability* 15, 2972. <https://doi.org/10.3390/su15042972>

Mastrucci, A., van Ruijven, B., Byers, E., Poblete-Cazenave, M., Pachauri, S., 2021. Global scenarios of residential heating and cooling energy demand and CO2 emissions. *Clim. Change* 168, 14. <https://doi.org/10.1007/s10584-021-03229-3>

McCartney, K., Humphreys, M., 2002. Thermal comfort and productivity. *Indoor Air*.

Sorknæs, P., Østergaard, P.A., Thellufsen, J.Z., Lund, H., Nielsen, S., Djørup, S., Sperling, K., 2020. The benefits of 4th generation district heating in a 100% renewable energy system. *Energy* 213, 119030. <https://doi.org/10.1016/j.energy.2020.119030>

Swedish Energy Agency, 2022. Energy in Sweden 2022 An Overview. Swedish Energy Agency.

---

# #232: Field monitoring of indoor air temperature of 3D-printed house in the hot climate of Saudi Arabia

## A case study of the 3D Studio 2030 in Riyadh

---

Khalid MIRZA<sup>1</sup>, Mohamed GADI<sup>2</sup>

<sup>1</sup> PhD candidate, Department of Architecture and Built Environment, University of Nottingham, Nottingham, [khalid.mirza@nottingham.ac.uk](mailto:khalid.mirza@nottingham.ac.uk)

<sup>2</sup> Associate Professor Department of Architecture and Built Environment, University of Nottingham, Nottingham, [mohamed.gadi@nottingham.ac.uk](mailto:mohamed.gadi@nottingham.ac.uk)

*Abstract: The residential sector in Saudi Arabia accounts for about 50% of the total energy consumption in the country, 70% of which is attributed to cooling requirements to satisfy indoor thermal comfort. To achieve the country's reform plan objectives, known as Vision 2030, Saudi Arabia aims to increase house ownership rates from 47% to 70% within a short time frame (between 2018 and 2030). Statistics suggest that the country must build millions of new residential units at a high rate to satisfy the rapidly growing housing demand. Thus, the country is being pushed to consider advanced construction technologies, robotic technologies, and large-scale 3D-printing techniques to accelerate housing ownership rates and achieve that 70% target. The growing housing demand is expected to increase the already high energy consumption, mainly produced from fossil fuels, in the next few years.*

*The work presented in this paper is a small part of a continuous study to assess the thermal performance of existing residential buildings constructed using 3D-printing technology in Saudi Arabia. The data discussed here were gathered from field monitoring of the indoor and outdoor temperature of a house constructed using 3D-printing technology in Riyadh City during the overheated season. The methodology included recording environmental variables inside different rooms, with different orientations, and measurements of external environmental variables to compare the thermal performance of individual rooms and the whole house in relation to the outdoor environment. Further, indoor thermal comfort was assessed using the adaptive method to evaluate the overall thermal performance of the house. The monitored data will later be used to validate a standard energy simulation software, which will, in turn, be utilized to carry out further investigations to assess and improve the overall thermal performance of 3D-printed houses.*

*Keywords: Thermal performance, 3D printing, Residential buildings, Indoor air temperature, thermal comfort*

## 1. INTRODUCTION

Saudi Arabia's rapid economic development, mainly driven by the oil boom, has led to considerable transformation and developments in several industries including, the infrastructure, building, and construction sectors. Accordingly, the construction industry has experienced swift growth and is considered one of the largest and most vital markets in the country (Alshahrani et al., 2023). However, modern buildings are characterized by excessive reliance on active systems instead of utilizing natural resources, resulting in significant energy demand (Abuhussain et al., 2019). Furthermore, statistics indicate that up to 65% of residential buildings lack thermal insulation, leading to inefficient thermal performance. These factors, combined with the country's severe climatic conditions, have contributed to the residential sector's significant energy consumption, which comprises about half of the total energy consumption in Saudi Arabia (Felimban et al., 2019; Alaboud and Gadi, 2019). Air conditioning contributes the most to the energy requirements in residential buildings and accounts for about 70% of household energy use (Al-Tamimi, 2021).

In 2016, Saudi Arabia unveiled its transformative economic and social reform plans, titled 'Vision 2030.' This governmental plan aims to diversify the country's economy, improve public services, and put an end to its long-term oil dependency (Saudi Vision 2030, 2022). However, the country is experiencing a severe housing shortage driven by the rapidly growing population at a growth rate of about 2% (Alabbasi et al., 2021). Delays in construction and a lack of construction workers have also contributed to insufficient housing offers in the market (Abdulmajeed et al., 2022). The construction market in Saudi Arabia is dominated by conventional building techniques, with reinforced concrete and hollow bricks being the most used construction materials across the country (General Authority of Statistics, 2023).

The Saudi government announced its ambitions to increase citizens' house ownership rate from 47%, reported in 2018, to 70% by 2030. The stated target has added a deficit of millions of houses to be constructed within a short time. Abdulmajeed et al. (2022) indicated that the conventional construction method can be time-consuming and inefficient in satisfying the rapidly growing housing demand. In this regard, the Saudi Ministry of Housing (now called the Ministry of Municipal, Rural Affairs and Housing) has introduced the 'Building Technology Stimulus Initiative,' which strive to transform the domestic construction market by implementing advanced, innovative, and sustainable construction technologies. In addition, the initiative seeks to cope with the Fourth Industrial Revolution by facilitating novel construction methods of robotic technologies and large-scale 3D printing, also known as additive manufacturing, to push the construction sector toward digitalization (Alabbasi et al., 2021). Therefore, investigating the thermal performance of 3D-printed concrete buildings in the hot climate context of Saudi Arabia is a critically important matter to assess such building's adaptability to the country's extreme climate conditions.

Three-dimensional concrete printing (3DCP) is a form of additive manufacturing considered a promising technique in the construction industry to fabricate buildings' elements or the whole building (Mahadevan et al., 2020). Although cementitious-base materials have been efficiently studied in additive manufacturing, Ghaffar et al. (2018) criticized the lack of guidelines and codes for evaluating the suitability of the fresh mixture for printing. Thus, a number of scholars, such as Bos et al. (2016); Di Carlo et al. (2013); Le et al. (2012), focused on evaluating and improving the properties of the fresh mixtures and their structural safety to ensure successful 3D printing of concrete.

The thermal performance in 3D concrete printing has gained many scholars' attention and has been investigated in various ways. Sun et al. (2021) calculated the thermal transmittance (U-value) of a 3D-printed concrete prototype house constructed indoors through thermographic testing and heat transfer monitoring. A similar study was carried out by Salandin et al. (2022) to investigate the suitability of an existing 3D-printed house to the climate features of Spain. By comparing the calculated U-value from the monitoring data with common construction materials (i.e., masonry blocks and concrete blocks), the study found that the insulated 3D-printed house had a similar thermal performance to the conventional construction typologies in Spain but may not satisfy building codes in other countries.

Using a computer simulation tool, Mahadevan et al. (2020) investigated the energy performance of a typical residential building in India by comparing three construction materials, namely a 3D printable concrete mixture, M25 concrete, and conventional brick masonry adopted from local code. The study indicates that the 3D printable concrete mixture used resulted in higher annual energy costs and operational carbon emissions than the other two materials. Ayegba et al. (2022) stated that 3D-printed walls are unfeasible with energy codes without adding additional thermal insulation, especially in cold climate zones. Compared with an uninsulated model, Kamel and Kazemian (2023) reported that 28% savings in energy usage intensity and up to 6.35 metric tons of carbon dioxide reduction can be achieved by improving the thermal performance of 3D-printed concrete buildings through the insulation material. Kaszynka et al. (2019) found that using high-performance concrete with mineral wool as an additional insulation layer in a 3D-printed wall led to similar thermal features to conventional, insulated walls despite being 8 cm and 14 cm less thick than conventional concrete and masonry wall systems, respectively. There are inefficient studies reporting measurements of environmental parameters from existing 3D-printed buildings that are directly exposed to the outdoor environment. In particular, there is a lack of research investigating the thermal performance of 3D-printed structures in hot regions. Analysing the thermal behaviour of such construction, especially in extreme environments, is crucial for indoor thermal comfort. Consequently, this research is part of an ongoing Ph.D. research level aiming to investigate the thermal performance of a 3D-printed house in the hot climate characteristics of Saudi Arabia.



## 2. METHODOLOGY

### 2.1. Climate conditions

Saudi Arabia is located between 16°N and 30°N, with a total area of about 2.15 million km<sup>2</sup> and a population of over 32 million. According to the Koppen-Geirger climate classification, Saudi Arabia falls within a hot, arid climate (BWh) (Al-Ahmadi and Al-Ahmadi, 2013). Riyadh, the capital city of Saudi Arabia, is the city investigated in this study. Riyadh's monthly mean of maximum and minimum air temperature (°C), precipitation (mm), and relative humidity (%) are presented in Figure 1. The overheated season extends from April to October, with July and August being the warmest periods of the year. During this time, the mean maximum air temperature in the city ranges from 33 °C in April to nearly 43 °C in June, July, and August. The mean minimum air temperature is generally above 20 °C during the entire season, reaching 29 °C in July and August. In the winter, however, the temperatures fall between approximately 20 °C and 10 °C. Thus, a significant variation in diurnal temperature can be found across the year, ranging between approximately 15 °C and 10 °C. On average, relative humidity levels are below 50%. Winter is the most humid season, with mean relative humidity levels above 35%. On the contrary, relative humidity is below 20% in the summer, averaging between 10% in July, which is the driest period of the year, and 20% in October.

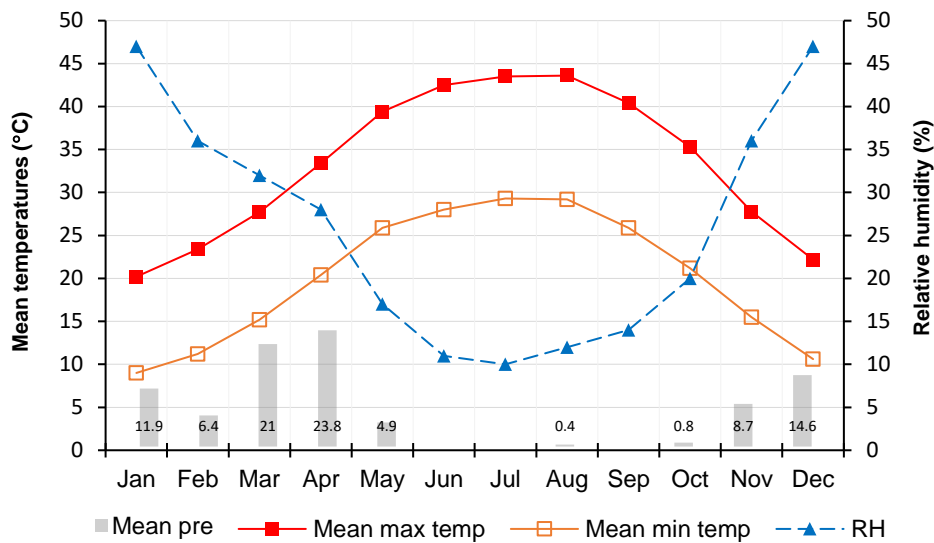


Figure 1 Climate conditions of Riyadh City. Reproduced from (Weather Atlas)

### 2.2. The case study building

The 3D Studio 2030 by CyBe is the case study building investigated in this study. The site falls within a new, raw district north of the city of Riyadh (Figure 2). The area is in a development phase, with some construction activities taking place during the study period as part of the massive housing projects announced by the government to increase dwelling stock. The building was constructed in 2018 utilizing a mobile robotic arm installed on a caterpillar by CyBe Construction, based in the Netherlands. It is a single one-story house with a total area of 80 m<sup>2</sup>. It comprises a living room, dining room, bedroom, bathroom, and kitchen. Such a small house was constructed to explore the potential of adopting new and efficient building techniques in the country. A total of 48 components were 3D printed in situ within one week. However, the construction of the entire house, including finishing work, was completed within five weeks (CyBe Construction, 2023). The studied 3D-printed house was the first of its kind in Saudi Arabia and became a mock-up of an in-situ large-scale 3D-printing technique for several housing projects set by the Ministry of Housing (Alabbasi et al., 2021). The house has a simple architectural geometry, with its main entrance facing due south. As shown in Figure 3, the building is directly exposed to the outdoor environment from all sides without any adjacent buildings. Notably, the house has been abandoned for a long time and left without being connected to the electricity grid.

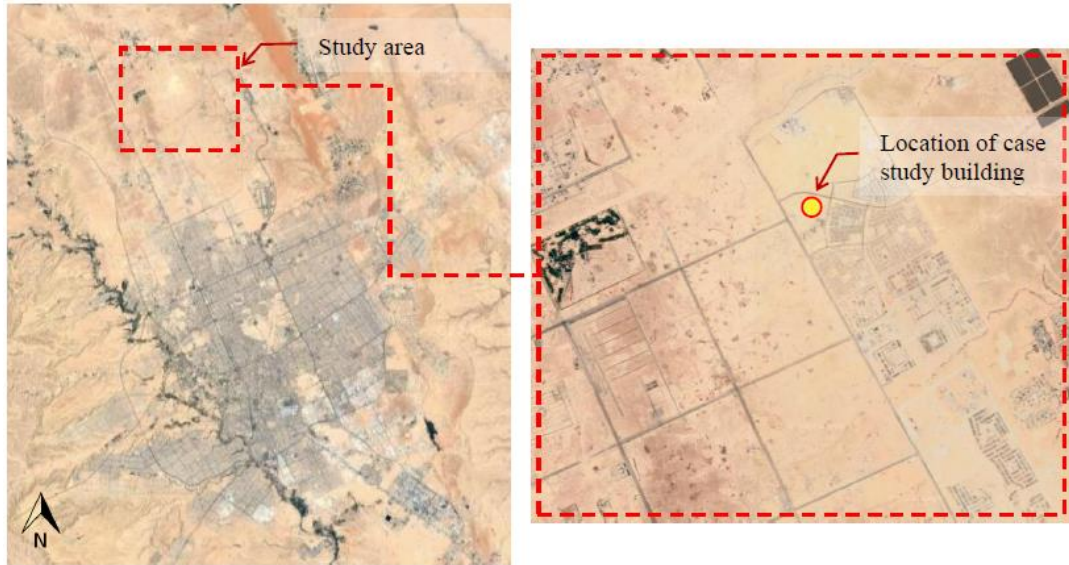


Figure 2 Maps illustrating the location of case study building in Riyadh. Modified from (Google, 2022)

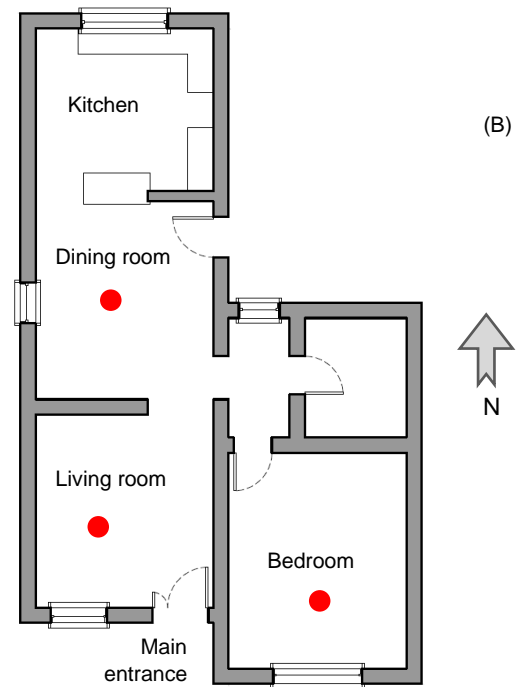


Figure 3 Illustrations of the case study building ; A. External view. B. Architectural drawing and selected rooms for fieldwork

### Construction details

External walls were 3D printed on-site using CyBe printable concrete mix. The walls are made from three layers: the outside layer, the inside layer, and the infill in between. Each layer was extruded layer by layer (a common method in 3D printing) at a width and height of 4 cm and 2 cm, respectively. Insulation material was used to fill the spaces in the core of the wall to improve its thermal resistance. The total thickness of the walls is approximately 30 cm. The roof was made of conventional precast hollow core slabs with insulation layers, and the floor was a grade slab covered with tiles. All rooms have a 10 mm gypsum board ceiling with a 10 cm air gap. Windows with tinted double glazing were used, with about 10 cm wooden egg-crate shading device from both sides.

### 2.3. Field measurements

Measurements were taken during the extreme summer of 2022 (from August 11<sup>th</sup> to 17<sup>th</sup>). A set of Tinytag data loggers were used to record air temperature and relative humidity from inside and outside the building. This allowed for investigating indoor thermal behaviour concerning the outdoor conditions in different rooms with different orientations, calculating indoor temperature fluctuation, and identifying peak times. A total of four instruments were used in this study (three loggers for indoor use and one for outdoor use).

Thus, three rooms with different orientations were selected in this study, as shown in Figure 3. The bedroom is located in the southeast corner of the house and has one window facing south. The living room is located in the southwest corner, with one window facing south. Finally, the dining room has two external walls oriented east and west, with one window facing west. It must be noted that all windows and doors were kept closed during monitoring to prevent convective thermal exchange. Further, the house was unoccupied over the study period to avoid any disturbance to the recorded data. Specifications of the instruments used are provided in Table 1.

For indoor measurements, the loggers were placed on a wooden stand previously designed for the purpose of this study. Each room was equipped with one Tinytag View-2 data logger. All three loggers were positioned as close to the centre of each room as possible to avoid radiant heat from the walls and at least 1.5 m away from the windows to protect them from direct solar heat input. Following ASHREA-55 (2017) guidelines for physical measurements, air temperature and relative humidity were recorded at a height of approximately 1.1 m from the floor level, whereas in the bedroom, the logger was placed at a height of 0.6 m from the floor level. The outdoor parameters were monitored from the roof of the house using Tinytag Plus-2. The logger was placed in a Stevenson screen, an enclosure to protect the data logger from precipitation and direct solar gain while allowing air circulation, at a height of approximately 1.3 m above the roof level. The four data loggers were programmed to take measurements at five-minute intervals during the testing period. Although the loggers were factory-calibrated, initial measurements were taken from one room. A negligible difference was found between the results, and accordingly, the loggers were positioned at their specified locations.

Table 1: Specifications of the instruments

Number of loggers	Instrument Model	Specifications	Application
1	Tinytag Plus-2 (TGP-4500)	<ul style="list-style-type: none"> <li>• Temperature range: -25 to 85 °C</li> <li>• Relative humidity range: 0 to 100 %</li> </ul>	Outdoor temperature and humidity
3	Tinytag View-2 (TV-4500)	<ul style="list-style-type: none"> <li>• Temperature range: -25 to 50 °C</li> <li>• Relative humidity range: 0 to 100 %</li> </ul>	Indoor temperature and humidity

### 2.4. Thermal comfort assessment

The adaptive method relates the indoor acceptable thermal ranges to the outdoor environmental conditions (ASHRAE, 2017). Adaptive thermal comfort suggests that when people experience thermal discomfort, they naturally respond in different ways to restore their comfort and adapt to changing conditions in their surroundings. The dynamic interaction between people and their surrounding environment was the idea behind developing the adaptive thermal comfort method. It was found that people living in hot regions favour warmer indoor conditions than people living in cold regions. People can control their thermal environment by adjusting their clothing levels, providing natural ventilation, and using shading systems without relying on mechanical cooling and heating systems to maintain thermal comfort. The neutrality temperature for a building under a free-running condition (i.e., without cooling and heating systems) can be computed using Equation 1 (de Dear and Brager, 2002). The comfort zone is referred to as the range of acceptable thermal conditions. The boundary limits of the comfort zone for 90% and 80% acceptability limits are calculated from the neutrality temperature using Equations 2 and 3, respectively (Albatayneh et al., 2016; ASHRAE, 2017). This study considered the 80% boundary limits to provide more flexibility in expanding the comfort zone inside the house.

Equation 1: Comfort temperature for non-airconditioned buildings

$$T_n = 17.8 + 0.31T_{out}$$

Where:

- $T_n$  = Neutrality temperature (comfort temperature)
- $T_{out}$  = Monthly outdoor temperature (average of daily outdoor temperature over at least seven and a maximum of 30 sequential days)

Equation 2: The upper and lower 90% acceptability limits ( $^{\circ}\text{C}$ )  
Where:

$$90\% \text{ acceptability limits} = T_n \pm 2.5^{\circ}\text{C}$$

- $T_n$  = Neutrality temperature (comfort temperature)

Equation 3: The upper and lower 80% acceptability limits ( $^{\circ}\text{C}$ )  
Where:

$$80\% \text{ acceptability limits} = T_n \pm 3.5^{\circ}\text{C}$$

- $T_n$  = Neutrality temperature (comfort temperature)

### 3. RESULTS AND DISCUSSION

In this study, the results of in-site air temperature measurements were analysed to provide insights into 3D-printed buildings' status regarding thermal performance in the harsh climate conditions of Saudi Arabia (Figure 4). The fieldwork data were collected in Riyadh during the hot summer. Environmental parameters were recorded every five minutes for seven days (11<sup>th</sup> to August 17<sup>th</sup>, 2022) from inside and outside the house. The results show that outdoor temperature ( $T_{out}$ ) ranges between 27  $^{\circ}\text{C}$  and 46  $^{\circ}\text{C}$  during the study period, with peak  $T_{out}$  occurring during daytime (14:00 and 15:00), whereas the lowest  $T_{out}$  values were recorded during the very early morning (3:00 to 6:00). The ranges of diurnal  $T_{out}$  reached 16  $^{\circ}\text{C}$ , which was expected in this climate. Relative humidity (RH) is generally below 20%, with an inverse relationship observed between  $T_{out}$  and RH curve lines. The mean outdoor temperature during the testing period was 37 $^{\circ}\text{C}$ .

As for the indoor environment, it was discovered that the thermal behaviour of all rooms is highly impacted by outdoor conditions. The indoor temperatures ( $T_a$ ) of the rooms began to rise between 6:00 and 7:00, slightly after sunrise, and peak between 14:00 and 15:00. A maximum of a three-hour lag between peak  $T_a$  and  $T_{out}$  was noticed. During peak outdoor temperature, the difference between  $T_a$  and  $T_{out}$  was less than 5  $^{\circ}\text{C}$ . In general, the  $T_a$  values of all rooms were found to be higher than the mean  $T_{out}$ . Moreover, a high level of agreement between the  $T_a$  values of each room can be noticed with less than a 1  $^{\circ}\text{C}$  variation between the results, even though each room has a different orientation. A nearly constant thermal status can be observed in all rooms with less than 2  $^{\circ}\text{C}$  temperature fluctuation. In general, indoor  $T_a$  values ranged between approximately 39  $^{\circ}\text{C}$  and 41  $^{\circ}\text{C}$ . The graph in Figure 5 illustrates the air temperature results for a 24-hour cycle (August 11<sup>th</sup>).

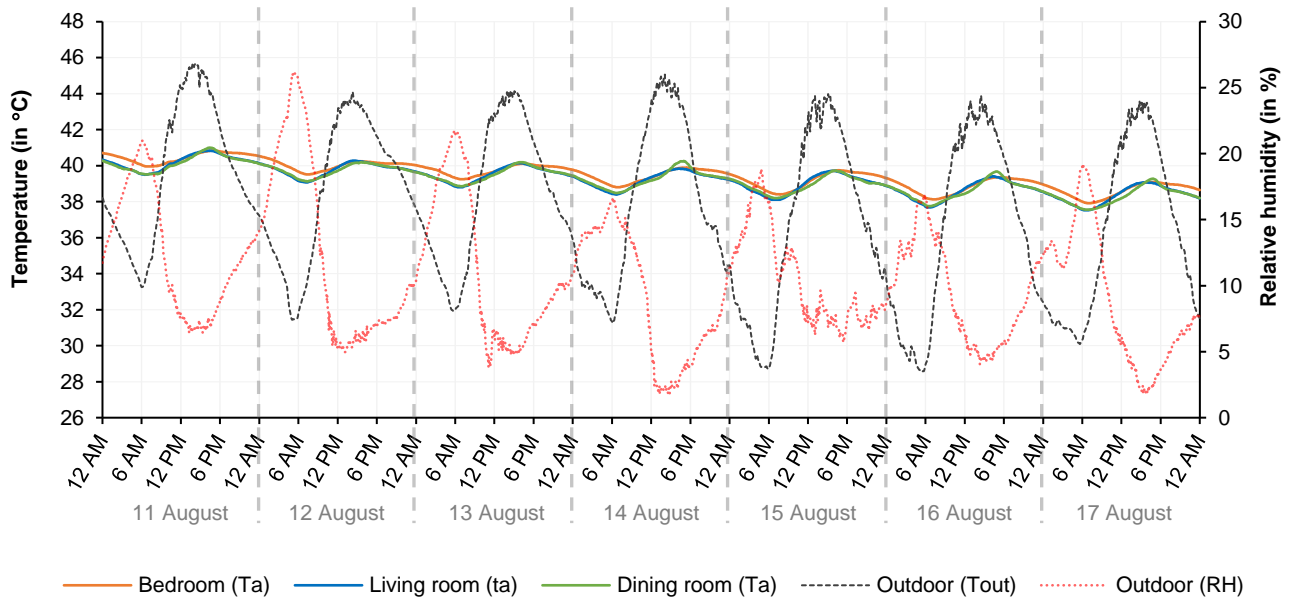


Figure 4 Outdoor and indoor monitored parameters for the complete period of the study

Based on the mean outdoor temperature value during the testing period, the computed neutrality temperature is 29.3 °C. The results of the adaptive thermal comfort for the 80% acceptability limits for the testing period for all rooms illustrated that thermal comfort was not achieved under the investigated conditions.  $T_a$  needs to be lowered by at least 6 °C and 8 °C in the morning and during the peak time, respectively, to fall within the identified 80% acceptability limits (from 25.8 °C to 32.8 °C).

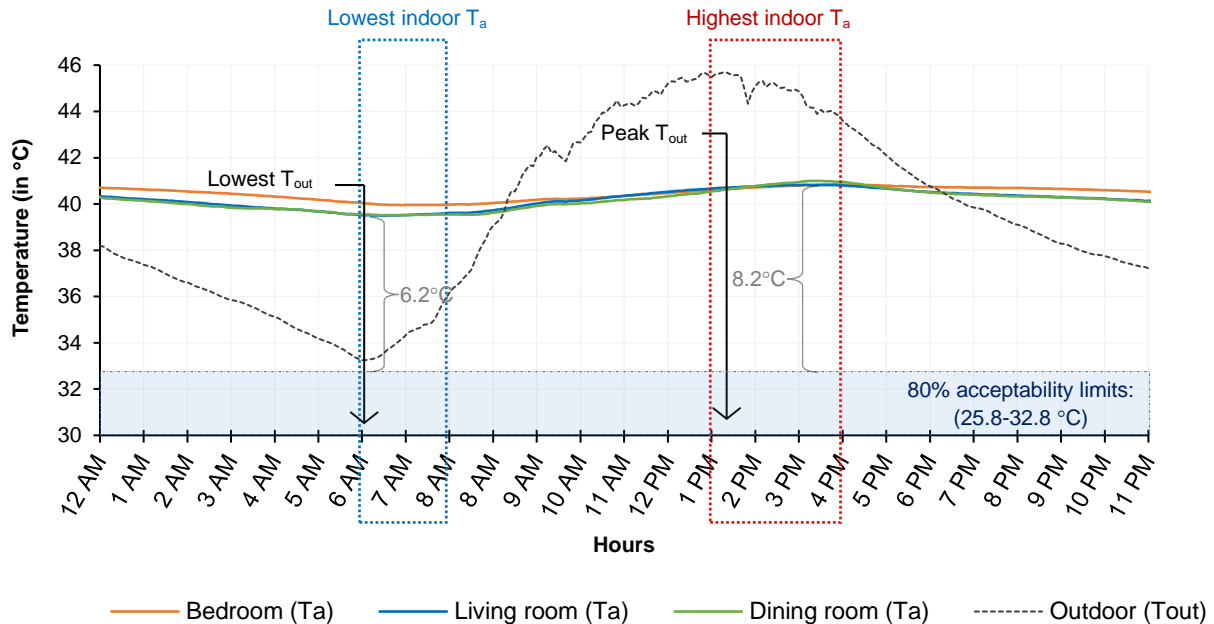


Figure 5 Outdoor and indoor temperatures for a 24-hour cycle (August 11<sup>th</sup>)

#### 4. CONCLUSION

The study provided analyses of field measurements of environmental variables collected in August 2021 to investigate the thermal performance of a residential building constructed using 3D concrete-printing technology in Riyadh, Saudi Arabia, during the summer. Indoor dry bulb temperature values were recorded at five-minute intervals over seven days (168 hours) in three different rooms with different orientations. A total of 6,048 pieces of data were analysed and compared with outdoor conditions to evaluate the impact of outdoor environmental conditions on indoor thermal performance, as the house was under a 'free-running condition' without any mechanical cooling system or natural ventilation. This was followed by a thermal comfort assessment using the adaptive method to evaluate the house's overall thermal performance during the specified period.

The results show nearly consistent indoor thermal behaviour compared to the significant variation in diurnal temperature recorded outside the house over the testing period. Indoor and outdoor temperatures ranged from 39 °C to 41 °C and from 27 °C to 46 °C, respectively. According to the adaptive thermal comfort method, the indoor environment condition is found to be at least 6°C above the 80% boundary of the acceptable temperature under the tested environmental conditions of the house. Therefore, various passive cooling strategies can be investigated to improve indoor thermal comfort.

#### 5. REFERENCES

Abdulmajeed A, Agkathidis A, Dounas T, et al. (2022) Developing a Design Framework for the Mass Customisation of Housing in Saudi Arabia: A Critical Review. In: 10th International Conference of the Arab Society for Computation in Architecture, Art and Design (ASCAAD 2022), Lebanon.

Abuhussain MA, Chow DHC and Sharples S (2019) Sensitivity energy analysis for the Saudi residential buildings envelope codes under future climate change scenarios: the case for the hot and humid region in Jeddah. In: IOP Conference Series: Earth and Environmental Science, pp.012039. IOP Publishing.

Al-Ahmadi K and Al-Ahmadi S (2013) 'Rainfall-Altitude Relationship in Saudi Arabia'. Advances in Meteorology 2013: 363029.

Al-Tamimi N (2021) 'Cost Benefit Analysis of Applying Thermal Insulation Alternatives to Saudi Residential Buildings'. Journal of Engineering Sciences 49(2): 156-177.

Alabbasi M, Chen H-M and Agkathidis A (2021) Assessing the effectivity of additive manufacturing techniques for the production of building components: Implementing innovation for housing construction in Saudi Arabia. In: 9th International Conference of the Arab Society for Computer Aided Architectural Design (ASCAAD 2021), Cairo.

Alaboud M and Gadi M (2019) Indoor environmental monitoring of residential buildings in Saudi Arabia, Makkah: a case study. IOP Conference Series: Materials Science and Engineering. IOP Publishing, 042044.

Albatayneh A, Alterman D, Page A, et al. (2016) 'Assessment of the Thermal Performance of Complete Buildings Using Adaptive Thermal Comfort'. *Procedia - Social and Behavioral Sciences* 216: 655-661.

Alshahrani A, Alaboud N, Leje MI, et al. (2023) 'Rating the significance of the factors influencing shortage of skilled labours for sustainable construction: a perception of Makkah construction practitioner'. *Journal of Umm Al-Qura University for Engineering and Architecture* 14(1): 13-25.

ASHRAE (2017) ANSI/ASHRAE Standard 55-2017. Thermal Environmental Conditions for Human Occupancy. Atlanta, GA: American Society of Heating, Refrigerating and Air-Conditioning Engineers.

Ayegba BO, Egbe K-JI, Matin Nazar A, et al. (2022) 'Resource Efficiency and Thermal Comfort of 3D Printable Concrete Building Envelopes Optimized by Performance Enhancing Insulation: A Numerical Study'. *Energies* 15(3).

Bos F, Wolfs R, Ahmed Z, et al. (2016) 'Additive manufacturing of concrete in construction: potentials and challenges of 3D concrete printing'. *Virtual and Physical Prototyping* 11(3): 209-225.

CyBe Construction (2023) 3D Studio 2030. Available at: <https://cybe.eu/> (accessed 24/06/2023).

de Dear R and Brager GS (2002) 'Thermal comfort in naturally ventilated buildings: revisions to ASHRAE Standard 55'. *Energy and Buildings* 34(6): 549-561.

Di Carlo T, Khoshnevis B and Chen Y (2013) Manufacturing Additively, With Fresh Concrete. ASME 2013 International Mechanical Engineering Congress and Exposition. San Diego, California, USA.

Felimban A, Prieto A, Knaack U, et al. (2019) 'Assessment of current energy consumption in residential buildings in Jeddah, Saudi Arabia'. *Buildings* 9(7).

General Authority of Statistics (2023) Dwellings & Housing. Available at: <https://www.stats.gov.sa/> (accessed 24/6/2023).

Ghaffar SH, Corker J and Fan M (2018) 'Additive manufacturing technology and its implementation in construction as an eco-innovative solution'. *Automation in Construction* 93: 1-11.

Google (2022) Riyadh City. Available at: <https://www.google.com/maps> (accessed 17/03/2022).

Kamel E and Kazemian A (2023) 'BIM-integrated thermal analysis and building energy modeling in 3D-printed residential buildings'. *Energy and Buildings* 279: 112670.

Kaszynka M, Olczyk N, Techman M, et al. (2019) 'Thermal-Humidity Parameters of 3D Printed Wall'. IOP Conference Series: Materials Science and Engineering 471(8): 082018.

Le TT, Austin SA, Lim S, et al. (2012) 'Hardened properties of high-performance printing concrete'. *Cement and Concrete Research* 42(3): 558-566.

Mahadevan M, Francis A and Thomas A (2020) 'A simulation-based investigation of sustainability aspects of 3D printed structures'. *Journal of Building Engineering* 32: 101735.

Salandin A, Quintana-Gallardo A, Gómez-Lozano V, et al. (2022) 'The First 3D-Printed Building in Spain: A Study on Its Acoustic, Thermal and Environmental Performance'. *Sustainability* 14(20).

Saudi Vision 2030 (2022) Vision 2030 Overview. Available at: <https://www.vision2030.gov.sa/> (accessed 24/6/2023).

Sun J, Xiao J, Li Z, et al. (2021) 'Experimental study on the thermal performance of a 3D printed concrete prototype building'. *Energy and Buildings* 241: 110965.

Weather Atlas Monthly weather forecast and climate (Riyadh, Saudi Arabia). Available at: <https://www.weather-atlas.com/> (accessed 11/5/2022).

---

## #233: Building retrofit- an active influence on the residential building's energy consumption by changing the size of the windows

---

Yue ZHANG<sup>1</sup>, Siddig OMER<sup>2</sup>

*1 Dept. of Architecture and Built Environment, Faculty of Engineering, the University of Nottingham, UK, laxyz69@nottingham.ac.uk*

*2 Dept. of Architecture and Built Environment, Faculty of Engineering, the University of Nottingham, UK, Lazsao@exmail.nottingham.ac.uk*

*Abstract: Heating buildings is a pressing issue in the UK given the UK's commitment to achieving net zero emissions targets. To solve this problem, a building strategy to effectively reduce energy consumption by simulating and modifying window size parameters is developed. This study mainly uses computer simulation experiments to evaluate the impact of optimizing window size on energy consumption during building renovation. For this purpose, a detached building located in Nottingham, UK was chosen as a model. The results of the study show that the south side of the building has the most significant impact on energy consumption. Therefore, by increasing the size of the south-facing windows, the overall energy consumption of the building can be significantly reduced. The study showed that the ideal window size increase was 1.6 times the original size, resulting in a window-to-wall ratio of 7.86% compared to 4.91% of the original size. When the technology of changing the window size is combined with multi-layer glass windows filled with xenon and Low-E vacuum windows, the building energy consumption can be better reduced, which can reduce the total energy consumption by 2.65% and 4.14% respectively. On the contrary, the study highlights that the presence of north-facing windows has a negative impact on the building's energy consumption. The findings have important implications for window reconstruction in British buildings. The research methodology and results can provide a valuable reference for architects and engineers seeking to optimize window design to minimize energy consumption in various types of residential buildings. By applying a similar window optimization approach, it is possible to determine optimal values for reducing energy consumption in different types of residential structures. The research demonstrates the potential to improve the energy efficiency of buildings and contribute to the UK's wider efforts to achieve net zero targets. Implementing these findings in building renovations could pave the way for a more sustainable future and promote energy awareness in the building industry.*

*Keywords: Net Zero Target, Building Retrofit, Window Size, Energy Simulation, Energy Consumption*



## 1. INTRODUCTION

### 1.1. Background

According to the UK government, as of 2019, the UK building sector accounts for around 37% of the country's total energy consumption, with residential buildings accounting for around 14% of the UK's total energy consumption. These figures show the importance of the UK building sector in terms of energy consumption and greenhouse gas emissions and reflect the importance of the UK government in reducing energy consumption in buildings." The total energy consumption of UK buildings in 2019 is 33.4 million gigawatt hours (kWh), with residential buildings accounting for about 28 percent and non-residential buildings accounting for about 72 percent. In addition, the UK's greenhouse gas emissions in 2019 are 480 million tons of CO<sub>2</sub>, of which the building sector accounts for approximately 19%. This indicates that the building sector plays an important role in the UK's energy consumption and greenhouse gas emissions. The UK has a wide range of residential buildings, from old stone buildings to modern high-rise apartments. There are different types of houses such as detached houses, apartments, townhouses, etc. in both urban and rural areas of the UK. According to the UK government, as of 2019, there are 28.5 million housing units in the UK, of which, about 60% are detached houses, 22% are apartments, and 18% are other types of houses. The UK also has several older buildings, some of which are hundreds of years old, and these buildings often need restoration and maintenance. Since UK residential buildings do not use air conditioning in summer, this study does not consider the effect of solar heat on the cooling load of the building in summer. In contrast, the solar heat gain in winter has a positive effect on the building so this study only considers the energy efficiency that can be improved by the windows in the building without shading conditions.

### 1.2. Literature Review

Some literature studies the optimal value of the window-wall ratio for buildings in European climates. For office buildings, although the optimal wall-window ratio exists for every climate and orientation, most of the ideal values can be found within a relatively narrow range ( $0.30 < WWR < 0.45$ ). (Goia, 2016) Total energy use may increase by 525% when the worst wall-window ratio is used, while energy efficiency is highest when the best wall-window ratio is used. Some literature studies the optimal WWR of office buildings in cold areas is 0.35, 0.3, 0.3, and 0.25 respectively in the south, north, east, and west. In general, the maximum energy-saving value of the south window wall ratio of the building in the cold area is relatively greater, while the north should be appropriately reduced under the allowed lighting and ventilation conditions. (Zhou et al., 2012) The paper also simulates the office building model, and the results show that the cooling energy use increases by 5.67% on average for every 10% increase in WWR. In addition, more than 20% of WWR buildings fail to provide comfortable temperatures. (Budhiyanto, 2017) These values can be used as a reference for us to study the optimal window-wall ratio of British buildings. There are also paper studies pointing out that for the university gymnasium in cold areas, the window design should use side Windows, with north and south lighting as the main, and east and west lighting as the auxiliary. (Caggiano et al., 2021) This is because buildings in the northern hemisphere get the most daylight from their southern Windows, while buildings in the southern hemisphere get the most daylight from their northern Windows. On the other hand, both the eastern and western surfaces are exposed to light in the morning or afternoon. Britain is in the northern hemisphere, and most of its energy consumption comes from heating buildings in winter. The influence of solar energy on building energy consumption should also be considered when designing the window-wall ratio. More sunlight reduces the building's heat load accordingly.

However, there is not much literature on the impact of modifying the window-to-wall ratio of windows in different directions on building energy consumption, which needs to be improved. Therefore, this project focuses on the impact of window sizes in different directions on the building. By modifying the size of windows to obtain an appropriate multiple of change, it is combined with multi-layer glass windows filled with xenon and Low E vacuum windows to reduce building energy consumption. This method can also be applied to other types of buildings, and it is believed that good results can also be obtained.

### 1.3. Influence of Windows on Residential Buildings

As the core component of a building, the importance of windows is often overlooked. However, windows play a key role in the overall energy consumption of a building while providing natural light and ventilation. When designing or selecting buildings, it is necessary to fully consider the configuration of windows to achieve the goals of environmental protection and energy saving. (Tummala et al., 2020, Lahmar et al., 2022, Albatayneh et al., 2021)

Read more about how window size and location can affect a building's energy efficiency. Too many windows are like opening too many holes in a building's insulation, causing massive heat loss and problems with air circulation inside the building. This will make it difficult to control the indoor temperature, which will increase the energy consumption of heating and cooling. Conversely, too few windows will result in poor indoor air circulation and poor indoor air quality, negatively impacting the health and comfort of occupants. (Shaeri et al., 2019, Dewi et al., 2022, Ma et al., 2015, Fathi and Kavooosi, 2021, Liu et al., 2021)

Therefore, a balance should be found that can make full use of the natural light and ventilation brought by the windows while effectively controlling energy consumption. This requires careful design and adjustment of window size and



placement. For example, south-facing windows can be enlarged to increase the illuminated area and maximize natural daylight. At the same time, the size of the windows on the north side can be reduced to reduce the intrusion of cold wind and the loss of heat.(Xue et al., 2019, Li et al., 2022)

In addition, the material selection of the window is equally important. Window materials with good thermal and acoustic properties, such as double or triple glazing, can be selected to further improve the building's energy efficiency.(Chiesa et al., 2019, Li et al., 2020)

In general, through the careful design of the size and location of windows and the selection of appropriate materials, not only can the energy consumption of buildings be reduced, the energy performance of buildings can be improved, but also a great contribution can be made to the improvement of the living environment.(Yang et al., 2015, Yu et al., 2013)

#### 1.4. Significance of This Study

In this study, by using computer software simulations, the windows that have a large impact on the building are found one by one by elimination, the size of the windows is modified, and the optimal value for reducing the energy consumption of the building is found by increasing the window area from 10% to 100% in the simulations. Based on this area, the window materials and construction can be modified to obtain a relatively optimal solution. In this project, the technology of changing the window size is combined with multi-layer glass windows filled with Xenon and Low-E vacuum windows. This method applies to all kinds of buildings that have windows, and the retrofitting of window sizes can have a positive impact. It can be used as a reference for the UK building energy efficiency program.

### 2. METHODOLOGY

#### 2.1. The Information of The Base Case Building

This research is based on a detached house in Belper, Derbyshire, England. The latitude is 53°01'07.8" and the longitude is 1°30'08.9". The building information is provided by Professor John Chilton.

The building is a double-story detached building. There are windows on all sides for good lighting.

Figure 1 shows the Building Simulation in Energyplus:

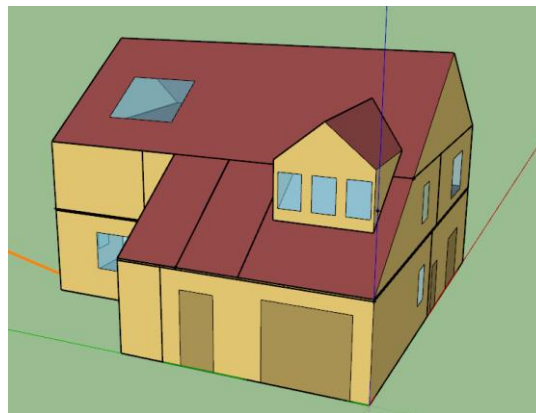


Figure 1 Building Simulation in Energyplus

#### 2.2. The Window-Wall Ratio

Window-to-Wall Ratio (WWR) is the proportion of the above-grade wall area covered by fenestration, calculated as the ratio of the wall's fenestration area to the total above-grade wall area. Since the ratio of Windows to walls can reflect the proportion of Windows in the envelope, the influence of Windows on building energy consumption is greater in buildings with a larger ratio of Windows to walls.

The Window-Wall Ratio on each side is shown below:

*Table 1: Window-Wall Ratio*

	Total(%)	North(%)	East(%)	South(%)	West(%)	Skylight-Roof Ratio(%)
Gross Window-Wall Ratio	5.14	4.16	4.69	4.91	7.39	6.25

### 2.3. The multi-layer glass windows filled with Xenon

Since the last 25 years of the 20th century, double-glazed windows have been widely manufactured in the UK. (Liu et al., 2017) They can reduce building energy consumption and improve the insulation properties of materials because the gaps between the panes are used as thermal barriers.(Aguilar et al., 2017)

Double-glazing is also known as an IGU, an insulated glazing unit. It is two sheets of glass that come as a sealed unit with a small air gap in between. The air gap acts as a buffer between the two materials that reduce the flow of heat energy through the IGU. The air gap is often filled with an inert gas, argon, as it further reduces the flow of heat. Double-glazing is very good at reducing heat flow, this works to keep heat inside a building in winter but also to reduce heat flow into a building in summer. This project will test both double-glazing windows with air and argon. The U-value of double-glazing windows is usually between 1.8-2.2 W/(m<sup>2</sup>K).

Triple glazing is an upgraded version of double glazing, with a lower U-value, but it is also more expensive. The U-value of triple-glazing windows is usually between 1.6-1.8 W/(m<sup>2</sup>K). If the windows are filled with argon, the U- value would be lower.

Aguilar studied four different double-glazed structures (using transparent, absorptive, low-e, and reflective glass) on an air gap. Studies have shown that reflective glass can save up to 72.9% of energy consumption. In hot and dry climates, the average payback period is 8.75 years.

An air gap is introduced between the glass plates as an insulation layer to reduce heat transfer through the window assembly. This also shows that compared with single-layer glass, the heat loss is reduced by 50%, and its advantage is that it maintains a relatively high visible light transmittance and g-value. In addition, the heat transfer rate of double-glazed windows is 2.5 times lower than that of single-glazed windows, so it can reduce heat by about 50-67% in warm climates.(Arıcı and Karabay, 2010)

Xenon were considered in this research. It was added to triple glazing window to simulate energy consumptions.

Table 2: Different Gas Parameters

Name	Air	Argon	Krypton	Xenon
Gas Type	Air	Argon	Krypton	Xenon
Thickness (m)	0.008	0.008	0.008	0.008
Conductivity Coefficient A	0.002873	0.002285	0.0009443	0.0004538
Conductivity Coefficient B	0.0000776	0.00005149	0.00002826	0.00001723
Conductivity Coefficient C	0	0	0	0
Viscosity Coefficient A	0.00000372	0.00000338	0.00000221	0.00000107
Viscosity Coefficient B	0.00000005	0.00000006	0.00000008	0.00000007
Viscosity Coefficient C	0	0	0	0
Specific Heat Coefficient A	1002.737	521.9285278	248.0906982	158.3397064
Specific Heat Coefficient B	0.012324	0	0	0
Specific Heat Coefficient C	0	0	0	0
Molecular Weight	28.97	39.948	83.8	131.3

### 2.4. The Low-E vacuum windows

The glass of the window is chosen in WINDOW and the calculation is done in WINDOW.

The Low-E windows with 40mm pillar spacing are chosen in this project.

The parameters of the vacuum Low-E window are shown below (Calculated by WINDOW software):

*Table 3: Vacuum Glass Window with Different Pillar Spacing*

Vacuum glass R0.25	20mm	25mm	30mm	40mm	50mm
U factor	1.304	1.036	0.875	0.702	0.617
SC	0.72	0.723	0.725	0.727	0.727
SHGC	0.627	0.629	0.631	0.632	0.633
Rel Ht Gain	465	465	465	464	464
Tvis	0.76	0.76	0.76	0.76	0.76
Keff	0.0177	0.0132	0.0108	0.0083	0.0072
Layer1 Keff	1	1	1	1	1
Gap1 Keff	0.0005	0.0004	0.0003	0.0002	0.0002
Layer2 Keff	1	1	1	1	1

## 2.5. The Steps of The Modelling

The model is built in Sketch and Openstudio software, and some of the technical retrofitting were made through Energyplus and Window software.

The geometry of the building was first created in Sketch, and then thermal zones were added. In openstudio, the weather files, constructions, schedules, and HVAC system can be set step by step.

### 1) Weather File

Watnall is the closest weather station, and the weather file GBR\_ENG\_Nottingham.Watnall.033540\_TMYx.epw and GBR\_ENG\_Nottingham.Watnall.033540\_TMYx.ddy are downloaded from the Energyplus weather file network.

### 2) Schedule Sets

The schedules include occupancy, lighting, and equipment. Since the owner lives with his wife and has retired, the schedule of each part is selected according to the description of the owner, and finally, the electricity loads for lighting and equipment are controlled at about 1GJ.

### 3) Construction Sets

The construction of the building is shown below:

*Table 4: Ground Floor Information of Building*

Ground floor	Conductivity (W/mK)
22mm Ceramic floor tiles (Kitchen and utility room)	0.6-1.7
50mm reinforced sand/cement screed on	1.05
50mm polystyrene insulation on	0.035
100mm concrete slab	1.05
20mm Damp proof membrane	1.15
150mm stone hardcore with sand blinding	2.9

*Table 5: First Floor Information of Building*

First floor	conductivity (W/mK)
22mm softwood floorboards on	0.12
220 x 50 mm timber joists	0.025
9.5mm plasterboard and 3mm skim ceiling	0.51

Table 6: Roof Information of Building

Roof 1980-2010	conductivity (W/mK)
165 x 265 mm clay tiles on	0.623
50mm Sarking felt on	0.06
100 x 50 treated timber rafters with purlins	0.12
100 x 50 mm treated timber ceiling joists with 100mm of glasswool insulation between	0.025

Table 7: Wall Information of Building

Walls 1980-2012	conductivity (W/mK)
100mm natural sandstone (external)	1
100mm cavity	0.024
100mm lightweight concrete block	1.046
100mm cavity filled with Shell blown polystyrene bead insulation	0.039
100mm lightweight concrete block	1.046
12mm lightweight plaster and skim (internal)	0.51

Table 8: Window information of Building

Windows 1981-2012 DGU	Thickness
Glass Out	4mm
air	8mm
Glass Inner	4mm

Table 9: Windows Glass Information of Building

Name	J WINDOW Glass
Optical Data Type	SpectralAverage
Thickness	0.004
Solar Transmittance at Normal Incidence	0.837
Front Side Solar Reflectance at Normal Incidence	0.075
Back Side Solar Reflectance at Normal Incidence	0
Visible Transmittance at Normal Incidence	0.898
Front Side Visible Reflectance at Normal Incidence	0.081
Back Side Visible Reflectance at Normal Incidence	0
Infrared Transmittance at Normal Incidence	0
Front Side Infrared Hemispherical Emissivity	0.84
Back Side Infrared Hemispherical Emissivity	0.84
Conductivity	0.9
Dirt Correction Factor for Solar and Visible Transmittance	1
Solar Diffusing	No

#### 4) Loads Definition

Table 10: Loads Information of Building

People Definition	
Number	2
Fraction Radiant	0.3
Carbon Dioxide Generation Rate	0.000038L/s·W
Lights Definition	

Watts Per Space Floor Area	4W/m2
Electric Equipment Definition	
Watts Per Space Floor Area	2W/m2
<b>Ventilation Definition</b>	
Outdoor Air Flow Per Person	9.44 L/s-Person
<b>Infiltration Definition</b>	
Flow Per Exterior Surface Area	0.000226568 m/s

## 2.6. Simulation Of Original Building and New Case Building

Since the three layers wall in the UK is not very common, in this study, the wall is changed into the common double-layer cavity wall. And the Energy consumption is shown below:

Table 11: Energy Consumption of Original Building and Base Case Building

Buildings	Gas Consumption (GJ)	Electricity Consumption (GJ)
Original Wall Building	55.5	22.95
Common Cavity Wall Building	67.1	30.69

## 2.7. The Steps of The Calculations

Step 1: Calculate the building energy consumption of the base case

Step 2: Derive the window heat gain and window heat loss for all windows and calculate the difference between heat gain and heat loss. Determine the impact of each window on the winter heating of the building. And classify the windows that have a positive impact on the building and the windows that have a negative impact. Table 12 shows that the windows on the north side dissipate more heat than they gain in winter, and the windows on the other three sides gain more heat than they dissipate in winter, with the largest difference for the windows on the south side. So, enlarging the south window or reducing the north window helps to reduce the winter energy consumption of the building.

Table 12: The Difference of Heat Gain Minus Heat Loss in Winter

Subsurface (window)	13 (N)	12 (N)	11 (N)	10 (N)	2 (S)	1 (S)	5 (S)	7 (E)	9 (E)	17 (W)	18 (W)	19 (W)	14 (W)	20 (Sky)
Difference of heat gain and loss in winter (GJ)	0.0 2	0.0 4	0.0 4	0.0 6	0.4 0	0.3 7	1.0 2	0.0 4	0.2 2	0.19	0.19	0.19	0.19	1.54

Step 3: By removing all the windows, the obtained gas load is 72.32GJ

Step 4: By deleting the north window, the result of the gas load is 67.14GJ

Step 5: Then is to delete the north and east windows, see the result gas load is 68.53GJ

Step 6: Then delete the north and east and west, leaving only the south window, the result of the gas load is 70.07GJ

Step 7: The south window has the greatest impact on the building's energy consumption, so consideration was given to increasing the area of the south window from 10% to 100%. Because it is a residential building, it must be considered that the building itself is not suitable for large windows like official buildings. So, consider increasing the area to 2 times.

Step 8: Replace the original double-glazed windows with multi-layer glass windows filled with Xenon and Low-E vacuum windows.

## 3. RESULTS AND ANALYSIS

Table 13 shows that the energy consumption of the building gradually increases as the windows are reduced, but the most significant increase in energy consumption is achieved when the windows on the south side are missing. The windows' heat gain and heat loss tables also show that the difference between heat gain and heat loss is greatest for the south-facing windows. This can also be attributed to the fact that buildings in the northern hemisphere have longer light hours on the south side, which results in higher heat gain.

Table 13: Energy Consumption of The Building Gradually Increases as The Windows Are Reduced

	Gas load (GJ)	Electricity (GJ)	Total (GJ)
With All windows	67.1	30.69	97.79
Without N windows	68.02	30.98	99.00
Without NE windows	68.53	30.92	99.45
Without NEW windows	70.07	29.12	99.19
No windows	72.32	28.44	100.76

Some subtle results can be obtained from the data:

No windows at all - Removing windows from the building has a positive effect on energy consumption.

Without north windows - Energy consumption increases, but not much

Without north and east windows - energy consumption increases

Without north and east-west windows (south side only) - increase in energy consumption

When comparing the difference between having only south-facing windows and no windows, it was found that removing south-facing windows increased energy consumption the most. The impact is also relatively larger for windows on other sides.

Result about expanding the area of south windows.

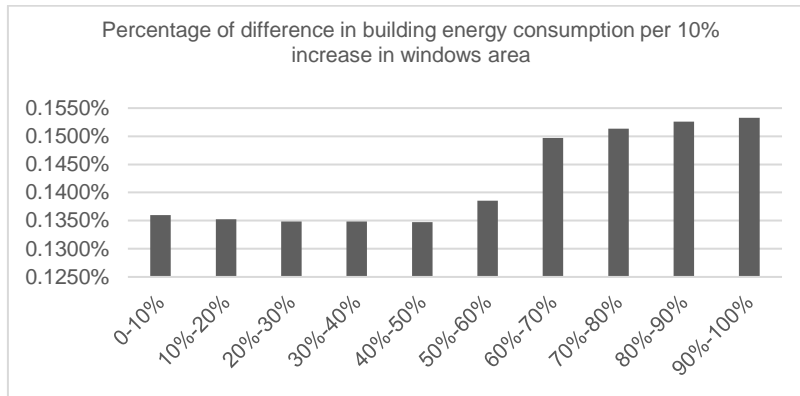


Figure 2 Percentage of Difference in Building Energy Consumption Per 10% Increase in Windows Area

By subtracting the energy consumption values of the windows after a 10%-100% increase in area, it can be concluded that the gas load reduction of the building increases gradually with the larger the area of the windows. However, the difference between the two adjacent values is not a stable value, but at 1.6-1.7 times there is a sudden huge increase and then a leveling off. Therefore, 1.7 times is the relatively optimal value for the current building area increase. Taking this value into account, and combining it with other window technology modifications, the effect of reducing the building's gas load can be maximised.

Table 14: Energy Consumption Increases with Window Area with Only South-Facing Windows

Window area multiple	Gas (GJ)	Elec (GJ)	Total (GJ)
1	70.07	29.12	99.19
1.1	69.97	29.18	99.15
1.2	69.88	29.23	99.11
1.3	69.78	29.28	99.06
1.4	69.69	29.33	99.02
1.5	69.59	29.40	98.99
1.6	69.50	29.48	98.98
1.7	69.39	29.61	99
1.8	69.29	29.74	99.03
1.9	69.18	29.87	99.05
2	69.07	30.01	99.08

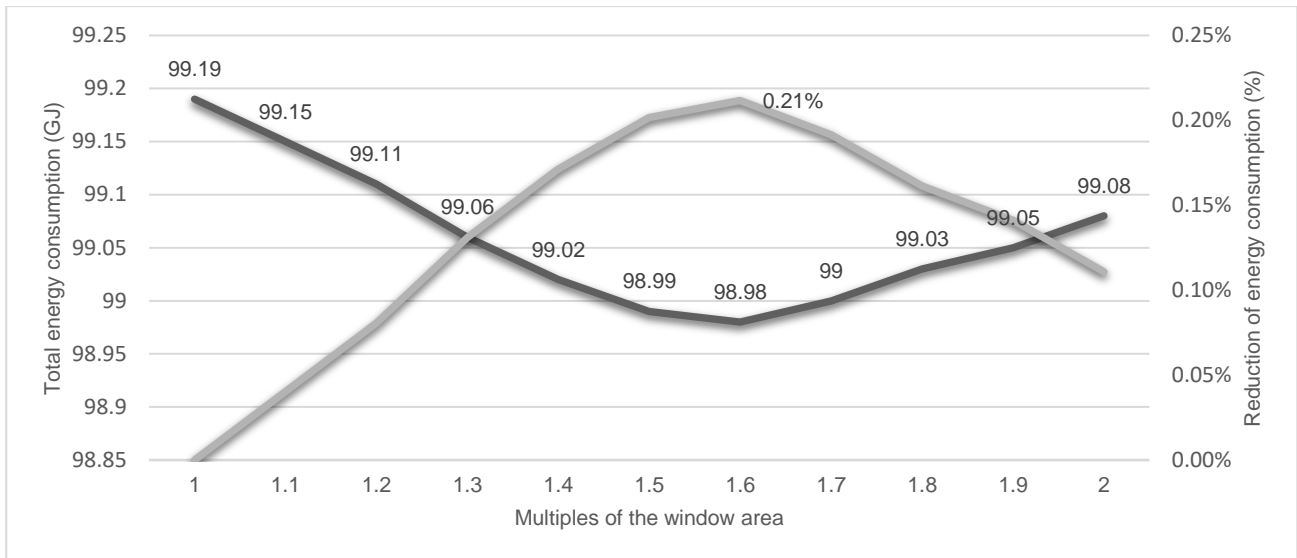


Figure 3 Total Energy Consumption with the Increase of Window Area with Only South-Facing Windows  
1 = current area ratio, and then increase the ratio

When considering not only the gas load of the building, but the total energy consumption (gas load+ electricity load) of the building, Figure 3 shows the value of the energy consumption of the building with the increase of the window area. It intuitively reflects that with the increase in the window area, building energy consumption gradually decreases and then increases slowly. The lowest point is when the window multiple is 1.6, and the total energy consumption of the building is 98.98GJ.

After determining that the increase ratio is 1.6 times, the south window of the original building is expanded, and the other Windows are retained. The result is that the gas load is 66.53GJ, the Electricity load is 31.08GJ, and the Total load is 97.61GJ. The reduction of total energy is  $97.79-97.61=0.18$ GJ (0.184%). When the technology of modifying the window size is combined with multi-layer glass windows filled with Xenon and Low-E vacuum windows, the energy consumption of the building can be better reduced.

Table 15: Summary results of the option window size

	Natural Gas Consumption (GJ)	Electricity Consumption (GJ)	Reduction of Gas Consumption (%)	Reduction of Electricity Consumption (%)	Reduction of Total Consumption (GJ)	Reduction of Total Consumption (%)
Original Common wall	67.1	30.69	0.00%	0.00%	0.00%	0.00%
Xenon-filled triple-glazed window with optimum ratio	65.36	29.84	2.59%	2.77%	2.59	2.65%
Vacuum window with optimum ratio	64.69	29.05	3.59%	5.34%	4.05	4.14%

#### 4. CONCLUSION

This project uses Sketchup, Openstudio, and Energyplus to simulate a detached building located in Nottingham, UK, and calculate its energy consumption. The report exported can obtain the heat gain and heat dissipation of each window of the building in winter. By calculating the difference between the heat and heat dissipation, it is concluded that the heat gain of the windows in the north of the building in winter is less than the heat dissipation, and the heat gain of the windows in the East and west south is greater than the heat dissipation. In winter, the sunshine time in the north is relatively short, and the heat of the sun is also low. Therefore, building energy consumption can be reduced by increasing the area of windows in the East, West, and South or reducing the area of windows in the north. In this project, considering the maximum difference between heat gain and heat dissipation in the south, an increase in the area of the south window is chosen. When considering the window area between 1 to 2 times its initial size on the southern side, a 60% increase in the window area leads to the lowest total energy consumption for the building, which amounts to 98.98 GJ, including both gas and electricity loads. When the windows on the other sides are retained and the south windows are expanded by 1.6 times, the building energy consumption is 97.61GJ. When the window sizing technique is combined with xenon-filled multi-glazing and Low-E vacuum Windows, building energy consumption can be even better reduced, which can reduce total energy consumption by 2.65% and 4.14%, respectively. By determining and comparing the direction in which the windows are oriented to have the greatest impact on energy consumption, and then increasing or decreasing the window area to achieve a reduction in the building's energy consumption, the optimal value for the building can be found. This method can be

applied to other types of buildings where windows have a positive impact on building energy consumption and can also provide a reference for building renovation.

## 5. REFERENCES

- aguiar, J. O., Xamán, J., Olazo-Gómez, Y., Hernández-López, I., Becerra, G. & Jaramillo, O. A. 2017. Thermal performance of a room with a double glazing window using glazing available in Mexican market. *Applied Thermal Engineering*, 119, 505-515.
- Albatayneh, A., Atieh, H., Jaradat, M., Al-Omary, M., Zaquot, M., Juaidi, A., Abdallah, R. & Manzano-Agugliaro, F. 2021. The Impact of Modern Artificial Lighting on the Optimum Window-to-Wall Ratio of Residential Buildings in Jordan. *Applied Sciences*, 11.
- Arci, M. & KARABAY, H. 2010. Determination of optimum thickness of double-glazed windows for the climatic regions of Turkey. *Energy and Buildings*, 42, 1773-1778.
- Budhiyanto, A. 2017. The Effect of the Window-to-Wall Ratio on Cooling Energy Usage and Comfort Temperature. *DIMENSI (Journal of Architecture and Built Environment)*, 44.
- Caggiano, A., Junlin, Z. & Longwei, Z. 2021. Multi objective optimization of window to wall ratio of University Gymnasium in severe cold area by coupling natural lighting and energy consumption. *E3S Web of Conferences*, 293.
- Chiesa, G., Acquaviva, A., Grosso, M., Bottaccioli, L., Florida, M., Pristeri, E. & Sanna, E. 2019. Parametric Optimization of Window-to-Wall Ratio for Passive Buildings Adopting A Scripting Methodology to Dynamic-Energy Simulation. *Sustainability*, 11.
- Dewi, O. C., Rahmasari, K., Hanjani, T. A., Ismoyo, A. D. & Dugar, A. M. 2022. Window-to-Wall Ratio as a Mode of Daylight Optimization for an Educational Building with Opaque Double-Skin Façade. *Journal of Sustainable Architecture and Civil Engineering*, 30, 142-152.
- Fathi, S. & Kavooosi, A. 2021. Optimal Window to Wall Ratio Ranges of Photovoltachromic Windows in High-Rise Office Buildings of Iran. *Journal of Daylighting*, 8, 134-148.
- Goia, F. 2016. Search for the optimal window-to-wall ratio in office buildings in different European climates and the implications on total energy saving potential. *Solar Energy*, 132, 467-492.
- Lahmar, I., Cannavale, A., Martellotta, F. & Zemmouri, N. 2022. The Impact of Building Orientation and Window-to-Wall Ratio on the Performance of Electrochromic Glazing in Hot Arid Climates: A Parametric Assessment. *Buildings*, 12.
- Li, A., Cheng, L., Tao, Q., Tang, Y., Olofsson, T. & Kosonen, R. 2022. Optimized design and energy consumption simulation of window-wall ratio in Yanqui Library, Jimei University. *E3S Web of Conferences*, 356.
- Li, J., Zheng, B., Chen, X., Zhou, Y., Rao, J. & Bedra, K. B. 2020. Research on Annual Thermal Environment of Non-Hvac Building Regulated by Window-to-Wall Ratio in a Chinese City (Chenzhou). *Sustainability*, 12.
- Liu, C., Wu, Y., Li, D., Zhou, Y., Wang, Z. & Liu, X. 2017. Effect of PCM thickness and melting temperature on thermal performance of double glazing units. *Journal of Building Engineering*, 11, 87-95.
- Liu, H., Zhang, Z., Ma, X., Lu, W., Li, D. & Kojima, S. 2021. Optimization Analysis of the Residential Window-to-Wall Ratio Based on Numerical Calculation of Energy Consumption in the Hot-Summer and Cold-Winter Zone of China. *Sustainability*, 13.
- Ma, P., Wang, L.-S. & Guo, N. 2015. Maximum window-to-wall ratio of a thermally autonomous building as a function of envelope U-value and ambient temperature amplitude. *Applied Energy*, 146, 84-91.
- Shaeri, J., Habibi, A., Yaghoubi, M. & Chokhachian, A. 2019. The Optimum Window-to-Wall Ratio in Office Buildings for Hot-Humid, Hot-Dry, and Cold Climates in Iran. *Environments*, 6.



Tummala, S., Kumar, D. R. V., N, S. K., K, N., K, S. R. R., E, V. K., Kosaraju, S., Bobba, P. & Singh, S. 2020. Spatial Day Light Autonomy and Energy Analysis of a Residential Building for Different Climatic Conditions and Window-to-Wall Ratios. *E3S Web of Conferences*, 184.

Xue, P., Li, Q., Xie, J., Zhao, M. & Liu, J. 2019. Optimization of window-to-wall ratio with sunshades in China low latitude region considering daylighting and energy saving requirements. *Applied Energy*, 233-234, 62-70.

Yang, Q., Liu, M., Shu, C., Mmereki, D., Uzzal Hossain, M. & Zhan, X. 2015. Impact Analysis of Window-Wall Ratio on Heating and Cooling Energy Consumption of Residential Buildings in Hot Summer and Cold Winter Zone in China. *Journal of Engineering*, 2015, 1-17.

Yu, Z., Zhang, W. L. & Fang, T. Y. 2013. Impact of Building Orientation and Window-Wall Ratio on the Office Building Energy Consumption. *Applied Mechanics and Materials*, 409-410, 606-611.

Zhou, Z. H., Hu, S. & Du, T. 2012. Study on Determination of Best Window-Wall Ratio of Office Building in Cold Area. *Applied Mechanics and Materials*, 260-261, 209-216.

---

## #235: A numerical study on the effect of different roof shapes on the performance of an oscillating aerofoil energy harvester integrated into a building structure

---

Katrina CALAUTIT<sup>1</sup>, Cameron JOHNSTONE<sup>2</sup>

<sup>1</sup> University of Strathclyde, Glasgow, United Kingdom, katrina.calautit@strath.ac.uk

<sup>2</sup> University of Strathclyde, Glasgow, United Kingdom, cameron.johnstone@strath.ac.uk

*Abstract: The increasing demand for sustainable building solutions has driven the exploration of renewable energy technologies integrated into buildings. One such approach involves harnessing wind energy around buildings through the integration of oscillating aerofoil-based energy harvesters. Whilst previous studies have investigated building-integrated wind energy devices, these technologies faced challenges such as low wind speeds, high turbulence levels, and cost concerns, hindering widespread adoption. To address these limitations, researchers have turned their attention to oscillating aerofoil energy harvesters. However, the integration of these devices onto building structures requires further investigation, as there exists a knowledge gap in this area. To fill this void, this study utilises computational fluid dynamics simulations and a one degrees of freedom solver in ANSYS Fluent to analyse the behaviour and performance of an oscillating aerofoil installed on a building's roof structure. The study's findings reveal promising results, demonstrating the prediction of the aerofoil's performance under varying conditions. In addition, the placement of oscillating aerofoils on pitched structure has shown to enhance the energy harvester's overall performance. This insight could drive future research to explore additional parameters to further optimise the energy extraction process. Through integrating oscillating aerofoil energy harvesters onto building structures, this study shows the method for the advancement of building-integrated wind energy technologies. This technology holds great promise in enhancing wind energy extraction from the built environment, contributing to more sustainable and eco-friendly energy solutions. As the demand for low-energy building design and renewable energy solutions continues to grow, this research aligns with the broader goal of promoting sustainable development and mitigating climate change. In conclusion, the integration of oscillating aerofoil energy harvesters onto building structures offers a promising approach to maximize wind energy extraction and foster the development of sustainable energy solutions in the built environment. As further research explores and refines this technology, it has the potential to revolutionize the way buildings generate and utilise clean energy, significantly reducing their environmental footprint.*

*Keywords: Building energy, Wind energy, Computational fluid dynamics, Oscillating aerofoil, Six degrees of freedom (DOF)*

## 1. INTRODUCTION

Wind energy harvesting systems have proven effective in integrating renewable energy solutions within the built environment. Conventional wind energy technologies, such as Horizontal Axis Wind Turbines (HAWT), Vertical Axis Wind Turbines (VAWT), and Ducted Augmented Wind Turbines (DAWT), have been commonly used (Sawant et al., 2021). However, researchers (Koliyabandara, N. and Mason, 2019; Hemida et al., 2020) have been interested in developing innovative wind capturing technologies that can generate energy from different Atmospheric Boundary Layer (ABL) conditions (Wang et al., 2016; Ntinis et al., 2014). Several studies (Koliyabandara, N. and Mason, 2019; Hemida et al., 2020; Tasneem et al., 2020; Kadivar et al., 2021; Bhat and Govardhan, 2013; Jingya et al., 2013) on building integrated wind turbine technologies have shown that pitched roof structures can accelerate wind velocities, leading to increased power output. However, challenges persist, including high equipment and installation costs, low wind speeds, and durability issues in turbulent environments (Aquino et al., 2017). To address these challenges, this study proposes a novel design of an oscillating aerofoil integrated into a building's roof structure. Existing studies (Poirel et al., 2008; Tang and Dowell, 2016; Shan et al., 2020; Tsushima and Weihua, 2017; Bibo and Daqaq 2013; Li et al., 2018; Chai et al., 2021; Quy et al., 2016; Zhang et al., 2020). in the literature for oscillating aerofoil only focuses on the design or its dynamic behaviour when it interacts with the wind flow, and not when it is integrated into the building roof structure. with no available study on exploring the integration of oscillating aerofoil technologies into buildings. The impact of roof shape on aerofoil flutter technology and power extraction performance remains unexplored.

Computational Fluid Dynamics (CFD) has become a primary tool for studying wind flow around various building structures and understanding aerodynamic characteristics (Abohela et al., 2012; Stathopoulos, T. and Wu, 2004). It offers a cost-effective approach to investigate different parameters at various wind and operating conditions (Abohela et al., 2012). The study aims to examine the aerodynamic behavior and power extraction performance of the proposed oscillating aerofoil design using CFD simulations with a six degrees of freedom (DOF) solver in ANSYS Fluent. The proposed 3D model of the oscillating aerofoil integrated into the building roof structure will be evaluated under different parameters to assess moment, angular velocity, and power output. This study seeks to provide a fundamental understanding of building-integrated energy harvesting systems and develop new data collection methods for power output and pitch oscillations.

Figure 1 depicts the operational mechanism of the proposed design, where the oscillating aerofoil interacts with the wind flow, resulting in motion due to torque forces. The building's roof shape is instrumental in enhancing wind velocities, potentially leading to increased power generation. To analyse wing movement and applied forces under various scenarios, the study will utilize the dynamic mesh method. In Figure 1, the mechanism of the proposed oscillating aerofoil integrated into the building's roof structure is shown. As the wind flow contacts the aerofoil (due to the inertia of the weight force), the wing starts to move around due to the torque force exerted by the current relative to the support rod. Simultaneously, the roof shape accelerates streamwise wind velocities over and around the buildings, intensifying turbulence in the vicinity (Abohela et al., 2012). The study aims to predict the motion, torque, angular velocity, and output power of the oscillating aerofoil. To achieve this, the dynamic mesh method will be employed to observe changes in the wing's movement and the forces applied in each case.

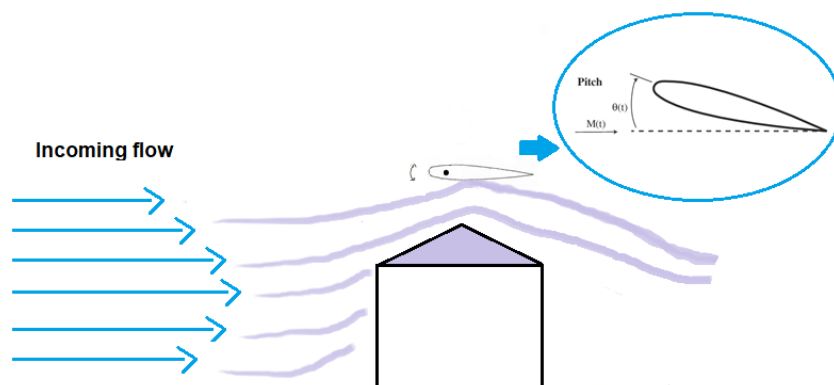


Figure 1 Schematic diagram of the building integrated wind energy harvesting system based on an oscillating aerofoil

## 2. METHOD

To investigate the performance of an oscillating aerofoil integrated into a building roof structure, a 3D Computational Fluid Dynamics (CFD) model was developed using ANSYS Designmodeler software. ANSYS meshing was utilized to generate grids for the simulations. Two distinct designs of oscillating aerofoils integrated into the roof building structure were considered. These designs encompassed a symmetrical NACA 0012 aerofoil integrated into two different roof shapes: a flat roof and a pitched roof building structure. The selection of the standard NACA 0012 aerofoil in this study was driven by its previous use in research on self-excited oscillations at low Reynolds numbers, proving its efficacy under such conditions. Additionally, the aerodynamic characteristics of the NACA 0012 aerofoil are well-documented, with a wealth of published research data available for this specific profile. Through incorporating these designs into the CFD model, the

study aimed to assess the aerodynamic performance and energy extraction capabilities of the oscillating aerofoil integrated into various building roof structures. The CFD simulations provided valuable insights into the behaviour of the aerofoil in different flow conditions, enabling a comprehensive evaluation of its potential as an innovative wind energy harvesting solution for building integration.

## 2.1. CFD geometry

The simulation geometry consists of three main components: the computational domain, the building roof structure, and the oscillating aerofoil, as depicted in Figure 2 and Figure 3. The computational domain measures 96.6 m x 66.6 m x 36 m, while the building roof structure has dimensions of 6 m x 6.6 m x 6 m. The selected aerofoil has a 1 m wingspan and a 1 m chord length. The dimensions of the roof building structure were determined based on the findings of a previous study (Tominaga et al., 2015), which also served as validation for the CFD model of the building with a pitched roof.

Figure 2 illustrates the symmetrical aerofoil used in the simulations, specifically the NACA 0012 profile. A support rod is strategically positioned at a quarter of the chord length ( $0.25c$ ) to allow the aerofoil to move in pitch directions. The support rod, with a diameter of 15 mm, provides stability for the oscillating aerofoil during motion. Whereas in figure 3, it showcases the integration of the oscillating aerofoils into the building roof structure. The aerofoils are precisely incorporated into the design to harness wind energy efficiently and enhance power extraction performance. These simulations form the basis for evaluating the aerodynamic behaviour and energy harvesting potential of the proposed building integrated wind energy system with oscillating aerofoils.

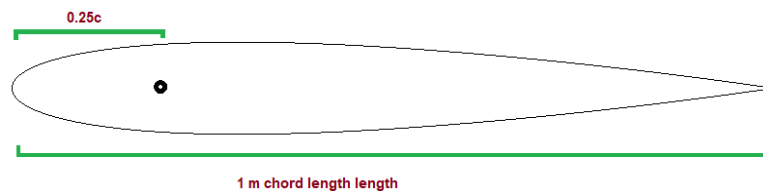


Figure 2 Centre of rotation of a (a) NACA 0012

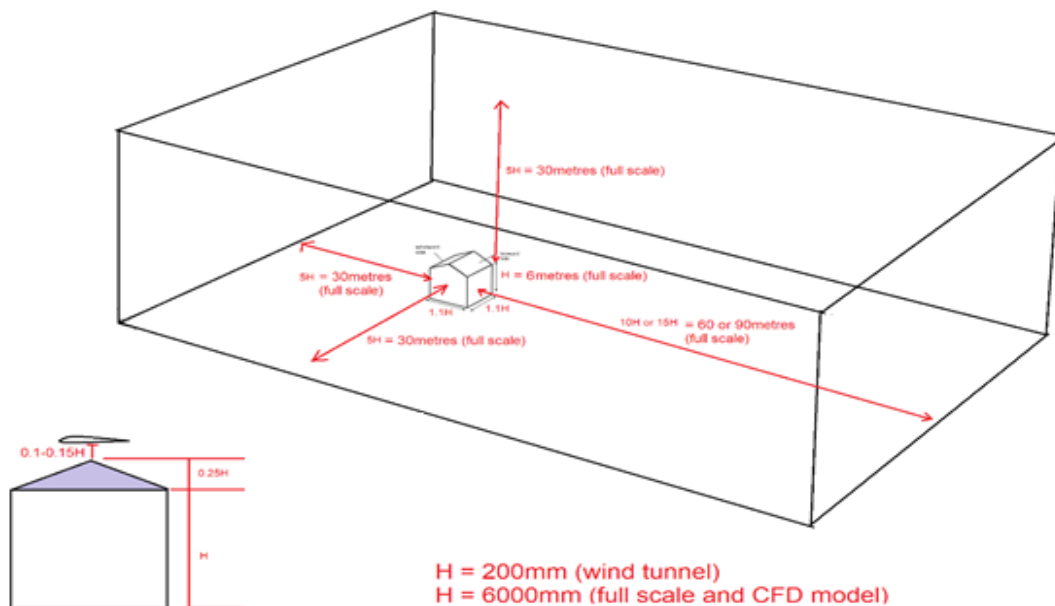


Figure 3 Schematic design of the computation model of the integrated design of building structure

## 2.2. Mesh and analysis

For the computational domain of the investigated CFD model, ANSYS Meshing software was employed for grid generation, resulting in 1,573,322 elements and 289,110 nodes. Given the complexity of the model, tetrahedral elements were used. To accommodate the dynamic nature of the simulation, a dynamic mesh method was applied, allowing automatic reconstruction of the mesh for new geometries as the model evolves. The dynamic mesh implementation utilized remeshing and smoothing commands to optimize mesh quality. During mesh analysis, key criteria such as skewness, orthogonality, aspect ratio, and negative volume were considered to ensure a suitable mesh configuration.

Figure 4 illustrates the meshing for the three designs of the model, showcasing the detailed mesh distribution. The skewness criterion was evaluated to have a maximum value of 0.95323, which remained within the limit for highly skewed cells and faces. Regarding orthogonality quality, a minimum value of 0.05 was achieved, indicating satisfactory mesh orthogonality. For aspect ratio mesh quality, a minimum value of 1.16 was obtained, implying a well-distributed and refined mesh across the computational domain. Overall, the grid generation and mesh analysis process played a vital role in preparing the CFD model for accurate simulations and reliable results, ensuring that the mesh configuration met the necessary criteria for a successful investigation.

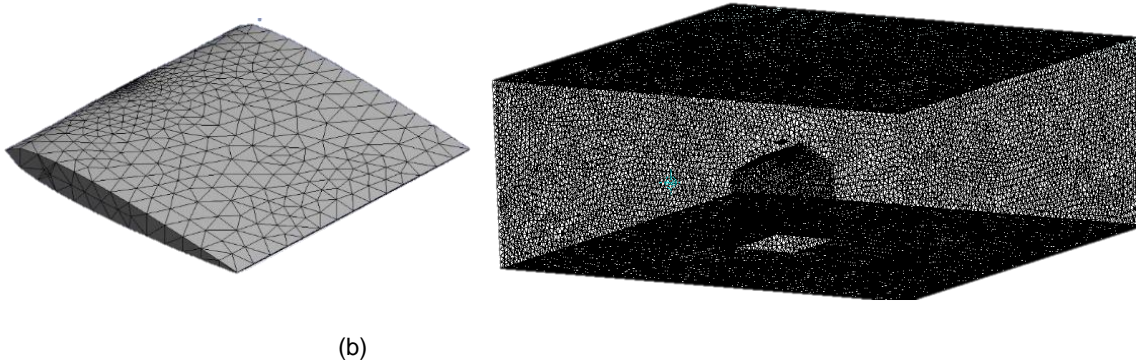


Figure 4 Meshing of (a) NACA 0012 (b) Computational domain and aerofoil integrated into the pitched roof building structure

The numerical simulations provided valuable insights into the interaction between the oscillating aerofoil and the wind flow in the building roof structure. ANSYS FLUENT's one degree of freedom solver accurately predicted pitch oscillations and power capture, considering forces and motion. The dynamic mesh method effectively modelled flow behaviours, accounting for changes in the computational domain's shape over time due to motion on its boundaries (Zhang et al., 2020; Fu et al., 2020; Sanderasagran et al., 2020; Dunbar et al., 2015; Wicaksono et al., 2021). This approach captured the intricate interactions between the aerofoil and wind flow, offering a comprehensive understanding of system behaviour. In addition, the simulations revealed the potential power output and performance of the oscillating aerofoil in the building-integrated wind energy system. The dynamic mesh method's success in accurately depicting complex fluid-solid interactions highlighted the effectiveness of this innovative technology. These results contribute significantly to advancing building-integrated wind energy technologies, offering sustainable energy solutions for the built environment.

### 2.3. CFD setup and boundary conditions

The analysis employed 3D Reynolds Averaged Navier-Stokes equations, momentum, and continuity equations to investigate the interaction between the wind flow and the aerofoil. The main goal was to calculate the motion, torque, and power output of the oscillating aerofoil. To achieve this, the dynamic mesh method was utilized to monitor the wing's movement and the forces during pitch motion. A 1 degree of freedom solver was employed to determine external forces, moments, and oscillations of the moving aerofoil. The power output was calculated using the mechanical power equation, considering the values of torque and angular velocity. The simulation was carried out in a pressure-based, time-dependent manner, considering gravitational forces. The study aimed to gain valuable insights into the performance of the oscillating aerofoil within the wind energy harvesting system.

#### Model Validation

The validation process involved comparing the simulation results with previous experimental studies on oscillating aerofoil and roof building structure. The comparison was performed separately for the frequency values of the oscillating aerofoil and the wind flow characteristics around the roof building structure.

### 2.4. Oscillating aerofoil

The 3D numerical model developed in this study was validated against wind tunnel experiment data conducted by (Poirel et al., 2008). The validation process utilized the dynamic mesh method with a 1 degree of freedom (DOF) solver in rotational motion (pitch). The numerical model was subjected to three different wind velocities: 6 m/s, 8 m/s, and 12 m/s. The obtained frequency values from the simulations were compared to the experimental data of (Poirel et al., 2008), and the results were presented in Table 1. The comparison showed that the frequency values from the current study exhibited a high level of agreement with the published data of (Poirel et al., 2008). Furthermore, the amount of aerofoil oscillation in the simulations closely resembled the values reported in the research paper, indicating a low error in the simulation results across all three different wind speeds. This validation process confirms the accuracy and reliability of the numerical model, instilling confidence in its ability to effectively analyse the behaviour of the oscillating aerofoil under varying wind conditions.

Table 1: Comparison of the current numerical results with the experimental data collected from the study of (Poirel et al., 2008)

	Velocity (m/s)		
	6	8	12
<b>Paper Frequency</b>	1.9	2.3	4.2
<b>Simulation Frequency</b>	1.95	2.4	4
<b>Error %</b>	2.6	4.3	4.7

## 2.5. Pitched roof building structure

The Computational Fluid Dynamics (CFD) modelling also encompassed the airflow around the pitched roof building structures. A comparison was made between the air flow distribution obtained from the experimental data in the work of Ntinis et al., (2014) and the CFD model of the pitched roof building structure. Figure 5 illustrates the experimental data as black dots and the current study's CFD results as blue (pitched roof). The findings revealed a minimal difference between the CFD results and the experimental data from Ntinis et al., (2014), indicating a low error in the simulation for the pitched roof building structure. A similar trend was observed across different wind profiles, further corroborating the accuracy and reliability of the CFD model.

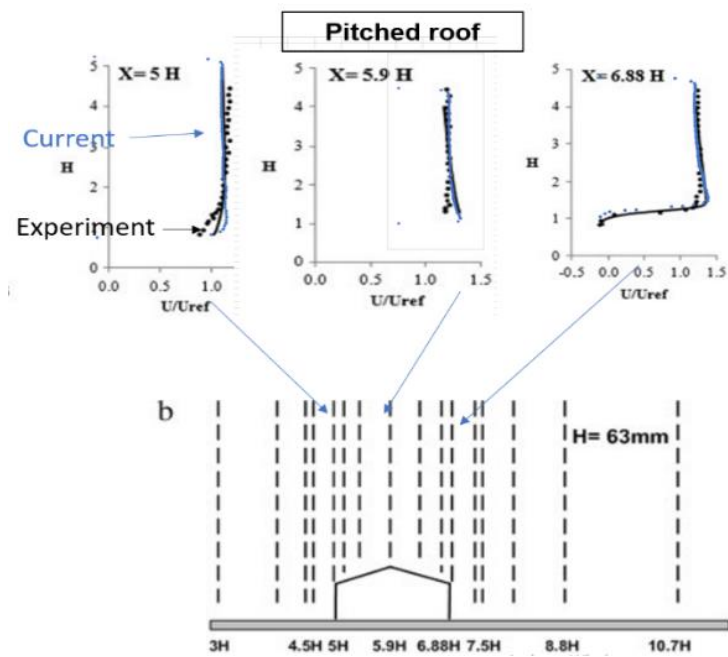


Figure 5 The comparison between numerical CFD results and experimental data of (Ntinis et al., 2014)

## 3. RESULTS AND DISCUSSION

The study aimed to compare the impact of urban wind flow and building roof structure on the performance of a proposed building integrated wind energy harvesting system under a wind speed of 3 m/s. The pitched roof building structure was found to accelerate wind velocities, providing an opportunity to enhance power extraction using an oscillating aerofoil. Various scenarios were analysed, and the values of torque, angular velocity, and power output were predicted using the six degrees of freedom (6 DOF) solver in a 1-degree rotational motion. Table 2 presents the specifications of the symmetrical aerofoil employed in the simulations. However, it was observed that the accelerated wind velocity imposed a significant wind load on the oscillating aerofoil, surpassing its handling capacity. To address this, a constraint was introduced in the ANSYS Fluent setup, limiting the model to a maximum reference angle of 23 degrees. This constraint was crucial in ensuring the stability and integrity of the simulation results.

Table 2: Specifications of the parameters of the NACA 0012 integrated to the building

Aerofoil	Dimension	Moment of inertia	Center of gravity (mass) (x,y)	Center of rotation
NACA 0012	1 m chord length and 1 m wingspan	0.04	(0.4182, 0)	(0.25, 0)

### 3.1. Pitch moment

The analysis of torque values revealed that placing the oscillating aerofoil on the roof building structure resulted in increased torque due to the accelerated wind velocity interacting with the pitched roof. Integration of the oscillating NACA 0012 with the pitched roof building structure showed improved performance compared to the flat roof building structure. This emphasizes the importance of building design in maximizing the efficiency and power output of the oscillating aerofoil within the building integrated wind energy harvesting system.

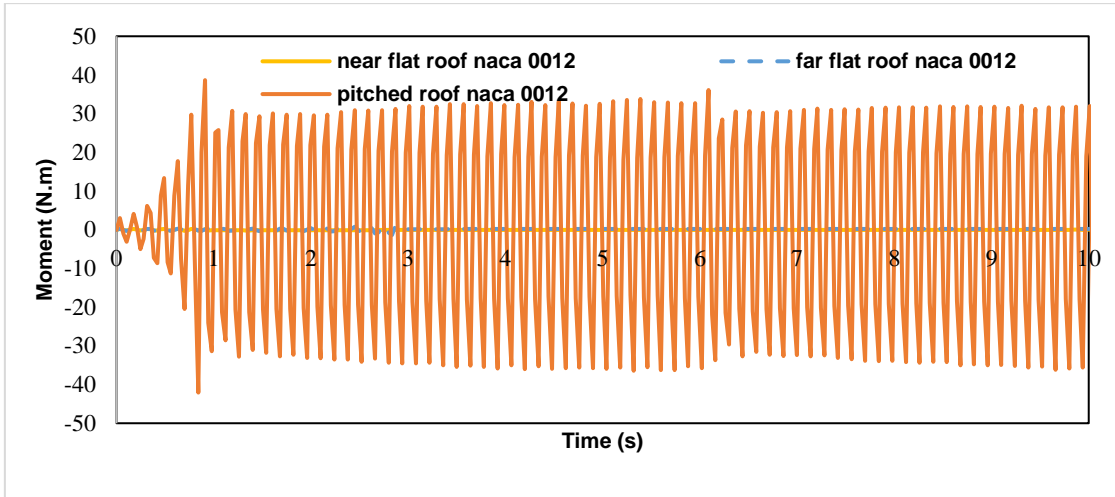


Figure 6 Comparison of the moment of torque between flat roof NACA placed near the roof and far from the roof, and a pitched roof at 3 m/s wind velocity

### 3.2. Angular velocity

Figure 7 presents the angular velocity values from a simulated sample for the pitched roof building structure, demonstrating a notable contrast with the flat roof integrated with the oscillating NACA aerofoil. The difference in angular velocity is attributed to the distinct pitch oscillation behaviour over time. The oscillations for the flat roof NACA 0012 aerofoil were relatively low compared to the specially designed pitched roof building integrated with the oscillating NACA aerofoil. This disparity arises from the lack of accelerated wind velocity advantage in the flat roof building structure, unlike the pitched roof building that effectively harnesses the wind flow to enhance the oscillating aerofoil's performance.

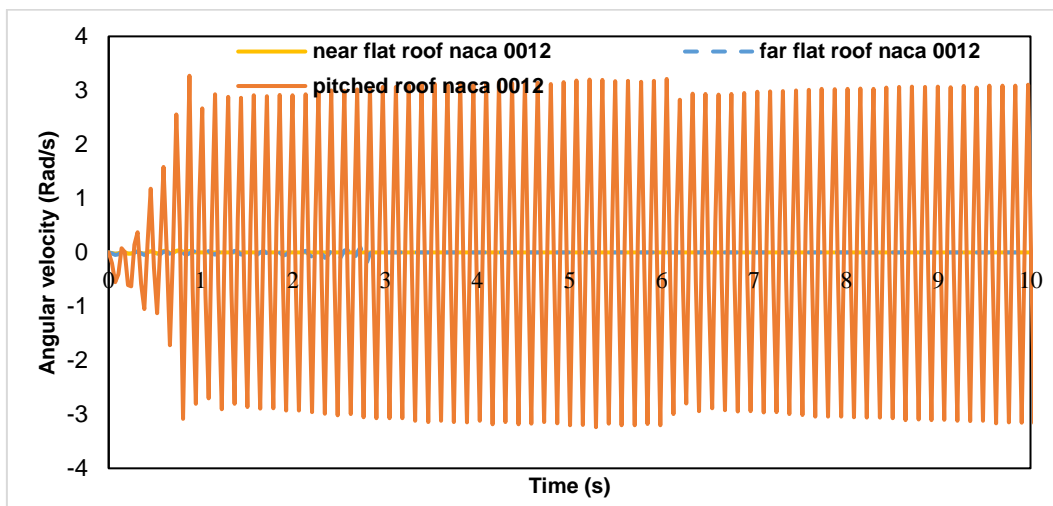


Figure 7 Comparison of the angular velocity between flat roof NACA placed near the roof and far from the roof, and pitched roof at 3m/s wind velocity

### 3.3. Power output

The power output was based on rotational motion from the result of torque ( $\tau$ ) and angular velocity ( $\omega$ ).

$$P = \tau \cdot \omega \quad (1)$$



Where:

- $P$  = Power
- $\tau$  = Torque
- $\omega$  = Angular velocity

The 1-DOF solver was used to analyze the pitch motion of the NACA 0012 aerofoil, positioned at the center of (0.25, 0) as shown in Table 3. The simulations revealed a substantial increase in power output when integrating the oscillating aerofoil onto the roof building structure. Table 4 presents the average power output values for the pitched roof design, demonstrating the influence of roof building structure on power generation. The highest average power output of 23.47353 watts was achieved with the integration of the NACA 0012 aerofoil into the pitched roof building structure.

In contrast, lower average power outputs of 0.00089 watts and 0.00243 watts were observed for the oscillating aerofoil placed near and far away from the roof, respectively. These findings underscore the significant impact of altering the placement of the oscillating aerofoil on the building roof structure and changing the roof shape, as they play a crucial role in enhancing the power performance of the designed model.

#### 4. CONCLUSION AND FUTURE WORKS

The paper proposes a building-integrated wind energy harvesting system and a methodology to study its power capture and fluid-solid interactions. The study fills a research gap by creating a CFD model of the system and investigating the power performance and pitch oscillation behaviour of an oscillating aerofoil integrated into the building's roof structure. This design presents a potential alternative to conventional wind turbines, offering lower equipment costs, easy installation on building roofs, and suitability for areas with lower wind speeds. Using a 1 degree of freedom (DOF) solver in rotational motion with ANSYS Fluent, the study accurately predicted moment, angular velocity, and power output.

In addition, the parametric analysis demonstrated that integrating an oscillating NACA 0012 aerofoil into a pitched roof building achieved the highest power output of 23.47353 watts, indicating improved performance. Future research in oscillating aerofoil integration within buildings should explore other roof geometries like curved surfaces, investigate alternative aerofoil shapes for higher power output, analyse the impact of different wind velocities and aerofoil dimensions, consider power performance under heave motion, study the influence of turbulence intensity on system operation and lifespan, and conduct a techno-economic analysis comparing the proposed design with conventional wind turbines.

#### 5. REFERENCES

- Sawant, M., Thakare, S., Rao, A. P., Feijóo-Lorenzo, A. E., Bokde, N. D., 2021. A Review on State-of-the-Art Reviews in Wind-Turbine- and Wind-Farm-Related Topics, *Energies*, 14(8), pp. 2041.
- Koliyabandara, N. and Mason, M., 2019. Wind loads on the roof of a low-rise building during flow acceleration, The 15th *International Conference on Wind Engineering*, Beijing, China.
- Hemida, H., Šarkić Glumac, A., Vita, G., Kostadinović Vranešević, K., Höffer, R., 2020. On the Flow over High-rise Building for Wind Energy Harvesting: An Experimental Investigation of Wind Speed and Surface Pressure, *Applied Science*, 10, pp. 5283.
- Wang, M., Huang, S., Lin, X., Novianto, D., Fan, L., Gao, W., Wang, Z., 2016. Research on Energy Consumption of Traditional Natural Villages in Transition: A Case Study in Zhejiang Province. *Energy and Power Engineering*, 8, pp. 34-50.
- Ntinis, G. K., Zhang, G., Fragos, V. P., Bochtis, D. D. Nikita-Martzopoulou, C., 2014. Airflow patterns around obstacles with arched and pitched roofs: Wind tunnel measurements and direct simulation. *European Journal of Mechanics - B/Fluids*, 43, pp. 216-229.
- Tasneem, Z., Al Noman, A., Das, S., Saha, D., Islam, M. R. Ali, M. F., Badal, M. F., Ahamed, M. H., Moyeen, S., Alam, F., 2020. An analytical review on the evaluation of wind resource and wind turbine for urban application: Prospect and challenges, *Developments in the Built Environment*, 4.
- Kadivar, M., Tormey, D., McGranaghan, G., 2021. A review on turbulent flow over rough surfaces: Fundamentals and theories, *International Journal of Thermofluids*, 10.
- Bhat, S. and Govardhan, R. 2013. Stall flutter of NACA 0012 airfoil at low Reynolds numbers. *Journal of Fluids and Structures*, 41, pp.166-174.
- Jingya, L., Lei, W., Kailing, W., Gong, K., Jian, H., 2013. Earthquake-resistant performance investigation for rural buildings in Zhongxiang area, China, *Geodesy and Geodynamics*, 4(1), pp. 55-60.



- Aquino, A., Calautit, J. K., Hughes, B., 2017. Urban Integration of Aeroelastic Belt for Low-Energy Wind Harvesting, *Energy Procedia*, 105, pp.738-743.
- Poirel, D., Harris, Y., Benaissa, A., 2008. Self-sustained aeroelastic oscillations of a NACA0012 airfoil at low-to-moderate Reynolds numbers, *Journal of Fluids and Structures*, 24(5), pp.700-719.
- Tang, D. and Dowell, E. H., 2016. Experimental Aeroelastic Models Design and Wind Tunnel Testing for Correlation with New Theory. *Aerospace*, 3(12).
- Shan, X., Tian, H., Cao, H., Feng, J., Xie, T., 2020. Experimental Investigation on a Novel Airfoil-Based Piezoelectric Energy Harvester for Aeroelastic Vibration. *Micromachines (Basel)*, 11(8), pp. 725.
- Tsushima, N, and Weihua, Su. 2017. Flutter suppression for highly flexible wings using passive and active piezoelectric effects, *Aerospace Science and Technology*, 65, pp. 78-89.
- Bibo, A., and Daqaq, M., 2013. Energy Harvesting Under Combined Aerodynamic and Base Excitations. *Journal of Sound Vibration*, 332, pp. 5086-5102.
- Li, K., Yang, Z., Gu, Y., He, S., Zhou, S., 2018. Nonlinear magnetic-coupled flutter-based aeroelastic energy harvester, Modeling, simulation and experimental verification. *Smart Materials and Structures*. 28.
- Chai, Y, Gao, W, Ankaý, B, Li, F, Zhang, C. 2021. Aeroelastic analysis and flutter control of wings and panels: A review. *International Journal of Mechanical System Dynamics*, 1(2), pp. 5- 34.
- Quy, V. D., Sy, N. V., Hung, D. T., Huy, V. Q., 2016. Wind tunnel and initial field tests of a micro generator powered by fluid-induced flutter, *Energy for Sustainable Development*, 33, pp. 75–83.
- Zhang, Y., Zhou, Z., Wang, K., Li, X., 2020. Aerodynamic Characteristics of Different Airfoils under Varied Turbulence Intensities at Low Reynolds Numbers. *Applied Science*, 10, 1706.
- Abohela, I., Hamza, N., Dudek, S., 2012. Roof Mounted Wind Turbines: The influence of roof shape, building height and urban location on wind speed.
- Stathopoulos, T. and Wu, H., 2004. Using computational fluid dynamics (CFD) for pedestrian winds. In: Proceedings of Structures, Building on the Past, Securing the Future.
- Tominaga, Y., Akabayashi, S., Kitahara, T., Arinami, Y., 2015. Air flow around isolated gable-roof buildings with different roof pitches: Wind tunnel experiments and CFD simulations. *Building and Environment*, 84, pp. 204-213.
- Fu, C., Uddin, M., Zhang, C., 2020. Computational Analyses of the Effects of Wind Tunnel Ground Simulation and Blockage Ratio on the Aerodynamic Prediction of Flow over a Passenger Vehicle. *Vehicles*, 2, pp. 318-341.
- Sanderasagan, A. Azizuddin, A., Oumer, A., 2020. Comparative CFD power extraction analysis of novel nature inspired vertical axis wind turbines Comparative CFD power extraction analysis of novel nature inspired vertical axis wind turbines. *IOP Conference Series Materials Science and Engineering*, 863.
- Dunbar, A., Craven, B., Paterson, E., 2015. Development and validation of a tightly coupled CFD/6-DOF solver for simulating floating offshore wind turbine platforms, *Ocean Engineering*, 110, pp. 98-105.
- Wicaksono, H., Hadi, S., Pranoto, B., Fakhrudin, M., 2021. Initial Rotation Characteristic Investigation of a Hybrid Savonius - Darrieus Wind Turbine using 6 DOF Computational Fluid Dynamics, *Mekanika: Majalah Ilmiah Mekanika*, 20(1).

---

## #236: A review on the state-of-the-art wind energy harvesting technologies and potential integration into building roof structure

---

Katrina CALAUTIT<sup>1</sup>, Cameron JOHNSTONE<sup>2</sup>

*1 University of Strathclyde, Glasgow, United Kingdom, katrina.calautit@strath.ac.uk*

*2 University of Strathclyde, Glasgow, United Kingdom, cameron.johnstone@strath.ac.uk*

*Abstract: In this study, the focus was on exploring alternative wind energy harvesting technologies that can overcome the limitations of conventional wind turbines in urban and rural areas. The conventional wind turbines have shown low power output in areas with low wind velocities, and their heavy installation on lightweight building structures can compromise the integrity of the structure and lead to a shorter lifespan of the turbines. To address these challenges, the study investigated the power and harvesting performance of various wind energy harvesting systems, particularly those employing oscillating mechanisms like galloping, flutter, and vortex-induced vibration. The objective was to provide a clean energy solution for off-grid areas to capture energy from the accelerated air flow on building roofs. The review analysed the technical features of each wind-induced vibration technology, considering non-uniform wind flow and a wide range of wind speeds that the energy harvester might encounter on the roof. The findings indicated that small-scale wind energy harvester devices achieved a power output of nanowatts to milliwatts. However, further improvements in power output were possible by integrating the energy harvester into roof building structures to create wind velocity acceleration, scaling up the harvester, and incorporating power management. The review revealed a lack of studies on the integration of small-scale energy harvesting devices with structures and buildings, indicating a crucial area for future research. Through exploring lightweight building integrated wind energy harvesting systems with longer lifespans, this study provides opportunity to sustainable energy solutions for off-grid areas, where conventional wind turbines may not be practical.*

*Keywords: Wind energy; Small-scale wind energy harvesting system; Building-integrated wind energy harvesting system; Buildings*

## 1. INTRODUCTION

The lack of access to electricity in developing countries, especially in tropical regions, calls for the development of affordable and sustainable renewable energy technologies. Conventional wind turbines face challenges in rural areas, making small-scale wind energy technologies a viable alternative. Wind-induced vibration technologies, such as galloping, flutter, and VIV, offer promising power capture capabilities, particularly in low wind speed areas. Integrating these technologies into building structures can lead to decentralised power supply, increased energy efficiency, and reduced dependence on energy companies.

However, there is a research gap in the integrated design of small-scale wind-induced vibration and roof building structures. Most existing studies focus on stand-alone wind-induced vibrations, neglecting their integration with buildings. To improve the power output, wind-induced vibration technologies should be placed on pitched or curved roofs, taking advantage of wind velocity acceleration. Additionally, upscaling the technology and improving its structure design can enhance power and harvesting performance.

Currently, there is limited research on small-scale wind-induced vibration technologies integrated into roof building structures, especially in rural communities in tropical regions. Most studies focus on Horizontal Axis Wind Turbines (HAWT), Vertical Axis Wind Turbines (VAWT), and Ducted Augmented Wind Turbines (DAWT) for building integrated wind energy harvesting systems. To fill this research gap, this study reviewed and evaluated the designs, efficiency, and power and harvesting performances of galloping, flutter, and VIV mechanisms for small-scale devices. Integrating these technologies into building structures could offer a cost-effective solution for power capture in areas with low wind speeds, making it a more practical option compared to conventional wind turbines.

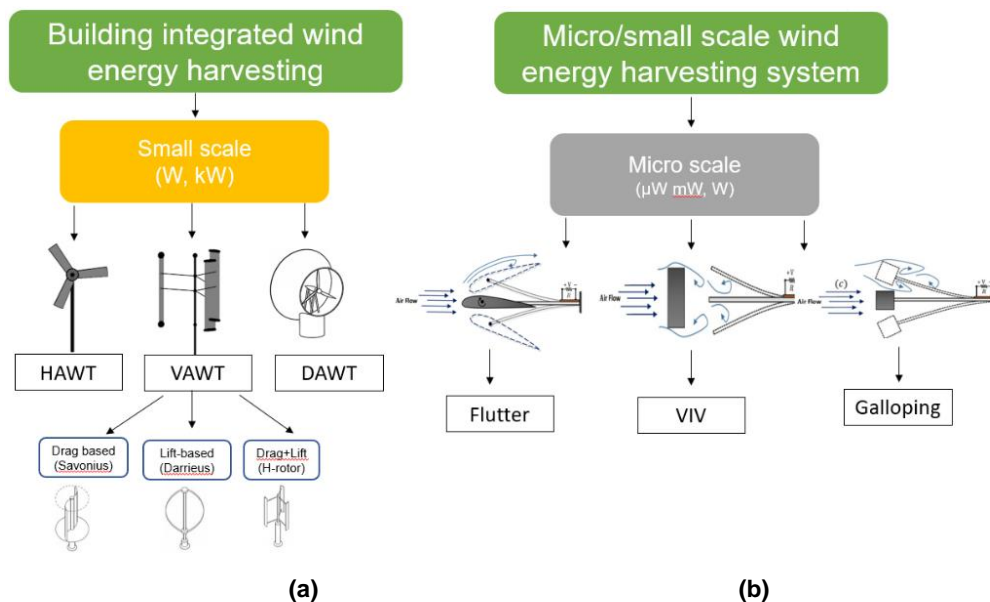


Figure 1 The designs of (a) conventional wind turbines and (b) wind induced vibration technologies

## 2. METHOD

A review of the state of the art was carried out on small-scale wind energy harvester and building integrated wind energy harvesting system. Since there are several research on these topics, the focus on this review was to examine the state-of-the-art-design, power and harvesting performance of lightweight small-scale wind energy harvesting system, which could potentially be integrated into rural buildings.

To gather the research materials for this review, the keyword search such as "wind induced vibration", "small-scale wind energy harvesting system", "building integrated wind energy harvesting system". The University of Strathclyde's "SUPrimo Library search tool, "Nature", "ScienceDirect", "Multidisciplinary Digital Publishing Institute (MDPI)" The selected papers are from the year 2011 to 2022 and books, chapter, thesis research paper are excluded from the review. Also, the papers selected are about the different design, mechanisms, method of analysis, and power and harvesting performance. After the review, each technology was analysed in terms of technical performance.

From the recent studies on the small-scale wind energy harvesting systems, there are three designs that are usually tested for wind induced vibration power and harvesting performance. These include the galloping, flutter, and vortex induced vibration-based wind energy harvester. Figure 2 shows the proposed designs for building integrated wind energy harvesting systems.

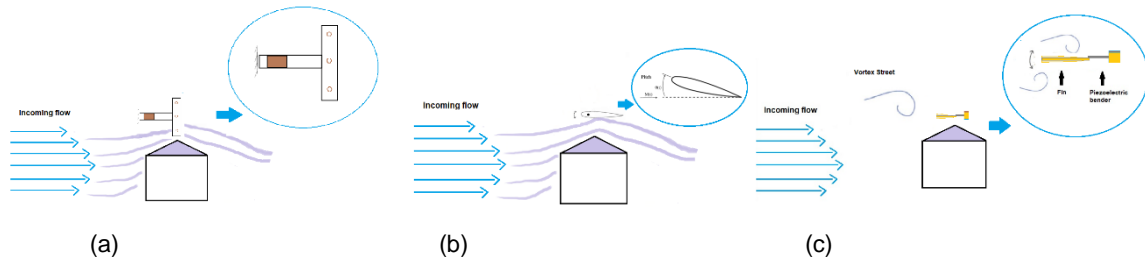


Figure 2 Schematic diagrams of proposed small-scale harvester for roof building integration (a) galloping (b) flutter (c) VIV

### 3. REVIEW OF THE STATE-OF-THE-ART

This section provides an overview of recent developments in small-scale wind-induced vibrations, focusing on their low cost, lightweight, simple structure, and compact design, which makes them suitable for installation on the roofs of rural houses and buildings to harness wind velocity acceleration.

Wen et al. (2021) analysed energy coupling mechanisms in wind energy harvesting systems, including galloping, flutter, and vortex-induced vibration (VIV). VIV demonstrated optimal efficiency at low wind speeds with suitable design, but its operational range is limited. Aeroelastic flutter, on the other hand, exhibits divergence and self-excitation, leading to negative damping at higher wind speeds. Galloping, combining positive features of VIV and flutter, offers a wide operational wind speed range, but lacks an established analytical model. The natural behaviour of wind-induced vibration utilizes combined lift and drag forces to convert wind flow energy. This mechanism proves more appropriate for low wind speed deployments, as vibrations are easily converted to electrical energy, unlike rotational motion. Flutter and VIV-based wind-induced vibrations share similar characteristics of dynamic instabilities from unsteady inertial, elastic, and aerodynamic forces, while galloping exhibits both aeroelastic flutter and VIV characteristics.

These small-scale wind-induced vibration systems can effectively operate at low wind speeds across a broad range of velocities, making them suitable for building-integrated wind energy harvesting. These technologies address the common challenge faced by conventional wind turbines, which become non-operational at low wind speeds. Thus, they show great potential for harvesting energy from building structures under low wind conditions and non-uniform wind flows.

#### 3.1. Galloping-type energy harvesting

Galloping is a self-excited vibration observed in slender body formations when exposed to static torsional moment, lift, and drag forces in crossflow direction. This phenomenon can lead to dynamic instability and negative dynamic damping (Wang et al., 2021). Integrating galloping technology into roof building requires further investigation to optimize design, considering non-uniform wind flow, effects of accelerated wind velocity on energy harvesting, and airflow distribution. Yang et al. (2013) conducted an experimental study on various tip cross sections for small-scale galloping energy harvesters. The square profile exhibited the best performance among rectangle, D-shape, and triangle, achieving a high peak power of 8.4 milliwatt. Zhao et al. (2020) investigated different shapes like funnel, triangle, and square, proposing a wind induced galloping energy harvester design with high normalized power densities under different wind speeds.

These studies demonstrate the potential of galloping-based systems for energy harvesting under various conditions, paving the way for their integration into buildings for effective wind energy utilization. Further research should focus on optimizing designs and evaluating the feasibility and cost-effectiveness of these systems for commercial deployment.

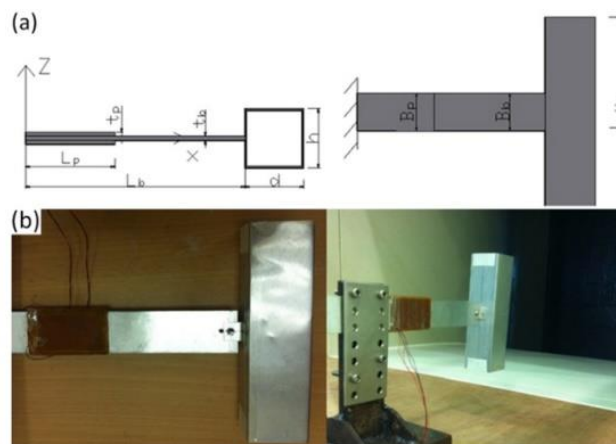


Figure 3 View at the top and side of the designed galloping energy harvesting system and (b) experimental setup (Yang et al., 2013)

The reviewed studies on galloping-based wind energy harvesting systems showcased diverse and innovative designs. Sirohi and Mahadik (2011) proposed a triangular cross-section connected to a cantilever beam, achieving a peak power output of 53 milliwatt in wind tunnel tests. Le and Kwon (2021) introduced a quadruple Halbach array for harvesting wind energy, achieving an 8 mW power output at 12 m/s wind speed. Wang et al. (2021) presented a cut-corner prism design, enhancing pressure differences and reaching a power output of 47.5 milliwatt with a windward side length of 0.6B.

These studies demonstrate the potential of galloping-based systems for power generation in various configurations and wind conditions. The designs offer promise for practical applications, such as powering wireless sensor nodes and other small-scale electronic devices in outdoor settings. The integration of these innovative energy harvesters with buildings or rooftops should be explored further to harness wind velocity acceleration and optimize power production. A techno-economic analysis would also be valuable to assess the feasibility of commercializing these systems and their cost-effectiveness compared to traditional wind turbines. Overall, galloping-based wind energy harvesting shows great potential for efficient and cost-efficient renewable energy generation in the future.

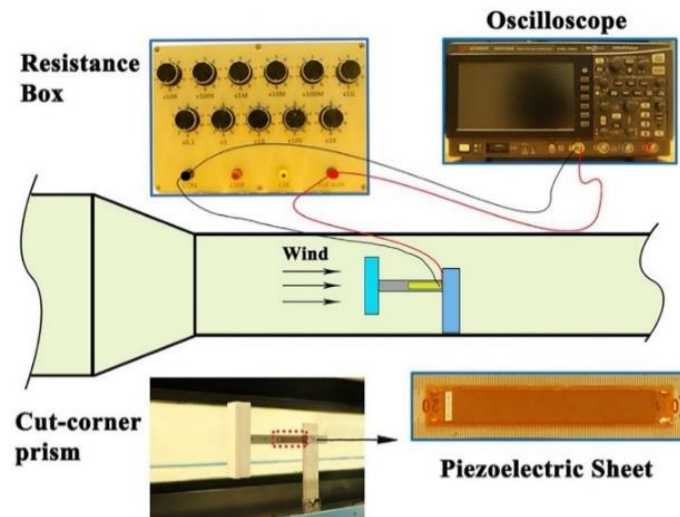


Figure 4 Schematic design of the cut corner prism energy harvesting system based on galloping mechanism (Wang et al., 2021)

The galloping-based wind induced vibration technology has been predominantly studied in laboratory settings or through numerical analysis, with no research exploring its integration into building structures. Table 1 summarizes the reviewed works and highlights the potential of this energy harvesting technology, showcasing its effectiveness in wind speeds ranging from 2 m/s to 13 m/s, particularly in non-uniform wind flows. This indicates its suitability for integration with buildings or roofs. Additionally, this technology offers the advantage of being lightweight and cost-effective compared to traditional wind turbines. However, a notable gap exists as none of the studies provided an evaluation of the capital costs, operational expenses, and maintenance costs associated with the energy harvester. A techno-economic analysis is crucial to gain insights into the commercial viability and market potential of the technology.

### 3.2. Flutter-type low energy harvesting

Flutter vibration mechanisms arise from self-excited aerodynamic forces and involve the interaction between solid structures and fluid, allowing for energy extraction to the harvester based on aerodynamic features. These technologies are primarily studied for stand-alone flutter wind energy harvesters, with most applications being wind tunnel experiments or numerical simulations. Integration of flutter-based wind energy harvesting systems into buildings is rare in the literature.

Recent developments in small-scale wind energy harvesting have shown the integration of flutter-based aeroelastic belts into urban building structures, as demonstrated by Aquino et al. (2016). The design utilizes electro-magnetic coils, tensioning membranes, and power conditioning devices with a simple structure, resulting in low costs and easy configuration with other technologies. The apex of the roof building at 45 degrees achieved the highest power output of 62.4 milliwatt under wind speeds of up to 6.2 m/s. Another design presented by Zhang et al. (2015) involves a cuboid chamber, piezo-electric cantilever, and resonant cavity for wind energy harvesting. The system exhibited a power output of 1.59 milliwatt at 11.2 m/s wind speed, demonstrating its potential for powering wireless sensor nodes. Whereas in the study of Chawdhury and Morgenthal (2018), the performance of a T-shaped cantilever beam for flutter-based wind-induced energy harvesting was investigated using a 2D CFD model. The system showed a maximum power output of 5.3 milliwatt at 8 m/s wind speed. Shan et al. (2020) proposed an aerofoil flutter-based aeroelastic wind energy harvesting system, which demonstrated limit cycle oscillation at high wind velocity. The maximum power output was 0.764 milliwatt at 16.32 m/s, outperforming existing aerofoil-based piezoelectric energy harvesters.

Overall, these studies highlight the potential of flutter-based wind energy harvesting systems for building integration, offering promising solutions for sustainable power generation in various applications.

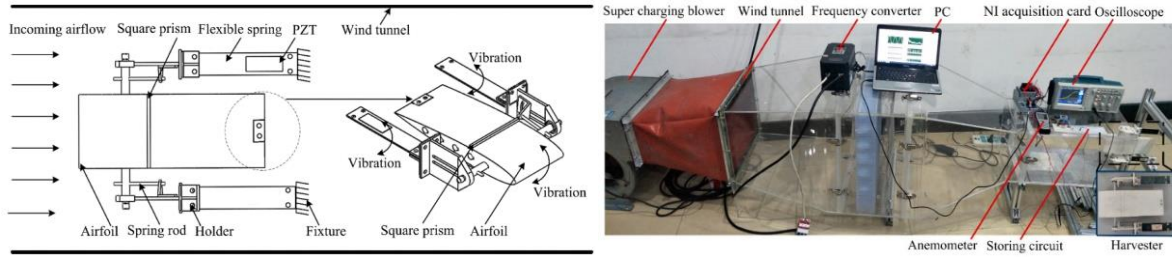


Figure 5 Schematic design of a piezo-electric energy harvesting system (Shan et al., 2020)

Sousa et al. (2015) investigated an aerofoil flutter-based wind energy harvesting system using numerical simulations. The design included aerofoil section with piezo-electric coupling and pseudo elastic hysteresis of shape memory springs to harvest wind energy. The study reported a power output of 120 mW with the best load resistance at 14 m/s-1 and 4.5 N. The addition of pseudo elastic hysteresis improved the power performance compared to hardened steel springs. Further evaluation is needed for real-world applications and techno-economic analysis.

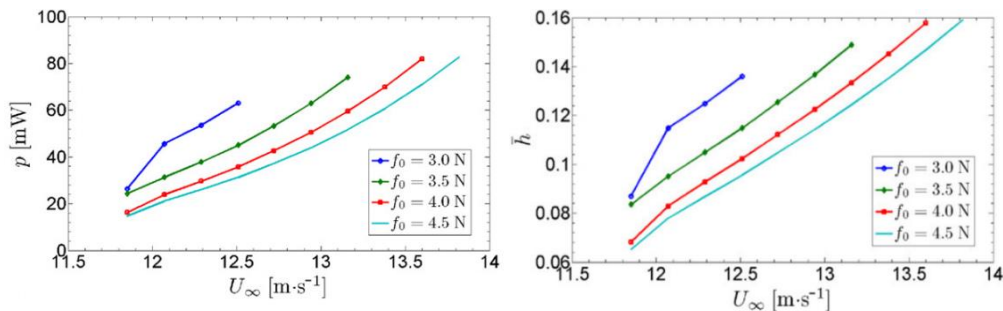


Figure 6 The results of peak electrical power output from the amplitude of plunge displacement (Sousa et al., 2015)

In Perez et al. (2015), a novel design of aeroelastic flutter wind energy harvesting system was introduced, attached to an electret transducer to convert membrane-induced motions into electric power. The prototype comprised a polymer membrane between two flat electrodes with Teflon Polytetrafluoroethylene electret coatings, with a bluff body inducing vortex shedding at the inlet. During tests, the membrane oscillated due to flutter effect, interacting with the flat electrodes. The continuous periodic movement directly transformed into electric power via the electret transducer. Multiple models were examined, with a 2.7 cm3 prototype generating 2.1 mW (782  $\mu\text{W cm}^{-3}$ ) at 30 m/s and 481  $\mu\text{W}$  (178  $\mu\text{W cm}^{-3}$ ) at 15 m/s with an electret charge of 650V. Further evaluation is necessary for real-world applications and techno-economic analysis.

### 3.3. Vortex-induced vibration-type low energy harvesting

Vortex-induced vibration (VIV) occurs when periodic vortices shed from a bluff body create oscillations due to resonance. A study by Lee et al. (2019) developed a microelectromechanical wind energy harvesting device based on VIV. The device consists of a cylindrical oscillator connected to a piezo-electric microelectromechanical system. The tests showed nanowatt power output, with higher power when the cylinders were connected, indicating potential for off-grid WSN. In another design by Weinsten et al. (2012), a piezo-electric cantilevered beam exposed to HVAC air flows generated milliwatts of power at flow excited resonance. Similarly, Jin et al. (2019) improved VIV amplitude and reduced the threshold wind velocity using bionic structure, obtaining milliwatt power output at higher wind speed. Another design by Hu et al. (2018) used e-shaped piezo-electric energy harvesting system from VIV, achieving highest power output of 3.35 mW when the mean fluid velocity, resistive load, and scale factor were configured to values of 1.5 m/s and 105  $\Omega$ .

Akaydin et al. (2012) introduced a design featuring a cylinder connected to a cantilevered beam partly covered with piezo-electric elements. The study examined a self-excited piezo-electric energy harvesting system exposed to steady and uniform wind flow. The system produced 0.1 milliwatt of non-rectified electric power at 1.192 m/s wind speed, highlighting its potential for building integration. Further research is needed to explore the integration of wind energy harvesters into building structures and optimize their power output in real-world conditions. 3D numerical model developed in this study was validated against wind tunnel experiment data conducted by (Poirel et al., 2008). The validation process utilized the dynamic mesh method with a 1 degree of freedom (DOF) solver in rotational motion (pitch). The numerical model was subjected to three different wind velocities: 6 m/s, 8 m/s, and 12 m/s. The obtained frequency values from the simulations were compared to the experimental data of (Poirel et al., 2008), and the results were presented in Table 1. The comparison showed that the frequency values from the current study exhibited a high level of agreement with the published data of (Poirel et al., 2008). Furthermore, the amount of aerofoil oscillation in the simulations closely resembled the values reported in the research paper, indicating a low error in the simulation results across all three different wind speeds. This validation process confirms the accuracy and reliability of the numerical model, instilling confidence in its ability to effectively analyse the behaviour of the oscillating aerofoil under varying wind conditions.



## 4. RESULTS AND DISCUSSION

The study aimed to compare the impact of urban wind flow and building roof structure on the performance of a proposed building integrated wind energy harvesting system under a wind speed of 3 m/s. The pitched roof building structure was found to accelerate wind velocities, providing an opportunity to enhance power extraction using an oscillating aerofoil. Various scenarios were analyzed, and the values of torque, angular velocity, and power output were predicted using the six degrees of freedom (6 DOF) solver in a 1-degree rotational motion. Table 2 presents the specifications of the symmetrical aerofoil employed in the simulations. However, it was observed that the accelerated wind velocity imposed a significant wind load on the oscillating aerofoil, surpassing its handling capacity. To address this, a constraint was introduced in the ANSYS Fluent setup, limiting the model to a maximum reference angle of 23 degrees. This constraint was crucial in ensuring the stability and integrity of the simulation. This analysis focuses on recent developments in wind-induced vibrations, including VIV, flutter, and galloping-based energy harvesters. Galloping-based wind energy harvesting systems have been tested in laboratories or through numerical simulations, demonstrating potential to produce power in the milliwatt range, suitable for powering wireless sensor nodes for environmental and structural health monitoring. However, further improvements are needed to transition from laboratory to real-world applications.

Both galloping and VIV-based wind-induced vibrations have shown promise in wind tunnel tests and numerical simulations for isolated wind energy harvesters, generating power output in the range of nanowatts to milliwatts. To improve power generation, these technologies can be scaled up and integrated into roof building structures with higher wind velocity acceleration. Only one recent study has investigated the flutter-based wind-induced vibration technology integrated into roof building structures, suggesting the optimal roof shape for maximizing power production.

The different designs of flutter-based wind energy harvesting systems showed their ability to generate power from wind-induced vibrations, proportional to wind speed. The simple structure, low cost, and lightweight materials make them suitable for powering LED lights, pedometers, and wireless temperature sensor nodes. The aerofoil-based piezo-electric design with pseudo elastic hysteresis achieved the highest power output of 120 milliwatts. VIV energy harvesting systems also demonstrated lower power output in the nano-watt to milliwatt range. VIV harvesters are affected by wind flow speed, capable of producing power at low wind speeds, but stability and performance should be considered at higher wind speeds in future studies.

## 5. CONCLUSION AND FUTURE WORKS

The field of building integrated wind energy harvesting systems has faced challenges in developing traditional wind turbines due to low wind speeds, turbulence, and high costs. This study reviews galloping, flutter, and VIV technologies for energy harvesting, focusing on small-scale devices that are cost-effective and suitable for installation in urban or rural areas. Stand-alone wind induced vibration technologies have shown potential in powering small-scale devices like wireless sensor nodes and LED lights. The aerofoil flutter design achieved the highest power output of 120 mW at 14 m/s wind speed, indicating that power output is correlated with wind velocity. The study recommends further testing under similar conditions for a comprehensive comparison of the three mechanisms. The power output can be improved through wind velocity acceleration, scaling up the harvester, and adding power management. Integrating wind energy harvesting systems onto roof buildings offers advantages like decentralized power supply and reduced transmission costs and reliance on diesel generators. Future work should investigate the effects of accelerated wind velocity, wind direction, and optimal location for energy harvesting. Additionally, economic, and environmental analyses are needed to assess operational performance, construction, and maintenance costs.

## 6. REFERENCES

- Gadonneix, P., Nadeau, M., Kim, Y. D., Birnbaum, L., Cho, H., Choudhury, A. R., Neto, J. C., Dager, J., Meyers, K., Sambo, A., Statham, B. A., World Energy Trilemma: Time to get real-the agenda for change. World Energy Council, United Kingdom, 2013.
- Borhanazad, H., Mekhilef, S., Saidur, R., Boroumandjazi, G., Potential application of renewable energy for rural electrification in Malaysia, *Renewable Energy*, Vol. 59, pp. 210-219, 2013.
- López-González, A., Domenech, B., Ferrer-Martí, L., Formative evaluation of sustainability in rural electrification programs from a management perspective: A case study from Venezuela. *Renewable and Sustainable Energy Reviews*, Vol. 1, No. 95, pp. 95-109, 2018.
- Leary, J., Schaube, P., Clementi, L., Rural electrification with household wind systems in remote high wind regions, *Energy for Sustainable Development*, Vol. 52, pp. 154-175, 2019.
- Toja-Silva, F., Lopez-Garcia, O., Peralta, C., Navarro, J. and Cruz, I., An empirical-heuristic optimization of the building-roof geometry for urban wind energy exploitation on high-rise buildings. *Applied Energy*, Vol.164, pp. 769-794, 2016.
- Kishore, R., Coudron, T., Priya, S., Small-scale wind energy portable turbine (SWEPT), *Journal of Wind Engineering and Industrial Aerodynamics*, Vol. 116. 21–31, 2013.

- Aquino, A., Calautit, J. K., Hughes, B., Urban Integration of Aeroelastic Belt for Low-Energy Wind Harvesting, *Energy Procedia*, Vol. 105, pp.738-743, 2017.
- Watson, S., Moro, A., Reis, V., Baniotopoulos, C., Barth, S., Bartoli, G., Bauer, F., Boelman, E., Bosse, D., Cherubini, A., Croce, A., Fagiano, L., Fontana, M., Gambier, A., Gkoumas, K., Golightly, C., Latour, M. I., Jamieson, P., Kaldellis, J., Macdonald, A., Murphy, J., Muskulus, M., Petrini, F., Pigolotti, L., Rasmussen, F., Schild, P., Schmehl, R., Stavridou, N., Tande, J., Taylor, N., Telsnig, T., Wiser, R., Future emerging technologies in the wind power sector: A European perspective, *Renewable and Sustainable Energy Reviews*, Vol. 113, 2019.
- Bošnjaković, M. Wind Power Buildings Integration, *Journal of Mechanics Engineering and Automation*. Vol. 3, pp. 221-226, 2013.
- Ledo, L., Kosasih, P. B., Cooper, P., Roof mounting site analysis for micro-wind turbines, *Renewable Energy*, Vol. 36, No. 5, pp. 1379-1391, 2011.
- International Energy Agency, Population without access to electricity falls below 1 billion, IEA, Paris, 2018 (Accessed at: <https://www.iea.org/commentaries/population-without-access-to-electricity-falls-below-1-billion> [Accessed: 10-Jan-2022]).
- Fei, F., Mai, J., Li, W. J., A wind-flutter energy converter for powering wireless sensors, *Sensors and Actuators A: Physical*, Vol. 173, No. 1, pp. 163-171, 2012.
- Yang, Y., Zhao, L., Tang, L., Comparative study of tip cross-sections for efficient galloping energy harvesting, *Applied Physics Letters*, Vol. 102, 064105, 2013.
- Jo, S., Sun, W., Son, C., Seok, J., Galloping-based energy harvester considering enclosure effect, *AIP Advances*, Vol. 8, 095309, 2018.
- Zhao, D., Hu, X., Tan, T., Yan, Z., Zhang, W., Piezoelectric galloping energy harvesting enhanced by topological equivalent aerodynamic design, *Energy Conversion and Management*, Vol. 222, 2020.
- Wen, Q., He, X., Lu, Z., Streiter, R., Otto, T., A comprehensive review of miniaturized wind energy harvesters, *Nano Materials Science*, Vol. 3, No. 2, pp. 170-185, 2021.
- Sirohi J, Mahadik R., Piezoelectric wind energy harvester for low-power sensors. *Journal of Intelligent Material Systems and Structures*, Vol. 22, No.18, pp. 2215-2228, 2011.
- Le, D. and Kwon, S. D., Design and Experiments of a Galloping-Based Wind Energy Harvester Using Quadruple Halbach Arrays. *Energies*. Vol. 14, pp. 6094, 2021.
- Wang, W., Huang, J., Yao, Z., Cut-corner prism piezoelectric energy harvester based on galloping enhancement mechanism, *Energy Reports*, Vol. 7, pp.6366-6374, 2021.
- Zhang, C., He, X. F., Li, S. Y., Cheng, Y. Q., Rao, Y., A Wind Energy Powered Wireless Temperature Sensor Node. *Sensors*, Vol. 15, pp. 5020-5031, 2015.
- Shan, X., Tian, H., Cao, H., Feng, J., Xie, T., Experimental Investigation on a Novel Airfoil-Based Piezoelectric Energy Harvester for Aeroelastic Vibration. *Micromachines (Basel)*, Vol. 11, No. 8, pp. 725, 2020.
- Chawdhury, S., Morgenthal G., Numerical simulations of aeroelastic instabilities to optimize the performance of flutter-based electromagnetic energy harvesters. *Journal of Intelligent Material Systems and Structures*, Vol. 29, No. 4, pp. 479-495, 2018.
- Vagner, C., Carlos, D., Airfoil-based piezoelectric energy harvesting by exploiting the pseudoelastic hysteresis of shape memory alloy springs. *Smart Materials and Structures*, Vol. 24, 2015.
- Perez, M., Boisseau, S., Gasnier, P., Willemin, J., Reboud, J. L., An electret-based aeroelastic flutter energy harvester, *Smart Materials and Structures*, Vol. 24, 035004, 2015.
- Lee, Y. J., Qi, Y., Zhou, G., Lua K. B., Vortex-induced vibration wind energy harvesting by piezoelectric MEMS device in formation. *Scientific Reports*, Vol. 9, 20404, 2019.
- Akaydin, H. D., Elvin, N., Andreopoulos, Y., The performance of a self-excited fluidic energy harvester. *Smart Materials and Structures*, Vol. 21, No. 2, Institute of Physics Publishing Limited, 2012.
- Jin, Z., Li, G., Wang, J., Zhang, Z., Design, Modeling, and Experiments of the Vortex-Induced Vibration Piezoelectric Energy Harvester with Bionic Attachments, *Complexity*, pp. 13, 2019.
- Weinstein, L., Cacan, M. R., So, P. M., Wright, P. K., Vortex shedding induced energy harvesting from piezoelectric materials in heating, ventilation, and air conditioning flows. *Smart Materials and Structures*, Vol. 21., 2012.
- Hu, Y., Yang, B., Chen, X., Wang, X., Liu, J., Modeling and experimental study of a piezoelectric energy harvester from vortex shedding-induced vibration, *Energy Conversion and Management*, Vol. 162, pp. 145-158, 2018.



Tasneem, Z., Al Noman, A., Das, S., Saha, D., Islam, M. R., Ali, M. F., Badal, M. F., Ahamed, M. H., Moyeen, S., Alam, F., An analytical review on the evaluation of wind resource and wind turbine for urban application: Prospect and challenges, *Developments in the Built Environment*, Vol. 4, 2020.

Laban, O., Maghanga, C., Joash, K., Determination of the Surface Roughness Parameter and Wind Shear Exponent of Kisii Region from the On-Site Measurement of Wind Profiles, *Journal of Energy*, 2019.

---

## #240: Inter-unit transmission of pollutants in naturally ventilated buildings adjoining a street canyon: a parametric study

A parametric study investigating the impact of ventilation strategies

---

Murtaza MOHAMMADI<sup>1</sup>, John CALAUTIT<sup>2</sup>

<sup>1</sup> University of Nottingham, University Park, Nottingham NG7 2RD, murtaza.mohammadi1@nottingham.ac.uk

<sup>2</sup> University of Nottingham, University Park, Nottingham NG7 2RD, john.calautit1@nottingham.ac.uk

*Abstract: The recent pandemic has accentuated the importance of clean indoor air and the risks associated with the airborne spread of pathogens. Outdoor meteorology and building configuration can spread pollutants and pathogens between different indoor units, deteriorating the air quality in the process. While previous studies have mainly focused on inter-unit pollutant crossflow in highrise buildings and isolated scenarios, the role of street canyon configurations in urban areas remains crucial for understanding ventilation characteristics and limiting the spread of contaminants. This research aims to evaluate the wind-driven transmission characteristics of pollutants between adjacent indoor units situated along a street canyon. By employing a numerical model, validated against experimental data, the study compares the impacts of five building ventilation strategies, each representing specific window opening combinations on the two buildings. Based on the environmental conditions set for the study, the results demonstrate that inter-unit transmission is reliant on both, the air change rate and the unit's specific location. By increasing the air change rate, cross-transmission decreases, offering an effective strategy to limit contaminants. However, units placed at the centre of the street canyon are more susceptible to contamination, requiring additional precautions for their occupants. Notably, the spatial arrangement of apartments (or units) within the canyon influences pollution diffusion along the street. Apartments at the canyon's edges may not directly contaminate units further down the street, but they still have a subtle influence, contributing small doses of pollutants. This study advances our understanding of inter-unit pollutant transmission in urban street canyons. Armed with these insights, residents can make informed decisions about adopting tailored ventilation strategies based on their apartment's location, proactively safeguarding their health. By employing the right ventilation strategies, residents can effectively minimize exposure to airborne pollutants, ensuring a healthier living environment in densely populated urban areas.*

*Keywords: Pollutant transmission, street canyon, inter-unit, CFD, natural ventilation*

## 1. INTRODUCTION

Indoor air quality has a determining role in the health and well-being of occupants. Previous epidemics and disease outbreaks have shown the vulnerability of indoor spaces, when the flow of contaminated air has led to the spread of airborne pathogens (Riley, 1974). Epidemiological studies have highlighted the long-range transmission routes of pathogens from infected patients to different locations, assisted by airflow. Additionally, chemicals such as ozone, carbon monoxide, oxides of nitrogen etc., also contribute to indoor air pollution and affect the health of occupants. Air movement greatly assists in their spread and transmission between different indoor spaces. The risk of contamination is higher in dense urban areas (Borck & Schrauth, 2021; Ganasegeran et al., 2021) and understanding the flow and pathways of transmission is paramount in designing safer urban habitats.

Consequently, several studies have been conducted to quantify the external routes of transmission of pollutants between apartments in a building. Mu et al. (Mu et al., 2018) studied the cross-floor transmission of pollutants, in a highrise building, under the influence of wind and solar radiation. They simulated the flow of pollutants in a single-side ventilated building and showed that the flow of pollutants from a source can vary depending on the wind speed. Under low wind speeds, the convective forces are dominant which transport the exhaust air upwards. Under high wind speed, however, pollutants are transported downward along the building if the source is located below the stagnation zone. The study highlights the risk of contamination of the leeward flats by windward sources under specific ambient conditions. Wang et al. (J. Wang et al., 2017, 2020) similarly concluded that, increasing the ambient wind speed leads to lower contamination potential. Additionally, their studies demonstrated that the choice of window type can play a role in limiting the cross-flow of pollutants.

Other studies on inter-unit transmissions, such as those by Ai et al. (2013), Dai et al. (2017) and Cui et al. (2016) etc., have carried out numerical simulations to understand the influence of wind forces. They showed that oblique wind angles help in dispersing the pollutants quickly, reducing the risk of inter-unit contamination. Whereas, the risk of contamination is significantly increased on the leeward face when the wind is blowing normal to the building, mainly due to the strong recirculation zone in the downwind section. The work also highlighted the role of surrounding buildings and their influence on the cross-transmission of pollutants. Similarly, wind tunnel tests (P. Y. Cui et al., 2021; Mu et al., 2016, 2017) have been conducted to estimate the contribution of source location and ventilation mode. Despite the limitations of each work, the results provide a good overview of the contamination risk and pathways of pollution flow in a building.

In general, the risk of inter-unit transmission in a single building has been examined by multiple studies. Nevertheless, the built environment is not only comprised of a single building or a highrise block, but also includes streets and avenues. Cross-transmission of pollutants in these scenarios has not been dealt with in sufficient detail and warrants more investigation. A street canyon consists of rows of buildings separated by a road or a street in between. The scale and dimensions of the configuration vary from street to street, in as much from city to city. Studies on urban pollution dispersion and ventilation (Ai & Mak, 2018; Buccolieri et al., 2009; Kastner-Klein & Plate, 1999; Mei et al., 2019; Morakinyo & Lam, 2016; Peng et al., 2017; Salim, 2011; Tominaga & Stathopoulos, 2011) have generally analysed outdoor conditions alone, usually involving the release of outdoor pollutants such as vehicles. Yang et al. (2015, 2016) have analysed the role of window opening strategy and building arrangement on the cross-flow of pollutants inside a street canyon. This study, however, looks at the inter-unit dispersion of pollutants inside indoor spaces rather than outdoor dispersion and attempts to identify the pathways of cross-flow of pollutants between different apartments (or units) inside buildings adjoining a street canyon.

Importantly, the following questions are raised:

- 1) Which is the safest location along the street canyon?
- 2) Can the ventilation mode offset the risk of inter-unit contamination?

A series of numerical simulations are performed to answer these research questions. The idealised street canyon configuration is simulated, being adopted from the wind tunnel tests conducted at the Karlsruhe Institute of Technology (2008). Five ventilation scenarios are explored in this paper, representing the different window opening strategies on the buildings. Normalised pollutant concentration and air changes per hour (ACH), described in the following section, are used to evaluate the ventilation performance and inter-unit transmission potential.

## 2. MATERIALS AND METHODS

The simulation domain consists of two parallel buildings with dimensions  $H = 10$  m,  $W = 10$  m and  $L = 100$  m. They are separated by a road of width 10 m in between. Indoor units were modelled at the centre and the two ends of the building, since previous studies have indicated the location of maximum and minimum concentration to be near the centre and ends of a street canyon, respectively (Buccolieri et al., 2009; Gromke & Blocken, 2015; Salim et al., 2011). The units' dimensions are  $H = 3$  m,  $W = 5$  m and  $D = 10$  m, with a window of 1 m  $\times$  1 m on the two facades perpendicular to the stream direction. The simulation domain is designed based on the recommendations of Franke et al. (2004) and Tominaga et al. (2008), wherein the front boundary is  $8H$  away from the upstream building, the rear boundary is  $19H$  from the downstream building, and the side faces are at a distance of  $7H$  from the building walls.  $H$  is the height of the building, equal to 10 m. Figure 2 shows the apartment naming convention used in the study.

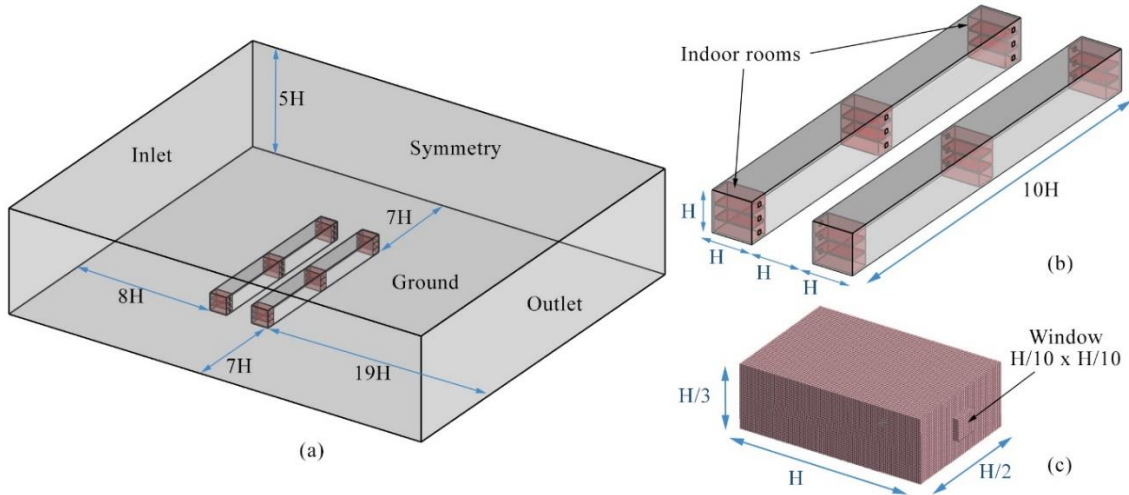


Figure 1 Domain configuration, (a) domain extent, (b) building dimension and (c) units' dimensions

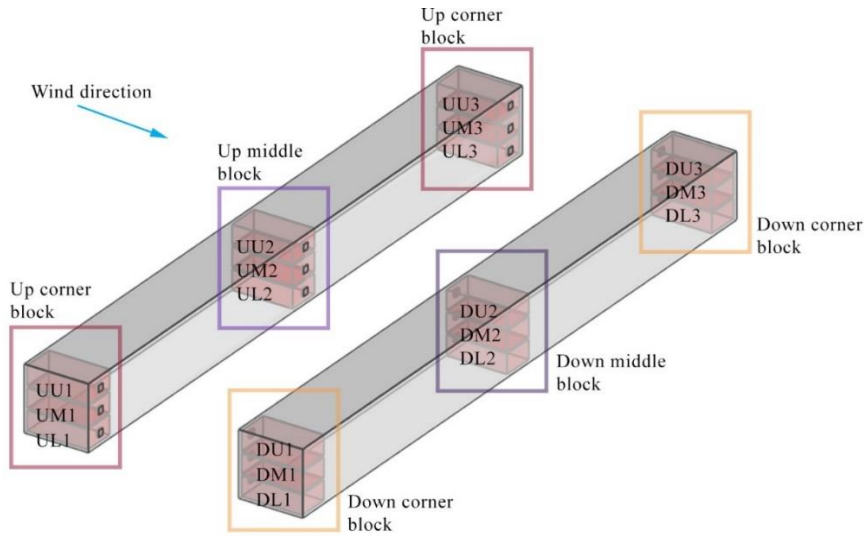


Figure 2 Apartment naming convention used in the study

The domain was discretised using a structured meshing technique, ensuring at least 10 cells across any building edge. The mesh sizing ensured that the smallest element, located in the indoor region, was  $0.01H$ . The inlet profile, describing an urban neighbourhood condition, was set according to the experiment by Gromke et al. (2015). The inlet velocity,  $u(z)$ , turbulence kinetic energy,  $TKE$ , and the dissipation rate,  $\varepsilon$ , were described by the following equations:

Equation 1: Inlet wind speed

$$u(z) = u_{ref} \left( \frac{z}{z_{ref}} \right)^\alpha$$

Equation 2: Turbulent kinetic energy at the inlet.

$$TKE = \frac{u_*^2}{\sqrt{C_\mu}} \left( 1 - \frac{z}{\delta} \right)$$

Equation 3: Turbulent dissipation rate at the inlet.

$$\varepsilon = \frac{u_*^3}{kz} \left( 1 - \frac{z}{\delta} \right)$$

Where:

- $z$  = height
- $u_{ref}$  = reference velocity at the reference height ( $z_{ref}$ )
- $\alpha$  = terrain feature set to 0.3, representing urban conditions
- $\delta$  = boundary layer depth set to 0.5 m
- $u_*$  = friction velocity set to 0.54 m/s
- $C_\mu$  = velocity field and turbulence function set to 0.09
- $k$  = von Karman constant set to 0.4.

Since the study focuses on only the wind-driven transmission, an isothermal condition was assumed with the SIMPLE scheme adopted for the pressure-velocity coupling. Pollution was represented by a neutrally buoyant gas, ethane, released

at the rate of  $Q = 0.182 \times 10^{-6}$  kg/s from a point source located at the centre of each apartment. The choice of turbulence was based on the ability of the model to predict the 3D flow features with sufficient accuracy within reasonable computational cost. RANS has been extensively used in previous studies to circumvent this problem, and the RSM closure model offers a good balance between accuracy and cost. Besides, the model is capable of resolving the flow in the wake of bluff bodies better than other RANS models (*Ansys® Fluent*; Gromke et al., 2008). Thus, the following study implements the RSM closure model, while the dispersion of the pollutant was determined by the steady-state advective-diffusion equation, given by:

$$\text{Equation 4: Dispersion modelling} \quad \vec{J}_l = -\left(\rho D_m + \frac{\mu_t}{Sc_t}\right) \nabla Y - D_T \frac{\nabla T}{T}$$

Where:

- $\vec{J}_l$  represents the mass diffusion of the pollutant,
- $D_m$  = mass diffusion coefficient
- $D_T$  = turbulent diffusivity respectively
- $\mu_t$  = turbulent viscosity
- $Sc_t$  = turbulent Schmidt number set to 0.3 (Gromke et al., 2008)
- $Y$  = mass fraction of the pollutant and
- $T$  = temperature.

## 2.1. Ventilation modes

Replicating real site conditions is difficult due to the variable usage of indoor spaces. Some assumptions were made to simplify the model, namely, five ventilation modes were assessed wherein all the apartments in a building were assumed to be ventilated from the same side. Only the wind-driven transmission was considered in this study and isothermal conditions were assumed. The 5 ventilation scenarios are described in Figure 3. The simulated pollutant concentration was normalised using Equation 3, and the air change rate in the apartment was calculated in terms of the purging flow rate, given by Equation 6.

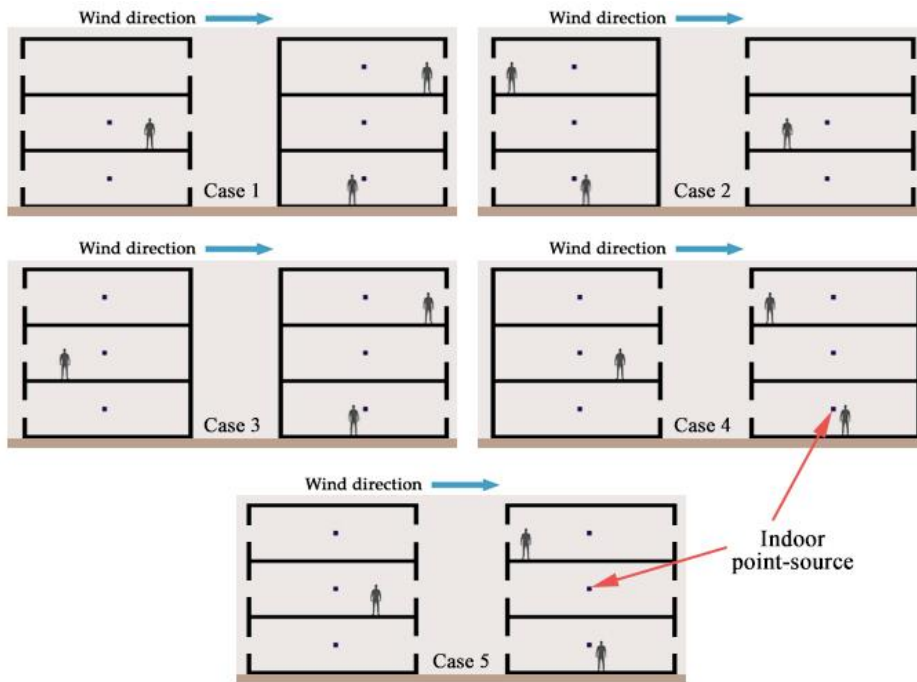


Figure 3 Ventilation modes simulated in the present study.

$$\text{Equation 5: Normalised pollutant concentration}$$

$$K = \frac{C Z_{ref}^2 U_{ref}}{Q}$$

$$\text{Equation 6: Purge air flow rate}$$

$$ACH = \frac{3600 * Q}{\int_0^V C \cdot dV}$$

Where:

- $C$  = measured concentration at a point inside the apartment
- $V$  = volume of the apartment

## 2.2. Validation

A decoupled validation method was adopted, wherein the indoor and outdoor domains were separately validated. The outdoor canyon model was compared against the study by Gromke et al. (2008) whereas the indoor domain was validated against the experimental work by Chen et al. (2006). The outdoor validation domain consists of an isolated street canyon model with two line-source of pollutants, located inside the street between the two buildings. Indoor apartments were not modelled for this part of the study. Figure 4 shows the normalised pollutant concentration ( $K$ ) values along the mid-height of the street-facing walls. In general, high  $K$  is observed near the centre of the wall ( $X = 0$ ), which gradually decreases towards the edges of the building ( $X = \pm 5$ ). The RNG  $k-\epsilon$  model consistently overpredicts  $K$  values along both walls A and B. The performance by other turbulence models is better but regions of small variations still exist. While the standard  $k-\epsilon$  slightly overpredicts near the centre of wall-A, the RSM underpredicts along the edges. Regardless, both models show good agreement along wall B. Analysis using four different validation metrics - correlation coefficient ( $R$ ), the normalised mean squared error (NMSE), the fractional bias (FB) and the fraction of predictions within a factor of two of the observations (FAC2), revealed the superior performance of RSM over other turbulence models.

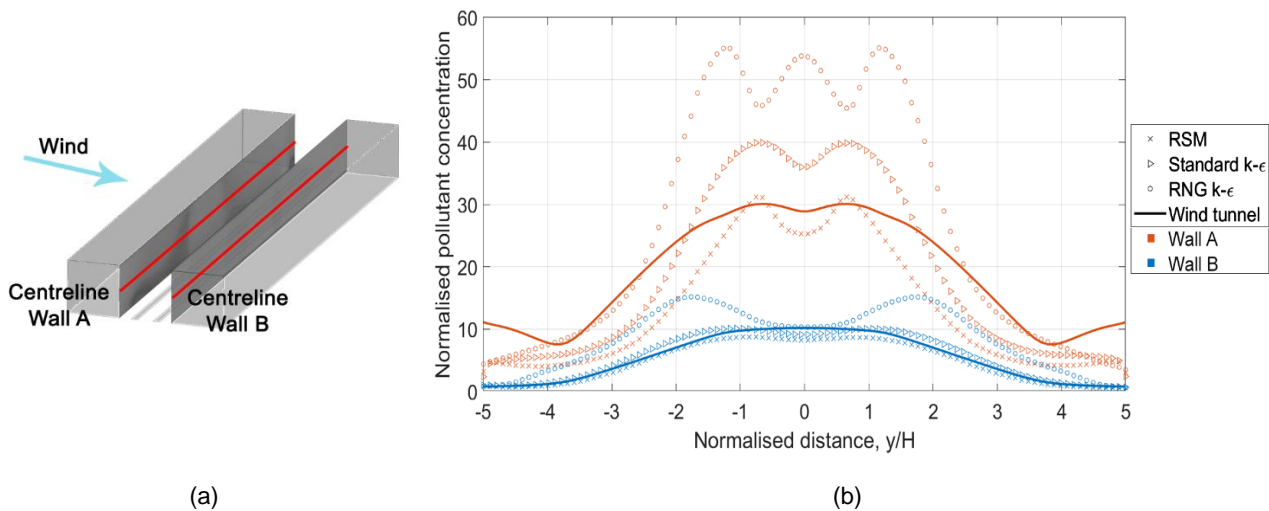


Figure 4 Outdoor pollutant dispersion validation, (a) The street canyon model showing the location of lines along which pollutant concentration values are plotted, (b) Comparison of normalised pollutant concentration ( $K$ ) between CFD and experimental results.

For the indoor domain validation, the physical experiment by Chen et al. (2006) was replicated in CFD. The validation model consisted of a room with height  $\times$  width  $\times$  depth = 0.4 m  $\times$  0.4 m  $\times$  0.8 m. Air was blown into the room at a speed of 0.45 m/s through a small opening, 0.04 m  $\times$  0.04 m wide, at a height of 0.34 m above the floor. While a similar opening located on the opposite face was set to 'pressure outlet', located at the height of 0.02 m. The x component of velocity is analysed at the central plane of the room, along three vertical lines at  $x = 0.2, 0.4$  and  $0.6$  m (indicated by the blue lines in Figure 5a). The standard  $k-\epsilon$ , RNG  $k-\epsilon$  and the RSM turbulence models were tested and compared. Figure 5 shows the comparison between physical observation and numerical prediction. Velocity is quite low near the floor, in the region from  $z = 0$  m to  $z = 0.3$  m, and is only noticeably near the top, from  $z = 0.3$  m to  $z = 0.4$  m. All three turbulence models can satisfactorily reproduce the physical observations within reasonable accuracy. Deviations are higher near the top of the room, above  $z = 0.3$  m, especially near the inlet - for the line  $x = 0.2$  m. The statistical significance tests revealed that all turbulence models are able to replicate the experimental observation. Nevertheless, we decided to proceed with the RSM turbulence model for further investigations as it generated reliable results for both the indoor and outdoor domains. The numerical calculations are satisfactory for the objectives of this study, which focuses on the global flow patterns inside the street canyon rather than a detailed analysis of the air movement inside the rooms.

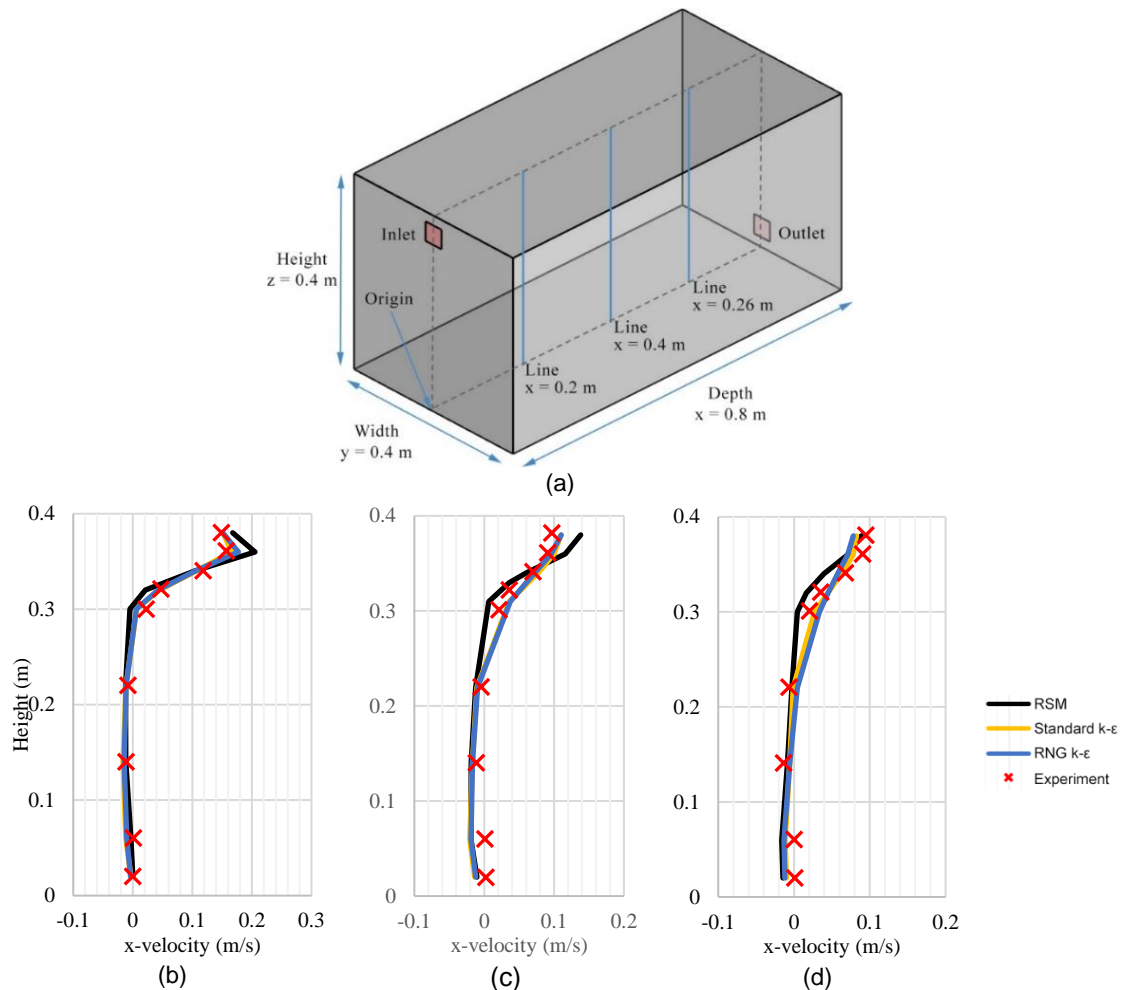


Figure 5 Indoor domain validation; a) CFD model; comparison of x-velocity along b)  $x = 0.2$  m; c)  $x = 0.4$  m; d)  $x = 0.6$  m.

### 3. RESULTS AND DISCUSSION

Results in terms of the normalised pollutant concentration ( $K$ ) and ACH is shown in Figure 6. The horizontal bars indicate the total pollution transmitted into the space from the neighbouring apartments, whereas the blue lines indicate the air exchange rate in the corresponding apartments. Evidently, the transmission of pollutants is dependent on the ventilation efficiency of the apartment. Under case 1, the downstream apartments are ventilated from the leeward side alone, resulting in low ACH, less than  $1.5 \text{ h}^{-1}$ . Low to medium pollutant concentration is observed in all downstream apartments, with the highest pollution in apartment DU2. The apartments on the upstream building, however, being under cross-ventilation experience higher ACH, in the range of  $40 - 80 \text{ h}^{-1}$ , which is accompanied by negligible infiltration of pollutants from the surrounding apartments. Under case 2, the ventilation mode is reversed on the two buildings, consequently, cross ventilation in the downstream apartments leads to higher ACH accompanied by lower infiltration of pollutants. On the upstream building, the reduced ACH does not lead to a significant increase in infiltration, and only a slight increase is observed in some apartments, especially for the ones in the centre of the canyon.

Cases 3 and 4 represent single-sided ventilation on both buildings, and therefore, the apartments have low ventilation efficiency. The average air change in the apartment is  $1.5 \text{ h}^{-1}$ , with the lowest and highest being  $0.4 \text{ h}^{-1}$  and  $4.3 \text{ h}^{-1}$ , observed in apartments DL2 (case 4) and UU1 (case 3), respectively. However, the transmission of pollutants is significantly higher in case 4, where the apartments are ventilated from the street side alone. In fact, the upstream building in case 4 has the highest concentration of transmitted pollutants (average  $K = 92$ ) among all ventilation scenarios. This is partly due to poor ACH and partly due to the recirculation of air and accumulation of pollutants in the street, which serves as the only region from where air exchange occurs between the indoor and outdoor domains. Comparatively, in case 3, pollutants are exhausted into the side away from the street, ensuring rapid dispersion and lowered infiltration in neighbouring apartments. Nevertheless, some vertical transmission does occur. Case 5 represents cross ventilation in both buildings, which promotes maximum air exchanges in all apartments. The average ACH is  $42 \text{ h}^{-1}$ , with relatively higher values in the upstream apartments. Corollary, negligible transmission occurs in the upstream apartments while slight infiltration of pollutants occurs in the downstream apartments. While it seems fair to conclude that a low ventilation rate produces higher transmission of pollutants, the relative location of the apartment is also important. For instance, in apartment DL1, pollutant concentration increases from 4.5 to 6.3 despite an increase in ACH from 0.5 to 1.8, in cases 1 and 4, respectively.

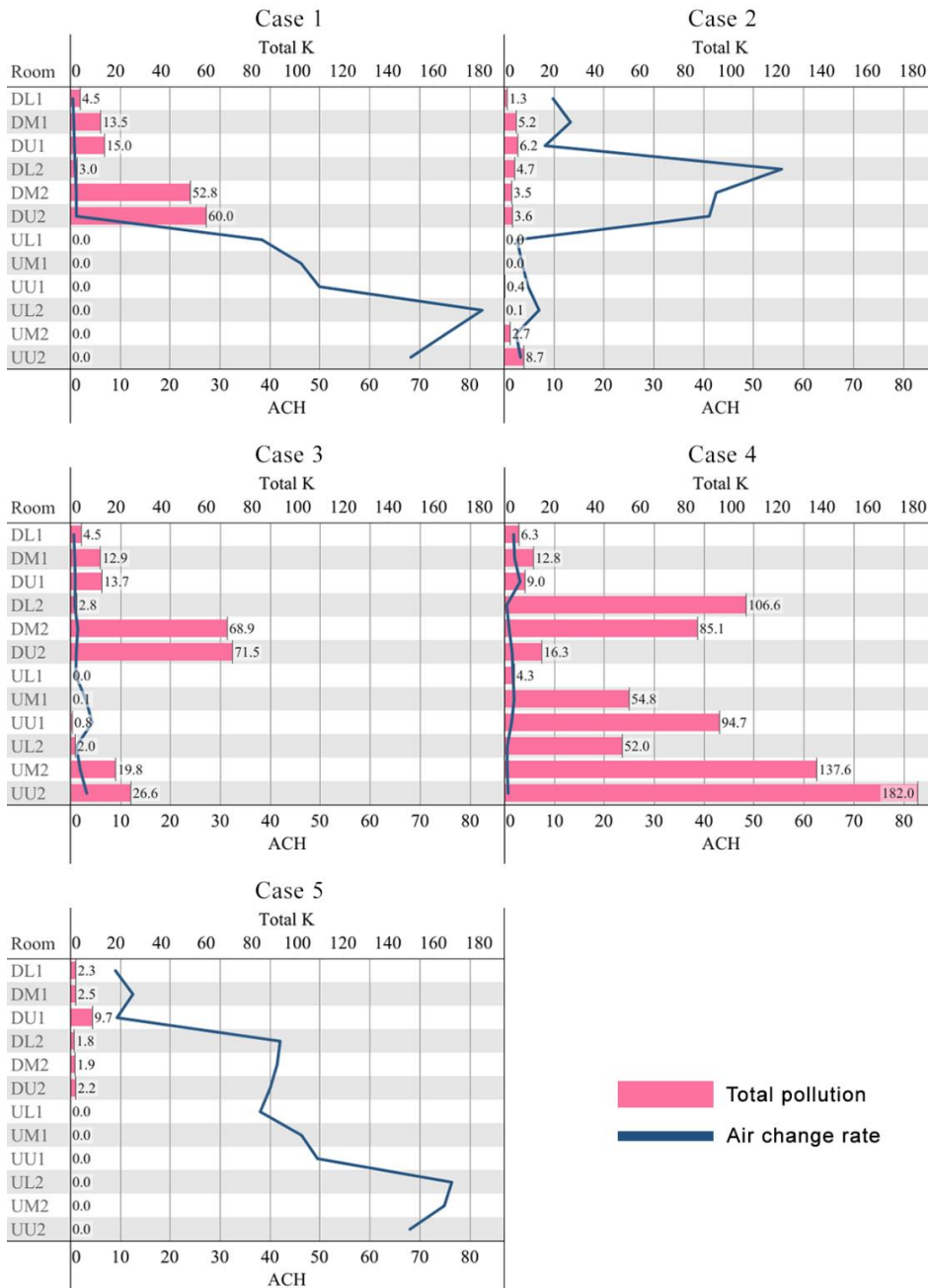


Figure 6 Total cross-transmitted pollutants in each apartment under various ventilation modes

### 3.1. Inter-block transmission

Figure 7 shows the bulk routes of transmission between the apartment blocks, where 'down' refers to downstream, 'up' refers to upstream, 'centre' refers to the apartments located in the centre of the canyon, and 'corner' refers to the apartments at one end of the canyon. The columns in the table indicate the locations from where pollutants are released, and the rows indicate the target location. Two patterns clearly emerge vis-a-vis, higher cross-transmission of pollutants is accompanied by low ACH, and the primary route of transmission occurs vertically within the same block. In general, downstream apartments are more contaminated than upstream apartments, especially with pollutants released from the downstream buildings. The downstream apartments at the centre of the canyon (DL2, DM2 and DU2) are highly contaminated when ventilated from a single side and are primarily concentrated with pollutants released from neighbouring central apartments. Conversely, transmission remains low on the upstream building even when ACH is reduced, as demonstrated by cases 2 and 3. In fact, ACH plays little effect on inter-block transmission between upstream apartments, suggesting vertical dispersion of exhausted pollutants.

In terms of contagion, emission from corner apartments is transferred more easily to surrounding units than the pollutants from central apartments. For instance, emission from the upstream corner block (apartments UL1, UM1 and UU1) is transported to both the downstream blocks while also leading to local transmission. In case 4, especially, pollutants from



corner blocks are transported to all apartments along the canyon. On the contrary, the central blocks are quite susceptible and are usually found to be contaminated by emissions released in other apartments. In principle, the contribution of corner apartments towards the contamination of central apartments is usually higher than the transmission of pollutants from central apartments to the corner apartments. This can be explained by the fact that the recirculating vortices near the canyon edges push air into the street canyon (towards the centre) transporting the pollutants towards the central of the canyon.

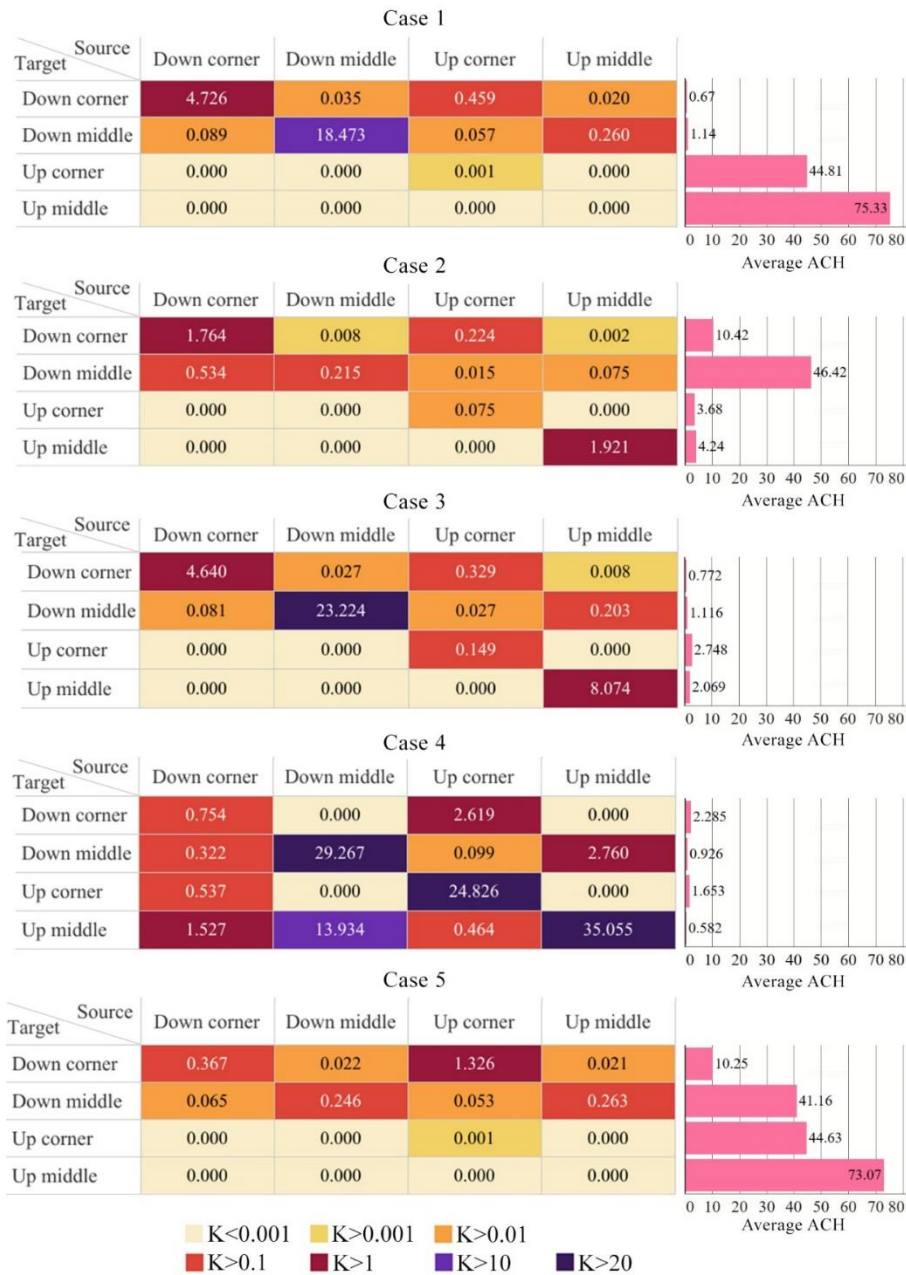


Figure 7 Inter-block transmission of pollutants

Cases 4 and 5 represent the two extreme scenarios of pollutant transmission and are further discussed below. Figure 8 shows the relative contribution of each source towards the contamination of an apartment under these two ventilation modes. The colour indicates the source of the pollutant, and its area represents the fraction of the total transported pollutant in that particular apartment. It can be observed that the primary source of pollution in corner apartments, for both ventilation modes, is the upstream corner block (UL1, UM1 and UU1) indicated by the warm colours in Figure 8, a and c. Whereas, there exists a wide range for the central apartments, indicated by a mix of blue and green shades (Figure 8, b and d). The presence of recirculating eddies in the street is the main reason for the transport of pollutants vertically as well as across the street. Moreover, as explained previously, some of the central apartments are slightly contaminated with pollutants from the far end of the canyon. For instance, the red and purple strips in the apartments DU2, DM2 and DL2, indicate the presence of corner pollutants (both the upstream and downstream corner apartments). The lateral flow of air, from the edges to the centre of the canyon, leads to the accumulation of pollutants in the central apartments.

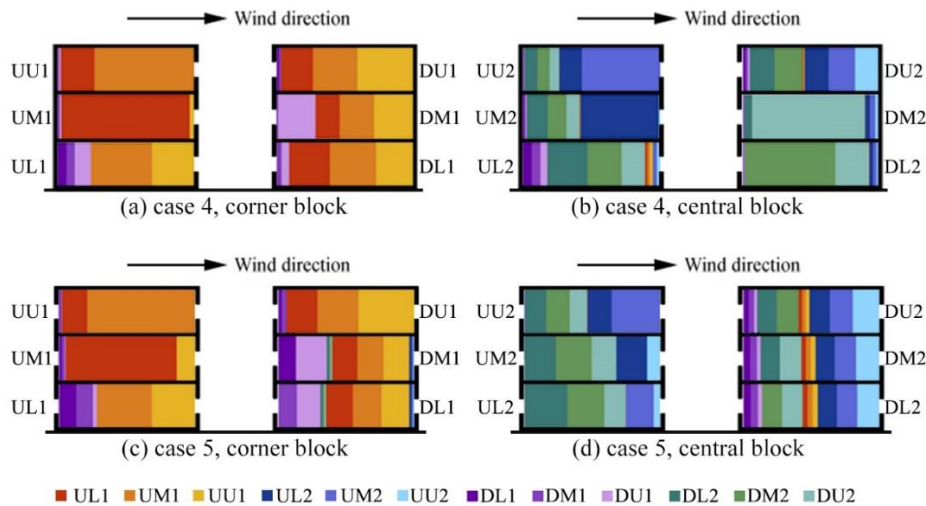


Figure 8 Relative contribution of pollutant sources in each of the apartments, for the cases 4 and 5

#### 4. CONCLUSION AND FUTURE WORK

The current study investigated the effect of ventilation mode on the inter-unit transmission of pollutants inside a street canyon, using numerical simulations. A decoupled validation of indoor and outdoor domains was performed, and the final model was implemented with five different ventilation strategies. The RSM turbulence model was used to close the set of RANS equations, and only the wind-driven transmission was considered. Importantly, the study attempted to answer two questions raised in the introduction, i.e., which is the least contaminated apartment in a street canyon, and can the ventilation mode offset inter-unit transmission? The results demonstrate that the cross-flow of pollutants is determined by both the ventilation efficiency in the apartment as well as the relative location inside the canyon. Under cross ventilation, the apartments in the centre of the canyon exhibit much higher ACH than the corner apartments, ensuring low infiltration. Whereas the single-sided ventilation mode generates comparable ACH in both locations, leading to higher contamination in the central apartments.

On average, the upstream corner blocks have a pollutant concentration of 10.3 and it represents the least polluted location. It is fair to conclude that the apartment on the top floor (UU1) presents the most ideal location as cross-transmission into the apartment is lowest and the ACH is sufficient to ensure good air quality. Despite the adverse scenario in case 4, the apartment is only contaminated by pollutants released from UL1 and UM1. Managing pollution in the lower apartments could serve as an easy method to limit transmission into UU1. The downstream central block shows, on average, the highest levels of pollutant concentration and poor ventilation. The block represents the worst location, with the highest average pollution in apartment DM2 (average  $K = 42.4$ ). Despite the peak pollutant concentration occurring in apartment UU2 under case 4 ( $K = 178$ ), the transmission in DM2 remains quite high for all cases and is accompanied by low ACH values as compared to the average upstream location.

Improving ACH alone does not lead to a reduction in transmission, but also depends on the relative location of the source. As can be seen in the downstream corner apartments, where the average ACH = 5, but the strategic location prevents the accumulation of pollutants from surrounding apartments. In brief, while pollutants released at the centre of the canyon disperse locally, the pollutants released at the edge of the canyon are dispersed along the length of the canyon, albeit in small concentrations.

The study looked at identifying the pathways of inter-unit transmission between apartments inside a street canyon, however, only limited test cases and environmental conditions were simulated, and several assumptions were made to simulate an ideal scenario. More work is needed to understand the role of environmental and spatial factors on the cross-flow of pollutants. The current work makes an important contribution in the domain of air quality in buildings, by establishing a critical relationship between the location of the apartment and the cross-transmission potential. Additional tests and analysis will help building planners introduce necessary intervention strategies to design safer indoor spaces and limit the transmission of pollutants.

#### 5. REFERENCES

Ai, Z. T., & Mak, C. M. (2018). Wind-induced single-sided natural ventilation in buildings near a long street canyon: CFD evaluation of street configuration and envelope design. *Journal of Wind Engineering and Industrial Aerodynamics*, 172, 96–106. <https://doi.org/10.1016/J.JWEIA.2017.10.024>

- Ai, Z. T., Mak, C. M., & Niu, J. L. (2013). Numerical investigation of wind-induced airflow and interunit dispersion characteristics in multistory residential buildings. *Indoor Air*, 23(5), 417–429. <https://doi.org/10.1111/ina.12041>
- Ansys® *Fluent* (Release 18.1). (n.d.).
- Borck, R., & Schrauth, P. (2021). Population density and urban air quality. *Regional Science and Urban Economics*, 86, 103596. <https://doi.org/10.1016/J.REGSCIURBECO.2020.103596>
- Buccolieri, R., Gromke, C., di Sabatino, S., & Ruck, B. (2009). Aerodynamic effects of trees on pollutant concentration in street canyons [Article]. *Science of The Total Environment*, 407(19), 5247–5256. <https://doi.org/10.1016/j.scitotenv.2009.06.016>
- Chen, F., Yu, S. C. M., & Lai, A. C. K. (2006). Modeling particle distribution and deposition in indoor environments with a new drift-flux model. *Atmospheric Environment*, 40(2), 357–367. <https://doi.org/10.1016/J.ATMOSENV.2005.09.044>
- Cui, D. J., Mak, C. M., Kwok, K. C. S., & Ai, Z. T. (2016). CFD simulation of the effect of an upstream building on the inter-unit dispersion in a multi-story building in two wind directions. *Journal of Wind Engineering and Industrial Aerodynamics*, 150, 31–41. <https://doi.org/10.1016/j.jweia.2016.01.007>
- Cui, P. Y., Zhang, Y., Chen, W. Q., Zhang, J. H., Luo, Y., & Huang, Y. D. (2021). Wind-tunnel studies on the characteristics of indoor/outdoor airflow and pollutant exchange in a building cluster. *Journal of Wind Engineering and Industrial Aerodynamics*, 214, 104645. <https://doi.org/10.1016/J.JWEIA.2021.104645>
- Dai, Y. W., Mak, C. M., & Ai, Z. T. (2017). Computational fluid dynamics simulation of wind-driven inter-unit dispersion around multi-storey buildings: Upstream building effect. <https://doi.org/10.1177/1420326X17745943>, 28(2), 217–234. <https://doi.org/10.1177/1420326X17745943>
- Franke, J., Hirsch, C., Jensen, G., Krüs, H. W., Miles, S. D., Schatzmann, M., Westbury, P. S., Wisse, J. A., & Wright, N. (2004). Recommendations on the use of CFD in wind engineering. *Proceedings of the International Conference on Urban Wind Engineering and Building Aerodynamics*, C.1.1–C1.11.
- Ganasegeran, K., Jamil, M. F. A., Ch'ng, A. S. H., Looi, I., & Peariasamy, K. M. (2021). Influence of population density for covid-19 spread in malaysia: An ecological study. *International Journal of Environmental Research and Public Health*, 18(18). <https://doi.org/10.3390/IJERPH18189866/S1>
- Gromke, C., & Blocken, B. (2015). Influence of avenue-trees on air quality at the urban neighborhood scale. Part II: Traffic pollutant concentrations at pedestrian level. *Environmental Pollution*, 196, 176–184. <https://doi.org/10.1016/J.ENVPOL.2014.10.015>
- Gromke, C., Buccolieri, R., Di Sabatino, S., & Ruck, B. (2008). Dispersion study in a street canyon with tree planting by means of wind tunnel and numerical investigations - Evaluation of CFD data with experimental data. *Atmospheric Environment*, 42(37), 8640–8650. <https://doi.org/10.1016/j.atmosenv.2008.08.019>
- Karlsruhe Institute of Technology. (2008). *CODASC (2008) Concentration Data of Street Canyons*. *Laboratory of Building- and Environmental Aerodynamics*. <https://www.windforschung.de/CODASC.htm>
- Kastner-Klein, P., & Plate, E. J. (1999). Wind-tunnel study of concentration fields in street canyons. *Atmospheric Environment*, 33(24–25), 3973–3979. [https://doi.org/10.1016/S1352-2310\(99\)00139-9](https://doi.org/10.1016/S1352-2310(99)00139-9)
- Mei, S. J., Luo, Z., Zhao, F. Y., & Wang, H. Q. (2019). Street canyon ventilation and airborne pollutant dispersion: 2-D versus 3-D CFD simulations. *Sustainable Cities and Society*, 50, 101700. <https://doi.org/10.1016/j.scs.2019.101700>
- Mohammadi, M., & Calautit, J. (2021). Impact of Ventilation Strategy on the Transmission of Outdoor Pollutants into Indoor Environment Using CFD. *Sustainability 2021, Vol. 13, Page 10343*, 13(18), 10343. <https://doi.org/10.3390/SU131810343>
- Morakinyo, T. E., & Lam, Y. F. (2016). Study of traffic-related pollutant removal from street canyon with trees: dispersion and deposition perspective. *Environmental Science and Pollution Research*, 23(21), 21652–21668. <https://doi.org/10.1007/s11356-016-7322-9>
- Mu, D., Gao, N., & Zhu, T. (2016). Wind tunnel tests of inter-flat pollutant transmission characteristics in a rectangular multi-storey residential building, part A: Effect of wind direction. *Building and Environment*, 108, 159–170. <https://doi.org/10.1016/j.buildenv.2016.08.032>
- Mu, D., Gao, N., & Zhu, T. (2018). CFD investigation on the effects of wind and thermal wall-flow on pollutant transmission in a high-rise building. *Building and Environment*, 137, 185–197. <https://doi.org/10.1016/j.buildenv.2018.03.051>

- Mu, D., Shu, C., Gao, N., & Zhu, T. (2017). Wind tunnel tests of inter-flat pollutant transmission characteristics in a rectangular multi-storey residential building, part B: Effect of source location. *Building and Environment*, 114, 281–292. <https://doi.org/10.1016/j.buildenv.2016.12.031>
- Peng, Y., Ma, X., Zhao, F., Liu, C., & Mei, S. (2017). Wind driven natural ventilation and pollutant dispersion in the dense street canyons: Wind Opening Percentage and its effects. *Procedia Engineering*, 205, 415–422. <https://doi.org/10.1016/j.proeng.2017.10.392>
- Riley, R. L. (1974). Airborne infection. *The American Journal of Medicine*, 57(3), 466–475. [https://doi.org/10.1016/0002-9343\(74\)90140-5](https://doi.org/10.1016/0002-9343(74)90140-5)
- Salim, S. M. (2011). *Computational study of wind flow and pollutant dispersion near tree canopies* [University of Nottingham]. [http://eprints.nottingham.ac.uk/12077/1/Thesis\\_-\\_Salim\\_M\\_Salim.pdf](http://eprints.nottingham.ac.uk/12077/1/Thesis_-_Salim_M_Salim.pdf)
- Salim, S. M., Buccolieri, R., Chan, A., & Di Sabatino, S. (2011). Numerical simulation of atmospheric pollutant dispersion in an urban street canyon: Comparison between RANS and LES. *Journal of Wind Engineering and Industrial Aerodynamics*, 99(2–3), 103–113. <https://doi.org/10.1016/j.jweia.2010.12.002>
- Tominaga, Y., Mochida, A., Yoshie, R., Kataoka, H., Nozu, T., Yoshikawa, M., & Shirasawa, T. (2008). AIJ guidelines for practical applications of CFD to pedestrian wind environment around buildings. *Journal of Wind Engineering and Industrial Aerodynamics*, 96(10–11), 1749–1761. <https://doi.org/10.1016/J.JWEIA.2008.02.058>
- Tominaga, Y., & Stathopoulos, T. (2011). CFD modeling of pollution dispersion in a street canyon: Comparison between LES and RANS. *Journal of Wind Engineering and Industrial Aerodynamics*, 99(4), 340–348. <https://doi.org/10.1016/J.JWEIA.2010.12.005>
- Wang, J., Huo, Q., Zhang, T., Wang, S., & Battaglia, F. (2020). Numerical investigation of gaseous pollutant cross-transmission for single-sided natural ventilation driven by buoyancy and wind. *Building and Environment*, 172, 106705. <https://doi.org/10.1016/j.buildenv.2020.106705>
- Wang, J., Zhang, T., Wang, S., & Battaglia, F. (2017). Gaseous pollutant transmission through windows between vertical floors in a multistory building with natural ventilation. *Energy and Buildings*, 153, 325–340. <https://doi.org/10.1016/j.enbuild.2017.08.025>
- Wang, Q., Sandberg, M., Lin, Y., Yin, S., & Hang, J. (2017). Impacts of Urban Layouts and Open Space on Urban Ventilation Evaluated by Concentration Decay Method. *Atmosphere 2017, Vol. 8, Page 169*, 8(9), 169. <https://doi.org/10.3390/ATMOS8090169>
- Yang, F., Gao, Y., Zhong, K., & Kang, Y. (2016). Impacts of cross-ventilation on the air quality in street canyons with different building arrangements. *Building and Environment*, 104, 1–12. <https://doi.org/10.1016/J.BUILDENV.2016.04.013>
- Yang, F., Kang, Y., Gao, Y., & Zhong, K. (2015). Numerical simulations of the effect of outdoor pollutants on indoor air quality of buildings next to a street canyon. *Building and Environment*, 87, 10–22. <https://doi.org/10.1016/j.buildenv.2015.01.008>

---

## #241: Operational tool for selecting energy systems for small buildings based on useful energy needs

---

Sérgio TADEU<sup>1</sup>

*1 Low Carbon & Resource Efficiency, R&Di, Instituto de Soldadura e Qualidade, 4415-491 Grijó, Portugal, sftadeu@isq.pt*

*Abstract: The European Union is constantly improving the energy performance of buildings directive (EPBD), one of its main objectives being to offer a methodological framework that allows identifying the cost-optimal of energy conservation measures, now with a very strong focus on retrofitting. The share of new buildings is very low, from 1 to 2% of the built stock, and it has become clear that the low renewal rate can jeopardize the assumed goals of reducing energy consumption and, consequently, mitigating the climate changes.*

*There are countless barriers to the energy retrofitting of buildings with an eco-efficiency approach, highlighting the lack of clarity in the strategy of policy makers at national level, complicated regulations of minimum requirements for intervention in the building envelope and renovation of energy systems, lack of information for building owners, corroborated by low quality energy performance certificates and need of simple decision-making support tools.*

*The complexity of analysing scenarios of possible interventions comes from the fact that the economic and environmental impact of a specific measure is influenced by other measures of the same package, which affect the cost optimality. For this reason, the best intervention option may not be a simple combination of individual retrofitting measures. Faced with this complexity, building owners are limited to replacing energy systems at the end of their life cycle.*

*This work proposes an operational tool for selecting energy systems for small buildings based on useful energy needs for domestic hot water preparation, space heating and cooling. Few input parameters are required: energy needs and costs, primary energy and greenhouse gas conversion factors, initial investment, efficiency and embodied impact of energy systems.*

*The methodology applied in this article is aligned with an eco-efficiency approach for the pre-selection of energy systems, integrating cost optimality and life cycle assessment to support decision-making on energy conservation measures. In order to demonstrate its applicability also in the pre-study of the competitiveness of new technologies, an example of an innovative heat pump is presented, in comparison with conventional energy systems in the Portuguese market, to meet useful energy needs in the consumption range of dwellings.*

*Keywords: buildings; energy retrofit; cost optimality; life-cycle assessment; eco-efficiency*

## 1. INTRODUCTION

The European Union is constantly improving the energy performance of buildings directive (EPBD, 2010), one of its main objectives being to offer a methodological framework that allows identifying the cost-optimal of energy conservation measures, now with a very strong focus on retrofitting. Several studies have carried out an economic assessment of energy efficiency retrofit measures, but very few include an environmental assessment of existing buildings. The share of new buildings is very low, from 1 to 2% of the built stock (European Commission, 2011), and it has become clear that the low renewal rate can jeopardize the assumed goals of reducing energy consumption and, consequently, mitigating the climate changes.

The economic and environmental assessments have mainly been applied to products/services and recently also to buildings (Zakula *et al.*, 2019). Thermal dynamic simulation has been included in life cycle assessment (LCA) studies to assess the potential contribution of the occupants' preferences not only to the operational energy use of buildings, but also to trade-offs between embodied and operational energy. The occupancy level of a building influences the operational energy use and the contribution of the different life cycle stages to the overall life span of a building. De Meester *et al.* and Azar and Menassa emphasised the need to properly take occupancy into account at the design stage, to arrive at more reliable building energy performance estimates.

There are countless barriers to the energy retrofitting of buildings with an eco-efficiency approach (Tadeu *et al.*, 2022). Among these, it is worth mentioning the lack of clarity in the strategy of policy makers at national level, complicated regulations of minimum requirements for intervention in the building envelope and renovation of energy systems (REH and RECS, 2013), lack of information for building owners, corroborated by low quality energy performance certificates and need of simple decision-making support tools.

The complexity of analysing scenarios of possible interventions comes from the fact that the economic and environmental impact of a specific measure is influenced by other measures of the same package, which affect the cost optimality. For this reason, the best intervention option may not be a simple combination of individual retrofitting measures (Tadeu *et al.*, 2019). Faced with this complexity, building owners are limited to replacing energy systems at the end of their life cycle (Tadeu *et al.*, 2018).

Lollini *et al.* studied the optimisation of opaque components regarding their energy, environmental and economic impacts. Kim *et al.* assessed the carbon emissions and related costs of apartment buildings, and Kneifel assessed energy efficiency measures in new commercial buildings. In the Portuguese context, Silvestre *et al.* performed an environmental, energy and economic assessment of building assemblies for new residential buildings. And Anastaselos *et al.* created a tool to perform an integrated energy, economic and environmental evaluation of thermal insulation solutions.

This work proposes an operational tool for selecting energy systems for small buildings based on useful energy needs for domestic hot water preparation, space heating and cooling. Few input parameters are required: energy needs and costs, primary energy and greenhouse gas conversion factors, initial investment and maintenance cost, efficiency and embodied impact of energy systems.

The methodology applied in this article is aligned with an eco-efficiency approach for the pre-selection of energy systems, integrating cost optimality and life cycle assessment to support decision-making on energy conservation measures. In order to demonstrate its applicability also in the pre-study of the competitiveness of new technologies, an example of an innovative heat pump is presented, in comparison with conventional energy systems in the Portuguese market, to meet useful energy needs in the consumption range of dwellings.

## 2. METHODOLOGY

The method applied by the operational tool presented in this paper consists of an incremental development based on a methodology with a life-cycle approach (Tadeu *et al.*, 2019 and 2022). In this study, only simplified analyses for selecting energy systems under separate economic and environmental criteria were explored. In the context of multi-objective optimization problems (MOP), it is recommended to apply the methodology presented in (Tadeu *et al.*, 2022).

The method allows the selection of energy systems according to the useful energy needs and can be applied to different buildings and climate regions. Construction building details are not required, but knowledge of the historical consumption data of dwellers is essential to estimate annual energy needs. Other necessary parameters are embodied impact and initial investment in each energy system, corresponding energy efficiency, primary energy and greenhouse gas conversion factors associated with each energy source and its respective supply cost.

## 2.1. Decision-making procedure

Adapting cost optimality concept (European Commission, 2012), the objective functions,  $f_1$  and  $f_2$  represent the total life cycle impact,  $LI$ , and the financial cost,  $FC$ , respectively. An optimization problem is applied in a minimization context for the two objective functions:

$$\text{Equation 1: Minimization context.} \quad \text{Min}\{f_1(\vec{x}), f_2(\vec{x})\}$$

Where:

- $f_1$  and  $f_2$  = objective functions
- $\vec{x}$  = vector of n decision variables

Each position of the  $\vec{x}$  vector corresponds to a decision variable, i.e., each position specifies both, the environmental and economic perspectives, and corresponding technical characteristic linked to each variable. For DHW, heating and cooling, the technical characteristic is efficiency.

The calculation procedures for the objective functions are described as follows. The subscripts represent: domestic hot water ( $w$ ), space heating ( $h$ ) and cooling ( $c$ ). It was considered in this study a calculation period  $\tau = 20$  years, which coincides with the lifespan ( $\tau_L = 20$ ) for all energy systems analysed in this work, as established by (EN 15459, 2007) for most technologies. This avoided having to deal with replacement costs and residual values in this application example.

## 2.2. Environmental impact

The first objective function,  $f_1$ , whose vector  $\vec{x}$  corresponds to a decision variable, is performed by the life-cycle impact of the energy systems,  $LI$ . Single DHW, space heating and cooling systems are considered ( $w, h, c$ ). Thus,  $LI(\vec{x}, \tau)$  is expressed by the sum of the embodied impacts of the systems,  $BI$ , and the impacts from useful energy needs provided ( $E_w, E_h, E_c$ ), referring to starting year,  $i = 1$ , over the calculation period  $\tau$ :

$$\text{Equation 2: First objective function.} \quad f_1(\vec{x}) = LI(\vec{x}, \tau) = \sum_{i=1}^{\tau} [BI + a_1 E_w + a_2 E_h + a_3 E_c](\vec{x}) \quad (\text{kgCO}_2\text{eq})$$

Where  $BI = BI_w + BI_h + BI_c$ ;  $a_1 = P_w/\eta_w$ ,  $a_2 = P_h/\eta_h$  and  $a_3 = P_c/\eta_c$ , with  $P_w, P_h$  and  $P_c$  being the greenhouse gas (GHG) emission factors for final energy and  $\eta_w, \eta_h$  and  $\eta_c$  the efficiency of the systems, which convert the useful into the final energy.

As the interest of this methodology is to provide an easy-to-interpret graphical interface, the objective function is partitioned into three straight line segments to be calculated. The first segment considers the embodied impact in all systems ( $BI$ ) that make up the set of solutions added to the impact proportional to energy consumption for DHW ( $a_1 E_w$ ):

$$\text{Equation 3: Life-cycle impact associating DHW.} \quad LI = BI + a_1 E_w \quad (\text{kgCO}_2\text{eq})$$

Assuming that after the DHW needs ( $E_w$ ) are satisfied, the increase in useful energy needs is associated with heating ( $E_h$ ):

$$\text{Equation 4: Life-cycle impact associating heating.} \quad LI = BI + (a_1 - a_2)E_w + a_2(E_w + E_h) \quad (\text{kgCO}_2\text{eq})$$

Finally, after the DHW and heating needs are satisfied, the following equation for cooling ( $E_c$ ) is obtained:

$$\text{Equation 5: Life-cycle impact associating cooling.} \quad LI = BI + (a_1 - a_2)E_w + (a_2 - a_3)(E_w + E_h) + a_3(E_w + E_h + E_c) \quad (\text{kgCO}_2\text{eq})$$

## 2.3. Financial cost

The undertaken costs and economic parameters are those established by the Delegated Regulation 244/2012 for a financial perspective (European Commission, 2012). Value-added tax (VAT) and other applicable taxes are included.

The second objective function,  $f_2$ , whose vector  $\vec{x}$  also corresponds to a decision variable, is performed by the financial cost of the energy systems,  $FC$ . Single DHW, space heating and cooling systems are considered ( $w, h, c$ ). Thus,  $FC(\vec{x}, \tau)$  is expressed by the sum of the initial investment for the combined systems,  $I$ , minus their possible residual values,  $V$ , plus respective maintenance costs and the costs from useful energy needs provided ( $E_w, E_h, E_c$ ), calculated by applying the discount factor  $D_\tau$ , referring to starting year,  $i = 1$ , over the calculation period  $\tau$ :

$$\text{Equation 6: Second objective function.} \quad f_2(\vec{x}) = FC(\vec{x}, \tau) = \sum_{i=1}^{\tau} [(I - V + M + b_1 E_w + b_2 E_h + b_3 E_c) D_\tau]^i(\vec{x}) \quad (\text{€})$$

Where  $I = I_w + I_h + I_c$ ;  $V = V_w + V_h + V_c$ ;  $M = M_w + M_h + M_c$ ;  $b_1 = C_w/\eta_w$ ,  $b_2 = C_h/\eta_h$  and  $b_3 = C_c/\eta_c$ , with  $C_w, C_h$  and  $C_c$  being the costs of final energy and  $\eta_w, \eta_h$  and  $\eta_c$  the efficiency of the energy systems, which convert the useful into final energy. The discount factor for year  $i$ ,  $D_\tau$ , is calculated by the following formula:

$$\text{Equation 7: Discount factor.} \quad D_\tau = \left( \frac{1}{1 + r/100} \right)^{i-1}$$

Where  $r$  is the real discount rate (%) that allows to calculate what the future payments added to the initial cost and minus the residual value discounted would be worth today.

Similar to what was explained for the first objective function, the second function,  $f_2$ , is partitioned into three straight line segments to be calculated. The first segment considers the overall costs of equipment,  $(I - V + M)$ , which make up the combined systems, added to the costs of final energy, proportionally to energy consumption for DHW ( $b_1 E_w$ ):

$$\text{Equation 8: Financial cost associating DHW.} \quad FC = I - V + M + b_1 E_w \quad (\text{€})$$

Assuming that after the DHW needs ( $E_w$ ) are satisfied, the increase in useful energy needs is associated with heating ( $E_h$ ):

$$\text{Equation 9: Financial cost associating heating.} \quad FC = I - V + M + (b_1 - b_2)E_w + b_2(E_w + E_h) \quad (\text{€})$$

Finally, after the DHW and heating needs are satisfied, the following equation for cooling ( $E_c$ ) is obtained:

$$\text{Equation 10: Life-cycle impact associating cooling.} \quad FC = I - V + M + (b_1 - b_2)E_w + (b_2 - b_3)(E_w + E_h) + b_3(E_w + E_h + E_c) \quad (\text{€})$$

## 2.4. Environmental assessment

LCA addresses the potential environmental life cycle (LC) impacts and consists of four interrelated steps: definition of goal and scope, life cycle inventory (LCI), life cycle impact assessment (LCIA) and interpretation (ISO 14040, 2006). The impact category of greenhouse gas emissions (GHG) was assessed, calculated using the IPCC assessment method (IPCC, 2013).

The emission and conversion factors are assessed seeking to be more accurate and updated than the national references, which still appropriately consider the evolution of the energy matrix towards renewables. Thus, the GHG emissions factors are 0.351, 0.250, and 0.031 kgCO<sub>2</sub>ep/kWh for electricity, natural gas and biomass, respectively. The final to primary energy conversion factors are 1.24, 1.12 and 0.12 kWh<sub>pe</sub>/kWh also for electricity, natural gas and biomass, respectively (Tadeu *et al.*, 2022).

## 2.5. Economic assessment

Economic parameters of the potential efficient technologies are those established by (EN 15459, 2007) and the Delegated Regulation 244 (European Commission, 2012). The technologies are selected and compared in common cost units, in €/kWh. The initial investment and maintenance costs (VAT and taxes included) are obtained through sampling from a market price database (CYPE Ingenieros, 2023).

The energy price trend is estimated by the EU covering the period up to 2050 (European Commission, 2021). The energy costs for electricity (Eurostat, 2023) and natural gas (Eurostat, 2023) are obtained from data provided by European Commission and the national regulator for energy services (ERSE, 2023). The energy cost for pellets is based on current market cost.

After the useful energy needs for all packages of measures are obtained, their costs are calculated in the financial perspective (considering interest of building owners). A discount rate is applied to the various costs incurred in the



economic life cycle of 20 years. Its value should reflect the most commonly offered rate to credit lines especially to the investment in energy efficiency projects (CGD, 2023).

### 3. CASE STUDY

To demonstrate the use of the proposed operational tool, a simulation was undertaken considering a typical range of useful energy needs for a 3-bedroom reference building (ADENE, 2023), in Portugal. The heating degree days (HDD = 947 °C) and cooling degree days (CDD = 61 °C) are compatible with climate data of cities located in the central region of the country (Eurostat, 2023). These parameters were adjusted to a location at an altitude of 160 m. The constructive characteristics of the reference building, together with the climate conditions of its location and the energy consumption patterns (Tadeu *et al.*, 2018: page 1417) of dwellers in Portugal (INE, 2011) were reflected in the estimates of useful energy needs DHW (2,400), space heating (2,000) and cooling (300 kWh/y).

The energy conservation measures associated 6 sets of different DHW, heating and cooling combined systems shown in Table 1. These packages of combinations were compared with the DHW, heating and cooling systems defined for the reference building (gas water heater, GWH, electric heater, EH, and compact device, CO).

Table 1: Set for DHW, heating and cooling systems

DHW System				Heating System				Cooling System			
<i>W,k</i>	Equipment	Fuel	$\eta$	<i>H,k</i>	Equipment	Fuel	$\eta$	<i>C,k</i>	Equipment	Fuel	$\eta$
<i>W,1</i>	Gas water heater	Gas	0.85	<i>H,1</i>	Electric heater	Electricity	1.00	<i>C,1</i>	Compact device	Electricity	1.00
<i>W,2</i>	Gas water heater	Gas	0.88	<i>H,2</i>	Air conditioner	Electricity	4.00	<i>C,2</i>	Air conditioner	Electricity	5.95
<i>W,3</i>	Gas boiler	Gas	0.83	<i>H,3</i>	Gas boiler	Gas	0.93	<i>C,3</i>	Compact device	Electricity	2.60
<i>W,4</i>	Biomass boiler	Pellets	0.85	<i>H,4</i>	Biomass boiler	Pellets	0.85	<i>C,4</i>	Compact device	Electricity	2.60
<i>W,5</i>	Water heater	Electricity	0.69	<i>H,5</i>	Air conditioner	Electricity	4.00	<i>C,5</i>	Air conditioner	Electricity	5.95
<i>W,6</i>	Heat pump	Electricity	3.00	<i>H,6</i>	Heat pump	Electricity	3.33	<i>C,6</i>	Heat pump	Electricity	2.68

Where:

- *W,k*, *H,k* and *C,k* identifies each DHW, heating or cooling system
- *W,1* combines only with *H,1* and *C,1*, and so on
- $\eta$  = system efficiency

The reference building had a DHW system with nominal efficiency of 0.85, heating and cooling systems with nominal efficiency of 1.00. The alternative systems pre-selected based on method applied by the operational tool were different GWH and CO equipment, an air conditioner (AC), a biomass boiler (BM), a gas boiler (GB), an electric water heater (WH) and a hypothetical innovative heat pump (HP). Such acronyms are presented in Figures 1 and 2 to separately identify DHW, heating and cooling equipment that make up the combined systems to provide respective energy needs.

Figure illustrates how the interaction between total life cycle impacts and useful energy consumption can be used to compare the eco-efficiency of each set of the energy retrofit systems. The total life cycle impact was assessed for 20 years, in order to avoid working with residual values, since it was assumed that the systems had the same life-cycle period. The solution of the most eco-efficient energy retrofit packages can be easily identified as a function of the DHW ( $E_{W,k}$ ), heating ( $E_{H,k}$ ) and cooling ( $E_{C,k}$ ) needs. It was considered that the initial point is the embodied energy impact related to each package ( $E_{W,k}+E_{H,k}+E_{C,k}$ ), as it is accountable, even if the systems are not used. The polygonal curve formed by the segments of the linear equations with the lowest impact, crossing at intersection points, identifies the most eco-efficient systems for each amount of useful energy needs. For the given useful energy needs indicated, the biomass boiler together with compact device performed better than all sets of energy systems, i.e., the energy retrofit package composed by BM+BM+CO would cause less environmental impact than the others.

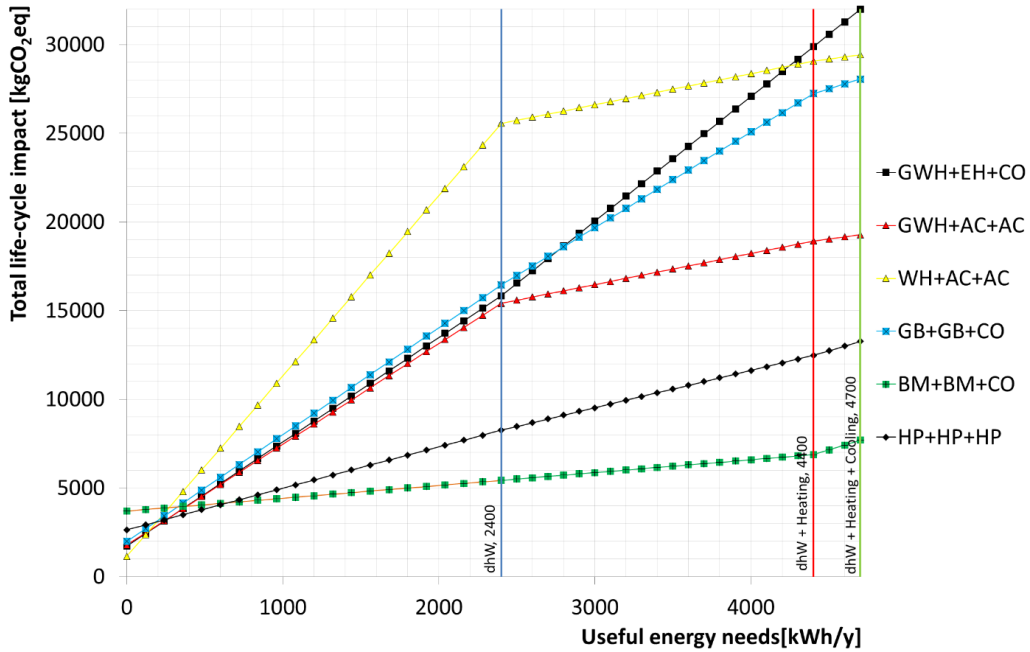


Figure 1 Results for total life cycle impact as a function of useful energy needs

Figure 2 shows the interaction between financial cost (also for 20 years and converted to net present value) and useful energy needs. Similarly, it is assumed that the initial point is the investment and maintenance costs that are related to each package, as they are accountable, even if not used. Note that is considered just the financial cost related exclusively to the systems and the respective energy used. The energy retrofit package composed by GWH+AC+AC turns out to be more economically attractive for the energy needs specified in the example. In short, the methodology applied for pre-selection of systems indicates that the most environmentally and economically attractive energy retrofit packages would not be the same. Therefore, the decision-maker can choose the solution that comes closest to the weighting given to these two decision criteria.

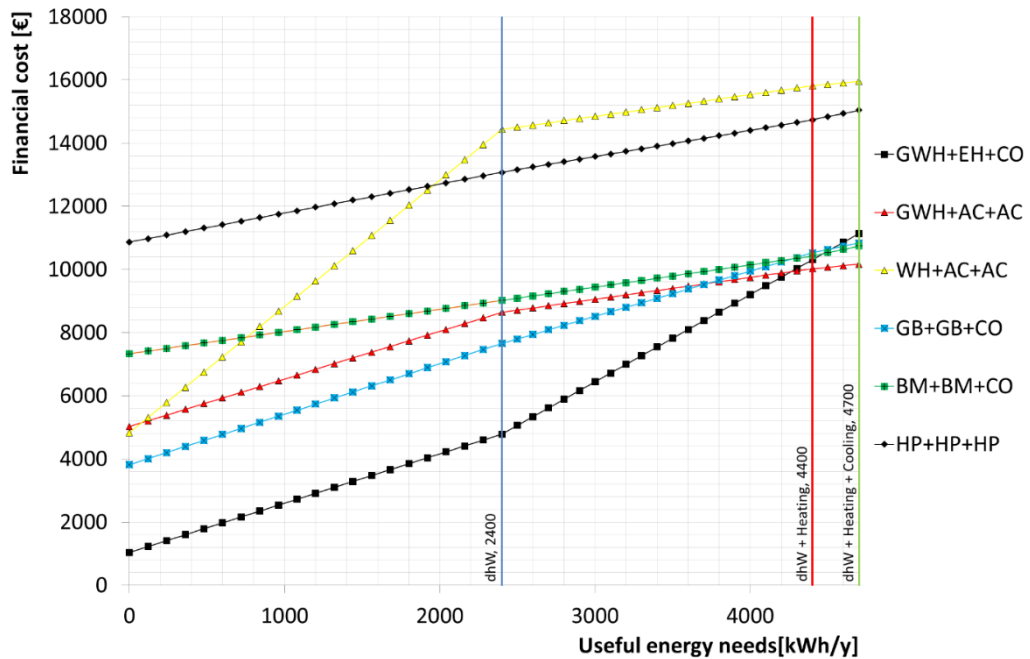


Figure 2 Results for financial cost as a function of useful energy needs

It is emphasized that the options must be analysed according to the specific characteristics of each building. For example, BM and HP depend on space for their installation, and BM still needs regular storage of pellets and additional precautions regarding fume extraction, which may not be in the interest of residents.

## 4. CONCLUSION

In this paper, an operational tool was presented to identify optimal energy systems for small buildings in terms of useful energy needs and considering the impact during the life cycle of these equipment. The applied methodology can be used to estimate the most economically attractive retrofit solutions, in addition to taking into account their environmental impact. Although this simplified methodology has been applied in this work to a housing representative of the Portuguese dwelling stock, it is equally applicable to different contexts, including small non-residential buildings and buildings in other climatic regions.

The simplicity of this tool allows its use by different stakeholders, such as: authorities (in policymaking), specialists (in recommending energy conservation measures), product and service providers (in market positioning) and building owners (in the investment decision).

## 5. ACKNOWLEDGEMENT

The SUREFIT project has received funding from the European Union's Horizon 2020 research and innovation programme under grant agreement No 894511. The author would like to thank the research partners of the SUREFIT project, Aalto University, AMSolutions, Fundación Santa Maria la Real, ISQ Group and the University of Nottingham, and also the industrial partners involved in R&D process of SUREFIT technologies, including CJR Renewables, Koester, Oncontrol Technologies, PCM Products, Solimpeks, and Winco Technologies.

## 6. REFERENCES

ADENE, 2023. Portal SCE - Sistema Certificação Energética dos Edifícios. [www.adene.pt/sce](http://www.adene.pt/sce).

Anastaselos, D., Giama, E. and Papadopoulos, A., 2009. An assessment tool for the energy, economic and environmental evaluation of thermal insulation solutions. *Energy and Buildings*, 41, p. 1165–1171.

Azar, E. and Menassa, C., 2012. A comprehensive analysis of the impact of occupancy parameters in energy simulation of office buildings. *Energy and Buildings*, 55, p. 841–853.

CGD, 2023. Caixa Geral de Depósitos - Credit for building retrofit. [www.cgd.pt/Particulares/Credito/Habitacao/Pages/Credito-Habitacao-Reabilitacao-Urbana-Compra.aspx](http://www.cgd.pt/Particulares/Credito/Habitacao/Pages/Credito-Habitacao-Reabilitacao-Urbana-Compra.aspx).

CYPE Ingenieros, 2023. Gerador de preços para construção civil. [www.geradordeprecos.info](http://www.geradordeprecos.info).

EN 15459, 2007. Energy Performance of Buildings - Economic Evaluation Procedure for Energy Systems in Buildings. European Committee for Standardization.

EPBD, 2010. Directive 2010/31/EU of the European Parliament and of the Council on the energy performance of buildings (recast), Off. J. Eur. Union L153, 13–15.

ERSE, 2023. Regulatory Authority for Energy Services. Portal ERSE. [www.erse.pt/pt/Paginas/home.aspx](http://www.erse.pt/pt/Paginas/home.aspx).

European Commission, 2011. A Roadmap for moving to a competitive low carbon economy in 2050.

European Commission, 2012. Commission Delegated Regulation No 244, Supplementing Directive 2010/31/EU by Establishing a Comparative Methodology Framework for Calculating Cost-Optimal Levels of Minimum Energy Performance Requirements for Buildings, C115, 1–38.

European Commission, 2021. EU reference scenario 2020 - Energy, transport and GHG emissions: trends to 2050. Publications Office.

Eurostat, 2023. Electricity price statistics. [http://ec.europa.eu/eurostat/statistics-explained/index.php/Electricity\\_price\\_statistics#Electricity\\_prices\\_for\\_household\\_consumers](http://ec.europa.eu/eurostat/statistics-explained/index.php/Electricity_price_statistics#Electricity_prices_for_household_consumers).

Eurostat, 2023. Heating and cooling degree days - statistics. [https://ec.europa.eu/eurostat/statistics-explained/index.php?title=Heating\\_and\\_cooling\\_degree\\_days\\_-\\_statistics](https://ec.europa.eu/eurostat/statistics-explained/index.php?title=Heating_and_cooling_degree_days_-_statistics).

Eurostat, 2023. Natural gas price statistics. [http://ec.europa.eu/eurostat/statistics-explained/index.php/Natural\\_gas\\_price\\_statistics#Natural\\_gas\\_prices\\_for\\_household\\_consumers](http://ec.europa.eu/eurostat/statistics-explained/index.php/Natural_gas_price_statistics#Natural_gas_prices_for_household_consumers).

INE, 2011. Instituto Nacional de Estatística and DGEG, Inquérito ao Consumo de Energia no Sector Doméstico 2010.

- IPCC, 2013. Climate Change 2013: the Physical Science Basis. Contribution of Working Group I to the Fifth Assessment Report of the Intergovernmental Panel on Climate Change, Cambridge University Press, Cambridge, United Kingdom and New York, NY, USA.
- ISO 14040, 2006. Environmental Management Life Cycle Assessment Principles and Framework, International Organization for Standardization.
- Kim, S., Lee, S., Na, Y. and Kim, J., 2013. Conceptual model for LCC-based LCCO<sub>2</sub> analysis of apartment buildings. *Energy and Buildings*, 64, p. 285–291.
- Kneifel, J., 2010. Life-cycle carbon and cost analysis of energy efficiency measures in new commercial buildings. *Energy and Buildings*, 42, p. 333–340.
- Lollini, Barozzi, Fasano, Meroni, and Zinzi, 2006. Optimization of opaque components of the building envelope. *Energy, economic and environmental issues. Building and Environment*, 41, p. 1001–1013.
- Meester, T., Marique, A., De Herde, A. and Reiter, S., 2013. Impacts of occupant behaviours on residential heating consumption for detached houses in a temperate climate in the northern part of Europe. *Energy and Buildings*, 57, p. 313–323.
- REH and RECS, 2013. DL 118 - Regulamento de Desempenho Energético dos Edifícios de Habitação, Comércio e Serviços, Code of the energy performance of buildings (residential and commercial), Ministry of Economy and Employment, 4988–5005.
- Silvestre, J., Brito, J. and Pinheiro, M., 2013. From the new European Standards to an environmental, energy and economic assessment of building assemblies from cradle-to- cradle (3E-C2C). *Energy and Buildings*, 64, p. 199–208.
- Tadeu, S., Tadeu, A., Simões, N. and Prado, R., 2018. A sensitivity analysis of a cost optimality study on the energy retrofit of a single-family reference building in Portugal, *Energy Efficiency*, 11, 1411–1432.
- Tadeu, S., Gonçalves, M., Simões, N. and Tadeu, A., 2019. Procedure to select combined heating and hot water systems: An expeditious cost optimality approach. *Journal of Building Engineering*, 25, 100838.
- Tadeu, S., Rodrigues, C., Marques, P. and Freire, F., 2022. Eco-efficiency to support selection of energy conservation measures for buildings: A life-cycle approach. *Journal of Building Engineering*, 61, 105142.
- Zakula, T., Bagaric, M., Ferdelji, N., Milovanovic, B., Mudrinic, S. and Ritosa, K., 2019. Comparison of dynamic simulations and the ISO 52016 standard for the assessment of building energy performance. *Applied Energy*, 254, 113553.

---

## #242: Power quality impacts of grid-tied PV inverters on low voltage distribution networks

### A smart OpenDSS model to find power quality threshold limits

---

Chinthaka ATTANAYAKE<sup>1</sup>, Nilupulee GUNATHILAKE<sup>2</sup>, Janaka EKANAYAKE<sup>3</sup>

<sup>1</sup> Generation Protection, Ceylon Electricity Board, Sri Lanka. [chinthaka.attanayake@ceb.lk](mailto:chinthaka.attanayake@ceb.lk)

<sup>2</sup> School of Computing, Engineering & the Built Environment, Edinburgh Napier University, UK.  
[n.gunathilake@napier.ac.uk](mailto:n.gunathilake@napier.ac.uk)

<sup>3</sup> Faculty of Engineering, University of Peradeniya. [ekanayakej@eng.pdn.ac.lk](mailto:ekanayakej@eng.pdn.ac.lk)

*Abstract: As a renewable initiative, risen attention can be seen in solar photovoltaic (PV) installations in the world. Since tropical countries and even many other countries during summer experience higher irradiance levels, there is great potential for PV generation in solar panels. However, power quality can be impacted when the number of PV modules is increased in a network due to the emergence of harmonics, unbalanced voltages, voltage flicker, neutral voltage variations, etc. Therefore, it is essential to empirically analyse power quality parameters, i.e., total harmonic distortion (THD), voltage unbalance, etc., and find threshold margins of PV capacities in a network.*

*Based on a case study conducted in Negombo, Sri Lanka, this work determines power quality impacts with reference to the number of PV interconnections in a distributed network. For the task, a low-voltage distribution network was chosen which was fed by a 250kVA, 11/0.4kV transformer with domestic loads and grid-tied PV inverters. A simulation model was developed in Open Distribution System Simulator (OpenDSS) with time-varying load patterns and PV generation. Consequently, a smart efficient method was introduced to model domestic loads with unique time-varying demand patterns. A determination criterion was established to derive snapshot load flow instants using time-varying load flow results to analyse voltage profiles along distribution feeders. Then, the model was enhanced to quantify the power quality parameters such as individual harmonic content, THD of voltage as well as current and neutral voltage variation. The results reveal that node voltage has improved with PV interception without violating the upper limit. The THD of voltage and current have slightly increased with the addition of PV inverters.*

*Keywords: Solar PV, renewable energy, low voltage distribution, power quality, OpenDSS*

## 1. INTRODUCTION

As a global initiative to address the energy crisis in the world, many countries are focusing on renewable energy resources, *i.e.*, solar, wind, hydropower, etc. Since solar is considered a dominant candidate, the implementation of photovoltaic (PV) which is the phenomenon of conversion of sunlight into electricity, is growing at an exponential rate. Large-scale PV power plants are connected to high voltage networks, whereas medium and small-scale PV plants are penetrated to distribution networks. Hence, the latter categories fall under the dispersed generation candidates. Small-scale PVs are mainly installed on rooftops that are connected to low-voltage (LV) distribution feeders. Due to the accelerated implementation of small-scale PVs into distribution networks, the impact of high penetration has become a challenge to maintain grid codes while harvesting this free solar energy. Figure 1 shows the basic components of a grid-tied PV system connected to an LV distribution network. PVs in such networks greatly affect phase voltage profile, neutral voltage variation, power flow patterns and power quality parameters because of the control schemes and non-dispatchable characteristics of these grid-tied systems. Although the individual impact of a small-scale rooftop PV is considerably small, the aggregated effect would be significant in terms of the operational behaviour of network components, protection coordination, and safety as well as the lifetime of home appliances.

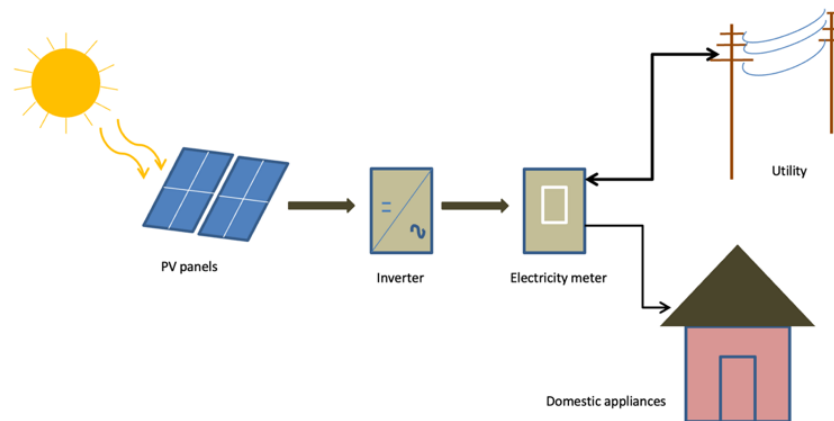


Figure 1 Basic grid-tied rooftop PV system

Modelling a PV system is a complex task since several external parameters such as ambient temperature, irradiance level, inverter control algorithms, and specifications of the solar panel and inverters affect the power output. As a result, it impacts power quality. Power quality is the availability of reliable and continuous electric power without causing intolerable electromagnetic disturbances to network components and appliances. Voltage sags and swells, momentary interruptions, voltage transients, harmonic voltages, frequency and voltage fluctuations are several power quality indices. In literature, many studies regarding PV impacts focus on the fact that PV arrays are constant current sources. Therefore, those work tends to gain lower accuracy. In addition, the majority of work was conducted considering a single LV feeder with synthetic consumer loads (Pillai et al., 2018), Institute of Electrical and Electronics Engineers (IEEE) standard test feeders (Dinh et al., 2021; Gupta et al., 2018), and single distribution transformer neglecting other medium-voltage (MV) loads connected to the MV feeder (Salimon, et al., 2023; Gupta et al., 2018). Thus, it is a necessity to develop a PV system with real-time characteristics including external conditions such as irradiance, ambient temperature, efficiency, etc., which govern the PV output and realistic consumer demand profiles (Daw, et al., 2021; Shen, et al., 2019). In an effort in filling a research gap mentioned above, proposing a real-time residential realistic load modelling methodology to derive power quality aspects was recognised as a core objective of this research.

### 1.1. Our Contribution

This study empirically analyses power quality to find threshold margins of small-scale PV capacities in distribution networks. Furthermore, this work introduces a smart efficient method to model domestic loads with unique time-varying demand patterns based on daily consumption. The case study was performed using a low voltage network of a 250kVA distribution transformer in Negombo, Sri Lanka with rooftop PV inverters. For the tasks, power quality impacts such as harmonics, total harmonic distortion (THD) of voltage as well as current, voltage unbalance, neutral voltage and phase voltage profiles were investigated. Harmonic voltages and currents were computed at several feeder nodes including point of common coupling (PCC) of PV inverters and transformer LV terminals. The effects of other MV loads too were considered for better approximation. This work:

- proposes an end-user domestic load modelling methodology with real-time demand profiles
- addresses methodologies for accurate determination of loading instants for power flows and harmonic analysis
- includes methodologies for modelling LV and MV lines, PV systems, domestic loads, and impacts of other loads such as transformers
- uses Open Distribution System Simulator (OpenDSS) for the analysis

During the LV distribution planning stage, the impact and the amount of PV penetration levels are not considered in Sri Lanka at present. That causes to deviate the expected operating conditions from the actual. Therefore, the importance of assessing distributed generation sources during LV planning is also addressed.

## 2. LITERATURE REVIEW

Distributed PVs are popular among retail electric consumers due to feed-in-tariff schemes and subsidised financial support for PV deployment in their houses. Therefore, studying their impact on distribution systems is an important subject of interest.

### 2.1. Modelling of PV Inverters, Loads and Distribution Feeders

PV system simulation comprises the modelling of PV arrays, direct current to alternating current (DC-AC) inverters, loads and distribution feeders. PV resources can be simulated as fixed current injectors (Castro et al., 2020). The main functions of inverters are maximum power point tracking (MPPT), grid synchronisation, energy storage and disconnection during grid anomalies (Cuello-Polo et al., 2021). Modern inverters use active power curtailment and reactive power absorption techniques to mitigate voltage problems in the network (Almeida et al., 2021). Volt/Var and Volt/Watt methods also contribute to overcoming voltage problems (Almeida et al., 2020). The most common practice of modelling loads is the ZIP<sup>1</sup> method. Determination of proper ZIP values and accurate diversity factors is a complex task (Bircan et al., 2020). In harmonic studies, an aggregate load is represented as a series or parallel combination of resistance and inductance. These resistance and inductance values are considered as constants throughout the frequency range (IEEE Std 399-1997, 1998). In Dugan et al., 2020, loads were designated with their measured harmonic spectra. The impedance of a four-wire low-voltage overhead power line is described by a 5x5 series impedance and shunt nodal capacitance matrix (Claeys et al., 2022). Both impedance and capacitance values have self and mutual components. Carson's equation can be used to simplify the impedance and capacitance matrices into 4x4 matrices such that the ground element had been removed and taking the effect of ground to the phase and neutral conductors (Raavi et al., 2021). If the voltage difference of the neutral wire between two adjacent nodes is zero, the simplified 4x4 matrices can be further reduced to 3x3 matrices using the Kron reduction (Claeys et al., 2022).

### 2.2. Load Flow Algorithms

Load flow methods such as Newton-Raphson (N-R), Gauss-Siedel and Fast decoupled methods are specifically formulated for load flow studies on transmission networks (Krishna et al., 2022; Mawuena et al., 2022). In Raavi et al., 2021, the bus number matrix has been used to develop a power flow algorithm for an unbalanced radial distribution network with renewable energy sources and distribution static compensators. Load flow methods in OpenDSS use bus admittance matrices. It consists of two algorithms known as normal algorithm and the Newton method. The normal algorithm is a fixed-point method as long as the initial voltage guess is closer to the final solution. For highly meshed networks, the Newton method is used with non-linear equations and complex voltage vectors (Dugan et al., 2020).

### 2.3. Impact of PV Deployments

The potential impact of small-scale residential PV deployment on distribution networks depends on feeder-specific parameters, *i.e.*, *feeder layout, voltage class, X/R ratio<sup>2</sup>, substation capacity, loading pattern.*, and PV-specific parameters, *i.e.*, *the capacity, location along the feeder, inverter control schemes, correlation of PV output with load, electrical proximity to other PV, variability of PV output depending on weather conditions* (Gimenes et al., 2022; Cuello-Polo et al., 2021; Sharma et al., 2020). Voltage magnitude is a crucial parameter that can be affected by the PV system. Voltage imbalance effects can be minimised by accommodating more single-phase PV systems connected to heavily loaded phases. How the penetration level of distributed generators affects the power loss and voltage profile to the network have been analysed in Salimon et al., 2023. A suitable location for distributed generators has been determined based on voltage profile index (VPI) which describes how close the actual voltage fits with the ideal value. Since the fault current contribution of PV inverters is negligible, the impact of PV deployment on power system faults can be neglected. In fact, large-scale PV penetration can cause unnecessary breaker tripping, protection under-reach and coordination conflicts (Liu et al., 2022; Pillai et al., 2018). Transient over-voltage due to the intermittent nature of PV inverters is also a power quality concern. During grid failures, local PV inverters are shut down by the activation of anti-islanding protection. During this disconnection period, local loads may experience higher voltages due to an abnormal rise in phase voltages. Voltage sags and swells can also be stated as another power quality parameter. Those determine the fault-ride-through capability of rooftop solar systems in some countries (Talha et al. 2021). Harmonic levels in distribution systems are growing due to harmonic-rich domestic loads such as the latest lighting accessories and electric vehicle chargers. PV inverter units are another source of harmonics to distribution networks due to pulse width modulation (PWM) techniques used in inverters. Subsequently, this may cause unacceptable voltage distortion (Sharma et al., 2020). THD in voltage (THD<sub>v</sub>) defines the distortion of

---

<sup>1</sup> Constant impedance (Z), constant current (I), constant power (P)

<sup>2</sup> X (reactance), R (resistance)

voltage due to higher order harmonic voltages, and it is measured by using Equation 1. THD in current (THD<sub>i</sub>) is defined in a similar manner to Equation 1.

Equation 1: THD of voltage.

$$THD_v = \frac{\sqrt{\sum_{n=2}^{50} V_n^2}}{V_1}$$

Where:

- THD<sub>v</sub> = THD of voltage related to fundamental voltage (%)
- V<sub>1</sub> = fundamental phase voltage (V)
- n = harmonic order

## 2.4. Power Quality Standards of Grid-Connected PV

International Electrotechnical Commission (IEC) 61727-2004 and IEEE 1547-2018 (IEEE Std 1547, 2018) provide guidance on grid-connected PV. IEEE 519-2022 (IEEE, 2022), IEEE 399-1997 (IEEE Std 399-1997, 1998) define harmonic generation, recommended limits and concepts involved in harmonic analysis. Apart from these, IEC 61000-4-7 (IEC 61000-4-7, 2021), IEC 61000-4-30 (IEC 61000-4-30, 2021), IEC 61000-4-15 and IEEE 1453 define power quality indices. All these standards specify parameters such as voltage deviation, frequency deviation, harmonic levels, three-phase unbalance, voltage flicker and allowable DC components (Barreto, 2023). With reference to the IEEE 519-2022, voltage distortion limits with reference to different bus voltage ranges at PCC are tabulated in Table 1 whereas current distortion limits are in Table 2. I<sub>sc</sub> is the maximum three-phase short circuit current, I<sub>L</sub> is the maximum fundamental current at the PCC, and thus I<sub>sc</sub>/I<sub>L</sub> is the short circuit ratio at the PCC. TDD is the total demand distortion. IEEE 3002.8-2018 standard (IEEE, 2018) further describes power system modelling techniques for harmonic analysis with two proposed methods. The first method is the harmonic power flow method which uses a nodal admittance matrix and fast Fourier transform (FFT). The second method is based on nonlinear device voltage-current characteristics which uses an iterative approach.

Table 1: Voltage distortion limits

Bus Voltage at PCC (kV)	Individual Harmonic Content	Total Harmonic Distortion
V < 1	5.0%	8%
1 ≤ V < 69	3.0%	5%
69 ≤ V ≤ 161	1.5%	2.5%
V > 161	1.0%	1.5%

Table 2: Current distortion limits

I <sub>sc</sub> /I <sub>L</sub>	Individual Odd Harmonic Order					TDD
	3 ≤ h < 11	11 ≤ h < 17	17 ≤ h < 23	23 ≤ h < 35	35 ≤ h < 50	
< 20	4.0	2.0	1.5	0.6	0.3	5.0
20 < 50	7.0	3.5	2.5	1.0	0.5	8.0
50 < 100	10.0	4.5	4.0	1.5	0.7	12.0
100 < 1000	12.0	5.5	5.0	2.0	1.0	15.0
1000 >	15.0	7.0	6.0	2.5	1.4	20.0

## 3. METHODOLOGY

The 250kVA, 11/0.4kV, Dyn11 distribution transformer chosen for the case study is named BZ520. It is located in Negombo, Sri Lanka where the area is progressively experiencing higher penetration levels of a large number of PV interconnections because of high irradiance levels. According to the consumer database of Lanka Electricity Company (LECO) in June, 2019, the BZ520 had the highest number of rooftop PV inverters and a variety of loads, such as single-phase and three-phase loads, with both residential and commercial consumers. This transformer has four LV aerial bundled conductor lines. Table 3 includes the connection details of the consumer loads and PV interconnections at that time. There are 371 load connections, and 13 roof-top PV inverters connected to it. PV inverter capacities and their feeder locations are presented in Figure 2.



Table 3: Connection details of consumer loads and PV inverters of BZ520 transformer

Feeder	Distance with spurs (m)	Consumers (unit)	PV (unit)
F1	542	68	4
F2	681	68	1
F3	608	105	3
F4	1082	130	5

The next task was to determine network boundaries for the simulation of the distribution system. The BZ520 is connected to Periyamulla-Cemetery (PERCM) feeder, which is one of the four 11kV overhead feeders of the primary substation (PSS) in Periyamulla. This PSS converts 33kV to 11kV via two 10MVA transformers. The distribution of other transformers of the PERCM feeder is illustrated in Figure 3. The impact of other transformers was also considered in the load flow solution. The two transformers which are upstream to the BZ520 were represented using 15-minute averaged demand values from the installed energy meters. To determine the combined effect of the remaining transformers, snapshot load flow was conducted using Neplan power system analysis software (Neplan, 2023). The voltage variation of the 11kV bus at the PSS at 15-minute intervals was used as the voltage profile, which reflects the effect of the upstream electrical network and other MV feeders of the PSS. Furthermore, the averaged active and reactive power profiles of the PERCM feeder were normalised and multiplied with the load flow results to quantify the demand profile of the lump load. For the acquisition of the network and operational parameters, the voltage profile and the demand profile were recorded at the PERCM feeder. A harmonic spectrum was also recorded at the same location using Sonel PQM711 power quality analyser (Sonel, 2023) and the measured harmonic spectrum was used as an input parameter to the simulation model. Both single-phase and three-phase short circuit levels at the 11kV terminals of the BZ520 were determined using ETAP 12.6.0 power system analysis software (ETAP, 2023) and were found out to be 60.58MVA and 42.31MVA, respectively.

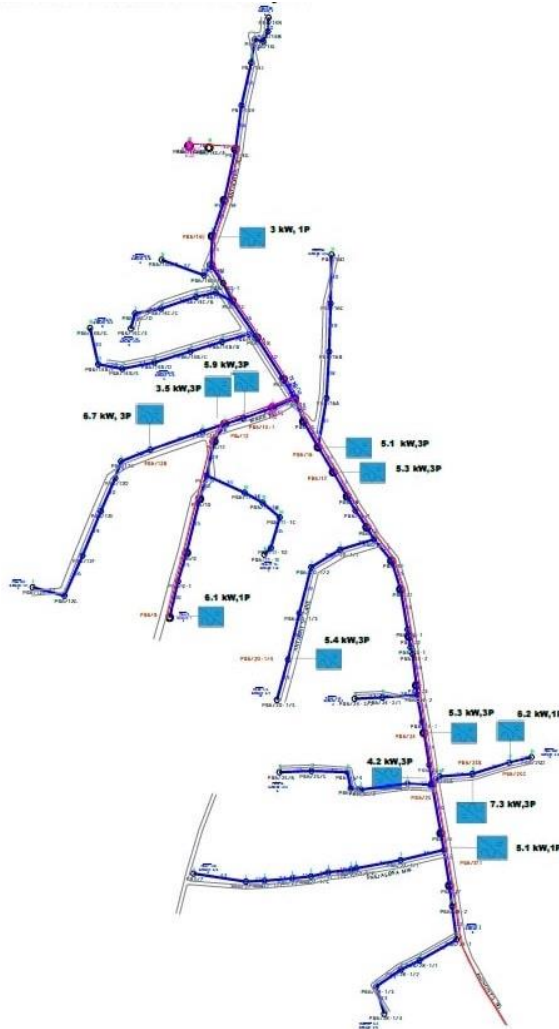


Figure 2 Dispersion of PV inverters connected to distribution network of BZ520

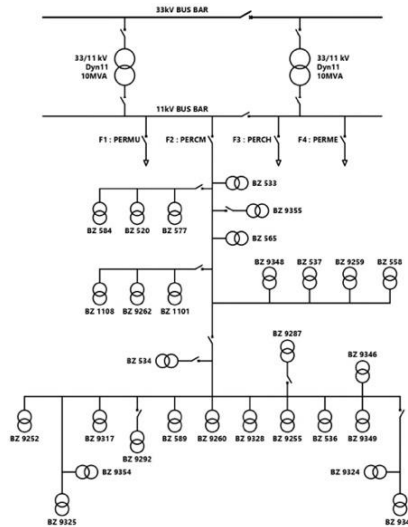


Figure 3 Transformer dispersion of PERCM feeder

### 3.1. Line Parameterisation

To model 11kV overhead conductors and 400V aerial bundled conductors, the OpenDSS generates line constants once their physical properties such as DC resistance, diameter, geometric mean radius, and x-y coordinates are given. The actual feeder topology was modelled by this method. This approach can be used where Carson's equations and Kron reduction methods cannot be used to model distribution circuits due to the fact that the neutral conductor is not grounded at every pole in Sri Lankan low-voltage distribution networks. LV feeders chosen for the study were equipped with 70mm<sup>2</sup> and 50mm<sup>2</sup> aerial bundled conductors. Line impedance and shunt nodal capacitance matrices were derived using Line Geometry and Line Constants libraries of the OpenDSS.

### 3.2. PV Modelling

The OpenDSS platform was used in this task due to extreme flexibility in PV modelling. It uses dedicated libraries for PV generators. The temperature coefficient factor of each PV array was obtained from manufacturer datasheets. Daily temperature variation at the 15-minute interval was obtained using a weather station located 5km away from the distribution network. Data logging was conducted for all PV inverters at the PCC using the power quality analyser. It was used to record the load flow and power quality parameters including the harmonic spectrum up to the 25<sup>th</sup> order. Inverter efficiency curves were obtained from inverter manufacturers' datasheets. Figure 4 visualises the PV system developed in the OpenDSS.

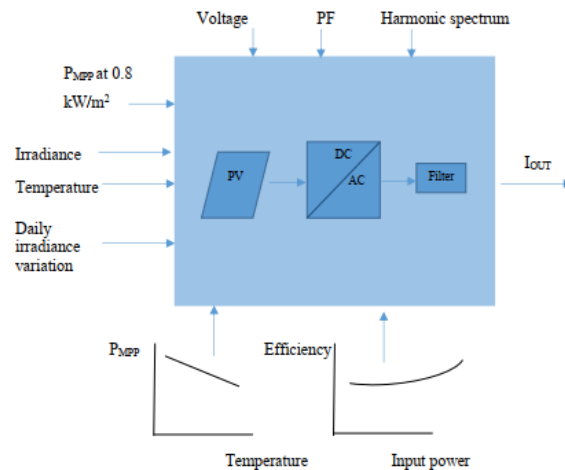


Figure 4 PV system block diagram used in OpenDSS

### 3.3. Load Categorisation

Three categories were defined based on monthly consumption. Hence, average monthly consumption was calculated by referring to 6-month records from January 2019 to June 2019 that are:

- **Category I:** Monthly consumption  $\leq 100\text{kWh}$
- **Category II:**  $100\text{kWh} < \text{Monthly consumption} \leq 200\text{kWh}$
- **Category III:** Monthly consumption  $> 200\text{kWh}$

All the consumers were put into one of the above categories based on the mentioned criteria. The average instantaneous demand per hour for each consumer was calculated using Equation 2. 720 is the number of hours for 30 days. Each consumer was represented by a unique average instantaneous value which was used as the multiplication factor. Field measurements were taken from three consumers of each category. Parametric values of terminal voltage, phase current, active power profile, reactive power profile, harmonic spectrum,  $\text{THD}_v$  and  $\text{THD}_i$  were recorded. Also, active and reactive power curves for the 24-hour duration were normalised by their corresponding highest value in the measurement matrices. These normalised active and reactive power curves were multiplied by previously determined average instantaneous demand for establishing a unique load profile for each consumer.

Equation 2: Average active power demand per hour.

$$AID = \frac{AMC}{720 \text{ Hours}}$$

Where:

- AID = average instantaneous demand per hour (kW)
- AMC = average monthly consumption (kWh)

### 3.4. Power Flow and Harmonic Analysis

A time series power flow solution was carried out for the developed OpenDSS model, including an 11kV busbar at the PSS, 11kV PERCM overhead feeder, MV lump load, PV inverters, domestic loads and low voltage lines. Using the solution derived at the LV terminals of the BZ520, three critical instants were identified called the maximum reverse power through the BZ520, the minimum active power demand instant and the maximum active power demand instant. Active and reactive power variation was extracted at important nodes in the network including the BZ520 transformer terminal, PV interconnection points, etc. Energy analysis was conducted to evaluate the transformer loss, the maximum demand, and energy flow with PV penetration. The voltage profile at each critical snapshot was determined for several nodes, such as PCC points, feeder starting points and feeder endpoints. Lastly, a harmonic analysis was conducted in the frequency domain with and without the presence of PV inverters to verify the power quality impact on the network. For that, PV inverters, domestic loads and an 11kV busbar were defined by their measured harmonic spectra during the harmonic simulation. During the harmonic simulation, the  $\text{THD}_v$ , the  $\text{THD}_i$ , individual harmonic voltages and the voltage unbalance factor (VUF) were calculated.

## 4. RESULTS & OBSERVATIONS

Figure 5 illustrates the active and reactive power flow variation at the MV terminals of BZ520 during the PV injection status. An important observation could be noticed that the reverse power flow had appeared through the BZ520 to the MV side. The neutral link voltage derived at the BZ520 remains below 0.1V without PV injection while it rises to 0.2V with PV injection. Neutral current variation along Feeder 1 is illustrated in Figure 6 for both with PV and without PV injection concerns. The neutral current reaches a maximum of 17.8A during the maximum PV generation. The amount of neutral current increment occurs when the existence of single-phase PV inverters.

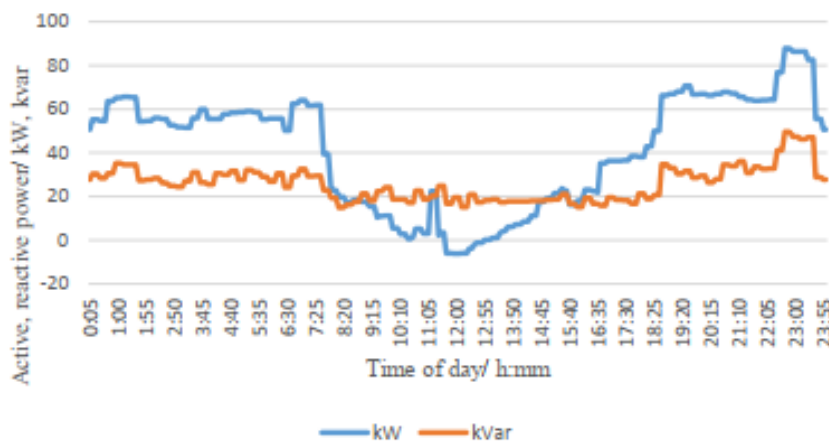


Figure 5 Power flow variation - 11kV terminals of BZ520 with PV injection

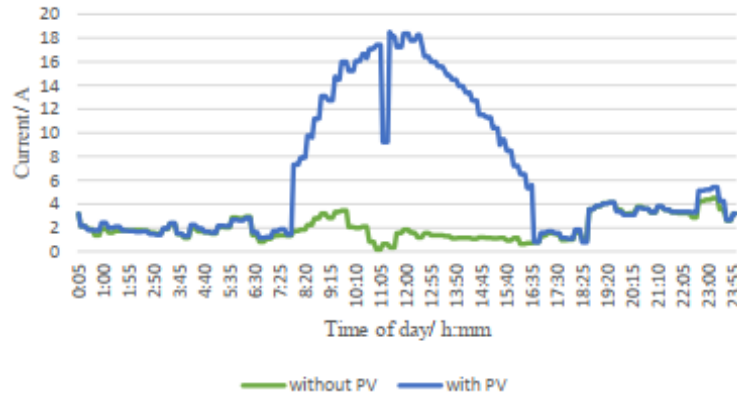


Figure 6 Neutral current variation at Feeder 1 with and without PV injection

It was found that the transformer had delivered 990kWh of energy per day when PV penetration existed. Transformer energy loss was evaluated as 17.6 kWh per day. When PV penetration did not exist, the transformer had delivered 1272kWh of energy, and the loss was 18.7kWh. Therefore, 282kWh of energy saving was achieved. The transformer's maximum demand was recorded as 100.83kVA. During the reverse power flow instant, 9.6kW active power was transferred to the MV side through the BZ520. Observed node voltages in each snapshot is shown in Figure 7. The maximum PV generation was observed to occur at 12:00h. When the PV generation is its maximum, the node voltage is higher.

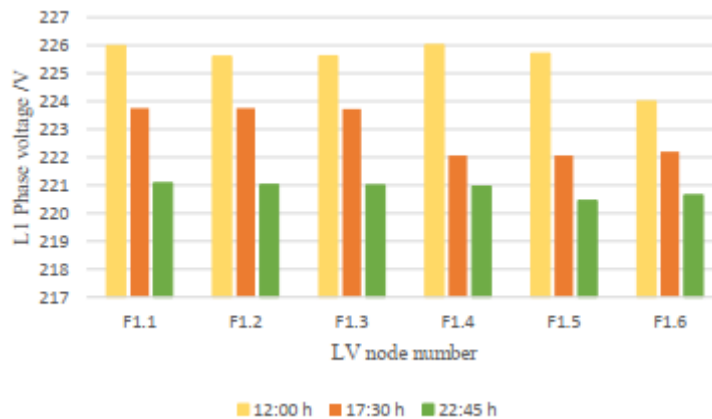


Figure 7 Phase voltage profiles of LV nodes of F1 at critical snapshots

Regarding the THD<sub>v</sub> results, F4 has higher values compared to F1, F2 and F3. The highest value of the THD<sub>v</sub> is 1.1%. During the non-PV inclusion scenario, the maximum THD<sub>v</sub> has reduced to 0.8% in phase L3. Phase L3 exhibits the highest THD<sub>v</sub> values compared to the remaining L1 and L2 phases. Results of the THD<sub>i</sub> assessed for the F4 nodes during the maximum PV generation instant show that the maximum evaluated THD<sub>i</sub> is 12.9% in phase L3. The maximum THD<sub>i</sub> was approximately 8% for the same phase when PV generation was excluded.

## 5. DISCUSSION

Modelling PV resources as fixed current injections reduces the accuracy due to the intermittent nature of solar irradiance, cloud transients, the power-temperature relationship of solar cells, inverter efficiency curves and ambient temperature variations. This study has considered all the above factors to increase the accuracy of PV modelling. Derivation of time-varying demand profile and power factor for domestic loads were achieved in this study using field measurements and an innovative load classification approach. Since it was realised that distribution system load modelling had not received the same level of attention as other power system components in general, this gap was appropriately filled by the methodology in this research, even though it is a combination of many variables, *i.e.* consumption pattern, living standards, type of equipment, etc. Load flow solutions such as N-R and Gauss-Siedel might encounter convergence problems and end up with anomalous nodal voltages because of radial feeder arrangement, low X/R ratio, unbalanced loading and single-phase distributed generation resources which are inherent characteristics in distribution networks. The OpenDSS platform uses a bus admittance matrix to solve load flow algorithms. Therefore, the nodal voltages are accurate.

Time series analysis was mainly conducted to analyse the voltage and power profile of the network with time. Since the domestic load consumption is higher than the PV generation, the reverse power flow could be observed from the LV side to the MV side through the BZ520 during 10:00h to 13:30h time period as shown in Figure 5. Reactive power is absorbed from the grid since PV inverters are operated at a unity power factor. When single-phase PV inverters are connected, the neutral link voltage increases significantly. LECO which is the distribution system operator in the Negombo area, practises

to connect the neutral conductor to the ground at feeder ends in addition to the transformer neutral link. Due to the fact that, the neutral link voltage remains at a lower value even the neutral conductor breaks at a midpoint. Neutral conductor current depends on various factors such as loading patterns of phase conductors, phase balancing, earthing impedance, and balanced and unbalanced injection of PV which will ultimately define the power quality. An increase of neutral current occurs during the existence of single-phase PV resources. In conclusion, it can be stated that PV generation has a clear impact on the neutral current along LV feeders. Three-phase PV inverters do not adversely affect the neutral current because of the balanced current injection. Nonetheless, the Sri Lankan Grid Code (PUC-LK, 2012) does not define threshold levels for neutral voltages and currents that shall be maintained by the utility. Single-phase PV and current harmonics (triplen harmonics) can be the reasons for having higher neutral currents.

According to the energy analysis of the network, PV modules have contributed to a total energy saving of 282kWh. The PV interconnections offer a total energy saving of 283kWh. However, the transformer loss has not improved by a considerable amount. This is mainly because the solar energy itself circulates among low-voltage feeders of the BZ520. Snapshot analysis helps to investigate voltage fluctuations, power flow along feeders, harmonic currents and voltages, capacity violations, etc., at specific time instants. As shown in Figure 7, the node voltage is higher at PV interconnection nodes during the maximum PV generation instants, whilst it is lower when PVs are not included. This reveals that higher voltages would exist in the vicinity of high PV penetrations. This phenomenon causes voltage regulation issues since distribution transformers are equipped with off-load tap changers. To mitigate voltage regulation issues, on-load tap changers or dedicated low-voltage feeders should be installed to absorb more PVs. The purpose of harmonic analysis is to examine the existing THD of PCC points of PV inverters. In THD<sub>v</sub> comparison between the statuses of with and without PV interconnections, the THD<sub>v</sub> remains below 8% of all nodes even with the maximum PV penetration instant. With reference to the simulation results, the THD<sub>v</sub> has increased with the presence of PV inverters. What is more, the THD<sub>i</sub> variations of the defined LV nodes of each feeder were determined with and without PV scenarios too. The THD<sub>i</sub> also surges with PV penetration compared to the non-PV application status. The allowable limit for the THD<sub>i</sub> depends on the short circuit ratio at each node. The short circuit level at the BZ520 low voltage terminals was calculated using the infinite bus method and the percentage impedance of the transformer which is 3.82% (nameplate data). Therefore, the short circuit level was found to be 9.45kA. The recommended THD<sub>i</sub> limits depend on the load currents at each PV inverter. The maximum load current among 13 PV inverters used for the study is 10.52A (7.29kW PV system). Consequently, the short circuit ratio became 898 for the worst-case scenario, and this ratio was compared with the recommended THD<sub>i</sub> values given in Table 2. According to the IEEE 519-2014, THD<sub>i</sub> should be lower than 15% for each node. The THD<sub>i</sub> has not increased beyond the recommended threshold of 15%.

Model validation was conducted to compare the simulated and the actual systems. A complete validation is impractical due to the complexity and large number of field measurements. Because of that reason, some locations were selected to validate the power profile of PV inverters and the power flow of the BZ520. Figure 8 represents the simulated and measured power flow of PV system 1. The actual power behaviour exhibits similar characteristics to the simulated power flow except for a few overshoots. The developed model can be adapted to any distribution network, which would be an added advantage to utilities to get insights about the real-time network behaviour. Before issuing the grid clearance certificate from the utility to PV developers, the operational performance and subsequent grid impacts of proposed PV systems can be analysed through flexible network conditions. If constraints exist, grid and feeder rehabilitations or augmentations can be identified in the early stage. This developed smart power quality analysis model can be utilised to evaluate PV penetration limits for a particular electricity network referring to the grid code.

### 5.1. Future Work

For a far better realisation of the simulation, the effect of other transformers in the 11kV PERCM feeder can be given as input functions. Even though the development of the entire 11kV feeder with all transformers in OpenDSS is a tedious coding process, more accurate results can be obtained. This model can be further improved to determine the optimum reactive power compensation and frequency support techniques. The benefits of integrating battery storage facilities with PV installations can be studied using the developed model. Such hybrid systems can be successfully promoted by introducing attractive feed-in tariff schemes.

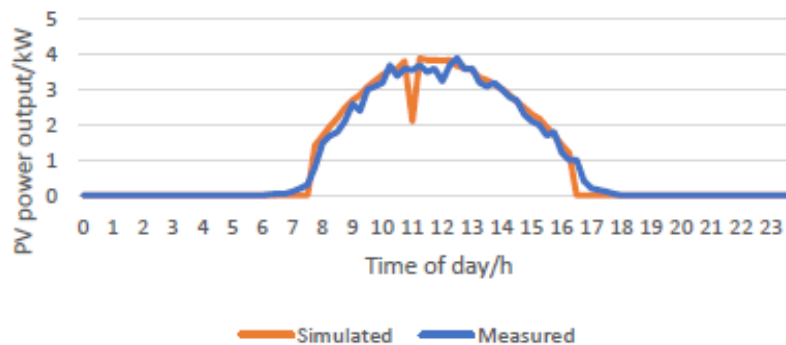


Figure 8 Simulated and measured power difference of PV system 1

## 6. CONCLUSION

The maximum absorption of distributed generation resources into the electricity distribution networks without compromising the power quality is an emerging research area nowadays. This study was conducted to evaluate the power quality impacts and operational behaviour of a selected distribution network empirically with inclusion of highly penetrated PV systems. For the task, modelling of a high PV penetrated low voltage distribution network was executed in the OpenDSS platform. A smart and accurate methodology was proposed for each consumer in a network to derive unique active and reactive power profiles. According to the results, single-phase PV inverters cause higher voltage imbalances. Neutral current also increases with the addition of PV which causes a risk of higher neutral conductor loss. The simulated power flow pattern at the BZ520 transformer node matches the field measurements in a similar pattern. The developed model was enhanced to quantify the power quality parameters such as individual harmonic content, the THD of voltage and current, and neutral current variation. The results reveal that node voltage has improved with PV interception without violating the upper limit. The THD<sub>v</sub> and THD<sub>i</sub> have increased with the addition of PV inverters without violating the upper limits.

## 7. REFERENCES

- Almeida, D., Pasupuleti, J., Ekanayake, J. and Karunarathne, E. (2020) "Mitigation of Overvoltage Due to High Penetration of Solar Photovoltaics using Smart Inverters Volt/Var Control", *Indonesian Journal of Electrical Engineering and Computer Science*, vol. 19, pp. 1259-1266, Apr., doi: 10.11591/ijeecs.v19.i3.pp1259-1266
- Almeida, D., Pasupuleti, J., Raveendran, S. K. and Basir Khan, R. (2021) "Performance Evaluation of Solar PV Inverter Controls for Overvoltage Mitigation in MV Distribution Networks", *Electronics*, vol. 10, no. 12, Jun., doi: 10.3390/electronics10121456
- Barreto, M., Guananga, A., Barragán, A., Zalamea, E. and Serrano, X. (2023) "Power Quality Analysis of Photovoltaic Systems", in 21<sup>st</sup> International Conference on Renewable Energies and Power Quality (ICREPQ), vol. 21, Spain, May, pp. 689-694, doi: 10.24084/repqj21.451
- Bircan, M., Durusu, A., Kakezoglu, B., Elma, O. and Selamogullari, U. S. (2020) "Experimental Determination of ZIP Coefficients for Residential Appliances and ZIP Model based Appliance Identification: The Case of YTU Smart Home", *Electric Power Systems Research*, vol. 179, p. 106070, Feb., doi: 10.1016/j.epsr.2019.106070
- Castro, L. M., Rodríguez-Rodríguez, and Martín-del Campo, C. (2020) "Modelling of PV Systems as Distributed Energy Resources for Steady-State Power Flow Studies", *International Journal of Electrical Power Energy Systems*, vol. 115, p. 105505, Feb. 2020, doi: 10.1016/j.ijepes.2019.105505
- Claeys, S., Geth, F. and Deconinck, G. (2022) "Optimal Power Flow in Four-Wire Distribution Networks: Formulation and Benchmarking", *Electric Power System Research*, vol. 213, Dec., doi: 10.1016/j.epsr.2022.108522
- Cuello-Polo, G. and O'Neill-Carrillo, E. (2021) "Power System Modelling for the Study of High Penetration of Distributed Photovoltaic Energy", *Designs*, vol. 5, no. 4, Sep. 2021, doi: 10.3390/designs5040062
- Daw, N. A. and Issa, A. A. (2021) "Sustainable Power Source for Off-Grid Domestic Load Modelling and Simulation using Matlab Software", in IEEE 1st International Maghreb Meeting of the Conference on Sciences and Techniques of Automatic Control and Computer Engineering (MI-STA). May, pp. 480-484, doi: 10.1109/MI-STA52233.2021.9464423
- Dinh, B. H., Nguyen, T. T., Nguyen, T. T. and Pham, T. D. (2021) "Optimal Location and Size of Photovoltaic Systems in High Voltage Transmission Power Networks", *Ain Shams Engineering Journal*, vol. 12, no. 3, pp 2839-2858, Sep., doi: 10.1016/j.asej.2020.12.015
- Dugan, R., Montenegro, D. and Ballanti, A. (2020) "Reference Guide – The Open Distribution System Simulator (OpenDSS)", Manual, pp. 1-232, Oct.
- ETAP (2023) "ETAP Products Solutions", Operation Technology, Inc., Belfast, UL (Date accessed: June 22, 2023) [Online] Available: <https://etap.com/product-list>
- Gimenes, T. K., da Silva, M. P. C., Ledesman, J. J. G. and Ando, O. H. (2022) "Impact of Distributed Energy Resources on Power Quality: Brazilian Scenario Analysis", *Electric Power Systems Research*, vol. 211, p. 108249, Oct., doi: 10.1016/j.epsr.2022.108249
- Gupta, S., Garg, S. Babbar, V., Saha, S. and Nagarwal N. (2018) "Modelling & Performance Investigation of PV Integrated IEEE 14 Bus Test System", in proc. international conference on Computing, Power and Communication Technologies (GUCON). Sep., pp. 275-279, doi: 10.1109/GUCON.2018.8674923

International Electrotechnical Commission (IEC) (2021) "IEC 61000-4-7:2002+AMD1:2008 CSV Consolidated Version", International Standard IEC 6100-4-15:2010, pp. 7-47, Oct. 2009 (Date accessed: June 17, 2023) [Online] Available: <https://webstore.iec.ch/publication/4228>

\_\_\_\_ (2021) "Electromagnetic Compatibility (EMC) – Part 4-30: Testing and Measurement Techniques – Power Quality Measurement Methods", International Standard IEC 61000-4-30:2015+AMD1:2021 CSV, pp. 7-292, Mar. (Date accessed: June 18, 2023) [Online] Available: <https://webstore.iec.ch/publication/68642#additionalinfo>

Institute of Electrical and Electronics Engineers (IEEE) (1998) "IEEE Recommended Practice for Industrial and Commercial Power Systems Analysis (Brown Book)", IEEE Std 399-1997, pp. 1-488, Aug., doi: 10.1109/IEEESTD.1998.88568

\_\_\_\_ (2018) "IEEE Recommended Practice for Conducting Harmonic Studies and Analysis of Industrial and Commercial Power Systems", IEEE Std 3002.8-2018, pp. 1-79, Oct., doi: 10.1109/IEEESTD.2018.8479357

\_\_\_\_ (2022) "IEEE Standard for Harmonic Control in Electric Power Systems", IEEE Std 519-2022 (Revision of IEEE Std 519-2014), pp. 1-31, Aug., doi: 10.1109/IEEESTD.2022.9848440

\_\_\_\_ (1998) "IEEE Standard for Interconnection and Interoperability of Distributed Energy Resources with Associated Electric Power Systems Interfaces", IEEE Std 1547-2018 (Revision of IEEE Std 1547-2003), pp. 1-138, Apr., doi: 10.1109/IEEESTD.2018.8332112

Krishna, P. V. N. M. and Sekhar, P. C. (2022) "Simplified Linear Load Flow Analysis for Transmission Networks", in proc. IEEE 16<sup>th</sup> International Conference on Compatibility, Power Electronics, and Power Engineering (CPE-POWERENG), Jun., pp. 1-5, doi: 10.1109/CPE-POWERENG54966.2022.9880889

Liu, S., Zhang, H., Zhang, P., Li, Z. and Wang, Z. (2022) "Equivalent Model of Photovoltaic Power Station Considering Different Generator Units' Fault Current Contributions", *Energies*, vol. 15, no. 1, Dec., doi: 10.3390/en15010229

Mawuena, M., Chetangny, P., Aredjodoun, J., Chamagne, D., Barbier, G., Houdedako, S. and Vianou, A. (2022) "Load Flow Study of Togo and Benin Transmission Power Network by the Newton-Raphson Method", *Advanced Engineering Forum*, vol. 44, pp. 49-71, Feb., doi: 10.4028/www.scientific.net/AEF.44.49

Pillai, D. S. and Rajasekar, N. (2018) "A Comprehensive Review on Protection Challenges and Fault Diagnosis in PV Systems", *Renewable and Sustainable Energy Reviews*, vol. 91, pp 18-40, Aug., doi: 10.1016/j.rser.2018.03.082

Public Utilities Commission of Sri Lanka (PUC-LK) (2012) "Distribution Code of Sri Lanka", Reports – Ceylon Electricity Board (CEB), pp. 3-74, Jul. (Date accessed: July 07, 2023) [Online] Available: [https://www.ceb.lk/front\\_img/img\\_reports/1532500020Distribution\\_Code.pdf](https://www.ceb.lk/front_img/img_reports/1532500020Distribution_Code.pdf)

PSI Neplan AG "NEPLAN | Downloads", Neplan AG 8700 Küsnacht, Zürich, Switzerland (Date accessed: June 20, 2023) [Online] Available: <https://www.neplan.ch/en-company>

Raavi, S., Vaisakh, K., Abdelaziz, A. and El-Shahat, A. (2021) "A Novel Three-Phase Power Flow Algorithm for the Evaluation of the Impact of Renewable Energy Sources and D-STATCOM Device on Unbalanced Radial Distribution Networks", *Energies*, vol. 12, Sep., doi: 10.3390/en14196152

Salimon, S. A., Adepoju G. A., Adebayo, I. G., Howlader, H. O. R., Ayanlade, S. O. and Adewuyi, O. B. (2023) "Impact of Distributed Generators Penetration Level on the Power Loss and Voltage Profile of Radial Distribution Networks", *Energies*, vol. 16, no. 4, p. 1943, Feb., doi: 10.3390/en16041943

Sonel S. A. (2023) "User Manuals", 2016-2023 Sonel S. A., Świdnica, Poland (Date accessed: June 21, 2023) [Online] Available" <https://www.sonel.pl/en/downloads/user-manuals/>

Sharma, V., Aziz, S., Heque, H. and Kauschke, T. (2020) "Effects of High Solar Photovoltaic Penetration on Distribution Feeders and the Economic Impact", *Renewable and Sustainable Energy Reviews*, vol. 131, p. 110021, Oct., doi: 10.1016/j.rser.2020.110021

Shen, Z., Wei, Z., Sun, G. and Chen, S. (2019) "Representing ZIP Loads in Convex Relaxations of Optimal Power Flow Problems", *International Journal of Electrical Power & Energy Systems*, vol. 110, pp. 372-385, Sep., doi: 10.1016/j.ijepes.2019.03.011

Talha, M., Raihan, S. R. S. and Rahim, N. A. (2021) "A Gried-Tied PV Inverter with Sag-Severity-Independent Low-Voltage Ride Through, Reactive Power Support, and Islanding Protection", *Journal of Modern Power Systems and Clean Energy*, vol. 9, no. 6, pp. 1300-1311, Nov., doi: 10.35833/MPCE.2021.000319

---

# #244: Exploring Sustainable Residential Building Solutions Through Green Engineering: A Saudi Arabian Case Study

---

Abdullah ALSHABANAT<sup>1</sup>, Siddig OMER<sup>2</sup>

<sup>1</sup>Department of Architecture and Built Environment, Faculty of Engineering, University of Nottingham, NG7 2RD  
University Park, Nottingham, UNITED KINGDOM

<sup>2</sup>Department of Architecture and Built Environment, Faculty of Engineering, University of Nottingham, NG7 2RD  
University Park, Nottingham, UNITED KINGDOM

*Abstract: The word “green” has become associated with sustainable products and environmental awareness, while the ‘green engineering’ term is used to describe building design that seeks to minimise pollution and promote human health, as well as promoting sustainability and nurturing the environment. Efficient green buildings can potentially boost economic growth, enhance social development, and promote the sustainability of the environment. Hence, buildings featuring minimal greenhouse gas (GHG) emissions and energy use while delivering thermal comfort are among the contemporary challenges of building design. The building industry plays a crucial role in Saudi Arabia due to its intricate national economy, as its growth is closely tied to the progress of various other economic sectors. Additionally, Saudi residential buildings consume almost half of the total national electricity consumption, so it will play a pivotal role in addressing energy and sustainability issues. Thus, ensuring the exploitation of the advantages of green engineering solutions to improve the energy consumption and thermal comfort performance of such residential buildings without impacting their architectural values should be a national goal. Therefore, in this study, the author aims to illustrate the integration of energy-efficiency strategies, renewable energy technologies (low-carbon technology), and passive traditional architectural design into the framework of sustainability principles. As a result, highly sustainable building methods are facilitated by designing in accordance with the three essential pillars of sustainability: social, economic, and environmental. This is achieved by combining the best features of traditional passive architectural design with low-carbon technologies, all while incorporating the latest energy-efficient measures.*

*Keywords: Green Buildings; Sustainability; Energy Consumption; Saudi Arabia.*



# 1. INTRODUCTION

The International Energy Agency (IEA, 2022) indicates that almost 15% of direct CO2 emissions and 30% of global energy consumption can be attributed to buildings and the construction sector combined. As developing countries engage in a greater number of construction projects and the floor area of global buildings grows, they make a greater contribution to these figures. Energy use in these countries is also affected by improved access to energy, increased ownership of energy-consuming appliances, and the growing demand for air conditioning in countries with hot climates. Lahn et al. (2011) explain that developing countries in hot climate regions including Saudi Arabia have also witnessed rapid population growth, which has led to greater resource consumption as a result of the increased demand for new buildings. Even though the Saudi Energy Efficiency Center (SEEC) seeks to rationalise energy production and consumption. The buildings and transport sectors account for 90% of domestic energy consumption in the country; almost a third of which is consumed by the building sector; as a proportion, this represents approximately 75% of Saudi Arabia’s electricity production. As shown in Figure 1, the Saudi residential sector consumes almost half of the total national electricity consumption, so it plays a pivotal role in addressing energy issues. Figure 2 illustrates that the desert climate prevalent in Saudi Arabia means that it has hot, dry summers, with temperatures reaching up to 38°C in coastal regions and 45°C in inland areas, sometimes reaching as high as 54°C. It is therefore essential that Saudi Arabia considers energy efficiency measures and adheres to sustainability principles due to the considerable amount of energy needed for cooling buildings.

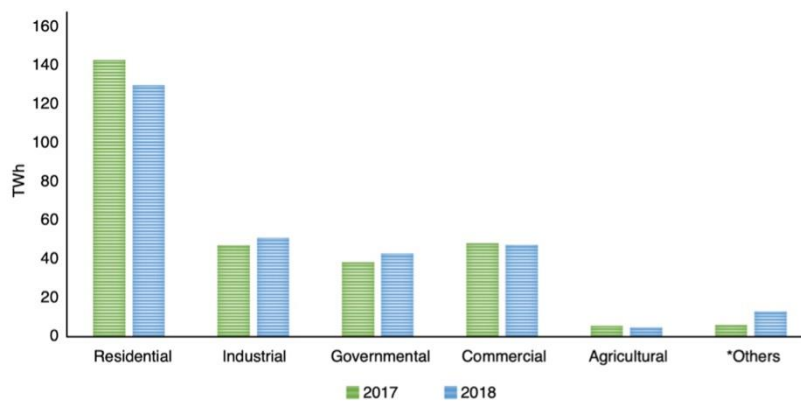


Figure 1 Electricity consumption by sector (2017-2018). (Source: Saudi Energy Efficiency Center (SEEC) 2020)

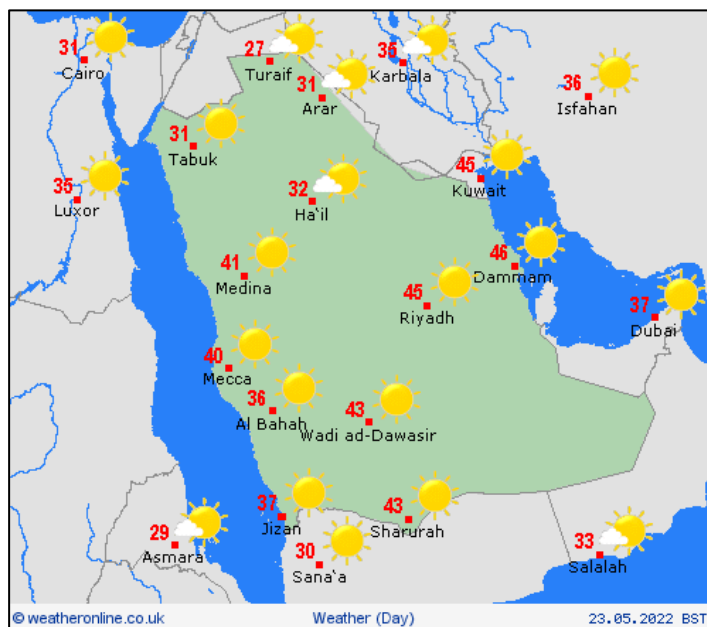


Figure 2 Saudi Arabia climate (23.05.2022), (Source: WeatherOnline Ltd)

The International Energy Agency (IEA, 2022) speculates that energy efficiency improvements in buildings could reduce global energy demand by about a third by 2050, which would have a significant impact on reducing global GHG emissions. However, such changes require the building sector to adopt then implement relevant energy consumption principles; for example, if the stated project goal is to implement sustainable design and preserve the environment around a development, then the most effective strategic solution would involve reducing the usage of non-renewable resources and increasing the use of renewable resources.

However, Saudi Arabia's Vision 2030 has set out several goals for the country to achieve by the stated date. The government's vision is particularly focused on environmental considerations and implementing more sustainable methods of buildings, industrialisation, and service delivery. As part of this vision to progress towards more sustainable development, the government not only intends to improve standards in the building industry in Saudi Arabia but also aims to make it more efficient and cost-effective. The improvements involve new regulations and codes of new building projects however the existing approach in Saudi Arabia tends to have scant regard for architectural design parameters and renewable energy usage and instead focuses on the building's thermal transmittance values for the opaque and transparent elements, aiming to meet the minimum requirements of the building envelope. However, according to Chwieduk (2003); and Alrashed, Asif (2014), the three core principles of sustainable energy buildings are sustainable design solutions, renewable energy technologies and energy-efficiency measures. As a result of the demand for more sustainable and energy-efficient architecture that meets community needs, interest in 'comprehensive design' is growing, while designers involved in the built environment including architects and engineers are pivotal to the achievement of the government's goals.

The United States Environmental Protection Agency (2022), stated that green engineering solutions involve the creation and implementation of approaches and practices aimed at decreasing pollution, fostering sustainability, and mitigating potential harm to both human well-being and the natural world, all while maintaining economic feasibility and effectiveness. In line with this, Figure 3 illustrates the current research project area, which will focus on these three fundamental dimensions. Therefore, in this study, the author aims to illustrate the integration of energy-efficiency strategies, renewable energy technologies (low-carbon technology), and passive traditional architectural design into the framework of sustainability principles.

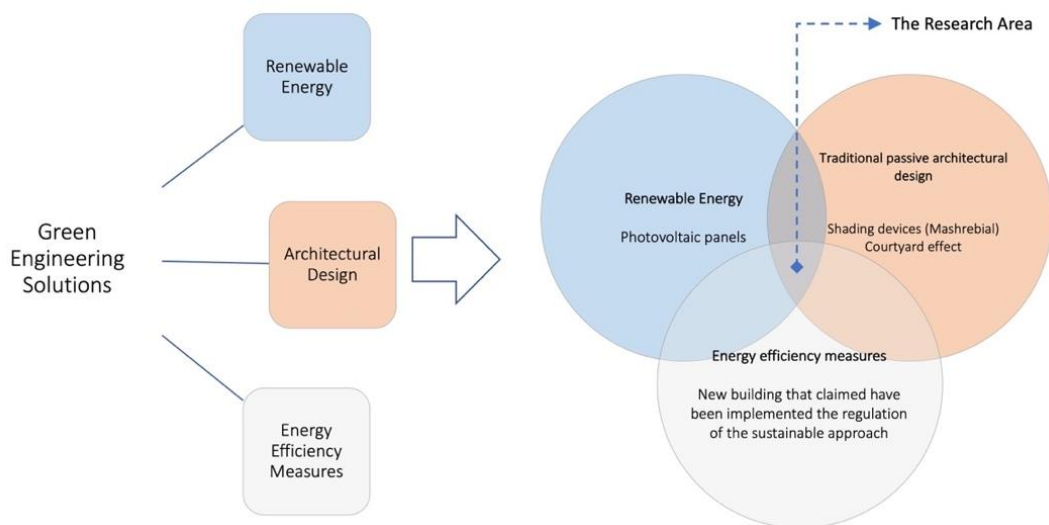


Figure 3 The research area.

## 2. BUILDING ENERGY CONSUMPTION IN SAUDI ARABIA

As the Saudi Electricity Company (2022) observed, the rise in the adoption of high-energy appliances, urbanisation, rapid population growth, subsidised tariff, and other such aspects, in Saudi Arabia, have contributed to the substantial elevations in energy consumption which principally rely upon fossil fuels. By 2025, a twofold increase in electricity demand is forecasted as a result of the aforementioned factors (Obaid, Mufti 2009). As illustrated in Figure 4, data collected by the King Abdulla Petroleum Studies and Research Centre (KAPSARC) between 2005 and 2020 on electricity consumption reflects the findings above. Significant quantities of electricity are consumed by air-conditioning units, and many contemporary buildings in Saudi Arabia intensively rely upon such cooling units, thereby ignoring fundamental sustainable design principles (Jamil et al. 2018). Consequently, refrigeration and air-cooling functions comprise almost 70% of household electricity due to the inadequately designed buildings in GCC nations like Saudi Arabia.

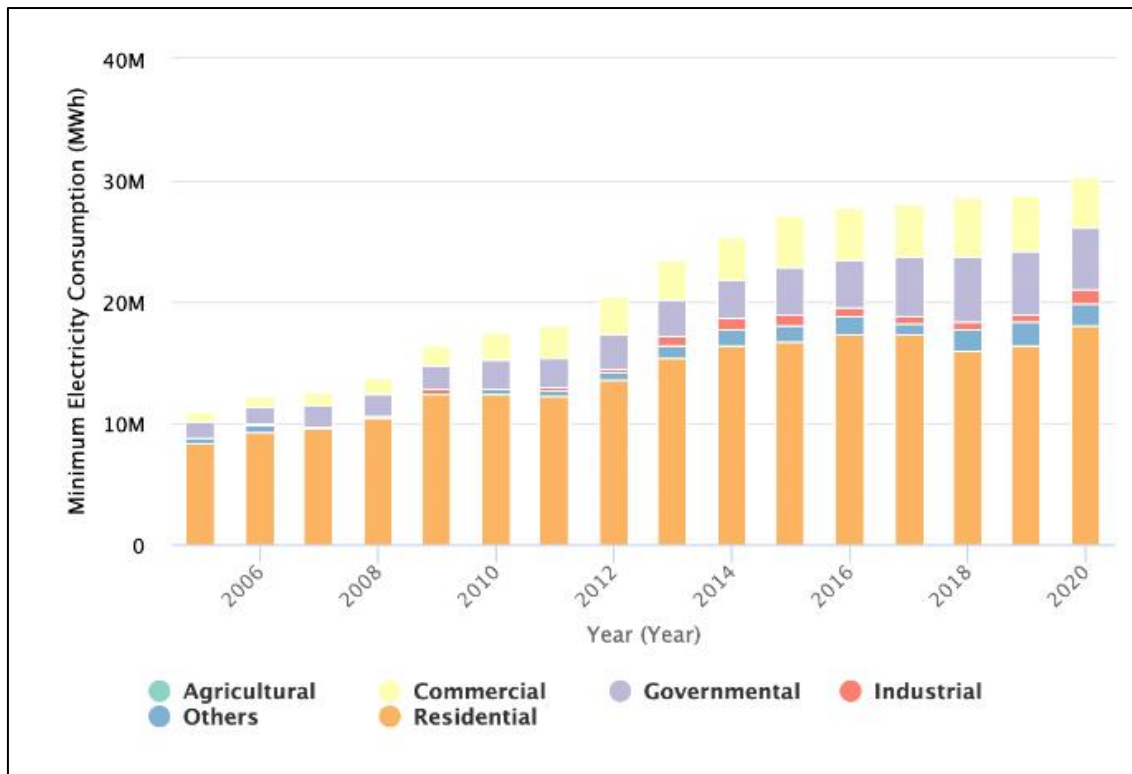


Figure 4 Electricity consumption by sector for Saudi Arabia from 2005-2020. (Source: KAPSARC)

The energy consumption of 191 houses in Saudi Arabia was statistically analysed to determine the most significant energy consumption markers in academic work (Esmaeil et al. 2019). Electrical energy consumption per unit area per inhabitant, and per house were among these markers. In addition, analysis was carried out on water heating, appliances, lighting and other such distinct high-energy domestic tools to ascertain their efficacy. Nonetheless, advanced optimisation, simulation, and geometry generation were not undertaken. Moreover, given that comparisons with published data and individual questionnaire responses serve as the basis for energy consumption reduction values and energy consumption results respectively, such results may not be entirely trustworthy. These findings held that 92.6 kWh/m<sup>2</sup>, 4704 kWh/capita, and 30,031 kWh/dwelling comprised the mean annual consumption energy performance parameters. Air conditioning, water heaters, lighting, and household appliances drew values of 66.5%, 10.3%, 8.5%, and 14.7% respectively which signify the end-use and kind of each domestic energy consumption source. A 43% decrease in the air-conditioning demand can be enabled by envelope insulation as the subsidised Saudi electricity tariff of 0.048\$/kWh and the worldwide power cost of 0.15\$/kWh produce an anticipated average simple payback time of 6.8 years and 2.2 years, respectively. Similarly, a 3% decrease in overall household energy consumption can occur via the adoption of efficacious lighting systems. Furthermore, a rapid payback period between 0.45 and 3.2 years is demonstrated in this area. As Al-Tamimi (2017) notes, Saudi buildings waste a substantial quantity of energy, as per his examination of the energy-saving techniques adopted in the Saudi building sector and the concurrent difficulties and prospects therein. Hence, renewable energy sources, such as wind and solar energy, energy-efficient conservation and design, green technology, and other such energy-efficient practices should be implemented by the national government. Taleb, and Sharples (2011) highlight the link between the significant levels of energy consumption in the country and the hot climate it experiences, provoking high usage of air-cooling systems. Solutions to diminishing energy consumption in buildings must factor in the distinct policies, economy, climate conditions, culture, and raw materials availability in distinct locations in order to maintain high levels of efficacy.

### 3. THE EFFECT OF CLIMATE ON SAUDI BUILDINGS

#### *Energy-Efficient Measures*

CO<sub>2</sub> emissions and energy consumption are significantly impacted by the extreme temperatures experienced in Saudi Arabia during the summer, with temperatures frequently superseding 40 °C, thereby highlighting the vital role of design in the construction process. Alshaikh et al. (2016) note that the status of being an air conditioning-reliant society is widely associated with Saudi Arabia. The adoption of energy retrofit strategies is hindered by various barriers such as the high costs and complexity involved and altering housing units to comply with the minimum energy efficacy guidelines. In addition, the benefits of climatic elements are ignored by novel building codes in the country that attempt to minimise energy consumption and enhance the sustainability and efficacy of buildings via only building envelopes. However, diminishing energy consumption can be enabled to a great extent via the adoption of energy-efficient measures.

### Low-Carbon Technology (Renewable Energy)

Even though, the harnessing of renewable energy sources is an appealing proposition in Saudi Arabia as multiple unique climatic and geographic locations exist. This is exemplified, as Yousef Etier et al. (2010) mentioned, that the country possesses one of the highest solar irradiation levels internationally, reaching annual values of 2080 kWh/m<sup>2</sup>, and Sheikh et al. (2021) highlight that the most widespread source of clean energy is the sun for the production of electricity. This Saudi climate benefit within the context of low-carbon technology has not been taken into account by residential building projects despite the establishment of multiple renewable energy plants by the Ministry of Energy to produce power for the industrial sector, as per Vision 2030. Hence, energy in residential buildings can be provided by the core green solution of solar energy in the country.

### Traditional Passive Architectural Design

On the other hand, the traditional architectural features of buildings in Saudi Arabia are characterised by the low number and small size of external openings, which usually start on the first floor to reduce the effect of the arid and hot climate on the house's internal spaces (Talib, 1984). Additionally, living spaces populate the periphery of several courtyards in other houses. Abdullah, Saleh (1998) and Al-Sayed (2011) note that the buildings are kept cool during the day from the cold air at night being maintained and the daytime shade that these courtyards provision, which also influences the interior temperature and offers natural ventilation and light. Furthermore, Mashrabiya exemplifies the shading devices still used in Arab countries that are found in conventional architecture and serve to diminish the influence of the dry and hot climate (Fathy, 1996). He adds safeguarding privacy, regulating the passage of light, heightening the humidity of the air current, and regulating the airflow are among the areas these devices enable. However, widespread adoption of such devices in buildings regulating climatic conditions did not occur in the country.

It is a reality that the climate is not considered enough in the contemporary design process of buildings in developing nations (La Roche, 2017). The manner in which the form and programme of a building interact with the external environment provokes the quantity of energy a building consumes. Minimal emissions and interior comfort in a building can be fulfilled by utilising the available energy and developing the capacity to manage exterior conditions. Hence, air movement, humidity, temperature, solar radiation, and the manner in which energy consumption is impacted by these features comprise the most significant climate variables in the design of buildings, given that they influence thermal comfort. The bioclimatic variables should determine the design process of a building in order to ensure suitability. Additionally, such suitability to the climate can be fomented by incorporating passive design methods which necessitate local climate knowledge, renewable energy technologies (low-carbon technology), and energy-efficiency strategies.

## 4. CURRENT SAUDI BUILDING CODES AND REGULATIONS.

The Saudi Building Code (SBC) is a collection of legal, administrative, and technical rules and specifications that outline the minimum building construction standards. Alayed et al. (2021) claim that the majority of the existing building envelopes in Saudi Arabia are made from reinforced concrete frames containing insulated concrete blockwork and they fail to meet the U-value specifications outlined in the most recent national building regulations. Nonetheless, new regulations implemented at the start of July 2021 mandate that new residential buildings must adhere to the new Saudi building code.

The Saudi Building Code Energy's Saudi Energy Conservation section (SBC-602) outlines the minimum performance standards for constructing energy-efficient buildings in KSA as shown in Table (1) below. These standards focus specifically on designing energy-efficient building envelopes. The requirements are established for three different climate zones as shown in Figure 5 below.

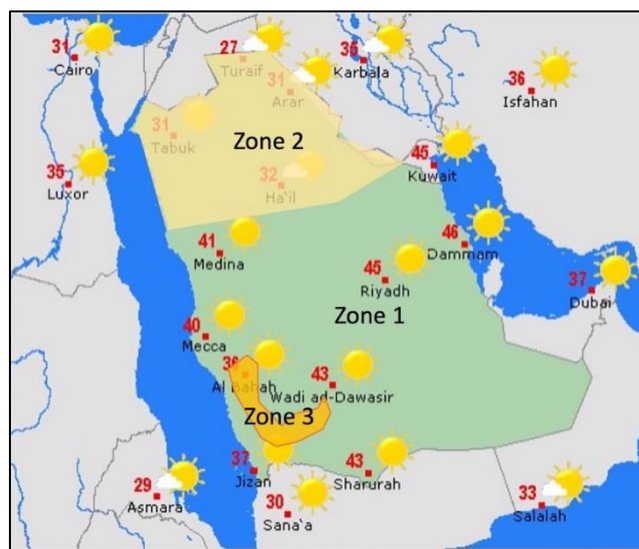


Figure 5 Climate zone map of the Saudi Building Code.

Furthermore, the Saudi Government established the Mostadam comprehensive sustainability rating and certification system to improve the long-term sustainability of residential buildings throughout Saudi Arabia (KSA). Mostadam is designed to achieve the goals of Vision 2030 and covers various sustainability issues relevant specifically to Saudi Arabia. Additionally, the ensure even greater sustainability for residential buildings, Mostadam is developed in alignment with the SBC and goes above and beyond the minimum SBC requirements. For example, Alardhi et al. (2020) point out that adhering to the SBC-602 requirement for buildings in Riyadh (located in zone 1 of SBC-602) can save as much as 17% of total electrical energy consumption for an entire building when the air conditioner is set at 25 C instead of 18 C. Moreover, Almasri et al. (2021) strongly advised that the SBC-602 code be fully applied when constructing new buildings in zones 1 and 2. Thus, one of the most effective and efficient methods of reducing total electrical energy consumption in Saudi buildings is adhering to the energy conservation requirements of the Saudi Building Code. However, integrating a number of passive architectural designs and renewable energy strategies for minimising energy consumption with these energy conservation measures would also be highly beneficial.

Table 1: Energy conservation requirements for Saudi residential buildings.

Item	REQUIREMENTS
Wall Overall heat transfer coefficient (U)	Wall: 0.454/0.511/0.591 for zones 1, 2,3
Roof U value	Roof: 0.272/0.340/0.397 for zones 1 ,2 ,3
Door U value	2.839 for all zones
Window Overall U value	2.668 for all zones
Window type	Aluminium frame with thermal breaks or PVC
Glass type	Double glazed with 12mm air space
External Colour	Light
solar heat gain coefficient (SHGC)	For all zones $\leq 0.25$
surface reflectance index (SRI)	Light colour with $SRI \geq 50$
Water absorption for insulation materials	$\leq 0.3\%$
Continuous insulation	Continuous across all building envelope
Ventilation	54.5L/s
Infiltration in fenestration	$\leq 1.5L/s/m^2$
Infiltration in floors	$\leq 2.5L/s/m^2$
Lighting power density	10W/m <sup>2</sup> ground floor, 6 W/m <sup>2</sup> first floor
Equipment power density	2.0kW ground floor, 1.0kW first floor
Vertical fenestration area	$\leq 25\%$ of the wall area
minimum energy efficiency ratio,	$\geq 11$

(SORCE: Saudi Energy Efficiency Centre, SBC 602).

## 5. EVALUATION OF PROPOSED GREEN ENGINEERING SOLUTIONS

The findings from the critical appraisal in relation to the literature review have led to the development of the initial concept of the research project, which is shown in Figure 6. The evaluation of energy consumption and thermal sense in terms of the indoor air temperature and should take place then applied energy efficiency measures with full consideration of the climate analysis using a climate consultant software as shown in Figure 7.

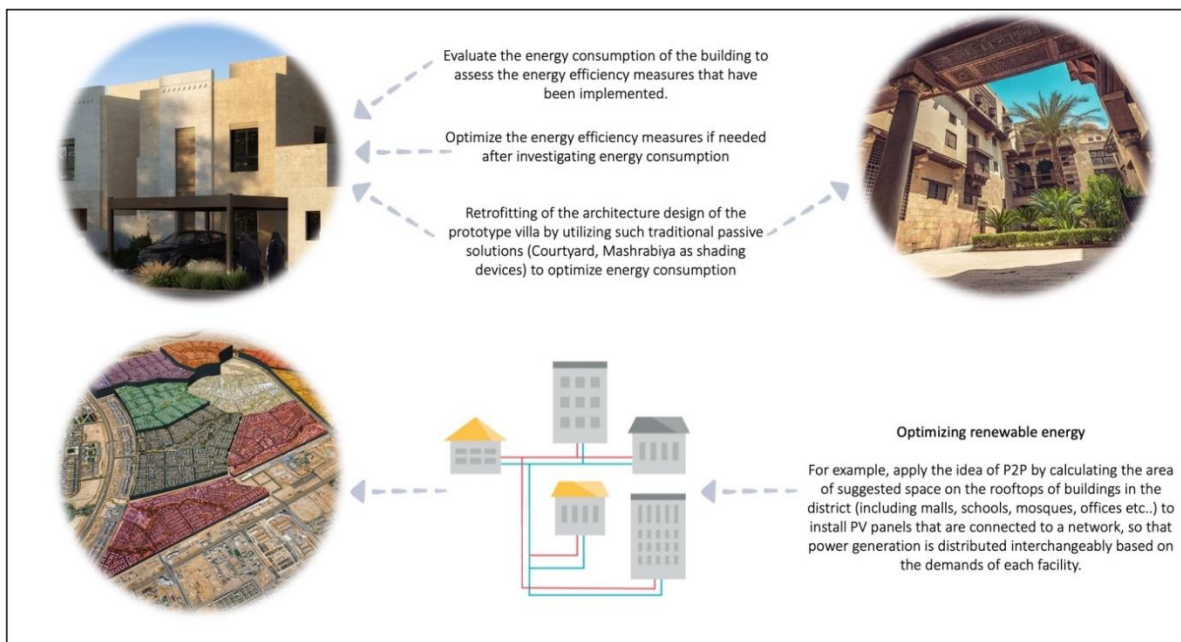


Figure 6 The proposed concept of the research project



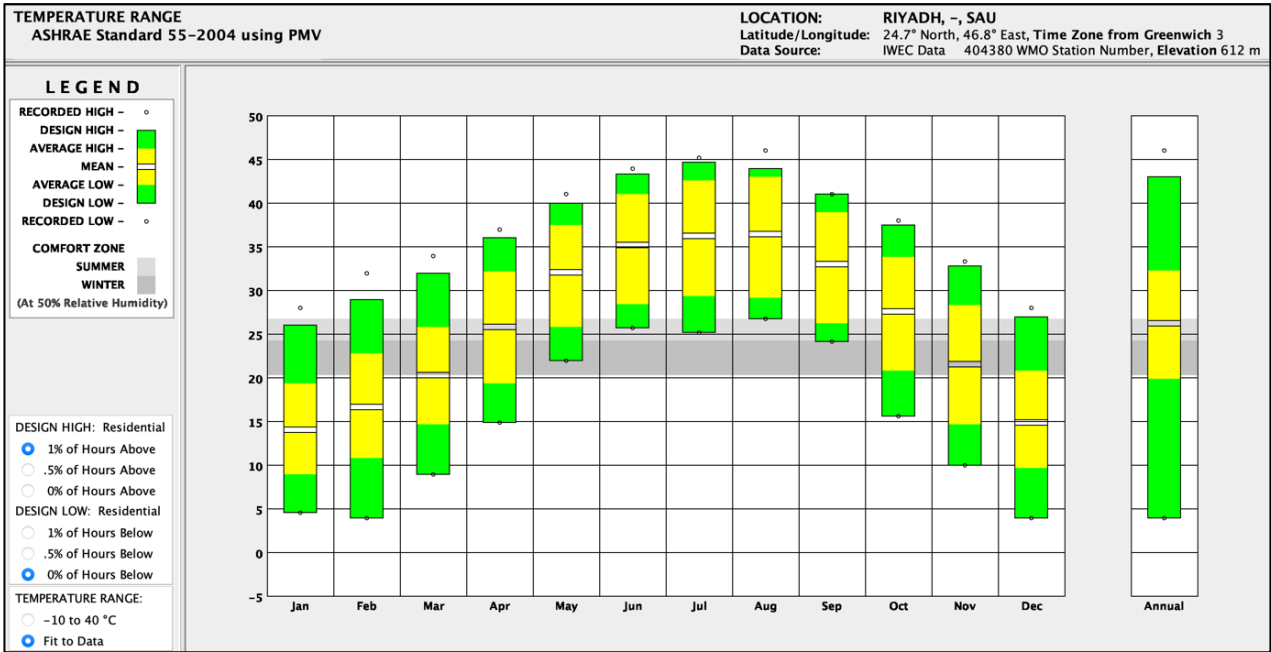


Figure 7 The climate analysis of the comfort zone

In addition, in the local context of applying knowledge from traditional passive architectural design solutions and bioclimatic design principles. However, in order to optimise the advantages of these components in this research project, their design should involve various creative parameters. For example, sunshade control above the courtyard could be exploited in order to minimise the direct sunlight of Saudi Arabia to cool the air prior to its introduction into the enclosed spaces of the building. The psychrometric chart in Figure 8 below depicts the design strategies for buildings in Riyadh city in Saudi Arabia by utilising a climate consultant's software, as well as the number of hours for cooling and heating that are within its climate condition.

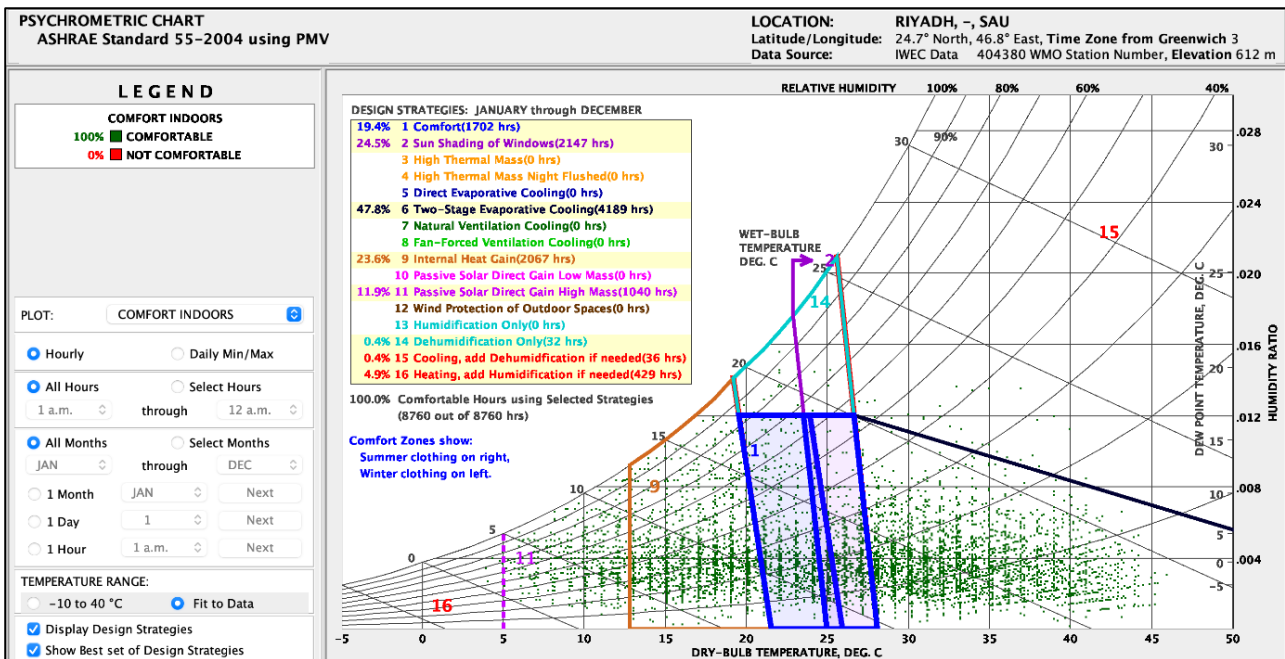


Figure 8 The psychrometric chart of Riyadh's buildings

Furthermore, the key benefit of solar energy is that it is a clean, renewable source of electricity. Additionally, solar energy can be scaled up, meaning that it could be used to power a single building or be implemented on a district scale. Extra electricity can then be fed back into the grid or stored in a battery when used on a smaller scale. Hence, Peer-to-Peer (P2P) renewable energy sharing among the buildings is a well proposed solution to generate power for each building from solar photovoltaics (PV), taking into consideration the radiation range as Figure 9 shows.

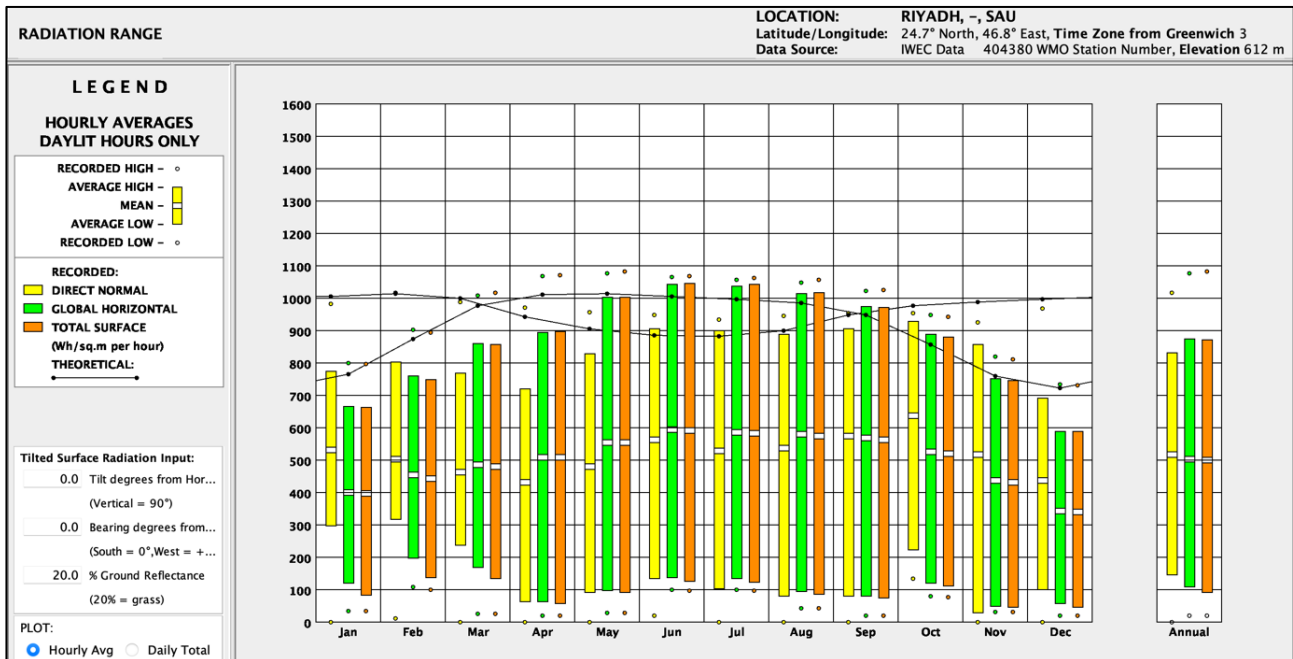


Figure 9 The radiation range of Riyadh City

## 6. FINDINGS AND CONCLUSION

As a result of the work carried out in relation to the literature review and how that connects with the study aim. It is evident that the three fundamental elements of the sustainable approach, with respect to the sphere of residential buildings within the Kingdom of Saudi Arabia (KSA), should be taken into account when designing a building, while climate effects and energy consumption serve as the focal aspects. Furthermore, the field of passive conventional architectural design, together with an elementary understanding of the behaviour and thermal comfort of a building, provides an opportunity for notable characteristics that could contribute to making the designs work successfully in relation to a building that offers appropriate thermal comfort with the least possible energy usage and greenhouse gas (GHG) emissions. Moreover, diminishing energy consumption can be enabled to a great extent via the adoption of energy-efficient measures, which should take into consideration efficient building regulation codes and the newest innovations in the field of green engineering solutions. In addition, solar energy should be considered a renewable source of energy with the greatest potential for use in KSA, as the sun generates more energy than consumers are likely to need. The promise of solar energy is simply restricted by the technical ability to transform it into electrical energy. Therefore, highly sustainable building methods are facilitated by designing in accordance with the three essential pillars of sustainability: social, economic, and environmental. This is achieved by combining the best features of traditional passive architectural design with low-carbon technologies, all while incorporating the latest energy-efficient measures. Figure 10 below illustrates a guideline extracted from the current study, including all the aforementioned aspects, which represent solutions from the field of green engineering.

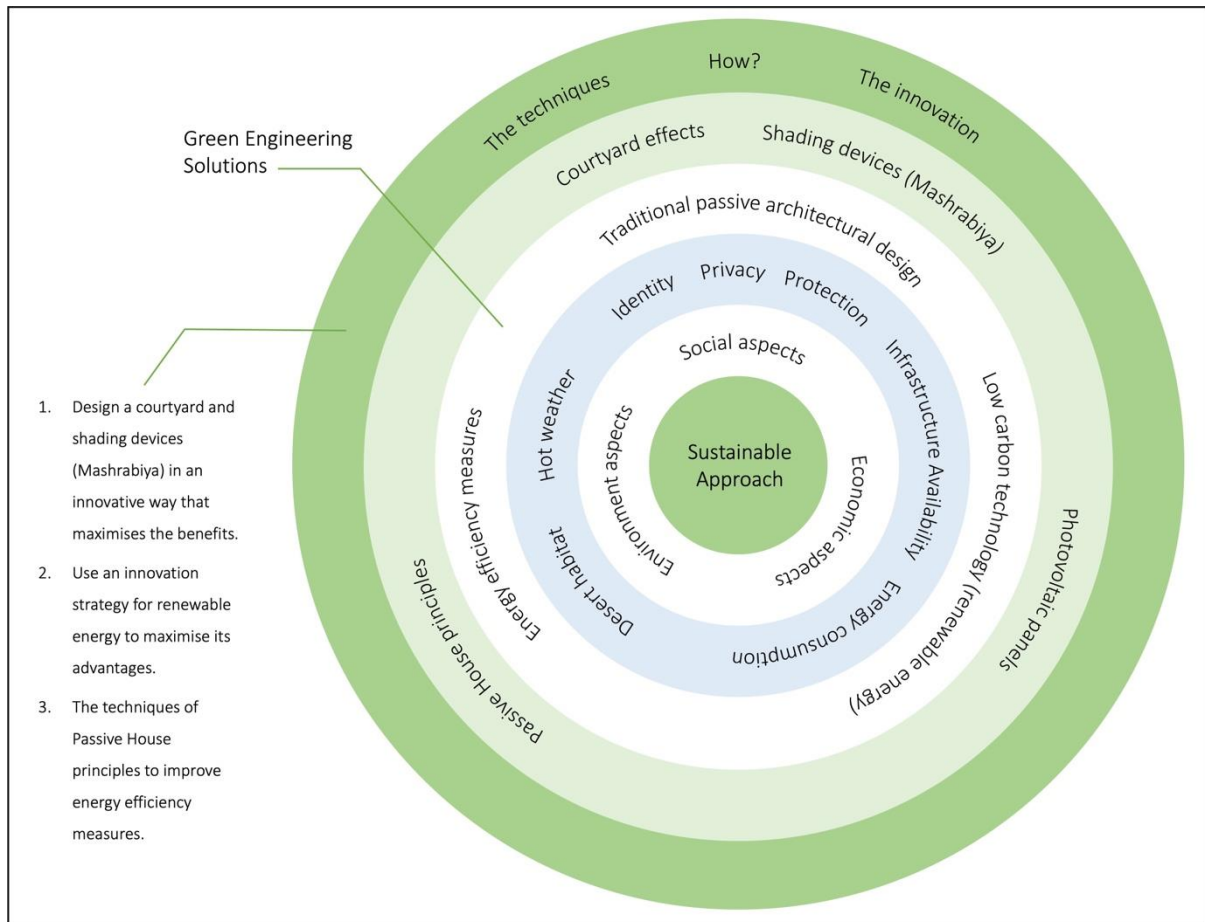


Figure 10 The current research project guidelines.

## 7. REFERENCES

- Abdullah, M., Saleh, E., 1998. Actual and Perceived Crime in Residential Environments: A Debatable Discourse in Saudi Arabia.
- Alayed, E., O'hegarty, R., Kinnane, O., 2021. Thermal envelope analysis for new code compliance of Saudi Arabian dwellings. *Energy and Buildings*, 243. 10.1016/j.enbuild.2021.110997.
- Almasri, R.A., Alardhi, A.A., Dilshad, S., 2021. Investigating the impact of the integration of the Saudi code of energy conservation with solar PV systems in residential buildings. *Sustainability (Switzerland)*, 13(6). 10.3390/su13063384.
- Alrashed, F., Asif, M., 2014. Saudi building industry's views on sustainability in buildings: Questionnaire survey. In: *Energy Procedia*. Elsevier Ltd, pp. 382–390. 10.1016/j.egypro.2014.12.400.
- Al-Sayed, W. (2011) 'Courtyard Phenomenon In Arab's Traditional Architecture'. Retrieved 9 April 2011, Available At: <http://lonaard.com/ar/articlearch-1.html> [Accessed 22 June 2022].
- Alshaikh, A.M., Alshaikh, A., Roaf, S., 2016. *Designing Comfortable, Low Carbon, Homes in Dammam, Saudi Arabia: The Roles of Buildings and Behaviours* [online]. Available at: <https://www.researchgate.net/publication/328306951>.
- Al-Tamimi, N., 2017. A state-of-the-art review of the sustainability and energy efficiency of buildings in Saudi Arabia. *Energy Efficiency*, 10(5), pp.1129–1141. 10.1007/s12053-017-9507-6.
- Chwieduk, D., 2003. Towards sustainable-energy buildings. *Applied Energy*, 76(1–3), pp.211–217. 10.1016/S0306-2619(03)00059-X.
- Esmail, K.K., Alshitawi, M.S., Almasri, R.A., 2019. Analysis of energy consumption pattern in Saudi Arabia's residential buildings with specific reference to Qassim region. *Energy Efficiency*, 12(8), pp.2123–2145. 10.1007/s12053-019-09806-x.



- Fathy, H., *Natural Energy and Vernacular Architecture: Principles And Examples With Reference To Hot Arid Climates*. 1986, Chicago: University of Chicago Press. Available At: <https://unu.edu/publications/books/natural-energy-and-vernacular-architecture-principles-and-examples-with-reference-to-hot-arid-climates.html> [Accessed 22 June 2022].
- King Abdulla Petroleum Studies and Research Center (KAPSARC), Saudi Arabia Energy Report –. <https://www.kapsarc.org/research/publications/saudi-arabia-energy-report/> [Accessed: 2022-08-04].
- IEA. 2022. Buildings – Topics - IEA. [Online] Available At: <https://www.iea.org/topics/buildings> [Accessed 14 May 2022].
- Jamil, R. et al., 2018. *Analysis of Challenges in Sustainable Construction Industry by Using Analytic Hierarchy Process: A Case Study of Jubail Industrial City, Saudi Arabia Green Building & Sustainable Technologies in Saudi Arabia View project Analysis of challenges in sustainable construction industry by using analytic hierarchy process: a case study of Jubail Industrial City, Saudi Arabia* [online]. Available at: <https://www.researchgate.net/publication/316597377>.
- Obaid, R.R., Mufti, A.H., 2009. Present State, Challenges, and Future of Power Generation in Saudi Arabia. In: Institute of Electrical and Electronics Engineers (IEEE), pp. 1–6. 10.1109/energy.2008.4781073.
- Sheikh, Y.A. et al., 2021. Impact of rooftop photovoltaic on energy demand of a building in a hot semi-arid climate. *Journal of Renewable and Sustainable Energy*, 13(6). 10.1063/5.0063044.
- Saudi Energy Efficiency Center (SEEC). Annual Report. Available At: <https://www.seec.gov.sa/> (Accessed: 4 August 2022).
- Saudi Electricity Company, 2022. [Online] Available At: <https://www.se.com.sa/en-us/pages/home.aspx> [Accessed 4 August 2022].
- Sheikh, Y.A. Et Al., 2021. Impact Of Rooftop Photovoltaic on Energy Demand of A Building In A Hot Semi-Arid Climate. *Journal Of Renewable and Sustainable Energy*, 13(6). 10.1063/5.0063044.
- Talib, K. (1984). *Shelter In Saudi Arabia*. New York: St. Martin's Press. Available At: <https://archive.org/details/shelterinsaudiar00tali/page/142/mode/2up> [Accessed 22 June 2022].
- Taleb, H.M., Sharples, S., 2011. Developing sustainable residential buildings in Saudi Arabia: A case study. *Applied Energy*, 88(1), pp.383–391. 10.1016/j.apenergy.2010.07.029.
- Lahn, Glada., Stevens, P., Royal Institute of International Affairs., 2011. *Burning Oil to Keep Cool: The Hidden Energy Crisis In Saudi Arabia*. Chatham House.
- La Roche, P., 2017. *Carbon-Neutral Architectural Design*. 2nd Ed. Boca Raton, Florida: Taylor & Francis Group.
- Yousef Etier, I. et al., 2010. *Analysis of Solar Radiation in Jordan Robust Control for a Chaotic System: Implementation and Testing View project Cooling Photovoltaic View Project Analysis of Solar Radiation in Jordan* [online]. Available at: <https://www.researchgate.net/publication/264887903>.
- VISION2030.GOV.SA. (2022). Saudi Vision 2030. [Online] Available At: <http://vision2030.gov.sa/en> [Accessed 28 May 2022].
- US EPA. 2022. U.S. Environmental Protection Agency | US EPA. [Online] Available At: <https://www.epa.gov/> [Accessed 31 May 2022].

---

## #245: A renewable multigeneration energy system for a public school in Denmark

---

August MAAHN SKYGGEJERG THOMSEN<sup>1</sup>, Alaa JALAL EL-AHMAD<sup>1</sup>, Ali IBRAHIM AL-BADRI<sup>1</sup>,  
Muhyiddine JRADI<sup>1,\*</sup>

<sup>1</sup> Center for Energy Informatics, University of Southern Denmark, Odense, Denmark, [mjr@mmmi.sdu.dk](mailto:mjr@mmmi.sdu.dk)

*Abstract: Distributed energy resources are becoming increasingly popular in times of energy volatility caused by large price fluctuations in the energy markets. It is therefore pro-actively interesting and advantageous for energy-heavy consumers if they establish renewable multigeneration systems to partly cover their own energy demand. Multigeneration systems create both low-emission energy and have the potential to yield positive impacts in terms of the total energy price and the economic feasibility of the energy generation solutions for the consumer. By implementing linear programming, a well-documented optimization method, this paper sets out to construct an open-source framework that can be used to evaluate different distributed renewable energy resource combinations for different types of consumers. This framework will make it possible to evaluate known and thoroughly tested technologies in combination with alternative technologies to determine the potential of investment. To showcase this possibility, scenarios containing different energy supply technologies were examined to determine the optimal technology mix and production plan for a public school located in Southern Denmark. The findings highlighted that the socioeconomic benefits of utilizing photovoltaic-thermal technology are very promising and have a large potential. Nevertheless, the combination of photovoltaic technology and heat pumps was the best overall scenario because of its ability to generate relatively cheaper energy while also maintaining socioeconomic benefits. This is especially important because it fits into the Danish plan for district heating expansion and reimbursement. The paper illustrated how the framework can be applied in combination with different technologies to determine the most efficient scenarios. The proposed technology combination of heat pumps, district heating, and photovoltaic units would, after implementation, be able to save the public school around 6.7 MDKK in a period of 20 years, with a payback period of around 9 years. It was shown that, within the specific multigenerational system proposed, heat pumps would cover 92% of the heat demand but would not be sufficient in peak load hours; therefore, district heating will be needed as a support.*

*Keywords: Linear optimization, production planning, multigeneration system, renewable energy, socioeconomic evaluation*

## 1. INTRODUCTION

In recent years, Denmark has been one of the world leaders in the field of sustainable energy policies (Jradi et al., 2018; Lund et al., 2009; Hagos et al., 2019), phasing out fossil fuels and transitioning to renewables. Even though Denmark is small by area, it's a country that strives to impact on a global perspective with its climate policies and innovation. Denmark is innovative in areas such as Wind Turbines, District Heating and -Cooling, as well as Biomass Recycling (Petersen, 2018; Lund et al., 2022). The country's striving has led to the implementation of various sustainable energy initiatives across the country, such as the Renewable Energy Directive (European Commission, 2023), the Energy Agreement of 2018 (Energi-, Forsyings- og Klimaministeriet, 2018), and the Climate Act of 2019 (The National Archives, 2019). Some municipalities in Denmark have taken significant steps towards achieving climate neutrality; this is the case for Odense Municipality. In the summer of 2020, the city council adopted a goal of achieving climate neutrality by 2030 at the latest (Odense Kommune, 2020). This goal depends on implementing new configurations for the existing DH network. One of the strategies chosen by the municipality of Odense relies heavily on heat pumps paired with PV systems to generate heat and power, which can significantly reduce CO<sub>2</sub> emissions. Schools, hospitals, and other public buildings are significant CO<sub>2</sub> emitters due to their high energy consumption pr. m<sup>2</sup>. Implementing sustainable energy systems in these institutions is necessary for achieving Denmark's long-term goal of phasing out fossil fuels. In this regard, Renewable Multigeneration Systems have emerged as a promising solution to this challenge (Jradi et al., 2014, Lykas et al., 2022; Mohammadi et al., 2020), allowing for the simultaneous production of heat and electricity using renewable energy sources. Renewable Multigeneration Systems involve the integration of various sustainable energy technologies such as photovoltaic, PV-Thermal, Heat Pumps, and thermal energy storage to provide buildings and facilities with a reliable and sustainable energy supply.

A public school in Odense is considered as a case study in this work to design, implement, and evaluate a multigeneration renewable energy driven system. The school is a large institution, covering an area of 11,000 m<sup>2</sup>, and has numerous classrooms, laboratories, offices, and other facilities which require heating and electricity constantly. Since it is a public institution, it is essential to ensure that the energy production is renewable to align with Denmark's ambitious renewable energy goals and that the decision positively impacts the socioeconomic bill. This paper will focus on establishing a sustainable solution that satisfies the school's heat and electricity demand and address the concerns about the system's economic and technical aspects. This will be done by determining the technologies which may fit the school's demand, considering the technical and socioeconomic perspectives. To implement this, scenarios with different energy technologies will be examined to determine the optimal mix and production plan for this public school.

## 2. METHODS AND STUDY DESIGN

The present study aims to develop a framework that focuses primarily on the economic benefit when identifying the optimal generation capacity for both individual heat and electricity production. The study leverages historical weather data, demand data and presents energy production technology data to achieve this. The economic analysis used to obtain and compare different scenarios includes:

- Cost-effectiveness Analysis (CEA)
- Socioeconomic Analysis (SEA)

This analysis will help determine the optimal scenarios with respect to a private economic perspective. The private financial view concentrates on using as little money as possible to cover the demand.

### 2.1. Framework Description

The method used to determine the optimal scenario is described in the flow chart presented in Figure 1. The flow chart visualizes the framework's four main parts, which are all implemented after the initial technology and scenario determination. Figure 1 is parted into Technology/Scenario determination, Data collection (1), Dynamic Lot Sizing Problem for each demand type (2), Capitated Lot Sizing problem (3), Economic evaluation (4), and comparison of scenarios. The technologies used can be determined by considering whether the technology is dispatchable, renewable, available in the area or beneficial for the specific location. The scenarios/combinations of the technologies are determined by considering which technologies complement each other, for example, PV & HP technologies.

In data collection (FW1), price data, technology efficiency, weather conditions, and technology prices, are all used to determine the operating cost pr. hour for each technology. The operational cost determination will also be based majorly on a simple modeling of each technology. The obtained prices pr. hour and the fixed cost pr. technology are used as inputs in the dynamic lot sizing problem (FW2). This is an optimization problem that determines both the optimal capacity and production plan for each technology. Because of a computational constraint, it is very complicated and costly to optimize both heat and electricity production in one problem, which is the reason for the separation. The optimal capacities from the dynamic lot sizing problem restrict the search for the optimal solution in the capitated lot sizing problem (FW3). By using the capitated lot sizing problem, the optimal solution is obtained by iteration. The optimal solution's production plan, and an hourly price for demand coverage, are then used to evaluate the scenario economically (FW4). These steps are repeated for all determined scenarios and hereafter compared.

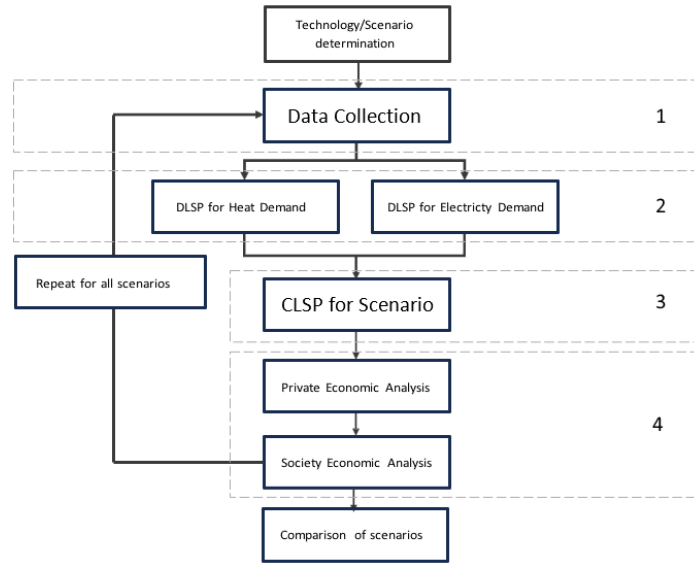


Figure. 1 Description of the adopted framework with the major steps and implementation phases

## 2.2. Scenario Description

The technologies within the scope of this paper have already been determined based on an initial scan as well as being renewable and fossil-free in nature. The four major technologies considered in this work are as follows: Air source heat pump (HP), biomass boiler (BM), photovoltaic (PV) and photovoltaic-thermal (PV-T). The selected combinations of technologies can be seen in Table 1. The patterns of these technologies enable the examination of the combination of HP and PV, which is the chosen strategy for both private heating and district heating rollout in Danish municipalities, including Odense where the considered school is located (Bormesterforvaltningen, 2021).

Table 1: Selected scenarios for examination

Scenario	Technology Mix
1	PV, BM, HP, Grid, DH
2	PV, HP, Grid, DH
3	PVT, BM, HP, Grid, DH
4	PVT, HP, Grid, DH

## 2.3. Modelling of Technologies

As mentioned in Section 2.1, each technology must be modelled and the efficiency in each hour needs to be calculated. The obtained efficiency can either be used to determine the hourly price pr. kWh generated or the maximum capacity in the same hour. All the technologies will therefore be modelled, except for the grid connection and the district heating network. These will behave as 'infinite bus'. In all scenarios, the COP of an air-to-water heat pump is used to determine the price pr. generated kWh pr. hour. According to the Danish technology catalogue for local heat production, the HP is modelled under the reference name: 'air to water heat pump - apartment complex - existing building (Danish Energy Agency, 2023). The COP of the HP is dependent on the temperature difference between the heat sink and heat source. Because the selected HP is of the type: Air-to-Water, and it is located outside the school, the source temperature can be defined as the ambient temperature at the HP location. The sink temperature is the supply temperature at which the heat must be delivered. To calculate the coefficient of performance (COP) for the HP, the equation for Carnot COP is utilized as follows:

Eq. 1. Calculation of heat pump COP

$$COP_{HP} = \frac{T_H}{T_H - T_C} \cdot \eta_{Carnot} \quad (1)$$

$T_H$  and  $T_C$  are the temperatures for the hot and cold reservoirs, respectively.  $\eta_{Carnot}$  is the Carnot Efficiency of the HP. The HP is used to supply domestic heating in the form of hot water. The sink temperature is defined as the required water temperature. It is assumed that the necessary water temperature at the outlet is fixed at 65°C (Statens Serum Institut, 2023). The Carnot Efficiency is adjusted so the SCOP during a reference year for the specific case study will be 3.40.

For the PV modelling, the photovoltaic module is simulated using a mathematical model based on the PV module Panasonic VBHN330SJ47 (Panasonic, 2022). The model itself is based on the electrical data sheet, the I-V curve, and the temperature characteristics of the module. Each module has a maximum power output of 330 W, at STC. The efficiency of the PV module is given in the electrical data from Panasonic as 19.7% at STC, and the temperature coefficient is defined as  $-0.258 \frac{\%}{^{\circ}\text{C}}$ . By implementing a linear regression, using the PV module data, the electricity output can be predicted at STC. Hereafter is the temperature coefficient implemented using Equation 2.

Eq. 2. PV Power output in relation to maximum output, temperature coefficient and ambient temperature.

$$P_{out} = P_{Max} + \left( (T_{coef} \cdot P_{Max}) \cdot \Delta T \right) \quad (2)$$

In addition, the PV-T was modelled using the same PV-module as above, the temperature coefficient was changed according to the actual PVT-module Abora aH72SK having a temperature coefficient of  $-0.36 \frac{\%}{^{\circ}\text{C}}$ . Hereafter, the correlation between electric efficiency and thermal efficiency from the Abora-datasheet was used to determine the thermal efficiency (Abora, 2022). This was done by implementing the electric efficiency in (j) and hereafter in (i). The obtained profiles can be seen in Figure 2.

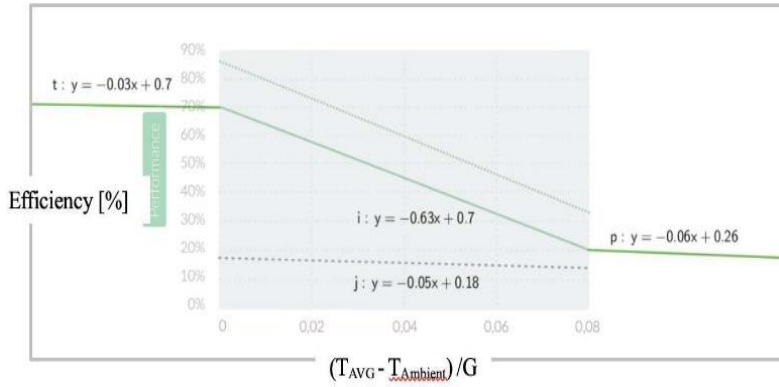


Figure 2 The line functions used to determine the thermal efficiency of the PV-T based on the electrical efficiency, original figure is from the Abora-aH72SK datasheet.

For the biomass boiler modelling, the price per kWh-heat produced by the biomass boiler is fixed for every hour in the year and can be found by multiplying the cost of the biomass with the heat capacity of the specific biomass used, employing Equation 3.

Eq. 3. Price pr. kWh\_heat producer by the biomass boiler.

$$Price \text{ pr. kWh} = B_{price} \cdot BM_{FuelCap} \cdot \eta_{boiler} \quad (3)$$

## 2.4. Linear-Programming

In this study, Linear programming was used to determine the optimal production mix of energy sources. The optimization problem will be parted into three different optimization phases, for each of the evaluated scenarios. The first two optimizations are of the type of dynamic lot sizing problems, where both the optimal capacity and hourly production mix are determined. These optimizations are made for the electrical demand and the heat demand separately. The combined system will be optimized using a capacitated lot sizing problem for each hour of the time horizon. An iterative process will hereafter be used to determine the optimal capacities of the local energy production units. By optimizing hour-by-hour, flexibility, real-time control, and precision are taken into account in the optimization. In terms of the dynamic lot sizing problem, the following presents the mathematical formulation of the DLSP. This problem aims to minimize both the cost of production and the capacity of the considered technologies. Optimization is utilized to determine the feasibility of different technology investments, accounting for the total cost of the capital and operational expenditures. In this regard, the DLSP is expressed as a LP, with the objective to minimize the total cost of operation and investment. The optimization does this as subject to constraints ensuring that the demand is met and technology capacities are not exceeded. The objective function is defined as the sum of the operational and capital costs for the entire timeframe. The operational costs (OpEx) represent the cost of producing energy per period and the capital cost (CapEx) represents the cost of investing in capacity for each technology. As mentioned, the constraints dictate that the total amount of energy in each period meets the demand, while ensuring that none of the technologies produce more energy than their rated energy output in the specific period. The mathematical formulation in Equation 4 serves as an algorithm, which can effectively determine the optimal production plan and capacities per technology.

Eq. 4. Linear problem for determining both capacities and optimal production schedule.

Minimize:

$$Z = \sum x_{j,i} \cdot c_{j,i} + \sum X_j \cdot C_j$$

Subject to:

$$x_{1,1} + x_{2,1} + x_{3,1} + x_{4,1} = D_i$$

$$x_{j,i} \leq X_j$$

$$-x_{j,(1,2,3,\dots,8760)} \leq 0$$

$$\begin{aligned}
i &= 1,2,3,4,5 \dots 8760 \\
j &= 1,2 \dots \text{Technologies}
\end{aligned}
\tag{4}$$

Furthermore, the capitated lot sizing problem (CLSP) is formulated in the same way as the DLSP, but with fixed capacities. This means that the algorithm after deployment only optimizes the production plan according to the capacities implemented as constraints. Therefore, Equation 5 presents the objective function formulated with no consideration of the CapEx, but only OpEx.

Eq. 5. Linear problem for determining the optimal production schedule with fixed technology capacities.

Minimize:  $Z = \sum x_{j,i} \cdot c_{j,i}$

Subject to:

$$\begin{aligned}
x_{1,1} + x_{2,1} + x_{3,1} + x_{4,1} &= D_i \\
x_{j,i} &\leq X_j \\
-x_{j,(1,2,3 \dots 8760)} &\leq 0 \\
i &= 1,2,3,4,5 \dots 8760 \\
j &= 1,2 \dots \text{Technologies}
\end{aligned}
\tag{5}$$

For both equations 4 and 5, it is applicable that:

- x = kWh produced per technology per hour
- c = price per produced kWh
- X = capacity of technology
- C = price per kW installed capacity per year
- D = kWh total demand per hour

### 3. SCENARIO OPTIMIZATION AND COMPONENT CONFIGURATION

When optimizing the heat and electricity production individually by using DLSP, Scenario 1 (S1) can be interpreted as shown in Figure 3. It is noted here that only two different primary energy inputs are exposed to conversion: Biomass and solar radiation. The primary energy is converted into either electricity or heat, where electricity can be defined as a secondary energy, but it is through the HP also used to generate heat. Excess electricity generated by the PV-module is in the optimization defined as all the electricity generated by the PV module, which is not used to cover the electricity demand. The excess electricity is sold to the grid.

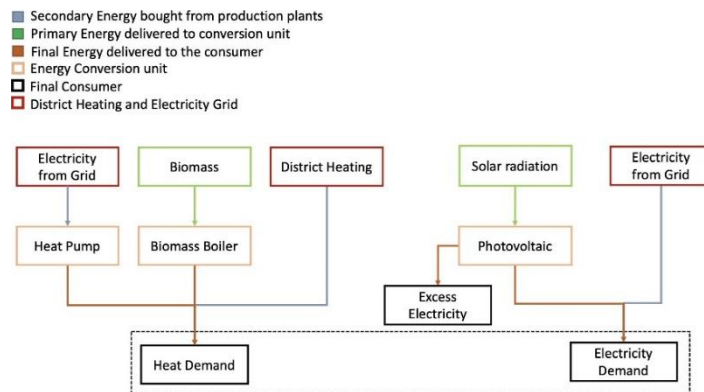


Figure 3 Overview of S1 as DLSP, optimised as two separate systems.

The system and optimization changes in configuration, when both electricity and heat productions are evaluated in the same system, can be seen in Figure 4. The major change to the configuration includes an electricity trade between the PV system and the heat pump, because LP does not allow for two different costs of the same unit. In the objective function, HP1 and HP2 are introduced, and the configuration behaves as follows: If excess electricity from the PV is available after covering the electricity demand, it can either be used as input to the heat pump or sold to the grid. The LP determines whether the cheapest solution in the specific hour is either to sell the electricity or use it for heat generation. The price for using the electricity to cover the electricity demand or to use the electricity in the heat pump is the alternative cost which could have been earned by selling the electricity to the system. In the optimization a control variable is introduced. This control unit buys electricity from the PV at the same price as it could be sold for in the grid. The control unit then distributes every bought kWh between the electricity load and HP1. Every kWh produced by the PV is by the optimization believed to be sold. Therefore, the control unit also ensures that it does not buy more than what the PV produces. In Figure 4, the control unit is labelled as: PV Electricity used in the system. The optimization does also ensure that the total production in one hour by HP1 and HP2 does not exceed the capacity limit of the heat pump. Production on both fictitious heat pumps at the same time can occur, but as HP1 can only produce heat from the excess electricity originating from the PV, HP2

can buy as much electricity from the grid as needed.

Scenarios S3 and S4 both introduce a new technology, photovoltaic-thermal (PV-T). PV-T's produce both electricity and heat from solar radiation on the panels and can assist in covering both the heat demand and the electricity demand. The CLSP component configuration for S3 and S4 is therefore changed so it adapts the generation of both thermal- and electric energy. The new configuration can be seen in Figure 5. This configuration applies for the heat production to only cover the heat demand. Sale of heat is out of the scope of this paper, meaning that excess heat generated by the PV-T cannot be sold to the district heating network. In this regard Equation 8 can be modified, so it is applicable for S3 and S4, by changing PV to:  $PV - T_{electricpart}$ , and incorporating a new constraint shown in Eq. 9. The objective function should include the  $PV T_{Thermal}$  part, meaning that the PVT in the objective function is parted into two separate units.

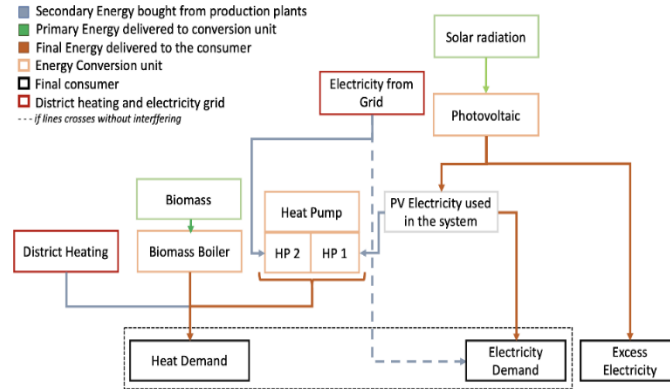


Figure 4 Overview of S1 as CLSP, optimised as one combined system.

$$PV T_{Thermal} \leq \eta_{Thermal} \cdot Cap_{PV T} \quad (6)$$

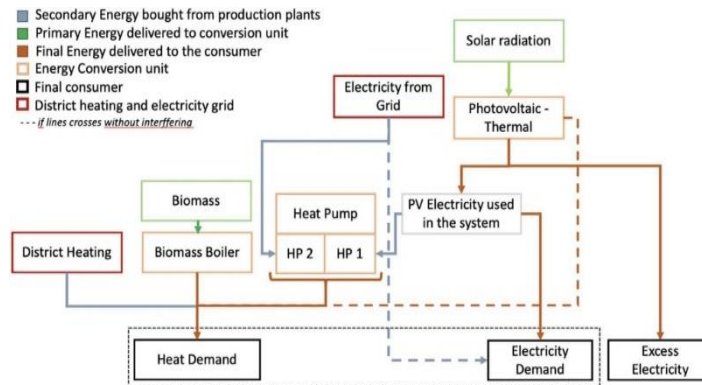


Figure 5 Overview of S3 as CLSP, optimised as one combined system containing both a Biomass Boiler and a PV-T

## 4. CASE STUDY AND RESULTS

In the following section the described methods are used to determine the solar optimal technology mix for a case study.

### 4.1. Baseline Scenario

To implement and evaluate the framework presented above, a public school in Odense is considered as a case study where the energy system will be designed and evaluated with respect to the baseline scenario, aiming to provide valuable insight into the performance and economic evaluation within scenarios 1-4. The school is a significant consumer of both heat and electricity, covering an area of 11,000  $m^2$ . The total heat consumption through the year is 1,165,995 kWh while the total electricity demand is 657,122 kWh. When examining the demand profiles, the peak for demand is determined to be 484.6 kWh and 199.8 kWh for heating and electricity, respectively. In the baseline scenario, it is assumed that neither the district heating network nor the electricity grid comes with any CapEx. This means that the grid and DH network are already constructed. This assumption is valid as the school is already utilizing the infrastructure.

### 4.2. Dynamic Lot Sizing Problem Results

When optimizing the capacities and the production plan as individual systems, the capacity of each technology depends on which scenario is examined. S1 and S2's electricity production in the DLSP is modeled the same way with the same

data, leading to the same capacity results. PV-T combines the separated systems because the investment price for installing PV-T comes with both electricity and heat production by converting solar irradiance. Because PV-T provides a combined generation of both heat and electricity, it is not possible to model it in the DLSP. It was expected that the DLSP for electricity production would show a maximum investment in PV modules, because of its high electricity production potential. The optimization confirmed this, as the optimal solution for the separated electricity system contains 990 kW of installed PV electricity generating capacity. The maximum electricity purchased from the grid is 191.5 kWh. The maximum production in one hour by the entire PV is 1141 kWh, and the total produced electricity is 1,220,314 kWh. The price of electricity, if the systems were separated, would be 0.34 DKK pr. kWh<sub>el</sub>.

Table 2: Electricity Results Overview.

LCOE [DKK/kWh]	0.34
Maximum Production [kWh]	1,141
Total Production [GWh]	1.22
Total Excess Electricity [GWh]	0.85
Renewable Penetration [%]	186

Even though there is a high penetration of solar power, and there is a lot of excess electricity generated throughout the year, the PV module generates non-dispatchable electricity. Hence, it is not guaranteed that the PV can cover the demand in each hour. By examining the load duration curve, and the technologies used to cover this demand, it is determined that both the Grid and the PV cover the needs at high-demand hours. It is also noticed that in some hours during the year, there is an electricity demand, but no PV generation. In these hours, the grid covers the entire load. When evaluating the heat production and electricity production separately, the optimal capacities for S1 and the economic results are shown in Table 3. Similarly, the capacities and prices for S2 are shown in Table 4.

Table 3: Optimal Capacities for Scenario 1.

Biomass Boiler Capacity [kW]	260
Heat Pump Capacity [kW]	27
Photovoltaic Capacity [kW]	990
LCOE of heat [DKK/kWh <sub>heat</sub> ]	0.230
LCOE of electricity [DKK/kWh <sub>electricity</sub> ]	0.338
Combined LCOE [DKK/kWh]	0.268

Table 4: Optimal Capacities for Scenario 2.

Biomass Boiler Capacity [kW]	-
Heat Pump Capacity [kW]	267
Photovoltaic Capacity [kW]	990
LCOE of heat [DKK/kWh <sub>heat</sub> ]	0.250
LCOE of electricity [DKK/kWh <sub>electricity</sub> ]	0.338
Combined LCOE [DKK/kWh]	0.282

### 4.3. Merging the electricity and heat production

By using the separated system capacities obtained in the DLSP and CLSP, the LCOE for the combined system can be obtained. This LCOE is what should be minimized when determining the optimal capacities for the combined system. With the specific capacities obtained in tables 3 and 4 can the LCOE of S1 and S2, as a combined system be determined to 0.266 and 0.272 DKK pr. kWh respectively. However, this is not an optimized result for the combined system, because the capacities were determined in the DLSP. These capacities are only used to limit the search for the optimal solution in the following section. By implementing an iterative method, the BM capacity is decreased compared to the optimal scenario from S1 DLSP, and the HP capacity is increased. By using this iterative method and implementing altered capacities in the CLSP, the optimal capacities for S1 are obtained. The capacities which generate the lowest LCOE for S1 are shown in Table 5.



Table 5: Three most beneficial capacity mix' for scenario 1 using iteration and how cost and LCOE is affected.

PV [kW]	HP [kW]	BM [kW]	Cost [MDKK/year]	LCOE [DKK/kWh]
990	125	180	0.478	0.262305
990	125	200	0.479	0.262463
990	100	200	0.479	0.262501

The cost difference per year between the cheapest scenario capacities and the third cheapest scenario capacities is about 350 DKK, which correlates to  $2 \cdot 10^{-4} \frac{DKK}{kWh}$ .

#### 4.4. Optimal Capacities & LCOE

The optimal capacities and the LCOE for each scenario are shown in Table 6.

Table 6: Optimal capacity, cost ned LCOE for each scenario using CLSP and iteration.

Scenarios	PV [kW]	PV-T [kW]	HP [kW]	BM [kW]	Cost [MDKK/year]	LCOE [DKK/kWh]
BS	-	-	-	-	0.798	0.437910
S1	990	-	125	180	0.478	0.262305
S2	990	-	240	-	0.495	0.271755
S3	-	400	50	240	0.543	0.297932
S4	-	400	250	-	0.566	0.310448

The optimization shows that S1 and S2, which both contain PV, produce cheaper energy than the PV-T scenarios. It is also noticed that all scenarios are cheaper than the baseline scenario pr. year, hence the optimized scenarios yield a positive impact.

#### 4.5. Break-Even Analysis

By evaluating the scenarios and their prices over a 20-year period, the break-even point for each scenario is determined. The break-even point describes the moment that the scenario has neither created revenue nor caused loss. The year after breaking even, the scenarios will be profitable. The break-even analysis will assume that the entire investment is made in the year 0.

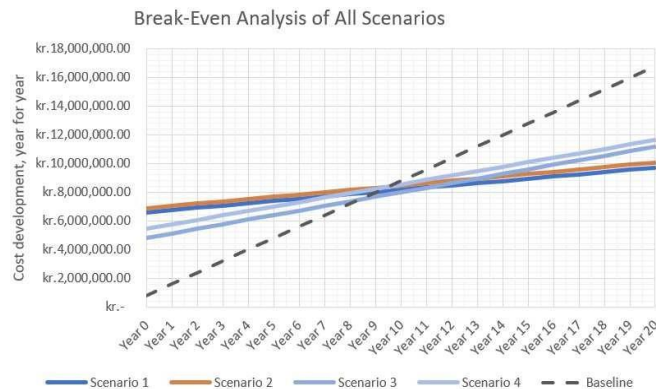


Figure 7 Break-Even Analysis of the different Scenarios in optimal capacity configurations.

In Figure 7, every scenario reaches the breakeven point between year 8 and year 10. The first scenario to reach break-even is S3, followed by S1. From the figure it can also be seen that on a 20-year period, it is expected that S1 will generate a surplus of 7 MDKK, a precise revenue overview can be seen in Table 7.

Table 7: Detailed overview of breakeven analysis.

Scenarios	Break even point [years]	Saving for 20 years [MDKK]	Savings of baseline [%]
S1	9	7.046	42
S2	9	6.698	40
S3	8	5.584	33
S4	9	5.137	31

#### 4.6. Examination of Optimal Scenario

When optimizing with respect to historical data for one year, the optimal scenario is found to be S1, generating the highest economic surplus. When examining the production plan of heat for this scenario, the HP primarily covers the base load 0-125 kWh. The BM covers the intermediate load of 125-310 kWh, and DH covers the excess load in peak demand hours. Even though HP primarily covers the base load, the order of technologies is not prioritized to their specific load in the production plan. In this regard, the optimization does always plan the production plan in the way allowing to generate the energy with the lowest LCOE. If the variable costs of either the BM or DH are cheaper than the HP, the cheaper technology will cover the demand at this specific hour. These specific load types of Base, Intermediate, and Peak loads are marked in Figure 8 as dotted lines. The full load hours of each technology can be used to illustrate this share of different loads, as presented in Table 8.

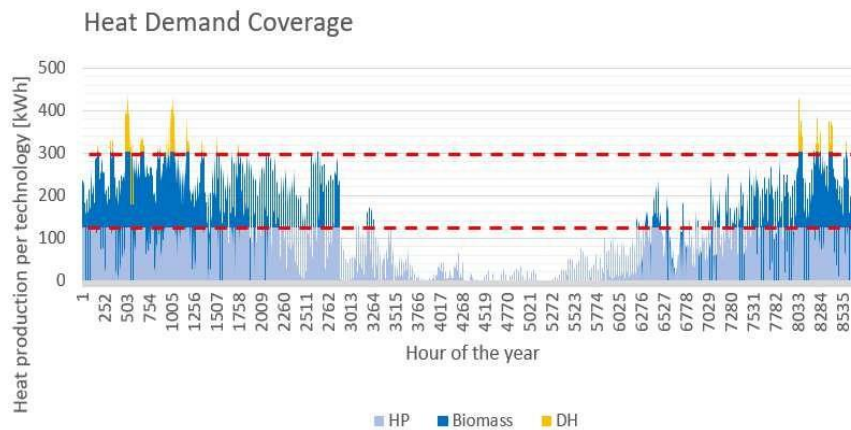


Figure 8 Scenario 1, Heat demand coverage during a year for scenario 1.

Table 8: Optimal scenario technologies and full load hours.

Technology	Total Production [MWh]	Full Load Hours [h]
Heat Pump	0.609	4873
Biomass Boiler	0.534	2887
District Heating	0.228	127

The HP has the largest number of full load hours and produces more heat throughout the year, even though it has a lower capacity than the BM. The largest number of full load hours is a sign of a higher utilization, which is typical for technologies that cover the base load. In most heat and electricity production plants, conversion technologies with a high CapEx and low OpEx are used to cover the base load. On the other hand, the peak load is often covered by a technology with a low CapEx, but high OpEx. This is very representative of DH since no investment cost is anticipated. When examining the evolution of the LCOE pr. hour through the year, it is noticed that the cheapest energy is generated in the summer period. This is because a lot of electricity is produced in this part of the year. The LCOE ranges from -4.633 to 0.833 DKK/KWh throughout the year. The LCOE is highly dependent on many external factors such as fuel prices, radiation from the sun, and the total demand. To understand how variables such as these influence the benefit of each scenario, a sensitivity analysis is implemented in the next section.

#### 4.7. Socioeconomic Evaluation

The socioeconomic parameters used to evaluate the most beneficial scenario socioeconomically are specified in the report 'Guidance in Socioeconomic Analyzes in the Field of Energy' by the Danish Energy Agency (DEA) (Danish Energy Agency, 2022). An overview of the determined socioeconomic costs is reflected in Figure 9 Here it is seen that the most socioeconomic beneficial scenarios are both S4 & S2 with a total cost being respectively, 692,377.72 DKK & 699,599.37 DKK. In comparison, the baseline scenario (BS) has a total cost of 1,230,677.84 DKK. By implementing multi criteria decision making, the optimal scenario for the specific case study is determined to be S2 if the socioeconomic criteria and private economic criteria are weighted equally. The decision is based on a pairwise comparison between each scenario, which is used in an analytical hierarchy process.

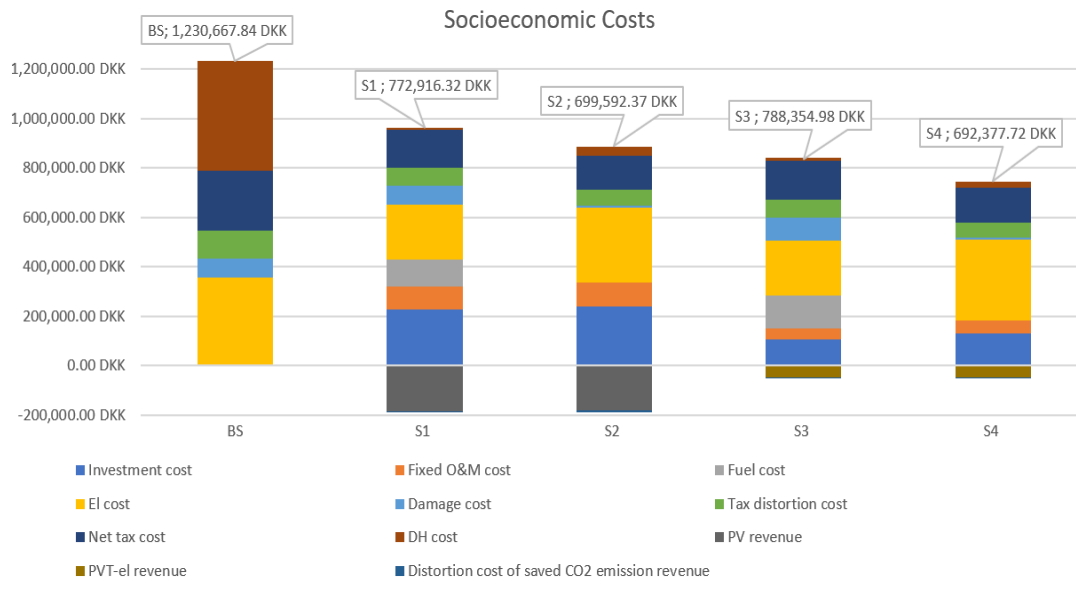


Figure 9 Socioeconomic Costs Comparison Between Scenarios

## 5. CONCLUSION

The paper set out to examine relevant scenarios consisting of different renewable energy production technologies and alternative conversion units, and hereafter determine the most profitable technology combinations, and the actual capacity of these units. By implementing two different linear programming methods, the optimal production plan and technology capacities were determined. In this paper a framework was established, enabling evaluating both the capacities and the optimal production plan. Furthermore, the framework did allow for further technological expansion, by making it possible to include own-modeled technologies and incorporating them, in a computationally effective way. The optimization and examination revealed that the most cost-efficient scenario for the case study was a combination of the technologies: photovoltaic/heat pump/biomass. On the other hand, the optimization also revealed that both the electricity grid and district heating were required for obtaining the cheapest production mix. Nevertheless, it was also shown that the photovoltaic-thermal technology can provide a more socioeconomic beneficial energy mix when combined with a heat pump, because of the low-emissions pr. kWh produced. This is also valid for the photovoltaic/heat pump combination, which ranks as the second-best scenario regarding both the business economic- and socioeconomic evaluation. With the combination of photovoltaic and heat pumps, from the perspectives of Scenario 2 in this paper, such transformation presents a good investment. It provides energy with a low LCOE and is also socioeconomically beneficial. For the public school, the technology combination would be able to save 6.7 MDKK in a period of 20 years, while breaking even after 9 years. It was shown that, within the specific multigenerational system proposed, heat pumps would cover 92% of the heat demand but would not be sufficient in peak load hours; therefore, district heating will be needed as a support.

## 6. ACKNOWLEDGEMENT

This work was carried out as part of the Danish participation in 'IEA EBC Annex 83 – Positive Energy Districts', no. 64020–1007, funded by the Danish Energy Agency under the Energy Technology Development and Demonstration Program (EUDP). We would also like to acknowledge the input from Athila Quaresma Santos for his guidance in the PV modeling part.

## 7. REFERENCES

Abora, 2022. Abora aH72SK, Datasheet. [Online], Available at: <https://solaractiva.es/wp-content/uploads/2022/01/AH72SK-EN.pdf>. [Accessed June 2023].

Bormesterforvaltningen, 2021. Gør hele energiforbruget i Odense CO2-neutralt. [Online], Available at: <https://www.odense.dk/byens-udvikling/klima/klimaneutral-2030/task-force-klimaneutral-2030/anbefaling2>. [Accessed June 2023].

Danish Energy Agency, 2022. Beregningsforudsætningerne. [Online], Available at: <https://ens.dk/sites/ens.dk/files/Analyser/soeb22.pdf>. [Accessed 05 May 2023].

Danish Energy Agency, 2023. Teknologikataloger. [Online], Available at: <https://ens.dk/service/fremskrivninger-analyser-modeller/teknologikataloger>. [Accessed 30 May 2023].

- E. D. Service, 2023. Consumption per de35 industry code per hour. [Online], Available at: <https://www.energidataservice.dk/tso-electricity/ConsumptionDE35Hour>. [Accessed 05 March 2023].
- Energi-, Forsyings- og Kimaministeriet, 2018. Energy Agreement 2018, Greener heating. [Online]. [Accessed June 2023].
- European Commission, 2023. Renewable Energy Directive. [Online], Available at: [https://energy.ec.europa.eu/topics/renewable-energy/renewable-energy-directive-targets-and-rules/renewable-energy-directive\\_en](https://energy.ec.europa.eu/topics/renewable-energy/renewable-energy-directive-targets-and-rules/renewable-energy-directive_en). [Accessed June 2023].
- Hagos, D.A., Ahlgren, E.O., Exploring cost-effective transitions to fossil independent transportation in the future energy system of Denmark. *Applied Energy*, 261 (2020), Article 114389.
- Jradi, M., Riffat, S., Tri-generation systems: energy policies, prime movers, cooling technologies, configurations and operation strategies. *Renew. Sustain. Energy Rev.*, 32 (2014), pp. 396-415.
- Jradi, M., Veje, C.T., Jorgensen, B.N., A dynamic energy performance-driven approach for assessment of building energy renovation – Danish case studies. *Energy Build.*, 158 (2018), pp. 62-76.
- Lund, H., Mathiesen, B.V., Energy system analysis of 100% renewable energy systems—the case of Denmark in years 2030 and 2050. *Energy*, 34 (5) (May 2009), pp. 524-531.
- Lund, H., Skov, I.R., Thellufsen, J.Z., Sorknæs, P., Korberg, A.D., Chang, M., Mathiesen, B.V., Kany, M.S., The role of sustainable bioenergy in a fully decarbonised society. *Renew Energy*, 196 (2022), pp. 195-203.
- Lykas, P., Georgousis, N. Bellos, E., Tzivanidis, C., A comprehensive review of solar-driven multigeneration systems with hydrogen production. *Int J Hydrogen Energy* (2022), Article S0360319922044640.
- Mohammadi, K., Khanmohammadi, S., Khorasanizadeh, H., Powell, K., A comprehensive review of solar only and hybrid solar driven multigeneration systems: Classifications, benefits, design and prospective. *Appl. Energy*, 268 (2020), Article 114940.
- Odense Kommune, 2020. Odense - Klimaneutral By Senest i 2030. [Online], Available at: [file:///C:/Users/alaaj/Downloads/Aftale\\_Klimaneutral\\_2030\\_Odense.pdf](file:///C:/Users/alaaj/Downloads/Aftale_Klimaneutral_2030_Odense.pdf). [Accessed June 2023].
- Panasonic, 2022. Photovoltaic module HIT@ VBHN330SJ47 / VBHN325SJ47. [Online], Available at: [https://www.europesolarshop.com/documents/panasonic/VBHN330\\_325SJ47\\_EN.pdf](https://www.europesolarshop.com/documents/panasonic/VBHN330_325SJ47_EN.pdf). [Accessed June 2023].
- Petersen, J.P., The application of municipal renewable energy policies at community level in Denmark: a taxonomy of implementation challenges, *Sustain. Cities Soc.*, 38 (2018), pp. 205-218.
- Statens Serum Institut, 2023. Legionærsygdom. [Online], Available at: <https://www.ssi.dk/sygdomme-beredskab-og-forskning/sygdomsleksikon//legionaersygdom>. [Accessed 15 March 2023].
- The National Archives, 2019. The Climate Change Act 2008 (2050 Target Amendment) Order 2019. [Online], Available at: <https://www.legislation.gov.uk/ukdsi/2019/9780111187654>. [Accessed June 2023].

---

# #247: The impact of applying the new Saudi Building Code on residential buildings' performance in Riyadh region

---

Abdulaziz ALADWANI <sup>1</sup>, Siddig OMER <sup>2</sup>

<sup>1</sup> Department of Architecture and Built Environment, the University of Nottingham, University Park, Nottingham, NG7 2RD, UK, ezxaa37@exmail.nottingham.ac.uk

<sup>2</sup> Department of Architecture and Built Environment, the University of Nottingham, University Park, Nottingham, NG7 2RD, UK, lazsa0@exmail.nottingham.ac.uk

*Abstract: The continual increase in energy consumption is of great concern to human wellbeing due to its environmental impact. Rapid population growth, fast urbanisation and high economic growth are the main causes of a considerable expansion in the building sector, whose extensive construction activities, especially with respect to domestic buildings, undoubtedly contribute to the overall increase in energy consumption. Worldwide, over a third of the total global energy consumption occurs in the building sector. Domestic energy consumption in particular has experienced fast growth in many developing countries during the last few decades. For example, in the Kingdom of Saudi Arabia (KSA), the energy demand in the domestic building sector has increased by approximately 7% annually since 1990, mostly due to air conditioning for cooling. One way to curb such energy consumption is through energy efficiency measures for buildings, and introducing effective energy standards and codes, which have been adopted in over 30 countries and regions around the world. This paper assesses and analyses the energy consumption patterns in residential buildings in the Riyadh region, the largest region in KSA in terms of population and housing density. The impact of applying the recently developed Saudi Building Code (SBC) on buildings' energy performance is investigated. This study includes 21 typical residential buildings within the Riyadh region, comprising villas and apartments, which are increasing rapidly in the Saudi building sector. The analysis is based on actual electricity bills, user behaviour, and results of a building simulation using DesignBuilder software. Results show that the application of the SBC and standards to the buildings' fabric can lead to an improvement in the energy consumption of villas and apartments by up to 19% and up to 40%, respectively. The variation is due to the impact of the various retrofitting strategies. The building fabric elements, in particular, are found to significantly influence the reduction of the buildings' energy consumption.*

*Keywords: Energy modelling, Residential buildings, KSA, Saudi Building Code (SBC)*

## 1. INTRODUCTION

The continuous growth of energy consumption is having an impact on the environment (Lee and Chen, 2008). According to Alrashed, Asif and Burek (2017), the world is facing serious energy and environmental challenges, and over 30% of total global energy consumption is caused by the building sector. An increase of 29% in global primary energy consumption between 2000 to 2010 has been reported. It is estimated that the residential, agricultural, and commercial sectors consume 11.8%, 43.4%, and 56.1% of the world's yearly energy from oil, natural gas, and hydropower, respectively (AlHashmi *et al.*, 2017). Moreover, energy consumption is considered to be the prime source of carbon dioxide (CO<sub>2</sub>) emissions (the residential sector is responsible for releasing 17% of the world's CO<sub>2</sub>) (AlHashmi *et al.*, 2017; Kim, Kim and Lee, 2019). Taleb and Sharples (2011) indicate that the increased greenhouse gas and CO<sub>2</sub> emissions are considered to be among the main causes of global warming (the fundamental source of these gases is fossil fuel burning). Therefore, urgent action must be taken to avoid the negative impact of this problem on future generations. Rapid population growth, increasing urbanisation and a high level of economic growth are the main reasons for considerable expansion in the building sector. According to AlHashmi *et al.* (2017), the residential sector in both developing and developed countries is expanding. Thus, the extensive construction activities in the building sector, especially concerning domestic buildings, is certainly a source of increasing energy consumption.

Domestic energy consumption has experienced accelerated growth in the Kingdom of Saudi Arabia (KSA) during the last few decades (Krarti, Dubey and Howarth, 2017a). Since 1990, the energy demand has increased by approximately 7% annually. The primary contributor to energy demand in KSA is the building sector, due to its dependence on air conditioning for cooling. In 2010, Saudi buildings consumed about 65% of KSA's total produced electricity; a proportion above the world average of approximately 50% (Shawk, 2018). Further research has confirmed that buildings consume up to 75% of the entire electricity generated (Abuhussain, Chow and Sharples, 2019). The ECRA's (2018) annual report revealed that nearly half of the electricity sold in 2018 was consumed by the residential sector, whereas this ratio is 25%, 19%, and 26% in the USA, Malaysia, and Japan, respectively (Al-Tamimi, 2017). A large number of developed countries have set buildings' energy efficiency as a target to reduce energy consumption and control pollution. Commonly, the provision of a comfortable environment for occupants and operation of building facilities are the main activities that consume energy (AlHashmi *et al.*, 2017). Energy efficiency can be defined as consuming less energy to provide the same or improved building services. In other words, it means to 'save energy consumption without compromising comfort, health and productivity levels' (Pérez-Lombard *et al.*, 2009). According to Galadanci *et al.* (2020), high-performance buildings can contribute to reducing environmental impacts and climate change, help reduce energy use, and improve indoor thermal conditions in buildings. Many studies indicate that a building's energy efficiency can be improved by implementing energy standards and codes, which have been adopted in over 30 countries and regions (Lee and Chen, 2008; Abuhussain, Chow and Sharples, 2019). The Ministry of Energy in KSA has studied the problem of increased energy demand and high CO<sub>2</sub> emissions, and has helped to establish many centres, programmes and standards to promote energy efficiency in buildings across the country (Krarti, Dubey and Howarth, 2017a). The introduction of the Saudi code is considered one of the most important contributions to achieving this goal.

## 2. SAUDI ARABIA'S BUILDING CODE

The Saudi Building Code (SBC) was developed in 2000, when a royal decree created the Saudi Building Code National Committee (SBCNC). The SBC is a set of legal, administrative and technical regulations and requirements that specify the minimum construction standards for a building, to ensure public safety and health (Al Surf, Susilawati and Trigunaryyah, 2014). In April 2003, after conducting preliminary studies and signing the agreement with the ICC, technical committees and sub-committees began to develop the SBC with adaptations to the base code, according to the cultural and social environment, soil types, natural and climatic conditions, and the properties of materials used in Saudi Arabia (SBCNC, 2007). In 2009 the code was optional, but it became mandatory in 2010 for new government buildings. At the end of 2013, a decision was outlined for a standard that regulates the maximum thermal transmittance U-values for the envelope of domestic buildings, for elements such as roofs, walls, and window glazing. These U-values became mandatory for residential buildings in the main cities. The implementation of this decision was in two stages: first, for residential buildings constructed after 2013; and Stage 2 introduced improved U-values for residential buildings constructed in 2017. The basis of this standard was SBC Chapter 601-Energy Conservation (Abuhussain, Chow and Sharples, 2018; AlFaraidy and Azzam, 2019). In 2018, an updated version of the SBC was released, with a new green building code category added. The updated SBC is being implemented in five phases. Phase one applies to administrative government buildings, tall buildings, hospitals, and hotels. Phase two applies to community buildings, educational buildings, commercial complexes, communications towers, industrial facilities, buildings less than 23 metres in height, and high-risk installations. Phase three, from August 2020, applies to community buildings, healthcare centres, serviced apartments, apartment buildings, and recreational buildings. Phase four, from August 2021, applies to business buildings. Phase five, from August 2022, applies to all other types of buildings (SBCNC, 2018). The code considers Saudi Arabia to have three climate zones. The climatic factors are the main determinant in this division, as Zone 1 is the warmest and Zone 3 is the coolest. Zone 1 is extremely hot, with a Cooling Degree Day (CDD) value greater than 5,000. Zone 2 is very hot, with a CDD above 3,500. Zone 3 is hot, for the remaining cities. Table 1 outlines the building envelope requirements for Zones 1, 2, and 3. This study focuses on the updated version of the energy conservation code for Zone 1 – specifically, the Riyadh region, which has the highest population density, the largest inhabited area, and is one of the hottest regions in the KSA.

Table 1: Building Envelope Requirements for Zones 1,2 and 3.

Climatic Zone	Areas	Properties of building envelope					
		U-value (W/m <sup>2</sup> .K)					SHGC
		Roof	Walls	Floor	Door	Window	Glazing
Zone 1	Riyadh, Makkah, Madinah, Najran, Jazan, Bisha, Eastern region	0.202	0.342	0.496	2.839	2.668	0.25
Zone 2	Gassim, Hail, Tabuk, Al-Jouf, Assir, Al-Taif, Al-Baha, Northern area	0.238	0.397	0.496	2.839	2.668	0.25
Zone 3	Abha, Khomis Moshet, Guriat, Tarif	0.273	0.453	0.496	2.839	2.668	0.25

### 3. METHODOLOGY

The multiple case study analyses 11 villas and 10 apartments in the Riyadh region. The aims of this study are: (i) to obtain the energy consumption breakdown; (ii) to measure the level of improvement in the residential buildings' performance after applying the updated SBC; and (iii) to determine which building fabric elements have a significant impact on the reduction of buildings' energy consumption. The methodology involved an analysis of the properties' design, construction fabric and materials. For each case study, the researchers obtained a set of official drawings, the ages and genders of residents, number and uses of rooms, types and sizes of windows and doors, types and numbers of air conditioners, inventories of electrical appliances used within the homes, types of hot water systems used, the number and types of lights used, and the monthly electricity consumption for three years (2018, 2019 and 2020). Household members of each of these dwellings were interviewed individually to understand the occupancy schedule.

#### 3.1. Study Sample Selection Criteria

It is important to set criteria for selecting the sample before collecting field data, to ensure that the study's results are reproducible and accurately represent the study population. The General Authority for Statistics (GASTAT) classified all KSA residential buildings into five types: apartment, villa, traditional house, floor in a villa, and floor in a traditional house. In order to choose the most suitable types, five criteria were developed. First, the selected types should form the largest proportion of residential buildings. Second, they should accommodate a high percentage of the population. Third, the total floor area in these types should be the largest. Fourth, the selected types should reflect future construction trends in the KSA. Fifth, they should represent the most significant percentage of energy consumption. After reviewing the five criteria, it was found that villas and apartments in Riyadh constituted the largest share among the different housing types. Thus, enhancing the energy performance of villas and apartments has the greatest potential to reduce electricity consumption.

Several standards were considered when selecting the villas and apartments to be studied, in order to represent typical housing. (i) The properties should be of the average housing size in the KSA. An average villa's gross floor area in Saudi Arabia is approximately 338 to 525 m<sup>2</sup>, whereas apartments are 100 to 250 m<sup>2</sup> (Monawar, 2001; Aldossary, Rezgui and Kwan, 2014a; AlHashmi *et al.*, 2017; Alshibani and Alshamrani, 2017; Krarti, Aldubyan and Williams, 2020). (ii) The number of occupants of the properties should reflect the average Saudi family. The average size of villa-dwelling Saudi families is seven members, and four members for apartment-dwelling families. In addition, 65% of the villas have 4–8 residents, while 75% of the apartments have 2–4 residents (GASTAT, 2023). (iii) The average monthly consumption of the selected cases should correspond to approximately 65% of the average monthly consumption of the subscribers of the Saudi Electricity Company, which is 1–4,000 kWh/month. In addition to the standards mentioned above, the case study buildings needed to match the buildings' typical characteristics (90% concrete) and have varying ages (GASTAT, 2023). These cases were examined individually using simulation software tools, in order to (i) obtain the monthly energy consumption and determine the annual consumption breakdown, and (ii) measure the percentage decrease in energy consumption after making the retrofit to meet the SBC requirements.

#### 3.2. Simulation Tool Selection

Various types of simulation software are available; they can be categorised in terms of complexity, from spreadsheet tools to more advanced, special-purpose simulation tools. Furthermore, simulation programs can also be classified by their integration with tools that address one aspect of building design, or with tools that integrate multiple aspects of building design (Trčka and Hensen, 2010). Galadanci *et al.* (2020) observed the successful and broad use of computer simulations in the building industry sector. An assessment to reduce energy consumption and environmental impact can be obtained by applying simulation-based design and building performance optimisation. Numerous types of simulation software were reviewed, in order to select appropriate software to fulfil the aims and objectives of this research. After reviewing a number of prior studies, a set of simulation programs were identified to analyse energy consumption in buildings. For instance, Aldossary, Rezgui and Kwan (2017) utilised Integrated Environmental Solutions (IES-VE) simulation tools. Meanwhile, Sefaira energy simulation software was used by Al-Kanani, Dawood and Vukovic (2017), while many authors employed EnergyPlus as their work simulation program (Alaidroos and Krarti, 2015; Krarti, Dubey and Howarth, 2017a; Alshahrani and Boait, 2019). Furthermore, Shwehdi *et al.* (2015) applied the VisualDOE energy simulation software, while Alshenaifi (2015) chose the ECOTECT simulation software to determine the ideal orientation for a house. Moreover, a recent study suggested using different simulation programs, such as the DesignBuilder® software, DOE-2, TRNSYS and ApacheSim

(Alshahrani and Boait, 2019). Analysis and predictions of energy consumption patterns in buildings could be obtained from these forms of simulation software.

After reviewing simulation software programs, the DesignBuilder® (DB) software from DB Software Ltd was chosen, as it met all the requirements of this research. This software is widely used for modelling and simulating energy-efficient building designs (Alshahrani and Boait, 2019). According to AlHashmi *et al.* (2017), DB is considered one of the most efficient graphical user interfaces for the EnergyPlus dynamic simulation engine. EnergyPlus can model buildings' heating, cooling, lighting, ventilation and domestic hot water (DHW). DB has useful built-in features that simplify energy performance comparisons. Moreover, DB contains some other features such as: (i) incorporating the issuance of energy performance certificates and the building regulations compliance certificate; (ii) carbon dioxide emissions calculation; and (iii) the program can perform optimisations based on cost, energy and comfort criteria (Chanchpara, 2019). DB software requires the specification of parameters to simulate a home's thermal performance. The parameters should describe the home's physical characteristics, installed appliances, occupancy behaviour, the building's location and climate, the nature of the surrounding environment, and other factors.

### 3.3. Modelling the Case Study Buildings

Building the simulation model for the case studies involved two main tasks: first, constructing a three-dimensional model for each property; then, an initial computer simulation for the building without retrofitting was run, and the model was validated. Second, an updated version of these case study buildings was developed to meet the retrofitting requirements of the SBC, in order to calculate the potential percentage of improvement in energy consumption for each case study.

For the first task, inputting data into the DB program included four main stages. The first involved determining the location coordinates of the study sample and the weather file. The second stage required entering the site details, such as the height of the location above sea level, defining the orientation of the main facade, and entering the monthly ground temperature. The third stage involved inputting the building materials characteristics for the exterior walls, roof, floor, windows, and doors. Subsequently, air conditioning and lighting data were entered, and the type of air conditioner was selected. The cooling set point temperature was 24°C, and the cooling setback was 26°C, based on the American Society of Heating, Ventilating, and Air Conditioning Engineers (ASHRAE) and SBC's recommendation (SBCNC, 2018; ASHRAE, 2021). The lighting type was then entered, and the lighting power density was specified according to Alrashed's (2015) study. The fourth stage involved entering occupancy information for each space in the dwellings. A new energy simulation was performed using the same user behaviour profiles, for the second task. Retrofitting was applied to envelope elements (exterior walls, roofs, floors, windows and doors) to validate the potential for energy consumption reduction.

## 4. CASE STUDY DESCRIPTION

This research was focused on residential buildings in the Riyadh region, which is located in the warmest zone of KSA. Thus, Riyadh consequently suffers more significantly from the energy consumption problem, due to the continuous use of air conditioning during summertime. Moreover, the Riyadh region has the highest percentages of population and housing in KSA: 26% and 28%, respectively (GASTAT, 2023). Table 2 presents the monthly maximum, minimum and average temperature in Riyadh (1985–2019) (NCM, 2023). The following section provides descriptions of the 21 properties that were chosen, as well as the occupants' user profiles.

Table 2: Riyadh region climate data

	January	February	March	April	May	June	July	August	September	October	November	December
Max. temperature	21	24	30	36	42	45	45	45	42	36	30	24
Min. temperature	9	9	15	21	24	27	27	27	24	18	15	9
Avg. temperature	15	18	21	27	33	36	36	36	33	24	21	18

### 4.1. Description of Villas

The 11 villas are located in the Riyadh region, in four cities (Riyadh, Marat, Shaqra, and Thadiq). The last three cities are located west and northwest of Riyadh. Villas 1, 5, 7, and 9 are in Riyadh, while Villas 3, 4, 6 and 10 are in Marat; Villas 2 and 8 are in Shaqra, and finally, Villa 11 is in Thadiq.

The main facade of six of the villas is facing north. Determining the building age is important, because it is expected that the more modern the building, the better the performance (for instance, new air conditioners and windows are more efficient). The villas' ages range from 2 to 20 years. Most villas consist of more than two floors. The villas' area in the KSA is often large and occupied by a large family. Furthermore, 65% of the villas have an area between 306 and 554 m<sup>2</sup>, and 73% have seven or more occupants. Most villas contain more than one guest room. A large building area, a high number of residents, and multiple guest rooms are part of Saudi culture. Most of the villas (82%) have split air conditioners. Table 3 presents a summary of the villas' main characteristics.



Table 3: The main elements summary of Villas.

Element	Villa 1	Villa 2	Villa 3	Villa 4	Villa 5	Villa 6	Villa 7	Villa 8	Villa 9	Villa 10	Villa 11
General information	Orientation	North	North	West	East	West	North	North	North	West	East
	Age	10	3	20	9	15	17	11	5	3	2
	Number of floors	2.5	2.5	2.2	2.3	2.4	2.2	2.1	1.9	2.1	2.3
	Built up area/ m <sup>2</sup>	495	634	554	619	669	380	664	337	375	518
	No. of occupiers	6	12	12	13	8	8	7	7	5	9
Appliance	No. of rooms	14	22	18	16	20	15	15	14	11	16
	Air conditioners	Split	Split	Window	Split	Central	Split	Split	Split	Split	Split
	Lights	LED	LED	Fluorescent	Halogen	LED	Fluorescent	LED	LED	LED	LED
	DHW	50 Litter	50 Litter	50 Litter	50 Litter	270 Litter*	50 Litter	50 Litter	50 Litter	50 Litter	50 Litter
	No. of fridges	3	4	3	3	6	4	5	2	2	2

Table 4: Villas' fabric thermal performance (U-value W/m<sup>2</sup>K).

Element	SBC Zone 1	Villa 1	Villa 2	Villa 3	Villa 4	Villa 5	Villa 6	Villa 7	Villa 8	Villa 9	Villa 10	Villa 11
EX wall	0.342	1.237	0.524	1.177	1.237	0.737	1.009	1.085	0.524	1.237	1.237	1.237
Roof	0.202	0.852	0.829	1.439	0.852	0.442	1.439	0.852	0.442	0.272	0.852	0.852
Floor	0.496	1.122	1.122	1.134	1.134	1.134	1.122	1.122	1.122	1.122	1.122	1.122
Glazing	2.668	5.778	2.665	5.778	3.159	3.159	5.778	3.159	3.159	3.159	3.159	3.159
Door	2.839	3.124	3.124	3.124	3.124	3.124	3.124	3.124	3.124	3.124	3.124	3.124

According to Alasmari (2019), three reasons have caused the large differences in building specifications in the KSA: (i) the rapid urban renaissance, (ii) the absence of a building code, and (iii) the arrival of workforce and engineers from different backgrounds to build housing projects. Therefore, nearly all the buildings in the study sample have different specifications, except for Villas 10 and 11. Villas 1, 4, 9, 10, and 11 have the same composition of the external wall. The roofs of Villas 1, 4, 7, and 10 have the same U-value (0.852 W/m<sup>2</sup>K). All villas are similar in their floor construction. Most of the old villas have single-pane glass windows, while 65% of the houses have double glazing. The details of the villas' fabric thermal performance are illustrated in Table 4.

## 4.2. Description of Apartments

All apartments are located in Riyadh and Marat (6 and 4 apartments, respectively). All apartments in the study sample have two or three external walls, facing different directions. Seven apartments have a roof that is not exposed to external factors (there is an apartment above it), while all apartments consist of a single story. Apartment 3 is the oldest, at 35 years old. The floor area of the smallest apartment is 108 m<sup>2</sup>, while the largest apartment is 171 m<sup>2</sup>. Nine residents occupy Apartment 3, while the numbers for the other apartments correspond to the average population of apartments in the KSA. Most of the apartments have a guest room, except for Apartment 3. Most of the apartments (80%) have split air conditioners. Table 5 presents detailed information about the elements of each apartment.

Table 5: The main elements summary of Apartments.

Element	Apart 1	Apart 2	Apart 3	Apart 4	Apart 5	Apart 6	Apart 7	Apart 8	Apart 9	Apart 10
General information	Orientation	East	North	South	North	West	West	East	East	East
	Age	10	2	35	2	11	11	2	3	5
	Roof	No	No	Yes	No	No	Yes	No	No	Yes
	Built up area/ m <sup>2</sup>	110	161	171	117	118	108	142	120	159
	No. of occupiers	3	5	9	2	4	5	6	4	2
Appliance	No. of rooms	5	6	7	7	6	5	7	7	7
	AC	Window	Split	Window	Split	Split	Split	Split	Split	Split
	Lights	LED	LED	Fluorescent	LED	LED	LED	LED	LED	LED
	DHW	50 Litter	50 Litter	70 Litter	50 Litter	50 Litter	50 Litter	50 Litter	50 Litter	50 Litter
	No. of fridges	1	1	2	1	1	1	1	1	1

Usually, apartments built by the same real estate developer are identical. Apartments 1, 2, 9, and 10 are identical; Apartments 6 and 7 have the same specifications. While Apartments 4, 7, and 8 are identical, each is in a different building. The (adiabatic) feature was used when the apartments were adjacent to other apartments, whether through the wall, ceiling, or floor. 'Adiabatic surfaces' means that they do not transfer heat beyond their outer surface and are often used for modelling boundaries with other spaces that can be considered to be at roughly the same temperature as the zone. Table 6 present the details of the apartments' envelope thermal performance. If the apartment door is made of wood, it opens to an internal area; thus, there is no heat transfer between the two spaces.

Table 6: Apartments' fabric thermal performance (U-value W/m<sup>2</sup>K).

Element	SBC Zone 1	Apart 1	Apart 2	Apart 3	Apart 4	Apart 5	Apart 6	Apart 7	Apart 8	Apart 9	Apart 10
EX wall	0.342	1.304	1.304	1.767	1.237	1.085	1.085	1.237	1.237	1.304	1.304
Roof	0.202	*	*	3.008	*	*	0.931	*	*	*	1.439
Floor	0.496	1.122	1.122	*	*	*	*	*	*	*	*
Glazing	2.668	5.778	5.778	5.778	3.159	3.159	3.159	3.159	3.159	5.778	5.778
Door	2.839	3.124	3.124	*	*	3.124	3.124	*	*	3.124	3.124

### 4.3. Operation Schedules

It is crucial to emphasise that one of the most significant variables in determining energy use is how family members behave. Thus, the daily profiles for occupancy, equipment/appliances and lighting were collected for each space. The properties have been divided into four main zones: guest zone, living zone, kitchen zone, and sleeping zone. The user profiles were found to be different for each property. The majority of the occupants are at work or school during the day. Guest rooms are rarely used during a month (approximately two to three times at maximum). The living area is used most of the day, and in some properties, the air conditioning is on for 24 hours during the summer months. Bedrooms are generally used during the night, and it is noted that bedrooms for girls are used for longer than boys' rooms. Unused bedrooms were observed in Villas 2, 3, 4, 6, and 10. These bedrooms have been allocated to their sons and daughters who visit at the weekend or holidays.

## 5. ANALYSIS AND RESULTS

Due to the change in temperatures and the difference in the residents' behaviour in the properties from year to year, the energy consumption bills for each building were collected for three years (2018, 2019, 2020), to obtain more accurate results. In general, energy consumption increases with increasing temperatures; see Figure 1. However, this may not be accurate when the occupancy schedule of the residential property varies. It is noticed that the consumption of some homes decreases during some summer months because the occupiers are away for a summer holiday, as an example. On the other hand, consumption increases significantly at some periods of the year due to the arrival of adult sons and daughters of the family, or guests, to spend time with the family during vacations. DB software was used to display the detailed consumption for each housing unit. The average consumption for three years was used to compare the actual and simulated consumption for each unit of villas and apartments. The analysis is divided into two parts, for villas and apartments.

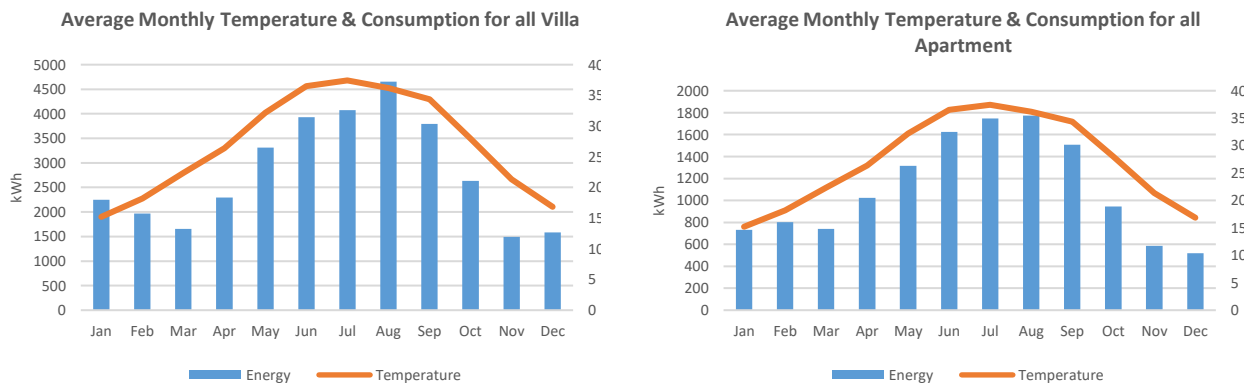


Figure 1 Average Monthly Temperature & Consumption for all Villa and Apartment

### 5.1. Analysis of the Villas

Based on three years' average billed consumption and simulation results, annual energy consumption varies between villas. The Energy Use Intensity (EUI) ranges from 23 to 103 kWh/m<sup>2</sup>/Yr. The study villas' average annual consumption and EUI are 33,635 kWh and 64.66 kWh/m<sup>2</sup>/Yr, respectively; see Figure 2.

It is noted that the summer months (June, July, August, and September) have the highest consumption, due to the high demand for air conditioning, with an average of 3,930, 4,070, 4,653, and 3,791 kWh, respectively. Villa 5 consumes the highest energy among the villas and has the highest EUI. It is expected that there are four main reasons for this: (i) the central air-conditioning type is used; (ii) central water heaters are used for domestic hot water (DHW); (iii) the villa has a large number of refrigerators; (iv) Villa 5's residents tend to spend a longer time during the day in the bedrooms, which leads to a large number of air conditioners operating for most of the day. On the other hand, Villa 11 is the least energy-consuming and the lowest EUI villa, because of the small number of occupants (only two people), and they are often at work during the day. In addition, they are away from the villa on weekends and holidays. It is also noted that the EUI of

Villa 8 is much higher than the average; this is probably because the villa's occupants are two elderly people, two maids, and a driver. Thus, they spend most of the day inside the villa, and 4–5 air conditioners often run for 24 hours.

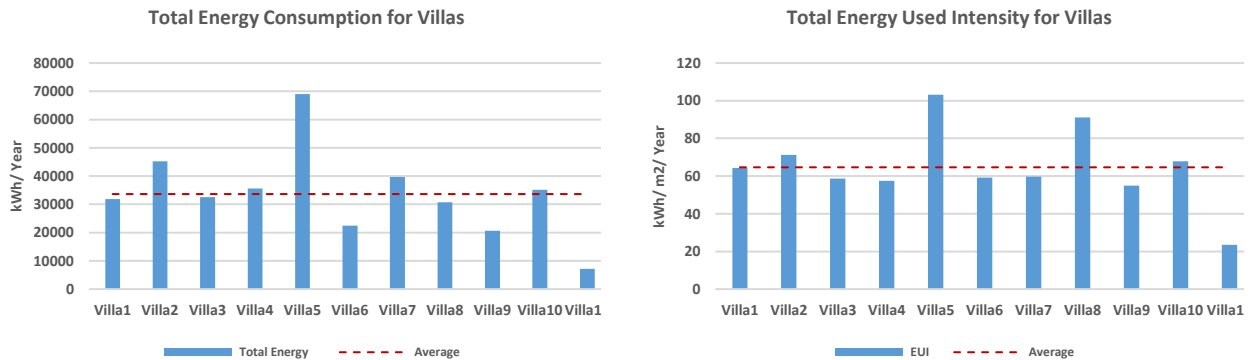


Figure 2 Annual consumption for Villas.

Simulation models were built, and a calibration process was conducted to obtain the energy consumption breakdown and measure the accuracy of the simulation models implemented for villas. DB software can break down the energy consumption into five categories: cooling, heating, lighting, DHW, and finally, equipment.

Verification of the validity of the models can be performed in several ways. According to Ruiz and Bandera (2017) and Alyami and Omer (2021), the uncertainty of models is determined using three main methods: ASHRAE Guideline 14, Federal Energy Management Program (FEMP) and International Performance Measurement and Verification Protocol (IPMVP). The principal uncertainty indices used are Normalised Mean Bias Error (NMBE), Coefficient of Variation of the Root Mean Square Error (CV(RMSE), and coefficient of determination ( $R^2$ ).

Each villa's model passed the three-method investigation test. Figure 3 shows the difference between actual and simulated total energy consumption. The highest difference between actual and simulated consumption was 2% in Villa 1. Figure 4 presents the energy consumption breakdown for villas. Air conditioning represents the highest percentage of energy consumption, ranging from 50% to 67%, due to the high temperatures in the Riyadh region.

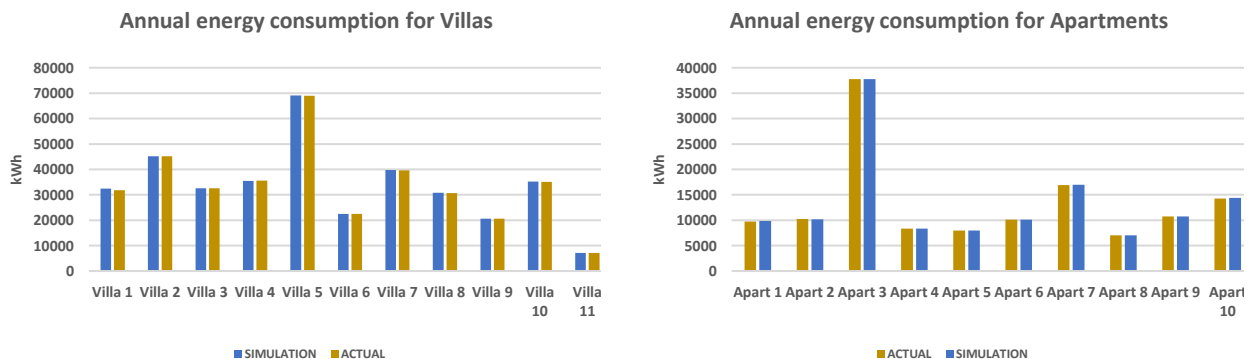


Figure 3 Actual and simulated annual energy consumption for villas & apartment.

## 5.2. Analysis of the Apartments

There is a wide variation in average EUI in the apartments. The highest annual energy consumption and EUI are seen in Apartment 3, at 37,763 kWh and 220.84 kWh/m<sup>2</sup>, respectively. In contrast, Apartment 8 has the lowest annual energy consumption. Apartment 3 has the highest consumption because it is the oldest; thus, it is expected that with the building's age, the efficiency of its equipment and materials, such as air conditioners and windows, will decrease. In addition, the apartment envelope is uninsulated. Moreover, the residents' number is large; they are all adults, and spend most of their time in the bedrooms, which leads to the operation of all air conditioners for almost 24 hours. The large difference in consumption between Apartment 3 and the other apartments leads to its high average annual consumption and EUI. Therefore, the average annual consumption and EUI were calculated twice: once for all apartments, and the other time for all apartments except Apartment 3. The average annual consumption for all apartments is 13,313 kWh and 10,597 kWh for all apartments except Apartment 3. Furthermore, the average EUI for all apartments and all apartments except for Apartment 3 is 94 and 80 kWh/m<sup>2</sup>, respectively; see Figure 5. It is noted that Apartments 3, 7, 6, and 10 have the highest EUI because their roofs are exposed to the outside atmosphere (i.e. no apartment above them), and all of them have a large number of residents, five or more. However, Apartment 7 differs in that its ceiling is not exposed to the outside

weather; but due to the behaviour of its occupants, who tend to leave the air conditioners running for 24 hours during the summer, it is still one of the apartments with the highest EUI.

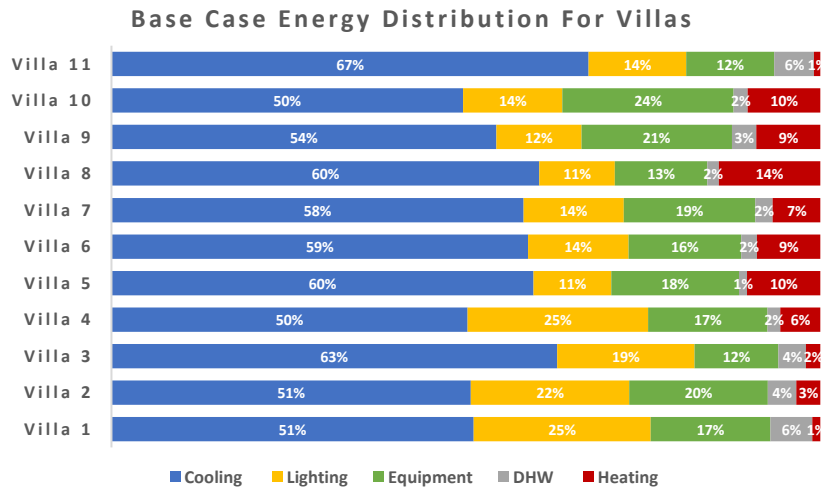


Figure 4 Annual consumption breakdown for villas (base case).

The summer months have the highest consumption. However, Apartments 7 and 10 consume more energy than other apartments (except Apartment 3) during January and February, considered the year's coldest months. Through interviewing the occupiers, it became clear that they use low-efficiency portable electric heaters to heat the apartment during the winter, which leads to high consumption. Simulation models were built for each apartment separately, and the occupancy schedule was entered. Figure 3 shows the actual and simulated consumption: they are almost identical, with the largest difference being 1%. Figure 6 displays the breakdown of energy consumption for each apartment. It can be seen that air conditioning represents the highest percentage of consumption, reaching 71% of the total in Apartment 3.

## 6. DISCUSSION

This section discusses the stages in the process of improving the case study buildings to meet the specifications of SBC-602. It also displays the percentage of improvement in each building. Three steps should be taken to execute the buildings' improvement. First, a comparison should be made between the U-value of the study buildings' fabric and the requirements of the code, to determine whether the buildings meet the code's requirements. Second, the buildings that do not conform to the specifications of the code should be improved. Finally, the level of improvement should be measured.

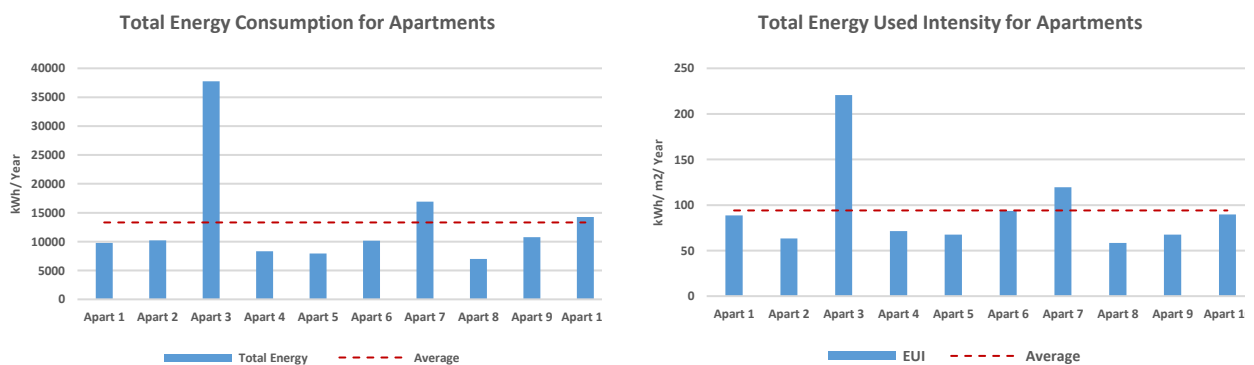
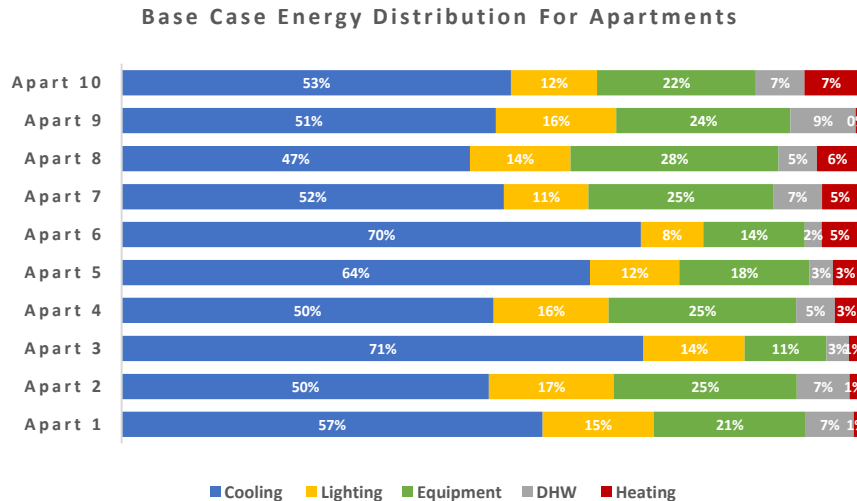


Figure 5 Annual consumption for Apartments.



*Figure 6 Annual consumption breakdown for Apartments.*

The roof, floor, external walls, windows and external doors of all the study buildings did not meet SBC requirements (see Table 4 and Table 6). Therefore, all buildings were improved to meet the code. Figure 7 shows the annual improvement in consumption for villas and apartments. Improving the villas' and apartments' fabric enhances the annual energy consumption by between 3% to 19% in villas and 1% to 40% in apartments. The overall improvement percentages for each property are shown in Figure 8.

A number of studies reported that adding or improving the level of insulation in the walls and roofs of various residential buildings in KSA can reduce annual energy consumption by 15–35% (Al-Homoud, 1997; Al-Sanea, 2002; Al-Sanea and Zedan, 2011; Alaidroos and Krarti, 2015; Abdul Mujeebu and Alshamrani, 2016; Krarti, Dubey and Howarth, 2017b). The area of the roofs and external walls was calculated for each property, to identify the relationship between its area and the level of improvement in its consumption: see Table 7 and Table 8.

The previous charts and tables show that for villas, the smallest consumption improvement is in Villas 2 and 9; this is because these two villas have the lowest U-value in external walls and roofs. It is also noted that when the U-values are identical between more than one villa or apartment, the improvement rate is approximately equal: 10% in Villas 1, 4, 10, and 11, and 6–7% in Apartments 4, 7, and 8. The higher U-value in external walls and roofs, in particular, led to Villa 6 having the highest improvement percentage in the total annual energy consumption, of 19%. The apartments' position (i.e. ground, middle or upper floor) and envelope U-value are crucial in influencing the improvement percentage of the apartments' energy consumption. Apartments 1, 2, and 9 have identical envelope specifications; however, Apartments 1 and 2 are located on the ground floor, so they show the lowest improvement rates of 1% and 3%, respectively. On the other hand, when the roof of the apartment is exposed to the outside weather, the roof area and the external walls are large; thus, the percentage of improvement in annual electricity consumption is high, as in Apartments 3, 6, and 10. Using the DB simulation program enables the determination of the average reduction from the detailed breakdown of energy consumption. After the improvement, the cooling and heating energy demands is reduced in villas by 14% and 45%, respectively, while this percentage is 58% in heating and 17% in cooling in apartments.

The saving percentage in energy consumption that was achieved in this research, of up to 19% and up to 40%, is considered to be acceptable, when compared with the previous studies' energy saving percentage, which was between 15% and 40% (Al-Homoud, 1997; Al-Sanea, 2002; Al-Ajlan *et al.*, 2006; Al-Mofeez, 2007; Al-Sanea and Zedan, 2011; Alaidroos and Krarti, 2015; Abdul Mujeebu and Alshamrani, 2016).

Reducing annual energy consumption by 12%, which was achieved as an average of energy conservation for villas and apartments in this research, can decrease the energy demand by 4890 GWh if the Riyadh region's residential buildings are retrofitted. The energy conservation percentage can be maximised by enacting various laws or government initiatives that motivate occupiers and homeowners. These include incentives and support to purchase high-efficiency electrical appliances, especially air conditioners; installing solar panels; shading building facades; and raising the residents' awareness of the behaviours that would increase consumption. According to Krarti, Dubey and Howarth (2017b), improving the efficiency of air conditioners can reduce energy consumption by up to 36%. In addition, installing solar panels amounting to 10–30% of the building area can generate 12–24% of the energy consumed (Aldossary, Rezgui and Kwan, 2014b). Shading the building facades in sections 20–100 cm long can reduce energy consumption by 3–6%. Furthermore, the behaviour of the residents has a significant impact on the energy consumption in the dwelling (Brounen, Kok and Quigley, 2012; Huang, 2012; Zhu *et al.*, 2013; Aldossary, 2015; Alshahrani and Boait, 2019).

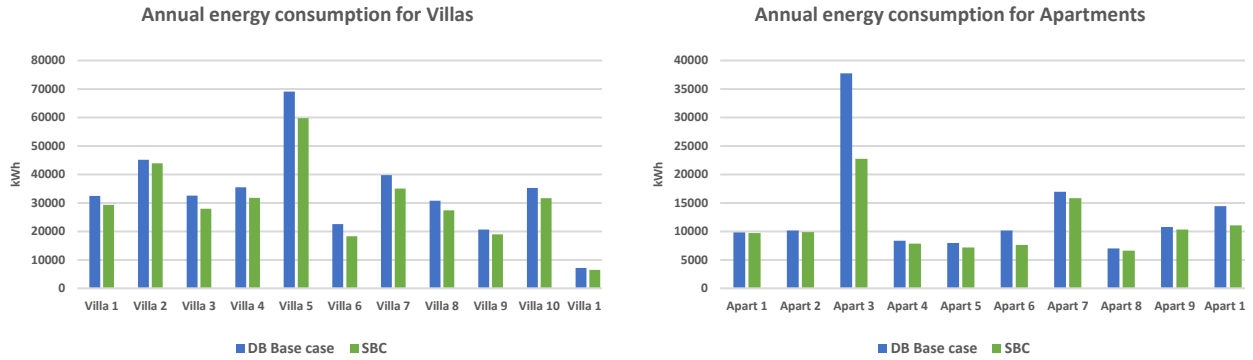


Figure 7 Comparison of annual energy consumption between the base case and after retrofitting as SBC

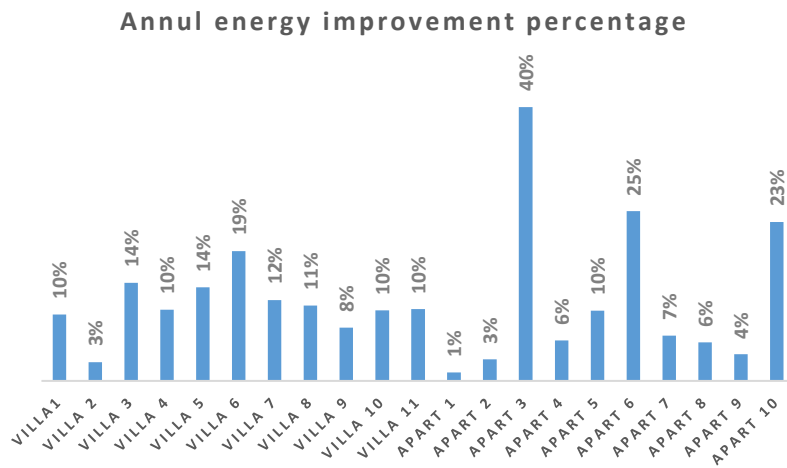


Figure 8 Annual energy improvement percentage for Villas and Apartments

Table 7: The area of the external walls and roof of the villas.

Element	Villa 1	Villa 2	Villa 3	Villa 4	Villa 5	Villa 6	Villa 7	Villa 8	Villa 9	Villa 10	Villa 11
EX wall	847.28	817.24	577.88	618.43	752.83	529.44	554.99	529.96	481.45	556.8	502.49
Roof	251.82	328.81	281.1	328.73	315	209.28	329.9	232.15	90.79	194.61	197.5

Table 8: The area of the external walls and roof of the apartments.

Element	Apartment 1	Apartment 2	Apartment 3	Apartment 4	Apartment 5	Apartment 6	Apartment 7	Apartment 8	Apartment 9	Apartment 10
EX wall	89.4	129.41	123	90.28	132.49	136.91	102.37	88.45	126.41	126.41
Roof	0	0	197.45	0	0	108.39	0	0	0	159.07

## 7. CONCLUSION

Energy consumption, particularly in the home, has experienced fast growth in many developing countries during the last few decades. Energy standards and codes are a way to curb buildings' energy consumption. The increasing demand for energy in KSA has led the government to update and apply the building code to all buildings. This study focuses on the updated version of the energy conservation code for Zone 1, specifically the Riyadh region, which has the highest percentages of KSA's total population and housing: 26% and 28%, respectively. Villas and apartments consume 32% and 31%, respectively, of total electricity use in the residential sector, and their EUI ranges from 23 to 220 kWh/m<sup>2</sup>/Yr. The average annual consumption is 33,635 kWh and 13,313 kWh for villas and apartments, respectively. Using DB simulation software, this study found that air conditioning represents the highest percentage of energy consumption, from 47% to 71%, due to the high temperatures in the Riyadh region. Applying the SBC improved the energy consumption in villas and apartments by up to 19% and up to 40%, respectively. The variation is due to the impact of the various retrofitting strategies. The building fabric elements, in particular, are found to significantly impact the reduction of buildings' energy consumption. Adding or improving the level of insulation in the walls and roofs is the most valuable factor for reducing energy consumption. Housing retrofitting in the Riyadh region can decrease the energy demand by 12%, amounting to 4,890 GWh annually. Furthermore, the energy conservation percentage can be maximised by up to 36% if high-efficiency electrical appliances, especially air conditioners, are purchased, or by up to 24% if solar panels are installed. Finally, raising people's awareness on how to reduce personal energy consumption can improve energy efficiency in the home.

## 8. REFERENCES

- Abdul Mujeebu, M. and Alshamrani, O. S. (2016) 'Prospects of energy conservation and management in buildings - The Saudi Arabian scenario versus global trends', *Renewable and Sustainable Energy Reviews*, 58(October), pp. 1647–1663. doi: 10.1016/j.rser.2015.12.327.
- Abuhussain, M. A., Chow, D. H. C. and Sharples, S. (2019) 'Sensitivity energy analysis for the Saudi residential buildings envelope codes under future climate change scenarios: The case for the hot and humid region in Jeddah', *IOP Conference Series: Earth and Environmental Science*, 329(1). doi: 10.1088/1755-1315/329/1/012039.
- Abuhussain, M. A., Chow, D. H. chi and Sharples, S. (2018) 'Assessing the adaptability of the Saudi residential building's energy code for future climate change scenarios', in *PLEA 2018 - Smart and Healthy within the Two-Degree Limit: Proceedings of the 34th International Conference on Passive and Low Energy Architecture*. HONG KONG, pp. 74–79.
- Al-Ajlan, S. A. *et al.* (2006) 'Developing sustainable energy policies for electrical energy conservation in Saudi Arabia', *Energy Policy*, 34(13), pp. 1556–1565. doi: 10.1016/j.enpol.2004.11.013.
- Al-Homoud, M. S. (1997) 'Optimum Thermal Design of Residential Buildings', *Building and Environment*, 32(3), pp. 203–210.
- Al-Mofeez, I. A. (2007) 'Electrical Energy Consumption Pre and Post Energy Conservation Measures: A Case Study of One-story House in Dhahran, Saudi Arabia', *King Saud Univ.*, 19(2), pp. 1–12.
- Al-Sanea, S. A. (2002) 'Thermal performance of building roof elements', *Building and Environment*, 37(7), pp. 665–675. doi: 10.1016/S0360-1323(01)00077-4.
- Al-Sanea, S. A. and Zedan, M. F. (2011) 'Improving thermal performance of building walls by optimizing insulation layer distribution and thickness for same thermal mass', *Applied Energy*, 88(9), pp. 3113–3124. doi: 10.1016/j.apenergy.2011.02.036.
- Al-Tamimi, N. (2017) 'A state-of-the-art review of the sustainability and energy efficiency of buildings in Saudi Arabia', *Energy Efficiency*, 10(5), pp. 1129–1141. doi: 10.1007/s12053-017-9507-6.
- Alaidroos, A. and Krarti, M. (2015) 'Optimal design of residential building envelope systems in the Kingdom of Saudi Arabia', *Energy and Buildings*, 86, pp. 104–117. doi: 10.1016/j.enbuild.2014.09.083.
- Alasmari, F. (2019) *An Institutional Analysis of State-Market Relations in the Saudi Arabian Housing System: A Case Study of Riyadh*. The University of Sydney.
- Aldossary, N. A. R. (2015) *Domestic Sustainable and Low Energy Design in Hot Climatic Regions*. Cardiff University.
- Aldossary, N. A., Rezgui, Y. and Kwan, A. (2014a) 'Domestic energy consumption patterns in a hot and arid climate: A multiple-case study analysis', *Renewable Energy*, 62, pp. 369–378. doi: 10.1016/j.renene.2013.07.042.
- Aldossary, N. A., Rezgui, Y. and Kwan, A. (2014b) 'Domestic energy consumption patterns in a hot and humid climate: A multiple-case study analysis', *Applied Energy*, 114, pp. 353–365. doi: 10.1016/j.apenergy.2013.09.061.
- Aldossary, N. A., Rezgui, Y. and Kwan, A. (2017) 'Establishing domestic low energy consumption reference levels for Saudi Arabia and the Wider Middle Eastern Region', *Sustainable Cities and Society*, 28, pp. 265–276. doi: 10.1016/j.scs.2016.09.015.
- AlFaraidy, F. A. and Azzam, S. (2019) 'Residential Buildings Thermal Performance to Comply With the Energy Conservation Code of Saudi Arabia', *Engineering, Technology & Applied Science Research*, 9(2), pp. 3949–3954. doi: 10.48084/etasr.2536.
- AlHashmi, M. *et al.* (2017) 'Energy Efficiency and Global Warming Potential in the Residential Sector: Comparative Evaluation of Canada and Saudi Arabia', *Journal of Architectural Engineering*, 23(3), p. 04017009. doi: 10.1061/(asce)ae.1943-5568.0000253.

- Alrashed, F. (2015) *DESIGN AND APPLICATION OF ZERO ENERGY HOMES IN SAUDI ARABIA*. Glasgow Caledonian University.
- Alrashed, F., Asif, M. and Burek, S. (2017) 'The role of vernacular construction techniques and materials for developing zero-energy homes in various desert climates', *Buildings*, 7(1). doi: 10.3390/buildings7010017.
- Alshahrani, J. and Boait, P. (2019) 'Reducing high energy demand associated with air-conditioning needs in Saudi Arabia', *Energies*, 12(1), pp. 0–15. doi: 10.3390/en12010087.
- Alshenaifi, M. A. (2015) *High Performance Homes in Saudi Arabia: Revised Passivhaus Principles for Hot and Arid Climates*.
- Alshibani, A. and Alshamrani, O. S. (2017) 'ANN/BIM-based model for predicting the energy cost of residential buildings in Saudi Arabia', *Journal of Taibah University for Science*, 11(6), pp. 1317–1329. doi: 10.1016/j.jtusci.2017.06.003.
- Alyami, M. and Omer, S. (2021) 'Building energy performance simulation: a case study of modelling an existing residential building in Saudi Arabia', *Environmental Research: Infrastructure and Sustainability*, 1(3), p. 035001. doi: 10.1088/2634-4505/ac241e.
- ASHRAE (2021) *ASHRAE handbook Fundamentals*. Available at: [www.ashrae.org](http://www.ashrae.org) (Accessed: 12 April 2022).
- Brounen, D., Kok, N. and Quigley, J. M. (2012) 'Residential energy use and conservation: Economics and demographics', *European Economic Review*, 56(5), pp. 931–945. doi: 10.1016/j.eurocorev.2012.02.007.
- Chanchpara, B. (2019) *ZERO ENERGY BUILDING*. New York Institute of Technology.
- ECRA (2018) *Statistical Booklet 2018*. Available at: <https://ecra.gov.sa/en-us/MediaCenter/doclib2/Pages/SubCategoryList.aspx?categoryID=5> (Accessed: 22 November 2022).
- Galadanci, A. S. et al. (2020) 'Energy investigation framework: Understanding buildings from an energy perspective view', *Journal of Building Engineering*, 28(November 2019), p. 101046. doi: 10.1016/j.jobe.2019.101046.
- GASTAT (2023) *Number of Household Members*. Available at: <https://portal.saudicensus.sa/portal/public/2/4/100747?type=TABLE> (Accessed: 12 June 2023).
- Huang, Y. (2012) *Energy Benchmarking And Energy Saving Assessment In High-Rise Multi-Unit Residential Buildings*. Ryerson University.
- Al kanani, A., Dawood, N. and Vukovic, V. (2017) 'Energy Efficiency in Residential Buildings in the Kingdom of Saudi Arabia', in Dastbaz, M., Gorse, C., and Moncaster, A. (eds) *Building Information Modelling, Building Performance, Design and Smart Construction*. Cham: Springer International Publishing, pp. 129–143. doi: 10.1007/978-3-319-50346-2\_10.
- Kim, D. W., Kim, Y. M. and Lee, S. E. (2019) 'Development of an energy benchmarking database based on cost-effective energy performance indicators: Case study on public buildings in South Korea', *Energy and Buildings*, 191, pp. 104–116. doi: 10.1016/j.enbuild.2019.03.009.
- Krarti, M., Aldubyan, M. and Williams, E. (2020) 'Residential building stock model for evaluating energy retrofit programs in Saudi Arabia', *Energy*, 195, p. 116980. doi: 10.1016/j.energy.2020.116980.
- Krarti, M., Dubey, K. and Howarth, N. (2017a) 'Evaluation of building energy efficiency investment options for the Kingdom of Saudi Arabia', *Energy*, 134, pp. 595–610. doi: 10.1016/j.energy.2017.05.084.
- Krarti, M., Dubey, K. and Howarth, N. (2017b) 'Evaluation of building energy efficiency investment options for the Kingdom of Saudi Arabia', *Energy*, 134(October 2016), pp. 595–610. doi: 10.1016/j.energy.2017.05.084.
- Lee, W. L. and Chen, H. (2008) 'Benchmarking Hong Kong and China energy codes for residential buildings', *Energy and Buildings*, 40(9), pp. 1628–1636. doi: 10.1016/j.enbuild.2008.02.018.



Monawar, A. H. (2001) 'A Study of Energy Conservation in the Existing Apartment Buildings in Makkah Region , Saudi Arabia', *PhD Thesis, School of Architecture, Planning & Landscape, University of Newcastle upon Tyne, United Kingdom*.

NCM (2023) *Saudi climate, National Center for Meteorology*. Available at: <https://ncm.gov.sa/Ar/Climate/KSAClimate/Pages/TemperatureAndPrecipitation.aspx> (Accessed: 12 June 2023).

Pérez-Lombard, L. *et al.* (2009) 'A review of benchmarking, rating and labelling concepts within the framework of building energy certification schemes', *Energy and Buildings*, 41(3), pp. 272–278. doi: 10.1016/j.enbuild.2008.10.004.

Ruiz, G. R. and Bandera, C. F. (2017) 'Validation of calibrated energy models: Common errors', *Energies*, 10(10). doi: 10.3390/en10101587.

SBCNC (2007) '601: Energy conservation requirements', in *Saudi Building Code*. Riyadh: Saudi Building Code National Committee.

SBCNC (2018) *Saudi Energy Conservation Code SBC 602- CR*.

Shawk, M. (2018) *Exploring the Energy Performance of the Residential Building Stock in 3 Regions in Saudi Arabia*. University of Southampton.

Shwehdi, M. H. *et al.* (2015) 'Energy savings approaches of buildings in hot-arid region, Saudi Arabia: case study', *Journal of Engineering Research*, 3(1), p. 7. doi: 10.7603/s40632-015-0007-6.

Al Surf, M. S., Susilawati, C. and Trigunaryah, B. (2014) 'The Role of the Saudi Government and the Saudi Building Code in Implementing Sustainable Housing Construction in Saudi Arabia', in *20th Annual Pacific-Rim Real Estate Society Conference*, pp. 19–22.

Taleb, H. M. and Sharples, S. (2011) 'Developing sustainable residential buildings in Saudi Arabia: A case study', *Applied Energy*, 88(1), pp. 383–391. doi: 10.1016/j.apenergy.2010.07.029.

Trčka, M. and Hensen, J. L. M. (2010) 'Overview of HVAC system simulation', *Automation in Construction*, 19(2), pp. 93–99. doi: 10.1016/j.autcon.2009.11.019.

Zhu, J. *et al.* (2013) 'Optimization method for building envelope design to minimize carbon emissions of building operational energy consumption using orthogonal experimental design (OED)', *Habitat International*, 37, pp. 148–154. doi: 10.1016/j.habitatint.2011.12.006.

---

## #249: A BIM-based framework for designing sustainable structures through the reuse of precast concrete components

---

Husam AL-JAWHAR<sup>1</sup>, Georgia THERMOU<sup>2</sup>, Carlos OSORIO-SANDOVAL<sup>3</sup>, SERIK TOKBOLAT<sup>4</sup>

<sup>1</sup> University of Nottingham, University Park, Nottingham NG7 2RD, UK, husam-aljawhar@uobaghdad.edu.iq

<sup>2</sup> University of Nottingham, University Park, Nottingham NG7 2RD, UK, georgia.thermou@nottingham.ac.uk

<sup>3</sup> University of Nottingham, University Park, Nottingham NG7 2RD, UK, carlos.osorio@nottingham.ac.uk

<sup>4</sup> University of Nottingham, University Park, Nottingham NG7 2RD, UK, serik.tokbolat@nottingham.ac.uk

*Abstract: The widespread use of concrete within the global construction sector is primarily attributed to its inherent qualities of resilience, versatility, longevity, and facilitation of economic growth. Nevertheless, it is noteworthy that this popular material is a significant contributor to the industry's greenhouse gas emissions, material depletion, and substantial waste production. Particularly in Europe, concrete constitutes the major component of demolition waste. Consequently, the practice of recycling and reemploying concrete components from pre-existing architectural structures harbours a considerable potential to attenuate the construction sector's ecological footprint substantially. This study presents a Building Information Modelling (BIM)-based reusability framework that aims to facilitate the reuse of precast concrete components in new sustainable structures, predicated on their performance and in line with specific matching criteria. This methodology involves utilising two distinct types of BIM models as input data. The first category, called 'Supply BIM', encapsulates data regarding existing components. In this category, the disassembly cost, the cost of each component, the disassembly durations, and the Life Cycle Analysis (LCA) of each component are calculated. Moreover, the load-bearing capacity of each component is analysed. The second category, termed 'Request' BIM, incorporates data necessary to reuse components during their subsequent lifecycle. The operational procedure relies on the BIM-based reusability model to aggregate matching concrete elements. Under the assumption that the Supply BIM possesses custom-built attributes equivalent to the Request BIM, the system will autonomously collect these components. This provides the foundation for a sustainable design for a new construction project. However, if the cost or LCA of the existing matching components exceeds that of the conventional new components, such components will be disregarded. This framework will underpin the development of a tool for designers that has the potential to reduce time and cost expenditures while minimising human error in sustainable design processes.*

*Keywords: Reusability Framework, BIM for Reusability, Circular Economy, Sustainable Structure, Precast Concrete Reuse.*

## 1. INTRODUCTION

The construction sector represents a vital component of the economic structure and a significant contributor to the gross domestic product of any given country. This industry is implicated in the generation of over 35% of total waste and is accountable for approximately 5-12% of the total Green House Gas (GHG) emissions across Europe (European Commission Brussels, 2020). Further compounding this issue, the construction industry consumes approximately half of all non-renewable raw materials and accounts for 36% of worldwide final energy utilisation (Norouzi et al., 2021). Given these environmental considerations, there is an imperative to identify sustainable alternative materials. Reutilised concrete elements from existing structures present one such promising alternative to traditional raw materials. ISO 20887:2020 defined reusable as 'the ability of a material, product, component or system to be used in its original form more than once and maintain its value and functional qualities during recovery to accommodate reapplication for the same or any purpose' (BS EN ISO 20887:2020).

Crother (2005) and Salama (2017) mention that the typical design paradigm for building components does not incorporate considerations for disassembly, refurbishment, or re-utilisation. Nonetheless, the existing building stock presents substantial potential that can be tapped into, effectively diminishing reliance on novel designs and concurrently reducing both greenhouse gas emissions and the consumption of raw materials. This potential has drawn considerable attention from both researchers and industry practitioners, leading to an emphasis on developing methodologies to facilitate the re-utilisation of building components. Despite these advancements, the field is marked by a notable absence of a common understanding regarding the pertinent design principles for reutilised load-bearing structures, and furthermore, the prevailing design norms fall short in their support for such an approach (Akinade et al., 2020).

To overcome the inherent limitations of certain strategies, numerous studies have endeavoured to address these obstacles. Some have concentrated on the deconstruction of a structure, subsequently reconstructing the building in a different location (Van den Berg et al., 2021), while others have directed their attention towards the reuse of specific architectural components, such as concrete facades (Salama, 2019), neglecting the remaining structural elements including slabs, beams, and columns. It is essential to consider that various factors during the lifespan of a building, including but not limited to corrosion, load capacity exceedance, and other deteriorating conditions, can potentially alter or diminish the functionality of concrete. Unfortunately, existing research models overlook this significant detail, which could negatively impact the performance of new structures that incorporate previously used concrete elements and may even lead to instances of structural failure.

To address these deficiencies, the development of a novel framework is needed. This framework should be designed to facilitate the effective reuse of significant precast concrete components from existing structures, based on their performance. Such a model could be seen as a viable alternative to new construction, with the potential to bolster both sustainability and circular economy initiatives.

## 2. REUSABILITY OF CONCRETE COMPONENTS AND THEIR IMPACT ON THE ENVIRONMENT

In the United Kingdom, the construction industry stands as the most prominent consumer of materials and the leading producer of waste by volume. Data compiled by the Department for Environment, Food & Rural Affairs (Defra) indicated that 63% of England's total waste output, amounting to 120 million tonnes out of 189 million tonnes in 2016, was linked to the construction, demolition, and excavation sectors (GCB, 2020).

The production process of concrete significantly contributes to environmental pollution. Key ingredients such as limestone, chalk, clay, gypsum, and sand are subjected to heating at roughly 1450 degrees Celsius. Other components of concrete include water, cement, and aggregate, the procurement of which involves several environmentally impactful processes such as water harvesting, stone extraction, crushing for aggregate, and large-scale mixing. These materials are then processed into a fine powder known as cement (Stacey, 2011). Following this, the concrete components are transported from the extraction site to the production plant, where precise measurements are combined to yield cast-in-situ concrete. This is then transferred to construction sites or formed into precast elements. Each stage of this process, from resource extraction to demolition, is characterised by significant energy use and CO<sub>2</sub> emissions. The incorporation of clinker in concrete elevates the embodied energy and CO<sub>2</sub> emissions, with every ton of clinker produced resulting in one ton of CO<sub>2</sub> emissions (Cabeza et al., 2013).

Crowther (2005) proposed a critique of the prevailing "Cradle-to-Grave" life cycle model of building materials and components, which ultimately leads to substantial waste production. In contrast, the study advocated for a cyclical "Cradle-to-Cradle" model. If applied to the production and utilisation of concrete, this model could potentially not only conserve the energy required for material manufacture but also mitigate the associated CO<sub>2</sub> emissions, solid waste, and dust pollutants that arise from the demolition process, as depicted in Figure 1.

In a life cycle assessment conducted by Morrison Hershfield Engineering examining reclaimed precast double-T concrete, it was revealed that such usage could result in significant environmental savings (Catalli, 2009). According to the ATHENA Life Cycle Assessment, benefits included an energy savings of 1.23 GJ, a reduction in CO<sub>2</sub> emissions by 147 kg, and a 50% decrease in water and air emissions for each cubic meter of precast double-T concrete, as compared to using a new double-T (Catalli, 2009).

Further evidence of the utility and benefits of reclaimed concrete can be found in a housing project situated in Mehrow, near Berlin. This venture involved the reuse of precast concrete elements from obsolete buildings, originally built using the 'Plattenbau' construction technique, in the creation of new residences. The approach resulted in a noteworthy cost reduction of 30% (Stacey, 2011) (refer to Figure 2).

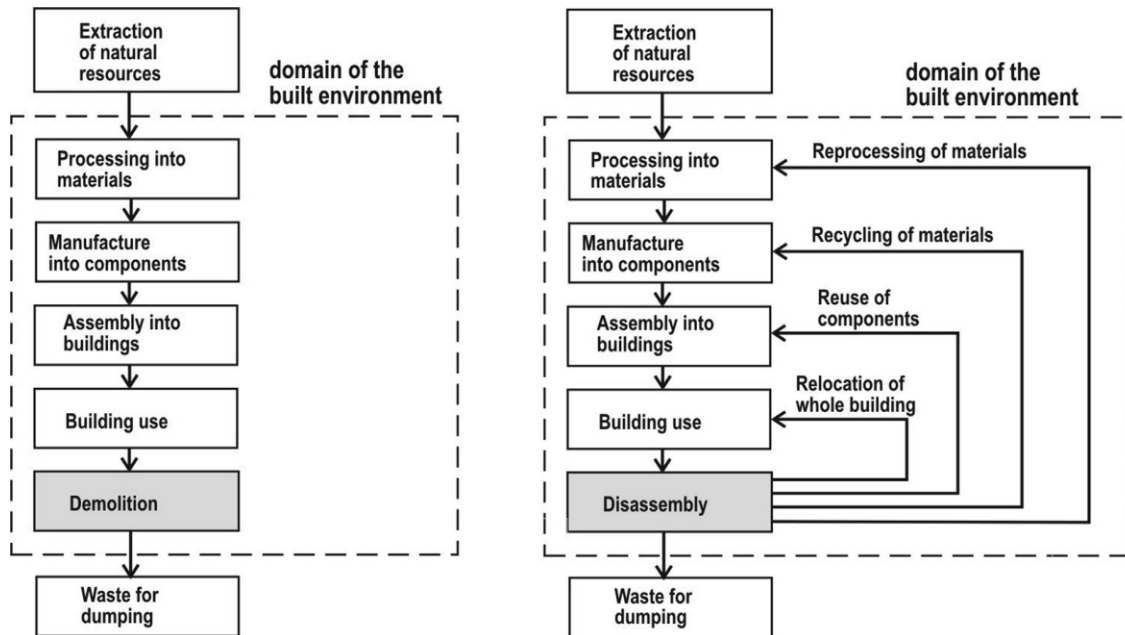


Figure 1 Changing the life cycle from linear to cyclic model through disassembly (source: Crowther, 2005)



Figure 2 Reuse of precast concrete slabs and panels for new housing construction in Mehrow, near Berlin (source: Stacey, 2011)

Moreover, a pragmatic study conducted by Piekko (2022) validated the economic and ecological viability of using reclaimed concrete in new construction. Their research demonstrated that new constructions using reclaimed concrete were less expensive and had a smaller environmental footprint compared to traditional construction methods (Table 1).

Table 1: Results of Demountable Three Different Construction (Source: Piekko, 2022)

Frame Type	Parts and Materials		Processes		New Building	
	Price (Euro)	Carbon footprint KgCo2	Price (Euro)	Carbon footprint KgCo2	Price (Euro)	Carbon footprint KgCo2
Conventional	8,754	5,712	0	0	8,754	5,712
Demountable "Wet"	8,908	5,734	2,235	15	98	179
Demountable "dry"	11,656	5,899	25	0	0	0
<b>As a result, the total prices and carbon footprints are as follows:</b>						
	Total Price (Euro)	Percentage %	Carbon footprint KgCo2	Percentage %		
Conventional	17,508	100	11,424	100		
Demountable "Wet"	11,241	64	5,928	52		
Demountable "dry"	11,681	67	5,899	52		

Components of concrete, such as beams, columns, and slabs, possess the potential for reuse, either for identical applications or for purposes that are similar. For instance, wall panels can be repurposed as fencing or noise barriers around highways proximate to residential zones, as well as walkways, platforms, and other landscaping elements. Concrete slabs could find renewed life as elevated flower beds, highway noise barriers, or fences, while beams and columns could be incorporated into landscapes and fences. Even suitable footings can be repurposed into structures such as retaining walls, dams, and water barriers (Salama, 2017).

Devenes et al. (2022) conducted an innovative study where they constructed a footbridge from 25 repurposed concrete blocks. These were interconnected through post-tensioning to generate a 10-metre span arch. The entire design and construction workflow of the prototype was documented, including sourcing of reusable concrete elements, structural design of the curve, and assembly. The non-destructive investigation, load testing, and Life-Cycle Assessment (LCA) were used to evaluate the mechanical properties and environmental impact of the Re: Crete arch prototype, Figure 3. Findings revealed that the reuse of concrete blocks yielded a structural behaviour analogous to an arch constructed from new or recycled concrete, yet it resulted in an environmental footprint that was more than 70% smaller.



Figure 3 Re:Crete footbridge prototype (source: Devenes et al., 2022)

There are currently few standards that acknowledge the deconstruction and subsequent reuse of structures. One such standard is ISO 20887:2020 (BS EN ISO 20887:2020), which defines reuse as the multiple uses of products or components without reprocessing for the same or different purposes. It excludes the preparation required for reuse, such as cleaning. A reused construction component should be functional in a different structure without the need for substantial repairs or modifications.

The principles of BS EN ISO 20887:2020 are applicable to assemblies and systems within a constructed asset, which can be deconstructed when the asset reaches the end of its lifespan or requires renovation. This allows for components to be repurposed. It is important to note that reusing older structures could be a significant strategy for addressing the current high carbon dioxide emissions and raw material consumption plaguing the construction industry. When construction components are deconstructed and reused, their total value, from both an economic and environmental perspective, is retained. Selling the same components multiple times effectively reduces their carbon footprint. Additionally, reusing these components decreases the need for virgin raw materials and new component production. For future reuse of new construction components to be possible, their connections must be designed for disassembly, in accordance with Design for Deconstruction principles.

Concrete, the predominant construction material, is responsible for significant waste and environmental impact (Crow, 2008). A growing global consensus has begun to view demolition as a design failure (Durmisevic, 2010). One prospective

solution to mitigate concrete waste lies in the conceptualisation of buildings that can be easily disassembled, thus promoting reuse and adaptation (Salama, 2017). Although extensive research has been conducted in this field, there is yet to be a method that facilitates the reuse of specific concrete elements from existing buildings based on their condition and performance to construct new facilities according to the updated design requirements instead of using new raw materials. Thus, it is necessary to devise a comprehensive strategy that allows for the quantification of the benefits of adaptive building reuse via a computational method.

### **3. PRESENTATION OF THE PROPOSED METHODOLOGY**

The proposed methodology utilises Building Information Modelling (BIM) environment to develop a framework for the reuse of precast concrete components in new, sustainable building construction. The main objective is to reclaim precast concrete components from existing buildings and prepare them for reuse in new construction, rather than disposing of them. To achieve this, a BIM framework is developed, and a computer-aided system will seamlessly integrate these reclaimed materials into the new construction project. The framework meticulously evaluates how well these elements align with the new requirements, highlighting the multitude of benefits associated with their reuse.

The challenges of the proposed research are:

1. Absence of previous research that focuses on reutilising individual structural elements and incorporating them into new buildings based on their performance. The bulk of prior research primarily investigates the possibility of reusing entire building components in different locations and functions or the potential for utilising specific portions of the existing building.
2. The lack of an effective automated method to ascertain which components of the existing building can be reused in the new building using a high-quality information model. Present studies often rely on the manual identification of features, which can result in delays, inflated costs, and inaccuracies.
3. Lack of information regarding the remaining structural integrity, physical degradation, or performance of reused components at the end of their life cycle or functional period.

#### **3.1. Proposed Methodology**

The primary function of this system is to evaluate the feasibility of reusing concrete components from existing pre-cast structures in new construction projects. The goal is to lessen dependence on fresh raw materials, enhancing environmental sustainability by reducing waste and lowering carbon emissions typically associated with new construction processes.

To achieve this, the system measures the performance of each precast concrete component, evaluating its current structural integrity and functionality. Factors such as durability, environmental resistance, and stability are considered. The objective is to determine whether the identified components can fulfil the functional requirements of a new design whilst maintaining their inherent performance characteristics.

The process that follows the identification stage involves creating a disassembly plan to assess the disassembly potential of each precast concrete component. This step necessitates an understanding of how a component can be safely removed from its current location without undermining its structural integrity. It is crucial to optimise the disassembly planning process, considering elements such as the type of bonding used, the component's design, and the potential impact of various disassembly techniques. Subsequently, operational costs, including disassembly, cost of components and the environmental impact of these operations, are calculated. All this information is then incorporated into the BIM system, known as the "Supply BIM," which serves as the initial input.

The design teams are then tasked with developing all the building details according to client requirements and needs. This information is entered into a secondary BIM, known as the "Request BIM," which serves as the second input.

To identify matching precast concrete components from the Supply BIM to the Request BIM, a matching function is utilised. This function facilitates the automatic reclaiming of substantial quantities based on size, performance, and other criteria. The Request BIM might require more than one Supply BIM, depending on the matching process. Therefore, this model is designed to minimise time, construction costs, and the expenses of examining the Supply and Request designs by each design team. It also mitigates potential human errors that may arise from manually investigating the cases for each building. Figure (4) illustrates the proposed framework, which comprises three modules as described in detail below:



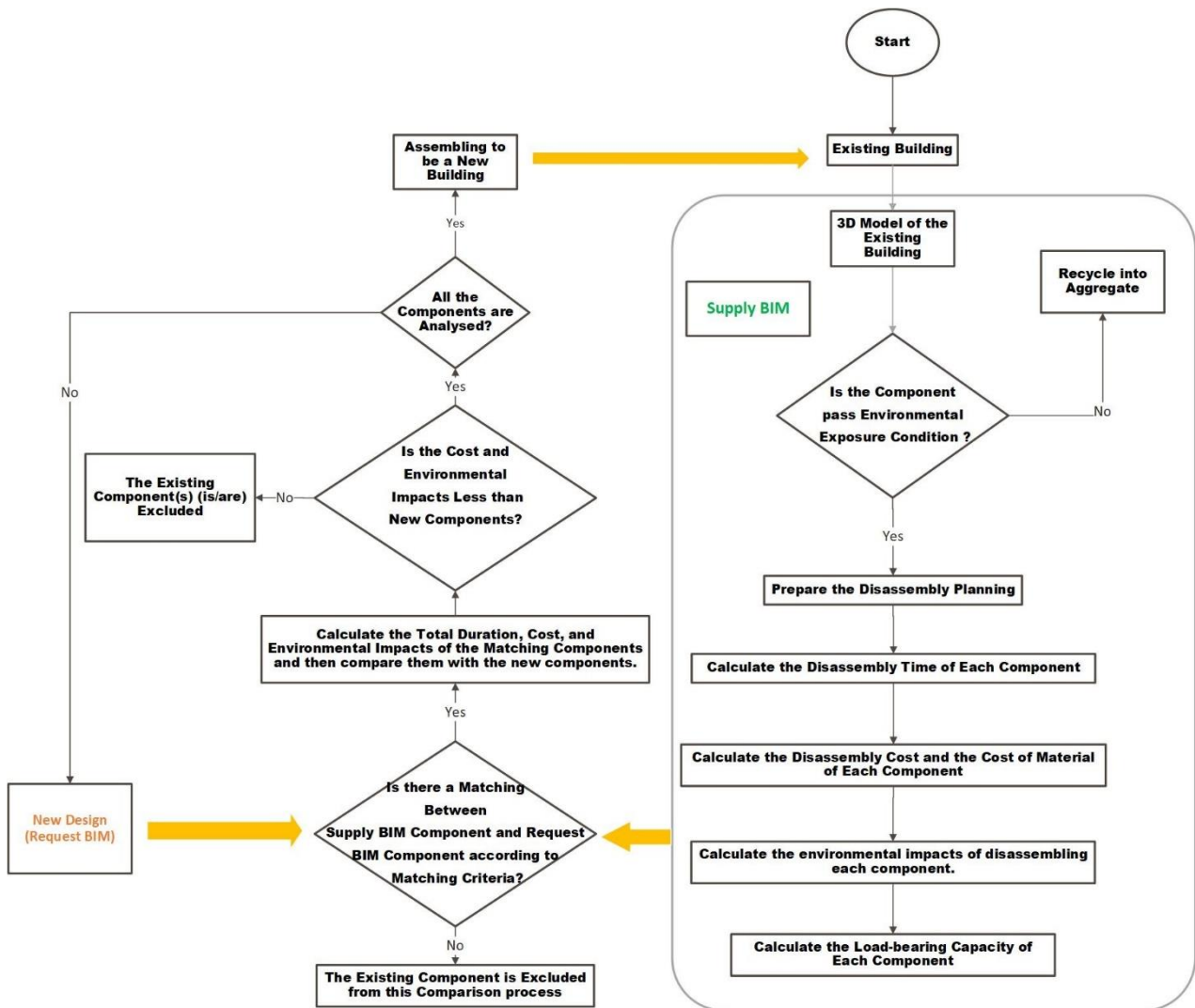


Figure 4 The Proposed BIM-based Reusability Framework

### Module one; Supply BIM

This module aims to redefine the lifecycle of buildings, shifting it from the current linear model to a cyclic one, achieved through the reuse of concrete components. This approach aligns with the principles of a circular economy, contributing to more sustainable and efficient resource utilisation, which is increasingly becoming a necessity in the contemporary construction industry.

The initial stage of this proposed process involves inspecting each concrete component for its condition (e.g., corroded reinforcement, cracking) and structural capacity (e.g., flexural capacity). One method used in these inspections is Non-destructive testing (NDT). NDT techniques such as ultrasound, radiography, or ground-penetrating radar can provide valuable insights into the health of the components, detecting any latent defects or degradation without causing further harm to the components (Spears and Taheri, 2023). If the component meets the requisite criteria for structural integrity and safety, it is deemed suitable for reuse in another construction project. Conversely, components that fail to meet these standards must be responsibly discarded or repurposed.

The subsequent stage of this proposed process entails a detailed planning phase for the disassembly of the building. This step, one of great importance, necessitates a careful and systematic deconstruction process. The objective is to prevent unnecessary damage to the concrete components, requiring precision and attention to detail. Avoiding such damage is crucial, as it could potentially compromise the integrity of these components, causing them unsuitable for future reuse, a consideration of ultimate significance in our aim to promote sustainability. Thus, this phase demands a comprehensive understanding of the building's structural interrelationships, each playing its unique role in maintaining the stability of the structure. Furthermore, knowledge of component properties is important, as the characteristics of each type of component determine its suitability for reuse. Connection methods, too, need to be thoroughly understood, as their improper handling can lead to irrevocable damage. Overall, this process stage is a delicate balance of precision, knowledge, and execution, aiming to preserve the reusability of as many building components as possible.

The assessment and quantification of disassembly time in deconstruction processes are critical for optimising efficiency and resource allocation and for minimising disruptions. This consideration extends beyond the physical act of deconstruction to include the planning, coordination, and preparation phases, as well as contingencies. Accurate estimations of disassembly time are paramount to avoid increased costs and project delays. A comprehensive analysis of each component within the deconstruction operation can provide insights into the overall time requirements for the project. This enables better resource allocation and strategy development. For instance, understanding these time frames can aid in scheduling activities during off-peak hours to minimise disturbances in urban areas. The evaluation and quantification of disassembly time provide valuable data for decision-making in resource management and the development of disassembly strategies.

Following this often referred to as the cost component, a detailed and nuanced financial evaluation is carried out. This process essentially aims to quantify the economic implications of disassembling the building, including each individual component that constitutes the structure. In the study, each precast concrete component, such as slabs, beams, and columns, is identified, and the cost of each component is then estimated. The cost to disassemble each of these components is also calculated. These costs encompass various factors such as labour, the equipment needed for the disassembly, transportation of the salvaged material, and any potential repair or refurbishment costs required to make the reclaimed materials usable again. After the individual cost of each component has been estimated, these costs are then summed up to determine the total cost of disassembly. This provides an overall financial estimate of the disassembly process. This financial assessment serves a dual purpose. On one hand, it helps stakeholders understand the magnitude of the financial commitment required for the disassembly process. On the other hand, it provides a basis to evaluate the economic viability of this approach. A comparative analysis is then conducted between this approach and traditional methods of constructing new buildings. Material sourcing costs under conventional construction, which involve procuring new materials and their transportation, are compared with the costs of reusing reclaimed materials. This comparison offers a holistic view of the economic feasibility of the reclamation process. If the cost of disassembly and reuse is less than or comparable to traditional methods and offers benefits of sustainability or other strategic advantages, the reclamation process can be considered economically viable.

Life Cycle Assessment (LCA) is a systematic method used to assess the environmental impacts of a product, service, or system throughout its life cycle (ISO 14040:2006). In the context of the BIM framework, it's often considered the mainstay of its sustainability dimension. An LCA offers an in-depth analysis of the environmental pros and cons related to the execution of a proposed cyclic building lifecycle. This analysis involves examining all the stages of a building's life, from its inception, construction, use, and maintenance, to its end of life, including decommissioning, deconstruction, and eventual disposal or recycling (ISO 14040:2006). However, for the specific investigation described in this study, the LCA begins with the deconstruction phase of the building, which includes carefully dismantling the building to salvage components for reuse. The energy usage, greenhouse gas emissions, and other environmental impacts associated with this phase are meticulously accounted for in the LCA. The LCA continues with other phases of the building's life cycle, such as the processes involved in preparing the components for reuse, transportation of these components, and the environmental impacts associated with these processes. The final phase in this LCA is the reconstitution of the building's subsequent lifecycle. Here, the salvaged components from the deconstruction phase are used to construct a new building or to refurbish an existing one. The energy required for this phase, the emissions produced, and any potential environmental benefits derived from the reuse of materials are thoroughly analysed and recorded in the LCA. The ultimate goal of an LCA in this context is to provide insights into the environmental impacts of a building's life cycle. This information is instrumental in the design and construction processes, enabling architects, engineers, and other stakeholders to make informed decisions to reuse these components again or use new components that can minimise the environmental footprint of buildings.

### *Module two; Request BIM*

In this stage of the process, the construction and design team engage in the critical task of translating the client's specifications into a coherent set of guidelines for the building construction. This phase is marked by a systematic approach that combines both established methods and significant considerations based on the unique aspects of each project.

The first step is to identify the needs and requirements of the client. This includes understanding the client's vision, goals, and practical needs for the building, taking into account factors such as the intended use of the building, target population, location, environmental conditions, budget, and timeframe. The team must gather, interpret, and confirm this information with the client to ensure alignment and prevent any miscommunication that could impact the project's success (Kamara et al., 2000).

Following this, the team embarks on the concept design stage. This is a creative phase where architects and designers formulate preliminary design solutions that fulfil the client's needs and requirements while adhering to regulatory constraints. The concept design usually involves creating sketches, drawings, and 3D models that visually represent the proposed building design. It is crucial at this point that the team effectively communicates these design ideas to the client for feedback and validation. Upon the completion of these stages, these detailed requirements are then integrated into the BIM system (Sarja, 2002).

The primary objective of this module is to act as a key input in the comparative analysis of BIM requests. This comparative process uses a variety of matching criteria to ensure accurate and useful comparisons. These criteria encompass a range of attributes, such as the geometric characteristics of the building design and its load-bearing capacity, along with a host



of other factors that are crucial in architectural modelling and construction planning. Request BIM plays a pivotal role in supporting the main function of the system, details of which will be elaborated in the subsequent section. This ensures an integrated and comprehensive approach to BIM request evaluation and management.

### *Module Three; The main function*

The third stage of this study involves identifying the desired functionality and architecture of a proposed method. Central to our proposed framework is the BIM-Based reusability concept.

To achieve this, two types of BIM are required: a 'Supply' BIM for existing buildings, which contains information relating to the existing precast concrete components, and a 'Request' BIM, which includes component reuse information for the second lifecycle (Yeoh et al., 2018). These were explained in the first and second modules, respectively. Components derived from the Supply BIM are incorporated into the process in a manner similar to those from the Request BIM. The process subsequently attempts to find a match between each existing component and the new design component based on specific matching criteria such as design life, load-bearing capacity, and geometry. If a component from the Request BIM satisfies all these criteria, it advances to the next stage.

At this stage, if both the cost and the environmental impact of the reused component are less than those of a new component, the process will select this component for assembly in the new building.

To develop this process, a sophisticated solution that harnesses the synergy of programming and technology is planned. Specifically, a computer-aided system using Autodesk Revit, a leading software in the architecture, engineering, and construction industry known for its BIM capabilities, is to be developed.

The deployment of Python, one of the most versatile and widely used programming languages, will be implemented in this endeavour. Python's extensive libraries and clear, readable syntax make it an ideal choice for such a project. With Python's integration into Revit, the automation of routine tasks, customisation of features, and innovation of new workflows are made possible.

By doing so, the efficiency, accuracy, and productivity of the work conducted within Revit are expected to be enhanced, thereby achieving the primary objective of this study.

## **4. CONCLUSION**

Concrete serves as a pivotal element within the construction sector, albeit with substantial environmental impact due to the generation of considerable waste. Addressing this issue calls for the exploration of innovative alternatives to the employment of raw materials. A potential solution lies in the utilisation of pre-existing building structure components.

Indeed, existing models and methodologies are in place that promote the recycling of concrete through the demonstration of its utility in design for deconstruction. However, no existing frameworks propose the use of concrete elements derived from the existing building in alignment with fresh design necessities. If the performance of the structure has been altered, the question then arises: where should these components find new applications, and how can we systematically gather these elements without additional costs, time burdens, or errors?

This study aims to bridge these gaps, developing a framework based on BIM tools. With the creation of this framework, designers will be equipped with a tool that substantially contributes to sustainability goals. This approach curtails dependence on virgin materials, consequently reducing the environmental impact tied to the extraction and transportation of new materials. Furthermore, it prevents the unnecessary disposal of valuable materials into landfills, promoting their potential repurposing.

The Framework consists of two input data, the process, and the output. The first input is the details of end-of-service life buildings needed to transform into a resource for constructing a new building. For each component, three requirements are required to intuitively introduce the features' performance, identification, and disassembly sequence. a BIM model with these requirements is used that helps the existing disassemble buildings at the end of their life cycle or the function to provide the fundamental requirements for reusing again; this BIM will call (Supply BIM).

The result will be a BIM containing a portfolio, structure performance and information relating to the existing building components. The design teams should develop all the building details according to the requirements and client needs. All this information will enrol to another BIM called (Request BIM), which represents the second input. To collect the matching concrete parts from Supply BIM to the Request BIM, a BIM-Based framework that supports automatically reclaiming substantial amounts according to size, performance, and other requirements is used.

The proposed framework will be developed into a computer-aided program. It will serve as an integrative plug-in for BIM software within Revit, all of which will be facilitated through the versatile medium of Python. This framework's adoption promises not only environmental benefits but also significant time and cost efficiencies, lowering expenses and time commitments related to acquiring raw materials, equipment, labour, and more. It also optimises expenditure associated with landfill taxes and needless transport.

However, a common preference among clients leans towards the inclusion of new elements within their buildings. Hence, prior to employing this framework, designers must effectively communicate the advantages of this approach to clients, ensuring that the end result will align with the outcomes achievable using raw materials. Additionally, it is vital for the designer to verify that the buildings chosen for reuse are able to disassemble.

## 5. ACKNOWLEDGEMENT

The authors would like to acknowledge the financial support provided by The Higher Committee for Education Development in Iraq (HCED) in the production of this work.

## 6. REFERENCES

- Akinade, O., Oyedele, L., Oyedele, A., Davila Delgado, J.M., Bilal, M., Akanbi, L., Ajayi, A. and Owolabi, H., 2020. Design for deconstruction using a circular economy approach: Barriers and strategies for improvement. *Production Planning & Control*, 31(10), pp.829-840. Available at: <https://doi.org/10.1080/09537287.2019.1695006>.
- BS EN ISO 20887:2020. Sustainability in buildings and civil engineering works — Design for disassembly and adaptability — Principles, requirements and guidance.
- Cabeza, L.F., Barreneche, C., Miró, L., Morera, J.M., Bartolí, E. and Fernández, A.I., 2013. Low carbon and low embodied energy materials in buildings: A review. *Renewable and Sustainable Energy Reviews*, 23, pp.536-542. Available at: <http://dx.doi.org/10.1016/j.rser.2013.03.017>.
- Catalli, V., 2009. Design for Disassembly: Early planning means an economic afterlife for buildings. *Sustainable Architecture and Building Magazine*, 27, pp.41-46. Available at: <http://www.sabmagazine.com/blog/2009/10/27/design-for-disassembly/>.
- Crow, J.M., 2008. The concrete conundrum. *Chemistry World*, 5(3), pp.62-66.
- Crowther, P., 2005. Design for disassembly—themes and principles. *Environment design guide*, pp.1-7.
- Devenes, J., Brütting, J., Küpfer, C., Bastien-Masse, M. and Fivet, C., 2022b, September. Re: Crete—Reuse of concrete blocks from cast-in-place building to arch footbridge. In *Structures* (Vol. 43, pp. 1854-1867). Elsevier. Available at: <https://doi.org/10.1016/j.istruc.2022.07.012>.
- Durmisevic, E., 2010. Green Design and Assembly of Buildings and Systems: Design for Disassembly a Key to Life Cycle Design of Buildings and Building Products. VDM Verlag Dr. Muller Aktiengesellschaft & Co. KG, Saarbrücken (Germany).
- European Commission, 2020, A New Circular Economy Action Plan; EUR-Lex COM/2020/98; European Commission: Brussels, Belgium.
- GCB, 2020, Zero Avoidable Waste in Construction: What do we mean by it and how best to interpret it. The Construction Products Association.
- Kamara, J.M., Anumba, C.J. and Evbuomwan, N.F.O., 2000. Establishing and processing client requirements—a key aspect of concurrent engineering in construction. *Engineering, Construction and Architectural Management*, 7(1), pp.15-28.
- Norouzi, M., Chàfer, M., Cabeza, L.F., Jiménez, L. and Boer, D., 2021. Circular economy in the building and construction sector: A scientific evolution analysis. *Journal of Building Engineering*, 44, p.102704. Available at: <https://doi.org/10.1016/j.jobbe.2021.102704>.
- Pieeko, 2022, White paper. Dismount and Reuse of Precast Concrete Frame. Available at: <https://www.peikko.com/news-events-media/magazines/white-papers/>
- Salama, W., 2017. Design of concrete buildings for disassembly: An explorative review. *International Journal of Sustainable Built Environment*, 6(2), pp.617-635. Elsevier B.V. Available at: <https://doi.org/10.1016/j.ijsbe.2017.03.005>.
- Salama, W., 2019. Design for disassembly as an alternative sustainable construction approach to life-cycle-design of concrete buildings. PhD Thesis. Leibniz University Hanover.
- Sarja, A., 2002. Integrated life cycle design of structures. CRC Press.
- Spears, M., Hedjazi, S. and Taheri, H., 2023. Ground penetrating radar applications and implementations in civil construction. *Journal of Structural Integrity and Maintenance*, 8(1), pp.36-49.
- Stacey, M., 2011. Concrete: a studio design guide. RIBA, London.
- Van den Berg, M., Voordijk, H. and Adriaanse, A., 2021. BIM uses for deconstruction: An activity-theoretical perspective on reorganising end-of-life practices. *Construction Management and Economics*, 39(4), pp.323-339. Available at: <https://doi.org/10.1080/01446193.2021.1876894>.
- Yeoh, J.K., Lee, S.L. and Ong, K.C.G., 2018. Development of a BIM-Based Framework to Support the Analysis of “Design-for-Disassembly” Strategies. In *Construction Research Congress 2018* (pp. 759-768).

---

## #251: The role of the informal sector towards sustainable waste management practices in developing countries: Case study in Jordan

---

Husam ABU HAJAR<sup>1</sup>, Ola AL-MAHASNEH<sup>2</sup>

*1 Civil Engineering Department, School of Engineering, The University of Jordan, Amman, 11942, Jordan, h.abuhajar@ju.edu.jo*

*2 Civil Engineering Department, School of Engineering, The University of Jordan, Amman, 11942, Jordan, olamahasneh@hotmail.com*

*Abstract: Waste management is a growing environmental concern worldwide due to its carbon footprint as well as the rising waste quantities coupled with the increasing global population. Waste management is particularly challenging in developing countries due to the inadequacy of waste collection and disposal practices. This study aims to characterize and investigate the role of the informal recycling sector in Jordan from technical, economic, and social perspectives. Informal recycling plays a vital role in Jordan's waste management sector; however, recent strategies have discussed eliminating or regulating this sector under the government's umbrella. Several interviews were conducted with government officials and workers in the informal recycling sector in Jordan, and it was concluded that recycling in Jordan does not exceed 10%, which is mainly attributed to informal recycling. It was also inferred that informal scavengers typically belong to socially marginalized groups in Jordan, and they experience harsh socioeconomic conditions because of this profession. Informal recycling workers also expressed their concerns towards the governmental plans to regulate their profession; as this may increase the financial burdens associated with taxing and social security.*

*Keywords: Informal recycling, Waste management, Sustainable development, Developing countries*

## 1. INTRODUCTION

Solid waste management is a growing concern worldwide due to the continuous rise in the global waste production. High per capita waste production rates are often witnessed in developed countries; however, such rates have been stable over recent years and are anticipated to decrease as a result of the effective implementation of recycling and recovery schemes in some countries. On the other hand, solid waste production is expected to keep rising in developing countries and it is speculated that the 2025 waste production in lower and middle income countries will be 38 – 67% greater than the 2016 figures. The gap between developed and developing countries in the context of solid waste management is obvious as developing countries struggle against technical and financial difficulties which prevents the adoption of sustainable practices (Abu Hajar & Abu Hajar, 2023; Abu Hajar et al., 2021; Lim et al., 2016). The solid waste management dilemma is complicated in developing countries where urbanization is rapid and resources are limited (Ahmed & Ali, 2004). This sector is often poorly operated and the services provided are usually inadequate and unreliable. Collection services in developing countries cover 50 – 80% in the cities, and the predominant waste management scheme is open disposal which lacks the minimum sanitary standards for the protection of the environment and ecosystems; hence, solid waste in developing countries is more readily available to informal scavengers whether in the streets or disposal sites (Lim et al., 2016; Wilson et al., 2006).

The informal recycling sector is an unregulated, labor-intensive, and low-technology sector which comprises waste picking and scavenging activities carried out by poor and marginalized individuals or family groups along the different stages of the waste management hierarchy. The purpose of such activities is to recover reusable and recyclable materials from the commingled waste stream. Workers in this sector often do not pay taxes, are not covered by governmental insurance programs, and have no trading licenses (Ahmed & Ali, 2004; Salau et al., 2017; Wilson et al., 2006). The informal sector is significant in low-income and developing countries due to poverty, unemployment, and underemployment (Ahmed & Ali, 2004). This sector brings social benefits by creating job opportunities for the poor and marginalized groups. According to previous studies, the livelihood of nearly 15 million people in developing countries is directly associated with informal recycling activities (Medina, 2008; Salau et al., 2017; Wilson et al., 2006). The informal recycling sector is a key player in developing countries which accounts for roughly 15-35% of waste collection (Salau et al., 2017). The structure and organization of the informal recycling sector begins with secondary materials being collected by pickers. These materials are sold locally to craftsmen and local industries through a chain of intermediate dealers (middlemen). The intermediate dealers can be formal and informal and can exist in different forms such as intermediate processors, junk shops, brokers and wholesalers. According to this organization, the pickers and scavengers exist at the bottom of this trade hierarchy making them the most vulnerable and economically stressed group (Wilson et al., 2006).

There are numerous challenges and difficulties facing the scavengers. Scavenging is often a family organized activity which results in the involvement and exposure of vulnerable groups including women, children, and the elderly to significant health risks. Industries often require large quantities of processed, baled, or granulated materials, and due to the lack of organized networks and the limited storage capacity, scavengers cannot sell directly to the industry leaving them easily exploited by the intermediate dealers. This is particularly true for those working in disposal sites which makes the transport of the recovered materials to the city a costly process. The profit margin for the middlemen is considerably higher than the scavengers' wages. Therefore, dodging the intermediate dealers and providing legitimate markets for recyclables will significantly increase the scavengers' income and enhance their social acceptance (Medina, 2008; Wilson et al., 2006). Another major challenge facing the informal sector in general and female scavengers in particular is the harassment by authorities, police, and the community; due to the fact that workers in this sector are from marginalized groups who are pushed to this type of work due to their harsh economic conditions and are often viewed as a lower unhygienic class (Medina, 2008; Wilson et al., 2006). Nevertheless, developing countries have recognized the importance of the informal recycling sector and the socioeconomic and environmental benefits this sector brings to the waste management services. This recognition has stimulated local, national, or international nongovernmental organizations (NGOs) to put pressure on the public authorities to shift their policies and legislation towards providing more support for those groups, enhancing their working conditions, and integrating the informal sector with the formal waste management system (Ahmed & Ali, 2004; Medina, 2008; Tilaye & Van Dijk, 2014; Wilson et al., 2006).

Jordan is a developing Middle Eastern country with limited natural resources and ambitious environmental protection goals. Jordan has ratified most recent international agreements and accords with the aim to mitigate the global greenhouse gas (GHG) emissions. Waste management sector in Jordan has evolved significantly over the past few decades in terms of collection and disposal. More than half of the country's solid waste is sanitary landfilled, while recycling accounts for less than 10% and is mostly undertaken by the informal sector. Regardless of the technological advancements, the informal sector is still and will remain a key player in the waste management sector in Jordan (Abu Hajar et al., 2021). This study aims to investigate the current situation of the informal waste sector in Jordan, and to highlight the key socio-economic challenges facing this sector. Several semi-structured interviews were conducted with governmental officials as well as workers from the field to identify the mechanism and structure of waste scavenging in Jordan, and to pinpoint the key socio-economic and technical challenges facing workers in this sector. Finally, recommendations for improving the working conditions and inclusion of the informal recycling activities under the official waste management sector were provided.

## 2. DATA AND METHODS

In this study, a systematic literature review was conducted to collect data and information on the waste management sector in Jordan in general and the informal recycling activities in particular. Reports by the Ministry of Environment (MoEnv), Department of Statistics (DOS), Greater Amman Municipality (GAM), and other relevant documents and published papers were thoroughly reviewed. Interviews were carried out with different governmental officials from the MoEnv, GAM, etc., to identify the key informants pertaining to the research topic, and to establish connections with landfill and disposal sites administrations to facilitate access for site visits and data collection. These interviews were also helpful in identifying the general hierarchy and structure of the informal sector, and the nature of relationship between the government and waste scavengers.

Site visits were carried out at Al-Humra disposal site (Al-Balqa Governorate), Al-Ghabawi landfill site (Amman Governorate), and Al-Baqa'a market for scraps-recycling (Al-Balqa Governorate) as shown in Figure 1. Al-Humrah disposal site is located nearly 40 km to the north west of the capital Amman. It has an area of 280,000 m<sup>2</sup> and it receives waste from 5 municipalities which are: Al-Salt, Ain Albasha, Al-Arda, Al-Fuhais, and Mahis. The total served population is nearly 750,000 individuals, and the total incoming daily waste ranges from 250-300 tons. This site is operated by the joint services council (JSC) of Al-Balqa Governorate. Al-Ghabawi is the largest landfill in Jordan which receives waste primarily from Amman and Zarqa Governorates. This sanitary landfill was established in 2003 to the east of the capital Amman and is operated and managed by GAM (Abu Hajar et al., 2021; Al-Mahasneh, 2020). Al-Baqa'a market is a well-known location for scrap dealers and workshops which is located in Al-Balqa governorate. The purpose of these site visits was to observe and inspect the informal recycling activities at the different stages.

Semi-structured interviews were then conducted to collect data from officials who are directly involved in the waste management activities as well as the scavengers and informal recyclers from the different study locations. The questions were prepared to cover a wide array of socioeconomic and demographic aspects related to the informal recycling industry. Examples of data collected included age, marital status, education, monthly income of workers in this field, recovered daily waste quantities and categories, destination of collected waste, past work experiences, informal recyclers present and future, economics of waste management at the facility or disposal site, limitations facing the operation in the facility, and the public perceptions and attitudes towards the workers in the informal sector. Some of the interviews (especially with workshop owners and scrap dealers) were carried out via phone due to the difficulty of face-to-face interviews. A non-probabilistic sampling was applied to interview as many workers in this sector as possible (the sample size in our study was 43 which included 18 people in Al-Humrah disposal site, and 25 scrap dealers and itinerary pickers), and the collected data were analysed qualitatively and quantitatively.

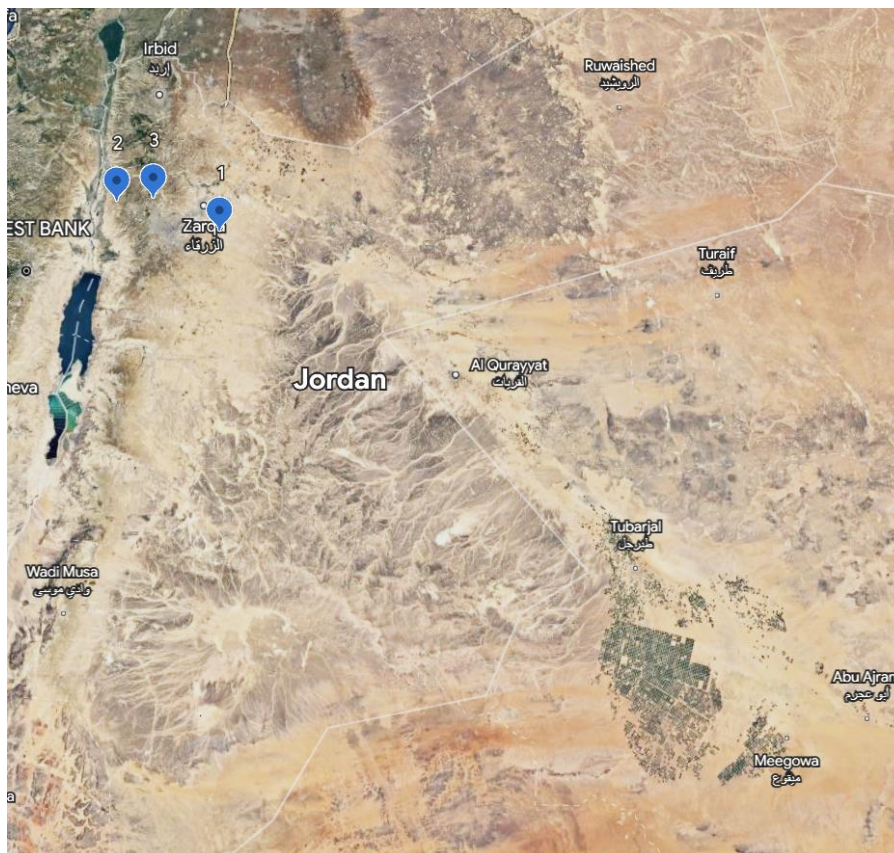


Figure 1 Study locations (1: Al-Ghabawi Sanitary Landfill; 2: Al-Humra Disposal Site; 3: Al-Baqa'a Market). Source: Google Earth, 2023



### 3. RESULTS AND DISCUSSION

#### 3.1. Landfill and disposal sites scavengers

In Jordan, nearly 50% of the solid waste is disposed in Al-Ghabawi Sanitary Landfill. During the site visit to Al-Ghabawi, there were some restrictions with respect to photography. According to the interviews with the landfill officials, informal scavenging activities are no longer permitted at this location due to security and safety considerations. Informal scavenging at Al-Ghabawi has caused serious conflicts in the past between the competing groups at the landfill. Informal scavenging has interfered with the daily activities at the landfill besides reported thefts of pipes and fabrics. Therefore, GAM has banned all recycling and scavenging activities at Al-Ghabawi Landfill since 2014. In fact, this location is currently secured by a police station to ensure that only personnel and authorized visitors are permitted to enter the landfill. Regardless, informal waste recycling activities exist in Amman and Zarqa governorates through a network of street pickers and waste dealers (Abu Hajar et al., 2021).

The other site investigation was carried out at Al-Humra Disposal Site, which is operated by Al-Balqa JSC, and is run by nearly 40 employees. This site is equipped with different heavy machinery such as loaders, bulldozers, and tractors to carry out the regular activities. The design of this disposal site, unlike Al-Ghabawi Landfill, is not according to sanitary landfilling standards, such that no gas recovery or leachate collection systems exist. The informal recycling activities are clearly present at Al-Humra location (Figure 2), where such activities are undertaken by a group of nearly 50 workers who are affiliated (informally) with a contractor. Nearly half of the scavengers at this site are children (below the age of 18) while the other half comprises males and females at approximately equal ratio. The researchers were able to interview 18 workers, nearly two thirds were in the 30-50 years age group. Only one interviewee was 70 years of age, who is a woman living and working at this location along with her children and grandchildren. Most of the interviewed scavengers are married and live along with their spouses and possibly other family members. The majority of the workers at this location are either illiterate or have dropped out of school prior to secondary education. Only one interviewee reported that he has successfully finished high school but with no further education. Children at this location are forced to drop out of school to accompany their families.



*Figure 2 Informal recycling activities at Al-Humra Disposal Site*

The typical work day at Al-Humra extends from sunrise to sunset, and scavengers start their day by digging into the waste piles to separate and collect different waste categories. The separated waste is then piled at different spots and dragged manually to the weighing scale. The contractor buys the separated waste from the workers, and then transfers the waste

via a small truck to Sahab Industrial City (to the east of the capital Amman). There is an agreement between the JSC and the contractor on the amount of time allocated for scavenging, so a truck load is often disposed onto a wide area where workers are given sufficient time to recover materials from the waste load. By the end of the day, the load is moved into the designated disposal location and covered with a thin layer of soil. Despite the competing interests among scavengers, there are minor problems or conflicts and each one typically works independently. The daily productivity varies based on age difference and experience, but the typical values range from 70 to 150 kg per person per day, and on average, one worker can collect 100 kg of recyclables per day. The average amount of waste recovered and transported out of this location is 3 tons per day, which typically includes plastic, mixed metal, nylon plastic, bread and legumes (often sold to herdsman), and other materials (copper, electric waste, etc.), as shown in Figure 3.

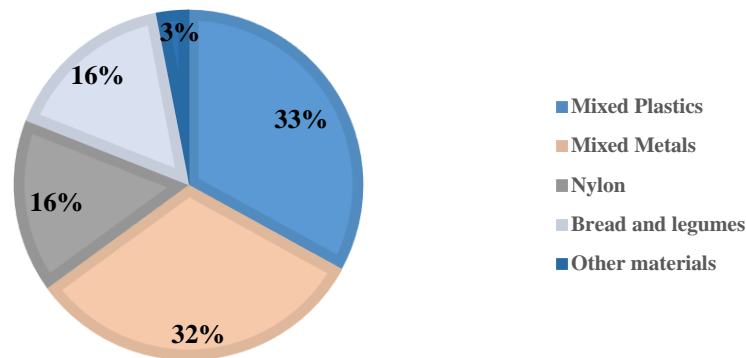


Figure 3 Categories of waste materials recovered from Al-Humra Disposal Site

Despite the fact that nearly 50% of the recyclables at this disposal site are paper and cardboard, these categories are no longer desirable in the remanufacturing industry. Hence, it is not feasible to collect and recycle paper and cardboard. In terms of income, those workers are paid based on the daily quantities they bring to the contractor, and the contractor pays the workers 5 JDs per 100 kg recyclables; thus, the average monthly income is JD 140 – 150 per worker. Nearly 85% of the workers live along with their families in tents at the disposal site location, while others live in different regions outside Al-Humra and travel daily to the disposal site. Scavengers often get their basic needs supply from the contractor in exchange for money but sometimes end up consuming food left-overs from the waste at the disposal site. Water is supplied to the scavengers by Al-Balqa JSC.

The interview questions covered several aspects related to the scavengers and the informal recycling profession in general. Two thirds of the interviewees reported that their only experience is in waste scavenging, which ranges from few months to more than 15 years. Other workers in this field were forced to switch careers and become scavengers due to the lack of opportunities and the fierce competition in other more rewarding professions (e.g. construction) where the more skilful labour is predominant, unlike waste scavenging which requires little to no qualifications or prior experience. Few of the interviewed workers believe that waste scavenging is a good profession which is indeed better compared to their previous work experiences, while others expressed their desire to change career if they find better opportunities. Therefore, it was deduced that most scavengers are satisfied with this profession, and are not seeking other opportunities; which can be attributed to the fact that scavenging at the disposal site is a regular job with a guaranteed daily income as opposed to other irregular job opportunities.

In terms of health and personal protection, only 17% stated that they use personal protective tools during waste scavenging such as gloves, which are often recovered from the piled waste at the disposal site. Although gloves are meant to provide protection, gloves recovered from wasted materials might originate from facilities with hazardous substances which is dangerous. Regarding health risks, most interviewees expressed their concerns because of the extreme hot and cold weather conditions, exposure to hazardous materials (e.g. broken glass, syringes, and chemicals), potential fires, cuts, and long-term injuries such as back pain. The lack of health insurance or the inability to pay for healthcare was one of the major challenges facing the scavengers given the high health risks associated with their jobs. On the other hand, scavengers expressed their fear of the unknown future due to the lack of social security. Any work-related injury will not be covered or compensated especially if such injury leaves them disabled or incapacitated. Another major challenge facing the informal scavengers is the low income which is far below the minimum wage according to the Jordanian Ministry of Labor. Perhaps the most serious challenge which was addressed by all interviewed workers was the poor housing conditions; as most scavengers live in tents at the disposal site making them vulnerable to extreme weather conditions (heat waves, storms, and floods). Hence, enhancing the socioeconomic conditions of the informal waste sector begins with providing suitable housing with electricity, water and sewer connections, in addition to social security and health insurance inclusion.

### 3.2. Scrap dealers

A total of 25 scrap dealers were interviewed, most of them via phone while only six were interviewed in-person. These interviewees were all males, 25-53 years of age, who mostly live in Amman and Zarqa due to the high economic activities

in these densely populated governorates. Some of the interviewed workers were willing to share information and details about their profession, and highlight the challenges facing their daily routine, while others were sceptical and shared very little details. Similar to waste scavenging, scrap dealing as a profession is often undermined by Jordanians despite the relatively high yield compared to other jobs and professions. The level of education varied among the interviewees; some had no educational background, while others had diploma or even bachelor's degree. Scrap dealing is also a family business which is carried out with relatives and acquaintances. This profession is highly dependent on the demand; thus, income varies significantly. Some interviewees reported that this is not their only profession, and that their net daily income of scrap dealing is JD 10 – 20, while others indicated that they make good income without revealing the actual figures. The amount of waste recovered and collected daily is highly variable, which could be as low as 100 kg but can reach up to 2 tons per day. Due to the lack of storage space, scrap dealers often sell to workshops who in turn have large storage spaces, and then the waste is sold by workshop owners to local factories or exported to other manufacturers abroad. Most of the workshops are located in Amman such as Al-Rajeeb, Wadi Al Qamar, and Marka. Scrap dealers who own shops, trucks, and storage spaces report that they have the capability of collecting up to 10 tons per day. Generally, materials are dismantled and processed at local manufacturers, while metals (e.g. iron, aluminium, and copper) are sold to local factories for remanufacturing or exported through three main export companies.

It was inferred based on the interviews that income earned by scrap dealing declined over recent years due to a variety of political and economic reasons such as the decline in oil prices, covid-19 pandemic, and the conflicts in neighbouring countries which affected the cross-boundary transport of different waste categories. In general, scrap dealers expressed more satisfaction compared to scavengers in landfills and disposal sites, which can be attributed to the simple and inexpensive scope and fast yield. For instance, one of the interviewees reported that he switched career from a blacksmith to a scrap dealer due to the decline of income in his former profession. On the other hand, nearly two thirds explained that they are limited to scrap dealing due to the lack of qualifications and education for other job opportunities. Thus, it was concluded that the majority of workers in this field do not intend to abandon this profession and seek other opportunities. It was also indicated that connections with enterprises is vital to ensure the regularity in the scrap dealing business. In fact, some of the most successful scrap dealers emphasized that random scavenging will likely lead to failure. Scrap dealers who reported working randomly by driving in the streets and calling residents through megaphones for unwanted recyclables often face trouble with authorities in addition to making very little income. Instead, scrap dealers need to focus on construction projects, factories, companies, or even residential areas with large waste quantities to maximize their yield and lower the operating expenses. Advertisements through e-commerce websites is also another approach to facilitate scrap dealing and enhance the economic return of this profession.

As for the health risks, 45% of the interviewees reported minor risks (cuts and injuries) which can be avoided if proper safety measures were applied. Nonetheless, there are several socio-economic risks associated with this profession such as recovering stolen items. This is due to the fact that informal recycling in general is an attractive profession for many outlaws; therefore, scrap dealers are often inspected or even harassed by authorities, particularly if working in high-end regions of the capital Amman; due to the stereotypical image and the premise that they collect stolen items. Nearly half of the interviewees reported that they do not possess health insurance or social security, while others pointed out that they have either social security, health insurance, or both from other jobs.

A summary of the key challenges facing the informal sector in Jordan is presented in Table 1.

*Table 1: Key challenges facing the informal recycling sector in Jordan.*

Scavengers at the disposal sites	Scrap dealers
<ul style="list-style-type: none"> <li>• Low income.</li> <li>• Lack of social security.</li> <li>• Lack of health insurance.</li> <li>• Social stigma.</li> <li>• Lack of proper housing.</li> <li>• Health risks (injuries, extreme weather).</li> <li>• Uncertain future.</li> </ul>	<ul style="list-style-type: none"> <li>• Vulnerable business and variable demand.</li> <li>• Social stigma.</li> <li>• Harassment by authorities.</li> <li>• Minor health risks.</li> <li>• Lower profit margins if operating on a small-scale.</li> </ul>

### 3.3. Integration of the informal sector

Despite the low recycling rates in Jordan, most recycling is undertaken by the informal recycling sector. As a result, it is vital to include the informal sector in future waste management strategies in Jordan in order to attain the sustainable development goals in this sector. The first step would be a paradigm shift in the public authorities and communities' perception towards those social groups to be viewed as part of the solution rather than a problem. The informal recycling should be recognized by the governments as an occupation and waste pickers should be considered as key stakeholders in the waste management sector. The economic conditions need to be enhanced by intervening in the informal sector hierarchy and improving market access of the informal pickers as well as establishing successful public-private partnerships (PPPs). These partnerships will be ideal in offsetting some of the budget-intensive collection costs. Such partnerships combine the dynamism, entrepreneurial spirit, technological advancements, and efficiency of the private sector with the social and environmental concerns of the public sector. Nonetheless, these arrangements should be investigated carefully to avoid potential conflicts with the formal sector activities such as the interference and delays caused by the presence of scavengers at the disposal sites, transfer stations, or even collection bins, and can introduce significant



risks to the scavengers. Such an issue can be resolved by investing in waste management infrastructure, such as dedicating separate areas for the informal recycling activities at the disposal sites or transfer stations without interfering with the heavy equipment activities. Also, PPPs have to take into account the undesirable impacts on the marginalized groups already working in the sector informally. Such partnerships should not aim to replace or leave waste pickers jobless; instead, the focus should be on integrating those groups in the newly introduced PPPs. Nonetheless, the weak legal and regulatory framework in developing countries and the lack of capacity amongst both sectors to cope with such new arrangements may hamper the integration of the public and private sectors (Ahmed & Ali, 2004; Medina, 2008; Tilaye & Van Dijk, 2014; Wilson et al., 2006). The establishment of national movements and associations of waste pickers have been successful in some developing countries to establish productive and fruitful communications with the public and private sectors.

#### 4. CONCLUSION AND RECOMMENDATIONS

This study aimed at investigating the situation and challenges of the informal recycling sector in Jordan. Recycling in Jordan is estimated at only 10% which is mainly undertaken by informal recyclers and scavengers throughout the streets, residential areas, and disposal sites. Three locations were investigated in this study which included Al-Ghabawi Sanitary Landfill, Al-Humra Disposal Site, and Al-Baq'a market. It was found that informal recycling activities have been banned at Al-Ghabawi due to safety and security considerations. The situation was different at Al-Humra, where a contractor is responsible for waste scavenging and recycling at this disposal site, and the contractor has a group of 50 scavengers who work on a daily basis to separate and collect waste materials. Those scavengers then sell to the contractor (by weight), who in turn transports the waste materials to workshops outside the disposal site. There are several socioeconomic challenges facing the scavengers at this location including low income, health risks, improper housing, lack of health insurance, lack of social security, social stigma, and the unclear future in this profession. The study also investigated scrap dealers who function primarily in the streets and collect waste from different residential, commercial, and industrial regions. This group of informal recyclers are relatively at a better position compared to the landfill scavengers in terms of economic yield and social status. However, some of the interviewed workers expressed concerns related to the business vulnerability and the social stigma associated with waste recycling and scavenging.

Although the informal recycling activities in Jordan are highly irregular, this sector can be highly effective and can complement the Jordanian strategies for sustainable waste management. Hence, it is key to capitalize on the experience of informal scavengers and waste dealers and include those groups under the official waste management sector in Jordan through proper regulatory and legal framework as well as public-private partnerships.

#### 5. REFERENCES

- Abu Hajar, H.A. and Abu Hajar, M.A., 2023. A Multi-dimension sustainability assessment of the economic growth in Jordan using the Sustainability Window Analysis. *Journal of the Knowledge Economy*, pp.1-23.
- Abu Hajar, H. A., Al-Qaraleh, L. A., Moqbel, S. Y., & Alhawarat, A. M. (2021). Prospects of sustainable waste management in developing countries: A case study from Jordan. *Environmental Monitoring and Assessment*, 193, 1-14.
- Ahmed, S.A. and Ali, M., 2004. Partnerships for solid waste management in developing countries: linking theories to realities. *Habitat international*, 28(3), pp.467-479.
- Al-Mahasneh, O. (2020). *Investigation of the Situation of Informal Sector in Solid Waste Management System in Jordan* (M.Sc. thesis, The University of Jordan).
- Lim, S.L., Lee, L.H. and Wu, T.Y., 2016. Sustainability of using composting and vermicomposting technologies for organic solid waste biotransformation: recent overview, greenhouse gases emissions and economic analysis. *Journal of Cleaner Production*, 111, pp.262-278.
- Medina, M. (2008). The informal recycling sector in developing countries: organizing waste pickers to enhance their impact. Note No. 44, The World Bank, Washington, D.C.
- Salau, O., Osho, S., Pizarro, R., Sen, L., Adejowo-Osho, O. and Osho, G., 2017. The Impacts of the Informal Sector on the Economics of the Municipal Waste Management System in Lagos State: An Overview of its Income Generation Potentials for the Vulnerable Urban Poor in Developing Countries.
- Tilaye, M., & Van Dijk, M. P. (2014). Private sector participation in solid waste collection in Addis Ababa (Ethiopia) by involving micro-enterprises. *Waste Management & Research*, 32(1), 79-87.
- Wilson, D.C., Velis, C. and Cheeseman, C., 2006. Role of informal sector recycling in waste management in developing countries. *Habitat international*, 30(4), pp.797-808.

---

## #253: The impact of courtyards and window designs on thermal and visual comfort conditions in adobe traditional buildings of Nigeria

---

Olutola F. ADEKEYE<sup>1,2</sup>, Sara MOHAMED<sup>3</sup>, Lorna KIAMBA<sup>4</sup>, Lucelia RODRIGUES<sup>5</sup>

*1 University of Nottingham, UK, olutola.adekeye@nottingham.ac.uk*

*2 Kwara State University, Malete, Kwara State, Nigeria., olutola.adekeye@kwasu.edu.ng*

*3 University of Nottingham, UK, sara.mohamed2@nottingham.ac.uk*

*4 University of Nottingham, UK, Lorna.Kiamba@nottingham.ac.uk*

*5 University of Nottingham, UK, lucelia.rodrigues@nottingham.ac.uk*

*Abstract: Most traditional buildings are designed based on factors such as ventilation, thermal comfort, wind flow, etc. Courtyards and windows are common features of Vernacular architecture and they play major roles in maintaining both Visual and thermal comfort in traditional building practices. The influence of courtyards and window designs on ventilation, daylighting, and thermal comfort is specific to a region shaped by local climate, culture, and available resources. This study analyzes the comfort conditions (thermal and visual) of Ilorin adobe Traditional buildings in the Warm Humid region of Nigeria, West Africa. This study aims to understand and analyze how courtyards, window sizes, designs, and arrangements affect occupants' comfort and overall environmental performance through a combination of case studies, fieldwork, and computer simulations (Optivent 2.1 and Andrewmarsh simulation tools). The study will evaluate the efficacy of various environmental and window design options to encourage natural ventilation, maximize daylight penetration, and improve thermal conditions. The performance predictions and output of simulations will help in identifying strategies for reducing energy consumption, provide a useful understanding of sustainable design principles for adobe traditional buildings, and also offer directions to designers, conservationists, and policymakers to preserve cultural heritage while maintaining comfort and healthy living conditions.*

*Keywords: Adobe Traditional buildings, window design, courtyards, ventilation, daylighting, thermal comfort.*

## 1. INTRODUCTION

Courtyards and window designs are two important elements of Nigerian vernacular architecture that can influence the thermal and visual comfort of the occupants. Thermal comfort is the degree of satisfaction with the temperature and humidity of the indoor environment, while visual comfort is the degree of satisfaction with the lighting and glare conditions. Both thermal and visual comfort have an impact on the health, well-being, and productivity of the occupants, as well as the energy consumption and environmental impact of the buildings.

Courtyards are open areas enclosed by walls or structures that can offer evaporative cooling, natural sunlight, ventilation, shading, and other benefits. They can also be used as social and practical places for a variety of ceremonies and activities. They can be used for a variety of ceremonies and activities as well as social and practical areas. The volume and direction of airflow, natural light, and heat gain and loss through the building envelope can all be influenced by the window designs. To achieve optimal thermal and visual comfort conditions, courtyards and window designs can be tailored to the orientation, temperature, and culture of the area.

For generations, Nigerian traditional architecture has used courtyards and window patterns as passive design techniques. For instance, the circular and rectangular courtyards seen in Yoruba architecture in the southwest of Nigeria serve to shade and cool the area while also fostering a sense of community and harmony (Foláránmí and Adémúleyá, 2018). Southeast Nigeria's Igbo culture is characterised by linear courtyards that link various rooms and purposes while enabling cross-ventilation and natural lighting (Okanlawon, 2022). Rectangular courtyards that serve as social and practical spaces as well as sources of natural ventilation and daylighting are a hallmark of Hausa architecture in northern Nigeria. It depends on the local materials, methods, and architectural styles, Nigerian traditional buildings feature different window patterns, but they typically include small openings that allow airflow through and daylighting (Okanlawon, 2022).

However, due to Nigeria's growing urbanisation and industrialization, many traditional buildings have been replaced with modern buildings that frequently disregard or ignore the passive design principles of courtyards and window designs. Many buildings have now resulted in thermal and visual discomfort conditions, which also has an adverse effect on the environment and increases energy use. Therefore, there is a need to revisit and revive the traditional wisdom of courtyards and window designs in Nigerian architecture and adapt them to meet the present-day needs of the climate condition and challenges of the society.

It was discovered in a prior study that almost 50% of the respondents, who were also occupants of Ilorin adobe traditional buildings, expressed dissatisfaction with the windows of their dwellings, indicating problems with thermal and visual comfort. This discovery prompted the need for further investigation to understand the precise causes of discomfort experienced by the occupants in relation to the windows of these traditional buildings. In this study, the researchers examined the research on how courtyards and window layouts affect the thermal and visual comfort of Ilorin adobe traditional buildings and provide some case studies of existing traditional buildings to analyse the effectiveness of these passive design strategies.

## 2. CLIMATIC CONDITIONS IN ILORIN

Ilorin is a city located in Kwara State, Nigeria. It lies in between the Northern and Southern states of Nigeria. Ilorin city is geographically placed 100km from Oyo and 40km from Ogbomosho, two important Yoruba cities respectively and it is classified under the Warm-Humid climate zone. (Szokolay and Koenigsberger, 1973), gives notable and important characteristics of Warm-humid climates as; "a climate that exhibits high temperature (hot), sticky conditions and the continual presence of dampness". A high humidity level of 75%, intense solar radiation as it is located close to the equator where the sun is usually at its peak, heavy annual rainfall that provides some coolness, air temperatures between 21 and 32°C, with negligible changes between days and night and moisture in the air is experienced in this climatic zone.

Tropical climates have the prevailing key issue of heat, where the major aim for professionals is to design buildings that will cool and dehumidify to provide appropriate thermal comfort levels for occupants where the annual mean temperature is greater than 20°C. Also, building designs should put into consideration occupants' thermal and visual comfort without any mechanical means which can be achieved by using local climate variables (Liedl et al., 2012), (Szokolay and Koenigsberger, 1973). The average daily dry bulb temperature for Ilorin peaks in March with a decline through to September. For the Wind speed an average daily wind speed of at least 1.8ms is recorded throughout the year with a peak value in June at 3.1 m/s see Figure 1(a and b). The analysis indicated that if passive strategies were considered, it would be possible to meet thermal comfort requirements for 44.3% of the entire year by keeping ambient temperatures within the predicted comfort range of 23.5°C to 29.8°C

Passive design guidelines recommended by ASHRAE-55 adaptive comfort via the psychrometric chart to provide comfort as derived from this analysis: Use of good natural ventilation, where windows are well-shaded and oriented to prevailing breezes(ASHRAE, 1992.).

- Capture natural ventilation, wind direction can be changed to up to 45 degrees toward the building by external wing walls and planting.
- Sun-shading is designed for the specific latitude to reduce or eliminate the need for air conditioning.
- Minimise or eliminate west-facing glazing to reduce heat gain in warmer periods and in the afternoons.

- Use of light-colored materials for walls and roofs (with high emissivity) to reduce heat gain through conduction.
- Use open-plan interiors to encourage cross ventilation.
- Use of high thermal mass indoor walls to provide coolth and provide time-lag.
- Use of passive design strategies developed by vernacular type architecture (where suitable)

From the psychometric chart, Ventilation is recognized as a key parameter that enhances thermal comfort and passive energy efficiency for naturally ventilated Ilorin traditional buildings Figure (1C).

(Vallejo, 2020) describes natural ventilation as a passive method in buildings that makes use of external factors like wind speed and atmospheric pressure differences to speed up the ventilation process. For the admission of air, this technique necessitates the use of apertures like windows. Natural ventilation is expected to be prioritized in passive buildings to reduce summertime cooling energy requirements.

Natural ventilation can be implemented in a variety of architectural contexts by selecting an appropriate guideline from the list below:

**Single-Sided Ventilation:** In this case, only one side of the wall has an air inflow and outflow.

**Cross-Ventilation:** Across the room, the air intake and outlet openings are located at opposing walls. Thereby creating a pressure difference across the space due to the openings at different heights.

**Atria:** A tall area is built next to the ventilated chamber, increasing the height difference and enhancing the stack effect.

Interestingly, Ilorin traditional Adobe unique building designs mostly rely on adaptive comfort as described above by making use of natural ventilation and passive cooling methods through the construction of small windows, courtyards, and either a single-sided or a combination of single-sided and cross-ventilation methods.

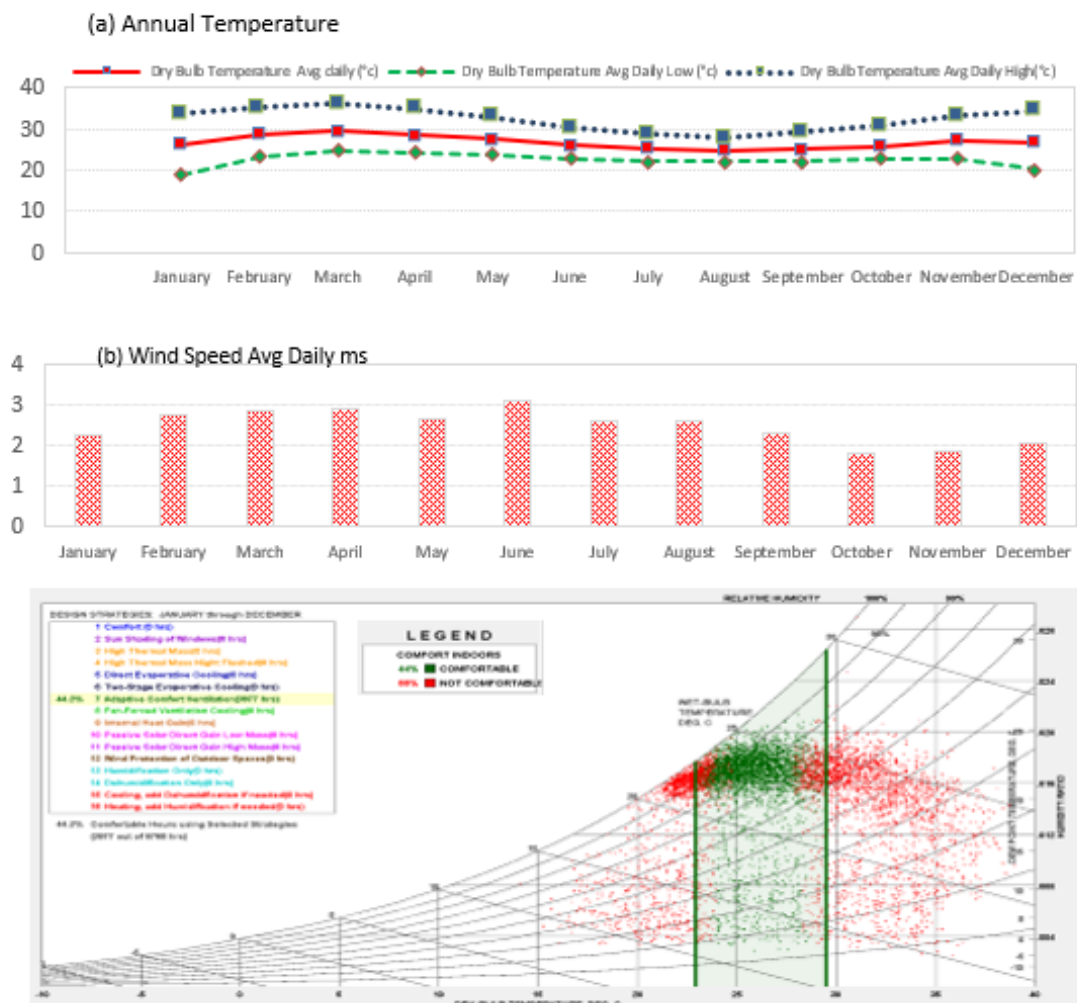


Figure 1 The climatic conditions for Ilorin city (a) Annual Temperature (b) Wind Speed (c) psychrometric chart with environmental strategies for Ilorin

### 3. METHODOLOGY

This study aims to analyse the thermal and visual comfort conditions of Ilorin adobe traditional buildings in the Warm Humid region of Nigeria. The methodology involves a combination of case studies, fieldwork, computer simulations using Optivent (version 2.1) simulation tool, and dynamic daylight calculation (Andrew Mash). Data was collected through architectural documentation, climate data collection, followed by physical measurements during fieldwork. Various variables related to thermal and visual comfort will be analysed, including the influence of window designs and sizes on natural ventilation and daylight penetration.

The study seeks to identify sustainable design strategies, reduce energy consumption, preserve cultural heritage, and provide valuable insights for designers to enhance occupants' comfort and maintain healthy living conditions in traditional buildings.

#### 3.1. Dynamic daylight calculation

The Andrew Marsh dynamic daylighting calculation tool is a deeply interactive software designed to address complexities in the design and analysis process. The software focuses on real-time dynamic daylight analysis within a rectangular room. With several characteristics including room size, windows, exterior shading devices, work plane height, etc., and instant updates on internal daylight distribution. Its main objective is to model the relationship between daylight distribution and factors like room size, window configuration, shading devices, and external obstructions in an engaging and user-friendly manner. The calculations are optimized for speed and accuracy, resulting in speedy and responsive interactions. This tool was used to analyze two rooms each within two case study buildings.(Andrewmarsh.com)

#### 3.2. Ventilation Optivent calculation software /Envelop flow model.

Envelope flow models are used to solve the equations governing the flow of air through openings in a building's envelope. They are based on assumptions about the distribution of the internal density (temperature). Consider an opening in the envelope to show the fundamental equations for a single cell. The essential formulae for an opening the link between the flow rate through an opening and the pressure differential across it is commonly expressed using the discharge coefficient and a defined geometric area equation:

Equation 1: 
$$q_i = \frac{C_{di} A_i \sqrt{2|\Delta p_i|}}{\rho}$$

Where:

- $i$  = identifies the opening/ inlet
- $q_i$  = is the flow rate through the opening ( $m^3/s$ )
- $C_{di}$  = is the discharge coefficient
- $A_i$  = is the area of the opening ( $m^2$ )
- $\Delta p_i$  = is the pressure difference (Pa)
- $\rho$  = is the air density ( $kg/m^3$ )

The discharge coefficient is defined and measured under still-air conditions with uniform density with flow being generated by wind. When the flow is generated by a density difference (i.e. in the absence of any wind effects), the pressure drop in equation (1) is given by:

Equation 2 
$$4\Delta p_i = P_{E0} - P_{I0} - \Delta P_0 g Z_i$$

Where

- $P_{E0} - P_{I0}$  = are the external and internal hydrostatic pressures respectively at the ground level (Pa)
- $\Delta P_0$  = is the density different at the ground level ( $kg/m^3$ )
- $g$  = is the gravitational force per unit mass  $m/s^3$
- $Z_i$  = is the height of the opening
- The density differences are defined by

Equation 3 
$$\Delta P_0 = P_E - P_I$$

Where:

- $P_E$  and  $P_I$  are the densities of the external and internal respectively ( $kg/m^3$ )

Equation 2 is applied to an opening aligned in any direction, irrespective of whether the flow is inward or outward, and whether the inside temperature is higher or lower than outside temperatures. However, it is important to note the height where the flows leave the opening  $Z_i$  i.e., the height of the outlet.

This follows from the outlet boundary condition, namely that the pressure at the outlet is determined by the pressure of the surrounding and the assumption that the temperature of the air remains unchanged as it flows through the opening. This means that for a long opening in the vertical direction, such as chimneys,  $z$  will change with the flow direction, (OPTIVENT.tools)

### Case studies description

**Case study One:** This building belongs to a district head also known as a Daudu and it is located at latitude  $8^{\circ}29'50.1''N$  and Longitude  $4^{\circ}33'09.4''E$ , built circa 1850 is a significant old residential traditional building that depicts unique Ilorin architectural and cultural styles that embraces influences from the Islamic religion and both Yoruba and Hausa ethnic groups. The first courtyard is the court of the men, where the men and older boys lived and entertained their friends. This court is also used to host visitors, especially those who were travellers and had arrived ahead of their appointment day to see the Emir. Separating the court of men from the rest of the house is the personal quarters of the Daudu which had a parlour and rooms for sleeping and storage for the Daudu. Behind the Daudu's quarters is the court of the women, where the four wives of the Daudu lived with the younger children and older female children. Behind the court of the women was the burial place for the family while the lavatory area opened from a passage to the left of the Daudu's quarters, see Figure 2.



Figure 2 Case study one

**Case study two:** This building is located in Ilorin East local government area of Ilorin with a latitude of  $8^{\circ}52'09.5''N$  and a Longitude of  $4^{\circ}53'58.3''E$ . This structure is a significant traditional adobe structure with extensive cultural and historical relevance to the Ilorin people, especially to those who reside in the okelele area of Ilorin. The pottery workshop in the courtyard is part of what makes the structure famous. The building was constructed around 1850, and its owners run a pottery company. The building and the craft industry have been passed on from generation to generation. The Yoruba ethnic group and the Islamic religion both have an impact on the building's architectural design. The structure consists of a number of bedrooms, a store, and a kitchen, all of which face a central courtyard that divides the male and female sections. The family members' graveyard is located behind the court of the women, see Figure 3.



Figure 3 Case study two

### 3.3. Courtyards and windows in Ilorin traditional buildings

The presence of courtyards in building design is an effective way of introducing passive cooling into buildings to enhance Passive energy efficiency, thermal comfort, ventilation, and lighting e.t.c, this passive cooling method is known to be adopted into Ilorin traditional building designs. According to (Myneni, 2013). The courtyard has a climate that is perfect for the tropics because it draws in cold air, which circulates inside the building and displaces stale air. Similarly, (Soflaei et al., 2017) explained further that when used as a passive cooling method, a central courtyard works as follows: as the day goes on and night falls, the air in the courtyard warms up. Natural convection layers of stored cool air in the courtyard flow into

the rooms around it as the temperature in the courtyard gently rises in the morning, keeping the courtyard cool until solar radiation hits it directly. Having one or two central courtyards is the predominant system seen in the two adobe traditional structures investigated.

As an illustration, one or two central courtyards is the predominant system seen in Ilorin adobe traditional building designs. Case one has two courtyards while case two has one courtyard. Traditional Ilorin buildings have a lease span that varies from 1.5 meters (Case two) to 1.8 meters (Case one). All buildings studied had an average lease span of 1.57 meters. In terms of floor-to-ceiling height, the buildings have an average floor-to-ceiling height of 2.2 meters. The window sizes of Ilorin traditional adobe buildings are small; findings report that the window sizes can be attributed to cultural privacy values, and thus, the window area of the buildings studied varied from 0.36m<sup>2</sup> to 0.72m<sup>2</sup>. Finally, these traditional buildings harness wind-driven natural ventilation. The ventilation technique(s) used spans from single-sided ventilation to the combination of cross and single-sided ventilation exclusively. Findings from the analysed buildings show that a single-sided ventilation system was used mostly in the structures.

## 4. RESULTS AND DISCUSSION

### 4.1. Daylight results

This section of the research analyses several daylight factors in existing case study buildings using different standards/rules of thumb and displays the daylight values across multiple lighting parameters appropriate for designs/buildings with effective visual and thermal comfort.

#### Rules-of-Thumb:

The Rules of Thumb is a set of practical guidelines that a space or an area must follow in order to be regarded as adequately day lit.

The building envelope, light admittance apertures, and light (luminance/illuminance) values distributed throughout the space serve as the foundation for these conditions. According to Rennie and Parand (1998), the guidelines to follow when developing a visually comfortable space are listed below.

- Effective daylighting can be obtained for any given space by varying the glass percentage of the window wall area within a particular room depth.
- The ratio of perceived light in a space to ambient skylight illumination is known as the daylight factor, as indicated in Equation 4

#### Rule of Thumb analysis

Rule of Thumb 1; Average Daylight Factor (Manual calculation) using:

$$\text{Equation 4} \quad \bar{D} = \frac{W}{A} \cdot \frac{T\theta}{(1-R^2)}$$

Where:

- D = average daylight factor
- W = net window area (Subtract 10% for frame)
- A = area of all surfaces of the room, including the window
- T = visible transmittance for the glass (subtract 10% to correct for dirt)
- $\theta$  = visible sky angle, in degrees
- R = R = average reflectance of room Surface
- (Rennie and Parand, 1998)

According to this "rule of thumb" (Average Daylight Factor), an average daylight factor of > 2% should be attained in order to meet the standards for the minimum average daylight factor necessary for a space to appear mainly illuminated. (CIBSE, 2015). Findings show that the Ilorin traditional adobe buildings under investigation do not have average natural daylight factor values that exceed or meet the threshold of > 2%, hence the condition is not adequate. This prediction validates the high number of dissatisfied occupants who reported to be experiencing visual discomfort. According to this general rule (Depth of Room), the window area given on existing Adobe Ilorin traditional buildings are less than 20% of the total window wall area, thus the criteria is not satisfied. This is most likely why the respondents reported visual discomfort.

Table 1: Average of daylight calculation for case studies one and two

Building	Space type	Number Of Windows	Window size	W	A	T	Θ	R	D = average daylight factor
Case study One	Livingroom	2	1.2*0.9	1.944	164	0.09	90	0.5	0.13
	Room	1	0.6 *0.6	0.324	101.5	0.09	90	0.5	0.03
Case study Two	Livingroom	1	0.6 *0.6	0.324	8.64	0.09	90	0.5	0.04
	Room	1	0.75*0.6	0.41	60.72	0.09	90	0.5	0.11

## Rule of Thumb 2: Depth of Room (Manual calculation)

Table 2: Rule of thumb depth of room rule

S/n	Building	Space type	Wall area	Criteria (%)	Existing window area	Minimum Window area (%)	Depth of Room rule
Case study One		Livingroom	24.4	30	2.16	7.3	Not successful
		Room	8.4	20	0.36	1.86	Not successful
Case study Two		Livingroom	11.85	20	0.36	2.4	Not successful
		Room	8.4	20	0.45	1.68	Not successful

Adekeye (2013), describes Ilorin adobe traditional buildings as built forms that have distinctive features and are distinguished by gothic-shaped doorways which are solely used as entrances and not as a security measure to keep off invaders because everyone coexisted amicably and there was no concern about expansion. On the sides and approach elevations of the houses, there are likewise only a few, very small window openings, leaving the interior spaces and the back side of the structure windowless. without having any. Based on findings and literature, two functional spaces within each case study building ( Palour and room ) both in case study one and two were chosen for analysis using the rule of thumb as seen in Table 1 and Table 2 and a basic parametric study revealing the level of visual comfort in the building through the Andrew mash simulation tool as shown in Figure 4.

## 4.2. Ventilation results (Optivent Simulation)

Figure 6 displays the air flow rate results for Case Study One, comparing the reference case (single-side ventilation) with a potential solution involving a shift to cross-side ventilation. The graphs depict the ventilation rates at different times of the day: 6:00 am (when all occupants are at home), noon (when only two occupants are at home and the rest are at work), and 8:00 pm (when all occupants are at home). Proper ventilation is crucial for maintaining indoor air quality and creating a comfortable environment. The recommended ventilation rates vary based on factors such as building type, occupancy, and activities conducted inside. For Residential Buildings, recommended by (CIBSE,2015) ventilation rates are as follows:

- Bedrooms: 0.35 to 0.5 m<sup>3</sup>/s per person.
- Living rooms and dining rooms: 0.35 to 0.5 m<sup>3</sup>/s per person.
- Kitchens: 0.7 to 1.0 m<sup>3</sup>/s per square meter of floor area.



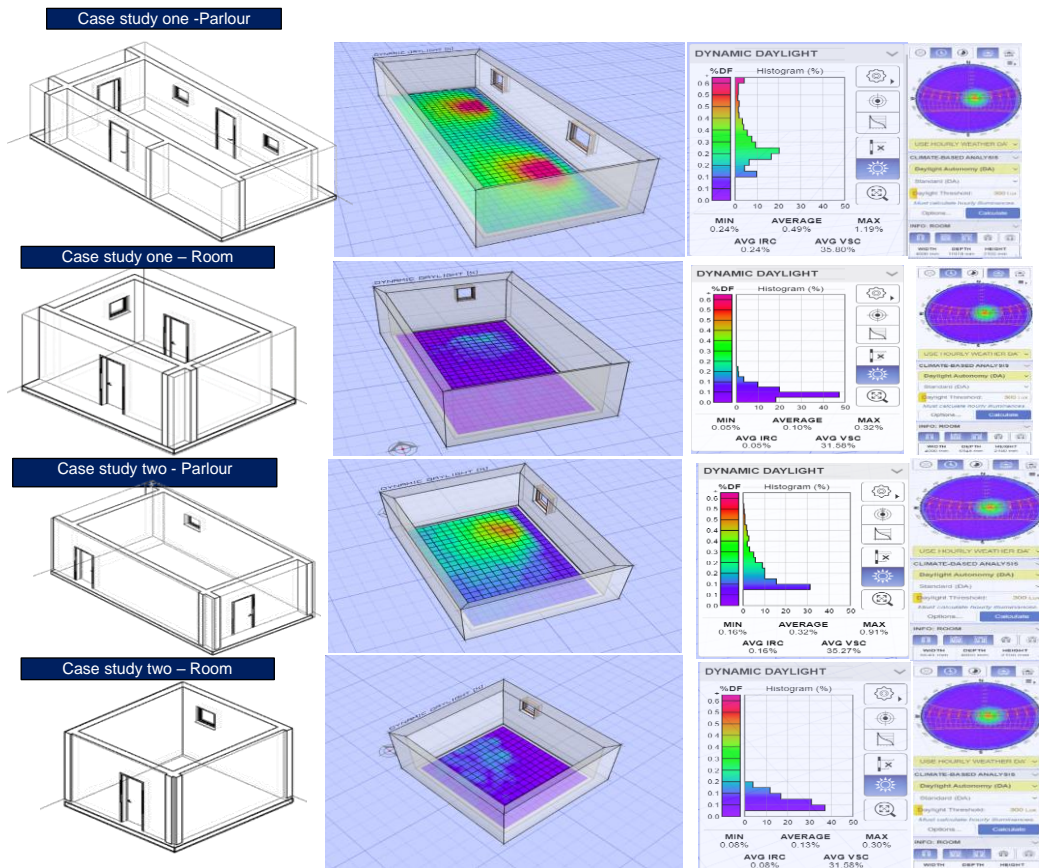


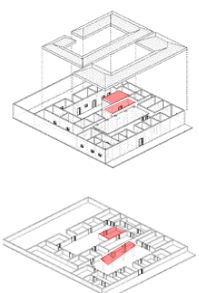
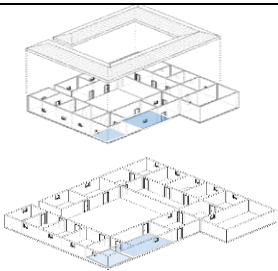
Figure 4 The results of dynamic daylight simulation of case study one and case study two (Andrewmarsh.com)

In the reference case (existing situation) of Case Study One for the Room Figure (5a) and Parlour Figure (5c) with only one window on a side (single side ventilation), the system failed to achieve the required ventilation rate throughout the day, even at 8:00 pm when the sun has set, and occupants could benefit from night cooling. Additionally, the figure indicates that the comfort temperature exceeded the ASHRAE standards' comfort zone (represented by the red dot outside the comfort zone).

In Case Study One, a promising potential solution has been proposed to improve room cooling by transitioning from a single-side ventilation system to cross ventilation and increasing the window size from 0.36m<sup>2</sup> to 4m<sup>2</sup>, see Figure (5b) and Figure (5d). This approach led to a substantial improvement in the achieved ventilation rate, reaching more than 4.40m<sup>3</sup>/s during the day from 6:00 am to 12:00 pm and at 8:00 pm, in stark contrast to the reference case that only achieved 0.06m<sup>3</sup>/s. Additionally, the figures revealed that the indoor temperatures, indicated by the red line, consistently remained within the comfort zone.

- Cross Ventilation System: The initial step in the potential solution involved replacing the existing single-side ventilation system with cross ventilation. This innovative design allowed fresh air to flow into the room from one side and exit from the opposite side. As a result, a continuous and efficient airflow pattern was established, effectively removing heat and improving room cooling.
- Increased Window Size: In tandem with cross ventilation, the window size was significantly enlarged from its original 0.36m<sup>2</sup> to an expansive four m<sup>2</sup>. This strategic enlargement enabled a higher volume of fresh air to enter the room during cross ventilation, thus enhancing the cooling effect and overall indoor air quality.
- Improved Ventilation Rate: The integration of cross ventilation and larger windows yielded remarkable results, as evidenced by the achieved ventilation rate. Specifically, during the designated daytime periods from 6:00 am to 12:00 pm and at 8:00 pm, the ventilation rate surged beyond 4.40m<sup>3</sup>/s. In stark contrast, the reference case could only manage a meager 0.06m<sup>3</sup>/s. This significant increase in airflow had a profound impact on cooling the room effectively.
- Consistent Comfort Temperatures: The figures displaying the indoor temperatures with a red line demonstrated that the proposed potential solution consistently maintained comfort temperatures within the acceptable range. This ensured that occupants experienced optimal comfort levels while benefiting from the improved room cooling achieved through cross ventilation and enlarged windows.

Table 3: shows the reference case studies and potential solutions.

Reference case one /existing situation	Potential Solution –Worst case sceneries	
<p>Area of the windows: 0.36m<sup>2</sup>                      Area of the windows: 1.08m<sup>2</sup>                      Floor Area (m<sup>2</sup>):48.8                      Room height 2.2m                      Volume (m<sup>3</sup>): 107.37                      Indoor temperature (°C): 31.7                      Inlet (surface) Azimuth: S, N</p>	<p>Change the system from single-side ventilation to cross ventilation.                      Increased the size of the windows (From 0.36m<sup>2</sup> to 4m<sup>2</sup>) please note the windows (2m<sup>2</sup>) worked for 6 am and 8 pm but not 12 noon                      Increased the size of the windows (From 0.36m<sup>2</sup> to 6m<sup>2</sup>) please note the windows (3m<sup>2</sup>) worked for 6 am, 8 pm, and 12 noon                      The area of the windows must be the same as the outlet of the windows. We reduced the stack height from 1.0 m to 0.8 m because the height of the room is only 2.2 m.                      In the living room                      The original windows size of 1.08m<sup>2</sup> worked for 6 am and 8 pm but not noon.                      Increased the size of the windows (From 1.08m<sup>2</sup> to 8.8m<sup>2</sup>) worked for 6 am, 8 pm, and 12 noonthe stack height from 1.0 m to 0.8 m because the height of the room is only 2.2</p>	
<p>Reference case two /existing situation</p> <p>Area of the windows (a): 0.45                      Area of the windows (b): 0.72                      Floor Area (m<sup>2</sup>):22.56                      Room height 2.2m                      Volume (m<sup>3</sup>): 49.63                      Indoor temperature (°C): 31.6                      Inlet (surface) Azimuth: W, S</p>	<p>Potential Solution –Worst-case scenarios</p> <p>Change the system from single-side ventilation to cross ventilation                      Increased the size of the windows (From 0.45m<sup>2</sup> to 8.6m<sup>2</sup>) please note the windows (2m<sup>2</sup>) worked for 6 am and 8 pm but not 12 noon                      Increased the windows size (From 0.72m<sup>2</sup> to 7.4m<sup>2</sup>) please note the windows (3.2m<sup>2</sup>)                      The area of the windows must be the same as the outlet of the windows                      We decreased the stack height from 1.0 m to 0.7 m.</p>	

Figures 6 and 7 present the reference and potential solutions for Case Study Two. The reference case demonstrates a lack of ventilation, resulting in overheating inside the room throughout the day and achieving only m<sup>3</sup>/s of ventilation rate. Consequently, the temperature remains outside the comfort zone. However, in Figures (6b) and (6d), upon applying the potential solution of cross ventilation, the temperature inside the space falls within the comfort zone. The achieved ventilation rate surpasses 10.88m<sup>3</sup>/s at noon when there are two occupants, reaching 5.43m<sup>3</sup>/s at 8:00 pm.

The results of both Case Study One and Case Study Two highlight the effectiveness of transitioning from single-side ventilation to cross-ventilation, along with the implementation of window size and stack height adjustments. These combined improvements significantly enhance the achieved ventilation rate, ensuring indoor temperatures remain within the comfort zone throughout the day. This emphasizes the critical importance of well-considered ventilation system design and appropriate window sizing, showcasing the advantages of cross-ventilation principles in indoor environments. These enhancements contribute to improved occupant comfort and support the development of sustainable cooling strategies.

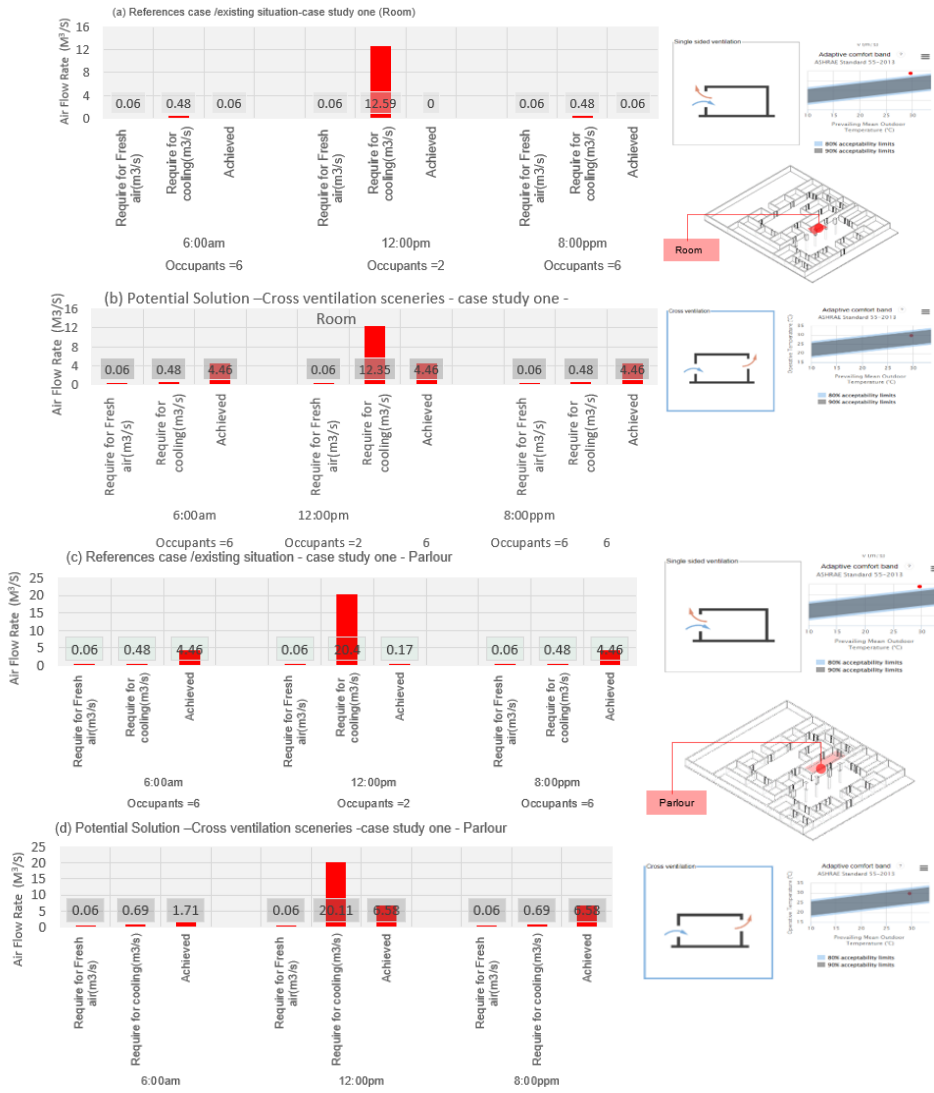


Figure 5 Optivent result showing the reference case and potential solutions for case study one for the room (a,b) and Parlour (c,d)

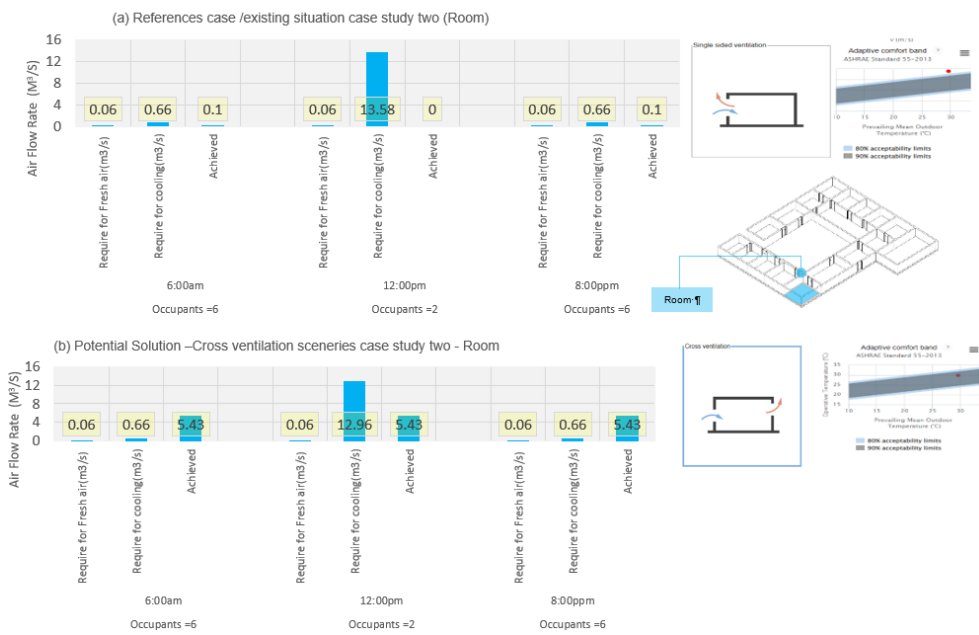


Figure 6 Optivent result showing the reference case and potential solutions for case study two(a,b).

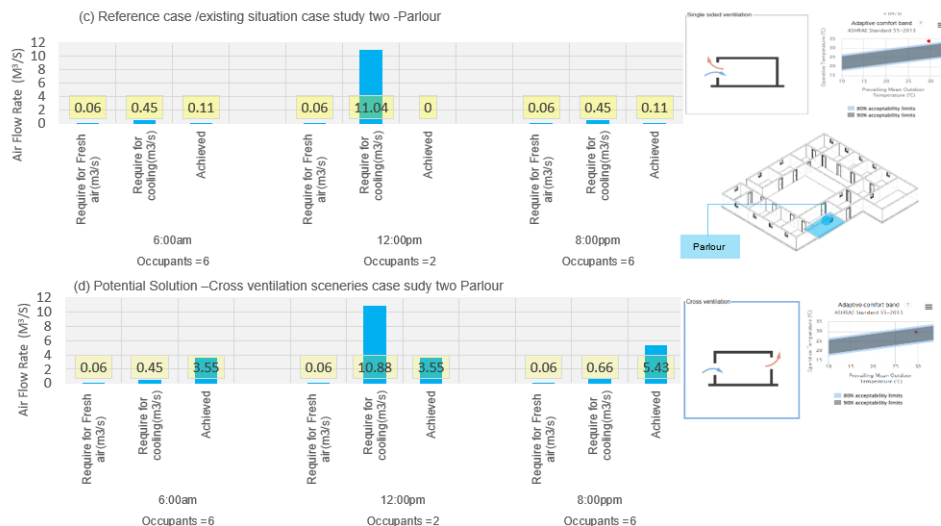


Figure 7 Optivent result showing the reference case and potential solutions for case study two (c,d)

## 5. CONCLUSION

Results from this study have shown that historically, tradition and climatic conditions played key roles in Ilorin architecture; hence Ilorin people build courtyards to enhance passive cooling to provide privacy and security by separating the female quarters from the male quarters and for social activities. Furthermore, Ilorin adobe traditional buildings have small windows to conserve their privacy but in turn this pose as a form of visual discomfort.

The ventilation of the studied buildings was calculated via Optivent tool (Version 2.1 - Building ventilation Simulation) and the study revealed that if the window sizes are increased from  $0.36\text{m}^2$  and  $0.72\text{m}^2$  respectively to  $3.2\text{m}^2$ , or additional windows with a total area of  $7.4\text{m}^2$  and the ventilation system changed completely from single-side ventilation to cross ventilation, the Ilorin adobe traditional building would deliver valuable visual & thermal comfort without compromising on the cultural values and privacy of the occupants. The potential solution of shifting to cross ventilation should be considered and evaluated to improve ventilation and maintain occupant comfort. The introduction of the cross-ventilation system could improve airflow rates and enhance indoor air quality and thermal comfort.

It is essential to carefully assess ventilation strategies and consider their impact on indoor conditions to optimize occupant well-being and energy efficiency. Future research and analysis will be crucial in identifying the most suitable ventilation approach for Case Study One to ensure a sustainable and comfortable living environment. Overall, this case study exemplifies the importance of thoughtful ventilation system design and window sizing in achieving effective room cooling and underscores the potential benefits of adopting cross-ventilation principles for indoor environments.

## 6. REFERENCES

- CIBSE (2015). *Cibse Guide A: Environmental Design 2015*. Cibse, 8th Eds, 402.
- Folàránmí, S. & Adémúleyá, B. (2018) 'Palace Courtyards In Iléjà: A Melting Point Of Traditional Yorùbá Architecture', *Yoruba Studies Review*, 2 (2), pp. 1-25.
- Liedl, P., Hausladen, G. & Saldanha, M. (2012). *Building To Suit The Climate: A Handbook*. Walter De Gruyter.
- Marsh,A.(2023) *AndrewMarsh.com*. Available at: <https://andrewmarsh.com>.(Accessed:23rd April 2023)
- Myneni, K. K. (2013) 'Courtyard As A Building Component; Its Role And Application In Developing A Traditional Built Form, Creating Comfort; A Case Of Athangudi Village, India', *International Journal Of Chemical, Environmental & Biological Sciences*, 1(4), pp. 633-639.
- Okanlawon, S. A., Odunjo, O. O And Adebeyejo, A. T (2022) 'Architecture Of Courtyards In The Indigenous Residential Areas Of nigerian Cities',*International Journal Of Humanities And Social Sciences (Ijhss)*, 11, pp. 11–22.
- Rennie, D. and Parand, F. (1998) *Environmental design guide for naturally ventilated and daylit offices*. Construction Research Communications.
- Standard, A.S.H.R.A.E., 1992. Thermal environmental conditions for human occupancy. *ANSI/ASHRAE*, 55, 5.

Soflaei, F., Shokouhian, M. & Soflaei, A.(2017) 'Traditional Courtyard Houses As A Model For Sustainable Design: A Case Study On Bwhs Mesoclimate Of Iran', *Frontiers Of Architectural Research*, 6(3), pp.329-345.

Szokolay, S. & Koenigsberger, O. 1973. *Manual Of Tropical Housing And Building*. Bombay: Orient Langman.

Vallejo, D. J. A. (2020). *Natural Ventilatio (Passive Cooling)*. Nottingham:University of nottingham,Department of Architecture and Built Environment.

Vallejo, J and Aparicio,P.(2003) *Optivent.Tools 2.1 Version*. Available at: <https://optivent.tools>.(Accessed : 28th March 2023)

---

# **#254: Advancing thermal comfort research: evaluating indices for naturally ventilated residential buildings in diverse climatic zones**

A data driven approach

---

Deepa Rani RANGASWAMY<sup>1</sup>

<sup>1</sup> Associate Professor, Department of Architecture and Planning, College of Engineering Trivandrum, Kerala, India  
deeparani.r@cet.ac.in

*Abstract: Thermal comfort research has taken a turn in the last decade with more focus on comfort models applicable to different climatic zones. Working home conditions due to pandemics added to it and started giving it a different direction altogether. Liveability and thermal comfort of houses of all income classes have hogged attention. There are several studies carried out in thermal comfort in naturally ventilated residential buildings specific to different regions and climatic conditions. Most of these thermal comfort studies are carried out in last two decades and used different thermal comfort indices to analyse the adaptiveness and other thermal comfort parameters of the occupants. This paper is an attempt towards that direction by reviewing the models or indices used for the evaluation of indoor thermal comfort specific to a climatic zone for naturally ventilated residential buildings and an evaluation of different indices are carried out based on the ASHRAE DB-RP884 specific to different climatic zone on the preview of the comfort indices used. The result of this study shows that the researchers preferred certain indices for each of the climatic zones. Based on the evaluation, a recommendation is made on the indices which gives the highest thermal comfort estimation of the occupants specific to the climatic zone. This result can guide future researchers on the selection of the indices specific to a climatic zone.*

*Keywords: Thermal Comfort Indices, Different climatic zones, Adaptiveness, NV Residential Buildings, ASHRAE DB-RP884*

## 1. INTRODUCTION

Thermal comfort research has taken a turn in the last decade with more focus on comfort models applicable to different climatic zones. Working home conditions due to pandemics added to it and started giving it a different direction altogether. Liveability and thermal comfort of houses of all income classes have hogged attention. This pandemic has raised huge concerns about the potential risk in mechanically cooled buildings. Scientists argue that mechanically cooled indoor temperatures and the air ducts of centrally air-conditioned buildings may enable the virus to thrive. Anticipating this risk, the scientific community recommends maintaining indoor environment with high levels of humidity, a high rate of air change, and higher air temperature. High humidity levels with high temperatures always cause thermal discomfort to the inhabitants. Hence thermal assessments cannot be done using universal evaluation methods. Each of the climatic zones has regional variations which need to be accounted for while doing indoor environmental assessments at least in residential buildings. This paper is an attempt in that direction to gather more information on this matter and bring out the various indices used in thermal comfort studies conducted in different climatic conditions and assess its applicability to the studied climatic zone.

## 2. LITERATURE REVIEW

Several researchers have tried to bring out the various aspects of thermal comfort through their reviews. Most of these reviews dealt with satisfaction levels of occupants through field surveys in various projects based on the post-occupancy evaluation. A comprehensive review of various thermal adaptations in buildings through post-occupancy evaluation studies and the different attributes contributing to the adaptations summarized the role of behavioural adjustments, physical acclimatization and expectation in improving thermal designs in buildings (de Dear, Richard J., Brager, 1998) (Gossauer and Wagner, 2007). A review on Forty years of Fanger's model of Thermal comfort clearly does an assessment of thermal comfort using the PMV model of Fanger and deals with the strengths and limitations of this model (van Hoof, 2008). A similar study reviewed various parameters influencing the effectiveness of occupant controlled natural ventilation, such as window opening type, window size, shape and placement, accessibility ((Roetzel *et al.*, 2010). Another review tried to compile the studies specifically in relation to thermal comfort and gender (Karjalainen, 2012). Significance of individual difference in the thermal comfort conditions such as age, gender, physical disabilities and fitness have been compiled by Wang in his review (Wang *et al.*, 2018).

A comparison of the data from the field surveys carried out by Humphreys in 1975-1981 with the data from later studies in terms of indices of thermal comfort, mean warmth response, temperatures found to be comfortable, sensitivity to temperature change, interpersonal variation, distribution of comfort with temperature, and the influence of outdoor temperature in the presence or absence of heating and cooling paved way to the role of adaptive approach in the formation of standards and guidelines (Humphreys, Nicol and Raja, 2013). Mishra and Ramgopal (2013) reviewed thermal comfort surveys of different climatic zone in terms of Neutral Temperature (Mishra and Ramgopal, 2013). Halawa and van Hoof (2012) proposed improvements to PMV/PPD model using adaptive field surveys (Halawa and van Hoof, 2012).

Looking at reviews conducted in residential buildings, researchers have reviewed micro-level comfortable temperature in bedrooms and bathrooms and other rooms in the context of various thermal comfort studies (Peeters *et al.*, 2009). Reviews included environmental conditions affecting thermal comfort in residential buildings (Frontczak and Wargocki, 2011), indoor thermal comfort based on heat balance and adaptive models with the focus on the current issues related with the PMV model (Harimi, Ming and Kumaresan, 2012), different factors affecting occupant comfort in Multi-unit residential building such as indoor conditions, outdoor conditions, building characteristics and occupant related characteristics (Andargie, Touchie and O'Brien, 2019) and studies in tropical climatic conditions (Rodriguez and D'Álessandro, 2019).

Some of reviews focused on various indices used for the long-term evaluation of the general thermal comfort conditions in buildings, the thermal comfort models developed so far, thermal comfort aspects in residential buildings, hospitals and so on. One of the reviews brought in a classification of occupant behaviour models based on review of the different occupant behaviour studies carried out in residential buildings (Balvedi, Ghisi and Lamberts, 2018). Djongyang *et al.* presented mathematical modelling of heat exchange between human body and environment along with thermal comfort approaches (Djongyang, Tchinda and Njomo, 2010). The review of different thermal comfort indices classified indices on the basis of their scientific model base (Carlucci and Pagliano, 2012). Review by Cheng *et al.* summarized thermal comfort models that addressed local thermal sensations and distinguished these models by their advantages, limitations, and suitable ranges of applications (Cheng, Niu and Gao, 2012). The authors (Taleghani *et al.*, 2013) thoroughly reviewed three thermal comfort standards ASHRAE 55-2010, European EN15251 standard, and the Dutch ATG guideline. Certain reviews addressed thermal comfort research on the context of its implications for building energy efficiency (Yang, Yan and Lam, 2014).

Hence it is understood that there is dearth of reviews which has attempted to explore thermal comfort in naturally ventilated residential buildings and comfort indices used to evaluate them based on the climatic zone to which they belong.

## 3. THERMAL COMFORT RESEARCH USING INDICES

The studies conducted by Humphreys and Nicol (1972), (1995) (1995) proved that comfort temperatures are never fixed and universal and showed good correlation with the mean outdoor temperature. This is mainly because of adaptive mechanisms which include personal adaptation, where alterations to metabolic rate, or to clothing will influence the heat



balance of the subject, and objective adaptation where the subject's subtle and usually unaccounted actions modify the local thermal environment. It is held that these adaptations are prompted by the subjects' expectations relating to the prevailing climate.

### 3.1. Methodology

The studies are evaluated and categorised according to the major climatic zones -Tropical, Dry zone, Temperate and Continental. Indices used to study the thermal comfort results are evaluated along with the study methodologies adopted.

### 3.2. ASHRAE – RP 884 database

ASHRAE-RP 884 database is one of the most popular public databases available for thermal comfort study. ASHRAE-RP 884 data set was collected to develop De Dears adaptive model and include 25,000 observations from 52 studies and 26 cities over different climatic zones all over the world (Gao *et al.*, 2021). This dataset was adapted for the thermal performance of indices studies in different climatic zones.

Table 1: Climatic zone and sub climatic zone data taken from ASHRAE-RP 884 database

#	Climatic Zone	Sub-Climatic Zone	No of Valid Data Entries	Min	Max	Mean	Standard Deviation
1	Tropical	Tropical Rainforest	438	26.5	35	30.97	1.56
		Cold Semi Arid	440	13.9	21	18.27	1.61
2	Dry (Desert and semi Arid)	Hot Desert	398	15.3	36	27.1	6.26
		Hot Semi Arid	430	15.2	37	25.74	5.12
		Humid Subtropical	252	27.2	35	30.64	0.13
3	Temperate	Hot Summer Mediterranean	64	19.2	32	27.43	1.96
		Temperate Oceanic	137	17.8	29	24.06	2.52
4	Continental	Warm Summer Humid Continental	437	23.4	28	25.24	1.5

### 3.3. Performance evaluation using ASHRAE-RP 884 database

Thermal comfort indices evaluated using the ASHRAE-RP 884 database in this study are Predicted mean Vote (PMV), Expected PMV (ePMV), Adaptive PMV (aPMV), Tropical Summer Index (TSI), Standard Effective Temperature (SET), Predicted Thermal Sensation (PTS), Adaptive Thermal Comfort Model, Indian Model of Adaptive Comfort (IMAC). Thermal comfort indices are evaluated based on its ability to estimate Actual Mean Vote (AMV) correctly. The methodology for evaluation is described in the paper by the same author (Rangaswamy and Ramamurthy, 2021). These indices values were converted to a common 7-point thermal sensation scale. The different indices are evaluated by the sensitivity and accuracy of its estimation of thermal sensation of the person in AMV scales. How close the estimations are made is calculated using the True Positive Rate (TPR) and Average Accuracy of Estimation (AAE).

## 4. TROPICAL CLIMATIC ZONE

Thermal comfort in humid tropics is mainly characterized by high humidity and high temperature with some provision for air movement. A comfort zone of 2–3° either side of the optimum can be taken as acceptable in hot humid tropics (Nicol, 2004). If fans are available to building occupants, another 2°C can be added to the predicted comfort temperature in hot conditions. In a humid climate or in conditions when the relative humidity is high, people may require temperatures that are about 1°C lower to remain comfortable, but the main effect of a higher humidity (or water vapour pressure) is to reduce the width of the comfort zone.

Studies conducted in the Tropical climatic zone have predominantly used Temperature as the primary index to investigate thermal comfort (Al-Tamimi and Fadzil, 2012), (Djamila, 2017), (Aflaki *et al.*, 2014), (Adunola, 2014). Some studies also employed PMV and SET as alternative indices for thermal comfort analysis (Nguyen, Singh and Reiter, 2012). Additionally, research in Composite climatic zones, which are subcategories of Tropical climates, utilized various indices such as AHRAE Adaptive and IMAC indices to compare thermal performance in buildings (Doctor-Pingel *et al.*, 2019). Moreover, Indraganti conducted multiple studies in both Tropical and Composite climatic zones, focusing on the impact of height on thermal comfort using Temperature, TSI, and PMV as key metrics (Indraganti and Rao, 2010) (Indraganti, 2010)

Figure 1 illustrates the usage of indices in Tropical climatic zone. Temperature and PMV are the most widely used indices in tropical climates which is followed by TSI and SET. Adaptive and IMAC are used by one study each. Figure 2 illustrates different methodologies used in Tropical climatic zone. Measurement or survey or the combination of both are mainly used for the study. Distribution of Air Temperature samples of ASHRAE-DB for Tropical climatic zone is given in Figure 3 which gives the profile of climatic condition in that area. Figure 4 shows the Average Accuracy and True Positive Rate estimated for each of the indices based on ASHRAE data showing how much percentage they are closer to the Actual Mean vote. TSI gives the highest performance in estimating AMV of occupants in Tropical climatic zone with average accuracy of 85% and sensitivity of 70%. This is followed by Adaptive and PTS with 82% Average accuracy and 62% Sensitivity. ePMV (with



an expectancy factor of 0.5) comes in third position in estimating AMV of occupants with 79% average accuracy and 57% sensitivity. TSI is mostly derived from survey data from Tropical climatic zones and accounts for Air Temperature, Humidity and Air velocity in the proportion of the influence (Rangaswamy and Ramamurthy, 2021). PTS is also derived from a large amount of survey data as an improvement over TSI. The correction factor ie. Expectancy factor of 0.5 puts the ePMV in range of the thermal adaptations of people in tropical climatic zone.

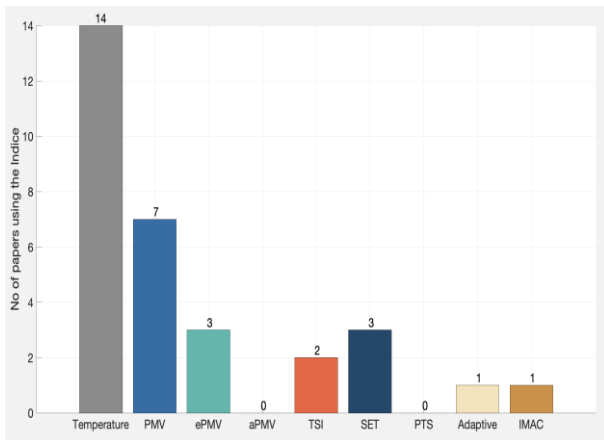


Figure 1 Usage of Indices in Tropical zone

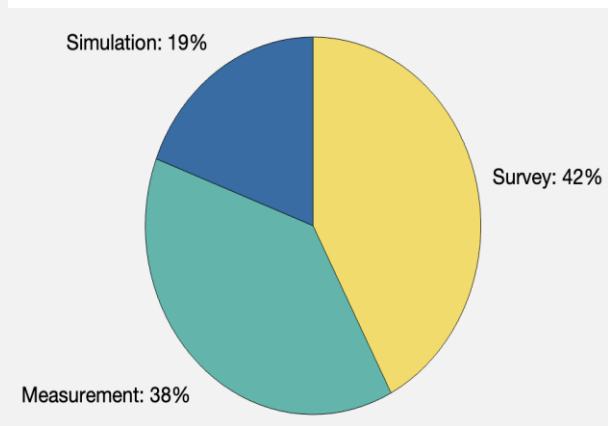


Figure 2 Usage of Methodologies in Tropical zone

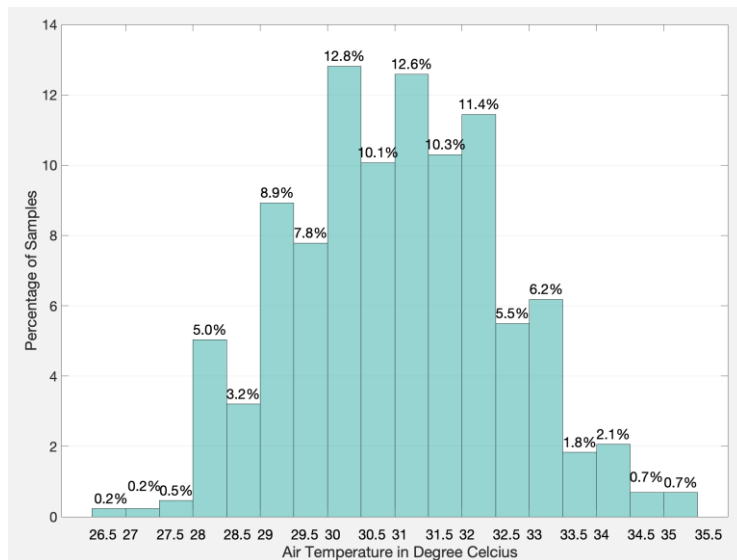


Figure 3 Distribution of Air Temperature in ASHRAE-DB data of Tropical Zone

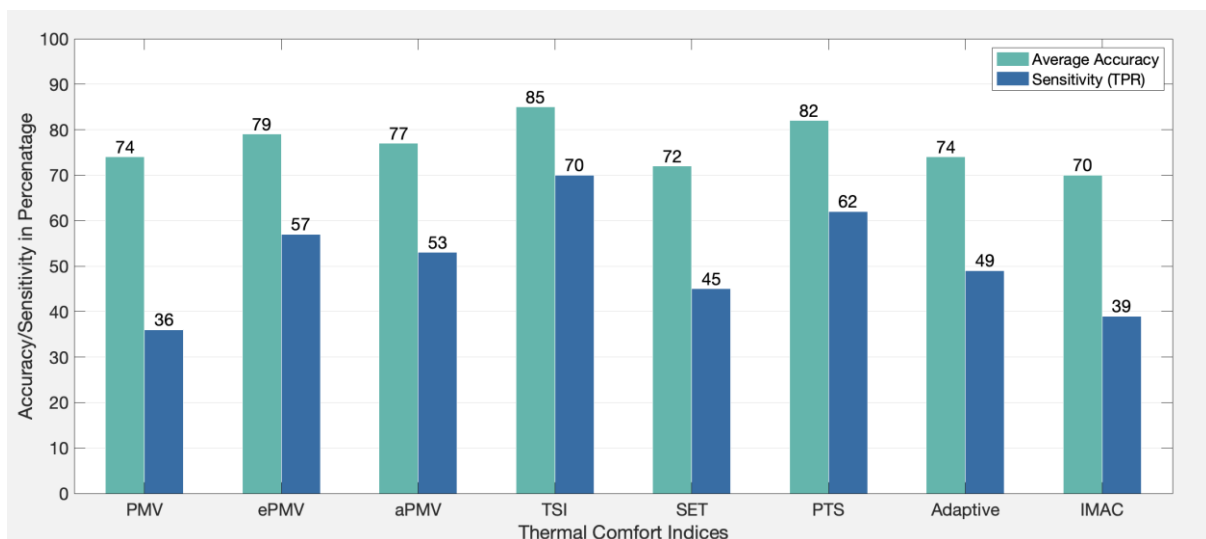


Figure 4 Analysis of Indices based on ASHRAE-DB for Tropical Zone

## 5. DRY (DESERT AND SEMI-ARID) CLIMATE ZONE

Dry climatic zones are characterised by very low precipitation, high evaporation rate that typically exceed precipitation and wide temperature which may occur daily and seasonally. This zone is mainly comprised of deserts and steppes and have hot summers, cool nights and moderate winters. Arid and semi-arid regions together make up 26 percent of the land area of Earth. The thermal comfort studies conducted in Arid climatic zones mainly used PMV, SET, PMV, ePMV, TSI as the indices. (Nematchoua *et al.*, 2014) used PMV and Temperature for their study and arrived at Neutral temperature calculation. PMV, ePMV and TSI were used together for the thermal comfort study conducted and to arrive at real time thermal performance of apartment buildings (Oudrane and Aour, 2019) evaluated the thermal comfort aspects of habitable architecture located in completely desert area. The study (Mohd Ariffin, Behaz and Denan, 2018) evaluated the thermal performance of traditional house in a desert climate using temperature as the index.

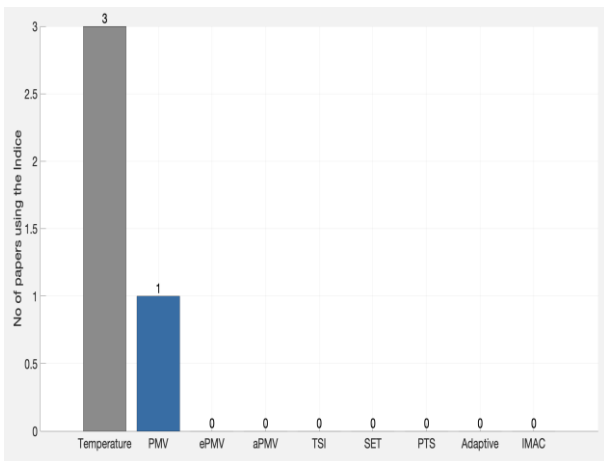


Figure 5 Usage of Indices in Dry zone

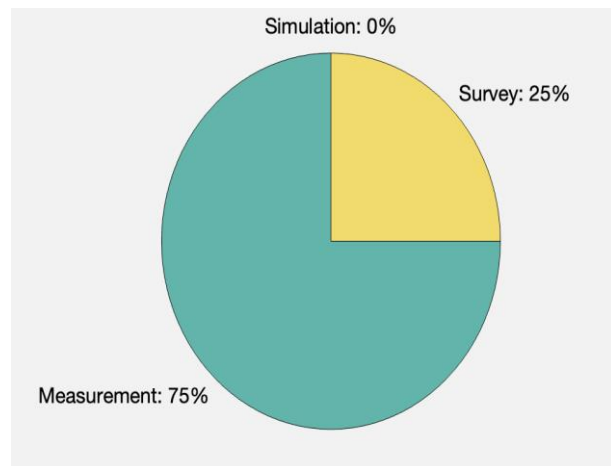


Figure 6 Usage of Methodologies in Dry zone.

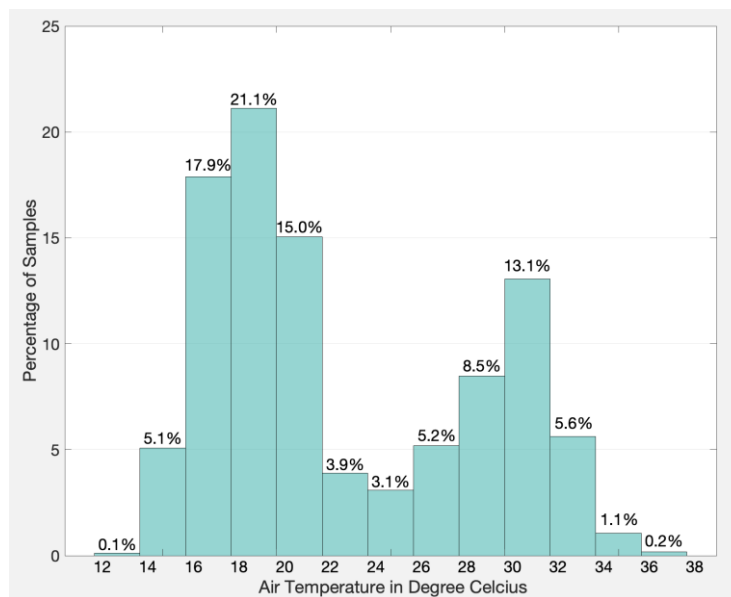


Figure 7 Descriptive statistics of Air Temperature of ASHRAE-DB data of Dry Zone

Figure 5 illustrates the usage of indices in Dry Zone and methodologies in dry zone is illustrated in Figure 6. Figure 7 shows the distribution of Temperature data in Dry climatic zone. Figure 8 illustrates the Average Accuracy and Sensitivity of AMV estimation by the different indices compared in Dry climatic zone. In Tropical climatic zone, SET and PTS gives the highest performance with Average Accuracy of 90 and 91 respectively. Sensitivity of the corresponding to SET and PTS is 45 and 59 respectively. SET and PTS are based on physiological strain, and it rightly accounts for environment factors, such as air temperature, relative humidity, air velocity metabolic rate, and external work and that could be the reason for better performance of SET and PTS in dry (desert) climatic conditions.

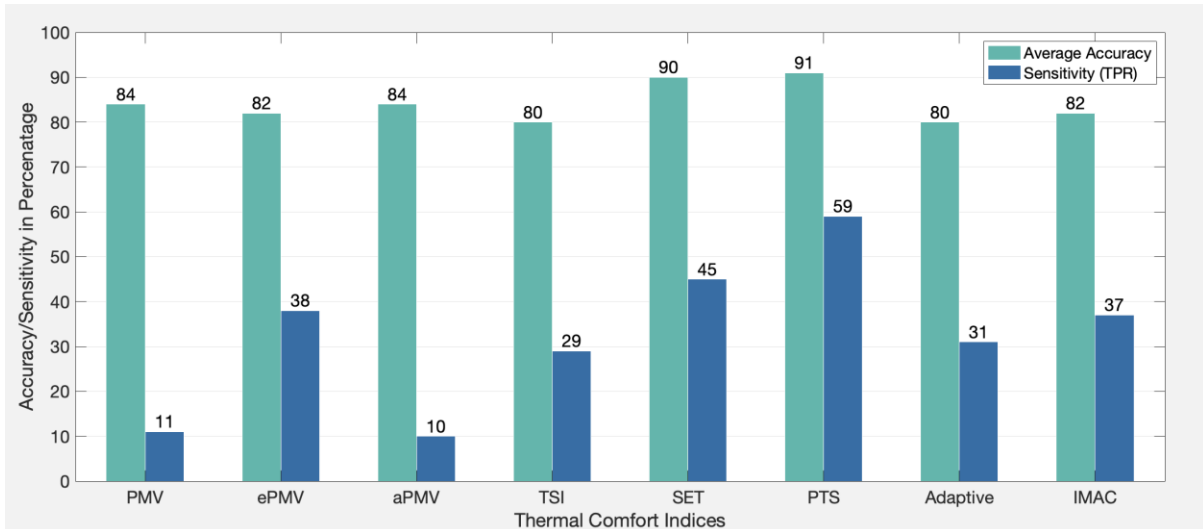


Figure 8 Analysis of Indices based on ASHRAE-DB for Dry Zone

## 6. TEMPERATE CLIMATE ZONE

The temperate climatic zone, where a significant portion of the global population resides, experiences four distinct seasons with considerable temperature variations between them. Studies conducted by various researchers, including Sharples and Malama (1997), Cheng and Ng (2006), Haase and Amato (2009), Guedes, Matias, and Santos (2009), Alves, Duarte, and Gonçalves (2016), and Peeters et al. (2009), have predominantly used PMV as the index for thermal comfort assessment in this climatic zone, followed by temperature (Sharples and Malama, 1997), (Cheng and Ng, 2006), (Haase and Amato, 2009), (Guedes, Matias and Santos, 2009), (Alves, Duarte and Gonçalves, 2016) and (Peeters et al., 2009). These studies have employed surveys and Thermal Sensation Vote (TSV) analysis, while others have utilized PMV for investigating the impact of climatic conditions, location, and orientation on thermal comfort, as seen in the works of Guedes et al. (2009), Becker and Paciuk (2009), Xu et al. (2018), and Kim et al. (2017) (Guedes, Matias and Santos, 2009), (Becker and Paciuk, 2009)(Xu et al., 2018) (Kim et al., 2017). Additionally, Zhang et al. (2010) conducted research using SET and PMV to derive a thermal sensation vote equation based on these indices (Zhang et al., 2010).

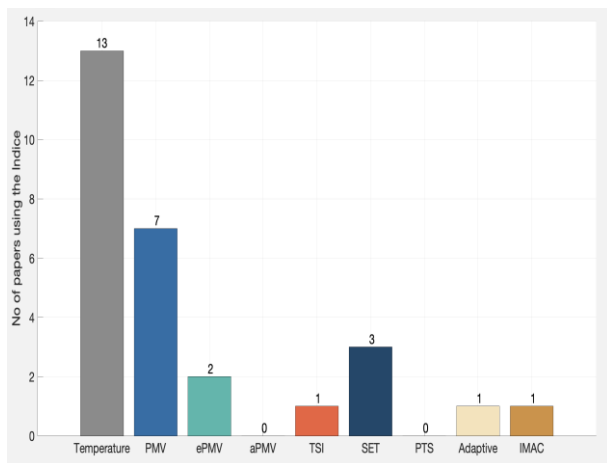


Figure 9 Usage of Indices in Temperate zone.

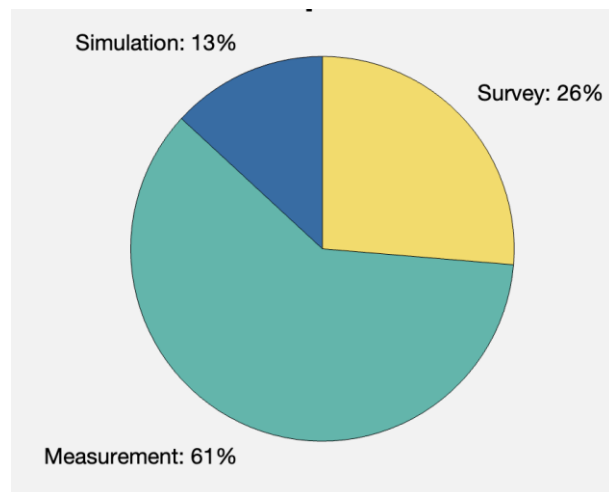


Figure 10 Study Methodology distribution in Temperate zone

The usage of indices in Temperate zone is illustrated in Figure 9. Temperature and PMV are the highest used indices in Temperate zone which is followed by SET and ePMV. TSI, Adaptive and IMAC are used by one study each. Figure 10 illustrates the methodologies used. Most of the studies (61%) uses measured data for the study. Figure 11 shows the distribution of temperature data in Temperate zone. Performance of Indices in Temperate zone is given in Figure 12 which indicates that SET and PTS have highest Average Accuracy and sensitivity in AMV estimation. The biological strain-based models - SET and PTS have coefficients derived for each of the climatic zone separately. That is the reason for higher performance of the SET and PTS In Temperate zone.

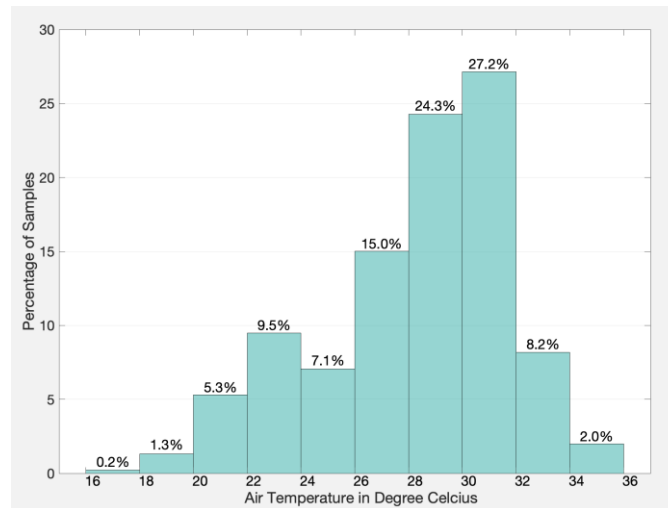


Figure 11 Descriptive statistics of Air Temperature of ASHRAE-DB data of Temperate Zone

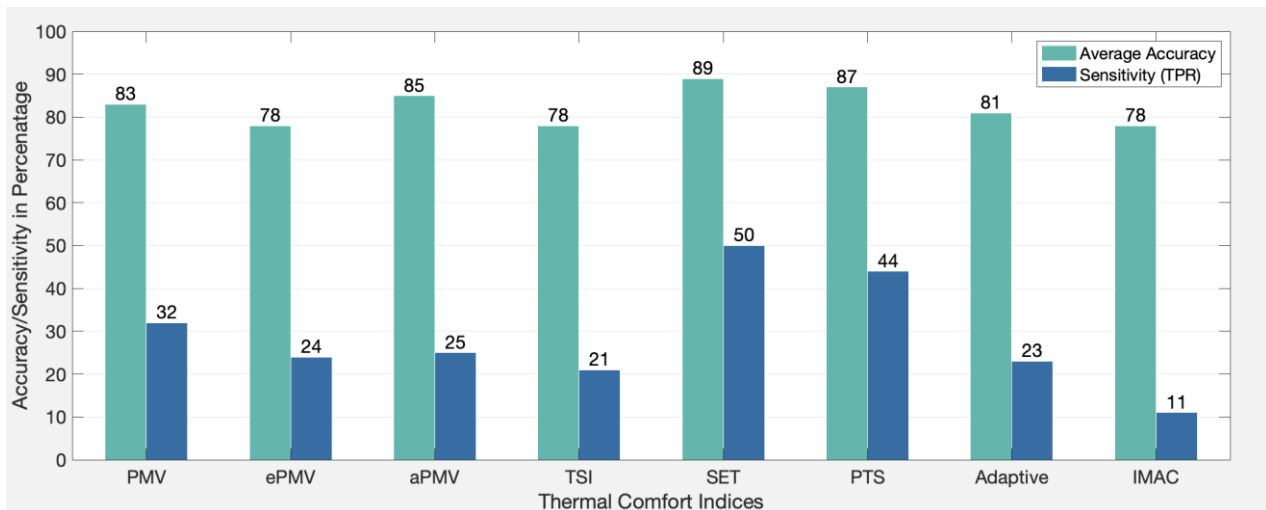


Figure 12 Analysis of Indices based on ASHRAE-DB for Temperate Zone

## 7. CONTINENTAL CLIMATE ZONE

Continental climates have significant variation in temperature characterised by hot summers and cold winters with extreme temperatures. Thermal comfort studies in Continental climatic zones used Temperature and PMV for the analysis. Borong compared the thermal performance between the traditional vernacular dwellings and the modern houses using Temperature and PMV as the index (Borong *et al.*, 2004). (Wang *et al.* 2010) conducted field study to determine both the neutral and the preferred air temperature and the acceptable range of thermal conditions for non-air-conditioned residential buildings of Harbin. The study was primarily based on Temperature and PMV and arrived at the Neutral temperature and preferred conditions of the inhabitants. (Ning *et al.*, 2015) used PMV model to arrive at the Neutral temperature of Harbin, China. (Yu *et al.*, 2017) evaluated the value of the PMV adaptive coefficient “ $\lambda$ ” in the adaptive thermal comfort model aPMV suitable to the Tibet area.

Usage of indices in Continental climate zone is illustrated in Figure 13. PMV is used the highest number of studies in Continental climate followed by SET whereas aPMV and Temperature are used by just one study each. Figure 10 shows that 57% of the studies used measurement as the methodology. Figure 11 gives the distribution of temperature data which shows that 60% of the time the temperatures lies between 28-32°C in continental zone. Performance of indices in estimating AMV for different indices in Continental climatic zone is given in Figure 12. PMV and its derived indices ePMV and aPMV have the highest Average Accuracy and Sensitivity in continental climatic zone. PMV was originally formed based on heat balance equations based on survey data from temperate and continental climatic zones. This accounts for the higher accuracy of the PMV based indices in Continental climatic zones.

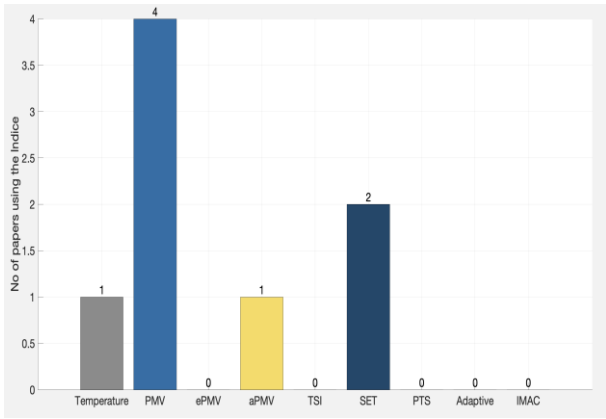


Figure 13 Usage of Indices in Continental

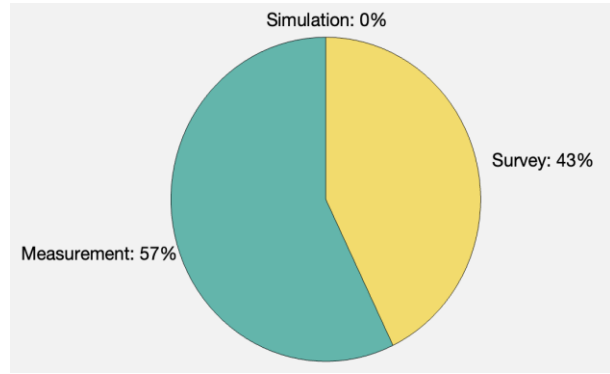


Figure 14 Study Methods distribution in Continental

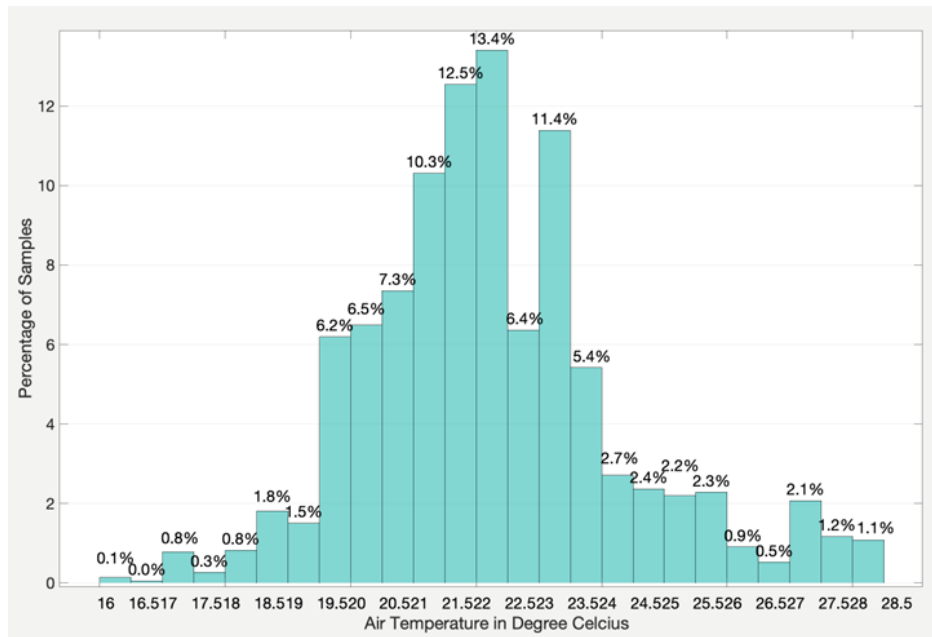


Figure 15 Descriptive statistics of Air Temperature of ASHRAE-DB data of Continental Zone

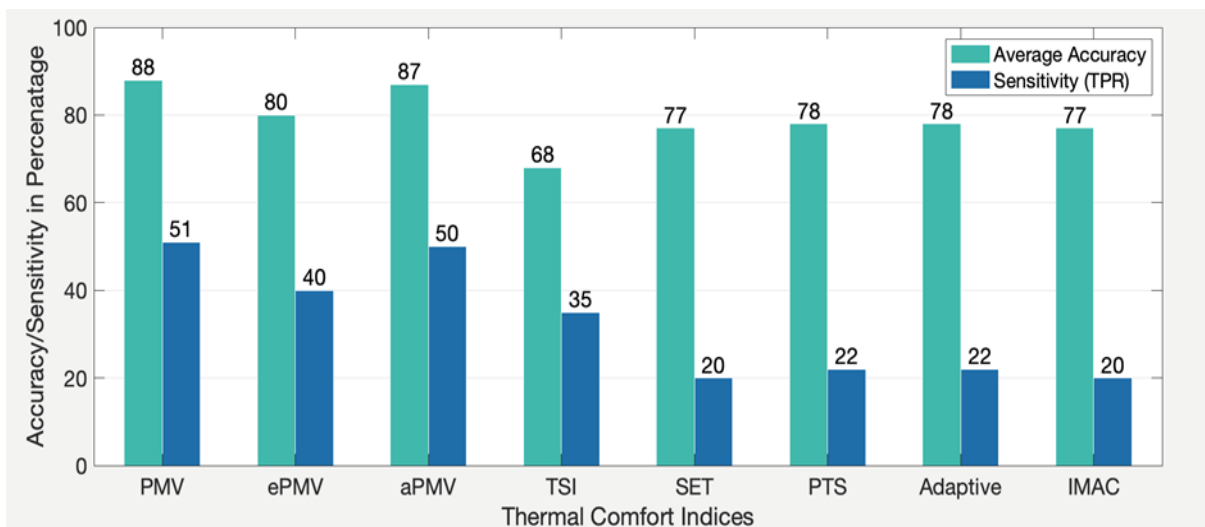


Figure 16 Analysis of Indices based on ASHRAE-DB for Continental Zone

## 8. DISCUSSIONS

Thermal performance of a building deals with the saving achieved in terms of energy through the building envelope features whereas Thermal comfort deals with thermal sensation experienced by the occupants when they start using the space. Thermal performance alone will not give a sufficient insight on actual performance of a building. Only in combination with thermal comfort characteristics can actually predict the overall performance of a building. It is revealed that the adaptive approach field investigations studied in the past focused significantly on temperature, without emphasizing on parameters such as mean radiant temperature, air velocity and humidity. But these indoor environmental parameters play a prominent role in occupants' preference and acceptance of the thermal environment in a given building. Hence a detailed study of these parameters is essential and such studies will contribute to energy savings in buildings.

Another aspect revealed from this study is that the indoor design temperatures as described by international standards (ISO 7730 and ASHRAE 55 - 1981, 1992, 2004) take no account of climatic variations and people's adaptive behaviour. The recommended temperature is assumed to apply irrespective of climate and people culture, way of life and kind of clothing, though with some recognition of difference between summer and winter. Studies conducted in different climatic zones of the world show that the ways in which people adapt to their thermal environment differ from place to place and thermal comfort conditions are always different in different parts of the world due to varying outdoor climate.

Each of the thermal indices are designed for some specific climatic zone even though the PMV based indices are developed for all kinds of climatic zone. The analysis results are summarized as follows.

- Temperature and PMV are the highest used thermal comfort models in Tropical climatic zone. Based on ASHRAE-DB analysis TSI gives the highest performance in AMV estimation followed by Adaptive and PTS in Tropical climatic zone.
- Dry (Desert) climatic studies also use Temperature and PMV indices. The analysis based on ASHRAE-DB proves that SET and PTS gives best estimates of AMV in Dry zone.
- Studies in Temperate climatic zone uses Temperature, PMV indices mostly followed by SET, ePMV and TSI. ASHRAE DB study indicates that SET and PTS gives the best results in AMV estimation in Temperate zone.
- Continental climatic zone studies are based on PMV, SET, aPMV and Temperature in the order of the number of studies. PMV based indices (PMV, ePMV and aPMV ) gives the best performance in AMV estimation in Continental climatic zone.

## 9. CONCLUSION

There have been valuable studies on thermal performance and comfort in residential buildings with respect to influencing parameters in different climatic zones of the world. Thermal performance parametric investigations with respect to factors such as shape and form of the building, orientation, ventilation pattern, fenestrations, shading effects and thermo-physical properties of building envelope have been studied extensively using either PMV model or universal adaptive model. But these models never been able to predict thermal comfort effectively due to variations in climatic zones. There have been no literature reports on thermal comfort indices used for evaluation of occupants' comfort in residential thermal environment based on its applicability to concerned climatic zone. Hence this work tried to bring together the major works done with respect to thermal comfort in residential buildings across the world in different climatic zones focusing on the thermal comfort indices used for its evaluation. Each of the thermal indices are designed for some specific climatic zone even though the PMV based indices are developed for all kinds of climatic zone. The study revealed that TSI gives the best estimate for thermal sensation in Tropical Zone, whereas SET and PTS gives the best estimate of AMV in Dry zone and Temperate zone. PMV based indices (PMV, ePMV and aPMV) gives the best performance in AMV estimation in Continental climatic zone. Thus, this study gives a recommendation on specific indices which provide higher accuracy in specific comfort zone.

## 10. REFERENCES

- Adunola, A. O. (2014) 'Evaluation of urban residential thermal comfort in relation to indoor and outdoor air temperatures in Ibadan, Nigeria', *Building and Environment*, 75, pp. 190–205. doi: 10.1016/j.buildenv.2014.02.007.
- Aflaki, A. *et al.* (2014) 'Building Height Effects on Indoor Air Temperature And Velocity in High Rise Residential Buildings in Tropical Climate', *OIDA International Journal of Sustainable Development*, 7(7), pp. 39–48.
- Al-Tamimi, N. and Fadzil, S. F. S. (2012) 'Energy-efficient envelope design for high-rise residential buildings in Malaysia', *Architectural Science Review*, 55(2), pp. 119–127. doi: 10.1080/00038628.2012.667938.
- Alves, C. A., Duarte, D. H. S. and Gonçalves, F. L. T. (2016) 'Residential buildings' thermal performance and comfort for the elderly under climate changes context in the city of São Paulo, Brazil', *Energy and Buildings*, 114, pp. 62–71. doi: 10.1016/j.enbuild.2015.06.044.

- Andargie, M. S., Touchie, M. and O'Brien, W. (2019) 'A review of factors affecting occupant comfort in multi-unit residential buildings', *Building and Environment*, 160, p. 106182. doi: 10.1016/j.buildenv.2019.106182.
- Balvedi, B. F., Ghisi, E. and Lamberts, R. (2018) 'A review of occupant behaviour in residential buildings', *Energy and Buildings*, 174, pp. 495–505. doi: 10.1016/j.enbuild.2018.06.049.
- Becker, R. and Paciuk, M. (2009) 'Thermal comfort in residential buildings – Failure to predict by Standard model', *Building and Environment*. Elsevier Ltd, 44(5), pp. 948–960. doi: 10.1016/j.buildenv.2008.06.011.
- Borong, L. *et al.* (2004) 'Study on the thermal performance of the Chinese traditional vernacular dwellings in Summer', *Energy and Buildings*, 36(1), pp. 73–79. doi: 10.1016/S0378-7788(03)00090-2.
- Carlucci, S. and Pagliano, L. (2012) 'A review of indices for the long-term evaluation of the general thermal comfort conditions in buildings', *Energy and Buildings*. Elsevier B.V., 53, pp. 194–205. doi: 10.1016/j.enbuild.2012.06.015.
- Cheng, V. and Ng, E. (2006) 'Comfort temperatures for naturally ventilated buildings in Hong Kong', *Architectural Science Review*, 49(2), pp. 179–182. doi: 10.3763/asre.2006.4924.
- Cheng, Y., Niu, J. and Gao, N. (2012) 'Thermal comfort models: A review and numerical investigation', *Building and Environment*. Elsevier Ltd, 47, pp. 13–22. doi: 10.1016/j.buildenv.2011.05.011.
- de Dear, Richard J., Brager, G. S. (1998) 'Developing an Adaptive Model of Thermal Comfort and Preference', *RP 884-ASHRAE Transactions*, 104(Part 1).
- Djamila, H. (2017) 'Indoor thermal comfort predictions: Selected issues and trends', *Renewable and Sustainable Energy Reviews*, pp. 569–580. doi: 10.1016/j.rser.2017.02.076.
- Djongyang, N., Tchinda, R. and Njomo, D. (2010) 'Thermal comfort: A review paper', *Renewable and Sustainable Energy Reviews*, 14(9), pp. 2626–2640. doi: 10.1016/j.rser.2010.07.040.
- Doctor-Pingel, M. *et al.* (2019) 'A study of indoor thermal parameters for naturally ventilated occupied buildings in the warm-humid climate of southern India', *Building and Environment*. Elsevier, 151(January), pp. 1–14. doi: 10.1016/j.buildenv.2019.01.026.
- Frontczak, M. and Wargocki, P. (2011) 'Literature survey on how different factors influence human comfort in indoor environments', *Building and Environment*. Elsevier Ltd, 46(4), pp. 922–937. doi: 10.1016/j.buildenv.2010.10.021.
- Gao, N. *et al.* (2021) 'Transfer learning for thermal comfort prediction in multiple cities', *Building and Environment*. Elsevier Ltd, 195(February), p. 107725. doi: 10.1016/j.buildenv.2021.107725.
- Gossauer, E. and Wagner, A. (2007) 'Post-occupancy evaluation and thermal comfort: State of the art and new approaches', *Advances in Building Energy Research*, 1(1), pp. 151–175. doi: 10.1080/17512549.2007.9687273.
- Guedes, M. C., Matias, L. and Santos, C. P. (2009) 'Thermal comfort criteria and building design: Field work in Portugal', *Renewable Energy*, 34(11), pp. 2357–2361. doi: 10.1016/j.renene.2009.03.004.
- Haase, M. and Amato, a. (2009) 'An investigation of the potential for natural ventilation and building orientation to achieve thermal comfort in warm and humid climates', *Solar Energy*. Elsevier Ltd, 83(3), pp. 389–399. doi: 10.1016/j.solener.2008.08.015.
- Halawa, E. and van Hoof, J. (2012) 'The adaptive approach to thermal comfort: A critical overview', *Energy and Buildings*. Elsevier B.V., 51, pp. 101–110. doi: 10.1016/j.enbuild.2012.04.011.
- Harimi, D., Ming, C. C. and Kumaresan, S. (2012) 'A Conceptual Review on Residential Thermal Comfort in the Humid Tropics', 1(6).
- van Hoof, J. (2008) 'Forty years of Fanger's model of thermal comfort: Comfort for all?', *Indoor Air*, 18(3), pp. 182–201. doi: 10.1111/j.1600-0668.2007.00516.x.
- Humphreys, M. A., Nicol, J. F. and Raja, I. A. (2013) 'Field studies of indoor thermal comfort and the progress of the adaptive approach', *Advances in Building Energy Research*, 1, pp. 55–88. doi: 10.4324/9781849770378-9.
- Indraganti, M. (2010) 'Adaptive use of natural ventilation for thermal comfort in Indian apartments', *Building and Environment*. Elsevier Ltd, 45(6), pp. 1490–1507. doi: 10.1016/j.buildenv.2009.12.013.
- Indraganti, M. and Rao, K. D. (2010) 'Effect of age, gender, economic group and tenure on thermal comfort: A field study in residential buildings in hot and dry climate with seasonal variations', *Energy and Buildings*, 42(3), pp. 273–281. doi: 10.1016/j.enbuild.2009.09.003.

- Karjalainen, S. (2012) 'Thermal comfort and gender: a literature review.', *Indoor air*, 22(2), pp. 96–109. doi: 10.1111/j.1600-0668.2011.00747.x.
- Kim, J. *et al.* (2017) 'Understanding patterns of adaptive comfort behaviour in the Sydney mixed-mode residential context', *Energy and Buildings*. Elsevier B.V., 141, pp. 274–283. doi: 10.1016/j.enbuild.2017.02.061.
- Mishra, A. K. and Ramgopal, M. (2013) 'Field studies on human thermal comfort - An overview', *Building and Environment*. Elsevier Ltd, 64, pp. 94–106. doi: 10.1016/j.buildenv.2013.02.015.
- Mohd Ariffin, N. A., Behaz, A. and Denan, Z. (2018) 'Thermal Comfort Studies on Houses in Hot Arid Climates', *IOP Conference Series: Materials Science and Engineering*, 401(1). doi: 10.1088/1757-899X/401/1/012028.
- Nematchoua, M. K. *et al.* (2014) 'A field study on thermal comfort in naturally-ventilated buildings located in the equatorial climatic region of Cameroon', *Renewable and Sustainable Energy Reviews*, 39, pp. 381–393. doi: 10.1016/j.rser.2014.07.010.
- Nguyen, A. T., Singh, M. K. and Reiter, S. (2012) 'An adaptive thermal comfort model for hot humid South-East Asia', *Building and Environment*. Elsevier Ltd, 56, pp. 291–300. doi: 10.1016/j.buildenv.2012.03.021.
- Nicol, F. (2004) 'Adaptive thermal comfort standards in the hot-humid tropics', *Energy and Buildings*, 36(7), pp. 628–637. doi: 10.1016/j.enbuild.2004.01.016.
- Ning, H. *et al.* (2015) 'Thermal Comfort and Thermal Adaptation between Residential and Office Buildings in Severe Cold Area of China', *Procedia Engineering*. Elsevier B.V., 121, pp. 365–373. doi: 10.1016/j.proeng.2015.08.1080.
- Oudrane, A. and Aour, B. (2019) 'Study and characterization of thermal comfort in a desert climate', *Advances in Systems Science and Applications*, 19(2), pp. 63–79. doi: 10.25728/assa.2019.19.2.667.
- Peeters, L. *et al.* (2009) 'Thermal comfort in residential buildings: Comfort values and scales for building energy simulation', *Applied Energy*. Elsevier Ltd, 86(5), pp. 772–780. doi: 10.1016/j.apenergy.2008.07.011.
- Rangaswamy, D. R. and Ramamurthy, K. (2021) 'Evaluation of Eight Thermal Comfort Indices Based on Perception Survey for a Hot-Humid Climate through a Naturally Ventilated Apartment', *Journal of Architectural Engineering*, 27(4). doi: 10.1061/(asce)ae.1943-5568.0000508.
- Rodriguez, C. and D'Álessandro, M. (2019) 'Indoor thermal comfort review: The tropics as the next frontier', *Renewable and Sustainable Energy Reviews*. Elsevier, 29(June), p. 100488. doi: 10.1016/j.uclim.2019.100488.
- Roetzel, A. *et al.* (2010) 'A review of occupant control on natural ventilation', *Renewable and Sustainable Energy Reviews*, 14(3), pp. 1001–1013. doi: 10.1016/j.rser.2009.11.005.
- Sharples, S. and Malama, A. (1997) 'A thermal comfort field survey in the cool season of Zambia', *Building and Environment*, 32(3), pp. 237–243. doi: 10.1016/S0360-1323(96)00063-7.
- Taleghani, M. *et al.* (2013) 'A review into thermal comfort in buildings', *Renewable and Sustainable Energy Reviews*. Elsevier, 26, pp. 201–215. doi: 10.1016/j.rser.2013.05.050.
- Wang, Z. *et al.* (2010) 'Thermal comfort for naturally ventilated residential buildings in Harbin', *Energy and Buildings*. Elsevier B.V., 42(12), pp. 2406–2415. doi: 10.1016/j.enbuild.2010.08.010.
- Wang, Z. *et al.* (2018) 'Individual difference in thermal comfort: A literature review', *Building and Environment*, 138(February), pp. 181–193. doi: 10.1016/j.buildenv.2018.04.040.
- Xu, C. *et al.* (2018) 'Thermal comfort and thermal adaptive behaviours in traditional dwellings: A case study in Nanjing, China', *Building and Environment*. Elsevier, 142(May), pp. 153–170. doi: 10.1016/j.buildenv.2018.06.006.
- Yang, L., Yan, H. and Lam, J. C. (2014) 'Thermal comfort and building energy consumption implications - A review', *Applied Energy*. doi: 10.1016/j.apenergy.2013.10.062.
- Yu, W. *et al.* (2017) 'A study of thermal comfort in residential buildings on the Tibetan Plateau, China', *Building and Environment*. Elsevier Ltd, 119, pp. 71–86. doi: 10.1016/j.buildenv.2017.04.009.
- Zhang, Y. *et al.* (2010) 'Thermal comfort in naturally ventilated buildings in hot-humid area of China', *Building and Environment*. Elsevier Ltd, 45(11), pp. 2562–2570. doi: 10.1016/j.buildenv.2010.05.024.



---

## #255: A hardware-in-the-loop simulation of a heat pump system for vehicle thermal management

---

Luca MURATORI<sup>1</sup>, Beatrice PULVIRENTI<sup>2</sup>, Lorenzo PERETTO<sup>3</sup>, Raffaella DI SANTE<sup>4</sup>, Giovanni BOTTIGLIERI<sup>5</sup>, Federico COIRO<sup>6</sup>

<sup>1</sup> University of Bologna, Viale del Risorgimento 2, 40136 Bologna, Italy, luca.muratori12@unibo.it

<sup>2</sup> University of Bologna, Viale del Risorgimento 2, 40136 Bologna, Italy, beatrice.pulvirenti@unibo.it

<sup>3</sup> University of Bologna, Viale del Risorgimento 2, 40136 Bologna, Italy, lorenzo.peretto@unibo.it

<sup>4</sup> University of Bologna, Viale del Risorgimento 2, 40136 Bologna, Italy, raffaella.disante@unibo.it

<sup>5</sup> Webasto Thermo & Comfort Italy Srl, Via E. Nobili 2, 40062 Molinella, Italy, giovanni.bottiglieri@webasto.com

<sup>6</sup> Webasto Thermo & Comfort Italy Srl, Via E. Nobili 2, 40062 Molinella, Italy, federico.coiro@webasto.com

*Abstract: The need to reduce vehicle emissions imposed by governments has led manufacturers to focus on the development of battery electric vehicles. Although this is a promising solution for improving air quality and reducing CO2 emissions, some limitations still hinder the widespread adoption of electric vehicles. The primary obstacle is the limited driving range compared to traditional internal combustion engine vehicles. This is due to the significant difference in energy density between the two technologies' energy storage systems and the longer charging time required for batteries compared to refuelling a tank of fuel. To address the limited driving range without increasing battery size (which would raise vehicle cost and weight), enhancing the energy efficiency of auxiliary systems, particularly the thermal management system, becomes crucial. Installing heat pumps and integrating them into a system that manages the thermal needs of the cabin, battery, power electronics and electric motor (PEEM) in a single unit can be an effective option for improving vehicle energy efficiency. The solution explored in this study is referred to as a single-liquid coolant loop. It consists of a primary refrigerant loop (a heat pump) that exchanges heat with a secondary liquid coolant loop. Through an intelligent valve system, the secondary loop delivers cold or hot coolant to various vehicle subsystems that require thermal management and allows for the recovery of the waste heat from the electronic components. Implementing control logic and defining the system's working modes necessitate simulating it using a mathematical model due to the high cost of conducting experimental tests on a real vehicle. To overcome the computational time required for simulating a model with a high level of accuracy, particularly regarding the refrigerant circuit, this paper presents the design of a hardware-in-the-loop (HIL) simulation. The HIL simulation allows testing the various functionalities of a vehicle-integrated thermal management system in real-time. The simulation focuses on the coolant loop and the models of cabin, battery, and PEEM, while a dedicated test bench replicates the thermal loads calculated in the simulation to evaluate the performance of the heat pump. The thermal loads are replicated by incorporating an electric heater into a coolant circuit connected to the evaporator and a radiator into a separate coolant circuit connected to the condenser. An important advantage of this HIL simulation is that we can verify the performance of the compressor's and electronic expansion valve's control systems on the real heat pump without assembling the entire vehicle thermal management system in the testing area. The results demonstrate the HIL system's ability to synchronize the test bench with the mathematical model by showcasing a battery electric bus driving in summer conditions. This HIL system demonstrates effective testing for the thermal management system of battery electric vehicles. However, certain limitations arise from the electric heater and radiator installed on the test bench. To accurately reproduce scenarios with the maximum thermal load on the evaporator, a more powerful electric heater is required. Similarly, for scenarios with the minimum thermal load on the condenser, without coolant temperature oscillations, a radiator with a smaller heat transfer area is needed. Addressing these hardware limitations would enhance the overall performance and accuracy of the HIL system for testing thermal management in electric vehicles.*

Keywords: Heat Pump, Hardware-in-the-Loop, Thermal Management, Battery Electric Vehicles

## 1. INTRODUCTION

In recent years, the automotive industry has placed significant emphasis on the development of battery electric vehicles (BEVs) to combat vehicle emissions and promote sustainability. While BEVs offer promising benefits such as improved air quality and reduced CO<sub>2</sub> emissions, they still face challenges that limit their widespread adoption among consumers. A critical hurdle is the limited driving range compared to traditional internal combustion engine vehicles (ICEVs). This discrepancy can be attributed to the substantial difference in energy density between the energy storage systems of these two technologies. While a gasoline tank boasts an energy density of approximately 8.76 kWh/l, a lithium-ion battery pack achieves only around 0.4 kWh/l. Moreover, the extended charging times required for BEVs, though mitigated by fast charging options, can accelerate the degradation of lithium-ion batteries (Edge *et al.*, 2021). Consequently, frequent fast charging is discouraged to ensure battery longevity.

Increasing the driving range by installing larger battery packs seems intuitive, but it comes at the cost of increased vehicle weight and expense. A more pragmatic approach lies in enhancing the energy efficiency of BEVs. Notably, the thermal management system plays a crucial role in influencing the driving range (Horrein *et al.*, 2017. Farrington and Rugh, 2000. Lee *et al.*, 2013). However, designing thermal management systems for BEVs is inherently more complex than for ICEVs, as they must cater to additional components that require thermal regulation. Aside from providing passenger comfort through HVAC (Heating, Ventilation, and Air Conditioning) heat exchangers, the system must also maintain the battery pack and power electronics and electric motor (PEEM) within their optimal thermal working conditions.

In pursuit of improved energy efficiency for thermal management systems, the implementation of heat pumps instead of electric heaters, as well as integrating cabin, battery, and PEEM thermal management into a single system to recover waste heat, have emerged as viable solutions (Leighton, 2015. Ma *et al.*, 2022. Tian *et al.*, 2018. Muratori *et al.*, 2022).

Given the complexity of electric vehicle thermal management systems, it becomes essential to develop accurate mathematical models that describe the physical behaviour of these systems for simulation purposes. Such simulations can verify the performance of various layouts and control logics, reducing development costs and time compared to assembling and testing full vehicle prototypes. However, when dealing with systems containing numerous components, dynamic simulations with high accuracy, such as driving scenarios in defined ambient conditions, can be time-consuming. In such cases, hardware-in-the-loop (HIL) simulations offer an advantageous solution, combining simulation models with specific hardware components that exchange data in real time.

In this study, we present the development of a HIL system that integrates the testing of a heat pump on a dedicated test bench with the simulation of the remaining vehicle thermal management system, encompassing models of the cabin, battery pack, and PEEM. This HIL system allows for comprehensive testing of various layouts and control logics for the vehicle's thermal management system without the need to modify the existing test bench setup. Our focus centres on simulating an electric bus operating in a summer condition to verify the HIL system's capability in maintaining consistent temperature, pressure, and volume flow at the interfaces between the test bench and the simulation environment. Through this integrated approach, we aim to contribute to the advancement of efficient and reliable thermal management systems for electric vehicles, paving the way towards a sustainable future for transportation.

## 2. HARDWARE-IN-THE-LOOP SIMULATION

The vehicle thermal management system analysed in this study consists in a refrigerant circuit that exchanges heat through the condenser and the evaporator with a liquid coolant loop. Figure 1 illustrates the schematic diagram of this system, referred to as a 'single liquid coolant loop system' because all the vehicle components are thermally managed using a liquid coolant loop. By employing a system of valves within the liquid coolant loop, heat transfer occurs between the hot and cold liquid (represented by the red and blue pipes in Figure 1) originating from the condenser and the evaporator, respectively, and the various vehicle devices (see Muratori *et al.*, 2022).

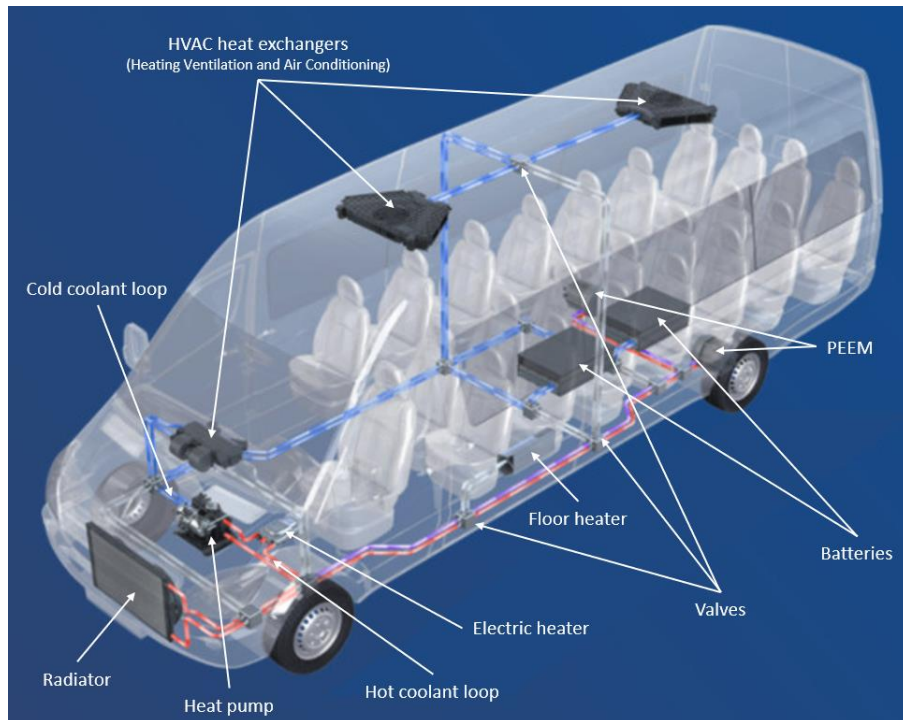


Figure 1 Illustration of the vehicle thermal management system

To execute the hardware-in-the-loop simulation, the integrated thermal management system of the vehicle was divided into two parts: the simulated part and the tested part. The tested part consists of the refrigerant circuit (which can also work as a heat pump), while the simulated part comprises the remainder of the system, including the liquid coolant loop, all associated heat exchangers (excluding the condenser and the evaporator), the cabin, the battery, and the power electronics and electric motor (PEEM). The reason behind this hardware-in-the-loop system design is rooted in the fact that the performance and the control system of the refrigerant circuit (i.e. the compressor's controller and the electronic expansion valve's controller) can be tested on a real heat pump operating as if it would be installed inside a vehicle, but without the need of assembling the entire vehicle thermal management system in the testing area. If we try to study the dynamic behaviour of our vehicle thermal management system using an accurate mathematical model, it is too time-consuming to compute the results relative to a standard driving cycle. Specifically, the solution is computed at a speed approximately ten times slower than real-time. The refrigerant circuit, being a two-phase domain, contributes significantly to reducing the time step and, consequently, the simulation speed. Consequently, a test bench was constructed to test the refrigerant circuit, enabling data exchange with the simulation environment to control the thermal loads imposed on the condenser and the evaporator.

## 2.1. Simulation environment

The vehicle thermal management system was developed using Simscape, a tool within Matlab that enables the creation of mathematical models for dynamic and steady-state simulations. Simscape utilizes pre-existing blocks containing equations that describe the physical phenomena.

The simulation environment incorporates models for the following components:

- Liquid coolant loop, including pipes, two-way and three-way valves, and T-joints. These elements compute the conservation of mass, momentum, and energy while neglecting fluid inertia and heat dissipation towards the ambient.
- Cabin volume, represented as a 0-D air volume where mass and energy conservation are calculated. To account for passenger presence, sources of heat, humidity, and CO<sub>2</sub> are imposed within the cabin volume.
- Battery pack and PEEM, modelled as thermal masses with heat generation corresponding to the driving cycle.
- Radiator and heat exchangers responsible for regulating the temperature of the cabin, battery, and PEEM. The effectiveness-NTU method is utilized to compute heat transfer between two fluids within each heat exchanger. During cooling conditions, the condensation of humidity is considered on the air side of the cabin heat exchanger.

The model for each component was calibrated to align with the data provided in the datasheet or experimental test reports from suppliers.

The system functionalities and, consequently, the configuration of coolant valves are defined to meet the requirements of each vehicle subsystem:

- Heating, cooling, ventilation, or dehumidification to maintain the cabin condition within the comfort curve defined in the VDV Nr. 236 standard (Truong, 2019).
- Heating, cooling, or equalization of the battery pack to maintain the temperature within the optimal range (10 °C – 35 °C). Equalization refers to a mode where no cooling or heating is required, but untreated coolant flows through the battery to ensure temperature uniformity.
- Cooling of the PEEM when any of its components exceed the maximum working temperature (typically around 65 °C) or to utilize the dissipated energy for heating the cabin or battery pack.

Finally, we verified that the model is capable of computing solutions at a speed faster than real-time, enabling real-time simulation synchronized with the refrigerant circuit test bench.

## 2.2. Test bench

The experimental setup used for testing the refrigeration circuit is illustrated in Figure 2. The refrigeration unit comprises five components: a compressor, a condenser, an expansion valve, an evaporator, and a receiver (not shown in Figure 2 as it is integrated into the condenser). Two liquid coolant loops are employed to control the operating conditions of the refrigeration unit, with one connected to the condenser and the other to the evaporator.

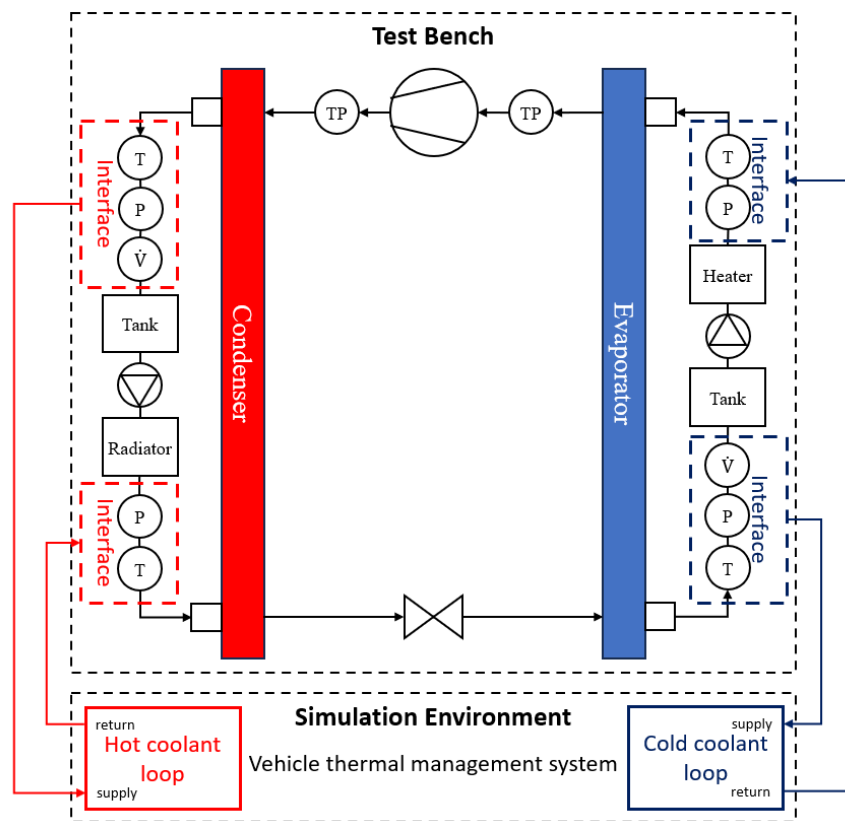


Figure 2 Layout of the HIL system. The sensors are identified as  $T$  = temperature,  $P$  = pressure,  $\dot{V}$  = volume flow rate,  $TP$  = temperature and pressure (a single sensor that measures both quantities)

Each loop includes a pump that is regulated to maintain a target liquid volume flow rate, measured using an electromagnetic flowmeter. The electromagnetic flowmeter is equipped with a measuring range of 0 – 10 m/s and an accuracy of  $0.2\% \pm 1$  mm/s. Upstream of each pump, an expansion tank is positioned to accommodate coolant expansion resulting from temperature and pressure increases. In the coolant loop on the right side of Figure 2, a radiator is installed to dissipate heat transferred to the coolant by the condenser. The rotational speed of the condenser fans is controlled using a PI controller for voltage regulation, thereby maintaining a target coolant temperature at the condenser inlet. In the other coolant loop, a high-voltage electric heater is incorporated to compensate for the heat absorbed by the evaporator from the coolant. The power of the electric heater is regulated to achieve a target temperature at the evaporator inlet. The electric heater includes a built-in temperature sensor to measure the liquid temperature within it, enabling automatic control of the absorbed power within a range of 0 W to a maximum value defined by the user, in order to attain the desired coolant temperature. To enhance the regulation of the coolant temperature at the evaporator inlet, the internal controller of the heater is not utilized, and instead, an external PI controller is employed. Consequently, a very high target temperature is set for the electric heater to operate at maximum power, while the PI controller regulates the limit to the maximum power to achieve the target coolant temperature measured by a sensor installed at the evaporator inlet. This approach is adopted for two reasons. Firstly, heat is absorbed by the fluid from the ambient environment along the pipe connecting the heater

to the evaporator, making the temperature measured by the built-in sensor not precisely representative of the evaporator inlet temperature. Secondly, the temperature sensor installed at the evaporator inlet provides higher accuracy. This PT100 sensor measures temperatures in the range of -50 – 450 °C with an accuracy of 0.25 °C. The same type of temperature sensor is utilized at the evaporator outlet and at the condenser inlet and outlet. Pressure sensors are also installed at these four locations, allowing the use of Coolprop (a thermophysical property database developed by Bell *et al.*, 2014) to determine density and specific heat based on both pressure and temperature readings. By combining these measurements with the coolant volume flow rate, the thermal power exchanged in the condenser and evaporator can be assessed using the following equation:

Equation 1: Thermal power exchanged at the evaporator/condenser

$$W = \rho \dot{V} (c_o T_o - c_i T_i)$$

Where:

- $W$  = Heat transfer rate (kW)
- $\rho$  = density of coolant calculated at the heat exchanger outlet as a function of temperature and pressure (kg/m<sup>3</sup>)
- $\dot{V}$  = volumetric flow rate of the coolant measured at the heat exchanger outlet (m<sup>3</sup>/s)
- $c_i$  = specific heat of the coolant at the heat exchanger inlet (kJ/kg K)
- $c_o$  = specific heat of the coolant at the heat exchanger outlet (kJ/kg K)
- $T_i$  = coolant temperature at the evaporator/condenser inlet (K)
- $T_o$  = coolant temperature at the evaporator/condenser outlet (K)

### 2.3. Data exchange and control logic

The hardware employed to enable data exchange between the simulation environment and the test bench is the Vector VN1670 CAN/LIN interface and the software that allows the interaction between the Simulink model and the Vector Hardware is CANoe. The simulation running on the laptop establishes communication with the Vector interface via an Ethernet bus. Subsequently, data are exchanged with the test bench, including sensors, data acquisition hardware, ECU (electronic control unit), and controlled devices, through CAN and LIN buses, as depicted in Figure 3.

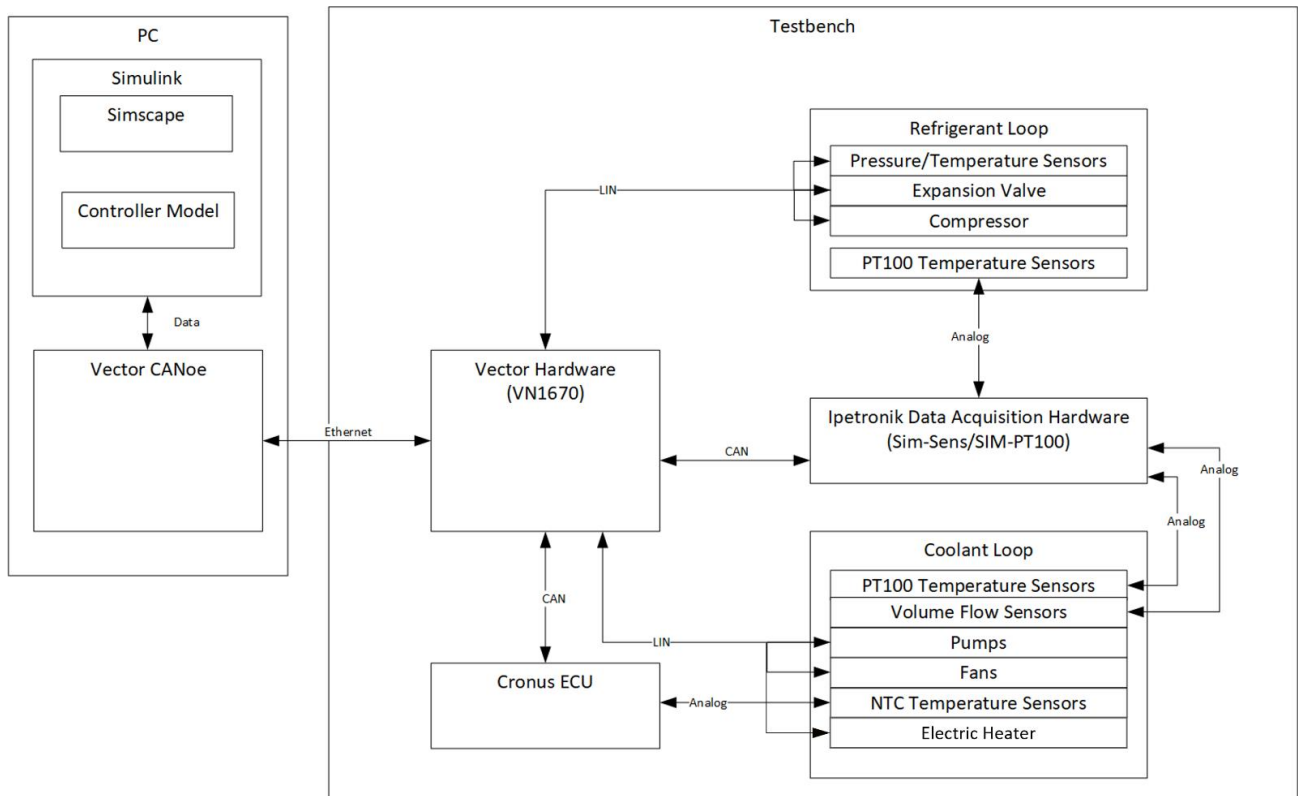


Figure 3 Communication scheme of the HIL system

The following data are exchanged between the simulation environment and the test bench:

- Compressor speed.
- Expansion valve opening steps.
- Radiator fans' voltage.

- Electric heater voltage limit and target temperature of the coolant inside it.
- Pump speeds.
- Temperature and pressure measurements in the refrigerant at the compressor inlet and outlet.
- Temperature and pressure measurements in the coolant at the evaporator inlet and outlet.
- Temperature and pressure measurements in the coolant at the condenser inlet and outlet.
- Coolant volumetric flow rates in the condenser and evaporator.

The interfaces for this system are the temperature, volume flow rate, and pressure of the coolant (as shown in Figure 2) at the:

- Condenser inlet
- Condenser outlet
- Evaporator inlet
- Evaporator outlet.

The coolant temperature measured in the test bench at the condenser outlet and at the evaporator outlet is the result of the regulation of the compressor speed, through a PI controller. These two values are imposed in the physical model, using a "Controlled Reservoir" block, to the coolant supply of the thermal management system in the hot coolant loop and cold coolant loop respectively. Then, thanks to the CANoe software that synchronizes the computation speed with the data acquisition, the physical model computes in real-time, every 0.1 s, the temperature of the coolant return from the thermal management system in both coolant loops. Consequently, these two values are used in the controller model as set points for the regulation of the radiator fans speed and of the electrical power absorbed by the heater, respectively. In this way, we can achieve the same temperature values at the condenser inlet and at the evaporator inlet on the test bench.

In the physical model, the volumetric flow rate is controlled in the two coolant loops using a "Controlled Volumetric Flow Rate Source" block positioned immediately after the "Controlled Reservoir" block. The volumetric flow rate is set equal to the measurements acquired in the two liquid coolant circuits of the test bench. To achieve this, the pumps installed in the test bench are controlled using a PI controller, ensuring a constant flow rate of 20 l/min in each loop.

The pressure is set as a constant value in the "Controlled reservoir" blocks, where the temperature of the coolant supply and return are also defined. The pressure value is determined based on measurements obtained from the test bench pipes when a coolant flow rate of 20 l/min is maintained. This simplification assumes that the variations of coolant pressure during the test are minimal due to the constant coolant flow. Consequently, when computing the energy flow using equation 1, the effects of density and specific heat variations with respect to pressure can be considered negligible (Incropera *et al.*, 2007).

## 2.4. Test conditions

The test was run setting in the physical model the simulation of an electric bus, with 10 passengers onboard, driving in summer climatic conditions, as described in the VDV Nr. 236 standard (Truong, 2019). The ambient temperature, relative humidity, and solar radiation are set at 35 °C, 50%, and 1000 W/m<sup>2</sup> respectively, while the target condition to be maintained in the cabin environment is 27 °C with a relative humidity < 50% and a CO<sub>2</sub> concentration < 1100 ppm, which corresponds to the comfort mode defined in the standard. The battery cooling is activated if the temperature of the cells is > 35 °C and then it is switched off, triggering the state of equalization, when the temperature reaches 30 °C. The PEEM in this simulation remains within the allowed working temperatures, therefore the request for active cooling is not triggered. The thermal generations inside the battery pack and PEEM are computed based on the selected driving cycle. Within the cabin, for each passenger 3 sources are imposed: 70 W of sensible heat, 0.01 g/s of CO<sub>2</sub>, and 0.04 g/s of moisture at 30 °C.

The simulation was carried out in a dynamic situation of the thermal management system to better verify the performance of the interface between the test bench and the physical model. In particular, we want to observe if the regulation of the radiator fans and of the electric heater is able to reproduce thermal loads on the condenser and evaporator, respectively, that make the heat pump work as if it was really installed inside the vehicle thermal management system. This point is assessed by checking if the coolant temperatures measured at the two refrigerant-liquid heat exchangers inlet follow closely the values computed for the coolant return temperatures in the physical model.

The simulation began with the vehicle being hot-soaked in the sun and concluded once all the vehicle's subsystems reached their target conditions, and the coolant temperature in both loops stabilized.

## 3. RESULTS

Figures 4 and 5 display the 4 temperature interfaces of the Hardware-in-the-Loop (HIL) system. In Figure 4, the dynamic profile of the coolant temperature at the outlet of the condenser and evaporator is depicted. The curves for the values measured on the test bench and those computed by the physical model in the simulation environment are perfectly superimposed. This agreement is expected since the simulation imposes identical coolant supply line temperatures as those acquired from the test bench. Figure 5 shows the same curves for the interfaces at the inlet of the condenser and

evaporator. This plot demonstrates the effective performance of the controller model in regulating the heat exchanged through the radiator and electric heater to achieve consistent temperatures at the inlet of the condenser and evaporator in both the test bench and simulation environment. The controller model performs well throughout the entire test duration.

As the battery temperature reaches 30 °C (Figure 6), and the battery thermal management subsystem shifts from cooling to equalization mode, the controller faces a sudden variation in the thermal load imposed on the evaporator and condenser, as represented in Figure 7. In this scenario, the temperature profiles (Figure 5) measured in the test bench closely follow the simulated profiles. The electric heater exhibits slightly better responsiveness compared to the radiator, with a maximum error of approximately 0.9 °C at the condenser inlet and about 0.5 °C at the evaporator inlet.

Figure 5 and Figure 7 also reveal two limitations of the test bench in terms of hardware. Initially, during the test's early stages, the measured coolant temperature is lower than the simulated one. Investigation reveals that the electric heater saturates during this phase (Figure 8), meaning it is not powerful enough to replicate the thermal load calculated in the simulation. Additionally, toward the end of the test, after the battery enters equalization mode, the temperature measured at the condenser inlet oscillates around the target with an amplitude of about 0.7 °C. This behaviour results from the radiator expelling excessive heat from the coolant when the fans are operating at minimum speed. The controller frequently switches the fan voltage supply between 0 V and the minimum value of 2.4 V to maintain the target coolant temperature (Figure 9).

Although the volume flow rate and pressure interfaces are not plotted, it is important to note that the volume flow rate is directly imposed in the simulation environment, matching the measured one at each time step. On the other hand, the pressure value is defined in the simulation as a constant, which is not updated during the test. While this value is close to the pressure measured in the test bench, it may not be exactly the same. Nevertheless, Figure 7 validates the hypothesis that the heat transfer at the heat exchangers is negligibly affected by small variations in pressure. The curves for the thermal power exchanged, computed in the simulation, align well with those obtained from measurements in the test bench when the simulated and measured coolant temperatures match.

Finally, Figure 6 showcases the performance of the heat pump in cooling down the cabin and battery pack when the ambient temperature is 35 °C, and the vehicle is exposed to significant solar radiation. Notably, the large thermal capacity of the bus battery pack is evident, as it takes nearly an hour to cool it down from 50 °C to 30 °C. Therefore, it is advisable to continually monitor the battery temperature and activate the cooling or heating mode even when the vehicle is parked, if the temperature falls outside the optimal working range.

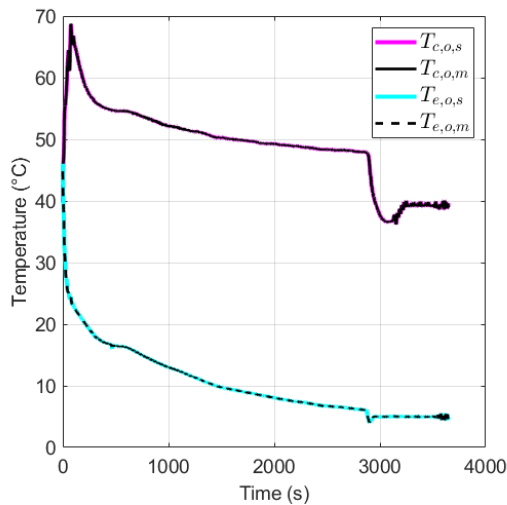


Figure 4 Interface between the test bench and the simulation environment at the outlet of the condenser and evaporator.  $T_{c,o,s}$  and  $T_{c,o,m}$  are respectively the coolant temperature at the condenser outlet computed in the simulation environment and measured on the test bench.  $T_{e,o,s}$  and  $T_{e,o,m}$  are respectively the coolant temperature at the evaporator outlet computed in the simulation environment and measured on the test bench.

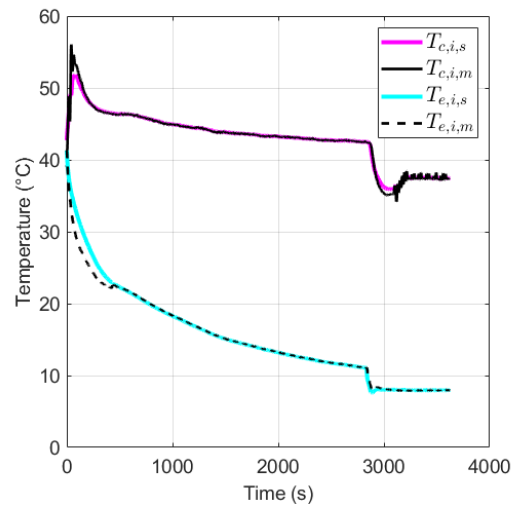


Figure 5 Interface between the test bench and the simulation environment at the inlet of the condenser and evaporator.  $T_{c,i,s}$  and  $T_{c,i,m}$  are respectively the coolant temperature at the condenser inlet computed in the simulation environment and measured on the test bench.  $T_{e,i,s}$  and  $T_{e,i,m}$  are respectively the coolant temperature at the evaporator inlet computed in the simulation environment and measured on the test bench.



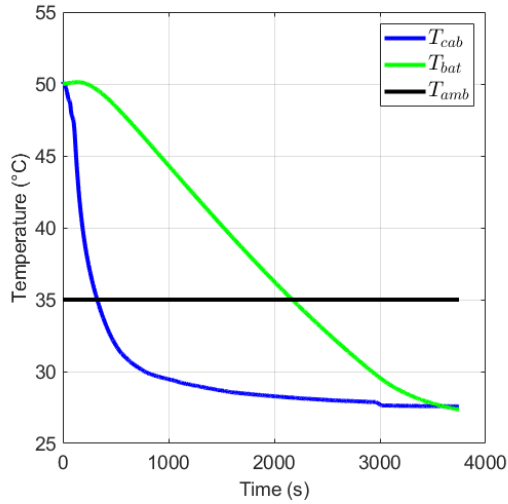


Figure 6 Evolution during the test of the cabin temperature ( $T_{cab}$ ) and battery temperature ( $T_{bat}$ ).  $T_{amb}$  represents the ambient temperature considered in the simulation environment.

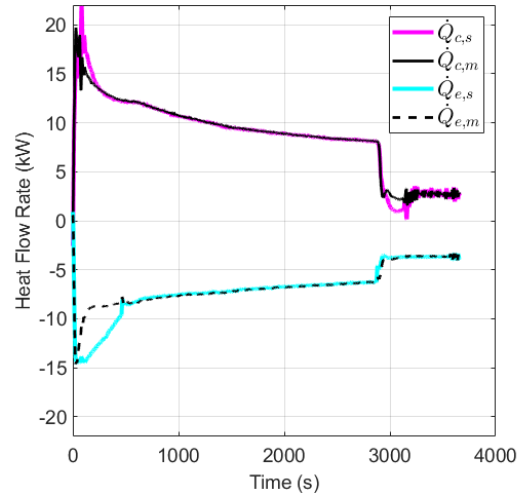


Figure 7 Comparison between the thermal power exchanged computed in the simulation environment and measured on the test bench through the condenser ( $\dot{Q}_{c,s}$  and  $\dot{Q}_{c,m}$ ) and the evaporator ( $\dot{Q}_{e,s}$  and  $\dot{Q}_{e,m}$ ).

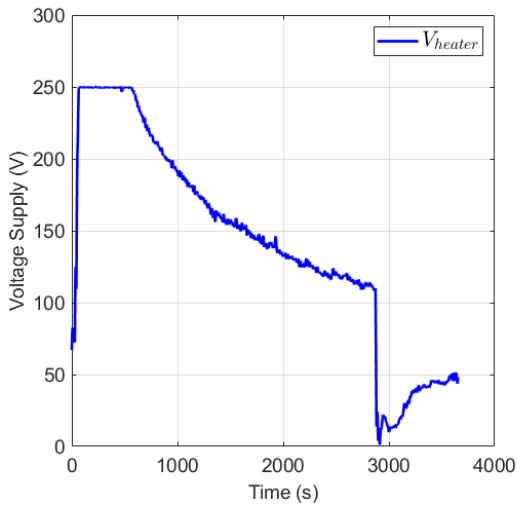


Figure 8 Regulation of the electric heater to maintain the target coolant temperature at the evaporator inlet on the test bench.

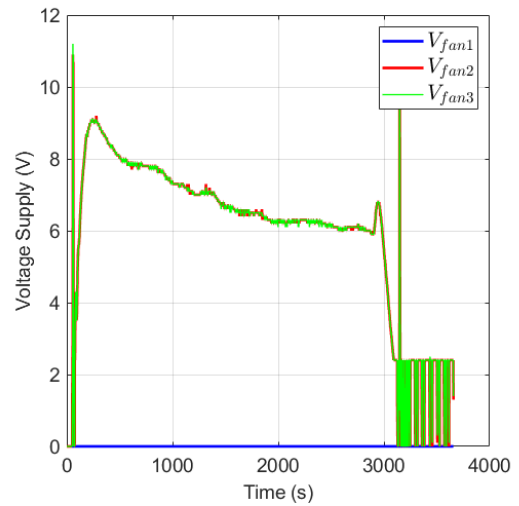


Figure 9 Regulation of the radiator fans to maintain the target coolant temperature at the evaporator inlet on the test bench.

#### 4. CONCLUSION

The thermal management system for battery electric vehicles presents greater complexity compared to traditional internal combustion engine vehicles due to the need to manage more components. As a result, simulation tools are increasingly adopted to streamline development processes and reduce costs. In this paper, we developed a Hardware-in-the-Loop (HIL) system that enables us to thoroughly test the performance and control logic of a real heat pump as if it were integrated into the thermal management system of an electric bus.

In our HIL system, the heat pump is connected to a radiator and an electric heater, while the vehicle cabin, battery pack, power electronics and electric motor (PEEM), and the overall vehicle thermal management system are modelled in Simscape. This comprehensive thermal management system encompasses two liquid coolant loops: a hot loop, heated by the condenser, and a cold loop, cooled by the evaporator. These loops distribute cold and hot coolant to the relevant heat exchangers through a system of valves.

We established interfaces before and after the condenser and evaporator on the liquid side, allowing us to exchange temperature, pressure, and volumetric flow rate data in real time between the HIL test bench and the simulation environment. A controller model effectively utilizes this data to regulate the thermal power exchanged through the radiator and heater, accurately reproducing the computed thermal load in the simulation for both coolant loops.



Our results demonstrate the overall efficacy of the controller model, indicating that it can effectively manage the thermal load. However, we also identified two limitations in terms of hardware for our HIL system. Firstly, the electric heater's power proved insufficient during certain phases of the test, suggesting the need for a more powerful alternative. Secondly, the radiator exhibited some limitations during the final phases of the test, with temperature oscillations occurring around the target temperature, implying the requirement for a smaller version of the radiator.

In conclusion, by addressing the identified hardware limitations, future iterations of the system could lead to more efficient and accurate testing, aiding in the advancement of thermal management systems for electric vehicles. The integration of HIL testing with advanced simulation models offers an effective and cost-efficient approach for ensuring the robustness and performance of such systems in the transition to a sustainable future of transportation.

## 5. REFERENCES

- Bell, I.H. *et al.* (2014) 'Pure and pseudo-pure fluid thermophysical property evaluation and the open-source Thermophysical Property Library coolprop', *Industrial & Engineering Chemistry Research*, 53(6), pp. 2498–2508. doi:10.1021/ie4033999.
- Edge, J.S. *et al.* (2021) 'Lithium ion battery degradation: What you need to know', *Physical Chemistry Chemical Physics*, 23(14), pp. 8200–8221. doi:10.1039/d1cp00359c.
- Farrington, R. and Rugh, J. (2000). 'Impact of Vehicle Air-Conditioning on Fuel Economy, Tailpipe Emissions, and Electric Vehicle Range', *Earth Technologies Forum*. Washington, D.C.
- Horrein, L. *et al.* (2017) 'Impact of heating system on the range of an electric vehicle', *IEEE Transactions on Vehicular Technology*, 66(6), pp. 4668–4677. doi:10.1109/tvt.2016.2615095.
- Incropera, F. P. *et al.* (2007), *Fundamentals of Heat and Mass Transfer*. 6<sup>th</sup> Edition. New York City, New York: John Wiley & Sons, Inc.
- Lee, J.T. *et al.* (2013) 'Effect of air-conditioning on driving range of electric vehicle for various driving modes', *SAE Technical Paper Series* [Preprint]. doi:10.4271/2013-01-0040.
- Leighton, D. (2015) 'Combined fluid loop thermal management for Electric Drive Vehicle Range Improvement', *SAE International Journal of Passenger Cars - Mechanical Systems*, 8(2), pp. 711–720. doi:10.4271/2015-01-1709.
- Ma, J. *et al.* (2022) 'Experimental study on the performance of Vehicle Integrated Thermal Management System for pure electric vehicles', *Energy Conversion and Management*, 253, p. 115183. doi:10.1016/j.enconman.2021.115183.
- Muratori, L. *et al.* (2022) 'A vehicle integrated thermal management system for electric busses', *2022 IEEE International Workshop on Metrology for Automotive (MetroAutomotive)*. doi:10.1109/metroautomotive54295.2022.9855156.
- Tian, Z. *et al.* (2018) 'Investigation on an integrated thermal management system with battery cooling and motor waste heat recovery for electric vehicle', *Applied Thermal Engineering*, 136, pp. 16–27. doi:10.1016/j.applthermaleng.2018.02.093.
- Truong, M.T. (2019). VDV-Schrift Nr. 236 - 'Air conditioning of buses of the classes I (Urban bus) and II (Suburban bus), for conventional diesel and gas buses as well as for hybrid, fuel cell and electric buses'. [online] Verband Deutscher Verkehrsunternehmen. Available at: <https://www.vdv.de/downloads/3054/236%20%20SEK/forced>.

---

## #256: The impact of PV, battery and Immersun on the Meadows community: data analysis of Project SENSIBLE

---

Jun GUAN<sup>1</sup>, Mark GILLOTT<sup>2</sup>, Mark SUMNER<sup>3</sup>, Eldar NAGHIYEV<sup>4</sup>

<sup>1</sup> University of Nottingham, Nottingham, UK, Jun.Guan@nottingham.ac.uk

<sup>2</sup> University of Nottingham, Nottingham, UK, mark.gillott@nottingham.ac.uk

<sup>3</sup> University of Nottingham, Nottingham, UK, mark.sumner@nottingham.ac.uk

<sup>4</sup> Siemens, Nottingham, UK, eldar.naghiyev@gmail.com

*Abstract: High energy prices and the goal of net zero by 2050 are putting pressure on the lives of people in the UK. Project SENSIBLE is a programme that ended five years ago with the goal of saving energy costs and carbon emissions by installing renewable energy devices in houses within the Meadows community in order to achieve self-consumption of electricity. In this paper, the data records of the project are collated and the relationship between PV, battery, Immersun and energy trading is analysed separately from the perspective of electricity exchange. The impact on economic and carbon emission indicators from different operating strategies of renewable energy devices is finally summarised. Firstly, the typical daily load profile of a single house is summarised in a regular manner and it is concluded that the peak energy use is almost entirely in periods of high rate. Secondly, the contribution of different control strategies to peak shaving is analysed, concluding that battery can reduce electricity sales by more than 60% and use this electricity for their own consumption, resulting in more efficient use of PV output. On this basis, by considering the change in electricity price during a day, it is concluded that the combination of PV and storage devices can reduce the amount of electricity bought during periods of high rate by more than 50%, with positive impact on the reduction of carbon emissions. Finally, a simulation of three houses with renewable energy equipment supporting one house with conventional energy sources is presented to show that the formation of a community energy network can further reduce the exported energy with very low income, improving the use of PV output and reducing energy cost. As there is still excess PV output, the use of heat pumps will be considered in the future to further improve energy efficiency.*

*Keywords: Self consumption; Energy cost; Carbon emission*

## 1. INTRODUCTION

Reducing carbon emissions in terms of electricity supply is significant in achieving the ambition of net zero (Vieira, Longo and Mura, 2021). After the Paris agreement in 2015, many countries around the world have been tending to reduce carbon emissions by replacing fossil energy sources with renewable energy sources (Taylor et al., 2022). However, the fact is that the goal of meeting the 2030 global warming temperature limit cannot be achieved with the current level of carbon reduction (UNEP, 2022). Therefore, expanding the proportion of renewable energy equipment installed as well as improving their energy efficiency has become a research hot spot. In 2022, wind power accounted for 26.8% of the electricity generated in the UK (NationalgridESO, 2023). About half of it came from offshore wind power (Energydashboard, 2023). However, the number of onshore wind turbines in the UK has decreased dramatically in recent years (Edward, 2022). Photovoltaic (PV) power generation in the UK accounted for 4.4% of total power generation in 2022, with the vast majority of PV power coming from small solar panels on residential buildings (Smartenergy, 2022).

Residential electricity consumption accounts for the largest share of total electricity consumption in the UK (Statista, 2023). The establishment of community-level integrated energy systems (IES) is one of the potential demand-side approaches that could achieve reductions in energy cost as well as carbon emissions. Ideally, a community-level IES would be able to self-manage and reduce the need to buy electricity from the grid. Mazzeo et al. (2021) adopted wind power and PV as the renewable energy generation component of the energy community and used Artificial Neural Networks methodology for output prediction. It was notable that the effects of different climates and geographic locations on power generation should be considered. Renewable energy generation is intermittent and voluntary. Electricity and heat storage technologies are commonly applied to improve the efficiency of renewable energy use in both the short and long term. Viteri et al. (2023) conducted a literature review on potential green hydrogen technologies for isolated energy community and concluded that hydrogen storage has advantages over batteries in terms of stability to maintain the balance between electricity supply and demand in the long term. However, the relationship between the location of hydrogen storage and safety should be considered. Ceglia et al. (2023) suggested that the incorporation of biomass into the cogeneration of energy communities could enhance the self-consumption of heat and electricity. Based on the results of a carbon simulation of a hypothetical post-electrification energy system. Jing, Zhou and Wu (2022) concluded that the widespread use of heat pumps would be a key step in the decarbonisation of thermal energy. However, the widespread use of heat pumps would increase peak electricity consumption and put pressure on the local grid. Consequently, energy management strategies should be used to reduce the costs associated with grid renovation.

The study of operation control strategies covers a wide range of aspects from long-term planning to short-term scheduling to ultra-short-term control. For example, Palmintier and Webster (2016) presented a planning method based on an integer-based clustering method in the field of long-term planning, and proposed planning for the allocation of renewable energy generation facilities from the perspectives of reducing operating costs and reducing carbon emissions respectively. Acha et al. (2018) proposed a planning method that enables the simultaneous capacity design, selection, and operation of multiple energy devices in a commercial building. Elkazaz et al. (2020) designed a two-layer smart home energy management system. The first layer is a day-ahead scheduling system, which functions to schedule the energy of the household power system for the next 24 hours, based on PV output forecasts and load forecasts, with the objective of minimum energy cost, updated every 15 minutes. The other layer is a real-time control system that adjusts the actual power exchange of the system by means of different control strategies for the batteries at different times of the day, updated every 1 minute. Through simulations and experiments, it was concluded that this home energy management system could increase the self-consumption of PV output and reduce energy costs. However, it only considered the use of PV and batteries and not the electrification of thermal energy. Furthermore, it was studied for a household level energy system, so the applicability to community level energy systems needs to be further investigated.

Project SENSIBLE aimed to improve the efficiency of energy use and reduce energy costs in the Meadows community by means of energy storage (Mendes et al., 2017). By categorising the electricity consumption data recorded by smart meters for several houses during the period 2018-2019, the houses installed with renewable energy related equipment could be divided into two groups, one with PV and batteries and the other with PV and Immersun. The data results are analysed in the following aspects in terms of changes in load demand during a typical day, impact of PV on energy exchange, impact of PV and battery on energy exchange, impact of PV and Immersun on energy exchange, contribution of renewable energy devices to the improvement of energy efficiency, contribution of renewable energy devices to the reduction of energy costs and carbon emissions. On this basis, the potential for the development of small energy community in the future is discussed.

## 2. METHODOLOGY

Project SENSIBLE was carried out in the Meadows community in Nottingham, UK. The houses participating in the research programme were installed with mainly three renewable energy devices - PV, batteries, and Immersun - in order to reduce the electricity costs incurred by buying electricity from the grid. The data analysed in this paper came from the 2018-2019 electricity power information recorded by the three-phase smart meters or three one-phase smart meters installed in each house. The data from the smart meters were uploaded in one-minute steps to the SENSIBLE data platform, which was available for download via MATLAB.

PV was chosen as the renewable energy generation facility, with battery and Immersun as the energy storage facility. In this case, two control strategies are available for the batteries. One strategy is to charge the batteries from the excess of

PV output to meet the house load when the irradiation is strong, and the stored electricity is discharged to maintain the balance of power when the PV is unable to meet the house demand. The other strategy is to purchase electricity from the grid for charging during periods of low tariffs and discharging at high tariffs time to cover the difference between the PV output and the house demand (TESLA, 2016). Immersun converts excess PV output into heat (Adamson et al., 2019). Compared to battery, Immersun has a simpler control structure and is cheaper to install, but requires a water storage device for example a hot water tank.

Electricity costs were calculated by dividing the rate into high and low tariffs over the duration of the whole day, as shown in Table 1.

Table 1: Electricity Prices

Low Unit Rate (00:00-07:30)	High Unit Rate (07:30-24:00)	Feed-in Tariff
6.83p/kWh	13.99p/kWh	2.16p/kWh

Carbon emissions were calculated based on the historical carbon intensity of the East Midlands at half-hourly steps on electricity info website. Figure 1 shows the change in carbon intensity for a random day in the summer of 2018 (Electricity Info, 2023).

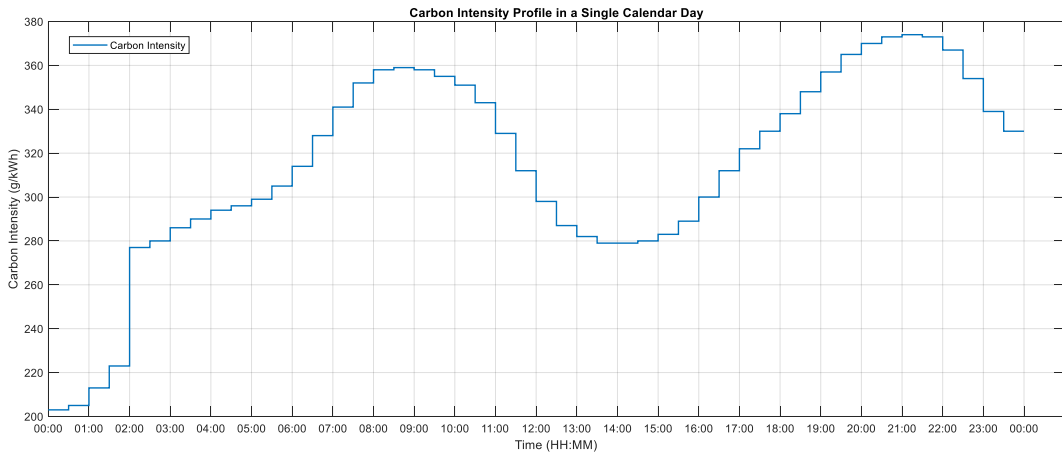


Figure 1 Carbon intensity profile for a summer day in 2018

A control strategy with a small energy community as the management object is used in order to maximise the self-consumption of the PV output. The control strategy focuses on setting the objective function and constraints for energy management, which in the case study of this paper includes PV, batteries, Immersun, grid trading, and load demand. The PV output and load profiles are taken from the data records of the smart meters. By considering only the electricity steady-state process, only the battery needs to be modelled.

The battery in charging and discharging process satisfies the constraint as shown in Equation 1. It indicates that both battery charging and discharging cannot exceed the maximum charging and discharging power limit. And battery can only be in one state among charge state, inactive state and discharge state at a certain moment.

Equation 1: Battery charging and discharging constraints.

$$\begin{cases} 0 \leq P_{cha}^{BT}(t) \leq B_{cha}^{BT}(t) \cdot P_{cha,max}^{BT} \\ 0 \leq P_{dis}^{BT}(t) \leq B_{dis}^{BT}(t) \cdot P_{dis,max}^{BT} \\ 0 \leq B_{cha}^{BT}(t) + B_{dis}^{BT}(t) \leq 1 \end{cases}$$

Where:

- $B_{cha}^{BT}(t)$  = 0-1 variables indicating the battery charging activity
- $B_{dis}^{BT}(t)$  = 0-1 variables indicating the battery discharging activity
- $P_{cha}^{BT}(t)$  = continuous variables that indicate the power of battery charging (W)
- $P_{dis}^{BT}(t)$  = continuous variables that indicate the power of battery discharging (W)
- $P_{cha,max}^{BT}$  = fixed quantities representing the maximum charging power of the battery (W)
- $P_{dis,max}^{BT}$  = fixed quantities representing the maximum discharging power of the battery (W)

Keeping the state of charge (SOC) within a certain range protects the battery from over charging and over discharging. SOC is defined as shown in Equation 2.

Equation 2: Battery SOC definition.

$$SOC^{BT}(t) = \frac{S^{BT}(t)}{S_R^{BT}}$$

Where:

- $S^{BT}(t)$  = remaining charge of the battery (kWh)
- $S_R^{BT}$  = rated capacity of the battery (kWh)
- $SOC^{BT}(t)$  = battery state of charge

The SOC satisfies the constraints as shown in Equation 3. It contains the upper and lower limits that the SOC values should meet and the consistency of the SOC value at the end of each run control with the SOC value at the start of the next run control.

$$\text{Equation 3: SOC constraints.} \quad \left\{ \begin{array}{l} SOC_{min}^{BT} \leq SOC^{BT}(t) \leq SOC_{max}^{BT} \\ SOC^{BT}(t) = SOC^{BT}(t-1) + \frac{P_{cha}^{BT}(t) \cdot \Delta T \cdot \eta_{cha}^{BT} - P_{dis}^{BT}(t) \cdot \Delta T \cdot \eta_{dis}^{BT}}{S_R^{BT}} \\ SOC^{BT}(0) = SOC^{BT}(1440) \end{array} \right.$$

Where:

- $SOC_{min}^{BT}$  = lower limit of SOC
- $SOC_{max}^{BT}$  = upper limit of SOC
- $\eta_{cha}^{BT}$  = charging efficiency of battery
- $\eta_{dis}^{BT}$  = discharging efficiency of battery
- $\Delta T$  = control interval (1 min)

The upper and lower limits on the buying and selling of electricity are constrained as shown in Equation 4.

$$\text{Equation 4: Grid trading constraints.} \quad \left\{ \begin{array}{l} 0 \leq P_{buy}^G(t) \leq B_{buy}^G(t) \cdot P_{buy,max}^G \\ 0 \leq P_{sell}^G(t) \leq B_{sell}^G(t) \cdot P_{sell,max}^G \\ B_{buy}^G(t) + B_{sell}^G(t) \leq 1 \end{array} \right.$$

Where:

- $P_{buy}^G(t)$  = imported power (W)
- $P_{buy,max}^G$  = upper limit of imported power (W)
- $B_{buy}^G(t)$  = 0-1 variable indicating if electricity is bought from grid
- $P_{sell}^G(t)$  = exported power (W)
- $P_{sell,max}^G$  = upper limit of exported power (W)
- $B_{sell}^G(t)$  = 0-1 variable indicating if electricity is sold to grid

In addition, the system should also satisfy the power balance constraint, as shown in Equation 5.

$$\text{Equation 5: Power balance constraint.} \quad P^{PV}(t) - P^L(t) + B_{buy}^G(t) \cdot P_{buy}^G(t) - B_{sell}^G(t) \cdot P_{sell}^G(t) + B_{dis}^{BT}(t) \cdot P_{dis}^{BT}(t) - B_{cha}^{BT}(t) \cdot P_{cha}^{BT}(t) = 0$$

Where:

- $P^{PV}(t)$  = positive PV output (W)
- $P^L(t)$  = positive load demand (W)

After modelling PV output, batteries, load profiles and power balance, an objective function needs to be presented. In this paper the lowest electricity cost is used as the objective function.

The cost of electricity for every time period is represented by Equation 6.

$$\text{Equation 6: Definition of energy cost.} \quad C^{step}(t) = \left( P_{buy}^G(t) \cdot \Delta T \cdot C_{buy}^{step}(t) - P_{sell}^G(t) \cdot \Delta T \cdot C_{sell}^{step}(t) \right) / 60000$$

Where:

- $C^{step}(t)$  = cost of electricity for every time period (pence)
- $C_{buy}^{step}(t)$  = unit rate of electricity bought (pence/kWh)
- $C_{sell}^{step}(t)$  = unit reward of electricity sold (pence/kWh)

Daily electricity costs are expressed by Equation 7.

Equation 7: Definition of daily electricity costs.

$$C_{total} = \sum_t^{1440} C^{step}(t)$$

Where:

- $C_{total}$  = daily electricity costs (pence)

It is evident that the problem is a Mixed Integer Linear Programming (MILP) which can be solved by Cplex via Yalmip.

### 3. ANALYSIS

The data recorded by Project SENSIBLE is analysed from the contribution of renewable energy devices to the reduction of energy costs and carbon emissions. Furthermore, the potential for the Meadows Community to develop into a small energy community in the future is also analysed.

#### 3.1. Smart meter data analysis

Figure 2 shows the load profile for a house on a typical summer day and a typical winter day. The time between 0:00 and 7:30 is the low unit rate period and the time between 7:30 and 24:00 is the high unit rate period. There are four peak points in a typical summer day, which could be probably cooking breakfast, cooking lunch, cooking dinner and evening bath. Beyond that the base line of power demand is caused by the fridge and the standby of various appliances. The load profile of typical winter day does not show significant differences compared to that of typical summer day, which is mainly because the house is heated entirely by gas rather than electricity.

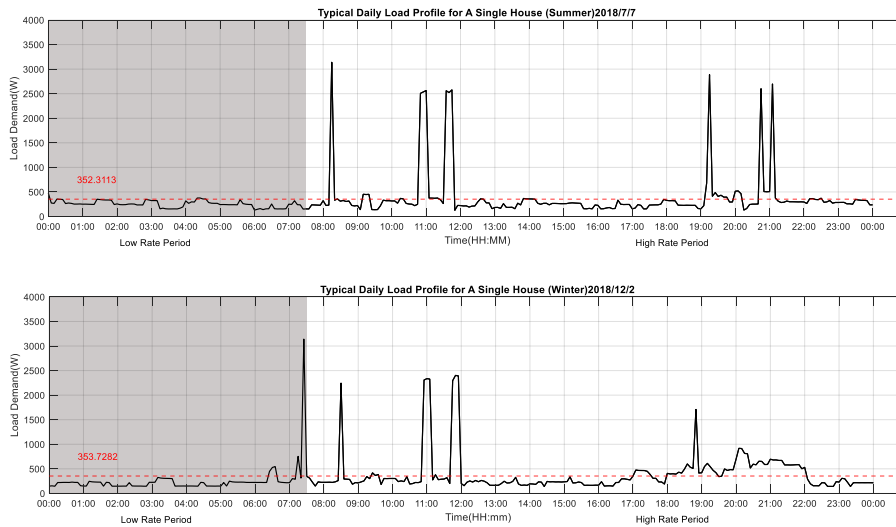


Figure 2 Two load profiles for a single house within typical days

In summary, most of the peaks in electricity consumption in the house occur during high rate time, which also means large energy costs. The access to renewable energy devices such as PV and batteries could change this situation.

Figure 3 illustrates the exchange of electricity during the day after the building is equipped with PV. The figure shows that the PV output peaks when the irradiance is high during the day, but the load demand does not reach its maximum at the same time. At this point, the excess PV output after meeting the load demand is sold to the grid. After the evening peak starting around 17:00 (one to two hours later in summer than in winter), which is also a period of high unit rate, the PV output decreases and almost all the electricity needed for the house is purchased from the grid. Therefore, PV can reduce the cost of electricity consumption to a certain extent, but there is still space for improvement.

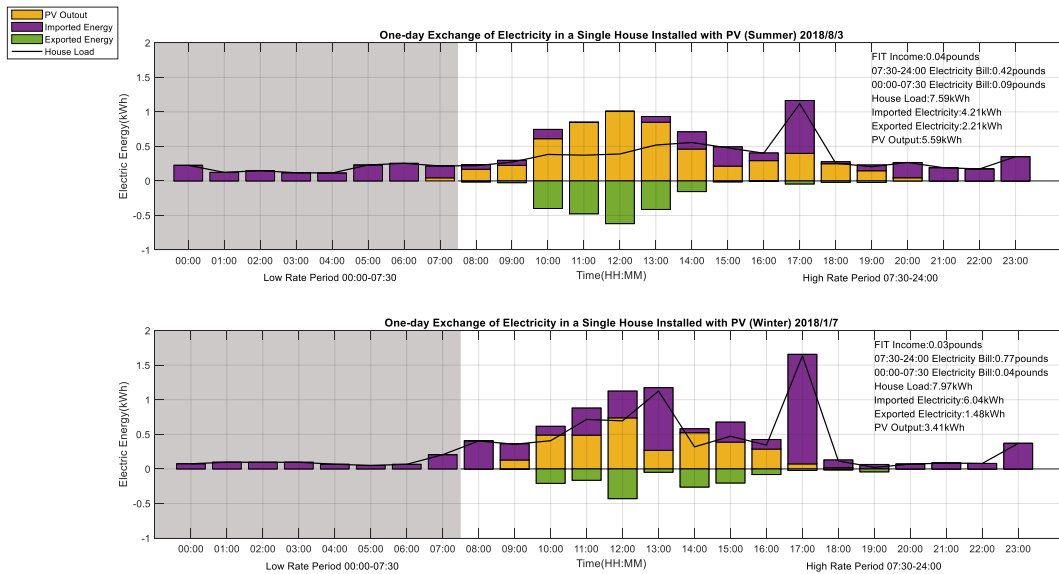


Figure 3 Daily electricity exchange in a single house installed with PV

Figure 4 illustrates the exchange of electricity within a day after the building is installed with the PV and the battery. The Figure shows that after the battery is installed, excess PV output charges the battery in preference to being sold to the grid. The charged battery is discharged when the PV output is insufficient, reducing the amount of power imported and achieving a reduction in energy cost. It should be noted that another type of battery control is to buy electricity from the grid for charging during periods of low electricity tariff and discharge it during periods of high electricity tariff. This type of control method can be used as a potential optimisation tool for community level energy systems.

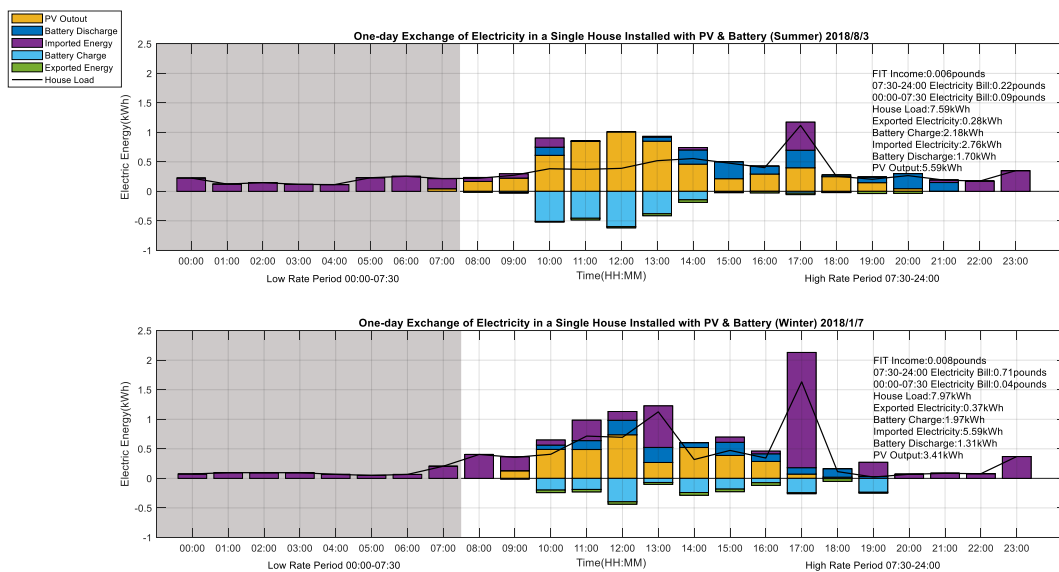


Figure 4 Daily electricity exchange in a single house installed with PV and battery

Immersun can be regarded as a battery without a discharge function. It reduces energy costs and increases energy efficiency by converting excess PV output into thermal energy to provide hot water for the house. It is worth noting that the Immersun can only convert electricity to thermal energy, not thermal energy to electrical energy, and has no direct connection to the grid. Therefore, there is no selling of electricity directly from the Immersun to the grid. The small amount of electricity exported shown in Figure 5 is the part of the PV output that is used to turn on the Immersun and keep it in operation, which is related to the internal control structure of Immersun. This part of the electricity is not involved in sales to the grid.

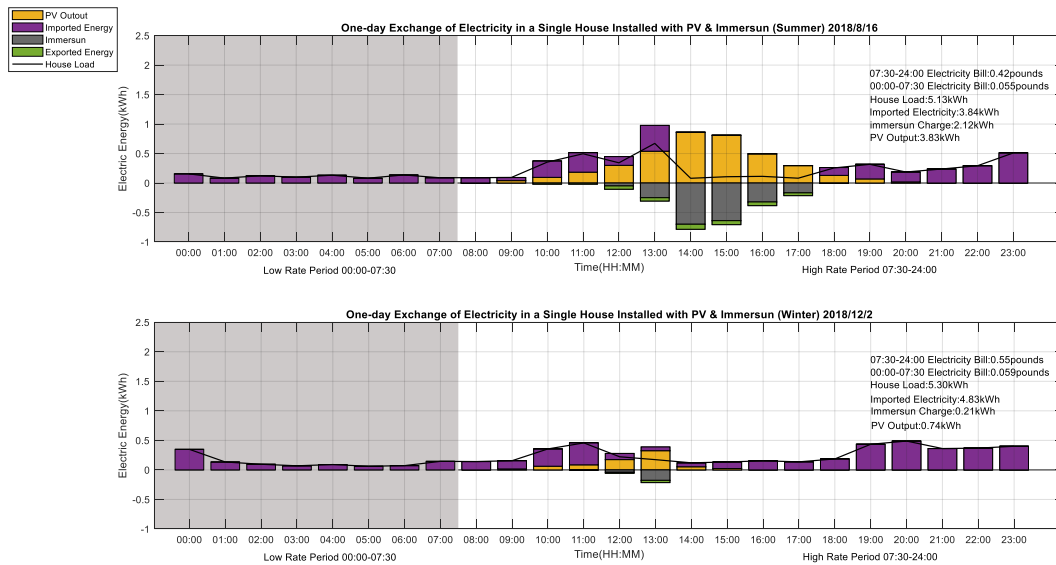


Figure 5 Daily electricity exchange in a single house installed with PV and Immersun

Using PV and battery as an example, the annual energy consumption of 7 houses installed with renewable energy equipment is calculated and the results are shown in Figure 6. As can be seen from the graph, the combination of PV and battery can effectively reduce the amount of electricity bought in times of high unit rate. The reduction in electricity selling during high rate periods means that more electricity is stored in the battery.

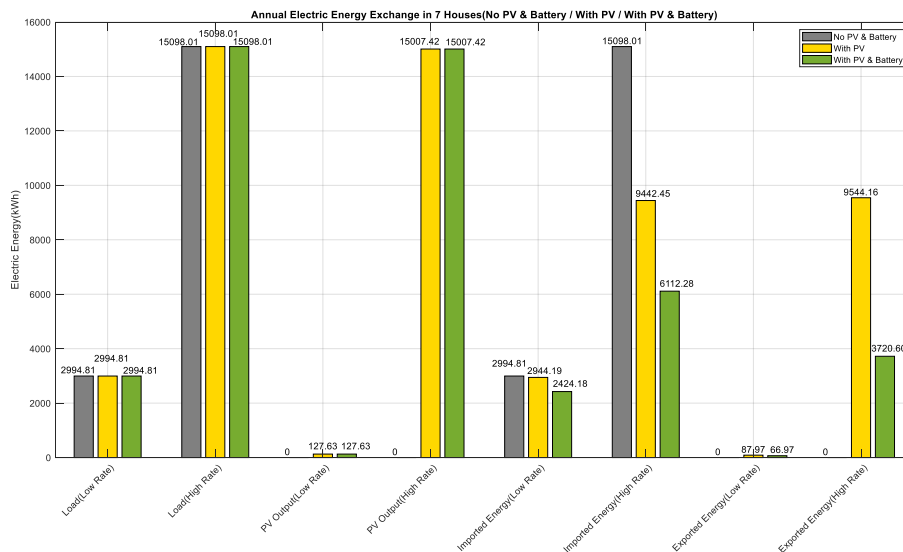


Figure 6 Annual electricity exchange and consumption of 7 houses

Using PVs and battery as an example, the annual energy costs and carbon emissions of 7 houses installed with renewable energy equipment are calculated and the results are shown in Figure 7. Table 2 further shows the detailed improvement.

Table 2: Contribution of renewable energy equipment to energy savings and carbon emissions

	Imported Reduction (High rate)	Imported Reduction (Low rate)	Exported Energy (High rate)	Exported Energy (Low rate)	Electricity Cost Savings	Carbon Emission Savings
PV Only	37.4%	1.7%	9544.1kWh	87.8kWh	1046.0pounds	1548.1kg
PV & Battery	59.5%	19.1%	3720.6kWh	66.9kWh	1394.8pounds	3185.3kg



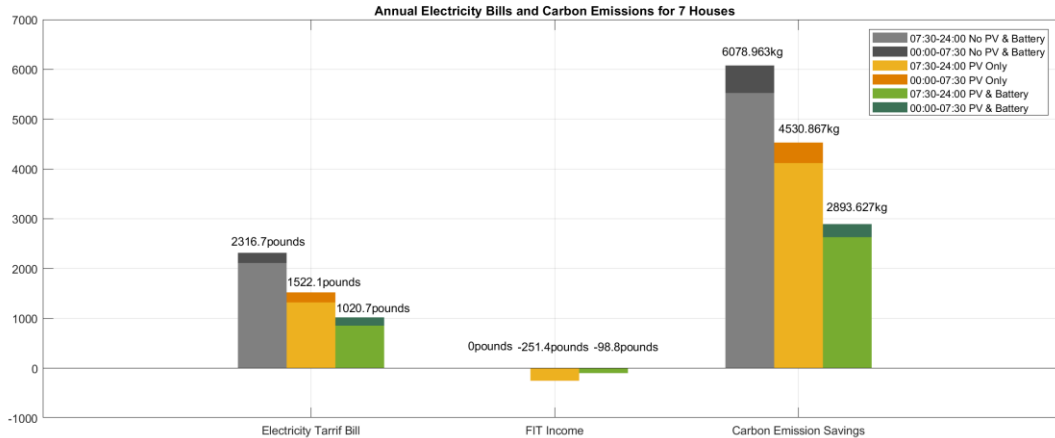


Figure 7 Annual electricity cost and carbon emissions of 7 houses

As can be seen from the graphs and table, both PV and battery devices can effectively improve energy efficiency, reduce energy costs and reduce carbon emissions by reducing the need to trade with the grid. The combination of PV and battery can provide greater benefits than PV alone.

### 3.2. Control strategy analysis

From the above analysis, it is clear that for a single house, even the use of both PV and battery storage will not completely consume all of the PV output. It means that some of the PV output is available for sale to the grid. Considering that the income from selling electricity to the grid is very low compared to the cost of purchasing electricity, it becomes a concern to utilise this PV output excess to the fullest. The establishment of community energy systems could be one answer to this problem.

In this case, it is attempted to consider houses without and with renewable energy devices as a micro-energy system and to investigate whether it is possible to reduce the cost of electricity in houses without renewable energy devices while ensuring that the inhabitants living in houses with renewable energy devices have normal access to electricity. Three houses equipped with PV and batteries and one house without any renewable energy equipment are chosen to solve for the operation of the micro-energy system formed by the four houses on a typical summer day, and the results are shown in Figures 8 to 10.

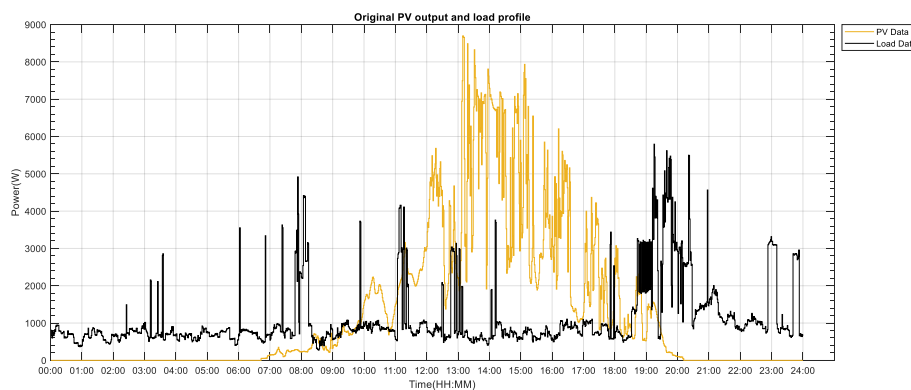


Figure 8 Original total PV output of 3 houses and load demand of 4 houses

Figure 8 illustrates the total PV output profile for the 3 houses versus the load profile for the 4 houses during a typical summer day. It is evident that the PV output of the three houses is sufficient to meet the demand of the four houses during the time period of high irradiation intensity at midday. The excess PV output offers the possibility for micro peer-to-peer energy systems to support each other and reduce electricity consumption.

Figure 9 illustrates the exchange of electricity in the small energy community. As can be seen from the Figure, the system uses significantly less power for sales to the grid than before the energy management occurred, initially meeting the objective of keeping as much energy as possible in the community. Battery charging and discharging activity is active, with load demand being met entirely by PV output and battery discharge during periods of high unit rate. During periods of low unit rate, the power balance is achieved by purchasing electricity from the grid only when discharging power from the battery is not sufficient to meet load demand, which helps to reduce electricity costs.

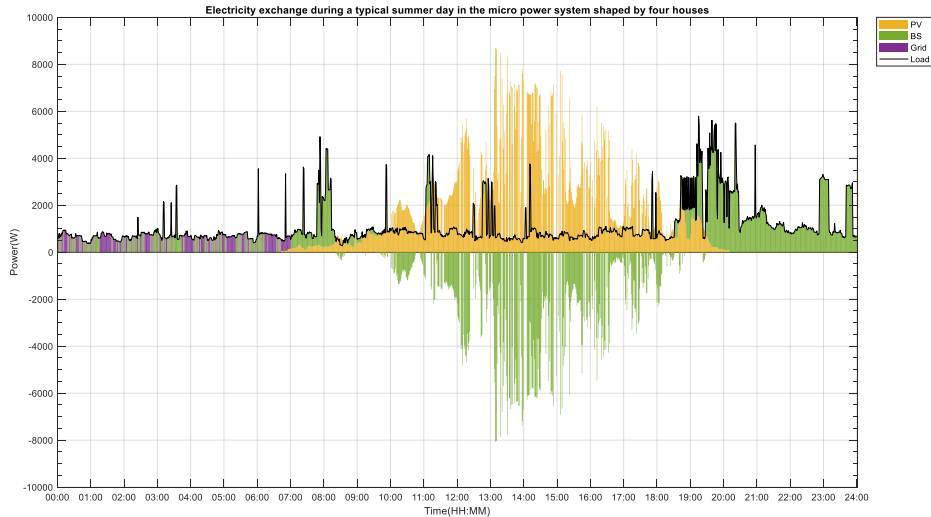


Figure 9 One-day electricity exchange after the implementation of an operating strategy targeting minimum electricity cost

The total cost of electricity for the four houses during a typical summer day before the small energy community is calculated to be 51.02 pence. After improvement, the cost of electricity for the 4 houses during a typical summer day is 18.78 pence. The results show that it is possible to reduce electricity consumption and increase energy efficiency by managing the combination of individual houses to form an energy community without installing additional renewable energy equipment.

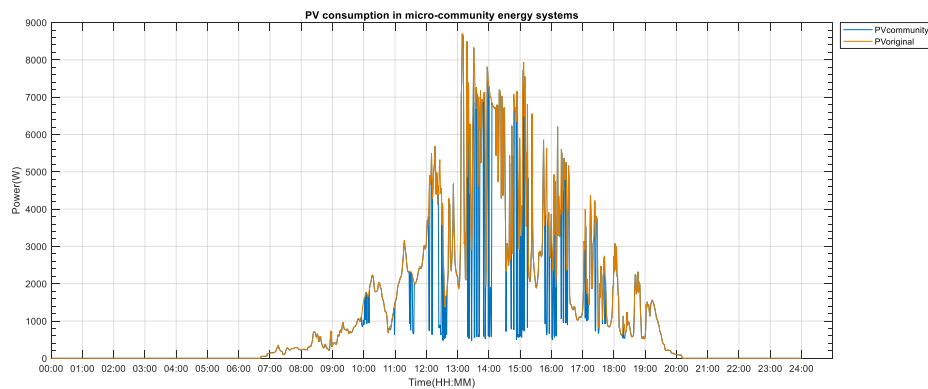


Figure 10 Comparison of PV output and actual PV output being used

As can be seen in Figure 10, after the development of energy community, there is still some excess PV output. To further utilise this excess PV output in the energy system, the installation of electrical energy conversion equipment such as heat pumps can be considered.

#### 4. CONCLUSION AND FUTURE WORK

In this study, the analysis of data records from Project SENSIBLE is used as an example to summarise the effect of the renewable energy storage equipment installed in the Meadows community on improving the energy efficiency of the house, reducing residential electricity costs and reducing carbon emissions. The potential for upgrading the houses in this community from an individual energy system to a micro-community energy system and the potential for the use of heat pumps are further analysed at the energy balance level. Specific conclusions are shown below.

PVs can relieve the pressure on load demand partially at times of high electricity prices, but excess PV output cannot be used locally. The combination of PVs and batteries makes it possible for the excess PV output to be utilised by the energy system in which it is located. Different methods of battery control correspond to different methods of energy storage. In this case, the battery is set to charge when there is a surplus of PV and discharge when the PV does not meet the load demand. It cannot be charged during periods of low electricity prices, which can lead to some economic losses.

By combining three renewable energy houses and one conventional energy house into a small energy community through MILP and performing an operation control analysis, it can be concluded that the energy community system has better economic benefits than a stand-alone house energy system. Issues related to heat pumps will be discussed in the next stage of the study.

## 5. REFERENCES

- Acha, S. et al. (2018) 'Optimal design and operation of distributed low-carbon energy technologies in commercial building', *Energy*, Volume 142, pp. 578-591.
- Adamson, M.A. et al. (2019) 'Development of a control system for a domestic grid-connected wind turbine', *Journal of computational and theoretical nanoscience*, 16(5-6), pp. 2249- 2258.
- Ceglia, F. et al. (2023) 'Energy and environmental assessment of a biomass-based renewable energy community including photovoltaic and hydroelectric systems', *Energy*, Volume 282, p. 128348.
- Edward, R. (2022) *The future of onshore wind turbines from 2022 onwards*. Available at: <https://www.boythorpewindenergy.co.uk/the-future-of-onshore-wind-turbines-from-2022-onwards/> (Accessed: 17 July 2023).
- Electricity Info (2023) *Regional Data Archive*. Available at: <https://electricityinfo.org/region-archive/> (Accessed: 17 July 2023).
- Elkazaz, M. et al. (2020) 'A hierarchical two-stage energy management for a home microgrid using model predictive and real-time controllers', *Applied Energy*, Volume 269, p. 115118.
- Energydashboard (2023) *Electricity Generation / Supply*. Available at: <https://www.energydashboard.co.uk/data> (Accessed: 17 July 2023).
- Jing, R., Zhou, Y. and Wu, J. (2022) 'Electrification with flexibility towards local energy decarbonization', *Advances in Applied Energy*, Volume 5, p. 100088.
- Mazzeo, D. et al. (2021) 'Artificial intelligence application for the performance prediction of a clean energy community', *Energy*, Volume 232, p.120999.
- Mendes, G. et al. (2017) 'SENSIBLE project community engagement both in Évora and Nottingham demonstrator sites', *24th International Conference on Electricity Distribution*, 2017(1), pp. 2897-2900.
- NationalgridESO (2023) *Britain's Electricity Explained: 2022 Review*. Available at: <https://www.nationalgrideso.com/news/britains-electricity-explained-2022-review> (Accessed: 17 July 2023).
- Palmintier, B. S. and Webster, M. D. (2016) 'Impact of operational flexibility on electricity generation planning with renewable and carbon targets', *IEEE Transactions on Sustainable Energy*, 7(2), pp. 672-684.
- Smartenergy (2022) *Solar panel statistics UK 2022: Everything you need to know*. Available at: <https://uk.smartenergy.co/blog/solar-panel-statistics-uk-2022/> (Accessed: 17 July 2023).
- Statista (2023) *Electricity demand in the United Kingdom (UK) 2000-2022*. Available at: <https://www.statista.com/statistics/323381/total-demand-for-electricity-in-the-united-kingdom-uk/> (Accessed: 17 July 2023).
- Taylor, P. C. et al. (2022) 'An interdisciplinary research perspective on the future of multi-vector energy networks', *International Journal of Electrical Power & Energy Systems*, Volume 135, p.107492.
- TESLA (2016) *TESLA Powerwall 1 Owner's Manual*. Available at: [https://www.tesla.com/en\\_gb/powerwall](https://www.tesla.com/en_gb/powerwall) (Accessed: 17 July 2023).
- UNEP (2022) *Emissions Gap Report 2022*. Available at: <https://www.unep.org/resources/emissions-gap-report-2022> (Accessed: 17 July 2023).
- Vieira, C.T., Longo, M. and Mura, M. (2021) 'Are the European manufacturing and energy sectors on track for achieving net-zero emissions in 2050? An empirical analysis', *Energy Policy*, Volume 156, p. 112464.
- Viteri, J.P. et al. (2023) 'A systematic review on green hydrogen for off-grid communities –technologies, advantages, and limitations', *International Journal of Hydrogen Energy*, 448(52), pp. 19751-19771.

---

## #260: Converting flood-risk areas to water-resilient and productive dryland production systems

### Example of flood water spreading weirs in Ethiopia

---

Gizaw DESTA<sup>1</sup>, Gizachew LEGESSE<sup>1</sup>

<sup>1</sup> International Crop Research Institute for the Semi-Arid Tropics (ICRISAT), ILRI Campus, Addis Ababa, [gizaw.desta@icrisat.org](mailto:gizaw.desta@icrisat.org); [gizachew.legesse@icrisat.org](mailto:gizachew.legesse@icrisat.org)

*Abstract: The drylands of Ethiopia are faced with recurrent droughts and an increasing frequency of flash floods that lead to disasters and shocks and severe food insecurity and malnutrition, resulting in humanitarian response actions. However, beyond humanitarian response, the strategies for drought and flood risk management, particularly the investment and development opportunities of using floods for dryland farming, are poorly understood. Historical flood risk information and remote sensing tools were used to assess suitable areas for flood recession areas. The tested flood water spreading weir (WSW) practice assisted in converting flash floods that emerge from adjacent mountains to divert and spread over the fields for productive use. WSWs established different farming zones based on the soil moisture regime and nutrient deposition distribution. The approach has enabled pastoralists to produce substantial amounts of biomass and grain during short and long rainy seasons, which would be stored and utilized during succeeding dry months. Highland-to-lowland geomorphological connectivity of landscape segments and characterizing their rainfall conditions can be useful frameworks for flood risk analysis and assessing floodplain farming. This case study suggests that flood risk can be managed through spreading weirs in the form of recession farming, negating the need for recurrent humanitarian response actions. Thus, addressing the knowledge and evidence gaps contributes to an informed decision towards unlocking the opportunities of flood farming to support livelihoods and agricultural development in drought-prone areas.*

*Keywords: flash flood, flood recession, flood risk, drought, landscape*

## 1. INTRODUCTION

Flooding has long been recognized as one of the major disasters affecting the lives and livelihoods of people. The recent trend of increasing incidents of floods in Ethiopia is disrupting the livelihoods of the population residing in the lowland areas (OCHA, 2007) (Amede, 2020). The humid highlands characterized by intense rainfalls, and steep and rugged terrain make the lowlands prone to floods (Barvels, 2021). Floods occur due to intense and sustained rainfall in the highlands, causing rivers to overflow and inundate areas along the riverbanks in lowland plains (Getnet, 2020) (Gumma, 2020). Flood hazard is part and parcel of living for many people in the lowlands, such as in districts in Afar located along the Awash River, in the Somali region along the Wabi Shebele River, in the South Omo along the Omo River, in Gambella along the Baro and Akobo Rivers, and in the floodplains surrounding Lake Tana (Desta, 2021). On the other hand, these regions have been known for recurrent droughts, leading to vulnerable situations in the communities. The cyclic occurrences of drought and flood imply the need to strategize flood risk management interventions that result in new and transformative opportunities. Traditional experience in recession farming and some pilot spate irrigation revealed the significance of flood farming for coping with shocks and alleviating livelihoods in drought-affected areas (Steenbergen, 2011). However, these opportunities are overlooked in the agriculture and water development strategies as potential solutions for drought risk management and the reduction of flood risks. Flash floods are distinguished by their unpredictability, increasing frequency, and magnitude of ephemeral and perennial streams, resulting in high uncertainty in determining the extent of flood-recession areas. Moreover, despite the growing number of seasonal flood hazards reported over the years (OCHA, 2007) (Mamo, 2019) (Desta, 2021), there is often a lack of infrastructure and strategic frameworks to convert flash floods into an opportunity for mitigating drought and boosting dryland agricultural production. This knowledge gap leads to low policy support for the technical, financial, and legal aspects of responding to the development of floodwater risk management measures and flood-based farming in drought-prone dryland systems.

## 2. CHARACTERISTICS AND TYPES OF FLOOD-BASED FARMING

Flood-based farming is a type of farming that does not use irrigation or rainwater. Flood farming is practiced globally under two conditions, which are driven by climate characteristics and geomorphological conditions. Flood-based farming usually occurs in relatively low-lying areas with gentle topography. First, it is practiced in moisture-stressed areas where rainfall variability and dry spells prevail. Flood-based farming, which is dependent on runoff generated from upstream areas, is possible in these circumstances if the upstream areas receive high rainfall as a source of floods receding in low-lying plains. Second, flood-based farming is practiced in areas that regularly receive floods, which can form the basis for either inundation or recession farming. It is a practice that depends on the residual soil moisture and soil nutrient deposits that remain after the flood recedes (Nederveen, 2011) (Balana, 2019). Four flood-based farming techniques are widely used, depending on the severity of the flooding and the local farming conditions. These include spate irrigation, inundation, recession farming, and flood spreading using weir structures. However, to determine the extent and duration of flood-based farming, the flood water supply is often difficult to predict due to uncertainties in the timing, duration, size, and frequency of floods from ephemeral and perennial streams (Steenbergen, 2011). Furthermore, to utilize riverine floods, the river courses are changing from season to season leading to changes in riverbed levels and sediment accumulations. As indicated in Figure 1, the distribution of flash floods and riverine floods shows the extent of occurrence of floods over the years with varying frequencies. The current flood farming in Ethiopia is estimated at 5.5 million ha (Alemayehu, 2008). According to a recent suitability mapping (Figure 2), 32.6 million hectares of land in the country (i.e., areas with rainfall less than 500 mm) are highly and moderately suitable for flood-based farming options (Desta, 2021).

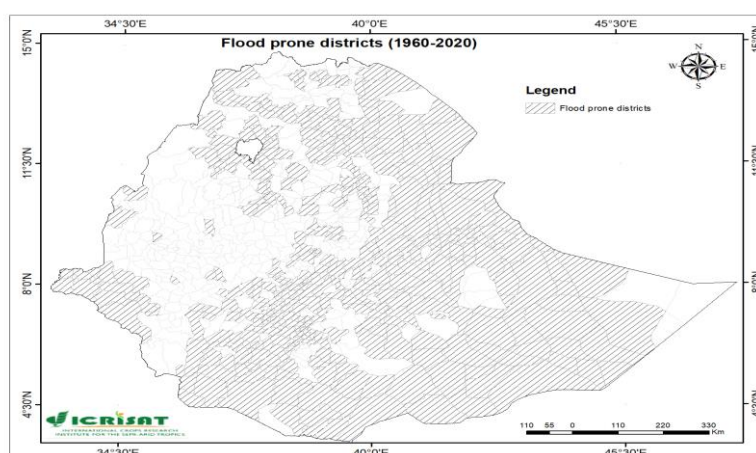


Figure 1 Flood-prone districts (shaded areas) in Ethiopia ranging from 4 to 25 frequency of flood occurrence per location from the 1960s to 2020s (Sources: Remapped from historical data records of UN-OCHA seasonal flood snapshots, <https://public.emdat.be/data>, and Mamo et al., 2019).

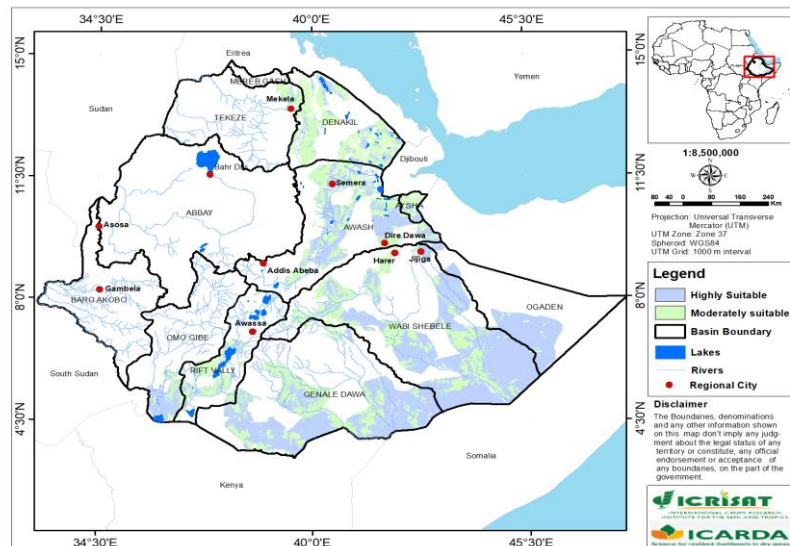


Figure 2 Map of socio-ecological suitability of flood-prone areas for flood-based farming in Ethiopia. The mapping is based on GIS-based multicriteria suitability analysis using expert knowledge (source: own publication, Desta et al., 2021).

### 3. BENEFITS OF FLOOD-BASED FARMING

Although flood-based farming is an uncertain type of farming, economically it is one of the potential entry points for agricultural production in the drought-affected drylands. It is the only source of water in an arid and semi-arid environment; thus, it has the potential to influence local livelihoods, economies, and biophysical systems (Steenbergen, 2011). It could serve a variety of functions, such as improving water-productive production systems in dryland areas, rangeland management for improved pasture production, livestock water supply, restoring soil and water resources, and creating a mosaic of green oases. Flood farming holds the potential, at least in the short term, to overcome the problem of crop and pasture failure. It also serves as a climate and water-smart practice to adapt to shocks and extremes. Flood-based farming is important for nutritional security and household coping mechanisms during the dry season when other food sources are depleted (Singh, 2021). Annual flood regimes of rivers are important in flood-affected areas, where flood-based farming could be an effective solution to meet food security and sustain livelihoods (Motsumi, 2012) (Balana, 2019) (Tariq, 2020). Overall, producing evidence on flood understanding and extent, flood impact on recharging and landscape water productivity, and flood-based agro-pastoral intensification options will result in more resilient agricultural production systems. Thus, addressing the knowledge and evidence gap on the potentials of flood farming contributes to an informed decision towards unlocking the opportunities of flood farming to support livelihoods and economic development in drought-prone areas.

### 4. A CASE STUDY OF FLOOD WATER SPREADING WEIRS

In partnership with local and bilateral partners, ICRISAT in Ethiopia has over the years deployed agro-pastoral intensification interventions using flood water spreading weirs (WSW). WSWs are weir structures built along the course of ephemeral and intermittent rivers to increase flood water heads and spread them horizontally on both sides of the river (Getnet, 2020). The cascading weirs along the river's course created flood-recession areas over crop and pasture fields. Since 2015, ICRISAT and its partners have introduced WSWs to convert flash floods that emerge from adjacent mountains to productive use (Amede, 2020). WSWs resulted in the deposition of sediments, with sand deposition being higher on the upside of the upstream weir whereas silt and clay deposition were prominent at the central location between the two weirs (Getnet, 2020). WSWs established various farming zones based on the soil moisture regime and distribution of nutrient depositions, which affected grain and biomass yields. In good potential zones with high moisture content, the WSW-based farming enabled higher food production, while in low moisture zones, there was a complete crop failure (Getnet, 2020). The approach has enabled pastoralists to produce huge amounts of biomass and grain during short and long rainy seasons, which would be stored and utilized during succeeding dry months.

The practice has also ensured a visible recovery of the dry and degraded rangeland ecosystems. Between 2010 and 2020, the coverage of crop cultivated, and vegetation-covered lands increased by 44% and 16%, respectively, and the bare lands decreased by 59% (from 87% to 28%) (Harawa, 2021). Farmers also reported increased livestock productivity, which is a major source of food and income for pastoral and agro-pastoral livelihoods, making WSW an important contributor to alleviating feed and water shortages. In 2020, 81.8 percent of the beneficiaries confirmed that livestock productivity increased after the construction of the WSWs. Project beneficiary agro-pastoralists earned a higher annual income (average 800 USD) than the non-beneficiaries (average 390 USD) (Harawa, 2021). The land use opportunity created by floodwater spreading weirs resulted in the expansion of crop and fodder farming and a huge social movement at the village

and district scales. The flood weirs restored the environment and transformed the land quality into productive land uses. The landscapes have been changed in terms of enhanced soil moisture, reduced peak flows, and minimized soil erosion and the formation of gully erosion.

## 5. INSIGHTS AND RECOMMENDED PRACTICES

*Integrated approach:* Flood risk management should be addressed by formulating an integrated approach embedded in the context of integrated water resources management and land use planning. The uncertainty of the flooding incidents, the local scale of the event, and the very short flood concentration time should be taken into consideration when developing flood risk management measures and an agronomic management strategy. Thus, flood management measures and intensification practices should be encouraged and supported with regular communication and technical backup on the rainfall forecasts, flash flood inventories, and coordinated land management and land use plans, which will enable the scaling-up of good practices.

*Process-oriented and holistic approach:* Realizing the potential of flood farming requires a process-oriented, holistic approach based on the inclusion of stakeholders and communities in the process. Use of the flash floods to boost agricultural production requires more than just designing and financing the construction of engineering measures. It requires a concerted effort and dedicated financial investment to support a process-oriented approach based on the coordinated efforts of stakeholders and communities at local and higher levels. The holistic approach will aim at increasing the response capacity of the local authorities and communities in flood-prone areas and the coordination of flood information services by institutions based on local community needs.

*Leveraging flood water investment opportunities:* The National Flood Response Plan currently aims to provide preparedness and emergency precautionary measures and develop an emergency response for flood-affected people with the coordinated effort of multiple stakeholders. Beyond the emergency flood response plan, there is a need for a national floodwater investment strategy to deal with flood risk management and economic production options within the overall integrated basin water management strategy that aims to unlock the potential of floodwater management and facilitate the actions of different actors to play their legitimate roles.

## 6. REFERENCES

- Alemayehu, T., 2008. Spate profile of Ethiopia (A preliminary assessment). Cairo, FAO.
- Amede, T. A. E. B. W. K. C. T. G. D. A. L. G. A. H., 2020. Facilitating livelihood diversification through flood-based land restoration in pastoral systems of Afar, Ethiopia.. *Renewable Agriculture and Food Systems*, pp. 1-12.
- Balana, B. S. S. B. B. W. T. K. S., 2019. Assessment of flood recession agriculture for food security in Northern Ghana: An optimization modeling approach. *Agricultural Systems*, Volume 173, pp. 536-543.
- Barvels, E. F. R., 2021. Earth Observation-Based Detectability of the Effects of Land Management Programmes to Counter Land Degradation: A Case Study from the Highlands of the Ethiopian Plateau.. *Remote Sensing*, 13(7), p. 1297.
- Desta, G. L. G. A. T. v. R. A. W. A., 2021. Unlocking the potential of flood farming to reduce flood risks and boost dryland production in Ethiopia.. Colombo, Sri Lanka: CGIAR Research Program on Water, Land and Ecosystems (WLE).
- Getnet, M. A. T. T. G. L. G. G. M. A. H. G. T. K. C. A. E., 2020. Water spreading weirs altering flood, nutrient distribution and crop productivity in upstream–downstream settings in dry lowlands of Afar, Ethiopia.. *Renewable Agriculture and Food System*, pp. 1-11.
- Gumma, M. A. T. G. M. P. B. P. L. G. T. G. V. d. A. E. B. W. K. C. S. M. W. A., 2020. Assessing potential locations for flood-based farming using satellite imagery: a case study of Afar region, Ethiopia. *Renewable Agriculture and Food System*, 37(S1), pp. 28-42.
- Harawa, R. W. C. O. G. (., 2021. Building resilient agri-food systems in East and Southern Africa. Research impact highlights 2020.. 2020 ed. Patancheru, India. : ICRISAT.
- Mamo, S. B. B. M. A., 2019. Historical Flood Events and Hydrological Extremes in Ethiopia. . In: A. A. W. S. G. E. Melesse, ed. *Extreme Hydrology and Climate Variability: Monitoring, Modelling, Adaptation, and Mitigation*. Amsterdam, The Netherlands: Elsevier, pp. 379-384.
- Motsumi, S. M. L. K. D., 2012. Indigenous knowledge and land use policy: Implications for livelihoods of flood recession farming communities in the Okavango Delta, Botswana.. *Physics and Chemistry of the Earth*, , Parts a/B/C(50-52), pp. 185-195.

Nederveen, S. M. H. S. V. A. T. G. Y., 2011. Flood-based farming practices in Ethiopia: Status and potential (Overview Paper #3).. Netherlands: Spate Irrigation Network.

OCHA, 2007. Reliefweb. [Online]  
Available at: <https://reliefweb.int/report/ethiopia/ocha-situation-update-no-2-flooding-ethiopia-1-31-aug-2007>  
[Accessed June 2023].

Singh, R. P. S. T. A. S. G., 2021. Assessment of flood recession farming for livelihood provision, food security, and environmental sustainability in the Ganga River Basin.. *Current Research in Environmental Sustainability*, 3(100038).

Steenbergen, F. H. A. A. T. A. T. G. Y., 2011. Status and Potential of Spate Irrigation in Ethiopia.. *Water Resources Management*, 25(7), pp. 1899-1913.

Tariq, M. F. R. v. d. G. N., 2020. A Critical Review of Flood Risk Management and the Selection of Suitable Measures.. *Applied Sciences*, 10(23), p. 8752.



---

## #261: Heat transfer optimization of a Carnot battery using a partial cascade organic-steam Rankine cycle

---

Pengcheng Li<sup>1</sup>, Jing Li<sup>2,\*</sup>, Xudong ZHAO<sup>2</sup>

<sup>1</sup>School of Automotive and Transportation Engineering, Hefei University of Technology, 193 Tunxi Road, Hefei, China

<sup>2</sup>Center for Sustainable Energy Technologies, Energy and Environment Institute, University of Hull, Hull, HU6 7RX, UK, Jing.Li@hull.ac.uk

*Abstract: Carnot battery is an emerging technology for low-cost, site-independent, environmentally friendly electricity storage and is also suitable for use in the heat sector. State-of-the-art Carnot battery uses subcritical steam Rankine cycles (SRC) for heat-to-power conversion because of the significant technical challenges of supercritical cycles, including increased leakage losses at high-pressure turbines and wetness at low-pressure turbines. The maximum operating temperature of about 565°C for molten salts limits the live steam pressure, water evaporation temperature (310-340°C) and power cycle efficiency. To increase the average temperature in the heating process and the cycle power efficiency, this paper proposes an innovative Carnot battery using a partial cascade organic-steam Rankine cycle integrated with molten salt storage. The organic fluid, a mixture of biphenyl and diphenyl oxide, absorbs heat from the molten salts and evaporates at a high temperature. It drives a turbine and then releases heat to generate steam for the bottom cycle. The steam is superheated and reheated by the molten salts. Fundamentals of the proposed system are illustrated, and mathematical models are built. Optimization is conducted. The results show the proposed Carnot battery has an efficiency of 8% higher than conventional ones.*

*Keywords: Carnot battery; Organic Rankine cycle; Steam Rankine cycle; Molten salts; Biphenyl/diphenyl oxide mixture*

# 1. INTRODUCTION

Carnot batteries, also known as pumped thermal electricity storage, are based on the use of electric heaters, heat pump, Rankine or Brayton heat engines (Dumonta, 2020). The Carnot battery buffers electrical energy by storing thermal energy (charge mode) from a resistive heater or a heat pump when the electricity production is redundant. Conversely, it generates power from the stored thermal energy (discharge mode) (Dumonta, 2020). Different prototypes have been developed, including a Liquid Air Energy Storage of 300 kW (Morgan, 2015), an electrical heater combined with a Rankine cycle (Siemens, 2019), a tested 150 kW Brayton cycle (Smallbone, 2017), and a 10 kW Carnot battery using a heat pump and a Rankine cycle (Chester, 2019).

A partial cascade organic-steam Rankine cycle (ORC-SRC) system integrated with dual-tank molten salt storage in Carnot battery applications has been proposed recently (Li, 2023). It is equipped with a top biphenyl/diphenyl oxide (BDO) mixture-driven organic Rankine cycle (ORC). The maximum thermal efficiency of 45.3% is achievable at a steam Rankine cycle (SRC) evaporation temperature of 290 °C, which is appreciably higher than the efficiencies of 41.2-41.98% obtained by the conventional plants. Nevertheless, the temperature drop between the two tanks of molten salts is smaller than the traditional value (219.6 °C vs. 275 °C), indicating a smaller storage capacity per mass of molten salts (Li, 2023).

In order to alleviate the above disadvantage, this paper proposes a novel heat exchange network (HEN) for the partial cascade ORC-SRC. The SRC superheater is divided into two stages to utilize the exergy in the molten salts more efficiently. The heat sources for the first and second stage SRC superheaters are molten salts from the outlets of ORC evaporator and high temperature tank (HTT), respectively. The novel HEN can enlarge the temperature difference between the hot and cold tanks. Its operating principles and characteristics are elaborated. Mathematical models are built, followed by heat transfer optimization at different nodes and a comparison between the two networks.

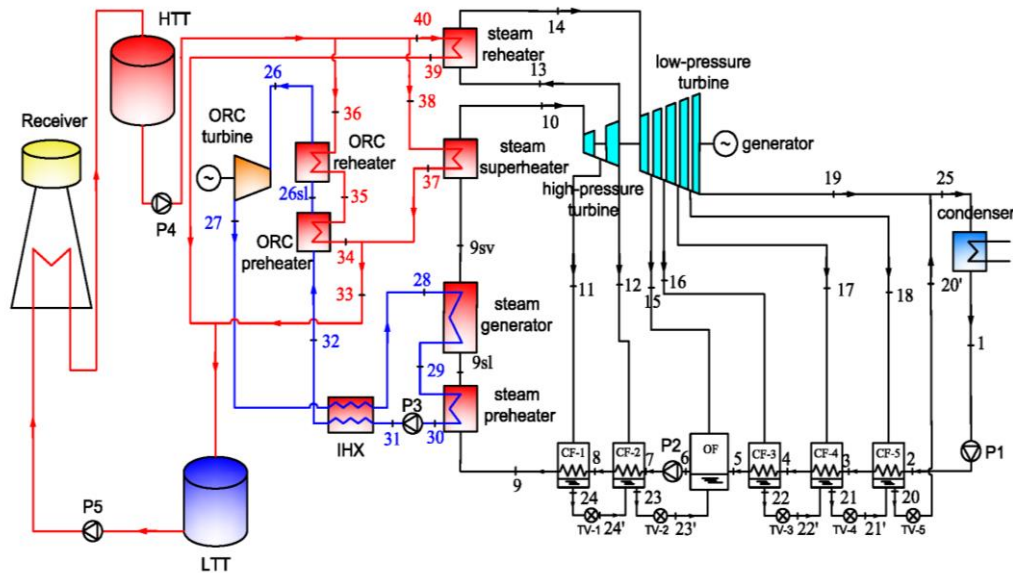


Figure 1 Partial cascade ORC-SRC with a simple HEN in Carnot battery applications (Li, 2023).

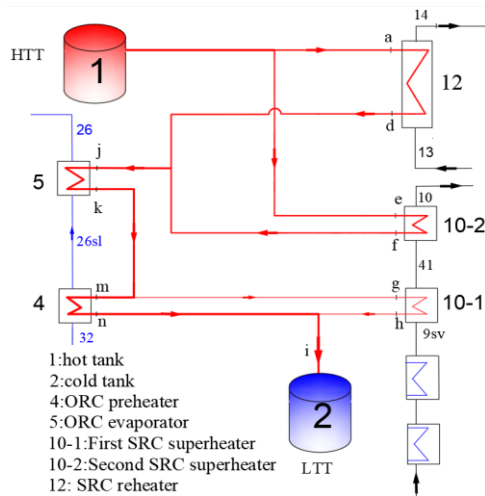


Figure 2 Improved HEN for the partial cascade ORC-SRC.

## 2. SYSTEM DESCRIPTION

The novel HEN for partial cascade ORC-SRC is depicted in Figure 2. The red, blue, and black lines represent the flows of molten salts, BDO mixture, and water/steam, respectively. The thickness of red lines distinguishes mass flow rates. The thinner the line, the smaller the molten salt flow.

Compared with a simple HEN structure in Figure 1, the improved design has two-stage SRC superheaters. The molten salt from the HTT is divided into two branches, which is less than that in Figure 1. The first SRC superheater is heated by a bypass of molten salt at the outlet of ORC evaporator. The second SRC superheater is heated by one molten salt branch from the HTT. The other branch supplies heat to the SRC reheater. The two molten salt branches converge and successively contribute to ORC evaporation and preheating. Finally, the molten salts at the outlets of ORC preheater and first SRC superheater converge and flow into the LTT.

## 3. MATHEMATICAL MODELS

The heat balance in the first SRC superheater, second SRC superheater, SRC reheater and ORC evaporator and ORC preheater is calculated as

$$\text{Equation 1: The heat balance in the first SRC superheater 1. } q_{10-1} = m_h \int_{t_h}^{t_g} c_p dt = m_{10}(h_{41} - h_{9_{sv}})$$

$$\text{Equation 2: The heat balance in the second SRC superheater 2. } q_{10-2} = m_f \int_{t_f}^{t_a} c_p dt = m_{10}(h_{10} - h_{41})$$

$$\text{Equation 3: The heat balance in the SRC reheater. } q_{12} = m_d \int_{t_d}^{t_a} c_p dt = m_{13}(h_{14} - h_{13})$$

$$\text{Equation 4: The heat balance in the ORC evaporator. } q_5 = m_k \int_{t_k}^{t_j} c_p dt = m_{\text{ORC}}(h_{26} - h_{26_{sl}})$$

$$\text{Equation 5: The heat balance in the ORC preheater. } q_4 = m_n \int_{t_n}^{t_k} c_p dt = m_{\text{ORC}}(h_{26_{sl}} - h_{32})$$

Where:

–  $c_p$  = specific heat capacity of molten salts [1]

$$\text{Equation 6: specific heat capacity of molten salts. } c_p = 0.172t + 1443$$

Given  $t_{9_{sv}}$ , all the parameters on the right side of the equal signs in Eqs. (1-5) can be calculated except  $h_{41}$ . The derivation process can be referred to the previous work [6].

$m_f$ ,  $m_d$  and  $m_n$  can be obtained by the above Eqs.  $m_k$  and  $m_h$  can be acquired by the conservation of mass.

$$\text{Equation 7: the conservation of mass. } m_{\text{tot}} = m_k = m_j = m_d + m_f$$

$$\text{Equation 8: the conservation of mass. } m_h = m_g = m_k - m_n$$

The flow lines represented by points d and f converge and flow into the ORC evaporator.  $t_j$  can be calculated by the law of conservation of energy.

$$\text{Equation 9: the law of conservation of energy. } m_d \int_{t_d}^{t_j} c_p dt = m_f \int_{t_f}^{t_j} c_p dt$$

Similarly, the low temperature tank temperature ( $t_{\text{LTT}}$ ) can be obtained from the conservation of energy.

$$\text{Equation 10: the law of conservation of energy. } m_h \int_{t_h}^{t_{\text{LTT}}} c_p dt = m_n \int_{t_{\text{LTT}}}^{t_n} c_p dt$$

## 4. RESULTS AND DISCUSSION

Table 1: Specific parameters for calculation

High pressure turbine inlet temperature (Li, 2019), $t_{10}$	540 °C
Low pressure turbine inlet temperature (Li, 2019), $t_{14}$	540 °C
HTT temperature (Xu, 2011), $t_{\text{HTT}}$	565 °C
ORC turbine inlet temperature (Chacartegui, 2016), $t_{26}$	400 °C
Minimum heat transfer temperature difference (Chacartegui, 2016), $\Delta T_{\text{min}}$	10 °C

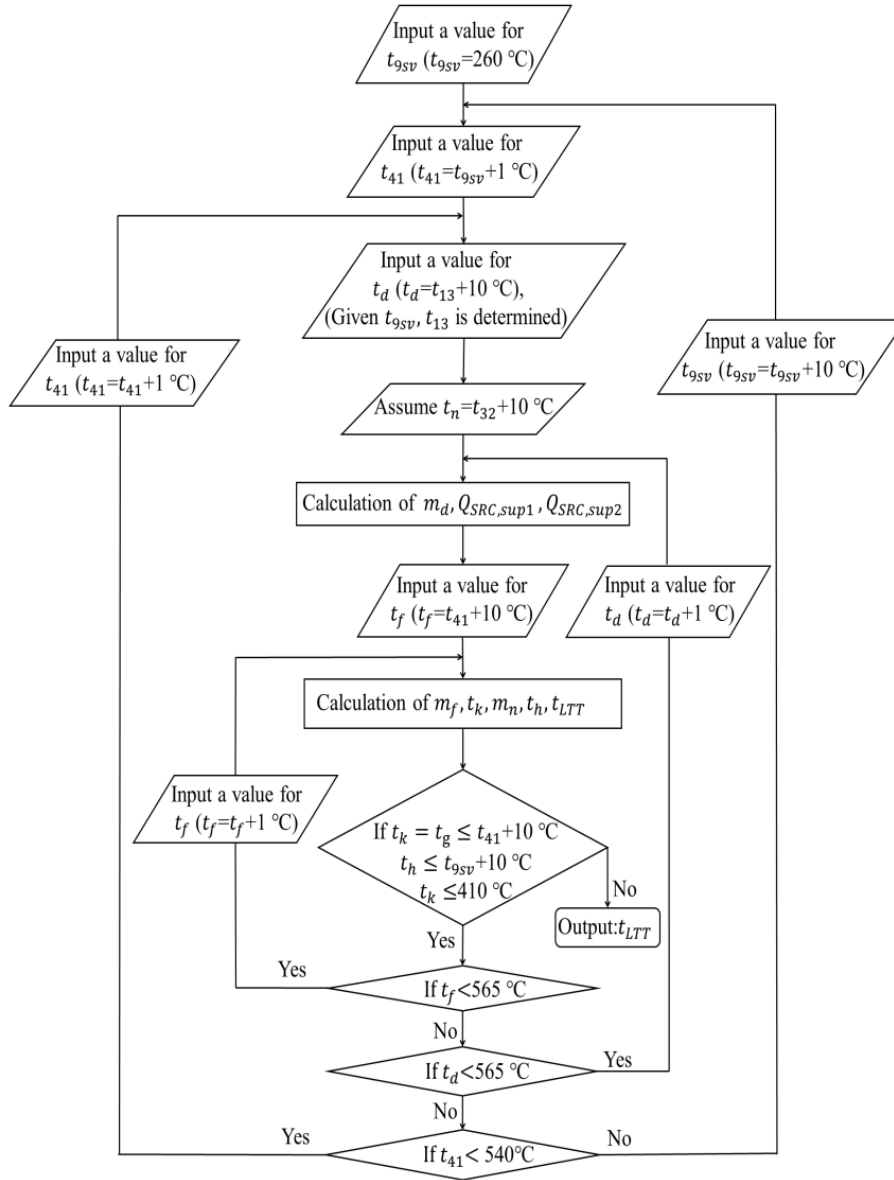


Figure 3 Determination of minimum  $t_{LTT}$  with  $t_{9sv}$ ,  $t_d$ ,  $t_f$  and  $t_{41}$ .

The specific parameters for simulation are listed in Table 1. The calculation procedure is exhibited in Figure 3.  $t_a = t_e = t_{HTT} = 565$  °C.  $t_{9sv}$ ,  $t_d$ ,  $t_f$  and  $t_{41}$  as denoted in Fig.2 are taken as independent variables, and the other parameters are dependent variables. The water evaporation temperature ( $t_{9sv}$ ) varies from 260 °C to 350 °C. Given  $t_{9sv}$ , the ranges of  $t_d$ ,  $t_f$  and  $t_{41}$  can be determined. Take  $t_{9sv} = 260$  °C as an example,  $h_{13} = h_{12} = 3284.89$  kJ/kg can be obtained according to the high-pressure turbine isentropic efficiency.  $t_{13} = 417.03$  °C can be obtained on condition that the pressure of extraction no. 2 is given ( $p_{13} = p_{12} = 2.06$  MPa [6]). Taking the minimum heat transfer temperature difference ( $\Delta t_{min}$ ) of 10 °C into consideration,  $t_d \geq t_{13} + 10$  °C in the SRC reheater. Meanwhile,  $t_d < t_{HTT}$ .  $427.03$  °C  $\leq t_d < 565$  °C can thus be determined. As  $t_{41}$  varies between  $t_{9sv}$  and  $t_{10}$ ,  $260$  °C  $< t_{41} < 540$  °C. Similar to  $t_d$ ,  $270$  °C  $< t_f < 565$  °C. The ranges of  $t_d$ ,  $t_f$  and  $t_{41}$  at different SRC evaporation temperatures can be deduced in the same way.

Figure 4 illustrates the variation of  $t_{LTT}$  with  $t_{41}$ ,  $t_f$  and  $t_d$  at  $t_{9sv} = 260$  °C. The interval between each surface is 50 °C. The results for  $t_{41} = 520$  °C are not presented because there are few eligible data. The variation in  $t_f$  and  $t_d$  are displayed both at 10 °C intervals to avoid too dense curves. At each  $t_{41}$ , a minimum LTT temperature ( $t_{LTT,min}$ ) can be achieved by optimizing  $t_f$  and  $t_d$ . They are 337.95, 332.21, 329.51, 325.57 and 392.13 °C when  $t_{41}$  is 270, 320, 370, 420 and 470 °C, respectively.  $t_{41} = 420$  °C corresponds to the lowest  $t_{LTT,min}$  among the five studied temperatures.

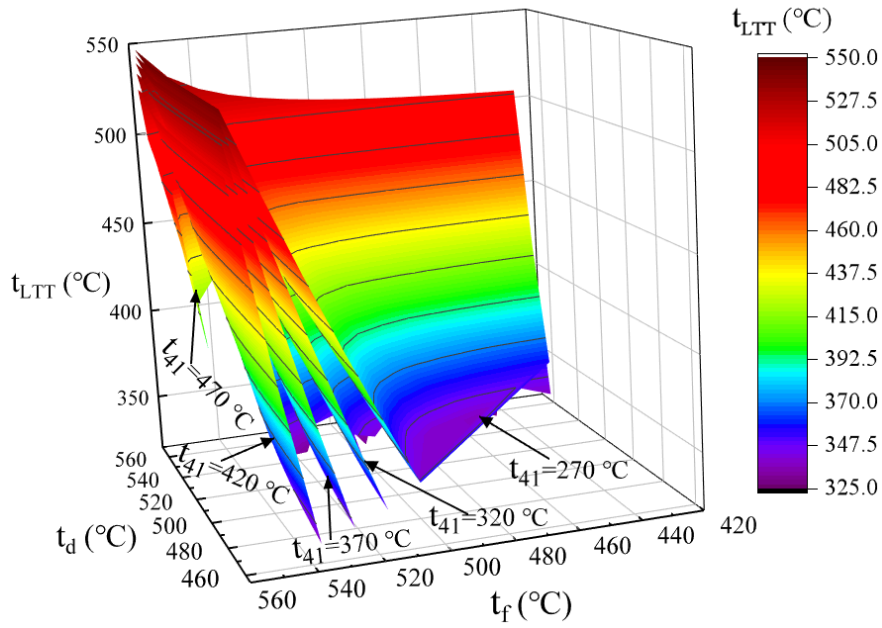


Figure 4 Variation of  $t_{LTT}$  with  $t_{41}$ ,  $t_f$ ,  $t_d$  at  $t_{9sv} = 260$  °C.

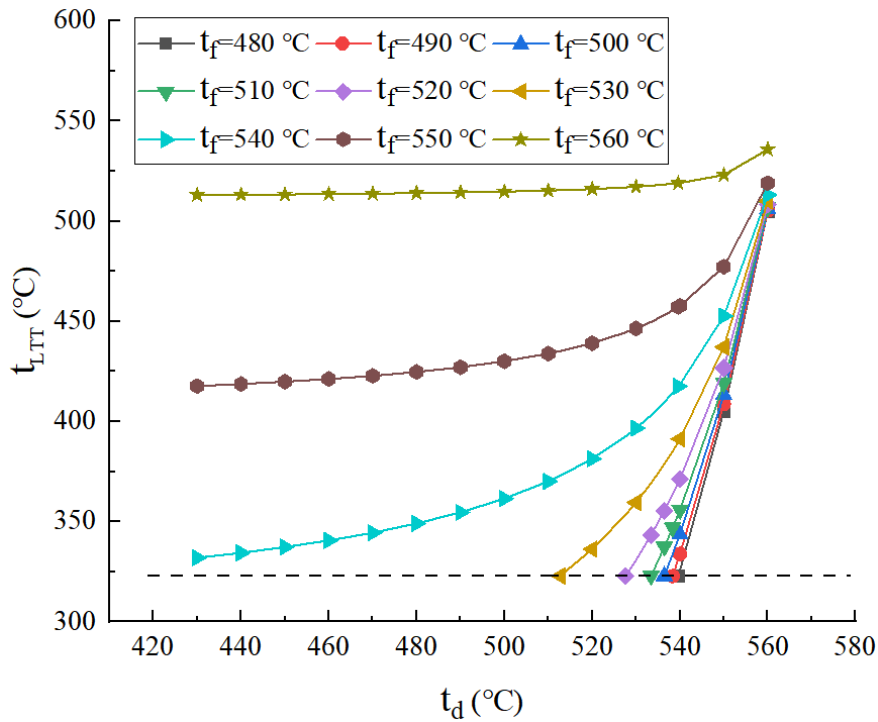


Figure 5 Variation of  $t_{LTT}$  with  $t_d$ ,  $t_f$  at  $t_{9sv} = 260$  °C and  $t_{41} = 420$  °C.

The variation of  $t_{LTT}$  with  $t_d$  and  $t_f$  at  $t_{9sv} = 260$  °C and  $t_{41} = 420$  °C is exhibited in Figure 5. Given  $t_f$ ,  $t_{LTT}$  increases with  $t_d$ . Lower  $t_f$  leads to more significant increment of  $t_{LTT}$ . There are six intersections between the curves and the horizontal dashed line of 322.8 °C, which indicates that the lowest LTT temperatures are the same when  $t_f$  rises from 480 °C to 530 °C. Notably, the lowest  $t_{LTT}$  of 322.8 °C is slightly lower than that of 325.57 °C in Figure 4. The reason is that  $t_d$  is calculated every 1 °C near the nadir in Figure 5, leading to more accurate results.

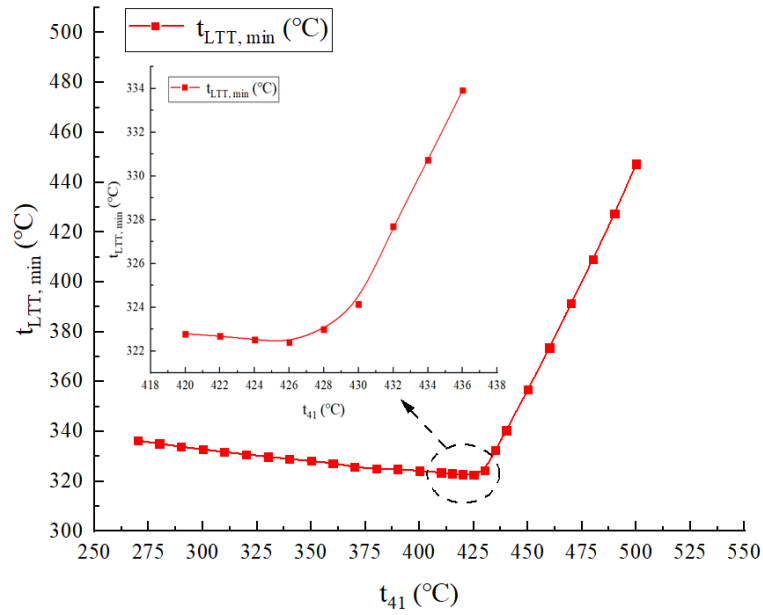


Figure 6 Variation of  $t_{LTT,min}$  with  $t_{41}$  at  $t_{9sv} = 260$  °C.

The variation of  $t_{LTT,min}$  with  $t_{41}$  at  $t_{9sv} = 260$  °C is shown in Figure 6. Each point is obtained by optimizing  $t_d$  and  $t_f$  at a given  $t_{41}$ .  $t_{LTT,min}$  first declines slightly and then increases remarkably. The lowest  $t_{LTT}$  of 322.41 °C is achieved at  $t_{41}$  of 426 °C.

Table 2: Parameters when the lowest  $t_{LTT}$  is obtained.

$q_{12}$	$q_{10-1}$	$q_{10-2}$	$q_5$	$q_4$
11271.90 MW	22704.00 MW	12898.00 MW	51901.94 MW	45794.55 MW
$t_d$	$t_f$	$t_k = t_m = t_g$	$t_h$	$t_{LTT}$
520.00 °C	528.37 °C	438.14 °C	270.06 °C	322.33 °C
$t_{9sv}$	$t_{41}$	$t_n$	$t_j$	$t_{13}$
260.00 °C	426.00 °C	337.80 °C	524.89 °C	417.03 °C
$m_d$	$m_f$	$m_{tot} = m_k = m_j$	$m_n$	$m_g$
163.03 kg/s	229.09 kg/s	392.12 kg/s	302.31 kg/s	89.82 kg/s

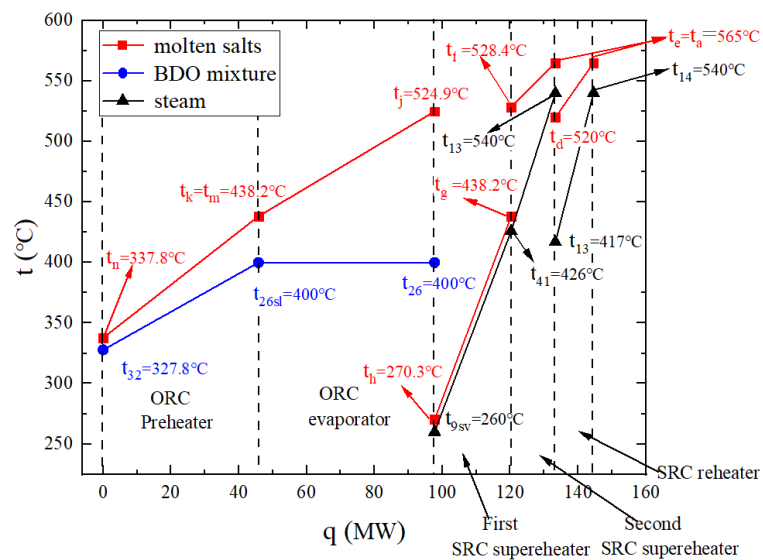


Figure 7  $t$ - $q$  diagram when the lowest  $t_{LTT}$  is obtained.

The parameters related to the lowest  $t_{LTT}$  are indexed in Table 2. The corresponding  $t$ - $q$  diagram is graphed in Figure 7. The dotted lines distinguish different heat exchangers. Notably, there are many groups of eligible  $t_f$ ,  $t_d$ ,  $m_f$  and  $m_d$  for a given  $t_{9sv}$ . The lowest  $t_{LTT}$  can be achieved under any group of parameters and only one of the results is presented in Table 2 and Figure 7. The reason can be explained by Figure 5. Given  $t_{9sv}$  of 260 °C and  $t_{41}$  of 420 °C, there are six  $t_d$

groups when  $t_f$  increases by 10 °C. More results will be deduced if  $t_f$  increases by 1 °C. The minimum heat transfer temperature differences are 10, 38.2, 10.3, 25 and 25 °C for the ORC preheater, ORC evaporator, first SRC superheater, second SRC superheater and SRC reheater, respectively.  $\Delta t_{min}$  occurs at the molten salt outlets of the first three heat exchangers, while at the molten salt inlets of the last two heat exchangers. The largest and smallest heat transfer takes place in the ORC evaporator and SRC reheater, respectively. The gradient utilization of molten salts energy is illustrated in Figure 8.

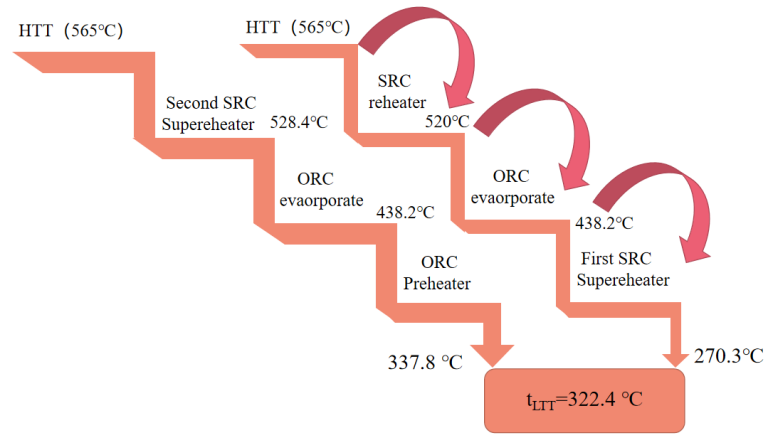


Figure 8 Gradient utilization of molten salts energy.

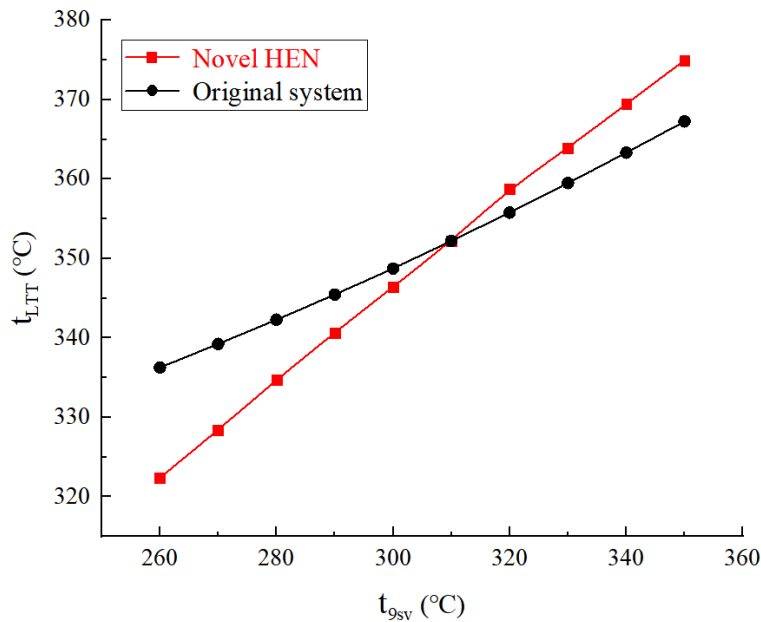


Figure 9 Comparison of LTT temperatures between the novel and original systems.

The comparison of LTT temperatures between the novel and original systems is depicted in Fig. 9. Both curves show an approximate linear increase. The two systems have the same  $t_{LTT}$  of 352.5 °C at  $t_{9SV}$  of 310 °C. A lower  $t_{9SV}$  results in a lower  $t_{LTT}$  of the novel HEN as compared with that of the original system. But  $t_{LTT}$  of the novel HEN is higher when  $t_{9SV}$  is above 310 °C. Notably, the maximum efficiency of 45.3% and  $t_{LTT}$  of 345.4 °C are achieved at  $t_{9SV}$  of 290 °C for the original system (Li, 2023). By comparison, it seems more advantageous for the novel HEN to operate at 260 °C because lower  $t_{LTT}$  and thus larger storage capacity can be realized at the slight sacrifice of power efficiency (45.04% vs. 45.3%). Besides, a lower  $t_{9SV}$  is more beneficial for the turbine design because various losses and cost can be reduced.

The comparison of total molten salt flow rates between the novel and original systems is presented in Figure 10. The total molten salt flow rate ( $m_{tot}$ ) rises as  $t_{9SV}$  increases for the novel HEN, while  $m_{tot}$  first descends and then climbs marginally for the original system. The two systems have the same  $m_{tot}$  of 395.6 kg/s when  $t_{9SV} = 285$  °C. The novel HEN has smaller total mass flow rates at low SRC evaporation temperatures. The mass flow of each molten salt branch is not plotted because there are many groups of eligible data at a given  $t_{9SV}$ .

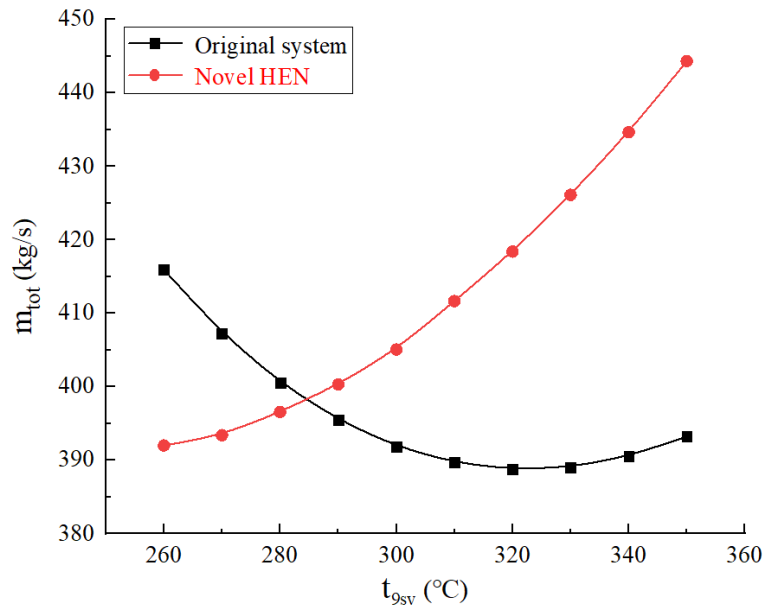


Figure 10 Comparison of  $m_{tot}$  between the novel and original systems.

## 5. CONCLUSION

A novel HEN for a partial cascade ORC-SRC is proposed in this paper. The SRC superheater is divided into two stages. The molten salt at the HTT outlet is divided into two branches to heat the SRC reheater and the second SRC superheater, respectively. The temperature of each node in the molten salt network is optimized. The results indicate that the lowest  $t_{LTT}$  is achieved at  $t_{41}$  of 426 °C and  $t_{9sv}$  of 260 °C. Despite a slight thermal efficiency decline as compared with the original system (45.04% vs. 45.3%), a lower  $t_{LTT}$  (322.41 °C vs. 345.4 °C) and a larger storage capacity can be realized by the novel HEN. Meanwhile, the moderate live steam pressure of 4.69 MPa in the SRC reduces the leakage loss of the high-pressure turbine and equipment costs.

<b>Nomenclature</b>		ORC	organic Rankine cycle
$c_p$	specific heat, J/kg.K	ORC-SRC	organic-steam Rankine cycle
$h$	enthalpy, kJ/kg	SRC	steam Rankine cycle
$m$	mass flow rate, kg/s	<b>Subscript</b>	
$p$	pressure, MPa	$min$	minimum
$q$	heat transfer, kW	$ori$	original
$t$	temperature, °C	$sl$	saturated liquid
<b>Abbreviation</b>		$sv$	saturated vapor
BDO	biphenyl/diphenyl oxide	$tot$	total
HTT	high temperature tank		
HEN	heat exchange network		
LTT	low temperature tank		



## 6. REFERENCES

- Analysis of two heat storage integrations for an Organic Rankine Cycle Parabolic trough solar power plant. *Energy Conversion and Management*, 125, 353-367.
- Chacartegui, R., Vigna, L., Becerra, J.A., Verda, V., 2016.
- Chester, 2019. <https://www.chester-project.eu/>, consulted on the 10/10/2019.
- Dumont, O., Frateb, G.F., Pillaic, A., Lecomptec, S., De paepec, M., Lemort, V., 2020. Carnot battery technology: A state-of-the-art review. *Journal of Energy Storage*, 32, 101756
- Morgan, R., Nelmes, S., Gibson, E., Brett, E., 2015. Liquid air energy storage - analysis and first results from a pilot scale demonstration plant. *Applied. Energy*, 137 845–853.
- Siemens, 2019. <https://www.siemensgamesa.com/products-and-services/hybridand-storage/thermal-energy-storage-with-etes> consulted on the 15/09/2017. Consulted on the 09/09/2019.
- Li, P.C., Qian, T.L., Li, J., Lin, H.W., Wang, Y.D. Pei, G., Jie, D.S., Liu, D.M., 2023. Thermo-economic analysis of a novel partial cascade organic-steam Rankine cycle. *Energy Conversion and Management*, 283, 116941.
- Li, X., Jin, J.x., Y, Yangt., Xu, N., Wang, Y.N., Mi, X.L., 2019. Comparison of tower and trough solar thermal power plant efficiencies in different regions of China based on SAM simulation. *SolarPACES 2018: International Conference on Concentrating Solar Power*, 2126, 030033
- Smallbone, A., Jülch, V., Wardle, R., Rskilly, P., 2017. Levelised cost of storage for pumped heat energy storage in comparison with other energy storage technologies. *Energy Conversion and Management*, 152, 221–228.
- Xu, C., Wang, Z.F., Li, X., Sun, F.H., 2011. Energy and exergy analysis of solar power tower plants. *Applied Thermal Engineering*, 31, 3904-3913.

---

# #263: An assessment of the value of V2X for commercial car parks: a case study for East Midlands Airport

---

Wenjie Yi<sup>1</sup>, Murtaza Turabbhai MOHAMMADI<sup>1</sup>, Mark GILLOTT<sup>1</sup>, Lucelia RODRIGUES<sup>1</sup>,  
Rob SHIPMAN<sup>1</sup>, Rong QU<sup>2</sup>, Tacis GAVOYANNIS<sup>3</sup>, Steve COWPER<sup>3</sup>,  
Charles BRADSHAW-SMITH<sup>4</sup>, Ash GUPTA<sup>5</sup>

*1 Department of Architecture and Built Environment, University of Nottingham, United Kingdom, {wenjie.yi1, murtaza.mohammadi1, mark.gillott, lucelia.rodrigues, rob.shipman} @nottingham.ac.uk*

*2 School of Computer Science, University of Nottingham, United Kingdom, rong.qu@nottingham.ac.uk*

*3 EVMobility, United Kingdom, {tacis, steve}@evmobility.com*

*4 SmartKlub, United Kingdom, charlesbs@smartklub.org*

*5 Gupta Smart Energy & EM Energy Solutions, Norway, ash@guptapartnership.com*

*Abstract: Registrations of electric vehicles (EVs) increased by a remarkable 40% globally in 2020, signalling a significant transition from internal combustion engines. In the UK, the number of EVs on the road is projected to reach a staggering 10 million units by 2030, constituting 30% of total vehicles on the road. However, this shift towards EVs poses challenges to the existing energy infrastructure if the demand of electricity is not effectively managed. Simultaneously, EV batteries' energy storage capacity opens up new prospects for bi-directional charging and Vehicle-to-Everything (V2X) services, which enable energy flexibility, trading and grid arbitrage. In this study, the authors assessed the impact of EVs on the future energy landscape for a large commercial parking facility at East Midlands Airport from 2022 to 2030, considering three EV charging scenarios: unmanaged charging, peak shaving, and grid arbitrage. Simulation results demonstrated that the peak shaving mode offered cost benefits by optimising charging during lower demand periods, resulting in a significantly reduced potential EV net costs due to charging (more than 20% savings compared to the unmanaged charging strategy in all years). The most promising solution was the bidirectional charging facility with grid arbitrage, enabling EVs to charge during periods of lower tariff and discharge during periods of higher tariff. This mode offered more than 200% savings compared to the unmanaged charging strategy in all years. The findings highlight the importance of investment in infrastructure and innovative technology today to prepare for future EV penetration, as a delayed deployment of necessary infrastructure will limit accessibility of the identified opportunity.*

*Keywords: electric vehicles, vehicle-to-everything, unmanaged charging, peak shaving, grid arbitrage.*

## 1. INTRODUCTION

In 2020, there were 10 million electric vehicles (EVs) on the road, which marked a decade of rapid growth despite the pandemic-induced downturn. Globally, EVs registrations increased by 41% in 2020 due to the supportive regulatory frameworks, additional incentives to safeguard EV sales, and the continuous expansion of EV models and decreasing battery costs. The majority of the world's top vehicle manufacturers have announced plans to extend their range of EV models and scale up production of light-duty EVs (International Energy Agency, 2021) .

The United Kingdom has set ambitious targets for the adoption of EVs as part of its broader strategy to achieve net-zero carbon emissions by 2050. The government's Transport Decarbonisation Package (Department for Transport, 2023b) aims to boost these ambitions by implementing a series of measures designed to accelerate the transition to EVs and decarbonise the transport sector. By 2030, the UK government expects Battery Electric Vehicles (BEVs) to account for 80% of the total vehicle sales in the country (Department for Transport, 2023a) . This is in line with the government's plan to end the sale of new petrol and diesel cars and vans by 2030. Furthermore, by 2040, it is expected that there will be 33.4 million EVs in the UK, equating to 72% of the nation's vehicles (EY, 2023) . This rapid increase in EV adoption underscores the urgent need for the development and optimisation of charging infrastructure and supply chains. A separate study by SMMT predicts the number of BEVs to increase to 30% by 2030 in the most optimistic scenario (i.e., high scenario), the details of the EV number projection are shown in Table 1.

Table 1: EV number projection (SMMT,2021).

Year	Low scenario		Central scenario		High scenario	
	Total BEV (x1000)	%BEV	Total BEV (x1000)	%BEV	Total BEV (x1000)	%BEV
2022	537	1.6	611	1.8	795	2.3
2023	740	2.2	953	2.8	1,449	4.2
2024	1,002	2.9	1,392	4.0	2,286	6.6
2025	1,335	3.9	1,951	5.6	3,342	9.5
2026	1,739	5.1	2,628	7.6	4,624	13.0
2027	2,229	6.6	3,447	9.9	5,973	16.7
2028	2,801	8.4	4,406	12.7	7,456	20.8
2029	3,484	10.6	5,553	16.0	9,072	25.3
2030	4,293	13.4	6,909	20.1	10,817	30.2

To support this transition, the UK government has proposed a Zero Emission Vehicle (ZEV) mandate (Department for Transport, 2023a) and CO2 emissions regulation for new cars and vans. This mandate requires an increasing share of zero-emission cars and vans, alongside a CO2 emissions regulation to ensure that new non-zero emission cars and vans do not become more polluting in future years.

The government has also identified six essentials for mainstream EV adoption. These include resilient supply chains and vital raw materials; clean and green power production; accessible charging infrastructure; the integration of EVs with smart grid technology; digital platforms and mobile applications to optimise EV charging; and finding and training the next-generation workforce. By 2040, the UK is expected to require a total of 20 million EV chargers, with about 2.4 million in public places (EY, 2023) .

The UK's transition to EVs is not without challenges. The infrastructure required for the widespread adoption of EVs is significant and requires collaboration across sectors. For instance, the application process for grid connections needs to be smoother and faster. Access to key potential sites for chargers must be easier. Once installed, chargers must be more reliable. A successful roll out of charging infrastructure is needed to encourage more consumers and corporates to make the transition and keep the UK on track to meet its ambitious targets. The penetration of higher numbers of EVs will have several impacts on the energy ecosystem, including increased demand for electricity, grid management and infrastructure upgrades, shift toward renewable energy sources and need for more charging stations.

While these challenges put significant burden on the original equipment manufacturers (OEMs), dealers and energy regulators, city planners and so forth, it also introduces fresh perspectives to market opportunities and diversifying revenue models. EVs offer a range of benefits beyond their zero-emission nature (Charles River Associates, 2023; Frankland, 2018; VIRTA, 2023). These benefits are largely tied to the Vehicle-to-Everything (V2X) concept, which allows EVs to interact with the power grid in a bidirectional manner, charging when demand is low and feeding power back into the grid when demand is high (Amamra et al., 2019; Jie et al.,2020; Singh et.al, 2022).

In this study, East Midlands Airport (EMA) has been selected as the case study for assessing the value of V2X for commercial car parks. Conducting the research within the airport context offers a range of advantages. Firstly, the long-stay car parks in the airport provide opportunities to explore and implement various sustainable and efficient energy solution. Moreover, the predictable dwell times of passengers enable the development of tailored energy management strategies. Additionally, airports are the place with large local energy demand to maintain their daily operations, and the existing car parks infrastructure presents a unique opportunity for integrating renewable energy technologies such as solar panels on rooftops or cartops without requiring significant changes to the physical layout. Overall, the long-stay

characteristic, predictable dwell times, large local energy demand and existing car park infrastructure create an ideal setting to assess the value of V2X at the airport.

This study aims to investigate the impact of different V2X technologies for a large commercial parking facility located at the EMA. Energy demand and associated cost predictions are made for the period 2022 to 2030 to understand the future EV landscape. Section 2 presents the background and the analysis results of the energy demand and energy tariff data, aiming to identify the potential opportunities for implementing V2X technologies. Based on these research findings, Section 3 further describes the proposed simulation algorithms for different charging scenarios, followed by the discussion on the simulation results on Section 4. Section 5 presents the conclusions and discusses the future work.

## 2. BACKGROUND

This section discusses background information at the facility to identify potential opportunities for implementing V2X technologies. The EMA is an 11kV customer connected to the Castle Donnington primary 33/11 kV substation and currently does not support electricity export. A private line exists within the site boundaries to power the buildings and other facilities. Half-hourly electricity data, covering the period from 1st January 2022 to 31st December 2022, was used to analyse the baseline demand of the main terminal and a few connected buildings. The electricity consumption of hangers, warehouses and several private facilities on site was not included in this dataset. Secondly, the cost associated with this energy usage was estimated using the half-hourly system sell/buy price data available on Elexon website (Elexon, 2023). Noted that this price does not represent the actual energy bill paid by the consumer but represents the cost incurred by the system operator in its role of managing system imbalances (Council of European Energy Regulations, 2023). The use of this parameter is justified since the tariff pattern would be similar between system sell/buy price and the cost to supplier. Moreover, the details of the energy contract at the airport are unknown and the system pricing provides a good estimate of the energy trading cost. For the remainder of the paper, tariff refers to system pricing.

Figure 1 shows the yearly-averaged half-hourly energy demand and tariff, over the course of a day, for the baseline year of 2022. The energy demand (red curve) is generally high from 3am to 3pm, with a steep increase from 6am onwards. After reaching the peak demand of nearly 1090 kWh, at around 7:30am, the demand gradually decreases. A small increase is observed later in the evening at 8pm. On the other hand, the energy tariff (blue curve) has on average two peaks during the day, corresponding to the high morning (6am-9am) and low afternoon (3pm-6pm) load. Two important conclusions can be drawn from the pattern. Firstly, the highest demand and tariff times are shifted by 9 hours, i.e., the highest energy demand occurs around 8am while tariff is highest later in the day at 5pm. Secondly, the peaks correlate only once during the day (mornings), while at other times the demand and tariff curves are unrelated. It is possible that an increase in demand by other consumers on the network could be driving this tariff peak. Analysis of the entire dataset revealed a low correlation coefficient ( $\rho = 0.19$ ) between the building demand and energy tariff, indicating a weak relationship between the two variables. Corollary, the tariff does not closely align with building demand, often resulting in high costs despite low demand levels at the airport. Given this observation, it is expected that the benefits offered by different smart charging strategies, namely peak shaving and grid arbitrage, will vary considerably.

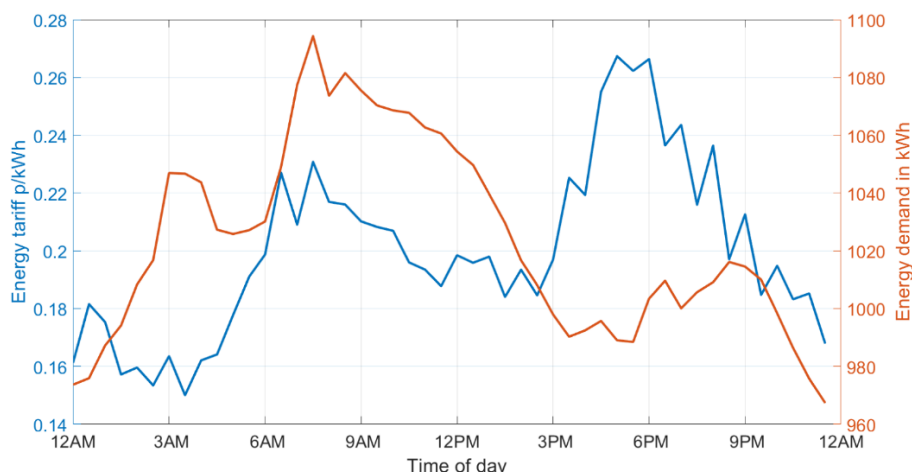


Figure 1 Average half-hourly electricity demand and tariff in the baseline year 2022

## 3. PROPOSED METHODS

Three charging scenarios were simulated: (1) unmanaged charging, (2) peak shaving, and (3) grid arbitrage. In the unmanaged charging scenario, EVs are charged at any time that is convenient for owners. In the peak shaving scenario, EVs serve to reduce the peak load by charging during off-peak times and supporting the grid during peak times. The grid arbitrage relies on the energy tariff to determine the optimal charging times of EVs. The unmanaged charging scenarios exhibits unidirectional energy flow, while the other scenarios facilitate bidirectional energy flow. The section is organised

as follows. Section 3.1 presents the model assumptions and limitations, and then section 3.2 outlines the renewable energy generation in EMA. Finally, section 3.3 presents the detailed methods used to simulate these three charging scenarios.

### 3.1. Model limitation and assumptions

This section outlines the specific assumptions made in the modelling process and the limitations. The simulation is sensitive towards two parameters: EV capacity and the energy tariff. Since no car parking information or EV data was available at the site, we assumed a certain percentage of parked vehicles to be EVs based on the forecasts by SMMT (2021), as shown in Table 2. The long-stay car parking facility at EMA can accommodate up to 2500 cars. In the central scenario, the number of EVs was varied from 50 in 2022 to 500 in 2030, i.e., of the total 2500 car parking spaces, 50 were earmarked for EVs in 2022 and 500 in 2030. Similarly, for the low and high scenarios, the number of EVs were increase from 50 in 2022 to 325 and 750 in 2030, respectively. Nevertheless, the model did not assume full capacity and the number of EVs varied each day, ranging between defined intervals as shown in Table 2.

Table 2: Estimated EV parking capacity at EMA.

Year	EV capacity scenarios at the airport			Weighted average battery size in kWh
	Low	Central	High	
2022 ( <i>baseline</i> )	10 - 50	20 - 50	30 - 50	50
2023	10 - 50	45 - 75	80 - 100	53
2024	35 - 75	70 - 100	155 - 175	56
2025	60 - 100	95 - 125	205 - 225	60
2026	85 - 125	145 - 175	305 - 325	64
2027	135 - 175	195 - 225	405 - 425	68
2028	160 - 200	270 - 300	505 - 525	72
2029	235 - 275	370 - 400	605 - 625	76
2030	285 - 325	470 - 500	730 - 750	80

Secondly, predicting building energy demand and energy tariff up to 2030 using machine learning algorithms was not possible due to limited dataset. Therefore, simple statistical methods were employed to estimate them. A growth of 1.06 was observed in the energy demand between the year 2021 and 2022, which was consequently applied for calculating building demand up to 2030. On the other hand, energy tariff at any time was derived by calculating the mean tariff of the corresponding times from the previous two years.

Since the aim of the study was to understand the broad impact of EV penetration, the EVs for each given year were assumed to have the same battery capacity. This was preferred over modelling every individual actor separately which would introduce unnecessary complexities in the model. The weighted average battery size was estimated based on the report by International Energy Agency (2020), such that the increment is proportional to the central scenario projection. Another limitation in the simulation was that the EV supply equipment (EVSE) was assumed to operate at a constant power of 22kW for the entire time frame. Finally, no differentiation was made between weekdays and weekends in estimating parked EV numbers.

### 3.2. Renewable energy generation

There are two wind turbines of 250 kW at the airport, located near the long-stay parking facility. The combined annual electricity generation of the two turbines amount to 370 MWh, which is approximately 2% of annual energy demand. Additional installation of wind turbines is a challenge at the site as the machinery interferes with aircraft operation. As for solar energy generation, we propose the design and installation of solar canopies over the car parking area. Figure 2 indicates the location of the two long-stay parking area at the airport, which cover an area of approximately 78,000 m<sup>2</sup>. Using a factor of 0.2 MW/acre, a ~3.5 MW plant can be installed at the airport to offset some of the grid imports. Our simulations indicate an annual generation of 3.3 GWh, which can offset 21% of the annual energy consumption through the grid. Peak production occurs during the summer months of May, June and July which can often be sufficient to meet the entire building demand during the daytime.

Note that the renewable energy generation will be primarily used to supply the airport daily operation instead of being sold to the grid. The term 'gross demand' mentioned in the below subsection refers to the airport's energy demand that remains unsatisfied after utilising the energy generated from renewable sources.



Figure 2 Parking area at the East Midlands Airport

### 3.3. Simulation models under different scenarios

The benefits and future impact of two smart charging methods, namely peak shaving and grid arbitrage were simulated in this work. The results from the two simulations were compared to a baseline energy demand, representing an unmanaged charging scenario. While the unmanaged charging mode may be convenient for owners, past studies have demonstrated that it will add significant load on distribution system and impact the grid performance (Anselmo et al.,2021). Flowcharts for the peak shaving and grid arbitrage simulation algorithms, for a 24-hour period, are shown in Figure 3.

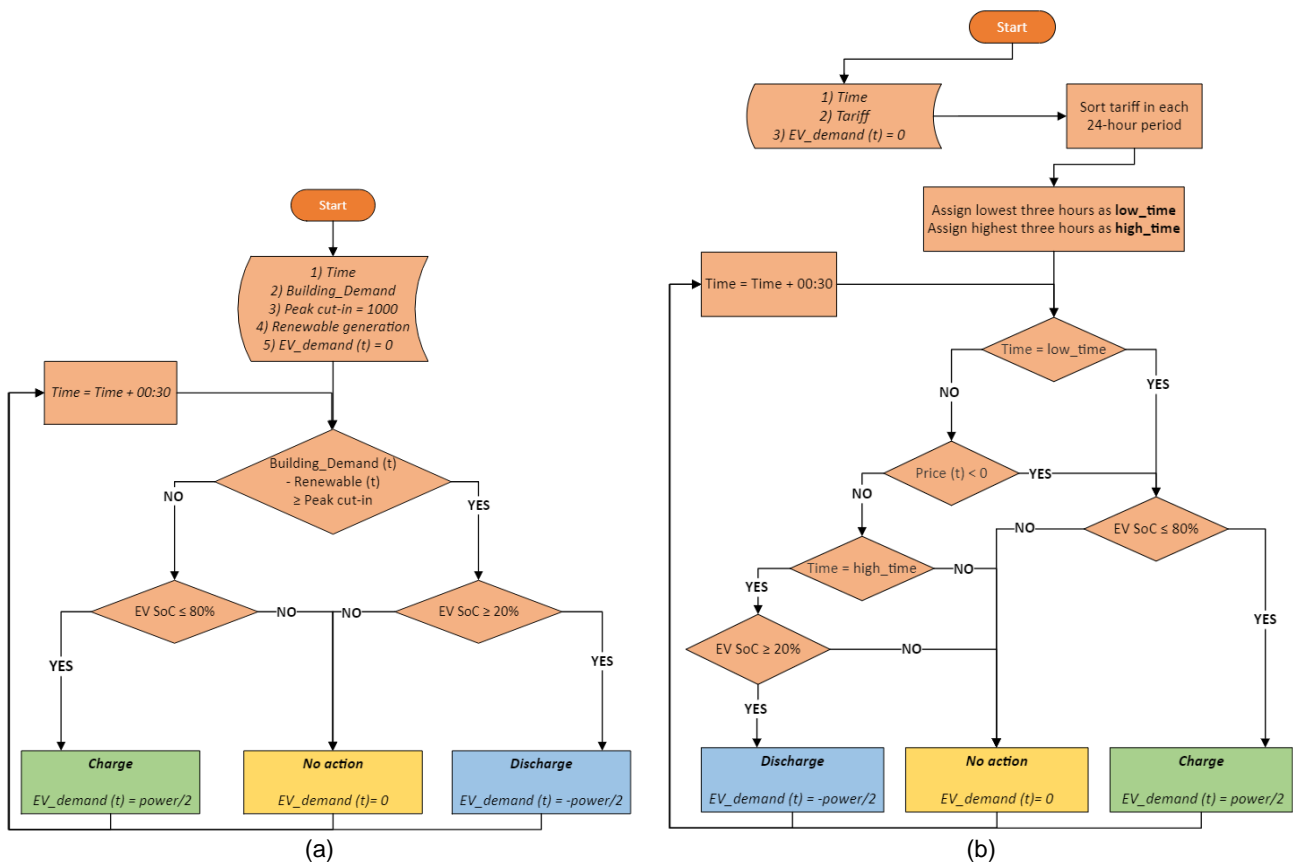


Figure 3 Flowcharts of simulation models (a) peak shaving (b) grid arbitrage

The following description provides details of each of the simulation methods.

- Unmanaged charging:** an annual EV parking dataset was generated, wherein the number of parked EVs was randomly assigned for each day depending on the year and EV penetration scenario (see Table 2). For example, in 2023, a random number between 45 and 75 was generated each day for central scenario, similarly in 2026 a random number between 305 to 325 was generated for high scenario. Following this, the algorithm iterated through each time step (i.e., through each half-hour period) and charged the vehicle up to 80% if their battery

state of charge (SoC) was below 80%. New EVs were introduced into the parking lot at 10am every day, which is the busiest time at the airport. The unmanaged model aims to maximise the cost for EV charging.

- **Peak shaving:** an annual EV parking dataset was created, wherein the number of EVs was randomly assigned (in the range shown in Table 2) for each day, similar to the previous scenario. New EVs were connected at 6am, just before the start of the morning peak. The choice of the changeover time is aimed towards incurring minimal cost under peak shaving scenario. The algorithm then iterated through each time step (i.e., through each half-hour period) and checked if the gross demand (building demand minus renewable generation) was greater than a threshold value, which is defined as the day average demand. If this condition was met, then the EVs were discharged to support the building demand. EVs were charged if the gross demand was lower than the day average.
- **Grid arbitrage:** an annual EV parking dataset was created, using the same approach described previously. The energy tariff for each 24-hour period was then analysed and classified. The lowest six tariff times in a day were assigned for charging while the highest six tariff times in the day were assigned for discharging. The algorithm then iterated through each time step and charged the EVs if the time-step belonged in the low tariff group and discharged if it belonged in the high tariff group. For all other time-step, no activity was assigned. New EVs were connected at the lowest tariff rate each day.

#### 4. RESULTS AND DISCUSSION

This section illustrates the benefits of V2X charging modes under different EV capacity scenarios (i.e., low, central, high). The charging cost associated with EV penetration in the baseline year (2022) under the central EV capacity scenario is shown in Figure 4. Note that the benefits we calculated here refer to the net costs due to charging. Capital costs of infrastructure and EVSE are not considered nor are ongoing maintenance and refresh. We are also assuming there are no constraint with regards to the number of available EVSE at any given time.

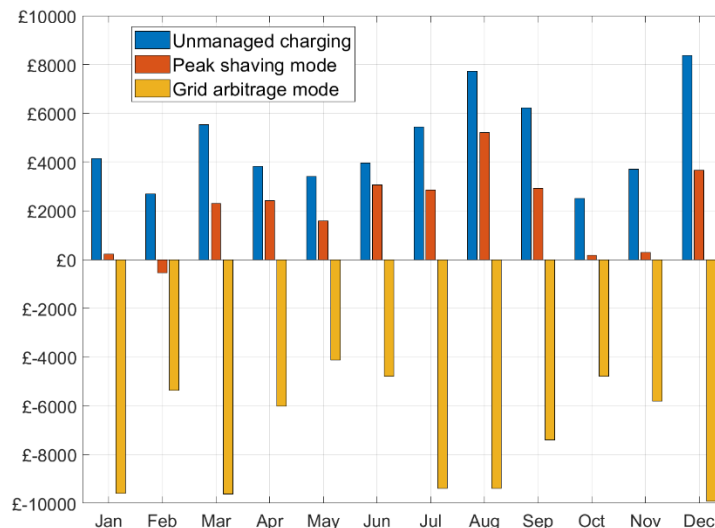


Figure 4 Results of different simulation models during the baseline year (central scenario)

As shown and Table 3, the annual net energy cost through parked EVs for the year 2022 is £56,626 if charging is unmanaged. Introducing peak shaving charging mode offsets some of the demand during peak times and consequently reduces the tariff associated during that time. The annual net cost in this mode is lowered to £37,479, a saving of nearly 34%. From a financial perspective, however, the grid arbitrage charging mode offers the maximum advantage. This mode charges vehicles during the low tariff times and feeds the energy back during high tariff times. This completely offsets the cost of vehicle charging, making an annual profit of £86,326, equal to a saving of nearly 252%. Similar observations are made for the low and high EV penetration scenarios during the period 2022 to 2030, as shown in Table 4 and Table 5, respectively.

Table 3: Simulation results during the period of 2022 to 2030 (central scenario)

Year	Unmanaged charging	V2G peak shaving		V2G grid arbitrage	
	Cost of EV operation	Cost of EV operation	Saving	Cost of EV operation	Saving
2022	56,626	37,479	34%	-86,326	252%
2023	78,026	56,941	27%	-115,796	248%
2024	136,462	97,097	29%	-182,114	233%
2025	174,987	130,897	25%	-234,152	234%
2026	285,863	206,925	28%	-367,246	228%
2027	386,368	280,421	27%	-446,130	215%
2028	564,333	422,325	25%	-646,091	214%
2029	790,904	588,435	26%	-900,019	214%
2030	1,225,000	894,149	27%	-1,360,405	211%

Table 4: Simulation results during the period of 2022 to 2030 (low scenario)

Year	Unmanaged charging	V2G peak shaving		V2G grid arbitrage	
	Cost of EV operation	Cost of EV operation	Saving	Cost of EV operation	Saving
2022	48,967	31,794	35%	-72,220	247%
2023	39,219	30,309	23%	-58,749	250%
2024	88,524	64,712	27%	-119,270	235%
2025	135,336	97,677	28%	-169,717	225%
2026	192,224	138,003	28%	-239,306	224%
2027	292,306	215,876	26%	-328,755	212%
2028	354,870	270,012	24%	-412,980	216%
2029	538,777	397,797	26%	-596,364	211%
2030	666,502	499,879	25%	-749,721	212%

Table 5: Simulation results during the period of 2022 to 2030 (high scenario)

Year	Unmanaged charging	V2G peak shaving		V2G grid arbitrage	
	Cost of EV operation	Cost of EV operation	Saving	Cost of EV operation	Saving
2022	63,687	41,482	35%	-98,303	254%
2023	117,525	84,019	29%	-173,681	248%
2024	264,243	187,217	29%	-363,456	238%
2025	347,547	256,127	26%	-463,066	233%
2026	552,753	395,588	28%	-740,326	234%
2027	769,465	563,033	27%	-872,013	213%
2028	1,000,749	751,146	25%	-1,179,094	218%
2029	1,244,250	908,071	27%	-1,463,335	218%
2030	1,592,731	1,211,836	24%	-1,798,663	213%

Figure 5 shows the growth in energy cost over the years under different charging modes and scenarios. The lines in Figure 5 represent the simulation result of the central scenarios, while the shaded area is formed by the simulation results of the high and low scenarios under each mode. The peak shaving and grid arbitrage modes offer potential benefits in terms of cost saving for EV operation in the future landscape, however, their impact is significantly different. While peak shaving creates a reduction in the import costs by 25%-35%, grid arbitrage generates income instead. From the very start of the simulation, the tariff-based charging mechanism ensures that the vehicles support the building demand in times of high import costs. The cumulative effect is that net energy is annually exported to the grid, generating income in the process. Under the peak shaving mode, benefits are mostly observed in winter months when the peak demand is significantly high. Over the course of other months, no major cost benefits are observed.

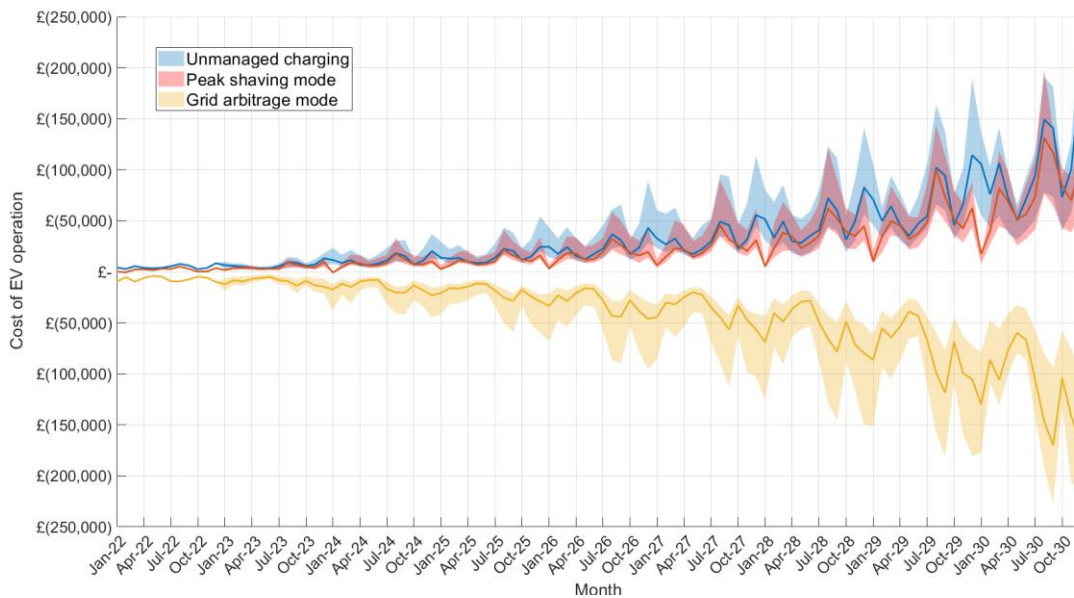


Figure 5 Results of different simulation models during the period of 2022-2030



## 5. CONCLUSION AND FUTURE WORK

This study investigated the potential benefits of implementing different V2X strategies, namely peak shaving and grid arbitrage, within the context of East Midlands Airport. The unmanaged charging mode is included as the baseline mode for comparison. Prior to simulating different charging modes, the data of the energy consumption and energy price was analysed to identify possible opportunities for V2X technologies implementation. The analysis revealed a weak relationship between energy consumption and energy price, which supported the feasibility of demand shifting to generate value for the airport. Simulation algorithms were devised for three EV charging modes: unmanaged, peak shaving, and grid arbitrage. The simulation experiments were conducted for three different EV capacity scenarios, namely low scenario, central scenario, and high scenario. The simulation results from 2022 to 2030 showed that both peak shaving and grid arbitrage charging modes can help reduce the EV charging costs, while grid arbitrage outperforms the other two strategies by generating a surplus income. For future work, the proposed simulation models can be further refined and extended using data from other airports such as Manchester Airport to further validate and generalise the findings.

## 6. REFERENCES

- International Energy Agency. (2021). Global EV Outlook 2021 Accelerating ambitions despite the pandemic. Available at: [www.iea.org/t&c/](http://www.iea.org/t&c/) (Accessed: 14 August 2023).
- Department for Transport. (2023b). Transport decarbonisation package to help boost net zero ambitions - GOV.UK. Available at: <https://www.gov.uk/government/news/transport-decarbonisation-package-to-help-boost-net-zero-ambitions> (Accessed: 14 August 2023).
- SMMT report (2021). Available at: <https://www.smmt.co.uk/wp-content/uploads/sites/2/SMMT-new-car-market-and-parc-outlook-to-2035-by-powertrain-type-11-06-21.pdf> (Accessed: 14 August 2023).
- Department for Transport. (2023a). Consultation on a zero-emission vehicle (ZEV) mandate and CO2 emissions regulation for new cars and vans in the UK. Available at: [www.gov.uk/government/organisations/department-for-transport](http://www.gov.uk/government/organisations/department-for-transport) (Accessed: 14 August 2023).
- EY (2023). UK-EV-success-hinges-on-six-essentials | EY UK. Available at: [https://www.ey.com/en\\_uk/news/2023/04/uk-ev-success-hinges-on-six-essentials](https://www.ey.com/en_uk/news/2023/04/uk-ev-success-hinges-on-six-essentials) (Accessed: 14 August 2023).
- Charles River Associates. (2023). Vehicle-to-Grid: The solution to our energy problem? Electric Reviews. Available at: <https://electricalreview.co.uk/2023/01/12/vehicle-to-grid-the-solution-to-our-energy-problem/> (Accessed: 14 August 2023).
- Frankland, O. (2018). The role of Electric Vehicles in a Smart Grid - Regen. Regen. Available at: <https://www.regen.co.uk/the-role-of-electric-vehicles-in-a-smart-grid/> (Accessed: 14 August 2023).
- VIRTA. (2023). Vehicle-to-Grid (V2G): Everything you need to know. Available at: <https://www.virta.global/vehicle-to-grid-v2g> (Accessed: 14 August 2023).
- Amamra, S. A., & Marco, J. (2019). Vehicle-to-grid aggregator to support power grid and reduce electric vehicle charging cost. *IEEE Access*, 7, 178528-178538.
- Jie, Y. A. N. G., Fan, G. U. O., & Zijian, C. A. O. (2020). Cost and benefit analysis of EV energy storage through V2G. *Energy Storage Science and Technology*, 9(S1), 45.
- Singh, K., & Singh, A. (2022). Behavioural modelling for personal and societal benefits of V2G/V2H integration on EV adoption. *Applied Energy*, 319, 119265.
- Elxon (2023). Available at: <https://www.bmreports.com/bmrs/?q=balancing/systemsellbuyprices> (Accessed: 14 August 2023).
- Anselmo, I., & Mahmood, H. (2021, September). Modelling and simulation of EV unscheduled charging and its impact on distribution systems. In *2021 IEEE PES Innovative Smart Grid Technologies Conference-Latin America (ISGT Latin America)* pp. 1-5). IEEE. Council of European Energy Regulations (2023). Available at: <https://www.ceer.eu/documents/104400/-/-/66369fc0-516c-7b67-7106-0fa6e12c0511> (Accessed: 14 August 2023).
- International Energy Agency (2020). Available at: <https://www.iea.org/reports/global-ev-outlook-2020> (Accessed: 14 August 2023).

---

## #266: Non-traditional social housing in the UK

---

Praveena POCHAMPALLI<sup>1</sup>, Lucelia RODRIGUES<sup>2</sup>, Renata TUBELO<sup>3</sup>

<sup>1</sup>University of Nottingham, University Park, Nottingham NG7 2RD, UK, Praveena.Pochampalli@nottingham.ac.uk

<sup>2</sup>University of Nottingham, University Park, Nottingham NG7 2RD, UK, Lucelia.Rodrigues@nottingham.ac.uk

<sup>3</sup>University of Nottingham, University Park, Nottingham NG7 2RD, UK, Renata.Tubelo@nottingham.ac.uk

*Abstract: Homes account for 26% of total greenhouse gas emissions in the UK, primarily arising from energy consumption. The UK's housing stock is among the oldest and least energy-efficient in the world, relying heavily on heating, typically powered by gas. As a result, meeting the UK's net zero greenhouse gas emissions target by 2050 relies on housing retrofitting for energy efficiency. Housing retrofit provides several benefits, such as reduced energy demand and costs, thereby reducing fuel poverty; improved comfort and wellbeing for occupants; and lower maintenance and repair costs. The social rented sector accounts for 4 million (17%) of England's projected 24 million households and approximately 5 million homes in the UK. Despite having a larger proportion of energy-efficient housing within its stock than other tenures, social housing has a significant decarbonisation challenge. The housing shortage at the end of the Second World War sparked a local-authority-driven house-building initiative across the nation. To meet the demand, in addition to 'traditional' brick-built homes, an estimated 1.5 million 'non-traditional' homes were constructed between the 1940s and the 1970s. Half of the stock is still in the social rented sector, which also falls under the Energy Saving Trust's subcategory group of 'hard-to-treat' homes. Precast reinforced concrete, in-situ concrete, and steel-framed construction were the most prevalent types of non-traditional construction. In spite of the fact that non-traditional housing comprises a significant portion of the social housing stock and exhibits greater improvement potential, due to its innate architectural complexities, it tends to be overlooked in favour of other traditional archetypes when it comes to retrofitting with energy-efficiency measures. Additionally, it remains a challenge to understand and identify the key characteristics of these typologies. This is, therefore, the focus of this work. The authors have explored the potential impact of retrofitting 'hard-to-treat' homes on the UK's net zero ambitions. The authors have identified and collated the most prevalent non-traditional housing archetypes' stock profile, general characteristics, features, and construction conditions. This comprehensive evaluation covered construction systems such as Wimpey No Fines, British Iron and Steel Federation Housing, and Cornish Unit type. This will aid in understanding the existing thermal performance and serve as a basis for suggesting practical and cost-effective retrofit alternatives for future research.*

*Keywords: Social housing, Non-traditional construction, Wimpey No-Fines, British Iron and Steel Federation Housing, Cornish Unit*

## 1. INTRODUCTION

Homes account for 26% of total greenhouse gas emissions in the UK, primarily arising from energy consumption (ONS, 2022). The UK housing stock is among the oldest and least energy-efficient in the world, relying heavily on heating, typically powered by gas (BRE, 2017; Passivhaus Retrofit in the UK, 2021) (Figure 1). According to the Office for National Statistics (2021) evaluation, the age of the property is the most important factor in determining its energy efficiency, ahead of fuel type and property type. As a result, attaining the UK's net zero greenhouse gas emissions target by 2050 is dependent on energy-efficient housing retrofitting (UK building Review, 2022). Housing retrofit has various advantages, including decreased energy consumption and expenditures, which reduces fuel poverty; enhanced occupant comfort and well-being; and reduced maintenance and repair expenses.

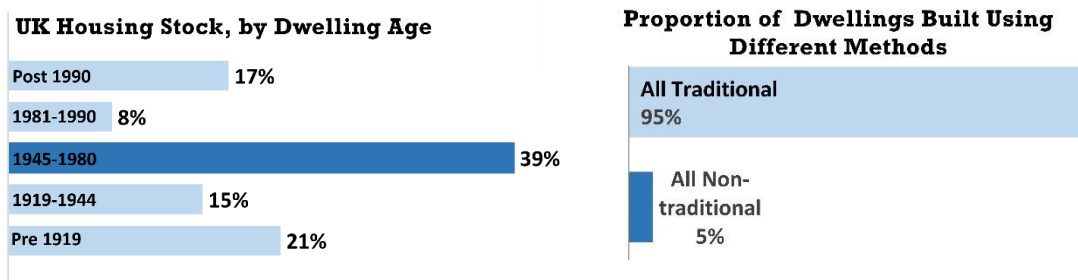


Figure 1 (Left) Housing stock built per age band, adapted from the *Housing stock of the United Kingdom*, BRE, 2017 and (Right) Traditional vs Non-traditional housing stock, adapted from EHS, 2008

Extensive research has been conducted on the general history of housing conditions in the United Kingdom (Bendixson, 1965; BRE, 2002; Bowley, 1945; Bullock, 2002; Burnett, 1993; Finimore, 1989; Harrison, H. et al., 2005; Hashemi, 2009; Holmans, 1987; Harvey & Ashworth, 1997; Mclean, S., 2009; Ross, Keith, 2002; Revell & Leather, 2002; Rodger, 1989; Sommerville, J. et al., 2011; White, 1965). However, less research has been conducted to review, highlight and summarise the most crucial factors with regards to non-traditional construction and system building, which not only changed the construction industry but also transformed the appearance of the UK cities and led to negative effects on the social and economic conditions of the country (Osborn, 1989). This paper intends to examine the historical context of housing in the United Kingdom, specifically focusing on non-traditional construction methods. The objective of this discussion is to examine the factors contributing to the development and subsequent lack of success of these approaches. The research approach employed in this article mostly consists of desktop research, wherein data is gathered from pertinent materials such as books, papers, and websites published by individual researchers, the UK government, and other research organisations. The subsequent analysis of the literature review is undertaken in order to ascertain the key determinants that influenced the non-traditional social housing stock in the United Kingdom.

### 1.1. Social Housing in the UK

The social rented sector accounts for 4 million (17%) of England's projected 24 million households and approximately 5 million homes in the UK (English Housing Survey 2021 to 2022: headline report, 2022; Beckett, 2014). Despite having a larger proportion of energy-efficient housing within its stock than other tenures, social housing has a significant decarbonisation challenge (English Housing survey, 2022). The housing shortage at the end of the Second World War sparked a local-authority-driven house-building initiative across the nation (BRE, 2017). To meet the demand, in addition to 'traditional' brick-built homes, an estimated 1.5 million 'non-traditional' homes were constructed between the 1940s and the 1970s (English housing survey- housing stock report, 2008). Around 72% of local authority housing stock and 47% of the housing association homes were built between 1945 and 1980. Only 8% of local authority stock and 37% of housing association homes were built after 1980 (Department for Communities and Local Government, 2017: p. 25). Approximately 50% of the stock remains within the social rented sector, which is also classified as a subset of 'hard-to-treat' homes by the Energy Saving Trust. Precast reinforced concrete, in-situ concrete, and steel-framed construction are the most prevalent types of non-traditional construction (English Housing Survey, 2008). In spite of the fact that non-traditional housing comprises a significant portion of the social housing stock and exhibits greater improvement potential, due to its innate architectural complexities, it tends to be overlooked in favour of other traditional archetypes when it comes to retrofitting with energy-efficiency measures (Energiesprong, 2022). It remains a challenge to understand and identify the key characteristics of these typologies (Mclean, S., 2009). As a result, this is the primary emphasis of this work.

## 2. NON-TRADITIONAL HOUSING (POST SECOND WORLD WAR)

Non-traditional housing construction can be classed as construction techniques that utilise systems of building, focused on speed and economy of construction. They differ widely from the traditional form of constructions that use bricks and mortar. It is the sort of construction that is used where a great deal of housing is required quickly, so it was often used by local authorities to mass build (Non-Traditional Housing in Calderdale, 2021). Non-traditional housing is often thought of as

being mainly for flats, however 40% of these dwellings were actually houses (EHS, Housing stock report, 2008) and 46% of such dwellings are located in the South East regions.

The onset of the Second World War necessitated a significant need for rapid building of houses. The government's goals, outlined in a white paper in 1945, included rebuilding homes damaged during the war as well as finishing the pre-war slum clearance programme and giving a separate residence to any family requesting one. Following the end of the Second World War, a notable surplus in the production of steel and aluminium emerged. These factors drove the move towards the use of prefabrication, as a result many new varieties of concrete, and steel framed systems emerged. Although the majority of systems were designed to offer permanent or long-term housing, a small number were specifically meant as emergency or temporary solutions (Non-Traditional Housing in Calderdale, 2021).

According to Ross et al. (2002), the Building Research Establishment (BRE) has documented more than 500 systems throughout the time period spanning from 1919 to 1976. Only a small number of these systems have been in continuous production for extended periods, specifically twenty years or more, and have been utilised in the construction of over 20,000 dwellings. Determining the precise quantity of residential structures constructed for various systems, as well as the duration of their production, presents challenges due to conflicting information from multiple sources (Mclean, 2009). However, the two charts in Figure 2 present data from the English House Condition Surveys carried out in 1986 and 1991, and attempts to list most of the systems that achieved notable production periods and numbers of dwellings built.

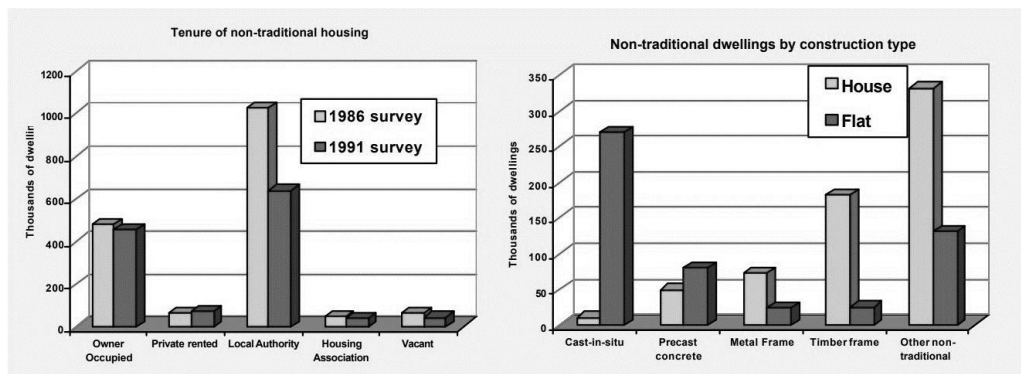


Figure 2 Non-traditional construction systems that achieved notable production periods and numbers of dwelling built (Source: English house Condition Surveys 1986 and 1991)

Today, the existing UK residential stock consists of approximately 26 million homes, of which some 8 million have solid walls (DCLG, 2008). Solid wall properties that include non-traditional forms of construction are in general considered to be 'Hard to Treat' (HTT) homes. HTT homes are defined by the Energy Saving Trust (BRE, 2008) as properties that cannot easily and cost-effectively be improved by conventional measures such as wall or loft insulation (Dowson et al., 2012). The insulation of HTT non-traditional houses can bring about significant emissions reductions from the building sector, thus making a significant impact on household energy consumption and play a large part in tackling fuel poverty (Changeworks, 2012). Calderdale Council, in their report on Non-Traditional Housing in Calderdale (2021) pointed out that Housing organisations and associations with large amounts of stock required properties to be brought up to a more modern standard for thermal efficiency, which normally involved a cladding system along with checks on structural elements.

In order to reach the housing sector decarbonisation targets, it is imperative to resolve the uncertainties surrounding the pre-retrofit thermal performance. This paper examines the hypothesis that the existing strategy, which primarily targets "Hard to Treat" (HTT) homes, is inadequate for achieving the United Kingdom's net zero goals. The authors propose a comprehensive analysis of the non-traditional housing stock, utilising available databases and literature, to identify key potential archetypes that have demonstrated notable production. Specifically, the authors suggest prioritising the retrofit of non-traditional social housing units such as Wimpey No Fines, British Iron and Steel Federation Housing (BISF), and Cornish Units, as these archetypes may offer greater potential for large-scale retrofitting.

## 2.1. Non-Traditional Construction Types and Performance

According to NHBC foundation (2015), the non-traditional properties are categorised within four groups: Timber frame construction; Metal frame construction; In situ concrete construction and Precast concrete construction. During the 1940s, 1950s, and 1960s, significant developments occurred in the field of residential construction, with a particular emphasis on productivity and innovative production techniques. As a result, an industrialised building ideology emerged. The philosophy shifted towards that of Industrialised building. This is based on the principle that as much work as possible is transferred from the site to the factory leaving a simple assembly system to be carried out on site. Construction methods that emerged in the years following World War II included the use of large panels, Wimpey no-fine concrete, Airey housing, and a few high-rise structures. In 1954, the United Kingdom reached its peak of housing construction, having completed just under 350,000 houses (Non-Traditional Housing in Calderdale, 2021).

Age, wear, lack of maintenance, and misuse made the buildings seem undesirable, yet many non-traditional housing systems initially supplied nice dwellings, and many still do. Most non-traditional housing systems are structurally sound;

however, some system-built homes have had issues. Some concrete system-built houses developed structural stability and durability issues in the 1980s. In the early 1980s, the Government commissioned the BRE to evaluate many housing styles with concerns. Defects in the design and construction of several dwelling types built before 1960 were declared fundamentally defective under the Housing Defects Legislation. The Housing Defects Act 1984 (now the Housing Act 1985) addressed these issues. Overall, the majority of non-traditional dwellings have provided levels of performance not very different from many traditionally built dwellings of the same age. However, there are inherent defects with several systems and repair may be impossible for some homes (Harrison et al., 2005).

The Centre for Sustainable Energy (CSE) investigated fuel poverty in non-traditionally built households. The Hard-to-Treat Homes subgroup of the Energy Efficiency Partnership for Homes commissioned the CSE study. The study calculated fuel poverty risk using House Condition Survey data. 52 local authorities with lots of non-traditional housing were studied. Running costs were compared to published income distribution statistics after each non-traditional home type's SAP scores were generated. The findings were that overall, low-rise non-traditional building is more energy efficient than solid-wall masonry but less so than cavity wall construction. Moreover, a new standard by The Energy Efficiency Standard in Social housing (EESH) now requires all social housing in Scotland to meet EPC Band B, or to be as energy efficient as practically possible by the end of December 2032. The UK government has also set a goal for fuel-poor home in England to reach EPC C or higher by 2030 contributing to the UK-wide net zero 2050 target (UK Housing Review, 2022). The Centre for Sustainable Energy (CSE) observed considerable improvements on all non-traditional stock in its possible case studies.

This initial study led to a comprehensive evaluation of the three principal non-traditional construction materials, namely in-situ concrete, steel framed, and precast concrete. Of the 500 different construction systems that were built using these non-traditional materials, the prominent ones representing each of the mentioned construction materials chosen for a preliminary literature study were the Wimpey No Fines, British Iron and Steel Federation Housing, and Cornish Unit housing types. The BRE historic archives provide a more extensive examination of various construction techniques. The primary goal of this preliminary investigation was not to provide comprehensive solutions for non-traditional housing, but rather to comprehend and identify the fundamental characteristics of these typologies, laying the groundwork for a subsequent examination of their thermal performance and retrofit solutions. As a result, the fundamental focus of this work is on this element.

### **3. IN-SITU POURED CONCRETE**

Concrete was widely employed as an alternative to brickwork in house construction beginning in the 1920s (Harrison, H. et al., 2005). They were created in an effort to cut costs by reducing construction time, but further study suggests that many cast-in-situ concrete buildings were actually more expensive to build than traditional modes of construction. Clinker aggregates and no-fines concrete were commonly used in the development of concrete mixes. In-situ concrete construction was used in about 450,000 of the approximately 1.5 million non-traditional houses produced in the UK up to 1975 (100,000 Easiform Type II and 300,000 Wimpey No-Fines were built up until the 1970s) (Harrison et al., 2005).

According to the BRE's investigations, no structurally unsafe conditions were discovered in these particular housing types. However, external wall disruption and cracking caused by imbedded metal corrosion may eventually lead to localised failure. Another source of concern in cast in-situ systems is the often poor thermal performance. Many concrete dwellings have been discovered to have significant heat loss, surface condensation that leads to mould growth, and rainwater penetration (Harrison et al., 2005).

#### **3.1. Wimpey No-Fines**

The housing system created by George Wimpey and Co involved the utilisation of rendered solid wall no-fines concrete and conventional construction techniques. Among the various non-traditional housing systems that emerged after the war, it can be observed that the Wimpey No-Fines system yielded the highest quantity of housing units. Between the 1940s and 1970s, a substantial number of dwellings were constructed, totalling over 300,000 (Harrison et al., 2005). These structures encompassed a variety of housing types, including bungalows, semi-detached and terraced houses, as well as low-rise blocks of flats. The architectural concept incorporated robust eaves beams made of reinforced concrete and precast concrete lintels positioned above the windows on the ground floor (Figure 3 (right)). The Wimpey technique employed the utilisation of no-fines concrete, a variant of lightweight concrete that possesses the advantageous properties of increased pourable height and enhanced compaction capabilities (Harrison et al., 2005). No-fines is a lightweight type of concrete without sand which does not separate and exerts less pressure when liquid, meaning formwork can be lighter and pour heights greater. Additionally, compaction can be achieved with the use of rods for tamping, eliminating the requirement for concrete vibrators. According to the report "Modern methods of construction: Building on experience" (2021), these distinctive characteristics resulted in a decreased demand for highly skilled workers. The dwellings were built utilising in-situ cast no-fines concrete, including external walls ranging from 8" to 12" in thickness. The notable exterior characteristics encompass walls with a render finish and the presence of circular ventilation points integrated within the external walls (Figure 3 (left)). Several key issues that have been identified in relation to this housing design include the occurrence of cracks in the external walls and the carbonation of dense aggregate concrete ring beams (Harrison, 2004).

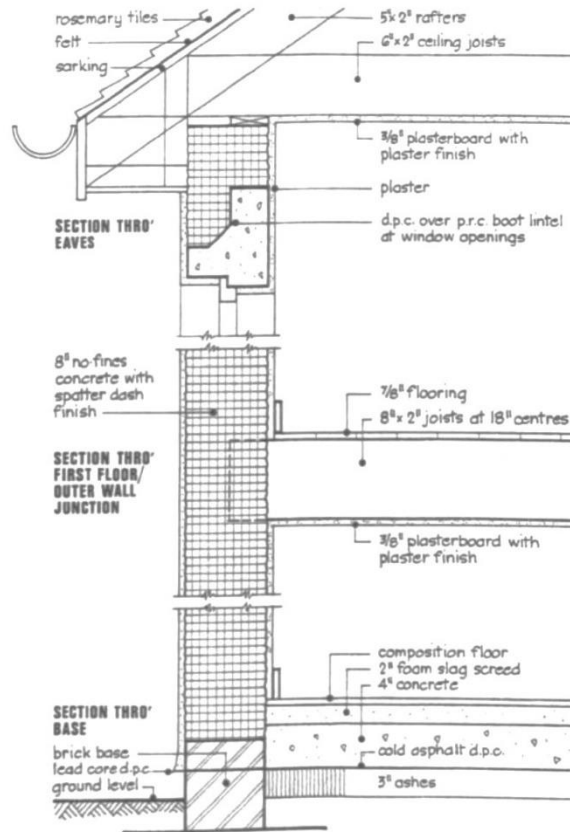


Figure 3 Wimpey No-Fines house (Source: Google Map data, 2023) (left) & Construction details (Source: Rutherford, 1996) (Right)

#### Technological Advancements and Scope for retrofit

A significant number of Wimpey No-Fines houses continue to be in existence. According to Harrison (2004), the simplistic nature of these forms renders them appropriate for the purpose of upgrading external wall insulation. During the 1970s, formwork methods such as Easiform and Wimpey No-Fines were substituted by light concrete blocks, which have since become a fundamental component in the construction of conventional houses. The concept was further advanced by the introduction of insulating concrete formwork (ICF) during the 1970s. The construction technique involves utilising hollow blocks made of polystyrene insulation, which may be stacked together to form a mould for pouring concrete. These blocks remain in place after the concrete has set, serving as a thermal insulation layer that envelops the building's structural core (NHBC, 2021).

#### 4. STEEL FRAMED HOUSES

In the UK, around 140,000 residential structures with steel frames and steel cladding have been built using a variety of system types. Certain residential constructions can be dated back to the interwar period, although the vast majority of residences were built after the Second World War ended. The British Iron and Steel Federation (BISF) was the principal supplier of steel-framed houses. While there may be some differences, a recurring feature is that the final dwelling was created to resemble a traditionally constructed building, integrating selected materials such as brick, imitation brick, or render (Harrison, H. et al., 2005). A number of causes prompted the comeback of steel frame building, including a severe shortage of skilled personnel and supplies, particularly timber, as well as an excess supply of steel and aluminium as a result of expanded manufacture for wartime needs.

Controversially, it is noteworthy to mention that the Housing Defects Act of 1984 did not classify any steel framed houses as defective. Nevertheless, it should be noted that this particular kind of building has indeed been linked to substandard performance, as indicated by Hobbs (2023).

The principal concern associated with steel-framed residences pertains to the susceptibility of the frame to corrosion, particularly in the vertical corner elements where the cladding or render may exhibit diminished effectiveness. Concerning indicators include the occurrence of cracks in rendered finishes or significant corrosion of steel cladding. Similar to concrete systems, steel framed systems might also face challenges in terms of thermal performance (Hobbs, 2023).



#### 4.1. British Iron and Steel Federation (BISF) House

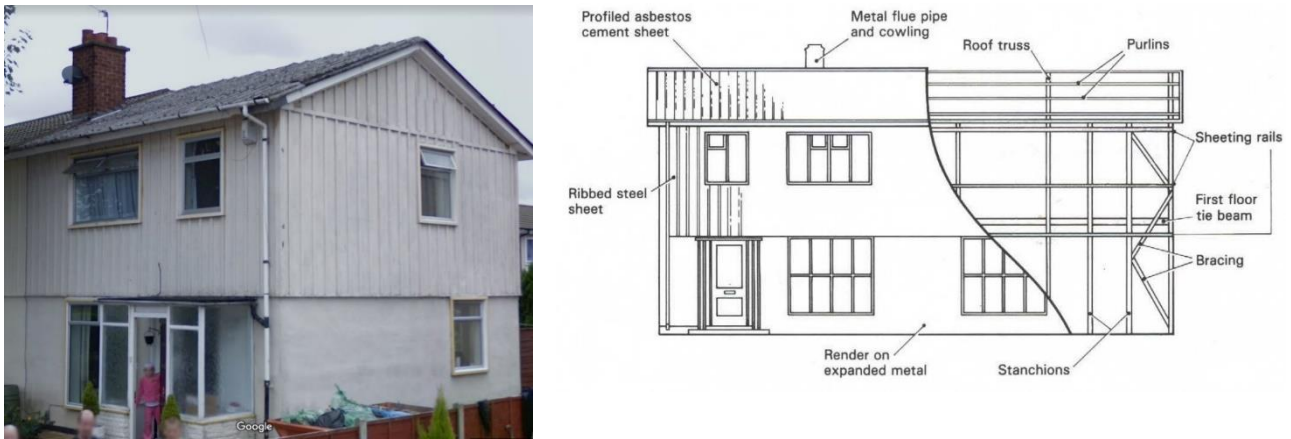


Figure 4 British Iron and Steel Federation house (Source: Google Map data, 2023) (left) and Front elevation showing the main structural elements (Source: BRE, 1986) (Right)

The BISF house, which was developed by the renowned architect Sir Frederick Gibberd, achieved considerable numerical success, with a total of 35,000 units constructed nationwide between the years 1944 and 1950. These houses were predominantly built as semi-detached, terraced dwellings, as well as flats. BISF houses were constructed as enduring residential structures, designed to possess a comparable lifespan to that of traditional brick-built houses. The residential structures were built on lightweight structural steel frames, incorporating distinctive exterior elements such as steel sheet cladding and metal trims (Figure 4 (right)). The steel frame was bolted together on site (BRE 469, 2004; Harrison, H., 2004; Modern methods of construction: Building on experience 2021). BISF residences that have not undergone subsequent modifications can be readily identified due to their distinctive feature of steel sheet cladding on the elevations (Figure 4 (left)).

##### *Technological Advancements and Scope for retrofit*

The report "BR 77 British Iron and Steel Federation steel framed house (1986)" presents findings derived from the investigation of numerous BISF houses in the UK. These observations indicate that while some houses remained in their original state, others had undergone or were now undergoing refurbishment. The report additionally observed that the degree of deterioration exhibits significant variation among individual houses and locations, lacking a consistent pattern. While severe deterioration of the steel framework has been detected in exposed sites, the number of affected houses seems to constitute a relatively small portion of the overall total. The structural integrity of the majority of BISF houses is generally intact, and any instances of deterioration within the structural framework can be remedied through a relatively straightforward process of removing and replacing the affected components. As per Hobbs (2023) findings, dwellings were equipped with roofing materials composed of asbestos, a substance recognised for its tendency to experience heightened fragility and reduced structural durability over time. This particular attribute not only poses a potential risk to the occupants residing, but also hinders the roofs' ability to adequately withstand various weather conditions and maintain their impermeability.

Steel-framed homes have inherent challenges in terms of detailing, such as the need to protect corrosion-prone components through the implementation of roof overhangs, flashings, and measures to isolate the construction from the ground, so ensuring the protection of the steel frame. Cold bridging was also an issue until details were technically improved to separate the steel frame thermal path from external face to internal leaf. In contemporary steel frame architecture, the entire structure is enveloped in insulation and kept on the warm side of the construction. The compatibility between steel framing and industrial manufacturing procedures allows for the application of high levels of precision and accuracy. According to the report "Modern methods of construction: Building on experience" (2021), light gauge steel refers to structural frames made from pressed cold formed steel sections that are both lightweight and galvanised. This construction approach provides advantages in terms of structural flexibility and material efficiency.

## 5. PRE-CAST CONCRETE

According to Harrison et al. (2005), until the mid-1970s, over 175,000 pre-cast concrete houses were built in the United Kingdom. Following the end of World War II, there was a significant demand for new housing. The Ministry of Defence and local authorities developed new precast concrete methods. Nonetheless, the use of precast concrete construction methods has resulted in a significant rise in flaws. At the time, three significant technological considerations were not well understood: A appropriate thickness of concrete is required to prevent the internal steel reinforcement from corrosion; The harmful consequences of various chemicals used to improve cure time over time; Building codes' failure to acknowledge the danger of panel systems if one panel fails, also known as progressive collapse. Hence some house types were

inherently defective (*Modern methods of construction: Building on experience* 2021). Throughout the 1980s, defects in these systems became apparent, leading government involvement and the designation of several of these systems as "defective" under the 1985 Housing Act (Hobbs, 2023).

The government subsequently established a corporation to licence "repairs" to these properties. This entailed removing the existing concrete and replacing it with brick and blockwork. This type of repair was costly, but it resulted in the house receiving a PRC Certificate (Holloway, 2018). As a result, these system-built dwellings can be difficult to identify. Many have been refurbished over the years, with new roofs and replacement windows, as well as rendered finishes, all of which might hide the original building's qualities (Hobbs, 2023).

The main concern in precast concrete houses is carbonation of the concrete, which can cause reinforcing steel to corrode and compromise the structural integrity of the building. Carbonation is more prevalent in precast reinforced concrete buildings, typically due to the use of poor-quality concrete and reinforcing steels placed at insufficient depths within the concrete. Water penetration accelerates the process, making structures in exposed sites or with poor weather-tightness particularly vulnerable (Hobbs, 2023). Calcium chloride, which was extensively used in concrete until the 1970s, can also generate carbonation. In extreme circumstances, the external walls may begin to bulge and lean as the structure begins to deteriorate (Hobbs, 2023). The poor thermal performance commonly observed in pre-cast concrete structures is an additional area of concern. Numerous instances have been documented wherein concrete houses exhibit significant heat loss, surface condensation resulting in mould, and penetration of rainwater.

### 5.1. Cornish Unit

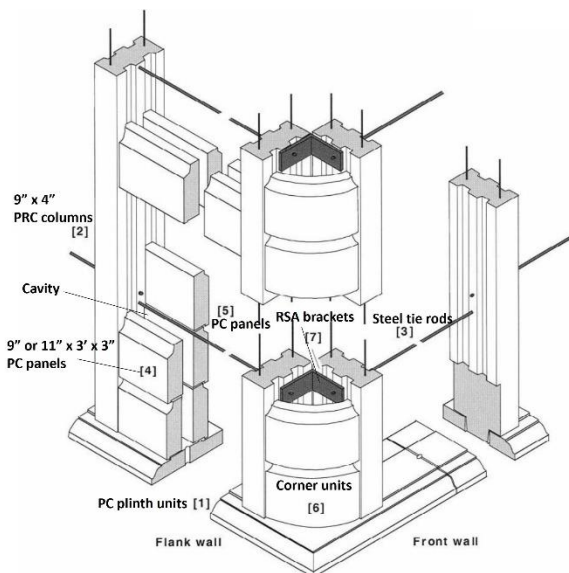


Figure 5 Cornish Unit house (Source: Google Map data, 2023) (Left) and construction details adapted from BR 469, BRE, 2004 (Right)

The Cornish Type 1 is widely acknowledged as one of the most easily identifiable precast concrete systems. The architectural feature of this structure is a unique mansard hipped roof, which is covered with vertically hanging tiles on its upper level (Figure 5). The mansard roof is characterised by its distinctive design, including sides that slope downwards with an increased steepness at the halfway point. The Type 1 architectural style bears resemblance to a bungalow, featuring dormer windows around the first floor (Holloway, 2018). The concrete modules were fabricated using a superior grade of white quartz aggregate, which is found in Cornwall and Devon as a byproduct of the china clay industry. The distinctive aspect of the external walling can be attributed to this particular aggregate. The construction of these units mostly took place in the South-Western region of the United Kingdom, as well as in the London area, commissioned by the London County Council (Selleck Nicholls & Co., 1951).

Selleck Nicholls & Co. and Central Cornwall Concrete & Artificial Stone Co. produced 30,000 homes during the 1950s over a 20-year production run (Holloway, 2018). These houses consisted of bungalows, two-story semi-detached houses, and terraced dwellings. Horizontal precast concrete panels and exposed PRC columns were used in the construction of the dwellings. Mansard roofs on Type I Cornish units and hipped roofs on Type II units, in addition to exposed concrete post and panel construction, were notable exterior features. Significant levels of chloride and cracking of PRC columns are the main causes of concern in these house types (Harrison, H., 2004). Both Cornish systems were declared as "defective" under the 1985 Housing Act and many were subsequently 'repaired'. Nevertheless, more than three decades following the passing of this legislation, a considerable number of units persist in their initial state (Holloway, 2018).



### *Designated defective house types*

The precast concrete building process frequently faced issues related to cold-bridges and inadequate reinforcement cover. During the early 1980s, an examination was conducted on an Airey house that had experienced fire damage. The analysis found the presence of cracks, which were attributed to insufficient protection of the reinforcement, as well as chemical alterations in the surrounding concrete. Subsequent inquiries revealed same structural deficiencies and the possibility of malfunction in more dwellings constructed using system-built methods. In the year 1984, the Secretary of State officially classified specific types of dwellings as inherently defective. The defective types were mainly precast concrete designs including Orlit and Cornish Unit, which were constructed in large numbers (Modern methods of construction: Building on experience, 2021).

### *Technological Advancements and Scope for retrofit*

The deterioration of reinforced concrete components and external finishes is a significant factor contributing to the many issues observed in pre-cast reinforced concrete (PRC) houses (Harrison, H. et al., 2005). The thermal performance of these building systems is significantly compromised. According to Holloway (2018), the initial insulation of the Mansard type roof was notably inadequate, with an approximate thickness of 25mm. If improvements have been done, it is often the case that only a thermal imaging camera can reveal them.

The majority of repairs were conducted with reinstatement systems that were licenced, inspected, and certified by PRC Homes Ltd, a subsidiary fully owned by NHBC. There is an increasing need for the renovation of low-rise dwelling units from this particular era. The process involves retrofitting and safeguarding pre-existing structures, while simultaneously upgrading them to meet current environmental regulations. Social housing constructed during the post-war era is frequently perceived as possessing both aesthetic and technological imperfections, and has never found popular acceptance in the UK. Nevertheless, the advancement of precast concrete construction has persisted, mostly for the purpose of developing buildings, both alone and in combination with other types of constructions. It is now a widely used and well understood technology (Modern methods of construction: Building on experience 2021).

## **6. CONCLUSION**

In this paper, the authors aimed to inform about non-traditional construction systems by explaining them through examples of widely explored construction types of the past and those of which are still in existence. It clarifies the long-held perception of postwar emergency housing, which, despite its negative repute, contained some brilliant engineering and long-lasting characteristics. It also emphasises the necessity for retrofitting as well as accelerating the delivery of a new generation of responsibly designed manufactured houses with aesthetic and technical build quality. Despite the fact that their initial design lives should have rendered them extinct, non-traditionally built houses have penetrated the housing market. When compared to regular dwellings, these houses have distinct construction forms, materials, inherent faults, and common difficulties. These can include flaws that could cause these houses to fail as well as flaws that would make them inferior to living in a traditional house. Identification is important to gain the understanding needed to appropriately assess their state and devise a suitable future prognosis.

The findings from this paper show the need for further research on evaluating the future value of these existing non-traditional homes through a detailed cost-benefit analysis. The cost-benefit analysis could compare the cost of refurbishing existing homes and the cost of building new homes. It is suggested that the cost analysis comparison will help social housing providers and construction managers to better understand the feasibility of refurbishing these homes. There is also a great scope for future work in assessing cost versus quality of life of the tenants within these existing properties.

The primary objective of the study was to examine the potential influence of retrofitting non-traditional homes on the United Kingdom's net zero goals. This was achieved by initially identifying the prevailing housing archetypes' stock profile, as well as their overall characteristics and construction conditions. However, it is recommended that future endeavours strive to incorporate a more extensive case study-based investigation. This would facilitate a thorough assessment of projects and ensure the availability of consistent data pertaining to costings and performance improvements.

## **7. REFERENCES**

- Bendixson, T. (1965). Industrialised building. Finding a winning system. *Design*, 200, 44 – 51.
- Bowley, M. (1945). *Housing and the State 1919-1944*. London: George Allen & Unwin.
- BRE. (2002). *Non-traditional housing in the UK – A brief review*. Garston: Building Research Establishment. Retrieved from [http://www.cml.org.uk/cml/filegrab/pdf/pub\\_misc\\_NontradhousingBR.pdf](http://www.cml.org.uk/cml/filegrab/pdf/pub_misc_NontradhousingBR.pdf).p df?ref=3595
- BRE, 2008. *Energy Analysis Focus Report. A study of Hard to Treat Homes Using the English House Condition Survey*. DEFRA Publications
- Bullock, N. (2002). *Building the Post-War World: Modern Architecture and Reconstruction in Britain*. London: Routledge.

- Burnett, J. (1993). *A social history of housing 1815-1985*. London: Routledge
- Changeworks, 2012. *Solid Wall Insulation in Scotland*. Changeworks
- Cornish Unit Construction part of the Selleck, Nicholls & Company, Ltd. (1951). Available from: <https://www.alamy.com/stock-photo-advert-for-cornish-unit-construction-part-of-the-selleck-nicholls-104177620.html>.
- Department for Business, I.& S. (2015) *Solid wall insulation: Future recommendations*, GOV.UK. Available at: <https://www.gov.uk/government/publications/solid-wall-insulation-future-recommendations> (Accessed: 31 August 2023).
- English Housing Survey 2021 to 2022: headline report* [online]. Available from: <https://www.gov.uk/government/statistics/english-housing-survey-2021-to-2022-headline-report>.
- Environmental Audit Committee (2021) *Energy Efficiency of Existing Homes*. House of Commons Environmental Audit Committee Fourth Report of Session 2019–21 [online]. Available from: <https://committees.parliament.uk/publications/5171/documents/52521/default/> (Accessed 2 November 2023).
- Fines in Public Housing. (1968). 68 (8), 1538. [online]. Available from: <http://dx.doi.org/10.2307/1121108>.
- Finnimore, B. (1989). *Houses from the factory: system building and the welfare state 1942-1974*. London: Rivers Oram Press.
- Hannah, Michelle and Nick Hunter, *NF82: Modern methods of construction: Who's doing what?* (Milton Keynes: NHBC Foundation, 2018) <https://www.nhbcfoundation.org/publication/modern-methods-of-construction-whosdoing-what/>
- Harrison, H. et al. (2005) Identification and assessment of non-traditional UK housing. *Structural Survey*. [Online] 23 (3), 172–179. [online]. Available from: <http://dx.doi.org/10.1108/02630800510610107>.
- Harrison, H. , Mullin , S. , Reeves , B. and Stevens, A. (2004) *Non-traditional Houses – Identifying Non-traditional Houses in the UK: 1918 – 75* . Bracknell: BRE Press.
- Harrison, R. (2009). Towards an Archaeology of the Welfare State in Britain, 1945– 2009. *Archaeologies*, 5(2), 238-262.
- Harvey, C. R. & Ashworth, A. (1997). *The Construction Industry of Great Britain* (2nd ed.). Oxford: Laxton's.
- Hashemi, A. (2006, November). *Modern Methods of Construction in the UK Housing Industry*. Third Research Student Conference, Cardiff, WSA
- Hobbs, S. (2023) *Houses of non-traditional construction – common property defects #6*, Peter Barry. Available at: <https://www.peterbarry.co.uk/blog/houses-of-non-traditional-construction-common-property-defects-6/> (Accessed: 29 October 2023).
- Holloway (2018) *Domestic surveys blog PRC and Cornish type1 non standard construction* [online]. Available from: <https://www.domesticsurveys.co.uk/2018/01/16/non-traditional-construction-part-2/>.
- McClean, S. (2009) "Surveying and Diagnosing Non-Traditionally Constructed Houses in the United Kingdom." *Journal of Building Appraisal*, 4(4), pp. 239–245. DOI: 10.1057/jba.2009.5.
- Ministry of Housing, C.& L.G. (2010) *English housing survey 2008: Housing stock report*, GOV.UK.
- Modern methods of construction: Building on experience* (2021) NHBC. Available at: <https://www.nhbc.co.uk/foundation/modern-methods-of-construction-building-on-experience> (Accessed: 20 October 2023).
- National-Statistics. *English Housing Survey 2021 to 2022*. Available online: <https://www.gov.uk/government/statistics/english-housing-survey-2021-to-2022-headline-report> (accessed on 10 August 2023).
- Nontraditional Houses in Calderdale*. (2021) [online]. Available from: <https://nonstandardhouse.com/non-traditional-houses-in-calderdale/>.
- OFFICE FOR NATIONAL STATISTICS 2022. *Climate change insights, families and households, UK: August 2022*.
- Report BR 153 *Structural condition of Wimpey no-fines low-rise dwellings*, BRE - Publication Index | NBS [online]. Available from: <https://www.thenbs.com/PublicationIndex/documents/details?Pub=BRE&DocID=83829>.
- Report BR 77 *British Iron and Steel Federation steel framed house* (1986). Bracknell, UK: BRE publications.

- Revell, K. & Leather, P. (2002). *The state of UK housing: a factfile on housing conditions and housing renewal policies in the UK* (2nd ed.), Bristol: The Policy Press.
- Rodger, R. (1989). *Housing in Urban Britain 1780-1914*. Cambridge: Press Syndicate of University of Cambridge.
- Ross, Keith, *Non-traditional housing in the UK: A Brief Review* (London: Council of Mortgage Lenders, 2002) [https://nanopdf.com/download/non-traditional-housing-inthe-uk\\_pdf](https://nanopdf.com/download/non-traditional-housing-inthe-uk_pdf)
- RUTHERFORD, H. R. (1996) *PUBLIC SECTOR HOUSING IN SCOTLAND 1940 to 1959*. University of Glasgow, Mackintosh School of Architecture [online]. Available from: <https://radar.gsa.ac.uk/4017/26/1996Rutherfordvol2GSA.pdf> (Accessed 5 November 2023).
- Sommerville, J. et al. (2011) No-fines concrete in the UK social housing stock: 50 years on. *Structural Survey*. [Online] 29 (4), 294–302. [online]. Available from: <http://dx.doi.org/10.1108/02630801111162369>.
- Turner, C. and Partington, R., 2015. *Homes through the decades. The making of modern housing*. NHBC Foundation, Milton Keynes.
- Understanding best practice in deploying external solid-wall insulation and internal wall insulation in the UK. (2017) [online]. Available from: <https://www.gov.uk/government/publications/understanding-best-practice-in-deploying-external-solid-wall-insulation-and-internal-wall-insulation-in-the-uk>.
- UK Housing Review 2022 shows faster progress is needed to tackle poor energy efficiency of older homes - Chartered Institute of Housing [online]. Available from: <https://www.cih.org/news/uk-housing-review-2022-shows-faster-progress-is-needed-to-tackle-poor-energy-efficiency-of-older-homes#:~:text=The%20UK%20government%20has%20set,rated%20EPC%20C%20or%20higher.>
- Way, Andrew, 'Benefits of light steel framing', *PBC Today*, 9 May 2019, <https://www.pbctoday.co.uk/news/planningconstruction-news/light-steel-framing/56740/>
- Wimpey No-Fines Concrete', *The Concrete Society*, <http://www.concrete.org.uk/fingertips-nuggets.asp?cmd=display&id=904>

---

## #267: Unlocking the potential of renewable energy: analysing energy storage deployment and policy in the EU

---

Kristiāna DOLGE<sup>1</sup>, Laura Kristiāna VIČMANE<sup>1</sup>, Dagnija BLUMBERGA<sup>1</sup>

<sup>1</sup> Institute of Energy Systems and Environment, Riga Technical University, Azenes iela 12/1, Riga, LV-1048, Latvia

*Abstract: The share of renewable energy utilized for power generation within the European countries will experience a substantial rise, ultimately attaining unprecedented levels in the forthcoming decades. The aforementioned trend can be attributed to the ambitious targets for renewable energy production and electrification set by the EU, which are stimulating investment and fostering innovation in the renewable energy sector. The incorporation of substantial amounts of renewable energy into the power grid poses various challenges, such as the intermittent and variable nature of renewable energy sources. To compensate for the volatile nature of renewable energy, energy storage and conversion (e.g. Power-to-X technologies) has been identified as a crucial factor in accelerating decarbonisation in the European Union. This study examines the current trends in energy storage deployment throughout the European countries and identifies the challenges and opportunities in energy storage policy. This study offers a comprehensive analysis of the installed capacities of energy storage facilities and investigates the energy storage policies that have been implemented in various European countries. The findings of this study provide valuable insights for policymakers in formulating energy policies that effectively promote the adoption and implementation of energy storage technologies.*

*Keywords: energy storage, renewable energy, energy policy, sustainability, energy transition*

## 1. INTRODUCTION

The share of renewable energy utilized for power generation within the European Union will experience a substantial rise, ultimately attaining unprecedented levels in the forthcoming decades. The aforementioned trend can be attributed to the ambitious targets for renewable energy production and electrification set by the EU, which are stimulating investment and fostering innovation in the renewable energy sector. It is projected that the proportion of renewable energy in the electricity system will reach 69% by the year 2030 (European Commission, 2023), up from 37% in 2021 (Eurostat, n.d.). The incorporation of substantial amounts of renewable energy into the power grid poses various challenges, such as the intermittent and variable nature of renewable energy sources. Supply and demand imbalances may lead to grid stability issues and require expensive grid enhancements. As a result, there is an urgent need for integration of flexibility technologies which will be a key element in decarbonized energy systems of the future.

The successful integration of renewable energy sources (RES) into the future energy system is projected to require a significant emphasis on the implementation of robust storage capacities. This is crucial in order to effectively manage and mitigate the inherent fluctuations associated with renewable energy generation (Directorate-General for Energy et al., 2023). According to estimates, the projected energy storage demand is approximately 200 GW by the year 2030 and 600 GW by the year 2050. If immediate action is not taken to increase the deployment of storage technologies, the current market trends in the energy sector will be insufficient to meet the system's requirements by 2030. A substantial increase in the adoption of storage capacity, amounting to a minimum of 14 GW per year, is necessary when compared to the previous rate of 1 GW per year (EASE, 2022).

In its recent publication, the European Commission acknowledges that implementing energy storage at the scale required is hindered by a number of obstacles that threaten its ability to effectively support the energy transition. Several of these obstacles relate to the need for long-term revenue clarity and predictability, which facilitates the acquisition of financial resources (European Commission, 2023).

The European Commission has made a commitment to persist in its efforts to develop suitable regulatory initiatives and policy instruments that will support in the progress and adoption of energy storage technologies within the European Union (Directorate-General for Energy et al., 2023). Nevertheless, it is the responsibility of each Member State to establish and execute the necessary regulatory framework and procedures in order to foster a conducive environment for the increased adoption of energy storage in their respective national electricity production sectors (European Commission, 2023). In order to stimulate Member States, the European Commission mandates that each Member State evaluate their electricity system's requirements for balancing and present concrete measures for cost-effective energy storage deployment in their revised national energy and climate plans (European Commission, 2023). While some member states have already implemented energy storage policies, for others there is still a great deal that is unknown. Therefore, it is necessary to comprehend what progress has been made in the implementation of energy storage policies in different EU countries and what examples of best practices can be identified.

The study presents a comprehensive compilation of the existing status of installed energy storage capacities across EU which identifies countries with higher installed capacities of energy storage facilities. This study analyzes the present status quo of energy storage policies across EU and evaluates the policy instruments implemented by various EU member states. An overview of the existing barriers and drivers in energy policy is performed in order to determine what measures could be implemented to eliminate the existing barriers and steer towards a greater energy storage penetration. The findings allow policymakers to develop effective energy policies based on examples of best practices uncovered by the research.

## 2. INSTALLED ENERGY STORAGE CAPACITIES IN EU

To examine the overall installed power capacities of energy storage technologies in the European Union, a statistical analysis was conducted using the database of European energy storage technologies and facilities published by the Directorate-General for Energy (Directorate-General For Energy, 2022). The analysis focused on the capacities of electrical energy storage, with the exclusion of thermal energy storage capacities. The dataset did not include projects that have been decommissioned or are currently offline. The data were compiled and analysed as of July 2023, while the database was published in November 2022. Hence, the information being presented does not encompass the recently disclosed energy storage initiatives. Data were compiled for 25 countries for which data were available in the database. For Latvia and Malta, no data on installed electrical storage capacity was reported in the database.

### 2.1. Total installations of energy storage technologies

A comprehensive examination of energy storage facilities in the European Union reveals a total of 730 facilities. Notably, Germany boasts the highest count with 161 facilities, followed by Spain with 101 facilities, and France with 74 facilities. Figure 1 depicts the overall quantity of electrical storage installations within the European Union member states. Figure 2 depicts the cumulative installed capacities of electrical storage facilities across European Union member states. The total installed power capacity amounts to 81,313 MW, with Spain (18,942 MW), Germany (16,253 MW), and Italy (8,801 MW) leading in terms of the highest capacities.

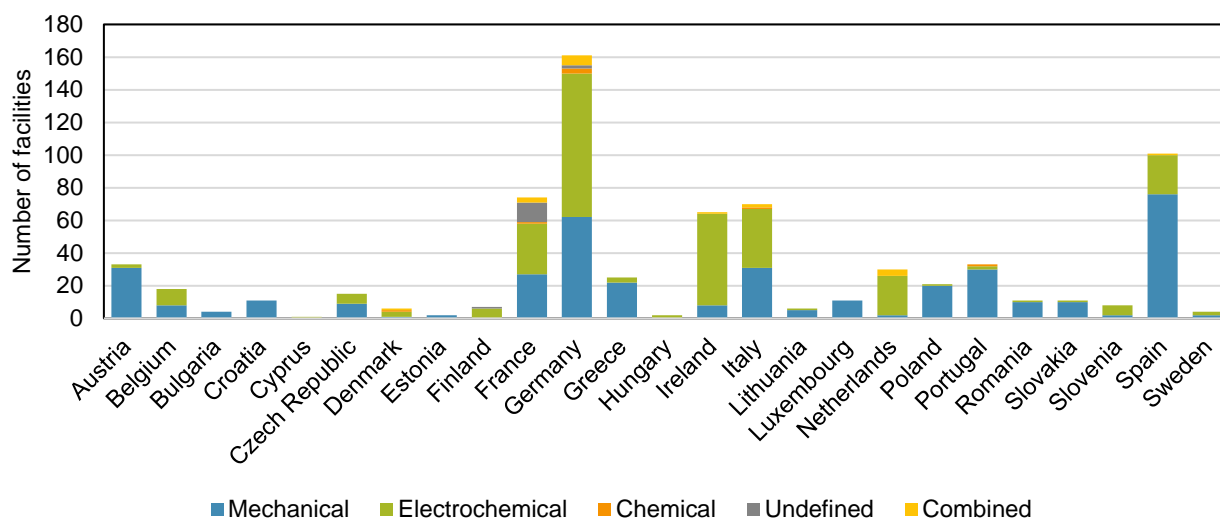


Figure 1 Number of electrical storage facilities in EU member states.

In terms of installed number of facilities (total of 384) and installed power capacity (total of 76,420 MW), mechanical storage facilities are the most prevalent in the European Union. There are a total of 306 electrochemical energy storage facilities in the European Union, with the highest concentrations in Germany, Ireland, Italy, France, and the Netherlands. In the European Union, the total installed capacity of electrochemical storage is 2,560 MW.

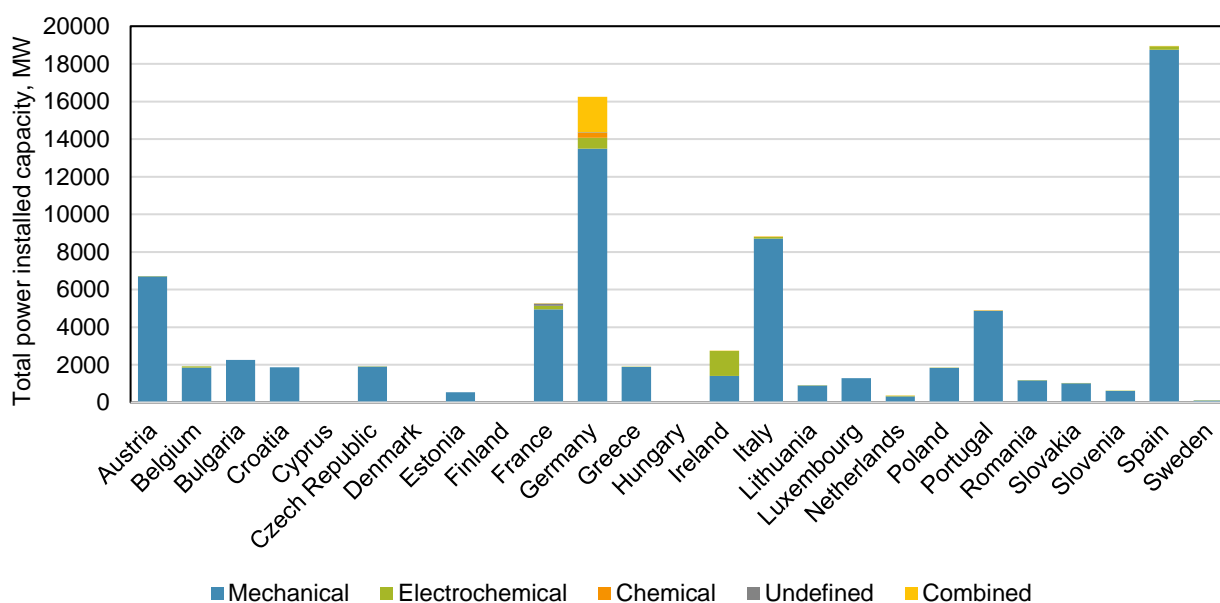


Figure 2 Total power installed capacity (MW) of electrical storage facilities in EU member states.

The majority of installed capacities for mechanical energy storage facilities are derived from pumped hydro storage (PHS), accounting for approximately 98% of the total. This is followed by compressed-air energy storage (CAES) with a capacity of 842 MW, and flywheel technology with a capacity of 463 MW. The predominant portion of electrochemical energy storage facilities consists of installed capacities utilising lithium-ion technology, accounting for approximately 89%. Additional electrochemical facilities encompass installations of sodium-sulfur (NaS), sodium-nickel chloride (NaNiCl), lead-acid electrochemical storages, electrochemical capacitors, and other technologies.

## 2.2. Status of the installed facilities

Out of the total installed power capacities, the majority of facilities, amounting to 48,093 MW, are presently operational. However, more than one fourth of the total installed power capacities of the facilities have been announced, suggesting a significant increase in energy storage implementation in recent years. Figure 3 depicts the status of electrical storage installations in EU member states.

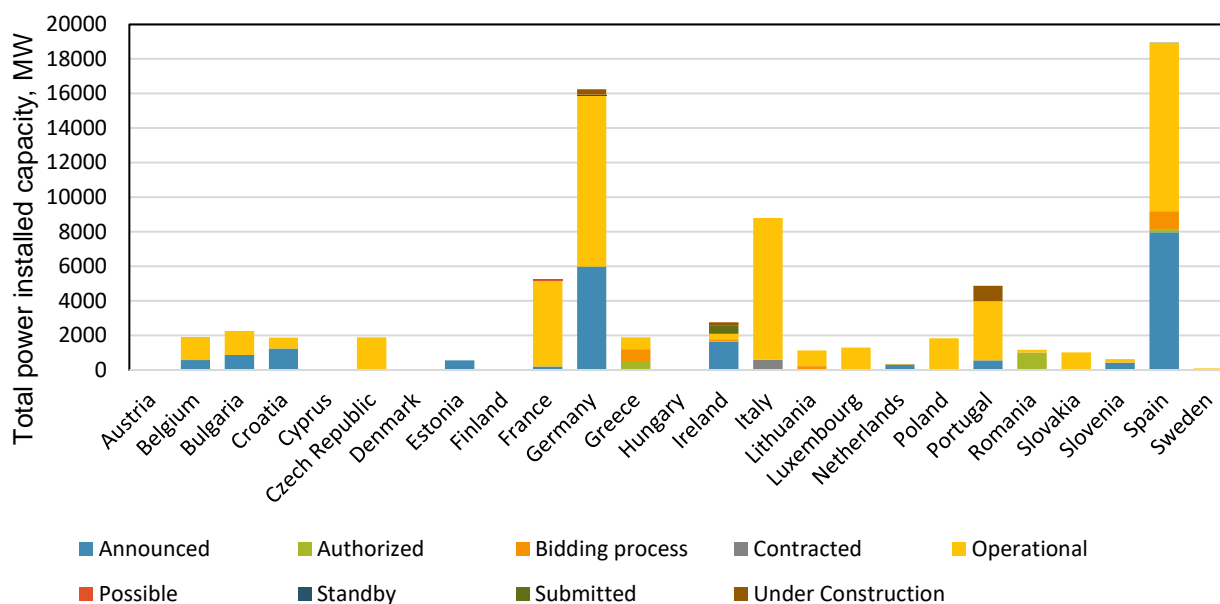


Figure 3 Status of electrical storage facilities in EU member states.

Germany (with 5,990 MW) and Spain (with 7,962 MW) are at the forefront in terms of announced energy storage capacities. In the case of Spain, Greece, and Lithuania, a substantial amount of capacities are presently undergoing the bidding process. Moreover, there are considerable capacities under construction in Germany, Portugal, and Ireland.

### 3. ENERGY STORAGE POLICIES ACROSS EUROPE

In order to assess the current state of energy storage policy implementation, it is crucial to comprehend the policy instruments and measures that have been implemented in European countries. Additionally, it is essential to identify the primary factors that have facilitated or hindered the deployment of energy storage in these countries. A comparative analysis has been conducted, utilising the latest literature and public information on energy storage policies and the energy policies database of the International Energy Agency (IEA) (IEA, n.d.), to examine the various policy instruments implemented in European nations. Furthermore, a comprehensive examination of the barriers and drivers in energy storage policy has been conducted.

#### 3.1. Cross country comparison of energy storage policies

There are various policy measures to incentivise the use of energy storage. The analysis identified six main groups of measures used in European countries - development of a sound regulatory framework, application of tax relief, financial incentives in the form of grants and subsidies, development of a comprehensive and structured strategy for the deployment of energy storage, provision of adequate funding for implementers and introduction of incentives for domestic manufacturing of energy storage technologies. A cross-country comparison was carried out, analysing 18 European countries. The countries were selected based on the information available from the literature review. The countries that were excluded from the comparison did not have enough public information to be used for the analysis. Table 1 presents an overview of the energy storage policy instruments employed in various European nations.

Table 1: Energy storage policy review across different countries in EU

	UK	Netherlands	Spain	France	Italy	Germany	Latvia	Hungary	Estonia	Romania	Portugal	Czechia	Belgium	Ireland	Austria	Croatia	Poland	Lithuania
Regulatory framework	X		X	X	X	X				X	X	X	X		X		X	X
Tax relief	X	X		X	X	X				X					X			X
Grants, subsidies	X		X		X	X	X	X	X	X	X	X	X	X	X	X	X	X
Comprehensive and structured strategy	X		X		X				X	X	X						X	
Funding	X		X	X		X	X	X	X	X		X	X		X	X	X	X
Domestic manufacturing incentive	X		X	X	X	X	X		X			X			X		X	X

Countries employ various policy instruments and methodologies to establish distinct priorities and objectives for their energy storage policies. According to Varela Soares (2023), at the moment the United Kingdom has successfully established the most comprehensive and efficiently structured electricity storage system in Europe. This system encompasses a comprehensive framework for the licencing and operation of storage assets. The primary aim of electricity storage is to offer flexibility services that are essential for the capacity market, with a primary focus on guaranteeing the reliability of the national energy supply in the United Kingdom (Varela Soares et al., 2023).

In the year 2015, the Netherlands implemented a temporary regulatory measure aimed at incentivizing investors to engage in electricity experimentation pertaining to both Energy Storage Systems (ESS) and renewable energy systems. Investors in renewable energy systems are granted preferential treatment, which encompasses various incentives such as tax exemptions and levy exemptions. However, in Netherlands the adoption of storage technology is experiencing a slow pace, primarily attributed to the existence of net-metering policies (Sani et al., 2020).

In Spain the establishment of regulations for electricity storage was undertaken to ensure harmonisation with the storage rules of the European Union (EU), resulting in the adoption of comparable definitions and competencies within both national and EU legislations. Electricity storage is acknowledged as a distinct undertaking, and it is further classified into two subcategories according to the nature of the services rendered. The classification of storage varies depending on its usage and connection. When storage is utilised for self-consumption and connected behind-the-meter, it is classified as an end user. On the other hand, storage is categorised as generation when it offers services to the grid. The recognition of storage that is dependent on consumption or generation requires the distinction between different types of storage services (Varela Soares et al., 2023).

The storage regulations in France are characterised by their broad and general nature, as they were established prior to the regulations of numerous other countries (Varela Soares et al., 2023). However, France lacks a dedicated legal framework pertaining to the advancement of energy storage systems. Feed-in tariffs typically exhibit a preference for the direct injection of electricity into the grid as opposed to storage implementation. The translation of roles leads to a duplication of charges when accessing the grid, thereby negatively impacting the adoption of energy storage systems.

In Italy, the regulatory framework pertaining to storage lacks a distinct and autonomous structure, as it is intricately linked to renewable-plus schemes (Varela Soares et al., 2023). In Germany there are several instruments introduced to support energy storage deployment. Germany has implemented a subsidy and loan programme with low interest rates to support the integration of Energy Storage Systems (ESS) batteries into the grid, particularly in conjunction with solar photovoltaic (PV) systems. The Ministry offers a coverage rate of 30% for the costs associated with the energy system. Additionally, grid tariffs and levies are exempted for energy storage system (ESS) facilities situated prior to the metre, on the condition that the stored energy is returned to the grid (Sani et al., 2020). However, the German framework pertaining to electricity storage exhibits a comprehensive nature; however, it is plagued by notable fragmentation due to the divergent definitions of storage found within different legislative and regulatory contexts (Varela Soares et al., 2023).

In Hungary investment support for utility-scale battery storage is being introduced. Hungary intends to establish a scheme that provides grants to support investments in utility-scale battery storage facilities (IEA, 2023b). Estonia has allocated EUR 7.8 million to support companies engaged in renewable energy production to invest in energy storage technologies. Companies that meet the criteria can receive funding up to one million euros, with a maximum subsidy amount of EUR 360,000 per megawatt-hour (MWh) of electricity storage (IEA, 2023a). Romania has introduced subsidies for battery storage manufacturing and deployment to encourage investments in electricity storage capacity. Under this support measure, costs incurred can be reimbursed up to EUR 167,000 per megawatt-hour (MWh) of storage or up to EUR 15 million per project (IEA, 2023c). At the national level in Belgium, there exist fundamental regulations that govern various aspects. However, the responsibility for formulating detailed protocols pertaining to licencing and operational procedures for storage facilities is delegated to the regional authorities in Belgium, namely Wallonia, Flanders, and Brussels. As a result, the national grid accommodates multiple regulatory regimes for storage in a coexisting manner (Varela Soares et al., 2023). Currently, Ireland lacks a comprehensive regulatory framework that specifically outlines the guidelines and regulations governing the storage of electricity (Varela Soares et al., 2023).

Poland has recently taken significant steps to promote the growth of batteries by implementing specific measures. One notable measure includes a substantial 50% reduction in grid connection fees for battery systems. Additionally, battery systems are now eligible to participate in renewable energy support programs, which opens up further avenues for their development. The amendment to the policy framework not only clarified the legal status of pumped hydro storage but also introduced effective mechanisms for regulating other energy storage technologies (IEA, 2022).

### **3.2. Drivers and barriers in energy storage policies**

Prior to identifying the factors that should be considered in the development of a successful energy storage policy, it is essential to investigate the barriers that currently exist in the energy storage industry. By accurately identifying any challenges, more effective policy incentives for the deployment of energy storage could be developed. According to Sani et al. (2020), before designing and adapting energy storage policies, national economies should identify all the benefits and functions of energy storage systems and determine the impact will they create to the entire power grid. The main objective of energy storage policy should be the ability to mitigate and remove existing barriers in the market (Sani et al., 2020). The existing barriers are detrimental to the sustainable development of the energy system in the long term, as they



create unnecessary bureaucratic burden which result in significant delays in development, inadequate price signals for the system, inefficient cost allocations, and compensations (Castagneto Gisse et al., 2018). For each group of identified energy storage policy barriers, a study by Castagneto Gisse et al. (2018) suggest measures that should be taken to unlock the potential of energy storage technologies in the future (Castagneto Gisse et al., 2018). This study examines the existing barriers and drivers of energy storage policy, which are summarized in Table 2.

Table 2: Summary of barriers and drivers in energy storage policy

Barriers	Drivers
Lack of concrete definition for energy storage	Transparency and predictability of revenues from energy storage
Insufficient conceptualization of energy storage in energy markets	Creation of new distinctive asset class for energy storage
Lack of a harmonised set of legal frameworks	Establishment of new markets for energy storage
Double grid charges	Implementation of subsidies and financial incentives
Inadequate compensation of storage technologies	Introducing investment tax credits for energy storage technologies
Unclear ownership rules	Support research and development (R&D) activities in energy storage
High capital costs of storage technologies	Legal certainty

A study conducted by Gisse et al. (2018) examines the primary barriers within the regulatory framework that hinder the implementation of energy storage innovations in the United Kingdom and the European Union in general. The research identifies four main categories of barriers within the energy storage policy of the European Union that impede the widespread adoption of energy storage technologies: (1) Inconsistency in market regulations for energy storage and its integration into the overall energy systems. (2) Energy storage being classified as an energy generation technology. (3) Insufficient ancillary service markets and ineffective balancing mechanisms. (4) Public perception and judgment of energy storage technologies. The common thread running through these barriers is the absence of direct support and clear incentives for strategic investments from regulatory bodies (Castagneto Gisse et al., 2018). In the absence of standardized regulation for energy storage within the European Union, energy storage technologies may face challenges in competing with power generation technologies, as well as other balancing and ancillary technologies, in terms of profitability. Due to the lack of established regulations, energy storage technologies are often categorized as energy generation technologies. Consequently, grid access charges for stored energy can be subject to double charges or uncertain fees (Parra & Mauger, 2022). Transmission and distribution network tariffs reflect double charges for energy storage systems, which are charged twice for energy storage (Castagneto Gisse et al., 2018). The lack of adequate understanding and acknowledgement of the advantages linked to energy storage plays a role in public scepticism and acts as a barrier to the swift adoption of flexibility measures. The limited comprehension is further intensified by the lack of well-defined roles in the market and the insufficient identification of long-term energy system needs (Castagneto Gisse et al., 2018).

The insufficient conceptualization of energy storage in global energy markets is another significant barrier. Current energy systems do not adequately position and conceptualize energy storage, preventing it from attaining its full potential and contributing maximally to the smart grid (Zame et al., 2018). Prior to this point, energy storage has been regarded solely as a depository for energy shortages and peak demands. However, energy storage technologies provide numerous non-energy benefits that should be considered in the development of future sustainable energy networks (Zame et al., 2018). The existing regulations governing electricity markets are ineffective as they fail to recognize the full potential of energy storage technologies in both traditional electricity systems and deregulated markets. The current tariff-based regulations imposed on energy storage systems limit their ability to generate income from auxiliary services in energy generation, transmission, and distribution. As a result, the integration of energy storage systems is hindered, slowing down the progress in this field (Zame et al., 2018). Ensuring fair treatment of energy storage technologies in electricity markets could expedite their widespread adoption (Tabari & Shaffer, 2020). According to a study conducted by Zame et al. (2018), the primary challenge in current energy storage policy is the absence of a well-defined pricing model and regulation for applied rates. This issue arises due to the multifunctionality of energy storage, which not only contributes to the power generation process of the energy system value chain but also provides benefits to transmission and distribution. Consequently, determining how the cost of energy storage should be allocated among these various grid components remains ambiguous (Zame et al., 2018).

Therefore, regulators should create distinctive asset class for energy storage for it to be viable in future smart energy grids (Zame et al., 2018). The new asset class definition for energy storage should take into account that energy storage can be applicable for ancillary services to optimize grid operations. This is also suggested by Zame et al. (2018) who argues that a separate asset category should be established for energy storage, and that appropriate policies and regulations should be implemented to encourage the use of energy storage systems (Zame et al., 2018). Energy storage systems are considered expensive when deployed as a one-dimensional technology with the sole objective of storing and using energy for load balancing and peak shaving, particularly when compared to fossil fuel-based power generation technologies. A study by Zame et al. (2018) suggests that current electricity and utility markets should be deregulated to expand creation of new markets that support energy storage with all its multifunctionalities. In turn, there should be support for stronger regulation and a market model in which energy storage would play a more inclusive role. New market structures would allow different energy storage owners, including third parties, to access the market independently, thus diversifying the existing energy market (Zame et al., 2018). At the moment there exist several constraints for energy storage to be connected to the grid such as waiting in the queue after generation technologies (Castagneto Gisse et al., 2018).

Distribution system operators could inform other grid customers of the benefits that could result from quicker energy storage connection to the grid such as avoiding reinforcement measures and reducing costs for end users. Energy storage would allow to balance the peak loads and avoid shortages in the power supply (Castagneto Gisse et al., 2018). However, if energy storage technologies are not incentivized, distribution system operators lack motivation to promote storage because it may reduce their own profitability (Castagneto Gisse et al., 2018).

Energy storage technologies cannot generate new energy themselves and rely on generators to generate revenue (Castagneto Gisse et al., 2018). For this reason, energy storage technologies have historically been classified as generation technologies. A study by Castagneto Gisse (2018) argues that a new definition for energy storage technologies should be introduced to remove existing barriers to energy storage deployment. Currently, the classification and treatment of electricity storage in the power system differs significantly from gas storage in the natural gas market (Castagneto Gisse et al., 2018). New markets should be created that reward energy storage technologies for the multiple benefits they provide to the general energy system, e.g., energy efficiency, avoided usage of fossil fuels, emissions savings, more sufficient utilization of generation and network assets, support for balancing renewable energy generation, rapid response time for backup power generation. Regulatory should acknowledge these non-energy benefits to create an enabling environment for energy storage technology exploitation (Castagneto Gisse et al., 2018). Due to high capital costs and unfavorable market conditions for generating returns, the installation of energy storage technologies is often not economically viable. As a result of high payback periods, investor confidence in energy storage systems is declining. Therefore, governments could introduce subsidies that reward the use of energy storage, as has been done to promote low-carbon power generation technologies such as PV panels and wind turbines. Experience with solar and wind power systems shows that financial incentives drive market growth, which in turn helps bring down the capital costs of new technologies such as energy storage more quickly (Castagneto Gisse et al., 2018).

Investment tax credits are one of the policy mechanisms that could be used to encourage investment in energy storage development projects (Zame et al., 2018). According to Zame et al. (2018), investment tax credits are one of the most effective ways to reduce the capital cost of energy storage technologies, mitigating the technology and investment risk of an emerging technology. Tax incentives for investment will help spur market demand for the technology and make energy storage technologies more competitive with other conventional energy system technologies (Zame et al., 2018). The study by Wesseh et al. (2022) suggests that climate policies solely cannot ensure that energy storage technology will be deployed as quickly as renewable generation technologies, so additional mechanisms in the form of tax incentives should be created (Wesseh et al., 2022).

Research and development (R&D) activities are a particularly important driver of energy storage system deployment because R&D creates knowledge, experience, and operational understanding needed to integrate new technologies into the system (Zame et al., 2018). More importantly, R&D activities help reduce the cost of technologies. Energy storage systems are emerging technologies, and numerous technology prototypes, demonstration and pilot projects are in the early stages of commercialization, so the cost of energy storage technologies is expected to decline (Zame et al., 2018). Supporting research and development in energy storage technologies would promote more rapid scaling up of pilot projects and continuously improve the benefits that energy storage systems provide to power grids (Zame et al., 2018).

#### **4. CONCLUSION**

This study provides a comprehensive overview of the installed capacities of energy storage facilities and examines the energy storage policies that have been implemented in different European countries. The data show that some countries are leading in the deployment of energy storage, while in other countries only a limited number of energy storage facilities are installed. The cumulative installed capacities of electrical storage facilities in European Union member states total 81,313 MW where Spain, Germany, and Italy have the highest capacities. In the European Union, mechanical storage facilities are the predominant form of energy storage in relation to installed power capacity, with electrochemical energy storage ranking second in prevalence. The predominant sources of installed capacities for mechanical energy storage facilities are pumped hydro storage (PHS), compressed-air energy storage (CAES), and flywheel technology. The majority of electrochemical energy storage facilities primarily employ lithium-ion technology, with other technologies such as sodium-sulfur (NaS), sodium-nickel chloride (NaNiCl), lead-acid electrochemical storages, electrochemical capacitors, and various other technologies also being utilised. The data on the status of installations showed that in recent years there has been an increase in the deployment of energy storage, which was reflected in a high number of projects announced and under construction. The availability of data on energy storage across European countries is currently extremely limited, posing a significant obstacle to research and development in this field. Therefore, regulatory bodies at both the national and international levels should take proactive measures to address this issue. One crucial step is the establishment of comprehensive data sets, such as within Eurostat, which would facilitate the collection of detailed information on installed energy storage capacities throughout Europe. Installed capacities should be recorded on an annual basis so that the dynamics of development can be studied.

A comprehensive comparative analysis has been undertaken, drawing upon the most recent scholarly literature on energy storage policies and the IEA energy policies database, in order to investigate the diverse policy instruments that have been implemented in eighteen European countries. There exist a variety of policy measures aimed at providing incentives for the adoption and utilisation of energy storage technologies. The analysis has identified six primary categories of measures that are employed in European countries. These measures include the establishment of a robust regulatory framework, the implementation of tax relief, the provision of financial incentives through grants and subsidies, the development of a

comprehensive and structured strategy for the deployment of energy storage, the allocation of sufficient funding for implementers, and the introduction of incentives to promote domestic manufacturing of energy storage technologies. The comparative analysis shows that subsidies and grants are the most commonly used policy instrument to incentivise the deployment of energy storage. In some countries, there is a lack of a comprehensive and robust strategy and regulatory framework, which significantly hinders the development of energy storage technology. In most countries, energy storage policies are still a relatively novel concept, and the first steps towards establishing a comprehensive energy storage policy have been taken by establishing a common definition for these technologies. In the coming years, it is anticipated that European countries will increase their efforts to develop policies for energy storage.

An investigation into the barriers and drivers in energy storage policy reveals that several factors hinder the rapid deployment of energy storage. These barriers include the lack of a clear and concrete definition for energy storage, insufficient conceptualization of energy storage within energy markets, the absence of a harmonized set of legal frameworks, double grid charges, inadequate compensation of storage technologies, unclear ownership rules, and high capital costs associated with storage technologies. To overcome these barriers and drive long-term development, various instruments can be employed. Firstly, ensuring transparency and predictability of revenues from energy storage is crucial. Additionally, establishing a new distinctive asset class specifically for energy storage can facilitate its integration into existing energy markets. Creating dedicated markets for energy storage and implementing subsidies and financial incentives can further incentivize its adoption. Furthermore, introducing investment tax credits for energy storage technologies can make them more economically viable. Supporting research and development (R&D) activities in energy storage is also essential for driving innovation and technological advancements in the field. Lastly, providing legal certainty and a stable regulatory environment can contribute to overcoming barriers and fostering a conducive landscape for energy storage deployment.

## 5. ACKNOWLEDGEMENT

This work has been supported by the European Social Fund within the Project No 8.2.2.0/20/I/008 «Strengthening of PhD students and academic personnel of Riga Technical University and BA School of Business and Finance in the strategic fields of specialization» of the Specific Objective 8.2.2 «To Strengthen Academic Staff of Higher Education Institutions in Strategic Specialization Areas» of the Operational Programme «Growth and Employment».

## 6. REFERENCES

- Castagneto Gisse, G., Dodds, P. E., & Radcliffe, J. (2018). Market and regulatory barriers to electrical energy storage innovation. *Renewable and Sustainable Energy Reviews*, 82, 781–790. <https://doi.org/10.1016/j.rser.2017.09.079>
- Directorate-General For Energy. (2022). *Database of the European energy storage technologies and facilities* [Data set]. Publications Office. <https://doi.org/10.2906/1011101101114/1>
- Directorate-General for Energy, Guidehouse., & Toegepast natuurwetenschappelijk onderzoek. (2023). *Staff working document on the energy storage—Underpinning a decarbonised and secure EU energy system*. [https://energy.ec.europa.eu/system/files/2023-03/SWD\\_2023\\_57\\_1\\_EN\\_document\\_travail\\_service\\_part1\\_v6.pdf](https://energy.ec.europa.eu/system/files/2023-03/SWD_2023_57_1_EN_document_travail_service_part1_v6.pdf)
- EASE. (2022). *Energy Storage Targets 2030 and 2050. Ensuring Europe's Energy Security in a Renewable Energy System*. <https://ease-storage.eu/wp-content/uploads/2022/06/Energy-Storage-Targets-2030-and-2050-Short-Summary.pdf>
- European Commission. (2023). *Commission Recommendation of 14 March 2023 on Energy Storage – Underpinning a decarbonised and secure EU energy system 2023/C 103/01*. <https://eur-lex.europa.eu/legal-content/EN/TXT/?uri=CELEX%3A32023H0320%2801%29&qid=1679302898964>
- Eurostat. (n.d.). *Share of renewable energy in gross final energy consumption by sector (NRG\_IND\_REN)*. Retrieved April 28, 2023, from [https://ec.europa.eu/eurostat/databrowser/view/SDG\\_07\\_40/default/table?lang=en](https://ec.europa.eu/eurostat/databrowser/view/SDG_07_40/default/table?lang=en)
- IEA. (n.d.). *Policy database*. <https://www.iea.org/policies>
- IEA. (2022). *Poland Electricity Security Policy*. <https://www.iea.org/articles/poland-electricity-security-policy>
- IEA. (2023a). *EUR 7.8 million in subsidies for renewable energy storage*. <https://www.iea.org/policies/17154-eur-78-million-in-subsidies-for-renewable-energy-storage>
- IEA. (2023b). *Investment support for utility-scale battery storage*. <https://www.iea.org/policies/17160-investment-support-for-utility-scale-battery-storage>
- IEA. (2023c). *Subsidies for battery and PV panel production and electricity storage*. <https://www.iea.org/policies/17404-subsidies-for-battery-and-pv-panel-production-and-electricity-storage>
- Parra, D., & Mauger, R. (2022). A new dawn for energy storage: An interdisciplinary legal and techno-economic analysis of the new EU legal framework. *Energy Policy*, 171, 113262. <https://doi.org/10.1016/j.enpol.2022.113262>

Sani, S. B., Celvakumaran, P., Ramachandaramurthy, V. K., Walker, S., Alrazi, B., Ying, Y. J., Dahlan, N. Y., & Rahman, M. H. A. (2020). Energy storage system policies: Way forward and opportunities for emerging economies. *Journal of Energy Storage*, 32, 101902. <https://doi.org/10.1016/j.est.2020.101902>

Tabari, M., & Shaffer, B. (2020). Paying for performance: The role of policy in energy storage deployment. *Energy Economics*, 92, 104949. <https://doi.org/10.1016/j.eneco.2020.104949>

Varela Soares, I., Mauger, R., & Santos, T. (2023). Considerations for benefit stacking policies in the EU electricity storage market. *Energy Policy*, 172, 113333. <https://doi.org/10.1016/j.enpol.2022.113333>

Wesseh, P. K., Benjamin, N. I., & Lin, B. (2022). The coordination of pumped hydro storage, electric vehicles, and climate policy in imperfect electricity markets: Insights from China. *Renewable and Sustainable Energy Reviews*, 160, 112275. <https://doi.org/10.1016/j.rser.2022.112275>

Zame, K. K., Brehm, C. A., Nitica, A. T., Richard, C. L., & Schweitzer Iii, G. D. (2018). Smart grid and energy storage: Policy recommendations. *Renewable and Sustainable Energy Reviews*, 82, 1646–1654. <https://doi.org/10.1016/j.rser.2017.07.011>

---

## #271: Maximizing solar power harvest: experimental analysis of vacuum insulated photovoltaic/thermal (PVT) power module in subtropical climates

---

OYIEKE, Andrew A Y.

Mangosuthu University of Technology, 511 Griffiths Mxenge Highway, Umlazi, KwaZulu-Natal, 4031, affiliation address, oyieke.andrew@mut.ac.za

*Abstract: The utilization of solar energy as a clean and sustainable source of power has gained significant attention in recent years. Photovoltaic/thermal (PVT) systems have emerged as a promising technology, integrating both electrical energy generation and thermal energy collection in a single device. This paper presents an experimental analysis of a solar vacuum insulated photovoltaic/thermal (VPVT) power module in a subtropical climate. This study seeks to assess the performance and energy efficiency of the VPVT system under realistic operating conditions and to evaluate its potential for solar energy harvesting in subtropical regions. The study included the measurement and analysis of various parameters such as solar radiation, electrical power output, thermal energy output, and overall system efficiency. Additionally, the impact of various factors, including ambient temperature, wind speed, and humidity, is considered in the analysis. The results indicate that the solar VPVT module exhibits favourable performance characteristics in subtropical climates. The electrical energy generation efficiency of the module remains high, even under high ambient temperatures. Moreover, the thermal energy collection efficiency is enhanced through the vacuum insulation, allowing for effective utilization of solar energy. The outcomes show that the solar VPVT panel operates well in subtropical temperatures, with a 16.01% gain in thermal efficiency and a 0.28% reduction in electrical effectiveness even after the PV cell coating was eliminated. As a result, overall efficiency improved by 9.16%. Total exergy and primary energy reduction efficiency improved by 2.74% and 4.25%, correspondingly. Furthermore, the study investigated the impact of various factors, such as ambient temperature, solar irradiance, and flow rate of the heat transfer fluid, on the performance of the VPVT module. It was observed that higher solar irradiance levels and lower ambient temperatures positively influenced the electrical and thermal efficiencies of the system. The findings from this experimental analysis provide valuable insights into the feasibility and effectiveness of utilizing solar vacuum insulated VPVT modules in subtropical climates and further assists engineers, researchers, and policymakers in making informed decisions regarding the deployment and integration of solar VPVT systems in subtropical regions. The results demonstrate the potential of this technology for renewable energy generation, especially in regions with abundant solar resources and a demand for both electricity and thermal energy.*

*Keywords: Solar energy, Photovoltaic/thermal (PVT) system, Vacuum insulation, Subtropical climate.*

## 1. INTRODUCTION

Given the vast untapped potential of renewable energy resources worldwide, solar energy harnessing systems face challenges in achieving their theoretical optimum due to the dispersed and irregular nature of the sun. The aim is to move towards greater effectiveness in power production and conversion methods while ensuring affordability and accessibility. Photovoltaic/thermal (PV/T) hybrid systems are now recognized as economically viable option and effective technologies for simultaneously converting solar energy into electrical and thermal energy within a single unit. These systems maximize energy output per unit area compared to separate thermal and PV modules (Agrawal and Tiwari, 2011). However, The attainment of optimal energy generation and thermal collection efficiency poses a notable challenge when it comes to using photovoltaic/thermal (PVT) systems in subtropical regions. Although PVT systems offer the advantageous capability of concurrently producing electrical and thermal energy, their thermal efficiency often falls short compared to individual solar thermal collectors due to the current emphasis placed primarily on electrical energy generation, consequently, reducing their competitiveness and application. Moreover, technical limitations, financial constraints, and commercial barriers obstruct solar energy from realizing its complete potential due to its decentralized and unpredictable characteristics in such regions. Accordingly, there arises a pressing need to address these hurdles effectively and cultivate improved solutions that perform competently and competitively amidst subtropical temperatures. One such technology is the vacuum insulated photovoltaic thermal (VIPVT) modules. Given that silicon PV cells have inherent limitations in electrical efficiency, typically between 15% and 20%, efforts to enhance overall PV/T system efficiency should prioritize thermal output. Recent studies have shown promising gains in overall system efficiency through performance evaluations of various PV/T configurations, geometric optimizations, and analysis of operational parameters. Experimental, simulation, and modelling analyses have utilized numerous procedures and software tools, leading to valuable outcomes (Aste et al., 2020; Diwania et al 2020; Jia et al 2019; Noxpanco et al 2020). Proposed thermal models, analytical expressions, design configurations, and simulation results have contributed to the advancement of hybrid PV/T technology. Validating simulated results through comparison with experimental data has provided insights into the accuracy of these models (Zhou et al 2020a; Zhou et al 2020b). In this study, the focus is on investigating vacuum insulation as a technique of enhancing thermal efficiency in a flat-plate hybrid PV/T mechanism with little effect on electrical efficiency.

The output of solar structures changes with the climatic settings of a specific locality. To examine the real operational behaviour of the hybrid VIPVT flat-plate collector system, it was essential to conduct experiments and acquire actual, dependable and realistic data with reference to the conventional hybrid PV/T. This encompassed measuring the current and voltage outputs, inflow and outflow water temperatures of the modules, as well as the average and nodal temperature circulation in the storage tank at identified consistent periods throughout the sunshine hours. The thermal and electrical efficiencies for both collectors and the electrical power was also determined and compared.

## 2. EXPERIMENTAL SETUP

The experiment made use of the tools and equipment whose characteristics are stated in Table 1. They included water tank, battery, charge-controller, circulation pump, data logger, thermocouples, and multimeter. In order to ensure that the outlets of the VIPVT collector and the traditional PVT collector discharging to the tank independently of one another, these collectors were installed adjacent to each other and linked in parallel. The entire assembly was exposed to the identical meteorological input parameters, including sun irradiance, wind speed, and air temperature that were measured and logged on location. To enable mobility and simple positional modification, the assembled combination of parts were mounted onto a portable support frame. The inclination angle was set at its maximum level of 35°. To minimize heat loss to the environment, the hot water side lagged 22 mm copper tubing and related fittings were used for the plumbing work. For simplicity of water flow and structural solidity, the water storage tank was positioned horizontally.

Solar insolation was measured using a thermopile SPN1 pyranometer with a sensitivity factor of 0.1, while wind velocity and air temperature were measured with R M Young and Campbell scientific CS215 sensors, both with 0.1 precision. The average temperature of the PV cells was measured using 5 surface-mounted Type-E thermocouple sensors distributed evenly over the panel, with observations logged and averaged concurrently. The water temperatures at the modules' inlets and outlets were measured using type-K thermocouples and recorded in the DataTaker DT80 linked to a computer. The charge-controller was attached to the electrical ports, enabling each panel's currents and voltages to be monitored and documented individually. The controllable valve lead-acid deep cycle battery was mounted and configured with a charge-controller that uses an algorithm for charging and tracking the battery's state of power. In order to convert DC to AC, a 300W inverter was attached to the battery.

Table 1: Experimental equipment characteristics and technical specifications

Equipment	Parameter	Sensitivity factor and accuracy
Thermopile SPN1 pyranometer	Irradiance (W/m <sup>2</sup> )	0.1 (0 to > 2000Wm <sup>-2</sup> )
	Accuracy	±5% ±10W/m <sup>2</sup> Hourly averages, Daily integrals, and individual readings of total radiation
R. M. Young Sensor	Wind speeds (m/s)	0.75
	Range:	0-100 m/s
	Accuracy:	± 0.3 m/s (0.6 mph) or 1% of reading , Wind direction: ± 3°
CS215 Sensor	Relative Humidity (%)	±2% (10% - 90%) at 25°C; ±4% (0% - 100%) at 25°C
ICS215 Sensor	Air Temperatures (°C)	±0.3°C (at 25°C); ±0.4°C (5° to 40°C); ±0.9°C (-40° to +70°C)

Component	Property	Value
Solar battery	Nominal voltage and capacity	Regulated valve sealed, 12V, 100Ah (20°C)
Solar circulation pump	Rated voltage ( $V_m$ ), total capacity, head, Power consumption and Max. flow rate	12V DC, 0.65A, 4 l/m, 8W, rated head 13m, max flow rate 10kg.f/cm <sup>2</sup>
Charge controller	Rated voltage and Maximum rated current	12,24,48V dc, 45A continuous
DataTaker DT80	System voltage, Analogue channels and Digital channels	10-30Vdc, 10 (analogue) and 8 (digital)
	Accuracy	±0.15 % (5oC to 40oC); ±0.35 % (-45°C to 70°C)

Table 2: The VIPV/T and VPT module characteristics.

Collector Property	VIP/T	PV/T
Collector area	1.42 m <sup>2</sup>	1.42 m <sup>2</sup>
Absorber type	Sheet and tube	Sheet and tube
Number of tubes	14	14
PV module power	180 W	180 W
PV cell type	Mono-crystalline	Mono-crystalline
No. of cells	72	72
PV cell encapsulation	Non-encapsulated	Encapsulated (0.002 m glass)
Packing factor	1.0	1.0
Top insulation medium	Vacuum	Air
Bottom insulation material	Fibre wool	Fibre wool
Insulation thickness	0.05 m	0.05 m
Glass cover	0.004 m low iron tempered	0.004 m low iron tempered

The data were configured to be recorded at 15-minute recurrent periods to obtain a substantial change in temperatures, a time-step big enough for solar energy to generate a significant difference in temperatures. Voltages and currents were minor at this period since they changed in milliseconds, but they were documented at the same periods as temperatures to determine efficiency. Measurements of currents, voltages, and temperatures were taken at pre-set, regular intervals during the day enabled the computation of electrical power generation, thermal output, and the correlation of the impact of vacuum insulation. The experimental setup is depicted schematically in Figure 1.

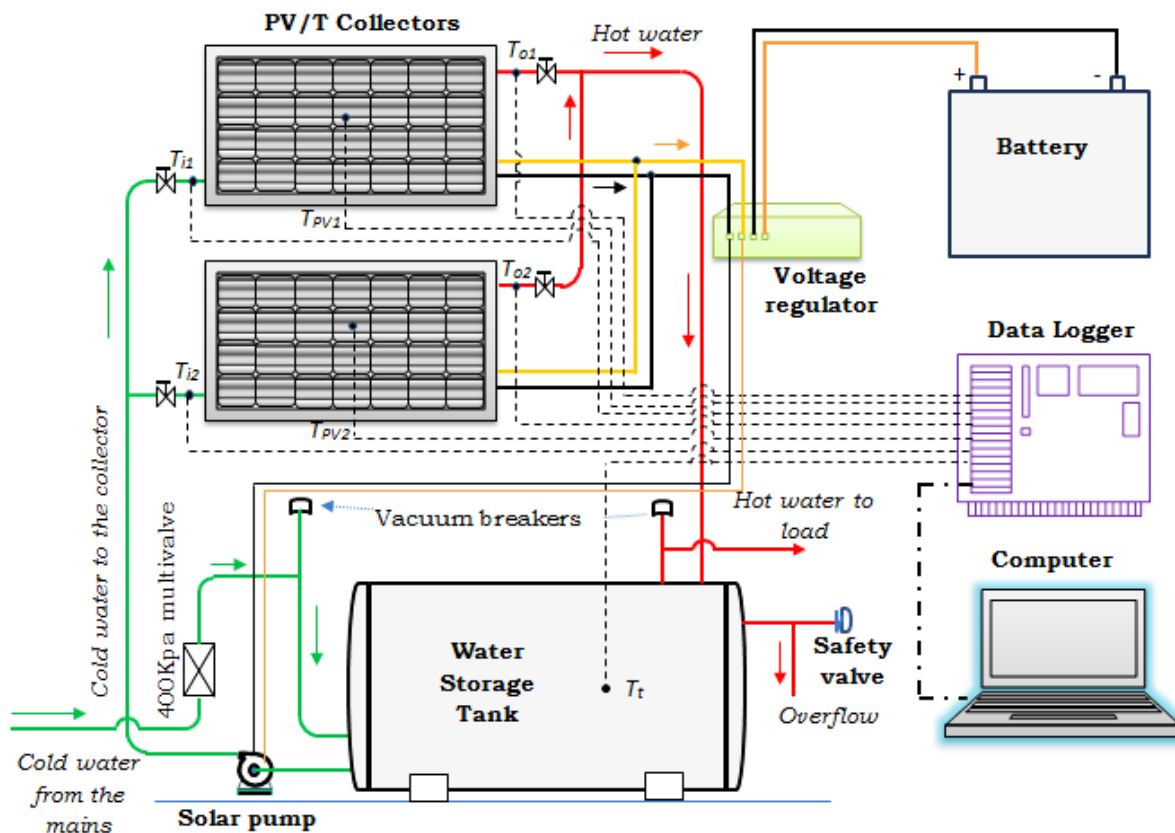


Figure 1 Schematic diagram of the experimental set up

## 2.1. Theoretical analysis

According to Oyieke and Inambao (2016), the experimental primary data were manipulated and theoretically analysed to give the secondary performance parameters. Subsequently, the proportion of the useable heat gained by the collector  $Q_u$  to the projected cumulative sun's radiation  $G$  gives the thermal efficiency  $\eta_{th}$  of a flat-plate collector as follows.

$$\eta_{th} = \frac{Q_u}{G} \quad (1)$$

The useful heat  $Q_u$  is the actual output defined as product of mass flow rate  $\dot{m}$  and specific heat capacity  $C_p$  of the cool-off fluid and the temperature change of the fluid at outlet  $T_o$  and inlet  $T_i$  given as;

$$Q_u = \dot{m}c_p(T_o - T_i) \quad (2)$$

Electrical efficiency  $\eta_{el}$  of the PV panel is mostly determined by incoming radiation from the sun and the photovoltaic (PV) module temperature  $T_{pv}$ . It is described as the ratio of maximal electrical power production to incident radiation and is inversely correlated to temperature, which means that it decreases as temperature rises. In this scenario, an equation from (Sadness and Rakstad, 2002) is adopted in this case to show the influence of temperature on PV efficiency, which is given as

$$\eta_{el} = \frac{I_m V_m}{G A_a} + \mu (T_o - T_i) \quad (3)$$

where  $I_m$  and  $V_m$  are the current and voltage of PV module at maximum power-point,  $T_{ref}$  is reference temperature taken as 25°C,  $A$  is area of the cell ( $m^2$ ), and  $\mu$  is the temperature coefficient of PV efficiency at reference conditions, while  $T_{pv}$  has been established by Dubey and Tiwari, (2009) in an equation commonly valid for typical pc-Si PV modules in terms of ambient temperature  $T_a$  as

$$T_{pv} = 30 + 0.0175(G - 30) + 1.14(T_a - 25) \quad (4)$$

According to Choi et al., (2020) and Erslan et al., (2020), the universally established expression for the total efficiency  $\eta_o$  of a PV/T panel is thus the summation of the electrical and thermal efficiencies given as

$$\eta_o = \eta_{th} + \eta_{el} \quad (5)$$

Additionally, the total energy efficiency, solar percentage, and primary energy-saving efficiencies are used to describe the VIPV/T collector effectiveness. By employing the Carnot-cycle theory to transform low quality heat energy into similar high quality electrical energy, the total energy efficiency considers the differences in thermal and electric energy qualities. Thus, according to Gholampour and Ameri (2016), the total exergy efficiency is defined as the sum of the electrical and thermal efficiencies.

$$\xi_o = \eta_c \eta_{th} + \eta_{el} \quad (6)$$

where  $\eta_c$  is the ultimate Carnot efficiency according to Adeli et al., (2012) and is given by

$$\eta_c = 1 - \frac{T_a}{T_o} \quad (7)$$

The solar fraction, or simply the entire energy demand met by solar energy, is the ratio of primary energy savings that a PV/T system may achieve to the overall energy requirement.

$$f = \frac{1}{2} \left( \frac{Q_{L,t} - Q_{Aux,t}}{Q_{L,t}} + \frac{Q_{L,e} - Q_{L,e}}{Q_{L,e}} \right) \quad (8)$$

where  $Q_{L,t}$  and  $Q_{Aux,t}$  represent the total thermal load and auxiliary heat required; and  $Q_{L,e}$  and  $Q_{Aux,e}$  represent the full electrical load and auxiliary electricity required. Li et al., (2019) presented the notion of primary energy saving efficiency as a metric that incorporates the thermo-electric energy quality proportions stated as

$$\eta_s = \frac{\eta_{el}}{\eta_{th} + \eta_{pgen}} \quad (9)$$

where  $\eta_{pgen}$  is the electrical power production efficiency for a typical power plant, usually taken to be 0.38.



### 3. EXPERIMENTAL RESULTS AND DISCUSSION

Multiple quantities of data were gathered throughout the experimental duration through measurements of weather-related variables, temperatures, voltages, and currents. These data were analysed and utilized for comparing the VIPV/T's performance attributes to those of the PV/T. A selection of the measurements acquired from the VPV/T are shown in Table 1. The next section analyses and discusses the findings.

Table 3: Selected experimental measurements and results

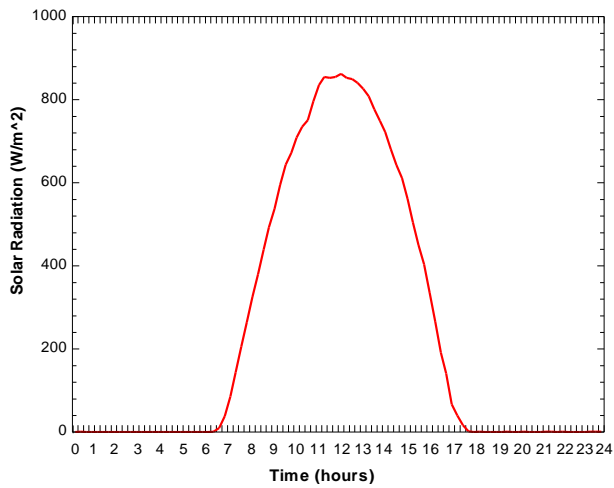
Time	Solar Radiation (W/m <sup>2</sup> )	Inlet Temp (°C)	Outlet Temp (°C)	Tank Temp (°C)	Voltage (V)	Current (A)	POWER (KW)	Wind speed V (m/s)	Ambient Temp Ta (°C)
07:30	62,3	20,03	20,92	20,68	12,58	1,67	21,00	1,055	18,47
08:00	130,04	21,69	21,32	20,99	17,64	2,35	41,37	1,313	19,02
08:30	311,3	20,83	25,41	22,45	24,29	3,23	78,44	1,15	19,48
09:00	501	20,83	26,55	23,68	31,53	4,19	132,22	1,087	21,46
09:30	590,2	20,83	27,97	23,92	33,96	4,52	153,35	0,848	23,00
10:00	655	20,83	30,51	25,08	33,25	4,42	147,05	1,763	22,35
10:30	702,6	20,89	34,87	26,08	34,54	4,59	158,69	1,288	23,19
11:00	757,5	20,83	44,93	32,10	36,28	4,82	175,03	1,638	23,21
11:30	814,3	21,67	52,99	42,09	34,97	4,65	162,69	1,368	22,93
12:00	830,4	21,42	55,97	48,66	35,33	4,69	166,05	2,463	22,97
12:30	811,6	22,35	54,82	54,69	34,21	4,55	155,69	1,061	23,46
13:00	776,2	23,27	53,37	56,29	33,64	4,47	150,53	2,163	22,88
13:30	727	23,29	52,75	56,08	33,59	4,47	150,13	2,063	22,79
14:00	676,5	24,17	49,03	56,96	33,89	4,51	152,75	2,513	22,40
14:30	566,5	23,96	44,47	55,99	33,63	4,47	150,41	4,662	22,20
15:00	540,6	22,08	35,49	55,77	32,32	4,29	138,91	3,875	21,70
15:30	417,4	21,53	29,50	55,12	29,12	3,87	112,79	4,587	21,32
16:00	262,2	21,91	25,62	52,36	18,39	2,45	45,02	2,987	20,95
16:30	153,85	20,40	24,14	50,63	15,81	2,10	33,26	2,338	20,94
17:00	33,59	20,61	23,11	49,06	12,38	1,65	20,37	2,238	20,61

#### 3.1. The weather parameters

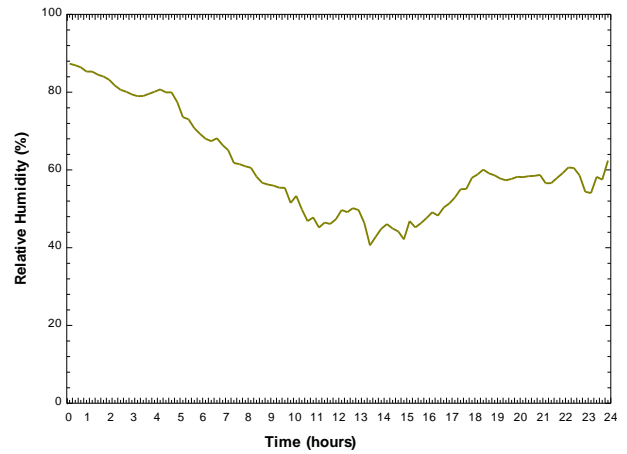
The amount of solar energy captured and put to use in a certain region depends on its climatic features. The major energy source used in this investigation and the most significant parameter was solar radiation. However, factors like relative humidity, wind speed, and ambient air temperature have an impact on its dissemination. The distributions of these variables were plotted to indicate the pattern of fluctuation throughout the test period at the Mangosuthu University of Technology weather station, which is a component of the South African Universities Radiation Network (SAURAN).

Figure 2(a) shows the fluctuation in solar radiation during the course of the experiment from which, it can be seen that the greatest value, 862.53 W/m<sup>2</sup>, was captured at midday. As seen in figure 2(b), the climate in Durban is rather humid. The greatest and lowest relative humidity variations for the day were 93.2% and 65.41%, respectively. The temperature of the surrounding air has a significant impact on the collector's ability to convert energy and thus, the hourly readings were plotted as displayed in Figure 2(c). The highest and lowest temperatures were 23.46°C and 17.78°C, respectively. Monitoring the variance in wind speeds is necessary to assess heat losses via the collector's top. The wind speed fluctuation curve presented in figure 2(d) shows that the mean speed was 2.17 m/s, falling within the permitted range set out in (Oyieke and Inambao, 2016), with the maximum and lowest values being 4.66 m/s and 0 m/s, respectively.

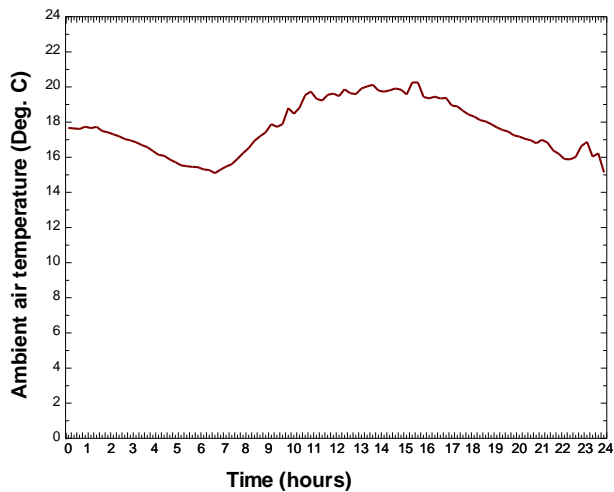
The fact that these values were observed and recorded throughout a 24-hour period every day should be emphasized. However, for the experimental analysis, only values that matched the solar exposure hours—most notably, from 7.30 am to 17.30 pm—were taken into account.



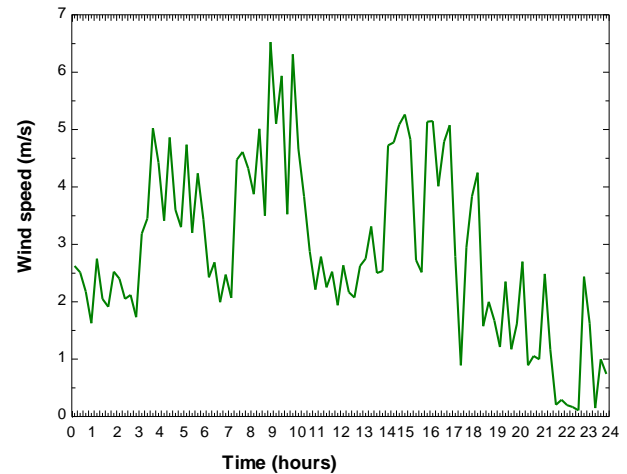
(a)



(b)



(c)



(d)

Figure 2 The variation of (a) solar radiation (b) relative humidity (c) ambient air temperatures (d) wind speeds during the test period 22nd August 2022

### 3.2. The daily thermal performance

A number of constants, measured variables, and computed variables were utilized to assess the thermal and electrical performance of the VIPV/T compared to PV/T. The various performance indicators were assessed using the numerical equations 1 through 9. In the next part, the thermal and electrical efficiency curves, useable heat energy, hot water temperature profiles, and other data for both modules were displayed and compared. The capacity of a solar collector to create water at high temperatures has a significant impact on its thermal characteristics. The increase in temperatures is caused by heat absorption, which, after accounting for all losses, results in usable heat ( $Q_u$ ). The module-generated variation of  $Q_u$  was assessed, and the resulting findings were displayed as seen in figure 3(a). With daily individual values of 5,376kJ/kg and 4,652.8kJ/kg, respectively, the VIPV/T produced 16.09% more usable heat energy than its PV/T counterpart.  $Q_u$  reached its greatest instantaneous levels of 208.87kJ/kg and 183.12kJ/kg during the day, respectively. These numbers, however, could change based on solar radiation.

In order to determine the change, the water temperatures were recorded at the modules' entrances and exits. The modules were supplied at the same temperature via a single inlet and discharged to the storage tank at various exits. Despite having the identical input temperatures, as seen in figure 3(b), the VIPV/T and PV/T reached their respective maximum temperatures of 57.97°C and 52.02°C around midday. The former produced an extra 12.8% increase in water temperature on average. The advantages of VIPV/T over PV/T may also be demonstrated in terms of heating rates. For example, a temperature of 45°C was reached for VIPV/T and PV/T at roughly 9.00 am and 9.45 am, respectively, indicating that the former required less time to heat up. Both the VIPV/T and PV/T released water at about the same temperature of 27°C at the conclusion of the measuring period.

The absorber plate's primary function is to take up any leftover heat that the PV cells have rejected. As a result, the temperatures of the plate increase, warming the water flowing through the tubes connecting beneath the plate. Because it controls how much water is heated, the plate temperature is a crucial factor in evaluating the heat transfer characteristics of the modules. Since it is frequently laborious to monitor the temperatures at each location on the plate, the study employed a mean value that was determined using equation 4. Figure 3(c) displays the variance of mean plate temperatures for both VIPV/T and PV/T. 181.75oC and 172.39oC, respectively, were the highest readings recorded. However, it was discovered that just 59.91°C and 56.02°C of water could be attained at these temperatures since only 8 mm of each tube's length made a direct connection with the absorber plate face.

The PV cells were exposed to identical average temperature as the plate itself because they were directly implanted on the upper exterior of the absorber plate. To prevent excessive stagnation temperatures that might harm the cells, these temperatures needed an extensive amount of controls. This made it necessary to take the cell encapsulation off. As shown, the storage tank was positioned horizontally at the base of the support structure. Although there may have been some stratification, the tank was regarded as totally-mixed for the duration of the investigation. Compared to the hot water inlet and outlet, the cold-water inlet and outlet were situated at a lower level. Water was originally pumped from the tank's full capacity to the collectors' inlets and then cycled back to the tank at heated temperatures. Hot water was released from both the VIPV/T and PV/T into a single tank intake. The average tank water temperature,  $T_t$ , was determined by measuring the temperature at the tank's centre. The temperature measurements were plotted as shown in figure 3(d), and it is clear from this that the water temperature rose steadily until reaching a high of 56.95oC at approximately 2:00 pm before gradually dropping as a result of a decline in the strength of the sun's radiation. By sundown, the tank was able to sustain water at adequate temperatures for domestic use at roughly 49°C because of its capacity to retain heat.

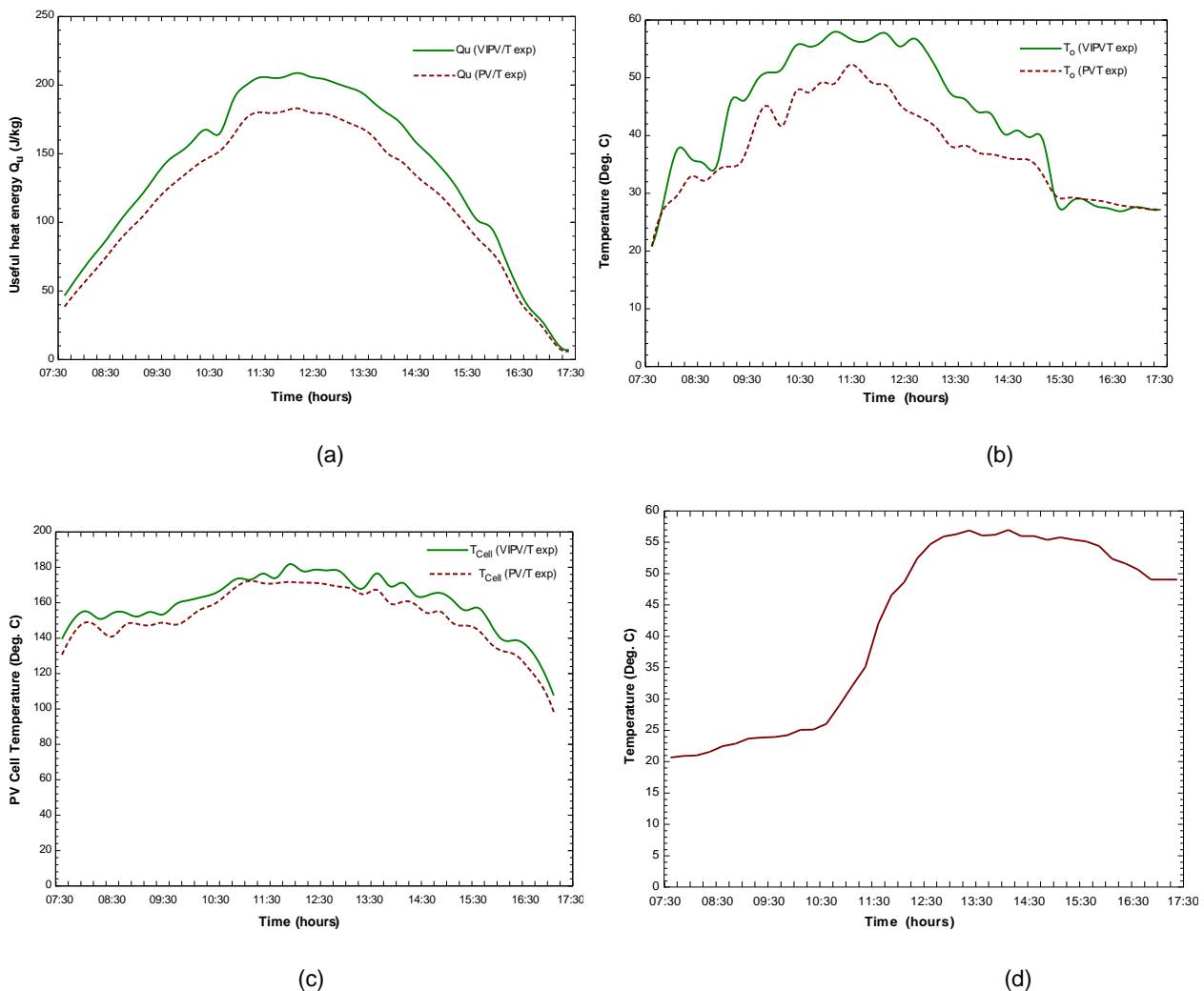


Figure 3 The hourly variation of (a) Useful heat (b) Outlet water temperature (c) Average PV cell temperatures (d) water storage tank temperatures for VIPV/T and PV/T

Figure 4(a) displays the plotted fluctuations in thermal, electrical, and total efficiency. In general, it was found that the VIPV/T provided better thermal performance than the PV/T. For VIPV/T and PV/T, the mean thermal efficiencies were 15.91% and 13.71%, respectively. This showed a 16.01% improvement in thermal efficiency. These results showed that the incorporation of the vacuum envelope had a favourable impact on the thermal characteristics. The vacuum envelope provided more thermal resistance to the radiative heat loss via the top side of the module, which is thought to be the cause of the difference in thermal efficiency. The thermal loss coefficient for the top ( $U_t$ ) indicated a considerable decrease in heat loss through the top as well. But it should be mentioned that the vacuum envelope shape and dimension was maintained throughout the investigation. Individual mean electrical efficiencies for the VIPV/T and PV/T both came in at 10.53 percent, a little improvement of 0.28%. The electrical efficiency curves were found to be flattened at midday, when radiation from the sun and the consequent rise in temperature were at their peak, and to be steepest in the early and late hours of the day. This illustrated how electrical efficiency is affected by temperature. The electrical efficiency was shown to increase above the mono-crystalline cells' maximum rated value during sunset after 17:00 hours. This occurred because there was no longer any solar energy, therefore the voltage regulator was pulling power from the batteries. Values tested after this point were getting close to 100%. For VIPV/T and PV/T, correspondingly, the total efficiencies as determined by equation 5 were estimated to be 26.44% and 24.25%, reflecting an increase of 9.16%.

Figure 4(b) displays a plot of the overall exergy, primary energy savings, and Carnot efficiencies. The variance of the Carnot efficiencies, which heavily dependent on the temperature differential between the surrounding air and the water flowing out of the modules, was estimated to be 2.74% higher than the average overall exergy efficiencies as specified by equation 6 and were found to be 11.33% and 11.59%, respectively. Subsequently, the average primary energy saving efficiencies for VIPV/T and PV/T modules, as determined by equation 9, were determined to be 20.48% and 19.63%, respectively. This indicated that a 4.25% improvement was attained. It was assumed that the traditional power generating efficiency was 0.38%. The adjustment was made as a consequence of improved thermal energy performance, which led to reductions in the supplemental energy needed for water heating during non-sunny hours. Since measuring the energy utilized for supplemental heating was not part of the experimental setup, the solar fraction as it is specified in equation 8 was not analysed. In addition, the experiment was only carried out in the daylight.

The energy efficiencies of the VIPV/T and PV/T modules were analysed and assessed using the Carnot efficiency, which is not one of the performance assessment markers. The average results were 6.53 percent and 5.6 percent, respectively.

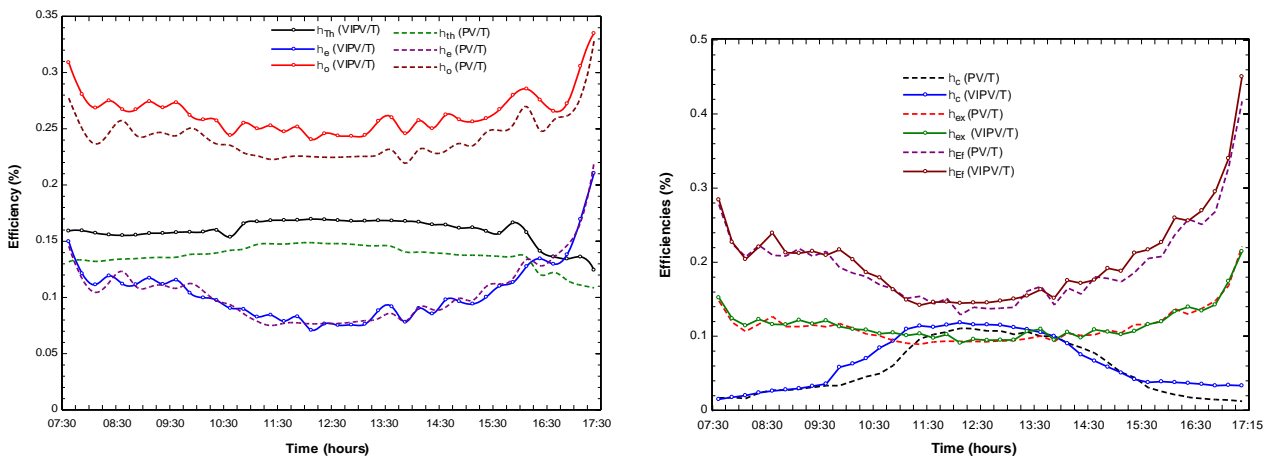


Figure 4 The variation of (a) thermal and electrical efficiencies (b) overall exergy, primary energy saving and Carnot efficiencies

Voltages, currents, and temperatures were monitored and recorded simultaneously in order to evaluate the electrical capacity of the modules. Each of the module's electrical power output was determined, and then its efficiencies were computed. Figure 5 displays the results of the electrical performance displayed. Figure 5(a) shows how voltage and current flows change over time, whereas Figure 5(b) shows the power created. For VIPV/T and PV/T, correspondingly, the highest voltages attained were 35.44V and 35.74V, whereas the highest possible current flows were 4.71A and 4.75A, respectively. This meant that the modules performed between 94% and 90% of their 36.16V and 4.98A rated capacities.

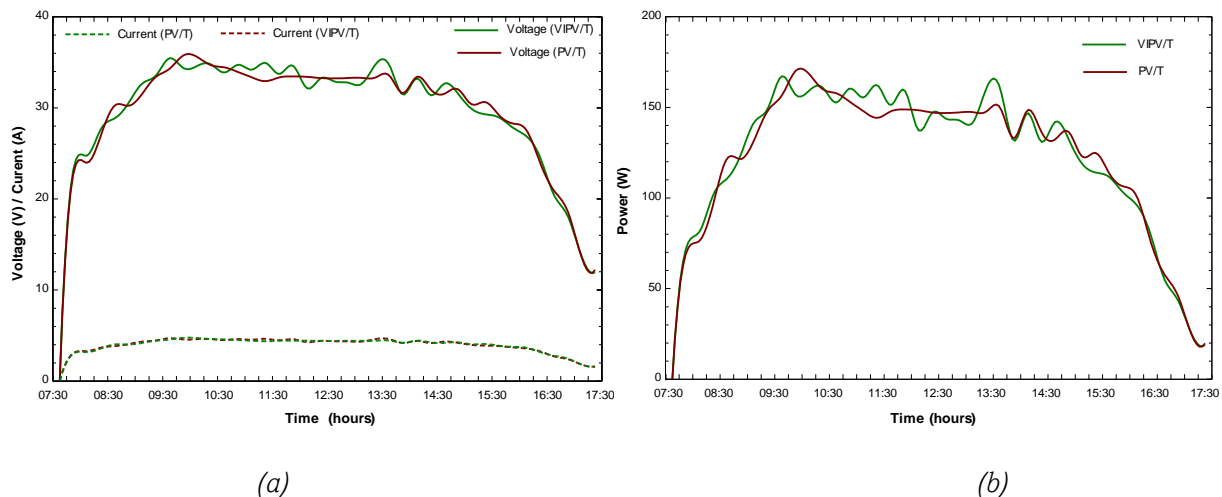


Figure 5 Electrical performance of the VIPV/T and PV/T modules (a) The variation of voltage and currents over time  
(b) The variation of electrical power generated

Although the modules' maximum power rating was 180W, the highest hourly power produced by VIPV/T and PV/T, respectively, was 167.10W and 169.92W. Within the 10-hour period, 4,851.90W and 4,835.66W, respectively, of total electricity were produced. 9,687.56W was realized for the two modules, which was enough to run the majority of home appliances. With the exception of the shift by a factor corresponding to the magnitude of the currents, the power curves were comparable to the voltage profile. It was noted that the amount of electrical power generated had barely changed.

#### 4. CONCLUSION

The vacuum insulation's impact on the PV/T's thermal and electrical characteristics was successfully studied experimentally. The measurements of temperatures, voltages, and currents needed in assessing power and heat fluxes were made possible by positioning the hybrid VIPV/T and PV/T modules next to one another and exposing them to the same climatic circumstances. It was proven that the VIPV/T outperformed the traditional PV/T in terms of performance. When the PV cell encapsulation was removed, it was determined that the vacuum inclusion improved thermal efficiency by roughly 16.01% while substantially maintaining electrical efficiency with a difference of 0.28%. As a result, efficiency increased overall by 9.16%. Additionally, by 2.74% and 4.25%, respectively, the total exergy and main energy saving efficiencies improved.

The findings of this study contribute to the understanding of the performance of solar vacuum insulated PVT modules in subtropical climates and provide valuable insights for the design and optimization of such systems. The experimental analysis demonstrates the potential of this technology in harnessing solar energy for both electrical power generation and thermal energy utilization in regions with abundant sunlight. The outcomes of this research can facilitate the development of sustainable and cost-effective solar energy solutions, particularly in subtropical regions. The integration of electrical and thermal energy production in a single module offers significant advantages in terms of space utilization and system efficiency. The experimental data presented in this study can serve as a basis for further research and development of solar vacuum insulated PVT modules, leading to their widespread adoption and contributing to the transition towards a clean energy future.

#### 5. REFERENCES

- Adeli, M, et al. 2012. 'Experimental Performance Evaluation of a Photovoltaic Thermal (PV/T) Air Collector and Its Optimization'. *Strojniški vestnik-Journal of Mechanical Engineering*, 58: 309–318. DOI: <https://doi.org/10.5545/sv-jme.2010.007>
- Agrawal S. and Tiwari A., "Experimental validation of glazed hybrid micro-channel solar cell thermal tile," *Solar Energy*, vol. 85, no. 11, pp. 3046–3056, 2011
- Arslan, E, Aktaş, M and Can, ÖF. 2020. 'Experimental and numerical investigation of a novel photovoltaic thermal (PV/T) collector with the energy and exergy analysis'. *Journal of Cleaner Production*, 276: 123255. Elsevier Ltd. DOI: <https://doi.org/10.1016/j.jclepro.2020.123255>
- Aste, N, del Pero, C and Leonforte, F. 2014. 'Water flat plate PV–thermal collectors: A review'. *Solar Energy*, 102: 98–115. Pergamon. DOI: <https://doi.org/10.1016/j.solener.2014.01.025>

- Choi, HU, et al. 2020. 'Experimental study on the performance of heat pump water heating system coupled with air type PV/T collector'. *Applied Thermal Engineering*, 178: 115427. Elsevier Ltd. DOI: <https://doi.org/10.1016/j.applthermaleng.2020.115427>
- Diwania, S, et al. 2020. 'Photovoltaic–thermal (PV/T) technology: a comprehensive review on applications and its advancement'. *International Journal of Energy and Environmental Engineering*, 11(1): 33–54. Berlin, Heidelberg: Springer. DOI: <https://doi.org/10.1007/s40095-019-00327-y>
- Dubey S, and Tiwari G.N., Analysis of PV/T flat plate water collectors connected in series, *Solar Energy*, Volume 83, Issue 9, 2009, Pages 1485-1498, ISSN 0038-092X, <https://doi.org/10.1016/j.solener.2009.04.002>.
- Gholampour, M and Ameri, M. 2016. 'Energy and exergy analyses of Photovoltaic/Thermal flat transpired collectors: Experimental and theoretical study'. *Applied Energy*, 164: 837–856. Elsevier. DOI: <https://doi.org/10.1016/j.apenergy.2015.12.042>
- Jia, Y, Alva, G and Fang, G. 2019. 'Development and applications of photovoltaic–thermal systems: A review'. *Renewable and Sustainable Energy Reviews*, 102: 249–265. Pergamon. DOI: <https://doi.org/10.1016/j.rser.2018.12.030>
- Li, Z, et al. 2019. 'Experimental study and performance analysis on solar photovoltaic panel integrated with phase change material'. *Energy*, 178: 471–486. Elsevier Ltd. DOI: <https://doi.org/10.1016/j.energy.2019.04.166>
- Noxpanco, MG, Wilkins, J and Riffat, S. 2020. A Review of the Recent Development of Photovoltaic/Thermal (PV/T) Systems and Their Applications. *Future Cities and Environment*, 6(1): 9, 1–16. DOI: <https://doi.org/10.5334/fce.97>
- Oyieke A Y. A., and Inambao F L., "Performance Characterisation of a Hybrid Flat-Plate Vacuum Insulated Photovoltaic/Thermal Solar Power Module in Subtropical Climate", *International Journal of Photoenergy*, vol. 2016, Article ID 6145127, 15 pages, 2016. <https://doi.org/10.1155/2016/6145127>
- Sandnes B. and Rekestad J., "A photovoltaic/thermal (PV/T) collector with a polymer absorber plate. Experimental study and analytical model," *Solar Energy*, vol. 72, no. 1, pp. 63–73, 2002.
- Zhou, J, Ma, X, et al. 2020. 'Numerical simulation and experimental validation of a micro-channel PV/T modules based direct-expansion solar heat pump system'. *Renewable Energy*, 145: 1992–2004. DOI: <https://doi.org/10.1016/j.renene.2019.07.049>
- Zhou, J, Zhu, Z, et al. 2020. 'Theoretical and experimental study of a novel solar indirect-expansion heat pump system employing mini channel PV/T and thermal panels'. *Renewable Energy*, 151: 674–686. Elsevier Ltd. DOI: <https://doi.org/10.1016/j.renene.2019.11.054>

---

## #275: Performance study for selected HVAC systems

---

Jiufa CHEN<sup>1,2</sup>, Jianchao MA<sup>3</sup>, Yibo CHEN<sup>4</sup>, Bing GUO<sup>5</sup>, Zhikai ZHAO<sup>6</sup>

<sup>1</sup> School of Energy and Environment, Southeast University, 2 Sipailou, Xuanwu District, Nanjing, China, chen.jiufa@126.com

<sup>2</sup> Purple Mountain Institute, 6 Fengxin Road, Yuhua District, Nanjing, China

<sup>3</sup> School of Urban Construction, Changzhou University, 21 Gehu Middle Road, Wujin District, China, jianchao\_ma@seu.edu.cn

<sup>4</sup> School of Civil Engineering, Zhengzhou University, Zhengzhou, China, yb\_chen77@163.com

<sup>5</sup> College of Water Conservancy and Civil Engineering, Shandong Agricultural University, Taian, China, 1977guobin@163.com

<sup>6</sup> National and Local Joint Engineering Laboratory of Internet Application Technology on Mine, China University of Mining and Technology, Xuzhou, China, zhikaizhao@163.com

*Abstract: This paper explores the effectiveness and energy consumption of three types of HVAC systems for summer cooling: fan cooling, split air conditioning (AC) system, and radiant system. The study focuses on evaluating the comfort level and energy efficiency of these systems using simulations. The simulations consider an office room with an occupant and analyse human body temperature distribution, air flow distribution, and energy consumption. Computational fluid dynamics (CFD) method is used for the simulations, considering various factors such as air conditioning equipment, room dimensions, and occupant characteristics. The findings provide valuable insights into the performance of different HVAC systems for achieving optimal comfort and energy efficiency in buildings.*

*Keywords: Comfort Level, Energy Efficiency, Fan Cooling, Split Air Conditioning System, Radiant System*

## 1. INTRODUCTION

The human body is a delicate thermal engine that requires precise temperature control (Adam et al., 2016). The normal body temperature is 37 °C, with rectal temperature being 0.3°C higher and axillary temperature 0.5°C lower than oral temperature. The body can tolerate daily temperature variations of 0.2 to 0.5°C with temperatures exceeding 41.1°C considered hyperpyrexia (Occupational Safety and Health Administration).

To maintain a healthy body temperature, buildings need to be equipped with heating, ventilation, and air conditioning (HVAC) systems (Agyenim et al., 2011, Deng et al., 2020, Fumo et al., 2018, Liu et al., 2009). This paper examines three types of HVAC systems for summer cooling: fan cooling, split air conditioning (AC) system, and radiant system. The study focuses on two aspects: comfort level and energy consumption.

## 2. SIMULATION SETUP

The simulation considers an office room with dimensions 4m wide, 7m long, and 2.7m high, as shown in Figure 1. The room is assumed to have an ambient air temperature of 30°C with one occupant. Three types of air conditioning equipment are evaluated: fan cooling, split air conditioner, and radiant air conditioning. The evaluations include human body temperature distribution, air flow distribution, and energy consumption features.

ANSYS Fluent 19.0 is used for simulating the room air conditioning and human body temperature distribution. Gambit software is used for grid division. The simulation considers the Boussinesq assumption for buoyancy effect, RNG k- $\epsilon$  model for turbulence flow, standard wall function model for wall functions, "simple" algorithm for pressure-velocity coupling, second-order upwind interpolation for convective terms, and second-order accuracy for variable solving. The convergence standard residual is set to  $10^{-5}$ .

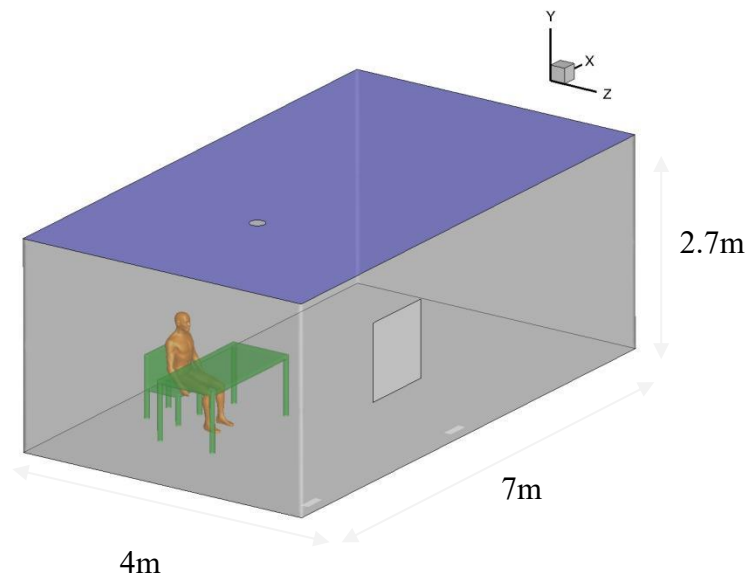


Figure 1 Simulated room, 4m wide, 7m long, and 2.7m high

A seated person is considered in the simulation with a height of 1.72m and body weight of 70kg. The metabolic rate is assumed to be 1.1 met, mean surface area (Du-Bois area) 1.65m<sup>2</sup>, and metabolic rate 65W/m<sup>2</sup>. The overall energy consumption rate is 107W.

All simulations are carried out in steady state.

## 3. FAN COOLING

In this scenario, a fan is used for air conditioning. The fan is positioned approximately 1.5m away from the person and has a front diameter of 500mm. It runs at 1000rpm, creating a driving force of 20Pa. The average indoor air flow velocity is found to be 0.42m/s.

As shown in Figure 2, the air flow is more dynamic in the central section compared to a location 2m away from the central plane. In the central section, a column of air flows at a velocity of 2.7m/s, directed towards the occupant's head, with an average velocity of 1.31m/s. As the distance from the central plane increases, the parallel air flow velocity decreases. At a distance of 2m from the central plane, the average air flow velocity is approximately 0.36m/s. The average air flow velocity for the whole room is approximately 0.42m/s.



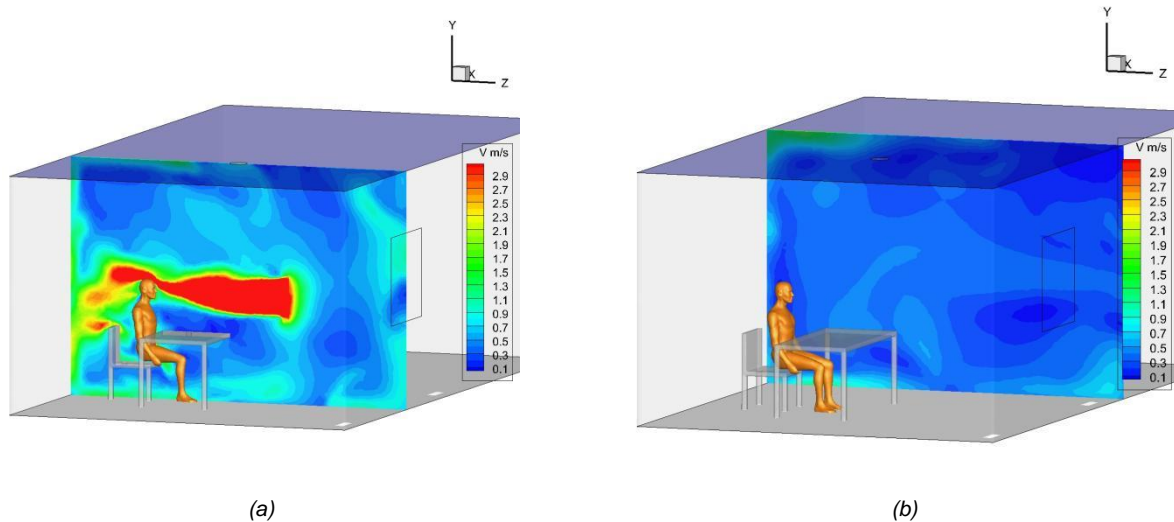


Figure 2 Air flow velocity profile for fan cooling method: (a) at occupant and fan's central section, (b) air velocity profile at the plane 2m away from the central section

As shown in Figure 3, the temperature distribution over the occupant's body shows that the head receives a direct air flow column with an average velocity of 3.5m/s, causing turbulence (turbulence intensity of 46.7%). As a result, the average head surface temperature drops to 31.8°C. Other parts of the body, away from the direct air flow, receive an average velocity of 0.66m/s and turbulence intensity of 27.7%, resulting in an average temperature of 33.5°C, 1.7°C higher than the head temperature. The simulation reveals the lowest surface temperature of the occupant as 31.5°C.

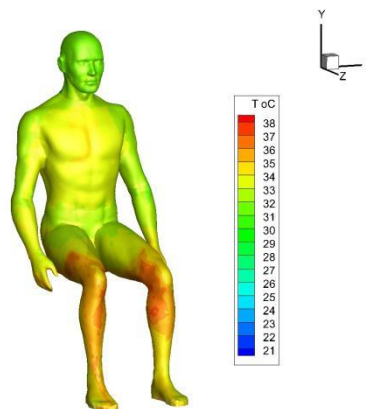


Figure 3 Temperature field for the air flow blown by the fan

#### 4. SPLIT AC SYSTEM

The split air conditioning (AC) system is widely used in residential and office buildings for both cooling and heating purposes. It consists of indoor and outdoor air handling units and operates as a heat pump system, utilizing refrigerant as the working fluid. This study focuses specifically on the system's performance during summer cooling operations.

In this investigation, the indoor air unit is positioned 3 meters away from the occupant, directly in front, with an air supply section featuring an opening of 100mm×500mm.

Figure 4 illustrates the velocity profile along the central line from the occupant to the indoor air unit, showcasing the airflow generated by the system. The conditioned air exits the air conditioner at a velocity of 2m/s with a temperature of 20°C. As it reaches the occupant, the average velocity decreases to 1.1m/s. Since the lower parts of the body do not receive direct airflow, the average air velocity for the entire body amounts to 0.14m/s. As we move further away from the air conditioning blast, the induced airflow in the room gradually diminishes. At a distance of 2m from the central plane, the average air velocity reduces to 0.07m/s.

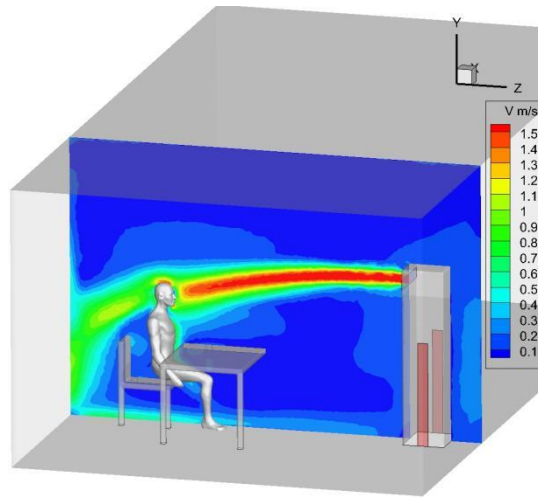


Figure 4 Air flow field induced by the air blast from the AC indoor unit

Figure 5 depicts the temperature distribution within the office room and for the occupant. The AC system delivers a stream of 20°C air towards the occupant, effectively removing heat from their surroundings. As a result of the cooling air blast, the occupant's head temperature is maintained at 26.7°C while a pool of cooler air accumulates at the lower body, leading to an average surface temperature of 23.7°C. The highest recorded surface temperature for the occupant was 38.3°C the lowest being 25.1°C, resulting in a temperature difference of 13 °C. Considering the entire room, the average temperature is 27.6 °C, with the central plane averaging 26.5°C and the plane 2m away from the central plane averaging 27.5°C.

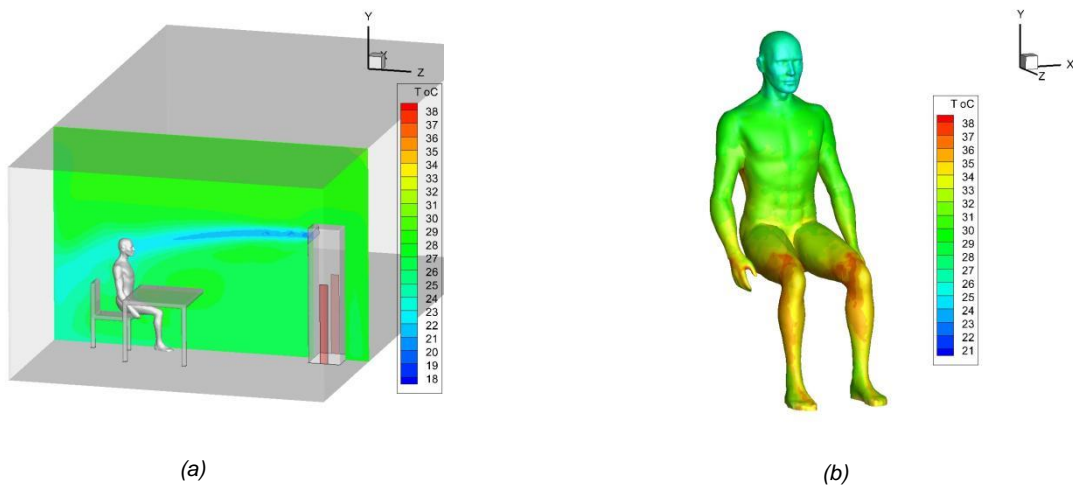


Figure 5 Air temperature distribution with the split AC system: (a) temperature distribution at the central plane, (b) temperature distribution over occupant's skin

## 5. RADIANT AIR CONDITIONING SYSTEM

A radiant air conditioning system, also known as radiant cooling, offers an alternative approach to cooling indoor spaces. Unlike traditional systems that rely on forced air or refrigerant, it utilizes radiant heat transfer to achieve cooling. This system is considered highly effective as it maintains a uniform and comfortable temperature throughout the entire room, thanks to the densely installed capillary tubes.

In this simulation, capillary tubes are installed in the ceiling (as depicted in Figure 6), through which chilled water at 18°C circulates. Fresh air is supplied to the room from a floor grid, with a volume flow rate of 30L/s and a temperature of 20°C, ensuring the maintenance of indoor air quality.



Figure 6 A photo taken during Installation of capillary tubes to the ceiling

With the radiant system, there is minimal noticeable air flow, apart from the diffused fresh air supply and the natural convection induced by the occupant's body heat, as illustrated in Figure 7. The fresh air supplied from the floor grid creates a pool of fresh air near the floor, with an average air flow velocity of 0.07m/s. The movement of air around the occupant is primarily driven by the convective heat from the body, resulting in an average air flow velocity of 0.13m/s over the head and 0.07m/s over the entire body surface.

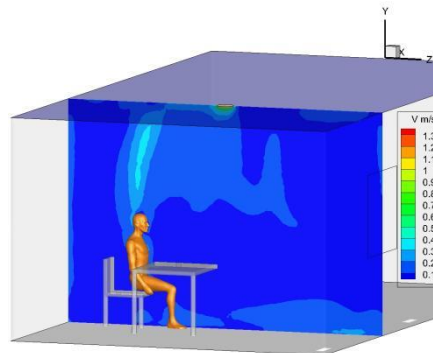


Figure 7 Air flow velocity field for the simulated radiant climate

Figure 8 demonstrates that the radiant system achieves a remarkably even temperature distribution. The capillary tubes cool the ceiling uniformly to 20°C. With the cooling effect from the ceiling, the room's air temperature is evenly distributed, reaching 26.0°C at the central plane and 23.6°C at planes located 2m away from the central plane. For the occupant, the simulation reveals a head temperature of 31.5°C and an average whole-body temperature of 31.7°C.

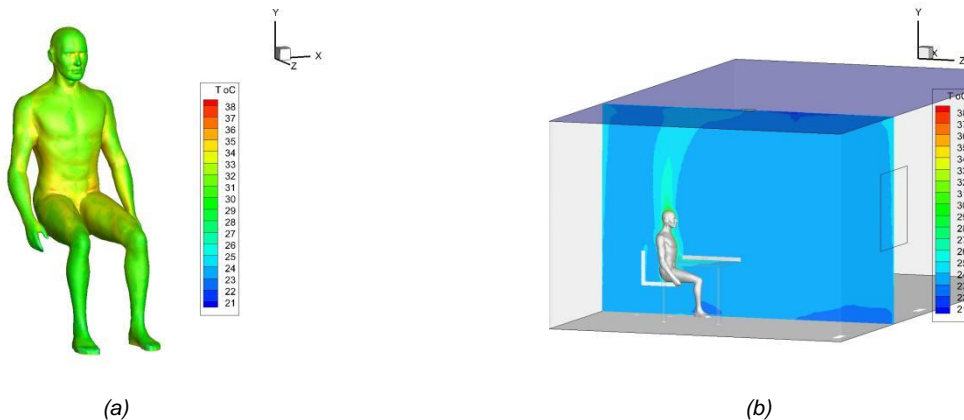


Figure 8 Radiant AC system: (a) temperature distribution over occupant's body surface, (b) temperature distribution for the central plane

## 6. COOLING PERFORMANCE AND ENERGY CONSUMPTION COMPARISON

Simulation results indicate that fan cooling alone is insufficient for maintaining comfortable conditions in an office environment. The simulation predicts that at a mild ambient temperature of 30°C the body temperature of occupants would exceed 33°C. If the ambient temperature rises further, such as to 35°C or higher, the elevated body temperature would cause sweating, fatigue, and a reduction in office work efficiency.

In contrast, the split AC system, the most popular choice for summer cooling, offers noticeable comfort for occupants. It can quickly respond to cool down indoor air, as observed in this simulation where the occupant's head temperature reached 26.7°C while the indoor air temperature stabilized at 27.6°C.

However, the split AC system is lacking in terms of overall body comfort. At an ambient temperature of 30°C the indoor unit must deliver air flow at 16°C or lower to the occupant, resulting in a significant 21°C temperature difference between the body core and the cooling airflow. The simulation also reveals a temperature difference of 13.2°C with the occupant experiencing low temperatures of 25.1°C and high temperatures of 38.3°C. These substantial temperature differences can lead to discomfort for the occupant.

A temperature difference of 12 °C between the body's core temperature and the external environment represents a significant shock to the body's thermoregulatory system. Prolonged exposure to such extreme temperatures could result in symptoms like dizziness, weakness, headache, nausea, vomiting, and in severe cases, pose a life-threatening situation. The specific effects of a 12 °C thermal shock depend on factors such as exposure duration, clothing, temperature range, and the individual's age and health.

Radiant systems offer improved thermal comfort for occupants. The simulation shows that the whole room temperature ranged from 23°C to 26°C. By uniformly cooling the surfaces, radiant systems maintain uniform air temperatures and building surface temperatures within the comfort range. This creates a pleasant indoor climate throughout the year, as evidenced by simulated head and body temperatures of 31.5°C and 31.7°C, respectively. Radiant systems also provide a constant level of oxygen supply through fresh air intake. Additionally, since radiant systems do not rely on air movement, they reduce the circulation of dust, allergens, and pollutants. These systems operate quietly, enhance air quality, and can significantly improve occupant work efficiency and quality of life.

Energy consumption in HVAC systems is a major concern in urban areas. Significant progress has been made in improving system efficiency and comfort for human occupants (Chen et al., 2020, Magdalena et al., 2019, Wang et al., 2019). Despite efforts to reduce energy consumption in split AC systems, the COP (Coefficient of Performance) typically ranges between 3 and 5. However, HVAC energy consumption still accounts for 40% to 60% of total energy consumption in urban areas.

In terms of energy consumption, radiant systems offer approximately 20% less energy consumption compared to split AC systems. Radiant cooling systems are more energy-efficient due to higher chilled water temperatures and the utilization of building structures, such as ceilings, walls, and floors, as radiant surfaces for heat exchange, resulting in reduced energy usage.

## 7. CONCLUSION

This study investigates three types of HVAC systems (fan cooling, split AC, and radiant system) for summer cooling in an office room. Through simulations using ANSYS Fluent software, the researchers analyse factors like human body temperature distribution, air flow distribution, and energy consumption. The simulations consider an occupant with specific characteristics and examine the performance of each HVAC system in terms of comfort level and energy efficiency. The results shed light on the effectiveness of different cooling systems and provide valuable information for designing HVAC systems that optimize both comfort and energy consumption in buildings.

## 8. REFERENCES

- Adam, E. & Bhat, S. R., 2016. Risk Assessment and Management of Thermal Shock for Human Safety in Spacecraft and Planetary Habitats. *Journal of Aerospace Engineering*, 29, 1.
- Agyenim, F., & Eames, P., 2011. Analysis of the energy consumption characteristics of HVAC and hot water systems in UK hotels. *Energy and Buildings*, 43(7), 1719-1727.
- Chen, Y., Zhang, X., et al., 2020. Performance evaluation of HVAC systems in a university building: A case study in China. *Energy and Buildings*, 211, 109820.
- Deng, S., Wang, S., et al., 2020. Energy performance of HVAC systems in different climates: A case study in residential buildings. *Energy and Buildings*, 225, 110381.
- Fumo, N., Gruber, P., et al., 2018. Energy performance assessment of HVAC systems: A data-driven methodology. *Energy and Buildings*, 177, 271-285.
- Liu Peng, Xie Junlong, Chen Huanxin, 2009. Comparison of Design Daily Energy Consumption between Independent Fresh Air Combined with Radiant Cooling Ceiling System and Other Air Conditioning Systems. 2009 Hubei Province HVAC Refrigeration and Thermal Power Academic Annual Conference. WUha, China (in Chinese).
- Magdalena, Z., & Zalewski, L., 2019. Energy performance assessment of HVAC system with radiant cooling in a public building. *Energy and Buildings*, 186, 116-126.

Occupational Safety and Health Administration. "Thermal Shock" by the Occupational Safety and Health Administration (OSHA). [https://www.osha.gov/SLTC/heatstress/thermal\\_shock.html](https://www.osha.gov/SLTC/heatstress/thermal_shock.html)

Wang, Z., Xu, X., et al., 2019. Energy performance analysis of HVAC systems in office buildings in different climate zones. *Energy Procedia*, 158, 3453-3459.

---

## #277: Challenges of climate change & resilient housing design solution

---

Afaq Hyder CHOHAN<sup>1,\*</sup>, Jihad AWAD<sup>1</sup>, Adi Irfan CHE ANI<sup>2</sup>, Bhai Khan SHER<sup>3</sup>

<sup>1</sup>Department of Architecture, College of Architecture, Art and Design, Ajman University, Ajman, United Arab Emirates, a.chohan@ajman.ac.ae

<sup>2</sup> Department of Architecture, University Kebangsaan Malaysia; <sup>3</sup>Shaheed Allah Buksh University, Jamshoro, Sindh, Pakistan.

*Abstract: The escalating challenges of climate change necessitate a novel approach to our built environments, especially housing, to foster adaptability and resilience. This investigation thoroughly scrutinizes academic literature to discern design strategies that bolster housing resilience amidst changing climate conditions. The analysis includes multiple case studies across Northern and Southern Pakistan, exploring the distinct challenges and environmental nuances in each area.*

*This multidisciplinary literature exploration delves into housing design resilience from architectural, environmental, health, and socio-economic perspectives. It critically assesses both established techniques and pioneering trends, merging traditional knowledge with contemporary advancements. This comprehensive approach emphasizes the role of community-driven design solutions, public engagement, and policy formulation in nurturing resilience.*

*The case studies from various Pakistani regions offer practical insights, revealing region-specific climate challenges and exploring housing design vulnerability in times of rain and flooding. Comparing these disparate climatic scenarios allows us to define tailored design and protection guidelines, promoting a resilient housing infrastructure capable of withstanding climate change.*

*In summary, this research highlights the necessity of immediate and future-oriented housing design strategies to combat climate change. By integrating insights from both the literature review and case studies, we provide recommendations for architects, urban planners, and policymakers to advance resilient housing design not only in Pakistan, but globally.*

*Keywords: Climate Change and Housing; Climate Resilience in Housing Design; Northern and Southern Regions of Pakistan.*

## 1. INTRODUCTION

Climate change poses a significant global challenge, with wide-ranging effects on the environment, society, and economy. Ensuring the resilience of affordable housing is crucial, as it houses millions of low-income individuals who are particularly vulnerable to climate change impacts. Baloch's study (2022) in *The Guardian* highlights that Pakistan's ongoing inundations are primarily linked to climate change, with rising temperatures intensifying monsoon precipitation and causing unprecedented floods in the Indus River basin. Climate change disproportionately affects monsoon-affected regions, making it imperative for nations, especially high carbon emitters, to develop sustainable adaptation strategies. Deforestation exacerbates flooding and landslides, and Pakistan's high deforestation rate underlines the need for long-term action to combat climate change-induced disasters (Hamid, M. 2022).

The study by Rannard (2022) emphasizes that the devastating floods in Pakistan serve as a wake-up call to the world about the threats of climate change. Although Pakistan is not a major contributor to global warming, its high growth trajectory of carbon emissions, linked to fossil fuel use, puts it at risk. Despite contributing less than 1% of global greenhouse gases, its geographical vulnerability makes it highly susceptible to the impacts of climate change.

Affordable housing faces increasing challenges due to climate change, as highlighted by the National Low-Income Housing Coalition (NLIHC, 2022) and the United Nations (UNDP, 2021). NLIHC's study reveals that affordable housing is disproportionately located in areas prone to natural disasters like floods, hurricanes, and wildfires. Similarly, the UN study warns that climate change will exacerbate the risks of displacement and homelessness, particularly affecting low-income communities. These findings underscore the urgent need to address the vulnerabilities of affordable housing to climate change and its potential impact on vulnerable populations (Cornell, C., Gurran, N., and Lea, T., 2020;). Another study conducted by the United Nations found that climate change will increase the risks of displacement and homelessness, particularly in low-income communities (UNDP, 2021).

The challenge of building resilience in affordable housing lies in the need to adapt to climate change impacts while considering limited resources. For instance, implementing climate-resilient measures like improved insulation or flood-proofing can be costly and difficult for low-income households. Adding to this challenge is the fact that many low-income households are located in areas most vulnerable to climate change effects, such as flood-prone regions and areas with extreme weather conditions. Pakistan is grappling with various housing-related issues, including a significant housing shortage and affordability concerns. Studies indicate that the country currently faces a housing deficit of 10 million units, with 24% of the population experiencing housing shortages. This deficit is higher than neighbouring countries like India and Bangladesh, making it crucial to address housing demand and availability (Qureshi et al., 2022).

Given the growing population and urbanization in Pakistan, the country's urban areas, which are already exposed to pollution and climate change, are expected to increase from 37% in 2020 to 60% in 2050. To create more liveable cities, urgent reforms are necessary, including integrated land use planning, increased investments in municipal services, and a focus on energy efficiency and clean transportation. Deforestation is a particularly concerning issue that needs attention (IIPS, 2022).

The issue of affordable housing and climate change resilience has gained significant attention in recent years due to the increasing recognition of the risks and impacts of climate change on vulnerable populations. Affordable housing is particularly vulnerable to the effects of climate change due to factors such as location, design, and materials used. Various studies have demonstrated the link between affordable housing and climate change resilience. For instance, a study conducted by the National Low-Income Housing Coalition (NLIHC) found that low-income households are disproportionately impacted by natural disasters, such as hurricanes and floods, which can cause significant damage to affordable housing (NLIHC, 2022;). Another study by the US Green Building Council (USGBC) found that green building strategies, such as energy-efficient design and the use of renewable materials, can improve the resilience of affordable housing to climate change impacts (USGBC, 2020; USGBC, 2021;).

Furthermore, the need to address climate resilience in affordable housing has been recognized by various international organizations and initiatives. For example, the United Nations has identified affordable housing as a critical area for climate change adaptation and has emphasized the need to integrate resilience strategies into housing policies and practices (UN-Habitat, 2022). Additionally, the 100 Resilient Cities initiative, which aims to build resilience in urban areas, has highlighted the importance of affordable housing in promoting resilience to climate change (100RC, 2020).

Despite these efforts, there are still challenges to achieving climate resilience in housing. One of the main challenges is the lack of funding and resources for implementing resilience measures in affordable housing. Another challenge is the difficulty of balancing the need for resilience with the cost of implementing measures, which can be particularly challenging for low-income households. In fact housing is a critical component of any society, as it provides shelter to low-income earners and other vulnerable populations. However, the challenge of resilience in affordable housing has become a significant issue in the face of climate change. Climate change has far-reaching impacts on the environment, society, and the economy, and the vulnerability of affordable housing to climate change is a threat to the livelihoods of these individuals.

Numerous studies have documented the risks associated with climate change and affordable housing. For instance, a study by the U.S. Department of Housing and Urban Development (HUD) found that affordable housing is disproportionately located in areas that are susceptible to natural disasters, such as floods, hurricanes, and wildfires (HUD,

2021). Another study conducted in the United Kingdom found that climate change will exacerbate existing inequalities in access to affordable housing and increase the risks of displacement and homelessness (Anderson et al., 2021).

The discussion above can be précised as that, at the moment we stand at the threshold of an increasingly uncertain future, humanity faces the dual challenge of mitigating the impacts of climate change and ensuring the availability of affordable housing. This confluence of crises demands a re-evaluation of our approach to urban planning, architecture, and policymaking, as we strive to create sustainable and equitable solutions that cater to the needs of a rapidly growing global population.

This study aims to address these intertwined challenges by examining the nexus between climate change and affordable housing. Through a synthesis of interdisciplinary research, case studies, and expert insights, the study aims to provide a comprehensive understanding of the multifaceted problem at hand and propose innovative strategies for tackling this dual crisis.

## **2. CLIMATE CHANGE AND CHALLENGES TO HOUSING**

Climate change is significantly impacting the built environment and housing infrastructure worldwide. Rising temperatures, extreme weather events, and sea-level rise pose threats to housing systems and exacerbate the need for affordable shelter amid economic disparities. The study by Adger, W. N., et al. (2018) highlights the vulnerability of housing structures to extreme weather events and rising sea levels, leading to physical and financial strain on homeowners, renters, and governments. Climate-related disasters, such as flooding, have profound psychological impacts, with rising rates of Common Mental Disorders (CMDs) observed among affected populations (Butler C., et.al 2016; Paranjothy S., et.al 2007; Tunstall S., et.al 2006; Convery and Bailey. 2008; Tempest E.L., et.al 2017; Milojevic A., et.al 2017; Fewtrell and Kay 2008).

Climate-related disasters can have profound psychological impacts, with the traumatic experience of witnessing one's home inundated leading to mental health disorders. Hence, a comprehensive response to climate change is crucial, encompassing mental health support alongside other strategies to address physical and infrastructural damage. Buchanan et al. (2020) emphasize the need for proper planning and building materials to minimize flood impacts on housing structures, including damage to foundations, walls, and overall integrity. Allstate Insurance highlights the multifaceted adverse effects of flooding, from structural damage to electrical hazards and biological concerns. Floodwaters can weaken floors, roofs, and walls, compromising the safety of inhabitants. Additionally, floodwater poses risks to electrical systems and household appliances, potentially leading to electrocution or fire. Post-flooding environments are conducive to mold growth, posing health risks and damaging building materials and personal belongings (Allstate. 2023).

Eves (2004) conducts a comprehensive analysis of housing defects caused by floods, examining factors like construction materials, building age, and local topography that influence vulnerability. Paulik et al. (2021) review the connection between climate change, increased flooding events, and resulting housing damage, proposing mitigation measures like improved building codes and flood-resistant designs. Mirza (2003) investigates the socio-economic consequences of flood-induced housing defects, including displacement, financial burdens, and health impacts, advocating for comprehensive policy interventions. Sanjit et al. (2017) presents a longitudinal study on climate change's impact in the eastern Himalayas, highlighting the negative effects on ecosystems and socioeconomics. Studies by Azuma et al. (2014) and Lowe et al. (2013) explore health implications of flood-induced housing defects, such as increased respiratory issues and mental health problems, stressing the need for timely remediation. Amini and Memari (2020) discuss challenges related to insuring properties vulnerable to flooding, proposing solutions like public-private partnerships and risk-based pricing for adequate coverage.

Besides the provision of indemnity to cover against the possible effect of climate change, Peacock et. al (2018) has compared different approaches to post-flood housing recovery, emphasizing the importance of community involvement and tailored efforts to meet affected populations' specific needs. Mostafiz et al. (2021) and Brody et al. (2007) highlight the sharp decline in property value in regions severely affected by climate change, leading to financial burdens and psychological distress. These studies stress the need for efficient flood risk control and housing durability strategies to alleviate economic repercussions. Dwellings in climate-impacted areas face financial strains, and studies by Eid & El-Adaway (2019) and Wahab & Kasim (2023) propose flood-resilient housing retrofits as a cost-effective solution to reduce flood risks and promote housing resilience through targeted investments.

Discussion under this section provides an overview of the multifaceted consequences of housing defects resulting from floods, including physical damage, health and safety risks, and economic and social impacts. Physical damage encompasses structural deterioration, compromised building integrity, and water damage to the interior and exterior of residential properties. This damage necessitates costly repairs and can render homes uninhabitable, forcing residents to find alternative shelter. Health and safety risks associated with flood-induced housing defects are significant, as they can lead to mold growth, poor indoor air quality, and contaminated water supplies. These conditions heighten the likelihood of respiratory illnesses, allergies, and other health complications, particularly for vulnerable populations, such as children and the elderly.

The economic impacts of flood-related housing defects are considerable, as they can decrease property values, increase insurance premiums, and strain financial resources due to repair and relocation costs. This burden disproportionately affects low-income households, exacerbating existing inequalities. Whereas social impacts of housing defects caused by



floods are diverse, ranging from displacement and homelessness to the disruption of community networks and the strain on local resources. Additionally, the psychological toll of losing one's home and the prolonged recovery process can lead to increased stress and mental health issues.

### 3. AIM & OBJECTIVES

This study aims to explore the link between climate change and the housing crisis, focusing on building resilient, sustainable housing systems. The research objectives include performing a comprehensive review of existing literature to comprehend the current knowledge of this relationship and conducting case studies in Pakistan from diverse geographical regions and climates to discern effective climate-adaptive strategies. By comparing these case studies, the study will identify common issues, influential factors, and vital success elements for developing resilient housing amidst climate change. Findings will be used to formulate evidence-based policy suggestions and practical guidelines for creating housing systems that can adapt to climate-induced challenges. The study will also pinpoint areas for future research to enhance our understanding of the complex interplay between climate change and housing crisis, fostering the creation of innovative, effective adaptation strategies.

### 4. METHODOLOGY

This study proposes a cross-disciplinary framework to explore the relationship between climate change and housing. It employs both theoretical and empirical evidence, focusing on reproducibility and broad applicability. The approach involves a literature review and theoretical synthesis, extracting theories from architecture, urban planning, environmental science, and more. Data collection involves primary and secondary sources, including climate datasets, housing market stats, governmental reports, and expert interviews. The study uses case studies representing diverse climates and housing systems in Pakistan to examine housing failure patterns and the effectiveness of existing climate-adaptive strategies. A comparative analysis will identify common factors influencing the success or failure of these strategies. The study will verify findings through comparative analyses and by comparing results with other relevant studies. Based on the results, the study will offer policy recommendations for resilient housing systems and will identify areas for further research to understand the complexity between climate change and housing

By implementing this methodological framework, the study aims to generate robust, reliable, and actionable insights that can inform policy decisions and practical interventions for addressing the challenges posed by climate change to the housing sector, as shown in Figure 1.

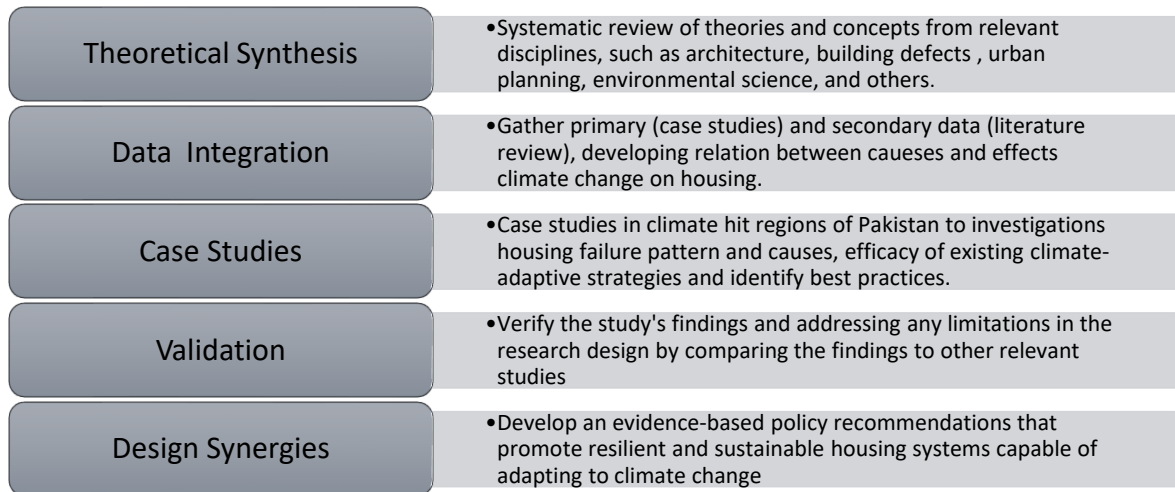


Figure 1 Methodical Flow

### 5. CLIMATE CHANGE IN PAKISTAN & STUDY OF HOUSING DISASTERS AND RESILIENCE

This study investigates the impact of climate change on housing in Pakistan, focusing on areas severely affected by climate-related disasters. It notes climate change as a major global concern with far-reaching consequences, evidenced by devastating floods in Pakistan that have disrupted millions of lives. Particularly, the districts of Dadu (Sindh), Swat (Khyber Pakhtunkhwa), and Pashin (Baluchistan) have been severely affected. Research (Baloch. 2022; Renard. 2022; UNDP. 2022) highlights climate change as a catalyst for the increased frequency and intensity of Pakistan's floods, driven by changing weather patterns, extreme temperatures, and glacier melting. These phenomena have escalated natural disasters, resulting in widespread housing and infrastructure destruction. Further studies (UNICEF. 2022; Sajid 2022; World Bank 2022) report the nationwide devastation from these climate-induced floods, particularly in Sindh, Baluchistan,

and Khyber Pakhtoon Khwa. The situation is aggravated by inadequate infrastructure and insufficient governmental support, necessitating urgent rehabilitation and reconstruction in these regions.

In addition, the reports (UNICEF. 2022; Sajid 2022; World Bank 2022) show that climate change-induced floods severely impacted Swat in Khyber Pakhtunkhwa and Pashin in Baluchistan, causing significant housing damage, displacement, and economic distress due to increased rainfall, glacial melting, and inadequate preparedness. These circumstances underscore the need for immediate intervention and sustainable solutions to mitigate climate change challenges. Consequently, this study focuses on three profoundly impacted areas in Pakistan: Dadu (Sindh), Pishin (Baluchistan), and Swat (Khyber Pakhtunkhwa), aiming to study the interplay between climate change, flooding, and housing destruction. Gul (2022) found that floodwaters devastated a third of the country, destroying or displacing over 2 million houses, killing 1.2 million livestock, and damaging 13,000 kilometers of roadways. With 8 million people displaced, standing floodwaters foster waterborne and vector-borne diseases, creating a growing health crisis. Sindh province sustained the majority of the damage (around 70%), followed by Balochistan, Khyber Pakhtunkhwa, and Punjab, with the poorest districts hit hardest.

This study highlights the need for adaptive strategies and resilient infrastructure in regions like Dadu (Sindh), Swat (KPK), and Pishin (Baluchistan), Pakistan, heavily affected by climate change. These locations will be explored in detail to understand flood origins and their impacts on housing and the built environment. For a comprehensive investigation, site visits were conducted to observe various destruction forms, alongside unstructured interviews and documentations of damage patterns. Traditional construction methods and materials used across different locales were also investigated. These efforts aim to mitigate climate change impacts and safeguard the welfare and livelihoods of affected communities.

### 5.1. House Design and Failure Pattern in District Dadu, Sindh.

Located on the Indus River's left bank, Dadu district is mainly agrarian, with features such as expansive agricultural lands, mountainous terrain, and a large natural freshwater reservoir, Manchar Lake. The district faced significant losses in 2022 due to climate change impacts on housing, health facilities, crops, livestock, and human lives (Shahzad, A., 2022).

Unprecedented monsoons and glacial melts affected 33 million people, causing 1,391 deaths and massive infrastructure destruction. Floodwaters submerged highways in several locations, causing weeks-long traffic disruptions. The district, housing 1.5 million people, experienced 466% above average rainfall, leading to 90% of the district submerging and more than 1,200 health facilities being inundated, resulting in the spread of numerous diseases (Hassan, 2022; Khushik, Q. A., & Shahid, J., 2022). Approximately 600 villages were submerged, stranding residents due to lack of boats, and around 30,000 houses were impacted by the floods and rain, as shown in Pictures (1-3). Dadu's traditional courtyard houses, combining adobe and industrial materials, signify a classic architectural approach. However, site visits and surveys revealed a striking picture of destruction and design failure, demonstrating the vulnerability of the community and built environment to climate change impacts. This underlines the urgent need for resilient infrastructure and adaptive strategies, necessitating architects, engineers, and policymakers to address shortcomings in building design and construction practices.

Climate change has exposed the vulnerability of traditional construction methods and materials. Structural failures due to soil erosion, water ponding on roofs, and high-water tables resulting in dampness are some challenges that need addressing to ensure building longevity and stability. Adapting resilient architectural designs and construction techniques to climate change challenges is thus crucial.



Picture 1: Making Flood Barriers    Picture 2: House after Rain & Flood Damage    Picture 3: Submerged Streets & Houses

### 5.2. House Design and Failure Pattern in District Swat, KPK.

Khyber Pakhtunkhwa (KPK), including the Swat district, is characterized by diverse topography and a significant tourism sector. Due to climate change, the region experienced unprecedented monsoons and landslides in 2022, causing severe damage (Ashfaq, 2022). Torrential rains and floods destroyed 35,123 houses and partially damaged 52,327, resulting in 289 fatalities and several injuries, with Swat accounting for 34 deaths (Ali, M., 2022). The floods also devastated

educational and health facilities and infrastructure, damaging 90 schools, 91 health facilities, and compromising over 1,455 kilometers of roads and 73 bridges, as shown in Picture 4.

In Swat, hotel and housing designs blend aesthetics and functionality with cultural considerations. Hotels typically feature reinforced concrete construction (RCC) for durability and structural integrity, energy-efficient systems, and advanced security features. However, heavy rains led to some collapses, indicating a need for climate-resilient infrastructure. Traditional houses incorporate the courtyard layout with south-facing orientations, RCC or load-bearing walls, and stone or cement block masonry, as shown in Pictures (5-6).

Design failures due to policy shortcomings, inadequate building control, and environmental challenges led to widespread destruction (Pictures 5). Overflows from rivers due to heavy rainfall caused soil erosion and landslides, leading to building collapses, especially in low-rise hotels (Picture 6). The lack of comprehensive environmental studies further contributed to these failures, emphasizing the need for rigorous policy implementation, effective building control, and environmental considerations.



Picture 4: District Swat Floods      Picture 5: RCC Construction in River Catchment      Picture 6: Damage to House in Landslide Rains & Submerged Bridge

### 5.3. House Design and Failure Pattern in District Pishin Baluchistan.

Pishin District, situated in Pakistan's largest province, Baluchistan, has suffered extensive flooding due to monsoonal rains (June-August 2022), causing significant damage and loss of life. The district is characterized by valleys, with elevations ranging from 1,370 to 1,680 meters, and the Lora River as its main water source. The severe rainfall across Baluchistan, Sindh, and Khyber Pakhtunkhwa provinces led to the loss of 244 lives, displaced thousands of families and affected approximately 430,416 people, as shown in Picture 8. Seven dam collapses worsened the situation, causing extensive damage to croplands and over 25,000 houses in Baluchistan, including around 2,000 in Pishin (OCHA. 2022; Nazir., Z. 2022).

House designs in Pishin incorporate traditional courtyard houses, made of sun-dried mud blocks and south-facing for optimal solar gain. These homes employ load-bearing clay or brick masonry walls, reinforced concrete, or I and T section steel frames, with either precast concrete or palm thatch roofs, finished with clay mortar. This design approach reflects the local context and environmentally conscious, culturally sensitive housing needs. However, like Swat and Dadu, Pishin suffers design failures due to its geographical and environmental challenges. These include compromised wall bonding, significant diagonal wall cracks, separation of joints at wall corners, soil erosion, water accumulation on rooftops, and material degradation, as shown in Pictures 7.



Picture 7: Total Collapse of Adobe Estate

Picture 8: Displaced People

Picture 9: Damaged House



Poor land levelling exacerbates surface water drainage, intensifying soil erosion and causing potential foundation damage. Pishin's hilly terrain, combined with policy deficiencies, inadequate building control measures, and heavy rainfall, result in widespread soil erosion and landslides, leading to the partial or total collapse of buildings as shown in Picture 9. This highlights the need for climate-resilient design and construction in the face of increasing climate change threats.

## 6. RESILIENT BUILDING DESIGN FOR A CHANGING CLIMATE

The study emphasizes the importance of adaptive, resilient design in affordable housing, accounting for climate change impact. This involves the potential of novel materials, construction methods, and sustainable technologies for reducing housing's environmental footprint and accessibility (Baudoin et.al, 2016). Mitigating disaster risk requires reducing vulnerability and increasing community resilience through structural and non-structural measures (Kreibich et. al, 2015). Structural measures involve enhancing design, enforcing construction standards and guidelines, and fortifying structures. Non-structural measures include hazard-based land-use planning, public awareness programs about hazard mitigation, and fostering disaster resilience (Adelekan, 2016).

Given the climate change risk, enhancing the resilience of affordable housing is necessary. A comprehensive strategy includes green infrastructure like green roofs and rain gardens, reducing flood risk, improving air quality, and enhancing biodiversity (Parker and Simpson 2020; Khodadad et.al 2023). Moreover, energy efficiency measures like energy-efficient appliances and better insulation reduce the environmental impact and energy costs (Kamal et al., 2021). Safe housing location involves comprehensive land-use planning, zoning regulations, and community engagement (Green, S. D. (2014).

Building houses in clusters or above floodplain levels can protect against floods. While elevated homes have higher construction costs, flood-resistant materials like concrete, bricks, and treated wood can minimize water damage (Shabani, S., Khan, A., & Amaratunga, D. (2019). Waterproofing techniques also enhance structural resilience during floods (Mitrani, H., & Sattary, S. (2021). Building flood barriers provide immediate protection, while floating homes and amphibious architecture respond effectively to rising water levels (O'Keefe, P., & Westgate, K. (2015).

Incorporating green infrastructure reduces stormwater runoff and alleviates flood risks. However, the cost can be prohibitive for low-income households, and there's a need to ensure interventions don't lead to gentrification or vulnerable population displacement (Streimikiene, D., et al., 2020). Hence, a comprehensive, multifaceted approach is crucial to creating resilient, affordable housing that withstands climate change impacts.

Innovative housing designs, together with effective urban planning and policy enforcement, can substantially improve the resilience of homes in flood-prone areas. The urgency of housing resilience against climate change necessitates policy interventions, community involvement, and technological solutions. It's vital to provide vulnerable populations access to safe, sustainable housing that can endure climate change impacts. Figure 2, derived from the previous discussion, illustrates a visual interpretation of the identified synergies to combat climate change in housing.

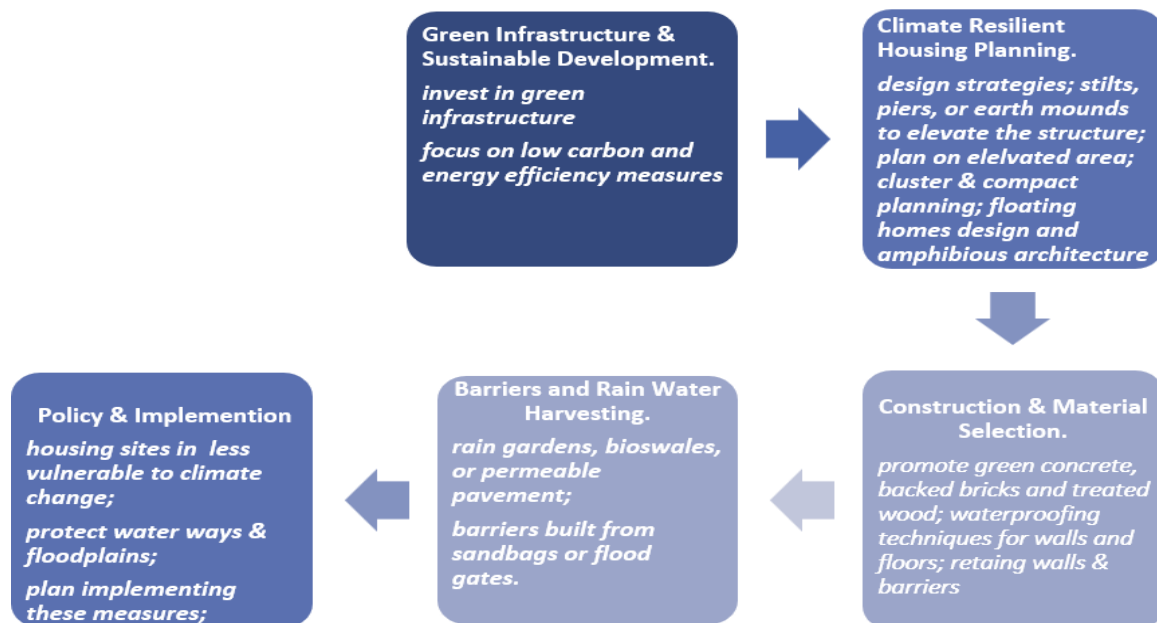


Figure 2 Resilient Design Initiatives

## 7. RECOMMENDATIONS FOR HOUSING DESIGN SYNERGIES AND CLIMATE RESILIENCE IN PAKISTAN.

Considering the obstacles outlined in Sections 7 of this study, along with the design possibilities presented in Section 8 it is crucial to incorporate climate change adaptation measures into Pakistan's housing policies and infrastructure development. This requires a strategic approach that incorporates both short-term and long-term planning measures. In the short term, immediate actions should focus on raising awareness and promoting resilience in vulnerable areas, while the long-term planning initiatives should involve developing comprehensive policy frameworks, such as climate change adaptation strategies, master planning, and climate-resilient building codes, to ensure sustainable housing and infrastructure development in the face of ongoing climate challenges, as shown in Figure 3.

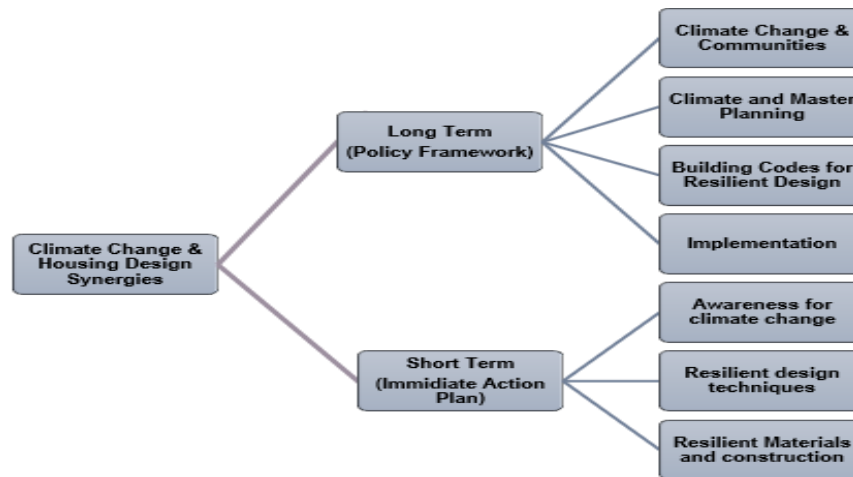


Figure 3 Climate Change & Housing Design Synergies

### 7.1. Long-Term Planning for Climate-Conscious Housing Design

To enhance housing resilience in the face of climate change, stakeholders must collaborate and exchange knowledge. They should develop climate-adaptive design policies and building codes, incorporating features like clustered housing, elevated lots, flood-resistant materials, and energy-efficient technologies. Sustainable urban planning can minimize environmental impact, while investments in climate-resilient infrastructure and upgraded housing systems bolster resilience. Advocacy for affordable, modular, and climate-resilient housing, along with financial aid and relocation assistance for climate-displaced individuals, is vital. Prioritizing vulnerable groups' needs, such as low-income communities, the elderly, and individuals with disabilities, ensures equitable urban adaptation strategies. These actions collectively promote long-term housing resilience and foster community cohesion in the face of climate challenges.

### 7.2. Short-Term Planning for Climate-Conscious Housing Design

To effectively address the multifaceted challenges of climate change on housing systems and settlements, a comprehensive approach is proposed. Firstly, utilizing social media, local context, and language can inform people about adaptive strategies, promoting long-term resilience. Secondly, incorporating an economic perspective involves sustainable materials, local construction, and green industry growth, creating jobs and aiding businesses to adopt climate-smart practices. Thirdly, a social dimension engages communities, enhancing capacity, and involving residents in decision-making, fostering cohesion and ownership. Lastly, assisting locals in learning climate-resistant housing design and construction techniques is crucial. By implementing short-term and long-term measures, governments and citizens can create mechanisms and resilience practices to safeguard infrastructure and communities, fostering inclusive and sustainable development.

## 8. CONCLUSION

This research started from the understanding that climate change poses significant challenges to housing resilience, especially impacting vulnerable populations such as low-income communities, the elderly, and disabled individuals. These groups often live in areas susceptible to climate risks with limited means for housing adaptation or relocation, highlighting the need for social equity in developing adaptive housing policies (Baloch. S, M. 2022; Rannard. G. 2022; IIPS 2022).

The study exposes the severe negative impacts of climate change on Pakistan, affecting housing, infrastructure, agriculture, and causing loss of human lives. It underscores the urgency for Pakistan to implement adaptive measures to mitigate climate change effects and safeguard vulnerable communities.

By examining housing loss through case studies in climate change hotspots in Pakistan, it was discovered that housing failure often stemmed from deficient design, the use of low-resilience materials, lack of building codes, compromised structural integrity, and homeowners' limited understanding of climate change risks. The housing types, ranging from adobe and hybrid constructions to Reinforced Cement Concrete (RCC) structures, all displayed unique vulnerabilities to flooding.

This study proposes both long-term and short-term initiatives for climate change and housing design, including investing in green infrastructure, energy efficiency measures, policy formulation, and involving multiple stakeholders in developing adaptation strategies (Figure 7). It also suggests fostering partnerships among governments, the private sector, and civil society organizations for comprehensive, innovative solutions.

While this research focused on climate change's impact on housing in Pakistan, it points to broader areas of study, such as sustainable design for climate-resilient housing in hot and arid climates or improving local materials and construction techniques for better climate resilience.

## 9. ACKNOWLEDGEMENT

The authors extend their appreciation to Ajman University for the APC assistance and the Healthy and Sustainable Built Environment Research Centre at Ajman University for offering an outstanding research setting. The authors are thankful to Ar. Abdul Manan in Baluchistan, Ar. Mohammed Kashif in KPK, and Engr. Niaz Mohammad Thebo in Sindh for their help in facilitating the case studies at the locations specified in the research.

## 10. REFERENCES

Baloch, S, M. 2022. There is nothing for us Pakistan's flood homeless start to despair. Sep 2020. Guardian UK. <https://www.theguardian.com/world/2022/sep/06/we-screamed-our-hearts-out-for-help-homeless-escape-pakistan-floods> (visited 25 April 2023).

Hamid, M. 2022. Climate change is a bigger threat to Pakistan than terrorism. Washington Post. July 14, 2022. <https://www.washingtonpost.com/opinions/2022/07/14/climate-change-pakistan-india-worse-threat-terrorism/>

Rannard, G. 2022. How Pakistan floods are linked to climate change. BBC News Climate and Science. Sep 2022. <https://www.bbc.com/news/science-environment-62758811> (visited 22 April 2023).

NLHIC. National Low Income Housing Coalition. (2022). On the front lines: Disaster Housing Recovery Coalition. <https://nlhlc.org/explore-issues/projects-campaigns/disaster-housing-recovery> (visited 8 May 2023)

Cornell, C., Gurrán, N., and Lea, T. (2020). Climate change, housing, and health: A scoping study on intersections between vulnerability, housing tenure, and potential adaptation responses. The University of Sydney, NSW Health, and the NSW Department of Planning, Industry and Environment. <https://www.hfhincubator.org/wp-content/uploads/2020/11/Cornell-et-al.-Climate-change-housing-and-health.pdf> (visited 22 April 2023).

UNDP. United Nations Development Program. (2021). Building resilience for sustainable development in Asia and the Pacific. <https://www.undp.org/publications/building-forward-together-towards-inclusive-and-resilient-asia-and-pacific> (visited 22 April 2023).

Qureshi et al. (2022). Climate Smart Housing in Pakistan. SDPI. SUSTAINABLE DEVELOPMENT POLICY INSTITUTE. [https://sdpi.org/sustainable-development-in-unusual-times-building-forward-better/publication\\_detail](https://sdpi.org/sustainable-development-in-unusual-times-building-forward-better/publication_detail) (visited 22 April 2023).

IIPS. Iqbal Institute of Policies Studies. 2022. NATIONAL HOUSING POLICY: ISSUES AND WAY FORWARD. <https://iips.com.pk/housing-policy-of-pakistan-issues-way-forward/> (visited 5 May 2023).

USGBC. US Green Building Council. (2020). Affordable Housing. <https://www.usgbc.org/resources/guiding-principles-green-affordable-housing> (visited 02 April 2023).

USGBC. US Green Building Council. (2021). Actions in Advocacy: High-performing affordable housing <https://www.usgbc.org/articles/actions-advocacy-high-performing-affordable-housing> (visited 02 April 2023).

100RC. (2019). Resilient Cities, Resilient Lives Learning from the 100RC Network. [https://resilientcitiesnetwork.org/downloadable\\_resources/UR/Resilient-Cities-Resilient-Lives-Learning-from-the-100RC-Network.pdf](https://resilientcitiesnetwork.org/downloadable_resources/UR/Resilient-Cities-Resilient-Lives-Learning-from-the-100RC-Network.pdf) (Visited 8 May 2023)

UN Habitat. (2022). Adequate Housing, Cities and Climate Change, and Localising the Sustainable Development Goals. [https://unhabitat.org/sites/default/files/2022/05/priorities\\_2022-2023\\_adequate\\_housing\\_cities\\_and\\_climate\\_change\\_and\\_localising\\_sdgs\\_04142022.pdf](https://unhabitat.org/sites/default/files/2022/05/priorities_2022-2023_adequate_housing_cities_and_climate_change_and_localising_sdgs_04142022.pdf) (Visited 8 May 2023)

- HUD. U.S. Department of Housing and Urban Development (2021). Climate Change Action Plan for Urban Development. <https://www.hud.gov/sites/dfiles/Main/documents/HUD-Climate-Action-Plan.pdf> (Visited 8 May 2023)
- Anderson, N.; Wedawatta, G.; Rathnayake, I.; Domingo, N.; Azizi, Z. Embodied Energy Consumption in the Residential Sector: A Case Study of Affordable Housing. *Sustainability* 2022, 14, 5051. <https://doi.org/10.3390/su14095051>.
- Adger, W. N., de Campos, R. S., Siddiqui, T., Gavonell, M. F., Szaboova, L., Rocky, M. H., ... & Billah, T. (2021). Human security of urban migrant populations affected by length of residence and environmental hazards. *Journal of Peace Research*, 58(1), 50-66.
- Butler C., Walker-Springett K., Adger W., Evans L., O'Neill S., Adger N. Social and Political Dynamics of Flood Risk, Recovery and Response. A Report of the Findings of the Winter Floods Project. University of Exeter; Exeter, UK: 2016. [Google Scholar]
- Paranjothy S., Gallacher J., Amlôt R., Rubin G.J., Page L., Baxter T., Wight J., Kirrage D., McNaught R., Palmer S.R. Psychosocial impact of the summer 2007 floods in England. *BMC Public Health*. 2011;11:145. doi: 10.1186/1471-2458-11-145. [PMC free article] [PubMed] [CrossRef] [Google Scholar]
- Tunstall S., Tapsell S., Green C., Floyd P., George C. The health effects of flooding: Social research results from England and Wales. *J. Water Health*. 2006;4:365–380. doi: 10.2166/wh.2006.031. [PubMed] [CrossRef] [Google Scholar]
- Convery I., Bailey C. After the flood: The health and social consequences of the 2005 Carlisle flood event. *J. Flood Risk Manag.* 2008;1:100–109. doi: 10.1111/j.1753-318X.2008.00012.x. [CrossRef] [Google Scholar]
- Tempest E.L., English National Study on Flooding. Health Study Group. Carter B., Beck C.R., Rubin G.J. Secondary stressors are associated with probable psychological morbidity after flooding: A cross-sectional analysis. *Eur. J. Public Health*. 2017;27:1042–1047. doi: 10.1093/eurpub/ckx182. [PMC free article] [PubMed] [CrossRef] [Google Scholar]
- Milojevic A., Armstrong B., Wilkinson P. Mental health impacts of flooding: A controlled interrupted time series analysis of prescribing data in England. *J. Epidemiol. Community Health*. 2017 doi: 10.1136/jech-2017-208899. [PMC free article] [PubMed] [CrossRef] [Google Scholar]
- Fewtrell L., Kay D. An attempt to quantify the health impacts of flooding in the UK using an urban case study. *Public Health*. 2008;122:446–451. doi: 10.1016/j.puhe.2007.09.010. [PubMed] [CrossRef] [Google Scholar]
- Buchanan, M. K., Kulp, S., Cushing, L., Morello-Frosch, R., Nedwick, T., & Strauss, B. (2020). Sea level rise and coastal flooding threaten affordable housing. *Environmental Research Letters*, 15(12), 124020.
- Allstate. 2023. What kind of home damage can a flood cause. Allstate Insurance Company. <https://www.allstate.com/resources/flood-insurance/home-flood-damage#:~:text=Floods%20can%20cause%20structural%20damage,your%20home%20after%20a%20flood.> (Visited 10 May 2023)
- Eves, C. (2004). The impact of flooding on residential property buyer behavior: an England and Australian comparison of flood affected property. *Structural Survey*, 22(2), 84-94.
- Paulik, R., Crowley, K., & Williams, S. (2021). Post-event Flood Damage Surveys: A New Zealand Experience and Implications for Flood Risk Analysis. In *FLOODrisk 2020-4th European Conference on Flood Risk Management*. Budapest University of Technology and Economics.
- Mirza, M.Q. 2003. Climate change and extreme weather events: can developing countries adapt. *Climate Policy*, Volume 3, Issue 3, 2003, [https://doi.org/10.1016/S1469-3062\(03\)00052-4](https://doi.org/10.1016/S1469-3062(03)00052-4)
- Sanjit Maiti, Sujeet Kumar Jha, Sanchita Garai, Arindam Nag, A.K. Bera, Vijay Paul, R.C. Upadhaya, S.M. Deb. An assessment of social vulnerability to climate change among the districts of Arunachal Pradesh, India, *Ecological Indicators*, Volume 77, 2017. <https://doi.org/10.1016/j.ecolind.2017.02.006>
- Azuma, K., Ikeda, K., Kagi, N., Yanagi, U., Hasegawa, K., & Osawa, H. (2014). Effects of water-damaged homes after flooding: health status of the residents and the environmental risk factors. *International journal of environmental health research*, 24(2), 158-175.
- Lowe, D., Ebi, K. L., & Forsberg, B. (2013). Factors increasing vulnerability to health effects before, during and after floods. *International journal of environmental research and public health*, 10(12), 7015-7067.
- Amini, M., & Memari, A. M. (2020). Performance of Residential Buildings in Hurricane Prone Coastal Regions and Lessons Learned for Damage Mitigation. In *Proceedings of the 5th Residential Building Design & Construction Conference*, Conference Center Hotel in State College, State College, PA, USA (pp. 4-6).

- Peacock, W.G., N. Dash, Y. Zhang, and S. Van Zandt. (2018). Post-Disaster Sheltering, Temporary Housing, and Permanent Housing Recovery. Pp. 569-594 in *Handbook of Disaster Research 2nd edition*, edited by H. Rodriguez, J. Trainor, and W. Donner. New York: Springer. [https://link.springer.com/chapter/10.1007/978-3-319-63254-4\\_27](https://link.springer.com/chapter/10.1007/978-3-319-63254-4_27)
- Mostafiz, R. B., Friedland, C. J., Rahman, M. A., Rohli, R. V., Tate, E., Bushra, N., & Taghinezhad, A. (2021). Comparison of neighborhood-scale, residential property flood-loss assessment methodologies. *Frontiers in environmental science*, 9, 734294.
- Brody, S. D., Zahran, S., Maghelal, P., Grover, H., & Highfield, W. E. (2007). The rising costs of floods: Examining the impact of planning and development decisions on property damage in Florida. *Journal of the American Planning Association*, 73(3), 330-345.
- Eid, M. S., & El-Adaway, I. H. (2019). Sustainable Disaster Recovery Framework: Reducing the Community Vulnerabilities throughout the Redevelopment Process. In *Computing in Civil Engineering 2019: Smart Cities, Sustainability, and Resilience* (pp. 498-506). Reston, VA: American Society of Civil Engineers.
- Wahab, B., & Kasim, O. (2023). Developing resilient cities in developing countries. *Handbook of Flood Risk Management in Developing Countries*.
- UNICEF. 2022. Devastating floods in Pakistan. <https://www.unicef.org/emergencies/devastating-floods-pakistan-2022> (Visited 9 May 2023)
- Sajid. I. (2022). Death toll, property damages from floods in Pakistan. <https://www.aa.com.tr/en/asia-pacific/death-toll-property-damages-from-floods-in-pakistan-keep-rising/2690677> (Visited 9 May 2023)
- Worldbank. 2022. Pakistan: Flood Damages and Economic Losses (press release)  
<https://www.worldbank.org/en/news/press-release/2022/10/28/pakistan-flood-damages-and-economic-losses-over-usd-30-billion-and-reconstruction-needs-over-usd-16-billion-new-assessme> (visited 5 May 2023)
- Gul. A (2022). Study: Pakistan Flood Damages, Economic Losses. *Voice of America*. October 2022. <https://www.voanews.com/a/study-pakistan-flood-damages-economic-losses-exceed-30-billion-6810207.html#:~:text=Floodwaters%20drenched%20one%2Dthird%20of,The%20U.N.> (visited 5 May 2023)
- Picture 1. [https://en.wikipedia.org/wiki/Dadu\\_District](https://en.wikipedia.org/wiki/Dadu_District) (Visited 5 May 2023)
- Picture 2. [https://en.wikipedia.org/wiki/Swat\\_District](https://en.wikipedia.org/wiki/Swat_District) (Visited 5 May 2023)
- Picture 3. [https://en.wikipedia.org/wiki/Quetta\\_Division](https://en.wikipedia.org/wiki/Quetta_Division) (Visited 5 May 2023)
- Ashfaq. M. (2022). PDMA: Monstrous floods, rains killed 289 in Khyber Pakhtunkhwa. Published in Dawn, September 5th, 2022. <https://www.dawn.com/news/1708450>
- Ali, M. (2022). Floods cost Khyber Pakhtunkhwa Rs68 billion, claims govt. Published in Dawn, September 2nd, 2022. <https://www.dawn.com/news/1707946>
- Shahzad., A. (2022). U.N. chief urges support for flood-hit Pakistan. *Reuters*. September, 11, 2022. <https://www.reuters.com/world/asia-pacific/un-chief-visits-areas-pakistan-devastated-by-floods-2022-09-10/>
- Hassan., R, A. (2022). Pakistan to breach main highway to protect town of Dadu from floods. *Reuters*. September, 11, 2022 <https://www.reuters.com/world/asia-pacific/pakistan-breach-main-highway-protect-town-dadu-floods-2022-09-11/>
- Khushik., Q. A., and Shahid., J. (2022). 110 districts hit by floods as locals race to save Dadu. Published in Dawn, September 2nd, 2022. <https://www.dawn.com/news/1708002>
- OCHA. ( 2022). Rapid Need Assessment Flood Emergency - Balochistan & Sind . United Nations Office for the Coordination of Humanitarian Affairs (OCHA). <https://reliefweb.int/report/pakistan/rapid-need-assessment-flood-emergency-balochistan-sind-28th-aug-2022>
- Nazir., Z. (2022). Pakistan floods threaten food security. *Deutsche Welle (DW) German international broadcaster*. September 13, 2022. <https://www.dw.com/en/pakistan-floods-threaten-food-security-as-critical-crops-destroyed/a-63104114>
- Baudoin, M. A., Henly-Shepard, S., Fernando, N., Sitati, A., & Zommers, Z. (2016). From top-down to “community-centric” approaches to early warning systems: Exploring pathways to improve disaster risk reduction through community participation. *International Journal of Disaster Risk Science*, 7, 163-174.



- Kreibich, H., Bubeck, P., Van Vliet, M., & De Moel, H. (2015). A review of damage-reducing measures to manage fluvial flood risks in a changing climate. *Mitigation and adaptation strategies for global change*, 20, 967-989.
- Adelekan, I. O. (2016). Flood risk management in the coastal city of Lagos, Nigeria. *Journal of Flood Risk Management*, 9(3), 255-264.
- Kamal, A. M., Sifa, S. F., Islam, S. M., Rafsan, M. A., Alve, M. I. H., Mahmud, T., ... & Rahman, M. Z. (2021). Climate Change Vulnerability Assessment of Patuakhali Municipality in Bangladesh. *The Dhaka University Journal of Earth and Environmental Sciences*, 187-198.
- Parker, J., & Zingoni de Baro, M. E. (2019). Green infrastructure in the urban environment: A systematic quantitative review. *Sustainability*, 11(11), 3182.
- Green, S. D. (2014). Building Resilient Communities in the Wake of Climate Change While Keeping Affordable Housing Safe from Sea Changes in Nature and Policy. *Washburn LJ*, 54, 527.
- Streimikiene, D., Lekavičius, V., Baležentis, T., Kyriakopoulos, G. L., & Abrahám, J. (2020). Climate change mitigation policies targeting households and addressing energy poverty in European Union. *Energies*, 13(13), 3389.
- Parker, J., & Simpson, G. D. (2020). A theoretical framework for bolstering human-nature connections and urban resilience via green infrastructure. *Land*, 9(8), 252.
- Khodadad, M., Aguilar-Barajas, I., & Khan, A. Z. (2023). Green Infrastructure for Urban Flood Resilience: A Review of Recent Literature on Bibliometrics, Methodologies, and Typologies. *Water*, 15(3), 523.
- Choia, C., Berrya, P., & Smitha, A. (2021). The climate benefits, co-benefits, and trade-offs of green infrastructure: A systematic. *Journal of Environmental Management*, 291, 112583.
- Ramyar, R., Ackerman, A., & Johnston, D. M. (2021). Adapting cities for climate change through urban green infrastructure planning. *Cities*, 117, 103316.
- Shabani, S., Khan, A., & Amaratunga, D. (2019). Flood resistant design of buildings: An investigation of the design consideration for flood resistant buildings. *Procedia Engineering*, 212, 1311-1318.
- Mitrani, H., & Sattary, S. (2021). Selection of materials in flood-prone areas: A sustainable approach. *Journal of Building Engineering*, 37, 102060.
- Penning-Rowsell, E., & Wilson, T. (2015). Gauging the performance of natural and engineered flood management interventions. *Journal of Flood Risk Management*, 8(3), 241-253.
- O'Keefe, P., & Westgate, K. (2015). Floating houses and amphibious houses: A solution to riverine and coastal flooding? *Environmental Hazards*, 14(4), 285-301.
- Coutts, A. M., & Hahn, M. (2015). Green infrastructure, ecosystem services, and human health. *International Journal of Environmental Research and Public Health*, 12(8), 9768-9798.

---

## #281: Smart responsive shading for enhanced energy efficiency in hot climates

---

Mahmoud ZMEEM<sup>1</sup>, Paolo BECCARELLI<sup>2</sup>, Christopher WOOD<sup>3</sup>

*University of Nottingham, University Park, Nottingham, NG7 2RD, UK,*

*<sup>1</sup>mahmoud.zameem@nottingham.ac.uk, <sup>2</sup>paolo.beccarelli@nottingham.ac.uk, <sup>3</sup>christopher.wood@nottingham.ac.uk*

*Abstract: Smart material technologies are integrated to promote dynamic structures for new buildings and energy retrofitting. The responsive shading system utilises a self-actuating Shape Memory Polymer (SMP) that dynamically activates and operates based on specific thermal conditions as required. The study's objective is to determine the most effective thermal activation stimulus for the adaptive shading system's mechanisms based on an SMP actuator on the performance of buildings, focusing on energy savings and interior comfort. In addition, the IES-VE dynamic building energy simulation was employed to analyse and evaluate the responsive shading performance. The findings were validated by comparing the existing glass facade of a high-rise apartment in Jeddah, Saudi Arabia. Results showed that the co-activation technique, combining solar radiation and air temperature triggers, proved to be the most efficient activation for improving the performance of responsive shading mechanisms in a hot climate. This system minimised solar heat gain, reduced glazed surface temperature, lowered indoor temperatures, reduced glare, and enhanced thermal comfort, resulting in notable energy savings and low-carbon emissions through reduced cooling consumption.*

*Keywords: Responsive Shading, SMPs Actuator, Thermal Activation, Energy Efficiency, IES Simulation*

## 1. INTRODUCTION

In Saudi Arabia, where the climate is sweltering, dwellings face several issues, such as discomfort and excessive cooling usage. With temperatures reaching record highs, using energy-intensive cooling techniques presents difficulties limiting energy use and cutting greenhouse gas emissions. This rising cooling demand causes environmental concerns such as global warming, economic instability, and generation capacity crises. Moreover, residential units alone contribute to approximately 70% of the overall energy usage in Saudi Arabia (Felimban *et al.*, 2019). As the country continues to seek sustainable solutions to these environmental challenges, incorporating “Smart Responsive Shading” appears as a potential technique to improve energy efficiency while controlling solar heat and providing ideal interior comfort. Adaptive shading dynamically responds to changing environmental conditions, optimising energy efficiency and building performance (Aelenei, Aelenei and Vieira, 2016). These systems use intelligent materials and technologies to adjust their configurations based on parameters like solar radiation, wind speed, and temperature (Loonen *et al.*, 2013). They align with the goal of near-zero energy buildings, significantly reducing energy consumption and CO<sub>2</sub> emissions while improving internal comfort. Studies have shown the potential advantages of responsive shading, including enhanced energy efficiency, improved comfort conditions, and minimised environmental impact (Attia, 2018).

The responsive system can be operated manually or automatically through sensors and actuators using intelligent materials like SMP, SMA, and PCM (Yoon, 2019). Smart material-based hinge actuator shading devices offer advanced technology without external sensors, responding naturally to environmental stimuli (Battisti, Persiani and Crespi, 2019). Integrating intelligent material actuators into building elements, such as adaptable envelopes and shading devices, enhances structure flexibility, indoor comfort, energy efficiency, and cost-effectiveness (Neuhaus *et al.*, 2020). This study proposes using SMP as an actuator, allowing the adaptive shading system to switch between open and closed positions based on thermoresponsive properties (Li *et al.*, 2018). SMPs are preferred over other thermoresponsive materials due to their unique reaction temperatures, shape memory effects, and flexible form options (Yoon and Bae, 2020).

SMPs are intelligent materials with unique capabilities such as shape-memory effect, thermoresponsive actuation, biocompatibility, programmable transition temperature, and quick reaction time. They are used in biomedical devices, adaptable constructions, intelligent fabrics, flexible electronics, aerospace, robotics, and other fields. The advanced properties of SMPs offer diverse possibilities in various industries and promise future innovations (Santo *et al.*, 2020). Previous SMP-based actuator applications in robotics and aerospace have shown promise. The feasibility, evaluation, and performance of their application in architecture are still in progress. For instance, Steven Beites (Beites, 2013) demonstrated the viability of SMP joints as actuator mechanisms for opening and closing, while J. Yoon (Yoon, 2019) created a hinge prototype utilising thermal stimuli for activation. These studies have highlighted the potential of integrating SMP actuators into structural systems. However, further research is needed to optimise the design and operation of these systems, including identifying optimal thermal activation parameters, conducting performance evaluations, material testing, assessing operational efficacy, and studying the adaptability of facade systems under varying climate conditions. The early design phase explores the performance of adaptable facades and how changing activation parameters can improve energy efficiency and thermal and visual comfort in hot climates. These cutting-edge, dynamic shading solutions for new construction and energy retrofits use advanced materials and technologies that change the environment dynamically.

## 2. SMP-BASED RESPONSIVE SHADING: MECHANISMS AND DESIGN

Implementing Shape Memory Polymer (SMP) as an actuator in adaptive shading systems allows dynamic management of the thermal response of the building, adjusting peak load times based on climatic variables and modulating seasonal energy needs. The activation parameters of the SMP material determine how the adaptive shading system works to achieve the desired building performance. The open/closed switching mechanism of an adaptive façade-based SMP is responsive to changes in external conditions. Therefore, selecting appropriate stimulus parameters is essential to ensure that the adaptive facade system operates efficiently and effectively in different weather conditions and is necessary to meet the needs of the building and its residents (Tabadkani *et al.*, 2021). Numerous investigations have explored various climatic variables for the activation of the adaptive system and have evaluated its effectiveness based on the goal of building performance and the specific location and climate zone of the building (Bonser *et al.*, 2019), including solar radiation (Yun, Park and Kim, 2017) (Evola, Gullo and Marletta, 2017) (Oh, Lee and Yoon, 2012), air temperature (Yoon, 2019), humidity (Nezamdoost, Van Den Wymelenberg and Mahic, 2018). Typically, researchers have implemented controls for the adaptive shading system that exceed specific thresholds, using solar radiation control to maintain comfort. However, each study had distinct objectives and climates; therefore, there is no agreement on the efficacy of the activation parameter.

This study investigates the optimal activation parameters for an adaptive facade system based on Shape-Memory Polymers (SMP) in a hot environment. An SMP strip sensitive to thermal changes controls the adaptive switching mechanism. The sun's heat is a thermal trigger for the SMP strip, causing it to bend and adjust the shading system. The sun shading module consists of triangular polycarbonate sheets attached to the SMP strip, which acts as the actuator. When exposed to the sun's heat, the SMP strip bends, closing the shading sheets to block sunlight. As the temperature drops, the SMP strip returns to its original position, reopening the shade. This adaptive shading system is designed to harmoniously synchronise building performance with environmental conditions, ensuring efficient and responsive shading based on the prevailing climate factors. Figure 1 illustrates the design and functioning of the system, showcasing its dynamic response to changing thermal conditions.

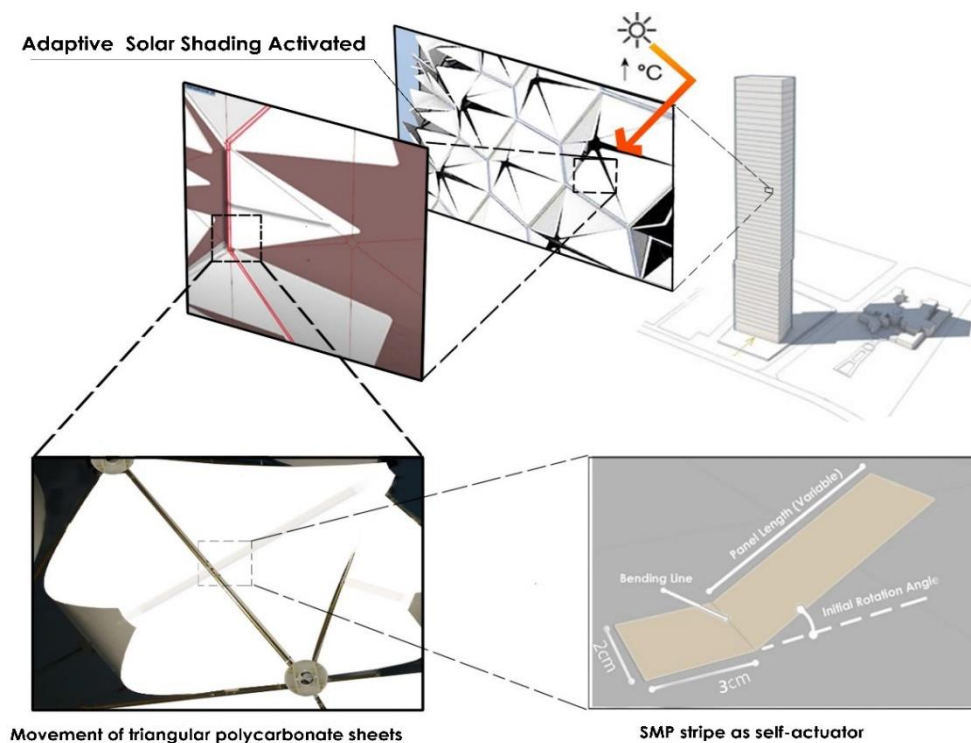


Figure 1 SMP actuator-based adaptive solar shading system

### 3. METHOD

#### 3.1. Thermal Activation

Determining the temperature or solar radiation threshold for the shade system's operation in hot climates is crucial for occupant comfort and energy savings. International standards like ASHRAE, ISO, and EN 15251 provide guidelines for indoor thermal comfort. In the UK, CIBSE offers meteorological data and static overheating criteria. The Passivhaus standard sets thresholds for occupied hours with temperatures above 25°C for living areas and 30°C for other regions (Passive House Institute, no date). Mostadam (Ministry of Housing, 2019) uses the PMV/PPD model based on ASHRAE 55 and ISO 7730 for thermal comfort in Saudi Arabia. However, adopting international standards in hot climates can lead to summer overcooling, causing discomfort and energy waste.

Furthermore, recent research by Nuaimi (Alnuaimi and Natarajan, 2020) showed that the international standards of PMV are in hot regions (such as the Global South) compared to field data from cities in India, the Philippines, and Thailand, causing 49% more discomfort due to overcooling than ideal interior temperatures. Another study by Elnaklah et al. (Elnaklah et al. 2021) found that the current international criteria for PMV thermal comfort do not predict thermal experience for 94% of the occupants, as shown by a meta-analysis of four cities in the Middle East (Jeddah, Amman, Dubai, Doha) with 39% discomfort due to overcooling in summer.

ASHRAE-55 presents an alternative approach for determining interior comfort, known as the adaptive thermal comfort model (Szokolay, 2014). This model considers the local climate's mean ambient temperature and occupants' preferences to establish interior temperature thresholds. Integrating this approach provides valuable information aligned with prevailing climatic conditions, essential in hot and humid climates like Jeddah, where outdoor temperatures can reach up to 45°C. Researchers and organisations have proposed several approaches to establish acceptable indoor temperature ranges based on outdoor conditions. Among these approaches, Nicol and Humphreys's widely used adaptive model integrates the theory of adaptive comfort and considers the impact of outdoor temperature and humidity on indoor comfort. Another frequently used model is the adaptive Szokolay model, which predicts acceptable indoor temperatures in hot and humid climates. Although both models provide valuable information on adaptive thermal comfort, the Nicol and Humphreys models offer a more comprehensive approach, accounting for a broader range of factors that influence thermal comfort. (Equations 1 and 2) are as follows: (1) Nicol and Humphreys, (2) Szokolay:

$$\text{Equation 1: } TC = 13.5 + 0.54 T_o$$

$$\text{Equation 2: } TC = 17.6 + 0.31 T_o$$

Where:  $T_o$  is monthly average outdoor temperatures

–  $TC$  = Thermal comfort (°C)

The Climate Consultant 6 software examined Jeddah weather using (EPW ) data covering (2007-2021). The software extracted data on average air temperature and relative humidity, as depicted in Figure 2, illustrating the annual averages. In particular, July and August emerged as the hottest, while January and February were the coldest.

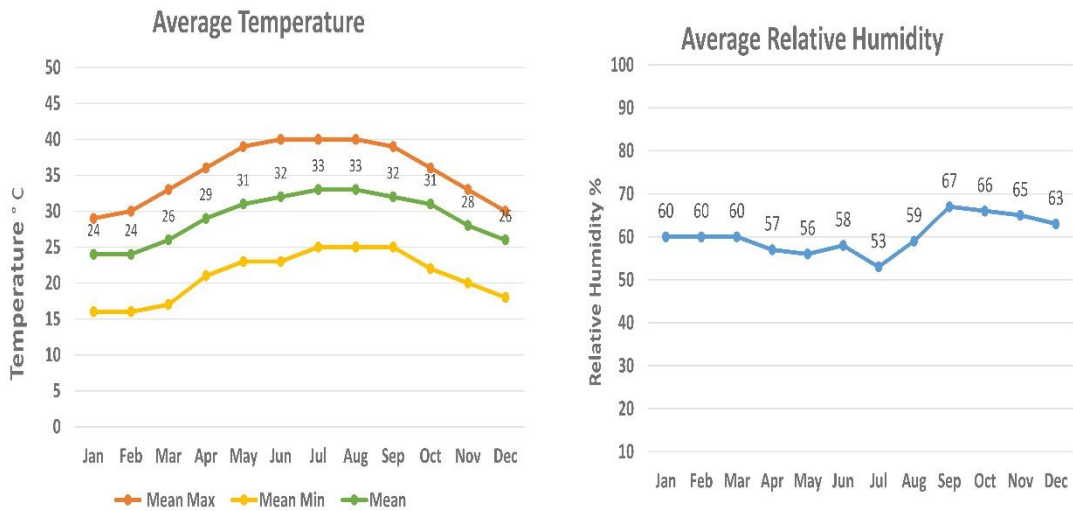


Figure 2 Jeddah's monthly mean air temperature and humidity levels

Table 1 presents the results of Szokolay, Nicol, and Humphreys's adaptive thermal comfort based on average outdoor temperatures in Jeddah city. These are calculated year-round and offer an alternate way of determining the appropriate range of indoor comfort temperatures in hot climates. The average outdoor temperature in July and August was 33°C. The Nicol and Humphreys equation yields a comfort temperature of 31.3 °C and a comfort range of 29.3 to 33.3 °C (+/- 2). The Szokolay equation-based examination found a comfort temperature of 28 °C and a comfort range of 25.5 to 30.5 °C (+/- 2.5).

Table 1: The adaptive thermal comfort limit in Jeddah by the Nicol and Szokolay formulae

Comfort limit Nicol and Humphreys (range +/- 2)°C					Comfort limit Szokolay (range +/- 2.5) °C				
Months	Outdoor Avg. Temp	Thermal Comfort	Lower	Upper	Months	Outdoor Avg. Temp	Thermal Comfort	Lower	Upper
Jan	24	26.4	24.4	28.4	Jan	24	25.0	22.5	27.5
Feb	25	27	25	29	Feb	25	25.3	22.8	27.8
Mar	26	27.5	25.5	29.5	Mar	26	25.6	23.1	28.1
Apr	29	29.1	27.1	31.1	Apr	29	26.5	24	29
May	31	30.2	28.2	32.2	May	31	27.2	24.7	29.7
Jun	32	31	29	33	Jun	32	27.5	25	30
July	33	31.3	29.3	33.3	July	33	28	25.5	30.5
Aug	33	31.3	29.3	33.3	Aug	33	28	25.5	30.5
Sep	32	31	29	33	Sep	32	27.5	25	30
Oct	30	29.7	27.7	31.7	Oct	30	26.9	24.4	29.4
Nov	28	28.6	26.6	30.6	Nov	28	26.2	23.7	28.7
Dec	25	27	25	29	Dec	25	25.3	22.8	27.8

Using the Nicol and Humphreys model, this investigation determined the activation point for the air temperature-activated adaptive shading system to be 33°C. This threshold was established based on data obtained in August, the hottest month in Jeddah. Figure 3 illustrates Jeddah's monthly mean adaptive thermal comfort relative to the outside temperature. Furthermore, the adaptive Nicol model also allows for a broader range of acceptable temperature variations, which may be particularly relevant in hot-humid climates such as Jeddah, where occupants prefer a slightly warmer indoor temperature. Furthermore, a study by Nicol and Humphreys found that people in hot-humid regions adapt to high temperatures, such as 33 °C in Pakistan and even 34 °C in Sri Lanka when the airspeed increases to 0.6m/s.

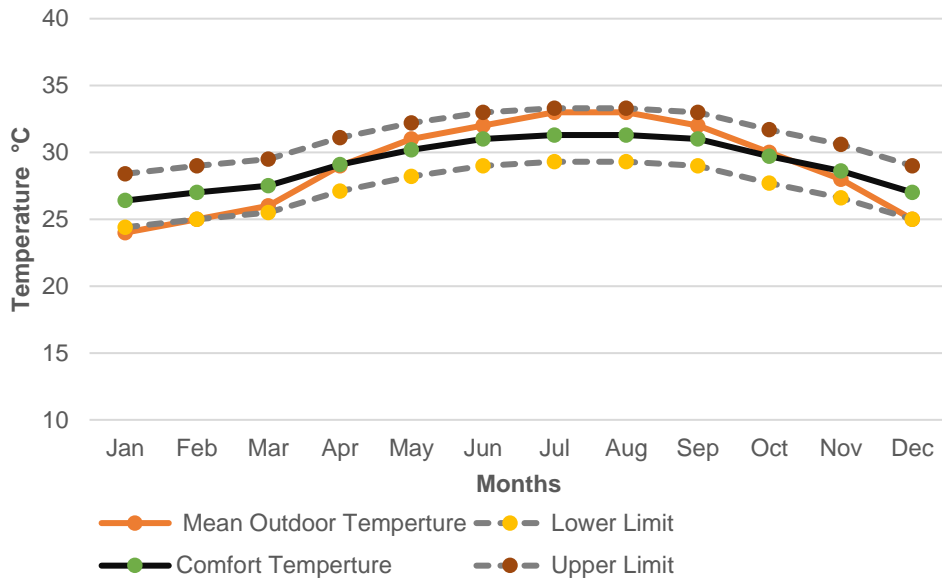


Figure 3 The monthly adaptive thermal comfort limit in Jeddah by the Nicol formula

However, accurately identifying the solar radiation threshold for activating the shading system is essential to optimise its operation, effectively balancing heat gain control and maximising the daylighting performance. Using IES-VE, the average direct sun radiation level in Jeddah was calculated to be 275 W/m<sup>2</sup>, which was applied to the system activation point. This approach involved estimating the direct solar radiation threshold, as shown in Figure 4, considering the average value measured in August.

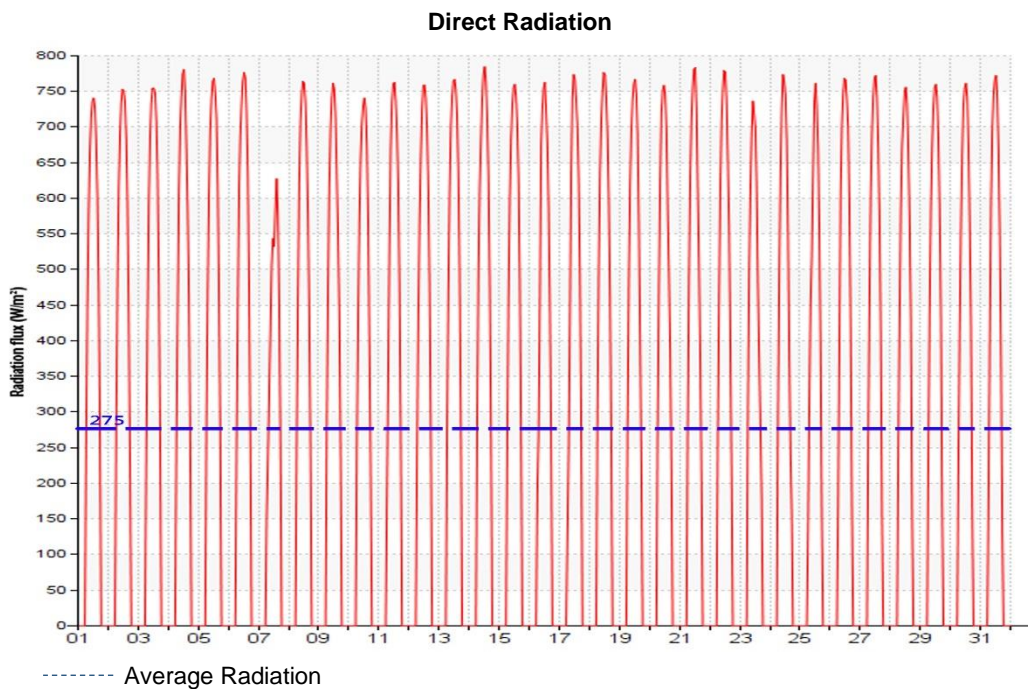


Figure 4 August's average levels of direct solar radiation in Jeddah

### 3.2. Simulation Tool and Weather Data

Building Performance Simulation (BPS) software is needed to study how responsive solar shading affects building energy and thermal comfort. Among the available options like EnergyPlus, ESP-r, ICE, and IES-VE, IES-VE was chosen for its dynamic simulation capabilities. It assesses the thermal performance of the adaptive facade and its effects on indoor conditions and energy usage, considering factors such as occupancy patterns, temperature, and solar radiation. The study utilises IES-VE and EPW files containing 15 years of precise weather data for Jeddah (2007 to 2021) to establish a baseline and evaluate performance under realistic historical climatic conditions. The evaluation will occur on August 24, the hottest day on record.



Jeddah, situated on the Red Sea coast in western Saudi Arabia, is located at coordinates (21°68'N and 39°16'E). It falls under the Kappen Climate Classification of BWH, indicating an arid desert-hot climate. However, due to its proximity to the Red Sea, Jeddah experiences a unique hot and humid climate. Using the IES software for analysis, Jeddah's highest temperatures were recorded in July and August, with a peak of 49 °C on August 24. Conversely, the coldest months are January and February, reaching a low of 15 °C on January 9. Figure 5, generated using the sun cast feature in IES-VE software, illustrates Jeddah's sun path and angle. It shows that the sun's path is oriented southward during the winter, moving towards the middle and northward during the summer.

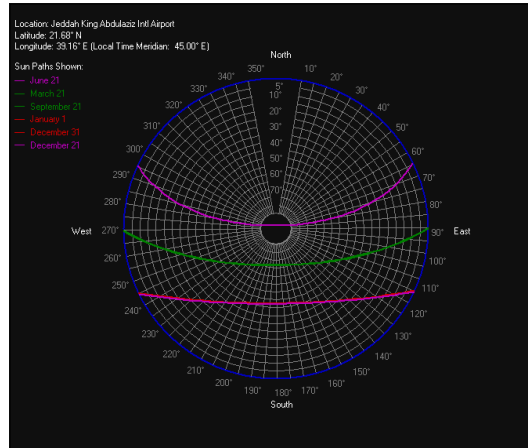


Figure 5 Jeddah Sun Path Diagram Generated by IES -VE Simulation

### 3.3. Case Study: Apartment Conditions

This study examines a high-rise apartment in the city of Jeddah. The building has a significant amount of glazing on its facade and a low thermal mass, representing the typical architectural style observed in the area. The “golden tower” skyscraper, which has a height of 205 metres, 48 storeys, and 78 residential flats, was built in 2017. Each floor comprises two identical apartments, each with an average area of 420 square metres, and the building offers apartments with three different orientations. Figure 6 shows the apartment layout on the 25th floor, which serves as the benchmark for evaluation and validation. The apartment has three different facade orientations: South, East and West. The living room (84m<sup>2</sup>) was selected for testing as it faces the west and south facades, representing the most challenging scenario with maximum sun exposure. As a result of the intense penetration of solar heat through these orientations, overheating and potential discomfort for residents are expected to increase.

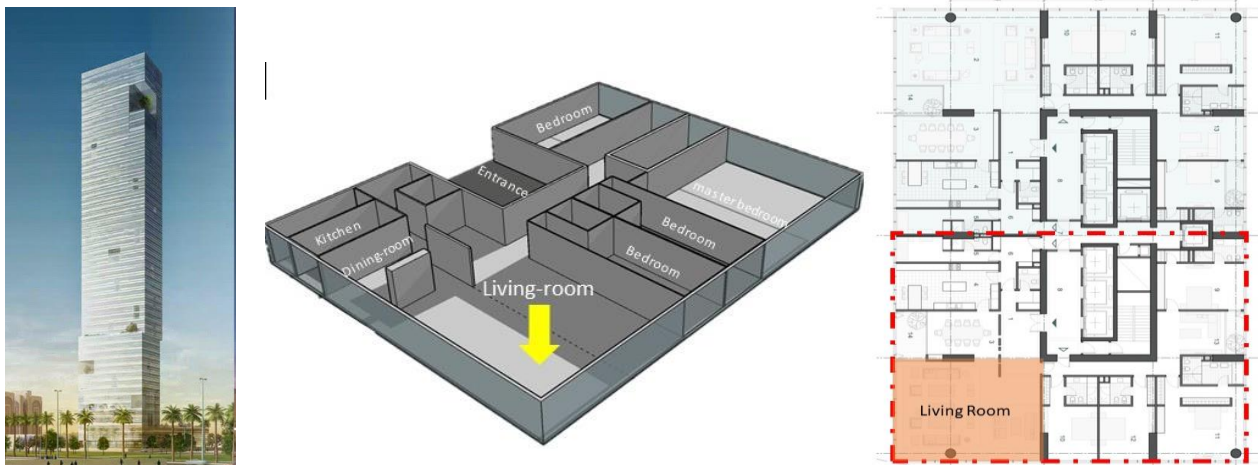


Figure 6 The layout and viewpoint of a skyscraper residence in Jeddah

The study conducted a detailed modelling of the living room, including its details, layout, building materials, interior finishes, lighting, and occupancy. These data were collected through site observations, resident interviews, and project management records. The thermal properties and construction materials of the existing apartment are applied. In addition, internal heat gain data was obtained from the ASHRAE Guide to ensure precision in the simulation. According to an operating profile, lighting, appliances and people (parents with three children), all contribute to the modelling of internal heat gain.

### 3.4. The Responsive Shading Operating Times

The responsive sun shading system uses an innovative SMP material as an actuator, dynamically adjusting to outdoor variables like solar radiation and air temperature. The switch system's open and closed mechanism is controlled through the IES-VE software using external louvre features and operational profile settings with control thresholds to calculate an operating schedule. The operational profile function in IES-VE manages this process with a daily thermal template manager defining the system's state control based on a thermal activation threshold. Three distinct activations guide the system's behaviour: operation based on outside air temperature ( $\geq 33\text{ }^{\circ}\text{C}$ ), operation based on direct solar radiation ( $\geq 275\text{ W/m}^2$ ), and a combination of both factors. Moreover, in the final step of the setting process, the exterior shading for the living room is selected using the project construction tool. The louvres respond to climatic activation factors based on control settings, enabling them to open or close accordingly. For instance, if the outdoor temperature exceeds  $33\text{ }^{\circ}\text{C}$ , the louvre device will be lowered and set to 0, providing maximum shading. Conversely, when the outdoor temperature falls below  $33\text{ }^{\circ}\text{C}$ , the louvre shading will increase and be set to 1, allowing more natural light and ventilation.

The following schedule outlines the operation of the responsive sun shading system based on the thermal activation described above. Figure 7 illustrates the dynamic behaviour of the shading system's operation on the west and south facades, estimated for August 24. Daily fluctuations influence the switching behaviour of the adaptive façade shading system in climatic conditions and activation thresholds. On the south face, the operating time shows that the adaptive shading will be closed for 8 hours between 8 a.m. and 16:00 and remain open for the rest of the day if the combination scenario is implemented. Alternatively, if the solar radiation activation scenario is selected, the system will be closed for 3 hours between 11:00 a.m. and 14:00 but remain open for the rest of the day. Lastly, the air temperature scenario will be closed for the entire day, except for 7 hours between 1 a.m. and 8:00 a.m. to be open.

However, the west façade timetable shows the exact period of operation by 8 hours in the combo scenario, while the closure time changed between 9:00 a.m. and 17:00. Furthermore, the air temperature-driven activation timeframe for adaptive shading aligns with that of the southern facade. However, there is a slight difference in the solar radiation scenario; the closure time is from 13:00 to 17:00, an hour longer than the southern facade.

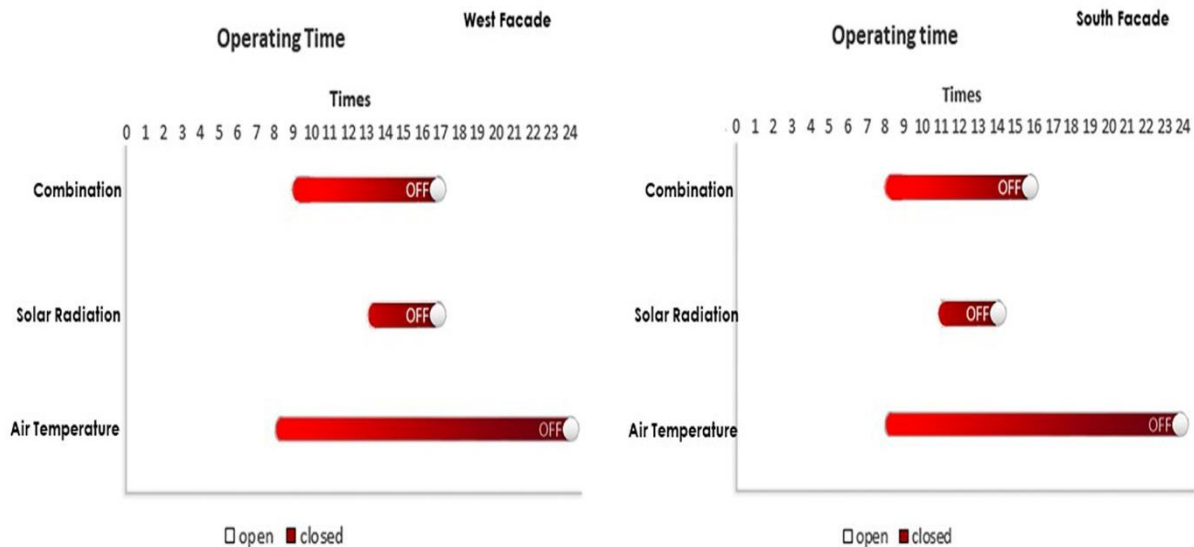


Figure 7 The system operating timeline under various activations on August 24

## 4. RESULTS AND DISCUSSION

The results validated the thermal performance of the adaptive facade by comparing it with the bare glazing facade on August 24, the hottest day. The study aimed to assess the efficacy of thermal activation factors by focusing on temperature control and energy savings. The assessment considered three activation scenarios: air temperature, solar radiation, and a combination. The living room was evaluated using IES-VE simulation with ApacheSim and Sun-Cast's model. The simulation calculated room temperature and thermal comfort under various climate control strategies, with the cooling system turned off to avoid interference with the overheating assessment. However, to evaluate the overall building performance, the cooling system was activated to a set temperature of  $23\text{ }^{\circ}\text{C}$ , following ASHRAE Standard 55 for indoor thermal comfort. Energy consumption and cooling load were analysed to determine the efficiency of the adaptive shading system. These results provide valuable insights into the effectiveness of activation parameter strategies considering thermal and energy efficiency.

On August 24, the study evaluated various thresholds for occupant comfort and energy efficiency. Relying on a single activation (e.g., a  $33^{\circ}\text{C}$  air temperature threshold) or solar radiation threshold ( $275\text{ W/m}^2$ ) was insufficient. However,



combining these thresholds resulted in an optimal operating schedule for 8 hours, achieving the desired balance between comfort and energy savings. The adaptive system effectively provides shading when needed, mitigating glare during intense solar radiation periods. This approach reduced solar gain, indoor temperature, and cooling demand and improved energy efficiency.

#### 4.1. Thermal Comfort Evaluation

##### Interior Temperature

In hot climates, controlling indoor temperature is vital for occupant comfort. Excessive solar gain leads to higher indoor temperatures, discomfort, and health risks due to heat. Responsive shading regulates solar gain and building temperature. This research employed operating temperature, which included air and average radiant temperature, to represent inside temperature. The simulation results of the three shading control factors were compared with a reference model of a living room that faces both south and west. This was done to see which factor improved the adaptive system's performance and energy. Simulations were conducted on August 24, a summer day, at various times (6 a.m., 9 a.m., 12 p.m., 3 p.m., and 6 p.m.) to account for the influence of solar gain at different periods.

The simulation results demonstrate the effectiveness of responsive shading activation variables in decreasing interior temperature throughout the day compared to the baseline facade. Figure 8 compares the current façade and the adaptive shading controlled by three different scenarios of climate variables in the operative temperature of the living room. The results showed that the combination scenario had the most notable improvement in indoor temperature and reduced overheating in the living room, followed by the air temperature scenario, while the solar radiation scenario was the worst, showing no change in the living room at any time. Table 4 illustrates that the combination scenario in the living room on August 24 achieved the most significant reduction in average indoor temperature, decreasing from 40.5°C to 35.3°C, resulting in a 5.2°C difference. At 9 a.m., the indoor temperature saw the highest reduction of 20%, dropping from the reference of 40.2°C to 31.9°C, representing an 8.3°C decline. Moreover, the living room's base model recorded a maximum temperature of 41.5°C at 3 p.m., while the combination scenario improved the temperature to 38.6°C, showing a difference of approximately 2.9°C, around 7%.

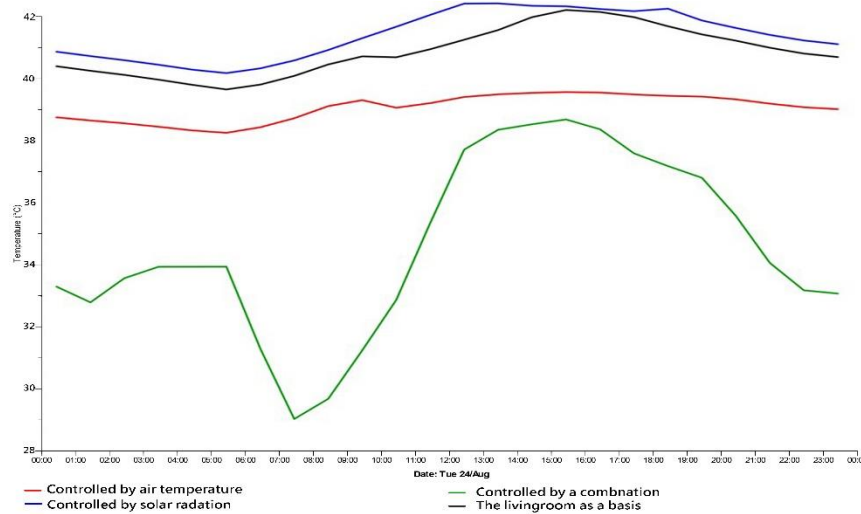


Figure 8 Interior temperature in baseline Vs. Adaptive shading by activation parameters on August 24

Table 2: Interior temperature in baseline Vs. Adaptive shading by activation parameters on August 24.

Type of Space	Living room °C					
	Time	6 a.m	9 a.m	12 p.m	3 p.m	6 p.m
The basic case		39.5	40.2	40.7	41.5	41.3
The Air Temperature		38.4	39.1	39.2	39.4	39.3
The Solar Radiation		40	40.5	41.3	41.7	41.5
The Combination		33.7	31.9	36.9	38.6	37.6

## Discomfort Hours

This study conducts the adaptive comfort method to evaluate overheating and discomfort hours, considering the dynamic interaction between occupants and the local climate. It offers a more flexible approach to thermal comfort. Based on the Nicol TC equation and using the mean outside temperature of August as a reference, the adaptive comfort levels in this study range from 33.3°C to 29.3°C. The operative temperature, which considers both air temperature and mean radiant temperature, is a helpful indicator for assessing interior comfort. Comparing adaptive facade activation options in the living room and bedroom helps identify the most effective solution for improving thermal comfort. Figure 9 compares hours above the comfort level in the living room on August 24.

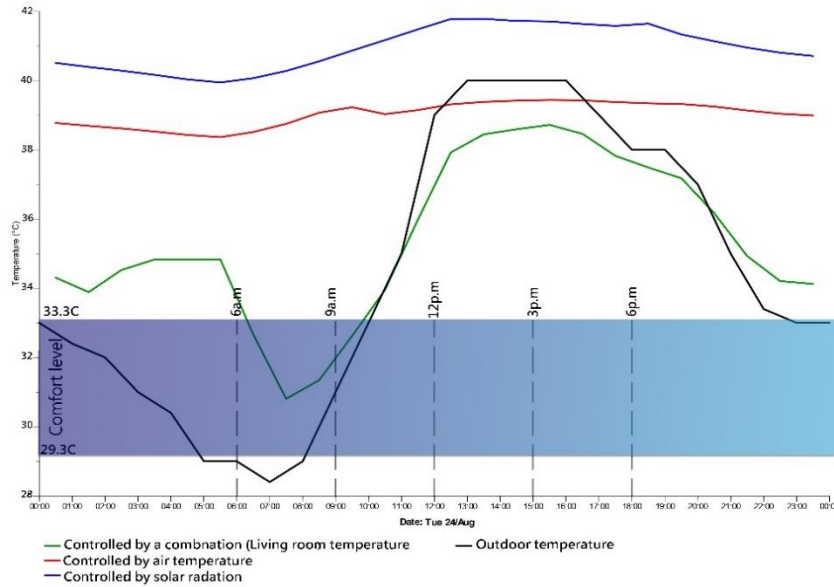


Figure 9 Comparing living room comfort hours under varying activation parameters on August 24

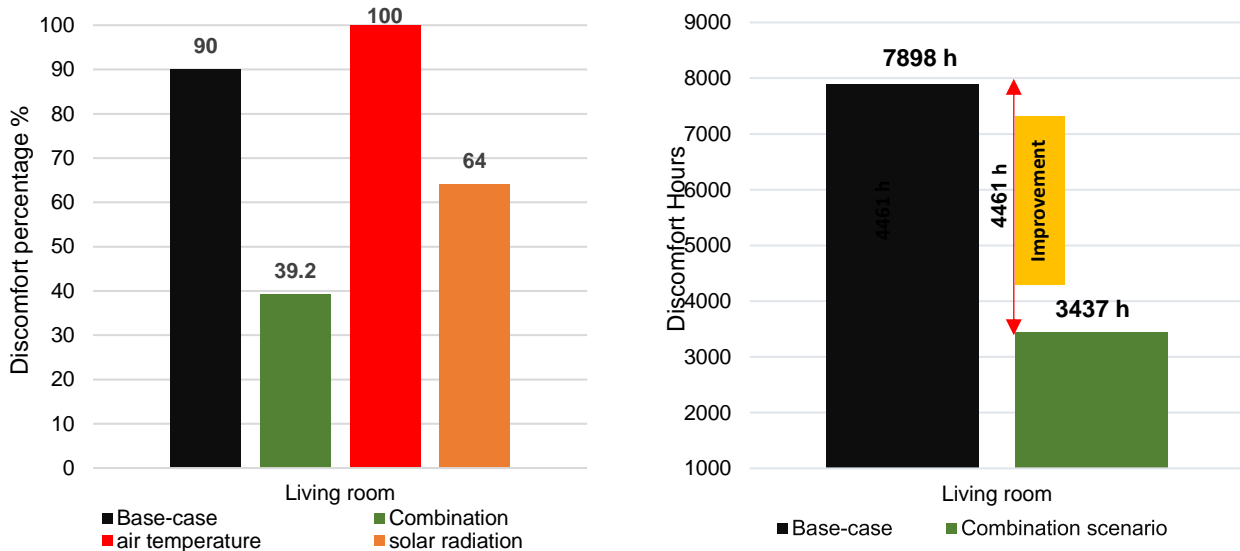


Figure 10 Comparing yearly discomfort ratios and improvement hours

Figure 10 demonstrates that the baseline living room had a discomfort ratio of 90% annually. Implementing the combined scenario leads to a substantial improvement in comfort hours, increasing them by 50.8%. This improvement in the integrated strategy amounts to 4644 hours out of 8760 occupation hours. Considering solar radiation, the second scenario also increases comfort hours by 26%. However, the air temperature scenario worsens comfort hours, increasing discomfort.

## 4.2. Energy Efficiency Evaluation

### Cooling Loads

Energy efficiency in hot climates is achieved by reducing cooling demand to maintain interior comfort. The simulation results demonstrate that the responsive sun shading system effectively reduces the solar heat gain and indoor temperature, reducing the cooling load. On August 24, the combination scenario resulted in the most effective cooling reduction in the living room. Figure 11a compares the cooling loads of the adaptive glazed facades activated by various environmental variables in the living room. The adaptive shading, triggered by the combination, reduced the cooling load by 38.5%, from (59.3 kWh) to (36.7 kWh). Followed by the air temperature control led to a 29% reduction to (42.1 kWh), while the solar radiation scenario resulted in a 21% reduction to (46.8 kWh). However, Figure 11b shows the annual cooling load (kWh) difference between the baseline and adaptive facades in the living room and bedroom. The adaptive system with integrated parameters achieved the highest reduction of 52% in the living room (6,882 kWh) and 40% in the solar radiation scenario (8,605 kWh). The air temperature scenario, with the lowest reduction, resulted in a 22% decrease in cooling load (11,185 kWh).

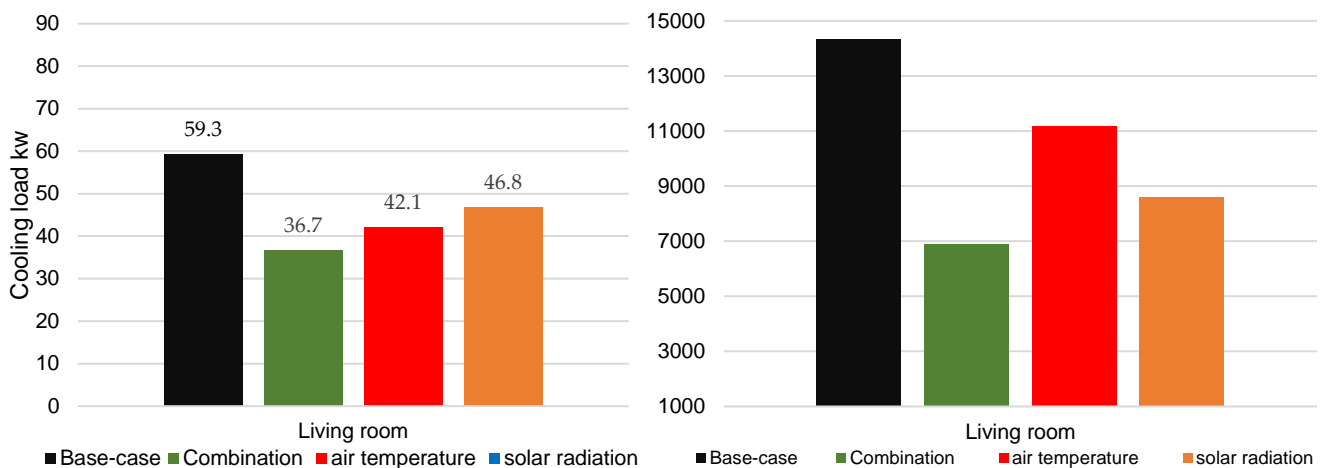


Figure 11 Cooling load in the base case Vs adaptive shading under all activations (a-left on August 24, b-right yearly)

## 5. CONCLUSION

This study focused on incorporating the smart thermoresponsive SMP actuator-based adaptive shading system cornubite to optimise energy efficiency and enhance thermal comfort for new buildings and retrofitted energy projects. Through extensive simulations using IES-VE software, we evaluated various activation scenarios, such as solar radiation-based, air temperature-based, and a combination of both, to determine the most effective approach. By utilising the capabilities of the responsive sun, shading dynamically responds to changes in environmental conditions, adjusting shading to optimise indoor comfort and energy usage. On the hottest day, the system demonstrated a remarkable 6°C reduction in the mean indoor temperature, resulting in improved hours of thermal comfort by 4644 hours out of 8760 occupation hours and significantly reduced cooling energy consumption. Implementing this energy-conserving approach can lead to substantial annual energy savings of approximately 39% and a decrease of 3,800 kg of CO<sub>2</sub> emissions for newly constructed buildings and retrofitted energy projects.

However, this study acknowledges certain limitations, such as evaluating daylighting performance constrained by the current capabilities of the IES-VE software. To address these limitations, future research should focus on scaling up the implementation of adaptive facades in real-world contexts to assess their long-term performance. Combining alternative simulation tools with innovative material properties can further optimise the thermal response of SMP materials. Continuous monitoring and feedback from occupants will be vital in refining the system's operation, striking a balance between comfort and energy efficiency. Additionally, incorporating natural or mechanical ventilation calculations will enhance thermal comfort and overall building performance for new and retrofitted energy projects.

## 6. REFERENCES

- Aelenei, D., Aelenei, L. and Vieira, C. P. (2016) 'Adaptive Façade: Concept, Applications, Research Questions', *Energy Procedia*, 91, pp. 269–275. doi: 10.1016/j.egypro.2016.06.218.
- Alnuaimi, A. N. and Natarajan, S. (2020) 'The energy cost of cold thermal discomfort in the global south', *Buildings*, 10(5). doi: 10.3390/BUILDINGS10050093.
- Attia, S. (2018) *Regenerative and positive impact architecture: Learning from case studies*. New York City. doi:

10.1007/978-3-319-66718-8.

Battisti, A., Persiani, S. G. L. and Crespi, M. (2019) 'Review and mapping of parameters for the early stage design of adaptive building technologies through life cycle assessment tools', *energy*, 12(9). doi: 10.3390/en12091729.

Beites, S. (2013) 'Morphological behavior of shape memory polymers toward a deployable, adaptive architecture', *ACADIA 2013: Adaptive Architecture - Proceedings of the 33rd Annual Conference of the Association for Computer Aided Design in Architecture*, pp. 121–128.

Bonser, S. *et al.* (2019) 'Biomimetic adaptive building skins : Energy and environmental regulation in buildings Energy & Buildings Biomimetic adaptive building skins : Energy and environmental regulation in buildings', *Energy & Buildings*, 205(October), p. 109544. doi: 10.1016/j.enbuild.2019.109544.

Elnaklah, R. *et al.* (2021) 'Thermal comfort standards in the Middle East: Current and future challenges', *Building and Environment*, 200(May), p. 107899. doi: 10.1016/j.buildenv.2021.107899.

Evola, G., Gullo, F. and Marletta, L. (2017) 'The role of shading devices to improve thermal and visual comfort in existing glazed buildings', *Energy Procedia*, 134, pp. 346–355. doi: 10.1016/j.egypro.2017.09.543.

Felimban, A. *et al.* (2019) 'Assessment of current energy consumption in residential buildings in Jeddah, Saudi Arabia', *Buildings*, 9(7). doi: 10.3390/buildings9070163.

Li, J. *et al.* (2018) 'Applications of shape memory polymers in kinetic buildings', *Advances in Materials Science and Engineering*. Hindawi Limited. doi: 10.1155/2018/7453698.

Loonen, R. C. G. M. *et al.* (2013) 'Climate adaptive building shells : state-of-the-art and future challenges', 25, pp. 483–493.

Ministry of Housing (2019) *Mostadam Rating System for Residential Buildings D + C*. Available at: <https://www.mostadam.sa/uploads/2019/09/5d91b53e0b866.pdf>.

Neuhaus, R. *et al.* (2020) 'Integrating Ionic Electroactive Polymer Actuators and Sensors Into Adaptive Building Skins – Potentials and Limitations', *Frontiers in Built Environment*, 6(July), pp. 1–22. doi: 10.3389/fbuil.2020.00095.

Nezamdoost, A., Van Den Wymelenberg, K. and Mahic, A. (2018) 'Assessing the energy and daylighting impacts of human behavior with window shades, a life-cycle comparison of manual and automated blinds', *Automation in Construction*, 92(April), pp. 133–150. doi: 10.1016/j.autcon.2018.03.033.

Oh, M. H., Lee, K. H. and Yoon, J. H. (2012) 'Automated control strategies of inside slat-type blind considering visual comfort and building energy performance', *Energy and Buildings*, 55, pp. 728–737. doi: 10.1016/j.enbuild.2012.09.019.

Passive House Institute (no date) 'Criteria for Buildings Passive House – EnerPHit –PHI Low Energy Building', (January). Available at: [www.passivehouse.com](http://www.passivehouse.com).

Santo, L. *et al.* (2020) 'Applications of Shape-Memory Polymers, and Their Blends and Composites BT - Shape Memory Polymers, Blends and Composites: Advances and Applications', in Parameswaranpillai, J. *et al.* (eds). Singapore: Springer Singapore, pp. 311–329. doi: 10.1007/978-981-13-8574-2\_13.

Szokolay, S. (2014) *Introduction to ARCHITECTURAL SCIENCE the basis of sustainable design*. 3rd Editio. London. doi: <https://doi.org/10.4324/9781315852409>.

Tabadkani, A. *et al.* (2021) 'Design approaches and typologies of adaptive facades: A review', *Automation in Construction*, 121(November 2020), p. 103450. doi: 10.1016/j.autcon.2020.103450.

Yoon, J. (2019) 'SMP Prototype Design and Fabrication for Thermo-responsive Façade Elements', *Journal of Facade Design and Engineering*, 7(1), pp. 41–61. doi: 10.7480/jfde.2019.1.2662.

Yoon, J. and Bae, S. (2020) 'Performance evaluation and design of thermo-responsive SMP shading prototypes', *Sustainability (Switzerland)*, 12(11). doi: 10.3390/su12114391.

Yun, G., Park, D. Y. and Kim, K. S. (2017) 'Appropriate activation threshold of the external blind for visual comfort and lighting energy saving in different climate conditions', *Building and Environment*, 113, pp. 247–266. doi: 10.1016/j.buildenv.2016.11.021.

---

# #283: Interpretable data-driven methods to automate energy model calibration

## Southampton UK Highfield Campus study case

---

Karla M. GONZALEZ-CARREON<sup>1</sup>, Massimiliano MANFREN<sup>2</sup>

<sup>1</sup> Faculty of Engineering and Physical Sciences, University of Southampton Boldrewood Campus SO16 7QF, UK,  
k.m.gonzalez-carreon@soton.ac.uk

<sup>2</sup> Faculty of Engineering and Physical Sciences, University of Southampton Boldrewood Campus SO16 7QF, UK,  
m.manfren@soton.ac.uk

*Abstract: In the journey towards zero emissions, the energy transition is a fundamental aspect of the transformation, and the construction industry is one of the most significant contributors to carbon emissions. Due to the magnitude of investments required to meet decarbonisation objectives and to achieve them within given temporal constraints, we must engage in medium/long-term planning. Consequently, a more in-depth understanding of energy consumption is required to facilitate effective decision-making and reduce uncertainty, which could undermine the effectiveness and credibility of measures. The present project leverages interpretable data-driven methods applied to building energy analytics. The case study is the Highfield Campus of the University of Southampton, where 48 buildings are currently served by a natural gas-fueled Combined Heat and Power (CHP) and District Heating (DH) system. As part of the research, individual energy signature models have been developed for the buildings monitored and the entire district energy system (CHP, DH). The observed data cover the periods before, during and after the COVID-19 pandemic, from 2017 to 2022. Two primary results have been achieved. First, by creating a novel formulation of energy signature regression, it is possible to find the best-fitting models and efficiently determine the actual building balance points (for degree-days consumption normalisation). The second was a counterfactual analysis of energy consumption patterns before, during, and after COVID-19 to detect potential changes. Future research will develop digital twins of building models that can analyse data at varying temporal and spatial resolutions to support the University's decarbonisation strategy.*

*Keywords: data-driven methods, interpretability, regression-based approaches, measurement and verification, energy analysis*

## 1. INTRODUCTION

According to the United Nations, climate change has become the main challenge that humankind has faced. The common goal to avoid a climate disaster is to reduce emissions and implement the net-zero policy (United Nations, 2023). Greenhouse gas (GHG) emissions are primarily caused by the energy sector, which accounts for about 75% of global emissions (IEA, 2023). In addition, approximately 80% of the world's energy supply is derived from fossil fuels such as natural gas, oil, and coal (IEA, 2020). Hence, energy transition is a priority. However, the urgency to cease the complete use of fossil fuels technologies and to implement decarbonisation measures led to reinventing energy efficiency implementations considering challenges such as renewables investments, energy efficiency and storage (Rosenow & Eyre, 2022). Still, there is the question of how to implement decarbonise measures in the building sector due to uncertainty in achieving optimal balance process and the problems related to the choice between investment in efficiency measures (i.e. reduction of demand) versus decarbonisation of supply (Rosenow & Hamels, 2023).

Therefore, it becomes necessary to look up a transformation that leads us to establish plans to focus on decarbonization for energy transitions and electrifications (Carayannis et al., 2012). Carayannis highlighted the necessity of radical shifts that could lead to different innovations (Elias G. Carayannis, 2011), and those shifts require flexibility and an improvement in the control energy demand to respond according to customer needs, grid conditions, climate (Junker et al., 2018). Those changes directly impact the energy demand, which is calculated to increase space cooling by over triple by 2050 (Gi et al., 2018; Isaac & van Vuuren, 2009). Energy transitions represent a complete change of mindset that requires a long-term planning perspective, then energy demand understanding becomes crucial. Staffell displayed that the way to reach a successful global energy transition is by understanding where, when and how much energy is required in a trusty and accurate way (Staffell et al., 2023).

## 2. LITERATURE REVIEW

Improving our understanding of energy demand in buildings is crucial for making better decisions and implementing solutions towards energy efficiency, M&V performance gaps, and renewable energy installation (de Wilde, 2014) (Omarov et al., 2023). The opportunity for improving this sector impacts the built environment in terms of raw resources, energy, and carbon emissions (Berardi, 2017), to exploit innovative technologies towards circular economy implementations (Barrie et al., 2017), and considering the fundamental domains as project, product, and services (Thuesen et al., 2018). Residential buildings are one of the biggest challenges due to the outsized influence of the stochastic nature of human behaviour (Kazmi et al., 2023). Additionally, weather and occupant behaviour have an impact on heating and cooling demand, which could vary over space and time (Pfenninger & Staffell, 2016), and an improvement in reducing thermostat changepoints could bring clear benefits such as lower energy bills, faster emissions savings compared with retrofit (Waite & Modi, 2020).

There are two main issues regarding energy and buildings, as identified by various authors. The first problem is that there needs to be a better understanding of our energy demand as consumers since it is non-stochastic data and varies significantly based on a person's lifestyle or end-use at a large scale (Manfren & Nastasi, 2019). The second problem is that the lack of data and understanding makes it very complicated to have an accurate representation of the energy demand for a single building (Andriamamonjy et al., 2019). As a result, it is crucial to have high-resolution energy demand data. According to Kazmi, energy demand forecasts could be used as a baseline for verification purposes, to optimize energy consumption and generation in real-time, for planning and operation of the grid, and for designing policies, model-driven optimization approaches to minimize emissions, costs, or grid impacts, to help predict cross-sectorial issues, and to reduce risks and implement better M&V and O&M (Kazmi et al., 2023). For these reasons, it is essential to create models that could facilitate energy demand, and advanced M&V 2.0 technologies are necessary (Granderson & Fernandes, 2017).

In order to create accurate energy predictions, different types of models have been classified. Paulus divided M&V's advanced mathematical techniques into three main classifications: white-box, grey-box, and black-box models (Paulus et al., 2015). Meanwhile, Staffell classified the four most common approaches for modelling energy demand in buildings into physical, statistical, surrogate and degree-days models (Staffell et al., 2023). The importance of creating these models is to gain a fair representation that allows for a better understanding, assessment, and prediction of energy demand. However, this process is complex as it involves multiple disciplines such as energy, buildings and infrastructure, computer sciences, and control processes. As Sibilla stated, this innovative process aims to create an interdisciplinary research environment (Sibilla, 2017).

Based on the different types of models, it was detected that essential features should be straightforward interpretation, trusty, simple, and facilitate comprehension. At this point, it is highlighted the necessity to have interpretability. *Interpretability* is an algorithm that could be logically inspected and can be understandable outputs by humans (Manfren et al., 2022). Rudin et al. also pointed out that choosing interpretability for a forecast model is extremely important to help the training and inference phase (Rudin et al., 2022). The nature of interpretability models is white-box type based on physical laws (Michalak, 2019). Therefore, some interpretable models can be easily understood by humans, like linear multivariate regression models (Asadi et al., 2014; Hygh et al., 2012; Lam et al., 2010) and decision trees (Ahmad et al., 2017; Araya et al., 2017).

This point becomes the essential part of this research, highlighting why working with interpretable data-driven energy demand modelling in buildings is crucial. As Nastasi stated, this new approach of rethinking energy efficiency requires a better understanding of the electricity and thermal profiles at hourly intervals using interpretable, reliable, and

straightforward techniques, with this data-driven modelling scope (Nastasi et al., 2022). The linear regression and change-point analysis methods are the main ones to consider for this research. Measurement and Verification (M&V) protocols are necessary due to their applicability to orient practical solutions created by various methods and best practices. The main reason is that the M&V scope is verifiable by different international protocols such as ASHRAE 14:2014 (ASHRAE, 2014), Efficiency Value Organization (EVO), and the International Performance Measurement and Verifications Protocols (IPMVP) (International EVO., 2017), Federal Energy Management Program (FEMP), and Investor Confidence Project (ICP). Those methods proposed have become a de-facto standard approach in measurement and verification (M&V), trusted based on field testing with rigorous rules (Kim & Haberl, 2018a, 2018c). Additionally, open-source software projects have been developed in recent years that contributes to the modelling integrated process such as Caltrack of the OpenEEMeter (OpenEEMeter, 2023), RMV2.0 (LBNL Energy Technologies Area, 2023), NMECR (KW Engineering, 2023), ECAM (SBW Consulting, 2023), etc.

Change-point models, also known as piecewise linear regression models (Paulus et al., 2015), become crucial because of their application first to predict heating and cooling energy consumption, second to estimate the balance point temperature (Hammarsten, 1987; Masuda & Claridge, 2014; Rabl & Rialhe, 1992) and finally, as part of the normalization measures for energy performance and applications (Kim & Haberl, 2018b). The change point models' process helps determine the energy signature and outdoor temperature coefficients (Paulus, 2017). The main input feature is the energy signature, which is the average power of the energy demand in an interval analysis, and the balance point temperature is the output variable of the temperature that is not needed for heating or cooling (Manfren et al., 2022). This model aims to impact directing on reducing the change points of gas demand in different scales (Kikstra et al., 2021).

Several authors have identified gaps in this field. For instance, there is an opportunity to create a consensus for modelling and techniques for the energy fields and building stock and at multiple scales for energy metering data (Grillone et al., 2020). They also generate a harmonized, temporally, and spatially scalable technique for large-scale analysis and long-term impact, enhancing transparency, comparability, and applicability (Spinoni et al., 2018), considering buildings energy performance (Omarov et al., 2023). Miller et al. distinguished that models should incorporate dynamic data sources and detect systematic disruptions (Miller et al., 2022). Staffell et al. associated generating high-resolution time series of demand could be used for system sizing to assess the need for infrastructure in national electricity systems and identified that few tools are available to study heating and cooling in an enormous scope (Staffell et al., 2023) to determine adequate space and time savings. Finally, Kazmi et al. concluded that no methodology, system, or process can help forecast models and unify energy demand to guide (Kazmi et al., 2023).

The model's analytics can effectively tackle the problems discussed in the introduction and provide a robust baseline for the case study (Qaisar & Zhao, 2022). Based on the literature review, it was identified that there is a gap in having automated models for energy analytics with a cross-sectorial perspective that considers physical constraints (Tronchin et al., 2019). It is possible to increase the level of automation and, at the same time, transparency. Also, considering information related to energy analytics and physical constraints, as shown in (Manfren et al., 2021)).

### 3. METHODS

Overall, the interpretable data-driven method is applied to building energy analytics. Two main methods with different approaches were used for this analysis. Starting in section 3.1 explains the automated code model. Then, the following section 3.2, defines the change-point regression method, which represents the basic model of analysis for energy consumption in the buildings. The second one will be described in section 3.2, the counterfactual analysis before, during and after COVID-19.

#### 3.1. Automated code model

This study aims to build a code model that can automatically be analysed using dynamic balance point analysis in Python and R. It assists in identifying the most suitable models and determining the most effective balance point for each building. Automating the process of finding the best-fitting models for dynamic analysis with different inputs, balance points, and analysis methods is crucial. Many authors have already applied and validated these models over the years. However, there is still more to explore in terms of practical applications. The goal is to take it further and devise a way to integrate all these features.

The following figure shows the process for the model with three main stages. The first stage is the input variables: the energy signatures and the out-air temperature. The second stage is the model itself, divided into three levels oriented to the 3P change point model. The first is to have the data sets divided in the period needed. It could be per building, per year, per type of benchmark, or counterfactual analysis. The second level is to make a loop for different balance points and select the best one based on the statistical evolution. Finally, the last level is the model. The main output variables obtained in this process are the best balance point, the coefficients model for a calibrated model, and a range of values based on the mean and the standard deviation.

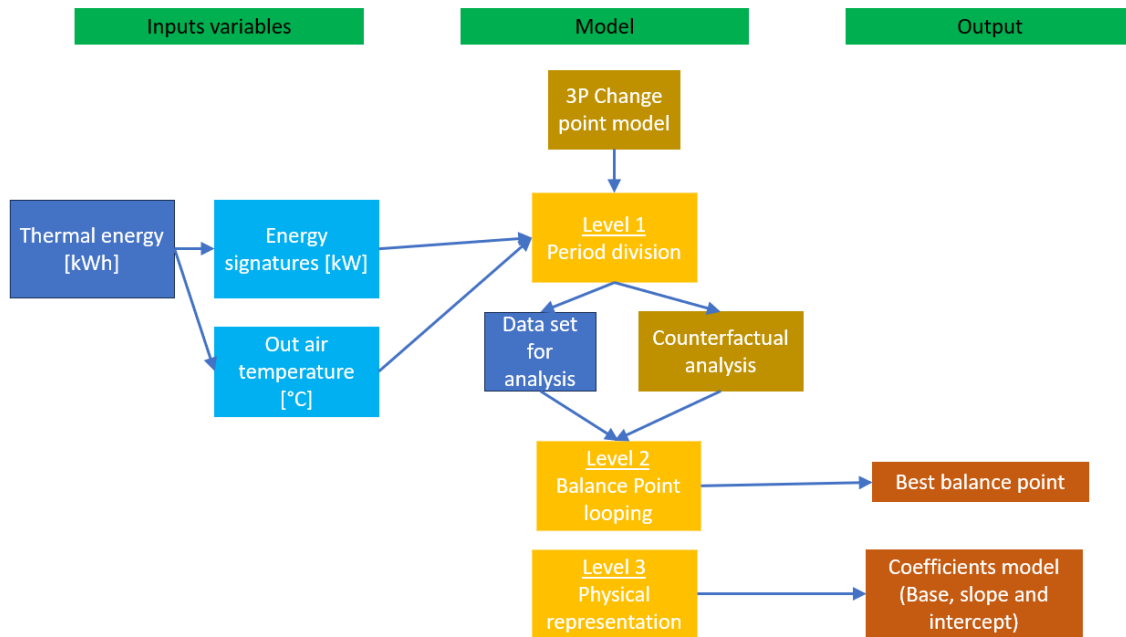


Figure 1 Flow diagram process.

### 3.2. Change-point regression method

This research uses a method called change-point regression to predict building energy consumption. The method uses dummy variables and interpretable regression-based analysis to generate piecewise linearization. This technique is widely used and is supported by variable-based degree-days regression algorithms and part of ASHRAE 14:2014. Specifically, the 3P change point is used for a heating model for CHP data.

The first approach was to combine the M&V measures and the equations with physical information that could be fundamental for a deeper understanding of the building. The step is to leverage the intercept and slope coefficients into possible physical interpretation to extract more information from the existing data and give those models practical visualisations. The next figure represents the three main coefficients based on the energy signature and outdoor air temperature.

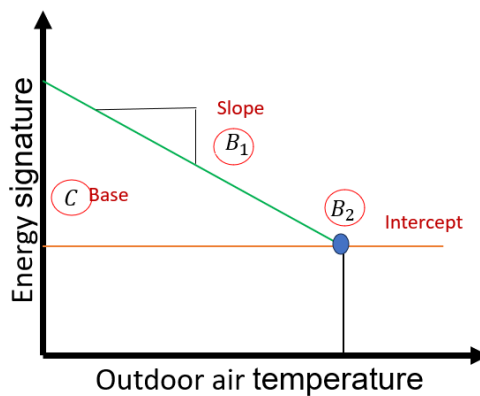


Figure 2 IMP change point model 3P heating models.

Equation 1: The mathematical model form for the 3P for heating

$$3P - H: E = C + B_1(B_2 - T)^+$$

Where:

- C is a Constant
- E is energy use
- T is the outdoor air dry-bulb temperature
- B's are regression coefficients.
- ( )<sup>+</sup> The parenthetic term evaluates to a negative number it is set to 0.



In this research, the E is the energy signature, the average power in a specific analysis interval, and the T is the outdoor temperature as the independent variable. Thanks to this step, the input data is normalised and eases the process to afterwards comparisons. These models are combined into different sub-models by introducing additional variables with dummy or 0-1 binary variables to the original datasets. Therefore, the dummy variable was a function of analysis to observe if the outdoor temperature was equal to or below the dynamic balance point. The balance point is when a building does not require heating or cooling, and it was a dynamic balance point analysis to get the best-fitted predicted model for each building. Highlighting dummy variables allows the piecewise form to adjust other behaviours in the same equation.

The result of the piecewise linear model combining Equation 1 for 3P change-point linear regression for heating with dummy variables helps to adjust the physical behaviour that the buildings have, considering the three coefficients set to real constraints such as the range of balance points allowed to be considered. These models' versatility, transparency and continuity aim for a better-fitted representation of the data and, therefore, contemplate the physical basis and interpretable outlook. Those ranges allow us to explore and reduce uncertainty and provide accurate predictions. Equation 2 shows the predicted model explained above.

Equation 2: Predicted model.

$$P_{model} = C + B_2 * \sum D_v + B_1 * \sum D_t$$

Where:

- $P_{model}$  is the predicted model output (kW)
- $C$  is the Base coefficient (°C)
- $B_2$  is the Intercept coefficient (kW/°C)
- $D_v$  is the Dummy variable dynamic balance point (°C)
- $B_1$  is the Slope coefficient (kW/°C)
- $D_T$  is the Dummy temperature dynamic balance point (°C)

Additionally, to measure the predicted model's performance, statistical indicators aimed to evaluate the models' adaptability based on ASHRAE 14:2014. For monthly data, the metric used was the minimum RMSE, and to select the calibrated models was CV(RMSE).

Equation 3: Root-mean-square error

$$RMSE = \sqrt{\frac{\sum_1^n E_i^2}{n - p}}$$

Equation 4: Coefficient of Root-mean-square error

$$CV(RMSE) = \frac{RMSE}{A} * 100$$

Where:

- E = Predicted – Measure models
- A is the average of the measured energy data.
- n is the total data

### 3.3. Counterfactual analysis

The counterfactual analysis is a way to track energy performance by comparing two different periods. This approach is widely used to standardise M&V and energy monitoring systems for energy models. In this case, the analysis has three periods: before, during and after COVID-19 to gain a better understanding of potential behavioural changes and shifts that occurred in the operation of the building. Those monthly periods are considered as follows:

Table 1: Counterfactual analysis periods.

Period	Dates	Notes
1. Before COVID-19 lockdown	From January 2017 to February 2020	Students and staff worked in presential schedules
2. During COVID-19 lockdown	From March 2020 to March 2021	Hard lockdown with no presence allowed, and after few allowed to enter buildings. Lectures were online.
3. After COVID-19 lockdown	From April 2021 to December 2022	Hybrid new normality between working home and office. Lectures are presential.

One of the most significant advantages of this method is that it enables comparisons of a building's performance under the same conditions, although there are different periods.

#### 4. CASE STUDY DESCRIPTION

The case of study is the central campus, “Highfield campus” of the University of Southampton in the southeast part of England, United Kingdom. There are three main features to highlight about this place.

- The Highfield campus has 48 buildings with different types of end-use purposes. Those purposes vary between academic purposes, such as lecture rooms or laboratories, and non-academic, such as administration and catering.
- Most of the buildings, in particular the largest ones, are connected to a District Heating (DH) system which is supplied by a natural gas fuelled Combined Heat and Power (CHP) with auxiliary boilers.
- Buildings not connected to CHP use natural gas boilers for heating.



Figure 3 Highfield campus 48 buildings University of Southampton UK (University of Southampton, 2023)

The following table shows the main features and characteristics of this case study. The main goal of this study is to have an interpretable data-driven model that could be applied to different study cases, so it becomes fundamental to identify the main input variables. Further, summarize to have a general process to apply to the 48 buildings independently.

Table 2: Input variables for the model.

Features	Characteristics	Notes
Spatial scale	Single buildings	48 buildings
Spatial scale	Cluster per type of benchmark	11 types
Temporal scale	Monthly data	
Temporal scale	Years	2017-2022
Energy input	Thermal CHP/DH	kWh
Energy input	Electricity	kWh
Other variables	Out air temperature	Monthly °C
Other variables	Occupancy	*
Other variables	Costs	Monthly \$

## 5. RESULTS AND DISCUSSION

### 5.1. Change-point regression method

The work was to determine the best balance point by an automated process. This analysis aims to know each building's most efficient balance point for the operation to help M&V. It was a dynamic balance point analysis to get the best-fitted predicted model for each building. The idea was to have a first approach to find a baseline to automate the 48 buildings to have each coefficient based on fitted balance points applying 3P change point linear regression models.

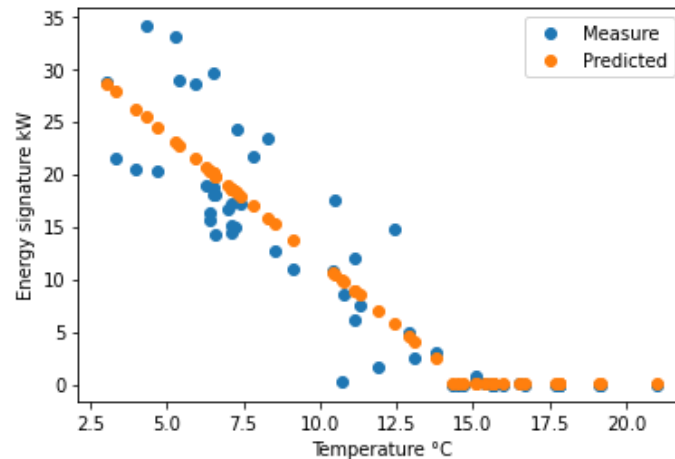


Figure 4 Sample measure vs. predicted data building 1

As preliminary results of the automated process, it was found physical constraints of the building with the optimized balance point. Thanks to the predicted models calculated above, it has interpretable results showing that 58% of the building's optimum balance point is below the UK's mean of 15.5 °C. The results represent an interesting outlook through analytics for modelling that allow us to obtain more contextual information. For instance, the direct meaning of this first sight is that the lower temperature is the balance point representing less natural gas consumption and, therefore, less GHG emissions.

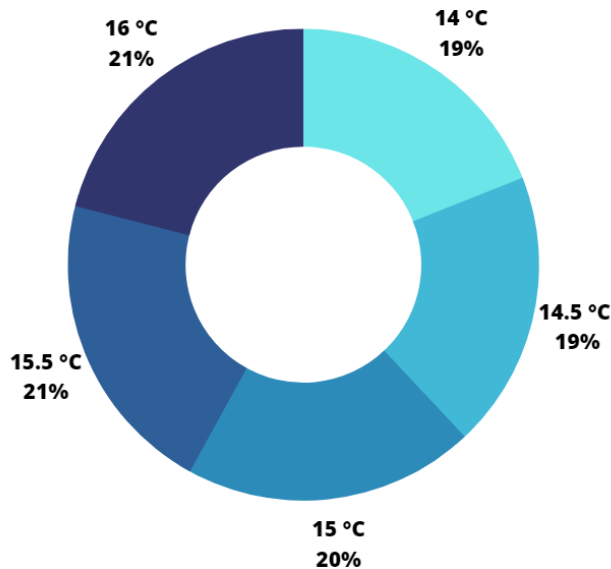


Figure 5 Different balance point results

### 5.2. Counterfactual analysis

The second part is the counterfactual analysis, which is based on the change point methodology explained before but considers three different energy consumption periods before, during and after COVID-19. The goal is to have initial steps to detect potential changes or patterns that could help the evolution of the buildings and help as a baseline for further research.

The results deploy an actual change in the thermal energy consumption system that, perhaps, happened due to a global pandemic and the mandatory lockdown. Nevertheless, this counterfactual analysis allows us to compare the impact of

different behaviours and find better solutions. The following figure shows the 48 best-fitted models for the three periods of analysis in the python code that ease the analysis. Some of the outcomes were that there are well-fitted models, but some are completely random prediction models that are assumed to be not reliable data.

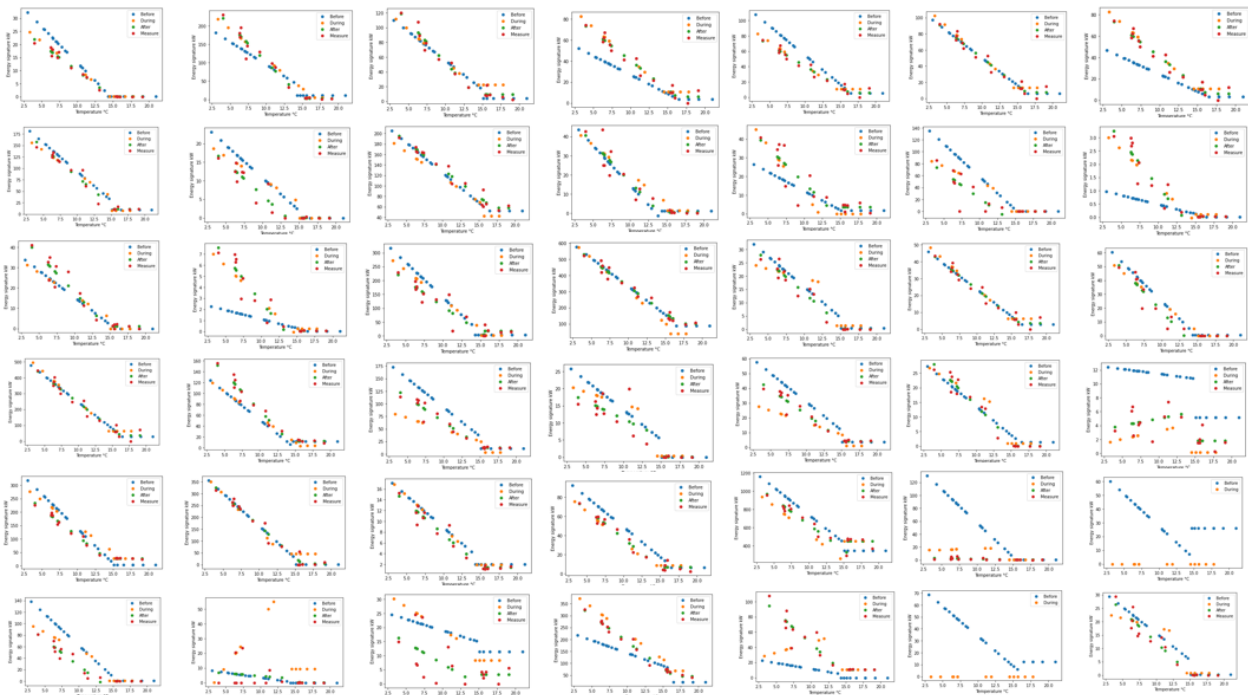


Figure 6 48 Building counterfactual change point model analysis.

The results obtained have an interpretable perspective that could enhance sustainable planning for the university transparently and clearly. Furthermore, using interpretable data-driven methods pushes to simplify and increase certainty in the decision-making process. Those solutions can be easily implemented in the university's sustainable energy management implementation program based on the Sustainable Building Design Standard ISO 50001.

## 6. CONCLUSION AND FUTURE WORK

The main conclusion obtained from this preliminary outcome is that the interpretable regression-based model provided practical solutions that could aim to ease the decision-making process to improve planning and enable confidence. Those methodologies help to detect opportunities from the data to reduce short- and long-term emissions and orient solutions to the energy transition. Part of the work is to apply those concise models in an automated process with physical interpretation for energy demand modelling. Part of the vision is to stick to simplicity. The simpler the implementation, the simpler it will be to have a successful deployment in actual buildings.

It is necessary to deploy models and automated processes in an overall way that extracts physical information that was difficult to get before. In this process, interpretable linear regression models can provide performance faster, more straightforwardly, and inexpensively. The regression-based data-driven methods are essential because they are validated, represent the entry-level solution for digitalising M&V solutions, and improve the understanding of energy performance. Another point is that although there are different techniques for modelling energy performance, it is fundamental to consider different spatial and temporal scales, from a single building to a complete district. Finally, this piecewise linear model represents a crucial step towards a deeper understanding of energy consumption and the opportunity to reduce uncertainty in the decision-making process.

This first approach represents the initial steps for evolving an automated process modelling for energy consumption. It is planned to go a step forward with an analysis based on the type of benchmark and a counterfactual analysis per scholar term to compare performance and measure the energy efficiency for each building on campus to support the University's decarbonisation strategy. Then, it is to develop a robust predicting model based on statistical analysis to have significant ranges to reduce uncertainty and improve decision-making long-term investments. However, the principal goal is to create digital twins for data-driven real-time analysis for each building considering different spatial and temporal scales. Also, it is to apply the process computed in multiple devices based on interoperability concepts.

## 7. REFERENCES

- Ahmad, M. W., Mourshed, M., & Rezgui, Y. (2017). Trees vs Neurons: Comparison between random forest and ANN for high-resolution prediction of building energy consumption. *Energy and Buildings*, *147*, 77–89. <https://doi.org/10.1016/j.enbuild.2017.04.038>
- Andriamamonjy, A., Klein, R., & Saelens, D. (2019). Automated grey box model implementation using BIM and Modelica. *Energy and Buildings*, *188–189*, 209–225. <https://doi.org/10.1016/j.enbuild.2019.01.046>
- Araya, D. B., Grolinger, K., ElYamany, H. F., Capretz, M. A. M., & Bitsuamlak, G. (2017). An ensemble learning framework for anomaly detection in building energy consumption. *Energy and Buildings*, *144*, 191–206. <https://doi.org/10.1016/j.enbuild.2017.02.058>
- Asadi, S., Amiri, S. S., & Mottahedi, M. (2014). On the development of multi-linear regression analysis to assess energy consumption in the early stages of building design. *Energy and Buildings*, *85*, 246–255. <https://doi.org/https://doi.org/10.1016/j.enbuild.2014.07.096>
- ASHRAE. (2014). *ASHRAE guideline 14:2014, Measurement of energy, demand, and water savings*.
- Barrie, J., Zawdie, G., & João, E. (2017). Leveraging triple helix and system intermediaries to enhance effectiveness of protected spaces and strategic niche management for transitioning to circular economy. *International Journal of Technology Management & Sustainable Development*, *16*(1), 25–47. [https://doi.org/10.1386/tmsd.16.1.25\\_1](https://doi.org/10.1386/tmsd.16.1.25_1)
- Berardi, U. (2017). A cross-country comparison of the building energy consumptions and their trends. *Resources, Conservation and Recycling*, *123*, 230–241. <https://doi.org/10.1016/j.resconrec.2016.03.014>
- Carayannis, E. G., Barth, T. D., & Campbell, D. F. (2012). The Quintuple Helix innovation model: global warming as a challenge and driver for innovation. *Journal of Innovation and Entrepreneurship*, *1*(1), 2. <https://doi.org/10.1186/2192-5372-1-2>
- de Wilde, P. (2014). The gap between predicted and measured energy performance of buildings: A framework for investigation. *Automation in Construction*, *41*, 40–49. <https://doi.org/10.1016/j.autcon.2014.02.009>
- Elias G. Carayannis, D. F. J. C. (2011). *Mode 3 Knowledge Production in Quadruple Helix Innovation Systems: 21st-Century Democracy, Innovation, and Entrepreneurship for Development*. Springer.
- Gi, K., Sano, F., Hayashi, A., Tomoda, T., & Akimoto, K. (2018). A global analysis of residential heating and cooling service demand and cost-effective energy consumption under different climate change scenarios up to 2050. *Mitigation and Adaptation Strategies for Global Change*, *23*(1), 51–79. <https://doi.org/10.1007/s11027-016-9728-6>
- Grillone, B., Danov, S., Sumper, A., Cipriano, J., & Mor, G. (2020). A review of deterministic and data-driven methods to quantify energy efficiency savings and to predict retrofitting scenarios in buildings. *Renewable and Sustainable Energy Reviews*, *131*, 110027. <https://doi.org/10.1016/j.rser.2020.110027>
- Hammarsten, S. (1987). A critical appraisal of energy-signature models. *Applied Energy*, *26*(2), 97–110. [https://doi.org/https://doi.org/10.1016/0306-2619\(87\)90012-2](https://doi.org/https://doi.org/10.1016/0306-2619(87)90012-2)
- Hygh, J. S., DeCarolis, J. F., Hill, D. B., & Ranji Ranjithan, S. (2012). Multivariate regression as an energy assessment tool in early building design. *Building and Environment*, *57*, 165–175. <https://doi.org/https://doi.org/10.1016/j.buildenv.2012.04.021>
- IEA. (2020). *World Energy Balances: Overview*. <https://www.iea.org/reports/world-energy-balances-overview/world>
- IEA. (2023). *Greenhouse Gas Emissions from Energy Data Explorer*. <https://www.iea.org/data-and-statistics/data-tools/greenhouse-gas-emissions-from-energy-data-explorer>
- International EVO. (2017). *Performance measurement and verification protocol. Tech report*.
- Isaac, M., & van Vuuren, D. P. (2009). Modeling global residential sector energy demand for heating and air conditioning in the context of climate change. *Energy Policy*, *37*(2), 507–521. <https://doi.org/10.1016/j.enpol.2008.09.051>
- Junker, R. G., Azar, A. G., Lopes, R. A., Lindberg, K. B., Reynders, G., Relan, R., & Madsen, H. (2018). Characterizing the energy flexibility of buildings and districts. *Applied Energy*, *225*, 175–182. <https://doi.org/10.1016/j.apenergy.2018.05.037>

- Kazmi, H., Fu, C., & Miller, C. (2023). Ten questions concerning data-driven modelling and forecasting of operational energy demand at building and urban scale. *Building and Environment*, 239, 110407. <https://doi.org/https://doi.org/10.1016/j.buildenv.2023.110407>
- Kikstra, J. S., Mastrucci, A., Min, J., Riahi, K., & Rao, N. D. (2021). Decent living gaps and energy needs around the world. *Environmental Research Letters*, 16(9), 095006. <https://doi.org/10.1088/1748-9326/ac1c27>
- Kim, H., & Haberl, J. (2018a). Field-test of the ASHRAE/CIBSE/USGBC performance measurement protocols: Part I intermediate level energy protocols. *Science and Technology for the Built Environment*, 24(3), 281–297. <https://doi.org/10.1080/23744731.2017.1368836>
- Kim, H., & Haberl, J. (2018b). Field-test of the ASHRAE/CIBSE/USGBC performance measurement protocols: Part I intermediate level energy protocols. *Science and Technology for the Built Environment*, 24(3), 281–297. <https://doi.org/10.1080/23744731.2017.1368836>
- Kim, H., & Haberl, J. (2018c). Field-test of the ASHRAE/CIBSE/USGBC performance measurement protocols: Part II advanced level energy protocols. *Science and Technology for the Built Environment*, 24(3), 298–315. <https://doi.org/10.1080/23744731.2017.1368837>
- KW Engineering. (2023). *NMECR*. <https://kw-labs.github.io/nmeocr/>
- Lam, J. C., Wan, K. K. W., Liu, D., & Tsang, C. L. (2010). Multiple regression models for energy use in air-conditioned office buildings in different climates. *Energy Conversion and Management*, 51(12), 2692–2697. <https://doi.org/https://doi.org/10.1016/j.enconman.2010.06.004>
- LBNL Energy Technologies Area. (2023). *RMV2.0*. <https://lbnl-eta.github.io/RMV2.0/>
- Manfren, M., James, P. A. B., & Tronchin, L. (2022). Data-driven building energy modelling – An analysis of the potential for generalisation through interpretable machine learning. *Renewable and Sustainable Energy Reviews*, 167, 112686. <https://doi.org/https://doi.org/10.1016/j.rser.2022.112686>
- Manfren, M., & Nastasi, B. (2019). *From in-situ measurement to regression and time series models: An overview of trends and prospects for building performance modelling*. 020100. <https://doi.org/10.1063/1.5117027>
- Manfren, M., Sibilla, M., & Tronchin, L. (2021). Energy Modelling and Analytics in the Built Environment—A Review of Their Role for Energy Transitions in the Construction Sector. In *Energies* (Vol. 14, Issue 3). <https://doi.org/10.3390/en14030679>
- Masuda, H., & Claridge, D. E. (2014). Statistical modeling of the building energy balance variable for screening of metered energy use in large commercial buildings. *Energy and Buildings*, 77, 292–303. <https://doi.org/https://doi.org/10.1016/j.enbuild.2014.03.070>
- Michalak, P. (2019). A thermal network model for the dynamic simulation of the energy performance of buildings with the time varying ventilation flow. *Energy and Buildings*, 202, 109337. <https://doi.org/10.1016/j.enbuild.2019.109337>
- Miller, C., Picchetti, B., Fu, C., & Pantelic, J. (2022). Limitations of machine learning for building energy prediction: ASHRAE Great Energy Predictor III Kaggle competition error analysis. *Science and Technology for the Built Environment*, 28(5), 610–627. <https://doi.org/10.1080/23744731.2022.2067466>
- Nastasi, B., Manfren, M., Groppi, D., Lamagna, M., Mancini, F., & Astiaso Garcia, D. (2022). Data-driven load profile modelling for advanced measurement and verification (M&V) in a fully electrified building. *Building and Environment*, 221, 109279. <https://doi.org/https://doi.org/10.1016/j.buildenv.2022.109279>
- Omarov, B., Memon, S. A., & Kim, J. (2023). A novel approach to develop climate classification based on degree days and building energy performance. *Energy*, 267, 126514. <https://doi.org/https://doi.org/10.1016/j.energy.2022.126514>
- OpenEEMeter. (2023). *Caltrack*. <https://www.caltrack.org/>
- Paulus, M. T. (2017). Algorithm for explicit solution to the three parameter linear change-point regression model. *Science and Technology for the Built Environment*, 23(6), 1026–1035. <https://doi.org/10.1080/23744731.2016.1267998>
- Paulus, M. T., Claridge, D. E., & Culp, C. (2015). Algorithm for automating the selection of a temperature dependent change point model. *Energy and Buildings*, 87, 95–104. <https://doi.org/https://doi.org/10.1016/j.enbuild.2014.11.033>
- Pfenninger, S., & Staffell, I. (2016). Long-term patterns of European PV output using 30 years of validated hourly reanalysis and satellite data. *Energy*, 114, 1251–1265. <https://doi.org/10.1016/j.energy.2016.08.060>

- Rabl, A., & Rialhe, A. (1992). Energy signature models for commercial buildings: test with measured data and interpretation. *Energy and Buildings*, 19(2), 143–154. [https://doi.org/https://doi.org/10.1016/0378-7788\(92\)90008-5](https://doi.org/https://doi.org/10.1016/0378-7788(92)90008-5)
- Rosenow, J., & Eyre, N. (2022). Reinventing energy efficiency for net zero. *Energy Research & Social Science*, 90, 102602. <https://doi.org/https://doi.org/10.1016/j.erss.2022.102602>
- Rosenow, J., & Hamels, S. (2023). Where to meet on heat? A conceptual framework for optimising demand reduction and decarbonised heat supply. *Energy Research & Social Science*, 104, 103223. <https://doi.org/https://doi.org/10.1016/j.erss.2023.103223>
- Rudin, C., Chen, C., Chen, Z., Huang, H., Semenova, L., & Zhong, C. (2022). Interpretable machine learning: Fundamental principles and 10 grand challenges. *Statistics Surveys*, 16, 1–85. <https://doi.org/10.1214/21-SS133>
- SBW Consulting. (2023). *ECAM*. <https://sbwconsulting.com/ecam/>
- Sibilla, M. (2017). *A meaningful mapping approach for the complex design*. Int. J. Des. Sci. Technol. <http://ijdst.europia.org/index.php/ijdst/article/view/2/1>
- Spinoni, J., Vogt, J. V., Barbosa, P., Dosio, A., McCormick, N., Bigano, A., & Füssel, H. M. (2018). Changes of heating and cooling degree-days in Europe from 1981 to 2100. *International Journal of Climatology*, 38, e191–e208. <https://doi.org/10.1002/joc.5362>
- Staffell, I., Pfenninger, S., & Johnson, N. (2023). A global model of hourly space heating and cooling demand at multiple spatial scales. *Nature Energy*. <https://doi.org/10.1038/s41560-023-01341-5>
- Thuesen, C., Koch-Ørvad, N., & Maslesa, E. (2018). *Organising Sustainable Transition: Understanding the Product, Project and Service Domain of the Built Environment Improving environmental building performance and workplace management through dynamic facilities management data View project PhD-"Radical improvements in sustainable building renovation based on new forms of collaboration and business models" View project*. <https://www.researchgate.net/publication/308337487>
- Tronchin, L., Manfren, M., & Nastasi, B. (2019). Energy analytics for supporting built environment decarbonisation. *Energy Procedia*, 157, 1486–1493. <https://doi.org/https://doi.org/10.1016/j.egypro.2018.11.313>
- United Nations. (2023). *Credibility and Accountability of Net-Zero Emissions Commitments of Non-State Entities*. [https://www.un.org/en/climatechange/high-level-expert-group?gclid=Cj0KCQjwsp6pBhCfARIsAD3GZuYouMn5K8HvZEa2tzzBeCA9L0heT2VV8bgqF4DTLwyXoOCgiDApbnsaAvLOEALw\\_wcB](https://www.un.org/en/climatechange/high-level-expert-group?gclid=Cj0KCQjwsp6pBhCfARIsAD3GZuYouMn5K8HvZEa2tzzBeCA9L0heT2VV8bgqF4DTLwyXoOCgiDApbnsaAvLOEALw_wcB)
- University of Southampton. (2023). *University of Southampton Map*. <https://maps.southampton.ac.uk/>
- Waite, M., & Modi, V. (2020). Electricity Load Implications of Space Heating Decarbonization Pathways. *Joule*, 4(2), 376–394. <https://doi.org/10.1016/j.joule.2019.11.011>

---

## #286: An Experimental Investigation on adsorption and regeneration performance of composite desiccants for building applications

---

Mariana VELASCO-CARRASCO<sup>1</sup>, Jorge Luis AGUILAR-SANTANA<sup>2</sup>, Saffa RIFFAT<sup>3</sup>

<sup>1</sup> Energy and Engineering, Nottingham Trent University, [mariana.velascocarrasco@ntu.ac.uk](mailto:mariana.velascocarrasco@ntu.ac.uk)

<sup>2</sup> Midlands Net Zero Hub, [jorge.santana@nottinghamcity.gov.uk](mailto:jorge.santana@nottinghamcity.gov.uk)

<sup>3</sup> Department of Architecture and Built Environment, Faculty of Engineering, University of Nottingham, UK; [saffa.riffat@nottingham.ac.uk](mailto:saffa.riffat@nottingham.ac.uk)

*Abstract: In recent years, composite desiccants have attracted significant attention for their effective dehumidification properties. These materials are created by impregnating hygroscopic salt into the pores of a host material. They are characterized for their exceptional moisture adsorption capacity and their ability to regenerate at low temperatures, making them suitable for building applications. This paper experimentally investigates novel composite desiccant materials designed for moisture control in buildings, where CaCl<sub>2</sub>, KHCO<sub>2</sub>, LiCl, and MgSO<sub>4</sub> - CaCl<sub>2</sub> salts mixtures were impregnated into raw vermiculite. The adsorption performance was evaluated within an environmental chamber, and the regeneration performance was assessed using an oven. The experimental results demonstrate the superior performance of the composite desiccants in comparison to the raw material. Furthermore, the experimental results reveal that the LiCl composite presents the highest adsorption performance. For the regeneration process, the LiCl composite presented the highest reduction in the short-term. However, in the long term, the CaCl<sub>2</sub> exhibited superior regeneration performance.*

*Keywords: building humidity control, composite desiccants, solid desiccants, vermiculites*



## 1. INTRODUCTION

Moisture control has become a worldwide concern due to the current construction practices and building operational controls. Energy saving has been prioritized and for this reason, buildings are better insulated, and airtightness has been reduced. This has increase moisture concerns in buildings that in many cases have been compensated by the incorporation of air-conditioning systems (Warwicker, 2010).

Similar to temperature, air humidity affects the thermal comfort perception and humidity (Kong et al., 2019). To achieve thermal comfort the relative humidity (RH) should range between 40 to 60%; below 40% increases the concentration of harmful chemicals in the air, which can cause respiratory infections and skin conditions. In contrast, having a relative humidity above 60% promotes the proliferation of viruses and mold spores (Cascione et al., 2019).

The application of air conditioning systems or humidifiers has been used as a method to obtain an optimal humidity level. Nevertheless, the implementation of these mechanisms increases the building energy demand and has limited ability to control the humidity (Luo, Yang and Lu, 2014; Wen et al., 2018; Lu, Kuok and Liu, 2020). In high-performance buildings, the energy consumption requirements for dehumidification control increase from 1.5% to 22.4%(Shehadi, 2018). In this regard, humidity-controlling materials provide a low-energy solution to help stabilize indoor relative humidity by absorbing or desorbing water molecules in the air.

Desiccants are a group of hygroscopic substances that can attract water-vapor molecules via adsorption or absorption (Yang, Rana and Lan, 2015). These materials, provide an alternative to traditional dehumidification methods that involve cooling air below the dew point (Longo and Gasparella, 2016), allowing independence to the humidity control.

There are two types of desiccants, liquid, and solid desiccants. In general liquid desiccants present more advantages over solid desiccants, having a higher adsorption capacity. Nevertheless, most of the liquid desiccants are unsuitable for building applications as they are considered toxic materials. Furthermore, liquid desiccant materials require a complicated packing system for dehumidification and regeneration (Huang and Zhang, 2013).

Examples of liquid desiccants include concentrated aqueous solutions of hygroscopic salts such as calcium chloride or lithium chloride, lithium bromide, triethylene glycols. Solid desiccants include a wide variety of materials such as silica gels, molecular sieves, metal-organic frameworks, polymers, activated carbon, among others.

Solid desiccant materials are considered an effective and economical approach for dehumidification and are less subject to corrosion compared to liquid desiccants. In general, they are considered environmentally friendly. Depending on the application, solid desiccant materials present higher advantages, due to their dryness, structure simplicity, chemical inertness, and ease of operation (Chua and Chou, 2003). Moreover, the application of solid desiccants can contribute to air cleanliness, which plays an important role in indoor air quality, as they can effectively remove several contaminants (Ge et al., 2018). The dehumidification and regeneration performance of a solid desiccant-based system is expected with high water adsorption capacity, good renewability at relatively low regeneration temperature, low desorption energy input, and high durability.

The impregnation of two or more hygroscopic salts into a porous desiccant is called a composite desiccant and is a common method to enhance the moisture performance capacity. Common host materials are silica gels, mesoporous silicate, active carbon, and natural rocks and are characterized by their low cost; nevertheless, they present low adsorption capacity. Natural rocks have brought attention as host materials, providing a wide variety, having a low regeneration temperature (50 °C to 80 °C) and a considerably low price (Jarimi et al., 2018).

Composite desiccants, create a balance between the stability of the porous desiccants and the high adsorption capacity of the hygroscopic salts (Zheng, Ge and Wang, 2014). However, the dehumidification performance of composite desiccant materials varies significantly depending on the host and immersed salts, which implies the importance of an optimal selection of the component materials and optimization of material composition. Composite desiccants have relatively lower regeneration temperatures (35 °C to 55 °C), which indicates that low-grade heat sources can be utilised for regeneration.

For building dehumidification purposes, the solid desiccant composite must possess the capacity to undergo regeneration at low temperatures, considering the limited sources available for this purpose. The desirable properties are described as follows:

- Compatibility between the desiccant and the hygroscopic salt
- Cheap and abundant
- Low desorption energy input
- Low regeneration temperature in the desired operating temperature range < 80 °C, to ensure the material full dehydration with a fixed temperature range (i.e., using a heat pump or fan).
- Long term stability

- Non toxic
- Non flammable
- Cost effective

## 2. MATERIALS AND METHODS

Vermiculites are composed of a group of hydrated laminar minerals which are aluminium, iron, and magnesium silicates. The subtract of the vermiculite is produced by heating to 1000 °C, converting the water to vapour at high temperatures creating a compact layer of the material. This process is referred as exfoliation and presents the expanded vermiculite that consists of granules of high porosity (Kipp, Wever and Kreji, 2000). These materials can present varying sizes, the most common being 0–2, 2–4, and 4–8 mm in diameter. Due to their porous structure, they have a strong capillary action, holding between 3 to 4 times their weight in water (Papadopoulos et al., 2008).

Humid air is a mixture of dry air and water vapor in which three variables are required, calculated by the dry bulb temperature, total pressure, and molar fraction of water. The total pressure is given by Dalton's Law as follows:

$$P_{tot} = P_{as} + P_{ve}$$

It is possible to characterize the water vapor quantity contained in kg dry air, as follow:

$$x = 0.622 \cdot \frac{P_{ve}}{P_{atm} - P_{ve}}$$

The relative humidity is defined as the ratio of the water vapor partial pressure at the saturated water vapor pressure.

$$\varphi \frac{100 \cdot P_{ve}}{P_{v,sat}} = \frac{100 \cdot x}{0.622 + x} \cdot \frac{P_{atm}}{P_{v,sat}}$$

Where the  $P_{v,sat}$  can be calculated in function of the temperature  $T > 0$ .

$$m_d = m - m_w$$

With a mass of water:  $m_w$  and a dry mass  $m_d$ .

The solution concentration  $C_s$  is defined as follow:

$$C_s = \frac{M_s}{M_{sol}} \text{ and } M_{sol} = M_s + M_w$$

### 2.1. Composite desiccant synthesis

To synthesize a composite desiccant, a base host matrix (vermiculite) and a hygroscopic additive are employed for their dehumidification potential. Four highly hygroscopic salts have been selected  $\text{KHCO}_2$ ,  $\text{CaCl}_2$ ,  $\text{MgSO}_4 - \text{CaCl}_2$ , and  $\text{LiCl}$ , to compare the effect as enhancement materials. These salts are deliquescent and will dissolve without proper containment within a host matrix. SIM composites were synthesized using the Insipient Wetness Technique (IWT) method.

The vermiculite contains a pore volume  $V_p$  of 2.84 ml/g (Jarimi et al., 2018). Further composite materials are prepared based on the (Casey et al., 2014), where the mass sample was calculated as follows:






$$m_{salt} = \frac{m_{SIM} - m_v}{m_{SIM}} \times 100(\%)$$

Where  $m_{SIM}$  indicates the mass of anhydrous SIM composite and  $m_v$  indicates the raw vermiculite. The relation between the vermiculite and the enhancement material is 1:3.

The hygroscopic salt was prepared individually by saturating water with the assistance of a magnetic stirrer. When the solution comprised multiple salts, the water saturation was carried out separately with equal volumes before being combined after each solution had settled.

Each salt was allowed to cool down for 24 hours before mixing it with the dry vermiculite. After this process, the composite was left to set for 24 hours before drying it in an oven to eliminate water molecules and ensure complete material dehydration. Table 1 presents the images of the testing samples, featuring the raw material as a comparison along with the four composite desiccants.

Table 1: Vermiculite testing samples.

	
<b>Raw vermiculite</b>	<b>Potassium Formate (KHCO<sub>2</sub>)</b>
	
<b>Magnesium Chloride (MgSo<sub>4</sub> - CaCl<sub>2</sub>)</b>	<b>Lithium Chloride (LiCl)</b>
	
<b>Calcium Chloride (CaCl<sub>2</sub>)</b>	

### 3. METHODOLOGY

#### 3.1. Method 1 - Performance comparison using a control box

The experimental evaluation was performed using a control box connected to an Environmental Climatic Chamber. The measurements were made using a humidity sensor (EK-H4 Sensirion) coupled with Digital Humidity Sensor SHT7x (RH/T), with a standard deviation of  $\pm 1.8\%$  RH and  $\pm 0.3$  °C. Sensors were placed in the inlet, outlet as shown in Figure 1, both the inlet and outlet had openings of 18 cm diameter, with airflow coming from the Environmental Chamber blown through with the assistance of an electric fan. The chamber temperature was set at 27 °C and the RH at 80%. The panels were placed on the top shelf of the control box, the experiment was monitored for 3 hours. The sample weight was compared before and after each test.

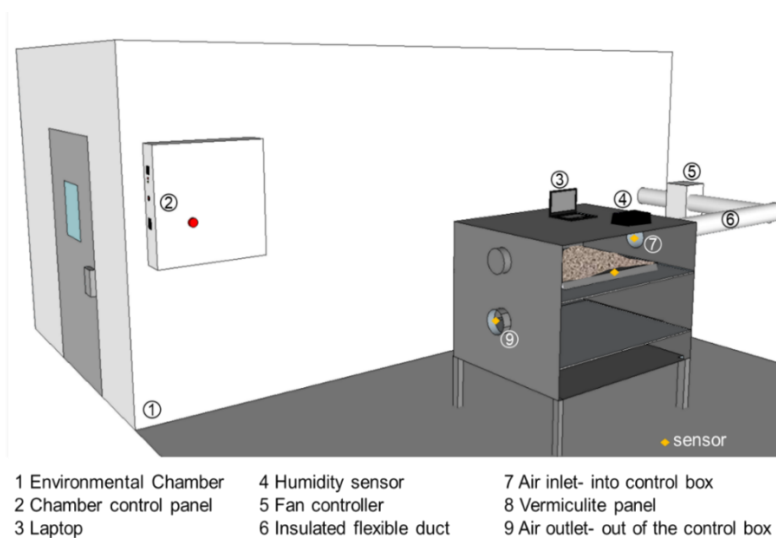


Figure 1 Method 1 schematic diagram of the experimental rig with a control box.

### 3.2. Method 2 – Performance comparison inside the Environmental Chamber

A second evaluation was conducted inside the Environmental Chamber. The samples were placed simultaneously. The contact area was selected as a key parameter to consider as the raw vermiculite presented greater volume. The samples were evenly distributed in a perforated metal tray as illustrated in Figure 2, with the aim of optimizing moisture adsorption. To achieve this, the trays were elevated 60cm above the floor. The chamber temperature was maintained at 27 °C and the relative humidity was set at 80%. The sample weight was monitored every 2 hours using a scale, with the testing period scheduled for 6 hours.

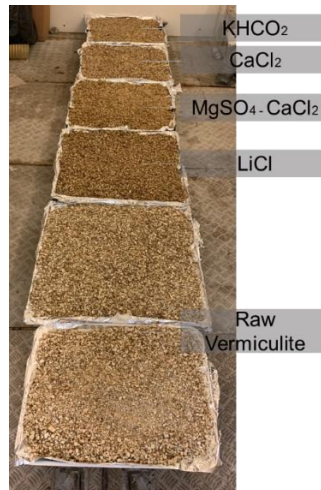


Figure 2 Environmental chamber performance comparison.

## 4. RESULTS AND DISCUSSION

### 4.1 Method 1 - Performance comparison using a control box

The moisture performance of all the tested samples was evaluated under the same environmental conditions, with the experiment being replicated twice and the average value duly recorded. As depicted in Figure 3, the composite materials demonstrated an improved adsorption capacity when compared to the raw vermiculite. Notably, the highest performance was exhibited by LiCl, closely followed by MgSO<sub>4</sub> - CaCl<sub>2</sub> and CaCl<sub>2</sub>. Out of all the hygroscopic salts, the KHCO<sub>2</sub> presented the lowest adsorption performance. The specific details concerning mass and adsorption percentages are outlined in Table 2. In this experimental evaluation, the initial sample weight was set at 1.5 kg.

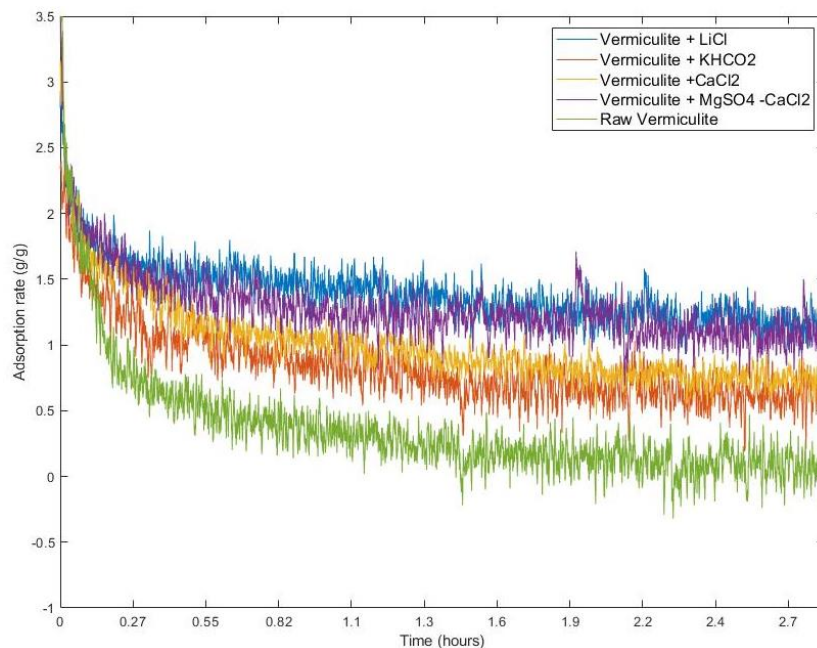


Figure 3 Desiccant adsorption performance at 1.5 kg.

*Table 2: Desiccant adsorption capacity at 1.5 kg.*

Material	Initial weight (kg)	Final Weight (kg)	Adsorption (kg)	Adsorption (%)
Vermiculite LiCl	1.5	1.634	0.134	8.93
Vermiculite MgSO <sub>4</sub> - CaCl <sub>2</sub>	1.5	1.624	0.124	8.27
Vermiculite CaCl <sub>2</sub>	1.5	1.621	0.121	8.07
Vermiculite KHCO <sub>2</sub>	1.5	1.612	0.112	7.47
Raw Vermiculite	1.5	1.562	0.062	4.13

#### 4.2 Method 2 – Performance comparison inside the Environmental Chamber

Table 3 illustrates the changes in mass volume variation during the experimental process. From all the testing samples, LiCl exhibited the highest mass increase with 28%, trailed by MgSO<sub>4</sub> - CaCl<sub>2</sub> and CaCl<sub>2</sub> with 21% and 16%, respectively. The composite with the lowest performance was KHCO<sub>2</sub> having a 13% increase. Finally, the raw vermiculite presented the lowest adsorption intake with 8%, in spite of presenting greater volume exposed to the environmental chamber conditions.

*Table 3: Desiccant adsorption capacity at 2 kg.*

Material (kg)	Time-lapse				Adsorption %		
	Initial weight	2hrs	4hrs	6hrs	2hrs	4hrs	6hrs
Vermiculite LiCl	2.00	2.299	2.451	2.571	14.61	22.18	28.17
Vermiculite MgSO <sub>4</sub> - CaCl <sub>2</sub>	2.00	2.207	2.333	2.425	10.24	16.53	21.13
Vermiculite CaCl <sub>2</sub>	2.00	2.145	2.227	2.331	7.25	11.35	16.55
Vermiculite KHCO <sub>2</sub>	2.00	2.147	2.225	2.271	7.35	11.25	13.55
Raw Vermiculite	2.00	2.098	2.116	2.130	6.04	7.17	8.01

#### 4.3 Regeneration performance results

The regeneration cycle is an important part of the moisture adsorbent to perform effectively. The enhancement materials have been selected based on their suitability to regenerate at low temperatures < 80 °C, making them suitable for building applications. To validate the effectiveness of the proposed materials the regeneration performance was tested using an electrical oven (AX Carbolite Gero) with a temperature range of 30 to 250 °C.

Table 4 presents the regeneration comparison of the tested samples at 0.6 kg. In this scenario, the oven temperature was set at 60 °C for 3 hours. The LiCl composite demonstrated a slightly higher reduction percentage in relation to the initial weight with 9.6%. Subsequently, both the CaCl<sub>2</sub> and the MgSO<sub>4</sub> - CaCl<sub>2</sub> displayed reductions of 9% and 8%, respectively. The KHCO<sub>2</sub> sample exhibited a 5% decrease, while the raw vermiculite showcased the lowest weight reduction, measuring at 3%.

*Table 4: Vermiculite oven regeneration at 0.6 kg.*

Material	Initial weight (kg)	End weight (kg)	Weight reduction (kg)	Reduction (%)
Vermiculite LiCl	0.6	0.542	0.58	9.66
Vermiculite CaCl <sub>2</sub>	0.6	0.546	0.54	9.00
Vermiculite MgSO <sub>4</sub> - CaCl <sub>2</sub>	0.6	0.551	0.49	8.17
Vermiculite KHCO <sub>2</sub>	0.6	0.568	0.32	5.33
Raw Vermiculite	0.6	0.584	0.16	2.67

Table 5 presents the comparison results of the samples over 24 hours. The initial weight was marked at 1 kg and the regeneration temperature was held constant at 60 °C. During this evaluation, the CaCl<sub>2</sub> exhibited the most significant reduction at 15%, closely followed by LiCl with 12%. MgSO<sub>4</sub> - CaCl<sub>2</sub> and KHCO<sub>2</sub> vermiculite composites experienced an 11% weight decrease, while the raw material showcased the smallest drop at 3%.

Table 5: Vermiculite oven regeneration at 1 kg.

Material	Initial weight (kg)	End weight (kg)	Weight reduction (kg)	Reduction (%)
Vermiculite CaCl <sub>2</sub>	1	0.847	0.15	15.35
Vermiculite LiCl	1	0.873	0.13	12.75
Vermiculite MgSO <sub>4</sub> - CaCl <sub>2</sub>	1	0.886	0.11	11.41
Vermiculite KHCO <sub>2</sub>	1	0.888	0.11	11.19
Raw Vermiculite	1	0.967	0.03	3.31

## 5. CONCLUSION

A selection of hygroscopic salts was coupled with raw vermiculite to create a novel composite material for moisture control in buildings. Vermiculite was chosen as a natural host material due to its notable characteristics such as high porosity, strong capillarity action, affordability, and widespread availability. The selection of LiCl, CaCl<sub>2</sub>, MgSO<sub>4</sub> - CaCl<sub>2</sub>, and KHCO<sub>2</sub> as the salt mixtures was informed by their capacity for low-temperature regeneration (< 80 °C) and their compatibility with the proposed desiccant material.

The experimental results underscore the ability of the hygroscopic salts to enhance the adsorption performance of the solid desiccant in comparison to the raw host matrix. Moreover, the composite materials exhibited the capability to dry efficiently at low temperatures (60 °C), making them suitable for building applications. The LiCl vermiculite composite presented the highest adsorption performance, having a mass gain up to 20% higher than that of the raw vermiculite.

During the regeneration process, the LiCl composite demonstrated the most effective short-term regeneration performance. However, over a 24-hour regeneration period, the CaCl<sub>2</sub> composite exhibited a higher regeneration performance, leading to a 12% greater reduction in vapor concentration compared to the raw vermiculite.

## 6. ACKNOWLEDGEMENT

The authors wish to gratefully acknowledge the support of Innovate UK (Grant Agreement ID 75704-501581).

## 7. REFERENCES

- Cascione, V. et al. (2019) 'A review of moisture buffering capacity: From laboratory testing to full-scale measurement', *Construction and Building Materials*. Elsevier Ltd, pp. 333–343. doi: 10.1016/j.conbuildmat.2018.12.094.
- Casey, S. P. et al. (2014) 'Salt impregnated desiccant matrices for "open" thermochemical energy storage - Selection, synthesis and characterisation of candidate materials', *Energy and Buildings*. Elsevier B.V., 84, pp. 412–425. doi: 10.1016/j.enbuild.2014.08.028.
- Chua, K. J. and Chou, S. K. (2003) 'Low-cost drying methods for developing countries', *Trends in Food Science and Technology*. Elsevier Ltd, pp. 519–528. doi: 10.1016/j.tifs.2003.07.003.
- Ge, T. S. et al. (2018) 'Experimental testing on contaminant and moisture removal performance of silica gel desiccant wheel', *Energy and Buildings*. Elsevier Ltd, 176, pp. 71–77. doi: 10.1016/j.enbuild.2018.07.033.
- Huang, S. M. and Zhang, L. Z. (2013) 'Researches and trends in membrane-based liquid desiccant air dehumidification', *Renewable and Sustainable Energy Reviews*. Pergamon, pp. 425–440. doi: 10.1016/j.rser.2013.08.005.
- Jarimi, H. et al. (2018) 'Materials characterization of innovative composite materials for solar-driven thermochemical heat storage (THS) suitable for building application', *International Journal of Low-Carbon Technologies*, 13(1), pp. 30–42. doi: 10.1093/ijlct/ctx017.
- Kipp, J. A. ., Wever, G. . and Kreji, C. (2000) 'International Substrate Manual Elsevier International Business Information Doetinchem', *International Substrate Manual Elsevier International Business Information Doetinchem*, the Netherlands.
- Kong, D. et al. (2019) 'Effects of indoor humidity on building occupants' thermal comfort and evidence in terms of climate adaptation', *Building and Environment*. Elsevier Ltd, 155, pp. 298–307. doi: 10.1016/j.buildenv.2019.02.039.
- Longo, G. A. and Gasparella, A. (2016) 'Experimental measurement of thermophysical properties of H<sub>2</sub>O/KCOOH (potassium formate) desiccant', *International Journal of Refrigeration*. Elsevier Ltd, 62, pp. 106–113. doi: 10.1016/j.ijrefrig.2015.10.004.
- Lu, H. C., Kuok, C. H. and Liu, S. H. (2020) 'High-performance humidity control coatings prepared from inorganic wastes', *Construction and Building Materials*. Elsevier Ltd, 263, p. 120169. doi: 10.1016/j.conbuildmat.2020.120169.

- Luo, Y., Yang, H. and Lu, L. (2014) 'Dynamic and microscopic simulation of the counter-current flow in a liquid desiccant dehumidifier', *Applied Energy*. Elsevier Ltd, 136, pp. 1018–1025. doi: 10.1016/j.apenergy.2014.06.023.
- Papadopoulos, A. P. et al. (2008) 'Inorganic and synthetic organic components of soilless culture and potting mixes', in *Soilless Culture: Theory and Practice*. Elsevier, pp. 505–543. doi: 10.1016/B978-044452975-6.50014-9.
- Shehadi, M. (2018) 'Review of humidity control technologies in buildings', *Journal of Building Engineering*. Elsevier Ltd, pp. 539–551. doi: 10.1016/j.jobe.2018.06.009.
- Warwicker, B. (2010) '15 - Desiccant materials for moisture control in buildings', in *Materials for energy efficiency and thermal comfort in buildings*. Elsevier Ltd, pp. 365–383. doi: 10.1533/9781845699277.2.365.
- Wen, T. et al. (2018) 'Investigation on the regeneration performance of liquid desiccant by adding surfactant PVP-K30', *International Journal of Heat and Mass Transfer*. Elsevier Ltd, 123, pp. 445–454. doi: 10.1016/j.ijheatmasstransfer.2018.03.005.
- Yang, Y., Rana, D. and Lan, C. (2015) 'Development of solid super desiccants based on a polymeric superabsorbent hydrogel composite', *RSC Adv.*, 5. doi: 10.1039/C5RA04346H.
- Zheng, X., Ge, T. S. and Wang, R. Z. (2014) 'Recent progress on desiccant materials for solid desiccant cooling systems', *Energy*. Elsevier Ltd, pp. 280–294. doi: 10.1016/j.energy.2014.07.027.

---

## #289: Investigation on a novel thermoelectric ventilator system for retrofit in heritage buildings

---

Qi XU<sup>1</sup>, Shihao ZHANG<sup>2</sup>, Saffa RIFFAT<sup>3</sup>

<sup>1</sup>College of Architecture, Nanjing Tech University, Nanjing, 210044, China, Email: xuqi@njtech.edu.cn

<sup>2</sup>School of Architecture and Urban Planning, Suzhou University of Science and Technology, Suzhou, 215011, China, shihaozhang@usts.edu.cn

<sup>3</sup>Department of Architecture and Built Environment, University of Nottingham, Nottingham NG7 2RD, UK, saffa.riffat@nottingham.ac.uk

*Abstract: In recent years, there has been a risen interest in retrofit in heritage buildings, especially energy and comfort retrofitting. Global governments pay much more attention on the preservation and reuse of heritage buildings. However, the retrofit might alter appearance of heritage building. In this paper, the investigation on a novel thermoelectric ventilator retrofit in heritage buildings has been undertaken. Firstly, an AHP methods-based survey has been conducted to identify appropriate component to apply the ventilator with minimum impact on the heritage features. Secondly, an overview of the prototype design, heat transfer model and experimental parameters would be presented. Finally, the MATLAB model along with Revit has been used to simulate the prototype's performance when installed in a sustainable house in the UK. According to the result, the prototype would supply 655 kWh heating energy for year-round operation and enhance the air change rate of the heritage buildings. This research would provide a new solution to reduce energy consumption during daily ventilation in heritage buildings.*

*Keywords: heat recovery system; thermoelectric module; heritage building*



## Nomenclature

A	Area	m <sup>2</sup>	Subscripts	
$\alpha$	Seebeck coefficient	V/K	c	cold side
$\alpha_1$	Heat transfer coefficient	W/(m <sup>2</sup> *K)	e	exhaust
$C_p$	Specific heat	J/(kg*K)	f	fresh
COP	Coefficient of performance		h	hot side
I	Current	A	hp	heat pipe
k	Thermal conductance	W/K	i	inside
$\dot{m}$	Mass flow rate	kg/s	in	inlet
P	Power	W	o	outside
Q	Heat dissipated	W	out	outlet
R	Thermal resistance	K/W	te / tec	thermoelectric module
r	Electrical resistance	$\Omega$		
T	Temperature	°C		
$\lambda$	Thermal conductivity	W/(m*K)		

## 1. INTRODUCTION

There is a huge stock of traditional buildings which hold significant historical and cultural value but often face challenges in terms of energy efficiency and indoor comfort. They provide us with a connection to the past and can help us to learn about our history and culture. However, heritage buildings can also be energy inefficient, which can lead to high energy bills and environmental impacts. It is of great social and economic significance to retrofit the traditional dwellings for better performance. Retrofitting these buildings is essential to ensure their preservation and continued use. However, traditional retrofitting methods may compromise the architectural integrity and appearance of these structures.

The global temperature increased by 0.2 °C in the past 100 years because of carbon emission. The spread of HVAC systems is regarded as a significant sector that contributes to building energy consumption and carbon emission. HVAC systems can provide a comfortable interior with suitable temperature, relative humidity, and ventilation rates. But they would also pose a greater risk of contamination. The HVAC systems with inadequate maintenance are also regarded as the main cause of illness related to buildings (Ganesh et al. 2019). It is noticed that the long-term air circulation of HVAC systems would contribute to a significant increase of illness for occupants (Huang et al. 2018)(Schieweck et al. 2018). In practice, reducing the frequency of heating, ventilation and air conditioning operation would be promising to achieve energy saving. However, due to the global coronavirus outbreak, adequate ventilation by opening windows is necessary, which would cause further energy consumption to maintain interior comfort. Hence, the challenge is to develop a low-carbon system coupled with the current technologies or explore an alternative system to the traditional one, which could satisfy the construction standards, regulations promoted by governments, and preserve the unique character of historic building as well.

The preservation and energy-efficient retrofit of heritage buildings have gained substantial attention worldwide (Choi et al. 2023; Yuk et al. 2023; Jiang et al. 2022). Governments and heritage organizations recognize the need to balance conservation efforts with sustainable building practices. However, there is limited research on retrofit solutions that specifically target energy-efficient ventilation while preserving the architectural and historical aspects of these buildings (Abdul Hamid et al. 2020). This research seeks to fill this gap by proposing a novel thermoelectric ventilator system. With the intention of reducing energy consumption during ventilation, the recirculation of return air may occur during operation especially under the cooling mode, which might further cause accumulation and spread of contaminated particles to increase the risk of illness. And from the literature, people living in a space with sealed windows or equipped with air conditioning were more likely to suffer from symptoms related to buildings compared to those living with enough natural ventilation (Ganesh et al. 2019). In the context of COVID-19, adequate ventilation by either opening windows or mechanical ventilation devices is essential to avoid suffering from diseases (Bhagat et al. 2020). However, necessary frequent ventilation would cause more energy use than normal. Hence, the aim of this paper is to develop a prototype to reduce energy consumption during ventilation.

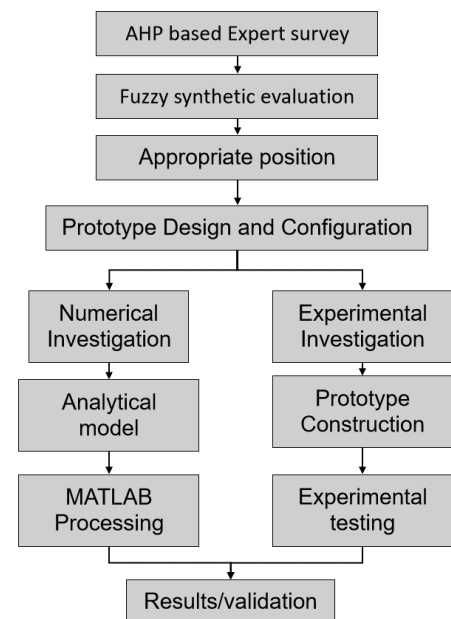


Figure 1 The framework of methodology

## 2. METHODOLOGY

The conventional heat recovery ventilation system for residential buildings is usually composed of a heat exchanger core, extractor fans, a fresh air inlet and a separate contaminated air exhaust outlet. The heat exchanger core is normally installed in attic space and requires a complicated and well-designed duct system to reach each room in the house (Fehrm et al. 2002), which will require extra time and are not suitable to apply in heritage building.

This research introduces a novel approach to heritage building retrofitting by proposing a thermoelectric ventilator system. Unlike traditional methods, this system aims to improve energy efficiency and indoor air quality without compromising the architectural and historical value of heritage buildings.

In order to integrate into the heritage buildings with minimally invasiveness, the location of the thermoelectric ventilator system should be carefully chosen so that it does not damage the heritage features of the building. And the design of the thermoelectric ventilator system should be sympathetic to the architectural style of the building. Hence, an Analytic Hierarchy Process (AHP) based fuzzy synthetic evaluation was conducted to identify the most suitable components for ventilator application which have the least impact on the heritage features of the building. Then, the design and construct a prototype of the thermoelectric ventilator system was demonstrated. Finally, MATLAB modelling and Revit simulation were utilized to assess the prototype's performance when integrated into a house in the UK.

## 3. PRIORITIZING APPROPRIATE COMPONENT

AHP-Based Fuzzy Evaluation, also named as FAHP (Fuzzy Analytic Hierarchy Process), is a decision-making method based on fuzzy mathematics and hierarchy analysis (Li et al. 2022). It combines the advantages of AHP and fuzzy comprehensive evaluation, while avoiding their disadvantages. It integrates hierarchical structure, weight analysis, consistency testing, and fuzzy evaluation. The evaluation process of FAHP generally involves determining the weight and factor set using the analytic hierarchy process, determining the evaluation set based on the actual situation, and then using fuzzy comprehensive evaluation to make a comprehensive evaluation.

### 3.1. Identifying Evaluation Criteria

As shown in Figure 2, an AHP was firstly implemented to establish a hierarchy structure with main evaluation criteria. The criteria, that were collected from previous studies such as (Yuk et al. 2023)(Marzouk et al. 2023)(Ge et al. 2022)(Zhang et al. 2021), are identified to compare and rank based on questionnaire retrieve from expert with rich project experience. All experts were invited to compare the impacts of various application components on the unique values of the historic building. There were 15 questionnaires sent out and 12 valid questionnaires were returned. Then, the pairwise comparison matrix was developed shown in Table 1.

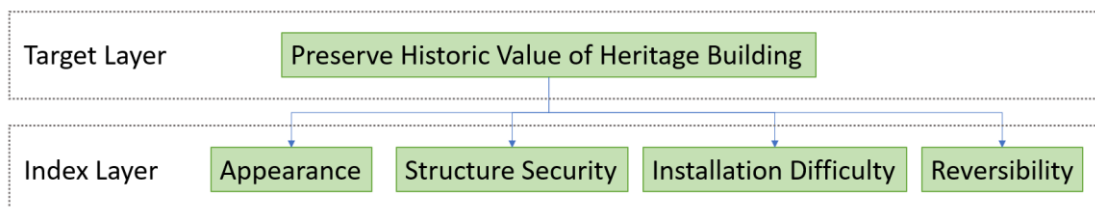


Figure 2 The hierarchy structure with main evaluation criteria

The consistency test of the current AHP showed a consistency ratio  $CR = 0.011 < 0.1$ , which meant the judgement matrix is acceptance. Table 1 shows impact weight of four indexes on the preservation of historic value, ranging from 0.095 to 0.397. The appearance and structure security had the highest impact weights, which suggests the retrofit solutions on the ventilation should be considered carefully in the view of the historic protection.

Table 1: Impact weights of various indexes

Index	Appearance	Structure Security	Installation difficulty	Reversibility
Impact weight	0.397	0.346	0.162	0.095

- Appearance: The components have been carefully selected to blend in with the building's aesthetics, minimizing any visual disruption.
- Structure Security: Showcase how the research considers building's structural safety to ensure that the proposed retrofitting solution is compatible with the existing structure.
- Installation difficulty: The installation is labour intensive and invasive on the structure, such as inaccessible components.
- Reversibility: The location is easy to install and capable of being reversed so that the original state of heritage is restored easily.

### 3.2. Fuzzy Evaluation

After the impact weight identified in the AHP, the fuzzy evaluation method which transfers the qualitative results to the quantitatively indicators is implemented to identify the most suitable components for ventilator application. The indicators for various index are divided into 5 ranks and ranges from 0-10. The grade 1 means the 'the invasive impacts on historic value; grade 9 represents the 'the least impact on the historic value'; the other level shows the intermediate impacts on the historic value. The results of the evaluation can be calculated by membership functions. The Triangle-shape grade of membership function of various levels have been shown below, from Rank 1 ( $R_1$ ) to Rank 9 ( $R_9$ ).

$$\begin{aligned}
 \text{Equation 1: Membership function of Rank 1} \quad R_1 &= \begin{cases} 1 & 0 < N \leq 1 \\ \frac{3-N}{2} & 1 < N \leq 3 \\ 0 & N > 3 \end{cases} \\
 \text{Equation 2: Membership function of Rank 2} \quad R_3 &= \begin{cases} \frac{N-1}{2} & 1 < N \leq 3 \\ \frac{5-N}{2} & 3 < N \leq 5 \\ 0 & N < 1 \text{ 或 } N > 5 \end{cases} \\
 \text{Equation 3: Membership function of Rank 5} \quad R_5 &= \begin{cases} \frac{N-3}{2} & 3 < N \leq 5 \\ \frac{7-N}{2} & 5 < N \leq 7 \\ 0 & N < 3 \text{ 或 } N > 7 \end{cases} \\
 \text{Equation 4: Membership function of Rank 7} \quad R_7 &= \begin{cases} \frac{N-5}{2} & 5 < N \leq 7 \\ \frac{9-N}{2} & 7 < N \leq 9 \\ 0 & N < 5 \text{ 或 } N > 9 \end{cases} \\
 \text{Equation 5: Membership function of Rank 9} \quad R_9 &= \begin{cases} \frac{1}{N-7} & 9 \leq N < 10 \\ \frac{2}{N-7} & 7 < N \leq 9 \\ 0 & N < 7 \end{cases}
 \end{aligned}$$

As shown in Figure 3, the components for ventilator application have been prioritized by the distribution of fuzzy evaluation. The results of window, door and lintel belonged to the relatively suitable rank, which means the greater potential on preservation of historic value. The foundation, wall and roof were relatively unsuitable for application. The foundation had advantages on the appearance preservation, however, it had a relatively low grades on the structure security, installation difficulty and reversibility. The results of wall and roof demonstrated unsuitability in perspective of all four indexes.

The current evaluation presented that the window, door and lintel can be the potential components for ventilator application. Also, the word, 'fenestration', can represented above components. In other words, this research should propose a novel ventilator for fenestration. Compare with conventional ventilators, the proposed prototype aims to improve the energy efficiency during ventilation without compromising the architectural integrity.

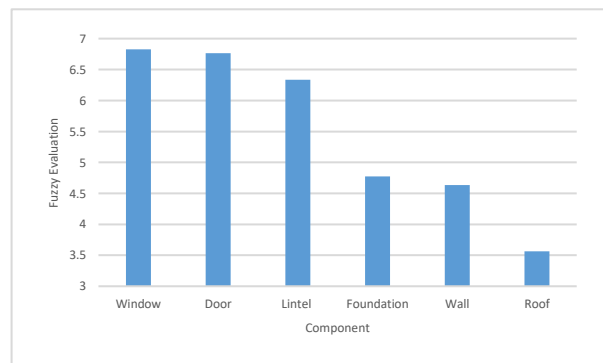


Figure 3 The distribution of fuzzy evaluation

### 4. PROTOTYPE DESCRIPTION

The applications of heat recovery systems make it possible to achieve above aim. An air-to-air heat recovery ventilator is commonly defined as one of the major energy-saving technologies that are essential to contribute to the reduction of consumption demands from HVAC systems (Mardiana-Idayu, Riffat 2012). In other words, it is based on preheating the incoming air to the interior through recycled waste heat from exhaust air. A representative heat recovery system in residential buildings is usually composed of a heat exchanger core, extractor fans, a fresh air inlet and a separate contaminated air exhaust outlet. The prototype is developed based on a TE module-based heat recovery system. Heat recovery system is commonly referred to as a device operating between two air sources at different temperatures which

transfers energy from one side to the other. In other words, it is based on preheating the incoming air to the interior through recycled waste heat.

#### 4.1. Peltier Effect

(Riffat, Gillott 2002) stated that the application of heat pump can enhance the heat transfer in heat recovery ventilator. As the refrigerants in most vapor-compression heat pump systems, such as CFCs and HFCs, have been regarded ozone-depleting substance, the interest on the application of thermoelectric heat pump for air conditioning and refrigerators has arisen (Riffat et al. 2006). Thermoelectric (TE) cooling modules are solid-state heat pumps based on the Peltier effect. With DC current flowing through the module, the heat transferred from one side to the other would occur, simultaneously creating a temperature gap between the two sides (Ioffe et al. 1959). Under suitable DC current supply, the temperature gap between the two sides of TE modules will be larger than the temperature gap between inlet and outlet air, which would enhance the heat transfer between heat sink and air flows. The applied thermoelectric module will reduce the number of moving parts in the system and aid the window heat recovery by helping move heat from the outgoing air into the incoming air stream, offering a backup heating system. The thermoelectric heat pump technique offers several advantages over other technologies:

- Solid-state without any moving parts, durable and long-life span.
- Small size, compact design, lightweight and easy installation without orientational limitations.
- Require no chlorofluorocarbon, environmentally friendly.
- Low-voltage DC power operation required which would be satisfied by photovoltaic (PV) solar cells, fuel cells and car DC electric sources (Zhao, Tan 2014), convenient control.
- Fully reversible by changing the direction of the DC power supply.
- Not much limited by operating environment even in severe and sensitive locations (Riffat, Ma 2004).

The prototype is developed based on the conventional TE module arrangement. The number of applied TE modules are adjustable depending on the actual requirement. The integrated system is introduced to reduce space heating consumption and maintain essential ventilation simultaneously. It takes the advantages of being energy-saving, environmentally friendly and compact which could be modular produced integrating with window frames. The prototype comprises four main components, heat exchanger core (TE module with aluminium plate fin heat sink); high density aerogel sheet, thermal insulating material panel and axial fans.

As the Figure 4 shown, the TE modules are positioned between two plate fin heat sinks to form a sandwich heat transfer structure. The highly efficient thermal bonding epoxy adhesive (ARCTIC MX-2 thermal compound paste) has been utilised between TE module surface and heat sink. Simultaneously, the TE module is bounded by the aerogel sheet which is positioned between heat sinks working as insulation pads to reduce heat convection and radiation between heat sinks on the cold side and hot side. Two expanded polystyrene insulation panels are attached to the inside surface of the housing case to reduce heat loss

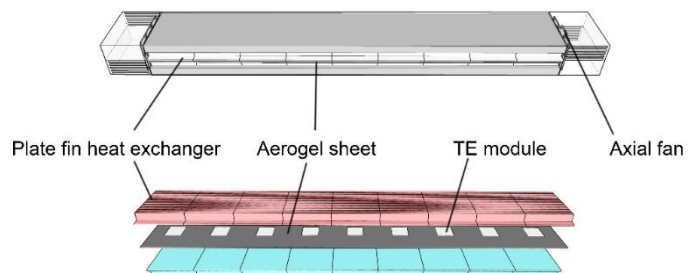


Figure 4 Schematic diagram of the WTEPFV design

through the casing and were incorporated with the plate fin heat sink to form the airflow exchanging channel. The axial fans are installed at the start and the end of heat sinks respectively, using negative pressure to draw air through the system. The housing case is made of engraved aluminium sheet or wood according to the features of heritage buildings.

In the winter period, with electric power supplied, the interior exhaust air will be firstly pumped into the cold side air channel by axial fans. And then, absorbing some heat across the cold side heat sink, it is exhausted to the ambient. Meanwhile, with a parallel flow arrangement, the outdoor fresh air will be sucked into another airflow channel attached to the TE module hot side. And then it would be heated through the hot side heat sink and be delivered into the room. The main desire is to reduce the heat loss during ventilation and provide pre-heated fresh air to assist the heating system to be more energy efficient. The proposed system could be powered by the PV generation system. In summary, the WTEPFV system would allow a pre-heated fresh air supply into the room in cold weather whilst reducing domestic building energy consumption during ventilation.

## 4.2. Installation

The concept of the decentralised heat recovery ventilator for single room application has been introduced, which would not require complicated duct systems like the traditional one. The proposed WTEPFV unit is designed as decentralised heat recovery ventilator. It is slim and compact design and could be installed on the new or existing room window frames or door frame for single room. The prototype could be utilised for a small-scale single room as a ventilator as well as a heater to assist existing heating devices. The application of the WTEPFV system could contribute to maintaining interior temperature and heat recovery from stale air during daily ventilation. And the whole unit might be running with PV and advanced intelligent building heating management systems for long-term operation which could contribute significantly to addressing energy supply-demand of a building.

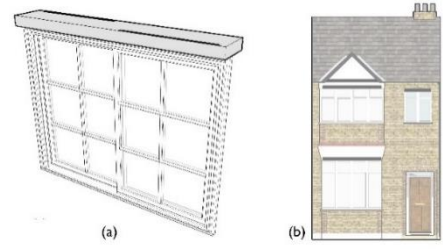


Figure 5 The schematic figure of prototype

## 5. MODELLING

The main aim of the model is to analyse the thermal performance of the system, predicting its heating generation rate and  $COP_h$  with different electric power input under the same environment condition (constant temperature of fresh air and exhaust air). For simplification, the following assumptions have been considered in the energy transfer analysis, including:

- The air velocity is assumed as constant, and the air pressure drop is not considered during the process.
- All the energy balance equations are for the steady state conditions. The heat loss of TE modules and plate fin heat sinks are neglected.
- The effect of temperature on the TE modules physical properties is ignored.
- The heating capacity of each TE module is constant.

## 6. CALCULATION OF PROTOTYPE OPERATION

### 6.1. Single thermoelectric module

From literature study, the heat generation rate at the hot side, the cooling capacity at the cold side of an individual TE module and its electrical power consumption can be calculated by Equation 6 to Equation 8 (Liu et al. 2018):

$$\text{Equation 6} \quad Q_h = \alpha I_{tec} (T_h + 273.15) + \frac{1}{2} I_{tec}^2 r_{te} - k_{te} (T_h - T_c)$$

$$\text{Equation 7} \quad Q_c = \alpha I_{tec} (T_c + 273.15) - \frac{1}{2} I_{tec}^2 r_{te} - k_{te} (T_h - T_c)$$

$$\text{Equation 8} \quad P_{te} = Q_h - Q_c = \alpha I_{tec} (T_h - T_c) + I_{tec}^2 r_{te}$$

Where  $Q_h$ ,  $Q_c$  are the heat dissipated at the hot side and the amount of heat absorbed at the cold side, respectively;  $P_{te}$  is the power input to TE module;  $T_h$ ,  $T_c$  are the temperature of hot side and cold side of TE module, respectively;  $I_{tec}$  is the selected current for TE module;  $\alpha$  is the TE module's Seebeck coefficient;  $r_{te}$  is the electrical resistance of TE module; and  $k_{te}$  is the thermal conductance of TE module. The value of  $\alpha$ ,  $r_{te}$  and  $k_{te}$  are related to the thermophysical properties of TE material. However, these characteristics are considered to be temperature independent to simplify the thermal transfer process. Here,  $\alpha$ ,  $r_{te}$  and  $k_{te}$  can be determined through the manufacturer's datasheet by Equation 9 to Equation 11 (Cai, Zhang, et al. 2019):

$$\text{Equation 9} \quad \alpha = \frac{V_{max}}{(T_{hot} + 273.15)}$$

$$\text{Equation 10} \quad r_{te} = \frac{V_{max}}{I_{max}} \left( 1 - \frac{\Delta T_{max}}{(T_{hot} + 273.15)} \right)$$

$$\text{Equation 11} \quad k_{te} = \frac{V_{max} I_{max} (T_{hot} + 273.15 - \Delta T_{max})}{2 T_h \Delta T_{max}}$$

Where  $V_{max}$  and  $I_{max}$  are the maximum voltage and current of TE module, respectively;  $\Delta T_{max}$  is the maximum temperature difference between hot and cold side of TE module; and  $T_{hot}$  is hot side reference temperature.

## 6.2. Calculation of plate fin heat sink

The widely used plate fin heat sink is the parallel plate structure heat sink, as shown in Figure 6. The thermal resistance of the plate fin heat sink could be estimated by its geometry structure and air flow rate.

For a basic plate fin heat sink in application, the overall thermal resistance  $R_{total}$  could be calculated as follows:

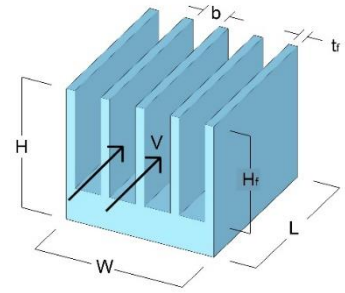


Figure 6 Diagram of typical parallel plate fin heat sink structure

$$R_{total} = \frac{H - H_f}{k_{base} \cdot W \cdot L} + \frac{1}{N_u \frac{k_{fin}}{b} \left[ (N_{fin} - 1)bL + 2N_{fin} \frac{\tanh\left(\sqrt{\frac{2N_u \frac{k_{fin}}{b}}{k_{fin}t_f}} H_f\right)}{\sqrt{\frac{2N_u \frac{k_{fin}}{b}}{k_{fin}t_f}} H_f} \right] H_f L}$$

Equation 12: overall thermal resistance

Where,  $R_{base}$  is the conductive thermal resistance between the TE module and the aluminium plate fin heat sink basement.  $R_{hs}$  is the heat transfer resistance of the plate fin heat sink.  $H$  is the total height of the plate fin heat sink;  $H_f$  is the height of fins;  $k_{base}$  is the thermal conductivity of the heat sink base;  $W$  is the width of the plate fin heat sink and  $L$  is the length of the heat sink.  $h$  is the convective heat transfer coefficient;  $A_{base}$  is the surface area of the basement which contacts airflow directly;  $N_{fin}$  is the number of fins;  $\eta_{fin}$  is the efficiency of heat sink;  $A_{fin}$  is the total area of fins;  $Nu$  is the airflow Nusselt number;  $k_{fin}$  is the thermal conductivity of heat sink fins;  $b$  is the fin spacing of heat sink;  $L$  is the length of heat sink;  $t_f$  is the thickness of heat sink fins; and  $H_f$  is the height of fins. The Nusselt formula  $Nu$  could be derived by the given Equation (4-4) from other similar experiments (Teertstra et al. 2000):

$$Nu = \left[ \frac{1}{\left[\frac{RePr}{2}\right]^3} + \frac{1}{\left[0.664\sqrt{RePr}^{0.33} \sqrt{1 + \frac{3.65}{\sqrt{Re}}}\right]^3} \right]^{-0.33}$$

Equation 13: Nusselt formula

$Re$  is the Reynolds number of the rectangular channel, related to fluid velocity, density and viscosity coefficient, and  $Pr$  is the airflow Prandtl number.

## 6.3. Heat balance of the system

The hot side of the TE module could supply heating to the fresh air and the cold side of TE module would supply cooling to the exhaust air. When the whole system operates under stable conditions, the hot and the cold side temperature of the TE module would keep approximately constant. According to the energy balance,  $Q_c$  is also the heat flow through the cold side heat exchanger and  $Q_h$  is the heat flow through the hot side heat exchanger. The method of the effectiveness-number of heat transfer units ( $\epsilon$ -NTU) for the hot and cold side heat exchanger is introduced to establish the heat transfer model, simplifying the analysis of the heat exchanging process. Therefore, the heat transfer rate ( $Q_h$ ,  $Q_c$ ) can also be simulated by the following equations (Cai, Wang, et al. 2019):

$$Q_h = \frac{T_h - T_{f-in}}{\frac{1}{\epsilon_h C_h}}$$

Equation 14:

$$Q_h = \frac{T_{e-in} - T_c}{\frac{1}{\epsilon_c C_c}}$$

Equation 15:

Where  $T_h$  and  $T_c$  represent the hot and the cold side temperature of TE module, respectively;  $T_{f-in}$  is the temperature of fresh air inlet;  $T_{e-in}$  is the exhaust air inlet temperature;  $C_h$  and  $C_c$  are the specific heat of airflow in the hot and the cold side,

respectively; and  $\varepsilon_h$  and  $\varepsilon_c$  are the heat exchanger effectiveness (functions of the hot and the cold side thermal conductance), which could be expressed as follows (Cai, Wang, et al. 2019)(Cai, Zhang, et al. 2019):

$$\text{Equation 16:} \quad \varepsilon_h = 1 - \exp\left(-\frac{U_h A_h}{C_h}\right)$$

$$\text{Equation 17:} \quad \varepsilon_c = 1 - \exp\left(-\frac{U_c A_c}{C_c}\right)$$

$$\text{Equation 18:} \quad U_h A_h = \frac{1}{R_h}$$

$$\text{Equation 19:} \quad U_c A_c = \frac{1}{R_c}$$

where  $U_h A_h$  and  $U_c A_c$  are the hot and the cold side thermal conductance, respectively;  $C_h$  and  $C_c$  represent the forced airflow specific heat in the hot and the cold side, respectively; and  $R_h$  and  $R_c$  are the hot and the cold side total thermal resistance, respectively, including convective thermal resistance of the flow and conductive thermal resistance of the heat sink.

Combining Equation (4-5) to (4-10), the heating capacity and cooling capacity could also be expressed as (Cai, Wang, et al. 2019),

$$\text{Equation 20:} \quad Q_h = \varphi_h U_h A_h (T_h - T_{f-in})$$

$$\text{Equation 21:} \quad Q_c = \varphi_c U_c A_c (T_{e-in} - T_c)$$

where  $\varphi$  is an introduced intermediate variable as a function of the hot/cold side thermal efficiency, which could be defined as

$$\text{Equation 22:} \quad \varphi_h = \frac{\varepsilon_h}{\ln \frac{1}{1 - \varepsilon_h}}$$

$$\text{Equation 23:} \quad \varphi_c = \frac{\varepsilon_c}{\ln \frac{1}{1 - \varepsilon_c}}$$

The heating and cooling loads could also be estimated by the following equations,

$$\text{Equation 24:} \quad Q_h = C_h (T_{f-out} - T_{f-in})$$

$$\text{Equation 25:} \quad Q_c = C_c (T_{e-in} - T_{e-out})$$

Here,  $T_{f-out}$  and  $T_{e-out}$  are the fresh air and exhaust air outlet temperature, respectively.

The WTEPFV prototype could be assumed as a set of multiple heating modules, connected in parallel electrically. Each module would operate with same working current input. Accordingly, the total heating capacity could be derived as,

$$\text{Equation 26:} \quad Q_h = \sum_1^n Q_h^i = Q_h^1 + Q_h^2 + \dots + Q_h^n$$

The coefficient of performance (COP) of the system for heating purpose ( $COP_h$ ) is given by:

$$\text{Equation 27:} \quad COP_h = \frac{\sum_1^n Q_h^i}{\sum_1^n P_{te}^i + P_{fan}}$$



Where  $n$  is the number of TE modules;  $P_{te}$  is the power consumption of TE modules and  $P_{fan}$  is the power supplied to the applied axial fans. A programme by MATLAB platform is built up to evaluate the heating performance of the system based on the thermodynamic model aforementioned. The simulation process is carried out following the flow chart as illustrated in Figure 7.

Eight TE modules were utilised in the system. The temperature of ingoing air and outgoing air during the modelling corresponded to the laboratory test condition where the ingoing cold air temperature of 18 °C and the outgoing air temperature of 30 °C were set. Due to the limitation of the applied wire with the maximum current rate of 18A for the construction, the total safe input current for TE modules is considered to be 16A, which means the maximum working current for each TE module during the testing is 2A. The laboratory scale investigation will be discussed in a later section. The modelling results of the system for heating performance under laboratory conditions are listed in Table 2.

With the increasing working current for TE modules, the higher estimated temperature changes would be obtained. However, excessive working current would cause the decrease of heat generation since the condition would exceed the rated heating capacity of the applied heat sink, further leading to the heat on the hot side flowing into the cold side. Moreover, the life span of the TE module would be affected with a large amount of heat gathered at the hot side. Therefore, to achieve operation with high current input, the modification should be conducted, reduce the amount of TE modules or optimise the heat sink design.

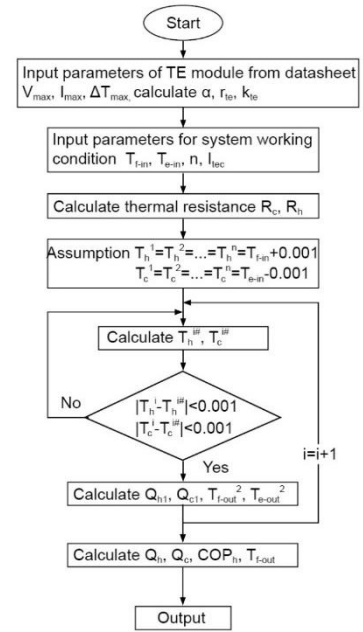


Figure 7 Modelling flow chart

## 7. EXPERIMENTAL INVESTIGATION

The prototype was tested in an environmental control chamber (HotBox) in the SRB building, University of Nottingham. Figure 8 shows the picture of the HotBox and testing rig. The system was mounted on one of the walls of the HotBox (1.8m\*1.8m\*1.2m), one side towards the chamber which acting as indoor condition, the other facing the laboratory that assuming as outdoor environment. Tests were carried out under various DC current to TE modules. The main temperature measurement tool, Data Taker DT80 Series 3, works as an interface between a laptop and the temperature sensors (thermocouples). And all the data were recorded when the Ecopump performed in a stable condition.



Figure 8 The photo of testing rigs

Table 2: Modelling results of the WTEPFV prototype.

Parameters	Value			Unit
Working current for each TE module	1A	1.5A	2A	
Ingoing air temperature (fresh air inlet)		18		°C
Temperature of fresh air after heat sink	28.8	33.6	39.1	°C
Temperature changes	10.8	15.6	21.1	°C
Total heating capacity	81.6	117.5	158.8	W
COP <sub>h</sub>	2.48	2.04	1.71	-



## 8. DISCUSSION OF MODELLING AND TESTING RESULTS

A comparison of modelling results and experimental results with similar operating conditions were conducted. Figure 9 shows the comparison of heating capacity and COP<sub>h</sub> between the modelling results and experimental results. In general, the modelling results and experimental results present a very similar trend under given current input. The comparisons indicate that the theoretical modelling results show an acceptable agreement with the test results; thus, the model can be used to predict the performance of the WTEPFV system for heating purposes.

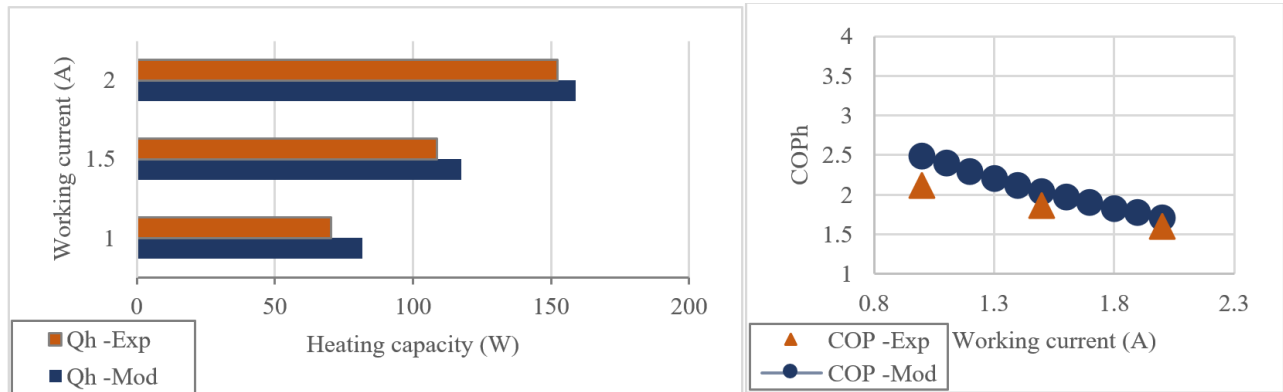


Figure 9 Comparison of heating capacity and COP<sub>h</sub> value between experiment and modelling

## 9. ANNUAL OPERATION PERFORMANCE, ECONOMIC AND ENVIRONMENTAL ANALYSIS

In this section, the annual operational performance of the proposed window TE module-based prototypes under real weather conditions is discussed according to software simulations. The performance of the units was obtained through the analytical model and experimental investigations conducted as reported in MATLAB.

The house located in Dunkirk, Nottingham will be employed to handle simulated operation of the prototypes. The house was built in mid of 20th century and it could provide for a family of two adults and one child. It is a two-floor house with sloping roof. The three-dimensional model with agreement of the sizing is built up in computer programme, as shown in Figure 10. (Bernier et al. 2010) stated that Britain's housing stock is among Europe's oldest and least energy efficient. In order to achieve goals on carbon emission saving, 80% of houses in stock, about 26 million homes, are required to retrofit like the selected house. This type of housing is common in the current housing stock in the UK.

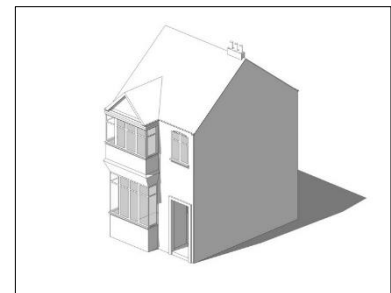


Figure 10 The visualisation model in software

In simulation, the minimum indoor temperature has been set to 18 °C, which means that the assumed temperature of exhaust air inlet for the prototypes is 18 °C. However, the outdoor temperature would change with time. 98% of the ambient temperature for annual operation time is below 18 °C. Based on the MATLAB programme, the heating performance of WTEPFV systems could be predicted under various operating conditions. From Yeler and Koseoglu, the TE system for heating purposes would be economically feasible when its COP could reach 1.4 or above (Yeler, Koseoglu 2020). Therefore, to obtain better energy efficiency, the minimum COP<sub>h</sub> for the systems are set to be above 1.4.

Based on the software simulation, the heat gains or heat losses of Bedroom in the house can be identified. Figure 11 (a) shows the heat gains or losses of Bedroom with different exterior temperature. According to the modelling of the WTEPFV unit, its heating capacity (Q<sub>h</sub>) under various ambient temperature could be obtained when the COP<sub>h</sub> has been set to be above 1.4.

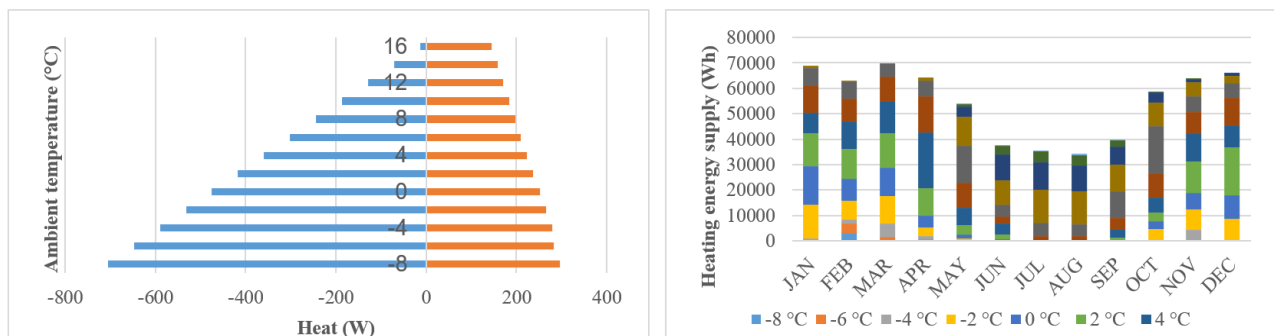


Figure 11 (a) Comparison of heat losses in Bedroom 2 and heat supplement from the WTEPFV under various ambient temperature; (b) Monthly heating energy supply from the WTEPFV

It can be found that the heat losses are reduced greatly when the temperature increase. And the heat losses would be less than the heat supplement from the WTEPFV unit when the outdoor temperature reaches 12°C or above, which means extra unnecessary heating exist. Therefore, the operation condition of prototype should be adjusted to avoid overheating and energy waste. The reasonable operating condition of the WTEPFV unit should meet both the requirement of COP<sub>h</sub> (above 1.4) and suitable heat loss compensation. Therefore, the optimal working current for the TE module satisfying the condition has been identified. After adjustment, the annual heating supply from the WTEPFV unit and annual power consumption can be calculated. Figure 11 (b) presents the monthly heating energy supplement from the WTEPFV. And the annual heat supply from the unit is calculated as about 655 kWh.

The annual energy consumption of the unit is calculated about 452 kWh, and the average operation COP<sub>h</sub> of the unit is calculated as 1.45. From simulation, the annual energy demand for space heating of Bedroom with installed WTEPFV is estimated to be 956 kWh. According to the abovementioned calculation, the WTEPFV system would supply 655 kWh heating energy for year-round operation. Therefore, extra 301 kWh energy is needed from other heating devices, i.e. electric heater. Although the WTEPFV system could supply basic ventilation, the extra energy demands to compensate the space heating are needed for Bedroom in the applied house.

The capital cost of the WTEPFV unit is about £564. While electric unit price is about 20p per kWh (Anon 2021b) and the average Inflation Rate in the UK is about 1.5% (Anon 2021a), the total operation cost (including electric energy consumption and capital costs) for the WTEPFV is calculated as £2,654 for a 20-year operation. Based on the abovementioned calculation, the average operation COP<sub>h</sub> is about 1.45, which means that the application of the WTEHPV unit can save energy consumption around 203 kWh every year. The total cost of energy saving after 13 years could cover the capital cost of the unit.

Furthermore, the carbon saving contribution of the WTEHPV could also be evaluated. (Hill et al. 2015) reported the average carbon emission factor of British grid energy consumption is about 0.46 kgCO<sub>2</sub>/kWh, which includes the carbon emission during electricity generation and transmission. The annual carbon emission caused by WTEHPV systems with grid energy system could be estimated, specified energy consumption multiply by corresponding carbon emission factor. Through calculation, the carbon emissions of Bedroom with installed WTEPFV could save 93.2 kg CO<sub>2</sub> emissions per year. And the total carbon emission saving of the WTEPFV application would account for around 21.1% of annual carbon emissions of Bedroom without the WTEPFV.

## 10. FUTURE WORK

Further investigation under real conditions and long-term schemes should be undertaken. The laboratory-based investigation could not imitate real operating performance. The field testing within the house has been interrupted by the COVID-19 pandemic. The results could be analysed to verify the simulated annual operation performance. Additionally, the systems would also be investigated with long term schemes and different climates to explore their real behaviour and applicability.

Theoretically, the common PV generation system could support the operation of TE module without extra national grid power supplies to achieve better energy efficiency performance. The energy generated by PV can be stored in the battery bank to power the unit and can also be consumed on other appliances. The investigation on the energy saving potential of proposed integrated systems powered by PV panels should also be carried out.

## 11. CONCLUSION

A comparison of modelling results and experimental results has been discussed. And decision parameters including working current, number of TE modules, the thermal resistance of heat sink and temperature differences between indoor and outdoor environment, are also numerically investigated to identify the optimization strategy. The major results are summarised below:

- The fenestration is the prioritized location to apply the novel ventilators. The novel ventilator should be slim and durable for minimal impact on historic features and maintenance.
- As the input current for TE modules increases, the heating capacity of the system will raise. However, the excessive current should be avoided due to the limitation of rated heat transfer capacity of the heat sink, especially for multiple TE module applications.
- According to lab-scale tests, the WTEPFV system could generate 70W to 152W heat with a working current ranging from 1A to 2A.
- For the WTEPFV system, it would provide annual heating of 655 kWh for Bedroom 2 at optimal working current, achieving an average COP<sub>h</sub> of about 1.45 with grid energy supply. From the calculation, the carbon emissions of Bedroom 2 with installed WTEPFV unit would reduce 93.2 kg CO<sub>2</sub> emissions per year.

## 12. REFERENCES

Abdul Hamid, A., Johansson, D., Bagge, H., 2020. Ventilation measures for heritage office buildings in temperate climate for improvement of energy performance and IEQ. *Energy and Buildings*, 211. 10.1016/j.enbuild.2020.109822.

Anon, 2021a. Office for National Statistics. Office for National Statistics.

Anon, 2021b. UK electricity prices. Power Compare.

Bernier, P., Fenner, R.A., Ainger, C., 2010. Assessing the sustainability merits of retrofitting existing homes. In: Proceedings of the Institution of Civil Engineers-Engineering Sustainability. Thomas Telford Ltd, pp. 197–207.

Bhagat, R.K. et al., 2020. Effects of ventilation on the indoor spread of COVID-19. *Journal of Fluid Mechanics*, 903.

Cai, Y., Zhang, D.D., et al., 2019. Air source thermoelectric heat pump for simultaneous cold air delivery and hot water supply: Full modeling and performance evaluation. *Renewable Energy*, 130, pp.968–981. 10.1016/j.renene.2018.07.007.

Cai, Y., Wang, L., et al., 2019. Thermal performance of an active thermoelectric ventilation system applied for built space cooling: Network model and finite time thermodynamic optimization. *Energy*, 170, pp.915–930. 10.1016/j.energy.2018.12.186.

Choi, J.Y. et al., 2023. Proposal of retrofit of historic buildings as cafes in Korea: Recycling biomaterials to improve building energy and acoustic performance [online]. *Energy and Buildings*, 287, p.112988. Available at: <https://www.sciencedirect.com/science/article/pii/S0378778823002189>.

Fehrm, M., Reiners, W., Ungemach, M., 2002. Exhaust air heat recovery in buildings. *International Journal of Refrigeration*, 25(4), pp.439–449.

Ganesh, H.S. et al., 2019. A model-based dynamic optimization strategy for control of indoor air pollutants. *Energy and Buildings*, 195, pp.168–179. 10.1016/j.enbuild.2019.04.022.

Ge, J. et al., 2022. Suitable and energy-saving retrofit technology research in traditional wooden houses in Jiangnan, South China [online]. *Journal of Building Engineering*, 45, p.103550. Available at: <https://www.sciencedirect.com/science/article/pii/S235271022101408X>.

Hill, N. et al., 2015. 2015 Government GHG Conversion Factors for Company Reporting: Methodology Paper for Emission Factors. Final Report. Department of Energy and Climate Change (DECC), London.

Huang, K. et al., 2018. Indoor air quality analysis of residential buildings in northeast China based on field measurements and longtime monitoring. *Building and Environment*, 144(July), pp.171–183. 10.1016/j.buildenv.2018.08.022.

Ioffe, A.F. et al., 1959. Semiconductor thermoelements and thermoelectric cooling. *Physics Today*, 12, p.42.

Jiang, W. et al., 2022. Protective energy-saving retrofits of rammed earth heritage buildings using multi-objective optimization [online]. *Case Studies in Thermal Engineering*, 38, p.102343. Available at: <https://www.sciencedirect.com/science/article/pii/S2214157X22005834>.

Li, Y. et al., 2022. Environment improvement and energy saving in Chinese rural housing based on the field study of thermal adaptability [online]. *Energy for Sustainable Development*, 71, pp.315–329. Available at: <https://www.sciencedirect.com/science/article/pii/S0973082622001879>.

Liu, Z. et al., 2018. Modeling and simulation of a photovoltaic thermal-compound thermoelectric ventilator system [online]. *Applied Energy*, 228, pp.1887–1900. Available at: <http://www.sciencedirect.com/science/article/pii/S030626191831033X>.

Mardiana-Idayu, A., Riffat, S.B., 2012. Review on heat recovery technologies for building applications [online]. *Renewable and Sustainable Energy Reviews*, 16(2), pp.1241–1255. Available at: <http://linkinghub.elsevier.com/retrieve/pii/S136403211100476X> [Accessed 24 June 2017].

Marzouk, M., El-Maraghy, M., Metawie, M., 2023. Assessing retrofit strategies for mosque buildings using TOPSIS [online]. *Energy Reports*, 9, pp.1397–1414. Available at: <https://www.sciencedirect.com/science/article/pii/S2352484722026749>.

Riffat, S.B., Gillott, M.C., 2002. Performance of a novel mechanical ventilation heat recovery heat pump system [online]. *Applied Thermal Engineering*, 22(7), pp.839–845. Available at: <https://www.sciencedirect.com/science/article/pii/S1359431102000248>.

Riffat, S.B., Ma, X., 2004. Optimum selection (design) of thermoelectric modules for large capacity heat pump applications. *International journal of energy research*, 28(14), pp.1231–1242.

Riffat, S.B., Ma, X., Wilson, R., 2006. Performance simulation and experimental testing of a novel thermoelectric heat pump system. *Applied Thermal Engineering*, 26(5–6), pp.494–501. 10.1016/j.applthermaleng.2005.07.016.

Schieweck, A. et al., 2018. Smart homes and the control of indoor air quality. *Renewable and Sustainable Energy Reviews*, 94(June 2017), pp.705–718. 10.1016/j.rser.2018.05.057.

Teertstra, P., Yovanovich, M.M., Culham, J.R., 2000. Analytical forced convection modeling of plate fin heat sinks. *Journal of Electronics Manufacturing*, 10(04), pp.253–261.

Yeler, O., Koseoglu, M.F., 2020. Optimization and experimental validation of a modular thermoelectric heat pump system for a premature baby incubator. *Journal of Electronic Materials*, pp.1–14.

Yuk, H. et al., 2023. Evaluation of suitability for passive retrofit of wooden roof considering the specificity of historic buildings [online]. *Building and Environment*, 242, p.110608. Available at: <https://www.sciencedirect.com/science/article/pii/S0360132323006352>.

Zhang, F. et al., 2021. A new framework to select energy-efficient retrofit schemes of external walls: A case study [online]. *Journal of Cleaner Production*, 289, p.125718. Available at: <https://www.sciencedirect.com/science/article/pii/S0959652620357644>.

Zhao, D., Tan, G., 2014. A review of thermoelectric cooling: Materials, modeling and applications. *Applied Thermal Engineering*, 66(1–2), pp.15–24. 10.1016/j.applthermaleng.2014.01.074.

---

## #290: Investigations on the retrofitting strategies coupling multiple targets on heritage dwellings located in Suzhou

---

Shihao ZHANG<sup>1</sup>, Qi XU<sup>2</sup>, Saffa RIFFAT<sup>3</sup>

*1 School of Architecture and Urban Planning, Suzhou University of Science and Technology, Suzhou, 215011, China, shihaozhang@usts.edu.cn*

*2 College of Architecture, Nanjing Tech University, Nanjing, 210044, China, Email: xuqi@njtech.edu.cn*

*3 Department of Architecture and Built Environment, University of Nottingham, Nottingham NG7 2RD, UK, saffa.riffat@nottingham.ac.uk*

*Abstract: Suzhou city is one of the national historical and cultural cities in China. There is a huge stock of heritage buildings built about 200 years ago. Heritage buildings, imbued with historical and cultural significance, pose unique challenges when it comes to retrofitting for modern energy efficiency and thermal comfort standards. The retrofit is essential for heritage conservation. However, the energy retrofit on the heritage dwelling without impacting on their characteristics, especially appearance, presents a major challenge for architects and policymaker. This research paper presents a comprehensive investigation into retrofitting strategies for heritage dwellings in Suzhou. The study prioritises retrofitting strategies that simultaneously address the multi-faceted goals of thermal comfort enhancement and energy consumption reduction. The research focuses on the imperative to reconcile heritage conservation with contemporary sustainability demands.*

*The paper begins by demonstrating the measurements process on the thermal properties and potential retrofit strategies of heritage buildings. Then, the Analytic Hierarchy Process (AHP) model would be implemented to evaluate the adaptability of potential retrofit strategies and select the strategies that preserves the uniqueness of historic building. After that, the selected strategies could be fully combined to form various scenarios, and the energy simulation for various scenarios would be carried out. The combination with least energy consumption is obtained. Finally, TOPSIS is employed to assess the performance of selected strategies across multiple criteria. This study contributes to the research on heritage building retrofitting, offering a systematic and integrated approach that can guide decision-makers, architects, and preservationists in safeguarding our architectural heritage while meeting the demands of the modern era.*

*Keywords: Multi targets; Retrofit; Heritage dwellings*

## 1. INTRODUCTION

Suzhou city, situated along the banks of the Grand Canal in Jiangsu Province, China, has a great reputation for its marvellous Chinese heritage buildings and landscape, which can be dated over 600 years ago. The heritage buildings in Suzhou have been carefully preserved as a UNESCO World Heritage List. In recent years, Suzhou's government is promoting the integration of its tangible cultural heritage with tourism, technology, fashion, and other creative fields (Wang 2014). However, there is a huge stock of traditional buildings which hold significant historical and cultural value but often face challenges in terms of energy efficiency and indoor comfort. They provide us with a connection to the past and can help us to learn about our history and culture. However, heritage buildings can also be energy inefficient, which can lead to high energy bills and environmental impacts. It is of great social and economic significance to retrofit the traditional dwellings for better performance. Retrofitting these buildings is essential to ensure their preservation and continued use. However, traditional retrofitting methods may compromise the architectural integrity and appearance of these structures.

The process of retrofitting existing buildings to improve overall performance has become a focus in the field of sustainable construction. Although retrofitting on modern buildings has been extensively studied in recent years, the retrofitting on heritage buildings introduces a series of complexity. Protecting its cultural and historical value requires a delicate balance between preservation and adaptation. The preservation and energy-efficient retrofit of heritage buildings have gained substantial attention worldwide (Choi et al. 2023; Yuk et al. 2023; Jiang et al. 2022). Governments and heritage organizations recognize the need to balance conservation efforts with sustainable building practices. However, there is limited research on retrofit solutions that specifically target energy-efficient ventilation while preserving the architectural and historical aspects of these buildings (Abdul Hamid et al. 2020).

This paper expands with a multidisciplinary exploration of transformation strategies that not only address these conflicting goals, but also provide templates for heritage preservation in other cities around the world. The research offers insights into how heritage buildings can embrace sustainable retrofitting, honouring their past while accommodating the needs of the present and future. Suzhou's heritage dwellings serve as a compelling case study, exemplifying the complicated choice between tradition and innovation, conservation and adaptation.

## 2. METHODOLOGY

The conventional heat recovery ventilation system for residential buildings is usually composed of a heat exchanger core, extractor fans, a fresh air inlet and a separate contaminated air exhaust outlet. The heat exchanger core is normally installed in attic space and requires a complicated and well-designed duct system to reach each room in the house (Fehrm et al. 2002), which will require extra time and are not suitable to apply in heritage building.

This research introduces a novel approach to heritage building retrofitting by proposing a thermoelectric ventilator system. Unlike traditional methods, this system aims to improve energy efficiency and indoor air quality without compromising the architectural and historical value of heritage buildings.

In order to integrate into the heritage buildings with minimally invasiveness, the location of the thermoelectric ventilator system should be carefully chosen so that it does not damage the heritage features of the building. And the design of the thermoelectric ventilator system should be sympathetic to the architectural style of the building. Hence, an Analytic Hierarchy Process (AHP) based fuzzy synthetic evaluation was conducted to identify the most suitable components for ventilator application which have the least impact on the heritage features of the building. Then, the design and construct a prototype of the thermoelectric ventilator system was demonstrated. Finally, MATLAB modelling and Revit simulation were utilized to assess the prototype's performance when integrated into a house in the UK.

This methodology of this research provides a holistic solution to the multiple challenges of heritage building renovation in Suzhou, and can serve as a model for similar conservation and sustainability efforts in other heritage-rich environments. It considers both qualitative and quantitative aspects, enabling a nuanced understanding of the complexities involved in achieving thermal comfort and energy efficiency in heritage residences while preserving their cultural and historical value.

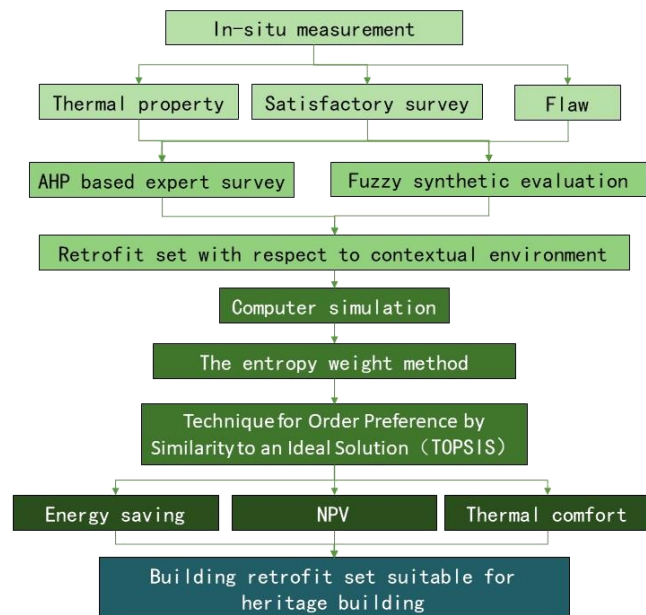


Figure 1 The framework of methodology

### 3. IN-SITU INVESTIGATION

#### 3.1. In-situ Measurement

A specific heritage building in Suzhou known as Dongshan, dating back to the Ming Dynasty, has been selected as the focal point of the in-situ investigation. This building is situated on Songyuannong Road in the Wuzhong area of Suzhou. While it possesses a fundamental level of protection, it is still in need of essential preservation and restoration measures. The Dongshan building has retained the structural elements and materials from its original construction during its last renovation. It boasts a construction area of 328.9 square meters and exhibits a body shape coefficient of 0.53 (Fu 2018).

It's important to note that there are numerous heritage buildings in the vicinity that share similar historical significance, architectural characteristics, and building materials. Therefore, the chosen Dongshan building can serve as a representative example of historic buildings in this particular region. While these buildings may not be subject to the same stringent protection measures as officially designated cultural heritage units, they still necessitate suitable protection and restoration efforts to preserve their historical appearance and cultural value.



Figure 2 Photo of Dongshan, Suzhou (Fu 2018)

The process of measurement plays a pivotal role in the evaluation of heritage buildings and the effectiveness of retrofitting strategies. It serves as a crucial source of empirical data that informs decision-making while striving to achieve retrofitting objectives and simultaneously preserve the building's historical significance. In the context of in-situ measurements, an extensive investigation is carried out to comprehensively assess various aspects of the building's performance, including thermal comfort and energy consumption, all while considering its unique features, materials, and existing conditions. Additionally, surveys and questionnaires are conducted with the occupants, providing real-world data that forms a solid basis for evaluating the retrofit strategies.

To facilitate this measurement process, a range of instruments is employed, which may include temperature sensors, humidity sensors, energy meters, data loggers, and environmental monitoring equipment. The temperature and humidity sensors are set to record data at regular intervals, typically every 15 minutes. Energy meters are utilized to monitor the electricity and gas consumption in the building, capturing data on a monthly basis. Data loggers, specifically the DT85 and CL11 models, collect data at 10-minute intervals, and results are retrieved monthly. A web-based data logger is employed to collect information from the various sensors and provide graphical representations for continuous monitoring.

To measure interior and exterior temperatures accurately, calibrated K-type thermocouples are used. These thermocouples are strategically positioned in locations such as the living room, kitchen, and bedroom, where occupants spend a substantial amount of time, and are distal to heat sources and direct sunlight. Additionally, the monitoring system incorporates ten thermocouples within a single house and a pyranometer placed on the southern wall. Furthermore, parameters related to exterior conditions are monitored using an Oregon Weather Station.

Table 1: The summary of the thermal performance of sample building

Building component or system	Thermal Performance and Structure
External Wall	1.58 W/ (m <sup>2</sup> K)
Roof	U-value: 2.3 W/ (m <sup>2</sup> K)
Windows	U-value: 5.1W/ (m <sup>2</sup> K)
Doors	U-value: 4.8 W/ (m <sup>2</sup> K)
Ventilation Strategy	Natural ventilation
Airt change rate	2.3/h
Heating or Cooling Method	Air Conditioning



### 3.2. Questionnaire

The data from questionnaires gathered responses from 10 occupants and landlords residing in heritage buildings, aimed at evaluating the appropriateness of various retrofitting approaches. These assessments considered multiple factors such as cost acceptability, preferences, and satisfaction levels. Furthermore, the investigation delved into occupant behaviors, including their usage of heating, cooling systems, lighting, and other energy-consuming devices. Figure 3 illustrates that the average acceptable retrofit cost hovers around 67,000 CNY, which can be categorized into four budget ranges: less than 40,000 CNY, 40,000-80,000 CNY, 80,000-120,000 CNY, and over 120,000 CNY. Notably, the two individuals willing to invest the highest amount of money also had the shortest acceptable payback period, both opting for a 3-5 year range. Conversely, those who were inclined to invest less money displayed greater patience for the payback period of residential green renovation, often choosing a longer timeframe.

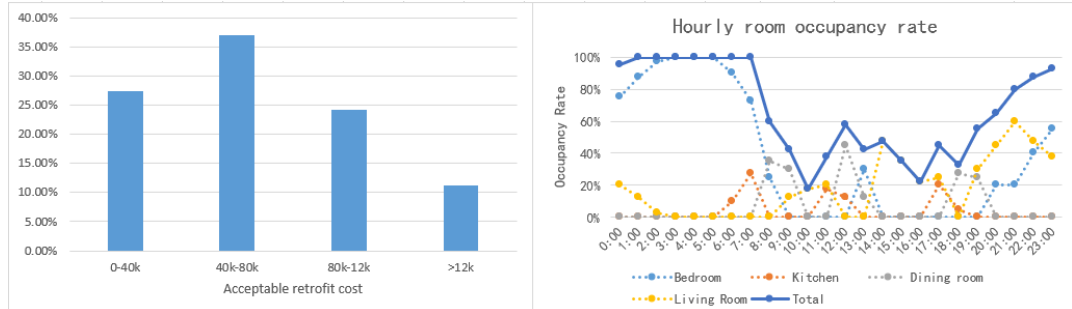


Figure 3 The feedback of the questionnaire

Consequently, it becomes imperative to conduct sensitivity analyses on conversion costs in multiple modes. One mode should focus on reducing the payback period, while the other should target lowering the conversion cost. This approach accommodates the diverse needs of different residents. Regarding annual energy expenditure in the surveyed households, it averages around 4,000 CNY, with a minimal difference of only 766 CNY among them. This suggests that the surveyed residents exhibit strikingly similar energy usage patterns. Moreover, the data pertaining to room occupancy rates reveals that 65% of residents primarily occupy their rooms during the evening hours from 21:00 to 07:00.

Prior to simulating the energy efficiency of different strategies, the initial step involved simulating the annual energy consumption of the building prior to any renovation. This served as the reference point for comparison. A three-dimensional model, as depicted in Figure 4, was created using computer software with accurate sizing information. During this phase, the Design Builder software was utilized to model the energy usage of the sample house being considered. It's worth noting that Suzhou is situated in a region classified as having 'hot summer and cold winter' conditions, characterized by a 90-day heating period and a 77-day cooling period.

### 3.3. Simulation on the Heritage Building

Before simulated the energy-saving performance of various strategies, the annual energy consumption of the building before renovation was simulated and regarded as the benchmark. The three-dimensional model with agreement of the sizing is built up in computer programme, as shown in Figure 4. In this stage, the Design Builder software has been employed to simulate the energy consumption of proposed sample house. Suzhou is located in area named as 'hot summer and cold winter', with heating and cooling periods are 90 days and 77 days, respectively.

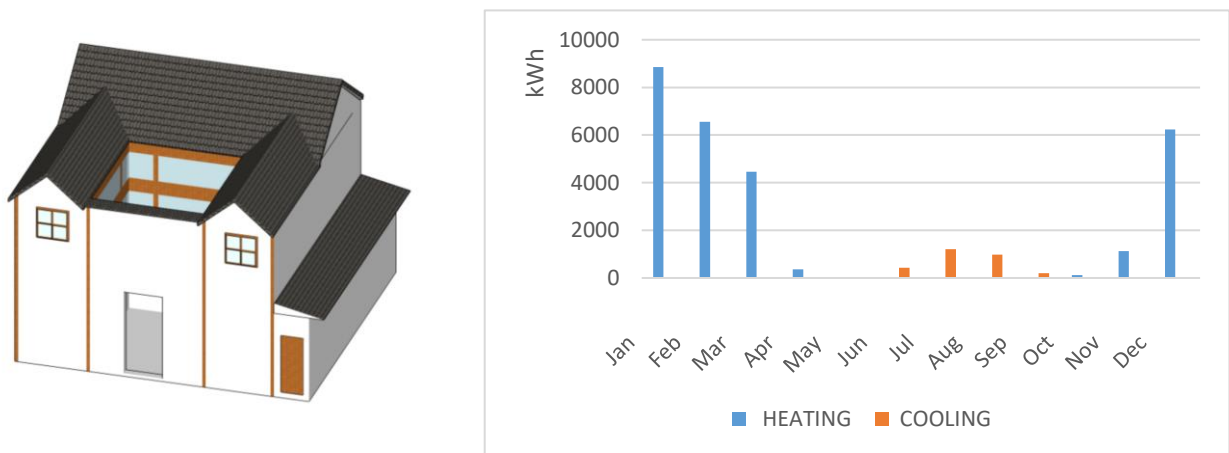


Figure 4 The image of the 3d model and heating and cooling energy consumption

The results of simulation indicate that the air tightness of sample building is poor and there are certain problems with energy consumption as the average energy consumption is over 100 kWh/m<sup>2</sup>. To solve this problem empirically, measures



should be taken to improve the air tightness and strengthen its insulation performance. For example, appropriate insulation materials can be added to the exterior walls, windows, doors and other parts; energy-saving equipment and technologies can be selected for ventilation systems to improve the efficiency of heating and cooling; in addition, regular maintenance and inspection should also be carried out to ensure the normal operation of the building's heating and cooling equipment.

#### 4. POTENTIAL STRATEGIES

The applicability of heritage building renovation strategies depends on various factors, including the historical significance, architectural style, structural conditions, and specific objectives of the renovation (e.g., improving thermal comfort, reducing energy consumption, preserving cultural heritage). The Table 2 shows a series of preferred renovation strategies that can be considered for heritage buildings mentioned in previous publications.

Table 2: Extraction of common retrofit strategies from previous publication

Components	Strategies	(Şahin et al. 2015)	(Mingkai 2016)	(Roberti et al. 2017)	(Silvero et al. 2018)	(Lu et al. 2021)	(He et al. 2021)	(Gupta, Deb 2022)	(Ge et al. 2022)	(Marzouk et al. 2023)	(Choi et al. 2023)
Exterior wall	Inner insulation	✓		✓	✓		✓	✓	✓		✓
	Outer insulation		✓			✓			✓		
Roof	Thermal mortar	✓	✓			✓					✓
	Thermal slab			✓	✓			✓	✓	✓	
Windows	Window frame										
	Glazing replace	✓	✓	✓	✓	✓	✓		✓	✓	
Air permeability	Air tightness	✓				✓					
Foundation	Insulation layer	✓									
Floor	Insulation layer	✓	✓		✓						
Interior wall	Insulation layer	✓	✓								
Device	Green energy					✓	✓				✓
	HVAC					✓	✓			✓	
	Light					✓	✓			✓	

It's worth noting that the majority of previously published papers have predominantly focused on passive design or building envelope improvements. These measures encompass actions like adding insulation, upgrading windows, and reducing air leakage, all of which have the potential to enhance thermal comfort and curtail energy consumption. Notably, the replacement of glazing was the second most frequently discussed strategy due to its high energy efficiency and cost-effectiveness. Some papers also introduce additional strategies, such as HVAC system upgrades, the integration of renewable energy sources, and the adoption of LED lighting.

This summary highlights the practical experiences regarding the prioritization of retrofitting strategies. However, it's essential to recognize that the choice of strategies can vary depending on the specific heritage building in question. Consequently, a more comprehensive evaluation is warranted. This evaluation should encompass historical and architectural considerations, energy audits, and economic calculations, as elaborated below.

#### 5. SUITABILITY OF RETROFITTING STRATEGIES ON HERITAGE BUILDING

AHP-Based Fuzzy Evaluation, also named as FAHP (Fuzzy Analytic Hierarchy Process), is a decision-making method based on fuzzy mathematics and hierarchy analysis (Li et al. 2022). It combines the advantages of AHP and fuzzy comprehensive evaluation, while avoiding their disadvantages. It integrates hierarchical structure, weight analysis, consistency testing, and fuzzy evaluation. The evaluation process of FAHP generally involves determining the weight and factor set using the analytic hierarchy process, determining the evaluation set based on the actual situation, and then using fuzzy comprehensive evaluation to make a comprehensive evaluation.

## 5.1. Identifying Evaluation Criteria

As shown in Figure 5, an AHP was firstly implemented to establish a hierarchy structure with main evaluation criteria. The criteria, that were collected from previous studies such as (Yuk et al. 2023)(Marzouk et al. 2023)(Ge et al. 2022)(Zhang et al. 2021), are identified to compare and rank based on questionnaire retrieve from expert with rich project experience. All

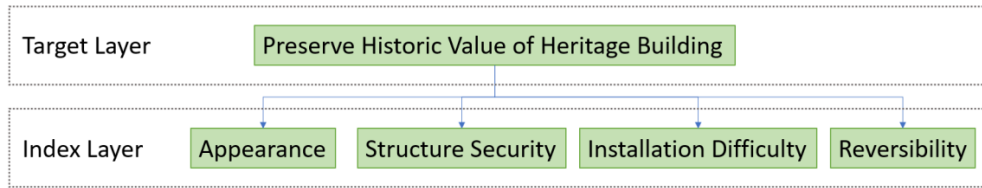


Figure 5 The hierarchy structure with main evaluation criteria

experts were invited to compare the impacts of various application components on the unique values of the historic building. There were 15 questionnaires sent out and 12 valid questionnaires were returned. Then, the pairwise comparison matrix was developed shown in Table 3.

The consistency test of the current AHP showed a consistency ratio  $CR = 0.011 < 0.1$ , which meant the judgement matrix is acceptance. Table 3 shows impact weight of four indexes on the preservation of historic value, ranging from 0.095 to 0.397. The appearance and structure security had the highest impact weights, which suggests the retrofit solutions on the ventilation should be considered carefully in the view of the historic protection.

Table 3: Impact weights of various indexes

Index	Appearance	Structure Security	Installation difficulty	Reversibility
Impact weight	0.397	0.346	0.162	0.095

- Appearance: The components have been carefully selected to blend in with the building's aesthetics, minimizing any visual disruption.
- Structure Security: Showcase how the research considers building's structural safety to ensure that the proposed retrofitting solution is compatible with the existing structure.
- Installation difficulty: The installation is labour intensive and invasive on the structure, such as inaccessible components.
- Reversibility: The location is easy to install and capable of being reversed so that the original state of heritage is restored easily.

## 5.2. Fuzzy Evaluation

After the impact weight identified in the AHP, the fuzzy evaluation method which transfers the qualitative results to the quantitatively indicators is implemented to identify the most suitable components for ventilator application. The indicators for various index are divided into 5 ranks and ranges from 0-10. The grade 1 means the 'the invasive impacts on historic value; grade 9 represents the 'the least impact on the historic value'; the other level shoes the intermediate impacts on the historic value. The results of the evaluation can be calculated by membership functions. The Triangle-shape grade of membership function of various levels have been shown below, from Rank 1 ( $R_1$ ) to Rank 9 ( $R_9$ ).

$$\begin{aligned}
 \text{Equation 1: Membership function of Rank 1} \quad R_1 &= \begin{cases} 1 & 0 < N \leq 1 \\ \frac{3-N}{2} & 1 < N \leq 3 \\ 0 & N > 3 \end{cases} \\
 \text{Equation 2: Membership function of Rank 2} \quad R_3 &= \begin{cases} \frac{N-1}{2} & 1 < N \leq 3 \\ \frac{5-N}{2} & 3 < N \leq 5 \\ 0 & N < 1 \text{ 或 } N > 5 \end{cases} \\
 \text{Equation 3: Membership function of Rank 5} \quad R_5 &= \begin{cases} \frac{N-3}{2} & 3 < N \leq 5 \\ \frac{7-N}{2} & 5 < N \leq 7 \\ 0 & N < 3 \text{ 或 } N > 7 \end{cases}
 \end{aligned}$$

Equation 4: Membership function of Rank 7

$$R_7 = \begin{cases} \frac{N-5}{2} & 5 < N \leq 7 \\ \frac{9-N}{2} & 7 < N \leq 9 \\ 0 & N < 5 \text{ 或 } N > 9 \end{cases}$$

Equation 5: Membership function of Rank 9

$$R_9 = \begin{cases} \frac{1}{N-7} & 9 \leq N < 10 \\ \frac{N-7}{2} & 7 < N \leq 9 \\ 0 & N < 7 \end{cases}$$

As shown in Figure 6, the components for ventilator application have been prioritized by the distribution of fuzzy evaluation. The results of LED replacement and airtightness belonged to the high adaptability, which means the greater potential on preservation of historic value. The fenestration, smart control and HP were relatively suitable for application. The inner insulation had advantages on the appearance preservation. As for other potential strategies, the score of evaluation demonstrated unsuitability in perspective of all four indexes.

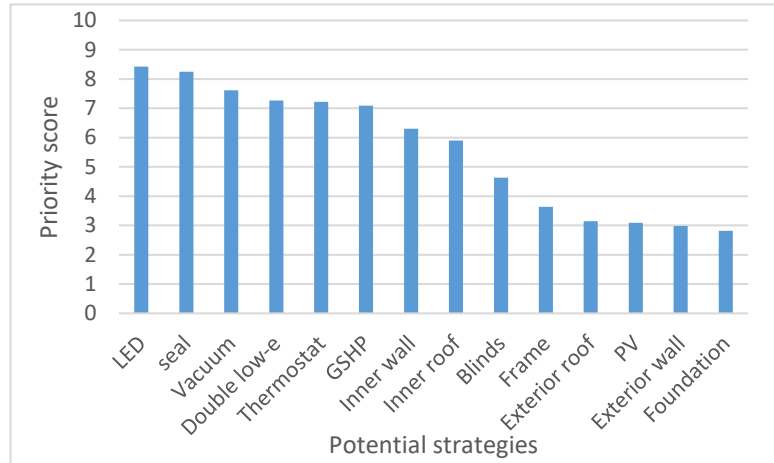


Figure 6 The priority score of fuzzy evaluation

Thus, the potential strategies for heritage building in Suzhou would be LED, seal strips, fenestration replacement, thermostat, high performance heating/cooling device and inner envelope insulation.

Based on the survey from the experts on historic building conservation, the thickness of insulation is limited below 40 mm to minimum the impacts on historic features. The available insulation materials are summarized in Table 4. The seal strips, always made of rubber or foam, are used to reduce the air leakage and protect the interior environment from exterior environment, such as temperature and humidity. The application of seal strips was assumed to reduce the air change rate to 1/h to 1.5/h (Ge et al. 2022). The potential retrofit choices for fenestration have also been listed in Table 4.

Table 4: Summary of available insulation material

Technology	Vacuum insulated Panel (VIPs)	Aerogel	Polyurethane (PUR)	Expanded polystyrene (EPS)	Vacuum Glazing	Double glazing	Double glazing low-e	LED Light
Thermal performance	0.007 W/m <sup>2</sup> *K	0.013 W/m <sup>2</sup> *K	0.025 W/m <sup>2</sup> *K	0.03 W/m <sup>2</sup> *K	0.9 W/m <sup>2</sup> *K	2.9 W/m <sup>2</sup> *K	2.3 W/m <sup>2</sup> *K	
Cost per m <sup>2</sup> (CNY)	600 (in 40mm thickness)	400 (in 40mm thickness)	65 (in 40mm thickness)	40 (in 40mm thickness)	800	180	260	18/Bulb

## 6. PRIORITY THE POTENTIAL STRATEGIES

Table 5: The summary of the potential choice for retrofit.

Insulation type								Light type		
I1	I2	I3	I4	I5	I6	I7	I8	I9	L1	L2
Original	EPS 30	EPS 35	PUR 30	EPS 40	PUR 35	PUR 40	Aerogel	VIP	Incandescent lamp	LED
Glazing type				Heating and cooling device						
A1	A2	G1	G2	G3	G4	HP1	HP2	HP3	HP4	
1/h	2.3/h	Original	Double	Double Low-e	Vacuum	Original	Heating device upgrade	All upgrade		Cooling device upgrade

In this section, a multi-criteria approach is employed to assess the suitability of various retrofitting strategies. These criteria encompass improvements in thermal comfort, reduction in energy consumption, and cost-effectiveness. The Technique of Order Preferences by Similarity to Ideal Solution (TOPSIS) is utilized to rank the retrofitting strategies based on their overall performance across these selected criteria. TOPSIS is particularly valuable in this research due to its ability to handle data uncertainty and imprecision.

There are more than 21 potential retrofitting options under consideration. When evaluating each individual retrofitting option, Table 6 displays the percentage of energy savings and associated costs. After weighing the potential energy

savings and costs, the priority retrofit option is found to be the replacement of heating devices and the application of air sealing measures, achieving energy savings of approximately 60% and 31%, respectively.

Considering that occupants have varying retrofit budgets, the 292 scenarios are categorized into four groups based on the total retrofit cost: less than 40,000 CNY, between 40,000 and 80,000 CNY, between 80,000 and 120,000 CNY, and over 120,000 CNY.

Table 6: The energy saving percentage for various options.

	OG	A1	G2	G3	G4	I2	I3	I4	I5	I6	I7	I8	I9	HP2	HP4
Energy Saving percentage (%)	0	31.68	3.57	4.69	6.59	5.89	7.29	7.60	8.43	8.83	9.65	12.66	14.17	60.52	2.58
Cost (CNY)	0	600	11520	16640	51200	21360	24920	39160	28480	42720	46280	284800	427200	6000	4800

For the group with a total cost of less than 40,000 CNY, there are 61 scenarios with total costs ranging from 600 CNY to 40,000 CNY. Figure 7 illustrates the simulated results for these scenarios, showing a total energy consumption ranging from 6,895 kWh to 30,546 kWh. The scenario with the lowest energy consumption involves the use of air sealing measures, 40mm inner insulation (EPS), and upgrades to heating and cooling devices. The total cost for this scenario is approximately 39,880 CNY, with an energy-saving rate of about 77%. However, when both cost and energy consumption are considered simultaneously, the TOPSIS results differ. Assuming that energy consumption and cost carry equal weight, the upgrade of heating devices and the application of air sealing measures receive the highest adaptability score. This results in a total energy consumption of around 8,640 kWh and an energy-saving rate of about 71%, which aligns with the findings from the single sensitivity analysis mentioned earlier. Thus, for retrofit budgets of less than 40,000 CNY, the preferred retrofit option is the upgrade of heating devices and the application of air sealing measures.

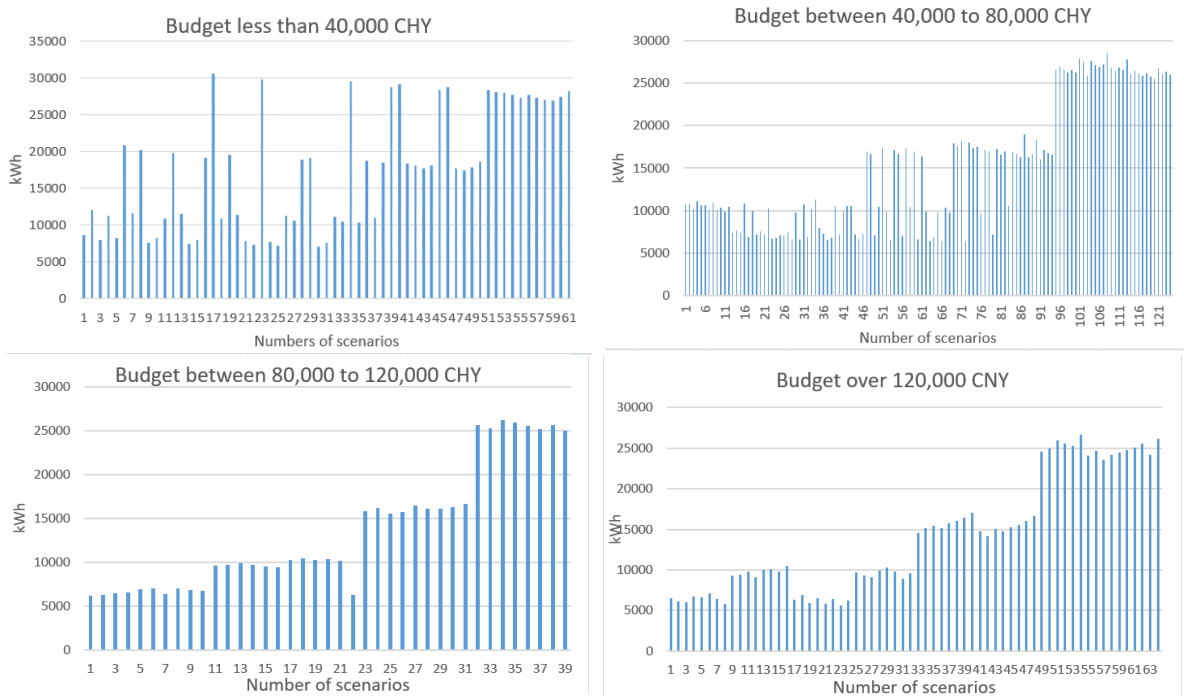


Figure 7 The result of energy consumption for various groups

For the group with a total cost ranging from 40,000 to 80,000 CNY, there are 124 scenarios, with total costs spanning from 40,600 CNY to 79,680 CNY. Figure 7 presents the simulated results for these scenarios, showing a total energy consumption between 6,362 kWh and 28,532 kWh. Overall, it's notable that the energy consumption in this group is lower than in the scenarios with a budget of less than 40,000 CNY. The scenarios with the least energy consumption involve the use of air sealing measures, double low-e glazing, 40mm PUR insulation, and upgrades to heating and cooling devices. This combination achieves an energy-saving rate of about 79% with a total retrofit cost of 74,320 CNY. Interestingly, the retrofit options promoted by TOPSIS analysis in this group are air sealing measures, double glazing, 35mm EPS insulation, and heating device upgrades, which differ from the scenarios with the least energy consumption. This configuration achieves an energy-saving rate of 76% with a total cost of 43,040 CNY.

As for the group with a total cost ranging from 80,000 to 120,000 CNY, there are 40 scenarios with energy consumption ranging from 6,165 kWh to 26,220 kWh. The scenarios with the least energy consumption involve the use of air sealing measures, vacuum glazing, 40mm PUR insulation, and upgrades to heating and cooling devices. This combination achieves an energy-saving rate of about 80% with a total retrofit cost of 108,880 CNY. The promoted retrofit options from TOPSIS analysis align with the scenarios with the least energy consumption in this group.

Lastly, there are 65 scenarios in the last group, with energy consumption ranging from 5,658 kWh to 26,679 kWh. The scenarios with the least energy consumption involve the application of air sealing measures, vacuum glazing, VIPs, and upgrades to heating and cooling devices. The promoted retrofit options from TOPSIS analysis in this group are air sealing measures, aerogel insulation, and heating/cooling device upgrades. These options achieve an energy-saving rate of about 78% with a total retrofit cost of 296,200 CNY.

It's evident that as the budget increases, the marginal effect on energy savings becomes more pronounced. The combination of air sealing measures, 40mm EPS inner insulation, and upgrades to heating and cooling devices can already achieve over 70% energy savings, making it unnecessary to consider more costly options when the budget is increased.

## 7. FUTURE WORK

This research offers an insightful tool for the ongoing exploration of strategies for renovating heritage houses, effectively balancing the preservation of cultural heritage with modern sustainable development objectives. However, it also points towards several avenues for future research and improvement:

### 1. Long-Term Monitoring and Evaluation

Extending the in-situ investigation over an extended period would yield insights into the long-term effectiveness of these strategies. This would ensure that the building continues to meet its thermal comfort and energy efficiency objectives over the years.

### 2. User-Centric Research

Instead of conducting a one-time survey and questionnaire, future research should adopt a more user-centric approach by collecting data from occupants and landlords over an extended period with specific intervals. This approach will enable the study of user behaviour changes over time, providing a more comprehensive understanding of evolving needs and preferences.

### 3. Heritage Building Typologies

Heritage buildings vary widely in terms of their preservation status and functions. Future research could categorize these buildings into typologies, each with its unique set of retrofitting challenges and opportunities. This approach would allow for more tailored and effective renovation strategies for different heritage building categories.

By addressing these areas, future research can contribute to a more holistic and nuanced approach to the preservation and sustainable development of heritage buildings.

## 8. CONCLUSION

The current research not only offers a comprehensive set of customized retrofit strategies tailored to the specific challenges faced by historic dwellings in Suzhou but also provides an in-depth understanding of their implications for thermal comfort and energy consumption. The article concludes by discussing the implications of the research findings for heritage conservation and sustainable urban development, while also outlining potential future research directions at the critical intersection of heritage preservation and environmental sustainability.

This research delved into the unique characteristics of heritage buildings in Suzhou and prioritized energy-saving retrofit strategies by considering energy consumption, economic factors, and the preservation of historic features. A representative historic building, the Dongshan house, underwent simulation and analysis to assess the suitability of various retrofit options. The most substantial energy savings were achieved through the upgrade of heating devices and the application of air sealing measures, while improvements in envelope insulation had a relatively smaller impact on energy conservation. LED lighting replacement and air sealing measures were identified as highly adaptable strategies for heritage buildings, indicating their potential for preserving historic value. Fenestration improvements, smart control systems, and heat pumps were also deemed relatively suitable for application. Inner insulation demonstrated advantages in terms of preserving the building's appearance. In contrast, other potential strategies scored poorly across all four evaluation criteria, indicating their unsuitability.

Based on various budget scenarios, a set of priority retrofit strategies was recommended:

1. For budgets less than 40,000 CNY, the top retrofit choices are the upgrade of heating devices and the application of air sealing measures, achieving an impressive energy-saving rate of 77%.
2. In the budget range of 40,000 to 80,000 CNY, the recommended strategies include air sealing measures, double low-e glazing, 40mm PUR insulation, and heating and cooling system upgrades, achieving a notable energy-saving rate of 79%.

3. For budgets between 80,000 and 120,000 CNY, the proposed options encompass air sealing measures, vacuum glazing, 40mm PUR insulation, and heating and cooling system upgrades, resulting in an energy-saving rate of 80%.
4. In scenarios with budgetary flexibility, the recommended strategies consist of air sealing measures, aerogel insulation, and heating/cooling system upgrades.

It is evident that the impact of increasing the budget is substantial. The application of air sealing measures, 40mm EPS inner insulation, and upgrades to heating and cooling systems can yield energy savings exceeding 70%, making further budget increases unnecessary to implement other options.

## 9. REFERENCES

Abdul Hamid, A., Johansson, D., Bagge, H., 2020. Ventilation measures for heritage office buildings in temperate climate for improvement of energy performance and IEQ. *Energy and Buildings*, 211. 10.1016/j.enbuild.2020.109822.

Choi, J.Y. et al., 2023. Proposal of retrofit of historic buildings as cafes in Korea: Recycling biomaterials to improve building energy and acoustic performance [online]. *Energy and Buildings*, 287, p.112988. Available at: <https://www.sciencedirect.com/science/article/pii/S0378778823002189>.

Fehrm, M., Reiners, W., Ungemach, M., 2002. Exhaust air heat recovery in buildings. *International Journal of Refrigeration*, 25(4), pp.439–449.

Fu, Y., 2018. The Preliminary Study of the Green Renovation on the Normally Traditional Folk Houses in the South of the Yangtze River [online]. *Architecture & Culture*, 3, pp.162–164. Available at: 1672-4909.

Ge, J. et al., 2022. Suitable and energy-saving retrofit technology research in traditional wooden houses in Jiangnan, South China [online]. *Journal of Building Engineering*, 45, p.103550. Available at: <https://www.sciencedirect.com/science/article/pii/S235271022101408X>.

Gupta, V., Deb, C., 2022. Energy retrofit analysis for an educational building in Mumbai [online]. *Sustainable Futures*, 4, p.100096. Available at: <https://www.sciencedirect.com/science/article/pii/S2666188822000302>.

He, Q. et al., 2021. A cost-effective building retrofit decision-making model – Example of China’s temperate and mixed climate zones [online]. *Journal of Cleaner Production*, 280, p.124370. Available at: <https://www.sciencedirect.com/science/article/pii/S0959652620344152>.

Jiang, W. et al., 2022. Protective energy-saving retrofits of rammed earth heritage buildings using multi-objective optimization [online]. *Case Studies in Thermal Engineering*, 38, p.102343. Available at: <https://www.sciencedirect.com/science/article/pii/S2214157X22005834>.

Li, Y. et al., 2022. Environment improvement and energy saving in Chinese rural housing based on the field study of thermal adaptability [online]. *Energy for Sustainable Development*, 71, pp.315–329. Available at: <https://www.sciencedirect.com/science/article/pii/S0973082622001879>.

Lu, Y. et al., 2021. An integrated decision-making framework for existing building retrofits based on energy simulation and cost-benefit analysis [online]. *Journal of Building Engineering*, 43, p.103200. Available at: <https://www.sciencedirect.com/science/article/pii/S2352710221010585>.

Marzouk, M., El-Maraghy, M., Metawie, M., 2023. Assessing retrofit strategies for mosque buildings using TOPSIS [online]. *Energy Reports*, 9, pp.1397–1414. Available at: <https://www.sciencedirect.com/science/article/pii/S2352484722026749>.

Mingkai, L., 2016. *Indoor thermal environment technology research of the ancient residential houses In the ancient city areas of Suzhou*. Suzhou University of Science and Technology. Available at: 2016-12-01-085213-14-006.

Roberti, F. et al., 2017. Energy retrofit and conservation of a historic building using multi-objective optimization and an analytic hierarchy process [online]. *Energy and Buildings*, 138, pp.1–10. Available at: <https://www.sciencedirect.com/science/article/pii/S0378778816318382>.

Şahin, C.D. et al., 2015. A transdisciplinary approach on the energy efficient retrofitting of a historic building in the Aegean Region of Turkey [online]. *Energy and Buildings*, 96, pp.128–139. Available at: <https://www.sciencedirect.com/science/article/pii/S0378778815002108>.

Silvero, F. et al., 2018. Energy retrofit solutions for heritage buildings located in hot-humid climates [online]. *Procedia Structural Integrity*, 11, pp.52–59. Available at: <https://www.sciencedirect.com/science/article/pii/S2452321618301094>.

Wang, Y., 2014. Suzhou | Creative Cities Network - UNESCO [online]. *Suzhou Intangible Cultural Heritage Conservation and Management Office*, p.1. Available at: <https://en.unesco.org/creative-cities/suzhou>.

Yuk, H. et al., 2023. Evaluation of suitability for passive retrofit of wooden roof considering the specificity of historic buildings [online]. *Building and Environment*, 242, p.110608. Available at: <https://www.sciencedirect.com/science/article/pii/S0360132323006352>.

Zhang, F. et al., 2021. A new framework to select energy-efficient retrofit schemes of external walls: A case study [online]. *Journal of Cleaner Production*, 289, p.125718. Available at: <https://www.sciencedirect.com/science/article/pii/S0959652620357644>.

---

## #291: Comparative study on a low-carbon house and common houses with post occupancy evaluation in rural area of China

---

Shihao ZHANG<sup>1</sup>, Qi XU<sup>2</sup>, Saffa RIFFAT<sup>3</sup>

<sup>1</sup>School of Architecture and Urban Planning, Suzhou University of Science and Technology, Suzhou, 215011, China, shihaozhang@usts.edu.cn

<sup>2</sup> College of Architecture, Nanjing Tech University, Nanjing, 210044, China, Email: xuqi@njtech.edu.cn

<sup>3</sup> Department of Architecture and Built Environment, University of Nottingham, Nottingham NG7 2RD, UK, saffa.riffat@nottingham.ac.uk

*Abstract: Nowadays, due to the construction of new buildings, global warming becomes more serious than ever before. In order to investigate the actual performance of low-carbon houses, post-occupancy evaluations have been undertaken on a low-carbon house and two typical normal houses in the rural areas of China. The result of the low-carbon house is compared with normal houses in perspective of indoor environment quality, energy consumption and satisfaction questionnaire. The result indicates the Eco-house enjoys advantages over the conventional houses in all respects. This paper also identifies the underlying factors that cause the gaps between predicted and recorded energy performance of the Eco-house. Most of the factors are associated with parameters regarding occupancy behaviour and facilities management in simulation.*

*Keywords: Low-carbon house, Energy benchmarks, post-occupancy evaluation*



## 1. INTRODUCTION

With the increasing evidence that greenhouse gas absorbs emitted radiant energy and causes the greenhouse effect, taking urgent measures to prevent the greenhouse effect in the future has become crucial (Taleb, Sharples 2011). The building sector takes an instrumental role in climate changes. The energy and material consumption by buildings accounts for about 40% of annual global consumption (Glass et al. 2008), (Zhao et al. 2015). With the development of real estate in Asia, total carbon emissions will increase greatly in the next 40 years. As for China, the situation is more urgent. The growth rate of energy consumption in buildings is about 10% in the past decades (Chang et al. 2014). In fact, Chinese people suffer from high carbon emissions. Thus, the Chinese government plans to achieve carbon neutrality by the 2060s (Li et al. 2022). And the building industry is one of the most important key factors to determine the success of a city's carbon neutralization.

With the rising demands to achieve an environmentally friendly world, increasing interest in sustainable buildings has been shown. In recent years, various low-carbon technologies have been promoted to support the sustainable revolution in the global building industry, such as passive design strategies (Zhang et al. 2011) and low waste technologies (Zhang et al. 2012). With the recent achievement of low-carbon technologies, many researchers in China have focused on the design and evaluation within various building types and climate zones (Pei et al. 2015), (Ma et al. 2020), (Laetitia et al. 2020).

The building regulation or certification systems have covered most kinds of buildings and climate zones. Furthermore, environmental and building regulations have become increasingly stringent, demanding higher energy-saving performance of buildings than ever before. For example, all new-built houses in the UK should be zero carbon emission, which means not only the combination of traditional passive solar energy devices but also the reduction in the heating requirement of the interior.

For most cases, the regulations are mainly applied during the design or construction phases. Actually, the most critical indicator determining if the building can provide a better interior environment with less energy consumption should be its in-situ performance. However, this is only addressed in a few building regulations or certification systems. With this end in view, post-occupancy evaluation (POE) is an important tool in the context of identifying if the building presents a similar performance as expected.

By undertaking the evaluation on the low-carbon house and normal houses, this paper investigates the benefits and advantages for occupants living in a low-carbon house in rural areas. Specifically, the objectives of this study include:

1. Explore the advantages of energy efficiency and interior air quality (IAQ) of the low-carbon house over normal houses through in-situ performance investigations.
2. Provide detailed insights on the gaps between predicted and actual energy consumptions.
3. Provide lessons and insights that can be captured and used in future practice.

## 2. POST-OCCUPANCY EVALUATION

The post-occupancy evaluation (POE) was firstly proposed in the 1960s (Li et al. 2018). Sim Van der Ryn from the University of California, Berkeley provided the systematic statements on the POE (SILVERSTEIN, MURRAY; VAN DER RYN 1967). The term 'POE' is defined as the evaluation of the building with a systemic method after construction and occupied for a while (Preiser, Wolfgang 1995). It also stated that the POE can be used to identify flaws in existing buildings and to test new building prototypes. POE always consists of measurements on the physical parameters, energy data collection, and the feedback from occupants via questionnaires or interviews. (Li et al. 2018) stated that there are few certification systems involved in-situ performance of the building. Therefore, POE becomes a necessary tool to provide feedback on the operation of a building and feedforward to the future building design. It is a crucial research methodology, which can be applied to both low-carbon and common buildings.

POE has become an important tool to improve the design and operation of a building. (Colclough et al. 2022) states that most of the research about POE includes energy consumption, air quality (such as temperature and carbon dioxide concentrations), lighting, and thermal comfort. Few papers focused on the occupants' comfort and satisfaction. The level of occupants' satisfaction in a questionnaire or interview is positively associated with environmental awareness (Deuble, de Dear 2012).

Most of the research about POE in China focus on public buildings, such as office buildings (Pei et al. 2015), (Liu et al. 2021), (Lin et al. 2016); college buildings (Yu et al. 2017), (Ding et al. 2019), (Zhang 2019) and terminal buildings (Huang et al. 2021). Few have investigated the actual performance of sustainable residential buildings in China, especially for rural areas. With the questionnaire survey and experimental investigation, this study intends to identify the discrepancies between the conventional house and the low-carbon house for rural areas and to find the gaps between the expected goal and in-situ performance.

### 3. MONITORING FRAMEWORK

This paper investigates several houses in the rural area of central China, including a low-carbon house and two normal built houses. The evaluation includes energy data, interior environment quality and satisfaction questionnaire.

#### 3.1. Case study buildings

In 2020, there are over 500 million people living in rural areas (Zeng et al. 2022). However, less than 10% of the houses in Chinese rural areas are sustainable buildings. China is adopting energy-saving building standards on the largest scale. There is almost no data about how these buildings operate. A low-carbon house and two typical normal houses are selected for the current research. The selected houses for analysis were as similar as possible, like similar size, occupancy hours and in a similar climate zone. All dwellings have been monitored for over one year.

##### *Eco-house*

This part introduces the design of the sustainable house named Eco-house. The Eco-house is an important attempt at sustainable building construction and operation in the rural regions in China. It was constructed to comply with the Passive House standard and Near-Zero Energy Building Technical Standards with a limited budget (€40,000). As Figure 1 shows, the layout of this building includes two bedrooms with one living room. The detailed parameters of the Eco-house have been listed in Table 1.



Figure 1 (a) The image of Eco-house; (b) the layout of Eco-house.

The Eco-house was constructed in 2019 with vacuum double glazing and mechanical heat recovery ventilators. The mechanical heat recovery can supply fresh air to the interior environment and reduce the heat loss during ventilation. The house contains one kitchen, one living room, two bedrooms, and one toilet on the ground floor.

##### *Normal house*

The selected normal houses are one-storey detached dwellings built six and twelve years ago. They are of brick wall construction but with various insulation materials. The structure of glazing and roof is various. The space heating/cooling demands are also met with air-conditioners. The houses in similar in size and layout, with two bedrooms, one living room, one kitchen, and one utility room. The detailed information of the normal houses can be found in Table 1.

Table 1: The summary of the parameters for Eco-house and normal houses

	Eco-house	Normal-1	Normal-2
<b>Usable Area (m<sup>2</sup>)</b>	61	69	73
<b>Construction Time</b>	2019	2010	2016
<b>Number of Occupants</b>	2	3	4
<b>External Wall W/ (m<sup>2</sup>·K)</b>	0.278	1.97	1.27
<b>Roof W/ (m<sup>2</sup>·K)</b>	0.39	1.56	0.87
<b>Windows W/ (m<sup>2</sup>·K)</b>	0.42	5.6	2.3
<b>Doors W/ (m<sup>2</sup>·K)</b>	1.9	2.3	2.4
<b>Ventilation Strategy</b>	Heat recovery ventilator	Natural Ventilation	Natural Ventilation

### 3.2. Measurement and analysis

The houses were monitored over an extended period of time. During the monitor period, the data loggers (DT85 and CL11) collected the data every 10 minutes. And the results were retrieved every single month. The web of the data logger collects the data from the sensor and provides the graphical for monitoring. The interior and exterior temperature is measured by calibrated K-type thermocouples. The monitor system included the 27 thermocouples placed in a single house and 1 pyranometer placed on the southern wall. Two of the thermocouples are placed for ambient temperature measurement. The thermocouples were placed in the living room, kitchen, and bedroom, where most occupants stay for a long time at home and away from heat sources and direct sunlight. The parameter of exterior space is monitored by Oregon Weather Station. The measured data of the weather station includes indoor/outdoor air temperature and relative humidity; CO<sub>2</sub> concentrations, at 10-min intervals.

The K-type thermocouples measure the temperature in the range 0 °C to 50 °C with an accuracy of  $\pm 0.4$ °C. The CO<sub>2</sub> sensor with a range from 0 to 5000 ppm and an accuracy of about  $\pm 5\%$ . The PM 2.5 sensor with a range of 0~999 $\mu\text{g}/\text{m}^3$  and accuracy of about  $\pm 5\%$ . The relative humidity sensors have an accuracy of about  $\pm 3\%$ . The data of overall energy consumption has been uploaded to the cloud.

The interior temperature recommended by Indoor Quality Standards GB/T18883 in China ranges from 22 °C to 28 °C during summer and 16 °C to 24 °C during winter. But in other standards, the preferred temperature is various. In Passive House Standards, the houses are designed under the same temperature, 20 °C. The British government proposed a temperature of 21 °C for the living room and 18 °C for the bedroom. The World Health Organization (WHO) suggests a minimum of 18 °C as the ideal home temperature. ASHARE suggested that thermal comfort temperature ranges from between approximately 19 °C and 28 °C (ASHRAE 2017).

Several evidence demonstrated that under UK climate, overheating is possible in low-carbon dwellings (Beizae et al. 2013), (Wright et al. 2005), (Jones et al. 2016), (Goncalves et al. 2021). Low-carbon buildings become more airtight and well insulated to reduce energy demand. The overheating risk is likely to further increase due to the effects of global warming. Furthermore, the average temperature in Hubei Province is higher than in the UK. Thus, the overheating risk is more likely to happen. As sustainable houses are emerging only in recent years, the actual indoor temperatures and risk of overheating in low-carbon houses are unknown. This paper is one of the first studies on overheating risk by the means of Post-occupancy Evaluation in China. However, there is no guidelines or definite thresholds for overheating in China. According to the CIBSE Guide A in the UK, overheating means the time when the temperature of the living room and bedroom exceeds 28 °C and 26 °C accounts for less than 1% of the annual occupied time. The passive house standards definite that the temperature in excess of 25 °C cannot occur for more than 10% of the annual occupied time.

Similar to the analysis of the thermal environment, the concentration of CO<sub>2</sub> in the sample houses has been measured and recorded to evaluate the interior air quality. The concentration level of CO<sub>2</sub> is regarded as an indicator of interior air quality in POE (Colclough et al. 2018). The Hygienic Standard for Carbon Dioxide in Indoor Air GB/T 17094 in China proposed that the daily average concentration of CO<sub>2</sub> should be less than 1000ppm. The maximum safety limit on the carbon dioxide concentration is 5000 ppm. If the air change rate can reach 8 litre/s/person, the interior space can maintain an acceptable level of CO<sub>2</sub> and pollutants (ASHRAE 2004). Indoor air quality can be categorized by typical ranges of CO<sub>2</sub> concentration indicating high to low indoor air quality as stated in BS EN 13779 (Colclough et al. 2018). IDA 1 means high indoor air quality with a CO<sub>2</sub> concentration of less than 400ppm. The worst air quality (IDA 4) indicates a CO<sub>2</sub> concentration of more than 1000 ppm.

Besides the common evaluation on carbon dioxide concentration in POE, this research also includes the measurements on PM 2.5 index to investigate the air quality. PM 2.5 is a severe air pollution problem in China (Pui et al. 2014), which leads to serious cardiovascular and respiratory diseases (US EPA National Center for Environmental Assessment Environmental Media Assessment Group, Sacks 2009). The maximum hourly PM 2.5 concentration is up to 700  $\mu\text{g}/\text{m}^3$ . The Indoor Air Quality Standards GB/T18883 states that the daily concentration of PM 2.5 should be less than 75  $\mu\text{g}/\text{m}^3$ .

#### *Questionnaire survey*

The qualitative appraise of the dwellings is also the main purpose of the POE, as the low-carbon houses aim to provide a comfortable environment with less energy consumption. It is an invaluable tool to judge if the low-carbon house has achieved its aims. Therefore, a satisfaction questionnaire has been distributed to the occupants of houses. The questionnaire has been undertaken in 2021 for all three dwellings.

The survey is made by anonymous questionnaire to make sure the truth of the answer. To mitigate the impact of subject factors, the number of a single house should be more than two participants. The questionnaire was carried out with concerning of thermal comfort and indoor air quality during winter and summer. To quantize the satisfaction level of occupants, the questionnaire used the internationally accepted ISO 7730 seven-point scale, from -3 to 3, for each of the criteria, representing the satisfaction level on thermal, air quality from Dissatisfied (-3) to Satisfied (+3), as shown in Table 2.

Table 2: The scale model of satisfaction level in the questionnaire

<b>Dissatisfied</b>	<b>-3</b>	<b>-2</b>	<b>-1</b>	<b>0</b>	<b>+1</b>	<b>+2</b>	<b>+3</b>	<b>Satisfied</b>
---------------------	-----------	-----------	-----------	----------	-----------	-----------	-----------	------------------

The list of the keywords in questionnaire is presented in Table 3.

Table 3 The list of keywords in the questionnaire

<b>Basic information</b>	Gender	Age	Job
<b>Occupants' habits</b>	Schedule in building	Time in bedroom	Time in living room
	Living habits		
<b>Indoor environmental quality</b>	Season profile	Winter	Summer
	Overall satisfaction		
	Thermal environment	Temperature	humidity
	IAQ	Odour intensity	
	Light	Illuminance	Control
<b>Facility</b>	Operating	Time	Control problem

#### 4. RESULTS

A detailed measurement is presented including the results of indoor environmental quality (IEQ), energy consumption, and satisfaction questionnaire from Eco-house and two normal houses. The results are presented in the form of tables and bar chart figures. The measured minimum and maximum outdoor temperature is  $-4.3^{\circ}\text{C}$  and  $44.2^{\circ}\text{C}$ , respectively. During summer, the outdoor temperature ranged from  $17.8^{\circ}\text{C}$  to  $44.2^{\circ}\text{C}$ . In August and September, there are 38 successive days with the maximum daily temperature exceeding  $35^{\circ}\text{C}$ . During winter, the outdoor temperature ranged from  $-4.3^{\circ}\text{C}$  to  $16^{\circ}\text{C}$ . The relative humidity is always over 60% all year round and would reach peak relative humidity in June, up to more than 80%. The heating, ventilation and air conditioning (HVAC) systems are applied for heating or cooling for all dwellings. Commonly, the HVAC systems are in operation from November to next March for heating and June to September for cooling.

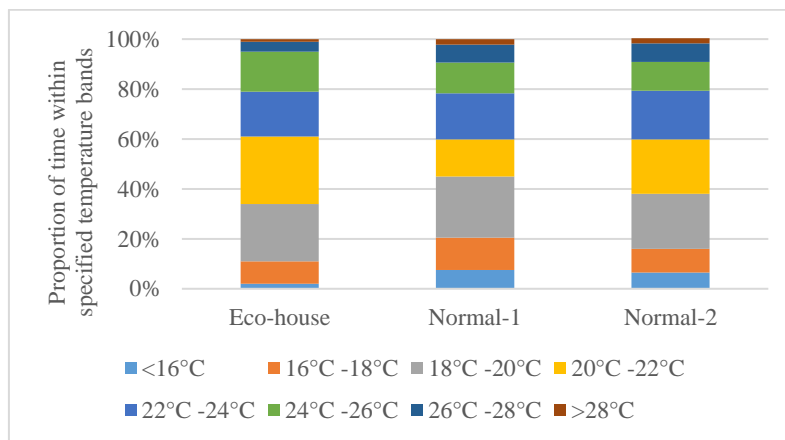


Figure 2 The interior temperature distribution in three sample dwellings

In consideration of the occupied hour of dwellings (18:00-8:00), the results of measured temperature during occupied houses are selected and analysed. In Figure 2, the distribution of interior temperature in three houses is presented. While the average interior temperature in Eco-house is the highest,  $21.9^{\circ}\text{C}$  and lower average temperatures have been recorded in Normal-1 ( $20.1^{\circ}\text{C}$ ) and Normal-2 ( $20.9^{\circ}\text{C}$ ). The mean temperature is similar among these sample dwellings. It can be noticed that the time when the temperature is less than  $16^{\circ}\text{C}$  and more than  $28^{\circ}\text{C}$  in Normal-1 and Normal-2 is much longer than Eco-house. The temperature variation in Normal-1 and Normal-2 is larger than Eco-house. About 80% of the time, the temperature of Eco-house belongs to the comfort temperature ranges suggested as ASHARE.

According to the requirements from ASHARE, the time when Eco-house is in the thermal comfort range accounts for over 75% of the occupied time. For Normal-1 and Normal-2, the value is about 68%. However, when discussing the overheating risk in Eco-house, the result changed considerably. No matter Passive house standards or CIBSE Guide A, there is a high overheating risk in Eco-house and likely to further increase. The time when internal temperature exceeds  $25^{\circ}\text{C}$  accounts for more than 13% of the year. The time when the temperature of the living room exceeds  $28^{\circ}\text{C}$  accounts for about 1% of the time, but for the bedroom the value is about 3%.

## Winter condition

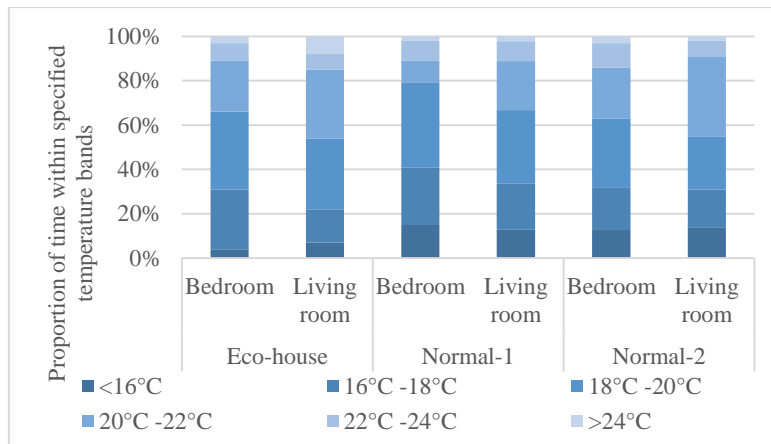


Figure 3 The temperatures in bedroom and living room across all monitored dwellings during winter

Similar to the previous statement, the Eco-house has the highest interior temperature in all sample dwellings. The recorded average temperature of the bedroom and the living room is 19.3 °C and 20.1 °C, respectively. As shown in Figure 3, the temperature in the bedroom of the Eco-house exceeding 16 °C takes for over 96% of the occupied time. And in the living room, the time accounts for 93% of the occupied time. The lowest temperatures were experienced in Normal-1, with an average temperature for the bedroom (18.5 °C) and the living room (18.8 °C). Only about 85 % of the time, the rooms in Normal-1 have recorded temperatures over 16 °C. Normal-2 have the second-highest temperatures with an average temperature of about 19.1 °C and 19.2 °C for the bedroom and the living room. In 87% of the occupied time, the temperature in Normal-2 is in the thermal comfort range as suggested by Indoor Quality Standards.

Table 4 shows the results of the questionnaire about IEQ during winter. The occupants of Eco-house are most satisfied with the living environment, reaching 2.5 in the questionnaire. As stated above, the average temperature in Eco-house is highest and temperature variation is the smallest.

The thermal comfort level of the Eco-house is much high, indicating that the performance of the house meets the requirements of the occupants. Because of the installation of heat recovery ventilators, the air quality in Eco-house is considerably higher than in other dwellings. The occupants in Normal-1 are most dissatisfied with the air freshness level because of closed windows. The relative temperature variation and air freshness are the main issues in Normal-1. As for Normal-2, the overall satisfaction level is higher than Normal-1. There is no obvious issue reported for Normal-2.

Table 4: The results of the questionnaire on IEQ during winter.

Satisfaction level (-3 to +3)	Eco-house		Normal-1			Normal-2	
	Adult 1	Adult 2	Adult 1	Adult 2	Children 1	Adult 1	Children 1
<b>Overall satisfaction</b>	2	2	-1	0	0	0	1
<b>Temperature</b>	2	3	-1	0	0	1	1
<b>Temperature variation</b>	3	2	0	1	-1	0	0
<b>Humidity</b>	2	2	1	0	1	1	0
<b>Air freshness</b>	2	3	-1	-1	1	0	0
<b>Odour density</b>	3	3	1	0	1	1	1
<b>Draughty</b>	2	3	-1	0	0	1	0

The parameters of air quality, carbon dioxide and PM 2.5 particles concentration, have been recorded and analysed. Figure 4 demonstrates the distribution of the carbon dioxide concentration in three sample houses during winter. It can be found that carbon dioxide concentrations of all houses below 1000 ppm account for more than 85% of the time. The average concentration of the bedrooms is higher than it in the living rooms. From the interview, the occupants prefer closing the window during night-time to reduce the heat loss via ventilation, which would reduce the fresh air supply and increase the carbon dioxide concentration in bedrooms.

The average carbon dioxide concentration for Eco-house, Normal-1 and Normal-2 is 618 ppm, 724 ppm and 746 ppm, respectively. Eco-house has the best performance among the three dwellings due to the application of the heat recovery ventilator. Based on the fundamental of carbon concentration regarded as an indicator for appropriate ventilation rates to determine the air quality (Rangel et al. 2020), the installed heat recovery ventilator appears to introduce sufficient fresh air to ensure the interior air quality in Eco-house.

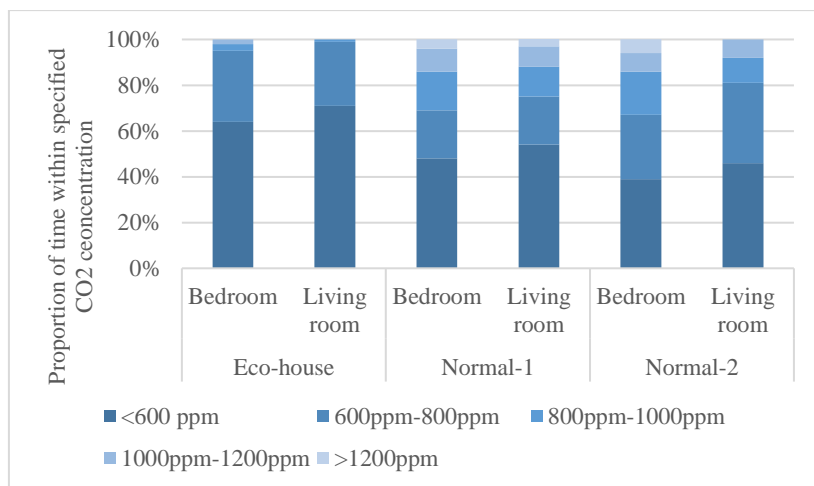


Figure 4 The carbon dioxide concentration levels in various rooms during winter.

### Summer condition

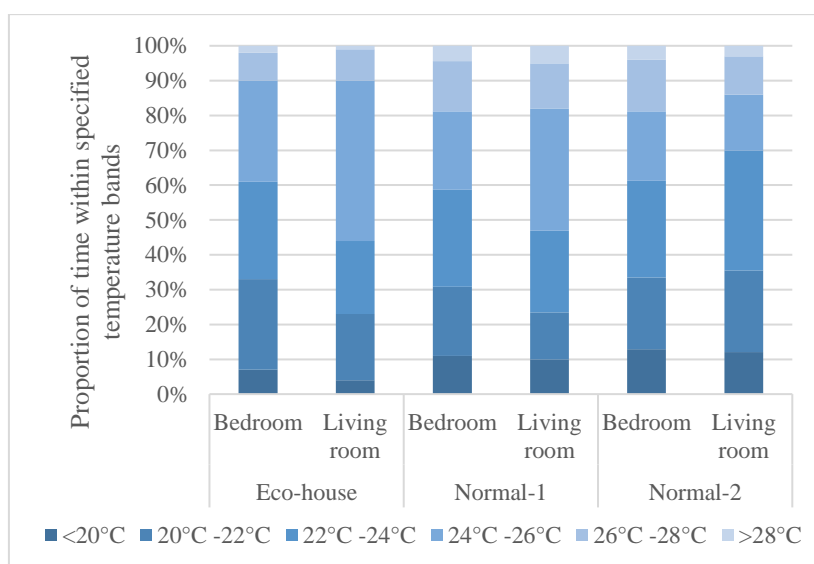


Figure 5 The temperatures in bedroom and living room across all monitored dwellings during summer.

Correspondingly, the Eco-house still have the highest temperature in summer, with an average temperature of 23.1 °C and 23.8 °C for the bedroom and the living room, respectively. About 72% of the occupied time, the interior temperatures of Eco-house are in thermal comfort range as suggested by Indoor Air Quality Standards. And the maximum temperature recorded in Eco-house is 31.2 °C. The recorded average temperature in Normal-1 is the second-highest, with 22.3 °C and 22.6 °C for the bedroom and the living room, respectively. For 68% of the occupied time, Normal-1 is in the thermal comfort range. The maximum recorded temperature in Normal-1 is about 30.2 °C. As for Normal-2, the recorded mean temperature is the lowest, with the bedroom of 21.8 °C and the living room of 22.0 °C. Only 61% of the time, the temperature in Normal-2 belongs to the thermal comfort range.

The overall satisfaction level during summer is much improved, as shown in Table 5. For Eco-house, the mean score for satisfaction level is increased from 2 to 3. Overheating is the main reported issue in Eco-house and get the lowest score among the three dwellings. As for the other two normal houses, the main issues mentioned in winter has not shown in summer. Normal-1 achieved the second-highest score on the overall satisfaction level. But both the occupants in Normal-1 and Normal-2 complained of mildew, mould growth in the toilet during summer. The mould in Normal-2 poses more serious moisture and mould issues than Normal-1. The moisture in the air provides an ideal environment for mould growth. Thus, the humidity, air freshness and odour density were the main unsatisfactory issues in the questionnaire for normal houses.

Figure 6 shows the distribution of the carbon dioxide concentration in three sample houses during summer. The carbon dioxide concentrations of all houses below 1000 ppm account for over 95% of the time. Compared with the index in winter, the carbon dioxide concentration during summer is much improved. Similar to winter, the average concentration of the bedrooms is higher than it in the living rooms. During summer, the occupants prefer to opening windows to enhance

ventilation cooling, as natural ventilation is the most energy-efficient way to cool buildings. The average carbon dioxide concentration for Eco-house, Normal-1 and Normal-2 are 602 ppm, 663 ppm and 692 ppm, respectively. As for Normal-1 and Normal-2, the readings on carbon dioxide concentration are higher than Eco-house, especially the meters of the bedrooms. The average concentration of Normal-2 is higher than Normal-1. Both of the two houses are not equipped with ventilators. The number of occupants might be the reason. There are 4 occupants living in Normal-2, and only 3 occupants in Normal-1.

Table 5: The results of questionnaire on air quality during summer.

Satisfaction level (-3 to +3)	Eco-house		Normal-1			Normal-2	
	Adult 1	Adult 2	Adult 1	Adult 2	Children	Adult 1	Children
<b>Overall satisfaction</b>	2	3	1	0	1	1	1
<b>Temperature</b>	1	2	1	2	1	2	1
<b>Temperature variation</b>	2	3	1	0	0	1	1
<b>Humidity</b>	2	3	-1	-1	0	-1	-1
<b>Air freshness</b>	3	3	-2	1	2	-3	-1
<b>Odour density</b>	3	2	0	-1	1	0	-2
<b>Draughty</b>	2	3	2	1	1	1	1

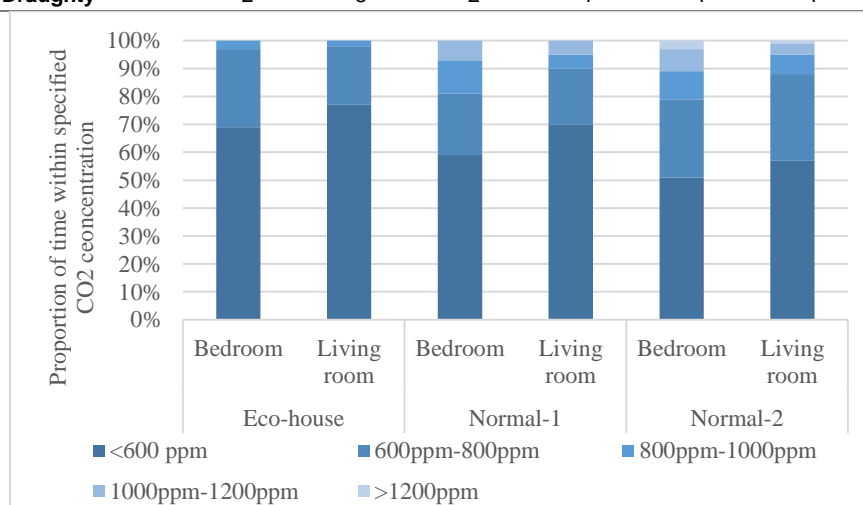


Figure 6 The carbon dioxide concentration levels in various rooms during summer

#### 4.1. Energy consumption

In order to mitigate the energy poverty and carbon emission, the global net human-caused emissions of carbon dioxide need to be reduced by 45% from 2010 levels by 2030 and to reach net zero by 2050. Near Zero Energy Building (nZEB) standards has been implemented in Europe since 2020. The British government required that certain new buildings are energy efficient and require all the new buildings to be zero carbon since 2016. To satisfy the passive house standards, the dwellings must consume less than 120 kWh/m<sup>2</sup>/year of primary energy on all building loads, including DHW, heating, cooling, auxiliary and household electricity. Energy use is typically measured per area and duration. Passive house standards deal with the energy use in the usable area, not the gross area of the building. The usable area excludes stairways and unheated areas. Furthermore, in 2019, the Ministry of Housing and Urban-Rural Development, PRC promoted the 'Near-Zero Energy Building Technical Standards' (GB/T51350). The guidelines stated the maximum energy consumption for heating should be less than 8 kWh/m<sup>2</sup>/year for the 'hot summer and cold winter area' in China. To comply with the Near-Zero Energy Building Technical Standards, dwellings must consume less than 55 kWh/m<sup>2</sup>/year primary energy for the regulated load only (such as space heating/cooling, DHW, fixed lighting and ventilation). The usable floor area has also been used to calculate the primary energy use. But the usable area includes all dwelling floor space as well as stairways and unheated areas. The conversion factor from electric to primary energy is assumed as 2.6.

Table 6: The energy consumption across all monitored dwellings.

	Eco-house	Normal-1	Normal-2
<b>Energy on space heating/cooling (kWh)</b>	783	1571	1108
<b>Total energy consumption on regulated loads (kWh)</b>	1360	2309	2005
<b>Usable floor Area (m<sup>2</sup>)</b>	61	69	73
<b>Average Primary Energy use (kWh/m<sup>2</sup>/year)</b>	58	87	71

As the appliances for regulated loads were powered by electricity in all dwellings, the energy consumed for regulated loads was in form of electricity. As shown in Table 6, the energy consumption on space heating/cooling accounts for about 60% of total energy consumed on regulated loads. The annual energy consumption on space heating/cooling of Normal-1 is the highest, 1571 kWh. Apart from energy on space heating/cooling, the Normal-2 consumed most energy, 897 kWh, on DHW and lighting for a year among three sample dwellings. Eco-house consumed the least energy on regulated loads. Moreover, it can be found that none of the sample dwellings can comply with near-zero energy building standards on average primary energy use. The average primary energy use in Eco-house, 58 kWh/m<sup>2</sup>/year, is closest to the requirements of standards. For Eco-house, the recorded total energy consumption for space heating/cooling is 782 kWh. During the spring, summer, and autumn, 103 kWh, 224 kWh and 95 kWh have been consumed by the air-conditioner. The figure in winter is significantly high, 359 kWh, corresponding with the heating action of the heat pump. Before the construction of Eco-house, a computer simulation has been undertaken to estimate the energy consumption on space heating/cooling in Eco-house. The predicted energy consumption on heating and cooling is 347 kWh and 165 kWh, respectively. And the disparity between predicted and actual energy consumption on heating and cooling is 98 kWh and 173 kWh. Eco-house consumed more energy than estimated by the computer programme. The predictive parameter for heating and cooling accounts for about 78% and 49% of the recorded energy consumption.

There is a great disparity between the predicted and the recorded data, especially the energy consumption for cooling. This summary is to identify the main causes of such discrepancies and the factors affecting unrealistic simulation results. (Menezes et al. 2012) stated the causes of discrepancies always includes the unreal data input to the software, occupancy behaviour, actual building quality, and facilities management level. The followed possible factors affecting the real performance have been identified:

1. The majority of the recorded temperature in winter is consistently higher than the expected in software. The average temperature of the bedroom during winter is 19.3 °C and 20.1 °C for the living room. However, the estimated mean temperatures are 18.01 °C and 17.74 °C. On contrary, the estimated mean temperature is higher than the recorded temperature during summer. The air-conditioner system consumed more energy to provide space cooling and heating than predicted.
2. The assumption on the daily occupied time in simulation starts from 20:00 to 7:00, which cannot reflect the actual occupied time. According to the interview, the typically occupied hour is from 18:00 to 8:00, and sometimes throughout all days. The air-conditioner will operate for more time than estimated.
3. The parameter of the weather file cannot match the recorded weather data well. For example, in the coldest month in China, January, the average temperature in the weather file is 3.9 °C but the recorded mean temperature is 4.6 °C. During summer, the temperature in the weather file is cooler than the recorded. This would be a possible factor resulting in the energy consumption in simulation lower than the real.
4. The actual Coefficient of Performance (COP) of the air-conditioner is difficult to specify. The COP of the air-conditioner is quite different under various cooling loads, temperature gaps and maintenance levels. But during the simulation, a fixed value is always inputted into the programme.
5. The performance of some building components is not satisfactory. The window frame of Eco-house is designed as the thermally broken aluminium window. The thermally broken aluminium window means the window frame is inserted into a reinforced polyamide bar, creating an insulated barrier within the window frame. But in practice, the window frame in Eco-house is the normal aluminium frame, which would allow more unwanted heat loss/gain via window frame, resulting in more energy consumption on space heating/cooling.

## 5. CONCLUSION

This paper evaluates the thermal comfort, IEQ and energy performance in Eco-house and two normal dwellings by post-occupancy evaluation. The physical parameters of the interior environment and energy consumption data have been collected and analysed. The key findings include:

1. The occupants in the Eco-house enjoy a very high level of thermal comfort in winter. But in summer, there is a high possibility of overheating risk. The occupants also reported hot feeling in Eco-house.
2. The occupants of Normal-1 have the lowest overall satisfaction level during winter. The relative temperature variation and air freshness during winter are the main issues in Normal-1. As for summer, mould growth is annoying in normal houses, especially in Normal-2.
3. The overall concentration in summer is lower than in winter for all dwellings due to the high frequency of ventilation. In terms of IEQ, the satisfaction level in Eco-house is higher than normal houses, especially for the air freshness. The heat recovery ventilator can improve the IEQ greatly over natural ventilation.
4. The carbon dioxide and PM 2.5 concentrations are within acceptable limits for Eco-house. The application of the air filter in the ventilator has been approved to successfully reduce the concentration of PM 2.5 particles.
5. It is worth mentioning that the satisfaction level on the interior air quality is positively correlated with odour density and draughtiness. The concentrations of CO<sub>2</sub> and PM 2.5 particles are perception weaknesses for occupants. The occupants have not complained about the issues about concentrations of CO<sub>2</sub> and PM 2.5 particles.
6. The energy consumption on regulated loads in Normal-1 is the highest. Except for the energy on space heating/cooling, Normal-2 consume the most energy. According to the calculation, none of the sample dwellings can comply with near-zero energy building standards on average primary energy use. But the parameter for Eco-house is the closest one, 58 kWh/m<sup>2</sup>/year.



7. The recorded energy consumption in Eco-house is higher than the simulated result. The causes of discrepancies in energy consumption are analysed. The identified factors, such as energy efficiency and operation time of air-conditioner, unrealistic data in the computer programme and building quality, would affect the gap between predicted and recorded ones.

Due to various factors affecting the perceptual IEQ and energy consumption, a detailed POE to increase the sample size and a longer time monitor on IEQ is needed in the future. Further work will seek to identify the specific issues or flaws which need to be addressed in Eco-house and normal houses. And monitoring more factors enable the use of more realistic parameters in simulation, bringing the more accurate predicted values.

## 6. REFERENCES

- ASHRAE, 2004. ASHRAE for standard ventilation for Acceptable air quality. *ANSI/ASHRAE Addendum n to ANSI/ASHRAE Standard 62-2001*, 8400.
- ASHRAE, 2017. Thermal environmental conditions for human occupancy. *ANSI/ASHRAE Standard 55-2017*.
- Beizaee, A., Lomas, K.J., Firth, S.K., 2013. National survey of summertime temperatures and overheating risk in English homes [online]. *Building and Environment*, 65, pp.1–17. Available at: <https://www.sciencedirect.com/science/article/pii/S0360132313000917>.
- Chang, Y. et al., 2014. Disaggregated I-O LCA model for building product chain energy quantification: A case from China [online]. *Energy and Buildings*, 72, pp.212–221. Available at: <http://www.sciencedirect.com/science/article/pii/S0378778813008426> [Accessed 28 May 2017].
- Colclough, S. et al., 2018. Investigation of nZEB social housing built to the Passive House standard [online]. *Energy and Buildings*, 179, pp.344–359. Available at: <https://www.sciencedirect.com/science/article/pii/S0378778818306765>.
- Colclough, S. et al., 2022. Post occupancy evaluation of 12 retrofit nZEB dwellings: The impact of occupants and high in-use interior temperatures on the predictive accuracy of the nZEB energy standard [online]. *Energy and Buildings*, 254, p.111563. Available at: <https://www.sciencedirect.com/science/article/pii/S0378778821008471>.
- Deuble, M.P., de Dear, R.J., 2012. Green occupants for green buildings: The missing link? [online]. *Building and Environment*, 56, pp.21–27. Available at: <https://www.sciencedirect.com/science/article/pii/S0360132312000741>.
- Ding, Y. et al., 2019. An occupancy-based model for building electricity consumption prediction: A case study of three campus buildings in Tianjin [online]. *Energy and Buildings*, 202, p.109412. Available at: <https://www.sciencedirect.com/science/article/pii/S0378778819317712>.
- Glass, J., Dainty, A.R.J., Gibb, A.G.F., 2008. New build: Materials, techniques, skills and innovation [online]. *Energy Policy*, 36(12), pp.4534–4538. Available at: <http://www.sciencedirect.com/science/article/pii/S0301421508004771> [Accessed 1 June 2017].
- Goncalves, V., Ogunjimi, Y., Heo, Y., 2021. Scrutinizing modeling and analysis methods for evaluating overheating risks in passive houses [online]. *Energy and Buildings*, 234, p.110701. Available at: <https://www.sciencedirect.com/science/article/pii/S0378778820334873>.
- Huang, Y. et al., 2021. Research on indoor spaces and passenger satisfaction with terminal buildings in China [online]. *Journal of Building Engineering*, 43, p.102873. Available at: <https://www.sciencedirect.com/science/article/pii/S2352710221007312>.
- Jones, R. V, Goodhew, S., de Wilde, P., 2016. Measured Indoor Temperatures, Thermal Comfort and Overheating Risk: Post-occupancy Evaluation of Low Energy Houses in the UK [online]. *Energy Procedia*, 88, pp.714–720. Available at: <https://www.sciencedirect.com/science/article/pii/S1876610216301138>.
- Laetitia, M. et al., 2020. The hot summer-cold winter region in China: Challenges in the low carbon adaptation of residential slab buildings to enhance comfort [online]. *Energy and Buildings*, 223, p.110181. Available at: <https://www.sciencedirect.com/science/article/pii/S0378778820305673>.
- Li, J. et al., 2022. China's flexibility challenge in achieving carbon neutrality by 2060 [online]. *Renewable and Sustainable Energy Reviews*, 158, p.112112. Available at: <https://www.sciencedirect.com/science/article/pii/S1364032122000417>.
- Li, P., Froese, T.M., Brager, G., 2018. Post-occupancy evaluation: State-of-the-art analysis and state-of-the-practice review [online]. *Building and Environment*, 133, pp.187–202. Available at: <https://www.sciencedirect.com/science/article/pii/S0360132318300957>.

- Lin, B. et al., 2016. Measured energy use and indoor environment quality in green office buildings in China [online]. *Energy and Buildings*, 129, pp.9–18. Available at: <https://www.sciencedirect.com/science/article/pii/S0378778816306673>.
- Liu, Y. et al., 2021. Thermal preference prediction based on occupants' adaptive behavior in indoor environments- A study of an air-conditioned multi-occupancy office in China [online]. *Building and Environment*, 206, p.108355. Available at: <https://www.sciencedirect.com/science/article/pii/S0360132321007526>.
- Ma, M. et al., 2020. Low carbon roadmap of residential building sector in China: Historical mitigation and prospective peak [online]. *Applied Energy*, 273, p.115247. Available at: <https://www.sciencedirect.com/science/article/pii/S0306261920307595>.
- Menezes, A.C. et al., 2012. Predicted vs. actual energy performance of non-domestic buildings: Using post-occupancy evaluation data to reduce the performance gap [online]. *Applied Energy*, 97, pp.355–364. Available at: <https://www.sciencedirect.com/science/article/pii/S0306261911007811>.
- Pei, Z. et al., 2015. Comparative study on the indoor environment quality of green office buildings in China with a long-term field measurement and investigation [online]. *Building and Environment*, 84, pp.80–88. Available at: <https://www.sciencedirect.com/science/article/pii/S0360132314003369>.
- Preiser, Wolfgang, F.E., 1995. Post-occupancy evaluation: how to make buildings work better. *Facilities*, 13(11), pp.19–28.
- Pui, D.Y.H., Chen, S.-C., Zuo, Z., 2014. PM2.5 in China: Measurements, sources, visibility and health effects, and mitigation [online]. *Particulate Matter*, 13, pp.1–26. Available at: <https://www.sciencedirect.com/science/article/pii/S1674200113002228>.
- Rangel, A.M. et al., 2020. Indoor Air Quality in Passivhaus Dwellings: A Literature Review. *International journal of environmental research and public health*, 17(4749).
- SILVERSTEIN, MURRAY; VAN DER RYN, S., 1967. *Dorms at Berkeley An Environmental Analysis* [eBook]. Berkeley. Available at: <http://files.eric.ed.gov/fulltext/ED018073.pdf>.
- Taleb, H.M., Sharples, S., 2011. Developing sustainable residential buildings in Saudi Arabia: A case study [online]. *Applied Energy*, 88(1), pp.383–391. Available at: <http://www.sciencedirect.com/science/article/pii/S0306261910002989> [Accessed 11 June 2017].
- US EPA National Center for Environmental Assessment Environmental Media Assessment Group, R.T.P.N., Sacks, J., 2009. Integrated Science Assessment for Particulate Matter (Final Report). *US EPA - Environmental Protection Agency*.
- Wright, A., Young, A., Natarajan, S., 2005. Dwelling temperatures and comfort during the August 2003 heat wave. *Building Services Engineering Research & Technology*, 26, pp.285–300. 10.1191/0143624405bt136oa.
- Yu, X. et al., 2017. On a Post-occupancy Evaluation Study of Effects of Occupant Behavior on Indoor Environment Quality in College Buildings in Chongqing [online]. *Procedia Engineering*, 205, pp.623–627. Available at: <https://www.sciencedirect.com/science/article/pii/S1877705817350877>.
- Zeng, C. et al., 2022. The exploration of residents' perception of eco-urbanization at community and driving factors in China [online]. *Cities*, 122, p.103513. Available at: <https://www.sciencedirect.com/science/article/pii/S0264275121004121>.
- Zhang, X., Platten, A., Shen, L., 2011. Green property development practice in China: Costs and barriers [online]. *Building and Environment*, 46(11), pp.2153–2160. Available at: <http://www.sciencedirect.com/science/article/pii/S0360132311001338> [Accessed 19 June 2017].
- Zhang, X., Wu, Y., Shen, L., 2012. Application of low waste technologies for design and construction: A case study in Hong Kong [online]. *Renewable and Sustainable Energy Reviews*, 16(5), pp.2973–2979. Available at: <http://www.sciencedirect.com/science/article/pii/S1364032112001141> [Accessed 19 June 2017].
- Zhang, Z., 2019. The effect of library indoor environments on occupant satisfaction and performance in Chinese universities using SEMs [online]. *Building and Environment*, 150, pp.322–329. Available at: <https://www.sciencedirect.com/science/article/pii/S0360132319300241>.
- Zhao, D.-X. et al., 2015. Social problems of green buildings: From the humanistic needs to social acceptance [online]. *Renewable and Sustainable Energy Reviews*, 51, pp.1594–1609. Available at: <http://www.sciencedirect.com/science/article/pii/S1364032115007194>.

---

## #293: Impact of various technologies on peak energy demand of residential building in the cold climate of UK

---

Sajan PREET<sup>1</sup>, Stefan Thor SMITH<sup>2</sup>

<sup>1</sup> School of Built Environment, University of Reading, Reading, RG6 6AH, UK, s.preet@reading.ac.uk

<sup>2</sup> School of Built Environment, University of Reading, Reading, RG6 6AH, UK, s.t.smith@reading.ac.uk

*Abstract: Residential buildings are the key contributors to the high electrical energy demand in the United Kingdom. Heat pumps mainly consume electricity to meet space heating and hot water demands. The Time-of-use tariffs have been introduced to enable consumers to time dependency of demand. However, peak energy demand, which occurs in a small percentage during a specific time of day, significantly impacts the overall power balance and stability of the utility grid. Investigation into integrating various demand-side management technologies to reduce peak heating demand has been increasing. In the present study, the impact of various technologies, such as photovoltaic panels with battery energy storage system (PV-BESS) (case 1), PV-BESS with the solar thermal system (case 2), and photovoltaic/thermal (PV/T) with BESS (case 3) system on peak energy demand and overall energy demand have been analyzed in cold climatic conditions. In the context of a residential building, a simulation model of David Wilson home was developed integrating various technologies, which was compared against the baseline model (case 0) integrated with an air source heat pump. The simulation was performed on DesignBuilder/EnergyPlus for the UK's winter month i.e., January. The Simulation results show that without any integration of technologies, the heating demand of David Wilson home in the month of January was 1531.6 kWh in case 0, which was reduced to 1456.1 kWh in case 1, 1318 kWh in case 2 and 1132.47 kWh in case 3. With the integration of the solar heating system, a maximum reduction in peak energy demand is observed with the PV/T-BESS (case 3) system.*

*Keywords: Building heating demand, Peak energy demand, Battery energy storage system, Solar assisted heat pump, photovoltaic/thermal system*

## 1. INTRODUCTION

Increment in the world population and high standard of living of people has increased the energy requirements of countries worldwide (Xia et al., 2022). For this reason, the energy consumption of buildings has notable consequences on the economy, energy generation capacity, and environment of specific countries (Preet et al., 2023). As per reports of the International Energy Agency (IEA) in 2022, around 32% of global energy consumption is specifically through residential buildings. In some countries, the energy consumption of residential buildings has exceeded the other sectors such as industries (Wilberforce et al., 2023). In the United Kingdom (UK), household buildings contribute to 32.5% of the entire nation's energy consumption among which around 68% of energy is consumed for space heating purposes (Ward et al., 2023) (F. Von Malmberg, 2021). The variability in energy demand of residential built space always remains non-linear, uncontrollable, and varies in an entire day from morning to evening. Its nature changed from static to dynamic with the introduction of smart and microgrid systems (Lamnatou et al., 2022). After the pandemic, the amplitude and frequency of Peak energy demand have increased due to the rise of several end users staying in built areas (Panda et al., 2022).

Fulfilling the time-vary electricity requirement of residential buildings at peak time is a key challenge for electricity suppliers. Within the United Kingdom, the residential sector accounts for approximately 60% of the maximum energy demand, with a predominant focus on addressing buildings' heating requirements (Dixon et al., 2022). Conventional power plants are used to generate more electricity so peak energy demand can be fulfilled (Ramirez-Mendoila., 2022). However, this approach is found inefficient and not economically feasible due to high fuel consumption, high maintenance cost, and high carbon emissions (Panda et al., 2022). During peak demand periods, electricity prices are up to eight times higher than during off-peak demand period (Ramirez-Mendoila., 2022). Thus, finding an effective solution for reducing peak energy demand and meeting the UK net zero emissions target has become an important area of research.

Demand-side management (DSM) stands out as the most efficient and sustainable solution for addressing the issue of peak energy demand in residential buildings (Uddin et al., 2018). It comprises a collection of techniques and strategies such as the incorporation of power-saving technologies, dynamic unit price, and Demand response-based programs for managing and mitigating both regular load and peak load instances (Kanakadhurga and Prabakaran, 2022). Implementation of time-based demand response programs such as time-of-use pricing, critical peak pricing, and real-time pricing has shown a reduction in peak energy demand. In the UK, a three-tier TOU tariff known as TIDE or RAG is implemented wherein, there exists a low-rate period from 23:00 to 6:00, offering a charge of 6.41 pence per kilowatt-hour (p/kWh). During the evening peak, spanning from 16:00 to 19:00, the rate increases to 29.99 p/kWh. For the remaining time slots, the rate is set at 14.02 p/kWh. (Green Energy UK). Additional DSM technologies, like the utilization of energy-efficient appliances, the incorporation of Distributed Energy Resources (DER) such as solar panels or wind turbines (Obi et al., 2020), and the deployment of energy storage systems such as electrical energy storage systems (EES) (Pimm et al., 2018) and thermal energy storage (TES) (Kutlu et al., 2022), have been applied to reduce the peak demand. In the present research work, an analysis has been conducted to assess how different Demand-Side Management (DSM) technologies, including solar-assisted heat pump systems, photovoltaic panels, photovoltaic/thermal systems, and battery energy storage systems, affect the peak energy demand of residential buildings in the cold climatic conditions of the UK.

### 1.1. Literature review

The incorporation of a solar thermal system into the heat pump arrangement has led to an enhancement in the system's Coefficient of Performance (COP). This improvement can be attributed to the higher evaporator temperature, resulting in a reduced compressor temperature when compared to conventional heat pump systems (Sezen and Gungor., 2023). Kim et al., 2018 conducted a parametric investigation on a solar-assisted heat pump system. Their study revealed that augmenting the collector area and absorption coefficient led to a notable improvement in overall performance. Bellos and Tzivanidis, 2019 conducted optimization studies for a solar-assisted heat pump system, specifically focusing on its performance in the mild winter climate of Athens. Their work involved exploring various working fluids to enhance the system's performance. Under steady-state conditions, maximum heat generation was 4.3 kW using R32 with R1234f working fluids. Bahman et al., 2022 developed a mathematical model of a photovoltaic thermal system-based heat pump to analyze its energy and exergy performance under different ambient conditions. A noticeable trend emerged where the average Coefficient of Performance (COP) exhibited an elevation in response to an increment in direct incident solar radiation. Zhang et al., 2019 performed a comparative analysis between solar thermal integrated serial indirect expansion-based heat pumps with parallel indirect expansion-based heat pumps during different seasons. The COP of Parallel ID-SAHP is 4.34 which is better than the COP of serial ID-SAHP which is 3.23.

Battery energy storage system is integrated into residential buildings to store electricity generated by photovoltaic panels and during off-peak periods that are utilized to run heat pump during peak hours. Pimm et al., 2018 examined the capability of battery energy storage systems to mitigate the peak energy demand. It was observed that the installation of 3 kW of battery storage per household can run the heat pump without an additional load of substations to meet peak demand. The above findings are corroborated by the research conducted by Schram et al., 2018. Leadbetter and Swan, 2012 suggested that the battery size of a typical residential home should vary from 2.6 kW with low electricity consumption to 5.2 kW with high electricity consumption to fulfill the requirement of space heating. Babacan et al., 2017 devised a convex optimization approach for orchestrating the storage of electricity. This method takes into account factors such as electricity tariff and demand. Lokeshgupta and Sivasubramani, 2019 observed from a study that all residential buildings can get back their BESS investment within the first three years of installation. Roberts et al., 2019 observed through a study that installation

of batteries between 2-3 kWh in residential apartments achieved up to 30% reduction in peak energy demand. Ghadimi et al., 2023 concluded that integration of photovoltaic panels with BESS can achieve higher reductions in energy savings which have been investigated in the present research article.

## 1.2. Research gap and objective

Reducing peak energy demand of residential buildings has become an important research topic due to the problem of grid stress, high carbon emissions, and elevated electricity prices. Researchers have put into practice a range of Demand-Side Management (DSM) strategies aimed at diminishing the peak energy demand of residential structures. Technologies such as energy-efficient heat pumps, photovoltaic panels, and electrical energy storage systems such as batteries have been implemented to meet peak heating and energy demand. Most of the researchers have implemented solar-assisted heat pumps and battery energy storage individually to reduce the peak heating demand. Nevertheless, the collective influence of the aforementioned technologies on the peak heating and energy demand of residential buildings in cold climates requires further examination, a subject that is addressed in the current study. In this ongoing research endeavour, the effectiveness of residential buildings incorporating DSM technologies is being examined. These technologies include the combination of solar PV panels with battery energy storage systems (PV-BESS) in case 1, PV-BESS along with a solar-assisted heat pump system in case 2, and a photovoltaic/thermal (PV/T) assisted heat pump system with BESS in case 3. These cases are being compared against a base case building (case 0) to assess their capability for reducing peak energy demand in the cold climate conditions of the UK.

## 2. METHODOLOGY

In this ongoing research study, an investigation has been conducted to evaluate the impact of various demand-side management technologies on diminishing the peak heating demand in residential buildings. The approach taken to achieve the goals of this research study is divided into three distinct stages as shown in Figure 1. In the first stage, a problem of high peak and overall energy demand of residential buildings i.e., high heating demand is identified that mainly occurs during the peak hours of the day. In the second stage, various demand-side management strategies have been identified that can potentially reduce the peak and overall energy demand. Technologies are on-site electricity generation systems (PVs and wind turbines), electrical energy storage systems (BESS), solar thermal systems, and Photovoltaic/thermal systems are mostly implemented to reduce the peak energy demand. In the third stage, an assessment is conducted regarding the thermal and energy performance of the residential building. This assessment involves evaluating the performance of residential buildings that integrate various technologies, as discussed earlier. These evaluations will be compared to the performance of residential buildings integrated with the base-case technology.

In the present research work, the DesignBuilder/EnergyPlus software is used to explore the potential of various technologies in reducing the peak energy demand of residential buildings. DesignBuilder is an energy simulation software that is mainly used to perform building simulations and analyse its thermal, lighting, and energy performance integrating various technologies and passive solutions (Martinez-Gracia et al., 2022). This software conducts thermal comfort analysis, environmental analysis, and cost analysis (Mujeebu et al., 2022). The software additionally calculates the shading caused by neighbouring buildings and assesses solar heat gain for each day across different months of the year. The thermal properties of the materials, ventilation rate, and occupancy profile can also be specified for different time periods. For the analysis, hourly meteorological data corresponding to a standard year and specific locations were employed as weather files. The accuracy of the computed values is notably reliable due to the proximity of the weather files to actual environmental conditions (Al-Huneidi et al., 2022).

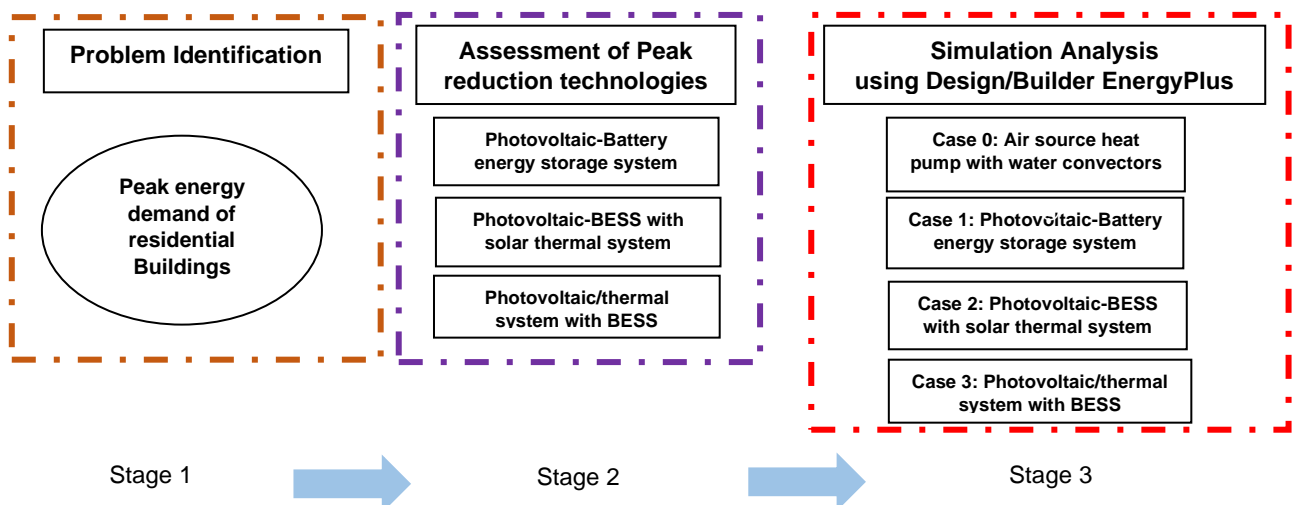


Figure 1 Methodology flow chart in the present study

### 3. SYSTEM DESCRIPTION AND MODELING

The modeling process encompasses the creation of representations for a residential building and its constituent elements, including the heat pump system, solar photovoltaic panels, solar thermal collectors, photovoltaic/thermal systems, and battery storage systems. These models were developed using the DesignBuilder and EnergyPlus software. Figure 2 depicts the selected David Wilson home, which is situated at the University of Nottingham. This two-story dwelling spans dimensions of 7.9 m × 7.9 m × 5.0 m and boasts a floor area of 62.41 m<sup>2</sup>. The construction materials utilized in the model are reflective of those used in the actual David Wilson home. The simulation model employs the London weather file. The home is conceptualized as a residence for a family of four, consisting of two working parents and two children. Specific parameters such as occupancy patterns, heating requirements, lighting usage, hot water consumption, ventilation rates, and appliance utilization are defined in the model to align with the behaviours of the four occupants.

Figure 3 shows the simulation model of David Wilson home with construction material and glazing. The glazing and construction materials with their thermal performance parameters are specified in the model. The U-values assigned to different construction elements are as follows: external wall 0.22 W/m<sup>2</sup>K, roof 0.19 W/m<sup>2</sup>K, glazing 1.8 W/m<sup>2</sup>K, door 2.2 W/m<sup>2</sup>K, and floor 0.2 W/m<sup>2</sup>K. The profiles include occupancy, heating, water consumption, and appliances are meticulously designed to replicate real-world scenarios. Separate profiles are defined for weekdays and weekends. During weekdays, all residents depart from the residence at 7:30 a.m. and return at 6:00 p.m. On weekends, however, all occupants remain within the home. The heat contributed by occupants consists of both sensible and latent components, with values around 90 watts per person and 60 watts per person, respectively. The operational patterns of lighting and appliances mimic the occupancy schedule, with the exception of sleeping hours. Heat gain from appliances remains consistent at approximately 530 watts, aligning with their usage. The Set temperature of the bedrooms is 18 °C from 10:00 p.m. to 5:30 a.m. as recommended by CIBSE guidelines (CIBSE). On weekdays, when all occupants are away from the residence, the set temperatures are lowered to 15°C, and heating might not be necessary during these unoccupied periods. Throughout the other hours, a set temperature of 21°C is maintained throughout the entire home.

In Case 1, Case 2, and Case 3, photovoltaic panels are positioned on the rooftop of the David Wilson residential building to produce electricity directly at the site. To store the electricity generated by the PV panels, 3 kW batteries are installed, aligning with the recommendation of Pimm et al., 2018. In both Case 2 and Case 3, the solar-assisted heat pump system comprises both solar thermal collectors and an air source heat pump unit. Solar thermal collectors harness solar energy to heat water, which is then stored in a collector tank for later use. The air source heat pump (ASHP), linked to the collector tank, utilizes the accumulated heat from the solar thermal system as a source of heat. Subsequently, this heat is raised to a higher temperature level and utilized to deliver warmth to the interior of the building. The incorporation of solar thermal collectors leads to an improvement in the Coefficient of Performance (COP) of the air source heat pump (ASHP). This enhancement is attributed to the diminished temperature difference between the heat source fluid and the heat sink fluid, as detailed by Olympos et al., 2022.

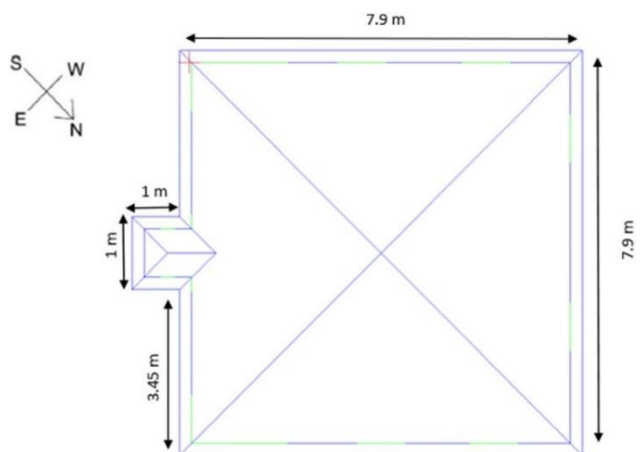


Figure 2 David Wilson home (left) located at the University of Nottingham and layout (right)



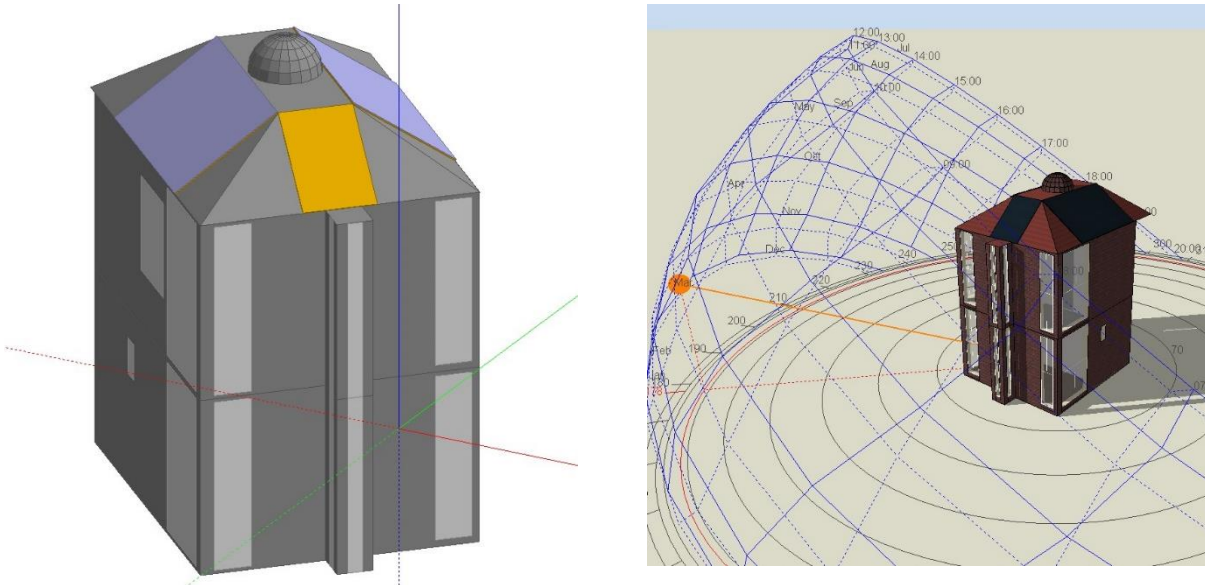


Figure 3 Simulation model of David Wilson home

In Case 1, Case 2, and Case 3, photovoltaic panels are positioned on the rooftop of the David Wilson residential building to produce electricity directly at the site. To store the electricity generated by the PV panels, 3 kW batteries are installed, aligning with the recommendation of Pimm et al., 2018. In both Case 2 and Case 3, the solar-assisted heat pump system comprises both solar thermal collectors and an air source heat pump unit. The schematic diagram of the solar assisted heat pump system integrated with water convectors for space heating is shown in figure 4. Solar thermal collectors harness solar energy to heat water, which is then stored in a collector tank for later use. The air source heat pump (ASHP), linked to the collector tank, utilizes the accumulated heat from the solar thermal system as a source of heat. Subsequently, this heat is raised to a higher temperature level and utilized to deliver warmth to the interior of the building. The incorporation of solar thermal collectors leads to an improvement in the Coefficient of Performance (COP) of the air source heat pump (ASHP). This enhancement is attributed to the diminished temperature difference between the heat source fluid and the heat sink fluid, as detailed by Olympios et al., 2022.

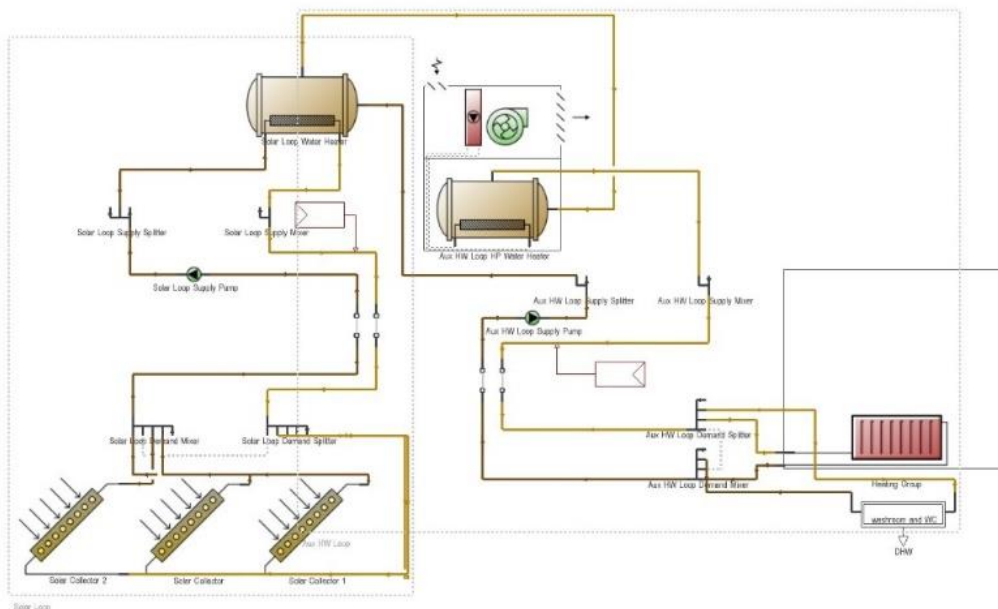


Figure 4 Detailed schematic diagram of solar-assisted heat pump components with water convectors

## 4. RESULT AND DISCUSSION

### 4.1. Heating and energy demand of the residential building

The heating load for the building, calculated for the month of January, is determined using the DesignBuilder/EnergyPlus software. According to the weather conditions prevailing in the UK during the month of January, the average dry bulb temperature is approximately 2°C as shown in Figure 5. In Figure 6 (a), the graph illustrates the heating demand profile of the residential building within the context of the base case model. During weekdays, the building's thermostat maintains the set temperature, particularly during occupancy periods, which corresponds to the morning and evening hours as depicted in Figure 6 (b). The peak heating demand during a single day is estimated to be around 15 kWh, while the total heating demand for the period is 1531.68 kWh, as shown in Figure 7 and Figure 8, respectively. A similar observation was reported by Kutlu et al., 2022, which validates the current simulation model. Their findings indicated a monthly heating demand of approximately 1498 kWh for the David Wilson home with an air source heat pump system, closely aligning with the heating demand observed in the current study. Considering room electricity, lighting electricity, fan energy consumption, and heating demand, the overall energy demand of the base case model amounts to 2452.61 kWh, as illustrated in Figure 9.

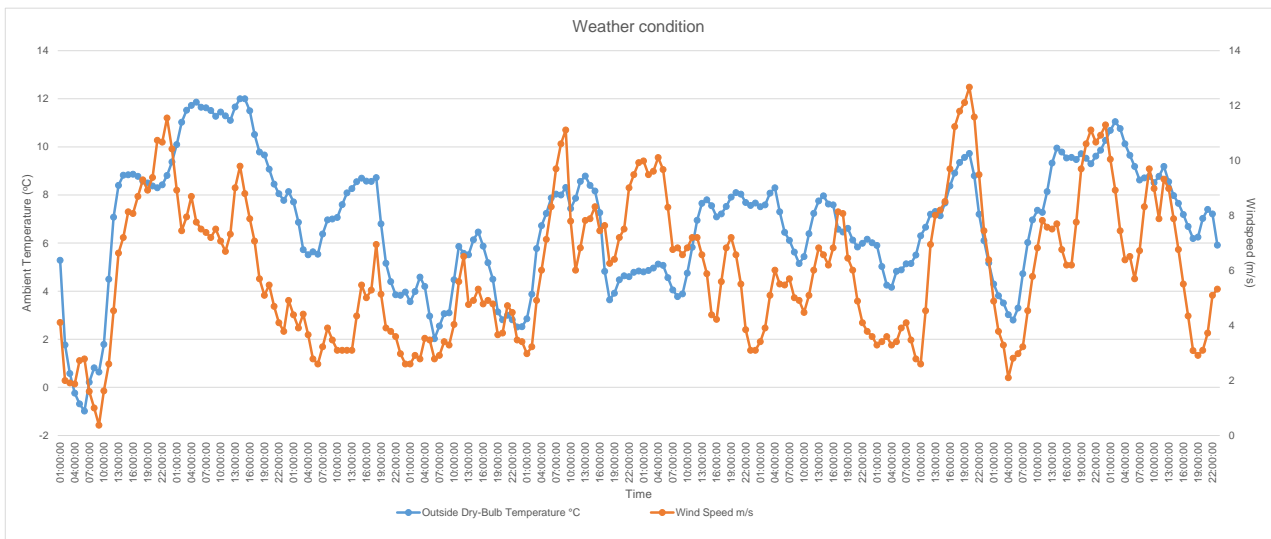


Figure 5 Ambient temperature and wind speed for one week

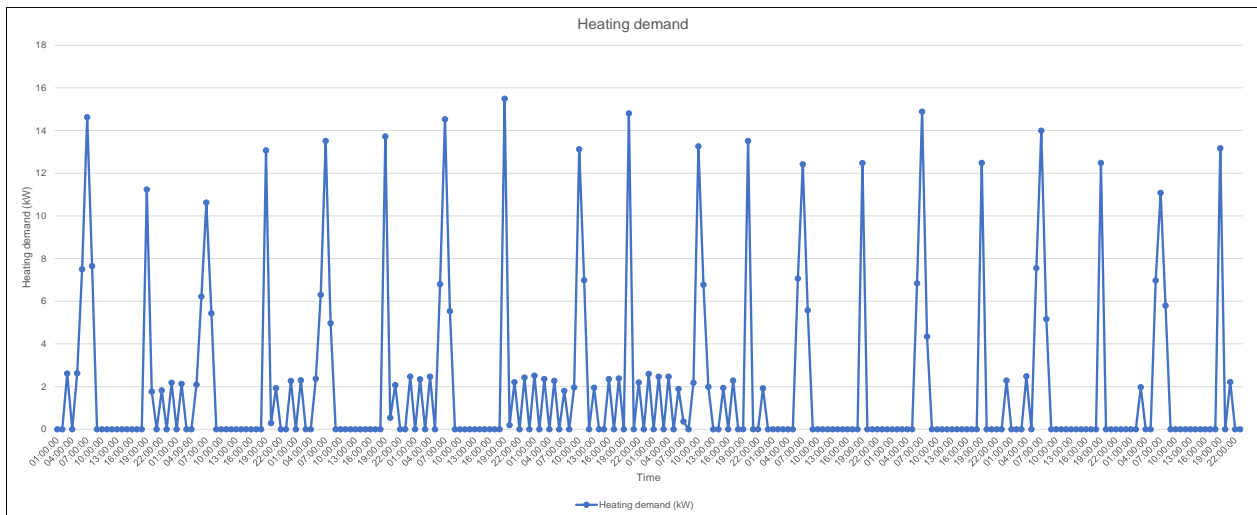


Figure 6 (a) Heating demand profile during one week in the baseline model



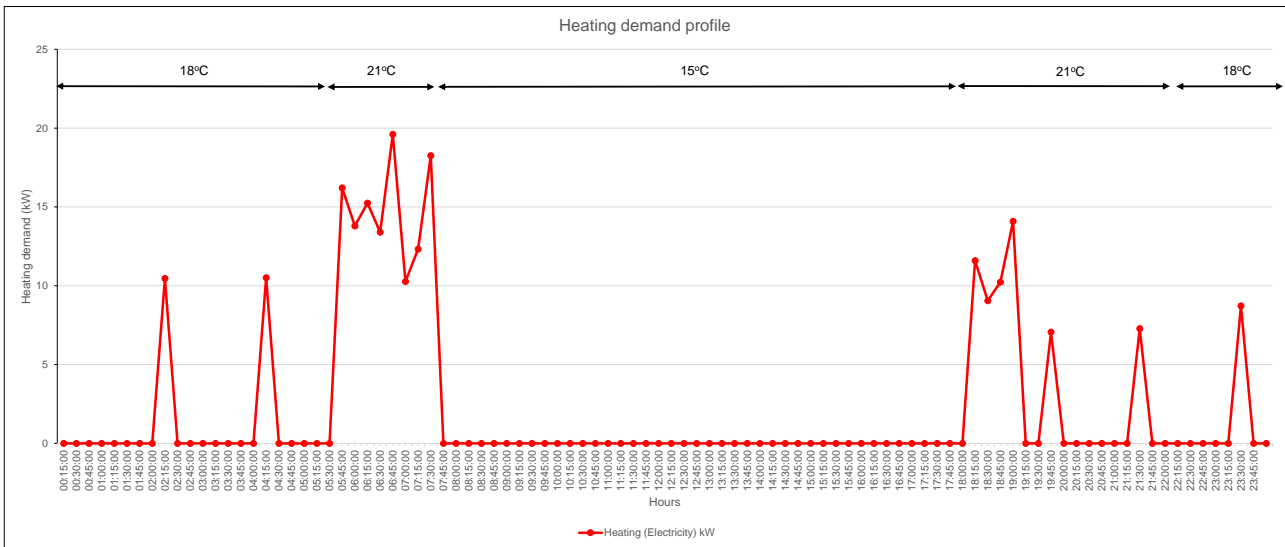


Figure 6 (b) Heating demand profile during a weekday in baseline model

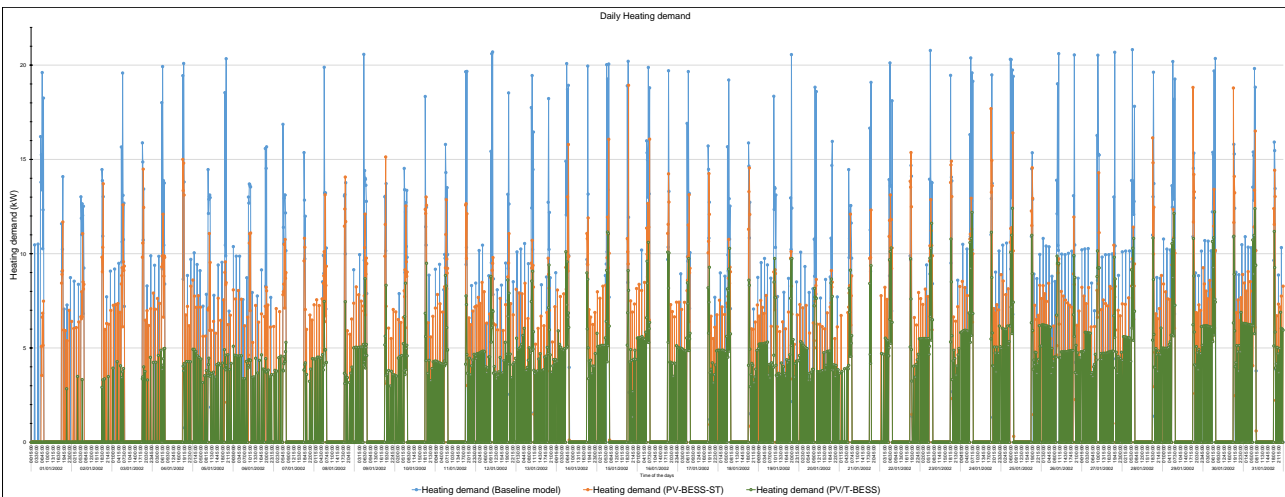


Figure 7 Daily heating demand profile with integration of different technologies during month of January

In Case 1, the integration of a photovoltaic panel with a 3 kW battery storage system into the residential building is aimed at reducing heating demand during peak hours. The photovoltaic panel generated approximately 75.53 kWh of electricity, which subsequently lowered the total heating demand to 1456.15 kWh, as illustrated in Figure 8. As a result, the overall energy demand for the Case 1 model was reduced to 2376.56 kWh, as depicted in Figure 9. Comparable findings were also observed by Pimm et al., 2018. In Case 2, through the integration of a solar thermal system with an air source heat pump, the peak daily heating demand was reduced to 12 kW as shown in Figure 7. The monthly fan energy consumption decreased to 142.98 kWh, and the total monthly heating demand was brought down to 1393.52 kWh. Leveraging the electricity generated by the PV panel, the heat pump's energy consumption was further reduced to 1318 kWh, leading to an overall monthly energy demand of 2223.81 kWh, as shown in Figures 8 and 9. These results align with similar observations made by Olympios et al., 2022 and Xu et al., 2021. With the utilization of photovoltaic/thermal system technology in Case 3, the peak heating demand was curtailed to 9 kW as illustrated in Figure 7. The monthly fan energy consumption decreased to 123.86 kWh, and the total heating demand dropped to 1208.45 kWh. By incorporating the power generated from the PV panels, this energy demand further decreased to 1132.47 kWh, as indicated in Figure 8. The cumulative effect of all the aforementioned technologies led to an overall energy demand reduction of 2019.61 kWh as indicated in Figure 9. Comparable patterns were noted in research conducted by Olympios et al., 2022 and Xu et al., 2021.

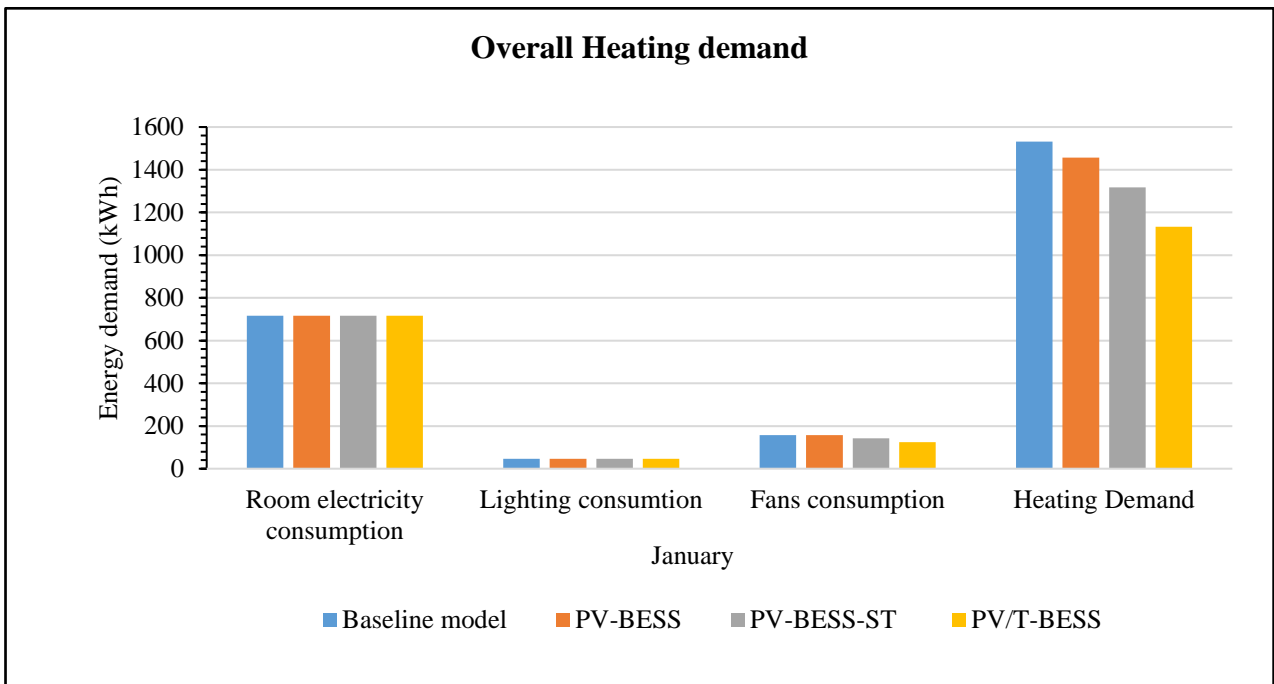


Figure 8 Heating demand of residential building with integration of different technologies

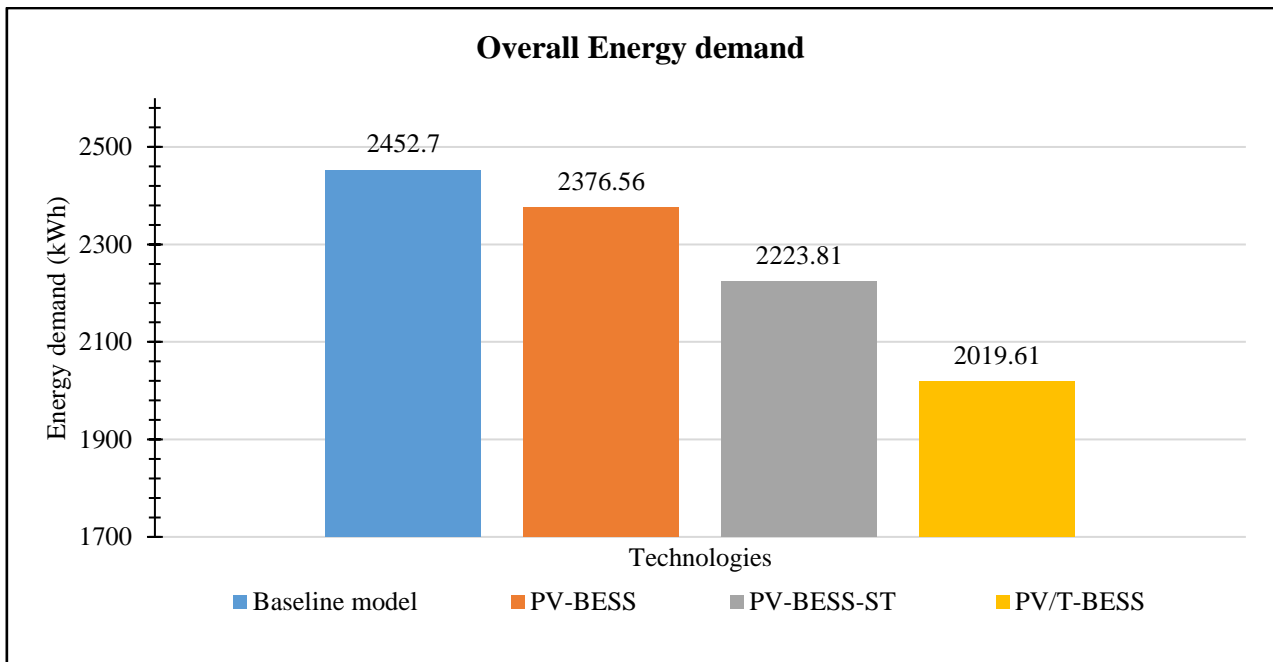


Figure 9 Overall energy demand of residential buildings during the month of January

## 5. CONCLUSION

In this current study, the effectiveness of incorporating various technologies into residential buildings has been explored. These technological strategies encompass the amalgamation of photovoltaic panels with battery energy storage systems (PV-BESS) in Case 1, the integration of PV-BESS with a solar thermal system in Case 2, and the photovoltaic/thermal (PV/T) with BESS in Case 3. These cases have been compared against a base case model (Case 0) to evaluate their potential for reducing peak energy demand within the cold climatic conditions of the UK. Focusing on a specific residential building, a simulation model of David Wilson's home was developed using the DesignBuilder/EnergyPlus software. The simulations were carried out for the entire month of January. This approach facilitated a thorough assessment of how the different technologies perform, particularly in terms of their influence on reducing peak energy demand. Based on the conducted analysis, several significant conclusions have been drawn:

- The precision of the simulation model's outcomes has been verified through a comparison with the results of the baseline model for the David Wilson residential building.
- The thermal and energy performance estimation of David Wilson's home, integrated with various technologies, has been successfully carried out for the cold climatic conditions in the UK, utilizing a simulation model.
- In the baseline model, the daily heating demand of the residential building reaches up to 15 kW. Through the incorporation of technologies, this demand was reduced to 12 kW with the PV-BESS-ST system and further down to 9 kW with the PV/T-BESS system.
- The heating demand for David Wilson's home in January, which was initially 1531.6 kWh in Case 0, experienced reductions to 1456.1 kWh with PV-BESS, 1318 kWh with PV-BESS-ST, and 1132.47 kWh with PV/T-BESS system.
- Among the considered options, the residential building integrated with a photovoltaic/thermal system with BESS achieved the most significant reduction in heating demand.

Additionally, it's suggested that the heating demand of residential buildings could potentially be further decreased by integrating thermal energy storage, particularly through the use of phase change materials, in conjunction with the air source heat pump. Excess heat generated by the photovoltaic/thermal system could be stored in these phase change materials, which could then fulfill the heating requirement of the residential space during peak hours. This approach could lead to even more efficient utilization of energy resources.

## 6. ACKNOWLEDGEMENT

The authors would like to acknowledge the Engineering and Physical Sciences Research Council (EP/T02318X/1) for the financial support of this research.

## 7. REFERENCES

- Xia, W., Apergis, N., Bashir, M. F., Ghosh, S., Doğan, B., & Shahzad, U. (2022). Investigating the role of globalization, and energy consumption for environmental externalities: empirical evidence from developed and developing economies. *Renewable Energy*, *183*, 219-228.
- Preet, S., Mathur, S., Mathur, J., Sharma, M. K., & Chowdhury, A. (2023). Energy characterization of forced ventilated Photovoltaic-DSF system in hot summer of composite climate. *Energy and Built Environment*.
- IEA. (2022). World energy outlook 2022. Paris, France: IEA.
- Wilberforce, T., Olabi, A. G., Sayed, E. T., Elsaid, K., Maghrabie, H. M., & Abdelkareem, M. A. (2023). A review on zero energy buildings—Pros and cons. *Energy and Built Environment*, *4*(1), 25-38.
- Ward, W. O., Li, X., Sun, Y., Dai, M., Arbabi, H., Tingley, D. D., & Mayfield, M. (2023). Estimating energy consumption of residential buildings at scale with drive-by image capture. *Building and Environment*, *234*, 110188.
- Von Malmberg, F. (2021). Exploring advocacy coalitions for energy efficiency: Policy change through internal shock and learning in the European Union. *Energy Research & Social Science*, *80*, 102248.
- Lamnatou, C., Chemisana, D., & Cristofari, C. (2022). Smart grids and smart technologies in relation to photovoltaics, storage systems, buildings and the environment. *Renewable Energy*, *185*, 1376-1391.
- Panda, S., Mohanty, S., Rout, P. K., Sahu, B. K., Bajaj, M., Zawbaa, H. M., & Kamel, S. (2022). Residential Demand Side Management model, optimization and future perspective: A review. *Energy Reports*, *8*, 3727-3766.
- Dixon, J., Bell, K., & Brush, S. (2022). Which way to net zero? a comparative analysis of seven UK 2050 decarbonisation pathways. *Renewable and Sustainable Energy Transition*, *2*, 100016.
- Ramirez-Mendiola, J. L., Mattioli, G., Anable, J., & Torriti, J. (2022). I'm coming home (to charge): The relation between commuting practices and peak energy demand in the United Kingdom. *Energy Research & Social Science*, *88*, 102502.
- Uddin, M., Romlie, M. F., Abdullah, M. F., Abd Halim, S., & Kwang, T. C. (2018). A review on peak load shaving strategies. *Renewable and Sustainable Energy Reviews*, *82*, 3323-3332.
- Kanakadhurga, D., & Prabakaran, N. (2022). Demand side management in microgrid: A critical review of key issues and recent trends. *Renewable and Sustainable Energy Reviews*, *156*, 111915.
- Pimm, A. J., Cockerill, T. T., & Taylor, P. G. (2018). Time-of-use and time-of-export tariffs for home batteries: Effects on low voltage distribution networks. *Journal of Energy Storage*, *18*, 447-458.

- Obi, M., Slay, T., & Bass, R. (2020). Distributed energy resource aggregation using customer-owned equipment: A review of literature and standards. *Energy Reports*, 6, 2358-2369.
- Kutlu, C., Tapia-Brito, E., Agbonaye, O., Su, Y., Smith, S. T., Hughes, B., & Riffat, S. (2022). Incorporation of controllable supercooled phase change material heat storage with a solar assisted heat pump: Testing of crystallization triggering and heating demand-based modelling study. *Journal of Energy Storage*, 55, 105744.
- Sezen, K., & Gungor, A. (2022). Performance analysis of air source heat pump according to outside temperature and relative humidity with mathematical modeling. *Energy Conversion and Management*, 263, 115702.
- Kim, T., Choi, B. I., Han, Y. S., & Do, K. H. (2018). A comparative investigation of solar-assisted heat pumps with solar thermal collectors for a hot water supply system. *Energy Conversion and Management*, 172, 472-484.
- Bellos, E., & Tzivanidis, C. (2019). Multi-objective optimization of a solar assisted heat pump-driven by hybrid PV. *Applied Thermal Engineering*, 149, 528-535.
- Bahman, A. M., Parikhani, T., & Ziviani, D. (2022). Multi-objective optimization of a cold-climate two-stage economized heat pump for residential heating applications. *Journal of Building Engineering*, 46, 103799.
- Zhang, H., Jiang, L., Zheng, W., You, S., Jiang, T., Shao, S., & Zhu, X. (2019). Experimental study on a novel thermal storage refrigerant-heated radiator coupled with air source heat pump heating system. *Building and Environment*, 164, 106341.
- Schram, W. L., Lampropoulos, I., & van Sark, W. G. (2018). Photovoltaic systems coupled with batteries that are optimally sized for household self-consumption: Assessment of peak shaving potential. *Applied energy*, 223, 69-81.
- Leadbetter, J., & Swan, L. (2012). Battery storage system for residential electricity peak demand shaving. *Energy and buildings*, 55, 685-692.
- Babacan, O., Ratnam, E. L., Disfani, V. R., & Kleissl, J. (2017). Distributed energy storage system scheduling considering tariff structure, energy arbitrage and solar PV penetration. *Applied energy*, 205, 1384-1393.
- Lokeshgupta, B., & Sivasubramani, S. (2019). Multi-objective home energy management with battery energy storage systems. *Sustainable Cities and Society*, 47, 101458.
- Roberts, M. B., Bruce, A., & MacGill, I. (2019). Impact of shared battery energy storage systems on photovoltaic self-consumption and electricity bills in apartment buildings. *Applied energy*, 245, 78-95.
- Ghadimi, N., Sedaghat, M., Azar, K. K., Arandian, B., Fathi, G., & Ghadamyari, M. (2023). An innovative technique for optimization and sensitivity analysis of a PV/DG/BESS based on converged Henry gas solubility optimizer: A case study. *IET Generation, Transmission & Distribution*.
- Mujeebu, M. A., & Bano, F. (2022). Energy-saving potential and cost-effectiveness of active energy-efficiency measures for residential building in warm-humid climate. *Energy for Sustainable Development*, 67, 163-176.
- Martínez-Gracia, A., Uche, J., del Amo, A., Bayod-Rújula, Á. A., Usón, S., & Arauzo, I. (2022). Energy and environmental benefits of an integrated solar photovoltaic and thermal hybrid, seasonal storage and heat pump system for social housing. *Applied Thermal Engineering*, 213, 118662.
- Al Huneidi, D. I., Tahir, F., & Al-Ghamdi, S. G. (2022). Energy modeling and photovoltaics integration as a mitigation measure for climate change impacts on energy demand. *Energy Reports*, 8, 166-171.
- CIBSE, CIBSE guide a: environmental design, in: Environmental Design, 2016 [Online]. Available: [www.cibse.org](http://www.cibse.org).
- Olympios, A. V., Sapin, P., Freeman, J., Olkis, C., & Markides, C. N. (2022). Operational optimisation of an air-source heat pump system with thermal energy storage for domestic applications. *Energy Conversion and Management*, 273, 116426.
- Xu, T., Humire, E. N., Chiu, J. N., & Sawalha, S. (2021). Latent heat storage integration into heat pump based heating systems for energy-efficient load shifting. *Energy Conversion and Management*, 236, 114042.

---

## #295: AI-based hourly electricity consumption prediction for households and residents

---

Mingrui ZHOU<sup>1</sup>, Xiao LI<sup>2</sup>, Somayajulu SRIPADA<sup>3</sup>, Yanan ZHANG<sup>4</sup>

<sup>1</sup> University of Aberdeen, r01mz23@abdn.ac.uk

<sup>2</sup> University of Aberdeen, xiao.li@abdn.ac.uk

<sup>3</sup> University of Aberdeen, yaji.sripada@abdn.ac.uk

<sup>4</sup> University of Nottingham, yanan.zhang1@nottingham.ac.uk

*Abstract: This research aims to develop an XGBoost-based predictive model for accurately forecasting hourly electricity consumption in diverse household scenarios. By leveraging household-specific details and time-specific data from the IDEAL dataset, which encompasses over 200 UK households, the study delves into precise electricity usage forecasting. Data pre-processing is employed to ensure data reliability and reduce the computational costs, while XGBoost's robust learning capability renders it particularly suitable for time series forecasting. Two training techniques, grid search and cross validation were introduced to find the most proper parameters, which assured the quality of the model. From the results, it is evident that the demand for electricity is primarily determined by temporal factors (hour, days, month, quarter, year, weekday) and marginally related to household features (number of residents, build era, income, install type). The developed model effectively captures the fundamental patterns of electricity demand, prompting both consumers and producers to embrace energy-efficient measures, paving the way for a more sustainable future. Meanwhile, energy experts could refer to the model with actual values to formulate an energy generating strategy based on the number of population and household for a specific location. This prediction can provide a dispatching basis for various smart grids.*

*Keywords: Electricity Consumption prediction; residential (household); Artificial Intelligence Models; XGBoost*

## 1. INTRODUCTION

In today's interconnected world, the digital revolution has transformed every facet of our lives, from how we communicate to how we commute. Electric vehicles (EVs), which were once considered a distant dream, are now becoming ubiquitous on our roads. The increasing prevalence of EVs is just one indicator of the larger trend: our world's ever-growing reliance on electrical energy (BloombergNEF, 2021). Such rapid technological transformation, while undoubtedly ushering in numerous benefits, also presents profound challenges—most notably, the strain on our global electrical grids and the environmental implications tied to increased electricity consumption. The numbers are telling. Predictions suggest that by 2040, the world will witness a staggering 30% surge in electricity demand compared to levels recorded in 2017 (Stanelyte, Radziukyniene, & Radziukynas, 2022). This exponential growth in electricity demand, a direct consequence of our technological progress, casts a shadow of increased environmental pressures, from the exacerbation of air pollution to the daunting challenges posed by global warming.

The ramifications of escalating electricity demand are manifold. As of 2020, power generation was responsible for 26% of global greenhouse gas emissions (IEA, 2022). The pressing need for precise electricity demand forecasting becomes evident in light of these statistics. Accurate predictions ensure that energy production aligns optimally with consumption patterns, thereby reducing the repercussions of superfluous energy production and storage (Suganthi & Samuel, 2012). A well-informed forecast not only minimizes waste but also provides an avenue for seamlessly incorporating renewable energy sources, lessening our reliance on fossil fuels (Zeng et al., 2017). Such meticulous integration can lead to a reduction of up to 25% in greenhouse gas emissions from power sectors by 2030 (Parmesan et al., 2022). Moreover, efficient energy production and consumption, guided by precise forecasting, can substantially mitigate the greenhouse gas emissions associated with energy production, especially from non-renewable sources (Al-Ghandoor et al., 2008). As the world grapples with the challenges of climate change, such forecasting becomes indispensable in steering our energy strategies towards a more sustainable and environmentally friendly direction.

As we stand on the cusp of a new era in energy management, smart grids emerge as a beacon of hope. Foreseen to cater to the anticipated rise in global electricity demand—from 22,126 TWh in 2019 to a staggering 34,454 TWh by 2040 (World Bank, 2021)—these grids will undoubtedly benefit from advanced predictive tools. The modern smart grid, characterized by its bidirectional channels and adaptability (Yu, Mirowski, & Ho, 2017), is positioned to reshape how we perceive and manage energy. With an accurate forecasting system in place, we can mitigate grid congestion, reduce the frequency of outages, and optimize production schedules. For example, data suggests that by 2030, with the adoption of predictive tools, we can reduce grid congestion by as much as 30%, a substantial leap from present capacities (Zhang et al., 2022). By modelling the consumption patterns of individual residents and households, the system can optimize electricity production schedules (Fallah et al., 2018). This not only ensures that electricity is generated precisely when and where it's needed, but also minimizes the strain on the grid during peak demand periods (Kim & Cho, 2019). Furthermore, with the integration of renewable energy sources like solar and wind into the smart grid, accurate demand forecasting becomes even more crucial (Wen et al., 2019). It allows for the seamless blending of these intermittent energy sources with traditional ones, ensuring a consistent and reliable power supply (Ahmad et al., 2014). In essence, by leveraging the capabilities of this forecasting model within the smart grid framework, we can achieve a more efficient, resilient, and sustainable energy ecosystem (Guo, O'Hanley, & Gibson, 2022).

In this paper, our mission is clear. We endeavor to develop an XGBoost model that stands as a beacon in predictive modeling for electricity demand. By tapping into the transformative power of artificial intelligence and machine learning, we hope to pave the way for a future where energy efficiency is a given, not a goal.

## 2. LITERATURE REVIEW

The quest for efficient and sustainable energy consumption is a defining challenge of our era. The fusion of global electricity demand spikes and pressing environmental concerns has catalysed significant research initiatives across both academic and industrial domains. These initiatives prioritize enhancing energy efficiency and staunchly combatting energy waste.

A panoramic view of recent literature delineates the trajectory of energy forecasting over the past two decades. Fallah et al. (2018) provided a comprehensive account of methodologies from 2001 to 2018, meticulously covering the evolution of forecasting techniques. Similarly, Hussain et al.'s review captures the essence of innovations spanning from 2011 to 2020 (2021). Various modeling strategies have surfaced over the years. These range from traditional statistical methodologies to cutting-edge AI-driven techniques, reflecting the discipline's evolution (Bianco et al., 2009). Based on the scholarly investigation centred on the development of a linear model for the electricity consumption in the Jordanian industrial sector, the Coefficient of Determination ( $R^2$ ) and adjusted- $(R^2)$  were found to be 99.3% and 99.2%, respectively. These findings underscore the robustness and suitability of linear AI models in predicting electricity consumption patterns (Al-Ghandoor et al., 2008). Two models, Support Vector Machine (SVM) and Artificial neural network (ANN), were constructed for forecasting building energy consumption, underscoring the significance of forecasting in energy conservation and strategic decision-making (Suganthi & Samuel, 2012). Subsequently, deep neural networks have also been widely used in prediction tasks. Ullah et al. (2019), who implemented a multi-layered Bi-LSTM for sequential analysis. Wen et al. (2019) combined a profound recurrent neural network with LSTM to forecast power loads in solar-driven microgrids. Kim and Cho (2019) employed CNN to extract features from energy consumption data, which were then relayed to a state expandable autoencoder for future consumption predictions at intervals of 15, 30, 45, and 60 minutes. Sajjad et al. (2021) introduced a hybrid sequential learning model for energy forecasting, integrating both CNN and GRU into a cohesive framework to

refine energy consumption prediction accuracy. Understanding household electricity usage patterns support policymakers, energy experts and power firms to have an overview of consumption and create strategies to increase electricity efficiency (Guo et al., 2022). Rahman et al. (2014) introduced a method employing both the simple regression model (SRM) and multiple linear regression (MLR), among other strategies, to effectively forecast India's overall energy consumption and assist policymakers in energy management decisions.

While much of the previous research has understandably focused on time series data for energy consumption predictions, this singular lens has often overshadowed the nuanced differences among consumer types. Many of these studies have been framed under architectures that might inadvertently render heterogeneous consumer behaviours and circumstances invisible, leading to generic predictive outcomes. The multifaceted nature of electricity consumption can't be accurately captured by time series data alone. After all, household energy usage isn't solely dictated by the hour of the day or the month of the year (Zhang et al., 2022). It is interwoven with a myriad of other influential factors that resonate with the daily lives of the inhabitants. Factors like the number of family members, the location of the house—whether it's nestled in a bustling city or spread across the tranquillity of the countryside - the income levels, and the distinct lifestyle choices made by urban versus rural residents, all play pivotal roles in determining energy consumption patterns.

In recognizing this intricate tapestry of factors, our work ventures beyond the traditional paradigm. While we certainly harness the predictive power of time series consumption data, we simultaneously integrate household-specific determinants into our predictive model. This enriched approach allows us to tailor our forecasts to different building typologies - from single-family homes in suburban locales to high-rise apartments in dense urban centres. Such granularity in prediction holds immense value, especially when charting power dispatch strategies for modern smart grids. For power grid operators and companies, this multifaceted prediction methodology offers an elevated layer of intelligence. Armed with insights into how specific consumer types correlate with their electricity consumption patterns, these entities are better positioned to anticipate and respond to fluctuating energy demands. They can streamline operations, enhance efficiency, and cultivate an energy landscape that is more attuned to the rhythms of its diverse consumer base. In essence, our approach promises a more tailored and responsive energy forecasting model, one that mirrors the complexities of real-world consumption behaviours.

### 3. DATASET

Having delved into the intricate landscape of energy consumption forecasting in the literature review, the success of any predictive model hinges critically on the quality and granularity of the data it is trained upon. A robust and comprehensive dataset not only facilitates the accuracy of predictions but also provides a profound understanding of the underlying patterns and trends that dictate energy consumption behaviours. Therefore, before presenting the technical intricacies of our proposed model, it is essential to first understand and appreciate the depth and breadth of the dataset we leveraged. This section offers a detailed exploration of the IDEAL Household Energy Dataset and the meticulous steps undertaken to pre-process and visualize this data, setting the stage for the subsequent modelling and evaluation phases.

#### 3.1. Dataset Description

The proposed models are trained and evaluated on the IDEAL Household Energy Dataset (Pullinger et al., 2021).

The IDEAL dataset, collected the information via sensors, encompasses electricity, gas, and contextual data from 255 British households. Spanning 23 months up to June 2018, the average participation lasted 286 days. Electricity readings were captured every second, while gas pulse data was recorded every 12 seconds. Additionally, the dataset offers insights into specific household details, such as the number of residents, days occupied during daylight and nights. This comprehensive dataset is valuable for studying energy consumption trends, building performance modelling, and non-intrusive load monitoring research.

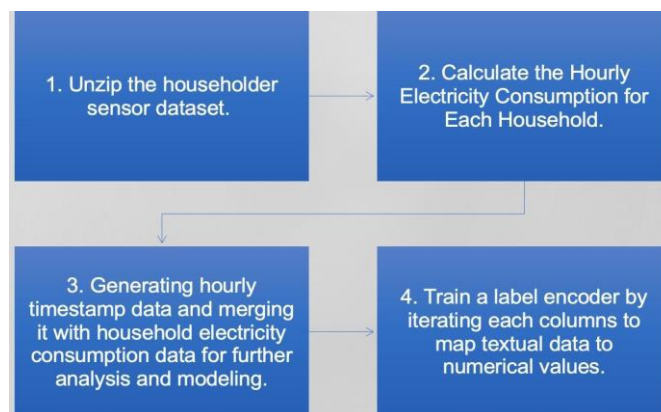


Figure 1 Steps for processing data to adapt to model training.

### 3.2. Data Pre-process

The figure1 describe the four steps transforming the raw data to training data.

*Unzip the dataset:* The dataset was downloaded via .zip document format. After unzipping, more than 200 subfolders are created under a folder. Each subfolder consists of several csv.gz documents describing energy consumption of households.

*Calculate the Hourly Electricity Consumption for Each Household:* Given that the electrical consumption data is captured second-by-second, leveraging this data for model training could lead to prohibitive computational costs due to the sheer volume of training instances (Chen et al. , 2023). Consequently, we aggregated the data hourly to facilitate more efficient predictive models.

*Generating timestamp home data and merging electricity consumption:* There is another document from the Ideal dataset describing the household information, such as number of residents, days occupied during daylight and nights. Each week, we randomly select "occupied days" where the resident count remains consistent from 7 am to 7 pm. On other days, it's zero. Similarly, for "occupied nights", residents are present from 7 pm to 7 am of the next day. On the non-selected nights, the count is zero. In order to assure every training data including the household information, we generated hourly timestamps for the data and merged it with the previous electricity consumption data.

*Train a label encoder to map textual data to numerical values:* Since some household related data are textual, it is necessary to discover a method to transfer text to numerical values in order to train a model. The label encoder scans through all CSV files to identify categorical columns and then creates label encoders for each of these columns. It returns a dictionary where keys are column names and values are their corresponding label encoders, also printing the label mappings for each column.

### 3.3. Data Visualization

Given the profound impact of data visualization on data comprehension as highlighted by Leung et al. (2021), we undertook a detailed visualization analysis of electricity consumption for a randomly selected household. The Figure 2 shows the electricity consumption for a random home.

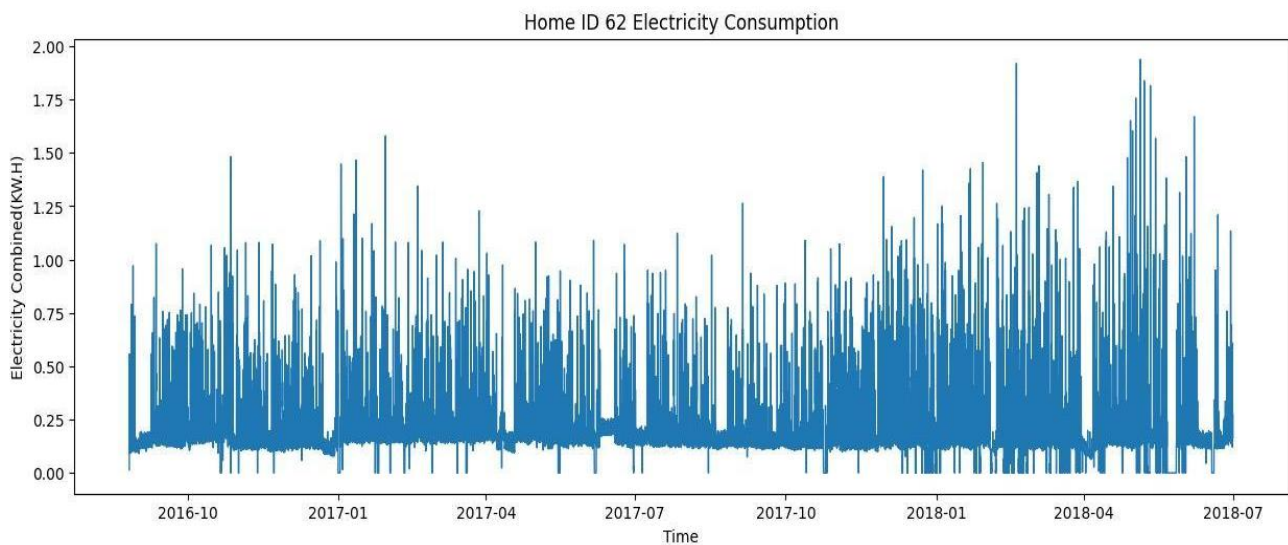


Figure 2 Electricity Consumption for Home No.62

The data was collected from around Aug 2016 to Aug 2018, which is almost two years. Therefore, an insight was yielded from the above figure. It is challenging to observe the performance of the predictive model directly because of giant data points.

### 3.4. Data Split

In artificial intelligence research, the preparation of datasets is paramount. Typically, datasets are divided into training (60%), validation (20%), and testing (20%) sets. The training set is foundational for model building, allowing the algorithm to adjust its parameters to capture data patterns. The validation set aids in model tuning. By evaluating the model's performance on the validation set, potential overfitting can be identified and adjustments made accordingly. Finally, the



testing set offers a true assessment of the model's performance in real-world scenarios, acting as a benchmark for its predictive capabilities.

## 4. MODEL

In the vast landscape of machine learning, predictive models stand out as invaluable assets, especially in sectors where understanding future trends can lead to optimized decision-making. The choice of model is paramount and hinges on several criteria, including the type and complexity of data at hand, the nature of the problem, computational constraints, and the desired accuracy of predictions. In this section, we delve into the intricacies of the XGBoost model, its mathematical underpinnings, its application in our study, and the results derived. Before diving deep into the specifics of the XGBoost model, it is beneficial to understand its foundational framework and how it distinguishes itself from other predictive models.

### 4.1. XGBoost

XGBoost is a kind of Artificial Intelligence model, which derives from the gradient boosting framework, optimizes loss functions by iteratively adding decision trees targeting preceding errors. The model structure and mathematical formula are displayed in Figure 3 and Equation 1. A weight function determined by former predictors would be implemented on data for the following predictors, which suggests the final output is determined by all predictors of the model.

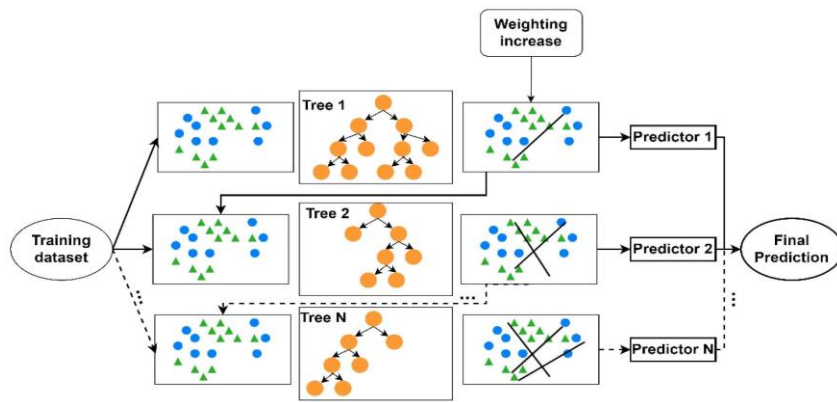


Figure 3 The structure of XGBoost model (Zhao, Zhao, Li, & Zhang, 2022)

$$\begin{aligned}
 \hat{y}_i^{(0)} &= 0 \\
 \hat{y}_i^{(1)} &= f_1(x_i) = \hat{y}_i^{(0)} + f_1(x_i) \\
 \hat{y}_i^{(2)} &= f_1(x_i) + f_2(x_i) = \hat{y}_i^{(1)} + f_2(x_i) \\
 &\dots \dots \\
 \hat{y}_i^{(t)} &= \sum_{k=1}^t f_k(x_i) = \hat{y}_i^{(t-1)} + f_t(x_i)
 \end{aligned}$$

Equation 1: Iteration formula of XGBoost model corresponding to Figure 3

It uniquely incorporates a regularization term to counter overfitting (Chen & Guestrin, 2016). Celebrated for its performance, XGBoost is scalable, handling vast datasets and offering parallel processing. It's compatible with major deep learning frameworks and supports diverse objective functions (Kavzoglu & Teke, 2022). However, its application on large datasets would be time- expensive, and optimal performance often demands meticulous parameter tuning (Yang, Wang, Yuan, & Liu, 2022).

### 4.2. Model training

In this paper, two techniques, grid search and cross validation were used in model training to improve accuracy and efficiency.

*Grid search:* is a systematic method employed in machine learning and data science to optimize hyperparameters. This technique involves defining a set of potential hyperparameter values and exhaustively evaluating every combination to identify the one that maximizes a model's performance (Liashchynskyi & Liashchynskyi, 2019). The process begins with the definition of a hyperparameter grid, followed by an exhaustive search where a model is trained for each combination. Each model's performance is then assessed, typically using a validation set or cross-validation (Zahedi et al., 2021). The significance of grid search lies in its ability to ensure optimal model performance through a structured approach. Its

simplicity and straightforwardness make it a preferred choice for hyperparameter tuning in various applications, especially when compared to other methods like differential evolution (Fu, Nair, & Menzies, 2016). Additionally, advancements in grid search techniques, such as adaptive grid search, further enhance its effectiveness in specific tasks like link prediction (Poštuvá et al., 2022).

*Cross-validation*: is a key technique in machine learning to assess model performance (Wilson, Kasy, & Mackey, 2020). It partitions data into subsets, training the model on one and validating on another. This method evaluates the model's generalization capability and reduces overfitting risks. While k-fold cross-validation is common, newer methods like blocked cross-validation offer precise error estimates with fewer runs (Merola, 2023). It's essential to understand that cross-validation may estimate the average prediction error across unseen training sets, not just the current model's error (Bates, Hastie, & Tibshirani, 2021).

### 4.3. Model Evaluation

In model assessment, it's crucial to evaluate out-of-sample performance. This study employs two methods: visualization inspection and the Mean Absolute Error metric (MAE, in Equation 2).

*Visualization inspection*: is a method by plotting the actual value and model prediction value in the same figure to explore whether the model is proper. However, based on the insight from the data visualization part, it is hard to observe the whole prediction period. Therefore, we introduce a data window. A continuous window of data from a randomly chosen home is selected from its' test set, and the prediction is visualized together with the actual value for that specific window.

*Mean Absolute Error (MAE)*: metric is widely recognized in quantifying the average absolute difference between predicted and actual values. It offers a straightforward measure of prediction errors, with a MAE of 0 indicating perfect predictions and a higher MAE signifying larger discrepancies. Given its direct interpretation and equal weighting to all errors irrespective of their direction, MAE is particularly apt for AI models. Specifically, MAE has been employed in model evaluation studies, highlighting its utility in assessing the accuracy of predictions in various contexts. (Chen et al., 2023).

$$MMAE = \frac{1}{n} \sum_{i=1}^n |y_i - \hat{y}_i|$$

Equation 2: MAE mathematical formula

In Equation 2:

$n$  is the number of observations.

$y_i$  is the  $i$ -th observed value.

$\hat{y}_i$  is the  $i$ -th predicted value.

$|y_i - \hat{y}_i|$  reflects the absolute difference between the  $i$ -th observed and predicted values.

## 5. RESULTS

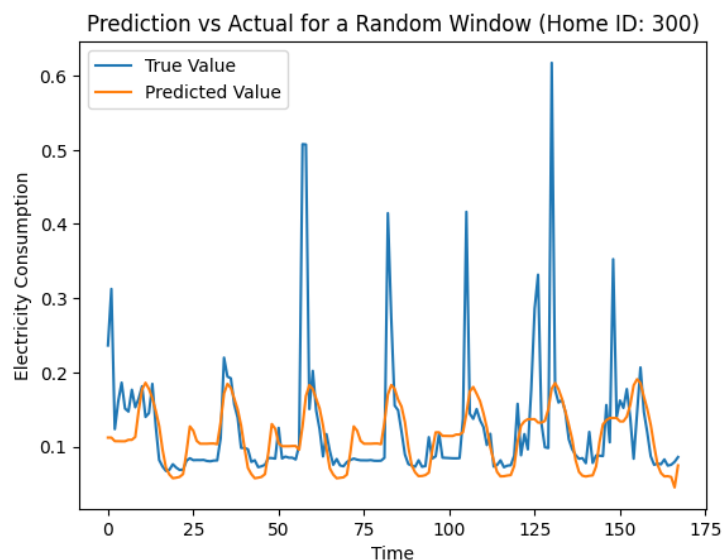


Figure 4 Prediction Visualization

## 5.1. Best parameter

Through a systematic grid search optimization of hyperparameters and with 5 times cross validation, we identified the optimal configuration for our model. The best-performing parameters were determined to be a learning rate of 0.2, a maximum tree depth of 7 and 150 predictors.

## 5.2. Visualization inspection & MAE

In order to facilitate a comprehensive assessment of the predictive model's efficacy through visual representation, we opted for a window size of 168. This encompasses the model's forecasting capabilities on an hourly basis for electricity consumption over a randomly selected week. From the graph, it's evident that the model effectively captures the fundamental trends and cyclical patterns in electricity consumption, aligning closely with the actual values in many areas. However, it is not sensitive enough when dealing with peak and trough points.

The MAE value of this model 0.0686 suggests that the model's predictions are within a margin of error of roughly  $\pm 7\%$  of the actual observed values on average.

Table 1: Features Importance

Feature	Living Room
Hour	53.5%
Month	11.8%
Quarter	10.0%
Day	8.4%
Weekday	7.7%
Year	6.3%
Residents	2.2%
Install type	0.0%
Income band	0.0%
Urban or rural	0.0%

## 5.3. Features Importance

XGBoost offers a function to display the importance of features from the dataset. The result is shown in the below table. The time related features, particularly the hour of the day, play a dominant role in the electricity consumption prediction model, accounting for nearly 48% of the importance, reflecting strong cyclical patterns in daily electricity usage. Housing-related features have a minor role in the model, suggesting that these features may have a relatively insignificant impact on the prediction of electricity consumption.

## 6. DISCUSSION

From the results presented earlier, it's clear that the model excels at capturing general trends in electricity consumption, but faces challenges when dealing with sharp peaks and troughs. One possible reason for this could be the static nature of certain input features. Specifically, while time-related variables evolve continuously, residential-related attributes remain constant for each household. This static nature could potentially inhibit the model from truly understanding and leveraging the impact of these residential features on consumption patterns. The interplay between these factors can be intricate, and a more dynamic representation might better capture the nuanced effects on electricity consumption. Beyond just hourly or daily changes, understanding the seasonal and annual variations in household consumption can offer deeper insights. Thus, for a more comprehensive examination of household-related features, it may be beneficial to explore broader temporal frameworks. For instance, assessing the influence of these variables over annual periods can highlight patterns and trends that aren't evident in shorter timeframes. This approach could elucidate the intricate interdependencies between household features and their subsequent impact on energy usage across various residential contexts.

Weather, undeniably, plays a pivotal role in shaping residential electricity consumption. The relationship between temperature and consumption isn't always linear. As noted by Guo et al. (2022), there exists a critical temperature threshold, specifically at 5°C, which significantly influences electricity demand. Consumption tends to rise sharply as temperatures dip below this point, but above it, the demand curve sees a subtle decrease. These observations suggest

the potential benefits of integrating hourly weather data for specific locations into our model. By doing so, we could account for the external climatic variables, thereby enhancing the predictive accuracy of the model. Such integrations can significantly improve the model's adaptability to real-world fluctuations and ensure more accurate forecasting in diverse scenarios.

## 7. CONCLUSION

In this research, our analytical framework delves deep into the intricate patterns of electricity consumption. Preliminary results indicate that time-associated parameters—such as hours of the day, weekdays versus weekends, and seasonal variations - are dominant factors governing electricity usage. In contrast, household-specific characteristics like family size, house location, or income bracket play a more peripheral, albeit still noteworthy, role in determining consumption patterns. The potency of our model lies in its ability to provide actionable insights for electricity generation scheduling based on these predictive trends. This is crucial in an era where real-time responsiveness in energy production can lead to considerable savings and enhanced efficiency. However, like all models, it's not without its limitations. To achieve a comprehensive and real-world application, further refinements are essential. Incorporating more related features, such as prevailing weather conditions or nuanced data on people's activities at different times of the day, can make the predictions more robust. As energy needs continue to evolve, capturing such granular details can be the key to creating a more adaptable and resilient energy forecasting model.

## 8. REFERENCES

- Ahmad, A. S. *et al.* (2014). A review on applications of ANN and SVM for building electrical energy consumption forecasting. *Renewable and Sustainable Energy Reviews*, 33, pp.102–109. doi:10.1016/j.rser.2014.01.069.
- Al-Ghandour, A. *et al.* (2008). Electricity consumption and associated GHG emissions of the Jordanian industrial sector: Empirical analysis and future projection. *Energy Policy*, 36(1), pp.258–267. Available at: <https://ideas.repec.org/a/eee/enepol/v36y2008i1p258-267.html> (Accessed: October 5, 2023).
- Alquthami, T. *et al.* (2022). A performance comparison of machine learning algorithms for load forecasting in smart grid. *IEEE access: practical innovations, open solutions*, 10, pp.48419–48433. doi:10.1109/access.2022.3171270.
- Bates, S., Hastie, T. and Tibshirani, R. (2023). Cross-validation: What does it estimate and how well does it do it?. *Journal of the American Statistical Association*, pp.1–12. doi:10.1080/01621459.2023.2197686.
- Bianco, V., Manca, O. and Nardini, S. (2009). Electricity consumption forecasting in Italy using linear regression models. *Energy (Oxford, England)*, 34(9), pp.1413–1421. doi:10.1016/j.energy.2009.06.034.
- BloombergNEF (2021). New Energy Outlook 2021 | Bloomberg NEF. [online] Bloomberg NEF. Available at: <https://about.bnef.com/new-energy-outlook/>.
- Chen, H. *et al.* (2023). Maybe only 0.5% data is needed: A preliminary exploration of Low Training Data Instruction Tuning. *arXiv [cs.AI]*. Available at: <http://arxiv.org/abs/2305.09246>.
- Chen, T. and Guestrin, C. (2016). XGBoost: A Scalable Tree Boosting System. in *Proceedings of the 22nd ACM SIGKDD International Conference on Knowledge Discovery and Data Mining*. New York, NY, USA: ACM.
- Parmesan, C., Morecroft, M. D., & Trisurat, Y. Climate Change 2022: Impacts, Adaptation and Vulnerability. [Research Report] GIEC. 2022. fahal-03774939f.
- Fallah, S. *et al.* (2018). Computational intelligence approaches for energy load forecasting in smart energy management grids: State of the art, future challenges, and research directions. *Energies*, 11(3), p.596. doi:10.3390/en11030596.
- Fatema, I., Kong, X. and Fang, G. (2021). Electricity demand and price forecasting model for sustainable smart grid using comprehensive long short term memory. *International journal of sustainable engineering*, 14(6), pp.1714–1732. doi:10.1080/19397038.2021.1951882.
- Fu, W., Nair, V. and Menzies, T. (2016). Why is differential evolution better than grid search for tuning defect predictors?. *arXiv [cs.SE]*. Available at: <http://arxiv.org/abs/1609.02613>.
- Guo, Z., O'Hanley, J. R. and Gibson, S. (2022). Predicting residential electricity consumption patterns based on smart meter and household data: A case study from the Republic of Ireland. *Utilities policy*, 79(101446), p.101446. doi:10.1016/j.jup.2022.101446.
- Hussain, T. *et al.* (2021). Smart and intelligent energy monitoring systems: A comprehensive literature survey and future research guidelines. *International journal of energy research*, 45(3), pp.3590–3614. doi:10.1002/er.6093.
- IEA (2022). Global Energy Review: CO2 Emissions in 2021. IEA, Paris <https://www.iea.org/reports/global-energy-review-co2-emissions-in-2021-2>, License: CC BY 4.0

- Jain, R. K. *et al.* (2014). Forecasting energy consumption of multi-family residential buildings using support vector regression: Investigating the impact of temporal and spatial monitoring granularity on performance accuracy. *Applied energy*, 123, pp.168–178. doi:10.1016/j.apenergy.2014.02.057.
- Kavzoglu, T. and Teke, A. (2022). Predictive performances of ensemble machine learning algorithms in landslide susceptibility mapping using random forest, extreme gradient boosting (XGBoost) and natural gradient boosting (NGBoost). *Arabian journal for science and engineering*, 47(6), pp.7367–7385. doi:10.1007/s13369-022-06560-8.
- Kim, J.-Y. and Cho, S.-B. (2019). Electric energy consumption prediction by deep learning with state explainable autoencoder. *Energies*, 12(4), p.739. doi:10.3390/en12040739.
- Leung, C. K. *et al.* (2021). A visual data science solution for visualization and visual analytics of big sequential data. in *2021 25th International Conference Information Visualisation (IV)*. IEEE.
- Liashchynskiy, Petro and Liashchynskiy, Pavlo (2019). Grid Search, Random Search, Genetic Algorithm: A big comparison for NAS. *arXiv [cs.LG]*. Available at: <http://arxiv.org/abs/1912.06059>.
- Merola, G. M. (2023). Blocked cross-validation: A precise and efficient method for hyperparameter tuning. *Research Square*. doi:10.21203/rs.3.rs-3221138/v1.
- Nguyen, V.-B., Duong, M.-T. and Le, M.-H. (2020). Electricity demand forecasting for smart grid based on deep learning approach. in *2020 5th International Conference on Green Technology and Sustainable Development (GTSD)*. IEEE.
- Poštuvan, T. *et al.* (2022). AdaGrid: Adaptive Grid Search for link prediction training objective. *arXiv [cs.LG]*. Available at: <http://arxiv.org/abs/2203.16162>.
- Pullinger, M. *et al.* (2021). The IDEAL household energy dataset, electricity, gas, contextual sensor data and survey data for 255 UK homes. *Scientific data*, 8(1), p.146. doi:10.1038/s41597-021-00921-y.
- Rakesh, K. and Rakesh, R. (2022). Electricity load forecasting in smart grid using web based geographic information systems (web GIS). *i-manager's Journal on Future Engineering and Technology*, 17(4), p.25. doi:10.26634/jfet.17.4.18971.
- Stanelyte, D., Radziukyniene, N. and Radziukynas, V. (2022). Overview of demand-response services: A review. *Energies*, 15(5), p.1659. doi:10.3390/en15051659.
- Suganthi, L. and Samuel, A. A. (2012). Energy models for demand forecasting—A review. *Renewable and Sustainable Energy Reviews*, 16(2), pp.1223–1240. doi:10.1016/j.rser.2011.08.014.
- Ullah, F. U. M. *et al.* (2020). Short-term prediction of residential power energy consumption via CNN and multi-layer bi-directional LSTM networks. *IEEE access: practical innovations, open solutions*, 8, pp.123369–123380. doi:10.1109/access.2019.2963045.
- Wang, Y. P. *et al.* (2012). Using relational analysis and multi-variable grey model for electricity demand forecasting in smart grid environment. *Power System Protection and Control*, 40(1), pp.96–100.
- Wen, L. *et al.* (2019). Optimal load dispatch of community microgrid with deep learning based solar power and load forecasting. *Energy (Oxford, England)*, 171, pp.1053–1065. doi:10.1016/j.energy.2019.01.075.
- Wilson, A., Kasy, M. and Mackey, L. (2020). Approximate cross-validation: Guarantees for model assessment and selection. *arXiv [stat.ML]*. Available at: <http://arxiv.org/abs/2003.00617>.
- Yang, Y. *et al.* (2022). Predicting freeway traffic crash severity using XGBoost-Bayesian Network Model with consideration of features interaction. *Journal of advanced transportation*, 2022, pp.1–16. doi:10.1155/2022/4257865.
- Yu, C.-N., Mirowski, P. and Ho, T. K. (2016). A sparse coding approach to household electricity demand forecasting in smart grids. *IEEE transactions on smart grid*, pp.1–11. doi:10.1109/tsg.2015.2513900.
- Zahedi, L. *et al.* (2021). Search algorithms for automated hyper-parameter tuning. *arXiv [cs.LG]*. Available at: <http://arxiv.org/abs/2104.14677>.
- Zeng, Y.-R. *et al.* (2017). Multifactor-influenced energy consumption forecasting using enhanced back-propagation neural network. *Energy (Oxford, England)*, 127, pp.381–396. doi:10.1016/j.energy.2017.03.094.
- Zhang, Y. *et al.* (2022). Investigation on a vermiculite-based solar thermochemical heat storage system for building applications. *Future cities and environment*, 8(1). doi:10.5334/fce.153.
- Zhao, H.-X. and Magoulès, F. (2012). A review on the prediction of building energy consumption. *Renewable and Sustainable Energy Reviews*, 16(6), pp.3586–3592. doi:10.1016/j.rser.2012.02.049.

---

## #298: How window opening behaviour affect thermal comfort of low-cost apartment in Indonesia

---

Irma Handayani LUBIS<sup>1</sup>, Lucelia RODRIGUES<sup>2</sup>, Lorna KIAMBA<sup>3</sup>

<sup>1</sup> University of Nottingham, University Park NG7 2RD, irma.lubis@nottingham.ac.uk

<sup>2</sup> University of Nottingham, University Park NG7 2RD, Lucelia.Rodrigues@nottingham.ac.uk

<sup>3</sup> University of Nottingham, University Park NG7 2RD, lorna.kiamba@nottingham.ac.uk

*Abstract: Indonesia has been experiencing population growth in the last few decades. On the other hand, achieving thermal comfort in a hot and humid climate is challenging. This paper aims to evaluate the effect of window-opening patterns on occupant thermal comfort in low-cost apartment buildings in Medan, Indonesia. The objectives of this research are: 1) to observe the window-opening pattern of occupants; 2) to investigate the effect on indoor air temperature, relative humidity, occupancy hour, activities, orientation, and the usage of active means; 3) to analyse the correlation between window-opening pattern and thermal comfort. The methodology used in this research is a survey of questionnaires and data logging on indoor temperature and humidity monitoring. One case study building was investigated in this study. It is called Rusunawa Kayu Putih, a publicly rented vertical housing unit operated and managed by the Ministry of Public Works and Human Settlement in Medan. The results showed that the opening window pattern was influenced by the occupancy hours, activities such as cooking, showering, sleeping, and smoking, and the praying time. It is also observed that the occupancy hours might not be correlated with the hourly indoor air temperature. In terms of thermal comfort, about 50% of participants experienced comfort during rainy and dry seasons, but only 20% of them opened their windows throughout the day. It is summarised that residents achieve thermal comfort by using mechanical ventilation rather than natural ventilation.*

*Keywords: Windows Opening, Low-cost Apartment, Climate Resilience, Indonesia*

## 1. INTRODUCTION

Indonesia has been experiencing population growth in the last few decades. According to the United Nations, Indonesia ranked second in the 2023 population growth rate. As the population keeps rising, the requirement for affordable and liveable housing is increasing. It is reported by The Ministry of Public Works and Housing of Indonesia that the total house backlog in 2019 was 6.8 million units, and the number of uninhabitable homes was 1.9 million units. Therefore, to increase access to decent, safe, and affordable housing for low-income people supported by adequate infrastructure, facilities, and utilities, the Ministry of Public Works and Housing plans to build more flats or affordable vertical housing for low-income people.

On the other hand, achieving thermal comfort in a hot and humid climate is challenging. People tend to rely on active means rather than using passive design strategies. Based on the Central Statistics Agency (BPS), it is stated that 80% of the population in Indonesia are low-middle-income people who cannot afford to install air conditioning in their houses during the global warming crisis. Alfata et al. (2015), who investigated the naturally ventilated apartment in Surabaya, found that the average air temperature in the master bedroom was approximately 30.1-31.8°C, higher at 1.8-3.5°C than the average outdoor temperature. Murtyas et al. (2020), who observed low-cost dwellings, summarised that more than 50% of participants responded to warm or hot sensations while only 20% felt comfort.

Natural ventilation by window opening is one of the passive design strategies that can help low-cost apartments achieve the occupants' thermal comfort. This strategy can be highly effective because it is costless, requires no artificial cooling, and consumes less energy. Alfata et al. (2015) concluded that full-day and night ventilation in public apartments can increase thermal comfort levels above 52-66%. Chünemann et al. (2021) argued that nocturnal window ventilation diminishes the possibility of overheating in dwellings during the days in a moderate climate. Kitagawa et al. (2021) believed that horizontal pivot windows could enhance high wind speed, thus promoting thermal comfort by reducing the convective heat transfer on the floor during the daytime.

This paper aims to evaluate the effect of window-opening patterns on occupant thermal comfort in low-cost apartment buildings in Medan, Indonesia. The objectives of this research are: 1) to observe the window-opening pattern of occupants; 2) to investigate the effect on indoor air temperature, relative humidity, occupancy hour, activities, orientation, and the usage of active means; 3) to analyse the correlation between window-opening pattern and thermal comfort. The methodology used in this research is a survey of questionnaires and data logging on indoor temperature and humidity monitoring. This paper includes the introduction, building thermal comfort, passive design strategies, methodology, results and discussions, and conclusions.

## 2. BUILDING THERMAL COMFORT

There are some standards that researchers have used to define the benchmark of thermal comfort, such as ASHRAE, CIBSE, and the National Standard of Indonesia. ASHRAE, CIBSE, and Szokolay are commonly used in the four-season countries that apply cooling and heating systems to promote thermal comfort. Indonesia National Standard has adopted ASHRAE Standard 55 to be more suitable for application in hot and humid climates. Table 1 summarises the comfort zone benchmarks from several building standards.

Table 1: Comfort Zone Standard

Standard	Comfort Zone
<b>ASHRAE Standard 55-2017</b> (ASHRAE, 2020)	A comfort zone is conditions falling within and including PMV levels from -0.5 PMV to +0.5 PMV. The average comfort temperature ranges between 23.5°C to 28.9°C.
<b>CIBSE Guide A 2016</b> (CIBSE, 2017)	<ul style="list-style-type: none"> <li>Adaptive comfort range = 23–27 °C (for London)</li> <li>In normal circumstances, humidity in the range of 40–70% RH is acceptable (Nevins et al., 1966)</li> </ul>
<b>Szokolay</b> (Szokolay, 2008)	The temperature limits of such a comfort zone can be taken relative to the above T <sub>n</sub> (neutrality temperature) for 90% acceptability from (T <sub>n</sub> - 2.5) °C to (T <sub>n</sub> + 2.5) °C.
<b>SNI T-14-1993-03</b> Indonesia National Standard	There are three parts to a comfort zone, namely: <ul style="list-style-type: none"> <li>Comfortable air condition, 20.5-22.8°C</li> <li>Optimal Comfort 22.8-25.8°C</li> <li>Nearly Convenient 25.8°C-27.1°C with relative air humidity of 50% -80%</li> </ul>
<b>SNI 03-6572-2001</b> Indonesia National Standard (SNI, 2020)	The thermal comfort zone for Indonesians as stated in <b>SNI T-14-1993-03</b> , and for design it is taken 25°C ± 1°C and relative humidity 55 % ± 10 %

In addition, some researchers have done several studies on thermal comfort in Indonesia. Karyono is one the most frequent researchers who did thermal comfort studies in some cities in Indonesia. He did thermal comfort studies with objects such as workers in the office, occupants of human settlements, college students, visitors in banks and cathedrals, market users, and primary schools (Harso Karyono, 2011). On the other hand, Alfata et al. did similar studies in offices in 4 big cities in Indonesia (Alfata, Muhammad Nur Fajri; Sujatmiko, Wahyu; Widyahantari, 2012).

In this research, the local standard from the government of Indonesia, which is written in SNI T-14- 1993-03, Procedures for Technical Planning of Energy Conservation in Buildings, is used. This standard is applied due to consideration of standard adaption that is more rational and applicable in hot and humid conditions. Therefore, I set the comfort temperature range between 20.5-27.1°C and with relative air humidity of 50% -80%.

### 3. WINDOWS OPENING BEHAVIOUR TO PROMOTE THERMAL COMFORT

Several studies on window-opening behaviour have been conducted in residential buildings. Some argued that window opening patterns promote thermal comfort, while others stated that it does not correlate with thermal comfort. There has been a debate about whether the window opening behaviour improves the occupants' thermal comfort. Some factors affect occupants' ability to open and close their windows. According to Dubrul (1988), two key factors motivate occupants' window opening behaviour, i.e., dwelling fabric factors (type of dwelling, rooms' orientation, window design, age of residence, insulation, heating and mechanical ventilation) and lifestyle (occupancy hours, smoking behaviour, activities, concern on energy saving, indoor climate preference, and moisture content). Identifying the key factors influencing occupants' behaviour on window opening and how they achieve thermal comfort is essential. Therefore, it can encourage people to use natural ventilation by opening windows as a passive design strategy to create a more sustainable environment.

Some research has proved that the timing of opening and closing the windows is related to thermal comfort. Brundrett (1977) summarised that the purpose of occupants opening their windows during winter was to obtain fresh air, avoid condensation, avoid stuffiness, remove smoke, remove cooking smells, and air room temperature conditions. Andersen et al. (2009) believed outdoor temperature significantly impacts window opening behaviour in Danish dwellings. Yao & Zhao (2017) summarised that the vital element that affects occupants to open their windows is the outdoor air temperature, and other factors are indoor CO<sub>2</sub> concentration, indoor air temperature, relative humidity, ambient PM<sub>2.5</sub> concentrations, wind direction, and wind speed. Du & Pan (2021) stated that five significant factors affect the variety of window opening patterns, i.e., orientation, floor, occupancy hour, indoor temperature, and behaviour on air conditioning usage. Schünemann et al. (2021), the combination of optimum window opening size and window opening time reduces the overheating risk in the building. Liu et al. (2022) investigated that indoor relative humidity was the most fundamental element affecting the high-intensity window-opening behaviour type.

On the other hand, some research summarised that window-opening behaviour has nothing to do with thermal comfort. Mori et al. (2020), who investigated public and private apartments in Indonesia, found that most occupants tend to open their windows during sunset and sunrise and shut them at night. They also added that the number of occupants, age, salary, and concerns about insects, safety, and rain were affecting the reason to open and close their windows. These reasons force them to use air conditioning and fans to achieve comfort during the nighttime. Verbruggen et al. (2021) and Cao et al. (2022) argued that occupants' habit of opening windows was related to room type and activity. Jayasree et al. (2022) mentioned that applying natural ventilation with limited airflow will not improve the thermal environment, and active means such as ceiling fans are needed to produce a prevalent air movement.

### 4. METHODOLOGY

The methodology used in this research is a survey of questionnaires and data logging on indoor temperature and humidity monitoring. One case study building was investigated in this study. It is called Rusunawa Kayu Putih, a publicly rented vertical housing unit operated and managed by the Ministry of Public Works and Human Settlement in Medan. Medan is located at 3.35°North and 98.40°East, and the elevation varies between 2.5 and 37.5 metres (8 ft 2 in and 123 ft 0 in) above sea level. According to the 2020 Census, Medan has a population of 2,435,252, making it the fourth largest urban area in Indonesia after Jakarta, Surabaya, and Bandung. It has a tropical rainforest climate with two typical wet and dry seasons. Hundreds of occupants answered general questions about their homes, occupancy hours, and thermal comfort sensation. This research tries to identify the correlations between data from the questionnaires and data observed by data logging.

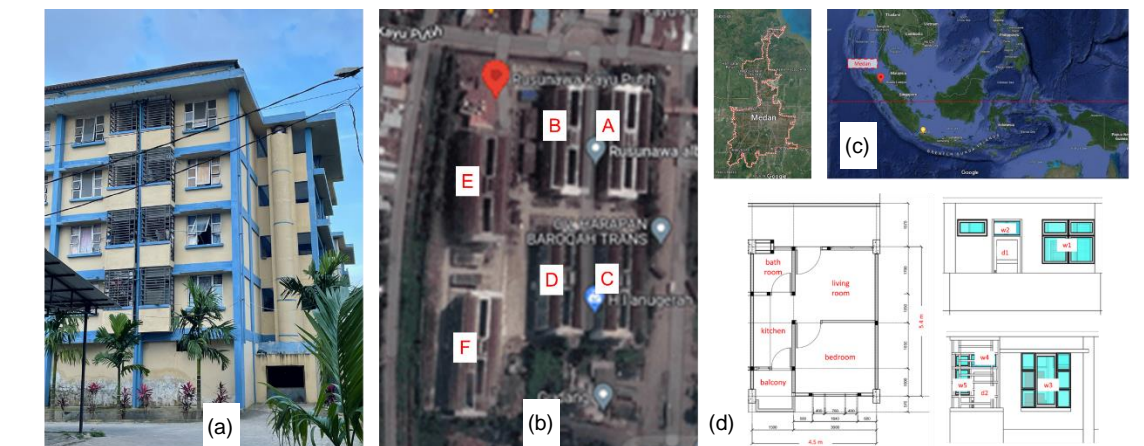


Figure 1 (a) The exterior view of Rusunawa Kayu Putih; (b) The block plan of Rusunawa Kayu Putih; (c) Map of Medan City, Indonesia (Google Map, n.d.); (d) The interior view of Rusunawa Kayu Putih



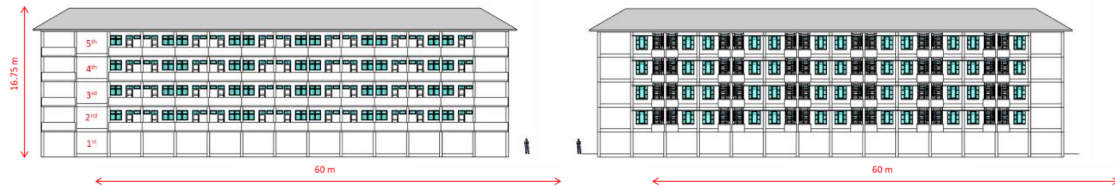


Figure 2 (a) Left - Corridor facing elevation; (b) Right - Outdoor facing elevation.

This section describes the overview of Rusunawa Kayu Putih, which is in the centre of Medan City. Rusunawa Kayu Putih consists of six building blocks (Block A, Block B, Block C, Block D, Block E, and Block F), and each of them has 96 apartments (each floor has 12 units). Blocks A, B, C, and D were first constructed in 2008; six years later, Block E & F were built as an extension. Each block has an equivalent size, which is approximately 60 m in length and 19.2 m wide. The building blocks are double-loaded buildings with an H-shape type (refer to Figure 2b). Each block is a 5-storey building where the 1st floor is allocated for commercial, and the 2nd to 5th floors are the living unit apartments. The total floor area of one building block is 3,894 m<sup>2</sup>, which is 778.8 m<sup>2</sup> on every floor. All blocks have a similar building orientation, which faces the west-east. The exterior and the interior view are depicted in Figure 2a and Figure 2b.

The survey was conducted in February 2023. Firstly, the questionnaires were distributed from 7-9 February 2023 and collected on 9 February 2023 in *Rusunawa Kayu Putih*. The questionnaire distribution and collection were helped by staff. The total number of questionnaires filled out by participants is 125 questionnaires. The questionnaires consist of three parts: part 1 is about occupants' homes, part 2 is about occupancy hours, and part 3 is about occupants' comfort. The questions in part 1 were about the home living time and the number of occupants in the apartment units. The second part included questions on occupancy hours during weekdays and weekends, the activities during the day and night, the doors and windows opening times, the reasons for opening and closing doors and windows, and the fan and air conditioner usage times. The questions in part 3 included gender, age, clothes level, and thermal sensation vote during the rainy and dry seasons. Even though the questionnaires were only delivered once, the questions involved the rainy and dry seasons to avoid biased and repeating answers and get an overall conclusion. (refer to Figure 3b).

The second part of the field study was the indoor climatic data measurement, which started on 9 February 2023 and will be running until January 2024. Four data loggers have been running in two case study buildings (each two units apartments), but this paper only explains one apartment building. The data logger used in this observation is tinytag Ultra 2, which can measure indoor air temperature and relative humidity. One data logger has been set in block B, 4th floor, number and the other one is in block F, 4th floor in Rusunawa Kayu Putih. The apartment has a living room, bedroom, bathroom, kitchen, and a small balcony. The number of occupants is three people. The occupants have been living in the apartment for more than 18 months. The data logger is placed around 170cm above the floor for safety reasons. Please refer to Figure 3b.



Figure 3 (a) Survey on questionnaires; (b) Indoor climatic measurements in Rusunawa Kayu Putih

## 5. RESULTS AND DISCUSSIONS

According to monitoring data on indoor air temperature and indoor relative humidity for eight months, it is found that the indoor air temperature has never achieved the comfort band while the relative humidity is predominantly in the comfort range. The hottest month is May, with the maximum temperature at 34.35 °C, and the coldest month since this research has been continuing was conducted in March, with the minimum temperature at 26 °C. The average indoor temperature is 30 °C. On the other hand, the months with the highest and the lowest indoor relative humidity are September and May, with 100% and 48.50%, respectively. The average indoor relative humidity is 74.72%.

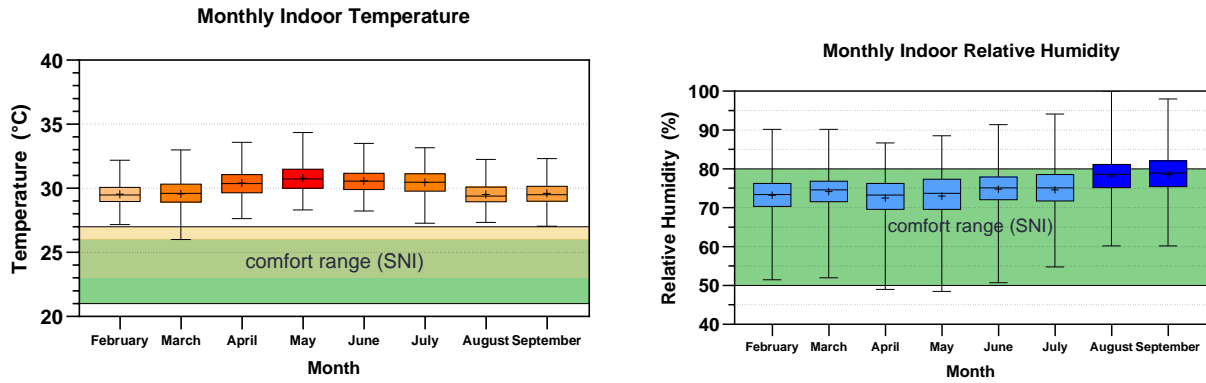


Figure 4 (a) Left - Monthly indoor air temperature chart; (b) Right – Monthly indoor relative humidity chart

**Relationship between Indoor Temperature and Indoor Relative Humidity**

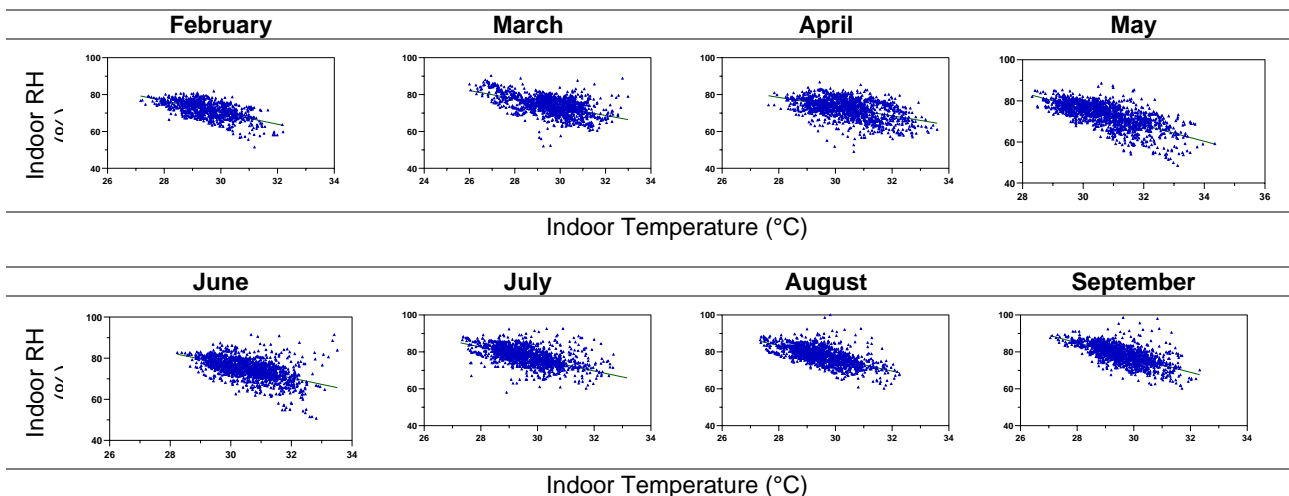
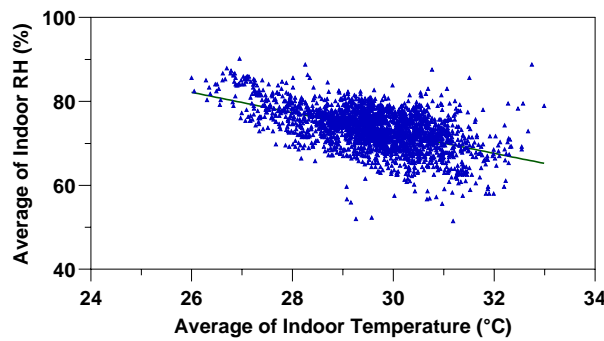


Figure 5 The correlation between indoor air temperature and indoor relative humidity

Figure 5 clearly shows that the correlation between indoor air temperature and relative humidity has a negative coherency. Faheem et al. (2022) also identified the negative regression between indoor air temperature and indoor relative humidity and outdoor temperature and outdoor relative humidity. The higher the indoor air temperature, the lower the indoor relative humidity is. It is noticeable that when the indoor air temperature has never reached the comfort range, the indoor relative humidity has always been in the comfort zone. May has the most significant discomfort conditions with the highest indoor air temperature and the lowest indoor relative humidity. The diverging state might be due to the minimum rainfall this month, resulting in the driest month of the year. This situation might challenge occupants in achieving thermal comfort in hot and humid regions. The range of indoor air temperature was between 26 °C and 34.35 °C, and the range of indoor relative humidity was between 48.50% and 100%. This result is in line with the statement of Toe & Kubota (2013), where hot and humid climates were focused on indoor operative temperatures higher than 25°C and indoor relative humidity greater than 45%. On the other hand, Murtyas et al. (2020) summarised similar results in outdoor temperature where the outdoor air temperature fluctuated from 23 °C to 36 °C, and the relative humidity ranged from 42% to 99%.

In terms of hourly monthly indoor temperature, the hotter hour was between 3 p.m. and 6 p.m. in March and April. The cooler hours was between 8 a.m. and 10 a.m. The hourly monthly indoor air temperatures were obviously different from the outdoor temperatures, where the hottest hours would be midday and the coolest hours would be early midnight. It is probably due to the time lag, which the time for heat to transfer from outside to inside the room.

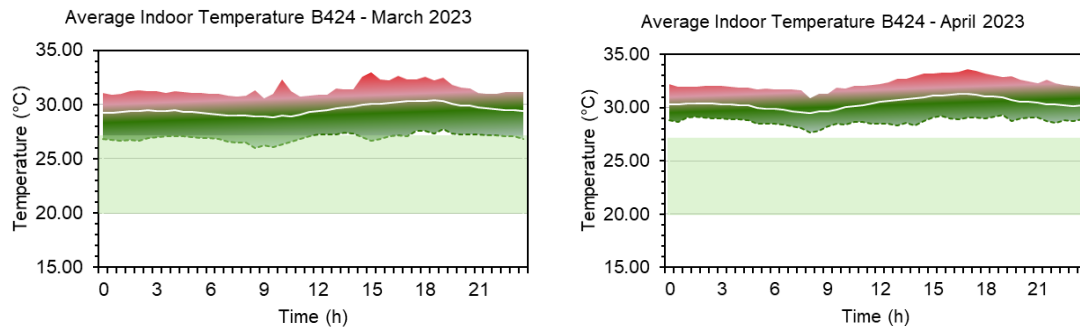


Figure 6 Fluctuation of the average hourly monthly indoor temperature in Rusunawa Kayu Putih on March 2023 and April 2023

According to the results of the survey, about 67% of participants have been living in the apartment for more than 18 months, and only 11% of them have been living for less than six months. Some of them have even survived for more than ten years. Most of the households that live in the apartment consist of four to five family members, that are parents and children. Some households that have more than four members usually rent two apartments. Some occupants also live alone without family.

According to the survey, the occupancy hours between weekdays and weekends showed no significant difference (see Figure 7). The similar trend in both occupancy hours is due to the relatively same activities during the weekdays and weekends, i.e., schools are still running on Saturday in Medan, and some people who work as fishermen or run a small business are still working during the weekends. Around 70% of the occupants leave their homes around 7 a.m. and return home around 7 p.m. Occupants tend to stay at home between 7 p.m. and 6 a.m. If it is referring to the hourly monthly indoor temperature, where the hotter hour was between 3 p.m. and 6 p.m., the occupancy hours were lower; which was not many people in the house during this hour, but the temperature was very high. It can be summarised that the occupancy hours might not be correlated with the hourly indoor air temperature. The indoor air temperature is presumably affected most by the outdoor temperature.

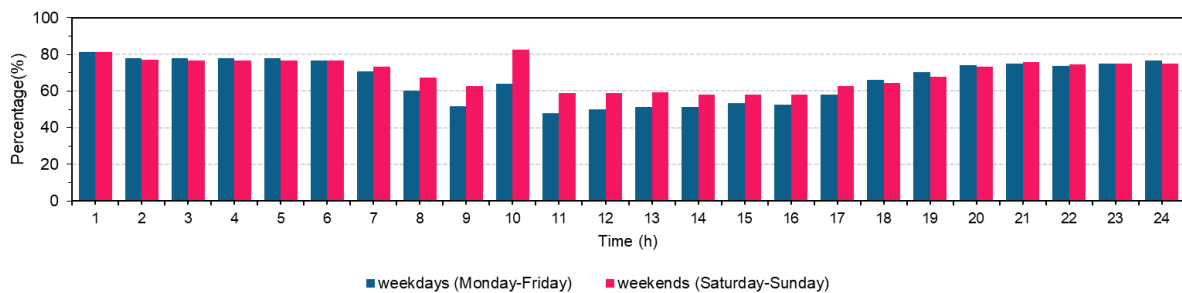


Figure 7 Typical occupancy hours in Rusunawa Kayu Putih

As depicted in Figure 8, the intensity of home activities was high during the morning. The cooking time was mostly between 5 a.m. and 11 a.m. According to the questionnaire results, there were two sleeping times: during the night and midday. Most of the occupants sleep during the night between 9 a.m. and 5 a.m. and take a nap between 11 a.m. and 4 p.m. In addition, due to the latitude of Medan, which is located at 3.35°North, the times for sunrise and sunset throughout the year are relatively the same. Sunrise usually begins from 6 a.m. to 7 a.m., and sunset starts from 6.30 a.m. to 7 p.m. It is also noticeable that occupants take a shower twice a day: in the early morning, between 5 a.m. and 10 a.m. and in the afternoon before sunset, between 4 p.m. and 7 p.m. Based on the interview, this habit is also related to morning and evening prayer times, which require cleanliness to perform; the times are around 5 a.m. and 6.30 p.m., respectively. The smoking times are varied from morning to evening.

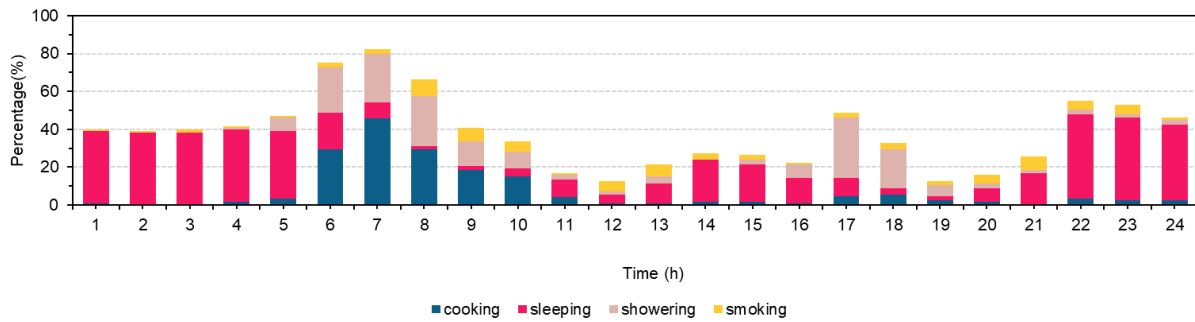


Figure 8 Typical activity hours in Rusunawa Kayu Putih

As illustrated in Figure 9 and Figure 10, only around 20% of participants open their windows throughout the day. This number was very limited if natural ventilation was applied to promote thermal comfort. It is also noticeable that the behaviour of opening and closing windows was relatively similar between the inner opening that faced the corridor and the outer opening that faced the external wall. The trend between building blocks that oriented to the East and the West also showed relatively identical results. Most of the residents open their windows in the morning, at 6 a.m. and close them before sunset, at 5 p.m. Residents in the west-orientated building blocks open the inner windows slightly more than the external windows. During the night, occupants tend to close their windows during sleeping time. This result is in accordance with Chai et al. (2020), where about 80% of the residents open their windows from 10 a.m. to 6 p.m., and only 10% apply it at night. It can be concluded that the passive design of harnessing nocturnal ventilation is not applicable in low-cost apartment buildings. In addition, Schünemann et al. (2021) also stated that there were some obstacles for occupants to open their windows during the night, such as noise, air pollution, safety, concern about insects or allergies, and leakage by the rain.

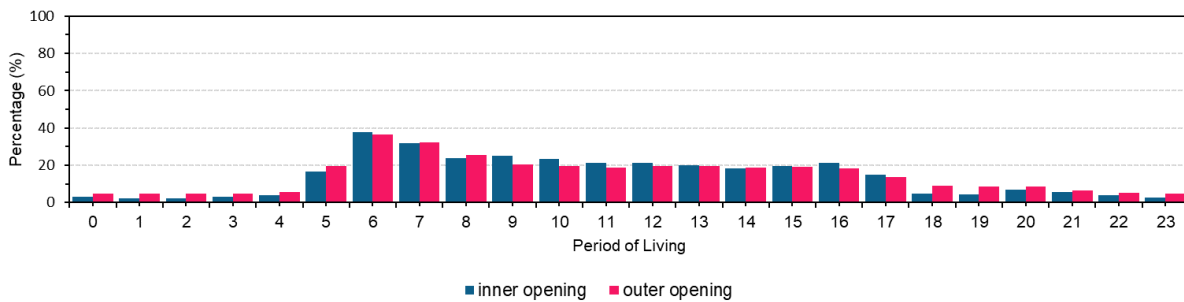


Figure 9 Doors and windows opening time in east-orientated units in Rusunawa Kayu Putih.

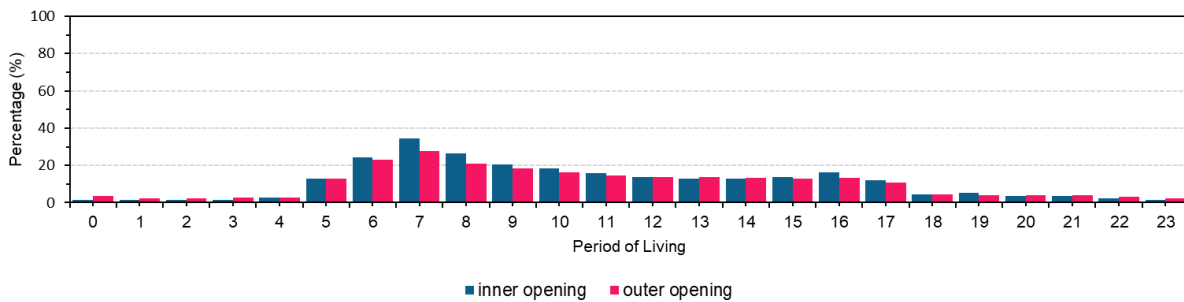


Figure 10 Doors and windows opening time in west-orientated-units in Rusunawa Kayu Putih

According to Figure 11, it can be concluded that occupants dominantly open their windows due to cooking and close them because of noise and rain. Another reason for opening the windows was due to smoking activity. It is also noticeable that there are other reasons for closing windows, i.e. privacy, safety, comfort, and praying times. Based on the results, it can be summed up that the morning opening windows were related to activities such as the morning prayer times, cooking times, showering times, and sunrise time. Meanwhile, according to the interview, the purpose of closing the windows during the night is for safety and resting time.

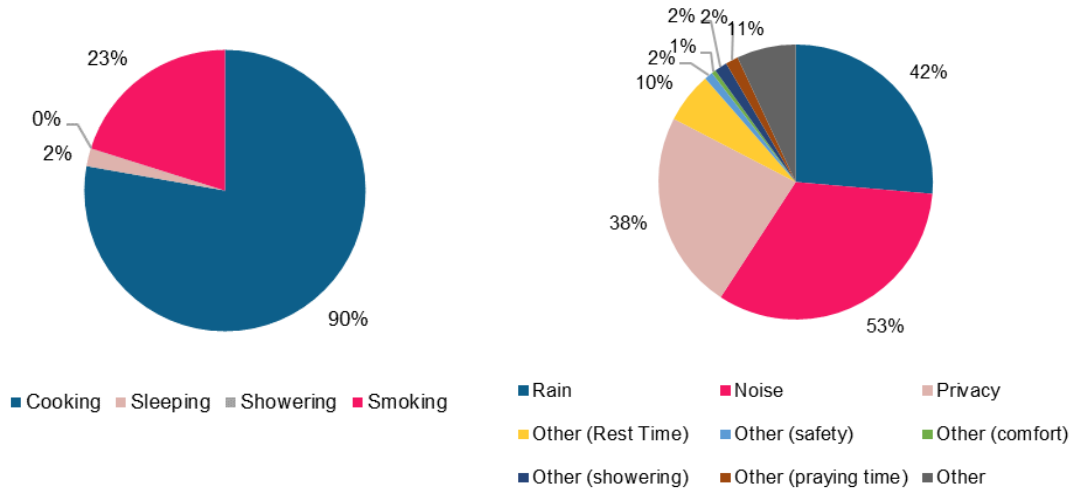


Figure 11 (a) Reasons for opening doors and windows (left); (b) reasons for closing doors and windows in Rusunawa Kayu Putih

As illustrated in Figure 12, almost 50% of participants use the fan throughout the day and night. According to the interview, most of them admit that the fan was on non-stop from morning to evening. On the other hand, the use of air conditioning units was mostly during the resting time, between 1 p.m. and 6 a.m. It is noticeable that residents rely most on mechanical ventilation rather than natural ventilation.

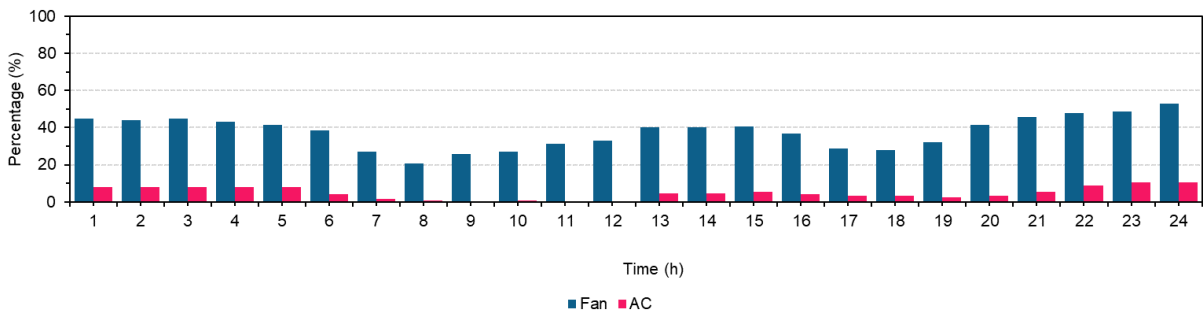


Figure 12 The usage time of fan and air conditioner in Rusunawa Kayu Putih

As depicted in Figure 13 and Figure 14, participants generally felt comfortable in the low-cost apartment building during rainy and dry seasons in terms of air temperature, humidity, air quality, and overall comfort. In terms of air temperature, most people sensed a neutral, slightly hot, and hot environment during the dry season and felt neutral, slightly cold, and cold during the rainy season. In terms of humidity, residents experienced between dry and neutral during the dry season and felt humid to neutral during the rainy season. In terms of air quality, most of the occupants experienced neutral and airy conditions during both seasons. For overall comfort, about 50% of participants stated that they achieved thermal comfort during their live in the apartment.

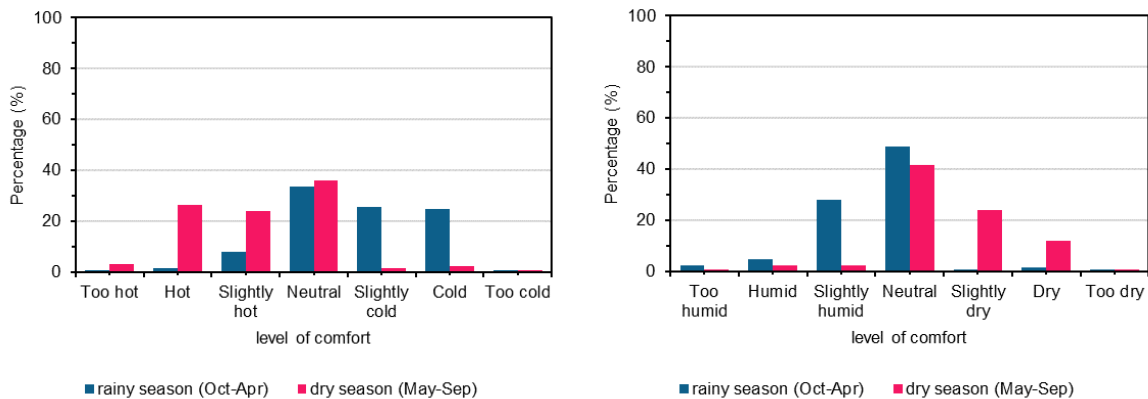


Figure 13 Occupants' comfort level of (a) air temperature (left); (b) relative humidity (right) in Rusunawa Kayu Putih

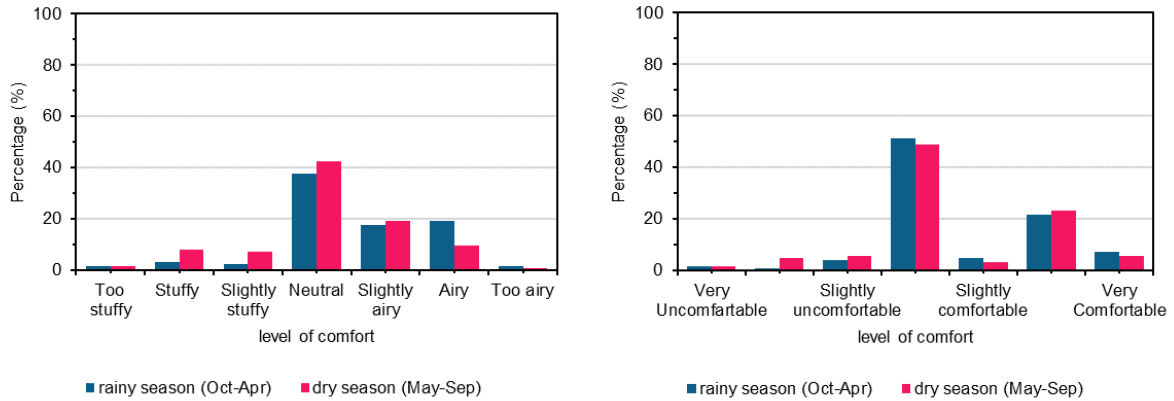


Figure 14 Occupants' comfort level of (a) air quality (left); (b) overall (right) in Rusunawa Kayu Putih

Their statement on mostly achieving thermal comfort is not related to the percentage of windows opening, which was only 20% of them who opened their windows throughout the day. The thermal comfort results were more in accordance with the usage hours on mechanical ventilation. It can be concluded that thermal comfort was achieved by active means such as fans and air conditioning.

## 6. FURTHER WORK

Some future work should be observed more to complete the whole research, such as producing adaptive thermal comfort range, identification of the comfort and discomfort hours, and interconnecting the comfort and discomfort hours to the usage of natural ventilation and mechanical ventilation. The comfort range used in this research was diverted from the Indonesian Nasional Standard, which might need to be adjusted. Future work on calculating the adaptive thermal comfort range must be calculated to identify the comfort and discomfort hours of the low-cost apartment buildings in Indonesia.

## 7. CONCLUSION

In general, it can be concluded that:

- 1) Most of the residents open their windows in the morning, at 6 a.m. and close them before sunset, at 5 p.m. This opening window pattern was influenced by the occupancy hours, activities such as cooking, showering, sleeping, and smoking, and the praying time.
- 2) Where the warmer hours were between 3 p.m. and 6 p.m., the occupancy hours were lower; which was not many people in the house during this hour, but the temperature was very high. It can be concluded that the occupancy hours might not be correlated with the hourly indoor air temperature. The indoor air temperature is presumably affected most by the outdoor temperature.
- 3) Most of the participants' perceptions of thermal comfort were not correlated with the percentage of windows opening during the day and night. The results showed that only 20% of participants opened their windows throughout the day, while around 50% of them experienced comfort during rainy and dry seasons. It should not be the opposite because natural ventilation is used to promote thermal comfort, which means that the more windows open during the day and night, the more comfortable hours are achieved.

## 8. ACKNOWLEDGEMENT

This research was supported by a Ph.D. studentship (Reference number: 42) funded by Indonesia Endowment Fund for Education (LPDP), Ministry of Finance, Republic of Indonesia and Puslapdik, Ministry of Education, Culture, Research, and Technology of Indonesia.

## 9. REFERENCES

- Alfata, Muhammad Nur Fajri; Sujatmiko, Wahyu; Widyahantari, R. (2012). Final Report of Innovation Research: The Effect of Air Movement on Thermal Comfort in Some Office Buildings in Some Big Cities in Indonesia. In *Thermal Comfort Study in the Office Buildings in Medan, Jakarta, Surabaya and Makassar*.
- Alfata, M. N. F., Hirata, N., Kubota, T., Nugroho, A. M., Uno, T., Antaryama, I. G. N., & Ekasiwi, S. N. (2015). Thermal Comfort in Naturally Ventilated Apartments in Surabaya, Indonesia. *Procedia Engineering*, 121, 459–467. <https://doi.org/10.1016/j.proeng.2015.08.1093>



- Andersen, R. V., Toftum, J., Andersen, K. K., & Olesen, B. W. (2009). Survey of occupant behaviour and control of indoor environment in Danish dwellings. *Energy and Buildings*, 41(1), 11–16. <https://doi.org/10.1016/j.enbuild.2008.07.004>
- ASHRAE. (2020). *Thermal Environmental Conditions for Human Occupancy*. [https://ashrae.iwrapper.com/ASHRAE\\_PREVIEW\\_ONLY\\_STANDARDS/STD\\_55\\_2020](https://ashrae.iwrapper.com/ASHRAE_PREVIEW_ONLY_STANDARDS/STD_55_2020)
- Brundrett, G. W. (1977). Ventilation: A behavioural approach. *International Journal of Energy Research*, 1(4), 289–298. <https://doi.org/10.1002/er.4440010403>
- Cao, Y., Pan, S., Liu, Y., Yu, H., Wang, X., Chang, L., Ni, M., & Liu, H. (2022). The window opening behavior of infant families: A case study during transition season in the cold region of China. *Energy and Buildings*, 254, 111588. <https://doi.org/10.1016/j.enbuild.2021.111588>
- Chai, Q., Wang, H., Zhai, Y., & Yang, L. (2020). Using machine learning algorithms to predict occupants' thermal comfort in naturally ventilated residential buildings. *Energy and Buildings*, 217, 109937. <https://doi.org/10.1016/J.ENBUILD.2020.109937>
- CIBSE. (2017). Environmental design. In *Environmental Design CIBSE Guide A*. <https://doi.org/10.5040/9781472596178-bed-e035>
- Du, J., & Pan, W. (2021). Diverse occupant behaviors and energy conservation opportunities for university student residences in Hong Kong. *Building and Environment*, 195, 107730. <https://doi.org/10.1016/j.buildenv.2021.107730>
- Dubrul, C. (1988). Inhabitant Behaviour with Respect to Ventilation - A Summary Report of IEA Annex VIII. *AIVC Technical Reports*, TN 23, 1–63. [http://www.aivc.org/Publications/publications.html#Technical-reports%5Cnhttp://www.aivc.org/Subscriptions/aivc\\_subscriptions.htm](http://www.aivc.org/Publications/publications.html#Technical-reports%5Cnhttp://www.aivc.org/Subscriptions/aivc_subscriptions.htm)
- Faheem, M., Bhandari, N., Tadepalli, S., & Abinaya, J. (2022). Investigation on window opening behavior in naturally ventilated hostels of warm and humid climate. *Energy and Buildings*, 268, 112184. <https://doi.org/10.1016/j.enbuild.2022.112184>
- Google Map. (n.d.). Retrieved June 19, 2022, from [google.com/maps](https://www.google.com/maps)
- Harso Karyono, T. (2011). Predicting Comfort Temperature in Indonesia, an Initial Step to Reduce Cooling Energy Consumption. *Buildings*, 5, 802–813. <https://doi.org/10.3390/buildings5030802>
- Jayasree, T. K., Jinshah, B. S., & Srinivas, T. (2022). The effect of opening windows on the airflow distribution inside naturally ventilated residential bedrooms with ceiling fans. *Building Services Engineering Research and Technology*, 43(1), 23–39. <https://doi.org/10.1177/01436244211024084>
- Kitagawa, H., Asawa, T., Kubota, T., Trihamdani, A. R., Sakurada, K., & Mori, H. (2021). Optimisation of window design for ventilative cooling with radiant floor cooling systems in the hot and humid climate of Indonesia. *Building and Environment*, 188(July 2020), 107483. <https://doi.org/10.1016/j.buildenv.2020.107483>
- Liu, Y., Chong, W. T., Cao, Y., Liu, H., Yu, H., Cui, T., Chang, L., & Pan, S. (2022). Characteristics analysis and modeling of occupants' window operation behavior in hot summer and cold winter region, China. *Building and Environment*, 216(November 2021), 108998. <https://doi.org/10.1016/j.buildenv.2022.108998>
- Mori, H., Kubota, T., Antaryama, G. N., Nastiti, S., & Ekasiwi, N. (2020). Analysis of Window-Opening Patterns and Air Conditioning Usage of Urban Residences in Tropical Southeast Asia. *Sustainability (Switzerland)*, Mori, H.,(20 December 2020). <https://doi.org/10.3390/su122410650>
- Murtyas, S., Hagishima, A., & Kusumaningdyah, N. H. (2020). On-site measurement and evaluations of indoor thermal environment in low-cost dwellings of urban Kampung district. *Building and Environment*, 184(June), 107239. <https://doi.org/10.1016/j.buildenv.2020.107239>
- Schünemann, C., Schiela, D., & Ortlepp, R. (2021). How window ventilation behaviour affects the heat resilience in multi-residential buildings. *Building and Environment*, 202, 107987. <https://doi.org/10.1016/J.BUILDENV.2021.107987>
- SNI. (2020). *SNI 6390:2020 Konservasi Energi Sistem Tata Udara pada Bangunan Gedung*.
- Szokolay, S. V. (2008). Introduction to architectural science: the basis of sustainable design. In *Journal of the American College of Radiology: JACR* (Vol. 8). <http://books.google.com/books?hl=en&lr=&id=VjwYnQ8q8I4C&oi=fnd&pg=PP2&dq=Introduction+to+Architectural+Science+the+basis+of+sustainable+design&ots=QJa9khbn7o&sig=ozEo4qjS0ICEY6z2OoDsbamwf50>
- Toe, D. H. C., & Kubota, T. (2013). Development of an adaptive thermal comfort equation for naturally ventilated buildings in hot-humid climates using ASHRAE RP-884 database. *Frontiers of Architectural Research*, 2(3), 278–291. <https://doi.org/10.1016/j.foar.2013.06.003>

Verbruggen, S., Delghust, M., Laverge, J., & Janssens, A. (2021). Habitual window opening behaviour in residential buildings. *Energy and Buildings*, 252, 111454. <https://doi.org/10.1016/j.enbuild.2021.111454>

Yao, M., & Zhao, B. (2017). Window opening behavior of occupants in residential buildings in Beijing. *Building and Environment*, 124, 441–449. <https://doi.org/10.1016/j.buildenv.2017.08.035>